

THE STRENGTH AND DEFORMATION CHARACTERISTICS OF A SOFT ALLUVIAL CLAY
UNDER FULL SCALE LOADING CONDITIONS

A Thesis Submitted to the
University of London
for the Degree of
Doctor of Philosophy in the Faculty of Engineering

by

Richard Stewart Pugh

Volume 1



June 1978

To my wife.

ABSTRACT

Extensive investigations into the strength and deformation characteristics of a soft alluvial clay have been made on a site adjacent to the River Thames at Stanford-le-hope in Essex.

The field investigations with which this work is primarily concerned, comprised both large diameter (from a test pit) and conventional piston sampling for laboratory testing purposes, vane shear and permeability testing and construction of five instrumented trial embankments.

The historical development of the Thames Tidal Defences and the geotechnical problems associated with their construction and maintenance are discussed. A geotechnical appraisal of the test site is presented together with a critical discussion of the laboratory test data and its relevance to the design of embankment foundations.

In view of current uncertainties regarding the use in design of shear strengths measured with the field vane apparatus a detailed study of this problem is made. Horizontal and vertical (small) vane tests were performed from, and adjacent to the test pit as part of a study of undrained strength anisotropy. A new (large) power driven vane was designed and used to investigate the effect of strain rate on the in-situ shear strength.

Construction, monitoring and instrumentation of the trial embankments are critically discussed and a new method of monitoring displacements during construction and failure is presented.

(ii)

The data from the foundation trials provide a detailed picture of the alluvial clay's behaviour under construction, failure and long-term loading conditions. The success achieved in the prediction of the various modes of behaviour, using both laboratory and small scale field test data, is critically assessed. Particular attention is paid to the determination of the field shear strength, in terms of total and effective stress, using limit equilibrium analyses and to the prediction of pore pressures and undrained displacements using finite element analyses.

ACKNOWLEDGEMENTS

The work described in this thesis was carried out as part of a project concerned with the influence of stress path on the strength and deformation characteristics of soils; financial support was provided by the Science Research Council and is gratefully acknowledged. The writer is particularly indebted to Professor A. W. Bishop for the opportunity to participate in the research work being performed within the Soil Mechanics Section of the Department of Civil Engineering at Imperial College of Science and Technology, University of London; and for his supervision and guidance throughout the course of the work.

A major part of the data presented herein was obtained in the field and therefore reflects the efforts of many people. Thanks are due to the following:-

The Anglian Water Authority under whose jurisdiction the Thames Tidal Defences fall, and their Consulting Engineers, Messrs. Binnie and Partners, for allowing the writer to actively participate in the foundation trials at Stanford-le-hope throughout the period of site work. Mr. D. L. Gudgeon was the Project Engineer (and is currently Deputy Chief Resident Engineer) for the main works, and Mr. A. J. Reid the Resident Engineer for the foundation trials. Particular thanks must go to Alan Reid, Arthur Harding and Mike Jeffries who, along with the writer, made most of the field observations presented in Chapters 4 and 5. The trial embankments were conscientiously constructed by the direct labour force of the A.W.A; the major part of the embankment instrumentation was installed by Messrs. Soil Instruments Ltd., whilst the photogrammetric work was carried out under the guidance of Messrs. Meridian Air Maps Ltd.

The conventional site investigation at Stanford-le-hope was performed by Messrs. Foundation Engineering Ltd., as was the boring associated with the large vane tests; in association with the latter Bob Skinner deserves mention for good organisation and Jeff Baty for good drilling practice. Alan Reid assisted the writer in the performance of the large vane tests and was also responsible for the sampling and in-situ vane testing from the test pit.

The carbon-14 dating of the peat layer encountered at the site was made by Dr. Harkness of the Scottish Universities Research and Reactor Centre.

The technical staff of the Soil Mechanics Section: Dave Evans, Fred Evans, Lou Spall, Ernie Harris and Eileen Gibbs have all been of great assistance throughout; their efforts in association with the design, construction and use of the various vane test calibration devices deserve particular mention.

Ernie Harris contributed greatly to the design of the large vane and Chris Pitches manufactured it to an admirable degree of precision. The carpentry work associated with the large vane was carried out by Bert Leete who also made the calibration apparatus for the Geonor vane.

Professor Francis kindly permitted the use of part of the hydraulics laboratory for testing and calibration of the large vane; calibration of the torsional load cell for the large vane was performed in the Department of Mechanical Engineering at Imperial College.

Joyce Gurr produced the photographs herein and also provided invaluable assistance with the time-lapse photography, both on and off site; Alf Kenney of City University processed the data.

Limit equilibrium computer programs were provided by Dr. S.K. Sarma of Imperial College and Mr. E. N. Bromhead of Kingston Polytechnic; the finite element computer program was provided by Dr. M.M.A.F. Hamza of Imperial College.

The academic staff at Imperial College; Professor J. N. Hutchinson, Dr. P. R. Vaughan, Dr. A. E. Skinner, Dr. R. J. Chandler, Dr. G. E. Green and Dr. S. K. Sarma, who always gave generously of their time and knowledge.

Also friends and colleagues: in particular Laurie Wesley with whom the writer worked closely in coordinating the field and laboratory work associated with the project, and behind whom (to his eternal shame) he trailed on many a lunchtime jog around Hyde Park; also Eddie Bromhead, Mauro Werneck, Mal Maguire, Mamdouh Hamza, Jane Walbancke, Ayad El-Ruwayih, Ufuk Ergun, James Apted, Sandro Sandroni, San Buri, Glen Truscott and Ian Symons for many helpful discussions throughout the course of the work.

Credit for the presentation of this thesis goes to Caryl Bromhead and Ula Schüler for tracing the majority of the figures and to Christine Sparrow for typing the text and the tables; all have stuck admirably to the task despite the passing years which the final preparation eventually spanned. John Goff kindly organised the photocopying at favourably commercial rates.

Special thanks must go to my wife Jane, who has endured for five years with alacrity; also to my parents, Ron and Ivy, and to my parents-in-law, John and Eileen Goff, without whom none of this would have been possible.

And, finally, to Sir William Halcrow and Partners for allowing me some leave of absence to enable my pen to reach this point.

CONTENTSVOLUME 1

	<u>Page</u>
Abstract	(i)
Acknowledgements	(iii)
Contents	(vii)
Notation	(xxiii)
(i) Symbols - general	(xxiii)
(ii) Subscripts/Superscripts	(xxviii)
(iii) Symbols - embankments and instruments	(xxix)
(iv) Abbreviations	(xxx)
<u>CHAPTER 1 - THE THAMES TIDAL DEFENCES</u>	1
1.1. Introduction	1
1.2. Historical Background	3
1.2.1. Pre-1953	3
1.2.2. Tides, Surges, the 1953 Floods and their Aftermath	7
1.3. Rebuilding the Defences after the 1953 Floods	10
1.4. The Current Improvement Scheme	16
1.4.1. General	16
1.4.2. Regional Geology	18
1.4.3. Site Investigation	21
(i) Field work	21
(ii) Laboratory work	22
1.4.4. The Role of Full Scale Field Tests in the Design	24

	<u>Page</u>
<u>CHAPTER 2 - MUCKING TEST SITE</u>	32
2.1. General	32
2.2. Site Investigation	33
2.3. Site Geology	35
2.4. The Alluvial Clay	38
2.4.1. General Description	38
2.4.2. Grading, Mineralogy and Index Properties	40
2.4.3. Consolidation Characteristics from Laboratory Tests	45
2.5. Ground-Water Conditions	48
2.6. In-Situ Stresses and Stress History	55
2.7. Laboratory Measurement of the Undrained Strength of, and Effective Stress Parameters for, the Soft Clay Foundation and their Use in Embankment Design	65
2.7.1. General	65
2.7.2. The Influence of Stress Path and Stress System	65
(i) Stress paths and stress system relating to embankment loading	65
(ii) Stress path and stress system influence on an isotropic elastic soil	68
(iii) Stress path and stress system influence on soft normally consolidated clays in nature	72
(iv) In-situ stress and stress history in relation to the laboratory measured undrained strength	75
2.7.3. Shear Strength Anisotropy	79
2.7.4. Sample Size and Strain Rate Effects	86
2.7.5. Undrained Strength/Depth Profile and Effective Stress Parameters	88
(i) Undrained strength	88
(ii) Shear strength of the desiccated layer	92
(iii) Effective stress parameters	93

	<u>Page</u>
2.7.6. Undrained Remoulded and Residual Strengths	94
2.8. Drained and Undrained Laboratory Deformation Characteristics of the Soft Clay Foundation	96
<u>CHAPTER 3 - FIELD VANE TESTS AT MUCKING</u>	135
3.1. The Field Vane Shear Test	135
3.1.1. Introduction	135
3.1.2. Factors Relevant to Vane Testing	136
(i) Soil disturbance	136
(ii) Number of blades	137
(iii) Vane shape and relative dimensions	138
(iv) Application and measurement of torque	139
(v) Rod friction	141
(vi) Relationship between applied torque and shear strength and shear modulus of soil	142
(vii) Undrained strength anisotropy	145
(viii) Rate of testing	148
(ix) Progressive failure	148
(x) Summary	149
3.2. Geonor Vane Tests	150
3.2.1. Introduction	150
3.2.2. The Equipment	154
3.2.3. Test Procedure	154
(i) Vertical tests	154
(ii) Horizontal tests	155
3.2.4. Discussion of Results	156
(i) Vertical tests	156
(ii) Horizontal tests	166
(iii) The undrained strength anisotropy of vertical and horizontal ' $\phi_u = 0$ ' planes in vane tests	172

	<u>Page</u>
(iv) Conclusions from, and uncertainties remaining after the performance and analysis of, the Geonor vane tests	184
3.3. Tests Carried Out with a New Large Vane Apparatus	188
3.3.1. Introduction	188
3.3.2. Testing Program	194
3.3.3. Testing Procedure	196
3.3.4. Test Results	200
3.3.5. Influence of Rotation Rate on the Measured Shear Strength	207
(i) Previous investigations into the effects of strain rate and consolidation on the field vane shear strength	207
(ii) Results obtained at Mucking	209
(iii) Implications with respect to Geonor vane test results	215
(iv) Conclusions	218
3.3.6. Stress-Strain Characteristics Measured in Vane Tests	219
3.4. Strain Rate Effects Observed in Laboratory and Field Tests Related to Full Scale Embankment Behaviour	222
3.4.1. Strain Rate Related to Fundamental Shear Strength Parameters	222
3.4.2. Observed Stress-Strain-Time Relationships	224
3.4.3. Application to Field Situations	226
3.5. The Selection of a Vane Shear Strength/Depth Design Profile and Factors Influencing that Selection	230

VOLUME 2Page

<u>CHAPTER 4 - CONSTRUCTION, INSTRUMENTATION AND FAILURE OF THE TRIAL EMBANKMENTS</u>	260
4.1. Descriptions and Aims of the Embankments	260
4.1.1. Bank 1, Stage 1	260
4.1.2. Bank 1, Stage 2	261
4.1.3. Bank 2	262
4.1.4. Bank 3	263
4.1.5. Bank 4	264
4.2. Site Work Prior to Instrument Installation and Embankment Construction	264
4.2.1. Prior to Instrument Installation	264
4.2.2. Prior to Embankment Construction	264
4.3. Construction, Monitoring and Failures	265
4.3.1. General	265
4.3.2. Bank 3	267
4.3.3. Bank 1, Stage 1	267
(i) Construction	267
(ii) Failure	268
4.3.4. Bank 1, Stage 2	268
(i) Construction	268
(ii) Failure	270
4.3.5. Bank 4	270
4.3.6. Bank 2	271
4.4. Discussion	271

	<u>Page</u>
<u>CHAPTER 5 - DETAILED RESULTS FROM THE INSTRUMENTATION OF THE TRIAL EMBANKMENTS</u>	287
5.1. Introduction	287
5.1.1. Overall Aims of the Instrumentation Program	287
5.1.2. Extent and Purpose of the Instrumentation Installed	287
5.1.3. The Presentation and Discussion of the Results	293
(i) General comments	293
(ii) Principles of measurement	294
(iii) Equipment	298
(iv) Application of instrumentation	298
(v) Interpretation of field observations	298
(vi) Final comments	298
5.2. Heave Pins	299
5.2.1. Bank 1	299
(i) Installation	299
(ii) Results	300
5.2.2. Bank 2 and Bank 4	301
(i) Installation	301
(ii) Results	302
(iii) Accuracy of observations	303
5.2.3. Final Comments	305
5.3. Horizontal Settlement Gauges (H.S.G. s)	309
5.3.1. Installation	309
5.3.2. Reading Equipment and Observational Procedure	310
(i) Reading equipment	310
(ii) Observational procedure	311
5.3.3. Accuracy of Vertical Displacements	316
(i) Precision of the equipment	316
(ii) Accuracy of measured displacements	319

	<u>Page</u>
5.3.4. Observed Vertical Displacements	321
(i) Bank 1, Stage 1	321
(ii) Bank 1, Stage 2	325
(iii) Bank 2	327
(iv) Final comments	331
5.3.5. Accuracy of Horizontal Displacements	333
(i) Precision of the equipment	333
(ii) Accuracy of measured displacements	333
5.3.6. Observed Horizontal Displacements	334
(i) Bank 1, Stage 1	334
(ii) Bank 1, Stage 2	335
(iii) Bank 2	336
(iv) Final comments	336
5.4. Inclinometers	343
5.4.1. Installation	343
5.4.2. Horizontal Displacement Observations	344
(i) Reading system	344
(ii) Reading process	347
5.4.3. Accuracy of Horizontal Displacements	349
(i) Precision of the instrument	349
(ii) Casing characteristics	349
(iii) Accuracy of the inclinometer system	350
(iv) Accuracy of the reading system	352
(v) Observational and data reduction errors	354
(vi) Summary	361
5.4.4. Observed Horizontal Displacements	362
(i) General	362
(ii) Face errors	364

	<u>Page</u>
(iii) Torpedo wheels in coupling when reading	366
(iv) Casing angles, angular changes, coupling readings and reading interval errors	366
(v) Vertical displacements of casings	373
(vi) Errors in keyway bearings	374
(vii) Horizontal displacements of casing bases	374
(viii) Final comments	375
5.4.5. Reading Process for Vertical Displacements	379
5.4.6. Accuracy of Vertical Displacement Observations	379
5.4.7. Observed Vertical Displacements	379
(i) Displacements of magnets in relation to soil	379
(ii) Observed displacements for Bank 1 and extrapolated data for Stage 1	382
(iii) Displacement profiles	386
(iv) Final comments	388
5.5. Piezometers	416
5.5.1. Installation	416
5.5.2. De-Airing	420
(i) General concepts	420
(ii) De-airing under initial hydrostatic conditions	422
(iii) De-airing during and after construction	423
5.5.3. Response Times	424
(i) General	424
(ii) Calculation from theory	427
(iii) Intake factors and system flexibility	431
(iv) Calculation of theoretical response times	435
(v) Summary	437
5.5.4. Site Procedure for Reading	437

	<u>Page</u>
5.5.5. Measured Pore-Water Pressures	438
(i) Equalisation after installation	438
(ii) Equalisation after de-airing	439
(iii) Performance of the system	439
(iv) Construction pore pressures	441
(v) Long-term observations - Bank 2, Bank 4	442
(vi) Summary	443
5.5.6. In-Situ Permeability Tests	443
(i) General	443
(ii) Theory for the constant head test	444
(iii) Test procedure	448
(iv) Discussion of results	450
(v) Summary	458
5.6. Slip Surface Indicators	478
5.6.1. Installation	478
5.6.2. Slip surface detection	478
5.7. Surface Movement Targets	480
5.7.1. General	480
5.7.2. Location by Triangulation Survey	481
(i) Procedure	481
(ii) Precision of target location	482
5.7.3. Location by Stereo Photogrammetry	484
(i) Introduction	484
(ii) Procedure	489
(iii) Precision of target location	491
5.7.4. Discussion of the Results	493
(i) During construction	493
(ii) During and after failure	495
5.7.5. Final Comments	498

	<u>Page</u>
5.8. Time-Lapse Photography	512
5.8.1. General	512
5.8.2. The Automatic Triggering System	513
5.8.3. Operation and Layout of the Photographic System	515
5.8.4. Analysis of the Results	516
(i) Determination of target image coordinates	516
(ii) Accuracy of measured coordinates	517
(iii) From image coordinates to field displacements	518
(iv) Precision of the observations	521
5.8.5. Discussion of the Results	521
(i) Bank 1, Stage 1	521
(ii) Bank 1, Stage 2	527
5.8.6. Final Comments	531
5.9. Temporary Bench Marks (T.B.M. s) and Level Surveys	554
5.9.1. Description and Installation	554
5.9.2. Level Surveying and Stability of Bench Marks	555
5.9.3. Accuracy of Level Survey	556
5.10. Vertical Settlement Gauges (Plates)	560
5.10.1. Description, Installation and Reading	560
5.10.2. Accuracy, and Assessment, of Results	561
5.10.3. Final Comments	562
5.11. Vertical Settlement Unit (V.S.U.)	567
5.11.1. Description, Installation and Reading	567
5.11.2. Accuracy, and Assessment, of Results	570
5.11.3. Final Comments	573
5.12. Conclusions	579

VOLUME 3

	<u>Page</u>
<u>CHAPTER 6 - BEHAVIOUR OF THE FOUNDATION MATERIAL UNDER THE APPLIED LOADING CONDITIONS</u>	583
6.1. Undrained Loading	583
6.1.1. Displacements	583
(i) Bank 1	583
(ii) Bank 2	587
(iii) Bank 4	588
6.1.2. Strains	588
(i) Horizontal strains	588
(ii) Vertical strains	594
(iii) Shear strains	597
(iv) Principal strains	599
6.1.3. Pore Pressures	602
(i) General	602
(ii) Pore-pressure predictions	610
6.1.4. Summary	641
6.2. Undrained Failure	689
6.2.1. Introduction	689
6.2.2. Bank 1, Stage 1	689
(i) General observations	689
(ii) Foundation instrumentation	691
(iii) Surface movements	692
(iv) Mechanism of failure	692
(v) Rates of movement	693
6.2.3. Bank 1, Stage 2	693
(i) General observations	693
(ii) Foundation instrumentation	694
(iii) Surface movements	696
(iv) Mechanism of failure	696

	<u>Page</u>
(v) Rates of movement	696
6.2.4. Summary	697
6.3. Consolidation, Settlement and Creep	709
6.3.1. Consolidation	709
(i) During construction	709
(ii) Post-construction	711
6.3.2. Settlement	712
6.3.3. Secondary Consolidation/Creep	713
6.3.4. Summary	715
6.4. The Direct Use of Field Measurements to Control Construction	734
6.4.1. Introduction	734
6.4.2. Displacements	734
6.4.3. Strains	736
6.4.4. Excess Pore Pressures	736
6.4.5. Summary	737
<u>CHAPTER 7 - ANALYSIS OF EMBANKMENT STABILITY USING LIMIT EQUILIBRIUM METHODS</u>	742
7.1. Methods, and Extent, of Analyses	742
7.1.1. Methods Used	742
7.1.2. Extent of Analyses	748
(i) Circular arc failure surfaces	748
(ii) Non-circular failure surfaces	749
7.2. Shear Strength Data for Limit Equilibrium Analyses	752
7.2.1. General	752
7.2.2. Summary of Data Used	758
(i) Total stress analyses	758
(ii) Effective stress analyses	759

	<u>Page</u>
7.3. Analysis of Bank 1, Stage 1 Failure	762
7.3.1. Maximum Fill Height-Total Stress Analyses	762
(i) General	762
(ii) Discussion of results	764
7.3.2. Maximum Fill Height-Effective Stress Analyses	766
(i) General	766
(ii) Discussion of results	768
7.3.3. Post-Failure Embankment Profile	769
7.4. Analysis of Bank 1, Stage 2 Failure	782
7.4.1. Maximum Fill Height-Total Stress Analyses	782
(i) General	782
(ii) Discussion of results	783
7.4.2. Maximum Fill Height-Effective Stress Analyses	786
(i) General	786
(ii) Discussion of results	787
7.4.3. Post-Failure Embankment Profile	789
7.5. Summary of Results of Stability Analyses for Bank 1	802
7.5.1. Introduction	802
7.5.2. Peak Shear Strength Parameters	806
(i) Total stress analyses	806
(ii) Effective stress analyses	809
7.5.3. Residual Shear Strength Parameters	811
7.5.4. Conclusions	813
7.6. Analysis of Bank 2	825
7.6.1. Introduction	825
7.6.2. Results of Analyses	825
7.7. Assessment of the Stability of Embankments on Very Soft Lightly Overconsolidated Clays	830
7.7.1. Introduction	830

	<u>Page</u>
7.7.2. Total Stress Analyses	831
7.7.3. Effective Stress Analyses	832
<u>CHAPTER 8 - ANALYSIS OF BANK 1, STAGE 1 USING THE FINITE ELEMENT METHOD</u>	834
8.1. Introduction	834
8.2. Method of Analysis	834
8.2.1. The Finite Element Method	834
8.2.2. Type of Elements	835
8.2.3. Constitutive Law	835
8.3. Analysis of Bank 1, Stage 1	836
8.3.1. Discretisation of the Continuum	836
8.3.2. Soil Properties	837
(i) The Mucking clay	837
(ii) The gravel	840
(iii) The sand fill	840
8.3.3. In-Situ Stresses	841
8.4. Results of Analyses	841
8.4.1. Comparison of Predicted and Observed Displacements	841
8.4.2. Predicted States of Stress Within the Foundation	846
8.5. Summary	848
<u>CHAPTER 9 - CONCLUSIONS</u>	853
References	862
<u>APPENDIX 1 - VANE TORQUE/SOIL SHEAR STRENGTH RELATIONSHIP: VERTICAL VANE TESTS</u>	A1
<u>APPENDIX 2 - CALIBRATION OF GEONOR VANE</u>	A2
A.2.1. Vertical Calibration	A2
A.2.2. Horizontal Calibration	A3
A.2.3. Discussion of Results	A3

	<u>Page</u>
<u>APPENDIX 3 - ANISOTROPIC ANALYSES FOR FIELD VANE TESTS</u>	A11
A.3.1. Analysis of Horizontal Vane Test Using Equation 2.15	A11
(i) The cylindrical surface	A11
(ii) The end surfaces	A12
A.3.2. Analysis of Horizontal Vane Test Using Equation 2.15(A)	A13
(i) The cylindrical surface	A13
(ii) The end surfaces	A13
A.3.3. Analysis of Horizontal Vane Test Using Equation 3.3	A14
(i) The cylindrical surface	A14
(ii) The end surfaces	A14
A.3.4. Analysis of Horizontal Vane Test Using Equation 3.3(A)	A15
(i) The cylindrical surface	A15
(ii) The end surfaces	A15
A.3.5. Analysis of Vertical Vane Test Using Equation 2.15	A16
A.3.6. Analysis of Combined Results of Horizontal and Vertical Vane Tests	A16
 <u>APPENDIX 4 - DESIGN, CONSTRUCTION, TESTING AND CALIBRATION OF THE LARGE VANE APPARATUS</u>	 A20
A.4.1. General	A20
A.4.2. Design of the Vane	A20
A.4.3. Construction of the Vane	A21
A.4.4. Design of the Vane Rods	A22
A.4.5. Design of the Loading Frame and Torque Measuring System	A24
(i) General	A24
(ii) Applied forces and component specifications	A27
A.4.6. Design of the Mechanical Drive System	A29
A.4.7. Testing and Calibration of the Large Vane Apparatus	A31
(i) Testing	A31
(ii) Calibration	A34

	<u>Page</u>
(iii) Calculations	A39
<u>APPENDIX 5 - STRESSES AND STRAINS ASSOCIATED WITH A VANE TEST IN AN ELASTIC SOIL</u>	A55
<u>APPENDIX 6 - DETAILED DATA RELATING TO LIMIT EQUILIBRIUM ANALYSES</u>	A58

NOTATION(i) Symbols - General

A	pore-pressure parameter
A	constant for horizontal vane test analysis (Chapter 3; Appendix 3)
A_r	area ratio of vane (Chapter 3)
a	parameter reflecting the influence of pore pressure on undrained strength anisotropy with rotation of principal stresses
a_α	parameter reflecting the influence of pore pressure on undrained strength anisotropy with rotation of shear plane (Chapter 3, Appendix 3)
a	cross-sectional area of standpipe (section 5.5)
a	pore-pressure parameter (Chapter 6)
a	curve fitting parameter (Chapter 8)
B	pore-pressure parameter
B	constant for vertical vane test analysis (Chapter 3; Appendix 3)
b	parameter reflecting the directional characteristics of c' and ϕ' , as well as pore pressure, on undrained strength anisotropy with rotation of principal stresses
b_α	parameter reflecting the directional characteristics of c' and ϕ' , as well as pore pressure on undrained strength anisotropy with rotation of shear plane
b	width of slice (Chapter 7)
b	curve fitting parameter (Chapter 8)
C_u	undrained shear strength
$C_{u\theta}$	C_u with the major principal stress at an angle θ° to the soil's vertical axis
C_{uV}	C_u with the major principal stress in the direction of the soil's vertical axis
C_{uH}	C_u with the major principal stress in the direction of the soil's horizontal axis
$C_{u\alpha}$	C_u associated with a shear plane at an angle α to the vertical
C_{uV}	C_u associated with a vertical shear plane
C_{uH}	C_u associated with a horizontal shear plane
C_{V1}	coefficient of consolidation (one-dimensional volume change)
C_{V3}	coefficient of consolidation (three-dimensional volume change)
C_c	virgin compression index
C_r	recompression index
C	constant for isotropic analysis of vane test (Chapter 3; Appendix 3)
C	load in jockey wheel pivot-large vane (Appendix 4)
C	coefficient of compressibility (Chapter 6)
c'	apparent effective cohesion intercept

D	diameter of vane
D	depth factor (Chapter 1)
D_{DW}	drive wheel diameter-large vane (Appendix 4)
D	outer diameter of piezometer cavity (section 5.5)
D	coefficient of dilation (Chapter 6)
d	differential or change
d_c	circumferential displacement of vane (Appendix 4)
d_{DW}	circumferential displacement of drive wheel-large vane (Appendix 4)
E	Young's Modulus
E_u	undrained deformation modulus
E_{u50}	undrained deformation modulus at 50% of axial failure strain in laboratory test
E_D	drained deformation modulus
E_H	Hvorslev's (1951) equalisation ratio
E_G	Gibson's (1963) equalisation ratio
E_X	Young's Modulus in the direction of the axis of soil symmetry (Chapter 2)
E_Z	Young's Modulus in any direction normal to the axis of soil symmetry (Chapter 2)
E	normal force on inter-slice boundary (Chapter 7)
e	void ratio
F	factor of safety
F	piezometer intake factor (section 5.5)
F_{OUT}	} outward and inward friction head losses in piezometer tubing
F_{IN}	
F_L	factor of safety against vertical shear (Chapter 7)
f()	function of
f(r)	function describing the distribution of mobilised shear stress across the ends of the vane 'cylinder'
fn	aperture size of lens
f	focal length of lens
f(x)	function defining the variation in the angle of the inter-slice resultant force in Morgenstern-Price stability analysis (Chapter 7)
f(x)	function defining the variation in the factor of safety against vertical shear in Sarma stability analysis (Chapter 7)
G	shear modulus
G_s	specific gravity
g	gravitational acceleration
H	drainage path length
H_c	critical height of embankment
H	height of vane (Chapter 3, Appendices 1 - 5)

h	height of fill, or foundation plus fill, above a point
h_w	head of water
h	distance over which G.W.L. is lowered (Chapter 2)
h	horizontal displacement error in inclinometer readings (section 5.4)
I	influence factor
I_B	brittleness index
I_p	plasticity index
I_{pm}	modified plasticity index
i	minimum angle between shear plane and vertical
i	slope angle of embankment (Chapter 1)
K_0	coefficient of earth pressure at rest
K_a	coefficient of active earth pressure
K_p	coefficient of passive earth pressure
K	bulk modulus
K_C	critical earthquake acceleration
k	coefficient of permeability
k_C	coefficient of permeability of piezometer ceramic
L	length of piezometer cavity
M	slope of critical state line in p'/q' stress space for triaxial conditions
M_{V1}	coefficient of volume compressibility (one-dimensional volume change)
M_{V3}	coefficient of volume compressibility (three-dimensional volume change)
m	ratio of intermediate principal effective stress to the sum of the major and minor principal effective stresses
m	permeability transformation factor (section 5.5)
n	r.p.m.
n	anisotropy ratio E_x/E_z (Chapter 2)
n	slice number (Chapter 7)
P	proving ring load
p	all round stress ($= \frac{\sigma_1 + \sigma_2 + \sigma_3}{3}$)
p_p	all round stress ($= \frac{\sigma_1 + \sigma_3}{2}$)
p_0	in-situ vertical stress
p_{op}	value of p_p corresponding to p_0' and $K_0 p_0'$
p_c	preconsolidation pressure

p_t'	maximum tensile effective stress soil can sustain
p_H	pressure head on inflow side of de-airing unit
Q	rate of flow or discharge
q'	deviator stress ($= \sigma_1' - \sigma_3'$)
R	resultant displacement
R	reading interval along inclinometer casing (section 5.4)
R_V	vertical reading interval for inclinometer (section 5.4)
R	radius of loaded area (Chapter 6)
r	radial dimension
r_c	radius of piezometer cavity
r_o	radius of vane
r_p	radius of piezometer
r_u	pore-pressure ratio
S_t	sensitivity
T	time factor
T_L	basic time lag
T_T	horizontal force - Geonor vane calibration (Appendix 2)
T_r	inclined force - Geonor vane calibration (Appendix 2)
T	drive chain tension - large vane (Appendix 4)
t	time
t_x	time for 'x' percent dissipation of pore pressure
U	percent dissipation of pore pressure
U_z	percent dissipation of pore pressure at depth 'z'
u	pore-water pressure
u_o	initial pore-water pressure
u_s	pore-water suction
u	object distance (sections 5.7 and 5.8)
V	volume
V	volume factor for piezometer system (section 5.5)
v	image distance
v	vertical location error in inclinometer readings (section 5.4)
v	velocity of flow through piezometer system (section 5.5)
v_H	vacuum head on outflow (return) side of de-airing unit (section 5.5)
W	weight
w	water content
X	shear force
x	C_{uH}/C_{uV}
x_α	C_{uH}/C_{uV}
x	$2(1 - A_f)$ (Chapter 2)

x_{hor}	horizontal displacement of inclinometer casing
x_{arc}	equivalent arc length to x_{hor}
z	depth
z_0	depth range over which horizontal normal stress is tensile
α	inclination of failure plane to vertical
α_v	vane test constant
α	factor reflecting effective stress changes consequent upon installation of push-in piezometer (section 5.5)
α	pore-pressure parameter (Chapter 6)
β	inclination of failure plane (minimum angle) to major principal plane
β	factor reflecting effective stress changes consequent upon installation of push-in piezometer (section 5.5)
Γ	critical void ratio
γ_B	bulk unit weight
γ_D	dry unit weight
γ_W	unit weight of water
γ	shear strain
γ_e	elastic shear strain
γ_p	plastic shear strain
γ_0	shear strain at vane circumference
γ_r	shear strain at radial distance 'r' from vane centre
Δ	change
δ	partial differential or change
δ	inclinometer casing twist or misalignment
ϵ	linear strain
θ	inclination of major principal stress to vertical
θ_c	inclination - Geonor vane calibration
θ_1, θ_2	inclinations of inclinometer casing to two vertical orthogonal planes
θ	inclination of inclinometer casing to vertical (section 5.5)
θ	angle of slip surface to horizontal (Chapter 7)
λ	factor reflecting influence of piezometer's permeability on results of C.H.T.
λ	scale factor in Morgenstern-Price stability analysis (Chapter 7)
λ	scale factor in Sarma stability analysis (Chapter 7)
μ	vane test correction factor
μ	piezometer/soil system flexibility function (section 5.5)
ν	Poisson's Ratio
ν_1	Poisson's Ratio for strains in the plane normal to the axis of soil symmetry caused by a strain increment in either direction

ν_3	Poisson's Ratio for strains in the plane normal to the axis of soil symmetry caused by a strain increment along the axis of soil symmetry
ρ	vertical settlement of inclinometer casing base
Σ	summation
σ	normal stress
σ_{OCT}	octahedral normal stress
σ_{θ}	circumferential (hoop) stress
σ_r	radial stress
σ_D	deviator stress
σ_r	deviator stress level (Chapter 8)
T	torque
T_{VER}	torque mobilised in vertical vane test
T_{HOR}	torque mobilised in horizontal vane test
T_c	component of torque deriving from 'cylindrical' vane surface
T_e	component of torque deriving from end surfaces of vane
τ	shear stress
τ_{OCT}	octahedral shear stress
τ_o	shear stress at vane circumference
τ_r	shear stress at radial distance 'r' from vane centre
τ_H	shear stress on horizontal plane
τ_V	shear stress on vertical plane
ϕ'	effective angle of shearing resistance
ϕ_u	undrained angle of shearing resistance
ω	angular rotation
ω_o	angular rotation of vane

(ii) Subscripts/Superscripts

A	axial
C	compression
CS	critical state
CR	critical
E	extension
FV	field vane
f	at failure
H	horizontal
h	horizontal
i	initial

MAX	maximum
MIN	minimum
MOB	mobilised
P	plane strain
PSA	plane strain active
PSP	plane strain passive
p	peak
r	residual
rm	remoulded
T	total
TC	triaxial compression
TE	triaxial extension
t	at time 't'
u	undrained
V	volumetric
v	vertical
x	horizontal coordinate direction in limit equilibrium analysis
1	major principal value
2	intermediate principal value
3	minor principal value
'	effective stress

(iii) Symbols - Embankments and Instruments

A	}	Section lines - Bank 1
Q		
B		
C	Section line (centre) - Bank 2	
D	Section line (centre) - Bank 3	
E	Section line (centre) - Bank 4	
X	horizontal (plane strain) site coordinate axis	
Y	horizontal site coordinate axis	
Z	vertical site coordinate axis	
H	heave pin	
H.S.G.	horizontal settlement gauge	
A-K	H.S.G. magnets	
I	inclinometer	
M1	upper magnet on casing	
M2	lower magnet on casing	
P	piezometer	

I piezometers installed to monitor seasonal pore-pressure changes
R.P.,R reference pin
SS slip surface indicator
SP vertical settlement gauge (plate)
S,ST surface target
T.B.M. temporary bench mark
t time-lapse camera target
V.S.U. vertical settlement unit
W observation well

(iv) Abbreviations

A.S.A. American Standards Association
A.O.D. Above Ordnance Datum
A.W.A. Anglian Water Authority
B.P. Before Present
B.G.L. Below Ground Level
B.S.K. British Standard Key
C.F. Calibration Factor
C.H.T. Constant Head Test
C.P.T. Cone Penetration Test
D.S.S. Direct Simple Shear
E.R.A. Essex River Authority
E.S.P. Effective Stress Path
F.o.S. Factor of Safety
F.E.Ltd. Foundation Engineering Ltd.,
F.V. Field Vane
F.E.M. Finite Element Method
G.L. Ground Level
G.L.C. Greater London Council
G.W.L. Ground-Water Level
G.V. Geonor Vane
H.P. Horse Power
H.W.S. High Water Spring (Tide Level)
I.D. Inner Diameter
I.G.S. Institute of Geological Sciences
K.R.A. Kent River Authority
L.L. Liquid Limit
L.V. Large Vane

M.A.F.F.	Ministry of Agriculture, Fisheries and Food
M.H.W.N.	Mean High Water Neap (Tide Level)
M.H.W.S.	Mean High Water Spring (Tide Level)
M.L.W.N.	Mean Low Water Neap (Tide Level)
M.L.W.S.	Mean Low Water Spring (Tide Level)
me	milli-equivalents
$\mu\epsilon$	micro-strain
N.T.S.	Not to Scale
O.C.R.	Overconsolidation Ratio
O.D.	Outer Diameter
O.G.L.	Original Ground Level
O.S.	Ordnance Survey
O ₂	Oxygen
P.C.D.	Pitch Circle Diameter
P.F.A.	Pulverised Fuel Ash
P.L.	Plastic Limit
p.p.m.	parts per million
P.S.A.	Plane Strain Active
P.S.P.	Plane Strain Passive
P.V.C.	Poly Vinyl Chloride
r.p.m.	revolutions per minute
S.P.T.	Standard Penetration Test
T.C.	Triaxial Compression
T.E.	Triaxial Extension
T.S.P.	Total Stress Path
S.H.A.N.S.E.P.	Stress History and Normalised Soil Engineering Properties
U.S.B.R.	United States Bureau of Reclamation
Y.L.I.G.H.T.	Yield Locus Influenced by Geological History and Time

CHAPTER 1

THE THAMES TIDAL DEFENCES

1.1. Introduction

The River Thames is fully tidal as far as Richmond Lock and semi-tidal to Teddington Lock (figure 1.1). The tidal defences to which the work in this thesis relates, however, are those from Barking in the west to Leigh-on-Sea in the east. The many tidal rivers and creeks in Essex are such that no part of the county is less than 55km from tidal waters. Protection from these is afforded by over 500km of man-made defences (almost entirely earth embankments) around the coast and tidal inlets from Barking Creek to the River Stour. The defences, behind which are 49,000 hectares of low lying ground, are the responsibility of the newly formed Anglian Water Authority (A.W.A.), which superseded the Essex River Authority in 1974.

The earth embankments along the Thames Estuary are founded on recent alluvium, deriving from material washed down into the Thames by numerous rivers and redeposited by tidal flows. Archaeological evidence from buried remains, dating from the Stone Age through to Roman times, indicates that the sea has advanced and retreated many times over the past 7000 years. Geological evidence, from the particle sizes deposited and dating of peat layers (Greensmith and

Tucker, 1973), reinforces this view, although the exact sequence of the various advances and retreats is uncertain. The general rise in sea level, in this area, since the end of the last glaciation appears, however, to be beyond doubt.

The deposition of the alluvium is continuing to this day and an insight into its variability can be had by viewing the present day environment of the intertidal mud flats. Deposition occurs, between high and low water levels, over a wide, fairly flat (intertidal) area. Due to the fall-off in the velocity of the tidal currents as they move across the intertidal area, coarser material is probably deposited towards low water level and finer material towards high water level (Evans, 1965). This is a fairly simple picture of the deposition of fine material (sand, silt and clay) as it occurs today, and indeed the majority of the alluvium is so constituted, with the gravels generally being of Pleistocene origins. The other material regularly encountered is peat, in various forms, representing advances of the sea; organic material generally is also in evidence.

The mud flats are traversed by a multitude of drainage courses, which range from very small streams to deep, steep sided creeks. The smaller streams which flow out across the mud flats are continually changing position and thus eroding and redepositing near surface material.

The tides which transport the soil particles also carry seeds of salt-resisting flora and these may grow on the mud flats, tending to trap additional material. Thus saltings are formed and the tidal ebb and flow becomes confined in a series of creeks. These creeks can form sizeable channels whose banks may slip and form shear surfaces in the alluvium. Eventually a salting may become so high that only the highest tides cover it, and with vegetation firmly established it starts to dry out. Such a salting is rich in mineral salts and forms ideal pasture for sheep. Much of the reclaimed land along the Essex coast has derived from the building of earth embankments around such saltings.

The downward flow of rainwater, where suitable ground-water conditions exist, may leach the salt from the pore water in the upper part of the clay to the extent where freshwater flora become predominant. Under these conditions the alluvium is converted to good arable land, although at depth the pore water tends to remain saline due to the presence of underlying, salt-water bearing, permeable strata (river gravels). Hence the general absence of trees and deep rooted vegetation on the marshland areas. Such a leaching process will increase the sensitivity of some alluvial deposits, depending on their grading and mineralogical content.

1.2. Historical Background

1.2.1. Pre-1953

This section provides a brief review of the historical development of the Essex marshlands and their sea defences. For a much fuller

account of this, as well as a detailed account of the 1953 floods, the reader is referred to Hilda Grieve's excellent book 'The Great Tide' (1959), from which much of this section is derived.

Although sheep are reported grazing on extensive areas of the Essex marshlands in the Domesday Book of 1086 (Grieve, 1959) there is no evidence of any sea defence works being instigated before the late 12th and early 13th century. Up to that time only wattle bridges over the creeks, and causeways of peat sods were provided to enable the sheep to flee in times of inundation. The first defences were referred to as fossatum (meaning dyke), implying a bank with a ditch from which the clay had been won or delved; hence the term delf or delph ditch as these are known locally. They are referred to on Ordnance Survey maps, and in parts of this thesis as drains. The present day defences are still mainly constructed from clay alluvium although the variability of this material means that in many cases it is far from ideal for such purposes. In particular, the clay is often highly plastic and prone to extensive shrinkage and cracking during prolonged dry periods.

From the time of these earliest defences, throughout the periods from the 12th to 16th century, the story is one of frequent floods caused by ever increasing tide levels: this period appears to have suffered particularly frequent periods of stormy weather (Peters, 1953). With each overtopping and/or breaching of the defences they were raised ever higher and many of today's embankments are the end product of work started centuries earlier. The seaward slopes were protected

by brushwood faggots, held down by wooden stakes, this practice gradually giving way to facings of chalk and claystones (from the London Clay) locked in position between rows of wooden piles. Some of the former, dating from the Middle Ages, were not replaced however, until well into the 19th century.

Canvey Island was reclaimed during a relatively floodless period in the calmer (meteorologically speaking) 17th century. Throughout the history of the defences cost has been a, if not the, major factor controlling their condition and, indeed, very existence, both in terms of funds available for their construction and upkeep, and the economic viability of protecting the land from flooding. In the past many breaches were left unrepaired, allowing the sea to reclaim thousands of hectares for long periods and some land was lost forever in this way. A striking example is the breach that occurred at Sandcreek Sluice, near Dagenham, on 29th October, 1707. This started as a 4m wide breach, but developed to 125m wide with the sea extending inland some 2.5km, and remained open for 13 years, finally costing £80,000 to repair.

The 18th century saw the introduction of hollow drainage (land drains) to the marshland, resulting in greater agricultural potential and thus increased value. Imported Kentish ragstone, pitched on chalk, was introduced as a facing material in this period. As the value of the land increased so did the economic desirability of protecting it. In this respect the 19th century brought not only further reclamation but also the dramatic effects of the Industrial Revolution. With the

railways, docks and industrial plants came a sudden increase in the population of the waterfront areas. Particularly industrialised was the area from London's dockland down river to Thames Haven, where the first petroleum storage tanks were built in 1880.

All the while the sequence of ever increasing tide levels and breaches in the defences continued unabated. Tidal records dating back to the early 19th century show that not only had mean sea level risen 230mm in the 120 years previous to 1953, but also that the frequency of exceptional surges* was increasing (Farquharson, 1953). A summary of the worst of these is presented in table 1.1.

DATE	HEIGHT OF SURGE	PREDICTED HEIGHT OF TIDE	MAXIMUM SEA LEVEL
	m.	m.A.O.D.	m.A.O.D.
Nov.1897	2.13	2.50	4.15
Jan.1928	1.65	2.52	4.15
Feb.1938	1.98	2.35	4.18
Mar.1949	2.29	2.47	4.21
Jan.1953	2.59	2.53	4.69

Table 1.1.

Exceptional Surges at Sheerness (after Farquharson, 1953)

N.B. M.H.W.S. = 2.71 m.A.O.D.)
H.W.S. = 3.20 m.A.O.D.) Sheerness

*as defined in 1.2.2.

With each instance of flooding plans were made to raise the sea defence levels. The Essex Rivers Catchment Board, formed in 1931, inherited defences which were generally in poor condition (Snell, 1953). After the 1938 floods, plans were implemented to raise the defences to between 300 and 600mm above that level. Many of the delph ditches were to be backfilled, and new ones dug, to leave a more substantial berm (6 to 9m wide) on the landward side. World War II delayed this work until 1946 and it was still incomplete in 1949 when another high tide level caused flooding. A new design level of between 300 and 600mm above the 1949 level was then adopted. As part of these improvements new revetments, comprising concrete blocks with bitumen-mortar joints, were introduced and landward slopes flattened to 1:2.5. The Essex River Board was formed in 1951/2 and assumed responsibility for the County's sea and tidal river defences, which were about to be subjected to the fiercest attack from the sea in recorded history.

1.2.2. Tides, Surges, the 1953 Floods and their Aftermath

Mean sea level is subject to both periodic and non-periodic fluctuations. The former category is confined to tidal variations, as the relative positions of sun, moon and earth vary, on a 28 day (lunar) cycle, with spring tides occurring every 15 days (2 days after full and new moon). Likewise neap tides occur every 15 days, interposed between the spring tides. The actual tide level and range also vary with the geometry of the coast line, and these variations may be quite considerable. Variations along the Thames Estuary are shown in table 1.2.

Non-periodic fluctuations are primarily due to the combined meteorological effects of wind and barometric pressure, but predominantly the former. Flow of water from inland rivers also contributes to this category. Tide data calculated for the Thames are based on average flows over Teddington Weir; extremely high flows can elevate the level at London Bridge by up to 300mm but their effects are negligible at Southend.

LOCATION	M.H.W.S.	M.H.W.N.	M.L.W.N.	M.L.W.S.	TIDAL RANGE (metres)	
	m.A.O.D.	m.A.O.D.	m.A.O.D.	m.A.O.D.	SPRING	NEAP
SHEERNESS	2.80	1.90	-1.40	-2.3	5.10	3.30
SOUTHEND	2.80	1.90	-1.50	-2.4	5.20	3.40
THAMES HAVEN	3.15	2.15	-1.65	-2.55	5.70	3.80
TILBURY	3.38	2.28	-1.72	-2.62	6.00	4.00
WOOLWICH	3.75	2.55	-1.95	-2.75	6.50	4.50
LONDON BRIDGE	3.90	2.70	-1.90	-2.70	6.60	4.60
CHELSEA BRIDGE	4.01	2.81	-1.49	-1.99	6.00	4.30
BARNES BRIDGE	4.13	3.13	-0.47	-0.87	5.00	3.60
RICHMOND LOCK	4.39	3.19	+0.49	+0.19	4.20	2.70

Table 1.2.

Tidal Variations in the Thames and its Estuary

(Data from Admiralty Tide Tables, Volume 1, 1972)

A surge is an elevation or depression of sea level by meteorological conditions, such occurrences being fairly common in the North Sea. Depressions of sea level (negative surges) are only a danger to navigation in shallow waters, whereas elevations (positive surges) present a major threat to coastal defences, being usually accompanied by high winds. Storm surges in the North Sea are generally associated with deep depressions moving from the north of Scotland towards southern Scandinavia and northern Germany (Peters, 1953).

From the continuous monitoring of tide levels at various ports, tide levels can be predicted according to location and astronomical conditions for average meteorological conditions and river flows. Storm surges are superimposed on the tidal elevations and cannot be predicted except as statistical probabilities. Table 1.1 provides a breakdown of previous exceptional sea levels into the maximum surge height and tidal elevation. This shows that the maximum height of surge does not coincide with high tide level or with a tide above M.H.W.S. on any of these occasions. Whether or not a surge results in sea elevation reaching danger level depends upon:-

- i. The force and duration of the winds causing the surge.
- ii. The predicted tide height.
- iii. The phasing of the tide and surge.

It is felt that there may be a limit on the height of a surge (3m approximately) arriving in the Thames Estuary at other than near low water, but that there appears to be no reason why smaller surges may not, in the future, be superimposed on tides above M.H.W.S. (Farquharson, 1953).

The depression of 31st January/1st February, 1953 (970 millibars minimum) brought winds of force 10 to 11 and a storm of unequalled ferocity since meteorological records were started. The height of the surge at Southend approached 2.75m and in addition was at a height of 1.80m and above for more than 15 hours. Sea elevations were up to 700mm higher than anything previously recorded in the Thames Estuary, although at Richmond the level was 150mm below that of 1928.

The storm left in its aftermath 839 separate breaches of the defences in Essex, totalling 108km of failed embankments. The breaches were up to 45m wide and between 1.5 and 6m deep. Tens of thousands of millions of litres of sea water poured through the breaches flooding a total area of 21,900 hectares, of which 16,600 hectares was agricultural land, as well as industrial and social service installations and homes, making 21,000 people homeless (compared to 86,549 in Essex during the whole of World War II). One hundred and twelve people lost their lives in Essex out of a national total in excess of 300. It is interesting to note that the design of flood defence embankments is not covered by the Reservoirs Act (1975), although their failure resulted in probably the greatest peacetime disaster known in Great Britain.

1.3. Rebuilding the Defences after the 1953 Floods

Extensive temporary repair work was carried out immediately after the floods to prevent further encroachment by the sea. This achieved, there were two main immediate objectives:-

- i. To assess the damage to defences and ascertain the causes of that damage.
- ii. To prepare new design standards and rebuild as soon as possible.

With respect to the former the Building Research Establishment (then Station) was asked to carry out an investigation into the soil-mechanics aspects of the failures (Cooling and Marsland, 1953) in conjunction with the Essex River Board (Snell, 1953). A variety of mechanisms of embankment failure were postulated, including those listed below:-

- i. Erosion of the seaward face by wave action, this being confined to very exposed locations.
- ii. Seepage through the fissured zone extending from high water mark on the seaward face, over the embankment crest and down the landward slope.
- iii. Overtopping followed by erosion of the landward slope and crest.
- iv. Uplift of the landward toe area due to artesian pressures in underlying permeable strata.
- v. Erosion through animal holes.
- vi. Erosion of new fill poorly bonded to an old embankment.

Inspection of partially breached sections showed that many shallow slips had occurred on the landward sides of the embankments. At the time these were attributed to seepage, with overtopping as a secondary factor causing further erosion. However, a full scale test to failure of an embankment showed that although considerable seepage occurred the bank did not fail until overtopped (Marsland, 1957(a) and 1966).

When marginally overtopped, erosion of the fissured backslope occurred, followed by a shallow slip. This in turn was followed by rapid erosion of the crest leading to a full scale breach. Another interesting point to arise was that very little seepage occurred through the body of the embankment although the 1m or so fissured surface layer had a permeability of the order of magnitude of a gravel. A trench excavated through an existing embankment at the Mucking test site (Chapter 2) also revealed the clay to be unfissured below a depth of about one metre.

Failure due to uplift pressures in underlying strata was not thought to have been a major occurrence, but where this mechanism did operate failure was very dramatic (Marsland, 1961). Where the overlying soils were impermeable (clays) failure was in the form of uplift and fracture whereas with more permeable soils (silts and sands) piping and quick conditions resulted.

The new design standard adopted by the Essex River Board was the 1953 tide level plus 600 to 900mm, according to local circumstances, but this was far from easy to achieve for various reasons:-

- i. Site conditions in many industrialised areas were unsuited to the raising of earth embankments because of frontage problems.
- ii. Likewise in agricultural areas where valuable land would need to be sacrificed, or high costs incurred if imported construction materials were used.

- iii. The weak foundation material meant that the combination of embankments, seaward creeks and landward delph ditches were, in many cases, close to limiting equilibrium.
- iv. On exposed coast lines earth embankments are very susceptible to frontal erosion.

The majority of the problems can be seen to stem directly or indirectly from the nature of the alluvial foundation material which is predominantly marsh clay. Typical geotechnical properties of the marsh clay are presented in table 1.3 which shows the clay to be typically very soft, very sensitive, organic and highly plastic, with the liquidity index close to unity. The stability problem associated with embankments on such a clay is illustrated in figure 1.3. This presents a much simplified version of the problem, wherein the embankment and foundation material have been considered as having a uniform undrained shear strength* and being underlain at some depth by a hard stratum. The curves illustrated in the figure are based on Taylor's (1948) stability numbers. For an average undrained strength of 12.5 kN/m^2 and an embankment slope of 1:2.5, the range of critical heights, H_c , (implying a factor of safety (F.o.S.) of unity) is from 7.15 to 4.5m as the depth ratio (D) increases from 1 to 4. With greater depths to a hard stratum (H_c/D) there is no significant decrease in the critical height which can be achieved.

The landward delph ditches and seaward river channels tend to reduce the allowable embankment height, and in the extreme case of the delph ditch extending to the embankment toe H_c is the height from the bottom

*the shear strength of the embankment material has little effect on the stability, as will be shown in Chapter 7.

LIQUID LIMIT	LL	80-120%	BULK UNIT WEIGHT	γ_B	15.7 kN/m ³
PLASTIC LIMIT	PL	33%	UNDRAINED SHEAR STRENGTH	C_u	10-15 kN/m ²
PLASTICITY INDEX	I_p	47-87%	SENSITIVITY	S_t	5
NATURAL MOISTURE CONTENT	w	LL%	EFFECTIVE ANGLE OF SHEAR RESISTANCE	ϕ'	24°
CLAY FRACTION	-	50%	PORE-PRESSURE PARAMETER	A_f	0.9
ORGANIC CONTENT	-	8%	COEFFICIENT OF CONSOLIDATION	C_v	1.42 m ² /yr

Table 1.3.

Typical Geotechnical Properties of Marsh Clay

(Data from Cooling and Marsland, 1953; Marsland, 1957(a) and 1966)

of the ditch to the embankment crest. The ditches are typically 1 to 2m deep and generally close enough to the embankments to affect their stability. Thus many of the embankments, post-1953, were close to limiting equilibrium, as are many at the present time, with no prospect of being able to accommodate flatter slopes or berms. In any event, figure 1.3 shows that even with very flat side slopes little is gained in terms of embankment height where there is a substantial thickness of soft clay foundation.

Thus, as might be expected, a large number of deep slips occurred during the heightening of the defences following the 1953 floods. A lesser number of failures occurred at various times up to eighteen months after the end of construction. This leads into a second major problem, namely the large post-construction displacements of embank-

ments constructed on the marsh clays. The end-of-construction stability may not be, as is commonly assumed, critical if the pore pressures generated by increasing shear strains are greater than those dissipated as consolidation proceeds (Marsland, 1957 (b)). In addition large settlements and lateral yields result in loss of freeboard and distortion of revetments.

The design work, in terms of end-of-construction stability, was based on shear strengths measured in undrained, unconfined and triaxial, compression tests on 38mm diameter samples and in-situ vane tests. Back-analyses using the laboratory results yielded F.o.S. values between 0.9 and 1.1 (Marsland, 1957(a) and 1966) whereas with the field vane the F.o.S. was about 1.2 (Golder, 1953). Failures occurring after the end of construction had F.o.S. values, based on laboratory results, of between 1.2 and 1.35.

The basic design principles adopted by the Essex River Board for post-1953 reconstruction work are outlined below (after Snell, 1953):-

- i. Flexible revetments (as described) on fissured clay banks.
- ii. Wave breaks where moderate wave action was anticipated.
- iii. A minimum crest width of 1.83m.
- iv. Raised rear berm levels.
- v. Drains to relieve uplift pressures.
- vi. Concrete capped and based, steel sheet piles to increase the height of earth embankments in industrial areas.

1.4. The Current Improvement Scheme

1.4.1. General

The Essex River Authority (E.R.A.) superseded the Essex River Board in 1965, at a time when the whole of the Thames Tidal Defences were being reviewed. In particular the idea of a barrage to protect London from storm surges coming up river has become a reality and work associated with its construction at Woolwich has already started. At the same time the tidal defences downstream of the barrage are being improved on both banks of the Thames and its estuary.

Binnie and Partners were appointed in 1971 as Consulting Engineers to the Essex River Authority, for the design and construction of improved tidal defences between Barking and Leigh-on-Sea. A major problem, in view of the trend in increasing tide levels and the possibility of tide/surge combinations worse than previously experienced was the adoption of a design crest level which would be adequate to prevent overtopping for a period of at least 60 years. The current heightening program in Essex will raise the defences on average about 1m (depending on locality) above existing levels; this implies design levels of 5.85, 6.05, 6.4 and 6.9 m.A.O.D., at Leigh-on-Sea, Thames Haven, Tilbury and Barking respectively. The height increase was based on the so-called M.A.F.F. (Ministry of Agriculture, Fisheries and Food) Line, which was drawn up from a consideration of the factors involved (the main ones being listed below) by a Committee representing the M.A.F.F., the Greater London Council (G.L.C.), the

E.R.A. and the Kent River Authority (K.R.A.).

The main factors requiring a higher defence level are as follows:-

- a. The increasing frequency of positive surges. The design criterion of a 1 in 1000 year surge under 2030 A.D. conditions was recommended by the Policy Committee for the Thames Barrier Project, and adopted in the 'M.A.F.F. Line'.
- b. The relative rise in sea level with respect to the land, being approximately 300mm per century.
- c. The increasing amplitude of the tidal cycle (60mm at Southend, 360mm at London Bridge).
- d. The confinement of the River Thames within a system of flood defence walls (300mm at Barking, 180mm at Tilbury).
- e. The reflected wave which would result from closure of the Thames Barrier. Closure 3 hours after low water is estimated to cause a 590mm wave between Barking and Tilbury, but only a 70mm wave at Canvey Island.

In addition the possibility of constructing barriers across the tidal creeks along this stretch of the defences was to be investigated by the Consultants.

The problems to be overcome were much the same as those facing the Essex River Board in 1953. Attention has particularly focused on the possibility of using light-weight fills, multi-stage construction and sheet piling to increase the height of existing embankments; in addition the use of anchored reinforced concrete walls in conjunction

with existing embankments around industrial and other limited frontage areas has been extensively studied (Picknett et al, 1974). Finally the design of the tidal creek barriers is another major facet of the works.

All of the preceding modes of construction are predominantly controlled by the strength and deformation characteristics of the soft alluvial clay foundation. Building up a comprehensive geotechnical picture of this material thus formed an integral, and major, part of the overall design.

1.4.2. Regional Geology

According to the Institute of Geological Sciences (1960) the larger divisions of strata present in the Thames Valley are as shown in table 1.4. The oldest strata to outcrop in the region are of Jurassic age and found to the north west, but the succession is generally unbroken only as far as the Lower Cretaceous. Thereafter a variety of different strata mark the boundary with the Palaeozoic. There are no deposits from Oligocene times in the Thames Valley whilst the Miocene was a non-depositional epoch in the British Isles. The main geological feature of the area is the chalk escarpment which traverses it approximately diagonally from south west to north east (figure 1.2).

The Thames Tidal Defence works are situated in the London Basin, a synclinal structure covered by Tertiary and extensive superficial deposits. Essex itself forms a low plateau within the region,

ERA	PERIOD	EPOCH	AGE FROM START
			MILLION YEARS
KAINOZOIC	QUATERNARY	RECENT	0.01
		PLEISTOCENE	2
	TERTIARY	PLIOCENE	7
		EOCENE	54
MESOZOIC	CRETACEOUS	UPPER	100
		LOWER	136
	JURASSIC	195	
PALAEOZOIC			

Table 1.4

Geological Succession in the Thames Valley - Major Divisions

sloping gently towards the North Sea and Thames Estuary, and likewise largely covered with superficial deposits. The structural picture of the basin, and the region as a whole, is completed further south by the chalk escarpment of the North Downs.

The sequence from the Cretaceous to Quaternary found in the Thames Valley may be enlarged as in table 1.5. The boundary between the Upper Cretaceous and the Eocene is marked by a

RECENT	Alluvium and Peat
PLEISTOCENE	River Gravel - Flood Plain Terrace Taplow Brickearth (Alluvium) River Gravel - Taplow Terrace Boyn Hill Brickearth (Alluvium) River Gravel - Boyn Hill Terrace
	Dry Valley Gravel; Gravel opposite chalk gaps; Coombe Deposits Boulder Clay; Glacial Sands & Gravels; Laminated Clay Plateau Gravel Clay-with-Flints, Pebbly Clay & Sand
PLIOCENE	Pebble Gravel and Crag Deposits
EOCENE	Barton Beds Bracklesham Beds Bagshot Beds
SOLID	Upper Bagshot Middle Bagshot Lower Bagshot
	London Clay and Claygate Beds Oldhaven, Woolwich, Reading and Blackheath Beds Thanet Beds
UPPER CRETACEOUS	Chalk - Upper Middle Lower Upper Greensand Gault Clay
LOWER CRETACEOUS	Lower Greensand Wealden Series

Table 1.5

Geological Succession in the Thames Valley - Detailed Sub-Divisions

considerable period of no deposition (Palaeocene). The succession of Pleistocene boulder clays and gravels, and to some extent the Pliocene, is not absolutely established and as presented in table 1.5 is to some extent speculative.

The solid deposits outcropping along the Thames from Barking to Leigh-on-Sea are Chalk, Thanet Beds, Woolwich Beds and the London Clay. The drift deposits comprise Thames Gravels and recent alluvium (figure 2.2). It is thought (I.G.S., 1960) that Boulder Clays once extended over the whole of Essex but in the area north of the Thames Estuary they have been largely eroded.

1.4.3. Site Investigation

(i) Field Work For the purposes of design and site investigation the river frontage was divided into three sectors as outlined in table 1.6, which also provides a summary of the field work.

Shell and auger borings were sunk at intervals of 500m or less along the line of the defences (both existing and proposed), all penetrating the Thames Gravels and many the underlying solid deposits. At important locations, e.g. proposed barrier sites, much closer spacings of boreholes were used. Sampling in the soft alluvial clays was carried out with thin walled, fixed piston samplers (102mm diameter x 1000mm (max) long) from the borings and with Delft samplers operated from a Dutch Deep Sounding rig. The

underlying firmer cohesive soils were sampled with conventional open drive U(100) sample tubes, and in granular materials S.P.T./C.P.T. s* were performed. In addition, a limited number of undisturbed samples of saturated sand were taken with a Bishop (1948) sampler.

In-situ shear strength measurements in the soft clay were made with both borehole and Geonor vanes. Piezometers were installed in boreholes, both in cohesive and granular strata, for long-term monitoring of ground-water conditions and in-situ permeability measurements. The latter were also carried out during the original boring. Additional driven piezometers (Little and Vail, 1960; Parry, 1971(c) and 1973) were installed in the soft clay at numerous locations.

(ii) Laboratory Work Index properties (moisture content, plasticity, unit weight, organic content and chemical concentrations) and gradings were established for all the major soil types encountered. Determination of strength and deformation characteristics was largely confined to the soft alluvium, with the following types of conventional laboratory tests being carried out on the piston samples:-

- a. Unconsolidated undrained triaxial compression tests with, and without, pore-pressure measurements.
- b. Consolidated undrained triaxial compression tests with pore-pressure measurements.

* Standard Penetration Test/Cone Penetration Test

SECTOR	FRONTAGE Km	FROM	TO	BOREHOLES	GEONOR VANES	DELFT SAMPLES	BOREHOLE PIEZOS	DRIVEN PIEZOS	REFERENCE
I	7	BARKING CREEK	RAINHAM	34	30	-	14	22	Foundation Engineering Ltd. (1973)
II	13	PURFLEET	TILBURY	48	20	-	22	1	Foundation Engineering Ltd. (1974(a))
III	25	MUCKING CREEK	LEIGH-ON- SEA	74	-	16	30	-	Soil Mechanics Ltd. (1972)

Table 1.6

Summary of Site Investigation for Thames Tidal Defences

- c. Consolidated drained triaxial compression tests.
- d. Triaxial pore-pressure dissipation tests.
- e. Consolidation tests (conventional and hydraulic oedometers).

1.4.4. The Role of Full Scale Field Tests in the Design

Extended works such as motorways and flood levees present particular problems with respect to site investigation, especially when constructed on variable foundation materials. Where major structures are involved (e.g. bridges, barriers) more detailed investigation is usually undertaken, but for the main part boreholes spaced at fairly large intervals form the basis for the geotechnical appraisal. Thus a fair measure of interpretation is involved, and the risk of unforeseen circumstances arising during construction is higher than in many other types of work.

With the data accrued from the site investigation stage the Engineer had a broad basis for design, comprising the following complementary approaches, as outlined by Bishop and Green (1973):-

- i. Empirical knowledge based on previous experience.
- ii. Index properties and a detailed geological description.
- iii. Appropriate engineering properties, derived from laboratory and in-situ tests, coupled with quantitative design methods.

At this stage, however, there were still considerable uncertainties which may be broadly grouped, again as outlined by Bishop and Green (1973), as follows:-

(i) Sampling and Testing The sampling of very soft clays is in itself a major problem (Ladd and Lambe, 1963; Davis and Poulos, 1967; Rowe, 1972(a)) and whether the laboratory specimen, following sampling, transportation, storage, extrusion, trimming and mounting is able to represent the field behaviour under the applied stresses is open to question. The physical act of performing tests at the very low stress levels associated with these materials also presents some difficulty (Wesley, 1975). The marsh clays are typically heterogeneous, fissured to some extent and may include pre-existing shear surfaces and therefore sample size may influence both strength and rate of pore-pressure dissipation. The total stress path and rate of testing will typically affect the measured undrained strength and anisotropy, whether structural or stress induced, similarly influences the strength determination as well as the consolidation characteristics.

(ii) Problems of Analysis

(a) Stability The marsh clay is typically brittle in terms of undrained strength and progressive failure may be important (Bishop, 1967 and 1971(b)). For sensitive clays the brittleness index (I_B) can be defined in terms of remoulded, rather than residual, strength (Bishop, 1971(a)):-

$$I_B \geq \frac{C_u - C_{urm}}{C_u} = 1 - \frac{1}{St} \dots\dots\dots(1.1)$$

where rm signifies remoulded

Thus for $St = 5$ (table 1.3) $I_B \geq 80\%$

Although the drained strength parameters are generally more readily defined than the undrained strength, the long-term factor of safety, when large amounts of creep are occurring, also presents an area of uncertainty as does the prediction of pore pressures for effective stress end-of-construction analysis.

(b) Settlement The construction process, in this case, typically imposes relatively small increments of stress upon the soil bringing it close to the preconsolidation pressure. Confident settlement predictions are thus made particularly difficult (Bjerrum, 1967 and 1973). Creep may also significantly affect the total settlement of the structures. Finally the drainage conditions and general geometry may impose taxing analytical problems on the designer, who is then forced to make simplifying assumptions.

(c) General Deformations Other than vertical settlement, these are not generally predicted in design because of both a lack of analytical methods and the difficulties of relating deformations to a failure condition, although lateral deformations may become unacceptable for flood defences well before failure. Finite element solutions are being increasingly used in this context (although still largely on a research basis); the problems associated with input data for such solutions are too complex and numerous to be covered here but typically laboratory deformation moduli and stress-strain functions present further uncertainties.

(iii) Physical Properties of New Types of Fill The proposed use of pulverised fuel ash (P.F.A.) and other waste products posed particular design problems in terms of stability and seepage.

(iv) Consequences of Various Geotechnical Processes The use of ground anchors and cut-off walls posed design problems, particularly with respect to development of anchor loads and passive earth pressures, as well as the stability and drainage characteristics of the existing embankments.

Some of the uncertainties included under 'sampling and testing' may be alleviated by testing large undisturbed samples (from test pits where possible), carrying out more elaborate laboratory testing and performing large scale in-situ tests. These are all expensive and do not obviate the need for design.

The geotechnical literature contains case histories, too numerous to mention, where either the predicted shear strength (e.g. Parry, 1971 (a)) and/or the settlement characteristics (e.g. Rowe, 1972(a)) based on the aforementioned design sequence (including conventional sampling and testing procedures) were unsatisfactory when compared to the behaviour of full scale structures. The F.o.S. of an embankment on soft clay is typically low (1.00 to 1.25) and the construction of trial embankments provides a welcome opportunity for the designer to check the geotechnical properties and method of design. For a project such as the Thames Tidal Defences (total 1972 (i.e. pre-inflation) projected cost of £40m) trial embankments would seem to make not only sound technical, but also economic, sense

(total site investigation cost of £600,000, including £100,000 for trial embankments and associated work) when compared to the considerable monetary cost of overdesigning, or failures during and after construction. Added to this is the enormous social and economic cost associated with failure of the new defences whilst under attack from the sea.

The trial embankments constructed to aid the design of the defences were not intended to simulate the construction of the actual clay embankments, but to provide detailed information on the behaviour of the foundation material under a variety of loading and drainage conditions, and the mechanism of failure. The loading (and drainage) conditions were, however, full scale in every sense, in that the foundation was stressed to similar levels and depths as would be experienced under the real embankments. This is particularly important with respect to the existence of a desiccated crust and the possibility of progressive failure being operational (Bishop and Green, 1973). The basic design methods could thus be checked and data obtained to facilitate monitoring of the main works.

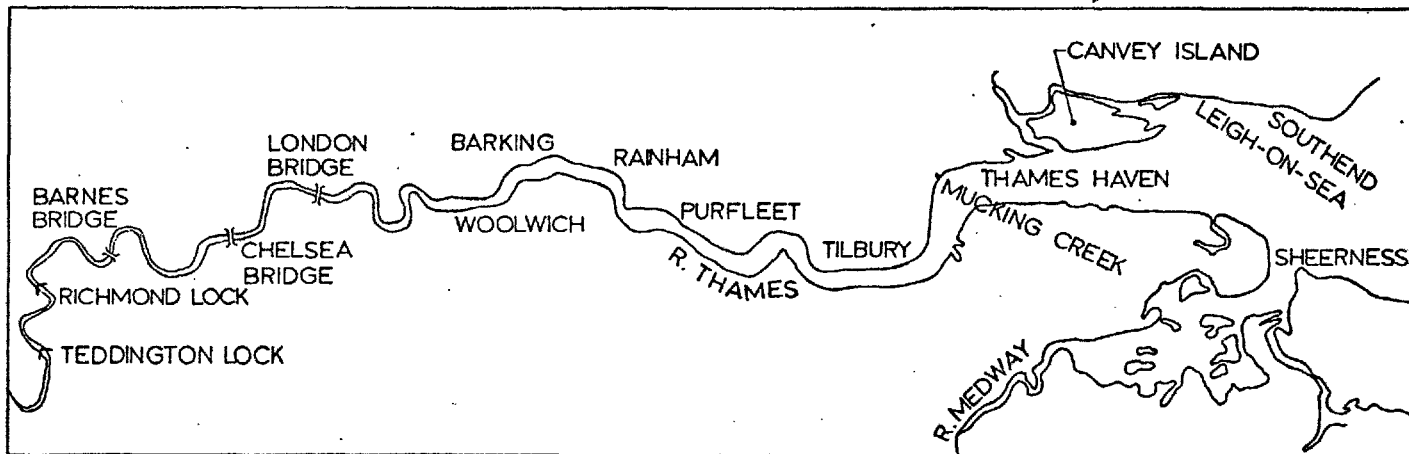
Two principal aspects of foundation behaviour were studied:-

- (i) End-of-construction stability (Bank 1, Stages 1 and 2). In particular, for extended works on soft clays the Geonor vane often provides a major source of undrained shear strength data. These data, however, cannot be confidently used unless calibrated against a full scale failure (Bjerrum, 1972).

- (ii) Settlement, deformation and pore-pressure characteristics including time dependence (Banks 1, 2 and 4).

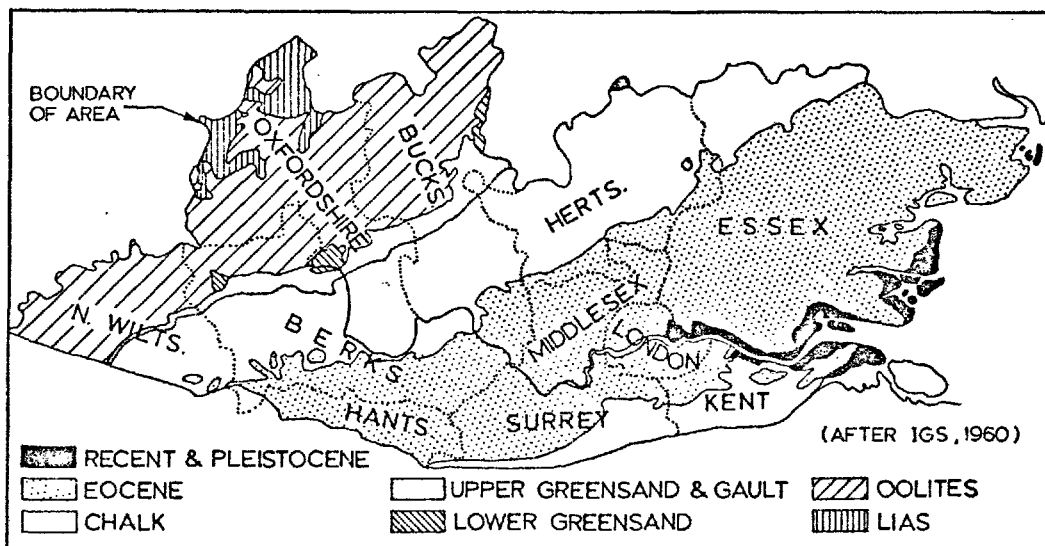
The use of trial embankments does not solve all the designer's problems, particularly on extended sites where the 'relationship' between predicted and observed behaviour may vary with soil conditions. They do, however, reduce the uncertainties by such a substantial amount that today most major projects of the type discussed are preceded by a full scale trial.

Many trial embankments have been constructed on soft clay, particularly for highway projects (Bourges et al, 1969; Justo, 1969; Ladd et al, 1969; Cox, 1971; Murray, 1971; Lambe et al, 1971; Ladd, 1972; Pilot, 1972; Wilkes, 1972 (a) and (b)) and flood levees (Kaufman and Weaver, 1967; Parry, 1968; Dascal et al, 1972; Taylor and Buchignani, 1972; Moh et al, 1972; Dascal and Tournier, 1975) as well as research (Bozuzuk and Leonards, 1972; Holtz and Broms, 1972; Holtz and Lindskog, 1972; Hoeg et al, 1969). There are also case records of highway embankments (Lacasse and Ladd, 1973; Lo and Stermac, 1965; Wu et al, 1975; Casagrande, 1960; Raymond, 1973) and flood levees (Golder and Palmer, 1955; Parry and McLeod, 1967; Marsland, 1957 (a) and 1966; Cooling and Marsland, 1953) which failed during or after construction. The findings from many of these case records will be discussed, in the light of the findings of the Thames Tidal Defence trial embankments, in later chapters.



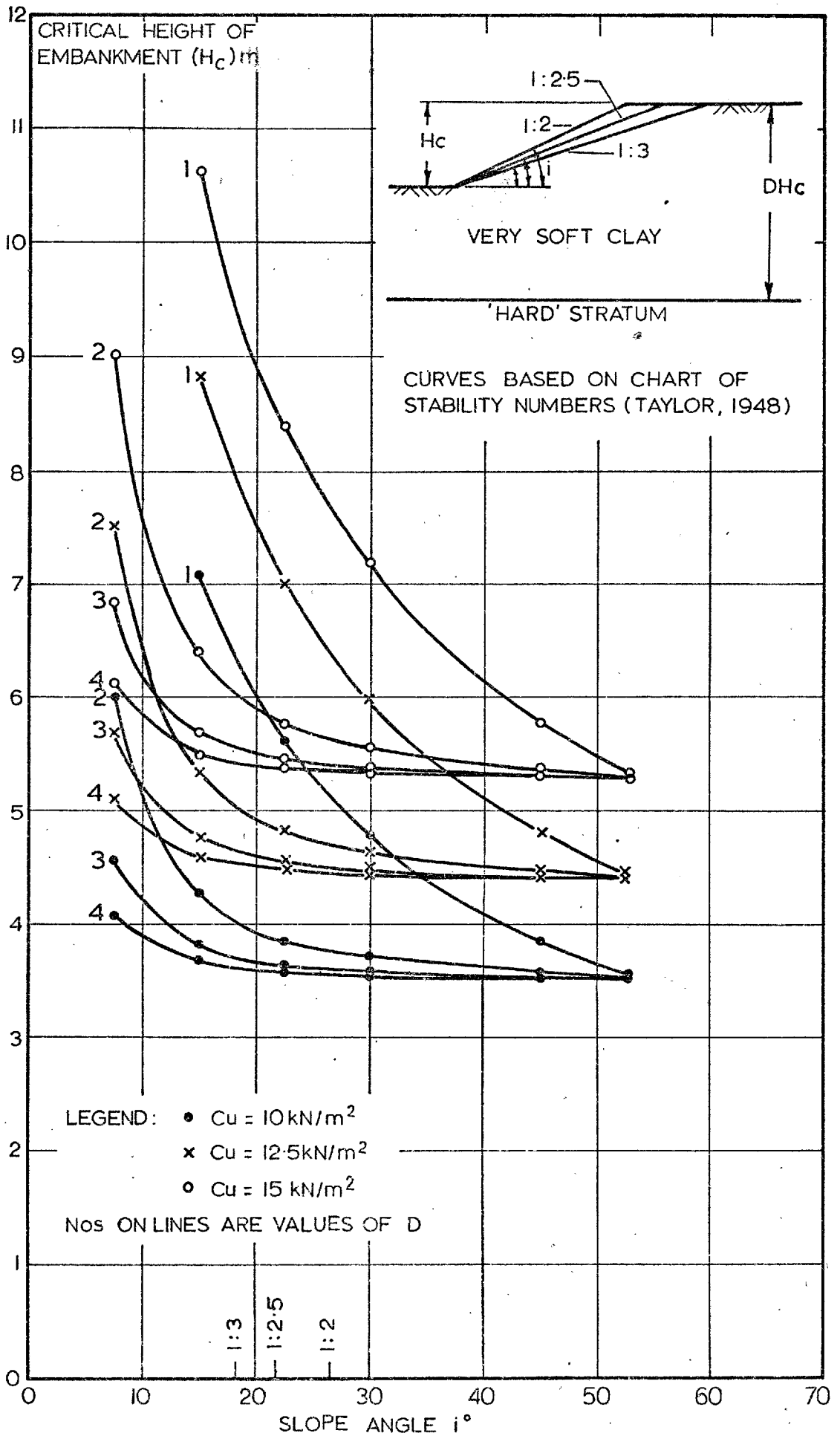
SKETCH MAP SHOWING TIDAL REACHES OF RIVER THAMES

Fig. 1.1



SKETCH MAP SHOWING GEOLOGY OF LONDON AND THAMES VALLEY.

Fig. 1.2



INTER-RELATIONSHIP OF SLOPE ANGLE, CRITICAL HEIGHT OF EMBANKMENT AND UNDRAINED SHEAR STRENGTH USING STABILITY NUMBERS.

CHAPTER 2

MUCKING TEST SITE

2.1. General

The site is to the south of Stanford-le-hope (figure 2.1) and is bounded by Mucking Creek and the River Thames to the west and south respectively (figure 2.3). The coastal landscape comprises a flat alluvial plain, about 500m wide, the land then rising gently inland. This alluvial plain, at an elevation of about 2m AOD, is largely arable land protected from inundation at high tide by the 3m high clay-embankment defences. These have delph ditches to the landward, and seaward slopes protected by revetments, being similar to the embankments described in Chapter 1. To their seaward side are, typically, intertidal mud flats many hundreds of metres wide. Oil refineries at Shellhaven and Coryton form an industrial complex extending from a kilometre or so to the east of the site, along the coast as far as Canvey Island. Land to the west of Mucking Creek is equally unattractive being an active refuse tip.

The geological map for the test site locality (figure 2.2) indicates that the succession in the test site vicinity is alluvium, river gravel, London Clay and Woolwich Beds. Before the selection of the test site at Mucking, many other sites were rejected because of the foundation conditions, surface filling, poor access or lack of availability. The thickness of alluvial clay at Mucking (6m or so) is towards the thin side of the range encountered along the overall site

(5 to 15m) but it is unusually free from silty or sandy partings or other major variations. It was felt that the site offered a particularly good opportunity for the correlation of laboratory and field behaviour of the clay. In addition, a ready supply of sand for embankment fill was available locally.

It might be argued that a site with more variable foundation conditions would be more representative of the foundation as a whole, and hence provide a better test for the design process. There is, however, no such thing as a typically varied foundation material, with sand, silt and peat layers interposed throughout the marsh clays which are themselves of variable composition and structure. By constructing the trial embankments on a relatively uniform deposit, the laboratory results and analytical procedures could be checked without any major doubts concerning the correct geotechnical modelling of the situation. The lessons learned could then be applied to other particular situations where the marsh clay was the main foundation material.

Five test embankments were constructed on the site, numbered and positioned as shown in figure 2.3 and described in Chapter 4.

2.2. Site Investigation

In addition to the investigation carried out in the vicinity of the test site, for sector III, a separate detailed investigation of the site was made (F.E.Ltd., 1974(b)). Shell and auger borings and

Geonor vane tests were carried out, mainly on embankment section lines (figure 2.3). The 203mm diameter borings were cased throughout their depths of between 7.50 and 20.00m. Undisturbed samples of the soft clay, 102mm diameter x 1000mm long, were taken with a fixed piston sampler and thin walled sample tubes. Normal open-drive 102mm diameter samples were taken in the firmer cohesive soils and S.P.T./C.P.T. s were carried out in granular materials as appropriate. The main laboratory testing program was confined to the samples of soft clay and followed the lines described for the main investigations in Chapter 1.

Five observation wells were installed into the gravel immediately underlying the alluvial clay and peat, and two deep bench marks were installed into the lower part of the same gravels, as described in Chapter 5 (see also figure 4.1). At a later stage five twin tube hydraulic piezometers were installed at various depths in the soft clay (figures 4.1, 2.4 and 2.12) to monitor seasonal ground-water variations, again as described in Chapter 5.

Finally, a test pit 4m long x 2m wide x 4.7m deep (figure 2.3) was excavated and 36, 254mm diameter x 305mm long, undisturbed cylinder samples were taken. These samples were used in a comprehensive laboratory study of the soft clay, carried out at Imperial College by Dr. L. D. Wesley, and the results used in this thesis are those reported by Wesley (1975) unless otherwise stated. The test pit was

excavated by a combination of mechanical grab and manual labour; the sample tubes were pushed into the soil by application of dead weight pressure and retrieved by manual excavation. Excavation of the test pit also enabled a detailed visual examination of the clay to be carried out and horizontal Geonor vane tests to be performed in situ. The pit, which was sheet piled and braced, was surrounded by well points jetted into the gravel and connected to a ring main and pump, in order to reduce uplift pressures at its base. Back-filling of the pit was carried out in 300mm layers, compacted by ramming. Although the test pit was very close to Bank 1 its size was such that any associated effects should have been minimal.

2.3. Site Geology

Borings at the test site and in the surrounding area showed the sequence of strata to be as follows:-

(i) Recent Alluvium

The uppermost alluvial clay is present to a thickness of 11m along the river frontage, but thins northward, the edge of the alluvial plain marking the inland limit of the outcrop. Below the test site it is typically 5 to 6m thick (6m thick under Banks 1 and 2, 5.2m under Bank 4) and underlain by a consistent peat layer. The peat also appears to thin northward being on average 600mm thick (500 to 750mm range) under Banks 1 and 2, but only 300mm thick under Bank 4.

Figure 2.4 shows the succession of alluvial deposits revealed beneath Banks 1 and 2. The peat has an essentially horizontal upper horizon but thickens slightly from west to east. Below the peat is a thin layer of clay, containing both gravel and organic matter, of near constant thickness (600mm). This layer thins rapidly northward and was not in evidence under Bank 4. A similar layer overlying the gravels at Shellhaven is described by Skempton and Henkel (1953) as a late glacial deposit. Below Banks 1 and 2 the junction of this clay with the gravel was dipping gently from west to east, the gravels being encountered at 15m depth at Shellhaven (Skempton and Henkel, 1953) and 17m depth at Canvey Island (George and Parry, 1973).

(ii) Pleistocene River Gravels

The uppermost part of these deposits are medium dense well graded gravel, from 750mm to 2.25m thick, with some sandy silty clay over the area of the test site. They reach a total thickness of 10m along the river frontage but thin northwards, outcropping on the higher ground beyond the edge of the alluvial plain where extensive old workings are now partly filled with water and used for fishing. They are, in the main, well graded flint gravels but also present in the succession are sandy gravels and sandy gravelly clays. The well graded fine-coarse sand used for the trial bank construction was worked from such a deposit, which is possibly a flood plain terrace (Skempton and Henkel, 1953) or older (Hutchinson and Gostelow, 1975; Hutchinson, 1975). The gravels, which are typically at 7m depth

and 8 to 9m thick under the trial embankments, die out to the north.

(iii) London Clay

The lower part of the London Clay outcrops beyond the north eastern part of the test area, and may even underlie part of the site but only to a thickness of a metre or so. The deposit is locally very silty, with beds of fine sand, silt, shells and some pebbles, and weathered for the top 1 to 3m.

(iv) Woolwich Beds

These underlie most, if not all, of the site, being encountered at depths of 15 to 16m and comprise a variable sequence of dense fine and medium sands interbedded with stiff clays and occasional gravels. The clays are dark brown or black, are frequently organic and often contain beds of stiff peat and lignite. The total thickness of Lower London Tertiaries beneath the area is thought to be about 50m, these being underlain by chalk.

The regional dip of the Cretaceous and Eocene deposits, resulting from the Alpine movements, is gently north eastwards; however beneath the test site area they are folded locally into a gentle syncline. Alluvial clays and gravels, having been laid down in more recent times, are horizontally 'bedded'.

Bulk samples of the peat layer were taken from 305mm diameter shell and auger borings (used in conjunction with the large vane tests; figure 2.3). These samples were dried out and dated, by carbon 14 analysis, at 5303 ± 45 years B.P. The peat contained fragments of wood and was relatively clay-free, inferring that it was probably laid down above normal high water. Its average depth below M.H.W.S. was 7.75m, which agrees well with the concept of a rising Holocene sea level as predicted by Walbancke (1968) and Greensmith and Tucker (1973), and also with data for peat of similar age at Tilbury (Godwin et al, 1965). The depositional elevation of the peat must have been very close to its present day one due to the presence of only a very thin layer of compressible material beneath it. The boundary between the Pleistocene and recent deposits represents a substantial period of time during which there was little or no deposition over the area.

2.4. The Alluvial Clay

2.4.1. General Description

During the last glaciation (Devensian) of the Pleistocene, sea level was depressed about 100m below its present day level. With moderating climatic conditions as the glacial period drew to a close, growth of vegetation increased and by 9000 years B.P. substantial forests covered what are now coastal areas (Kidson and Heyworth, 1975). The rise in sea level consequential upon the melting of the glaciers subsequently swamped such forests, and peats, similar to those at Mucking, were

formed. As the sea level continued to rise, sand, silt and clay particles, probably deriving largely from the London Clay and Lower London Tertiaries, were deposited in this salt-water environment wherein the clay size particles formed an open flocculated structure with a water content close to the liquid limit. In a marine environment, such flocculated materials may be relatively homogeneous (Bjerrum, 1954), but the estuarine clays are typically more varied. Deposition thus continued until recent time when the land was reclaimed; consolidation taking place under the self-weight of the material only, with no subsequent erosion or filling.

The present day geotechnical profile shown in figure 2.4 is based on visual inspection of the test pit, and samples therefrom, as well as disturbed and undisturbed samples from the shell and auger borings. Also included are the extremes of ground-water conditions recorded over a complete seasonal cycle, indicating that ground-water levels fluctuate between the ground surface and 1.5m depth. The top 1 to 1.5m of the profile is a firm desiccated clay with an increasing amount of organic matter towards the surface. Underlying the desiccated zone, the clay is very soft with very little organic matter below 2m depth. The main feature of the soft clay's fabric is a pattern of root holes which extend, mainly vertically, throughout its depth although decreasing in size and intensity with depth. Slight traces of organic matter in the lower part of the clay are confined to these root holes. The fabric was also examined after drying of the

material but no additional features were noted except the absence of any structure. Above 2m depth, however, there were numerous shear surfaces in the clay at the test pit location, and evidence of substantial movements having occurred on some of these (Wesley, 1975). The fabric of the desiccated zone is dominated by extensive open fissures which are in evidence throughout the summer months, and to some extent throughout the seasonal cycle.

2.4.2. Grading, Mineralogy and Index Properties

The data in this section come from two sources, namely tests performed by the writer on disturbed samples from the large diameter (305mm) boreholes and tests performed by Wesley (1975) on the undisturbed test pit samples, the latter being labelled where comparisons have been made.

Grading curves from sedimentation tests (figure 2.5) show that there are little or no sand size particles in the alluvial clay and only 15% in the lower clay. The silt sizes are well graded in the alluvial clay and the variation in clay fraction with depth, from about 30 to 60%, can be seen, this latter point being better illustrated in figure 2.7. From being 60% near the surface the clay fraction drops to around 30% between 3.25 and 4.50m depth and then increases to nearly 50% just above the peat layer. Based on the mechanism of deposition discussed in Chapter 1 the increase in silt content may mark a change in the relative position of the area to high and low water marks. The clay fraction of the lower clay was just under 30%.

The relative proportions of the various clay minerals within the clay fraction were determined for samples from 2 and 4m depth, using X-ray diffraction techniques, as listed in table 2.1. The clay mineral composition was nearly identical for both samples. Data from a nearby deposit of London Clay (from clay pits at South Ockendon) are also presented in this table, and in figure 2.8, for comparison.

The salinity of the pore water within the alluvial clay was not determined but for the adjacent Shellhaven alluvial clay the pore-water salinity was 25gm/litre compared to the 31gm/litre of the river at Shellhaven and 35gm/litre for sea water (Skempton and Henkel, 1953). It would seem likely that the Mucking clay has been similarly leached, due to the downward flow of ground-water in the vicinity (section 2.5).

Several moisture content and Atterberg Limit determinations were made at regular depth intervals throughout the clay, as shown in figure 2.6. Scatter is quite considerable near the surface, but noticeably decreases with depth; the increasing consistency in the results with depth can also be seen in figure 2.7, where the water contents, Atterberg Limits, liquidity index and clay fraction are compared for the two sets of test results. Despite the variations in the Atterberg Limits and water contents above 3m depth, the trends are similar for the two locations and thus the plasticity (figure 3.3) and liquidity indices compare well.

Clay Mineral	Mucking Clay			London Clay*	
	% of Clay Fraction	% of Whole		% of Clay Fraction	% of Whole 50% < 2 μ
		60% < 2 μ	30% < 2 μ		
Kaolinite	12.5	7.6	3.8	12.8	6.4
Illite	41.5	24.8	12.4	41.7	20.9
Montmorillonite	46.0	27.6	13.8	45.5	22.7

Table 2.1.

Clay Mineralogy of Mucking Clay and London Clay

*Data from Apted (1977)

The above variations and relationships were further demonstrated by examining a sample from 3.18 to 3.48m on the basis of water contents taken on a 25mm grid across vertical and horizontal sections (Wesley, 1975). This showed a variation in water content of about 20% over the length of the sample and 15% across the diameter. However, the Atterberg Limits also varied from top to bottom of the sample indicating compositional changes and the heterogenous nature of the clay. Thus the changes in water content of the clay cannot be linked *per se* to changes in undrained strength and compressibility.

The plasticity index is noticeably dependent on the clay fraction, varying with it from 70% near the surface down to 40% and then up to around 60% just above the peat (figure 3.3). This dependency is best

illustrated by the activity chart (figure 2.8) which also reflects the constant mineralogical composition of the clay fraction. The activity of the Mucking clay averages out at 1.15 and is, therefore, in the normally active range defined by Skempton (1953), whose data for the Shellhaven and London Clays are also shown. It is interesting to see that the London Clay, with its similar clay mineralogical constitution to the Mucking clay, is inactive due to almost complete leaching of its pore water.

Figure 2.8 also shows Mucking clay and London Clay data on a plasticity chart. The Mucking data plot sensibly along a line above, and parallel to, the A-line, indicating an inorganic highly plastic clay. The lower clay is inactive and of low plasticity indicating a different mineralogical composition and hence supporting the supposition that this is a late glacial, rather than recent, deposit. The one point below the A-line is the sample from 300 to 600mm which has much higher Atterberg Limits but unchanged plasticity, reflecting the increased organic content.

The liquidity index (figure 2.7) increases from about 0.1 near the surface to near unity between 3 and 5m depth, and then drops to 0.8 just above the peat. These values confirm that only slight leaching has occurred and the activity chart shows that any related effects are uniformly distributed through the alluvial clay layer. Where leaching has occurred as a result of downward percolation of rain water, weathering of the upper layers may take place (Bjerrum 1967,

1973). In addition to the removal of sodium cations, the oxygen and carbon dioxide in rain-water may result in oxidation of the clay with consequential lowering of the pH of the ground-waters. This results in weathering of micas and feldspars with subsequent release of cations having higher valencies than sodium (e.g. aluminium and iron), which then attach themselves to clay minerals with adequate base exchange capacities. Such a weathering process results in increased plasticity, activity and undrained strength in the upper zone of a clay, as well as a reduced compressibility due to increased inter-particle attraction. The base exchange capacity of the Mucking clay is almost certainly adequate (31me for Shellhaven clay as opposed to 4, 8 and 100me for kaolinite, illite and bentonite respectively (Skempton and Northey, 1952)) for this mechanism to be feasible, but the plasticity and activity charts repudiate such an occurrence. The other main mechanisms responsible for weathered crusts in clay deposits are frost penetration and drying (Bjerrum, 1973). The 1 to 1.5m thick weathered zone at Mucking would thus appear to be truly desiccated.

As stated earlier, below 2m the organic content was minimal and even in the upper part of the crust was only 1 or 2%, and thus much less than the 8% quoted in table 1.3. Thus no pretreatment was carried out prior to sedimentation tests and the Atterberg Limits were determined without any drying. Drying reduced the liquid limit of the Shellhaven clay by a few per cent (Gibson, 1953).

Bulk unit weights (γ_B) were determined from triaxial test specimens as shown in figure 2.23, there being a slight increase from about 14.5 kN/m^3 to 15.5 kN/m^3 with depth. Based on these results, and the fact that the samples were fully saturated below the crust, the water contents indicated a specific gravity (G_s) of 2.70. A limited number of specific gravity determinations yielded a figure of 2.73.

2.4.3. Consolidation Characteristics from Laboratory Tests

The laboratory investigation was largely confined to the 10 samples taken from the 3.18 to 3.48m depth level, this being selected as an appropriate horizon for detailed studies because of the relative uniformity of the clay. Data obtained on the consolidation characteristics were initially limited to those from one oedometer test, one triaxial dissipation test and the results of the consolidation stages of triaxial tests all carried out at this level. In addition oedometer tests were carried out on four of the borehole piston samples taken from depths of 1.1, 2.4, 2.9 and 4.35m.

The triaxial specimens were consolidated to an average in-situ stress (p_p^*) of 21 kN/m^2 (calculated assuming the coefficient of earth pressure at rest (K_0) to be 0.55) at which C_{v3} was $94.7 \text{ m}^2/\text{year}$ compared to $63.1 \text{ m}^2/\text{year}$ for C_{v1} from the oedometer test at an in-situ vertical effective stress (P_0') of 27 kN/m^2 . These high values

* $p' = \frac{\sigma_1' + \sigma_2' + \sigma_3'}{3}$, but in the laboratory tests was taken as

$\frac{\sigma_1' + \sigma_3'}{2}$ for the in-situ conditions ($= p'_p$)

were attributed to the presence of the root holes in the soil, which although open at low effective stress levels may close at higher effective stress levels (Wesley, 1975) resulting in the observed rapid decrease in C_v with increasing effective stress (on average approximately one order of magnitude decrease at p'_p or $p'_o = 80 \text{ kN/m}^2$).

Additional oedometer tests performed to investigate the relative stiffness of horizontal and vertical samples at the main test level produced similar C_{v1} values for the vertical samples ($45 \text{ m}^2/\text{year}$) but reduced values for the horizontal samples ($11 \text{ m}^2/\text{year}$). These tests also showed the coefficient of one dimensional volume compressibility (M_{v1}) in the horizontal direction to be twice that of the vertical direction over the in-situ stress range (15 to 30 kN/m^2 increment). This was also demonstrated by the larger volume changes under isotropic as compared to K_o^* consolidation in triaxial tests at low stress levels. At higher stress levels (somewhat in excess of twice the apparent preconsolidation pressure (p'_c)) similar M_v and C_v values were observed for vertical and horizontal samples.

C_v is linked to M_v and the coefficient of permeability (k) as follows:-

$$C_v = \frac{k}{M_v \gamma_w} \dots\dots\dots(2.1)$$

where γ_w is the unit weight of water. Thus if 'H' and 'V' denote horizontal and vertical directions respectively, for in-situ stress levels, using the

* K_o consolidation herein denotes consolidation to the in-situ stresses and does not imply conditions of zero lateral yield.

following relationship:-

$$\frac{k_v}{k_H} = \frac{C_{vv} M_{vv}}{M_{vH} C_{vH}} \dots\dots\dots(2.2)$$

$\frac{k_v}{k_H} = 2$, this anisotropy of the permeability being in the opposite

sense to that often encountered in soft clays (Rowe, 1968 and 1972(a) and (b)) and confirming the predominantly vertical influence of the root holes.

Results from the oedometer tests on the borehole samples showed the same tendency for decrease in C_v values with increasing effective stress, but much lower C_v values (4.7×10^{-1} to $3.2 \text{ m}^2/\text{year}$) at the same value of p_o' . Sample disturbance, resulting in a reduction in the effectiveness of the preferential drainage paths, is the only explanation that can be advanced to account for these anomalous results.

All the plots of void ratio (e) versus $\log \sigma_v'$ exhibited an apparent preconsolidation pressure (p_c') as shown in figure 2.13 and discussed in section 2.6. Sample disturbance appears to lower the soil's void ratio and hence also lower the initial part of the $e - \log \sigma_v'$ curve (Schmertmann, 1955 ; Bromham, 1971). The overall effect is to reduce C_v at low stress levels without much change in M_v (Davis and Poulos, 1967) and also to mask the p_c' effect and lower its apparent value.

2.5. Ground-Water Conditions

The ground-water conditions under each embankment prior to construction were monitored by numerous piezometers in the clay. However, as mentioned in section 2.2 a particular study of ground-water conditions at the site was made using the observation wells adjacent to Bank 1 and below Bank 3, and the five hydraulic twin tube piezometers (PI1-5) especially installed in the clay well away from any construction activity.

The piezometric elevation in the gravel was tidal to some extent, as shown in figures 2.9 and 2.10. The former shows the piezometric elevations recorded by the four observation wells adjacent to Bank 1 during a spring tide cycle, the latter being a similar plot for the well beneath Bank 3 during a neap tide cycle. All the tidal responses are relatively small, indicating that the gravel does not make a clean outcrop in the river. Extrapolating the piezometric elevations to the design tide level at Mucking (6.05 m.A.O.D.) produces pressures which are, at worst, artesian by about 250mm of head (see inserts to figures 2.9 and 2.10). These readings were taken during the summer only, due to the loss of the wells during embankment failures, and it is probable that during the winter months the mean piezometric elevation in the gravel rises due to its outcropping in water-filled pits further inland. However, the total soil weight beneath Bank 1 is equivalent to an artesian pressure in the gravel of about 3.75m above original ground level (O.G.L.), so that uplift is not a problem at the test site.

The larger tidal response of well W.A.S., adjacent to Bank 1 compared to the other three wells is difficult to account for, but two possible explanations are advanced:-

- (i) The other three installations are faulty.
- (ii) W.A.S. is located in material with more direct access to tidal waters.

The average levels recorded in the wells over a 12 hour cycle are very close to mean tide level as shown in table 2.2. These average levels indicate flow through the gravel into the river as do the individual values for the wells shown in the same table. The implied hydraulic gradient towards the river is approximately 0.0015 which, if linearly extrapolated to mean tide level, suggests the gravel outcrops in the river some 100m or so from the shoreline, (see also O' Riordan, 1978).

Well Number	Mean Piezometric Elevation (mAOD)	Mean Tide Level (mAOD)
WAN WAS WBN WBS	0.52) 0.44) 0.48) 0.49) 0.47) 0.45)	0.240
W3	0.41	0.19

Table 2.2.

Mean Piezometric Elevations in the Gravel and Mean Tide Levels

The results of one year's observations of the ground-water conditions in the clay are shown in figure 2.11 together with the monthly rainfall figures for the same period. A number of interesting points arise from these data, summarised as follows:-

- (i) There is a variation in the apparent ground-water level of about 1.5m between summer and winter.
- (ii) The pattern of ground-water level changes follows the rainfall pattern, but with varying amounts of time lag. The ground-water level dropped steadily between March and August although the minimum rainfall was recorded in April, after which it steadily increased, the time lag between them thus being 3 to 4 months. On the other hand the ground-water level rose very rapidly during September and October although there is still a time lag of about 2 months between maximum rainfall and ground-water level.
- (iii) The rising and falling of the ground-water table was virtually effective throughout the depth of clay monitored i.e. the body of clay consolidated and swelled during a complete seasonal cycle.
- (iv) Consolidation appears to have progressed equally at all depths (i.e. the isochrones moved parallel to the initial 'hydrostatic' line) whereas swelling was greater, initially, near to the ground surface.
- (v) The mean piezometric elevations recorded in the gravel have been plotted on figure 2.11 (although the readings were taken in 1973) indicating under-drainage of the clay by about 500mm below hydrostatic conditions.

Points (iii) and (iv) are better illustrated in figure 2.12 which shows ground-water profiles at various times during the year as well as the preconstruction ground-water profiles beneath Bank 1 (August 1973) and Bank 2 (January 1974). These latter two sets of data confirm point (iii) which may have been attributed to poor sealing of the piezometers. There is no doubt concerning this point for the installations beneath any of the embankments as will be shown in Chapter 5 where the piezometer results are discussed in detail. However, there is some doubt attached to the readings for P11 as it was very close to ground level and monitored suctions during the summer without being de-aired during the year. Thus the pore pressures recorded on P11 during the winter months are almost certainly too high, although water was standing to some depth (100 to 200mm approximately) above ground level during that period at the piezometer installation locations.

The complete ground-water profile through the clay and into the gravel, for Bank 1, as shown in figure 2.12 confirms the underdrainage, being in this case 400mm below hydrostatic compared to the 600mm recorded at Shellhaven by Skempton and Ward (1952).

The seasonal movement of ground-water levels is a complex phenomenon, governed largely by the combined effects of rainfall and evaporation/transpiration, the permeability and compressibility of the soil and the pore-pressure changes which occur as a result of total stress changes in the upper layers. In typical clay strata, especially grass

covered deposits, the term ground-water level (G.W.L.) merely implies the change point from negative to positive pore pressures in a permanently saturated medium, there being no physical line above which the ground is dry and below which it is saturated. However, at Mucking the high permeability of the desiccated zone (see also Marsland, 1957 (a), 1966) means that there is a physical water table movement above a certain permanently saturated horizon. There can be either positive or negative pore pressures in both of these zones at different times of the year. Within the desiccated zone there are blocks of saturated material with water contents close to the plastic limit in summer and of higher liquidity index in winter.

A major point of interest, particularly with respect to stress history, is that the pore-pressure changes become effective throughout the clay layer. This at first seems surprising, although seasonal equilibration of pore pressures to depths of several metres, in grass covered London Clay slopes has been reported by Walbancke (1976). The feasibility of the observed rapid equilibration with depth in terms of the measured soil parameters is now examined.

The total stress changes due to water level movement in the crust can be approximately examined by considering an initially saturated layer which dries out completely (as opposed to saturated blocks with low liquidity indices, separated by open fissures).

Thus for a 1.5m deep desiccated layer with the G.W.L. at the surface, initial bulk unit weight (γ_{B1}) = 15 kN/m³ and initial water content (w_1) = 84% (implying $G_s = 2.70$ and full saturation), the total stress at depth (Z) = 1.5m is 22.5 kN/m² = p_{o1} . After a 1.5m drop (h) in the G.W.L. and complete drying of the crust the new bulk unit weight (γ_{B2}) is equal to the dry unit weight (γ_D):-

$$\gamma_{B2} = \gamma_D = \frac{\gamma_{B1}}{1 + w_1} = 8.15 \text{ kN/m}^3$$

Thus the new total stress (p_{o2}) at 1.5m depth is 12.20 kN/m² representing a total stress change (Δp_o) of -10.3 kN/m² and resulting in an undrained pore-pressure change of the same magnitude. The total pore-pressure change required for equilibration of a 1.5m G.W.L. change is -14.75 kN/m² and therefore that required by consolidation is only -4.45 kN/m² or -450mm of water. Thus less than 33% of the G.W.L. change would need to be accounted for by consolidation (or swelling with a rising level), for full equilibration throughout the strata. The total stress changes considered are exaggerated but this simple calculation does indicate that the immediate pore-pressure change, consequential upon the total stress change in the desiccated layer, may be a significant component of the overall pore-pressure change in such materials.

The consolidation component may be investigated by considering the time necessary for varying degrees of consolidation at depth intervals throughout the strata as shown in table 2.3. The calculations have been based on consolidation (or swelling) proceeding simultaneously from the surface and base of the clay layer (i.e. assuming similar seasonal variations in the piezometric elevations of the clay and gravel) and the in-situ C_{v1} of $63 \text{ m}^2/\text{year}$. This value relates to axisymmetric conditions, zero lateral yield, vertical flow only and a p_0' of 27 kN/m^2 . Swelling would obviously be expected to proceed even more rapidly than consolidation, which is represented in table 2.3.

Depth Below Ground Level z.m.	$\frac{Z}{H}$	T $U_z = 30\%$	t_{30} days	T $U_z = 50\%$	t_{50} days	T $U_z = 80\%$	t_{80} days
1.5	0.41	0.08	1.0	0.17	2.2	0.53	6.9
2.5	0.69	0.19	6.9	0.32	11.6	0.70	25.5
3.5	0.97	0.24	17.0	0.38	27.0	0.75	53.0

Table 2.3

Consolidation Characteristics of the Clay Layer at In-Situ Stress Levels

where H is the maximum drainage path length = stratum thickness/2

T is the time factor

U_z is the percentage consolidation at depth z

t_x is the time for x percent consolidation

and $T = \frac{C_v t}{H^2}$, all values being taken from Taylor (1948).

The C_v values corresponding to the lower in-situ effective stresses associated with winter conditions are approximately 30% higher and thus the figures in table 2.3 represent an upper bound for equilibration times. The consolidation times indicated would allow rapid equilibration of pore-pressure changes as a consequence of the high in-situ C_v values, and the sort of ground-water profile movements observed. The rather more rapid swelling of the surface layers is probably a result of the more rapid advancement of infiltration compared to evaporation in the winter and summer months respectively.

2.6. In-Situ Stresses and Stress History

Figure 2.13 shows the vertical total (p_0) and effective (p_0') stresses and pore-water pressure (u) profile relating to the foundation material below Bank 1 prior to construction. As can be seen from figures 2.4 and 2.12 the pore pressures are typical of the lowest seasonal values and hence p_0' is near to its maximum present day value. The total stress profile has been assumed to remain constant, despite the observations of the previous section, as there are no data on which to base any seasonal total stress changes in the upper part of the crust. Thus, in fact, the p_0' profile shown probably represents the maximum attainable values under normal climatic conditions. The maximum seasonally observed pore pressures (u_{\max}) are included in figure 2.13 (see also figures 2.4 and 2.12) and extrapolated to a ground level water table, thus producing a seasonal minimum profile for the vertical effective stress ($p_0'_{\min}$). Finally the preconsolidation pressures

obtained from the oedometer tests have been plotted and a p_c' line drawn, this being approximately equidistant from the two p_o' lines such that:-

$$p_c' - p_o' = 13 \text{ kN/m}^2 \quad \text{and}$$

$$p_c' - p_o'_{\min} = 25 \text{ kN/m}^2 \quad (\text{see also table 2.8})$$

Values of p_o' relating to suctions above G.W.L. could not be determined because of the unknown contribution of desiccation stresses to these suctions, no pore-pressure measurements being made above 1m depth. The p_c' value from the horizontal oedometer sample has also been plotted although this test did not represent K_o conditions in the ground.

The existence of a preconsolidation pressure in a 'geologically normally consolidated'* soft clay layer is probably due to the combined effects of secondary consolidation (Bjerrum, 1967), a previously lower ground-water level and near surface stresses caused by evaporation. Parry (1970) examined the theoretical implications of a previously lower G.W.L., showing that where suctions were developed above this low level it coincides with the minimum value of the undrained strength (C_u). Thus, based on the following assumptions:-

(i) $C_u = f(p_c')$

(ii) No desiccation effects below the previous lowest G.W.L.

* i.e. no erosion of overlying strata.

(iii) Suctions greater than, or equal to, hydrostatic conditions extended to this level.

(iv) Lowering of the G.W.L. is the only mechanism of overconsolidation.

it is possible to estimate the amount of overconsolidation which has occurred in a soft clay layer.

In almost any soft clay some degree of secondary consolidation will have occurred, the amount appearing to be a function of the soil's plasticity (Bjerrum, 1973). Laboratory creep tests show that the Mucking clay undergoes secondary consolidation at both in-situ and higher stress levels, although the ultimate creep rates appear to be independent of stress level. In addition a preconsolidation effect may develop due to the formation of cohesive bonds (Bjerrum, 1967 and 1973). The chemical weathering process described in section 2.4.2. is the sort of mechanism envisaged to produce such bonds. However, in *thin* deposits of reasonably uniform plasticity the value of $p_c' - p_o'$ would be expected to remain essentially constant, as in the case of ground-water lowering. Never-the-less, these typical causes of overconsolidation below the previous lowest G.W.L. may be to some extent overlapping i.e. not mutually additive (Parry, 1970). Thus laboratory measurement of the variation in p_c' and C_u , plus a knowledge of p_o' , does not enable the components of overconsolidation to be separated with any certainty.

At Mucking the $p_c' - p_o'$ value of 13 kN/m^2 indicates that an additional lowering of the G.W.L. by 1.3m (i.e. to 2.8m depth) would achieve the estimated amount of overconsolidation. As will be shown in section 2.7.5.

(figure 2.23) the minimum value of C_u occurs between 1.5 and 2.5m depth. Previous G.W.L.s at these depths would imply effective stresses of respectively 13 and 3 kN/m^2 below the existing p_c' values. Thus ground-water table movements may account for a substantial proportion of the overconsolidation. The implied subordinate role of secondary consolidation must be qualified by the aforementioned overlapping effects as well as any reduction in the p_c' values as a result of sample disturbance.

Figure 2.13 also shows the variation in overconsolidation ratio (O.C.R. = $\frac{p_c'}{p_o'}$) with depth for the two extremes of pore pressure

considered. Due to the uncertainties associated with the determination of p_c' , and the total stress profile associated with low G.W.L.s, the values of O.C.R. must be regarded as representative rather than definitive. The variation in O.C.R. with the seasonal pore-pressure variations is of particular interest, being significant throughout the layer, the values relating to maximum pore pressures agreeing broadly with those presented by Parry (1970, 1971(a)). Figure 2.24(A) shows a comparison of the Mucking results with those from some late glacial clays (Bjerrum, 1973) which have been overconsolidated predominantly by secondary consolidation (aged normally consolidated clays). The values of O.C.R. for the Mucking clay corresponding to maximum p_o' are in reasonable agreement with Bjerrum's results, although the contribution to p_c' of secondary consolidation would appear to be less for the Mucking clay.

The light overconsolidation of the Mucking clay implies that K_0 will be higher than the values associated with truly normally consolidated clays. Typical values for the latter may be obtained using the expressions suggested by Jaky (1944 and 1948):-

$$K_0 = 1 - \sin \phi' \quad \dots\dots\dots(2.3)$$

and by Brooker and Ireland (1965):-

$$K_0 = 0.95 - \sin \phi' \quad \dots\dots\dots(2.4)$$

Both of these expressions have been linked to the ϕ' values of 25° and 32° , respectively relating to the overconsolidated and normally consolidated parts of the effective stress failure envelope (section 2.7.5), and the ensuing K_0 values plotted in the third diagram of figure 2.13. This figure also shows the variations in K_0 with depth, predicted on the basis of O.C.R. and plasticity index from the charts of Brooker and Ireland (1965). These were derived from tests on remoulded soils and the overconsolidation was thus entirely a result of stress history. The three prediction methods, coupled with the different ϕ' and O.C.R. values, produce a wide range of K_0 values. Two indirect assessments of K_0 , deriving from a study of the undrained strengths measured using horizontal and vertical vane tests, are also included in the diagram. These values will be discussed in Chapter 3, but it would appear that equations 2.3 and 2.4 predict K_0 values which are too low in this case.

No direct measurements of K_0 were made in the field during the site program. Indeed such measurements are fraught with difficulty (Bishop, 1958), although the recently devised Camkometer (Wroth and

Hughes, 1973) appears to give promising results (Wilkes, 1974; Hughes et al, 1975) and has recently been used on the Mucking site. The results from these tests were not available at the time of writing. Indirect estimates of the field K_0 values have been made in the laboratory by relating the measured suctions, in samples assumed to be perfect, to the in-situ effective stresses via Skempton's (1954) pore-pressure parameters 'A' and 'B':-

$$\Delta u = B (\Delta \sigma_3 + A (\Delta \sigma_1 - \Delta \sigma_3)) \dots\dots\dots(2.5)$$

where σ_1 , σ_2 and σ_3 are the major, intermediate and minor principal stresses respectively, and Δ denotes change.

Such estimates (Skempton, 1961) also rely on a knowledge of the relevant value of 'A' and the in-situ vertical effective stress. Suctions have also been estimated indirectly by finding the effective stress for zero volume change in consolidation (Bishop et al, 1965) and K_0 from c' , ϕ' and A_f related to $\frac{dC_u}{dz}$ from quick undrained triaxial tests (Werneck, 1974).

The test pit samples at Mucking were taken mainly during January 1973 when the vertical effective stress profile probably approximated to $p_{o'}'_{min}$ (figure 2.13). At the main testing level (3.18 to 3.48m) the $p_{o'}'$ value was thus about 18 kN/m². Suction values reported by Wesley (1975) show a near normal distribution from 0 to 30 kN/m² with a mean value of about 11 kN/m².

During the sampling of soft clays the effective stresses may change as a consequence of moisture movement within the sample. This is consequential upon the remoulding of a thin zone around the circumference of the sample and the associated positive pore pressures. The periphery of the sample thus tends to consolidate whilst the central area swells with subsequent loss of suction (Bjerrum, 1973). Such a mechanism has been shown to be valid for the Mucking clay by Apted (1977) who measured water contents 4 to 10% higher at the centre than at the periphery of 102mm diameter piston samples. The loss of suction is probably less for the larger (254mm) diameter, more carefully taken, cylinder samples. A study of suctions in the latter showed that evaporation during trimming could lead to substantial moisture losses and increased suctions. On the other hand, water released from root holes and other inclusions (e.g. shells) could result in swelling and reduced suctions. Suctions tended to increase slightly during sample storage, and thus the overall post-sampling effect appears to be an increase in effective stress.

For a sample of soft clay (i.e. $K_0 < 1$) the suction (u_s) in a perfect sample is given as follows:-

$$u_s = -K_0 p_0' - A (1 - K_0) p_0' \dots\dots\dots(2.6)$$

Using an 'A' value of 0.19 (Wesley, 1975) this implies $K_0 = 0.52$ (for $u_s = -11 \text{ kN/m}^2$) compared to the predicted value of 0.92 (figure 2.13).

The latter figure would, in turn, imply a suction of 17 kN/m^2 , the calculation not being very sensitive within a reasonable range of 'A' values (0.1 to 0.3; see e.g. Ladd and Lambe, 1963). The measurement of K_0 from sample suctions in soft clays is thus very sensitive to small changes in these suctions and the procedure would seem better suited to the higher average effective stresses typical of more heavily overconsolidated soils.

The measurement of K_0 in the laboratory can also be made directly, by using the K_0 triaxial test (Bishop 1958; Bishop and Henkel, 1962) wherein the sample is subjected to drained increments of axial and lateral stress such that no lateral yield occurs. The test may be controlled by the use of lateral strain belts or by monitoring axial and volumetric strains. The latter procedure was used in the one such test carried out on the Mucking clay. The suction in the particular sample was 14.5 kN/m^2 corresponding to $K_0 = 0.76$, which decreased to a normally consolidated value of 0.42 at a p_c' of 45 kN/m^2 (figure 2.13). The latter K_0 value is exactly that predicted by Brooker and Ireland (1965) for the normally consolidated clay ($\phi' = 32^\circ$), whilst the p_c' value is identical to that from the oedometer test. It should be noted at this point that the following expression for K_0 :-

$$K_0 = \frac{\Delta \sigma_H}{\Delta \sigma_V} = \frac{\Delta \sigma'_H}{\Delta \sigma'_V} \dots\dots\dots(2.7)$$

where σ_H and σ_V are respectively horizontal and vertical normal stresses, only applies to consolidation on initial drained loading

with no lateral yield i.e. on the virgin consolidation curve (Bishop, 1958), and not for the overconsolidated state in the ground or in the laboratory.

A loss of suction in the K_0 triaxial sample means that, on application of the initial all-round pressure, the sample consolidates rather than swells as a perfect sample may have done. The test is thus better suited to determining the normally consolidated K_0 value for soft clays, for which the overconsolidation effects may only manifest themselves at low effective stresses. However, the K_0 triaxial test does show the lightly overconsolidated nature of the clay and that the field predicted K_0 values are probably not unreasonable.

Having established the normally consolidated value of K_0 with a fair degree of certainty it is of interest to examine the effect on the horizontal total stresses of lowering the G.W.L. by some distance (h) with the soil in the normally consolidated condition (G.W.L. at ground surface). Assuming p_0 remains constant it can easily be shown that the total horizontal stress becomes negative above a certain depth (Z_0) defined as follows:-

$$Z_0 = h \left[\frac{1}{1 + \frac{K_0}{1-K_0} \frac{\gamma_B}{\gamma_w}} \right] \dots\dots\dots(2.8)$$

where γ_w is the unit weight of water (Bishop, 1958), as long as the suctions between the depths of Z_0 and h are hydrostatic. Thus for

$h = 2\text{m}$, $Z_0 = 0.95\text{m}$ and tension cracks would be formed in the clay to about this depth, which agrees well with the observed fabric of the desiccated layer.

The in-situ stress variations within the 6m thick clay layer can be seen to be fairly significant. The light overconsolidation of the material means that C_u is largely dependent on p_c' and hence independent of these variations. Likewise overall settlements are largely controlled by whether or not p_c' is exceeded (Bjerrum, 1967). Typically for the Mucking clay at the main test elevation $M_{v1} = 4.6 \times 10^{-4} \text{ m}^2/\text{kN}$ for the stress increment covering the in-situ stress range (15 to 30 kN/m^2) whereas for an increment (60 - 120 kN/m^2) in excess of p_c' ($= 45 \text{ kN/m}^2$), $M_{v1} = 1.2 \times 10^{-3} \text{ m}^2/\text{kN}$.

The variations in the in-situ stresses do, however, change the starting point of the field stress paths and hence the degree of strength mobilisation prior to construction loading. The foundation beneath an embankment is subjected to a range of stress paths with the principal stress directions varying from vertical through to horizontal. Thus the variance in K_0 either side of unity determines whether active or passive loading conditions will be most critical e.g. for $K_0 < 1$ passive conditions will initially reduce the maximum shear stress whereas for active conditions the maximum shear stress mobilised in the soil is already somewhat towards the failure condition. For $K_0 > 1$ the reverse is obviously true. Likewise the deformations

resulting from the various stress paths are dependent on the initial starting in-situ stress conditions (Lambe, 1967), the active and passive cases providing the extremes of such deformations (Henkel, 1970).

2.7 Laboratory Measurement of the Undrained Strength of, and Effective Stress Parameters for, the Soft Clay Foundation and their Use in Embankment Design

2.7.1. General

The laboratory study of the Mucking clay was mainly directed towards an investigation of the effects of stress path, shear strength anisotropy and applied stress system (viz triaxial and plane strain) on the shear strength characteristics, and in particular for the undrained case. This work has enabled the parameters to be used in design to be considered in some depth, and their adequacy in predicting field behaviour to be studied in detail. In particular some of the more recently advocated design procedures for the undrained stability analysis of soft clay foundations (Bjerrum, 1972 and 1973; Ladd and Foott, 1974) will be considered in this section and in Chapter 7.

2.7.2. The Influence of Stress Path and Stress System

(i) Stress paths and stress system relating to embankment loading

Figure 2.14(A) shows an idealised embankment failure situation, with a circular arc failure surface passing through the foundation. Approximate principal stress directions are shown for three locations as follows:-

- a. under the centre of the embankment,
- b. under the embankment toe,
- c. close to the toe of the slip,

based on the simplifying assumption that the failure surface is at a constant angle to the major principal plane (after Lo, 1965). More recently finite element analyses have shown the general sense of these directions to be correct (see e.g. Hamza, 1976 and Chapter 8).

The stress paths followed within any soil element of a loaded foundation will generally involve some rotation of the principal stress directions. Stress paths plotted on the basis of principal stress magnitudes determined by finite element analysis will include the effects of such rotations, but these as yet cannot be incorporated in laboratory testing. Laboratory stress paths are thus generally limited to applying changes in magnitude approximating to the in-situ conditions with the directions of the principal stresses corresponding to those at failure. In addition the foundation beneath an embankment is typically loaded under plane strain conditions (Banks 1 and 2 at Mucking) whereas laboratory tests are commonly carried out under axisymmetric stress conditions.

The stress space used for the plots in this particular section is that suggested by Lambe (1967) wherein the vertical and horizontal normal (σ_v and σ_H) stresses are used, as opposed to the principal stresses. This plot is largely confined to those cases where the

former and latter coincide, but is advantageous in separating the stress space into a compression and extension region, a feature which cannot be achieved with principal stresses. Extension is thus defined as 'extension of the soil element with respect to its in-situ vertical axis'. The passive earth pressure situation (path 'e', figure 2.15(A)) typifies this definition, which does not imply a reduction in principal stresses.

Figure 2.15(A) shows typical field (plane strain) stress paths associated with embankments and foundations, and a normally consolidated soil ($K_0 < 1$)*. It can be seen that for the increasing stress levels relevant to the construction of a conventional embankment, a range of undrained loading paths from the compression situation of foundation loading to the extension situation of passive earth pressure may be expected. Paths 'a', 'b' and 'c' in figure 2.15(A) are analogous to locations 'a', 'b' and 'c' in figure 2.14(A). In the figure a single effective stress path (E.S.P.) for all cases of undrained foundation compression, and another for extension, is shown, although the fact that the undrained strength in plane strain extension is generally less than in compression (table 2.6) indicates that the E.S.P. s are dependent on the T.S.P. s.

Corresponding laboratory stress paths are shown in figure 2.15(B) in the form of the two main compression and extension paths. The diagram again relates to a normally consolidated clay and zero

*The total stress paths, which may in reality be curved, have been approximated to straight lines and the in-situ pore pressure neglected for simplicity.

initial pore pressure. A different E.S.P. for triaxial and plane strain conditions is shown, indicating the lower undrained strengths associated with the triaxial condition, particularly in extension (table 2.6).

(ii) Stress path and stress system influence on an isotropic elastic soil

Thus far it has been indicated that various field and laboratory stress paths and systems can result in the mobilisation of different C_u values. In order to understand why this should be it is instructive to consider the influence of the four total stress paths (T.S.P.s) in figure 2.15(B) coupled with both triaxial, and plane strain, stress systems on an isotropic elastic soil. All of these stress paths involve a change in either the horizontal, or the vertical, principal stress only (i.e. $+\Delta\sigma_1$ or $-\Delta\sigma_3$) such that the resulting change in total normal stress ($\Delta\sigma$) is equal in magnitude to $2C_u$ (starting from isotropic conditions).

The pore-pressure change (Δu) in a saturated isotropic elastic soil may be expressed as follows:-

$$\Delta u = \frac{1}{3} (\Delta\sigma_1 + \Delta\sigma_2 + \Delta\sigma_3) = \Delta\sigma_{OCT} \dots\dots\dots(2.9)$$

where $\Delta\sigma_{OCT}$ is the octahedral normal stress, this expression leading directly to equation 2.5 when $A = \frac{1}{3}$ (Skempton, 1954). For the triaxial case $\Delta\sigma_2 = \Delta\sigma_3$ or $\Delta\sigma_1$. Alternatively, when a saturated isotropic elastic material is loaded under undrained

(Poisson's Ratio, $\nu = 0.5$) plane strain conditions it can be readily shown that:-

$$\Delta\sigma_2 = \frac{1}{2} (\Delta\sigma_1 + \Delta\sigma_3) \dots\dots\dots(2.10)$$

which when substituted into equation 2.9 yields:-

$$\Delta u = \frac{1}{2} (\Delta\sigma_1 + \Delta\sigma_3) = \Delta\sigma_2 \dots\dots\dots(2.11)$$

and thus there is no change in the intermediate effective principal stress in such a test.*

The details of the various stress paths, starting from an isotropically consolidated state (p'), the total normal stress change, induced pore-pressure change and constant 'A' value ($=A_f$) are given in table 2.4. Inspection of the results shows that elastic theory predicts unique triaxial compression and extension E.S.P.s, but with differing inclinations, whereas a unique vertical plane strain E.S.P. exists for compression and extension. The differences are entirely consequential upon the different pore pressures induced by the various total stress combinations, as reflected in the 'A' values.

If the Mohr-Coulomb failure criterion is now incorporated assuming a zero apparent cohesion intercept (c') and a unique ϕ' for compression and extension such that:-

$$C_u = p'_{pf} \sin \phi' \dots\dots\dots(2.12)$$

where $p'_{pf} = \frac{\sigma_1' + \sigma_3'}{2}$ at failure, which leads to:-

*these conclusions can alternatively be arrived at by a consideration of the changes in effective stress coupled with elastic pore-pressure changes (Bishop and Hight, 1977).

Test Type	$\Delta\sigma_A^*$	$\Delta\sigma_H^*$	$= \frac{\Delta\sigma}{2} C_u$	Δu	A_f	$x = (1 - 2A_f)$
Triaxial Compression	$+\Delta\sigma_1$ $0 = \Delta\sigma_1$	$0 = \Delta\sigma_2 = \Delta\sigma_3$ $-\Delta\sigma_2 = -\Delta\sigma_3$	$+\Delta\sigma_1$ $-\Delta\sigma_3$	$+\frac{1}{3}\Delta\sigma_1$ $-\frac{2}{3}\Delta\sigma_3$	$+\frac{1}{3}$ $+\frac{1}{3}$	$+\frac{1}{3}$ $+\frac{1}{3}$
Triaxial Extension	$-\Delta\sigma_3$ $0 = \Delta\sigma_3$	$0 = \Delta\sigma_1 = \Delta\sigma_2$ $+\Delta\sigma_1 = +\Delta\sigma_2$	$-\Delta\sigma_3$ $+\Delta\sigma_1$	$-\frac{1}{3}\Delta\sigma_3$ $+\frac{2}{3}\Delta\sigma_1$	$+\frac{2}{3}$ $+\frac{2}{3}$	$-\frac{1}{3}$ $-\frac{1}{3}$
Plane Strain Compression	$+\Delta\sigma_1$ $0 = \Delta\sigma_1$	$0 = \Delta\sigma_3$ $-\Delta\sigma_3$	$+\Delta\sigma_1$ $-\Delta\sigma_3$	$+\frac{1}{2}\Delta\sigma_1$ $-\frac{1}{2}\Delta\sigma_3$	$+\frac{1}{2}$ $+\frac{1}{2}$	0 0
Plane Strain Extension	$-\Delta\sigma_3$ $0 = \Delta\sigma_3$	$0 = \Delta\sigma_1$ $+\Delta\sigma_1$	$-\Delta\sigma_3$ $+\Delta\sigma_1$	$-\frac{1}{2}\Delta\sigma_3$ $+\frac{1}{2}\Delta\sigma_1$	$+\frac{1}{2}$ $+\frac{1}{2}$	0 0

Table 2.4

Variation in Pore-Pressure Response in an Isotropic Elastic Soil, with Stress Path and Stress System

*A denotes axial and H horizontal with respect to the testing machine axis.

ϕ'	C_{UTE}/C_{UTC}		$C_{UPSA/P}/C_{UTC}$	
	A†	B†	A	B
20	0.80	0.80	0.89	0.95
22.5	0.775	-	0.87	-
25	0.75	0.75	0.86	0.92
27.5	0.73	-	0.84	-
30	0.71	0.71	0.83	0.89

Table 2.5

Variations in Undrained Strength of an Isotropic Soil with Stress Path and Stress System, as Predicted by Elastic and Critical State Theories

†A. Elastic theory plus Mohr-Coulomb

B. Critical state theory (results from Parry, 1971(b))

$$\frac{C_u}{p_{p0}'} = \frac{\sin \phi'}{1 - x \sin \phi'} \dots\dots\dots(2.13)$$

where $x = (1 - 2A_f)$, (values being given in table 2.4), the values in table 2.5 are produced. Thus a combination of Mohr-Coulomb and isotropic elasticity leads to different undrained strengths in triaxial extension and compression for any particular ϕ' , but a unique value in plane strain. The difference between the three values of undrained strength increases with ϕ' , and thus possibly with decreasing plasticity. For the range of ϕ' values considered triaxial extension strengths are 20 to 30% lower than triaxial compression whilst the plane strain values are intermediate, being 11 to 17% below those from triaxial compression. The differences are entirely dependent on the intermediate principal stress, the value of which is truly intermediate in the elastic plane strain situation, but an upper bound ($= \sigma_1$) in triaxial extension, and a lower bound ($= \sigma_3$) in triaxial compression.

Also shown in table 2.5 are data presented by Parry (1971(b)) based on the following critical state assumptions:-

- a. $c' = 0$ and ϕ' independent of stress path.
- b. $\frac{\sigma_1'}{\sigma_3'} = \frac{1 + \sin \phi'}{1 - \sin \phi'}$ at the critical state(2.14)
- c. Samples at the same initial value of σ'_{OCT} reach the critical state at a common value of σ'_{OCT} regardless of stress path.

The values are exactly the same as those predicted from elasticity and Mohr-Coulomb for the triaxial tests, which is not surprising as

equation 2.14 is Mohr-Coulomb (with $c' = 0$) and the use of equation 2.9 results in $\Delta\sigma'_{OCT} = 0$ which is a particular form of condition (c). In addition the same values of ϕ' have been used for both sets of calculations implying $\phi' = \phi'_{cs}$

(cs denotes critical state) which is only true in limited circumstances. The difference in the plane strain predictions is due to the assumption by Parry that $\frac{\sigma_2'}{\sigma_1' + \sigma_3'} = 0.4$

whereas from elastic theory this ratio is a constant equal to 0.5 for the isotropic case.

Thus both of these theoretical approaches indicate that the undrained strength in plane strain field conditions will be overestimated by triaxial compression (T.C.) tests and underestimated by triaxial extension (T.E.) tests although the mean of these latter two may give a reasonable approximation to the former.

(iii) Stress path and stress system influence on soft normally consolidated clays in nature

Table 2.6 presents a summary of some of the more recent experimental data on this topic for undisturbed samples consolidated back to the in-situ stresses. The exception to this latter condition are the Mucking samples which were isotropically consolidated, although it will be shown in the next sub-section that this was of little consequence. A number of comparisons can immediately be made with table 2.5. The results of plane strain active* (P.S.A.) and plane strain passive* (P.S.P.) tests show significantly lower strengths

*P.S.A: compression test with $\Delta\sigma_1$ positive and $\Delta\sigma_3 = 0$, $\Delta\sigma_1 = \Delta\sigma_A$

P.S.P: extension test with $\Delta\sigma_1$ positive and $\Delta\sigma_3 = 0$, $\Delta\sigma_1 = \Delta\sigma_H$

A denotes axial, and H horizontal, with respect to the axis of the testing machine.

REFERENCE	Ip %	$\phi^{\circ} E^{\circ}$		$\phi^{\circ} C^{\circ}$		<u>CUTE</u>	<u>CUPSA</u>	<u>CUPSP</u>	<u>CUDSS</u>	<u>CUPSA</u>
		TE	PSP	TC	PSA	CUTC	CUTC	CUTC	CUTC	CUPSP
Drammen(Lean)Clay Berre & Bjerrum,1973	10	-	-	30	-	0.21	-	-	0.65	-
Sensitive Marine Clay Ladd, 1972	15	-	-	20	-	-	1.18	0.52	0.80	0.44
Boston Blue Clay Ladd & Foott, 1974	24	-	-	27	-	0.47	1.03	0.57	0.61	0.55
Haney Clay Vaid & Campanella, 1974	26	33.8	34.3	29.8	31.6	0.63	1.11	0.79	-	0.71
Drammen(Plastic)Clay Berre & Bjerrum,1973	31	-	-	31.7	-	0.40	-	-	0.80	-
Matagami Clay Dascal et al, 1972	47	-	-	-	-	0.74	-	-	-	-
Mucking Clay Wesley, 1975	40-70	25	25	25	25	0.56	1.09*	0.76*	-	0.70*
Bangkok Clay Berre & Bjerrum,1973	88	-	-	39.8	-	0.52	-	-	0.59	-

Table 2.6.

Variations in the Undrained Strength of Undisturbed Samples of 'Normally' Consolidated Clays with Stress Path and Stress System (All Samples ' K_0 Consolidated' Except*)

*isotropically consolidated to mean in-situ stress level.

REFERENCE	Ip%	ϕ°	CUH1/CUV1		CU(45)1 /CUV1	
			TC	PSA	TC	PSA
Welland Clay, Lo, 1965	15	29	0.75	-	0.84	-
Welland Clay, Delory & Lai, 1971	15	29	0.70	-	0.81	-
Mucking Clay Wesley, 1975	40-70	25	0.70	0.70	0.80	0.80

Table 2.7.

Variations in the Undrained Strength of Undisturbed Samples of Lightly Overconsolidated Clays with Sample Orientation

for the latter whilst the P.S.A. results are very similar to, although generally slightly higher than, the T.C. ($+\Delta\sigma_1 = \Delta\sigma_A$, $\Delta\sigma_3 = 0$) results. The undrained strengths from the T.E. ($-\Delta\sigma_3 = \Delta\sigma_A$, $\Delta\sigma_1 = 0$) tests are always the lowest and significantly lower than those from the P.S.P. tests. These trends are consistent throughout the tabulated data, which refer to samples whose in-situ vertical axis corresponds to the vertical axis of the testing machine. The differences between the P.S.P. and P.S.A. results is due both to the inappropriateness of elasticity as a model for soil behaviour, and, probably predominantly, anisotropy. The latter would thus appear to be an important factor in determining the mobilised undrained strength of all the clays considered in table 2.6. The closeness of the T.C. and P.S.A. undrained strengths is largely because in reality the intermediate principal stress tends towards the minor, rather than the major, principal stress (see e.g. Wesley, 1975) and hence the critical state predictions are rather closer to the mark than those based on elasticity.

A comparison of all the undrained results, including the full depth range and various sample orientations, for the Mucking clay shows the plane strain values (P.S.A.) to be even closer overall to the T.C. values than indicated by the results in table 2.6. These latter values refer to isotropically consolidated undrained tests carried out at the main test level. Thus for the Mucking clay undrained triaxial compression tests resulted in C_u values closely approximating to the plane strain values.

The results of direct simple shear (D.S.S.) tests performed with the Geonor simple shear apparatus (Bjerrum and Landva, 1966) are also included in table 2.6. The stress path and stress system associated with this test are somewhat indeterminate, but it is generally held to be representative of position (b) in figure 2.14(A) (Bjerrum, 1972; Ladd and Foott, 1974). The results are typically intermediate between those from the two types of compression and extension tests.

The effective stress parameters (c' and ϕ') are generally assumed to be stress path, and stress system, independent and for most normally consolidated clays, isotropic. This is the case for the Mucking clay under triaxial and plane strain conditions, although the only other comprehensive set of data on this aspect in table 2.6 (Vaid and Campanella, 1974) showed 4.5° difference between ϕ' from T.C. and P.S.P. tests, and 4° difference between T.E. and T.C. tests.

(iv) In-situ stress and stress history in relation to the laboratory measured undrained strength

Another important aspect of stress path influence on the undrained strength is the starting stress system i.e. whether the sample is sheared undrained, isotropically consolidated to a mean (p'), or the vertical (p_0'), in-situ stress or consolidated anisotropically to the estimated in-situ stresses (p_0' and $K_0 p_0'$). The latter procedure necessitates a knowledge of K_0 which, as has been shown in the previous

section, is open to considerable uncertainty. Davis and Poulos (1967), Bjerrum (1973), and Berre and Bjerrum (1973) consider it essential to consolidate samples to the in-situ stresses for a correct prediction of the undrained strength, whereas Ladd and Lambe (1963) maintain that the ensuing reduction in void ratio will result in an overestimate of the undrained strength.

According to Bjerrum (1973) the change in void ratio is partly compensated for by the earlier swelling of the sample, consequent upon its extraction from the ground. The quality of the sample, and particularly the proportion of the mean in-situ effective stress represented by the pore suction, is obviously an important factor in this argument.

Ladd and Foott (1974) have proposed a procedure for normalising the effects of stress history. The method is based on the assumption that for a particular soil two samples having the same O.C.R., but different p_c' and p_o' values, exhibit a common value of the normalised parameter C_u/p_o' . Firstly oedometer tests are carried out over the depth range being investigated and p_c' is determined, and hence from p_o' the O.C.R. variation with depth is established. Samples are then consolidated to various stress levels in excess of p_o' and sheared undrained to provide a relationship between C_u and p_o' , as shown for the Mucking clay in figure 2.16. The method relies on the soil exhibiting a constant value of C_u/p_o' when $p_o' > p_c'$. Additional samples are consolidated to various stresses in excess of p_c' , then unloaded back to $p_o' = p_c'$ and

sheared undrained to provide a relationship between C_u/p_o' and O.C.R. From this relationship the undrained strength can be found for any particular p_o' value.

The method can be seen to take the soil to elevated stress levels such that it behaves once more as a normally consolidated deposit.* The effects of overconsolidation at the in-situ stress levels are then back-extrapolated from the effects of stress reductions at the higher stress levels. The main disadvantages of the technique are that no strength measurements are made at the in-situ stress levels and that the overconsolidation effects are modelled only by stress relief. A consequence of testing at high stress levels may be to destroy structural features, which in fact contribute to the lightly overconsolidated behaviour, in the form of interparticle bonding caused by chemical changes or particle orientation resulting from the in-situ stress system (Bishop, 1971(a)). In addition the sensitivity of C_u/p_o' to O.C.R. necessitates the accurate determination of p_c' , a feat which is often as difficult to achieve as a reliable measurement of C_u (Mesri, 1975).

It should be noted at this point that the p_c' indicated by figure 2.16 is almost identical to that from the oedometer tests on a vertical sample (assuming $K_o = 0.42$ applied at p_c'), and also that the normally consolidated part of the C_u/p' plot does not extrapolate to the origin. Wesley (1975) attributes this latter fact to the relatively short consolidation period used precluding any secondary consolidation.†

*The assumption, implicit in the method, that once p_c' has been exceeded the soil's behaviour is independent of its previous stress history, does not appear to be correct for the Mucking clay (see e.g. section 2.4.3).

†see, also, Buri (1978).

Samples of Mucking clay were tested in undrained triaxial compression in the unconsolidated state, after isotropic consolidation to the mean in-situ stress level and after K_0 consolidation. Tests were performed in extension and compression as well as unloading from the in-situ deviator stress followed by compression loading. The tests showed no significant undrained strength variation with the initial stress system, in either the extension or compression results. The reasons for this are partly illustrated in figures 2.16 and 2.17, the latter showing that the effective stress paths at low stress levels tend to converge at failure, despite different starting stresses, due to the variation in pore-pressure response, and particularly A_f , with consolidation pressure (figure 2.18). This results in the relatively small gain in undrained strength with consolidation pressure over the sub- p_c' stress range, as shown in figure 2.16. Thus the variations in initial suction (typically 50 to 65% of that for a perfect sample) were not responsible for any major variations in the undrained strength. The samples which were unloaded from the in-situ deviator stress, and subsequently loaded in compression, showed that even for a perfect sampling operation there is a slight loss in undrained strength, due to the irreversible nature of the soil's stress-strain behaviour (Bishop, 1971(a)). The 'A' value of 0.19 relating to sampling, as used in the previous section to calculate K_0 , was derived from these tests.

Thus the results of the unconsolidated undrained triaxial tests were considered to give C_u values relating to the in-situ stresses. In qualifying this conclusion it must be remembered that the K_0 value

of 0.55 used for the laboratory work appears low on the basis of the field evidence, and that no tests were carried out from different K_0 values. Such tests would have been of value in ascertaining the effect of variations in K_0 *per se*, and as a result of seasonal in-situ effective stress changes. The laboratory data, however, indicate that variation in K_0 would have little effect on the measured value of C_u .

In addition Wesley (1975) points out that the samples were of high quality (based on the suction measurements, as defined by Ladd and Lambe (1963)) and from relatively shallow depths, so that the effect of the initial consolidation pressure may be greater in other situations.

2.7.3. Shear Strength Anisotropy

The undrained strength of a soil may be anisotropic as a consequence of predominant structural features, stress history or the in-situ stresses (Parry, 1971(a)). Anisotropy associated with the latter circumstances is that most commonly occurring in soft clays and probably results from preferred particle orientations causing the structural stiffness of the material to vary with the direction of the applied stress.

The failure plane orientation within a soil mass depends upon the applied stress system, including boundary conditions, as well as the material's structure. All of these factors combine to influence the

pore pressures generated under load, and the undrained strength (Duncan and Seed, 1966(a) and (b); Duncan, 1967). This overlapping of the effects of stress path, stress system and undrained strength anisotropy (as typified by the results in table 2.6) has led to some confusion in the literature of the latter's contribution to the discrepancies observed between laboratory measurements and back-analysed field values of undrained strength.

The variation in undrained strength with in-situ stress, principal stress directions and failure plane orientation was predicted theoretically by Hansen and Gibson (1949), and more recently by Bjerrum (1973), who neglected the effect of pore pressures which was implicit in Hansen and Gibson's work and appears to be a major factor in undrained strength anisotropy (Bishop, 1966(a)).

For a plane strain field situation the difference between the P.S.A. and P.S.P. tests provides a good indication of the importance of anisotropy (table 2.6), but there is no *a priori* reason to take these test conditions as representing the extremes of anisotropy that the soil may exhibit. In order to further investigate this phenomenon, P.S.A. tests could be carried out on samples prepared with their in-situ axes at varying inclinations to the major principal stress. The assessment of undrained strength anisotropy from a comparison of T.E. and T. C. tests, as suggested by Bjerrum (1972, 1973), is not possible unless some account is taken of the stress path/system effects inherent in such a comparison.

Because of the difficulties associated with carrying out large numbers of plane strain tests, most undrained strength anisotropy studies on samples prepared at various inclinations have been performed using the triaxial apparatus (e.g. Lo, 1965; Agarwal, 1967; Maguire, 1975; Wesley, 1975). Such studies, whether carried out using the triaxial or plane strain apparatus, are open to interpretation difficulties arising from the ambiguity in failure plane orientations as shown in figure 2.14(B).1. This ambiguity is more pronounced in triaxial specimens, a particular example being horizontal samples (as pointed out by Bishop (1966(a)) and Wesley (1975)) which may fail on planes that were vertical in the ground, with the direction of movement being horizontal (figure 2.14(B).2) and thus not related to the movements on a typical field failure surface. Such difficulties are particularly relevant when stability analyses are carried out taking anisotropy into account by assigning to each segment of the slip surface an undrained strength according to its inclination (i.e. $C_u = f(\theta)$, see figure 2.14(A)).*

Results presented by Lo (1965) and Delory and Lai (1971) for the lightly overconsolidated Welland Clay show a steady drop in undrained strength from vertical to horizontal samples with a minimum ratio of between 75 and 84% (table 2.7). The semi-confined tests of Delory and Lai (1971) restricted the failure plane to a particular direction (whilst maintaining freedom of inclination), yet the results were almost identical to those of Lo (1965). However, by testing samples at inclinations through 180° as opposed to 90° , Delory and Lai's

*Noting that $\beta = 45^\circ$ for a correct interpretation of the $\phi_u = 0$ analysis (Skempton, 1948(c)) and not $45^\circ + \phi'/2$ as proposed by Lo (1965).

results emphasised that different undrained strengths can be obtained on planes having the same inclination to the vertical. Although unique values of undrained strength cannot be assigned to particular planes, there appears to be an unambiguous relationship between the principal stress direction and undrained strength. An anisotropic stability analysis such as that suggested by Lo (1965), wherein the most likely failure planes associated with the various principal stress directions are considered, would seem to be an improvement on current practice (figure 2.14(A)).

Bjerrum and Kenney (1967) suggested that the undrained strength on a particular plane will depend on whether the direction of shear is the same (active), or opposite (passive), sense to that which it carried in situ (figure 3.8(A)). This is in fact another definition of planes at the same inclination to the vertical having different undrained strengths, being a function of the inclination of the principal stresses to the soil structure, as shown by Delory and Lai (1971) and predicted by Hansen and Gibson (1949).

Ladd and Foott (1974) suggest that the average undrained strength obtained from P.S.A. and P.S.P. tests, or the results of D.S.S. tests (which appear to approximate to this average), may account for undrained strength anisotropy in stability calculations. They also suggest the average from T.E. and T.C. tests may be applicable, and although isotropic elastic theory casts some doubt on the justification for such an assumption, the approach may provide an

acceptable approximation in design. The average undrained strength mobilised around a slip surface in an anisotropic soil will depend upon the orientation of that surface (or vice versa) and thus any averaging technique can only be approximate, although preferable to the use of the maximum or minimum values.

Figures 2.19 and 2.20 show the results of unconsolidated undrained triaxial and plane strain compression tests carried out on samples of Mucking clay cut at varying inclinations from vertical to horizontal (15° intervals). The samples in figure 2.19 were from 3.78 to 4.08m depth and tested at an axial strain rate of 0.3% per hour. Plane strain tests were performed only on vertical, horizontal and 45° samples. The 'end-on' plane strain tests refer to samples with the plane strain axis in the vertical direction such that failure had to occur on a vertical plane with the movement in a horizontal direction. The fact that these tests produced undrained strengths almost identical to the horizontal triaxial and plane strain tests indicates that the inclination of the failure plane was not of major importance, and reinforces the view that the direction of the major principal stress is of prime importance.

Figure 2.20 shows averaged values for all the undrained results over the depth range from 2.58 to 4.58m. These additional results are from unconsolidated undrained triaxial tests carried out on vertical, horizontal and 45° samples. They generally represent an average from four tests, carried out at an axial strain rate of 0.2% per minute.

The results show the strength to drop steadily from vertical to horizontal, with a minimum ratio of between 64 and 78%. An average strength reduction to 70% of the vertical strength is typical of the results (table 2.7) including the consolidated undrained series quoted in table 2.6. These latter tests were carried out at an axial strain rate of 0.3% per hour. The P.S.P. results quoted in table 2.6 were in fact P.S.A. tests carried out on horizontal samples, this being a legitimate method of carrying out plane strain extension tests. The ratio C_{UPSP}/C_{UPSA} is seen to be 70%, thus predicting undrained strength anisotropy of the same order as the T.C. tests. The ratio of C_{UTE}/C_{UTC} is 56%, which is 14% lower still, this drop being attributable to stress path/system effects not related to the plane strain situation.

The steady drop in strength from vertical to horizontal is very similar to that reported for the Welland Clay (table 2.7) and can be readily modelled using the expression suggested by Bishop (1966(a)) as follows:-

$$C_{U\theta 1} = C_{UV1} (1 - a \sin^2 \theta) (1 - b \sin^2 2\theta) \dots\dots\dots(2.15)$$

where $C_{U\theta 1}$ is C_U when the major principal stress is at an angle θ^0 to the soil's vertical axis.

C_{UV1} is C_U with $\theta = 0$

a is a parameter reflecting the influence of pore pressure

b is a parameter reflecting the directional characteristics of c' and ϕ' as well as pore pressure.

with a = 0.3 and b = 0.065 as shown in figure 2.20.

The fact that 'b' is close to zero indicates the predominant influence of pore pressure on the anisotropic undrained strength response of the Mucking clay, as well as the essentially isotropic nature of c' and ϕ' .

The data in figures 2.19 and 2.20 show that the P.S.A. and P.S.P. tests do represent the extremes of undrained strength anisotropy for the Mucking clay, suggesting that the averaging technique of Ladd and Foott (1974) may be very reasonable in this case. However, the strength on the 45° samples is still only about 80% of the vertical samples (81 to 85% for the Welland Clay, table 2.7) so that an average of the vertical and horizontal cases may be an over-estimate.

Consolidated undrained tests, carried out under triaxial and plane strain conditions, on samples at varying inclinations to the vertical showed the undrained strength anisotropy to be a function of pore-pressure response with c' and ϕ' essentially constant. The strain at failure for the different inclinations of sample only varied slightly, but the relationship between strain and pore pressure varied significantly. This is in contrast to the Welland Clay for which Lo (1965) found the anisotropy to be a function of differing failure strains, the pore pressure-strain relationship remaining unchanged with sample inclination. The differing pore-pressure response of the Mucking clay with principal stress direction is primarily due to the reduction in soil skeleton stiffness from vertical to horizontal loading conditions.

The fact that this anisotropic skeleton stiffness effect disappears at higher stress levels emphasises the need for tests at the in-situ stress levels. Thus the pattern of decreasing undrained strength as the principal stress direction rotates from vertical to horizontal may be a common feature for soft lightly overconsolidated clays where the anisotropy is mainly a function of soil skeleton stiffness differences, resulting from the in-situ, and previous, horizontal and vertical principal stresses.

Finally, Berre and Bjerrum (1973) have suggested that undrained strength anisotropy decreases with increasing plasticity on the basis of the ratio C_{UTE}/C_{UTC} , which has been shown to increase with decreasing ϕ' for an isotropic elastic soil. The data in table 2.6 have been arranged in order of increasing plasticity but there does not appear to be any strong correlation with anisotropy, although the very low values of C_{UTE}/C_{UTC} and C_{UPSA}/C_{UPSP} are associated with clays of very low plasticity. In addition the minimum ratio of C_u from the horizontal and vertical samples of Mucking clay was associated with the depth range over which the plasticity was a minimum.

2.7.4. Sample Size and Strain Rate Effects

The tests described thus far were all performed on 38mm diameter by 76mm high triaxial, and 38mm wide by 76mm high by 203mm long plane strain samples. In addition triaxial tests were performed on 102mm diameter by 203mm high vertical samples; a comparison of these latter tests with those on the small vertical triaxial samples showed no discernable sample size effects.

Two rates of axial strain were primarily used in the test program, viz:-

- a. 0.2% per minute for the unconsolidated undrained triaxial and plane strain tests. These tests only formed a small part of the overall program but are the only ones covering the full depth range of the test pit. The time to failure was typically 10 to 15 minutes.
- b. 0.33% per hour (= 0.0056% per minute) used for the consolidated undrained tests and a limited number of unconsolidated undrained tests on samples at varying inclinations (figure 2.19). The time to failure was typically 9 hours.

In order to investigate the influence of strain rate on the undrained shear strength a series of isotropically consolidated undrained triaxial tests were carried out at varying strain rates. The results are presented in figure 2.21 normalised to the undrained strength at 10 minutes failure time as are some very similar results for Drammen (plastic) Clay (Berre & Bjerrum, 1973; see also table 2.6) anisotropically consolidated to the in-situ stresses.

The Mucking clay can be seen to exhibit a considerable strain rate effect, this being in excess of 20% per log cycle from 1 to 10 minutes, dropping to about 8% per log cycle between 1000 and 10,000 minutes, to failure. Strain rate is further discussed in Chapter 3 in relation to strain rate influence on the field undrained strength mobilised by a new large vane apparatus. The difficulties associated with relating

laboratory, and field, measurements of strain rate effects to the undrained strength which can be mobilised at field loading rates are also discussed in the same chapter.

Strain rate also influences the effective stress parameters, as shown in figure 2.22, but the effect is rather less than in the undrained case due to the influence of the pore-pressure response. Thus, although the drop in undrained strength from the 513 to 6160 minute test is 2.45 kN/m^2 , it can be represented by a reduction in c' of 1.6 kN/m^2 with $\phi' = 25^\circ$. Bjerrum (1973) associated the time dependent drop in available undrained strength with a tendency for the transfer of load from cohesive to frictional components within the soil mass, and hence with materials of higher plasticity.

2.7.5. Undrained Strength/Depth Profile and Effective Stress Parameters

(i) Undrained Strength

Figure 2.23 shows the average undrained strength plotted versus depth as a full line. This represents a straight average taken from the results of vertical, 45° and horizontal triaxial samples, the approximate magnitude and depth range of these tests being given by the long chain-dotted lines. Both these lines and the full one are best fit approximations, although the scatter was not great except for the top 2m or so where the in-situ shear surfaces and general non-homogeneity were reflected in the results. The averaging technique was thus similar to that proposed by Ladd and Foott (1974).

The upper part of the main strength/depth curve (solid line) is based on vertical tests only, whilst the extreme upper and lower segments (hatched lines) are straight line extrapolations.

Included for comparison is the design curve arrived at by the Consulting Engineers on the basis of the commercially tested piston samples. These samples were vertical 38 x 76mm triaxial specimens tested under unconsolidated undrained conditions at an axial strain rate of 0.2% per minute, as were all the samples represented in figure 2.23. The undrained strength of the piston sample specimens, which were trimmed from the bottom of the tubes, is on average 2 kN/m² less than the vertical test pit samples (see also figure 3.7). This doubtless reflects a drop in sample quality, comprising a high degree of suction loss and some mechanical disturbance. Specimens taken from the top of the 1m long piston sample tubes exhibited substantially lower undrained strengths than those from the bottom, indicating a high degree of mechanical disturbance.

In arriving at the undrained strength design curve,* sample size, sample disturbance, stress path, stress system and anisotropy have all been taken into consideration, and account, where necessary. However, major uncertainties still remain regarding the possible influence of strain rate† and progressive failure on the field undrained strength which can be mobilised under full scale loading conditions.

*the laboratory average design curve.

†the proposed field average design curve (figure 2.23) is corrected for strain rate by direct extrapolation of t_f (lab) to t_f (field) - see also table 3.11.

Finally, the dependence of the undrained strength on p_c' has been shown in figure 2.16, this aspect being further examined in figure 2.24(B). Curves (3) and (4) show the variation in C_u/p_o' with plasticity predicted by field vane (F.V.) tests, for aged and young normally consolidated clays respectively, presented by Bjerrum (1973). It has been pointed out by Mesri (1975) that, because of the relationship between p_c'/p_o' and plasticity (figure 2.24(A)) for the same clays, curve (4) is also a common curve of C_{UFV}/p_c' for both aged and young clays. A young clay is a genuine normally consolidated one ($p_o' = p_c'$) and as might be expected curve (4) is very similar to line (6) which represents Skempton's (1957) empirical relationship:-

$$C_u/p_o' = 0.11 + 0.0037 I_p \dots\dots\dots(2.16)$$

It should be noted that Skempton's equation is based primarily on laboratory data whereas Bjerrum's curve is for the field vane, and according to Bjerrum (1972, 1973) the field vane strength needs to be corrected according to plasticity, to produce the true field strength as follows:-

$$C_u(\text{FIELD}) = C_{UFV} \cdot \mu \dots\dots\dots(2.17)$$

where μ is a correction factor related to plasticity index as described in Chapter 3 and shown in figure 3.3. Thus if curve (4) is corrected for plasticity, curve (5) is obtained (Mesri, 1975) which indicates the field C_u/p_c^{-1} to be independent of plasticity. This implies that the slope of line (6) is a function of p_c' (i.e. it contains C_u/p_o' values relating to lightly overconsolidated soils)

Z	$P'_{o\min}$	P'_o	P'_c	$\frac{P'_{o\min}}{P'_o}$	$\frac{P'_c}{P'_o}$	I_p	C_{uvi}	$\frac{C_{uvi}}{P'_{o\min}}$	$\frac{C_{uvi}}{P'_o}$	$\frac{C_{uvi}}{P'_c}$	$C_{uFV(V)}$	$\frac{C_{uFV(V)}}{P'_o}$	$\frac{C_{uFV(V)}}{P'_c}$	$C_{uFV(V)}$	$\frac{C_{uFV(V)}}{P'_c}$
m	kN/m ²	kN/m ²	kN/m ²	—	—	%	kN/m ²	—	—	—	kN/m ²	—	—	kN/m ²	
1.5	7.75	22.25	34.0	4.38	1.53	73	-	-	-	-	15.8	0.70	0.46	10.70	0.31
1.53	8.00	22.50	34.50	4.31	1.53	73	13.10	1.64	0.58	0.38	-	-	-	-	-
2.0	10.50	24.0	36.00	3.43	1.50	68	-	-	-	-	17.7	0.74	0.49	12.40	0.34
2.13	11.50	24.50	37.00	3.22	1.50	66	14.65	1.28	0.60	0.40	-	-	-	-	-
2.5	13.00	26.00	39.00	3.00	1.50	60	-	-	-	-	18.4	0.71	0.47	13.40	0.34
2.73	14.00	27.00	40.00	2.85	1.48	55	15.45	1.10	0.57	0.39	-	-	-	-	-
3.0	16.00	28.00	41.50	2.59	1.48	48	-	-	-	-	19.0	0.68	0.46	15.00	0.36
3.33	18.00	30.00	43.00	2.39	1.44	40	17.5	0.97	0.58	0.41	-	-	-	-	-
3.5	19.00	31.00	44.00	2.32	1.42	37	-	-	-	-	17.8	0.57	0.40	15.30	0.33
3.93	21.50	33.50	46.00	2.15	1.38	39	18.65	0.87	0.59	0.41	-	-	-	-	-
4.0	22.00	34.00	47.50	2.15	1.38	40	-	-	-	-	17.7	0.52	0.37	14.90	0.31
4.5	25.00	36.00	49.50	1.98	1.37	46	-	-	-	-	17.7	0.49	0.35	14.30	0.29
4.53	25.50	36.50	50.00	1.97	1.37	47	19.35	0.76	0.53	0.39	-	-	-	-	-
5.0	28.00	39.50	52.50	1.87	1.33	56	-	-	-	-	18.6	0.47	0.35	14.00	0.27
5.5	31.50	42.50	55.50	1.76	1.31	61	-	-	-	-	20.5	0.48	0.37	15.00	0.27
6.0	35.00	45.00	58.5	1.67	1.30	63	-	-	-	-	21.6	0.48	0.37	15.60	0.27

Table 2.8. Field and Laboratory Measurements of Undrained Strength Related to In-Situ Stress and Stress History

and/or strain rate effects. Bjerrum's data tend to support the latter, particularly at the lower I_p values. If field vane tests require rate corrections (which μ is supposed to predominantly be (Bjerrum, 1972)) it seems logical to suppose that so do quick undrained laboratory tests, the results from which led to equation 2.16.

Table 2.8 and figure 2.24(B) show that for the Mucking clay C_{uVI}/p'_y is nearly constant for $p'_y = p'_c$ or p'_o and that the respective values are approximately 0.4 and 0.58, the latter being in good agreement with curve (3). The former value is higher than predicted by equation 2.16 and curve (4) for the range of plasticity encountered, although this may be partly due to an underestimate of p'_c . No inferences can be drawn from the relatively consistent values of $C_{uVI}/p'_{(o,c)}$ over a fairly wide range of plasticity, as these changes are associated with mineralogical and water content changes, and, as pointed out in section 2.3, need not lead to changes in C_u .

The value of $C_{uVI}/p'_{o \min}$ is not constant, reflecting the much higher range and magnitude of the O.C.R. values associated with $p'_{o \min}$. The F.V. data in figure 2.24(B) are discussed in section 3.2.4.

(ii) Shear strength of the desiccated layer

The fissured nature of this material precluded the preparation of laboratory triaxial samples and the only shear strength data were obtained using the small (12.6mm diameter by 19mm high) laboratory

vane, indicating $C_u = 50 \text{ kN/m}^2$. This is of the order of magnitude suggested by visual examination in the field of the intact material, but does not take into account its fabric.

Desiccated layers pose a major problem in analyses involving soft clay foundations, as no sensible strength measurement can generally be made in either the laboratory or the field.

Seymour-Jones (1975) suggests the use of at least two tentative values for the undrained strength of the crust in any design, in order to study its influence. The difficulty in selecting realistic values led to the adoption of a two-stage embankment at Mucking; this was intended to induce one failure surface passing through the crust (Bank 1, Stage 2) and another through undesiccated clay only (Bank 1, Stage 1), as described in Chapter 4.

Effective stress analyses are equally uncertain in this layer as accurate pore-pressure readings of suctions close to ground level are very hard to achieve. This problem is not alleviated if the pore pressures become positive during construction, as will be discussed in Chapter 5.

(iii) Effective stress parameters

These have been discussed to some extent in passing and the effective stress envelope in the low stress range was presented in figure 2.17. The effective stress envelope for the stress range investigated is presented in figure 2.25 and can be seen to have been divided into

two segments as follows:-

- a. $c' = 8 \text{ kN/m}^2$ } representing the lightly overconsolidated
 $\phi' = 25^\circ$ } behaviour at low stress levels.
- b. $c' = 3.5 \text{ kN/m}^2$ } representing the normally consolidated
 $\phi' = 32^\circ$ } behaviour at higher stress levels.

The uncertainty of the envelope's shape at very low stress levels is indicated in figure 2.17. The abrupt change from the 'overconsolidated' to the 'normally consolidated' envelope is obviously an approximation to the gradual transition which probably occurs in reality.*

Similarly to the undrained strength the major uncertainties regarding the effective stress values are the influences of strain rate and progressive failure.

2.7.6. Undrained Remoulded and Residual Strengths

Laboratory vane tests on remoulded samples resulted in the values of sensitivity shown in figure 2.23. The sensitivity is closely linked to the liquidity index as a comparison with figure 2.7 shows; likewise figure 2.26, where the results can be seen to sensibly follow the relationship postulated by Bjerrum (1954) for clays whose sensitivities derive mainly from leaching and secondary consolidation. The sensitivity increases from unity in the desiccated zone to nine at a depth of about 5m, thus spanning the range from insensitive to slightly quick. These

*This does not mean that abrupt changes in behaviour cannot occur when the preconsolidation pressure is exceeded.

results are further discussed in section 3.2.4. in relation to the field vane values of sensitivity. There does not appear to have been a common classification of sensitivity adopted in the literature and the terms used herein are as defined by Bjerrum (1954) and indicated in figure 2.24. Using equation 1.1. to define the brittleness in terms of sensitivity, the lower bound for the value of I_B , using the maximum value of sensitivity is 89%.

In addition a number of 'undrained' ring shear tests were performed on undisturbed (with and without a pre-cut plane) and remoulded samples. These are summarised in figure 2.27 and the residual strength compared to the remoulded strength measured with the laboratory vane and in triaxial tests. The agreement between the various data sources is very good and for the test level the undrained brittleness index from the undisturbed ring shear sample was 80%, compared to 83% corresponding to a sensitivity of 6, the former deriving from equation 2.18 as follows:-

$$I_B = \frac{C_u - C_{ur}}{C_u} \dots\dots\dots(2.18)$$

where r denotes residual (Bishop, 1971(a)).

The data in this section would thus suggest that the Mucking clay is a brittle material and that progressive failure may be an important factor in design calculations. However, the application of this information in design requires a knowledge of both the pre-and post-

peak stress-strain behaviour of the soil, as well as the stress distribution within the soil mass (Bishop, 1971(b)). As pointed out in Chapter 1, this uncertainty regarding the influence of progressive failure in a truly brittle material is one of the main reasons for a trial embankment construction.

2.8. Drained and Undrained Laboratory Deformation Characteristics of the Soft Clay Foundation

The value of the initial undrained deformation modulus (E_u) and axial failure strains (ϵ_{Af}) for the undrained tests are presented in table 2.9. for the various consolidation histories, sample orientations and stress paths considered. The unconsolidated tests were performed on samples from 3.78 to 4.08m depth, whereas the remainder of the tests were on samples from the main test level (3.18 to 3.48m). The axial strains at failure are in general small (2 to 4%) being greater for the horizontal compression samples, and extension tests on vertical samples, than for the vertical compression samples, and slightly less in plane strain than in triaxial conditions.

From isotropic elastic theory the slope of the undrained stress - strain curve can be predicted for triaxial conditions:-

$$\frac{\Delta\sigma_A}{\Delta\epsilon_A} = E_u = E^T \dots\dots\dots(2.19)$$

where E is Young's Modulus and T denotes total stress, and for plane strain conditons:-

$$\frac{\Delta\sigma_A - \nu\Delta\sigma_p}{\Delta\epsilon_A} = E^T \dots\dots\dots(2.20)$$

where p denotes the plane strain axis in the testing machine.

From equation 2.10 $\Delta\sigma_p = \Delta\sigma_2 = \frac{1}{2}\Delta\sigma_1 = \frac{1}{2}\Delta\sigma_A$ ($\Delta\sigma_3 = \Delta\sigma_H = 0$)
and therefore as $\nu = 0.5$:-

$$\frac{\Delta\sigma_A}{\Delta\epsilon_A} = E_u = \frac{4}{3} E^T \dots\dots\dots(2.21)$$

Thus elastic theory predicts the slope of the plane strain stress-strain plot to be $\frac{4}{3}$ of that for the triaxial case. The relationships may also be expressed in terms of the drained deformation parameters by using the relationship:-

$$E^T = \frac{3E'}{2(1 + \nu')} \dots\dots\dots(2.22)$$

The E_u values in the table are based on $\epsilon_A = 0.25\%$ so that a direct comparison may be made with the results quoted by Wesley (1975) for drained tests. The results show the horizontal undrained deformation modulus to be generally less than the vertical and the values from the consolidated samples to be higher than those which were unconsolidated. The measurement of E_u is not very precise, however, especially at small strains, and there was considerable scatter in the results. This is typified in table 2.9 by the plane strain values being less than the triaxial ones for the consolidated tests but greater for the unconsolidated tests.

TEST TYPE	SAMPLE ORIENTATION	STRESS PATH	E_u kN/m ²	ϵ_{Af} %
Unconsolidated: 3.78 to 4.08m				
Triaxial	V	$+\Delta\sigma_A$	2400	2-4
	H	$+\Delta\sigma_A$	2100	3-5
Plane Strain	V	$+\Delta\sigma_A$	3680	1.5-3.5
	H	$+\Delta\sigma_A$	2960	4-5
Isotropically Consolidated: 3.18 to 3.48m				
Triaxial	V	$+\Delta\sigma_A$	4800	2-4
	V	$-\Delta\sigma_A$	4000	3-7
	H	$+\Delta\sigma_A$	3720	2-5
	H	$-\Delta\sigma_A$	3600	2-3
Plane Strain	V	$+\Delta\sigma_A$	3920	1.5-2
	H	$+\Delta\sigma_A$	2500	2-3
Anisotropically (K_0) Consolidated: 3.18 to 3.48m				
Triaxial	V	$+\Delta\sigma_A$	5000	1-2
	V	$-\Delta\sigma_A$	5000	4-6

Table 2.9.

Deformation Characteristics in Undrained Shear

Triaxial samples consolidated to the in-situ stresses produced similar results. However, the initial modulus over the first 0.1% or so axial strain for compression loading was about twice that for extension and isotropically consolidated samples. As can be seen this effect disappears by 0.25% axial strain. The failure strain in this case is also slightly lower.

The considerable number of unconsolidated undrained triaxial tests on samples at varying inclinations carried out over the depth range of the test pit exhibited similar E_{U50} values, this being defined as the secant modulus at 50% of ϵ_{Af} . The stress-strain curves generally did not diverge significantly from linear, or from each other, until between 33 and 50% of ϵ_{Af} , after which they exhibited markedly different behaviour. The horizontal samples produced a smooth, flat topped, curve whereas those for the vertical samples were steeper with a pronounced peak, and a post-peak drop in strength. The intermediate inclinations exhibited intermediate behaviour and there was a tendency for the stress-strain curves to converge at higher strains in some cases.

The unconsolidated undrained plane strain tests carried out over the full depth range showed no definite trend within the scatter of the triaxial results, although there was a tendency for a slightly higher E_u value. However, the $\Delta\sigma_p$ values in the plane strain tests were only between 10 and 20% of $\Delta\sigma_A$ at 50% of ϵ_{Af} (compared to 50% of $\Delta\sigma_A$ predicted by elastic theory), and thus a stress-strain curve 5 to 10% steeper than the triaxial would

predict a similar value of E^T . The averaged curves from the vertical, horizontal and 45° samples resulted in a range of E_{U50} values between 2100 and 3350 kN/m^2 , showing no trend with depth and having a mean value of 2700 kN/m^2 . The E_{U50} values from the other undrained tests also fall into this pattern and range of results.

Figure 2.28 shows E_{U50} versus p'_p for the isotropically consolidated undrained triaxial test series, the relationship being very similar to that of C_u versus p'_p from the same tests (figure 2.16). E_{U50} is also apparently not much affected by consolidation pressure below a certain p'_p value (corresponding to p'_c) although there is a much sharper fall off below $p'_p = 10 \text{ kN/m}^2$ than is apparent in figure 2.16. Thus loss of suction may have resulted in lower values of E_u being obtained in some of the unconsolidated tests, although the values at 50% of ϵ_{Af} are not vastly different to those from the consolidated tests.

In relation to undrained strength anisotropy resulting from in-situ stress, and stress history, Bjerrum (1973) has postulated that the soil has a certain reserve of shear strength, known as the critical shear stress (τ_{cr}). The value of τ_{cr} that can be mobilised in the field (i.e. C_u) depends on whether the shear stress is applied in the same (active) or opposite (passive) sense to that mobilised in nature (Bjerrum and Kenney, 1967). As described in section 2.7.2.

Wesley (1975) has shown that the soil skeleton of the Mucking clay is stiffer in the vertical than horizontal direction (2:1 ratio approximately) and that the anisotropic stiffness results in higher pore pressures being generated in undrained shear on horizontal

samples. This varying stiffness concept appears to corroborate Bjerrum's (1973) hypothesis of shear strength reserve.

Bjerrum (1973) also showed that for vertical samples of lightly overconsolidated Drammen (plastic) Clay, consolidated to the in-situ stresses, the drained and undrained stress-strain curves were very similar up to τ_{cr} , at which point the undrained sample failed and the drained stress-strain curve became less steep. The undrained curve exhibited a pronounced peak strength and post-peak strength loss, whilst the drained sample underwent an increase in consolidation at shear stresses in excess of τ_{cr} . Furthermore, samples consolidated to the normally consolidated stress range, or tested unconsolidated, produced lower E_u values at small strains, flat topped stress-strain curves and no τ_{cr} point in the drained tests.

The Mucking clay results agree with these findings in respect of the initial high E_u values for compression loading from the in-situ stress state, loss of anisotropic effects at higher stress levels and lower E_u values for unconsolidated samples. The Drammen Clay also exhibits a flatter stress-strain curve and a lower E_u in triaxial extension tests starting from the in-situ stresses, with larger strains to failure and a lower value of τ_{cr} (table 2.6). These characteristics are also exhibited by the Mucking clay in extension tests carried out on vertical samples.

Drained tests on isotropically consolidated samples of Mucking clay showed the initial drained deformation modulus (E_D) for vertical samples to be twice that for horizontal samples (at 0.25% axial strain), as predicted by the aforementioned oedometer tests. The stress-strain curves also exhibited a τ_{cr} value close to the undrained strength, and corresponding to a vertical effective stress (for the vertical samples) close to p_c' from the oedometer tests, but this was not accompanied by any pronounced change in the strain path. These tests were carried out to an axial strain of 10% at which point failure had not been reached.

Drained tests were also carried out on K_0 consolidated samples, incorporating six stress paths comprising those described in table 2.10 plus tests at constant deviator stress with increasing and decreasing normal stress level. An interesting point to arise from these latter tests was that for the loading case the soil behaved isotropically whereas in unloading the behaviour was markedly anisotropic with the axial strain close to zero.

The data from the isotropically, and K_0 , consolidated drained triaxial tests are presented in table 2.10, the interpretation being based on simple anisotropic and isotropic elasticity respectively wherein:-

E'_x is Young's Modulus in the direction of the axis of soil symmetry (vertical).

n is the anisotropy ratio E'_x/E'_z where E'_z is Young's Modulus in any direction normal to the axis of soil symmetry.

ν_1' is the ratio of two orthogonal strains, both in the plane normal to the axis of soil symmetry, caused by a strain increment in one of these orthogonal axes.

ν_3' is the ratio of the strain in any z direction to the strain in the x axis caused by a strain increment in the x direction.

This notation coincides with that adopted by Atkinson (1973(a)) and Wesley (1975). The four independent elastic constants are sufficient to describe the behaviour of a cross-anisotropic elastic material when the principal stress axes coincide with the axes of soil symmetry.

It can be seen that different parameters appear to be required for decreasing, as opposed to increasing, principal stress situations. However, all the vertical compression tests predict E'_x between 3050 and 3300 kN/m^2 with ν_3' from 0.07 to 0.10. The values of E'_z and ν_1' can be obtained using the results of the horizontal tests as shown in table 2.10; simple anisotropic elastic theory can then be used to predict the initial deformation modulus (E_u) and effective stress path for isotropically consolidated undrained tests on vertical and horizontal samples (Atkinson, 1973(a)). Table 2.11 shows the results of such a prediction, compared to observed values of E_u and 'A'.

The values of 'A' predicted for the triaxial tests are low but for the plane strain tests are not inconsistent with the observations. The predicted values of E_u for the triaxial test are low but show a correct trend from horizontal to vertical. The anisotropic elastic theory predicts the same E_u for vertical and horizontal directions

TEST TYPE	SAMPLE ORIENTATION	STRESS PATH	E'_x kN/m ²	n	ν'_1	ν'_3	$\epsilon_{Af}\%$
Isotropically Consolidated: 3.18 to 3.48m							
Triaxial	V	$+\Delta\sigma_A$	3200	-	-	0.10	-
	H	$+\Delta\sigma_A$	-	2	0.15	-	-
Anisotropically (K_0) Consolidated: 3.18 to 3.48m							
Triaxial	V	$+\Delta\sigma_A$	3300	-	-	0.10	13+
	V	$-\Delta\sigma_A$	5100	-	-	0.35	3
	V	$+\Delta\sigma_H$	3050	-	-	0.07	14+
	V	$-\Delta\sigma_H$	1630	-	-	0.33	2.5

Table 2.10.

Deformation Characteristics During Drained Shear

TYPE OF LOADING	INITIAL DEFORMATION MODULUS			A_f	
	PREDICTED*		OBSERVED	PREDICTED*	OBSERVED
	DRAINED	UNDRAINED	UNDRAINED		
Triaxial Vertical	E'_x	$1.190E'_x$	$1.5E'_x$	0.20	0.40
Triaxial Horizontal	$0.5E'_x$	$0.735E'_x$	$1.16E'_x$	0.40	0.70
Plane Strain Vertical	$1.01E'_x$	$1.409E'_x$	$1.23E'_x$	0.32	0.40
Plane Strain Horizontal	$0.51E'_x$	$1.409E'_x$	$0.78E'_x$	0.67	0.72

Table 2.11.

Initial Deformation Modulus and Pore-Pressure Parameter A_f For Isotropically Consolidated Undrained Compression Tests ($+\Delta\sigma_A$) Predicted by Anisotropic Elastic Theory and Compared to Observed Values

*n = 2, $\nu'_3 = 0.10$, $\nu'_1 = 0.15$

in plane strain whereas the observed horizontal value is significantly lower. However, this result also appears low in comparison to the other results. It is felt that the results in table 2.11 present a rather misleading picture in that any agreement, or disagreement between observed and predicted is largely fortuitous because of the scatter in the test results.

For an isotropic elastic material the predicted value of E^T (equation 2.22) is $1.36 E'$ which is sensibly close to all the observed triaxial values of E_u . As stated previously no significant trend in the triaxial E_{U50} values could be detected within the scatter of results. This would suggest that the E_{U50} values from these tests could be taken as E^T for the foundation in an isotropic elastic analysis. Certainly there is no evidence to suggest that the further sophistication of anisotropic elasticity is warranted. In addition Hamza (1976) has shown that, for non-linear elasticity, overall deformations are much more sensitive to small changes in C_u , than in E^T , at higher stress levels.

Finally, for an isotropic elastic material the one-dimensional coefficient of volume compressibility is given by:-

$$M_{V1} = \frac{(1 + \nu')}{(1 - \nu')} \frac{(1 - 2\nu')}{E'} = \frac{3(1 - 2\nu')}{2(1 - \nu')} \frac{1}{E^T} \dots\dots\dots(2.23)$$

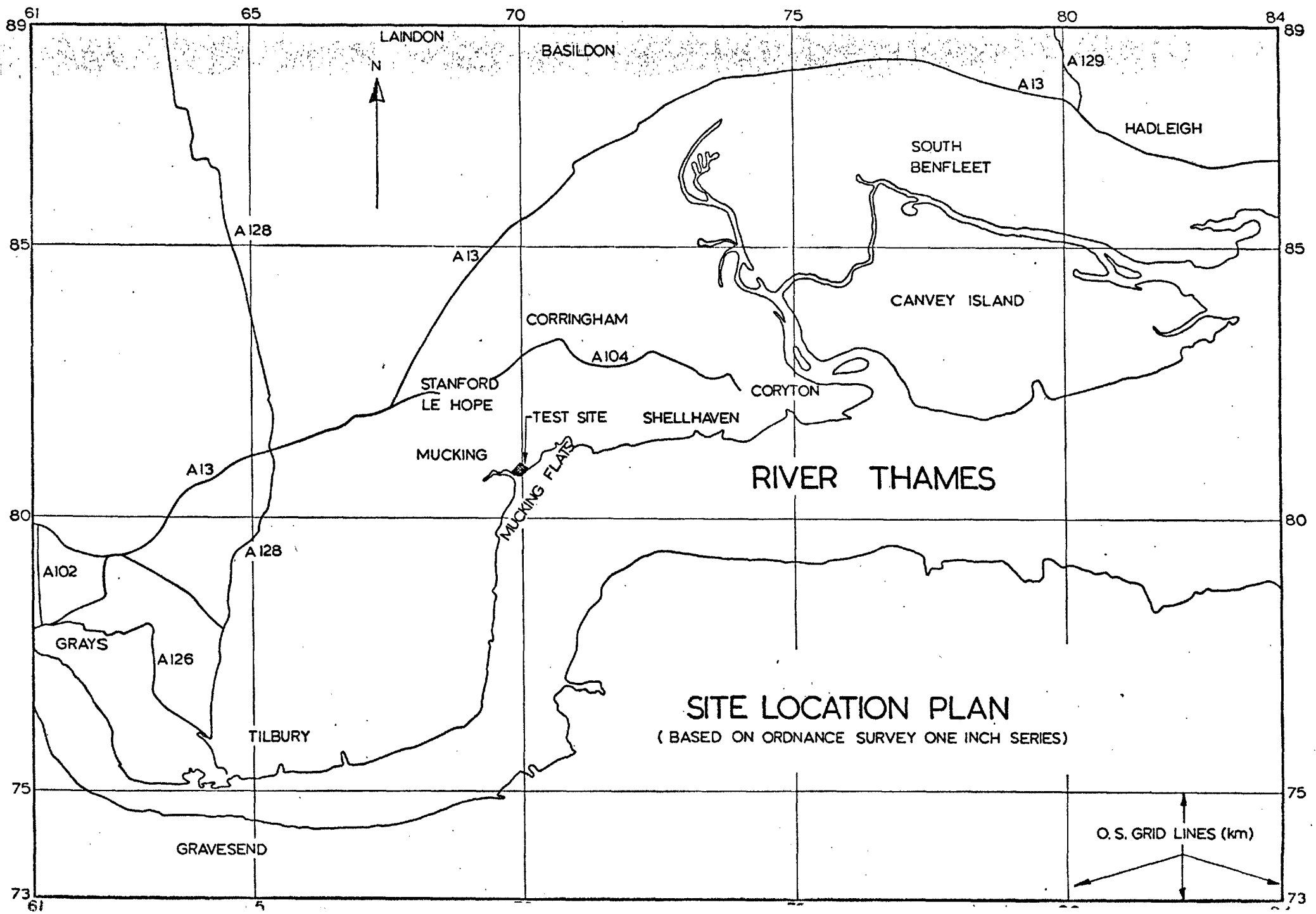
With $E' = 3200 \text{ kN/m}^2$ and $\nu' = 0.10$ $M_{V1} = 3.06 \times 10^{-4} \text{ m}^2/\text{kN}$ compared to $4.6 \times 10^{-4} \text{ m}^2/\text{kN}$ from oedometer tests over the in-situ stress range (15 - 30 kN/m^2). The three-dimensional coefficient of

volume compressibility may be predicted from:-

$$M_{V3} = \frac{3(1 - 2\nu')}{E'} = \frac{9(1 - 2\nu')}{2(1 + \nu')} \frac{1}{E'} = \frac{1}{K} \dots\dots\dots(2.24)$$

where K is the bulk modulus for isotropic compression.

Again with $E' = 3200 \text{ kN/m}^2$ and $\nu' = 0.10$, $M_{V3} = 7.5 \times 10^{-4} \text{ m}^2/\text{kN}$ compared to $6.95 \times 10^{-4} \text{ m}^2/\text{kN}$ from the triaxial dissipation test over the stress increment 0 to 25 kN/m^2 .



SITE LOCATION PLAN

(BASED ON ORDNANCE SURVEY ONE INCH SERIES)

Fig 2.1

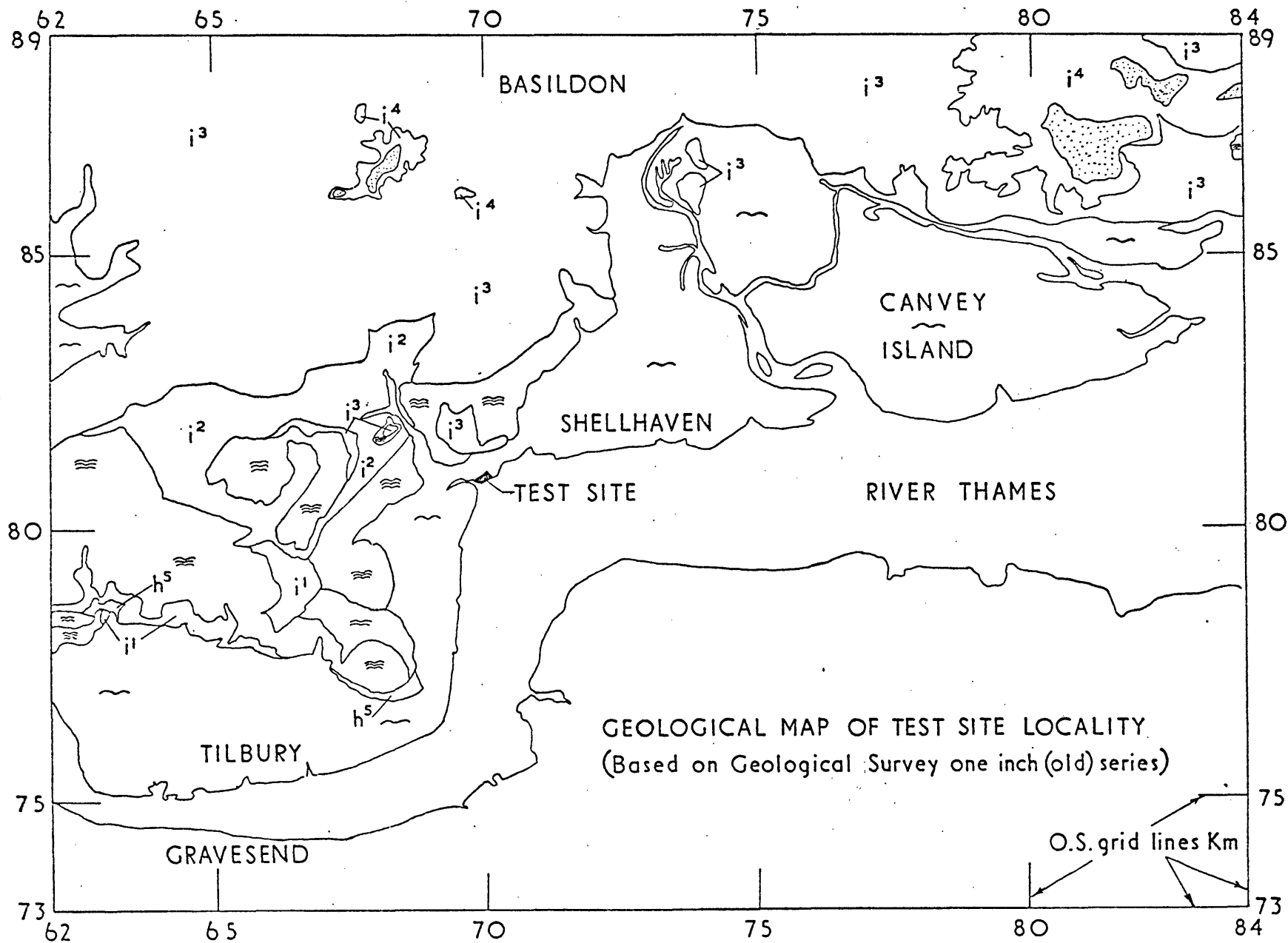


Fig. 2.2

Legend

- | | | | | |
|----------------------------|----------------------------------|------------------------------|----------------------------|-----------------------------------|
| Alluvium | Brickearth | River Gravel | Pebbly Gravel | i ⁴ Lower Bagshot Beds |
| i ³ London Clay | (i ² ' Oldhaven Beds) | i ² Woolwich Beds | i ¹ Thanet Sand | h ⁵ Chalk |

697

698

699

700

701

SITE PLAN

(BASED ON ORDNANCE SURVEY 1/1250 SERIES)

- LEGEND:**
- BOREHOLE
 - GEONOR VANE TEST
 - + LARGE VANE TEST

810

O.S. GRID LINES (100m)



APPROXIMATE LINE OF SITE BOUNDARY FENCE

DRAIN

BANK 4

BANK 2

ACCESS ROADS

809

PIPE

DRAIN BACKFILLED PRIOR TO BANK 4 CONSTRUCTION

BANK 1

TEST PIT

BANK 3

INSTRUMENT HUT

SITE OFFICES

808

MUCKING CREEK

ACCESS ROAD

FOOTPATH ON TOP OF EXISTING FLOOD BANK

DRAIN

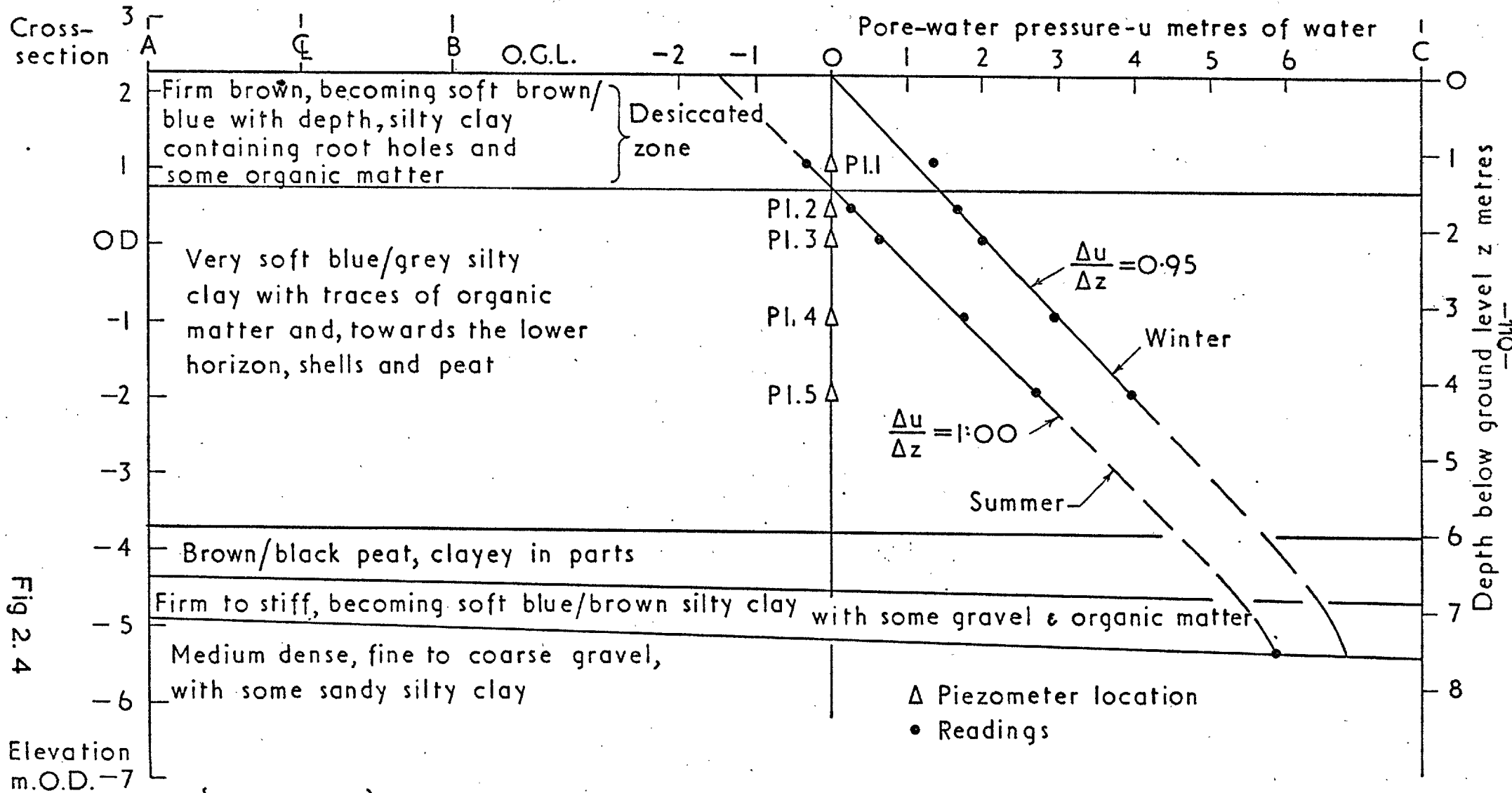
DRAIN

HIGH WATER MARK OF MEDIUM TIDES

LOW WATER MARK OF MEDIUM TIDES

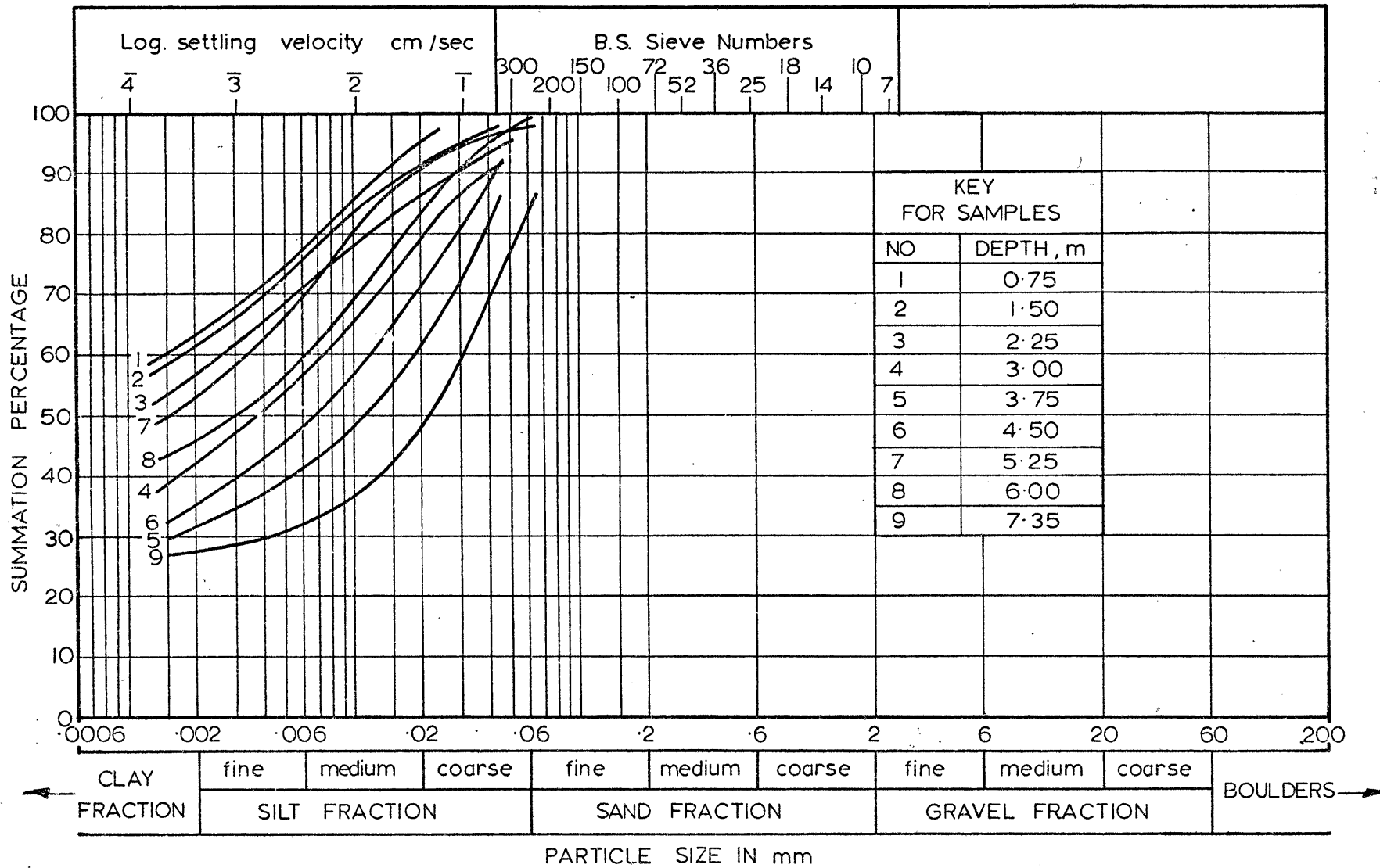
RIVER THAMES

Fig 2.3



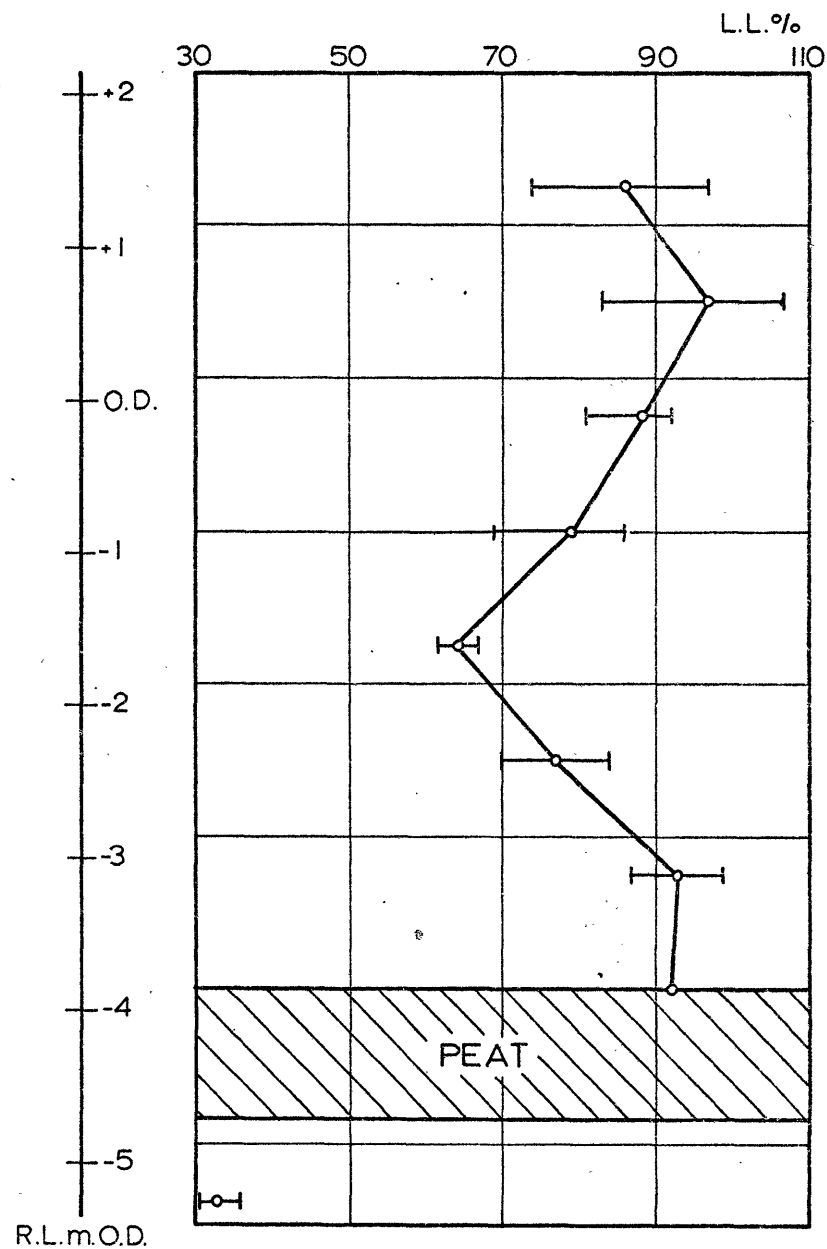
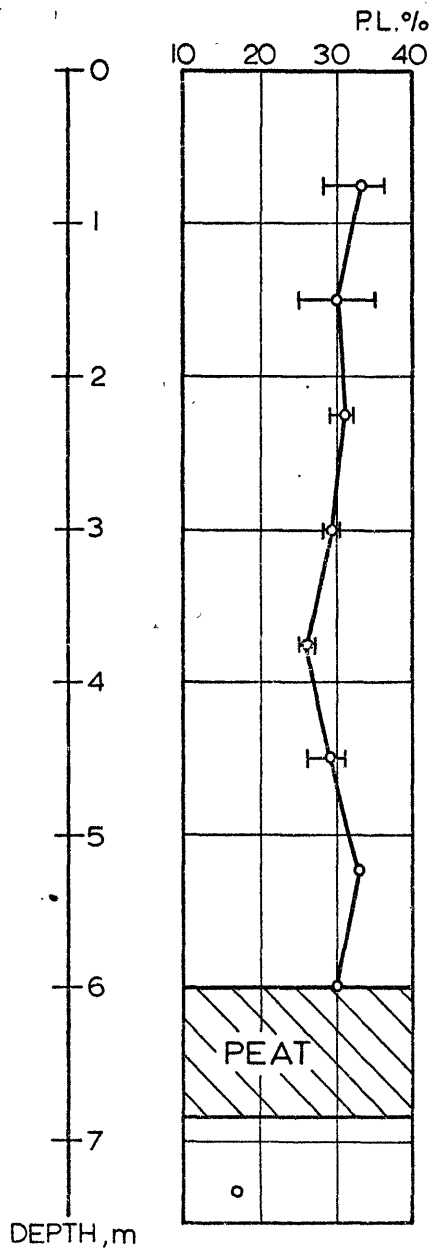
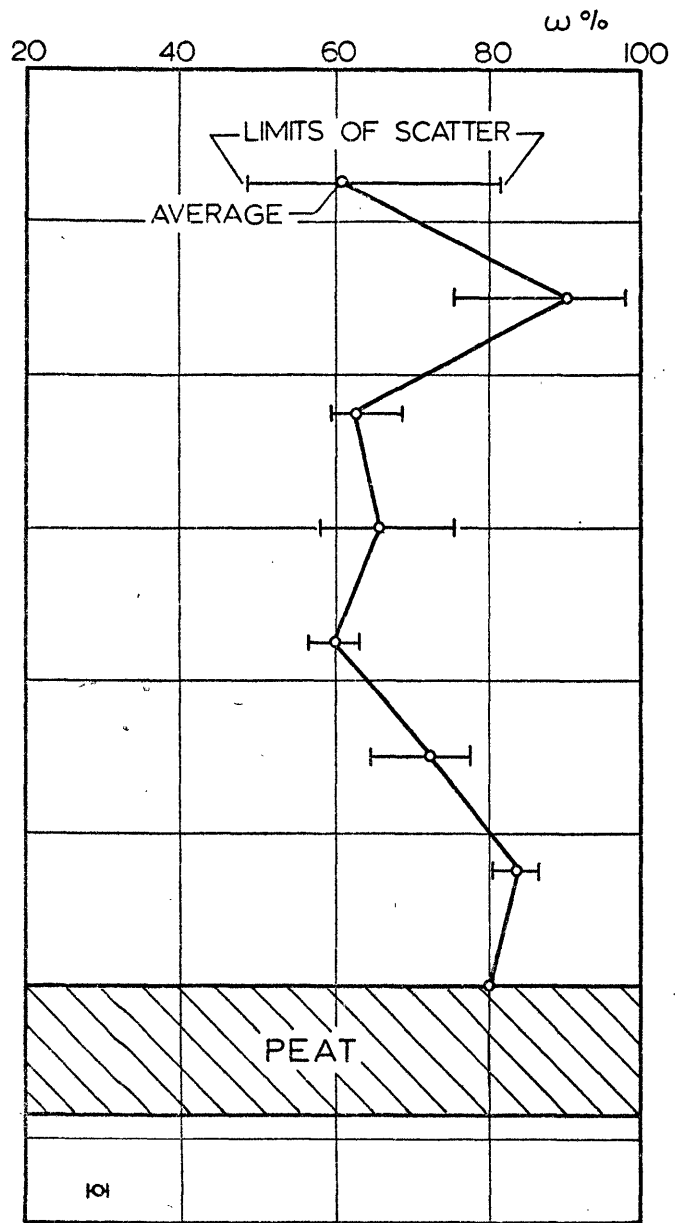
'EAST-WEST' SOIL PROFILE BENEATH BANKS 1 & 2 & EXTREMES OF GROUND WATER PROFILE MEASURED OVER A ONE YEAR CYCLE

Fig 2.4



PARTICLE SIZE DISTRIBUTION

Fig 2.5



WATER CONTENT AND ATTERBERG LIMITS

Fig 2.6

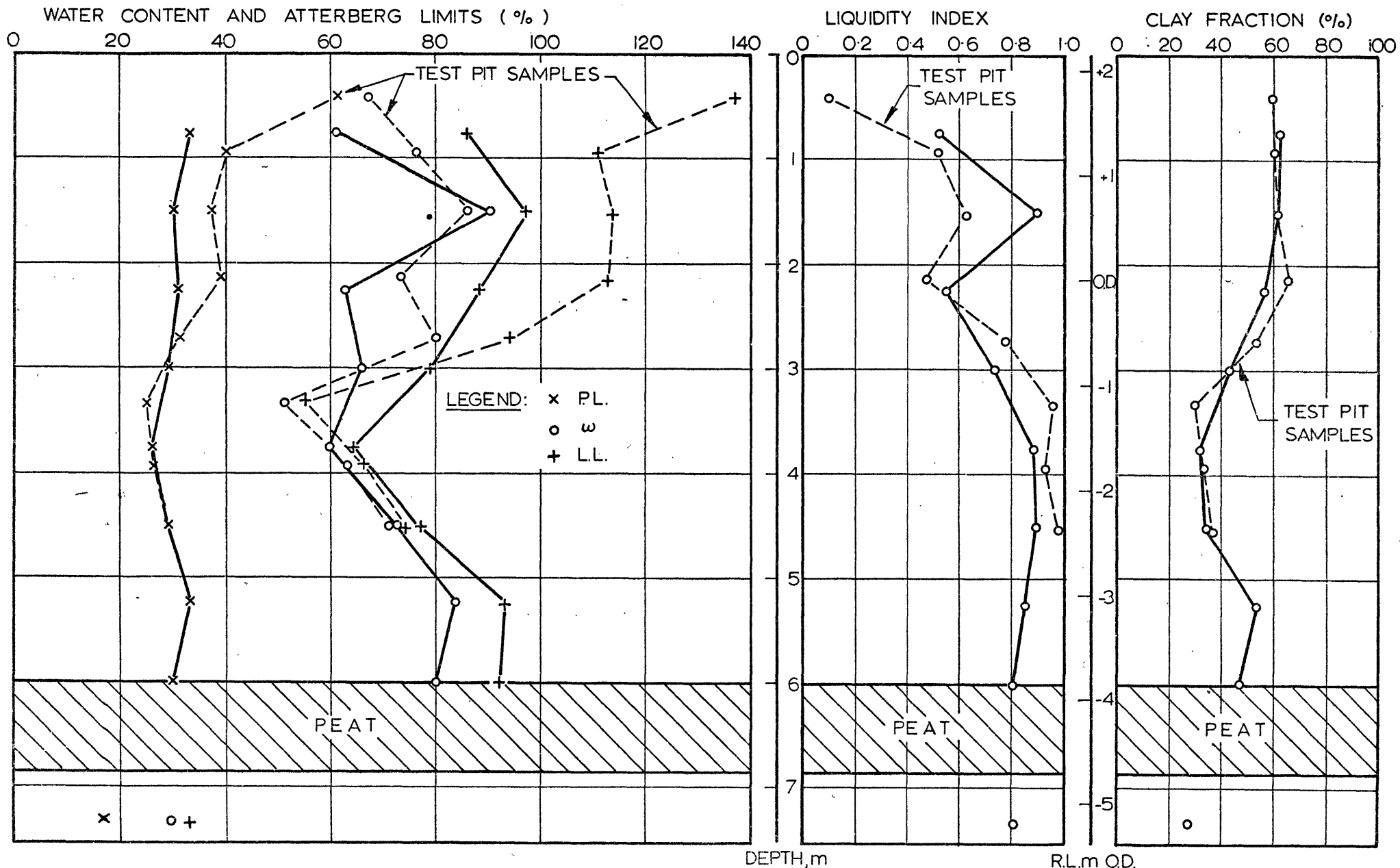


Fig 2.7

INDEX PROPERTIES AND CLAY FRACTION

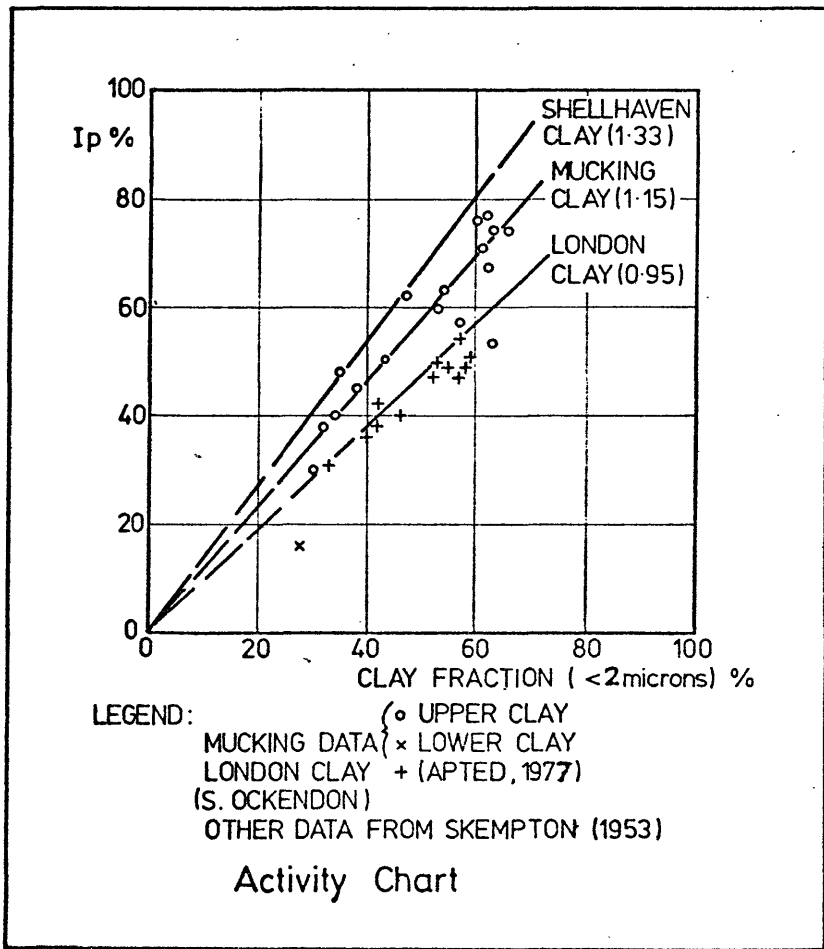
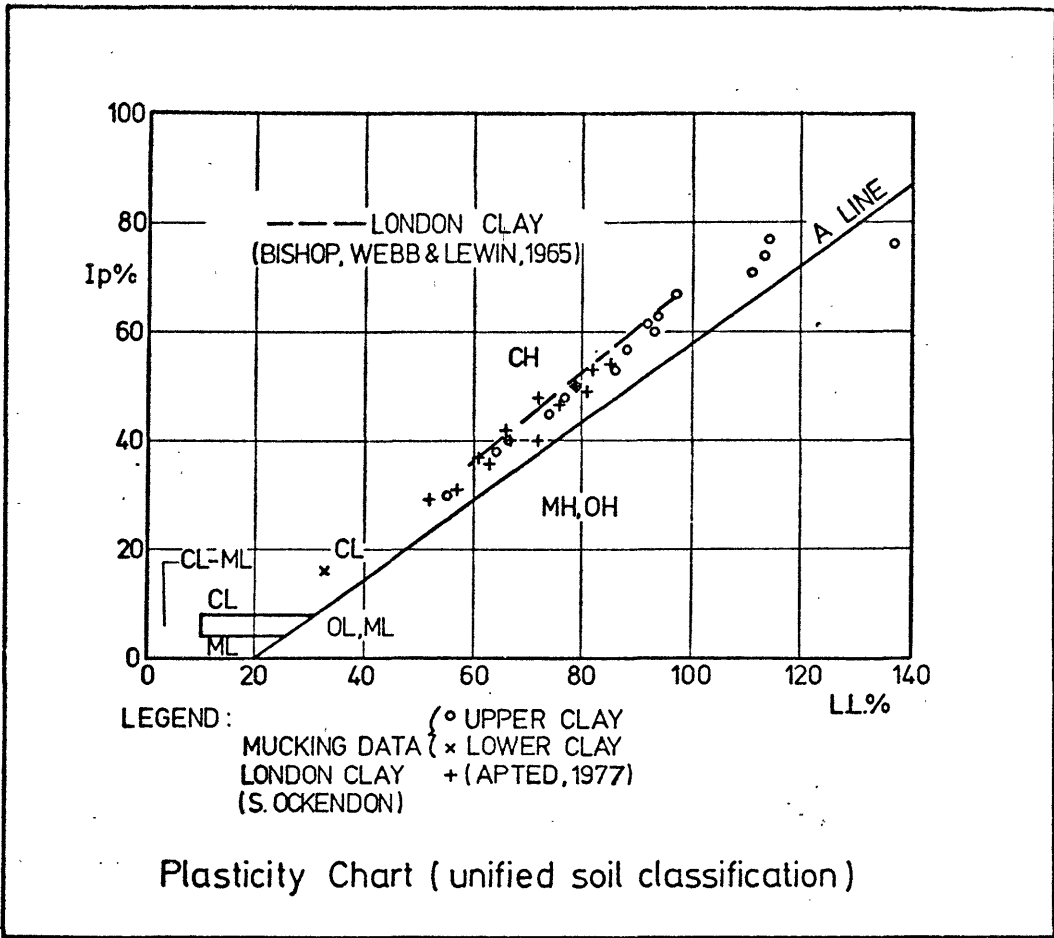


Fig 2.8

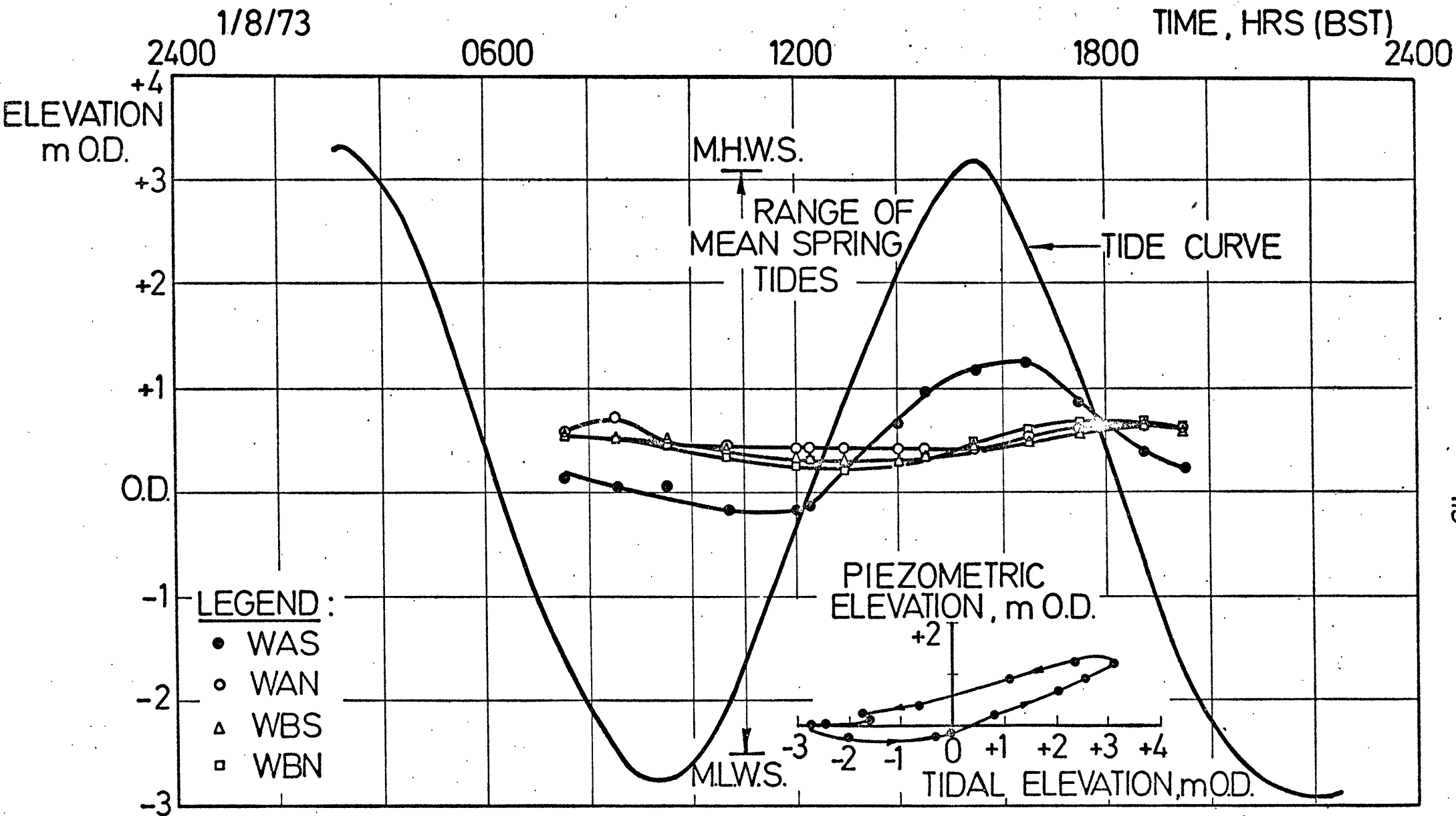
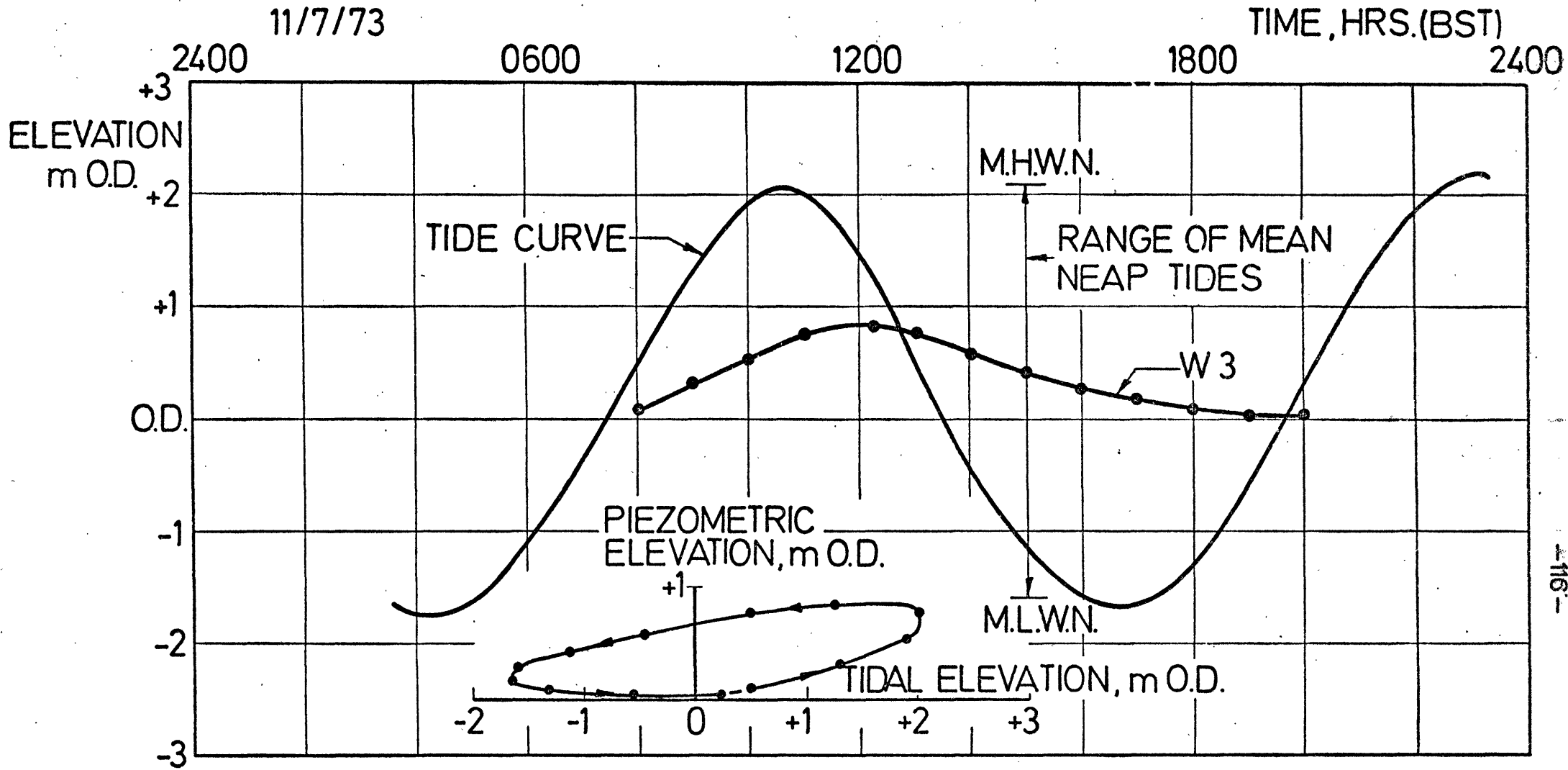
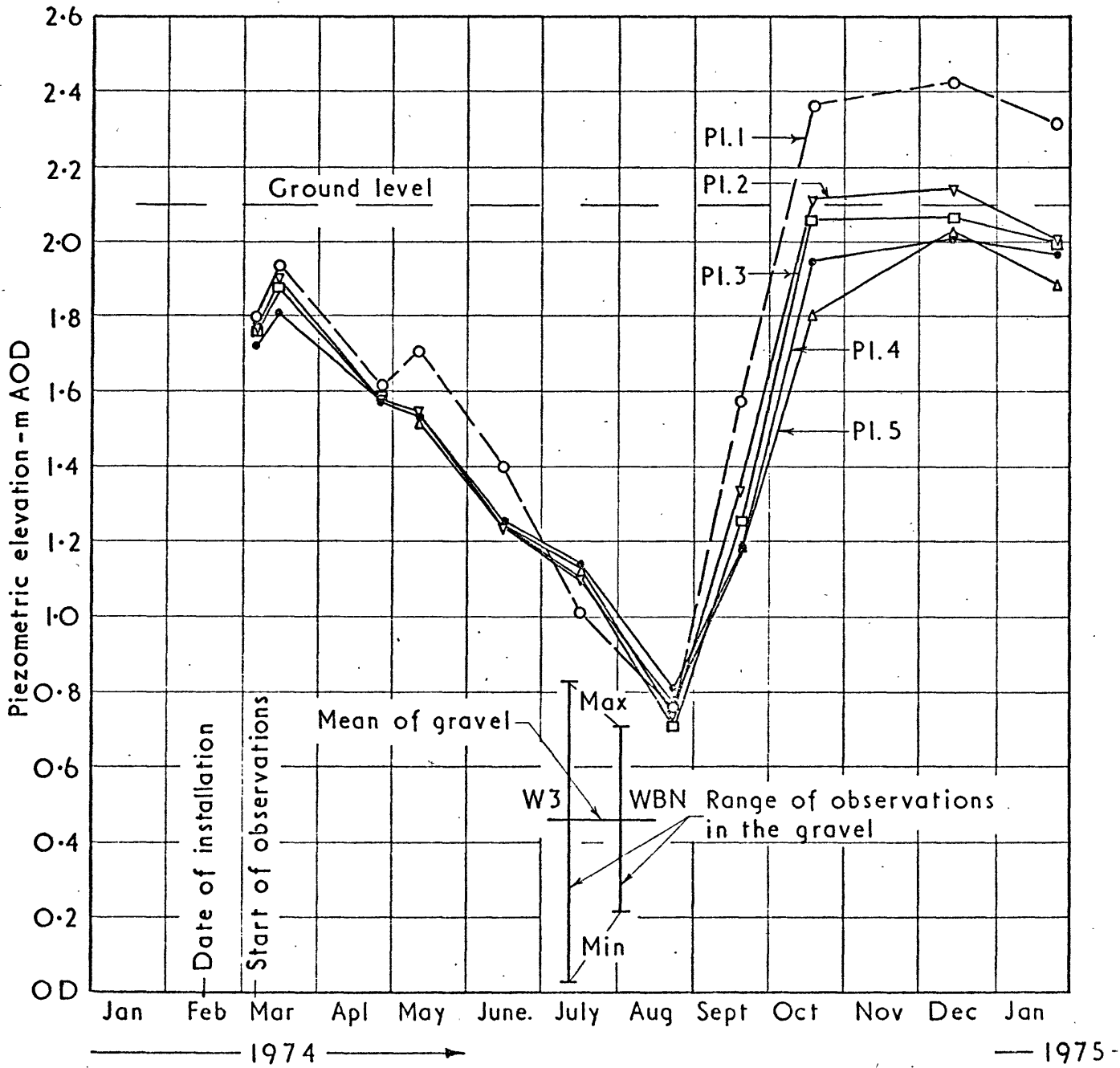
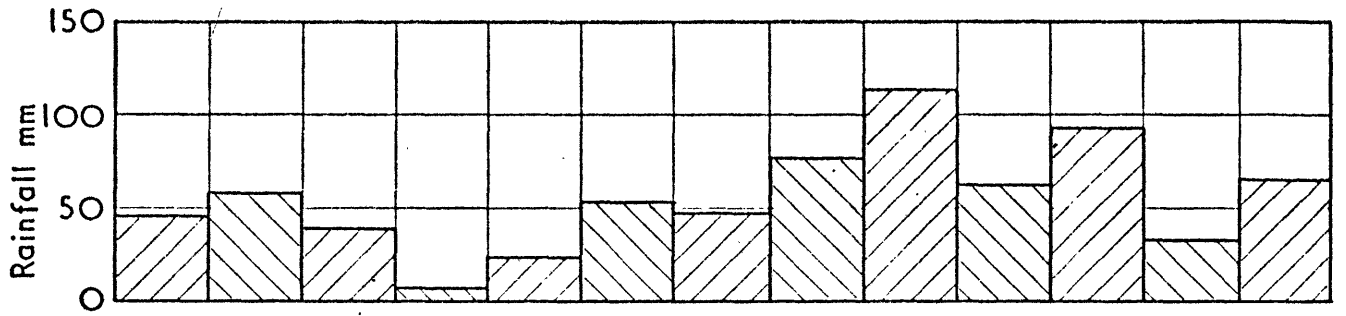


Fig 2.9

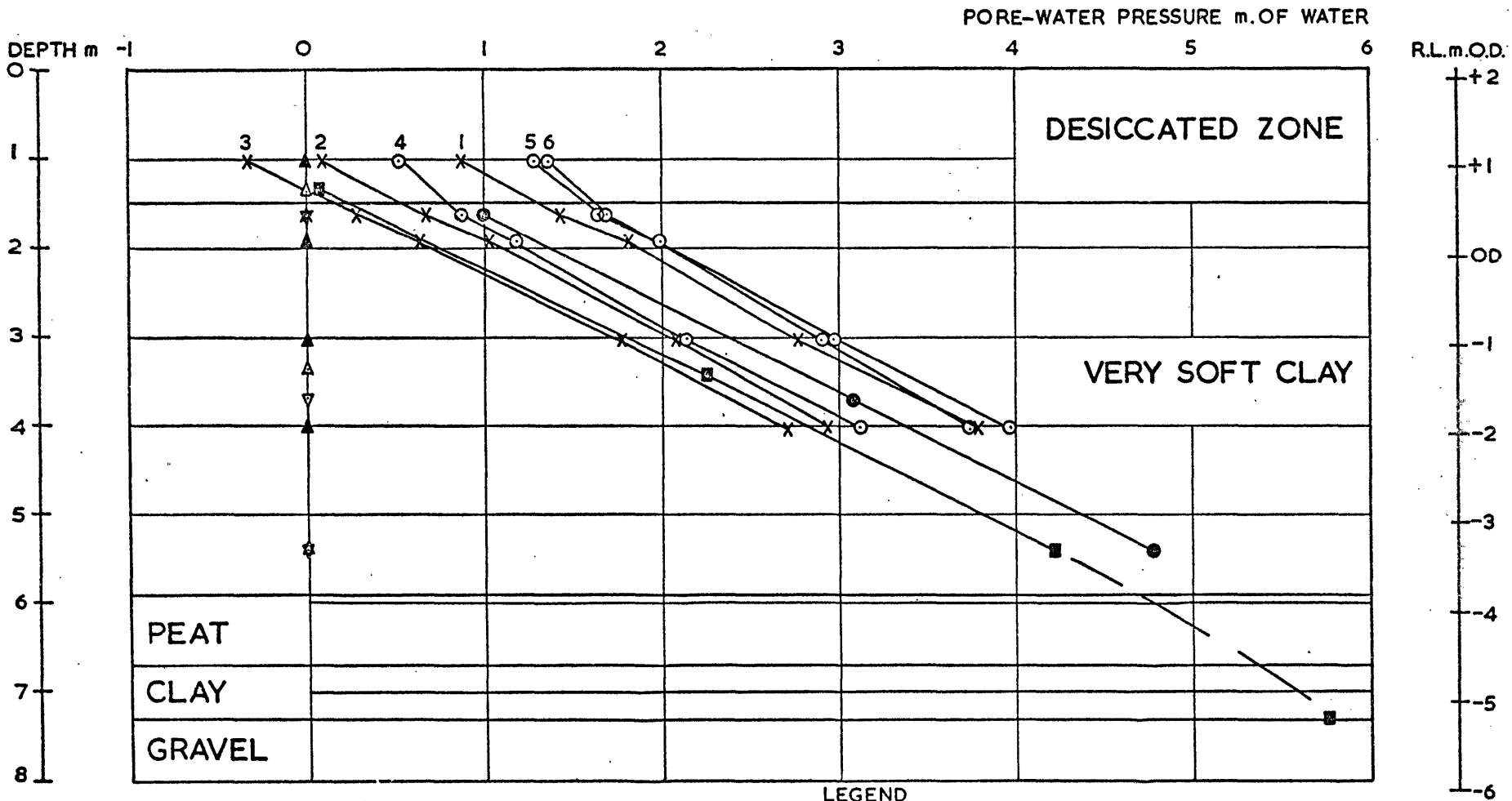
Comparison of tidal elevation and piezometric elevation in the gravel beneath Bank 1.



Comparison of tidal elevation and piezometric elevation in the gravel beneath Bank 3.



SEASONAL CHANGES IN PIEZOMETRIC ELEVATIONS IN THE CLAY
 Fig 2.11



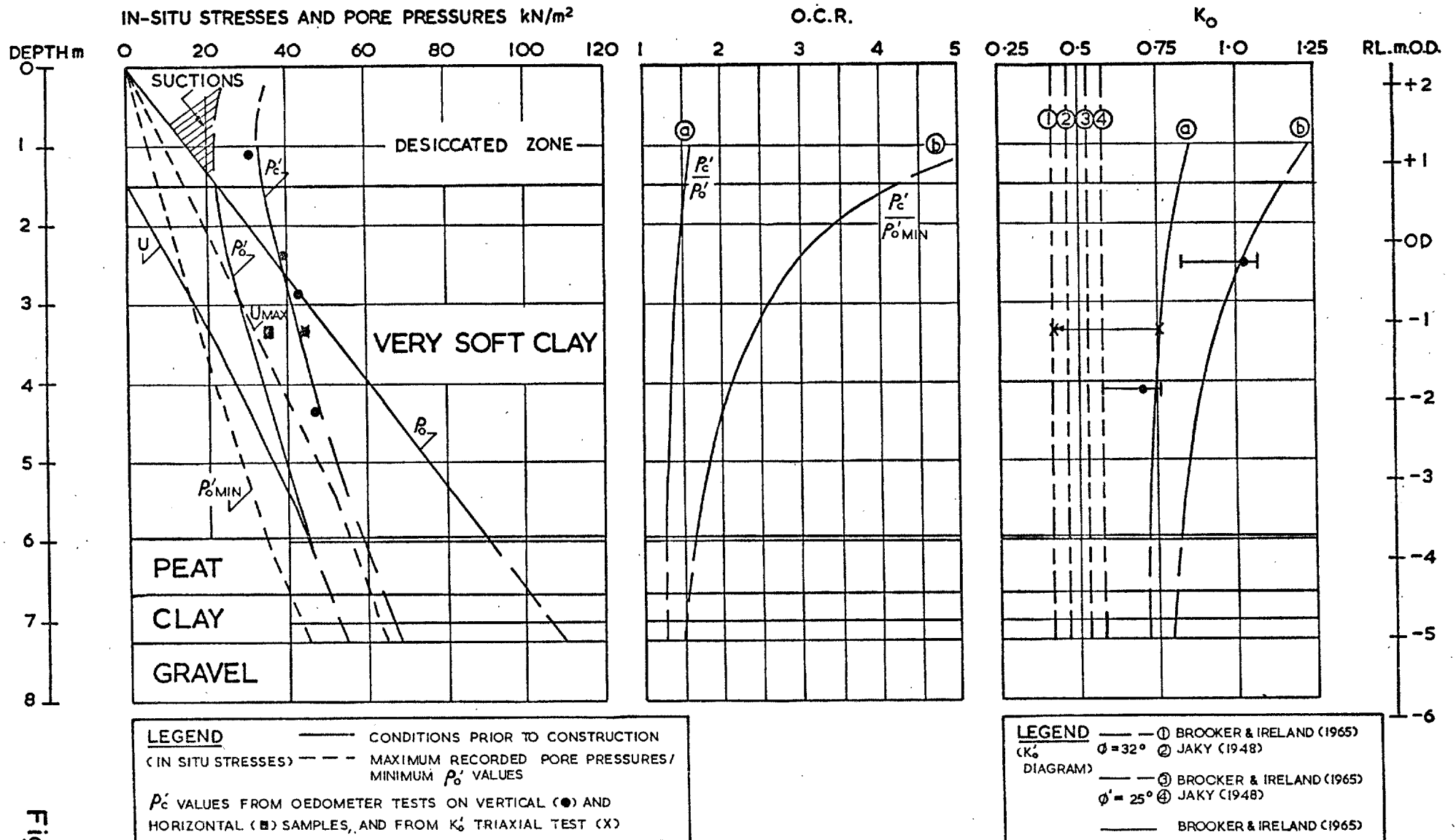
SEASONAL VARIATIONS IN THE
GROUND-WATER PROFILE

N.B. HORIZONTAL SCALE IS 2 X VERTICAL

LEGEND

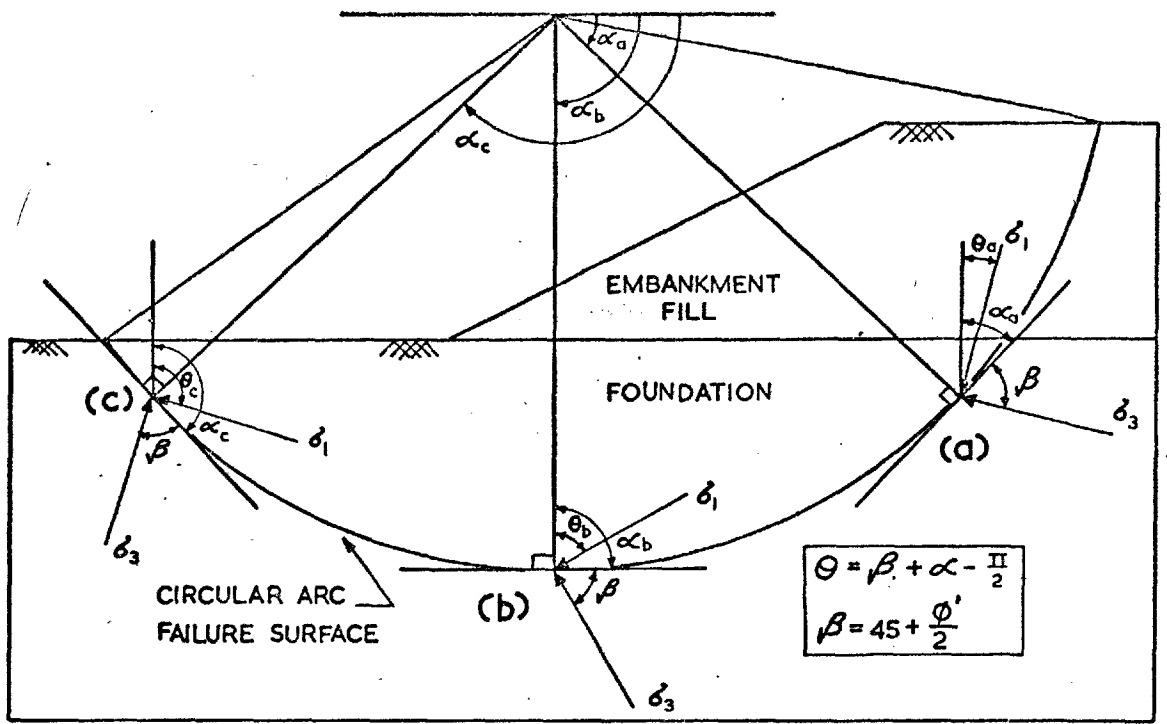
- ▲ I PIEZOMETERS
- X G.W.L. FALLING 1. MARCH '74 2. JULY '74 3. AUG '74
- G.W.L. RISING 4. SEPT. '74 5. OCT '74 6. DEC '74
- △ BANK 1 PIEZOMETERS PAI - 3
- AUGUST '73
- ▽ BANK 2 PIEZOMETERS PC 4-6
- JANUARY '74

Fig. 2.12

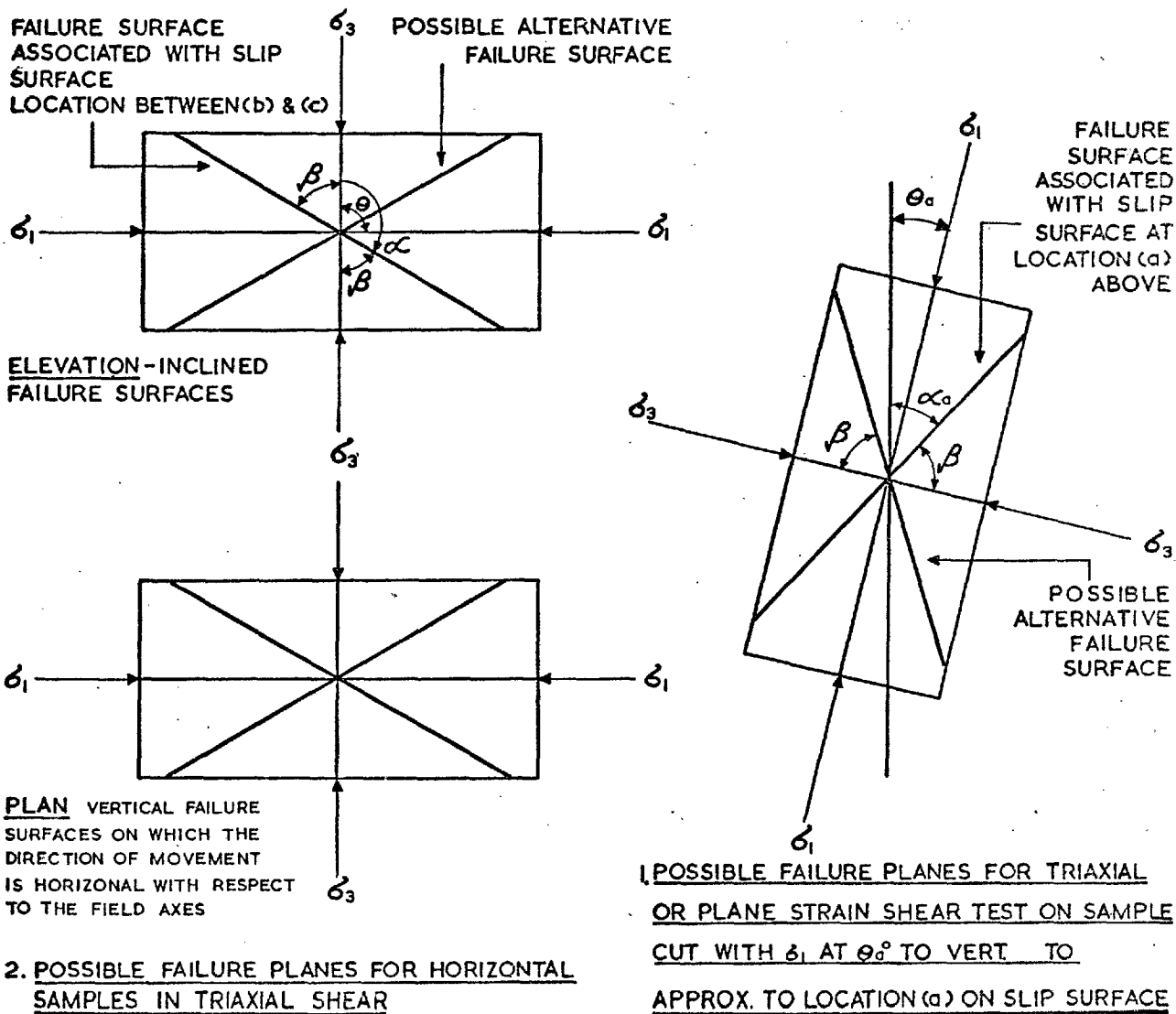


IN-SITU STRESSES FOR THE FOUNDATION
BENEATH BANK I

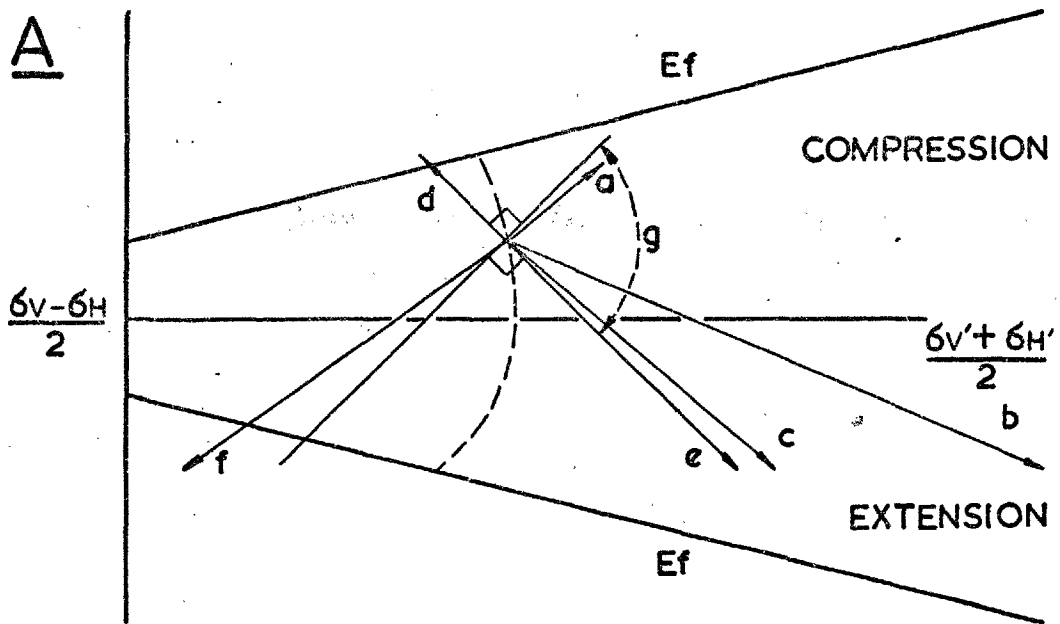
Fig. 2.13



(A) PRINCIPAL STRESS DIRECTIONS AT FAILURE LINKED TO SLIP SURFACE ORIENTATION (after Lo, 1965)

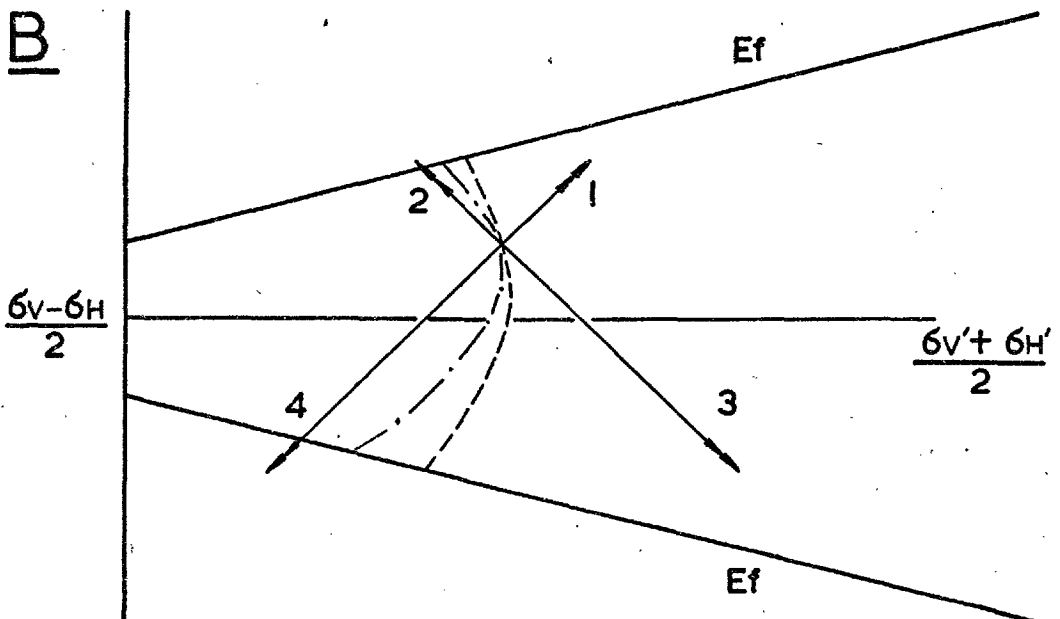


(B) TYPICAL AMBIGUITIES ASSOCIATED WITH FAILURE PLANES IN TRIAXIAL AND PLANE STRAIN TESTS ON SAMPLES AT VARIOUS INCLINATIONS TO VERTICAL WHEN COMPARED TO THE FIELD SITUATION



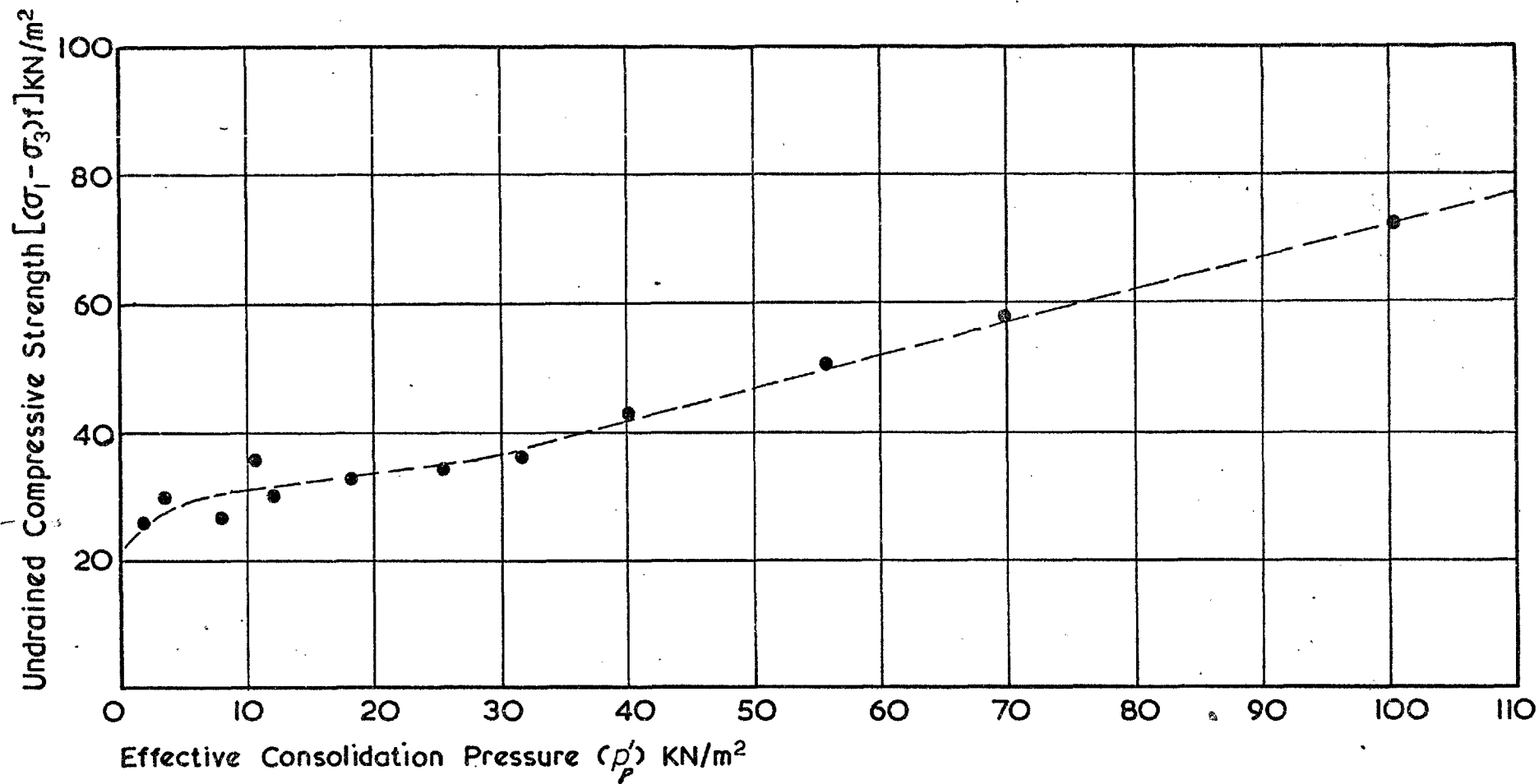
- KEY :**
- a - FOUNDATION LOADING; BENEATH CENTRE OF EMBANKMENT
 - b - BENEATH TOE OF EMBANKMENT
 - c - NEAR TOE OF SLIP
 - d - ACTIVE EARTH PRESSURE
 - e - PASSIVE EARTH PRESSURE
 - f - FOUNDATION UNLOADING; EXCAVATION
 - g - RANGE OF ENTIRELY LOADING T.S.Ps
- } 45° LINES

- COMMON NOMENCLATURE - Ef-EFFECTIVE STRESS FAILURE ENVELOPE**
- T.S.P. ——— TOTAL STRESS PATH (PLANE STRAIN & TRIAXIAL)
 - E.S.P. - - - EFFECTIVE STRESS PATH (PLANE STRAIN)
 - E.S.P. - . . . EFFECTIVE STRESS PATH (TRIAXIAL)



- KEY:**
- 1, + $\Delta\sigma_v$, $\Delta\sigma_h = 0$
 - 2, - $\Delta\sigma_h$, $\Delta\sigma_v = 0$
 - 3, + $\Delta\sigma_h$, $\Delta\sigma_v = 0$
 - 4, - $\Delta\sigma_v$, $\Delta\sigma_h = 0$

FIELD (A) AND LABORATORY (B) STRESS PATHS FOR A NORMALLY CONSOLIDATED CLAY UNDER UNDRAINED CONDITIONS



UNDRAINED COMPRESSIVE STRENGTH VERSUS CONSOLIDATION PRESSURE (3.18-3.48m)
(after Wesley, 1975)

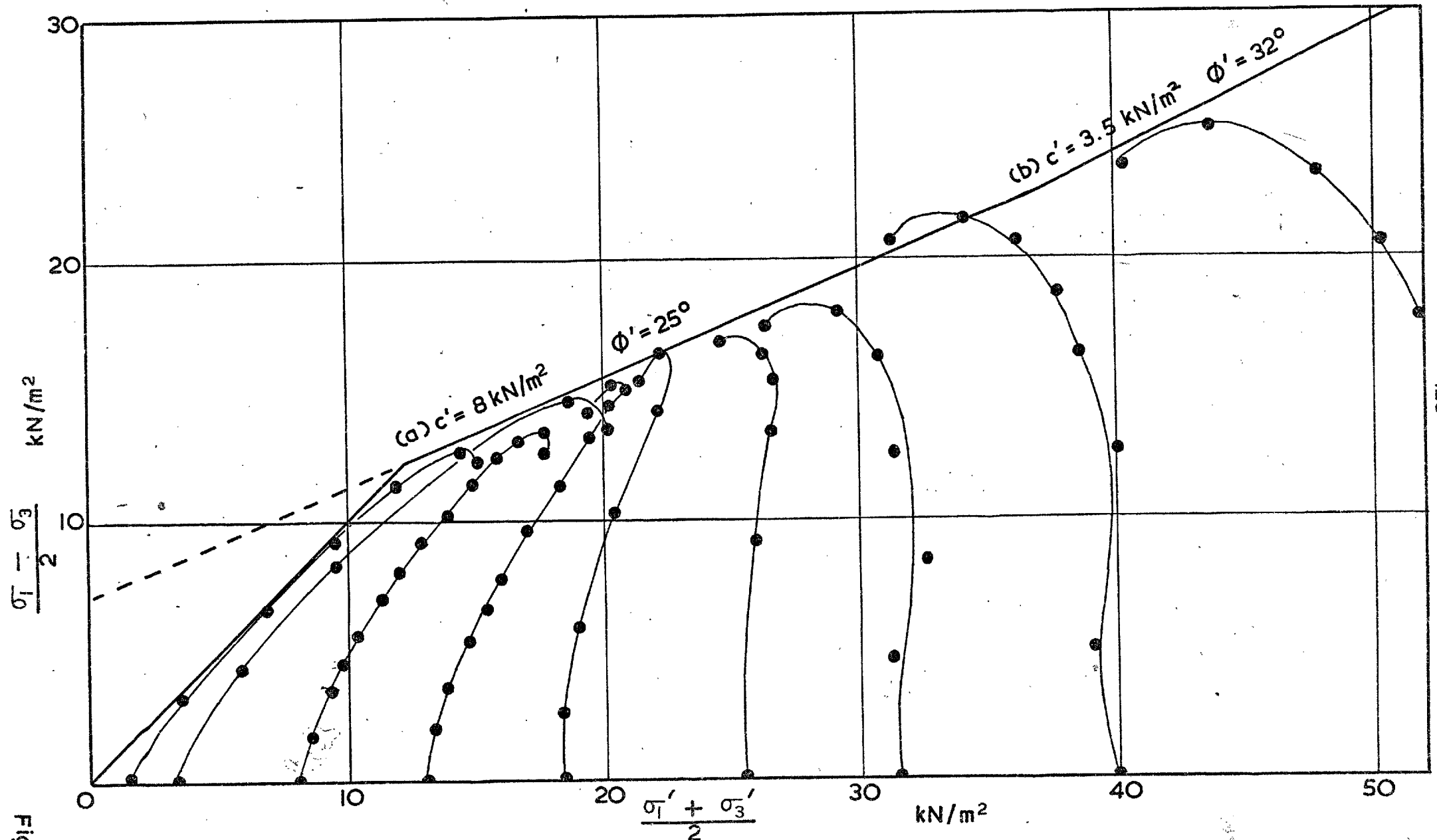
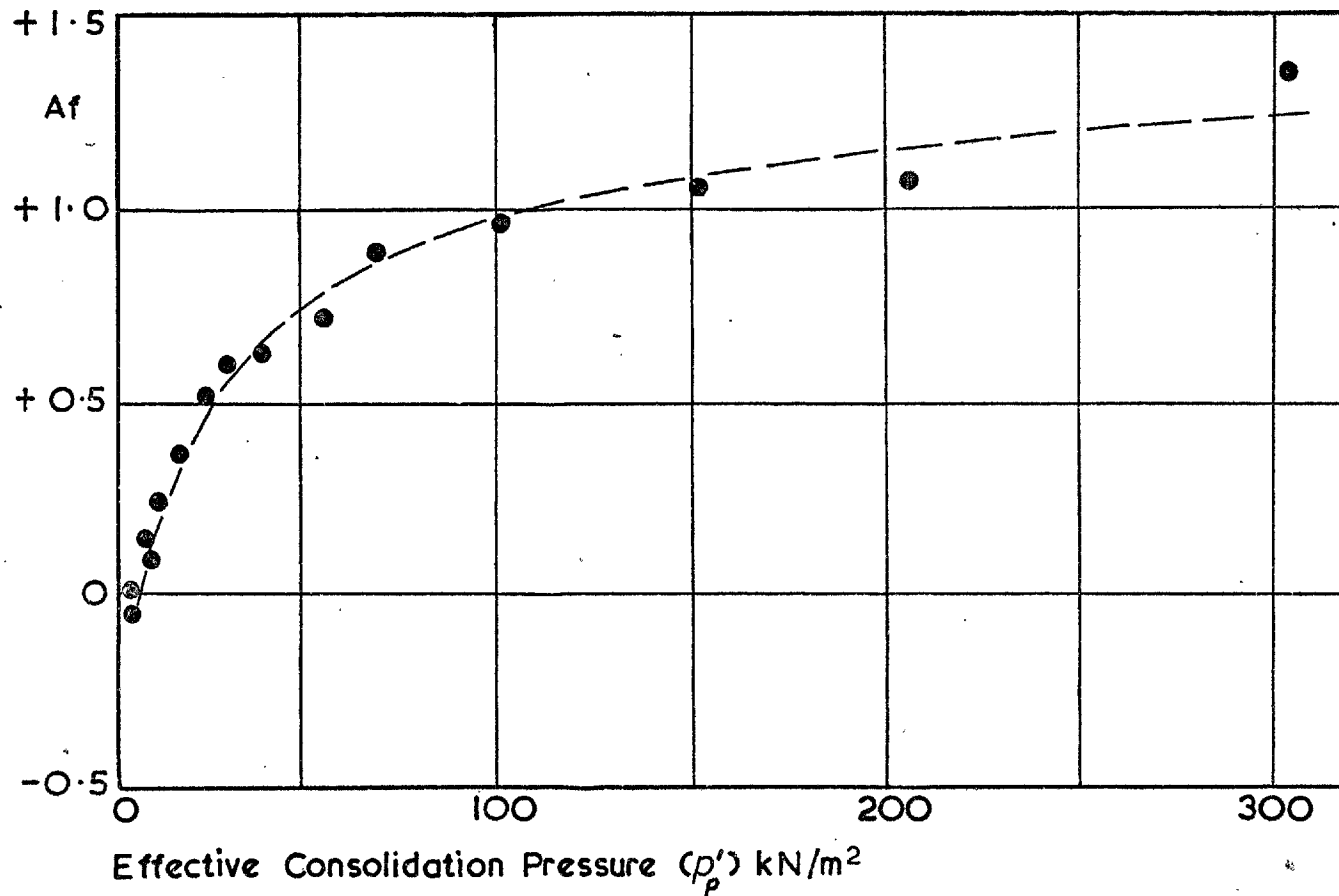


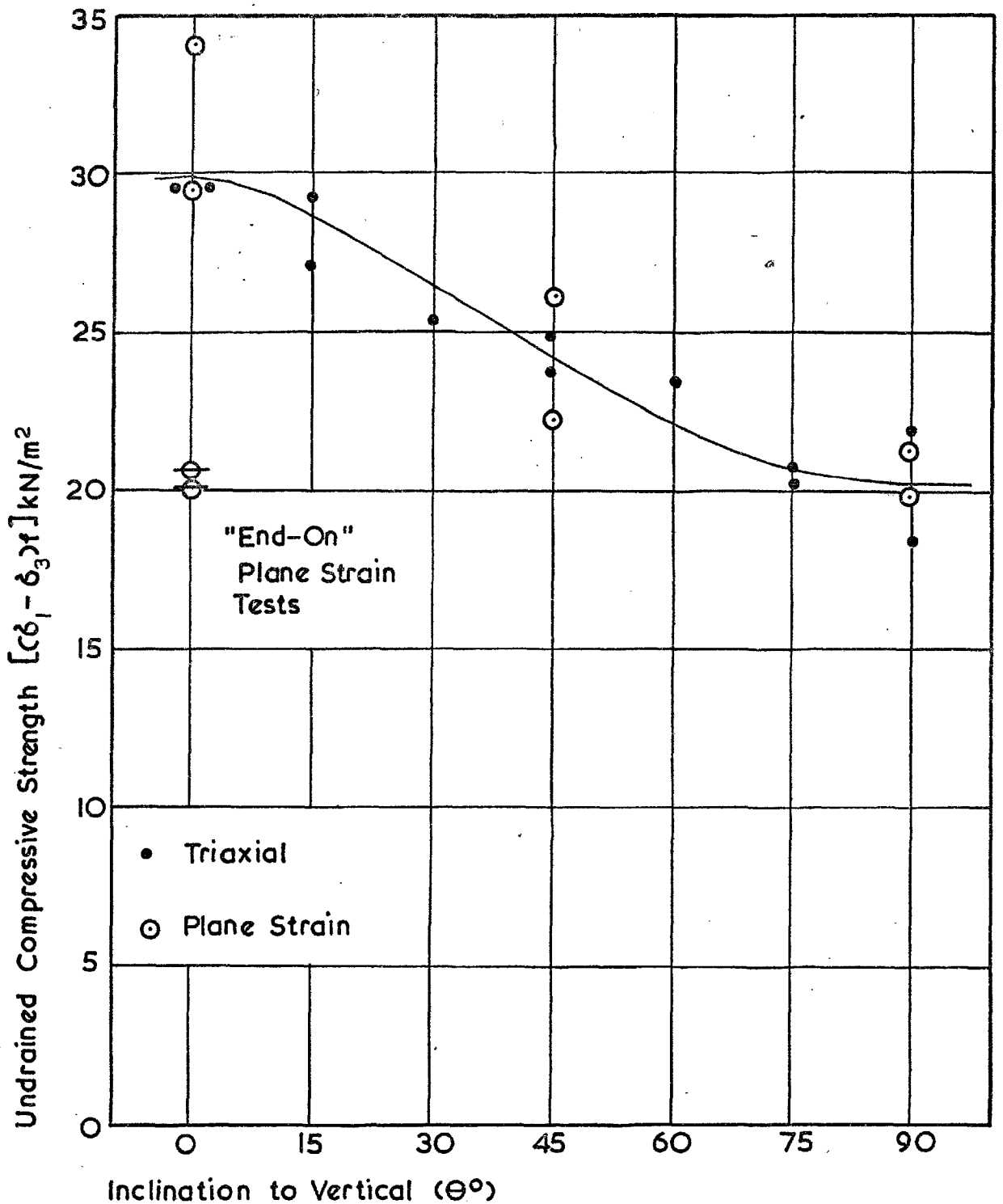
Fig. 2.17

CONSOLIDATED UNDRAINED TRIAXIAL TESTS: EFFECTIVE STRESS PATHS AT LOW STRESS LEVELS (3.18 to 3.48m) (After Wesley 1975)



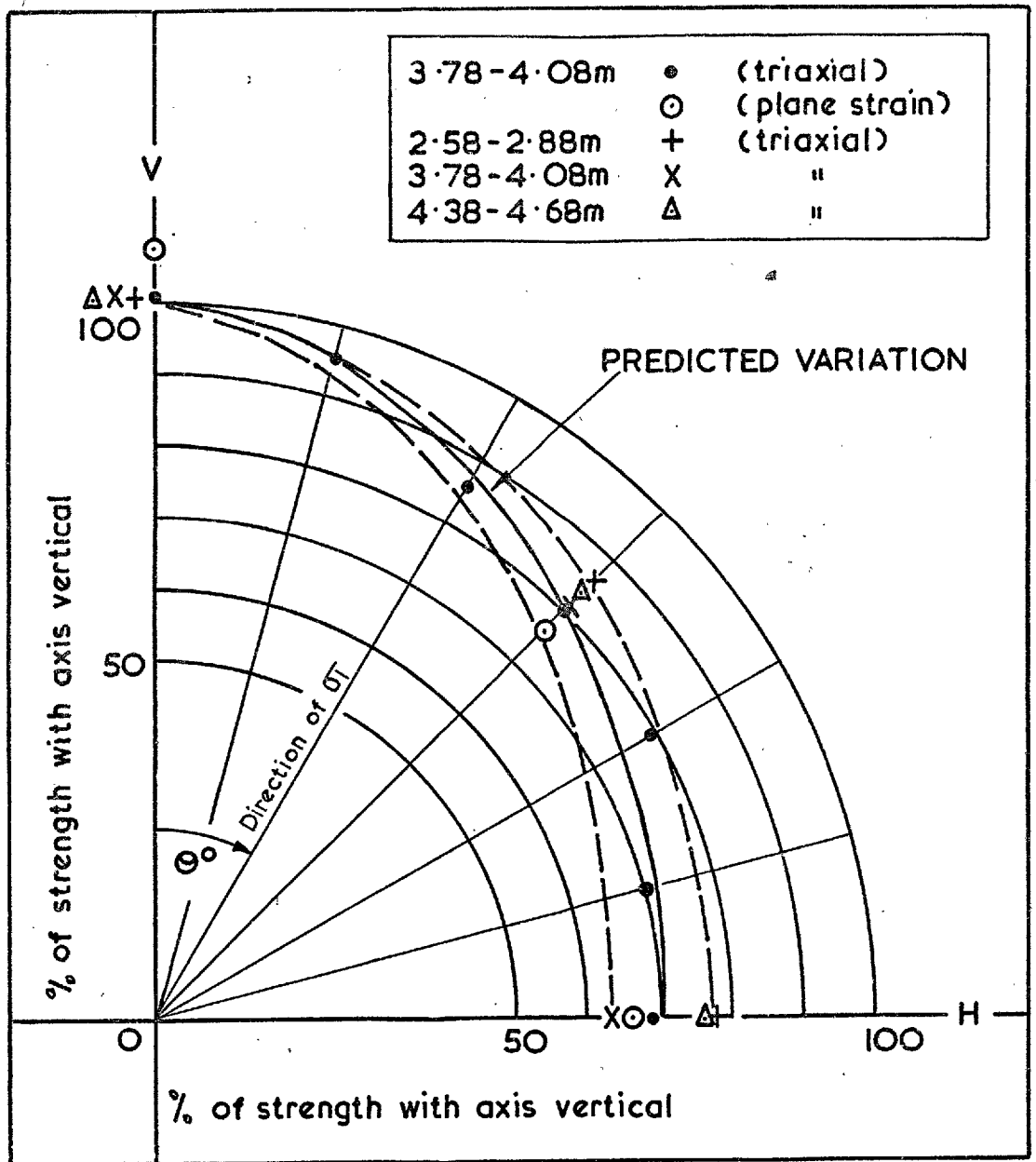
**CONSOLIDATED UNDRAINED TRIAXIAL TESTS:
VALUES OF A_f (3.18-3.48m) (after Wesley 1975)**

Fig. 2.18



UNDRAINED TRIAXIAL AND PLANE STRAIN TESTS AT VARYING ORIENTATIONS (3.78 - 4.08m) (after Wesley, 1975)

Fig.2.19



PREDICTED VARIATION GIVEN BY BISHOP'S (1966) EQUATION (2.15):-

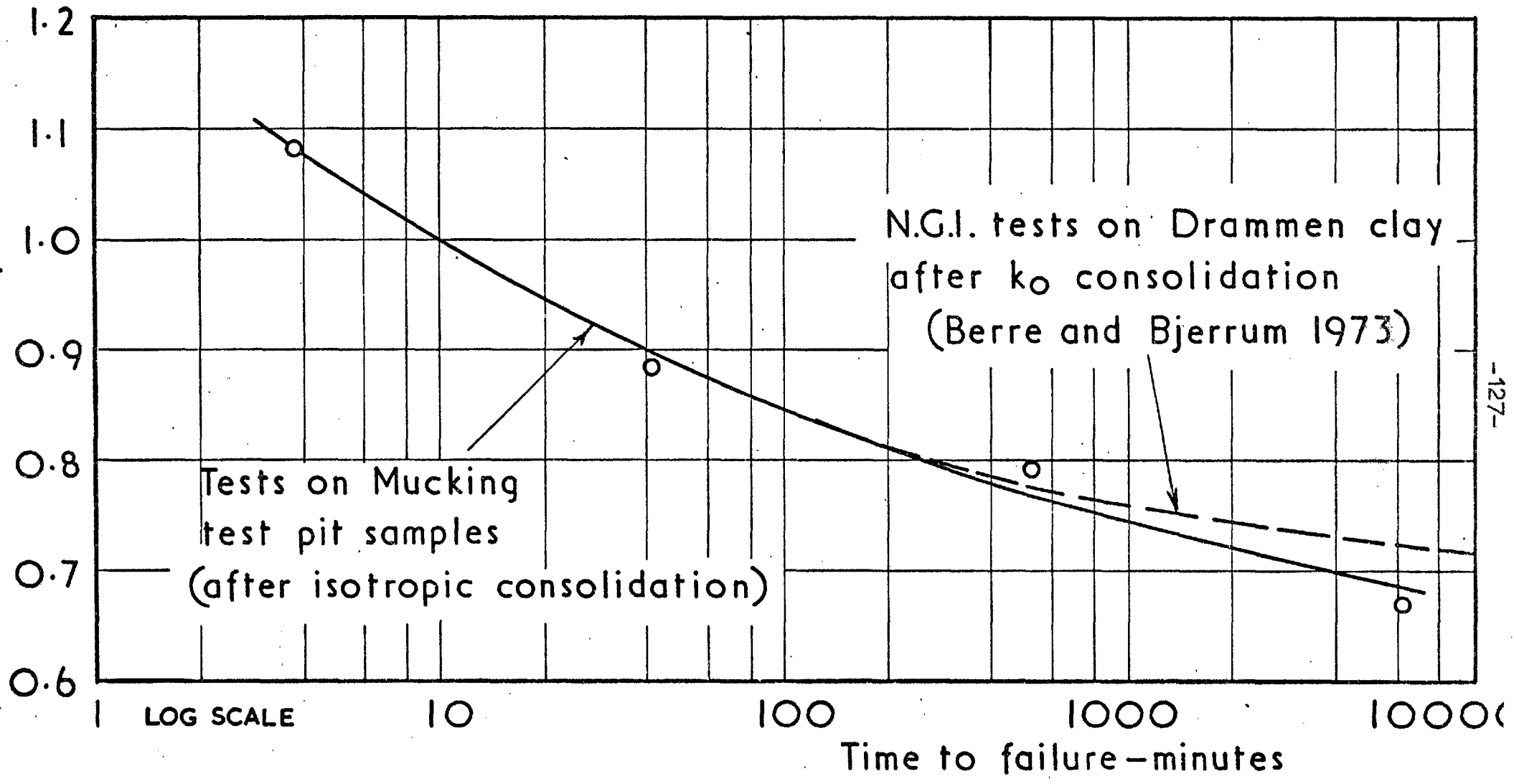
$$C_{\theta H} = C_{UVI} (1 - a \sin^2 \theta) (1 - b \sin^2 2\theta)$$

with $a = 0.3$, $b = 0.065$

**POLAR DIAGRAM SHOWING RESULTS OF
UNDRAINED TESTS AT VARYING
INCLINATIONS** (after Wesley, 1975)

Fig. 2.20

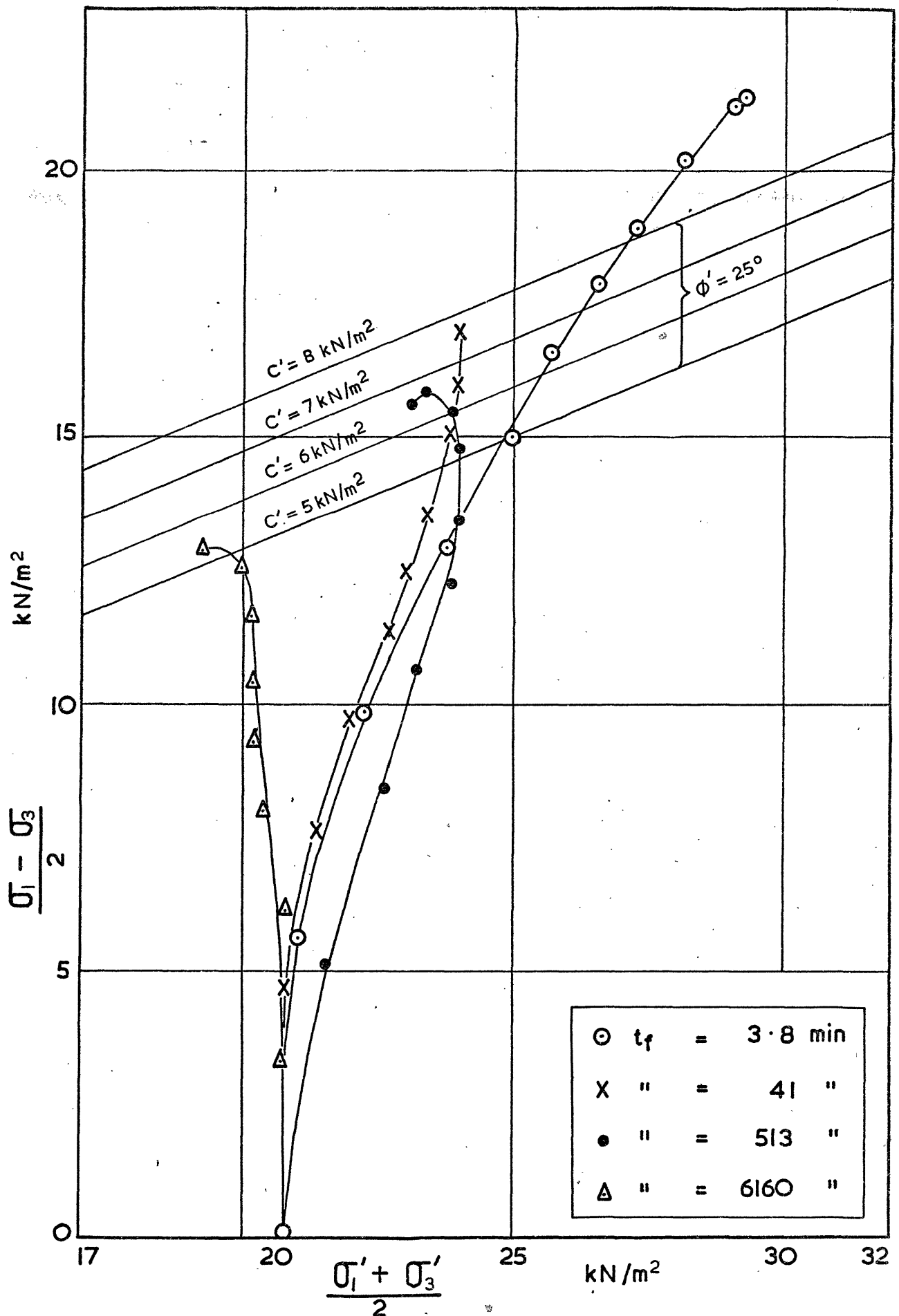
$(\sigma_1 - \sigma_3) \text{ at } t_f = 10 \text{ min}$



-127-

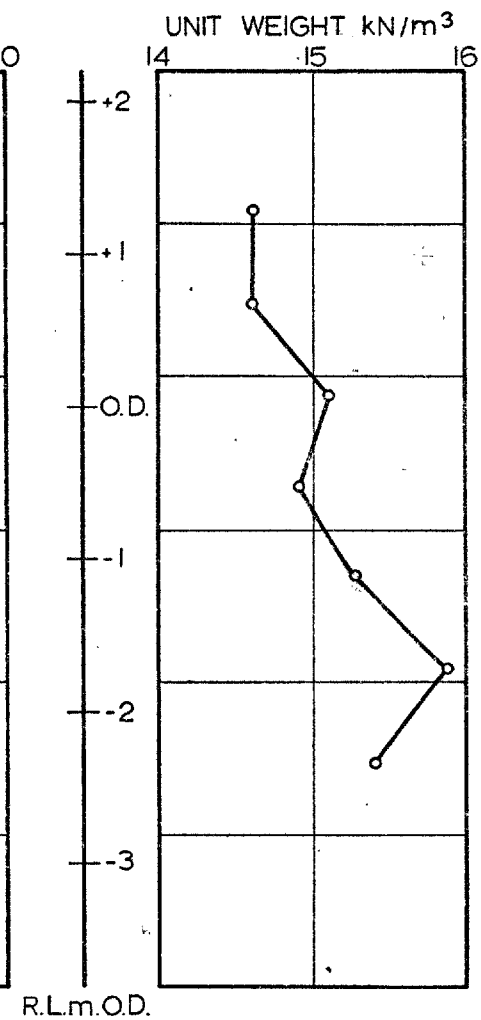
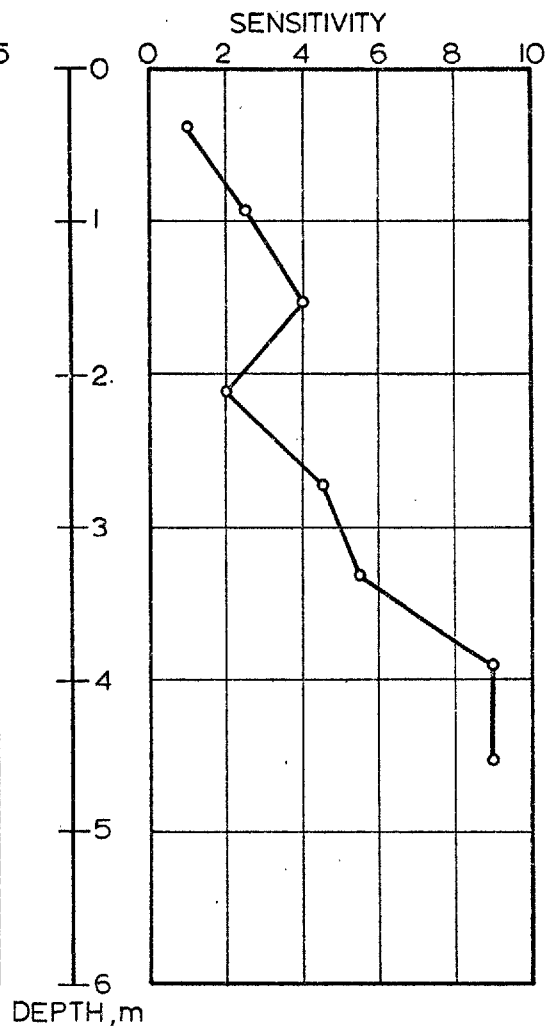
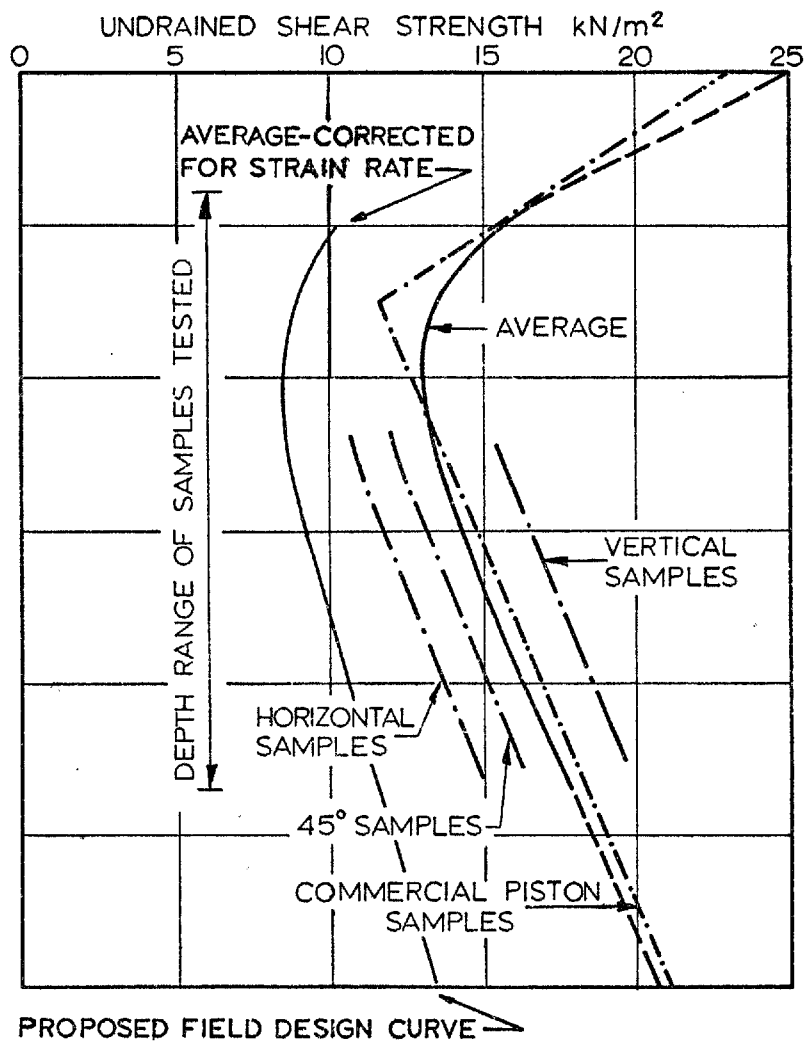
Fig 2.21

STRAIN RATE INFLUENCE ON UNDRAINED STRENGTH



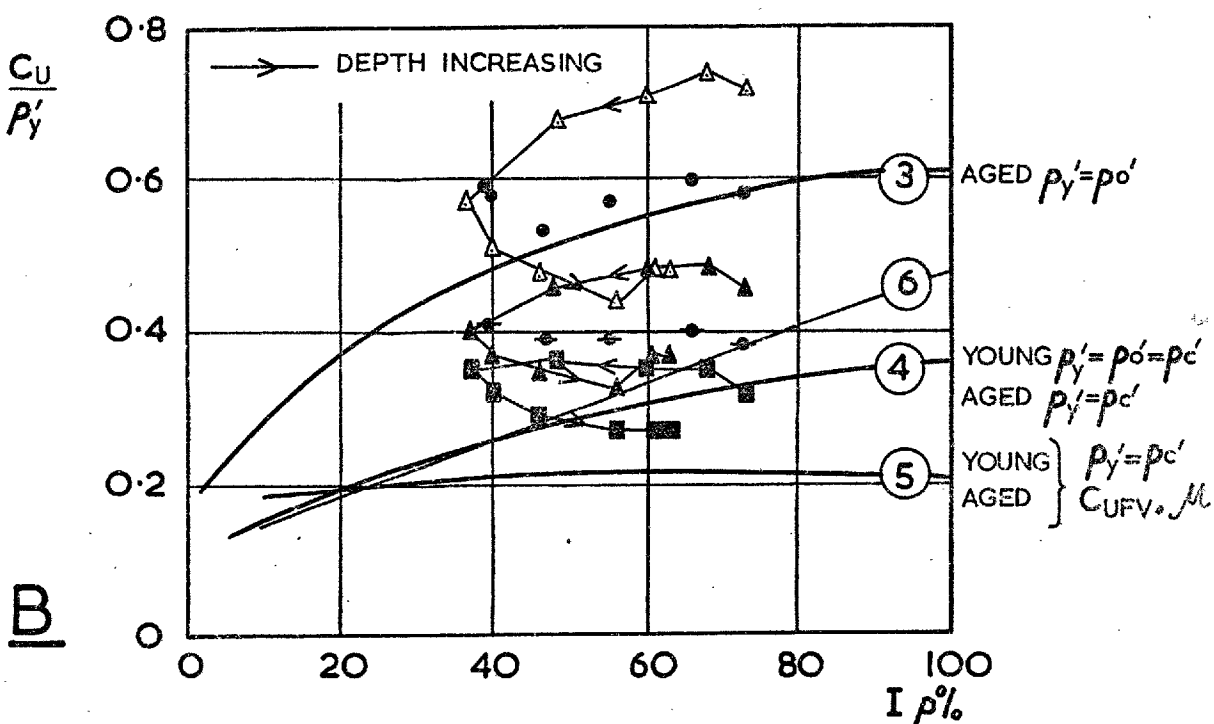
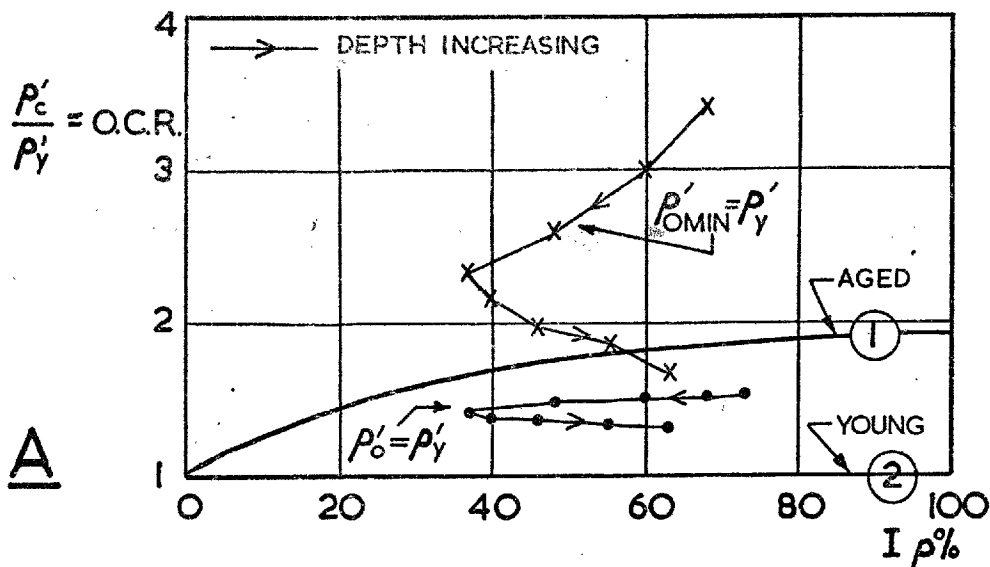
STRAIN RATE INFLUENCE : STRESS PATHS FROM TESTS AT DIFFERENT SPEEDS (3.18 - 3.48m)
 (after Wesley, 1975)

Fig. 2.22



TEST PIT SAMPLES: UNDRAINED SHEAR STRENGTH, SENSITIVITY AND UNIT WEIGHT

Fig 2.23



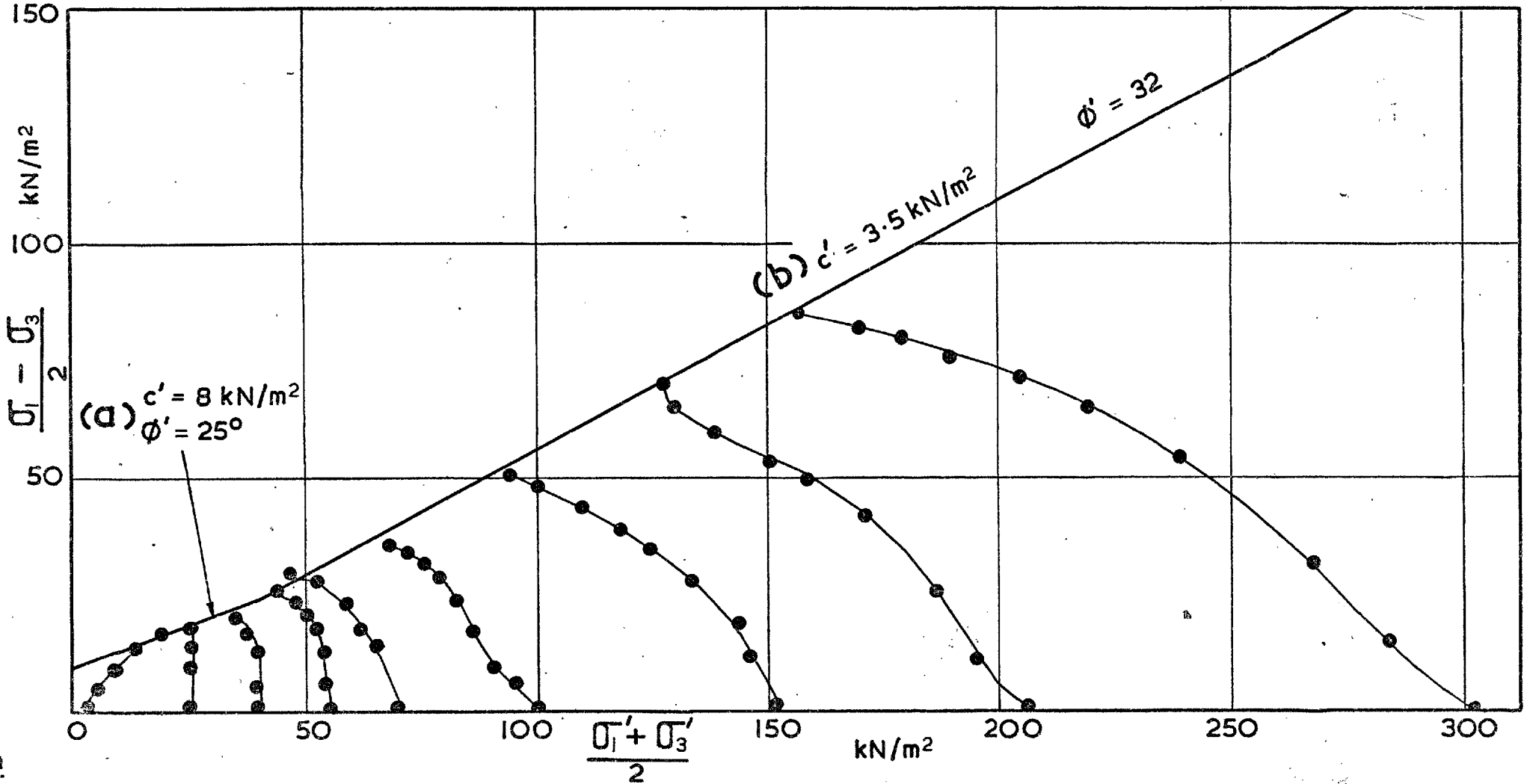
LEGEND

• C_{UVI}, P'_o	◊ C_{UVI}, P'_c
△ $C_{UFV(V)}, P'_o$	▲ $C_{UFV(V)}, P'_c$
	■ $C_{UFV(V), \mu}, P'_c$

(1) → (5) DATA FROM BJERRUM (1973) & MESRI (1975) FOR N.C. LATE GLACIAL CLAYS (C_{UFV})

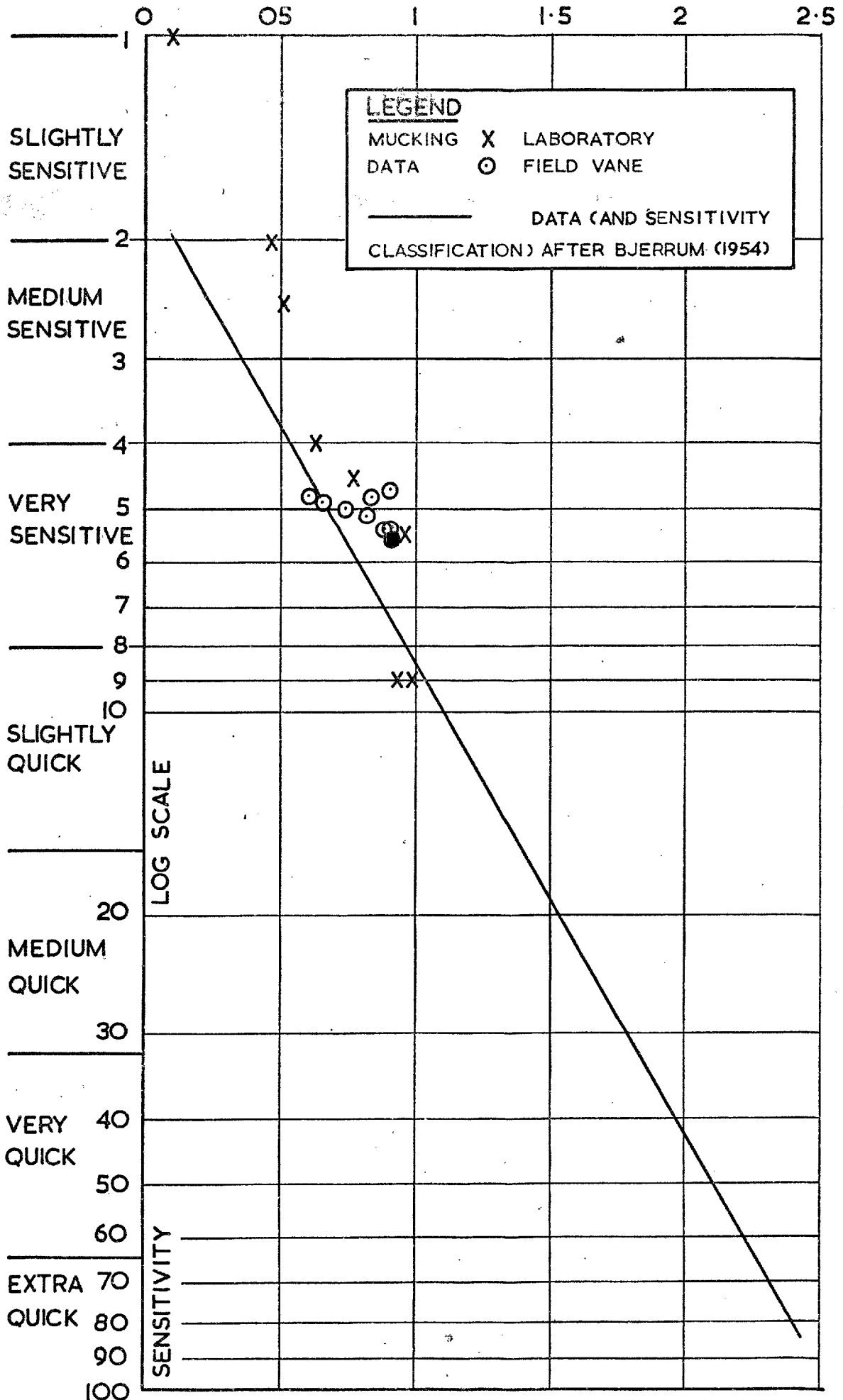
(6) $\frac{C_u}{P'_o} = 0.11 + 0.0037 I_p$ FOR N.C. CLAYS (SKEMPTON, 1957)

RELATIONSHIPS BETWEEN PLASTICITY INDEX, O.C.R. AND UNDRAINED STRENGTH

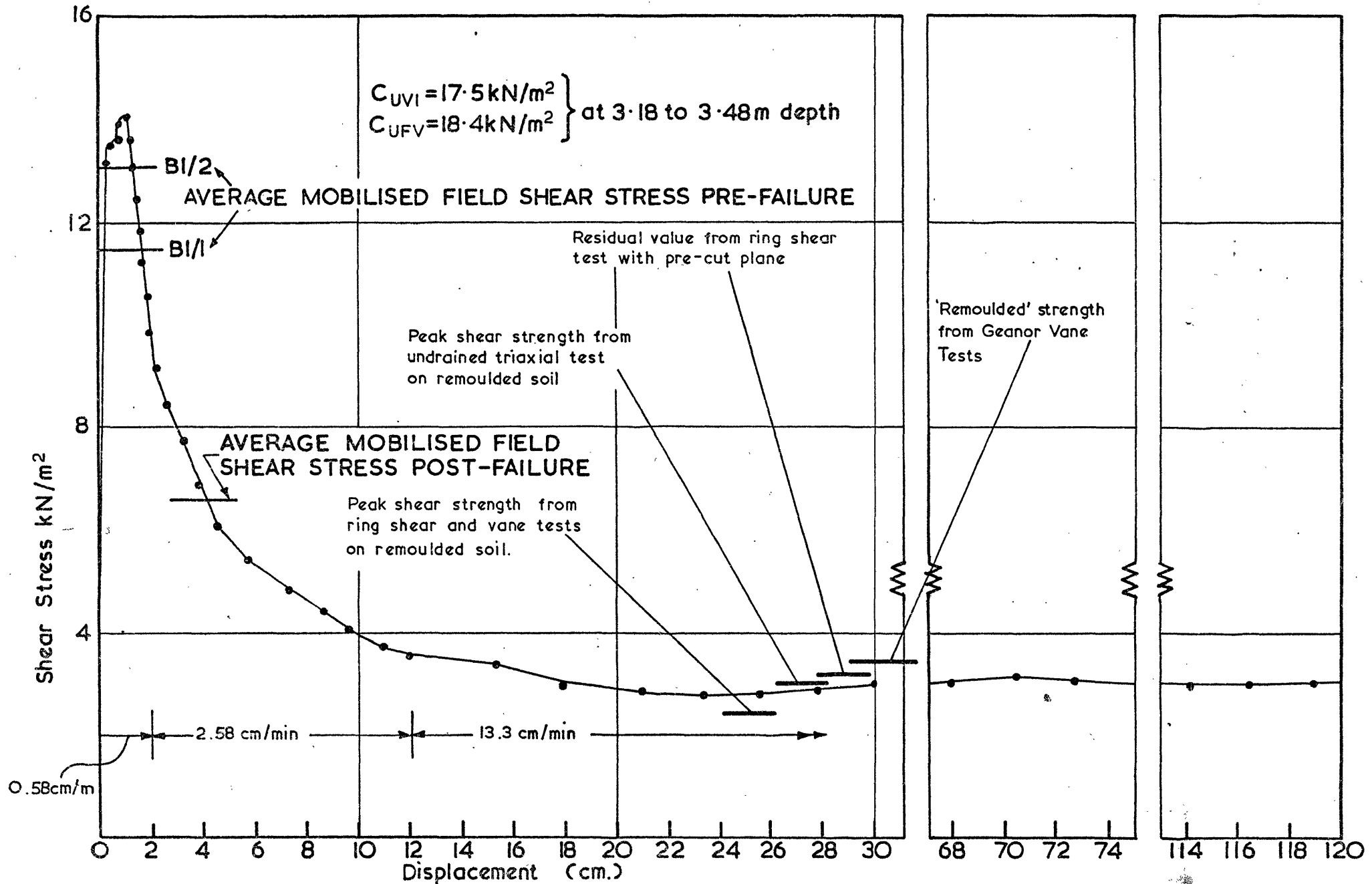


CONSOLIDATED UNDRAINED TRIAXIAL TESTS: EFFECTIVE STRESS PATHS
 (3.18 - 3.48 m) (after Wesley, 1975)

Fig 2.25



RELATIONSHIP BETWEEN LIQUIDITY INDEX & SENSITIVITY AS MEASURED IN THE LABORATORY AND FROM FIELD VANE TESTS Fig 2.26



UNDRAINED RING SHEAR TEST SHOWING PEAK STRENGTHS COMPARED WITH REMOULDED AND RESIDUAL VALUES (3.18-3.48 m) (laboratory data from Wesley, 1975)

Fig 2.27

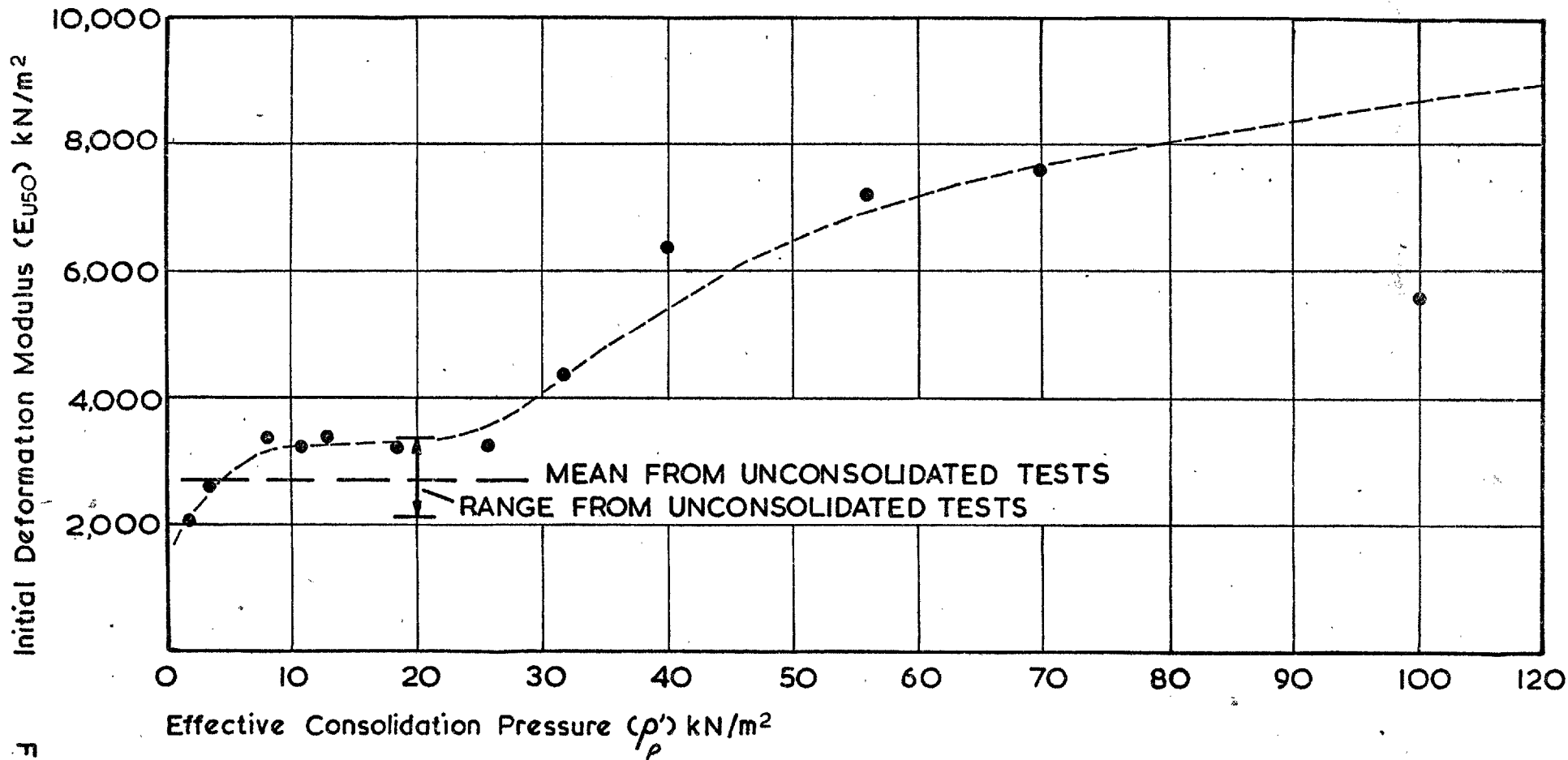


Fig 2.28

UNDRAINED DEFORMATION MODULUS VERSUS CONSOLIDATION PRESSURE (3.18 - 3.48m)
 (after Wesley, 1975)

CHAPTER 3

FIELD VANE TESTS AT MUCKING

3.1. The Field Vane Shear Test

3.1.1. Introduction

The in-situ vane test appears to have been developed simultaneously in Great Britain and Sweden during the 1940.s* (Smith, 1945; Smith, 1947; Skempton, 1948(b); Cadling and Odenstad, 1950) in order to overcome the problem of sampling in soft clays. The introduction of the vane test seemed to indicate that sample disturbance was indeed the primary cause of the previously observed discrepancies between laboratory undrained strengths and field values obtained from back-analyses (e.g. Skempton and Golder, 1948; Cadling and Odenstad, 1950; Cadling and Linskog, 1957; Andresen and Bjerrum, 1957; Bjerrum and Kjaernsli, 1957; Lo and Stermac, 1965).

However, with the passage of time it became clear that discrepancies could exist between the field undrained strength as determined from vane tests and the back-analysis of failures of full scale structures (e.g. Golder and Palmer, 1955; Casagrande, 1960; Parry and McLeod, 1967; Eide, 1968; Ladd, 1969; Bjerrum, 1972; Lacasse and Ladd, 1973; Dasca1 and Tournier, 1975). The case histories reported in these and other references indicate that the vane test often overestimates the undrained strength but in some cases may underestimate it (e.g. Ladd, 1972). Thus the field (and indeed laboratory) measurement

* Similar equipment is reported to have been used in Sweden and Germany during the earlier part of the century (Cadling and Odenstad, 1950; Osterberg, 1957; Kallstenius, 1957; Cox, 1967).

of this quantity is still subject to considerable uncertainty for soft clays, this being reflected in the increasing number of trial embankments constructed on such materials (Bjerrum, 1972; Bishop and Green, 1973). In view of the circumstances it was decided to devote part of this research to a critical appraisal of the field vane shear test.

3.1.2. Factors Relevant to Vane Testing

(i) Soil Disturbance

(a) Due to Advancement to Test Position

This may be by boring (borehole vane, see e.g. Skempton, 1948(b)) or jacking inside a casing (Cadling and Odenstad, 1950; e.g. Geonor vane). In either case between three and five diameters (of the boring or casing respectively) is generally allowed between the base of the borehole/casing and the top of the vane after the latter has been pushed ahead of the former. Cadling and Odenstad (1950) found that a distance of five diameters was sufficient for a quick clay and suggested that three diameters might be sufficient for less sensitive materials.

(b) Due to Insertion of the Vane

The soil disturbance caused by the presence of the vane itself is to some extent a function of the area ratio of the vane where:-

$$\text{Area Ratio} = A_r = \frac{\text{average cross-sectional area of vane}}{\text{cross-sectional area of equivalent soil cylinder}}$$

Additional disturbance is caused by the downdrag forces on the blade faces as the vane is inserted.

The area ratio of most vanes in common use is less than 10% (Osterberg, 1957). Typical examples of area ratio are 8% for the Bishop vane (75mm diameter; Skempton, 1948(b)) and 9% for the Geonor vane (65mm diameter). It is obviously a compromise between the need to minimise soil disturbance and yet have sufficient vane blades of adequate stiffness, and a rod capable of transmitting the required torque without excessive twist.

The insertion of the vane also sets up pore pressures in the soil and these will affect the measured shear strength. Aas (1965) found an increase in strength of 30 to 50% resulted if one to three days were allowed to elapse between vane insertion and testing ('consolidated undrained' vane tests).

(ii) Number of Blades

This factor influences the stress distribution set up during the vane test and hence the effect of progressive failure on the rupture surface. A small number of blades may result in a less uniform stress distribution on any surface, whereas a large number may be unacceptable on the grounds of excessive area ratio.

Cadling and Odenstad (1950) performed tests with two and four bladed vanes, the latter resulting in higher measured strengths.

Vanes with four blades have been used almost exclusively ever since although eight blades have been incorporated to provide additional stiffness in vanes with large height/diameter ratios (Weisel, 1973).

(iii) Vane Shape and Relative Dimensions

The minimum vane diameter is predetermined by the necessity to place the vertical rupture surface outside the area influenced by the vane rod. The total rupture surface also needs to be large enough to produce a shear force measurably greater than the rod friction.

The ratio of height (H) to diameter (D) reflects the relative importance of the assumed mobilised shear stress distribution across the horizontal and vertical rupture surfaces. The commonly adhered to H/D ratio of 2/1 ensures that the main contribution to the shear force at failure, in an isotropic soil, comes from the vertical surface. In such a case the assumed mobilised shear stress distribution on the horizontal surfaces does not much affect the results (figure 3.1.). Under some conditions of undrained strength anisotropy and with lower H/D ratios it becomes more significant. Common vane test practice is to use vanes with $H/D = 2/1$ and assume isotropic soil strength conditions and uniform mobilised shear stress distributions.

The maximum physical vane dimensions have generally been controlled by the amount of torque (T) which can be applied by a piece of equipment essentially portable and easy to operate, as well as the size of vane and rods which can be readily handled and advanced into position. Vane sizes of the order 55 x 110mm and 65 x 130mm are

commonly used in Great Britain and Scandinavia, although vane sizes up to 130 x 130mm are reported by Aas (1967) and Weisel (1973). The standard American design (A.S.T.M., 1964) caters for vanes up to 100 x 200mm, these being intended for use in firmer soils.

The dimensions of the vane are also important in respect of the zone of soil which is stressed during the test, and hence the pore-pressure regime and drainage pattern which result. For larger volumes of soil under test the scatter of results may be reduced due to better representation of the soil conditions.

(iv) Application and Measurement of Torque

The original Swedish vane incorporated direct drive by means of a bar which was turned manually against spring balances, the rotation being recorded by a large protractor (Cadling and Odenstad, 1950). Alternative arrangements abound (e.g. see A.S.T.M., 1957) and have included a tennis-net winder and spring balance (Skempton, 1948(b)).

The commonly used Geonor equipment incorporates a torque head which is clamped to the outer casing, this providing the reaction against which the torsion is applied. The outer casing is usually locked against the jacking frame to ensure it does not rotate in the ground. A square-section drive shaft in the torque head slide fits into a like female adaptor screwed into the top vane rod. This adaptor also has a horizontal hole to accommodate the tommy bar, by means of which the vane can be advanced to and pulled from the test position.

Torque is applied to the shaft via a gear wheel at whose centre it is located by four blade springs. The wheel is rotated by a worm gear, which is in turn rotated by means of a small detachable handle, the reduction being 1/3600. The shaft rotates in a bearing seated in the main housing, this bearing taking out the horizontal force applied by the worm so that a pure torque is applied to the vane rods.

The magnitude of the torque is indicated by a pointer which registers a magnified version of the relative displacement between the central shaft and the gear wheel (i.e. the deformation of the blade springs). The torque applied to the wheel, and indicated by the pointer, includes a frictional component in the bearing, which must increase as the applied torque increases. This friction is eliminated from consideration by Geonor's calibration device wherein a known torque is applied to the shaft on the underside of the bearing.

In this respect the Geonor vane is inferior to the American design (Gibbs, 1957; A.S.T.M., 1964) wherein the torque is measured on the 'right' side of the bearing, within the apparatus. This is achieved by the gear wheel bearing directly onto the main housing. A split ring mounted around the gear wheel's centre applies a pure torsion to the vane rods, this being measured by means of a dial gauge recording the ring's deformation. The design is a borehole vane and the housing is simply a plate which attaches directly to the borehole lining.

Rotation of the vane is usually back-calculated from the time elapsed, the rotation at ground level being applied manually at a set rate. In this respect the operator's skill at maintaining the set rate is relied

upon. A recent development in vane design (Weisel, 1973) eliminates many of the previous inadequacies. It incorporates mechanical drive via a gearbox and measurement of applied torque at the vane itself by means of strain gauges on the lower rod. The angular rotation was measured at the base of the vane casing by means of a displacement transducer, thus enabling an accurate determination of the true angular rotation of the vane. Whether such a recording system is robust enough for normal commercial use will only be proven by experience.

(v) Rod Friction

(a) In the Apparatus

Vanes jacked into position independently of a boring will have bearings between the casing and inner rod. Borehole vanes may be cased or uncased, and may also have spacers to locate the rods in the borehole. Any bearings or spacers in contact with the drive rods will result in an additional frictional component in the measured torsion.

The Geonor vane has a protection shoe at the base of the outer casing, into which the vane itself is locked during driving. Locking is facilitated by a spring, in the coupling piece, which engages in a sleeve inside the outer casing. The coupling piece, which joins the vane assembly to the vane rods incorporates a thrust bearing to minimise friction with the base of the outer casing. This is the only bearing below ground level; it is packed with grease and fitted with a grease

nipple. Just prior to testing the vane is pushed out of the protection shoe, a distance of 500mm whence the coupling piece is at the base of the outer casing. The close fit of the protection shoe also serves to clean the vane blades on re-entry.

(b) In the Ground

Skin friction on the rod directly above the vane must either be eliminated or separately measured. The Geonor vane incorporates a separate outer casing for the rod. It is attached to the coupling piece and terminates directly above the vane, where a seal prevents ingress of soil and moisture. The gap between the rod and its casing is also filled with grease. Clay is removed from the outer rod as it is withdrawn, by a brass ring immediately above the protection shoe.

(vi) Relationship between Applied Torque and Shear Strength and Shear Modulus of the Soil

(a) Assumed Rupture Surface

This is generally taken as a cylinder having the same height and diameter as the vane. Attempts have been made to predict a cylindrical rupture surface of larger diameter than the vane (Skempton, 1948(b)); although deformation certainly occurs outside the diameter and height of the vane (Cadling and Odenstad, 1950) there is no quantitative evidence on which to base such a prediction. Indeed, where samples have been recovered which contain shear surfaces generated during a vane test, the former assumption appears to be

close to the truth (Jain and Mohan, 1957; Gibbs, 1960). Recent work at Cambridge University, using X-ray techniques to monitor the development of the rupture surface in vane tests, indicates a very thin zone, approximating also to the commonly accepted soil cylinder. In fact the rupture surface appears to propagate perpendicularly from the blade tips and is thus slightly non-cylindrical (Wroth, 1975(a)).*

(b) Assumed Distribution of Shear Stresses

In order to relate the maximum applied torsion to the shear strength of the soil, having assumed a cylindrical rupture surface as described above, the shear stress distribution on the surfaces of the cylinder must be known. Inspection of soil samples which have been sheared in vane tests reveals an apparent variation in shear strain around the vertical failure surface (maximum values occurring near the vane blades) whilst an elastic analysis, based on an infinitely long cylinder shearing in clay, supports a uniform shear stress distribution (Cadling and Odenstad, 1950).

Shear stress distributions across the ends of the vane are equally uncertain, but generally less important within the normal ranges of H/D and C_{UH}/C_{UV} where 'H' and 'V' respectively denote horizontal and vertical planes (figure 3.1.). Uniform shear stress mobilisation is commonly assumed over the whole surface area of the cylinder. Alternative distributions across the horizontal (end) surfaces are linear and parabolic variations from zero at the centre to peak at the circumference. As the shear strains on any horizontal plane might be expected to increase radially one of these alternatives

*Whilst testing the large vane (section 3.3) in the laboratory the writer made similar observations; in fact the failure surfaces appeared to be a series of tangents to a circle passing through the rupture zone.

would seem intuitively more reasonable. A simplified elastic analysis (Cadling and Odenstad, 1950) supports the latter, whilst the former has been used in this work. The uniform distribution across the end surfaces has the attraction of being conservative in the estimation of soil strength. The inclusion of the rod on the upper surface is generally ignored; in the case of a linear distribution this is of even less import than for the uniform distribution, the omission again being conservative in the prediction of soil shear strength.

(c) Vane Test Formulae for Determination of Soil Shear Strength

The standard formulation is derived in Appendix 1* and is as below:-

$$T_{VER} = \frac{\pi D^2 \cdot H}{2} (C_{UV} + \frac{\alpha_V D}{H} C_{UH}) \dots\dots\dots(A.1.1.)$$

where VER signifies a vertical vane test, and α_V is a vane test constant.

(d) Determination of Shear Modulus of Soil

For an elastic isotropic soil approximate analyses can be made (Cadling and Odenstad, 1950) in order to link the angular rotation of the vane (ω) and the mobilised shear stress (τ) to the shear modulus of the soil (G). The simplified representation of the vane varies from an infinite cylinder (Appendix 5) to a sphere, providing respectively upper and lower bounds for the shear modulus. The following formulation, derived from the spherical assumption, lies between these limits and is considered reasonably realistic (Weisel, 1973):-

*Noting that the undrained strength C_u is assumed to apply to the cylindrical rupture surface.

$$G = \frac{\tau}{2.25\omega_0} \dots\dots\dots(3.1.)$$

This formula may be applied to vane test results, expressed in terms of angular rotation (in radians) of the vane versus mobilised shear stress, over the linear (elastic) portion of the relationship. In order to attempt the determination of the shear modulus it is thus necessary to either measure rotation of the vane directly, or to be able to account for rod and vane twist and other deformation within the torque applying and recording device. The applied angular rotation must also be known, in the latter case, at any time and this implies mechanical rather than manual drive. For these reasons, plus the general uncertainty regarding what is actually happening to the soil during the test, the vane is not commonly used in this context.

(vii) Undrained Stength Anisotropy

The vane test imposes failure surfaces upon the soil, which are of little relevance to occurrences in reality, under conditions approximating to constant total normal stress. The results of section 2.7.2. ((i) and (ii)) suggest that even in an elastic isotropic soil the 'undrained strength' measured by the field vane may be different to that measured in a plane strain laboratory test. In addition the shear strength mobilised on horizontal (C_{UH}) and vertical (C_{UV}) planes may also be different in this idealised case. It is thus not justifiable to use the relationship C_{UH}/C_{UV} from vane tests as a measure of undrained strength anisotropy any more than it is to use the ratio C_{UTE}/C_{UTC} .

It was also shown in section 2.7.3. that it is not feasible, in general, to associate unique values of C_u with shear planes at particular inclinations, but that unique values of C_u appear to be linked with particular principal stress directions. In the vertical vane test the shear stress is applied to planes which are principal planes in situ (and thus carry no in-situ shear stress), but the ensuing principal stress vectors during the test are not known. If, for any reason, the undrained strength of the soil is different for vertical and horizontal shear planes, the measured soil strength (assuming isotropic undrained strength for calculation purposes; Appendix 1., equation A.1.2.) will be a weighted average, the value depending on the vane dimensions, the degree of shear strength mobilisation in each direction and the assumed shear stress distributions.

By using vanes having various H/D ratios the mobilised shear stress on the horizontal and vertical planes can be separately determined. Inspection of equation A.1.1. shows that by plotting $2T/\pi D^2 H$ as ordinate versus $\alpha_v D/H$ as abscissa, the intercept of the ordinate is C_{UV} and the slope C_{UH} . This approach (figure 3.2) proposed by Aas (1965, 1967) assumes that the peak shear strength is simultaneously mobilised on the horizontal and vertical shear surfaces, at the same time as maximum torque is recorded by the vane apparatus. In soils exhibiting undrained strength anisotropy this may not be the case; the effective stress parameters may also exhibit different degrees of mobilisation on different planes (Bishop, 1966(a)).

In addition as 'D' and/or 'H' are varied the mobilised shear stress ratio at peak torque may also vary, because the relative contributions from the vertical and horizontal planes are a function of these dimensions and hence so is the angular rotation. This is illustrated in figure 3.2. which shows that the plot proposed by Aas (1965) will only be a straight line in the special case when the undrained strength is mobilised simultaneously on both planes. This was realised by Weisel (1968, 1971) who proposed the alternative procedure of varying 'H' with 'D' constant, and plotting T (ordinate) versus 'H' (abscissa) which (from equation A.1.1.) leads to an ordinate intercept of $(\pi\alpha_V D^3)\tau_H$ and slope $(\frac{\pi D^2}{2})\tau_V$ (Weisel, 1973; figure 3.2.). The significant difference in Weisel's approach was the plotting of torque, for each 'H' (or H/D), at intervals of angular rotation and thus relating the mobilised horizontal (τ_H) and vertical (τ_V) shear stresses to shear strain (γ). In this way $\tau_{H(MAX)} = C_{UH}$ and $\tau_{V(MAX)} = C_{UV}$ can be evaluated even though they are mobilised at different shear strains.

Menzies and Mailey (1976) studied undrained strength anisotropy using a series of diamond shaped vanes (similar to the 45° vane described by Aas, 1967) producing conical shear surfaces inclined at varying angles to the vertical. In this way each vane only records the strength on one inclination and the degree of mobilisation problem only arises in the assumption of a shear stress distribution along the shear surfaces. In common with the previously described methods this approach is very sensitive to this assumption. Figure 3.1.(1) shows that for a particular measured torque, with C_{UV} constant and for any H/D, a variation in C_{UH}/C_{UV} of 33% (from 1.00 to 1.33) can be accommodated within the range between a linearly varying and uniform end shear stress distribution.

(viii) Rate of Testing

The vane test is not a constant rate of strain test, due to rod twist etc., but approximates to this definition. The pioneer work of Cadling and Odenstad (1950) led them to adopt a rate of rotation of 0.1 degrees/second, which has remained as standard ever since. Undrained laboratory triaxial tests have shown that the measured undrained strength decreases with increasing time to failure for certain soils (Casagrande and Wilson, 1951; Lo and Stermac, 1966; Berre and Bjerrum, 1973; Wesley, 1975). That such a decrease also occurs in the field vane test has been shown by Skempton (1948(b)) and Weisel (1973). The vane test, however, is open to uncertainties in this respect as the onset of partial drainage cannot be predicted. Aas (1965) reports consolidated undrained tests (vane left in position for 1 to 3 days before the test) and drained tests. The latter were stress controlled tests taking 2 to 4 days for failure and gave results 17 to 38% lower than the former. Failure in the drained tests occurred some hours after the addition of the final load increment. These tests were performed in a quick clay of low plasticity and no measurable variation in strength was observed if the rate of rotation, in the normal vane tests, was varied by a factor of ten either side of standard.

(ix) Progressive Failure

Progressive failure may be of importance in determining the average strength which can be mobilised on shear surfaces in soft clays under full scale loading conditions in the field (Bishop, 1971(b)).

Whether or not this mechanism is operative in the field vane test (or in any instance of a soil subjected to shear stress) depends upon the uniformity of the shear stress distributions, and its influence depends upon the brittleness index of the soil where:-

$$\text{Brittleness Index} = I_B = \frac{\tau_p - \tau_r}{\tau_p} \dots\dots\dots(3.2.) \text{ (Bishop, 1967),}$$

where p denotes peak (for undrained conditions, $\tau_p = C_u$ and $\tau_r = C_{ur}$ as in equation 2.18), and the rate of post-peak strength loss with increasing strain.

Although in theory progressive failure is not a time dependent phenomenon, field observations indicate that the development of shear strains is (Bjerrum, 1972) and duration time of the test may thus influence also the effect of progressive failure.

(x) Summary

It can be seen that what is essentially a simple field test is not so easy to interpret, and the application of the results therefrom to stability analyses is still open to considerable uncertainty. Bjerrum (1972) attempted to resolve some of these uncertainties by investigating a number of case histories where vane tests had been used to predict the stability of embankments on soft clay with varying degrees of success. From this study emerged a correction factor, μ , to be applied to field vane test results before their use in stability analyses.

$$\text{i.e. } C_u(\text{FIELD}) = \mu \cdot C_{uFV} \dots\dots\dots(2.17)$$

where $\mu = f(I_p)$ as in figure 3.3.

This factor, which is a reduction one except at very low plasticity indices, obviously includes all the effects, discussed previously, which cause the field vane strength to differ to that back-calculated by circular arc limit equilibrium analyses of embankments which have failed. In addition it will include allowances for any deficiencies in this model of soil behaviour. It is an empirical formulation and as such its validity is likely to be far from universal. Certainly factors other than plasticity index must influence the relative effects of loading rate, undrained strength anisotropy, progressive failure and relevance of the analytical method on the ability of the vane test to predict a reliable undrained strength value for design purposes.

3.2. Geonor Vane Tests

3.2.1. Introduction

The Geonor vane tests carried out at the Mucking test site (figure 2.3) can be sub-divided as below:-

- (i) 21 tests in the vicinity of the trial embankments, generally along the instrumented section lines.
- (ii) 8 vertical and 9 horizontal tests adjacent to, and from respectively, the test pit.
- (iii) 4 tests adjacent to the large vane test boreholes.

The first category of tests were carried out to relate directly to the observed stability of the embankments and to the conventional laboratory tests on the piston and test pit samples. The second group were to compare results with the laboratory test results on the large cylinder samples from the test pit. The final tests for comparison with the large vane test results, are discussed in the section pertaining to the latter (i.e. 3.3.5. (iii)).

It has been pointed out that the direction of shear in vertical vane tests is not relevant to typical shear surfaces generated by embankment failures (Bishop, 1966(a)). If a soil is considered which exhibits shear strength anisotropy, and this anisotropy is physically represented, for illustrative purposes, by horizontal bedding, certain directions of shear can be envisaged which may result in different shear strengths being measured (Menziés & Mailey, 1976). These, as illustrated in figure 3.4, are summarised below:-

1. type 1 planes - shearing is parallel to, and along the bedding.
2. type 2 planes - shearing is perpendicular to, and along the bedding.
3. type 3 planes - shearing is perpendicular to, and across the bedding.

If horizontal and vertical vane tests, and an embankment failure are now considered in relation to this model, the various shear surfaces may be described as below:-

1. Vertical vane test (i) horizontal surfaces - type 1
(ii) vertical surface - type 2

2. Horizontal vane test (i) vertical surfaces - type 2 — type 3
(ii) cylindrical surface - type 1 — type 3
3. Embankment failure type 1 — type 3

The type 2 planes are those envisaged as possible failure planes for horizontal triaxial samples (Bishop, 1966(a); see also figure 2.14(B)2.) and investigated by Wesley (1975) in the 'end-on' plane strain tests. Figure 3.8 is intended to illustrate some of the difficulties associated with assigning unique strengths to planes, and the important difference between type 2 and type 3 failure planes. Part (c) of figure 3.8 shows the relationship, between the undrained strength and the minimum angle which can be measured between the failure plane and the vertical, obtained by Delory and Lai (1971) for the Welland Clay. For each failure plane inclination, except vertical and horizontal, there are two undrained strength values, one relating to active, and one to passive, shear (figure 3.8(A), wherein the 45° planes (A to D) can be directly related to the active and passive shear strengths on 45° planes in figure 3.8(c)). The vertical and horizontal planes in this case are associated with undrained strengths which are independent of the direction of shear; this agrees with the concept of active and passive shearing (Bjerrum, 1973), there being no in-situ shear stress on these (initially) principal planes.*

The results of the inclined triaxial tests on Mucking clay (figures 2.19 and 2.20) have been plotted on figure 3.8(c), assuming $\beta = \text{constant} = 60^{\circ}$ (Wesley, 1975) and thus that $\alpha = \theta^{\circ} + 30^{\circ}$, and are in good agreement with the Welland Clay results. Also shown is the variation

* likewise the $\phi_u = 0$ planes are each associated with two values of C_u except for the vertical and horizontal directions; however these latter planes are also associated with a unique value of C_u and thus $C_{uH}/C_{uV} = 1$ although the soil is far from isotropic.

in undrained strength over a 180° range of θ (and α) predicted by equation 2.15 (see section 2.7.3. and figure 2.20), this again agreeing well with Delory and Lai's results, the predicted variation in strength from $\theta = 90^{\circ}$ to 180° being identical to that from 90° to 0° .

The 'end-on' plane strain tests, however, represent failure of a horizontal sample on a vertical (type 2) failure plane, on which the shear direction is horizontal. The results correspond well to the results of the triaxial tests on horizontal samples (as indicated by the arrow in figure 3.8(c)) and thus to the principal stress directions but do not conform to the results for vertical (type 3) failure planes. Thus type 2 failure planes may result in very different undrained strengths to type 3 failure planes, according to the principal stress directions about which nothing is known in the vane test.

The vertical vane test results in shear failure on predominantly type 2 failure planes* and may thus give results which are at variance to laboratory triaxial tests, whereas the horizontal vane test predominantly induces type 1 to type 3 failure planes, thus corresponding to a typical foundation failure surface.†

*for an isotropic soil, and $\alpha_v = 0.25$, it can be seen from equation A.1.1. that the end surfaces of the vane cylinder only contribute 11% of the mobilised shear stress.

†similarly to the conventional vertical vane test, the diamond shaped vanes of Aas (1967) and Menzies and Mailey (1976) induce failure by shearing in directions which are not relevant to typical field situations.

In order to try and resolve some of the uncertainties regarding the shear directions and failure planes involved in vane tests, and their relationship with those in laboratory tests and field failures, it was decided to take advantage of the test pit by carrying out the program of horizontal vane tests outlined previously.

3.2.2. The Equipment

The Geonor vane equipment has been largely described, by way of example, in the previous sections. The vane size used was 65 x 130mm ($A_r = 8.8\%$). The rods (20mm O.D.) and casing (42mm O.D., 35mm, I.D.) were extended in metre lengths from the 1m long main section incorporating the vane assembly.

The equipment as supplied by the manufacturer came complete with a calibration curve (C_u versus dial divisions) for the torsion head. It was decided to recalibrate the equipment before use, and as the torque is ideally measured at the vane, thus eliminating all frictional components deriving from the apparatus, this was done. A simple calibration frame was designed and constructed and the vane calibrated in both the horizontal and vertical position as described in Appendix 2.

3.2.3. Test Procedure

(i) Vertical Tests

These were carried out in the conventional way. A small pit was dug to accommodate the vane head (which is oversize for the jack) and the jacking frame positioned and held down by pickets. The first test was

performed at 1.5m and further tests throughout the soft clay layer at 500mm intervals. The maximum depth was usually 5.5 or 6.0m (approximately -3.25 or -3.75m O.D.), penetration of the peat being impossible with the vane equipment.

The tests were carried out at the conventional rate of 0.1 degree/second (60 revolutions/minute of the crank handle), with time to failure varying from 2.5 to 10 minutes, averaging out at about 5 minutes. The tests were sometimes rather hesitant, in respect of the applied rotation, at first due to taking up of the 'lock' between the outer casing and the jacking frame.

Having recorded a peak the vane was rotated 25 times using the handles supplied with the torsion head. These fit into the upper part of the head, which is attached to the gear wheel and rotates independently of the lower main casing. The test was then repeated; the peak mobilised shear stress measured is commonly referred to as a remoulded value and used to estimate the material's sensitivity. Obviously it is rather something approaching, if still somewhat, in many cases, a residual undrained strength.

(ii) Horizontal Tests

Holes were cut in the sheet piles supporting the trial pit side to enable the vane to be advanced into the soil. The casing was positioned in the jack, which was lain horizontally on supporting timbers. Another timber, across the test pit, transferred reaction from the top of the jack to support struts in the excavation wall. The casing was clamped

in position with Stilsons: this total configuration was found to be perfectly satisfactory. Tests were carried out at 500mm intervals horizontally, generally being between 3.5 and 5.5m from the pit so as to be beyond its zone of disturbance. The remaining test procedure was as for the vertical tests.

Great care was taken to keep the alignment of the vertical and horizontal tests, adjacent to and from the test pit, correct. This was very important as test positions were only 1m apart in order to have a reasonable chance of measuring any strength difference between the two axes.

3.2.4. Discussion of Results

(i) Vertical Tests

(a) Peak Strengths

The results of these tests are shown in figures 3.5, 3.6, and 3.17. Each profile relates to a particular embankment cross-section (e.g. A, C, B, C; see also figure 4.1) or location (e.g. test pit, large vane test site; see also figure 2.3) and is the average from between 3 and 8 tests. The various profiles are remarkably similar in shape with shear strengths most commonly within the range 15 to 20 kN/m². It is encouraging that the average shear strength appears to increase eastwards along the site of Bank 1 (i.e. from Section A, through Section C to Section B) as this is supported by the failures of this embankment which were always least pronounced to the eastern end (see Chapter 6). The higher strengths and large range of scatter

encountered at some locations (e.g. test pit at just below 3m depth and large vane test site at 2.5m depth) were initially thought to reflect the inherent non-homogeneity of the material although an alternative explanation is advanced in section 3.3.5 (iii). The range of scatter of the results in general (average approximately 3 kN/m^2) may similarly reflect this aspect of the material; the results typically become more consistent with depth (again see also section 3.3.5 (iii)).

The shape of the undrained shear strength/depth profile produced by the average of all the vertical Geonor vane test results, is compared to the laboratory average design curve*(figure 2.23) in figure 3.7. Below 4m depth agreement with the average (which is a linear extrapolation below 4.7m depth) and with the commercial piston samples is very good. The vertical triaxial samples from the test pit exhibit higher C_u values(C_{UV1}) than the vertical vane tests ($C_{u.FV(V)}$) below 3.5m depth, but above this the results from the Geonor vane tests are considerably higher than those from the test pit (approximately $+ 3 \text{ kN/m}^2$), and the piston sample (approximately $+ 5 \text{ kN/m}^2$) vertical triaxial samples.

The actual values of $C_{u.FV(V)}$ and C_{UV1} (test pit samples) are also given in table 2.8 together with values of $C_{u.FV(V)}/p_o'$ and $C_{u.FV(V)}/p_c'$ for comparison with the equivalent values for C_{UV1} . This comparison is graphically represented in figure 2.24 wherein $C_{u.FV(V)}/p_o'$ and $C_{u.FV(V)}/p_c'$ can be seen to be much more variable than either C_{UV1}/p_o'

*the laboratory average design curve is uncorrected for strain rate effect; the proposed field average design curve is corrected for strain rate (see section 2.7.5. and figures 2.23 and 3.7).

or C_{uV1}/p_c' , both of which are essentially constant. However, below 3.5m depth $C_{u.FV(V)}/p_c'$ is nearly constant (approximately 0.375) and comparable in value to C_{uV1}/p_c' which is approximately constant at 0.390 throughout the soft clay layer.

Thus the high Geonor vane strengths measured over the top 3.5m of the soft clay layer appear to be independent of p_c' and would seem to result from a mechanism which is not operational in the triaxial test samples. The Geonor vane tests were carried out in approximately $\frac{1}{3}$ to $\frac{1}{2}$ of the time to failure of the triaxial tests and thus the strain rate effect (section 2.7.4.) must be considered in any comparison; figure 2.21, which relates to the 3.18 to 3.48m depth range, indicates that the vane strengths may be up to 10% high, thus complicating any direct comparison. Never-the-less at this depth $C_{u.FV(V)}$ and C_{uV1} are nearly identical, whilst above and below it the two values diverge. Figure 3.3(B) shows the variation in plasticity index with depth, the strain rate investigation carried out by Wesley (1975) coinciding approximately with the depth at which the plasticity is a minimum. According to Bjerrum (1972, 1973) the strain rate effect increases with increasing plasticity, as indicated by the correction factor μ (figure 3.3(A)) which is predominantly a rate effect factor (Bjerrum, 1972). Thus $C_{u.FV(V)}$ would be expected to be increasingly closer to C_{uV1} both above and below 3.5m.* The fact that $C_{u.FV(V)}$ is so much greater than C_{uV1} above 3.5m depth, and less than it below this depth, indicates that strain rate effects are not predominantly responsible for the differences.

*Noting that theory (Hansen & Gibson, 1949; see also herein) predicts $C_{u.FV(V)}$ to be less than C_{uV1} .

The variation of the vane shear strength correction factor (μ) (Bjerrum, 1972) with depth for the Mucking site is shown in figure 3.3(B). The maximum variation in plasticity index between the borehole and test pit samples is 15%. The value of μ varies from 0.68 to 0.86, the variation in plasticity index resulting in a range of uncertainty for μ of 0.06 (or 6% of $C_{u.FV(V)}$). All of the vane shear strength profiles have been correspondingly corrected and the corrected values plotted (figures 3.5, 3.6, 3.7 and 3.23), the average strength reduction being about 24%. The corrected average values of $C_{u.FV(V)}$ (i.e. $C_{u.FV(V)} \cdot \mu$) as shown in figure 3.7 can be seen to be everywhere lower than the values of C_{uV1} , particularly below 3.5m depth. Above 3.5m $C_{u.FV(V)} \cdot \mu$ is very close to the values from the piston samples and the average design curve, whereas below 3.5m depth it is substantially (4.5 to 5 kN/m²) lower than both. Thus the corrected field vane undrained strength profile diverges from the laboratory data by a similar amount (although of opposite sign) to the uncorrected version, but over a different depth range. The use of the correction factor certainly does not 'iron out' the tendency for the results from the upper half of the strata to appear high in comparison to those from the lower half, particularly with respect to the proposed field average design curve.

Figure 2.24 also shows the influence of the correction factor μ on the field vane strength in the form of $C_{u.FV(V)} \mu / p_c'$. The range of scatter of $C_{u.FV(V)} \mu / p_c'$ is the least for the three field vane combinations plotted, but not as consistent as C_{uV1} / p_c' . The values of $C_{u.FV(V)} \cdot \mu / p_c'$ in fact straddle line 6 (Skempton, 1957) and curve 4 (Bjerrum, 1973; Mesri, 1975) but are considerably higher than Mesri's (1975) normalised line (5).

(b) Remoulded Strengths

The remoulded shear strength profiles are similar from one location to another, as were the peak strengths, C_{urm} being essentially constant with depth (approximately 3.5 kN/m^2). The Geonor vane is not suited to the measurement of such low shear strength values, and typically underestimates the sensitivity due to frictional influences within the apparatus (Bjerrum, 1973). The calibration of the Geonor vane precluded such frictional effects but even so, as can be seen from figure A.2.3., the apparatus is not suitable for such measurements. As stated in Appendix 2, the use of an average calibration factor may have resulted in errors of about 30% on the high side in the remoulded strength measurements, which although not significant in absolute terms (i.e. only about 1 kN/m^2) will have resulted in an underestimation of the sensitivity recorded by the field vane test.

However a comparison of the average value of C_{urm} from the field vane tests with those from laboratory triaxial, vane and ring shear tests as well as with the ring shear residual value (C_{ur}) for undisturbed material (figure 2.27) shows close agreement between all the data sources (all values being between 2.5 and 3.5 kN/m^2). Such agreement between the peak remoulded strength and the residual strength is typical of the more sensitive clays (Bishop, 1971(a)). The field vane C_{urm} and $C_{u.FV}$ values lead to sensitivity values which are everywhere between 4 and 8. In some instances there is a trend for the sensitivity to increase with the liquidity index (e.g. cross-section A and the test pit), but in other cases, and

for the overall average, the field vane sensitivity is independent of depth and liquidity index. This may be a consequence of apparatus effects as described previously.

The overall average value of S_t from the field vane tests (figure 3.7) is about 5. This independence of liquidity index is in marked contrast to the laboratory values (section 2.7.6. and figures 2.7, 2.23, 2.26 and 3.7) although figure 2.26 shows all the S_t measurements to sensibly follow the relationship, postulated by Bjerrum (1954), between sensitivity and liquidity index. Agreement between laboratory and field vane measurements of the sensitivity of soft clays appears to be better for insensitive clays (Skempton, 1948(b), Skempton and Northey, 1952) than for sensitive clays (Eden and Hamilton, 1957; Bjerrum, 1971). This observation can best be examined by a discussion of the factors influencing sensitivity.

Sensitivity, as defined by Bishop (1971(a)), 'is the ratio of the peak undisturbed strength to the peak remoulded strength and is a measure of the breakdown in structure and change in pore pressure caused by very large strains'. The structural breakdown results in reduced contributions to the strength of its two constitutive components, viz:-

1. The cohesive component which can be sub-divided into:-
 - (a) cohesive bonds which have developed within the soil during its geological history,
 - (b) the void ratio effect of adsorbed water layers.
2. The frictional component.

In a remoulded soil specimen cohesive component 1(b) will be present but not 1(a) and the frictional component may be reduced. Continuous shearing, towards the residual strength value (in the ring shear apparatus, field vane test or under full scale loading conditions), of a natural soil deposit results in reduced, or zero, contributions from the cohesive components and a reduced frictional component.

For soils whose sensitivity is solely the result of consolidation, and whose cohesion derives entirely from source 1(b) above, a unique water content/undrained strength relationship may exist regardless of stress history (Hvorslev, 1960), and likewise an undrained remoulded strength/water content relationship. The sensitivity of such materials is not much affected by stress history (Bishop 1971(a)), and therefore by liquidity index either, and S_t might be in the range 1 to 2. The residual strength on the other hand may be much lower than the remoulded value, and a vane test, after large strains in the undisturbed material, might measure an intermediate value.

Typical soft clays derive their cohesion from sources 1(a) and 1(b) and often have high sensitivities as a result of secondary consolidation, inter-particle bonds and leaching of the pore fluid. In such clays the peak undrained strength may be largely dependent on p_c' and the remoulded strength on the liquidity index. Where leaching is not a major factor (i.e. the clay is not quick) the field vane 'residual'

strength appears to approximate to the laboratory residual and remoulded values, the destruction of the 'cohesive' bonds and generation of positive pore pressures being primarily responsible for the strength loss.

The meta-stable structure of quick clays, which is destroyed by remoulding and during field failures, results in sensitivities which may be one to two orders of magnitude greater than for the normal soft clays described previously. For such materials the field vane does not appear to be able to achieve the measurement of this ultimate residual/remoulded value which is largely consequential upon the very high liquidity indices.

The vane test is always open to question with regard to the state of drainage, and if any consolidation takes place the measured undrained strength will obviously be affected. Partial dissipation of the excess positive pore pressures generated by remoulding, or shearing towards the residual strength value, will result in an increased undrained strength being measured and this could significantly lower the calculated sensitivity in materials with very low peak strengths. A second possibility is that the very narrow failure zone generated in the vane test (Wroth, 1975(a)) may not be representative of the circumstances created by remoulding or a full scale failure.

(c) Test Pit Results Related to Laboratory Tests on Inclined Triaxial, and 'End-On' Plane Strain Tests

The averaged results of the vertical, and the horizontal, vane tests (figure 3.6) carried out adjacent to, and from, the test pit are

presented in table 3.1. where a direct comparison can be made with the overall average values of $C_{u.FV(V)}$ (figure 3.7) and C_{uV1} (figure 3.6 and 3.7). The values of the latter in table 3.1 have been interpolated to coincide with the depths of the test pit Geonor vane tests. The results from the test pit are generally close to the average results, particularly below 3.5m depth, and the comments made in sub-section (a) also apply in this case.

The high $C_{u.FV(V)}$ results above 3.5m depth have been preliminarily discussed, and obviously do not agree with the lower strength on a type 2 plane predicted by the 'end-on' plane strain tests, or the strengths from any of the triaxial tests. However, if attention is confined to the results below 3.5m depth, and in particular to the very consistent (with regards to repeatability, magnitude and overall trend) grouping of results from 3.80 to 4.40m depth a more meaningful comparison with the laboratory results appears possible. The range and mean value of $C_{u.FV(V)}/C_{uV1}$ for this depth range in the test pit have been plotted on figure 3.8(c)* which essentially relates to the depth range 3.78 to 4.08m, although the relationship determined in the laboratory has been shown to apply from 2.58 to 4.68m depth (figure 2.20). The vertical vane test results appear to closely correspond to C_{uV1} and are considerably higher than the 'end-on' plane strain results. If the vane test results are reduced by 10% to correct for the rate effect difference with their laboratory

*the question mark in the figure indicating that there is a contribution from the horizontal plane also.

DEPTH	$C_{u.FV(V)}$ AVERAGE OF ALL RESULTS	C_{uV1}	ISOTROPIC ANALYSES OF TEST PIT RESULTS		ANISOTROPIC ANALYSES OF HORIZONTAL TESTS					
					EQUATION 2.15, $\alpha_v = 0.25$			EQUATION 3.3, $\alpha_v = 0.25$		
			$C_{u.FV(V)}$	$C_{u.FV(H)}$	C_{uV1}	C_{uV}	C_{uH}	C_{uV1}	C_{uV}	C_{uH}
m	kN/m ²	kN/m ²	kN/m ²	kN/m ²	kN/m ²	kN/m ²	kN/m ²	kN/m ²	kN/m ²	kN/m ²
1.35	-	-	16.3	-	-	-	-	-	-	-
1.65	16.5	13.75	15.9	18.0	21.4	18.8	15.7	20.8	18.7	16.6
2.25	18.0	14.75	19.8	17.3	20.6	18.1	15.1	20.0	18.0	16.0
2.45	18.25	15.00	18.3	19.3	22.9	20.2	16.9	22.3	20.1	17.8
2.75	18.75	15.75	20.0	18.8	22.3	19.6	16.4	21.7	19.5	17.4
3.20	18.5	17.00	24.5	21.5	25.5	22.4	18.8	24.8	22.3	19.9
3.50	17.75	17.75	18.6	24.9	29.6	26.0	21.8	28.8	25.9	23.0
3.80	17.50	18.25	18.3	20.0	23.8	20.9	17.5	23.1	20.8	18.5
4.10	17.50	18.50	17.6	18.3	21.7	19.1	16.0	21.1	19.0	16.9
4.40	17.50	19.00	18.5	19.6	23.3	20.5	17.1	22.6	20.4	18.1

Table 3.1. Horizontal and Vertical Geonor Vane Test Results

counterparts, the mean value of $C_{u.FV(V)}/C_{uV1}$ reduces to 86%, approximately equal to C_{uV} from the laboratory tests.* The shear strength mobilised on type 2 failure planes in the vertical vane test thus appears to be more closely related to the type 3 planes associated with the triaxial tests than the type 2 planes in the 'end-on' plane strain tests.

(ii) Horizontal Tests

(a) General

The horizontal vane test results are shown in table 3.1 and figure 3.6, the undrained strength ($C_{u.FV(H)}$) being based on isotropic behaviour (equation A.1.1., with $C_{uV} = C_{uH}$). The differences between the values of $C_{u.FV(V)}$ and $C_{u.FV(H)}$ are not great, the latter also being well in excess of C_{uV1} over the upper part of the clay stratum, and mostly less than the scatter of the results. This obviously makes any confident analysis of the relationship between $C_{u.FV(V)}$, $C_{u.FV(H)}$ and C_{uV1} rather difficult. However, there does appear to be a trend, perhaps better illustrated by the torque difference ratio $\frac{T_{max} - T_{min}}{T_{max}}$ diagram (figure 3.6), for the vertical and horizontal tests to respectively yield higher values of $C_{u.FV}$ in the upper and lower parts of the clay layer.

(b) Analysis Using Anisotropic Undrained Strength Model

As stated previously the cylindrical failure surface for a horizontal vane test is comparable to a typical cylindrical foundation failure

*in sub-section (ii) it is shown that equation 2.15 leads to $C_{u.FV(V)} = 0.98 C_u$ for vertical failure planes and to $C_{u.FV(H)} = 0.80 C_{uV1} = 0.91 C_{uV}$ for vertical $\phi_u = 0$ planes ($C_{uV} = 0.88 C_{uV1}$).

surface, and therefore following on from Lo (1965; see also figure 2.14) it would not seem unreasonable to analyse this failure surface in terms of the undrained strength variation predicted by equation 2.15. However, the assignment of an undrained strength to a particular plane has been shown to imply a particular principal stress vector: whilst this may not be unreasonable in situations where the principal stresses determine the orientation of the failure surface, in cases, such as the shear box and vane tests, where the failure plane orientation is imposed by the testing machine this implicit assumption may be far from valid (see e.g. Morgenstern and Tchalenko, 1967).

Figure 3.8(c) shows the variation in undrained strength of the Mucking clay with inclination of the failure plane from the vertical, predicted by equation 2.15, over 180° . For a horizontal vane test four quadrants may be considered, as in figure 3.8(B), and each failure plane inclination between (and including) 0° and 90° occurs once in each quadrant. Figure 3.8(B) demonstrates by way of 45° planes that there are two active and two passive (figure 3.8(A)) quadrants involved in such a test and therefore that the integration of equation 2.15 (with $\theta = \alpha - 30^{\circ}$) from $\alpha = 0^{\circ}$ to 180° models the laboratory behaviour in the vane test analysis.* This integration may start at point 'W' (figure 3.8(B) and (C)) on a vertical plane ($\alpha = 0^{\circ}$) and involves active shearing to point 'N' on a horizontal plane ($\alpha = 90^{\circ}$) and then passive shearing to point 'E' on the second vertical plane ($\alpha = 180^{\circ}$). The complete component of undrained strength mobilised on the cylindrical surface of a horizontal vane test is obviously twice that obtained from such an integration.

Appendix A.3.1. gives the mathematical derivation of the torque developed in a horizontal vane test (T_{HOR}), in a soil where the

*as the cylindrical surface is assumed coincident with $\phi_u = 0$ conditions the actual distribution is strictly given by $\theta = \alpha - 45^{\circ}$ from $\alpha = 15^{\circ}$ to 195° ; this being mathematically identical to that above.

undrained strength varies with failure plane according to equation 2.15, as follows:-

$$T_{HOR} = \frac{\pi D^2 H C_{uV1}}{2} \left[\left(1 - \frac{a}{2}\right) \left(1 - \frac{b}{2}\right) + \left(1 - \frac{a}{4}\right) \left(1 - \frac{3b}{4}\right) \frac{\alpha_V D}{H} \right] \dots\dots\dots(A.3.1)$$

In common with all the vane test analyses carried out during this reasearch, the analysis assumes that the undrained strength is fully mobilised simultaneously on all planes. For a 65mm (D) by 130mm (H) vane, with a = 0.30 and b = 0.065 (as derived in 2.7.3.):-

$$T_{HOR} = 0.806 C_{uV1} \text{ for } \alpha_V = 0.25 \text{ and}$$

$T_{HOR} = 0.837 C_{uV1}$ for $\alpha_V = 0.33$ where T_{HOR} has units of N.m and C_{uV1} of kN/m^2 . The influence of the anisotropy can be assessed by comparison with the corresponding expressions for an actual, or assumed, isotropic soil (equation A.1.1, with $C_{uV} = C_{uH}$) as follows:-

$$T_{HOR} (=T_{VER}) = 0.971 C_{u.FV(H)} \text{ for } \alpha_V = 0.25 \text{ and}$$

$$T_{HOR} (=T_{VER}) = 1.007 C_{u.FV(H)} \text{ for } \alpha_V = 0.33, \text{ using the same units.}$$

Therefore the results from the isotropic analyses of the horizontal vane tests can be directly related to the anisotropic analyses as follows:-

$$C_{uV1} = \frac{0.971}{0.806} C_{u.FV(H)} = 1.205 C_{u.FV(H)}, \text{ for } \alpha_V = 0.25 \text{ and}$$

$$C_{uV1} = \frac{1.007}{0.837} C_{u.FV(H)} = 1.203 C_{u.FV(H)}, \text{ for } \alpha_V = 0.33 \text{ or}$$

$$C_{u.FV(H)} = 0.830 C_{uV1} \text{ and } 0.831 C_{uV1} \text{ respectively.*}$$

*it will be shown in Chapter 7 that the use of equation 2.15 and the critical $\phi_u = 0$ slip surface produces an average undrained shear strength of $0.82 C_{uV1}$.

The values of C_{uV1} implied by this analysis of the horizontal vane test are presented in table 3.1 for $\alpha_v = 0.25$. The use of $\alpha_v = 0.33$ would reduce the values of C_{uV1} by less than 4%. The values from the vane test are everywhere in excess of those from the laboratory tests, particularly at the higher elevations. Considering the results from 3.80 to 4.40m depth the C_{uV1} values are 17 to 30% higher than those from the laboratory, reducing to a range from 6 to 17%* if a 10% rate effect correction is applied. This suggests that the horizontal vane test may reproduce an undrained strength which represents a weighted average of the anisotropic strength variations, and therefore is compatible with the laboratory triaxial test results.

The analysis can be extended by substituting the derived values for C_{uV1} and θ into equation 2.15 to find the C_u values associated with horizontal ($\theta = 60^\circ$, $\alpha = 90^\circ$) and vertical ($\theta = 150^\circ$, $\alpha = 180^\circ$) planes as shown in table 3.1. The values of C_{uV} are on the whole slightly greater than $C_{u.FV.(V)}$ and for the range 3.80 to 4.80m the difference is +9 to +14%.*

If the vertical vane test is analysed using equation 2.15 to predict the undrained strengths on the vertical and horizontal planes, the torque may be expressed as follows:-

$$T_{VER} = \frac{\pi D^2 H}{2} C_{uV1} \left[\left(1 - \frac{a}{4}\right) \left(1 - \frac{3b}{4}\right) + \left(1 - \frac{3a}{4}\right) \left(1 - \frac{3b}{4}\right) \frac{\alpha_v D}{H} \right] \dots\dots(A.3.3)$$

this expression being derived in Appendix A.3.5.

*both of these sets of data suggest that $C_{uFV(V)}$ is approximately 0.78 C_{uV1} ; now for vertical $\phi_u = 0$ planes $C_u = 0.80 C_{uV1}$ and from the 'end-on' plane strain tests was about 0.65 C_{uV1} .

For a 65mm (D) by 130mm (H) vane, with $a = 0.30$ and $b = 0.065$:-

$$T_{VER} = 0.839 C_{uV1} \text{ for } \alpha_V = 0.25, \text{ and}$$

$T_{VER} = 0.865 C_{uV1}$ for $\alpha_V = 0.33$, where T_{VER} has units of N.m and C_{uV1} of kN/m^2 . Therefore, using the previously derived expressions for an isotropic analysis it follows that:-

$$C_{u.FV(V)} = \frac{0.839}{0.971} C_{uV1} = 0.864 C_{uV1} \text{ for } \alpha_V = 0.25, \text{ and}$$

$$C_{u.FV(V)} = \frac{0.865}{1.007} C_{uV1} = 0.859 C_{uV1} \text{ for } \alpha_V = 0.33$$

Thus, noting that from equation 2.15 $C_{uV} = 0.88 C_{uV1}$, for $\alpha_V = 0.25$, $C_{u.FV(V)} = 0.982 C_{uV}$ and for $\alpha_V = 0.33$, $C_{u.FV(V)} = 0.976 C_{uV}$.^{*} This confirms that for vane tests the strength of type 3 planes will be greater than for type 2 but, as suggested by the earlier comparisons with the laboratory tests, the difference is not as great as suggested by the 'end-on' plane strain tests.

Thus, in conclusion, a theoretical analysis of the horizontal and vertical vane test predicts undrained strengths which are 83% and 86%^{*} respectively, of those for vertical triaxial tests. Using those results considered most reliable, i.e. from 3.80 to 4.40m depth, the inter-relation between the two types of vane test suggests that $C_{u.FV(V)}$ is in fact less than $C_{u.FV(H)}$, and that this is at least partly because of the difference in the C_u values associated with Type 2 and Type 3 shear planes.

The data thus indicate that the results of vertical vane tests require correction for anisotropy, as suggested by Bjerrum (1972 and 1973) and illustrated in figure 3.3. Using the latter the relevant correction factor

*again noting that based on horizontal and vertical $\phi_u = 0$ planes $C_{u.FV(V)} = 0.80 C_{uV1} = 0.91 C_{uV}$.

is 1.08, which if applied to $C_{u.FV(V)} = 0.78 C_{uV1}$ produces an undrained shear strength equal to $0.84 C_{uV1}$; this is in good agreement with the results of the stability analyses (Chapter 7) and the horizontal vane tests.

The simplest assumption regarding the variation of C_u with θ over a single quadrant, from vertical ($\theta = 0^\circ$) to horizontal ($\theta = 90^\circ$) is obviously linear, hence:-

$$C_{u\theta1} = f(\theta, C_{uV1}, x) \text{ where } x = \frac{C_{uH1}}{C_{uV1}} = 1 - a$$

with limiting conditions:-

$$\theta = 0, C_{u\theta1} = C_{uV1}$$

$$\theta = \frac{\pi}{2}, C_{u\theta1} = x \cdot C_{uV1} = C_{uH1}$$

which are satisfied by:-

$$C_{u\theta1} = C_{uV1} \left[1 - \frac{2}{\pi} \theta^r (1 - x) \right]^* \dots\dots\dots(3.3)$$

Figure 3.9 shows a comparison between equations 2.15 and 3.3 over a vertical to horizontal quadrant. The latter predicts undrained strengths which are larger than those predicted by the former over 7/9 of the quadrant. Thus values of C_{uH1} and C_{uV1} calculated from measured vane torques would be lower using equation 3.3.

Similarly to equation 2.15, equation 3.3 can be used to model the variation in undrained strength through a 90° segment (from $\alpha = 30^\circ$ to $\alpha = 120^\circ$) of the horizontal vane test, as shown in Appendix A.3.3.,

*this crude expression was only studied in order to assess the importance of the assumed variation, having determined C_{uV1} and C_{uH1} , on the torque measured in the vane tests.

Leading to:-

$$T_{HOR} = \frac{\pi D^2 H C_{uV1}}{2} \left[1 - \frac{1}{2} (1 - x) + \left(1 - \frac{1}{3} (1 - x)\right) \frac{\alpha_V D}{H} \right] \dots\dots\dots(A.3.2.)$$

Thus for a 65mm (D) by 130mm (H) vane with $x = 0.70$:-

$$T_{HOR} = 0.831 C_{uV1} \text{ for } \alpha_V = 0.25, \text{ and}$$

$T_{HOR} = 0.863 C_{uV1}$ for $\alpha_V = 0.33$, again where T_{HOR} has units of N.m, and C_{uV1} of KN/m^2 . These results may also be related to the isotropic analyses as follows:-

$$C_{uV1} = \frac{0.971}{0.831} C_{u.FV(H)} = 1.168 C_{u.FV(H)}, \text{ for } \alpha_V = 0.25, \text{ and}$$

$$C_{uV1} = \frac{1.007}{0.863} C_{u.FV(H)} = 1.167 C_{u.FV(H)}, \text{ for } \alpha_V = 0.33$$

or $C_{u.FV(H)} = 0.856 C_{uV1}$ and $0.857 C_{uV1}$ respectively.

The values of C_{uV1} , C_{uV} and C_{uH} resulting from this analysis of the horizontal vane tests are presented in table 3.1, with $\alpha_V = 0.25$, for comparison with the results of the previous analysis. The analysis is not particularly sensitive to the change in function describing the variation in C_u with θ , particularly as far as C_{uV} is concerned.

(iii) The 'Undrained Strength Anisotropy' of Vertical and Horizontal

' $\phi_u = 0$ ' Planes in Vane Tests

(a) Previous Investigations

The initial studies by Aas (1965, 1967) on highly sensitive Norwegian marine clays indicated C_{uH}/C_{uV} values most commonly between 1.5 and 2

whereas Weisel (1973) reports values of between 0.68 and 0.8, increasing to greater than unity with depth, for the soft normally consolidated Ska Edeby clay. Results from a 45° diamond shaped vane (Aas, 1967) indicated that the strength of the Norwegian clays dropped steadily from the horizontal to vertical shear surfaces. Menzies and Mailey (1976) used a series of diamond shaped vanes with varying blade inclinations to investigate the variation in undrained strength with shear plane angle of two soft clays of medium plasticity. This comprehensive series of tests again produced maximum and minimum undrained strengths on horizontal and vertical planes, but such that C_{uH}/C_{uV} was approximately 0.5.

The results of these vane test studies are obviously not compatible with the results of the laboratory tests presented previously, for which the maximum strength occurs on a plane at approximately 30° to the vertical.* However, considering the difference in the tests, this is not surprising.

Bjerrum (1973) reported values of C_u measured in the D.S.S. apparatus for samples cut at inclinations such that α varied from 0° to 90°. For each value of α two samples were prepared, both of which were consolidated under the in-situ normal and shear stresses applying to that plane. One sample was then sheared actively and one passively such that a plot of $C_{u\alpha}$ (C_u for a plane at α° to the vertical) versus α could be plotted over 180° similarly to figure 3.8(C). In these

*the $\phi_u = 0$ plane being at 45° to the vertical; in addition the anisotropy depicted in figure 3.8(C), based on equation 2.15, predicts a unique value of C_u for horizontal and vertical $\phi_u = 0$ planes.

tests the maximum and minimum $C_{u\alpha}$ values were generally recorded respectively, at approximately $\alpha = 45^\circ$, active and passive. The strengths on horizontal and vertical planes were thus not maxima or minima. In fact C_{uH} was always greater than or equal to C_{uV} and Bjerrum shows these values to closely correspond to those of Aas (1965, 1967) for the same clays, indicating good agreement between the F.V. and D.S.S. tests. This agreement conveniently ignores the fact that in Aas's tests C_{uH} and C_{uV} were maximum and minimum values, as they were, also in the F.V. tests of Menzies and Mailey (1976). The D.S.S. tests thus do not actually agree with the results of triaxial, plane strain or F.V. tests, which is again hardly surprising in view of the different stress system involved, and the unknown principal stress vectors and true failure plane inclination.

The work of Aas (1965, 1967) and Denness and Green (1971) led them to the conclusion that the variation in undrained strength from the horizontal to the vertical plane was best modelled by an ellipse whereas Menzies and Mailey (1976) employed Casagrande and Carillo's (1944) equation. The laboratory measured variation in undrained strength with the major principal stress direction has been represented by various equations (e.g. Casagrande and Carillo, 1944; Hansen and Gibson, 1949; Bishop, 1966(a); Davis and Christian, 1971). The latter used a number of equations to predict the undrained strength variation of a wide variety of soils. They concluded that only an elliptical variation (their model based on previous work by Hill (1950) and Scott (1963)) and Bishop's (1966(a)) equation (2.15) were satisfactory over the whole range of soil types considered.

(b) Analysis of Results

The direct use of equation 2.15, with $\theta = \alpha$ may thus be considered as an alternative solution in the horizontal vane test analysis as follows:-

$$C_{u\alpha} = C_{uV} (1 - a_{\alpha} \sin^2\alpha) (1 - b_{\alpha} \sin^2 2\alpha) \dots\dots\dots(2.15(A))$$

where a_{α} and b_{α} are constants, with $a_{\alpha} = 1 - \frac{C_{uH}}{C_{uV}}$

Likewise the simple equation 3.3 can be related directly to failure planes as follows:-

$$C_{u\alpha} = C_{uV} \left[1 - \frac{2}{\pi} \alpha^r (1 - x_{\alpha}) \right] \dots\dots\dots(3.3(A))$$

where $x_{\alpha} = \frac{C_{uH}}{C_{uV}} = 1 - a_{\alpha}$

Figure 3.8(C) shows a comparison between the predictions of equations 2.15 and 2.15(A) for the undrained strength variation with failure plane inclination (α) from $\alpha = 0^{\circ}$ to 180° . The two equations represent the same distribution of undrained strength, but are 30° ($90^{\circ} - \beta^{\circ}$) out of phase. Integration of either expression over the range $\alpha = 0^{\circ}$ to 180° thus results in the same average undrained strength, although they represent different values of C_{uV} and C_{uH} .*
 Figure 3.9 can also be used to provide a comparison between equations 2.15(A) and 3.3(A) if α is substituted for θ and planes for principal stress directions.

As shown in Appendices A.3.2. and A.3.4. the use of equations 2.15(A) and 3.3(A) in the analysis of horizontal vane tests leads, respectively,

*also significant is the complete dissimilarity of the C_u distribution on the laboratory $\phi_u = 0$ planes (equation 2.15) to the type of distribution associated with anisotropy studies using the field vane (equation 2.15(A)).

to the following:-

$$T_{HOR} = \frac{\pi D^2 H C_{UV}}{2} \left[\left(1 - \frac{a}{2\alpha}\right) \left(1 - \frac{b}{2\alpha}\right) + \frac{\alpha_V D}{H} \right] \dots\dots\dots(A.3.1(A))$$

and

$$T_{HOR} = \frac{\pi D^2 H C_{UV}}{2} \left[1 - \frac{1}{2} (1 - x_{\alpha}) + \frac{\alpha_V D}{H} \right] \dots\dots\dots(A.3.2(A))$$

In the previous analyses of the horizontal vane tests the representation has included a value of 'a' or 'x'. However, this formulation merely implies maximum and minimum C_u values on horizontal and vertical planes, and that there is a certain variation in C_u with α . In order to solve the two unknowns C_{uH} and C_{uV} an additional equation is required, and is supplied by the formulation for the vertical vane test. This is dependent only on the values of C_{uH} and C_{uV} as can be seen from an inspection of equation A.1.1., which can be rearranged (Appendix A.3.6) as follows:-

$$T_{VER} = \frac{\pi D^2 H C_{UV}}{2} \left(1 + \frac{x_{\alpha} \alpha_V D}{H} \right) \dots\dots\dots(A.3.5)$$

The use of a combination of equations A.3.1(A) or A.3.2(A) and equation A.3.5, to solve for C_{uV} and C_{uH} implies that these two values uniquely apply, irrespective of the direction of shear, and in particular that shear on type 2 planes mobilises a similar undrained strength to shear on type 3 planes. The laboratory data have suggested that this is not so, but under a different stress system to the vane test. The vane test results are variable, but the individual analysis of the horizontal and vertical tests indicates likewise, although the difference would not appear quite so great as indicated by the laboratory tests. The errors

implicit in the combined analysis may thus not be as great as might be thought on first inspection. Nevertheless the combined analysis will predict a value of C_{uV} which is strongly influenced by shearing on type 2 planes.

As is shown in Appendix A.3.6., using equations A.3.1(A), or A.3.2(A) and A.3.5., a relationship between the torsion ratio for adjacent horizontal and vertical tests can be simply related to $x_\alpha = \frac{C_{uH}}{C_{uV}}$, such a relationship being graphically represented by figure 3.10.

(c) Results Related to Those From Analyses of Individual Horizontal and Vertical Tests

Table 3.2 shows values of x_α , C_{uH} and C_{uV} obtained from the combined analyses of the horizontal and vertical tests, incorporating $\alpha_v = 0.25$ and 0.33. The results are influenced by the choice of both α_v and the undrained strength distribution selected for the horizontal tests. In the former instance the influence is not as great as for previous studies using vertical vane tests with various H/D ratios. In the range $C_{uH}/C_{uV} = 0.5$ to 2.0 the maximum variation in C_{uH}/C_{uV} is approximately 14%, and for conditions approaching isotropy is negligible (see figure 3.10). The maximum variation in C_{uH}/C_{uV} , for the same range, due to the combined effects of α_v and anisotropic strength representation is a maximum of 28% decreasing to 10% for an isotropic soil (see Appendix A.3.6).

DEPTH	EQUATION 2.15(A)						EQUATION 3.3(A)					
	$\alpha_v = 0.25$			$\alpha_v = 0.33$			$\alpha_v = 0.25$			$\alpha_v = 0.33$		
	x_α	C_{uV}	C_{uH}	x_α	C_{uV}	C_{uH}	x_α	C_{uV}	C_{uH}	x_α	C_{uV}	C_{uH}
m	-	kN/m ²	kN/m ²	-	kN/m ²	kN/m ²	-	kN/m ²	kN/m ²	-	kN/m ²	kN/m ²
1.65	1.56	15.0	23.4	1.63	15.8	25.8	1.46	15.1	22.1	1.50	14.8	22.3
2.25	0.70	20.5	14.3	0.66	20.8	13.7	0.64	20.6	13.2	0.59	21.0	12.4
2.45	1.28	17.7	22.7	1.29	17.6	22.7	1.16	18.0	20.9	1.19	17.8	21.2
2.75	0.90	20.2	18.2	0.90	20.3	18.3	0.83	20.4	16.9	0.80	20.6	16.5
3.20	0.70	25.3	17.7	0.66	25.8	17.0	0.64	25.5	16.3	0.59	26.0	15.4
3.50	2.30	16.3	37.4	2.60	15.1	39.4	2.15	16.5	35.5	2.38	15.5	37.0
3.80	1.43	17.5	25.0	1.48	17.1	25.3	1.31	17.7	23.2	1.36	17.4	23.7
4.10	1.20	17.2	20.7	1.20	17.1	20.5	1.10	17.4	19.2	1.11	17.3	19.2
4.40	1.30	17.9	23.3	1.34	17.6	23.6	1.20	18.1	21.7	1.23	17.9	22.0

Table 3.2.

Values of C_{uV} and C_{uH} From Anisotropic Analysis of Horizontal and Vertical Geonor Vane Test Results

The results in table 3.2 show, as would be expected, that although the various combinations of α_v and undrained strength distribution lead to some variation in x_α the values of C_{uv} are very similar in each case. The C_{uv} values are generally lower than predicted by the horizontal vane test alone,*and slightly lower than the values of $C_{u.FV(V)}$ which they closely approximate to.

The C_{uh} values which evolve from the combined analysis are completely different to those from the horizontal test, the analysis of which involved the prior assumption of C_{uh}/C_{uv} .* The combined analysis leads to C_{uh}/C_{uv} values which are both greater and less than unity. The values from 3.80 to 4.40m depth are again very consistent and all exceed unity, whereas there is a tendency for values less than unity to occur at higher elevations (e.g. 2.25, 2.75 and 3.25m depth). This is illustrated by the tendency for the horizontal tests to record higher torques than the vertical at increasing depths (figure 3.6).

(d) Strengths on Planes Related to In-Situ Stresses

Aas (1967) concluded that the ratio C_{uh}/C_{uv} was closely linked to the in-situ vertical and horizontal effective stresses, whilst Kenney and Landva (1965) performed laboratory vane tests on isotropically and anisotropically consolidated samples which indicated that K_0 influenced the measured value of $C_{u.FV(V)}$. On the other hand the laboratory tests have shown (section 2.7.2) that for the Mucking clay C_u is not much affected by variations in the initial stress state below p_c' . If the vane strength is influenced by the in-situ effective stresses, this may be a cause of discrepancy between the laboratory and field vane data.

*noting that in this analysis the planes are $\phi_u = 0$ planes, whereas previously the undrained strengths associated with vertical and horizontal failure

In order to investigate this aspect a simple analysis was carried out using two sets of results from the combined horizontal and vertical vane test analyses. The most consistent set of results throughout has been that from 3.80 to 4.40m depth, and this was considered first. Using equation 2.15(A) and $\alpha_v = 0.25$ leads to an average C_{uH}/C_{uV} of 1.31, with $C_{uV} = 17.5 \text{ kN/m}^2$ and $C_{uH} = 23.0 \text{ kN/m}^2$. A second, less obvious and less consistent, grouping is for the tests between 2.25 and 2.75m depth. The results at 1.65 and 3.20m depth were not considered because of their greater scatter, and also to enable the average C_{uH}/C_{uV} to be related to a relatively small depth range in both cases ($\pm 300\text{mm}$ from an average of 4.1m previously). Those tests ($\pm 250\text{mm}$ from an average of 2.5m depth) produced a larger range of C_{uH}/C_{uV} (0.70 to 1.28 with an average of 0.96) but reflect the measurement of values less than unity at the higher elevations. The actual values of C_{uH} and C_{uV} were, respectively, 18.7 and 19.5 kN/m^2 . For both the sets of data considered the variations in measured torque were relatively small (figure 3.6).

The results are summarised in table 3.3 together with an approximate analysis to determine the initial vertical and horizontal effective stresses. The analyses are based on the assumption that the shear strengths on horizontal and vertical failure planes are respectively given by the Mohr-Coulomb failure criterion as follows:-

$$\tau_{uH} = c' + \sigma_{Hf}' \tan \phi' \dots\dots\dots(3.4)$$

$$\tau_{uV} = c' + \sigma_{Vf}' \tan \phi' \dots\dots\dots(3.5)$$

where σ_H' and σ_V' are the normal effective stresses on horizontal and vertical planes respectively, 'f' denoting at failure and 'i' (table 3.3) denoting initially.*

The effective stress parameters for the soil were defined in section 2.7.5 and were shown not to be significantly anisotropic. Using $\phi' = 25^\circ$, σ_{Hf}' and σ_{Vf}' have been calculated from τ_{uH} and τ_{uV} respectively, as presented in table 3.3, and σ_{Hi}' being known the pore-pressure change (Δu_f) pertaining to the horizontal plane can be evaluated. The undrained strength anisotropy of the Mucking clay is partly the result of the pore pressures generated during shear, and the excess pore-pressure distribution created by a vane test may be, locally, complex. In order to evaluate σ_{Vi}' it has been assumed that Δu_f applies to both the planes considered.

The calculations show that the value of c' chosen does not affect the predicted values of σ_{Vi}' or K_0 but varies the value of Δu_f . In both cases the predicted pore-pressure changes are negative, the smallest changes being associated with the higher values of c' , which are closer to those predicted by back-analysing the trial embankment failures (Chapter 7). These smaller pore-pressure changes are also more compatible with the magnitudes observed in the laboratory

*It is generally assumed, and has been herein, that the F.V. shear strength is C_u , and not $C_u \cos \phi'$ as proposed by Hansen and Gibson (1949). In the above analyses τ_u associated with horizontal and vertical failure planes was derived from the relevant $\phi_u = 0$ planes using the assumed variation as defined by equation 2.15(A).

Data Set	A			B		
Depths m	3.80	4.10	4.40	2.25	2.45	2.75
Average depth m	4.10			2.50		
c_{UH}/c_{UV}	1.31			0.96		
τ_{UV} kN/m ²	16.0			17.3		
τ_{UH} kN/m ²	20.0			16.7		
$\sigma'_{Hi} = P'_o$ kN/m ²	29.1			20.8		
C' kN/m ²	0	3	6	0	3	6
σ'_{Hf} kN/m ²	42.9	36.5	30.0	35.8	29.4	22.9
ΔU_f kN/m ²	-13.8	-7.4	-0.9	-15.0	-8.6	-2.1
σ'_{Vf} kN/m ²	34.3	27.9	21.4	37.1	30.7	24.2
$\sigma'_{Vi} = K_o P'_o$ kN/m ²	20.5			22.1		
K_o	0.70			1.06		
$K_o (P'_o = P'_{o \max})$	0.58			0.85		
$K_o (P'_o = P'_{o \min})$	0.77			1.11		

Table 3.3.

Undrained Strengths on Horizontal and Vertical Planes, As Derived From Field Vane Tests, Related to In-Situ Stresses

tests. The σ_{Hi}' values were based on figure 2.13 but with the G.W.L. at 750mm depth. The vane tests were carried out in the early part of 1973, for which no piezometric levels were available. Consideration of $P'_{o \max}$ and $p'_{o \min}$ does not greatly influence the predicted values of K_0 (see table 3.3) although the implied negative pore-pressure changes are respectively lesser and greater than those reported.

The K_0 values obtained have been plotted in figure 2.13 and sensibly follow the trend of light overconsolidation predicted by the laboratory data. Whilst it is not suggested that the vane test can be used as a method of predicting K_0 , the results of this analysis tend to support the observations of previous workers (e.g. Aas, 1967) that the strengths on horizontal and vertical planes, and thus the overall average strength, measured in vane tests may be closely related to the in-situ principal stresses on these planes.

If the data in table 3.1., relating to the anisotropic analysis of the horizontal vane tests on the basis of the laboratory measured undrained strength anisotropy, are examined similarly to that in table 3.3, K_0 values of 1.33 and 1.24 are obtained for 2.50 and 4.10m depth respectively. Thus the hypothesis that the strength measured in the vane test is dependent on the in-situ normal stresses acting on the shear planes, demands undrained strength anisotropy of the kind depicted by equations 2.15(A) and 3.3(A), as might be expected.

(iv) Conclusions From, and Uncertainties Remaining After the Performance and Analysis of, the Geonor Vane Tests

The main points arising from the vane test data may be conveniently summarised as follows:-

(1) An accurate calibration of the Geonor vane apparatus is essential, particularly when it is to be used in very soft clays. The equipment is not really suitable for the measurement of very low remoulded strengths, the calibration curve for the particular vane used indicating an overestimate of C_{urm} and hence an underestimate of S_t . This may be a particularly important factor for very sensitive clays.

(2) The undrained strength/depth profile obtained from the vertical vane test results was very similar over the whole site. There is, however, considerable scatter in the results which, nevertheless, become more consistent with depth. Where slightly higher undrained strengths (overall) were recorded with the vane greater mobilised full scale field strengths were implied by the observed failures (Chapter 6).

(3) The Geonor vane tests predict substantially higher undrained strengths than the laboratory tests over the first 3m or so of the soft clay layer. Below this depth the vane test results approximate to the laboratory design profile and are thus lower than those from the vertical triaxial samples. The values of $C_{u.FV(V)}$ appear to be independent of p'_c , although the ratio of these two values becomes more consistent with depth.

(4) The average time to failure in the Geonor vane tests was $\frac{1}{3}$ to $\frac{1}{2}$ of the laboratory values; laboratory studies indicate that this may result in vane strengths up to 10% higher than their laboratory counterparts.

(5) The value of Bjerrum's (1972) correction factor μ is between 0.68 and 0.86 for the Mucking clay. This implies that the full scale field undrained strength is between 68 and 86% of the field vane strength. Correction of the Geonor vane test results does not appear to rationalise them with respect to the laboratory data, which are also influenced by strain rate.

(6) The measured values of $C_{u.FV(V)}$ below 3.5m depth suggest that the undrained strength corresponding to Type 2 planes in the F.V. test is lower than that corresponding to Type 3 planes in the laboratory, but not as low as that corresponding to Type 2 planes in the laboratory.

(7) Isotropic analyses of the horizontal and vertical vane tests show a tendency for the latter to measure higher C_u values in the upper part of the clay, while at depth the reverse is true.

(8) Two analyses were carried out, in terms of anisotropic undrained strengths, using the results of horizontal and vertical tests.

(a) Separate analyses of the results of the horizontal and vertical tests, based on the laboratory variation of undrained strength with failure plane inclination, suggest that for the more consistent vane

test results in the lower half of the clay layer both types of test were compatible with this assumption if strain rate effects are taken into consideration. Whilst theory predicted undrained strengths which were 83% ($C_{uFV(H)}$) and 80% ($C_{uFV(V)}$) of C_{uV1} the data suggest that $C_{uFV(V)}$ may be about 0.78 C_{uV1} . After correction for anisotropy (Bjerrum, 1973) this latter figure was in good agreement with the data from the stability analyses and with $C_{uFV(H)}$.

(b) Analyses of the combined results of the horizontal and vertical vane tests, based on the very different assumption that the shear strengths measured on the horizontal and vertical rupture surfaces are maximum and/or minimum values, were used to predict the degree of undrained strength anisotropy. Further analysis, assuming that the measured shear strengths are directly related to the effective normal stresses led to values of the in-situ lateral effective stresses which appear acceptable for a lightly overconsolidated clay. The latter analysis was in fact similar in logic to that performed by Hansen and Gibson (1949) (using Skempton's (1948(e)) ' λ theory'), who also considered the vane shear strength as equal to $C_u \cos \phi'$. If the vane tests in general were analysed on this basis, with $\phi' = 25^\circ$, then the true undrained strength would be 1.10 $C_{u.FV}$, where $C_{u.FV}$ is derived directly from equation A.1.1. as previously.

The two different approaches to the incorporation of undrained strength anisotropy in vane test results predict similar values of C_{uV} , but very different values of C_{uH} , the basic assumptions

in each analysis being more important than the type of undrained strength variation used therein. Hansen and Gibson's (1949) analysis interestingly predicted that for a typical British post-glacial clay the ratio $(\sigma_1 - \sigma_3)f.FV(V)/(\sigma_1 - \sigma_3)f.TC$ would be 0.89 and therefore that $C_{u.FV(V)}/C_{u.TC}$ would be 0.80. Thus, in common with the methods used, this analysis also predicts that the average shear strength measured in a vertical vane test may be significantly influenced by undrained strength anisotropy and, therefore, that allowance should be made for this factor when using the results in stability analyses. This view point is supported by Berre and Bjerrum's (1973) observation that corrected vane test results are generally close to the average undrained strength from T.E., D.S.S. and T.C., tests.*

The main uncertainties may be briefly summarised as follows:-

- (1) What is the cause of the high C_u values, and considerable scatter, recorded in the upper 3m of the clay layer?
- (2) Are the more consistent vane test results obtained in the lower 3m of the clay representative?
- (3) Is the rate effect for the vane test the same as indicated by the laboratory tests? Parry 1971(a) considered not, due to the different strain conditions in the two types of test.
- (4) The answers to questions (2) and (3) will influence the confidence with which the conclusions on vane test anisotropy can be regarded.
- (5) The vane test, and laboratory sample sizes are reasonably compatible, but are the vane test results sample size independent?

*noting that the anisotropy correction to $C_{u.FV(V)}$ is small and that the laboratory data will also require correction for strain rate effects.

(6) Is Bjerrum's (1972) correction factor (μ) valid in this case, and if so what factors is it accounting for?

(7) Does the standard field vane test result in the measurement of a shear strength which is truly undrained? Near surface vane strengths up to 20% higher than the laboratory triaxial values were measured in a varved clay (Lo and Stermac, 1965) and attributed to dissipation of pore pressures (Townsend, 1965). Varved clays are obviously a special case, but many soft clays have fabrics which permit rapid drainage at low in-situ effective stresses (Rowe, 1968, and 1972(a) and (b)).

(8) What is the undrained strength profile that would be used in design, based on the vane test results and having considered all the influencing factors?

3.3. Tests Carried Out with a New Large Vane Apparatus

3.3.1. Introduction

The large vane test was conceived in the hope that it might resolve some of the previously listed uncertainties raised by the results of the Geonor vane tests. It was also hoped to further investigate the relationship between field vane and laboratory measurements of undrained strength. In particular the high undrained strengths measured using the Geonor vane, as opposed to the laboratory triaxial apparatus, above 3.5m depth could be attributed to:-

(1) High lateral stresses resulting from overconsolidation.

(2) The fact that the shear surfaces in a vane test are predetermined, whereas the laboratory sample may fail on preferential shear surfaces (determined by the structure and fabric of the soil).

(3) Partial dissipation of excess pore-water pressures, generated by the insertion of the vane and/or during shear.

This latter factor particularly, together with the field vane strain rate effect, has received little attention to date. Bjerrum (1972) has suggested that the rate of undrained loading is the major factor causing discrepancies between field vane and back-analysed undrained strengths, particularly in plastic clays, with anisotropy and progressive failure being factors of secondary importance (Dascalescu and Tournier, 1975). However, the conditions of drainage under which a standard field vane test is carried out are somewhat uncertain and it is instructive at this point to consider the stresses and strains associated with the test.

A simple elastic analysis can be carried out, assuming the vane to be a rigid cylinder having the same diameter as the vane and extending axially to infinity, the clay adhering to the surface of the cylinder. Cadling and Odenstad (1950) carried out such an analysis, and also performed tests which showed that the rigid body motion, assumed therein to represent the clay within the circular section defined by the vane blades, was not unreasonable. As shown in Appendix 5 the simplified analysis leads to equation A.5.1. as follows:-

$$\tau_r = \frac{r_0^2}{r^2} \tau_0 \dots\dots\dots(A.5.1.)$$

where τ_0 is the mobilised shear stress at a distance from the vane centre equal to its radius, r_0 , and τ_r is the mobilised shear stress at a radial distance, r . The analysis can be extended, as shown in Appendix 5., to express the shear strain (γ_r) as a function of the angle subtended at the vane's centre (ω), as follows:-

$$\omega = \frac{1}{2} \frac{r_0^2}{r^2} \gamma_r \dots\dots\dots(A.5.2.)$$

and therefore the shear strain at the vane circumference (γ_0 , $r = r_0$) as a function of the vane's rotation (ω), as follows:-

$$\omega_0 = \frac{1}{2} \gamma_0 \dots\dots\dots(A.5.3.)$$

Equation A.5.3. leads directly to a definition of the shear modulus in terms of the vane's angular rotation and the mobilised shear stress for an elastic soil:-

$$G = \frac{\tau_0}{2\omega_0} = \frac{\tau}{2\omega} \dots\dots\dots(A.5.4.)$$

Equations A.5.1. and A.5.2. show that, for a particular vane size, the radial distance (r) from its centre at which a particular value of shear stress (τ_r), shear strain (γ_r) and angle subtended at the vane's centre (ω) occur are directly related to the vane's radius (r_0).

As the shear strain (γ_0) and shear stress mobilised (τ_0) in an elastic soil are directly related to the vane's angular rotation ($\omega_0 = \omega$), and not to its dimensions, it follows that the stress gradient set up is directly related to the vane's radius. Thus for two vanes, the diametric ratio of which is 2:1, the radial distance over which the soil is stressed to a particular level will also be in the ratio 2:1.

In order to investigate the undrained strain rate effect in the field vane test it is necessary to stress a soil sample of such a size that minimal drainage occurs during the test. The vane size (254mm (D) x 508mm (H)) selected was such that the linear dimensions were approximately 4 x (3.908 to be exact) those of the Geonor vane used. Considering drainage to occur radially outwards into the soil, consolidation time being proportional to the square of the drainage path length, it should be possible to carry out a test with the large vane approximately 16 x more slowly than with the Geonor vane, the same amount of consolidation occurring in both tests. Therefore, if the 5 minute vane test is the upper time limit for an undrained Geonor vane test (Cadling and Odenstad, 1950) the large vane equivalent would be 80 minutes.

The conditions of stress and drainage relating to a vane test are doubtless more complex than assumed in the preceding discussion.

In particular, for the Mucking clay drainage may be predominantly in the vertical direction, and in general may also take place radially inwards towards the centre of the vane. However, as the height and diameter of the large vane are both 4 x greater than for the Geonor vane, the drainage paths in these directions are also correspondingly longer as will be the increase in consolidation time.

The new apparatus would not be able to separately investigate factors (1) and (2), outlined previously, which should similarly influence the results obtained with both large and small vanes, having the same geometrical configuration and H/D ratio. The laboratory test program did not reveal any sample size effects (section 2.7.4) and on this basis it seemed unlikely that this would be a major factor in a comparison of the results from the Geonor and large vane tests. However the largest laboratory samples tested were 102mm diameter and it was thus possible that the larger volume of soil tested could be advantageous in measuring a more representative undrained strength, bearing in mind the inherent non-homogeneity of the deposit.

The two major initial decisions to be made, regarding the design and construction of the large vane, were the type of vane apparatus and the type and size of vane. Practical considerations led to the selection of a borehole vane, and as direct comparisons were to be made with Geonor vane test results, a standard cruciform

shape was adopted, with $H/D = 2/1$. The selected dimensions were particularly convenient for use in conjunction with a 305mm (12 ins) diameter cable tool boring. It will by now have been noted that the design was carried out in Imperial units, this being because the existing components utilised, particularly the drilling equipment, were manufactured under that system.

The adoption of the cable tool as a boring method in preference to a flight auger (which might be expected to cause less soil disturbance), was based largely on the adaptability of the former for use with the in-situ vane test. In particular the large working space around the borehole, plus the lifting and jacking capabilities of a small cable tool rig were considered very desirable. Such rigs also enable conventional sampling, and plate loading tests, to be carried out in conjunction with vane tests, and are of course readily available. Experience with flight augers at the Mucking site had shown that it was not easy to achieve a 'clean' borehole and therefore that a lined borehole was necessary.

Having decided to operate the vane apparatus from a lined 305mm cable tool boring, the borehole lining could be used to provide partial or total reaction to the torque applied to the vane. In line with the approach of using readily available commercial site investigation equipment and techniques, the obvious choice for drive rods was some form of standard rotary core drilling rods. Finally, as the principal object of the exercise was to investigate strain rate effects, a motorised drive system was essential. Details of the design, (figure 3.11)

construction, testing and calibration of the large vane apparatus are given in Appendix 4.

3.3.2. Testing Program

In order to avoid the main area of disturbance below the boring, the vane was advanced 1.422m (4ft. 8ins) into the ground at the base of the borehole, thus placing the top of the vane 914mm (3ft) (i.e. three diameters of the boring) below the borehole base, as suggested by Cadling and Odenstad (1950). To enable the performance of as many tests as possible within the 6m thick soft clay layer, the borehole was not advanced to the lowest level of the previous test before reinserting the vane. Instead, the borehole was advanced by 1.117m (3ft. 8ins), thus leaving 305mm (1ft) of disturbed clay below the base of the borehole. When advanced to its new position the top of the vane was therefore 609mm (2ft) below the level of its base in the previous test. In this way 508mm high x 254mm diameter samples could be tested with only 609mm separating them (figures 3.12 and 3.17) and, hopefully, without any additional disturbance at the test locations.

This testing sequence permitted four large vane tests to be carried out per borehole in the soft clay, as illustrated in figure 3.12, the testing sequence being identical for all the boreholes. The need for the borehole to be cased from the start limited the first vane test to a minimum average depth (i.e. the depth to the mid-height of the vane) of 1.956m, this depth only being achieved by

the use of a special short (864mm) length of casing. All the other casing lengths were 'standard' and, as shown in figure 3.12, their use necessitated that a short length at the base of the borehole be unlined in some instances.

Nine borings were sunk at the locations indicated in figure 2.3 and therefore 36 large vane tests were performed, of which 35 were successfully concluded. At each of the four test levels (figure 3.12) a series of tests was carried out using different rates of applied angular rotation. Three tests were carried out at what was denoted the standard rate (1.81° per minute, using gear 2; Appendix 4., table A.4.3.), two tests at each of 5 x slower (gear 3) and 25 x slower (gear 4) than standard and one test at each of 5 x faster (gear 1) and 125 x slower (gear 5) than standard. In addition, following the measurement of a peak torque in tests carried out at the two slower rates, the load was removed and a reloading test carried out at the fastest rate. These tests were denoted rapid reloading tests. No attempt was made to directly measure the remoulded strength as in the Geonor vane tests, but tests carried out at the standard and fastest rates were continued post-peak until the jack reached the end of its travel.

In order to measure the rod friction component of the applied torque two tests were performed (at test levels 2 and 4) with the drill rods only, these being advanced 914mm beyond the base of the borehole.

From the results of these tests it was also possible to approximately determine the remoulded strength. Finally, four Geonor vane tests were carried out adjacent to the large vane test boreholes (figure 2.3) so that as direct a comparison as possible could be made between the results from the two types of vane test.

3.3.3. Testing Procedure

With the rig set up, the borehole was advanced to its first depth and the short length of casing installed. Great care was taken to ensure that the initial line and position of the borehole was correct in order to avoid any problems when positioning the vane. At this point the reaction members for the jacking operations were installed, these being held down by two 500mm diameter helical auger type pickets installed to 2m depth. The reaction members were installed close to the borehole so that the flanges of the casing clamps reacted against them and thus further resisted any tendency for the casing to rotate under the torque applied by the loading frame (plate 3.1). They were positioned to run at right angles to the rig so that timbers could be lain between them, providing a working surface for the location of the loading frame, drive frame and generator, as well as leaving maximum working space around the apparatus.

The vane, plus the appropriate lengths of N W drilling rods and the drive rod (all fully tightened) were then lowered into position using the rig, the lifting swivels etc., used with the piston sample jacking equipment all being N W threaded. This operation was carefully

carried out, to ensure that the vane was vertical, and centrally positioned, within the borehole, although the care taken during the drilling process ensured that it was achieved without any difficulty. Before the vane was jacked into position the uppermost N W drilling rod was always above the level of the hanger head so that the borehole top plate could not be positioned. In order to ensure the vane's verticality during jacking, a wooden borehole top plate, with a central 66.675mm diameter hole, was placed in the hanger head. The 'T-piece', ropes and pulleys comprising the jacking equipment were then assembled and connected to the drive rod and reaction members (plate 3.1) and the vane jacked the 1.422m to the test position. The mechanical advantage of the jacking system can be seen to have been 4, and with 4 people on the ropes the vane was successfully jacked into position on all occasions, and generally (although not always) without undue effort. Assuming the remoulded strength to act on the faces of the vane blades a jacking load (deriving from skin friction only) of 1.30 kN (290 lb.f) would be required and thus only 80N (18lb.f) per person. If the peak strength were mobilised these loads would increase approximately 5 times (average S_t) and thus the effort actually required for jacking suggests that the remoulding edge of the vane was fully effective.

With the vane in position the loading frame could be positioned, the apparatus set up and the test carried out as described in Appendix A.4.7. The electric motor was powered by a portable, petrol driven 3kW generator (plate 3.1.)

During the drilling operations the boreholes were kept full of water in order to at least partially maintain the previous in-situ stress levels at their bases (particularly the vertical total stresses; see e.g. Hansen and Gibson, 1949). Before positioning the borehole top plate the borehole was finally topped up with water prior to the test being performed. Upon completion of the test the apparatus was dismantled and the vane pulled clear using the drilling rig. A considerable amount of clay was generally found to have adhered to the vane blades, this being cleaned off before further use. The adhesion of clay to the vane blades during advancement must increase the disturbance caused, especially where a number of vane tests are carried out from one borehole level (Flaate, 1966).

The borehole was then advanced to the next level and the test procedure repeated. Disturbed samples were taken from the borings and used for the determination of gradings and index properties, as described in Chapter 2. The boreholes were logged in detail and continued until the gravel layer was encountered. A borehole was only advanced to a new depth if a vane test was to be performed immediately afterwards. Having advanced the borehole the vane was inserted, the apparatus assembled and the test started as soon as practicable. Thus a vane test comprised a complete operation of drilling, installation, assembly and testing, the operation up to the start of the test taking about an hour. The time delay between advancing the vane into position and commencing the test was about 15 minutes and therefore considerably longer than for the Geonor vane test.

No major problems arose during the performance of the tests, mainly due to the thorough proving tests carried out beforehand. The site work was carried out in mid-winter when conditions were very wet and muddy, the components of the apparatus needing frequent washing down; oiling and greasing of the moving parts was also carried out at least once per borehole. The proving ring dial gauge was not well suited to site conditions and, although protected as far as possible it stuck on one occasion, resulting in the loss of a test, as mentioned previously. For any future use of the large vane apparatus a suitable all weather dial gauge would be an improvement.

The Geonor vane tests were carried out in the manner described previously, advantage being taken of the spare time available during the very slow large vane tests and the rig moves, to perform them. The crew of the rig very soon became accustomed to the large vane apparatus, and the associated boring and testing procedure, and were able to rapidly advance the boring and set up the equipment unaided. Close supervision of both of these activities was, of course, maintained and the tests themselves performed by the writer and Mr. A. J. Reid of Binnie and Partners. The 36 large vane tests and 4 Geonor vane test probings were carried out in a four week period, the rig operating on an 8 hour day under winter conditions. By carrying out tests at different rotation rates at the various levels in the same borehole, rig standing time was kept to a minimum. The slower tests

were carried out, to a large extent, outside of normal working hours and the very slow ones involved the vane apparatus being operational throughout the night.

A better overall field performance of the new equipment could not have been hoped for. On the basis of the site work it is anticipated that 6 large vane tests could be performed at the standard testing rate, starting from ground level, in a full working day. Ideally future use of the apparatus could be combined with large diameter piston sampling and plate bearing tests all being performed in the same borehole.

3.3.4. Test Results

The results from the series of large vane tests are presented in table 3.4., wherein it can be seen that the times to failure ranged from just over 1 minute to 1260 minutes, with the standard rotation rate of 1.81° per minute producing failure times between 5.5 and 13.25 minutes. Inspection of the results reveals that the repeatability at a particular level and rotation rate is very good. For example, the 3 standard rate tests performed at each level exhibited maximum and average scatters of 2.1 kN/m^2 (i.e. ± 1.05) and 1.37 kN/m^2 respectively. The times to failure are likewise very consistent for each grouping. The mobilised shear stresses and angular rotations were all calculated as described in Appendix A.4.7. (iii).

During the performance of the tests readings were taken at 0.25, 0.5, 1, 5 and 30 minute intervals respectively for the five rotation rates from fastest to slowest, enabling the mobilised shear stress to be plotted against angular rotation for each test, as in figures 3.13 to 3.16. Where more than one test was conducted the results have been normalised to produce an average stress-strain curve. Also shown in the figures is the rod friction component of the shear stresses plotted, this being on average about 0.25 kN/m^2 , and mobilised at very small strains. From the rod friction tests the remoulded strength can be calculated (this being very approximate as maximum readings of the order of 10 dial divisions were recorded), giving a value of 3 kN/m^2 which is in excellent agreement with the previously discussed results from the laboratory, and Geonor vane, tests.

The averaged results from each test level and rotation rate are presented in table 3.5., the maximum shear stresses having been corrected for rod friction (as are those in table 3.4), and some of the angular rotations at failure (ω_f) for bedding errors. These latter errors resulted from there being some initial slack in the loading system and only occurred on two occasions (figures 3.15 and 3.16). As the test procedure largely eliminated such possibilities from the main loading system, these errors are probably due to final tightening of the drive rod (which could not be tightened with the wrenches for fear of damage) onto the uppermost drilling rod. The results of the rapid reloading tests are presented in table 3.6., together with the results of the initial slow tests for comparison.

Level No. (Depth Range and Average)	Displacement Rate of Jack	Maximum Shear Stress T_{max}	Angular Rotation At Failure, ω_f	Time to Failure t_f
metres	mm/minute	kN/m ²	degrees	minutes
1 (1.702-2.210, 1.956)	24.13	17.62	12.54	1.67
	4.826	13.47+ 14.10 13.19	4.43+ 21.91 8.97	3.5+ 13.25 6.00
	0.965	18.36 18.47	10.77 16.92	37.0 54.0
	0.193	13.19 10.70	8.96 11.47	150 180
	0.039	13.39	9.50	780
2 (2.819-3.327, 3.073)	24.13	13.81	10.73	1.40
	4.826	11.06 13.16 12.32	8.29 10.32 10.92	5.50 6.75 7.00
	0.965	15.01 13.13	14.90 10.05	47.0 33.0
	0.193	17.82 16.62	13.93 14.61	228 235
	0.039	13.13	11.27	930
3 (4.140-4.648, 4.394)	24.13	15.45	7.81	1.25
	4.826	15.81 13.87 14.67	- 6.39 12.05	9.50 5.25 8.50
	0.965	13.90 13.22	5.94 7.18	25.0 28.0
	0.193	14.45 13.48	7.51 7.41	150 145
	0.039	14.39	7.63	750
4 (5.257-5.765, 5.511)	24.13	17.72	19.45	2.75
	4.826	15.68 16.94	13.19 16.39	10.00 12.00
	0.965	14.97 15.19	11.93 13.05	46.0 49.0
	0.193	16.94 14.32	12.56 7.16	245 160
	0.039	17.30	13.03	1260

†reloading test after unloading from just below maximum shear stress indicated

Table 3.4 Results Summary For Large Vane Tests

Level No. (Depth Range and Average)	Displacement Rate of Jack	Maximum Shear Stress τ_{max}	Angular Rotation at Failure, ω_f	Time to Failure t_f
metres	mm/minute	kN/m ²	degrees	minutes
1 (1.702-2.210, 1.956)	24.13 4.826 0.965 0.193 0.039	17.62 13.59 18.42 11.95 13.39	12.54 15.44 ⁺ 13.85 10.22 9.50	1.67 9.63 ⁺ 45.5 165 780
2 (2.819-3.327, 3.073)	24.13 4.826 0.965 0.193 0.039	13.81 12.18 14.07 17.22 13.13	10.73 9.84 12.48 14.27 11.27	1.40 6.42 40.0 231.5 930
3 (4.140-4.648, 4.394)	24.13 4.826 0.965 0.193 0.039	15.45 14.78 13.56 13.97 14.39	7.81 9.22 ⁺ 6.56 7.46 6.83 Δ	1.25 7.75 26.5 147.5 750
4 (5.257-5.765, 5.511)	24.13 4.826 0.965 0.193 0.039	17.72 16.31 15.08 15.63 17.30	16.15 Δ 14.79 12.49 9.86 13.03	2.75 11.00 47.5 202.5 1260

+ 2 tests only (out of 3) considered

Δ corrected for initial bedding errors

Table 3.5

Large Vane Tests: Results Averaged for Each Strain Rate At Each Depth

The results from the 4 Geonor vane tests are presented in table 3.7., together with average values of $C_{u.FV}$ and times to failure (t_f). The individual values of t_f only vary between 2.5 and 8 minutes, but there is considerable scatter in the shear strengths at each location (figure 3.17). As with the previously reported results, this scatter decreases with depth and in addition appears to be related to t_f (figure 3.22). The scatter in these latter values also decreases with depth.

A comparison of the Geonor vane test results with the average values for the whole site (figure 3.17) shows the former to be close to, but slightly less than, the latter. An initial comparison between the results from the large and Geonor vane tests, therefore, reveals a greater consistency in the measured shear strengths for a particular range of failure times, for the former. This appears to be because the shear strength measured in the Geonor vane tests is more sensitive to small changes in the failure time, particularly at the shallower depths, although the influence of sample size cannot be discounted.

An initial comparison between the large vane test shear strengths and those from the laboratory, and Geonor vane, tests is presented in figure 3.18. This shows that much lower strengths were obtained from the large vane tests than from the Geonor vane tests and laboratory triaxial tests on vertical samples.

Level No. (Depth Range and Average)	Displacement Rate of Jack	Maximum Shear Stress τ_{max}	Time to Failure t_f
metres	mm/minute	kN/m ²	minutes
1 (1.702-2.210, 1.956)	0.193 24.13	13.19 14.97	150 2.00
	0.193 24.13	10.70 12.42	180 0.67
	0.039 24.13	13.39 13.87	780 1.00
2 (2.819-3.327, 3.073)	0.193 24.13	17.82 20.08	228 1.25
	0.193 24.13	16.62 19.60	235 1.50
	0.039 24.13	13.13 14.26	930 1.00
3 (4.140-4.648, 4.394)	0.193 24.13	14.45 15.55	150 1.00
	0.193 24.13	13.48 14.06	145 1.00
	0.039 24.13	14.39 16.10	750 1.00
4 (5.257-5.765, 5.511)	0.193 24.13	16.94 17.81	245 1.25
	0.193 24.13	14.32 15.13	160 1.00
	0.039 24.13	17.30 17.23	12.60 1.25

Table 3.6

Large Vane Tests: Results of Rapid Reloading Tests Carried Out
After Initial Slow Loading To Failure

Depth	Shear Strength $C_{u.FV}$	Time to Failure t_f	$C_{u.FV}$ AVGE	t_f AVGE
metres	kN/m^2	minutes	kN/m^2	minutes
1.5	13.0 16.0 17.5 11.75	2.5 8.0 4.5 5.0	14.56	5.0
2.0	17.5 17.5 19.5 18.5	2.5 5.5 7.5 5.0	18.25	5.1
2.5	17.0 14.5 26.0 23.0	2.5 3.0 8.5 7.0	20.13	5.25
3.0	17.0 16.0 21.0 19.0	4.0 4.0 6.5 5.5	18.25	5.0
3.5	17.5 16.0 16.0 18.0	4.0 4.5 4.0 5.5	16.13	4.5
4.0	20.0 18.0 15.5 15.5	5.5 4.5 3.5 3.5	17.25	4.25
4.5	19.0 18.0 16.0 17.0	4.0 4.5 4.0 6.0	17.50	4.6
5.0	18.5 17.5 17.5 17.5	4.5 3.5 5.0 5.5	17.75	4.6
5.5	20.5 20.5 18.0 20.5	6.0 6.0 5.0 6.0	19.88	5.75
6.0	19.0 17.5	5.5 5.0	18.25	5.25

Table 3.7

Results of Geonor Vane Tests Carried Out Adjacent to Large Vane Tests

3.3.5. Influence of Rotation Rate on the Measured Shear Strength

(i) Previous Investigations into the Effects of Strain Rate and Consolidation on the Field Vane Shear Strength

The rather limited data on this subject have been outlined previously in section 3.2 (viii). Using a vane with $H = 200\text{mm}$ and $D = 80\text{mm}$, Cadling and Odenstad (1950) found that the measured shear strength of a number of Swedish clays (various I_p 's) decreased over a range of rotation rates from 60 to 6 degrees per minute, but increased at still slower rates. This behaviour was attributed to an undrained rate effect at the higher rates, this being superseded by consolidation at the slower rates. On this basis it would certainly seem possible for consolidation to influence the results of Geonor vane ($H = 130\text{mm}$, $D = 65\text{mm}$) tests in certain soils.

Weisel (1973) performed a comprehensive series of tests, using a motorised vane ($H = 130\text{mm}$, $D = 65\text{mm}$), in the plastic ($I_p \approx 50$) Ska Edeby clay. The results from these tests (figure 3.21) showed a continuous drop in strength from a strain rate 10 x faster, to 100 x slower, than standard. There was no evidence of consolidation influencing these results although the maximum time to failure was only of the order of 60 minutes.†

† The results plotted in figure 3.21 are derived from the limited data presented by Weisel (1973), the times to failure being based on average failure strains. As these did not vary significantly the shape of the curve is correct; $t_f = 60$ minutes is probably near to the upper limit for the duration of the slowest tests.

In contrast to both of these findings Aas (1965) reported no variation in the measured shear strength of a low plasticity ($I_p < 20$) Norwegian marine clay when the testing rate was varied by a factor of 10 either side of standard. However, stress controlled 'drained' tests in the same material produced shear strengths between 0.9 and 1.4 times the conventionally obtained values whilst for 'consolidated undrained' tests the results were 1.3 to 1.5 times the latter. As the pore pressures set up by the insertion of the vane had approximately the same time to dissipate in both types of test, the results mean that the increase in strength with the dissipation of both the initial and shear generated pore pressures (assuming these to be positive) in the drained tests has been counteracted to some extent by a time dependent strength loss.

Flaate (1966) also reports a series of 'consolidated undrained' vane tests, with consolidation times (i.e. the delay between inserting the vane and starting the test) varying from 3 (taken as normal) to 480 minutes, in a Norwegian marine clay. These results (figure 3.19) showed a fairly rapid initial increase in strength, followed by a decrease in strength between 15 and 60 minutes and then a further increase up to 480 minutes. There is no evidence to suggest that these rather unexpected variations were due to scatter as the results are all averages from a number of tests, the scatter being within fairly close limits. The tests performed directly after insertion of the vane gave the lowest strengths; such tests correspond to normal vane practice. The longest delay of 8 hours resulted in a strength 1.2 times higher,

compared to the ratios of between 1.3 and 1.5 reported by Aas (1965) after between 1 and 3 days delay.

Therefore, in conclusion, the shear strength measured in a vane test may be influenced by strain rate effects and dissipation of pore pressures generated by both the insertion and rotation of the vane. The relative influence of these factors will depend primarily on the type and size of vane used, the rate of testing and the nature of the soil. For normal vane practice it would appear to be advisable to perform the test immediately after the vane has been advanced to the test position. Thus far it has been assumed that the pore pressures generated during insertion and shear are both positive. The data of Aas (1965) and Flaate (1966) suggest for insertion that this is the case, but there is no definite evidence regarding the shear generated pore pressures. Indeed the analysis of the horizontal and vertical vane tests presented in table 3.3 suggests that small negative pore pressures may be generated by vane shear tests. The elastic analysis performed by Cadling and Odenstad (1950) predicted positive pore pressures in front of each vane blade, varying linearly to negative pore pressures of equal magnitude behind each blade, and thus no change in the average pore pressure around the shear surface.

(ii) Results Obtained at Mucking

The variations in the measured shear strengths with time to failure for the four test levels are presented in figure 3.20 for:-

(A) All the tests carried out (see also table 3.4)

(B) The average shear strength and time to failure at each strain rate, for each depth (see also table 3.5).

(C) The average shear strength and time to failure at each strain rate, for all the depths (see also table 3.8).

Considering the results at each level there appear to be two distinct shear strength - time to failure relationships. At test levels 3 and 4 the measured shear strength initially drops with increasing time to failure, but reaches a minimum between 50 and 100 minutes and thereafter gradually increases. These data can be interpreted as representing an initial strain rate effect, upon which the influence of positive pore-pressure dissipation is superimposed with increasing time. The rapid reloading tests (table 3.6) at these levels show relatively small increases in strength, varying from -0.5% to +12.5% (5.75% average), the average absolute values being marginally less than those obtained in the rapid loading tests. The soil has thus undergone a permanent strength reduction, as the increase in strength due to consolidation cannot be directly added to the higher strength associated with the very rapid rate of rotation. The results also indicate that if negative pore pressures are generated under conditions of undrained shear then their influence is not as significant as that of the dissipation of positive pressures caused by the vane's insertion.

The results at test levels 1 and 2, whether considered individually (figure 3.20(A)) or on average (figure 3.20(B)) exhibit a very different relationship. An initial, rather more rapid, drop in

Displacement Rate of Jack	Maximum Shear Stress τ_{max}	Time to Failure t_f
mm/minute	kN/m ²	minutes
24.13	16.15	1.77
4.826	14.22	8.70
0.965	15.28	39.88
0.193	14.69	186.63
0.039	14.55	930
LARGE VANE TESTS		
- *	16.57	4.93
- †	18.47	5.11
GEONOR VANE TESTS		

* All Geonor vane test results

† Geonor vane test results corresponding to large vane test elevations only.

Table 3.8

Large and Geonor Vane Tests: All Results Averaged At Each Strain Rate

LARGE VANE			GEONOR VANE		
Test Level	Average Depth	$C_{u.LV}$	Depth	$C_{u.GV}$	$\frac{C_{u.GV} - C_{u.LV}}{C_{u.LV}}$
	m	kN/m ²	m	kN/m ²	%
1	1.956	14.4	2.0	18.25	+26.7
2	3.073	12.2	3.0	18.25	+49.6
3	4.394	15.5*	4.5	17.50	+16.7
4	5.511	17.3	5.5	19.88	+14.8

Table 3.9

Comparison of Large and Geonor Vane Test Results At Same Time To Failure

* with rate effect differences considered $C_{uLV} = 0.73 C_{uV1}$

strength with time is followed by an increase (again more dramatic than at levels 3 and 4) and subsequently a further decrease. The single test results at the very slow and very fast rates are obviously open to question, although all the test levels show a high strength for the rapid tests. The intermediate testing rates were all used two or three times, with very consistent results, and thus the shear strength - t_f relationship would seem well defined to at least the 200 to 300 minute region. Again the initial strength drop may be interpreted as a strain rate effect upon which, subsequently, the influence of pore-pressure dissipation is dominantly superimposed. It is interesting to note that the strength increase is almost identical in magnitude (it is also similar for levels 3 and 4) and that the upturn in the shear strengths occurs firstly at level 1 and lastly at levels 3 and 4. Furthermore the strength reaches a peak between 40 and 50 minutes for level 1 and at about 150 minutes for level 2, whereas the strengths at levels 3 and 4 were still continuing to rise at $t_f = 1000$ minutes. It would seem likely that the observed initial increase in strength is mainly a function of the dissipation of positive pore pressures generated by the vanes insertion and that this is dominant over the strain rate effect up to a certain point, after which the result is a net drop in strength.* This interpretation is thus similar to that required to explain the results obtained by Aas (1965).

The rapid reloading tests performed at level 1 showed strength increases of between 3.6 and 13.8% (10.3% average) but the average strength attained was substantially (5 kN/m^2) lower than that

*i.e. an undrained strain rate effect followed by a strength increase as a result of consolidation, followed by a drained rate effect.

obtained in the rapid loading tests. In common with the tests at levels 3 and 4 these results show that although some consolidation has occurred there has been a permanent reduction in the strength of the soil. In contrast the results of the rapid reloading tests at level 2 show increases in strength of between 8.6 and 17.9% (13.1% average) resulting in an average strength 2 kN/m^2 greater than recorded in the rapid loading test. Thus in this case the loss in strength is not as great as the gain resulting from consolidation.*

The rapid reloading tests have thus far been considered in average terms for each test level. Closer examination of table 3.6 reveals that in all cases the increase upon rapid reloading decreases with increasing time to failure. This further illustrates the continuing strength loss with time to failure due to the decreasing strain rate, despite the superimposed consolidation effects. It should be noted, however, that the rapid reloading tests are doubtless influenced by how close to the peak strength the original test was stopped, although generally there was not a significant post-peak strength loss in the slow tests (figures 3.13 to 3.16).

The effect of consolidation at levels 3 and 4 is more dramatically illustrated in figure 3.21 where the variation in shear strength with time to failure, in laboratory and field tests, is shown over 5 log cycles of time; all the results have been normalised to a failure time of 10 minutes. On this basis a combination of Weisel's (1973) field

*Reference to figures 3.12 and 3.3 indicates that I_p decreases in the order-test levels 1, 4, 3, 2 and therefore that the undrained rate effect should likewise decrease (Bjerrum, 1972) in the same order.

vane results with the laboratory results for the Mucking clay (and hence for the Drammen (plastic) clay as shown in figure 2.21) indicates a steady drop in strength with time to failure, although the field vane results could be interpreted as showing some signs of consolidation towards the maximum times considered. The large vane tests at levels 3 and 4 can be seen to initially follow the trend of the other two sets of data and then diverge sharply from the laboratory results as consolidation becomes predominant over the strain rate effect in influencing the measured shear strengths. This occurs at a time to failure of between 40 and 50 minutes, suggesting that a Geonor vane test may need to be performed in about 3 minutes to be truly undrained at these lower levels. At a t_f of 80 minutes (corresponding to $t_f = 5$ minutes for the Geonor vane; see section 3.3.1) the strength has increased by about 5% over the laboratory values, even at these levels.

Averaging the data for all the test levels, at each strain rate (figure 3.20 (c) and table 3.8) produces a shear strength (14.5 kN/m^2 approximately) which is independent of the testing rate beyond 10 minutes to failure. The same data, as presented in figure 3.21, could be interpreted as an initial strength loss due to strain rate effects, this being exactly compensated for by an increase due to consolidation at increasing times to failure.

Figure 3.17 shows the shear strength profiles obtained from the large vane tests at the various rotation rates. Only at levels 3 and 4 was the maximum strength recorded at the fastest rate, and the slowest rate

did not correspond to a minimum strength at any level. The profiles corresponding to the fastest and slowest rates have also been plotted alongside the Geonor results to enable a direct comparison to be made between the latter and the various large vane test profiles. Taking these in order from the fastest to the slowest (profiles 1 to 5) the following comments can be made:-

(1 to 2) The strength drops throughout the layer (the drop being most marked nearest to the surface), the profiles retaining the 'classic' shape associated with soft clay deposits, the minimum strength being at level 2.

(2 to 3) The strength continues to drop in the lower half of the deposit but increases in the upper half, the largest increase being at level 1. The profile shape could still be described as 'classic' but the minimum strength is now at level 3.

(3 to 4) The strength increases at levels 2, 3 and 4 whilst decreasing at level 1, producing a profile rather similar in shape to that of the Geonor vane tests (figures 3.7 and 3.17).

(4 to 5) The strength continues to rise at levels 3 and 4 whilst rising slightly at level 1 and decreasing at level 2, thus producing a 'classic' profile (similar to 2) with the minimum strength at level 2.

(iii) Implications with Respect to Geonor Vane Test Results

The Geonor vane test results, corresponding to the average vane depth at each test level, have been plotted in figure 3.20 at the relevant failure

times. At all levels the Geonor results are high (as shown in table 3.9), particularly for the upper half of the clay layer (see also figure 3.18). It would thus appear that the Geonor vane test results have been influenced by consolidation at all levels, and as indicated by the large vane test results, this influence is more pronounced at the upper levels. The rapid consolidation of the upper half of the clay layer is consistent with the nature of the soil's fabric, as described in Chapter 2.

It is interesting to note at this point that the data for levels 3 and 4 in table 3.9 indicate the Geonor vane strengths to be about 15% higher than those from the large vane at $t_f = 5$ minutes. In contrast the data presented in the previous sub-section (figure 3.21) suggested that the increase in strength due to consolidation for a 5 minute Geonor vane test might be about 5%*. It is thus possible that part of the difference is due to sample size influences or additional soil disturbance in the large vane tests.

At levels 1 and 2 shear strengths were measured with the large vane approximating to the Geonor results, at failure times of about 45 and 250 minutes respectively, whereas at levels 3 and 4 the large vane strengths are always less than the Geonor values. This would appear to be because in the upper part of the clay consolidation could occur during the large vane tests, rapidly enough to produce a strength increase significantly greater than the loss due to the strain rate effect, plus any sample size or disturbance losses, whereas at depth the reverse was true.

*it will be remembered that analysis of the horizontal and vertical vane tests at this level suggested that both $C_{uFV(V)}$ and $C_{uFV(H)}$ were some 6 to 17% on the high side.

In this context large vane strength-depth profile number 4, where significant consolidation has occurred at levels 1 and 2, is interesting in that it closely resembles the shape of the Geonor vane profile. Thus a profile could be obtained from the large vane test results, which closely resembles the Geonor profile, by considering the maximum strengths attained after some evidence of consolidation (i.e. excluding the very rapid tests). Such a profile is presented in figure 3.23(A), the maximum difference between the two profiles occurring at the depths where the large vane results have been affected by the slow strain rates necessary before significant consolidation occurred. It should be reiterated that the consolidation necessary to achieve these strengths at any test level is probably significantly greater than occurred in the Geonor vane tests due to the previously mentioned strain rate effect as well as any additional factors such as sample size and disturbance.

Further evidence that the high strengths measured in the Geonor vane tests are the result of consolidation, particularly at the higher elevations, is presented in figure 3.22. This shows that even within the small range of failure times which resulted in the Geonor vane tests that there is a definite trend for higher strengths to be associated with increasing failure times. This increase is, again, probably largely due to dissipation of positive pressures generated by the vane's insertion. The findings are in agreement with the results of Flaate (1966), presented in

figure 3.19, wherein significant increases in strength can be seen to result from time delays of a few minutes (i.e. between the times of 3 and 15 minutes). Despite the much longer delay between insertion of the vane and the start of a test using the large vane, there is no sign of increasing strength with time to failure over the initial time scale at any of the test levels.

(iv) Conclusions

(1) The shear strengths measured in the Geonor vane tests appear to be influenced to various degrees by the dissipation of positive pore pressures generated during insertion of the vane. The more rapid dissipation of these pore pressures at the higher elevations results in the greatest increases in strength occurring in these locations. The measured shear strengths appear to be sensitive to small changes in the failure times and it is these changes which may be largely responsible for the wide range of scatter observed, again particularly at higher elevations. The variation in time to failure and the scatter in the shear strength data decreases with depth, as does the influence of the root holes in the soft clay on the consolidation characteristics.

(2) The results from the large vane tests are not significantly influenced by small changes in the time to failure and therefore the results at any particular strain rate are very consistent. Despite the longer delay between the vane's insertion and the actual test all the results show an initial drop in strength with

time. The minimum strengths recorded are significantly lower than those from the Geonor vane tests, and only the results from those large vane tests where substantial consolidation is indicated approach those of the Geonor tests.

(3) The large vane test results indicate that vane test shear strengths are influenced by strain rate effects and the dissipation of positive pore pressures. These latter may be predominantly the result of the vane's insertion. The rapid reloading tests indicated that at slow strain rates the soil underwent a strength loss,*despite consolidation, which could not be recovered upon increasing the strain rate.

(4) With the Geonor vane it would not seem possible to perform an undrained test in the Mucking clay (particularly in the upper parts) even at high strain rates. With the new large vane apparatus it was possible to perform undrained tests at strain rates corresponding to normal laboratory practice.

3.3.6. Stress-Strain Characteristics Measured in Vane Tests

Although there was no relationship between strain rate and angular rotation to failure (table 3.5), the shear stress-angular rotation relationships obtained with the large vane apparatus (figures 3.13 to 3.16) were very consistent. The tests performed at the faster strain rates were continued after a peak stress was recorded; the

*initially undrained, at all test levels, and subsequently drained at the upper test levels.

shear stress-angular rotation relationships thus obtained had a distinct peak followed by a steady drop in the mobilised shear stress with increasing strain.

From the linear 'elastic' part of such shear stress-angular rotation relationships a value of the shear modulus can be computed using the formulations developed by Cadling and Odenstad (1950), as described in section 3.2(vi)(d) and Appendix

5. The initial parts of all the stress-rotation plots were very similar, the results from the rapid loading tests being used in conjunction with equation 3.1 for the computations of 'G' presented in table 3.10. For the purposes of limiting the data to the 'elastic' part of the plots all the calculations relate to a shear stress of 5 kN/m².

For an isotropic elastic soil the shear modulus is related to Young's Modulus as follows:-

$$G = \frac{E}{2(1 + \nu)} \dots\dots\dots(3.6)$$

Test Level	ω		G kN/m ²	Vane Travel mm
	Degs.	Rads.		
1	2.3	0.0401	50	4.3
2	2.5	0.0436	46	4.7
3	1.9	0.0332	60	3.6
4	3.1	0.05	37	5.8

Table 3.10
Shear Modulus From Large Vane Tests

and therefore for undrained shear the value of E_{u50} from the quick undrained laboratory tests (section 2.8), of 2700 kN/m^2 leads to a 'G' of 900 kN/m^2 . The average value from the large vane tests is thus lower than this by a factor of 18.

A 'G' value of 900 kN/m^2 implies (via equation 3.1) an angular rotation of 2.225×10^{-3} radians or approximately 0.15° . This corresponds to a circumferential vane travel of about 0.2mm. The accurate measurement of such small displacements (or rotations) is beyond the scope of the large vane apparatus. In the calculation of the angular rotations the deflection of the proving ring was directly, and the rod twist and deflection of the vane blades indirectly, accounted for whilst the jack travel was indirectly measured. For future attempts to monitor the angular rotation of the vane it is suggested that direct observation of the main drive wheel would be preferable, thus leaving only the rod twist to indirect assessment. Other possible sources of discrepancy in measurements of 'G' are soil disturbance resulting from the vane's insertion and inadequacy of the theoretical model (Appendix 5.) used for the calculation.

The use of equation 3.1 to calculate 'G' from vane test data has also been reported by Cadling and Odenstad (1950) and Weisel (1973). The former recorded values between 50 and 1500 kN/m^2 for soft clay deposits in Sweden, these being from 3 to 12 times lower than estimated from E_u , for the cases where this was measured. The vane used by the latter

incorporated a displacement transducer to record angular rotations, 'G' values between 200 and 800 kN/m² being obtained for the 'Ska Edeby clay. Thus although equation 3.1 may give 'G' to a reasonable approximation in the latter case, the vane test in general does not appear to be well suited to this application. This is largely due to the inadequacy of the angular rotation measurements.

3.4. Strain Rate Effects Observed in Laboratory and Field Tests Related to Full Scale Embankment Behaviour

3.4.1. Strain Rate Related to Fundamental Shear Strength Parameters

The resistance to shear which a soil can provide comprises both frictional and cohesive components. The former is developed at mineral to mineral contact points (especially between silt size particles and larger) and the latter between clay minerals which are separated by adsorbed water layers (see e.g. Hvorslev, 1960; Bishop 1971(a)). These two components of shear strength also appear to be mobilised at different strains: Schmertmann and Osterberg (1960) showed (from tests on Boston Blue Clay) that cohesion was fully mobilised at very small strains whilst the frictional component was fully developed only at much larger strains, by which point the cohesive component had diminished considerably. Under the in-situ stresses the mobilised shear strength of a soft clay is therefore, probably, predominantly cohesive. Bjerrum (1972, 1973) used this simple outline of a very complex behaviour pattern to postulate a qualitative theory of strain rate effects in soft clays, as outlined in the following paragraph.

Under a given stress system both types of interparticle contact creep. The cohesive contact is of a viscous nature and the associated creep movements are many times greater than for the frictional contacts. In addition, the creep associated with the viscous component may be expected to be greater for the more plastic clays. The cohesive component will also initially exist under higher stresses due to its more rapid mobilisation. After a certain finite strain has occurred in a cohesive bond it will fail, the time necessary to reach this strain being quite short at high stress levels but very long at low stress levels. With the continuing failure of cohesive contacts within a soil mass, load will be transferred increasingly to the frictional contacts with a corresponding decrease in the creep rate. Bjerrum postulated two alternative stable configurations which could eventually develop, as follows:-

(1) The entire load is gradually transferred to the frictional contacts with the creep rate decreasing and ultimately reaching zero.

(2) The frictional component is unable to sustain the full load and the cohesive bonds cannot be fully relieved: the creep rate decreases as load is initially transferred and ultimately reaches a constant value.

Bjerrum (1973) also linked this strain rate concept to the existence of a critical shear stress (τ_{CR} ; section 2.8) by postulating that at the critical value of shear strain large numbers of cohesive bonds have failed, resulting in pore-pressure generation and undrained failure or, in the drained case, large deformations.

3.4.2. Observed Stress-Strain-Time Relationships

As mentioned previously, many investigators have reported a reduction in undrained strength with increasing time to failure. Berre and Bjerrum's (1973) results for the Drammen (plastic) Clay (figure 2.21) were also presented as in figure 3.24., showing the inter-relationship of shear strain rate, shear strain and shear stress (for small strains; $\tau < \tau_{CR}$). A number of interesting points arise from this representation of the undrained strain rate effect, outlined as follows:-

- (1) The rate of drop of shear strength decreases with decreasing shear strain rate, and is nearly linear on a semi logarithmic plot (i.e. exponential).
- (2) Under constant strain rate conditions the relationship between shear stress and strain is again approximately exponential.
- (3) If, at any stress level, an increment of shear stress is applied, the rate of shear strain increases approximately exponentially.
- (4) At the new stress level attained in (3) the shear strain rate decreases with increasing strain.

The results of drained tests obviously only correspond to the slower rates of shear strain, but show similar behaviour in this region to the undrained tests, over the same range of axial strains.

Bjerrum et al (1958) found, however, that the drained strength of a soft marine clay was independent of strain rate for failure times between 1 and 30 days. This was attributed to an increase in cohesion (resulting from secondary consolidation) compensating for the time dependent strength losses.

Bishop and Lovenbury (1969) performed drained creep tests on the normally consolidated Pancone Clay (from Pisa) which revealed the following main points:-

- (1) Axial strains increased throughout the test period at all stress levels.
- (2) The proportional increase in axial strains tended to be greater at lower stress levels, with increasing time.

The overall effect was decreasing creep rates with time at all stress levels, and a tendency to ultimately reach common creep rates; similar behaviour was observed for the Mucking clay in long-term oedometer tests (see section 2.6). As pointed out by Bishop and Lovenbury (1969) the shear stress level in an oedometer test on a material with $c' = 0$ is 50% of the failure value in a drained test having the same value of σ'_3 , irrespective of ϕ' . Both clays also exhibited periods of instability during which the creep rates rose, these possibly being associated with a structural rearrangement of the soil particles (Bishop and Lovenbury, 1969).

The results of both drained and undrained tests appear compatible with Bjerrum's (1973) hypothesis; however, there is no evidence in the long-term (1 - 3 years) drained, or short term undrained, tests reported of constant (secondary creep) or zero creep rates being attained on an engineering time scale.

Parry (1971(a)) noted that in some cases the high undrained strengths obtained using high strain rates for tests on soft clays were associated with 'peaking' of the stress-strain curves, this phenomenon

disappearing to produce smoother curves at lower strain rates, with a corresponding decrease in the rate of strength loss. The high strengths under rapid loading were attributed to "structural features in the soil or pore-pressure behaviour" while the less marked strength loss at the slower strain rates was attributed to creep. The tests on the Mucking clay (section 2.7.4.) produced relatively flat topped stress-strain curves at all strain rates.

3.4.3. Application to Field Situations

Embankments built on soft clay foundations are generally constructed in layers, each of which corresponds to an applied increment of shear stress. Accepting Bjerrum's (1973) hypothesis that the development of shear strains within the soft clay foundation is time dependent, it can be seen from figure 3.24 that if the loading increments are applied rapidly, the critical shear strain will be approached at a high strain rate and correspondingly a high shear stress is mobilised at failure. Typical embankment geometries involve a reduction in fill volume per layer as the height increases and therefore an increasing rate of construction as time proceeds (figure 4.6). Thus the critical strain may again be reached at a high strain rate even though the overall construction time was fairly long. This does not imply that an embankment constructed initially relatively slowly, followed by more rapid filling will be able to attain the same height (or 'undrained' strength) as an embankment constructed very rapidly. Reference to figure 3.24 indicates this to be because the shear strength of the foundation ultimately depends not only on the shear strain rate

at failure but also on the shear strains developed during the overall loading process i.e. on the stress-strain-time path followed. This is illustrated by the results from the large vane tests where the increase in strain rate imposed in the rapid reloading tests was not sufficient to mobilise the strength obtained in an entirely rapid test plus the strength increases gained by consolidation. It therefore follows that strain rate effects may not be accounted for in design by direct recourse to the variation in the laboratory undrained strength with time to failure illustrated in figure 2.21, which when extrapolated from a 10-15 minute triaxial test to a 70 day construction period (figure 4.6) would indicate a drop in strength of 35% for the Mucking clay (table 3.11).

It is therefore possible to mobilise different undrained strengths in the field according to the construction program. A trial embankment constructed to failure will mobilise an undrained strength which has been reduced to some extent (below the laboratory value) by strain rate influences and, if the other major uncertainties in determining the field C_u can be appraised, it may be possible to evaluate this reduction. Thus far the discussion has been limited to the undrained case, but in general this is only part of the overall design problem, the aim being to arrive at a design height which can be successfully constructed and subsequently will afford a factor of safety in excess of unity.

The indications are (Bjerrum et al, 1958; Bishop and Lovenbury, 1969) that the loss in strength under completely drained conditions is not significant* on an engineering time scale. However, the important period for an embankment on a soft clay foundation may

*The limited data from the large vane tests at levels 1 and 2 tend to contradict this view, however.

be the period following the end of construction. Having established an undrained strength for the foundation, typical embankments on soft clay are designed with relatively low factors of safety (Casagrande, 1960; Parry, 1971(a)) and therefore impose high shear stress levels. After the end of construction shear strains can be expected to continue to develop and, if undrained conditions were maintained, the embankment would fail after a certain time interval, the length of which would depend on the stress level and stress-strain-time path during construction. Eventual failure is only averted if the increase in the soil's available shear strength, due to consolidation, is greater than the time dependent loss. The consolidation process involves not only the pore pressures generated during construction, but also those developed as a consequence of the continuing shear strains. The post-construction stability of the embankment is thus largely determined by the outcome of a 'race' between consolidation and strain rate.

There would not appear to be any way in which the observed laboratory rate effect can be directly incorporated in the design.* The existence of a pronounced rate effect is, however, a warning that the end of construction condition is not necessarily the most critical point, as far as stability is concerned, and that even in the short term the available field shear strength will probably be substantially less than indicated by quick laboratory tests. As indicated previously, the construction of a trial embankment to failure will, at best, only indicate what portion of the time dependent strength loss can be

*i.e. other than by direct extrapolation of the laboratory data on a t_f basis, as used to derive the proposed field average design curve.

expected during construction, and therefore what percentage may have to be offset by post-construction consolidation. For many soft clays the influence of progressive failure will not be readily separable from the strain rate effects, and of course may be to some extent instrumental in determining the influence of the latter, and vice versa.

Having constructed a trial embankment to failure and arrived at a field undrained strength, and effective stress parameters, the determination of a factor of safety adequate to ensure long-term stability of prototype embankments is therefore by no means easy. It is thus desirable to construct a test section corresponding to the design height of the prototype to check that the assumptions made regarding the strain rate effects (and progressive failure) are adequate. The post-construction stability will probably be analysed in terms of effective stresses, the parameters for which were shown in section 2.7.4. (figure 2.22) to be strain rate dependent for the Mucking clay. The analysis of short term (undrained) failure in terms of effective stress may afford an advantage in this respect, in that c' and ϕ' for soft clays may not be significantly anisotropic (section 2.7.3.) and in addition the strain rate influence may be to some extent pore-pressure related. Thus the difference between the predicted soil strength and that back-analysed (using measured pore pressures) may be a more definite indication of strain rate effects, particularly in less brittle materials.

3.5. The Selection of a Vane Shear Strength/Depth Design Profile and Factors Influencing that Selection

The results presented in section 3.3. have largely resolved the uncertainties listed in sub section 3.2.4.(iv). In particular the high strengths, and wide range of scatter, of the Geonor vane test results in the upper part of the clay appear to be due to consolidation influences. The evidence presented suggests that the Geonor vane tests in the lower part of the clay were not greatly affected by this mechanism, and therefore that the conclusions reached in section 3.2.4. are valid. In addition the effect of strain rate appears to similarly influence the values of undrained strength measured in the laboratory and with the field vane.*

The best estimate of the field vane undrained strength would seem to be provided by the large vane test results. A number of alternative profiles could be adopted, but two suggest themselves as more obvious these being as follows:-

- (1) the minimum values obtained,
- (2) the results at the same time to failure as the Geonor tests.

The former is the most conservative, but some of the minimum values were recorded at fairly high values of failure time and were thus influenced by both consolidation and strain rate effects. The latter, however, were almost certainly undrained and the failure time means that Bjerrum's (1972) correction factor is applicable. Therefore these results, which require interpolation from figure 3.20, with the

*and also similarly to influence the drained strengths measured in the laboratory and with the field vane.

appropriate correction factor applied, were selected as the best possible design values (figure 3.23(B)). As with the laboratory data the main uncertainties regarding the vane test undrained strengths are the effects of strain rate and progressive failure, although Bjerrum's work at least enables a positive allowance for the former to be made in the design vane shear strength.

Since the original conception of a plasticity related correction factor for the vane test (Pilot, 1972; Bjerrum, 1972) the relative influence of strain rate, anisotropy and progressive failure have been further investigated. Bjerrum (1973) proposed that the results of vane tests were substantially influenced by undrained strength anisotropy, particularly in soils of low plasticity. This led to the sub-division of the correction factor μ into a strain rate effect (reduction component at all I_p values) and an anisotropy effect (addition component at all I_p values) as indicated in figure 3.3(A). Thus for the Mucking clay the average μ of 0.76 is composed of a 0.70 strain rate effect reduction factor times a 1.08 anisotropy addition factor. This agrees with the conclusion reached in the earlier part of this chapter that the vane tests in the Mucking clay provide a good account of undrained strength anisotropy. It is important to note, however, that the influence of this anisotropy on the average shear strength which can be mobilised in the field under full scale loading conditions will depend on the principal stress directions (figure 2.14(A)). The relationship between field vane and laboratory undrained strengths, and the field value may thus vary considerably with the geometry of the situation (Eide and Holmberg, 1972; see also Chapter 7).

Dascal and Tournier (1975) related F.o.S. to I_p for the case histories studied by Bjerrum (1972), by means of a regression analysis and concluded that Bjerrum's relationship excluded the influence of those failures for sensitive clays, and therefore also of progressive failure. They proposed an alternative relationship for sensitive clays (liquidity index > 1.1 , and therefore $S_t > 10$ from figure 2.26) again based on a regression analysis. This produced a new correction factor supposedly embracing the effects of progressive failure, as well as strain rate and anisotropy. Dascal and Tournier (1975) also suggested the use of a modified plasticity index, defined as follows:-

$$I_{pm} = w - P.L. \dots\dots\dots(3.7)$$

to account for rate effects in sensitive (leached) clays (see also Dascal et al, 1972). On this evidence no reduction factor would need to be applied to the Mucking clay results to account for progressive failure.

The various reductions which can be applied to both the laboratory and field vane undrained strengths are summarised in table 3.11. The laboratory strain rate correction, based on the vane test correction factor μ was derived by calculating the time to failure implied by μ for the vane test results using figure 2.21. Ranges of values for the effects of anisotropy and strain rate given by Parry (1971(a)) are also shown. Finally figure 3.18 and table 3.9 show that even in the lower clay the undrained strengths from the large vane tests are about 15% lower than those from the Geonor vane tests, and it has been suggested that the large vane test results

may have been influenced by sample size or disturbance effects.

On the basis of table 3.11 and the preceding comments it might be expected that the 5 minute duration large vane tests, corrected for strain rate and anisotropy, would produce undrained strengths equal to or less than the average field value. The acceptance of the validity of the strain rate correction factor implies that the laboratory design curve is about 35% higher than the field undrained strengths. Both of these 'predictions' assume progressive failure to have negligible influence on the mobilised undrained strength.

It is interesting to note that the rate effect component of μ implies 75% of the reduction which would be given on the basis of a straight extrapolation of t_f , from the quick laboratory test to the full scale field situation. The assertion by Parry 1971(a) that undrained strength anisotropy is not a major factor in the prediction of the field undrained would seem inappropriate in this case.

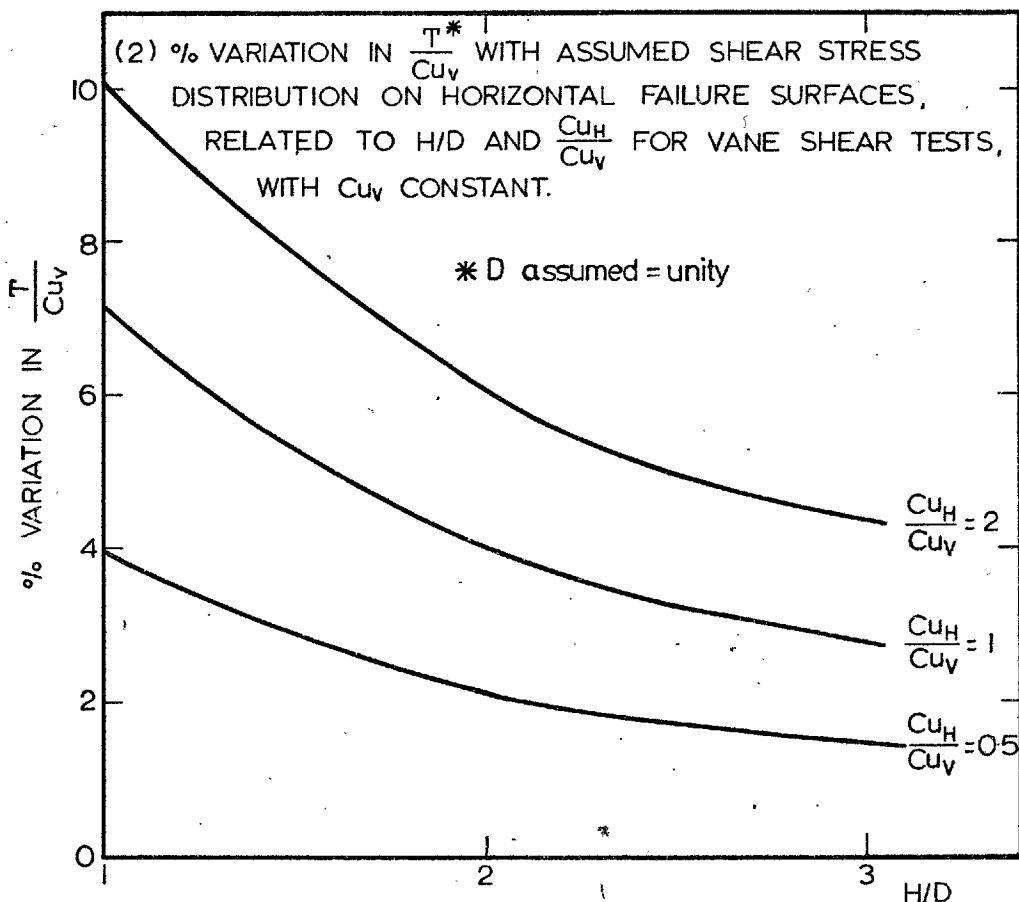
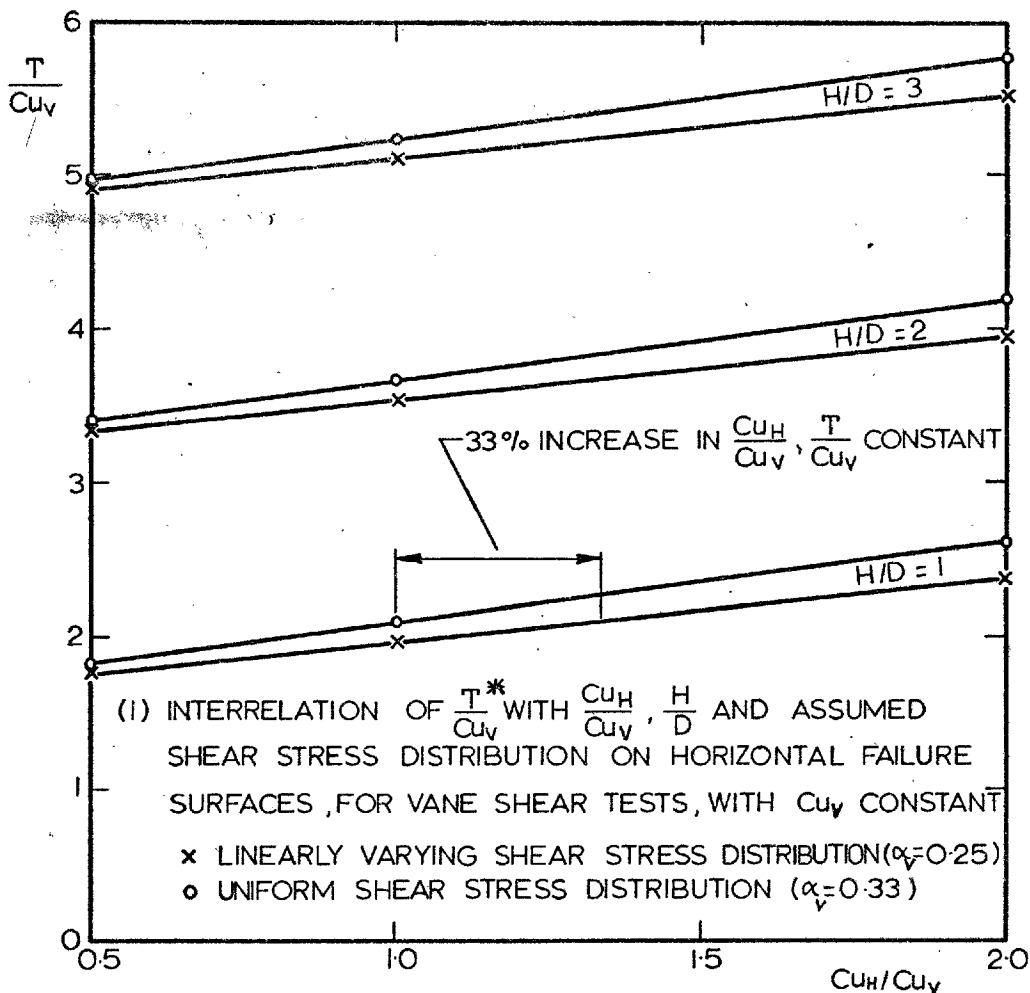
TEST	POSSIBLE REDUCTION FACTORS			APPLIED TO DESIGN STRENGTH
	ANISOTROPY	STRAIN RATE	PROGRESSIVE FAILURE	
FIELD VANE ($t_f = 5$ minutes)	1.00 (anisotropic analyses; Hansen & Gibson, 1949)	0.61 (t_f extrapolated to t_f in field using lab. data, fig. 2.21)	0.20 maximum (undrained I_B from field vane = 80%)	1.08 x 0.70 x 1.00 = 0.76 = μ
	1.08 (anisotropy component of μ ; Bjerrum, 1972 and 1973)	0.70 (rate effect component of μ ; Bjerrum, 1972 and 1973)	1.00 (Dasal and Tournier, 1975)	
LABORATORY TRIAXIAL ($t_f = 10-15$ mins- vertical samples)	0.87 (average from C_{UV1} , C_{U451} , C_{UH1} tests)	0.65 (t_f extrapolated to t_f in field using lab. data, fig. 2.21)	0.20 maximum (undrained I_B from lab. tests = 80%)	0.87 x 0.65 = 0.57
	0.82 (use of equation 2.15 and critical slip surface for $\phi_u = 0$ analysis)	0.75 (assuming $t_f = 800$ mins in lab corresponds to $C_{u, FIELD}$, based on $\mu = 0.70$)		
	0.90 - 1.00 (Parry, 1971(a))	0.85 - 1.00 (Parry, 1971(a))		

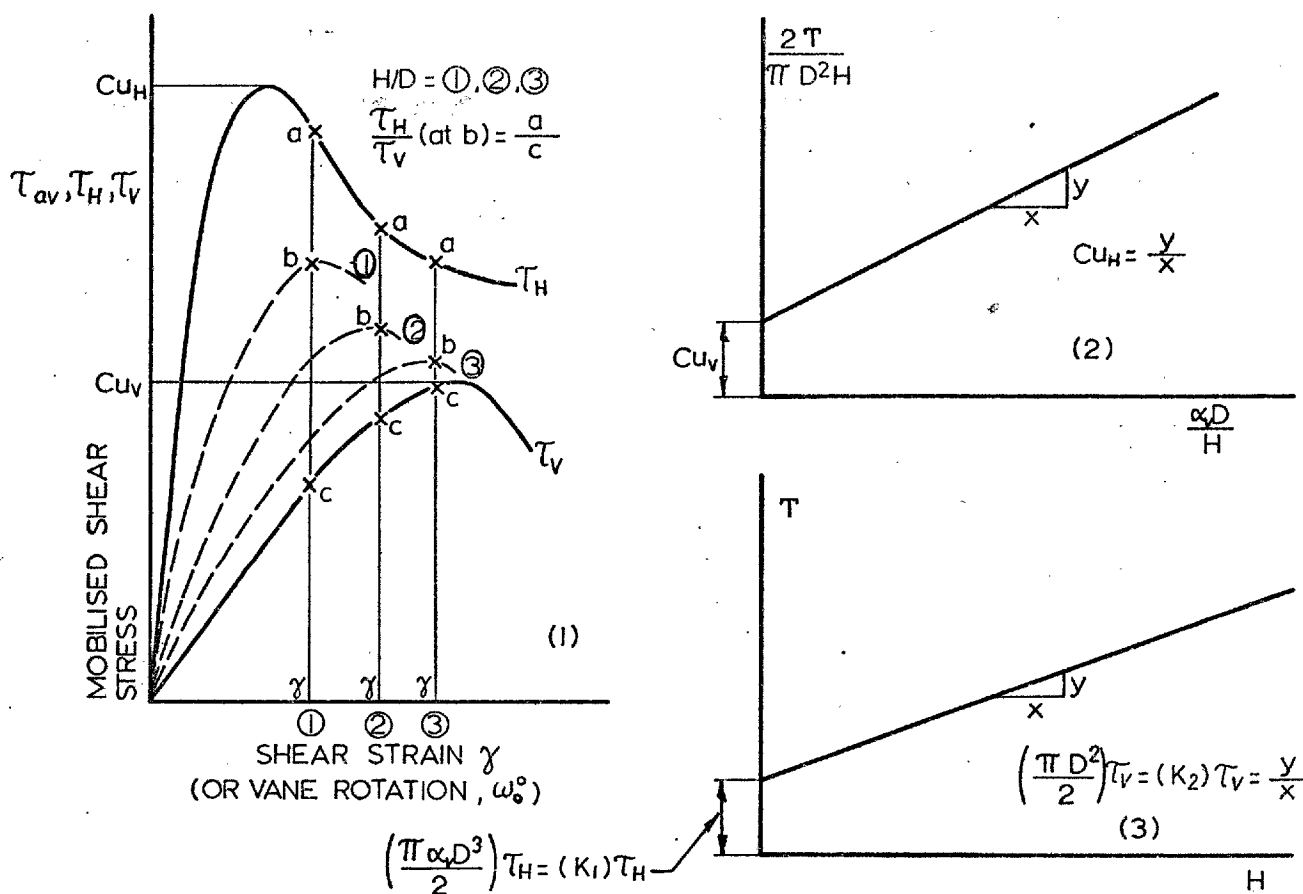
Table 3.11

Possible Reduction Factors For Field Vane And Laboratory Measurements Of Undrained Strength



PLATE 3.1 FIELD OPERATION OF LARGE VANE

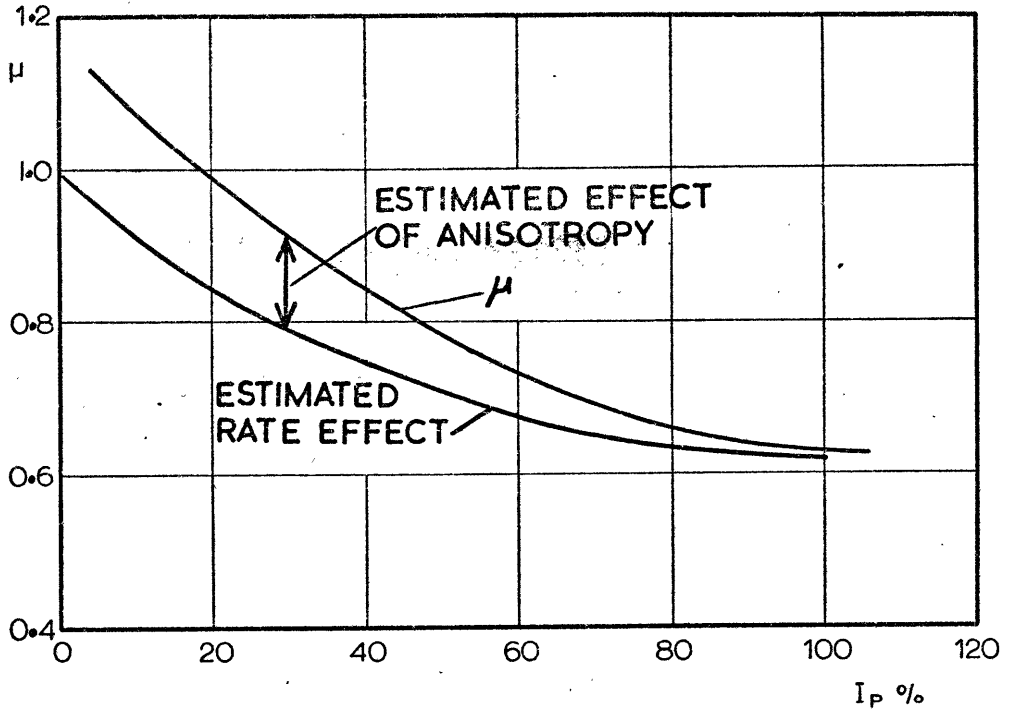




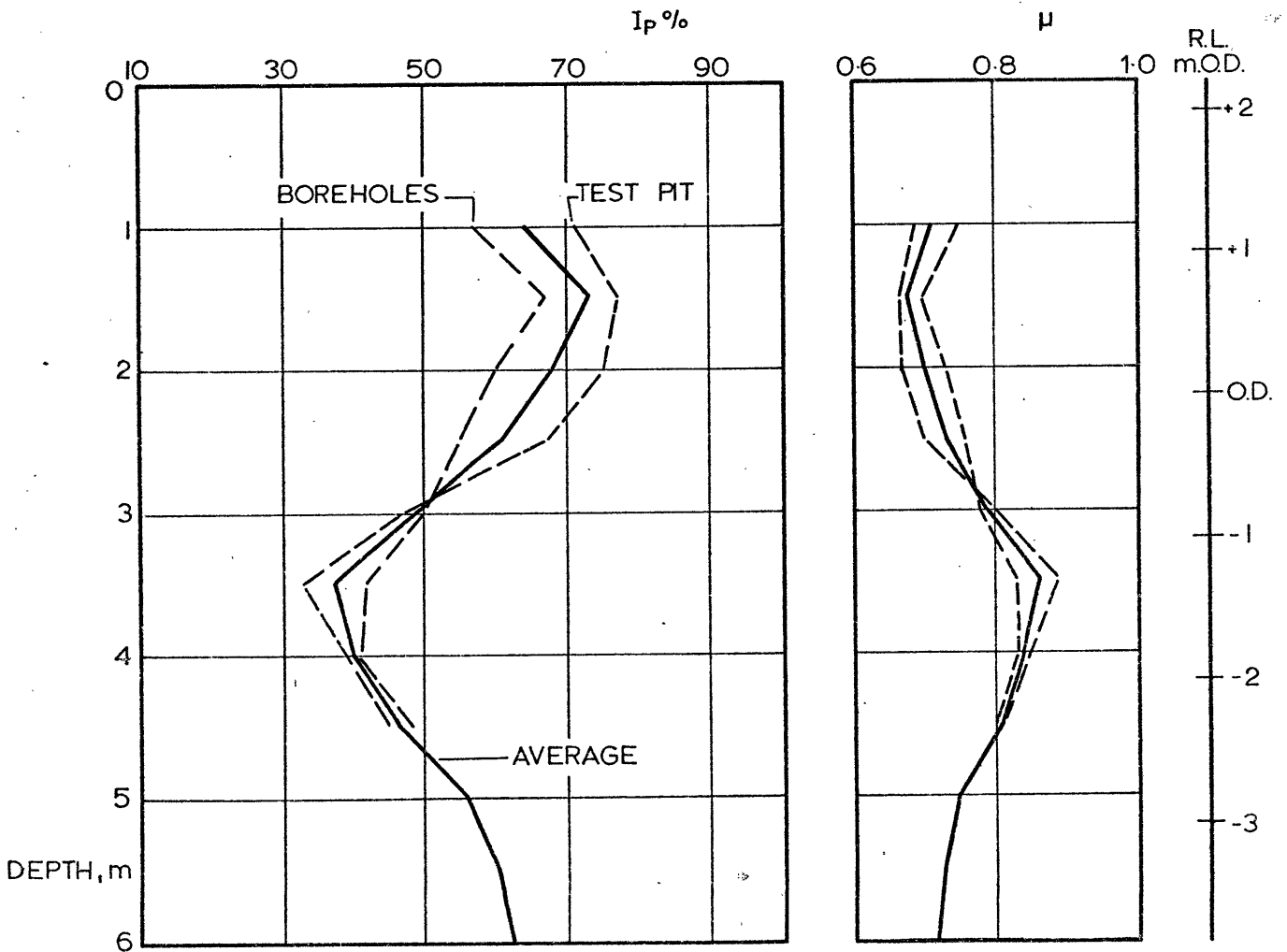
- (1) SHEAR STRESS (τ) / SHEAR STRAIN (γ) RELATIONSHIP FOR HORIZONTAL (H) AND VERTICAL (V) PLANES IN A THEORETICAL SOIL EXHIBITING UNDRAINED STRENGTH ANISOTROPY, PLUS AVERAGE SHEAR STRESS / SHEAR STRAIN RELATIONSHIPS (HATCHED LINES) WHICH MIGHT BE OBTAINED FROM VANE TESTS WITH VARYING H/D RATIO
- (2) DETERMINATION OF Cu_H/Cu_V FROM VANE TESTS, AS DESCRIBED IN (1), AFTER AAS (1967)
- (3) DETERMINATION OF τ_H/τ_V FROM VANE TESTS, AS DESCRIBED IN (1), AFTER WEISEL (1973)

UNDRAINED SHEAR STRENGTH ANISOTROPY IN RELATION TO VANE SHEAR TESTS

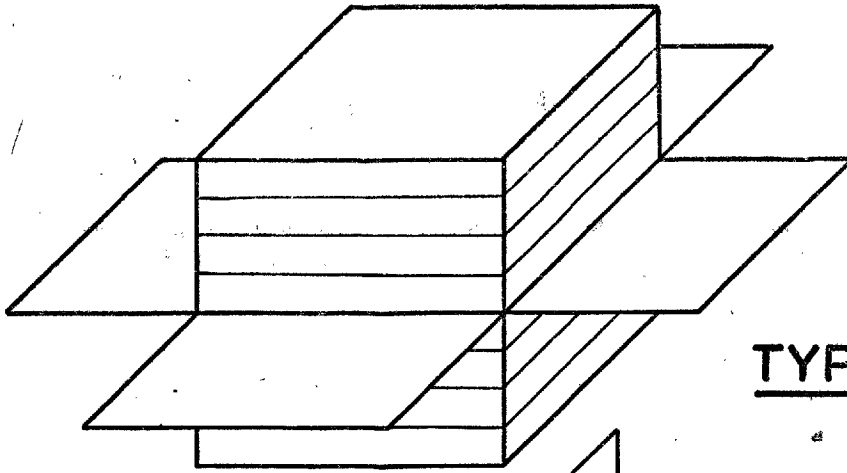
Fig. 3.2



(A) RELATIONSHIP BETWEEN VANE SHEAR STRENGTH CORRECTION FACTOR, μ , AND PLASTICITY INDEX (after Bjerrum, 1972 and 1973)

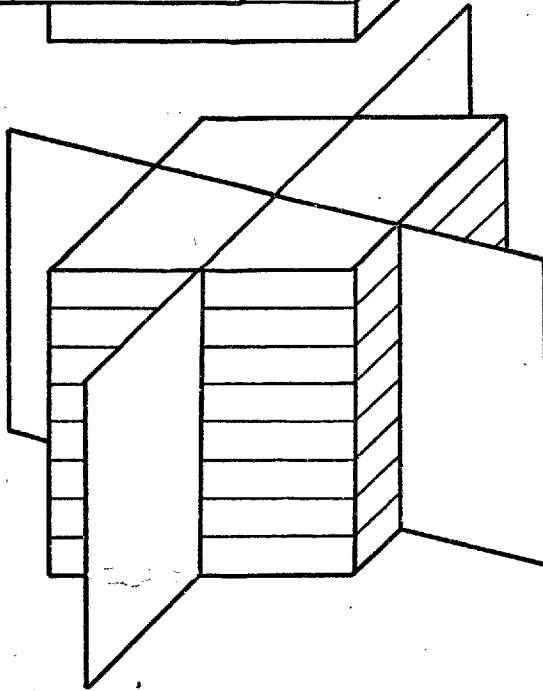


(B) VARIATION OF PLASTICITY INDEX AND VANE SHEAR STRENGTH CORRECTION FACTOR WITH DEPTH

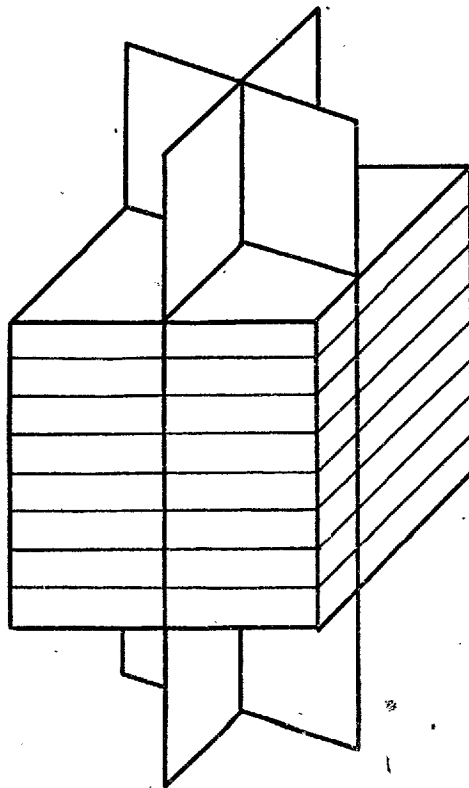


TYPE 1 PLANES

NB SHEARING IS IN THE DIRECTION THE PLANE PROTRUDES FROM THE CUBE

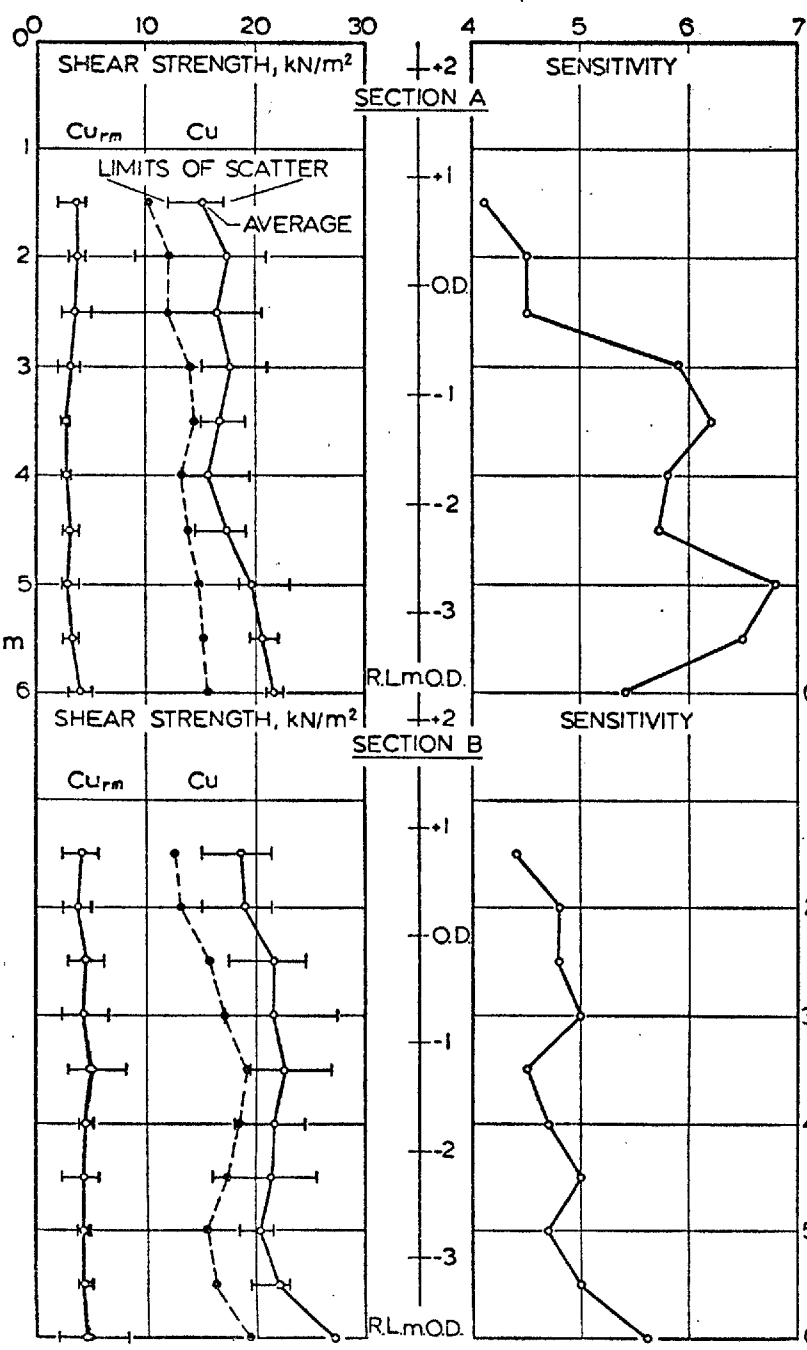


TYPE 2 PLANES



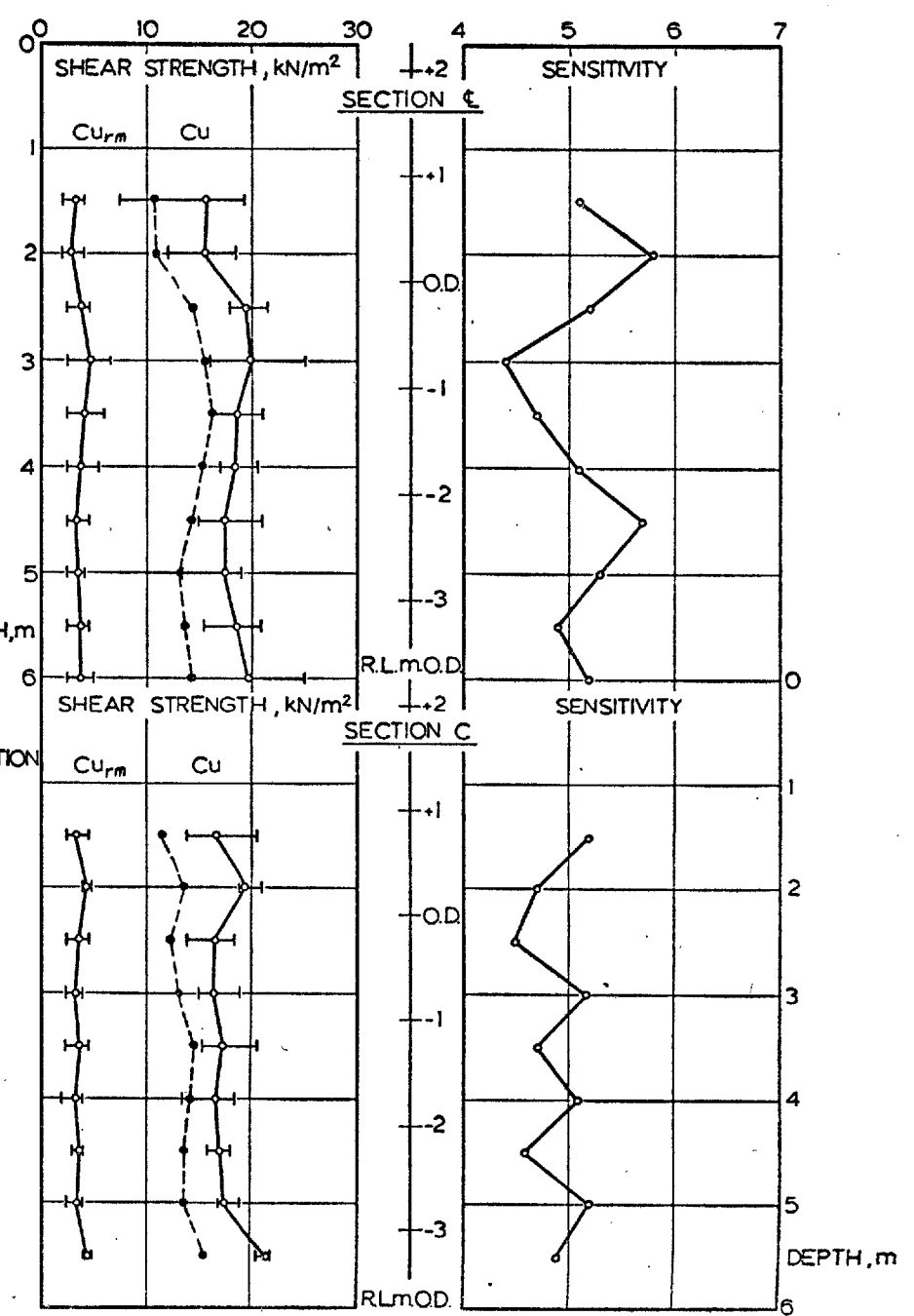
TYPE 3 PLANES

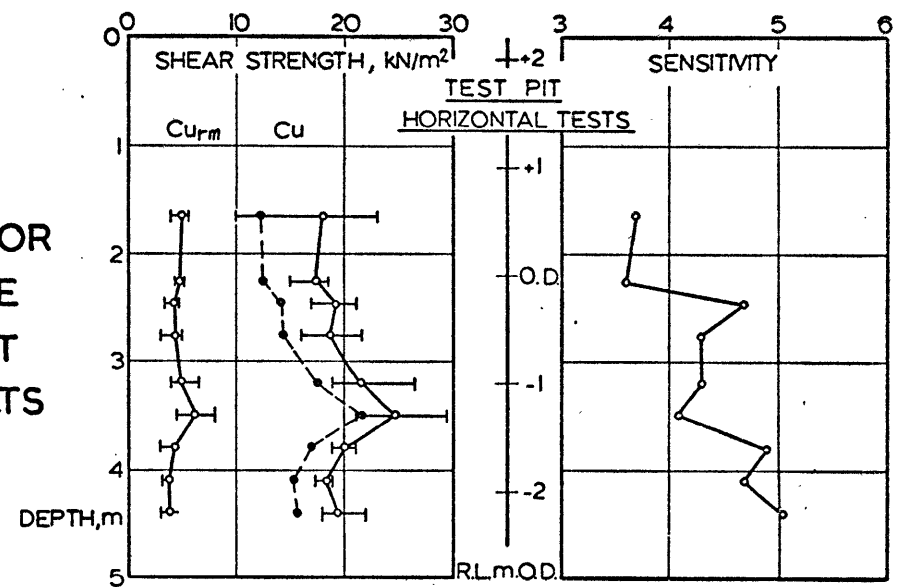
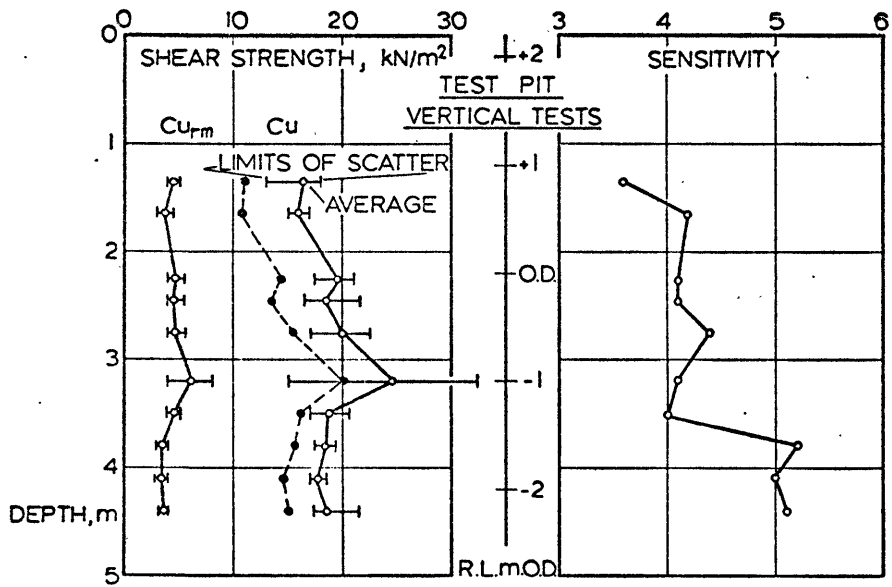
SHEAR PLANES IN HORIZONTALLY BEDDED DEPOSIT



LEGEND
 • IS PEAK STRENGTH
 x BJERRUM'S CORRECTION FACTOR, μ

GEONOR VANE TEST RESULTS

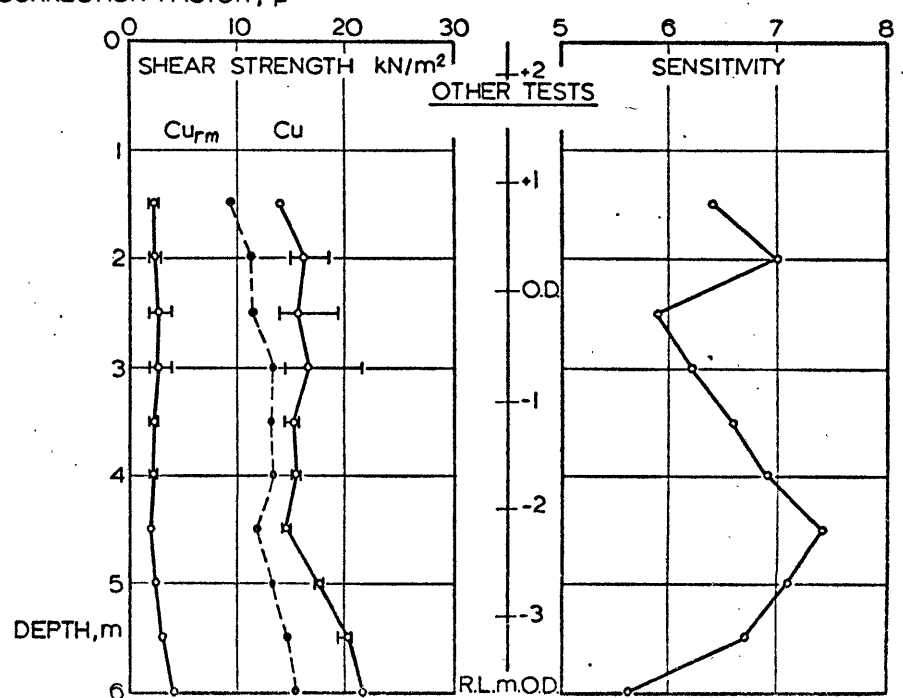
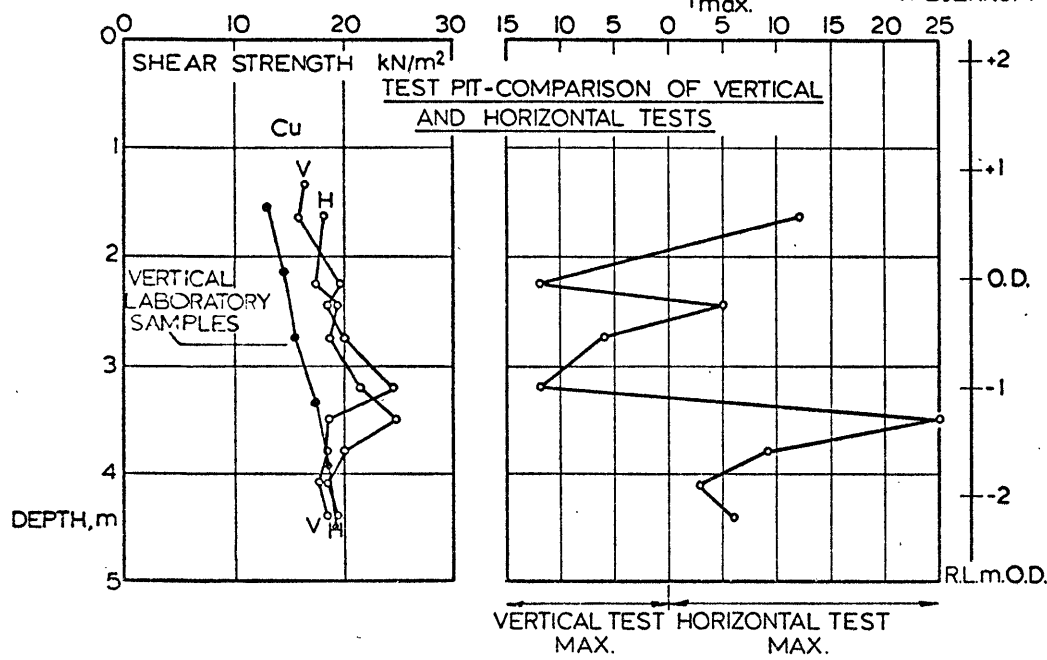


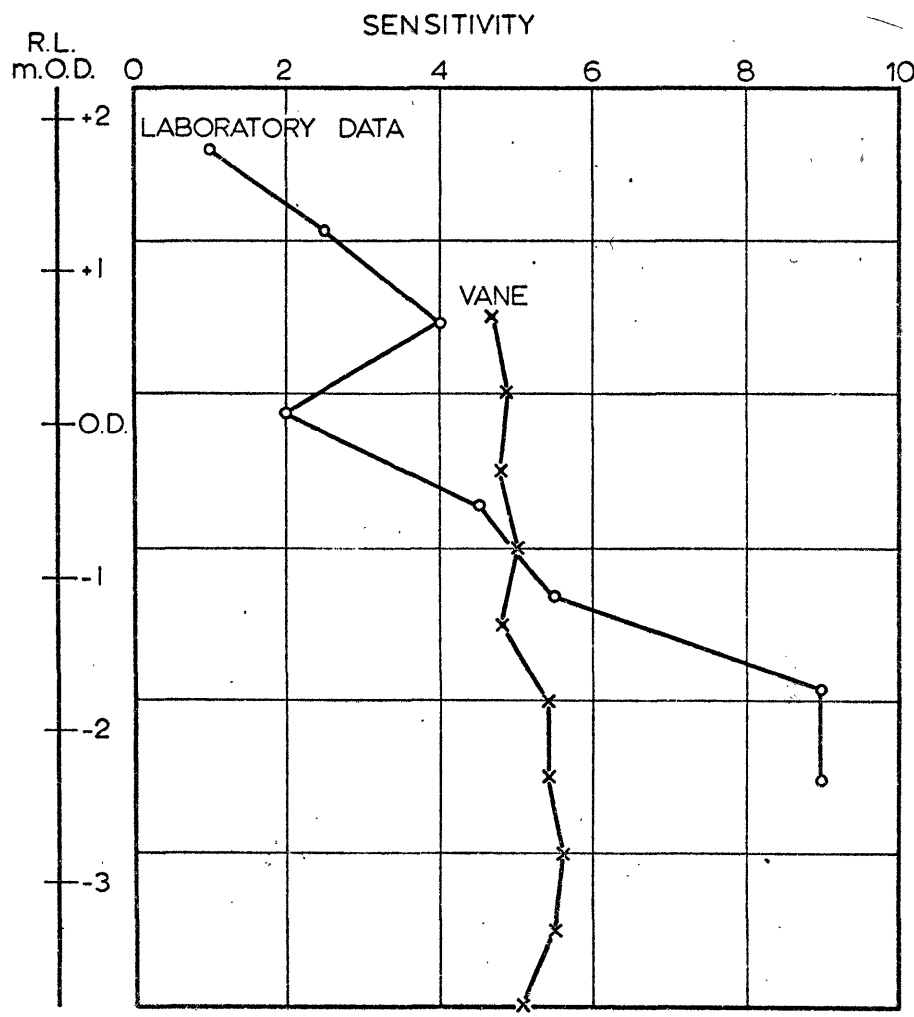
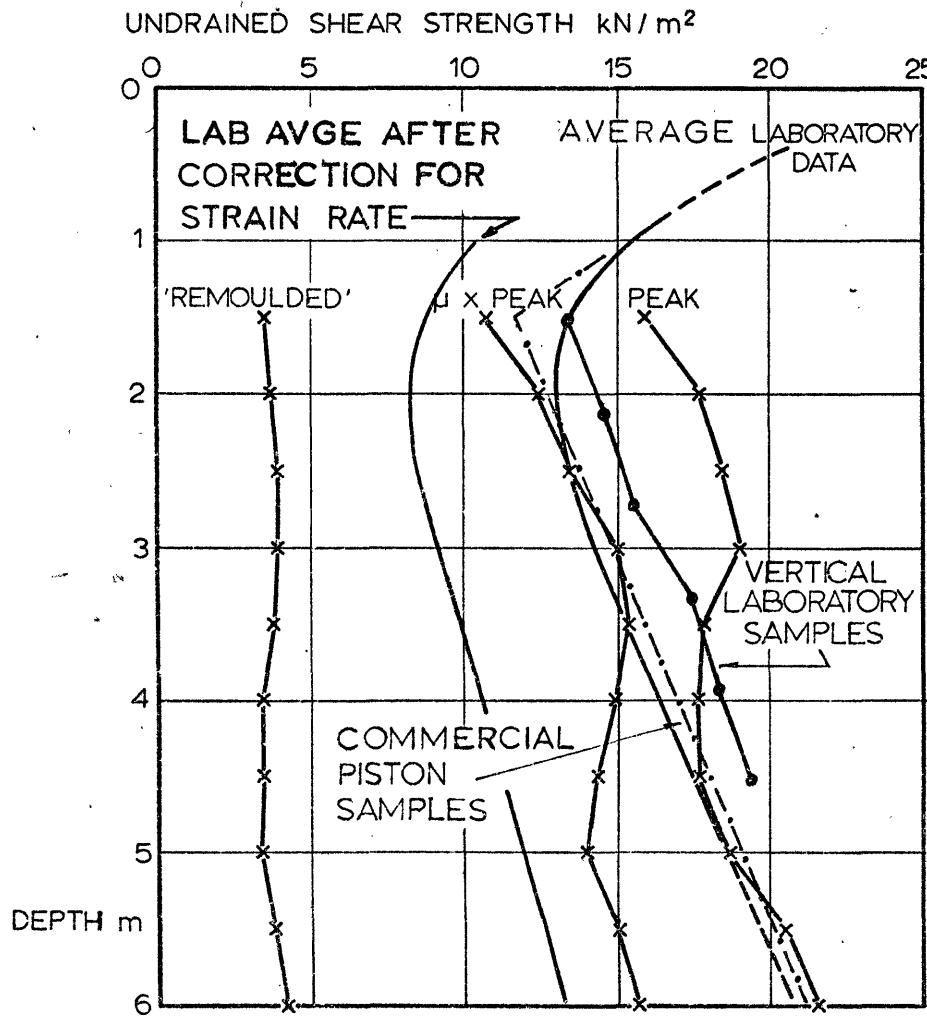


GEONOR VANE TEST RESULTS

LEGEND

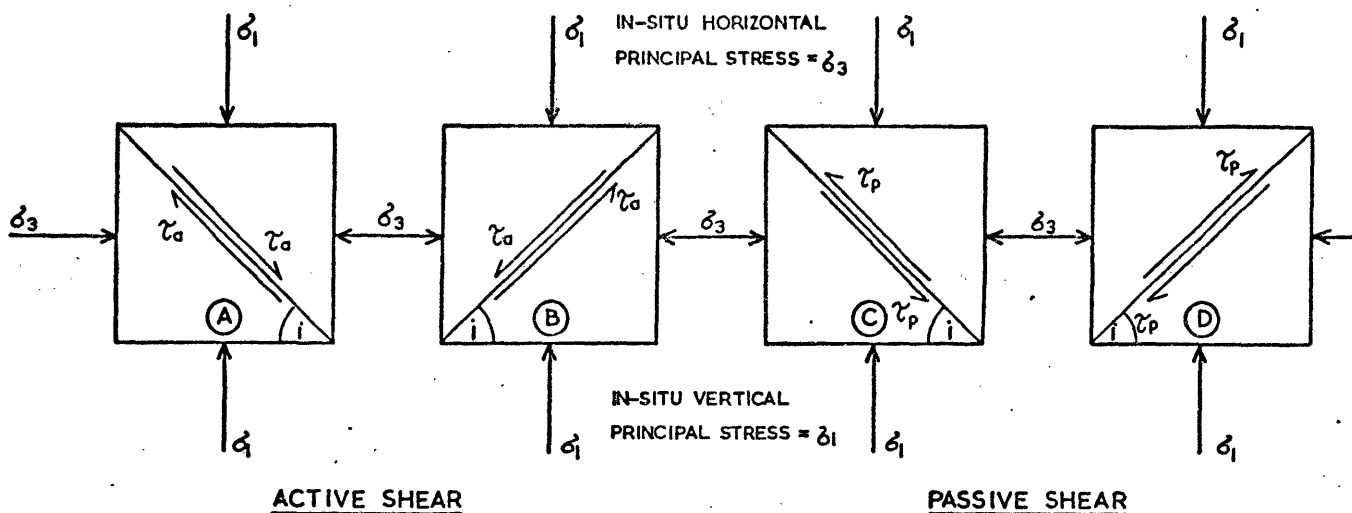
$\frac{T_{max} - T_{min}}{T_{max}} \%$ • IS PEAK STRENGTH
 x BJERRUM'S CORRECTION FACTOR, μ



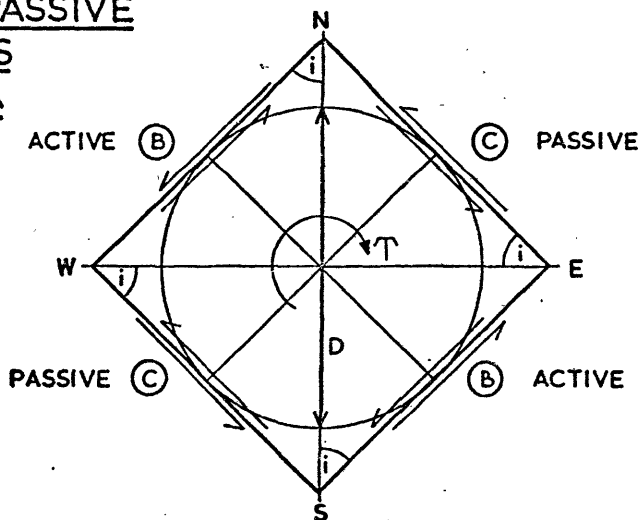


VERTICAL GEONOR VANE TESTS : AVERAGE OF ALL RESULTS

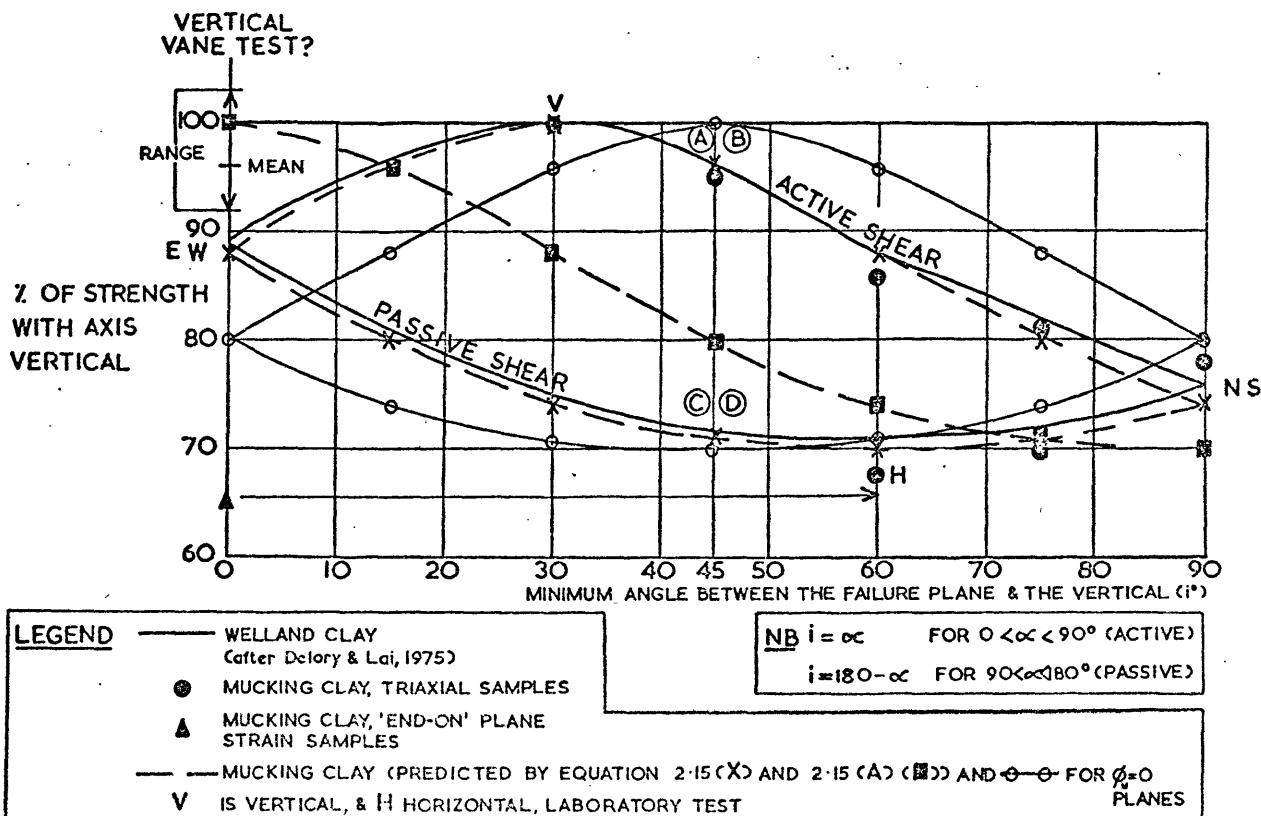
Fig. 3.7



B) ACTIVE AND PASSIVE SHEAR PLANES RELATED TO A HORIZONTAL VANE TEST

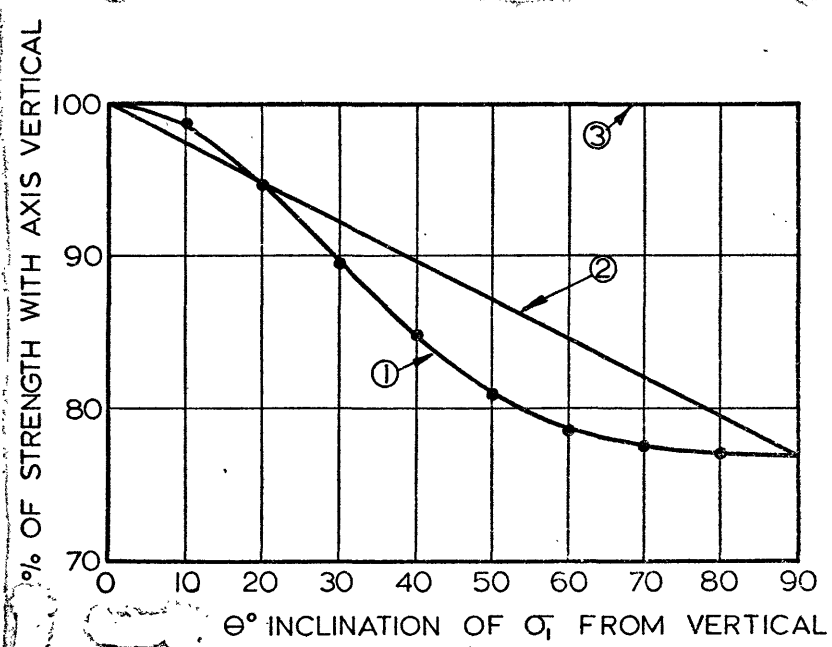
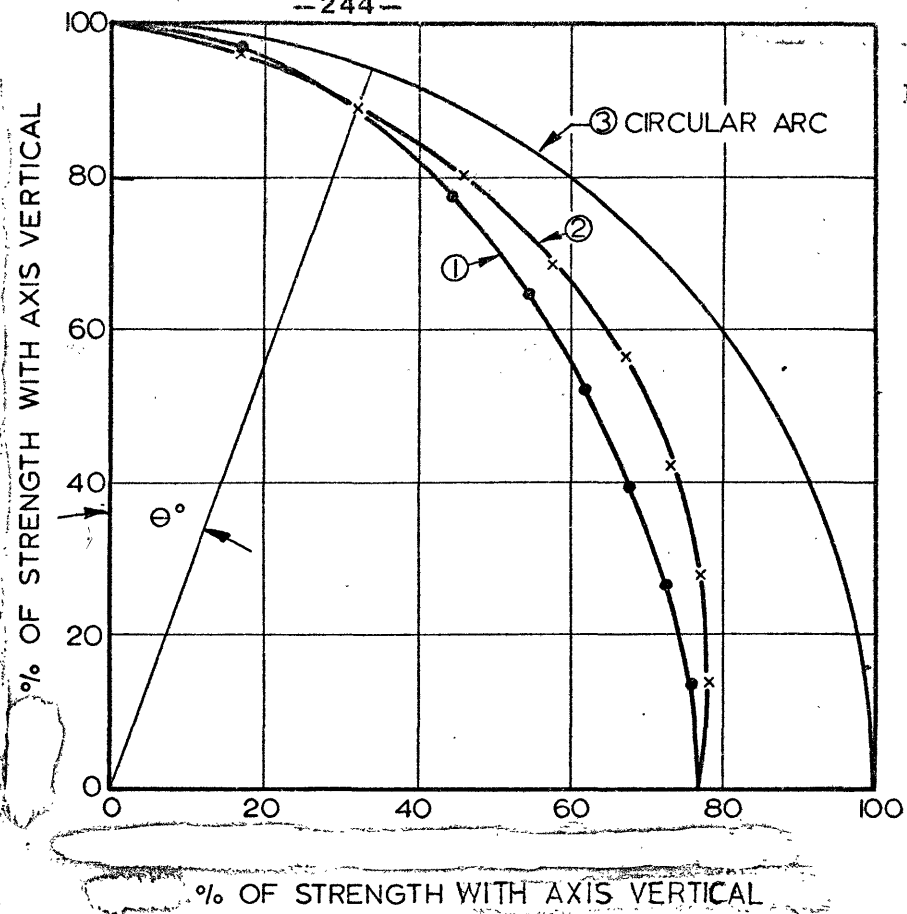


C) ACTIVE AND PASSIVE SHEAR PLANES IN LABORATORY TESTS



UNDRAINED STRENGTH ANISOTROPY RELATED TO INCLINATION OF SHEAR PLANE & SHEAR DIRECTION

FIG. 3.9



(1) θ = Inclination of major principal stress with respect to vertical axis. Variation of undrained strength with θ given by Bishop's equation (2.15)

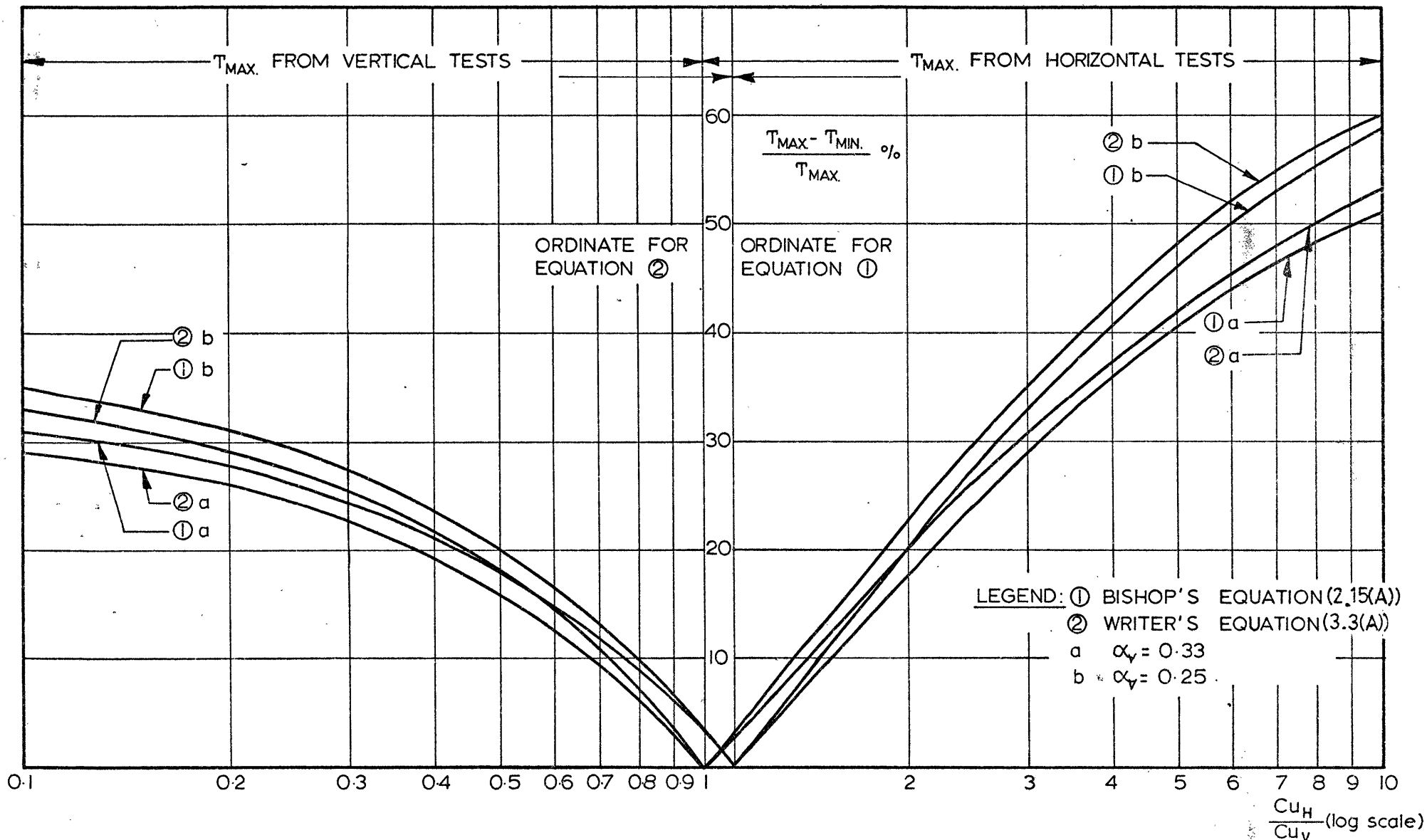
$$C_{u\theta 1} = C_{uv1} (1 - a \sin^2 \theta) (1 - b \sin^2 2\theta) \quad (a = 0.23, \quad b = 0.065 \text{ from laboratory data})$$

(2) θ = Inclination of shear surface to vertical. Variation of undrained strength with θ given by equation assumed for vane analysis (3.3)

$$C_{u\theta 1} = C_{uv1} \left[1 - \frac{2}{\pi} \theta^r (1 - x) \right] \quad x = \frac{C_{uH1}}{C_{uv1}} \text{ (Assumed = 0.77 for comparison with (1))}$$

(3) Undrained strength constant for all θ .

DIAGRAMS SHOWING VARIATION OF UNDRAINED STRENGTH



DETERMINATION OF C_{uH}/C_{uV} FROM RESULTS OF HORIZONTAL AND VERTICAL VANE TESTS

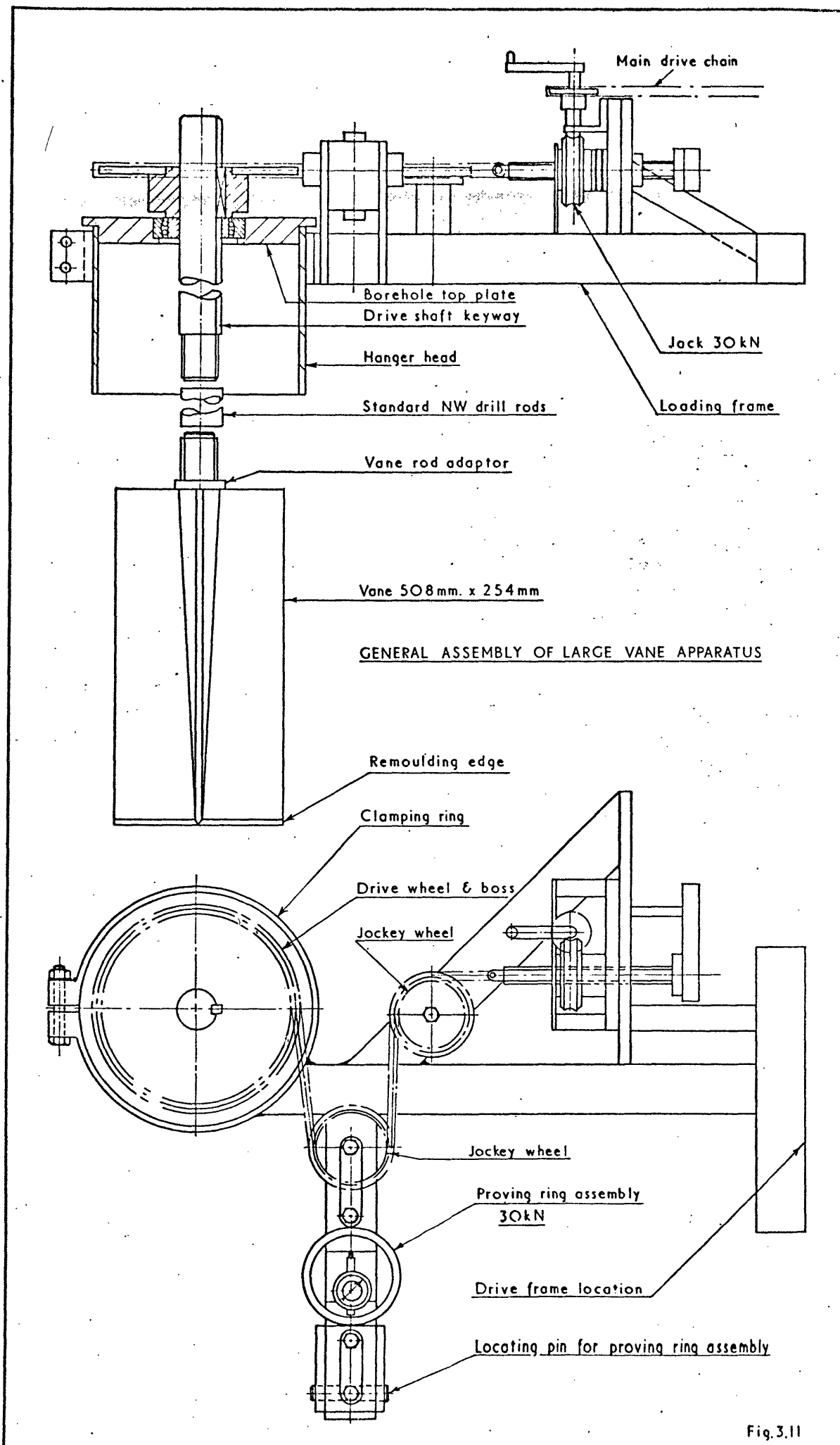


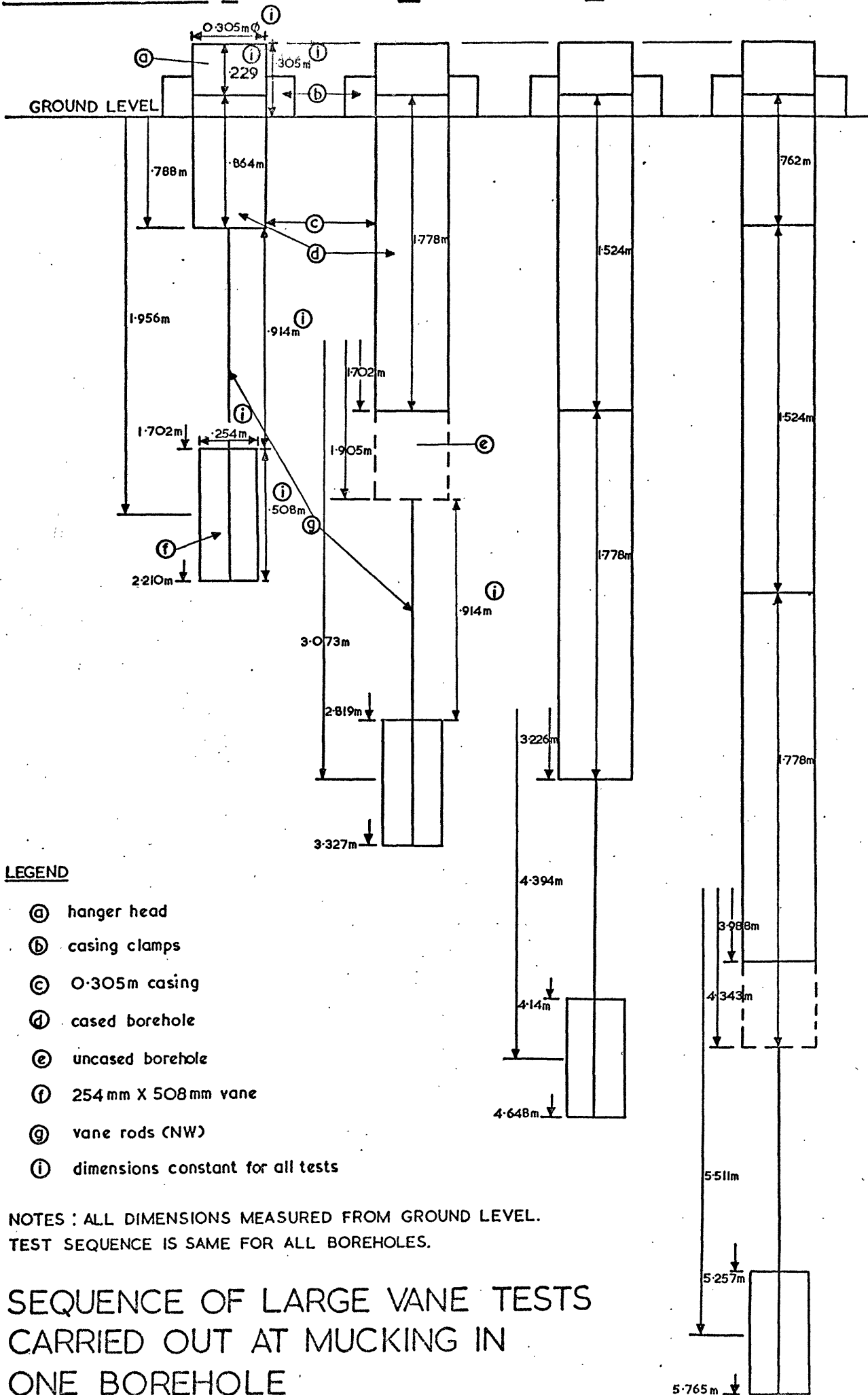
Fig.3.11

TEST LEVEL No. 1

2

3

4

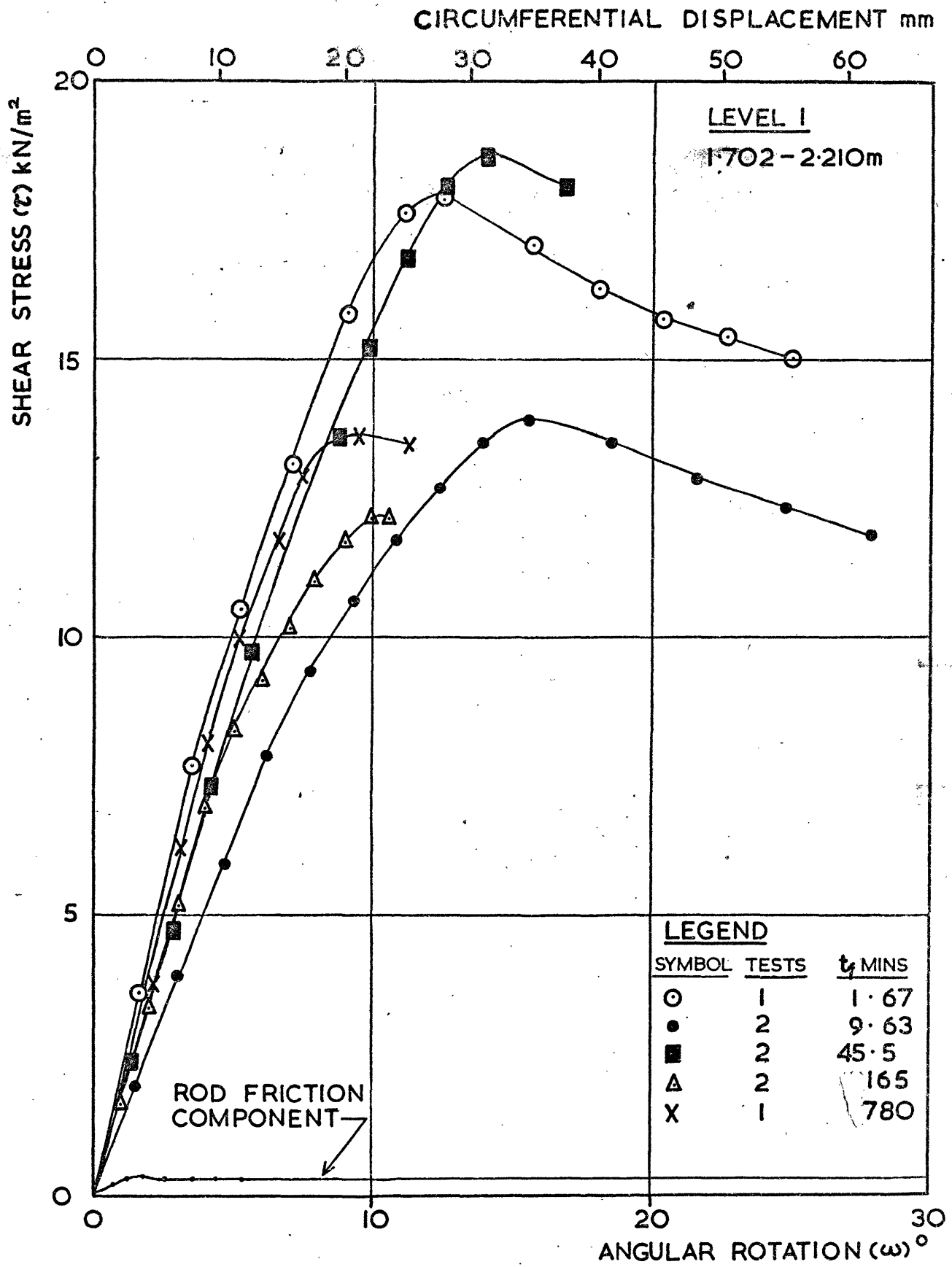


LEGEND

- (a) hanger head
- (b) casing clamps
- (c) 0.305m casing
- (d) cased borehole
- (e) uncased borehole
- (f) 254 mm X 508mm vane
- (g) vane rods (NW)
- (i) dimensions constant for all tests

NOTES : ALL DIMENSIONS MEASURED FROM GROUND LEVEL.
TEST SEQUENCE IS SAME FOR ALL BOREHOLES.

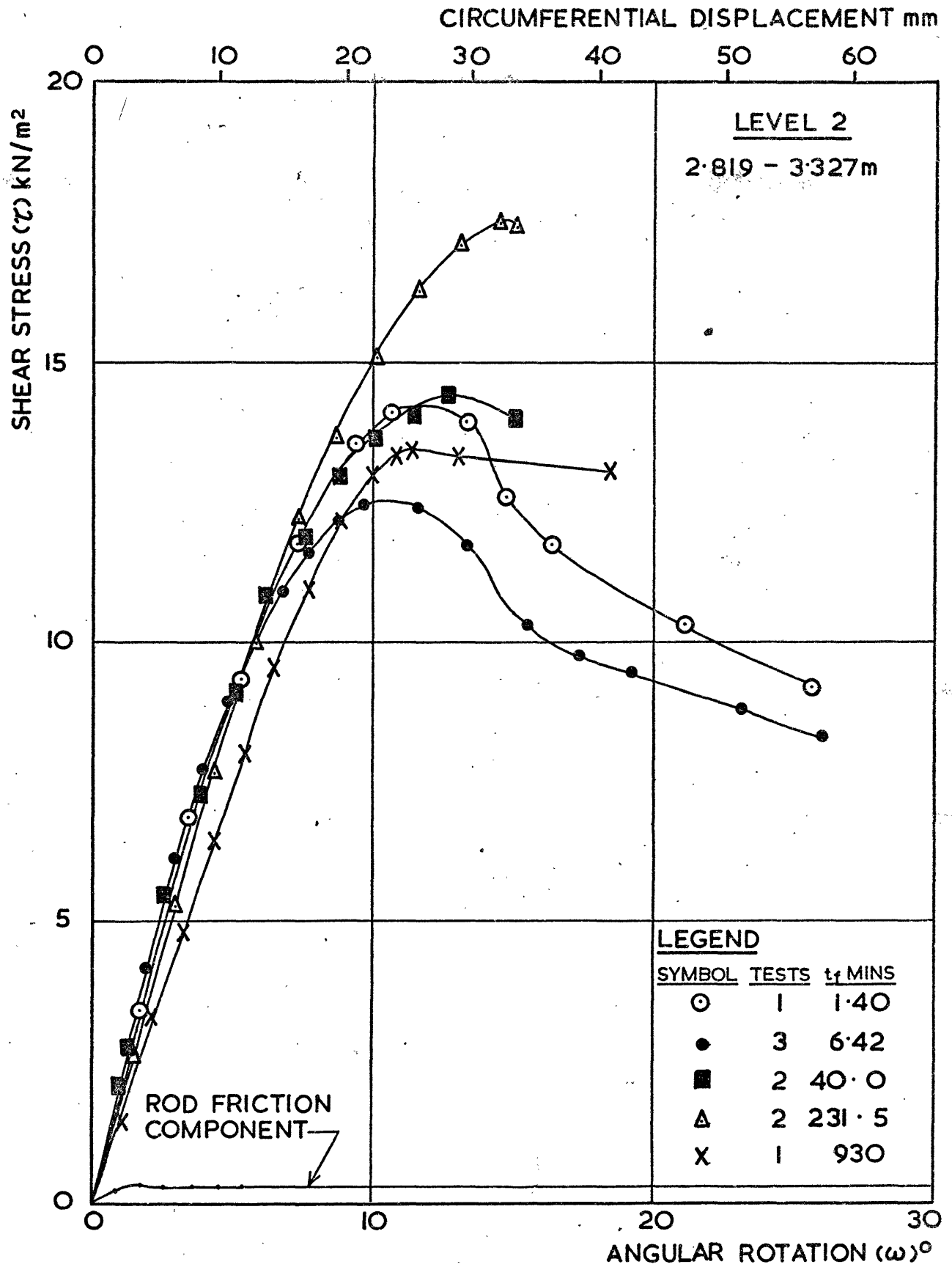
SEQUENCE OF LARGE VANE TESTS
CARRIED OUT AT MUCKING IN
ONE BOREHOLE



LARGE VANE TESTS

MOBILISED SHEAR STRESS VERSUS ANGULAR ROTATION

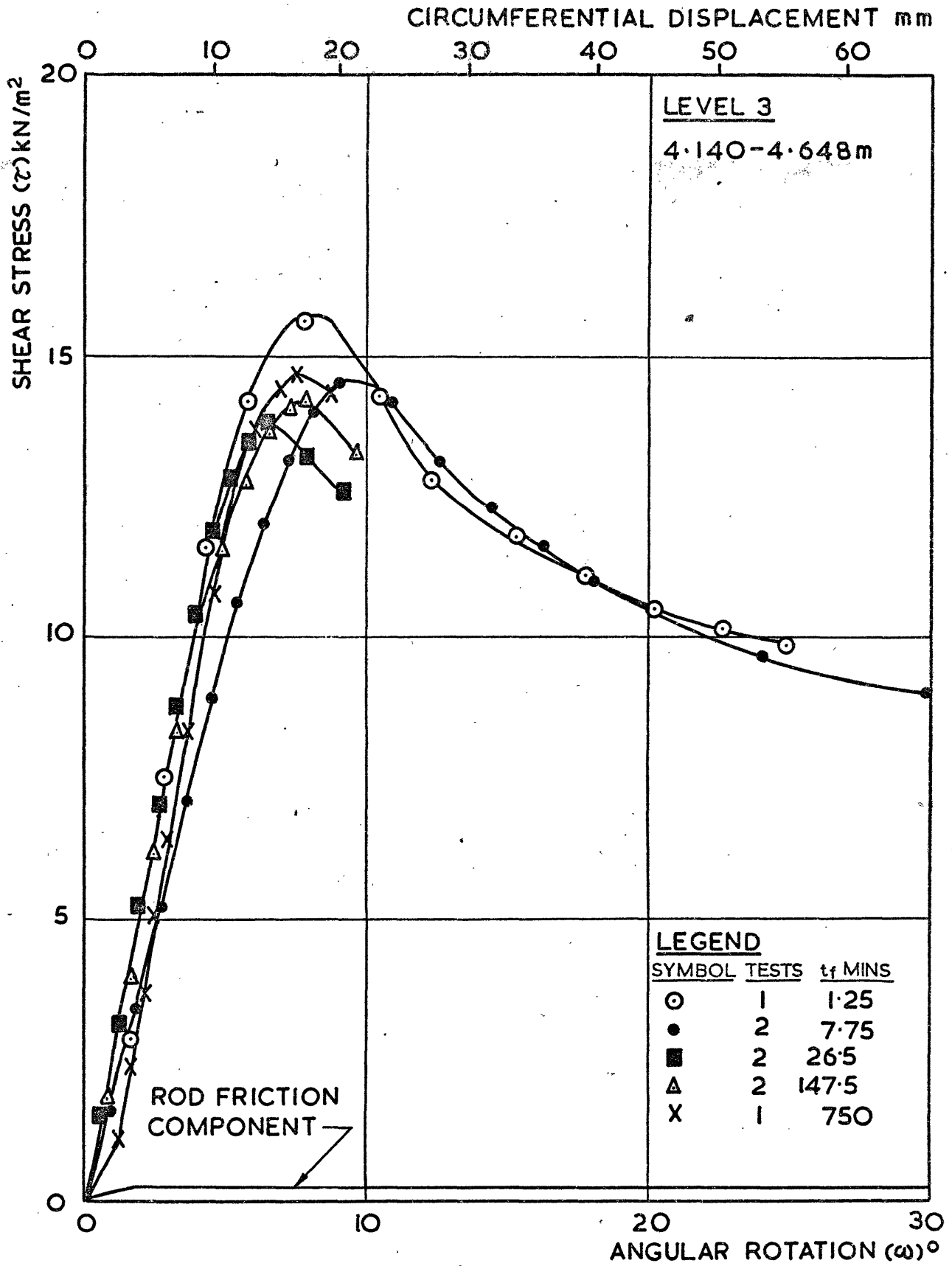
Fig. 3-13



LARGE VANE TESTS

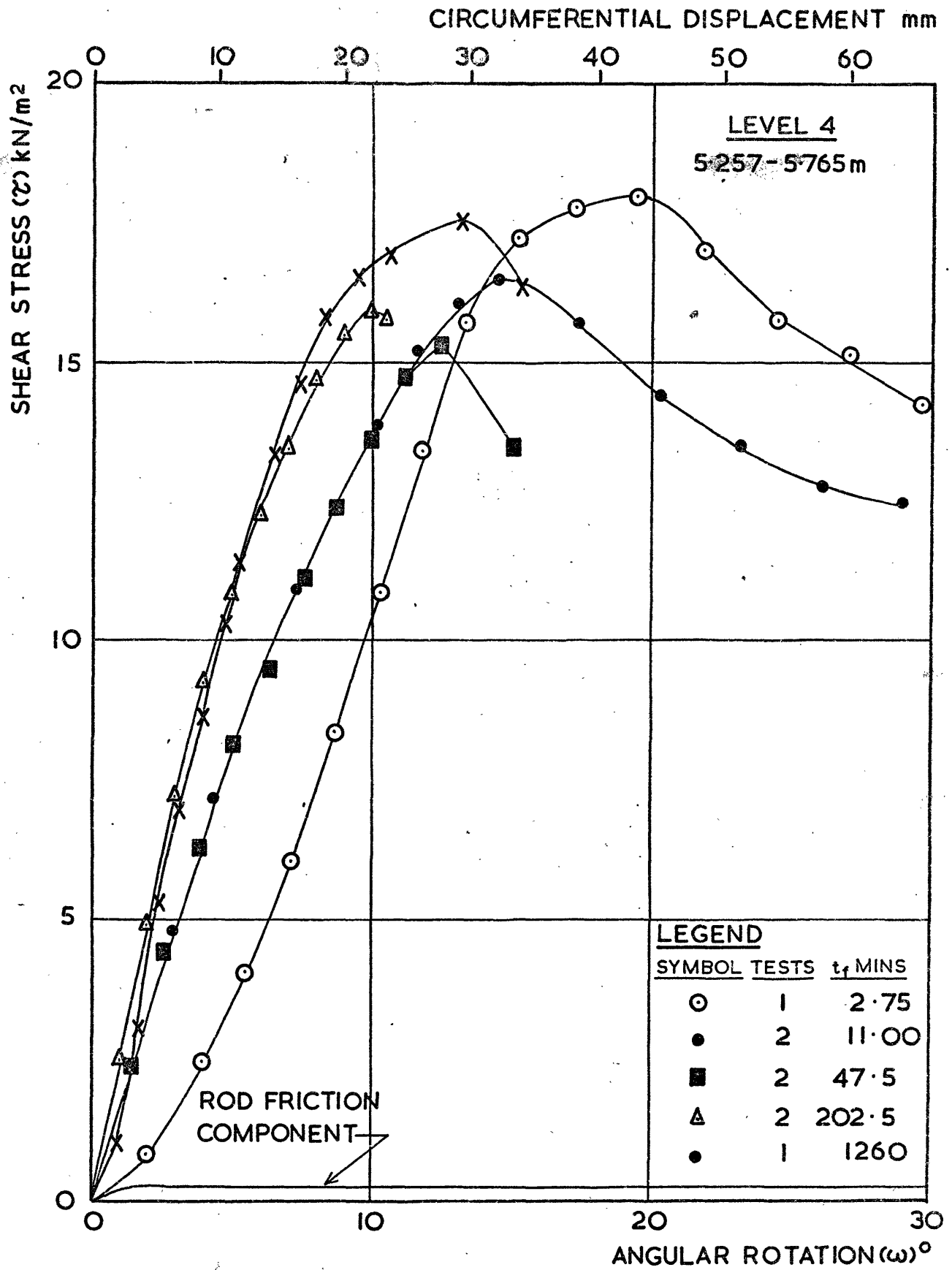
MOBILISED SHEAR STRESS VERSUS ANGULAR ROTATION

Fig. 3.14



LARGE VANE TESTS

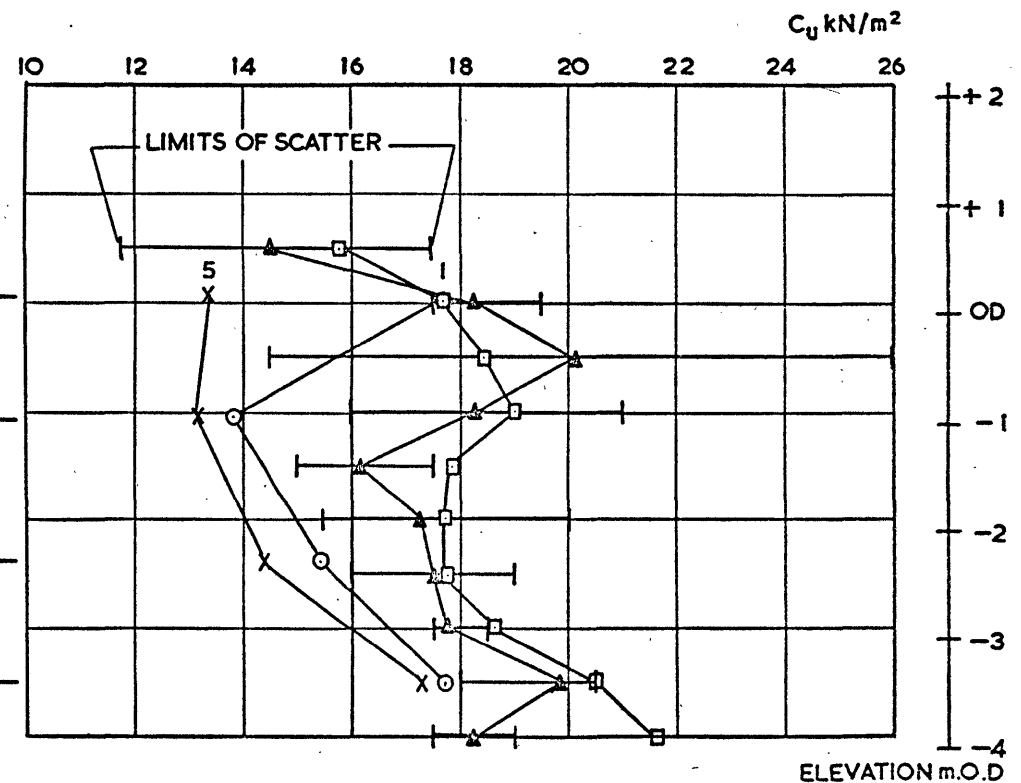
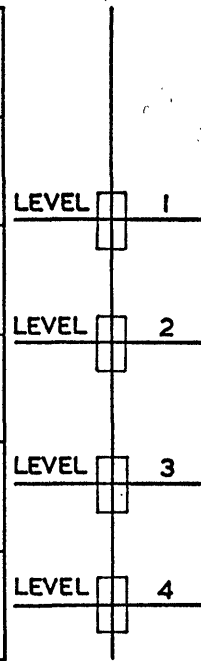
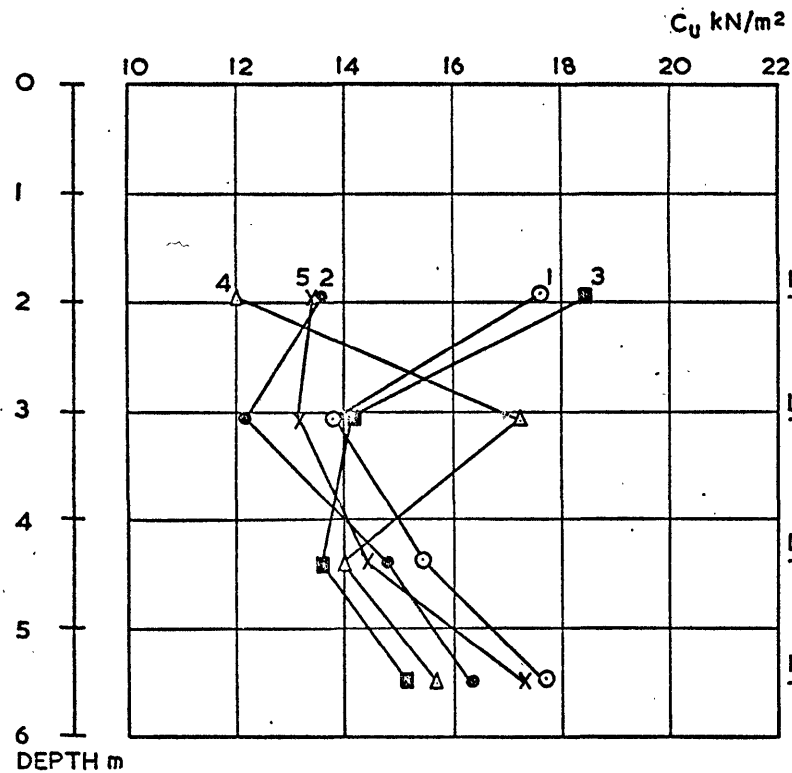
MOBILISED SHEAR STRESS VERSUS ANGULAR ROTATION



LARGE VANE TESTS

MOBILISED SHEAR STRESS VERSUS ANGULAR ROTATION

Fig 3.16

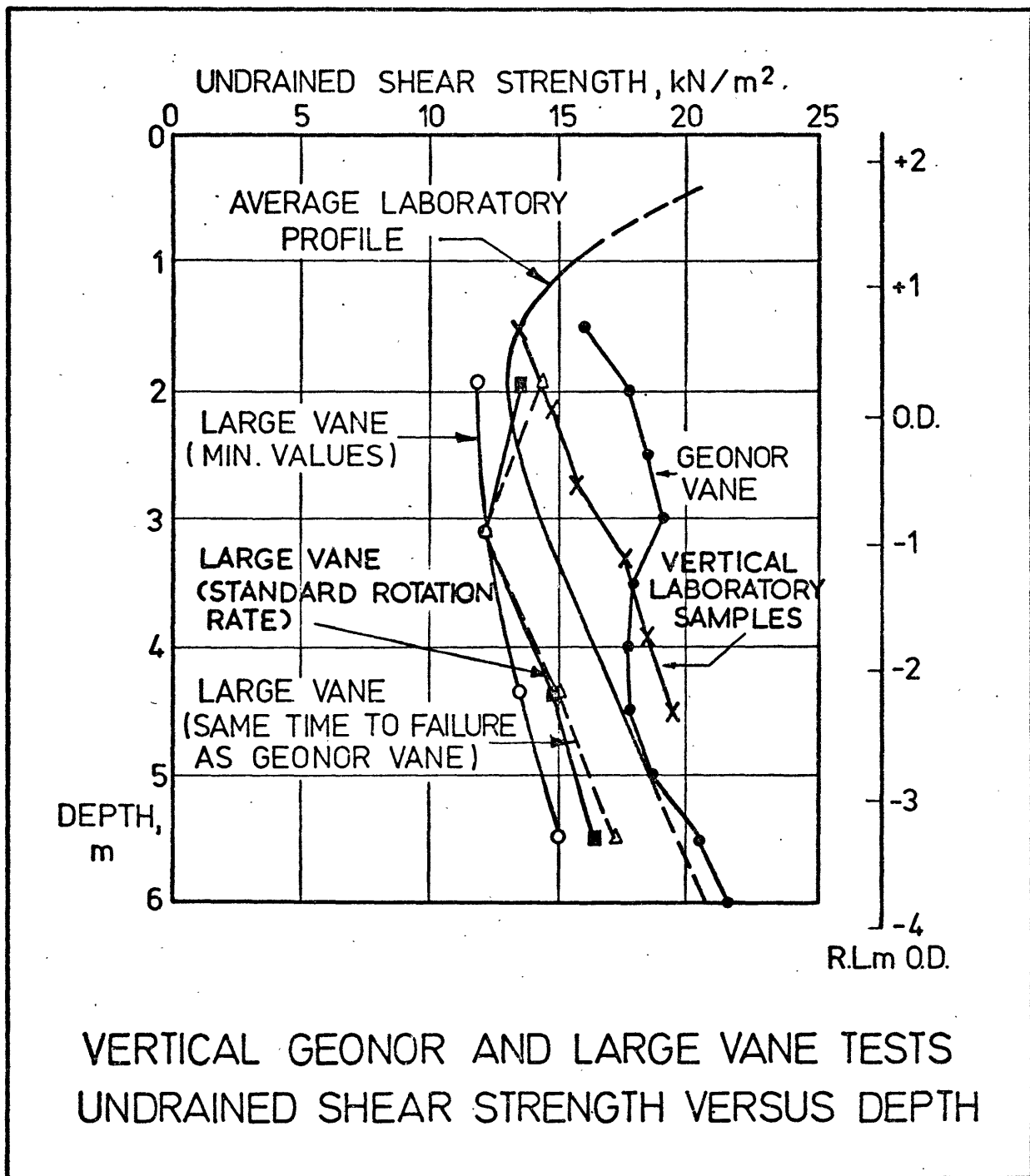


LEGEND				
PROFILE	SYMBOL	VANE SIZE mm	1/2 AVERAGE MINS	COMMENTS
1	○	254 x 508	1.77	LARGE VANE
2	●	"	8.70	"
3	■	"	39.88	"
4	▲	"	186.63	"
5	X	"	930	"

LEGEND			
SYMBOL	VANE SIZE mm	1/2 AVERAGE MINS	COMMENTS
▲	65 x 130	5	GEONOR TESTS ADJACENT TO LARGE VANE TESTS
□	"	5	AVERAGE OF ALL GEONOR VANE TESTS
○	254 x 508	1.77	LARGE VANE
X	"	930	"

COMPARISON BETWEEN AVERAGE RESULTS OF LARGE (254 x 508mm) AND GEONOR (65 x 130mm) VANE TESTS

Fig. 3.17



VERTICAL GEONOR AND LARGE VANE TESTS
UNDRAINED SHEAR STRENGTH VERSUS DEPTH

Fig 3.18

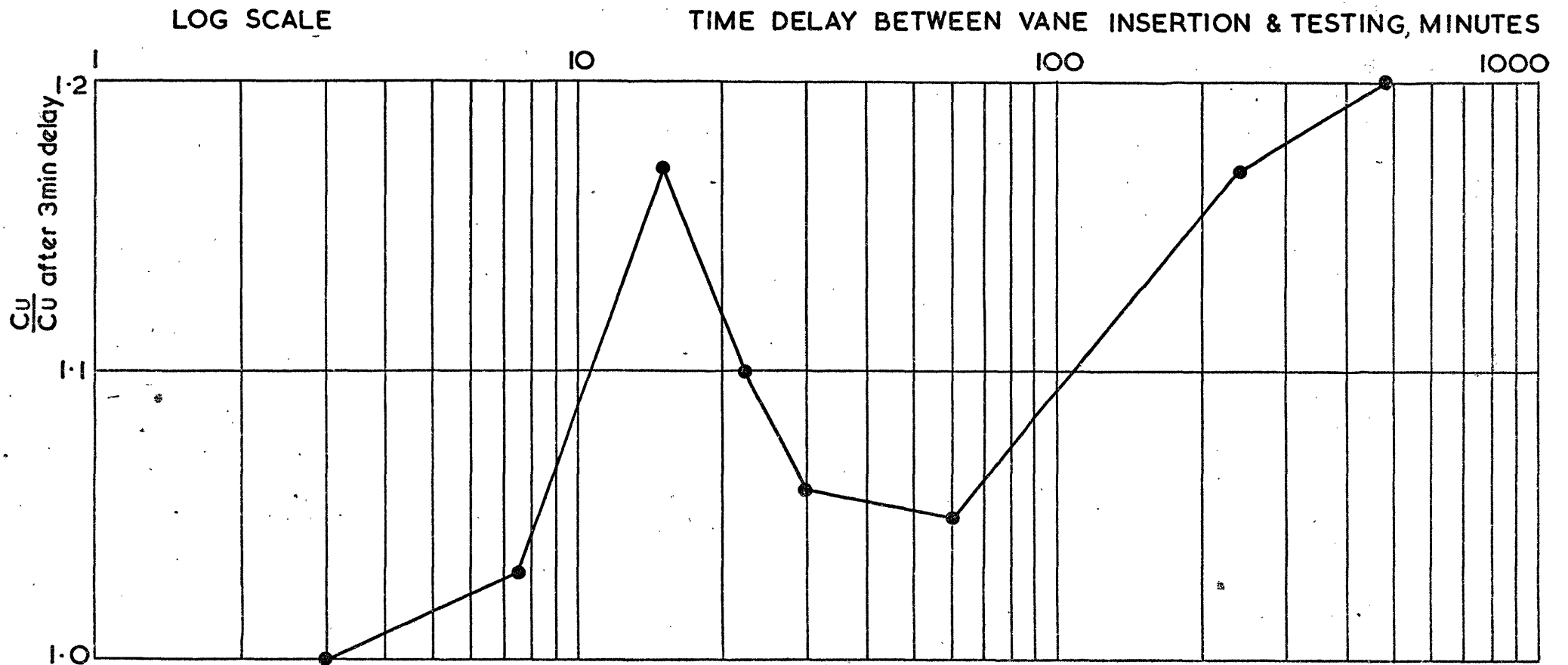
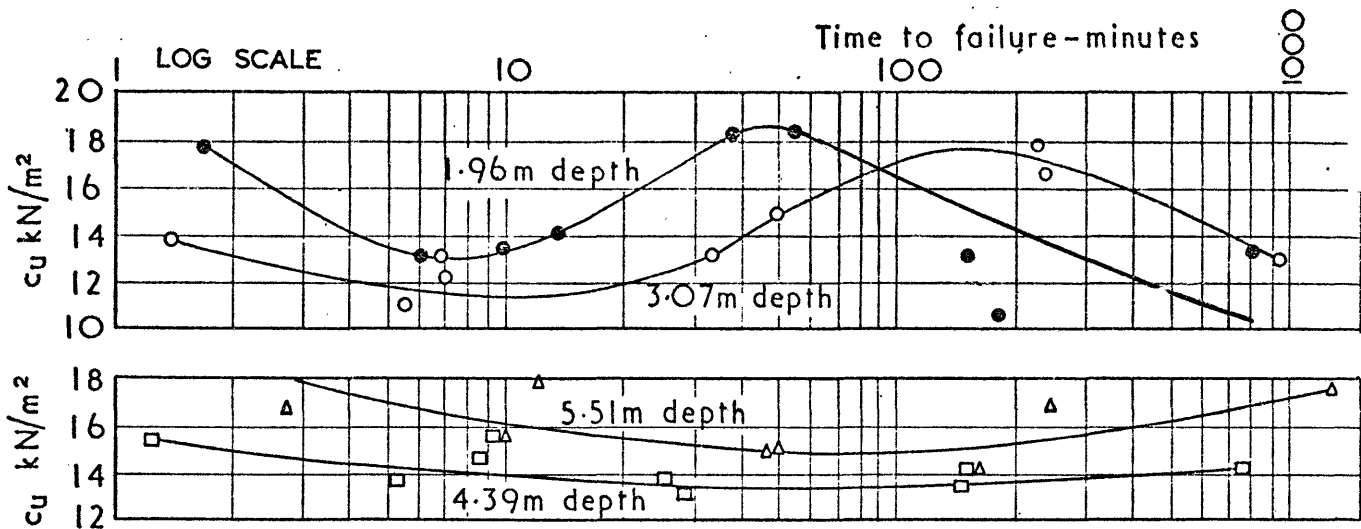
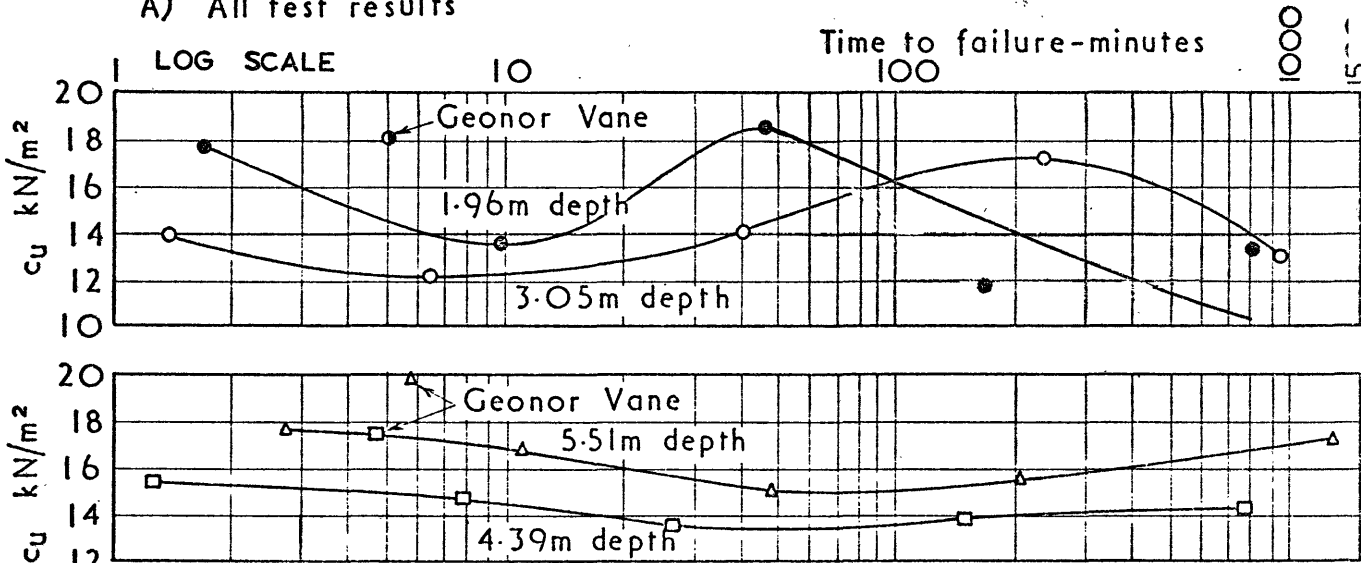


Fig 3.19

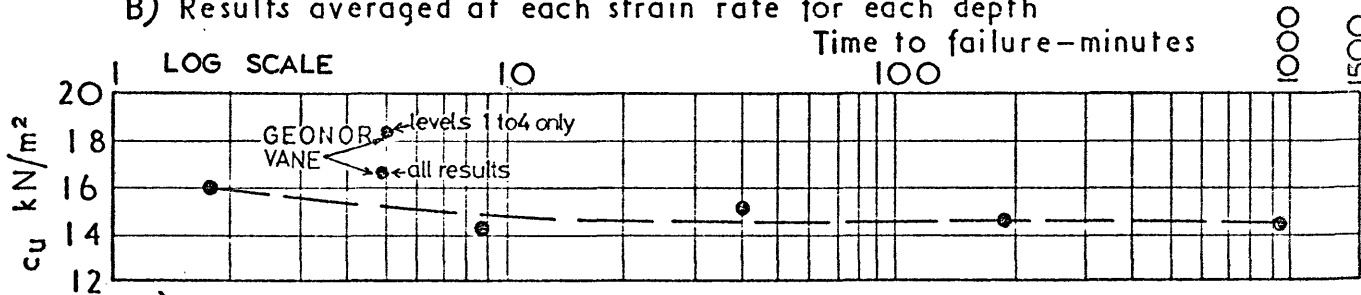
RESULTS OF 'CONSOLIDATED UNDRAINED' VANE TESTS FOR A NORWEGIAN MARINE CLAY (after Flaate, 1966)



A) All test results



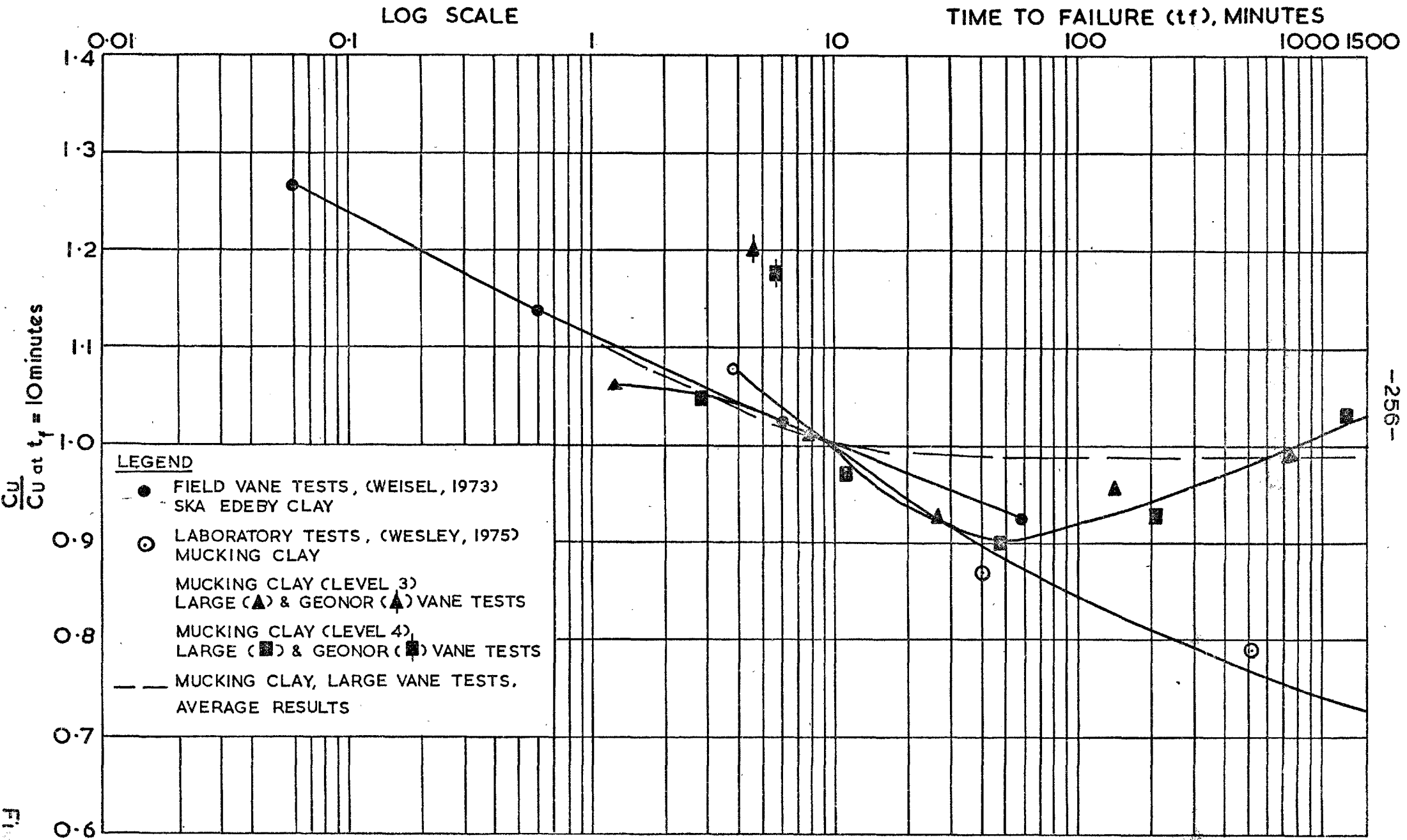
B) Results averaged at each strain rate for each depth



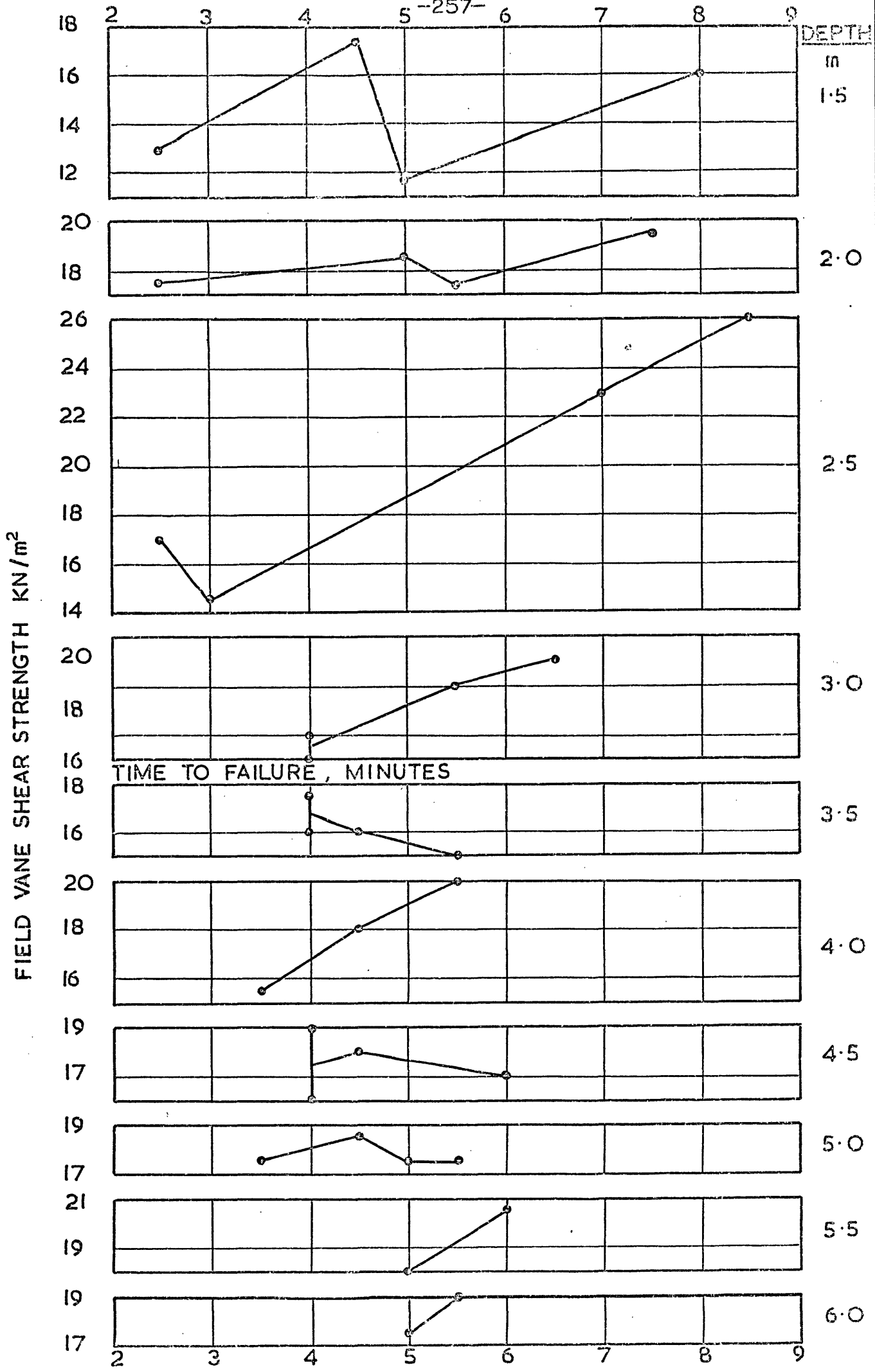
C) All results averaged at each strain rate

LARGE VANE TESTS - UNDRAINED STRENGTH VERSUS LOG TIME TO FAILURE

Fig. 3.20

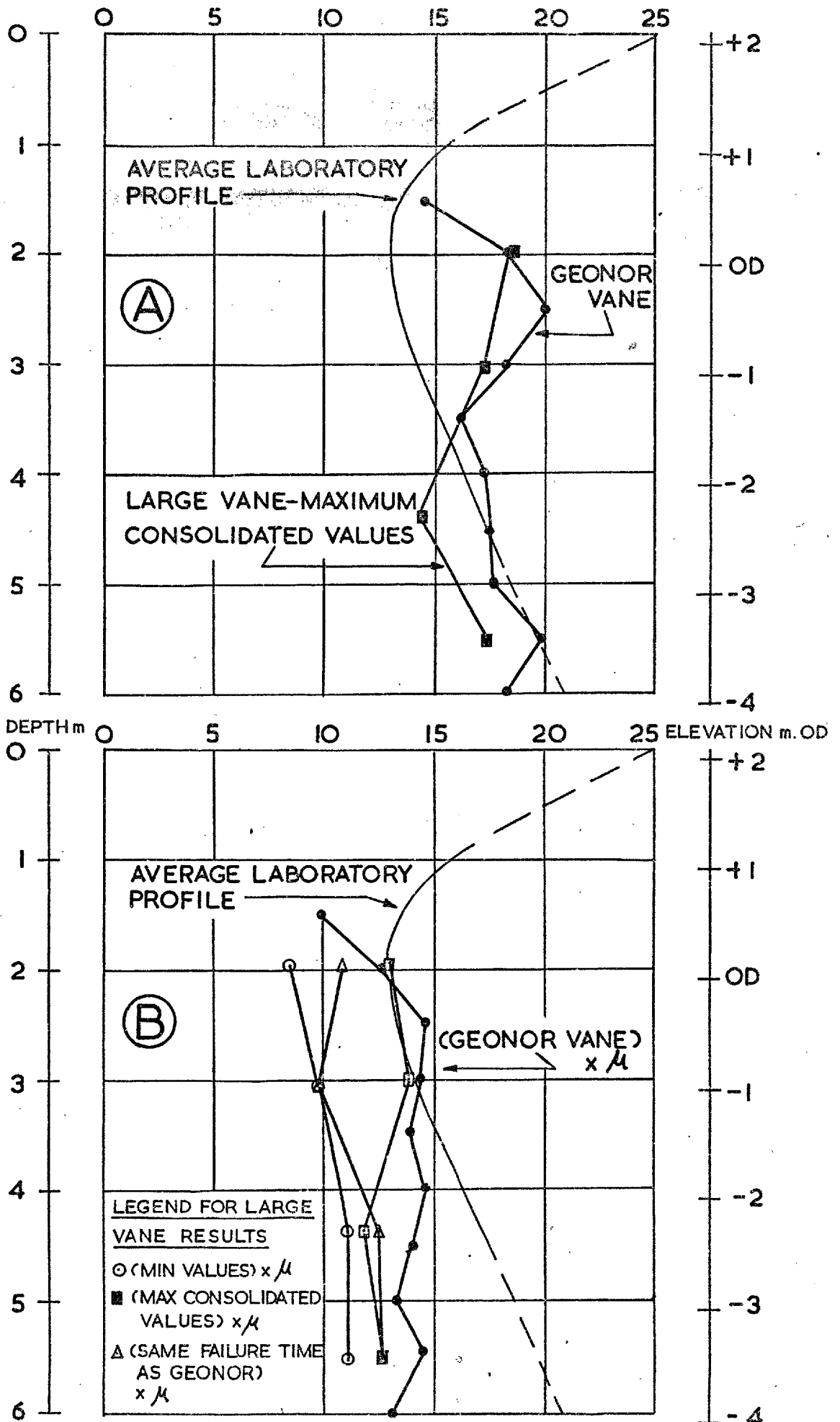


STRAIN RATE INFLUENCE ON LABORATORY AND FIELD VANE UNDRAINED STRENGTHS

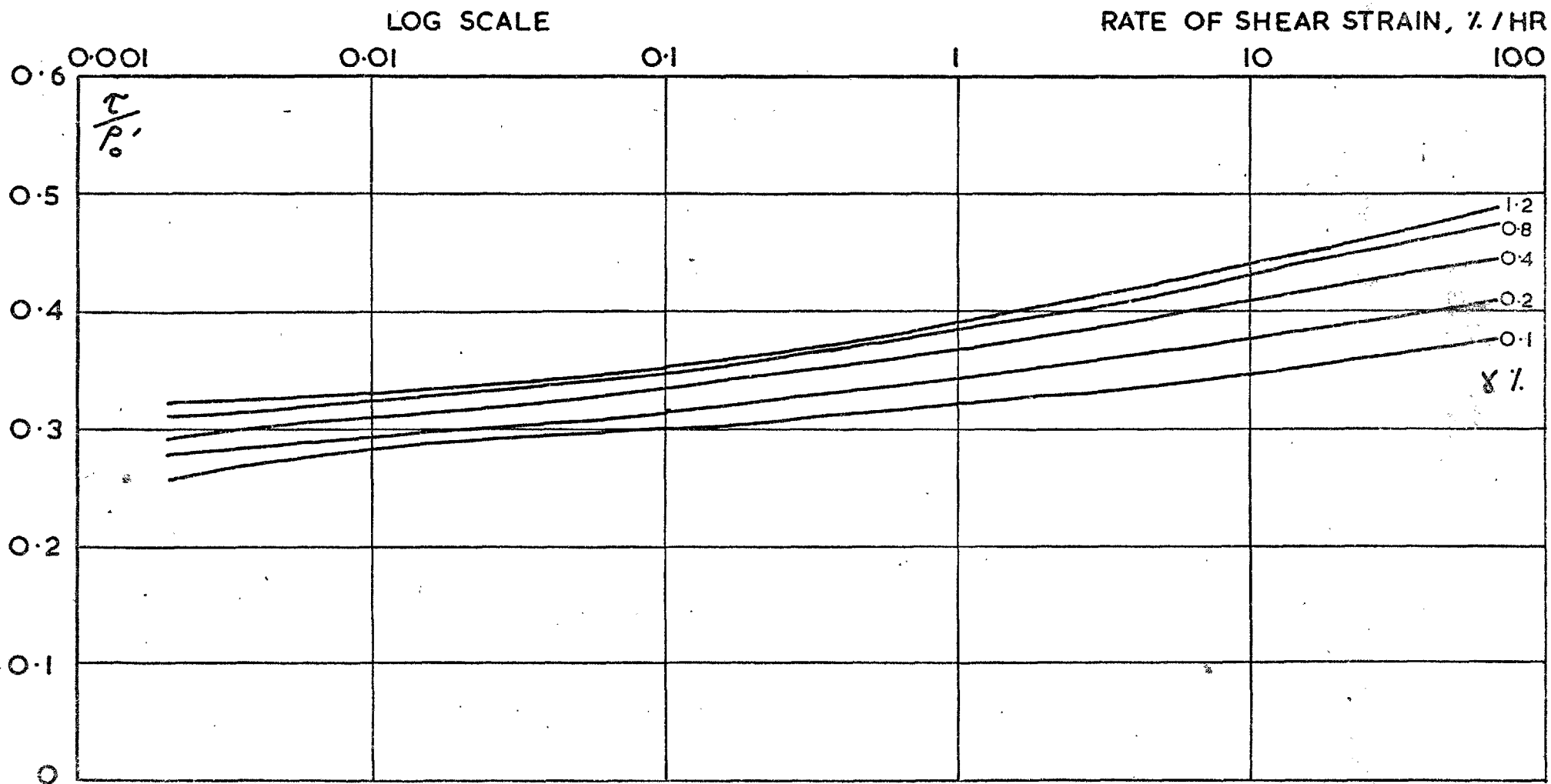


GEONOR VANE TESTS - c_{UFV} VERSUS t_f

Fig. 3.22



INFLUENCE OF (A) CONSOLIDATION AND (B) BJERRUM'S CORRECTION FACTOR ON LARGE VANE TESTS



RATE OF SHEAR STRAIN OBSERVED IN TRIAXIAL COMPRESSION TESTS ON PLASTIC CLAY FROM DRAMMEN, SHOWN AS A FUNCTION OF SHEAR STRESS AND SHEAR STRAIN

(AFTER BERRE AND BJERRUM, 1973)

THE STRENGTH AND DEFORMATION CHARACTERISTICS OF A SOFT ALLUVIAL CLAY
UNDER FULL SCALE LOADING CONDITIONS

A Thesis Submitted to the
University of London
for the Degree of
Doctor of Philosophy in the Faculty of Engineering

by

Richard Stewart Pugh

Volume II



June 1978

CHAPTER 4

CONSTRUCTION, INSTRUMENTATION AND FAILURE OF THE TRIAL EMBANKMENTS

4.1. Descriptions and Aims of the Embankments

It was initially intended to construct four trial embankments on the site, as outlined below:-

4.1.1. Bank 1, Stage 1 (figures 4.1, 4.2 and 4.3)

A rectangular in plan (90m x 34m) embankment designed to induce a plane strain (cylindrical) failure within the 'normally consolidated' foundation material only, and to the southern side of the embankment. These objectives were achieved by the excavation of two 1m deep trenches through the desiccated crust, and the sectional geometry of the embankment fill. At this point it should be noted that the 'east-west' centre line was 14m from the southern toe, the 'north-south' centre line was a true centre line and the embankment failed at a height of 4m. Both trenches were symmetrical about the 'north-south' centre line, the central one being 70m x 10m with its long sides 3.5m and 6.5m to the southern and northern sides respectively of the 'east-west' centre line. This trench was excavated prior to construction. The final cross-section consisted, running from 'north' to 'south', of a 1:2.5 slope up to a height of 2.25m followed by a 3m wide berm and then another 1:2.5 slope up to final crest level of 4m. The final crest width of 10m followed by a 1:2 slope back to original ground level completes the picture of the embankment fill section. The toe trench,

40m x 4m at the surface and 38m x 2m at 1m depth, had its 'east-west' centre line 8m from the southern toe of the embankment and was excavated at a fill height of 2.75m.

The principal aims of this embankment are listed below:-

- a) To enable the determination of the undrained strength of, and the effective stress parameters for, the 'normally consolidated' material under full scale loading conditions.
- b) To assess the laboratory and in-situ shear strength measurements in the light of a) and hence examine the significance of undrained loading rates, shear strength anisotropy and progressive failure.
- c) To study the deformations and excess pore-water pressures generated during the construction, and prior to, during and after the failure of such an embankment.
- d) By means of finite element analyses to assess the laboratory deformation moduli (undrained) and pore-pressure parameters and to investigate the effects of stress paths predicted by the analyses.
- e) To study the performance of various types of instrumentation with regard to the future monitoring of actual structures.
- f) To assess which, if any, of the measured quantities provided the best warning of approaching failure.

4.1.2. Bank 1, Stage 2 (figures 4.1, 4.3 and 4.4)

The follow up to Bank 1, Stage 1 designed to induce a plane strain (cylindrical) failure passing through both the 'normally consolidated' and desiccated foundation material, and to the northern side of the

embankment. This was achieved by means of the sectional geometry alone. The embankment was again rectangular in plan (90m x 47.5m) with the same centre lines and eastern and western toes as for Stage 1, these latter again having a 2:1 slope, and failed at a fill height of 4.5m. The final cross-section along the 'north-south' centre line, again running from 'north' to 'south', consisted of a 2:1 slope up to final crest height of 4.5m, a crest width of 7m and then a 1:2.5 slope down to fill height 2.75m and a 7.5m wide berm. From this berm another 2.5:1 slope led down to a fill height of 1m, this being an approximately 15m wide berm of clay fill covering the heave and toe-trench areas of the Stage 1 failure.

The principal aims of this embankment were as for Stage 1 but including the effect of the desiccated crust, and with no finite element work intended.

4.1.3. Bank 2 (figures 4.1 and 4.5)

A rectangular in plan (75m x 25m) embankment designed to load the foundation, with the desiccated crust intact, in plane strain conditions to the stress levels imposed by a working factor of safety (1.4 to 1.6)*. The embankment was constructed to the 'east' of Bank 1 and on the same 'east-west' centre line, about which it was symmetrical. The final fill height was 2.80m, with a computed factor of safety of approximately 1.5*at the end of construction, all side slopes being 1:2.

*in terms of effective stress

The main aims of this embankment are listed below:-

- a) To monitor pore-water pressures and deformations, both during and after construction, within the foundation material at working stress levels.
- b) To thus compare the settlement, deformation and pore-pressure characteristics (including time dependence) with those predicted by laboratory tests.
- c) To measure the long-term settlements and lateral displacements which would be incurred by a working structure, with subsequent loss of free board.
- d) To assess the ability of selected instrumentation, on a much reduced scale compared to Bank 1, to monitor a working structure over a long time period.

4.1.4. Bank 3 (figure 2.3)

A circular in plan (axisymmetric) embankment constructed to a fill height of 4m to study the consolidation characteristics of the foundation material. The height of this embankment was based on laboratory undrained strengths measured in quick undrained tests on vertical piston samples (section 2.4.3) and the embankment was the first to be constructed. It subsequently failed and is described in the text but is not quantitatively analysed.

Due to this unforeseen failure it was necessary to construct a second consolidation study embankment, designated Bank 4.

4.1.5. Bank 4 (figures 4.1. and 4.5)

A circular in plan (axisymmetric) embankment with a base diameter of 24m, crest diameter of 16.5m, fill height of 2.5m and side slopes of 1:1.5. This embankment, similarly to Bank 2, was designed with the knowledge gained from Bank 1.

All the embankments were constructed from a clean, well graded, fine to coarse sand, this being a local Thames Terrace deposit. It was hoped that the use of this material would avoid complications in the analyses (limit equilibrium and finite element).

4.2. Site Work Prior to Instrument Installation and Embankment Construction

4.2.1. Prior to Instrument Installation

The positions of the five embankments are shown on the site plan (figure 2.3) as well as the hard-cored roadways which were constructed at this stage. Topsoil was stripped across the site of each embankment to a depth of about 200mm and the central, vertically sided, trench for Bank 1 was excavated to a depth of 1m. Sand fill was then placed over these areas to a level about 100mm proud of original ground level, to provide a working surface for the installation of the instruments. The topsoil was stored for reinstatement purposes.

4.2.2. Prior to Embankment Construction

The instrumentation installations carried out by Soil Instruments Ltd., under contract, were completed first. These comprised the inclinometer

casings, slip surface indicators, horizontal settlement gauges, vertical settlement unit, temporary bench marks, piezometers and the gauge house. Great care was taken wherever instruments or their connection leads crossed roadways and wooden mats were used to protect such installations. Except on the actual embankments, plant movements were restricted to the roadways as far as practicable. The contract instrumentation was installed under the direct supervision, and to the satisfaction of, the Engineer's staff.

The remaining instrumentation, comprising the vertical settlement plates, surface movement targets, heave pins and survey stations, was installed by the Engineer's staff. This pre-construction work was completed in a 12 week period from the end of April until the end of July, 1973. The pre-construction work for Bank 4 followed similar lines, being carried out in the last week of August, 1973.

A large part of the survey installations was obviously carried out during construction. Full details of the instrumentation, installations and performance are given in the next chapter whilst layouts and locations are shown in the plans and sections (figures 4.1 to 4.5).

4.3. Construction, Monitoring and Failures

4.3.1. General

The construction of each embankment was preceded by the initial reading of all the instruments. This entailed obtaining three sets

of readings, consistent within the accuracy of the measurements, for each instrument. The piezometers were read as often as possible prior to construction, in order to be sure that 'steady state' conditions were being monitored.

The basic construction sequence of each embankment was in layers, of variable thickness but on average about 500mm. Instrument readings were generally taken after the completion of each lift, and more frequently if deemed necessary. This approach was largely necessitated by the amount of vibration set up by plant movements (particularly sand delivery lorries), the horizontal settlement gauges and the surveying equipment being most susceptible to such disturbances.

The construction was carefully controlled as regards level and line, accuracies of better than $\pm 50\text{mm}$ and $\pm 20\text{mm}$ being respectively aimed for. The embankments were constructed as near to profile as possible and carefully hand trimmed to exact profile after completion of each lift. In-situ density tests were carried out in the sand fill by a water replacement method (using a polythene liner) after each lift. Grading tests were performed on sand samples taken at intervals throughout the construction program.

The following outline of the construction and failure sequences has been condensed as far as possible by the use of tabulation.

The embankments are considered in chronological order.

4.3.2. Bank 3 (table 4.1)

The sand was delivered directly to the location by lorry, placed by dragline (1m³ bucket) and spread by dozer. This embankment was constructed first in order to provide all round experience for the construction of Bank 1; in this it was very successful! The failure can, in hindsight, be attributed to two causes:-

- a) the embankment was constructed too close to the nearby drainage ditch,
- b) the height was calculated on the basis of an overestimate of the undrained strength of the foundation. The embankment had a factor of safety of 1.28 at 4m height on this basis with level ground all around.

Circular arc analyses (in plane strain) of this axisymmetric structure are obviously approximate but subsequent analyses using the undrained strength data derived from Bank 1 and the correct geometry yielded a factor of safety of 1.0 ± 0.05 for Bank 3.

4.3.3. Bank 1, Stage 1

(i) Construction (table 4.2)

The sand was again delivered to the bank location by lorry. The dragline operated along the entire southern toe of the embankment, initially, and placed the fill for spreading by two dozers. As the embankment height increased the dragline was restricted to the south-eastern end of the bank.

(ii) Failure (table 4.3)

The fill level was at 4m over the central parts of the embankment, dropping away slightly to the eastern and western ends by 1730 hours on 9.10.73 when construction finished for the day. The embankment had been properly trimmed to profile and the top was raked flat. The only cracks observed were tension cracks in the base of the toe trench. At 1930 hours, just after an inspection of the bank had revealed nothing untoward, the alarm bell sounded, and tension cracks were visible on the crest. It is worth noting at this point the efficiency of the triggering device and alarm system. The alarm bell sounded and the photographic records (both automatic and manual) were started 15 minutes before visible vertical displacement of the crest occurred, and almost certainly at the instant of formation of the first tension crack.

4.3.4. Bank 1, Stage 2

(i) Construction (table 4.4)

This section includes the transition period between the failure of Stage 1 and the true starting of Stage 2 construction. Firstly the changes in instrumentation are outlined:-

Horizontal Settlement Gauges 'A' and 'B' were both severely distorted in the area of the toe trench. However, the buckled sections were cut out and the access tubes rejoined using oversize collars. These repairs allowed the passage of the draw cords and tape but not the probes. This meant that the probes could not pass under the embankment at all on H.S.G.A. and so only H.S.G.B. was operational during Stage 2.

Inclinometers IA/B 1-3 inclusive were lost during the Stage 1 failure.

Piezometers PA1, 10, 11, 12, 25, 26 and 27 plus PB 10, 11 and 12 were all lost during Stage 1. The piezometers were de-aired as necessary between Stages 1 and 2.

Slip Surface Indicators SA/B 1-5 inclusive were lost during Stage 1 failure.

Heave Pins, Triangulation/Photogrammetry Stations and Targets, the Alarm System, and Time-Lapse Photography Installations were all re-established for Stage 2 in corresponding locations to Stage 1.

Vertical Settlement Gauges A further plate, SPB/2 was installed.

The first stage in the transition was the construction of a clay berm, to a height approximately 1m above original ground level, from the original toe position of Stage 1 to the southern edge of the toe trench. The clay was near surface material excavated by the drag line from an area to the west of Bank 3, and then transported by lorry and spread by the two dozers, these items of plant providing the only compaction effort applied. The embankment itself was then levelled by the dozers to the initial profile for Stage 2. Fill for Stage 2 was brought by lorries to the south-eastern corner of the bank and then placed by the drag line, which was situated on the first construction level (later to become the upper berm) throughout the construction period.

(ii) Failure (table 4.5)

By 1700 hours on the 16.11.73 the fill height over the central area of the embankment was 4.5m grading down to 3.75m at the eastern and western ends, at which time construction finished for the day. At 1705 hours the alarm bell sounded and the time-lapse camera was triggered; however, an inspection of the bank revealed no visible signs of cracking of the fill or heave of the foundation although the crest appeared to be dipping towards the 'east-west' centre line. Inspection of the crest at this time was difficult as it had not been raked flat although the embankment profile had been trimmed to shape. The crest was thus raked flat and smooth and the alarm system re-set. Observation of the mercury pots in the triggering device, and subsequent photographic and photogrammetric data, indicated that the bank was moving quite substantially during this period.

At 2240 hours the alarm bell again sounded and the time-lapse camera was set into motion. Inspection of the embankment revealed that failure had started, there being vertical displacements right from the start in this case. Once more the triggering device and alarm system proved an unqualified success.

4.3.5. Bank 4 (table 4.6)

Prior to the construction of this embankment the drain to the west of its site was infilled with clay, passage of the water being facilitated by concrete pipes in the base of the fill. The sand fill for the embankment was taken from the western end of Bank 1. One

dozer was employed pushing sand from Bank 1 to the drag line, situated between Banks 1 and 4, which then placed it on Bank 4 where it was spread by the second dozer.

After the end of construction readings were taken daily, as far as possible, up to 10 days then every other day for a further 10 days or so and then weekly until the end of permanent site work (end of March, 1974). Thereafter readings were initially taken monthly but this period eventually lapsed to two to three month intervals.

4.3.6. Bank 2 (table 4.7)

The sand for Bank 2 was pushed directly from the position of Bank 1 by the two dozers. The monitoring of the embankment after the end of construction was as described for Bank 4.

4.4. Discussion

The instrumentation, and results obtained from trial embankments 1, 2 and 4, are discussed in detail in subsequent chapters. This section is limited to a discussion of the construction and instrument reading processes. The alternative to the adopted method was to build and read continuously, and this was only rejected, really, because of the difficulties associated with plant movements. The writer now feels, however, that the chosen method had much to commend it over the latter one even if this had been practicable. The site staff, typically on such projects, was small, being only four persons who had to do all the setting-out, supervision of

construction, maintenance and reading of instruments, reading and plotting of data as well as organising the day to day running of the job (which was carried out by direct labour).

The system adopted allowed for the setting-out work, construction supervision, data reduction and plotting and general site work to be carried out whilst construction was in process. At the end of a particular construction lift all hands could be turned to the reading of the instruments, which generally took between four and eight hours for Bank 1. At the same time any final trimming of the banks could be carried out and the plant was free for maintenance or the inevitable small jobs which required doing (mainly keeping the access roads open!). Readings were thus taken regularly and at well defined stages in the construction. The rates of construction are presented in figure 4.6 which shows that there was no appreciable loss in time incurred by the method.

The adoption of twenty four hour site manning, with two extra people carrying out the night shifts, was essential to the monitoring of the failures, and also eased the burden of instrument reading as some could be read at night. However, as will be discussed in the next chapter, this was not always successful. The night shifts were only operated for the last five days before the failures.

With regard to the actual construction it was found that the use of simple batter boards and level posts enabled an accurate profile to

be achieved. The writer has seen trial embankments where it was difficult to imagine what form the geometry was supposed to take. It is obviously fruitless to indulge in such exercises, with vast amounts of expensive instrumentation, if the embankment is not constructed to the standards normally expected in civil engineering earthworks.

LIFT NO.	DATES	DAY NOS	FILL HT AT END OF LIFT	OBSERVATIONS
	1973		m	
1	16/7 - 18/7	1-3	0.5	Weather: unsettled, some rain.
2	19/7 - 23/7	4-8	1.0	Weather: fine
3	24/7 - 25/7	9-10	1.5	Weather: fine
4	26/7 - 27/7	11-12	2.0	Weather: fine
5	30/7 - 31/7	15-16	2.5	Weather: fine
6	31/7 - 1/8	16-17	3.0	Weather: fine
7	2/8 - 3/8	18-19	3.5	Weather: fine. Signs of accelerating vertical movements.
8	6/8 - 7/8	22-23	4.0	Weather: rain. Construction complete. Bank still settling rapidly.
	8/8	24	4.0	Weather: fine. Rate of settlement increasing, pore pressures rising. Damp spots observed around toe of embankment with water ponding in places. This restricted to southern half of embankment toe.
	9/8	25	4.0	Weather: fine. Damp spots worsened overnight and in evidence all around southern part of toe. Cracking and bulging of the fill on S.E. face of embankment. Water observed piping from foundation near western toe area. The cracks in the fill worsened during day until by evening they extended from S.E. toe, up back, across top and down to S.W. toe. Water table at southern toe area was up to 300mm below O.G.L. although surface of foundation still dried and cracked. Pore pressures rising at toe, steady in centre of loaded area.
	10/8	26		Bank failed at about 0400 hours along line of cracks in fill, failure extending into the drain.

Table 4.1. Bank 3 : Construction and Failure

LIFT NO.	DATES	DAY NOS	FILL HT AT END OF LIFT	OBSERVATIONS
	1973		m	
1	20/8 - 22/8	1-3	0.5	Weather: hot & dry.
2	24/8 - 30/8	5-11	1.25	Weather: hot & dry. Delay in construction due to Bank Holiday.
3	5/9 - 8/9	17-20	1.75	Weather: hot & dry.
4	12/9 - 14/9	24-26	2.25	Weather: hot & dry.
5	17/9 - 19/9	29-31	2.75	Weather: changeable, heavy rain. Parts of site flooded. Berm formed on northern side of bank at 2.25m fill height (5.00m AOD). Phototheodolites installed. First mercury line for triggering device installed at 2.50m AOD.
	20/9 - 28/9	32-40	2.75	Weather: changeable. Site very wet, still some flooding. Alarm system installed & tested; also time-lapse camera & target bulbs. Floodlights in position.
	29/9 - 1/10	41-43	2.75	Weather: mild. Site drying out. Toe trench excavated.
6	3/10- 4/10	45-46	3.25	Weather: changeable. Site still wet. Some water standing at bank toes & base of sand fill saturated. 24 hour watch started on bank. Second mercury line installed at 4.00m AOD.
7	5/10- 6/10	47-48	3.50	Weather: heavy rain. Toe areas very wet along whole of embankment.
	7/10	49	3.50	Weather: changeable. First visible evidence of increasing horizontal displacements in form of buckling of HSG tubes in toe trench (A, 74mm: B, 35mm).
8	8/10	50	3.75	Weather: changeable. Final mercury line installed at 6.00m AOD. HSG s continue to buckle; 0530 hrs (A, 89mm: B, 42mm), 1800 hrs (A, 105mm: B, 60mm), 2100 hrs (A, 120mm: B, 66mm).
9	9/10	51	4.00	0345 hrs (A, 128mm: B, 75mm), 0730 hrs (A, 133mm: B, 80mm), 1500 hrs (A, 160mm: B, 100mm). Tension cracks noticed in base of toe trench in the afternoon. 1930 hrs, alarm sounded heralding start of failure.

Table 4.2. Bank 1, Stage 1 : Construction

DATE	TIME	TIME ELAPSED	OBSERVATIONS
1973	hours	minutes	
9/10	1930	0	Alarm triggered. First cracks in fill observed on bank top (50mm wide maximum) extending along 20-25m of crest about 3m from southern edge. No vertical displacement across cracks.
	1945	15	Cracks up to 100mm wide with first signs of vertical displacement around C/S A.
	1950	20	Vertical displacements across cracks 70-100mm maximum.
	1955	25	HSG tubes 'A' & 'B' displaced 340mm & 140mm respectively.
	2005	35	Movement not visible to naked eye but could hear inclinometer tubes buckling. Vertical displacements now 120-150mm near C/S A.
	2008	38	Vertical displacements accelerated to 300 - 500mm. Heave visible in toe trench, especially towards western end. Cracks appearing in foundation between toe & trench.
	2016	46	Heave extending past west end of trench; 500mm of heave in trench.
	2024	54	Maximum vertical displacement of crest 640mm. Heave well developed.
	2026	56	Vertical displacement 750mm.
	2030	60	Signs of secondary movements; crack formed 3m from northern crest, 3.5 m from main crack; 160mm of vertical displacement across new crack. Other intermediate cracks becoming visible.
	2035	65	Cracks extend to within 20m of eastern end & right up to western end of bank crest.
	2100	90	Maximum vertical displacement is 840mm, 5m west of centre line.
	2300	210	Vertical displacement 1m.
10/10	0100	330	Base of toe trench at original ground level.

Table 4.3. Bank 1, Stage 1 : Failure

LIFT NO.	DATES	DAY NOS	FILL HT AT END OF LIFT	OBSERVATIONS
	1973		m	
	9/10	51	4.00	Failure of Stage 1.
	15/10-22/10	57-64	4.00	Weather: cold, wet. Placing toe weight over heaved area.
	23/10-27/10	65-69	2.75	Weather: changeable. Bank to first level for Stage 2.
	27/10- 1/11	69-74	2.75	Weather: warm, dry. Established survey stations, surface targets & time-lapse targets as far as possible. Phototheodolites, time-lapse camera, alarm system & lower mercury line installed. Reading, repairing (& de-airing (9/10 - 1/11) instruments.
1	1/11- 3/11	74-76	3.15	Weather: cold, dry. Start of construction proper.
2	6/11- 7/11	79-80	3.55	Weather: cold, dry. Middle mercury line installed.
3	9/11-10/11	82-83	3.85	Weather: mild, dry. Alarm system connected up.
	11/11	84	3.85	Weather: changeable. False alarm sounded. 24 hr site duty started.
4	13/11	86	4.05	Weather: cold, windy. Max fill height over central area of bank only. Ends 500mm lower from now on.
	14/11	87	4.05	Weather: cold, dry. Final mercury line installed & connected to alarm system.
5	15/11	88	4.25	Weather: cold, dry.
6	16/11	89	4.50	Weather: cold, dry. At 1705 hrs alarm sounded. No cracks visible but crest of bank appeared to be slumping. Mercury pots reset. 2240 hrs alarm sounded again, start of failure.

Table 4.4. Bank 1, Stage 2 : Construction

DATE	TIME	TIME ELAPSED	OBSERVATIONS
1973	hours	minutes	
16/11	2240	0	Alarm triggered. Crack between c/s A & C.
	2250	10	Crack extended west of c/s A & eastwards to c/s B. 60mm vertical displacement at C.
	2305	25	Secondary cracking developing west of c/s A. Toe heave now visible.
	2310	30	Vertical displacements 100mm across crack to west of c/s A.
	2315	35	Heave zone becoming more clearly defined. Tension cracks up to 5mm wide in heaved part of foundation.
	2330	50	160mm, 300mm & 550mm of vertical displacement on c/s B, C & A respectively. Single failure surface through fill at c/s B, but double stepped formation at C & A.
	2335	55	Well defined graben formed to west of c/s A with multiple failure surfaces visible & maximum of 600mm vertical displacement across them. Failure surface extends to western end of bank.
	2340	60	Time-lapse camera failed, possibly due to cold (Temp $\approx 0^{\circ}\text{C}$)
	2345	65	500mm vertical displacement at C.
	2350	70	900mm vertical displacement 11m west of c/s A with multiple failure surfaces forming steps in fill. Stepped formation now extends to C but passes into single failure surface as c/s B is approached.
2400	80	800mm vertical displacement at c/s A, 650mm on C.	

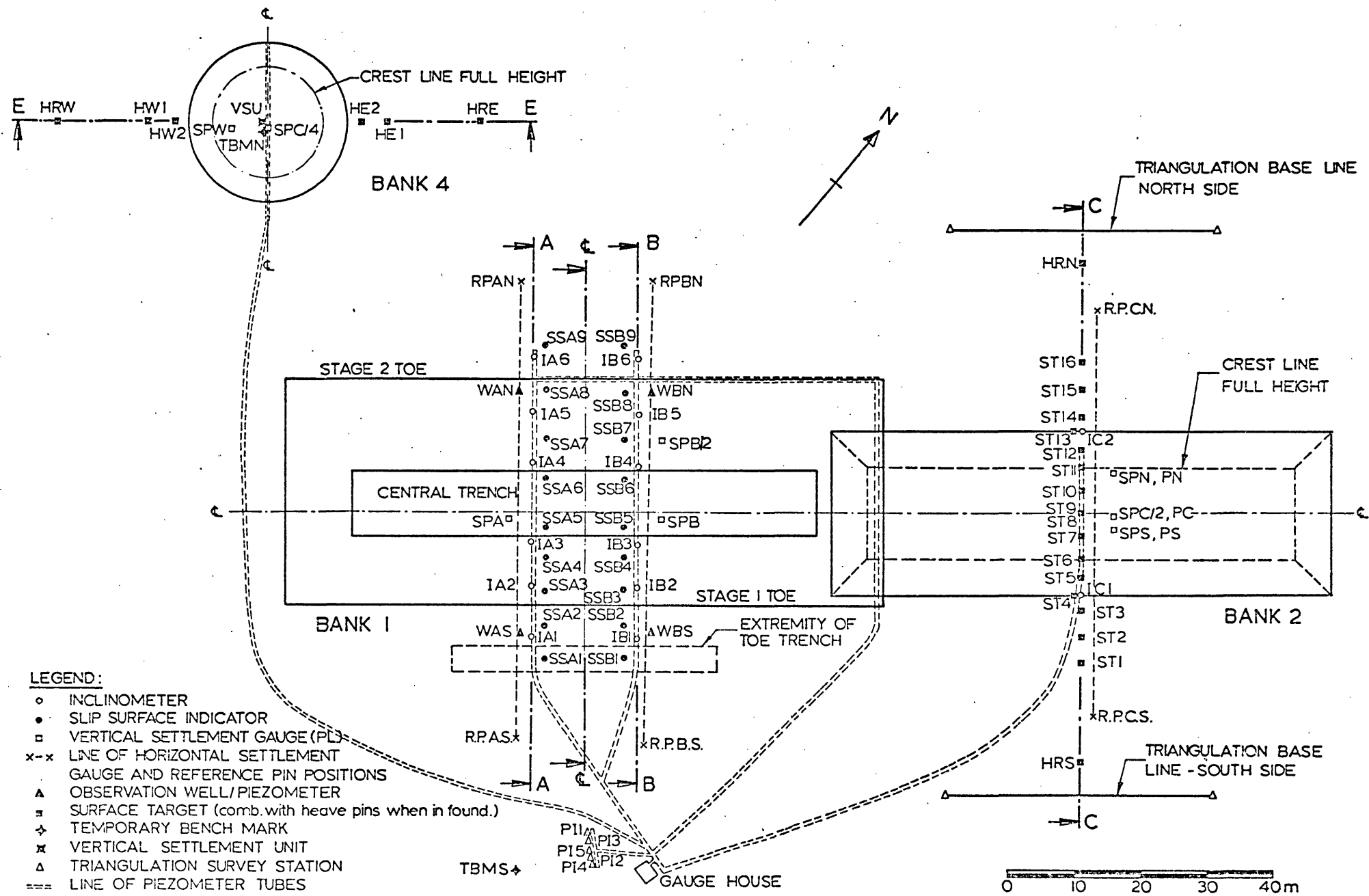
Table 4.5. Bank 1, Stage 2 : Failure

LIFT NO.	DATES	DAY NOS	FILL HT AT END OF LIFT	OBSERVATIONS
	1973		m	
1	4/12 - 5/12	1-2	0.85	Weather: V. cold, wet.
2	5/12 - 6/12	2-3	1.45	Weather: cold, dry. Site starting to dry out, very wet previously.
3	7/12 -10/12	4-7	1.90	Weather: mild, dry.
	11/12 -12/12	8-9	1.90	Weather: heavy rain. Readings at end of lift 3 repeated. No sign of increasing settlement or pore pressures with time.
4	12/12 -13/12	9-10	2.50	Weather: fine. Construction complete.

Table 4.6. Bank 4

LIFT NO.	DATES	DAY NOS	FILL HT AT END OF LIFT	OBSERVATIONS
	1974		m	
1	9/1 - 10/1	1-2	0.5	Weather: cold, very wet. Large areas of site flooded.
2	11/1 - 15/1	3-7	0.95	Weather: wet, & windy. Site still largely flooded.
	16/1 - 17/1	8-9	0.95	Weather: gale force winds. HSG shelter blown down.
3	18/1 - 21/1	10-13	1.25	Weather: mild. Site drying out.
4	23/1 - 25/1	15-17	1.85	Weather: mild, dry.
5	30/1 - 2/2	22-25	2.50	Weather: mild.
6	4/2 - 5/2	27-28	2.80	Weather: clear, sunny. Construction completed.
	6/2	29	2.80	Weather: cold, dry. Plates installed on bank top to monitor settlement.

Table 4.7. Bank 2



MUCKING TEST SITE - DETAILS OF FOUNDATION INSTRUMENTATION

PLUS AS-BUILT PLANS AND SURVEY INSTALLATIONS FOR BANKS 2 AND 4

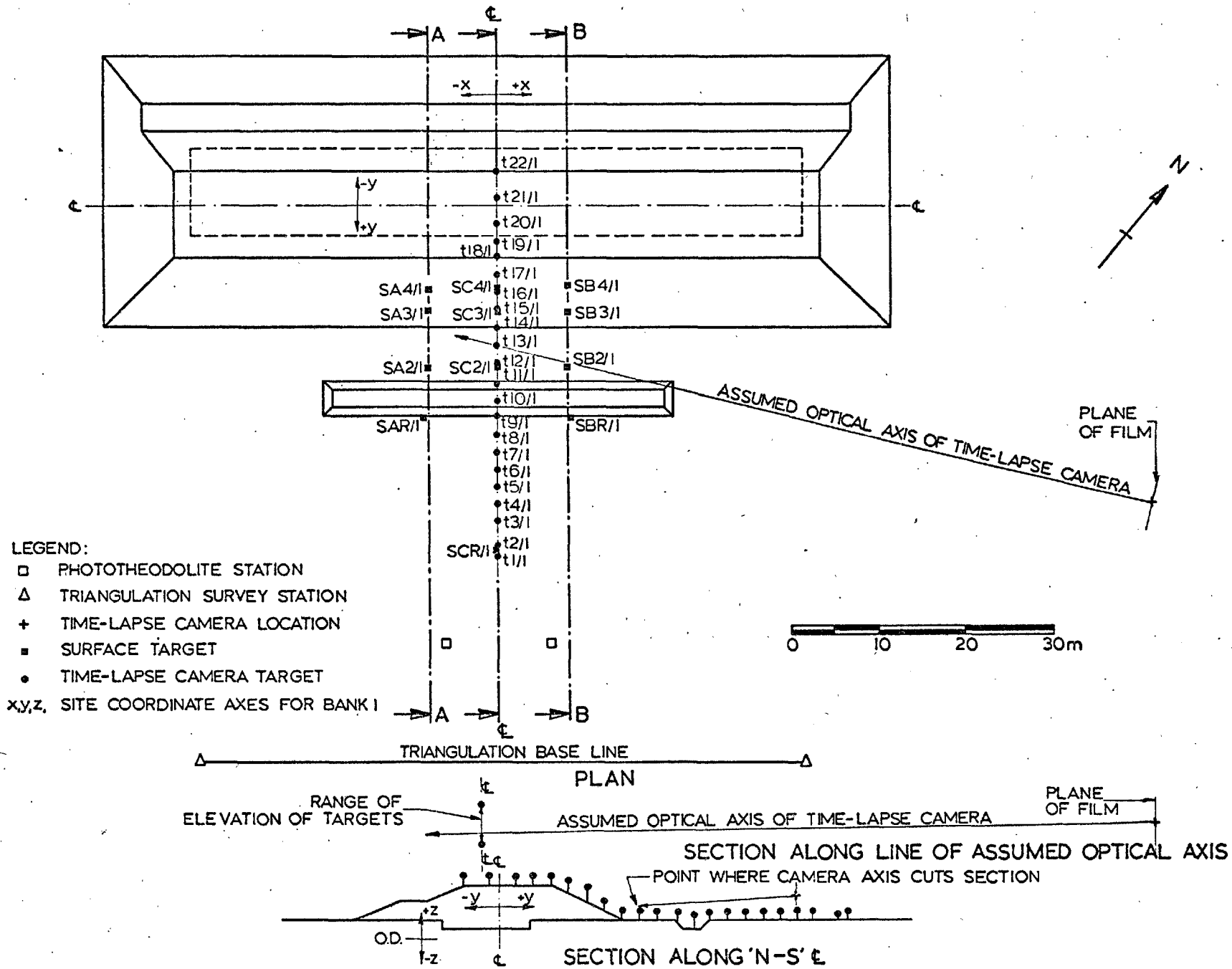
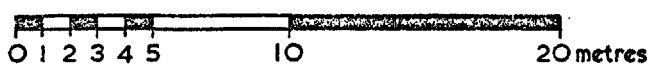
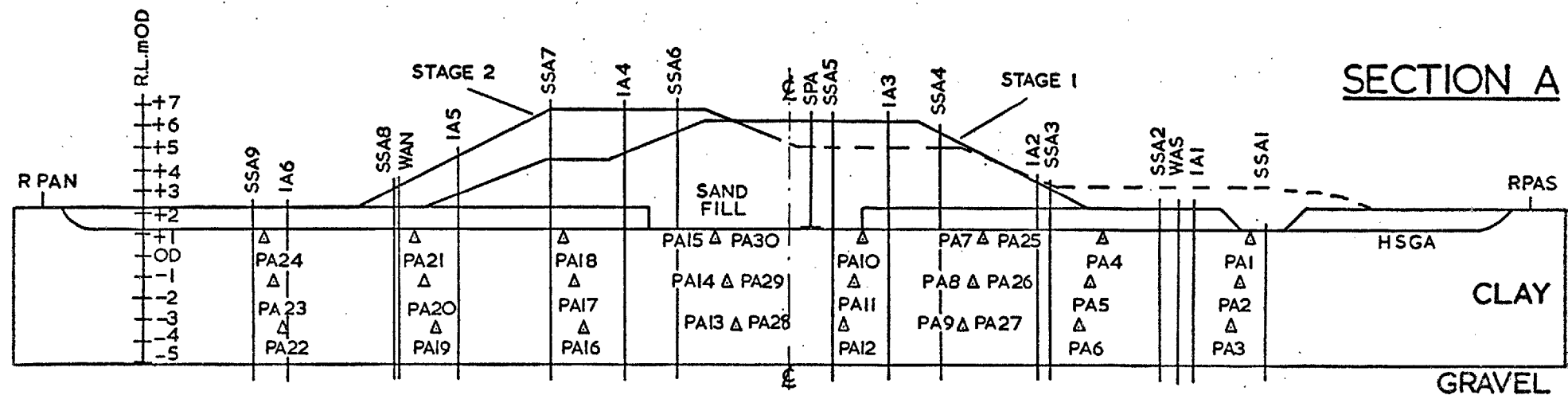
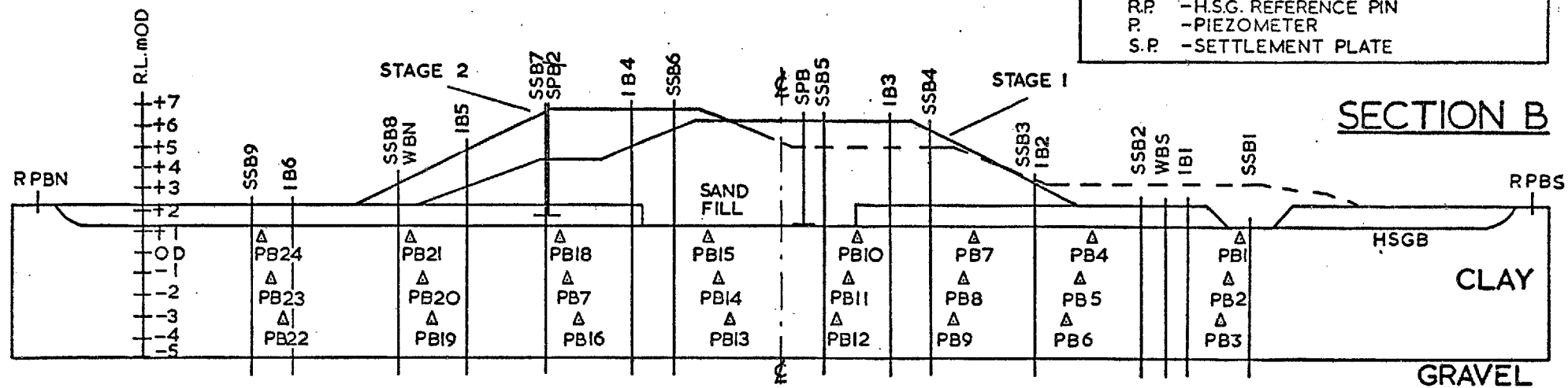


Fig.4.2

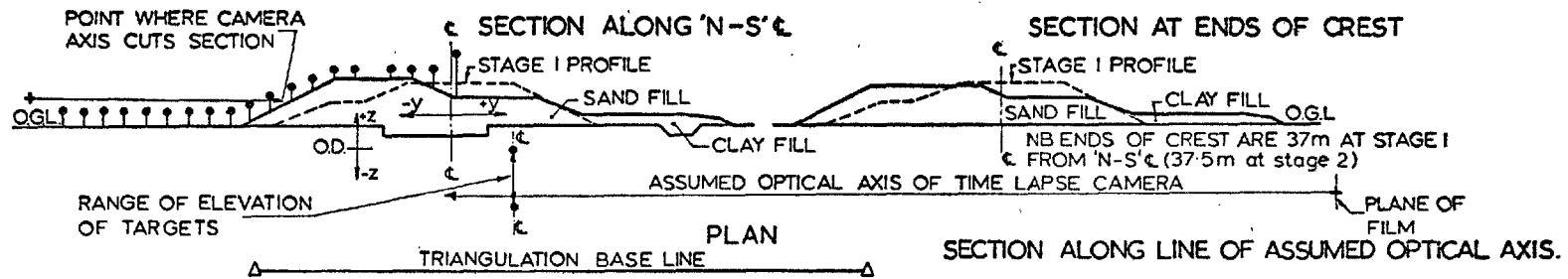
BANK I, STAGE I: PRE-FAILURE PLAN AND SECTION SHOWING PHOTOGRAPHIC AND SURVEY INSTALLATIONS.



KEY: I.	- INCLINOMETER
S.S.	- SLIP SURFACE INDICATOR
W.	- OBSERVATION WELL
H.S.G.	- HORIZONTAL SETTLEMENT GAUGE
R.P.	- H.S.G. REFERENCE PIN
P.	- PIEZOMETER
S.P.	- SETTLEMENT PLATE



BANK I, SECTIONS A & B : DETAILS OF FOUNDATION INSTRUMENTATION



LEGEND:

- PHOTO THEODOLITE STATION
- △ TRIANGULATION SURVEY STATION
- + TIME-LAPSE CAMERA LOCATION
- SURFACE TARGET
- TIME-LAPSE CAMERA TARGET
- x,y,z, SITE COORDINATE AXES FOR BANK 1

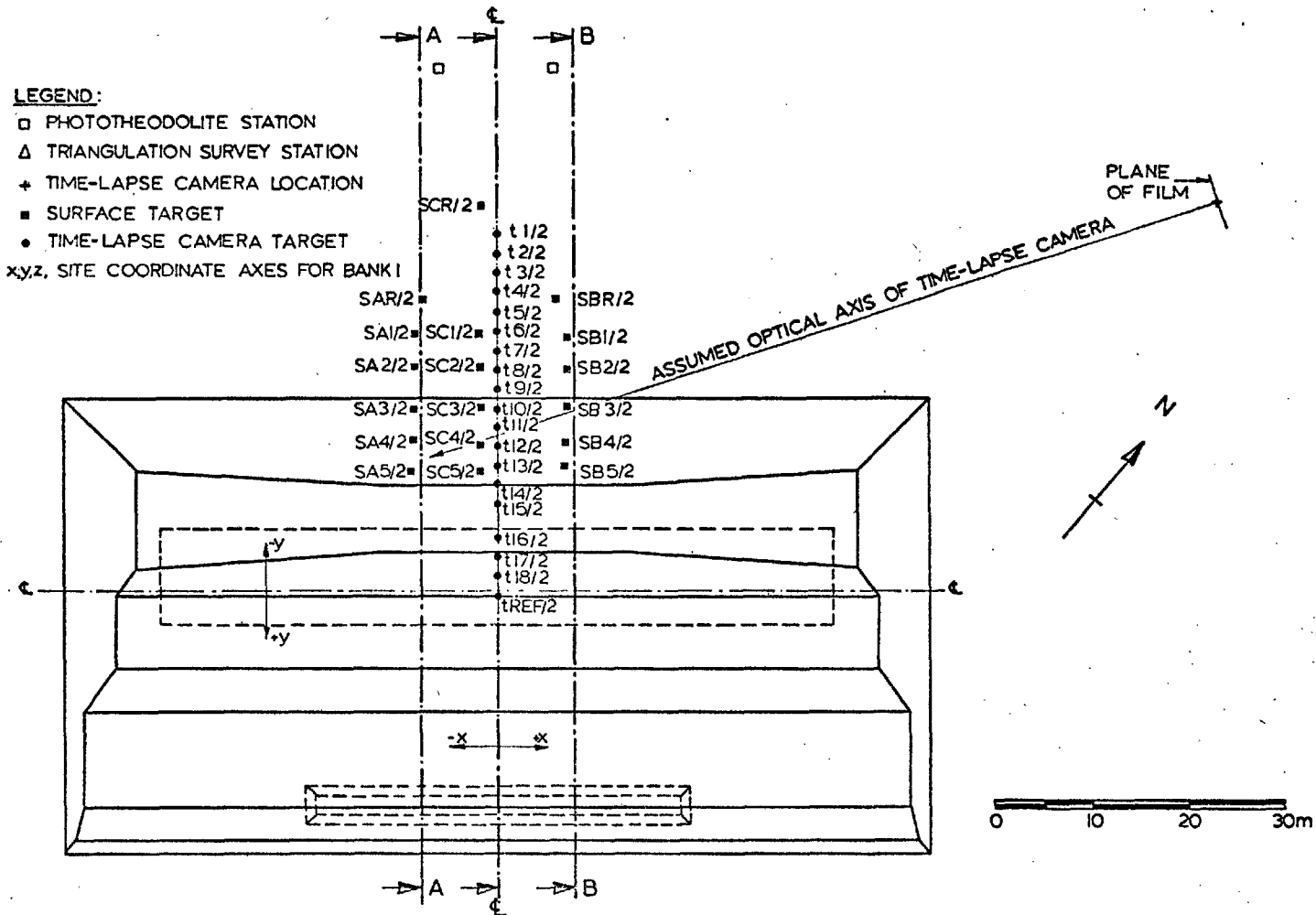
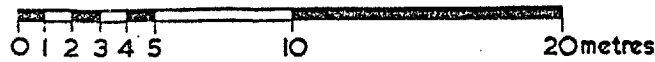
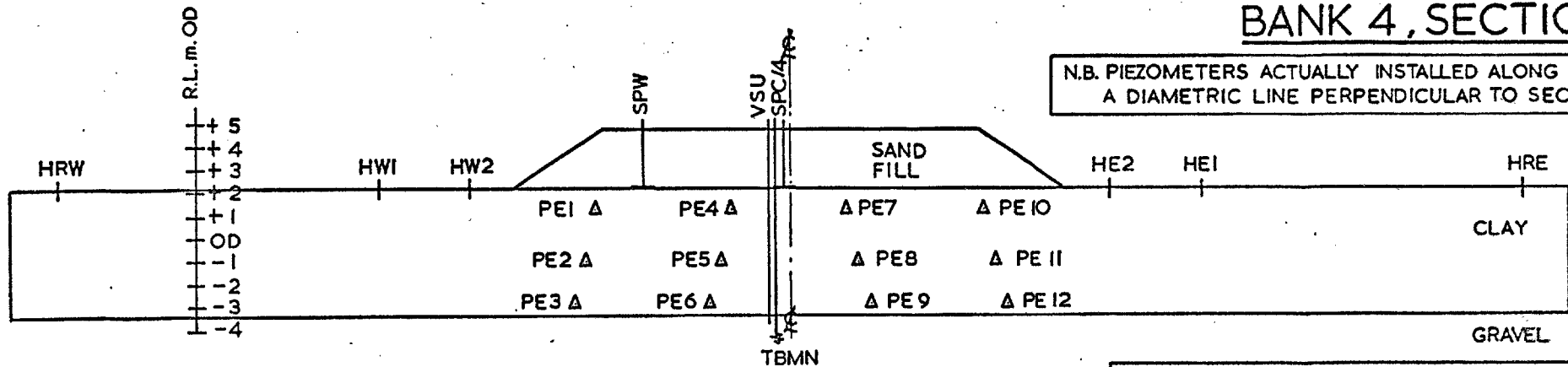


Fig. 4.4

BANK 1, STAGE 2: PRE-FAILURE PLAN AND SECTIONS SHOWING PHOTOGRAPHIC AND SURVEY INSTALLATIONS.

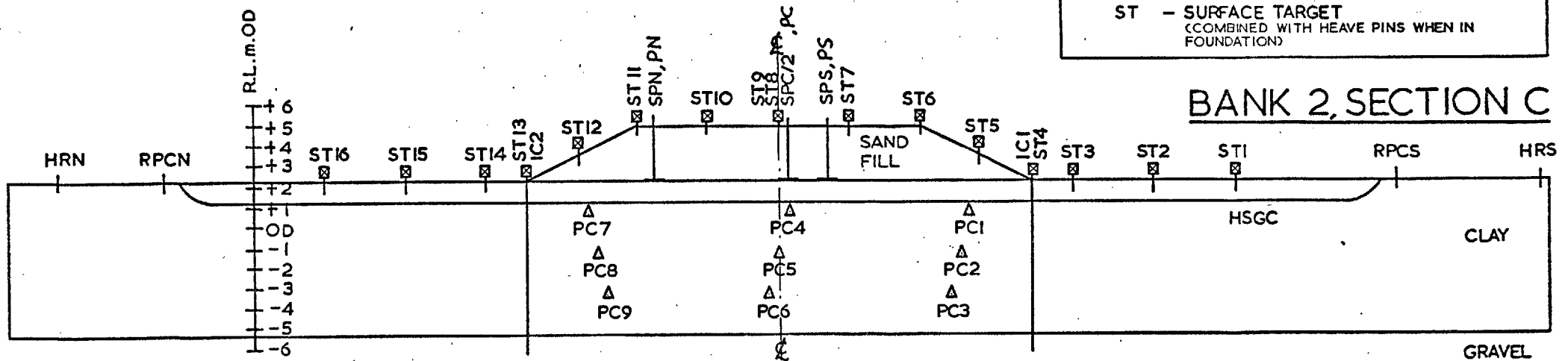
BANK 4, SECTION E

N.B. PIEZOMETERS ACTUALLY INSTALLED ALONG A DIAMETRIC LINE PERPENDICULAR TO SECTION E

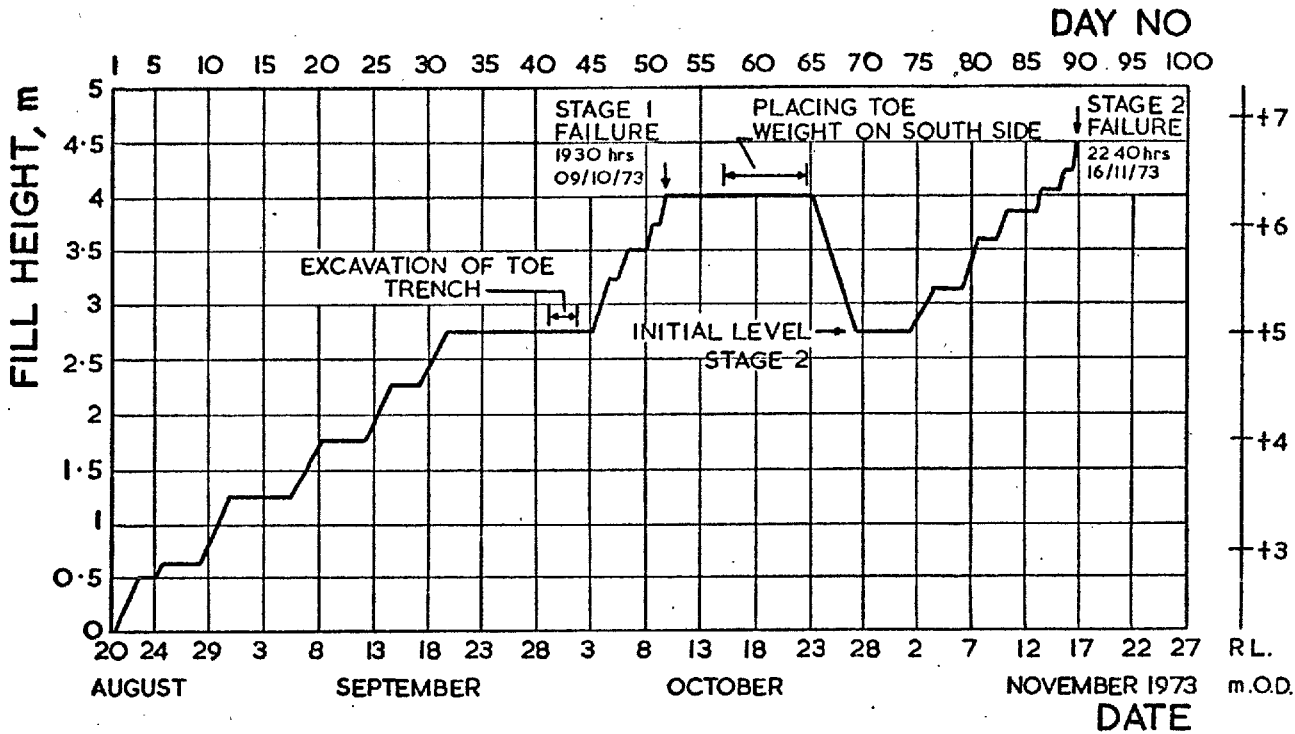


- KEY:**
- I - INCLINOMETER
 - HSG - HORIZONTAL SETTLEMENT GAUGE
 - RP - HSG REFERENCE PIN
 - P - PIEZOMETER
 - SP, P - SETTLEMENT PLATE
 - H - HEAVE PIN
 - ST - SURFACE TARGET
(COMBINED WITH HEAVE PINS WHEN IN FOUNDATION)

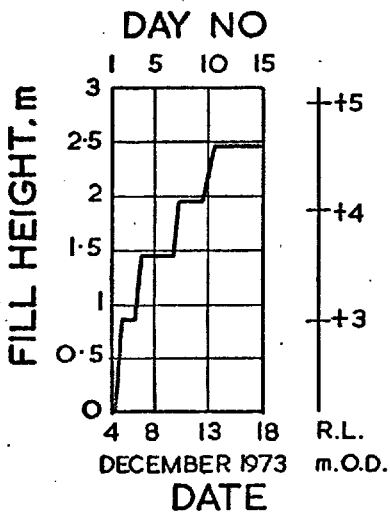
BANK 2, SECTION C



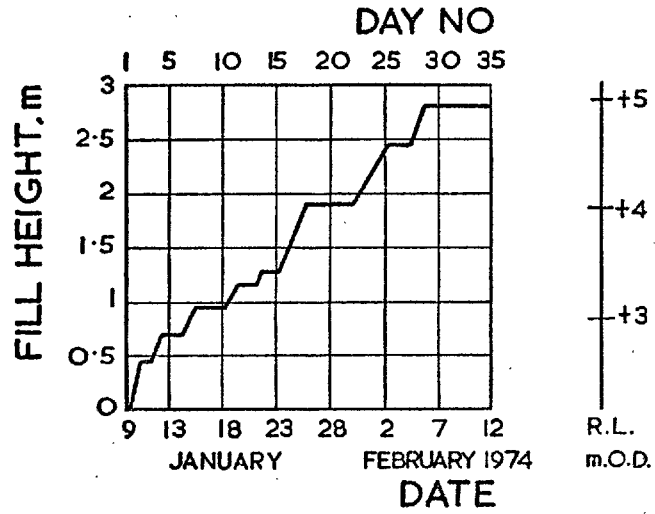
BANK 2, SECTION C & BANK 4, SECTION E:
 DETAILS OF FOUNDATION INSTRUMENTATION AND SURVEY INSTALLATIONS



BANK 1, STAGES 1/2



BANK 4



BANK 2

RATES OF CONSTRUCTION

Fig.4.6

CHAPTER 5

DETAILED RESULTS FROM THE INSTRUMENTATION OF THE TRIAL EMBANKMENTS

5.1. Introduction

5.1.1. Overall Aims of the Instrumentation Program

In Chapter 1 the reasons for the construction of the trial embankments were outlined, as was their purpose in providing detailed information on the behaviour of the foundation material under a variety of loading and drainage conditions, including failure.

The individual test fills and their specific purposes have been discussed in detail in Chapter 4, together with a broad outline of the site construction program.

The overall aim of the instrumentation program was thus to provide data to enable a detailed assessment of the foundation behaviour as well as providing guide lines for the future use of field instrumentation in monitoring the performance of the prototype structures. The selection of the appropriate variables and instruments for long-term observations required particular study (Vaughan, 1973(d)).

5.1.2. Extent and Purpose of the Instrumentation Installed

The instrumentation locations are shown on the site plans and sections presented in figures 4.1 to 4.5 and the extent of, and nomenclature used for, the instrumentation is summarised in table 5.1.1., which also

SECTION/TYPE OF INSTRUMENT	BANK 1 STAGE 1				BANK 1 STAGE 2				BANK 2				BANK 4			
	NO	KEY	PLAN	SECTN	NO	KEY	PLAN	SECTN	NO	KEY	PLAN	SECTN	NO	KEY	PLAN	SECTN
5.2.Heave Pins									10	ST1-4, ST13-16 HRS,HRN	4.1.	4.5.	6	HRE, HRW HE1,2, HW1,2	4.1.	4.5.
5.3.Horizontal Settlement Gauges	2	H.S.G.A. H.S.G.B.	4.1.	4.3.	1	H.S.G.B.	4.1.	4.3.	1	H.S.G.C.	4.1.	4.5.				
5.4.Inclinometers	12	IA1-6 IB1-6	4.1.	4.3.	6	IA4-6 IB4-6	4.1.	4.3.	2	IC1, IC2	4.1.	4.5.				
5.5.Piezometers	54	PA1-30 PB1-24	-	4.3.	44	PA2-9, 13-24, 28-30, PB1-9, 13-24	-	4.3.	9	PC1-9	-	4.5.	12	PE1-12	-	4.5.
5.6.Slip Surface Indicators	18	SSA1-9 SSB1-9	4.1.	4.3.	8	SSA6-9 SSB6-9	4.1.	4.3.								
5.7.Surface Movement Targets	12	SAR/1, SCR/1, SBR/1, SA/B/C2- 4/1	4.2.	-	18	SA/B/CR/2 SA/B/C1- 5/2	4.4.	-	16	ST1-16	4.1.	4.5.				
5.8.Time-Lapse Camera Targets	22	t1-22/1	4.2.	4.2.	19	tref/2 t1-18/2	4.4.	4.4.								
5.9.Temporary Bench Marks	1	T.B.M.S.	4.1.	-	1	T.B.M.S.	4.1.	-	1	T.B.M.S.	4.1.	-	1	T.B.M.N.	4.1.	4.5.

TABLE 5.5.1.

Key To Extent Of, and Nomenclature For, Instrumentation Plus Location Plans and Sections and the Layout of Chapter 5

TABLE 5.1.1. Continued.

Key to Extent Of, and Nomenclature For, Instrumentation Plus Location Plans and Sections and the Layout of Chapter 5

SECTION/TYPE OF INSTRUMENT	BANK 1 STAGE 1				BANK 1 STAGE 2				BANK 2				BANK 4			
	NO	KEY	PLAN	SECTN	NO	KEY	PLAN	SECTN	NO	KEY	PLAN	SECTN	NO	KEY	PLAN	SECTN
5.10. Vertical Settlement Gauges/ Surface Settlement Plates	2	S.P.A. S.P.B.	4.1	4.3	3	S.P.A. S.P.B. S.P.B/2	4.1	4.3	3/3	SPN/PN SPC/2/PC SPS/PS	4.1.	4.5	2	SPC/4 SPW	4.1	4.5
5.11. Vertical Settlement Units													1	V.S.U.	4.1	4.5

provides a key to the location drawings and the detailed discussion of each instrument in this chapter.

The main embankment instrumentation lines were designated as follows:-

Bank 1, Sections A, C, B

Bank 2, Section C

Bank 4, Section E

The coordinate axes used throughout this thesis for Banks 1 and 2 are shown on figures 4.2 and 4.4: 'X' denotes the plane strain direction, 'Y' the horizontal axis perpendicular to the 'X' axis and 'Z' the vertical direction. The horizontal axes have their origins at the intersections of the embankments' 'N-S' and 'E-W' centre lines, whilst the 'Z' axis relates to Ordnance Datum.

The specific purposes of the instruments, in relation to the aims of the trial embankments, as set out in Chapter 4, were considered as follows:-

Bank 1

(1) The measurement of horizontal and vertical displacements during construction (inclinedometers, horizontal settlement gauges, vertical settlement gauges, surface movement targets, heave pins). Such measurements would lead, via simple calculations, to linear and shear strains.

(2) The measurement of horizontal and vertical displacements during and after failure (surface movement, and time-lapse camera, targets), leading to displacement/time relationships for the embankment failures.

(3) The detection of the zones of maximum shear strain at the time of failure (slip surface indicators) enabling the location of the actual failure surface to be determined.

(4) The measurement of pore pressures during construction and, possibly, during and after failure (hydraulic piezometers). From these measurements the pore-pressure ratio (r_u), defined as:-

$$r_u = u/\gamma_B h \dots\dots\dots(5.1.1.)$$

where γ_B and 'h' represent the bulk unit weight and height, respectively, of the material above the point at which the pore pressure 'u' applies, can be readily determined.

The measurements would, therefore, enable limit equilibrium analyses of the failures to be performed and in addition provide very interesting 'four-dimensional' data on the mechanism of the failure, both with (Bank 1, Stage 2) and without (Bank 1, Stage 1) the desiccated crust in position.

It was also hoped to investigate the relationship between the measured pore pressures and the applied total stresses, the latter being determined for Stage 1 by finite element analyses. The predictions of displacement and strain provided by the latter could be compared to field observations whilst the stresses, in conjunction with measured pore pressures, could

be used to study the effective stress paths followed by the loaded foundation. It was also hoped these analyses would prove useful in studying the influence of K_0 , both in the laboratory and the field.

Bank 2

(1) The measurement of horizontal and vertical displacements during, and post, construction (inclinometers, horizontal settlement gauges, vertical settlement gauges and plates, surface movement targets and heave pins) enabling field estimates of the drained compressibility.

(2) The measurement of pore pressures during, and post, construction (hydraulic piezometers) enabling the field C_v to be determined.

Linear horizontal strains and pore-pressure ratios could also be readily derived from the measured data.

Bank 4

(1) The measurement of vertical displacements throughout the foundation (vertical settlement unit, vertical settlement gauges and temporary bench mark) during, and post, construction enabling a more detailed study of the field drained compressibility and the ready determination of linear vertical strains.

(2) The measurement of pore pressures during, and post, construction (hydraulic piezometers), again enabling the field C_v to be readily assessed at prototype stress levels.

In addition, piezometers were used to monitor seasonal and tidal fluctuations as described in Chapter 2, and for the determination of in-situ permeabilities.

Finally, the various displacement and pore-pressure measurements would be studied to see which, if any, and in what location, provided the best indication of impending failure. The performance of the instruments up to, and in some cases during and after, failure would be studied with a view to their future use and in order to make improvements in the equipment and/or monitoring and data reduction processes where possible.

5.1.3. The Presentation and Discussion of the Results

(i) General Comments

The writer was very fortunate in that his time on site was preceded by the British Geotechnical Society's Symposium on Field Instrumentation in Geotechnical Engineering (1973); the four general reports to this symposium provide a convenient framework for the discussion of the main aspects of geotechnical field instrumentation, being as follows:-

- (1) Principles of Measurement (Arthur, 1973)
- (2) Equipment (Green, 1973(b))
- (3) Applications of Instrumentation (Vaughan, 1973(d))
- (4) Interpretation of Field Observations (Burland, 1973(a))

In Chapter 5 these four aspects will be considered in varying degrees of detail, and have been adopted as sub-section headings in the following discussion.

(ii) Principles of Measurement

As stated by Arthur (1973), the reasons for making the measurements and their relative value are not included herein, the basic considerations being calibration and error. The latter depend on the ability to eliminate, or account for, the unwanted variables inherent in the measurements. Following the guide lines set down by Arthur (1973) the basic factors to be considered are as follows:-

(1) Only two variables were measured at Mucking, being displacements and pore-water pressures.

(2) The physical phenomena used to make the measurements are particularly important in geotechnical instrumentation with its associated harsh environmental conditions, and the performance of various of these, as employed at Mucking, are discussed.

(3) Robustness is always emphasised as a priority aspect of instrumentation schemes; Green (1973(b)) quotes the three "R's" of instrumentation as resolution, reliability and ruggedness. However, increasingly sophisticated systems are being developed, with an upsurge in automatic and remote reading systems (Irwin, 1973; Wilson, 1973) and additionally direct links to computers (Sherwood and Currey, 1973).

(4) Sensitivity, as referred to in this thesis, relates to the calibration of the measuring devices and is taken to be synonymous with resolution i.e. the smallest measurement unit detectable by the instrument.

(5) The response time of an instrument under essentially static loading conditions particularly relates to piezometers, although most instrument installations disturb the soil and in so doing generate excess pore pressures.

(6) The range of measurement units over which an instrument can function and its sensitivity are often closely related (Hutchinson, 1973), and the selection of a reasonable compromise presents a real problem to the geotechnical engineer designing an instrumentation system. For example, embankments on soft clay foundations may induce pre-failure lateral displacements in the foundation which range from very small (Ladd, 1972) to quite large (as reported herein) and inclinometer casings may become inaccessible prior to failure (Werneck, 1974). In particular, devices for measuring settlements in soft clays have to be capable of monitoring large displacements (Wilkes, 1972(a)) Piezometer tubing has to be able to cope with large displacements under such circumstances, especially if during and post-failure pore pressures are to be monitored.

(7) Environmental calibration, or the soil/instrument interaction problem, is one of the most difficult to resolve, particularly in soft clays. Much attention has been paid in the following sections to the ability of the instruments to measure the true displacements and pore pressures associated with the loaded foundation in the absence of the instrument, this aspect reflecting the accuracy of the measurements as is now discussed.

(8) The accuracy of the measurements reflects all of the foregoing aspects, but it is fair to say that environmental calibration may often be the major factor. Accuracy may be defined as the closeness of approach of a measurement to the true value of the quantity measured, being thus the degree of correctness (Gould and Dunnicliff, 1972) and indicating the error, whereas precision is the closeness of approach of each of a number of similar measurements to the arithmetic mean. Thus accuracy requires precision, but not vice versa, and in field geotechnical instrumentation precision generally refers to the instrument and accuracy to the measured quantity. The use of the terms sensitivity, precision and accuracy in Chapter 5 adheres to these definitions.

In the case of displacement measurements the instrument usually consists of a probe or sensor which is used to monitor the displacements of objects placed in the foundation or fill. In the absence of environmental calibration, only in the case of simple surface installations located by survey techniques do accuracy and precision tend to become synonymous. The best estimate of accuracy in such cases is usually a second measurement of the same quantity using an entirely different instrument, such duplication being achieved at many locations for the trial embankments. The physical connection of horizontally and vertically installed instruments at various points, as suggested by Wilkes (1973), although posing a possible interaction problem, would be a valuable attribute to the assessment of accuracy.

The sensitivity, precision and accuracy of each type of instrument installed at Mucking have been considered in as much detail as possible in Chapter 5; without such an assessment of the accuracy of the observations any analyses assume less meaningful proportions. Where possible, standard deviations (standard errors) have been assessed and precisions/accuracies presented in terms of 99% confidence levels (i.e. 1 in 100 readings will be worse than the quoted value). Alternatively, an accuracy expressed as $\pm 'x'$ implies the probable maximum deviation from the true value.

Finally, it should be noted that displacement measurements involve the location of points in space, and as such the absolute accuracy of location may be less important than the precise assessment of the change in position.

(9) The reliability of the data may be impaired by such things as the de-airing (or lack of it) of piezometers, damage of (and repairs to) instruments, staff changes and inadequate data reduction procedures. The latter are particularly important when, as is often the case, large amounts of data rapidly accrue. Sophisticated instrumentation still requires readings to be taken and analysed by competent personnel and automatic readouts may obscure parts of the data reduction process, thus inscreasing the possibility of unobserved errors (Green, 1973(b)).

The reading procedure itself is very important and involves an understanding of the fundamental variables being measured; detailed attention has been paid to this aspect of the instrumentation.

(iii) Equipment

Much of the instrumentation installed was available commercially and only brief descriptions have been given; instrumentation developed particularly for the site has been discussed in more detail. Installation techniques have been covered in some detail as they are often more important than the instrument itself. Green (1973(b)) has pointed out the desirability of a personal commitment to the success of the instrumentation by the installation personnel.

(iv) Application of Instrumentation

The application of the instrumentation to the Mucking foundation tests has been previously considered in Chapter 4 and section 5.1.2.

(v) Interpretation of Field Observations

In Chapter 5 the data have been reduced rather than interpreted, in that the first aim was to arrive at values of the fundamental variables (i.e. pore pressures and displacements) which could be relied on to a certain accuracy. Interpretation of the measured variables with respect to the soil behaviour has been largely left to subsequent chapters.

(vi) Final Comments

The main aims of Chapter 5 are thus to describe the instruments, the installation, reading and data reduction procedures, plus the precision and accuracy of the measurements, leading to an overall assessment of their performance.

Some measurements have been discussed in more detail than others. For example, if some dissipation of pore pressure occurred during the construction of Bank 1, Stage 1, this would have had a far greater influence on the vertical than horizontal displacements (see e.g. Hamza, 1976). The latter are thus usually favoured for comparisons with undrained finite element analyses and hence the particular attention paid to the horizontal displacements recorded by the inclinometers.

Although it is agreed that the successful application of field instrumentation schemes requires not inconsiderable experience, there is relatively little in the way of detailed practical advice or assessments of observed accuracy (Arthur, 1973) available in the literature to aid the newcomer to this field. To these ends the writer has sought to provide guide lines for the use of commercial and non-commercial instrumentation in soft clay foundations. A summary of much of the available literature has been presented by Robertson (1974).

5.2. Heave Pins

5.2.1. Bank 1

(i) Installation

Heave pins were installed in the foundation (on Section lines A and B), to monitor horizontal and vertical movements of the ground surface during construction. Reference heave pins were similarly installed distant from the bank; these served to monitor repeatability of vertical

location and as datums for the horizontal location of the other pins.

The installation procedure consisted of digging a small hole, about 300mm deep, into the base of which a 1m length of 20mm O.D. steel rod was driven a further 300mm. The hole was then concreted up and the top of the pin marked with a saw cut to enable accurate horizontal location. These installations were cheap, and easy to install and monitor and it was hoped that they would not only provide a useful additional source of data during the construction of the trial banks, but also be incorporated in the monitoring of the prototype structures.

(ii) Results

The vertical (Z) and horizontal (Y) displacements of the heave pins, during the construction of Stage 1 and Stage 2, were monitored by level survey and tape measurements respectively. The latter were performed with a steel band calibrated in 'mm'; the measurements were direct, over relatively short horizontal distances, and no corrections were made. The readings taken during both construction stages were very erratic with respect to both horizontal and vertical displacements; in particular the reference pins underwent heave movements of up to 35mm. Data from other sources (primarily surface movement targets) indicated that the heave movements prior to failure were not greatly in excess of this figure, particularly for Stage 1. The surface target observations for both stages of construction in fact indicated pre-failure heaves of the order of 50 to 75mm, of which an appreciable amount occurred during the addition of the final 500mm of fill prior to failure. Finally, the failures of Bank 1, Stages 1 and 2, extended approximately 10m from the embankment toes and in both cases this meant that only one heave pin,

the pre-failure displacements of which were not significantly different from the reference pins, was sited in the failure zone.

The results of the heave pin displacements for Bank 1 have, therefore, not been presented herein, but displacements of the surface targets in the foundation are shown in section 5.7. The latter were of similar dimensions to the heave pins and installed to a slightly greater depth, their performance being far superior in terms of stability. It is thought that the significant difference between the two types of installation was the concrete block, the surface targets being simply pushed into position. During the construction period of Bank 1, especially for Stage 1, site conditions transformed from very dry, after a hot dry summer, to very wet in the autumn (as indicated in tables 4.2 and 4.4). This transformation obviously resulted in volume changes in the upper desiccated layer of the foundation, which were reflected in the heave of the reference pins (typically 35mm between the start of Stage 1 and the end of Stage 2). The fact that the surface targets did not respond so dramatically to these volume changes suggested that the heave pin displacements were those of the concrete block installed in the top 300mm of the foundation, whereas the surface targets were responding to the undrained heave of the foundation nearer to their bases.

5.2.2. Bank 2 and Bank 4

(i) Installation

The experiences with the Bank 1 installations necessitated a modified design for those used to monitor Bank 2 and Bank 4. A smaller diameter (102mm) hole was hand augered to a depth of 1m (approximating therefore

to the base of the desiccated zone proper): the steel pin was then pushed a few centimetres into the clay and concreted in to a depth of 150mm (maximum) from the base of the hole. The remainder of the hole was filled with sand, compacted in layers, to give the installation horizontal stability. It was hoped that the heave pin would monitor the displacements of the concrete block, but that this would now predominantly reflect embankment associated foundation displacements rather than seasonal volume changes.

Heave pins were thus installed in the foundation adjacent to, and on the centre lines of, Bank 2 and Bank 4, together with distant reference pins (figures 4.1. and 4.5.). Also, based on the experiences of Bank 1, the heave pins were all installed within 10m of the embankment toes. The heave pins for Bank 2 (ST1 to ST4 and ST13 to ST16) had surface targets clamped to them and were located horizontally by both tape measurements and triangulation.

(ii) Results

(a) During Construction

The results for Bank 2 and Bank 4 are shown in figures 5.2.1. and 5.2.3. respectively, and appear satisfactory in both cases. The vertical and horizontal displacements were small for both embankments, but particularly so in the case of Bank 4, where the heave pins provided the only horizontal displacement data for the foundation. In figure 5.2.1. the horizontal displacements of the Bank 2 heave pins, as located by tape measurements and triangulation, can be compared to the ground level movements at the toe recorded by inclinometer ICl. The three sources of horizontal displacement produced fully compatible results.

Only the results from the south side of Bank 2 (ST1 to ST4) and the east side of Bank 4 (HE1 and HE2) have been presented, the displacements for the opposite faces of each embankment being much smaller. However, the results were equally satisfactory and, in the case of the horizontal displacements for Bank 2, compatible with the results of inclinometer IC2.

(b) Post-Construction—Long-Term Observations

The long-term observation of the heave pins adjacent to Bank 2 and Bank 4 are presented in figures 5.2.2. and 5.2.3. respectively, these being discontinued as indicated in the figures. In the case of Bank 2 this was because it was felt that the inclinometers provided adequate data, and in the case of Bank 4 because the heave pins were intended primarily to monitor the displacements during construction. The results for Bank 2 are very good; in particular the close agreement between the horizontal displacements of surface target ST4 and inclinometer IC1 suggests that both installations were successful in monitoring the displacements of the foundation. The results for Bank 4 appear equally satisfactory.

(iii) Accuracy of Observations

(a) Vertical Location By Level Survey

The accuracy of this aspect of the heave measurements is a function of the accuracy of the level survey itself, this being fully discussed in section 5.9, and the stability of the installations with respect to seasonal volume changes. The long-term behaviour of the four reference pins installed for Bank 2 and Bank 4 is represented statistically in table 5.2.1. The standard errors are of the order associated with the

accuracy of the level survey and thus indicate that the reference pins were stable over the periods of observation, which, for both embankments, spanned a complete cycle of seasonal changes. However, the overall accuracy indicated by the results in table 5.2.1. is $\pm 9.5\text{mm}$; although the results as plotted are very acceptable a more precise level survey is really needed to accurately measure vertical displacements which ranged from less than 5mm during construction to a maximum of 33mm post-construction.

BANK NO.	2		4	
	HRS	HRN	HRE	HRW
Reference Pin				
Observations	22	22	24	24
Standard Error mm	± 2.61	± 2.93	± 5.37	± 4.57
99% Confidence Limit mm	± 6.53	± 7.33	± 13.43	± 11.43

Table 5.2.1.

Accuracy of Location of Heave Reference Pins by Level Survey

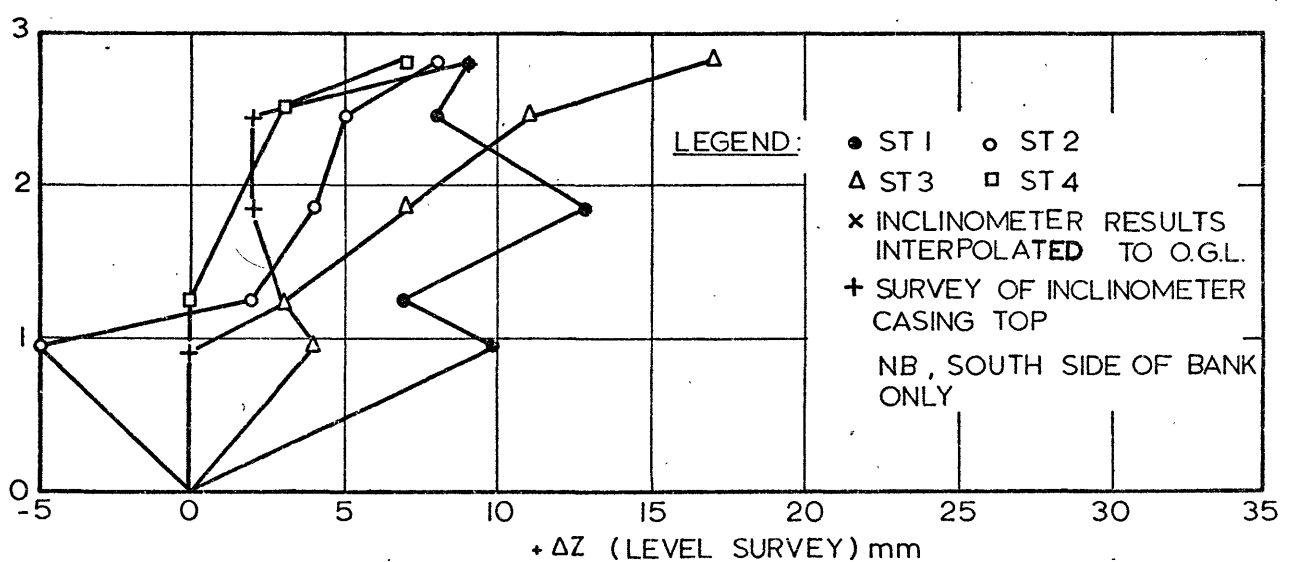
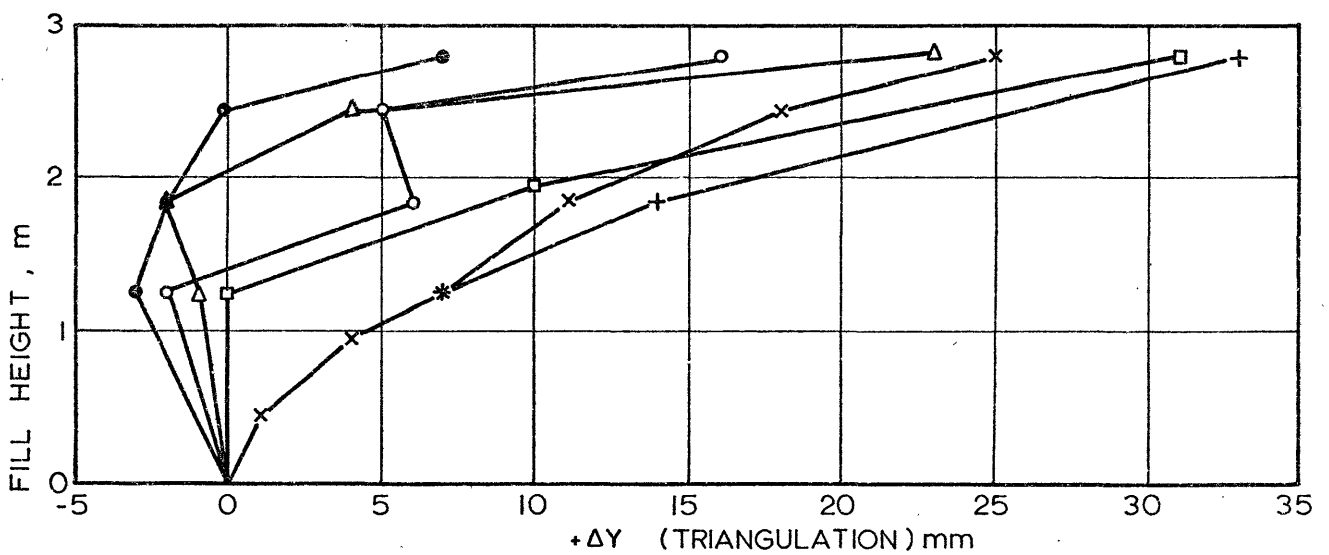
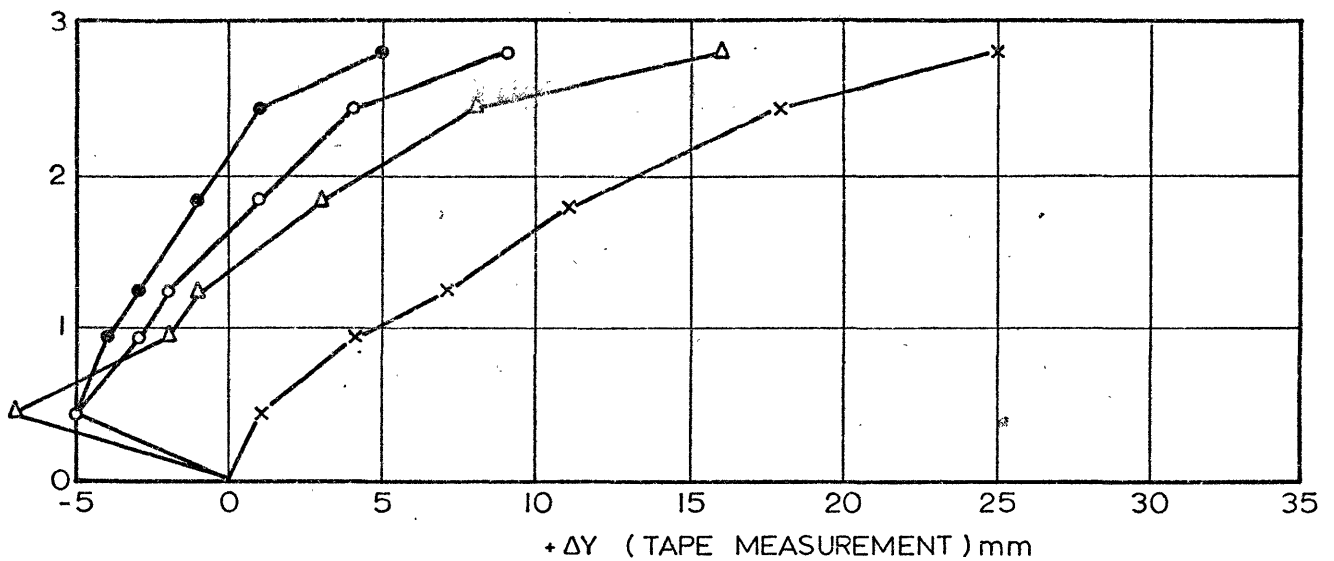
(b) Horizontal Location by Tape Measurements

The only repeated measurements to stationary heave pins were the initial readings. These indicated that location could be achieved to within $\pm 2\text{mm}$, which is in agreement with the suggested accuracy for uncorrected steel tape measurements of $\pm 1/5000$ suggested by Gould and Dunicliff (1971), the maximum measuring distance being about 25m. The construction observations for Bank 2 are certainly in reasonable agreement with the

triangulation results. Horizontal location by tape measurement can thus produce results accurate enough for relatively small construction displacements as well as the larger post-construction values observed. These measurements are simple to take, and in view of the short times involved it is suggested that they could be repeated once or twice to further improve the accuracy.

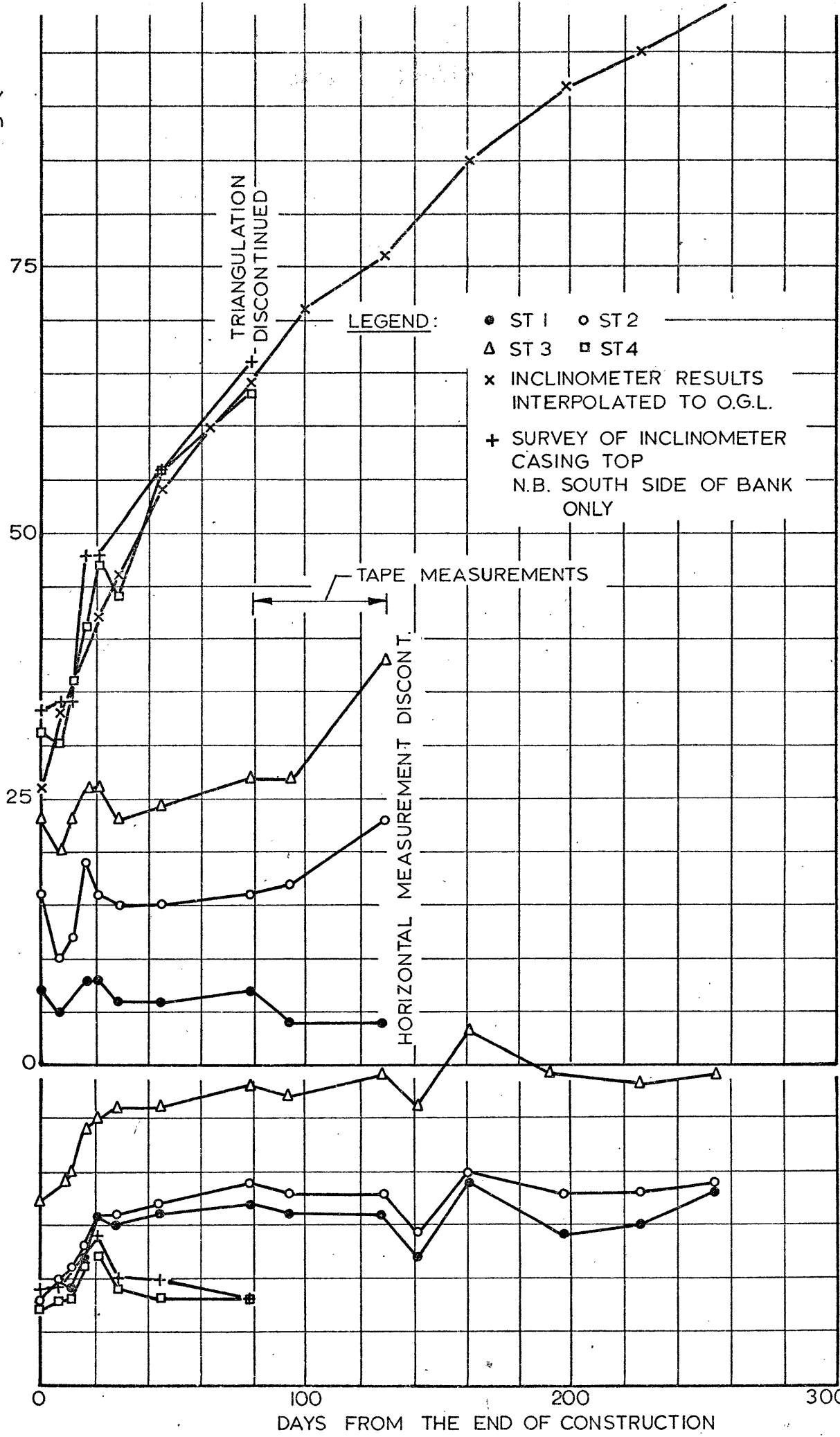
5.2.3. Final Comments

The modified design of heave pin used for Bank 2 and Bank 4 performed perfectly satisfactorily over a long period. For the small amounts of undrained foundation heave associated with the soft clay, a level survey with an accuracy better than $\pm 5\text{mm}$ would be recommended for future installations. Although the installations performed satisfactorily, they could possibly be improved by sleeving the auger hole above the concrete with a plastic liner and filling around the pin with a weak bentonite: cement grout. A gap, filled with compressible polystyrene, could be left to prevent the sleeve acting on the concrete base.

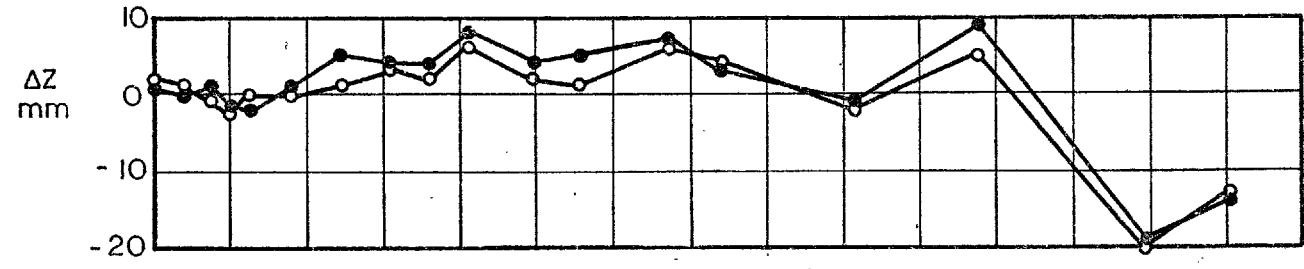
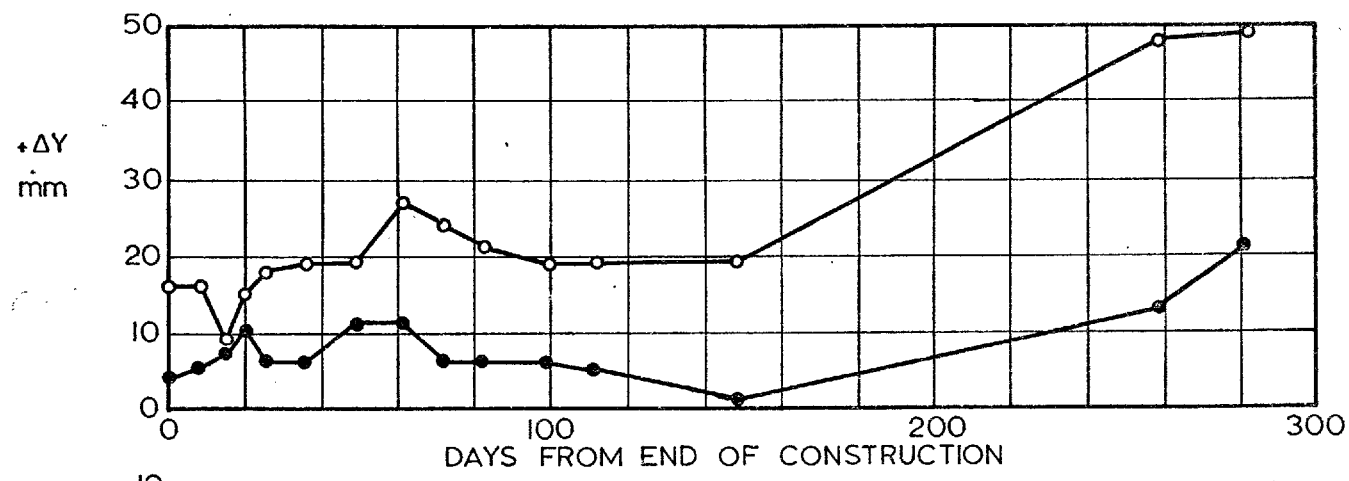
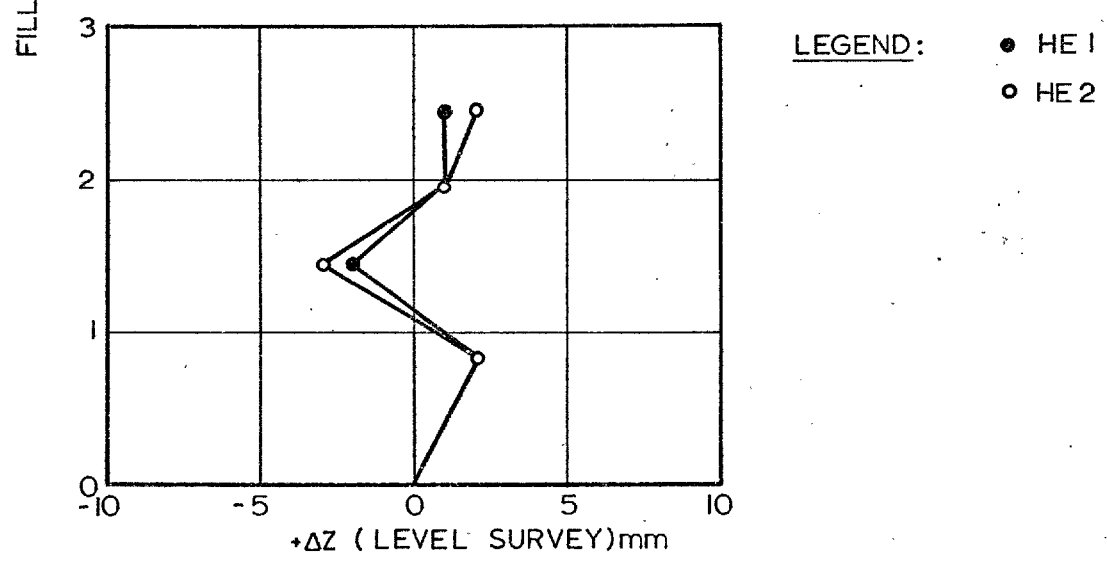
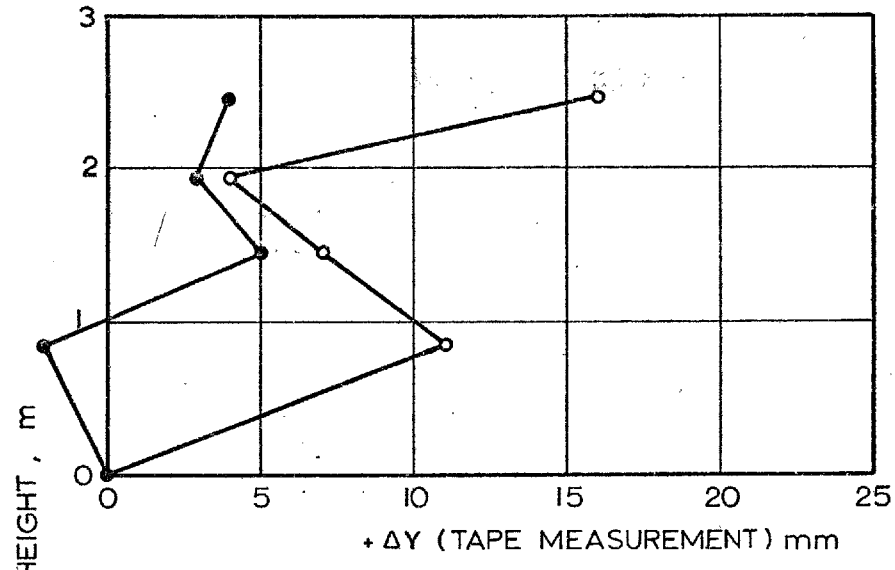


BANK 2: Surface Targets in the Foundation (Heave Pins) - Displacements during construction versus fill height.

+ΔY
mm



BANK 2: Surface Targets in the Foundation (Heave Pins) - Post-construction displacements.



BANK 4: Heave Pins - Displacements during and post-Construction

Fig. 5.2.3

5.3. Horizontal Settlement Gauges (H.S.G. s)

5.3.1. Installation

Three H.S.G. s were installed on the site, the locations being Section lines A, B (Bank 1; figures 4.1 and 4.3) and C (Bank 2; figures 4.1 and 4.5). The basic installation comprised a near horizontal, flexible, polypropylene access tube (48mm O.D., 35mm I.D.) buried in the foundation at the section along which a settlement profile was required. Aluminium plates containing permanent ring magnets were positioned at intervals around the access tube. The vertical profile of the access tube was surveyed using a hydraulic probe, and horizontal movements of the magnets recorded by a sensing probe; both probes were connected on a composite cable, and were passed through the access tube (figure 5.3.1.), their mode of operation being described in the next section.

The three access tubes were installed in straight trenches excavated to a depth of 1m along the appropriate section lines. With the tube positioned along the base of the trench the ring magnets were passed over and along it to the required locations. The magnet plates were individually backfilled to ensure their original position perpendicular to the tube, and care was taken to bring the access tube ends to ground level in a relatively shallow, smooth, curve. The trench was then backfilled in layers (approximately 300mm) and compacted using a rammer. The ends of the access tube were terminated in concrete pads through which were installed steel reference pins to provide vertical and horizontal control for the H.S.G. measurements (figure 5.3.1.). These reference pins were similarly installed to the heave pins used for Bank 1.

The installations used for Bank 2 incorporated two refinements in the light of difficulties experienced during observations made with the Bank 1 H.S.G. s. Firstly, weatherproof shelters, similar to those erected at the triangulation and phototheodolite stations (section 5.7), were constructed at the H.S.G. observation stations and, secondly, the reference pins were installed to the modified heave pin design used for Bank 2 and Bank 4.

5.3.2. Reading Equipment and Observational Procedure

(i) Reading Equipment (figure 5.3.1.)

The settlement probe was a brass cylinder, vented to atmospheric pressure and containing a bladder filled with de-aired water. The bladder was linked to a pressure transducer and the probe to atmospheric pressure, by standard nylon piezometer tubing. The horizontal movement probe was also a brass cylinder, but this time containing a reed switch connected within an electrical circuit comprising a battery and a buzzer. The two probes were positioned about 750mm apart on a strong composite cable, which carried the tubes from the settlement probe and the wires from the reed switch to a cable drum: this served not only to store the cable but also to house the transducer, air vent, buzzer and battery.

The changes in elevation of the settlement probe were registered as resistance changes of the transducer, which formed the active arm of a conventional bridge arrangement housed in a portable read-out unit. This was powered by a 6 volt battery and linked to the transducer by a jack-plug connection. The unit incorporated a digital read-out

display, calibrated directly in metres (head of water) relative to a datum, and had battery checking facilities. Horizontal location of the magnets was signalled by the buzzer and recorded by means of a steel band (1mm divisions) connected to the forward (settlement) probe and passed out of the opposite end of the access tube to the main cable (figure 5.3.1). The H.S.G. equipment was manufactured and supplied by Soil Instruments Ltd.

(ii) Observational Procedure

(a) Bank 1

The settlement observations were made to the southern side of the embankment and the horizontal displacements recorded to the north. The cable drum and read-out unit were set up, and interconnected, at the southern station. The read-out unit was found to require at least 5 minutes warm-up time and was therefore switched on at this point.

Meanwhile the operator at the northern station connected the tape to a draw cord, which was left in position through the access tube when the latter was not in use, and secured to the reference pins. The tape was pulled through the access tube by the operator at the southern station and connected to the nose of the settlement probe. Prior to this, all the cable was unreeled from the drum and covered with a tarpaulin; this being intended to minimise temperature effects by obtaining a uniform cable temperature prior to operation and also to protect the cable not in use from meteorological factors in general.

If the draw cord indicated that there was water in the access tube, this was removed using a compressed air source; the initial insertion of the draw cord was also by this method. The access tube on Section A had been joined, for economic reasons, and the joint sealed with denso tape; however, the joint leaked and it was necessary to de-water the access tube on a number of occasions. This again was to prevent temperature influences, which would manifest themselves if the probe were to pass from air into water and back into air again whilst in the access tube.

With the equipment set up ready for use the settlement probe was placed on the southern reference pin (R.P.A.S. or R.P.B.S.) and the read-out unit zeroed. The probe was then passed through the access tube, the operator to the south pushing the cable and the operator to the north pulling in the tape. The vertical elevation of the access tube was recorded at intervals between the southern and northern stations, the operator to the north controlling the reading positions. Each of these was set to correspond to a whole number of metres at the northern reference pin (R.P.A.N. or R.P.B.N.). With the tape held in position on the reference pin the northern operator signalled (communication being by walky-talky radio sets) to his southern counterpart, who pulled gently on the cable until the tape/cable system was taut. The vertical elevation of the access tube was then recorded directly from the read-out unit; generally about 30 seconds response time was allowed although sometimes this was inadequate.

Initially it was intended to isolate the transducer from the settlement probe whilst the latter was in motion, in order to protect the former from any pressure surges that might occur. However, using this system

it was found that, when the transducer was switched in to the circuit to take a reading, the response time was much longer than when the transducer was left permanently switched in. Continuous observations of the pressure (head) readings during the travel of the probe through the access tube revealed that there were no strong pressure surges. This was probably because the passage of the probe was very smooth (i.e. it was not difficult to pull through and did not stick) and the changes in elevation were mostly small.

The above finding was the result of a number of proving runs carried out using the H.S.G. prior to taking the initial readings. These trials also led to the adoption of the tape/cable configuration used. An alternative system which can be used, and has to be in situations with zero or limited access at one end of the tube (see e.g. Werneck, 1974) is for the horizontal and vertical measurements to be made at one station. Readings were taken with the tape and settlement measurements both being recorded at the southern station, the probe initially being pulled through to the north using the draw cord. It was found to be much more difficult to operate this system both externally (i.e. at the stations) and internally due to the extra tightness caused by the tape passing alongside the probes. It is also very easy, using this system, for the tape to become twisted or kinked within the access tube, and hence break.

The reading interval for the vertical elevations was selected as 3m. When the probe reached the northern station it was positioned on the reference pin and a reading taken. Thus the relative elevations of the reference pins were determined using the settlement probe and its

performance could be checked against their 'true' relative elevations as determined by the level survey. The probe was then pulled back to the southern station, readings again being taken at 3m intervals to obtain a duplicate set. The final reading on the southern reference pin provided an indication of any drift that might have occurred during the observations.

At the same time as the settlement readings were being taken the magnet locations were recorded. When the buzzer was heard the probe was pulled back a short distance and the cable/tape system gently pulled taut by both operators. When the probe was passing from the south to the north the tape operator at the northern station would pull the tape, the southern operator providing gentle resistance until the buzzer signal started and the start point of the signal was recorded; likewise the end of the signal was also recorded. The magnets were similarly located with the probe travelling from north to south except that the probe was pulled by the southern operator, against gentle resistance provided by the northern operator. The start and end of signal was thus recorded with the probe passing through each magnet in both directions. Upon completion of a set of readings the draw cord was pulled back through the access tube using the tape, and its ends secured to the two reference pins. The access tube was fitted with lockable end caps, when not in use, as such installations are particularly susceptible to blockage by animals as well as vandals.

(b) Bank 2

In the writer's opinion the accuracy of field observations, with a particular instrument of known precision, is determined to a considerable extent by environmental factors in so much as these affect not only the

instrument but also the operating personnel. To this end the H.S.G. stations were protected by weatherproof shelters as described previously. These not only enabled readings to be taken irrespective of weather conditions but, also meant that the operation could be carried out in 'relative comfort'.

The readings for Bank 2 were otherwise similarly taken to those for Bank 1 with the major exception that the cable was kept on the cable drum when not in use. This made the reading operation far easier (about 1 hour from start to finish including setting up), and with the shelters in position temperature effects were probably less than for Bank 1. However, this mode of operation required some care as the transducer was not located centrally within the cable drum, which, being rotated as the cable passed through the access tube, had to be correctly positioned before each reading.

Water in the access tube was more of a problem for H.S.G.C., particularly during the post-construction period when the site was frequently flooded. Water was able to run into the observation stations and down the access tube, which had thus to be blown out before nearly every set of readings. This problem could have been avoided by constructing the station bases at a slightly higher level, a point worth noting for future installations.

(c) General

It will have been noted that the observational procedure adopted entailed the monitoring of vertical displacements at particular points in the cross-section, and horizontal displacements at other points. Whereas,

the horizontal displacement measurements followed a particular point in the soil (although its settlement was unknown) the vertical displacement readings were always taken at the same horizontal location. The most correct observational process would have been to monitor settlements at the magnet locations and thus to follow the displacement vector of a particular soil element. In order to do this, sufficient magnets need to be installed to provide an adequate settlement profile.

The procedure adopted was thus deficient in that displacement vectors could not be directly plotted (i.e. without some degree of interpolation) and that the settlement readings did not follow the progress of a particular soil element. This may be of particular importance for the foundation area beneath the embankment slopes where both the vertical component of shear strain (i.e. change in vertical displacement per unit length of cross-section) and the horizontal component of shear strain (i.e. change in horizontal displacement per unit depth) may be large. However, these inadequacies in observational approach did not seriously affect the accuracy of the measured vertical displacements as, in conjunction with the measured horizontal displacements, they indicated that errors from this source would be far less than the accuracy of the measurements (as discussed in the next section).

5.3.3. Accuracy of Vertical Displacements

(i) Precision of the Equipment

The manufacturers quote an 'overall accuracy' of $\pm 10\text{mm}$, and a range of 3.5m for the determination of settlements, whilst the sensitivity of the read-out unit is 1mm. The precision of the instrument and the

accuracy of the settlement determinations are influenced by a number of factors, these being primarily as follows:-

(1) The elevation measurements are such that the hydraulic system is in tension. The practical application of the instrument is therefore limited by cavitation problems.

(2) Small amounts of air in the system will result in long response times and erroneous short-term pressure measurements (Vaughan, 1973(a)). The tension in the hydraulic system accentuates this problem and the use of properly de-aired water (2 p.p.m.* of dissolved O_2^{\dagger}) is essential. The use of tap water (10 p.p.m. of dissolved O_2) would be expected to cause major problems; even water de-aired by boiling under a vacuum and allowed to cool whilst in contact with air (5 p.p.m. of dissolved O_2) is considered inappropriate by Gould and Dunnicliff (1971).

(3) The specific gravity of water varies between 1.0000 at 39^oF (4^oC) and 0.9971 at 77^oF (25^oC) and temperature changes will therefore affect the measured pressures.

The original version of this instrument, developed at the Swedish Geotechnical Institute (Bergdahl and Broms, 1967), incorporated an air filled bladder and a water filled probe. Elevations were determined by the application of air pressure sufficient to return the water to a read-out level, at which point expansion of the bladder and air/water pressure balance are assumed. The instrument thus has the advantage that the hydraulic system is not in tension but otherwise the factors influencing its accuracy are as described for the H.S.G.

*p.p.m. - parts per million

$\dagger O_2$ - oxygen

Gould and Dunicliff (1971) reported data from a later version of this instrument and suggested that, where ambient temperature did not differ from subsurface temperature by more than 20°F (11°C), pressure balance could be achieved in 30 seconds to an accuracy of ± 5 mm. However, in hot weather, with temperature differences of between 40°F (22°C) and 80°F (44°C), equalisation times increased to 5 minutes or more. The combination of temperature change and reading before equalisation reduced accuracy to between ± 10 and ± 50 mm for the aforementioned temperature variations respectively.

An identical instrument to that used at Mucking was used to record settlements beneath a trial embankment at the Empingham Dam site (Werneck, 1974). Initial results revealed drifts of up to 50mm when the probe was returned to the reference pin. Subsequent calibration of the instrument using known level changes (on the side of the site office) indicated an accuracy of ± 10 mm, but considerable drift was observed when the probe was left stationary for any length of time. The equipment was returned to the manufacturer and the transducer found to be faulty.

This experience led to the design and construction of a simple calibration frame for use at the Mucking test site. The frame comprised a steel ladder, the rungs of which were pieces of angle section spaced at about 300mm intervals, bolted to the side of the instrument hut. The instrument could thus be calibrated by setting up the drum and read-out unit on the roof of the hut and comparing the level differences of the rungs obtained using the hydraulic probe and from a level survey. Calibrations carried out prior to the construction of the trial embankments indicated an accuracy better

than $\pm 10\text{mm}$ with some drift.

An estimate of the precision of the instrument in the field was also obtained prior to construction, by taking four sets of readings in one day along H.S.G.B. The standard error of a single observation, as determined from these trials, was $\pm 4.7\text{mm}$ and the precision expressed as a 99% confidence level was $\pm 11.75\text{mm}$. However, all of the H.S.G. readings were repeated and the mean result used; the standard error of the mean was $\pm 3.3\text{mm}$ corresponding to a 99% confidence limit of $\pm 8.25\text{mm}$. A maximum drift of 25mm was recorded on returning to the southern reference pin during the field trials (i.e. $\pm 12.5\text{mm}$ from the mean). These figures thus agreed with the manufacturer's claim of overall accuracy and the simple calibration tests

(ii) Accuracy of Measured Displacements

This depends on the ability of the flexible access tube to model the soil displacements and the accuracy of location of the probe within the access tube as well as the elevation measuring accuracy of the hydraulic system.

Horizontal control of the probe position using the observational procedure described was initially, with the access tube near horizontal, a function of the tape measurements. This, as described in section 5.3.5., was of the order of $\pm 2\text{mm}$. As the access tube deforms during construction there is a loss of horizontal location control, this being a function of the inclination of the access tube. H.S.G. s 'A' and 'B' were approximately 70m long, with H.S.G.C. slightly shorter at 60m . Considering half a gauge length (i.e. 35m), with 500mm settlement at the embankment centre decreasing linearly to zero

at the reference pin locations, produces an access tube inclination to the horizontal of $0^{\circ} 49'$. The corresponding horizontal distance error is 3.5mm which would produce a settlement error of 0.06mm.

In order to produce a settlement error of the magnitude of the measurement accuracy (i.e. 10mm) would require a horizontal mislocation error of 700mm. It was, therefore, not anticipated that horizontal location of the probe would result in a significant loss of accuracy even if inclination corrections were not made. Finally on this point, the probe is not a tight fit in the access tube and this may result in differences of level being recorded at the same location, but these should not exceed a few millimetres.

The overall accuracy of the vertical displacement measurements can only be assessed by comparisons with other measurements of settlement. Gould and Dunnicliff (1971) report such a comparison where the precision of the readings was better than $\pm 25\text{mm}$ for settlements of 1200mm in a rubbish tip; agreement with adjacent settlement plates was to within 90mm (or 7% of the total) although the comparison was impaired by the variability of the material and positional differences between the instruments. Despite the calibrated precision of $\pm 10\text{mm}$ Werneck (1974) considered the H.S.G. settlements to have an overall accuracy of only $\pm 30\text{mm}$ which, at Empingham, represented between 10 and 15% of the measured settlements. Dunnicliff (1971) suggested an accuracy range of between ± 5 and $\pm 25\text{mm}$ to be applicable to this type of instrument.

5.3.4. Observed Vertical Displacements

(i) Bank 1, Stage 1

The initial readings were, in general, highly satisfactory and indicated the precision of the instrument to be within the limits defined by the pre-construction trials. However, on two occasions very strange readings were obtained but as the operators were inexperienced this was not attributed to apparatus malfunction.

The readings taken during construction varied from very good, with repeatability better than $\pm 10\text{mm}$ and minimal drift, to very poor, with repeatability worse than, and drift in excess of, 50mm .

Table 5.3.1. shows the average repeatability of the vertical location measurements (within the access tube) with respect to the mean of each pair, for the H.S.G. readings taken during construction of Bank 1. The values are much worse than obtained pre-construction, and lead to a standard error of $\pm 9\text{mm}$ and 99% confidence limit of $\pm 22\text{mm}$ for the mean of a pair of readings. Also presented in table 5.3.1. are the level differences between the northern and southern reference pins indicated by the hydraulic probe travelling in both directions, and the drift in the datum level obtained when the probe was returned to the southern pin. There is no apparent correlation in the data between repeatability, drift and the level difference error in relation to the survey values. The results were typified by repeatability variations, between two adjacent reading points, from a few millimetres to 30 or 40mm.

When the vertical displacements were plotted, direct comparisons could be made with the results from the settlement plates, which were at the same level and very close to the access tubes. These comparisons

revealed differences in the measured settlements of between 15 and 85mm, with the H.S.G. results indicating the smaller settlements in each case. At some locations the H.S.G. profiles indicated heave of the foundation beneath the embankment after substantial amounts of fill had been placed. Approximate comparisons could also be made with the heave movements of the foundation, as recorded by the inclinometers and surface targets. These indicated that pre-failure heave of the foundation was small, being about 50mm maximum and only 20 to 30mm at a fill height of 3.5m. In contrast the H.S.G. results indicated heaves in excess of 100mm in some instances.

The results of the vertical settlement plates and the order of magnitude of the heave movements thus enabled an attempt to be made to 'fit' the settlement profiles at certain locations. Due to the close proximity of the H.S.G. s and the settlement plates, and the high degree of confidence in the data from the latter (section 5.10) it was decided to fit the vertical displacement profiles to the plate settlements as shown in figures 5.3.2. and 5.3.3. The amount of vertical downward shift applied to each set of observations is included in table 5.3.1., indicating, again, no trend between the apparent precision of the observations and the observed accuracy.

A constriction in the access tube of H.S.G.A. prevented the probe from travelling beyond the rear berm after the readings of 17/9/73, although the tape would still pass through. Due to the difficulties being

H.S.G.	DATE	AVGE. PRECISION OF READINGS	LEVEL DIFFERENCE OF REFERENCE PINS, mm				DRIFT ON RETURN	COMMENTS
			S to N	N to S	AVGE	LEVEL SURVEY		
	1973	±mm					mm	
A	4/9	21	-98	-103	-100	-131	+5	Readings Rejected
A	17/9	7	-135	-135	-135	-131	0	Lowered 17mm to fit
A	3/10	15	-	-	-	-	+40	40mm
A	5/10	9	-	-	-	-	+46	44mm
A	9/10	15	-	-	-	-	-58	80mm
B	5/9	10	+195	+169	+182	+170	+26	75mm
B	17/9	4	+171	+166	+169	+165	+5	20mm
B	24/9	8	+135	+171	+153	+159	-36	50mm
B	2/10	12	+143	+160	+152	+162	-17	86mm
B	6/10	10	+165	+123	+144	+162	+42	Not plotted
B	8/10	13	+212	+151	+182	+162	+61	Lowered 20mm to fit

TABLE 5.3.1.

Bank 1: Accuracy and Precision of Vertical Displacement Measurements Deriving from the H.S.G. s

experienced with the H.S.G. readings at that time, no attempt was made to survey the remaining part of the access tube from the northern station and hence the limited data in figure 5.3.2.

Also included in figures 5.3.2. and 5.3.3., for comparison with the H.S.G. data, are the vertical displacements of the uppermost inclinometer magnets and the surface targets in the foundation. The results suggest that the measured settlement profiles were 'relatively' correct although 'absolutely' in error. Agreement between the three data sources is particularly good for H.S.G.A. and the southern part of the profile for H.S.G.B. The lack of compatibility between the inclinometer magnet displacements and the settlement profile for the northern part of H.S.G.B., particularly with increasing fill height, may well be due to the inaccuracy of the former (as discussed in section 5.4).

The relatively low degree of accuracy of the vertical displacements measured with the H.S.G. s is reflected in the profiles, particularly in the areas outside the embankment. Bearing in mind the magnitude of the pre-failure heave the profiles suggest that the overall accuracy of the vertical displacements as plotted is about $\pm 25\text{mm}$. This is close to the accuracy of the actual measurements recorded (table 5.3.1.), as would be expected if the errors in absolute level have been removed by the fitting process, and represents about 15% of the total measured settlements. Such an order of accuracy is less than was hoped for, and is inadequate with respect to the observed displacements, particularly in the heave zones.

It was thus accepted that the measured vertical displacement profiles were in error by differing constant amounts, but no positive explanation was available. The level survey of the reference pins could not be faulted,* so that the main possibilities were a faulty transducer, faulty read-out unit, air in the hydraulic system or temperature effects. The apparatus was therefore returned to the manufacturer for checking and de-airing after the completion of Bank 1, Stage 1. No faults were found.

(ii) Bank 1, Stage 2

Failure of Bank 1, Stage 1 caused both H.S.G. access tubes to buckle, so that the probe could not pass beneath the embankment from the southern side. The tubes were cut, straightened, joined and re-buried beneath the clay berm constructed to the south of Bank 1 between construction stages (figure 4.3). Despite this work, only the tape and draw cord would pass through the jointed section, suggesting that the initial constriction in H.S.G.A. was the installation joint. It would thus not appear advisable to install jointed sections of access tube, even though it may be financially desirable so to do. The probe could therefore not pass beneath the embankment on Section A, from either side and H.S.G.A. was abandoned.

H.S.G.B. was monitored from the northern side during Stage 2, horizontal and vertical measurements being recorded together. The probe was initially pulled as far as it would go using the draw cord by an

*Although the reference pins underwent level changes as a result of near surface volume changes these were not as large as those experienced by the heave pins; in any event the reference pins were surveyed on each occasion that the H.S.G. s were read.

operator at the southern station. The original reduced levels at the new measurement points were interpolated from the initial readings and three settlement profiles obtained. These produced even more erratic results than those for Stage 1; the profiles were inaccurate in comparison to the observations of the two settlement plates on Section B, and could not be reconciled with these measurements. No data has been presented for the Stage 2 observations of H.S.G.B. and no ready explanation could be advanced for the disappointing results.

The equipment was again returned to the manufacturers, checked and de-aired. Although the equipment was found to be working properly there was air in the hydraulic system. The apparatus was then calibrated under the writer's supervision, in the manufacturer's workshop, and over the full working range showed an accuracy of better than ± 5 mm, with no drift. This was under constant temperature conditions and it remained to be seen if this performance could be reproduced under field conditions.

Other users of this equipment have encountered similar problems. McKenna and Roy (1973) and Cole (1973) found that frequent de-airing was necessary under field conditions. This could be due to the use of inadequately de-aired water or water loss at the bladder and through the uncovered nylon tubing. George and Parry (1973) reported errors of up to 70% in measuring 200mm of settlement; these errors were attributed to temperature effects and subsequently they also exposed the whole of the cable to ambient temperature before use. This produced some improvement, but satisfactory results were only finally

obtained when the readings were taken at night.* It is interesting to note that these results, as shown by George and Parry (1973), produced very reasonable looking settlement profiles but that the absolute values of settlement were greater than indicated by other instruments. In contrast the daytime results at Mucking (during a very hot summer) produced reasonable profiles but with low absolute values of settlement. These occurrences could both be the result of temperature difference effects on the water's specific gravity, although such effects also manifest themselves due to volume changes of the tubing.

(iii) Bank 2

It was hoped that the modifications to the observational system would minimise any temperature effects and that the de-airing would improve the performance of the equipment in monitoring vertical displacements of the Bank 2 foundation.

Three sets of initial readings were taken for Bank 2, statistical analysis of these producing a standard error of $\pm 6\text{mm}$ and a 99% confidence limit of $\pm 15\text{mm}$ for the mean of a pair of observations. Thus despite everything these were slightly less precise than the results obtained during the proving trials for Bank 1. However, the drift in the zero position upon returning the probe to the southern reference pin was only between 5 and 12mm, with the average predicted level difference between the reference pins differing from the level survey by between 7 and 18mm.

*readings taken during the summer.

Readings on H.S.G.C. were subsequently taken during and post-construction, the records for 18 months of observations being presented in figure 5.3.5. A summary of the results, similar to that for Bank 1 (table 5.3.1.), is presented in table 5.3.2. At first glance it can be seen that the results are much more precise and that the drift and level difference errors are much smaller than for Bank 1. The standard error of the mean readings within the access tube was $\pm 3.5\text{mm}$ with a 99% confidence limit of $\pm 8.75\text{mm}$, which is of the order claimed by the manufacturers. In addition it became apparent that even when relatively large zero shifts occurred on return to the southern reference pin that the repeatability of the measurements within the access tube was unaffected. On reflection, table 5.3.1. also showed that the drifts recorded at the reference pin were far larger than the average repeatability of the access tube measurements. This implied that whereas the readings within the access tube were reasonably accurate that those for the reference pins could be subject to much larger errors. As the latter determine the absolute level of the profile, any errors would result in the measured profile, although relatively correct, being incorrectly located in space and lead to incorrect displacement values. The shifts necessary to tie in the Bank 1 profiles to the settlement plate data were therefore probably due to incorrect reference pin measurements.

Further examination of the Bank 2 data also revealed that, even when drift and level difference errors occurred, either the north to south, or south to north difference might be very close to the surveyed value. Thus if the south to north difference was much

closer, the return measurement on the southern reference pin (and hence any drift) was ignored. If, however, the north to south difference was closest, the average value at the southern reference pin was used. In the former case the reduced level of the profile was tied in to the northern reference pin, and in the latter the southern reference pin was used. The final column of table 5.3.2. indicates the implied level difference errors using this procedure, these being between +10 and -22mm with an average of -6mm. These figures indicate, as do the overall results in table 5.3.2, that the level difference errors and drift were within acceptable limits considering the precision of the equipment ($\pm 9\text{mm}$) and the accuracy of the level survey ($\pm 6\text{mm}$; see section 5.9).

The H.S.G. results, although having a basic precision of $\pm 9\text{mm}$, would thus appear to be subjected to additional errors, over and above that due to inaccuracies in the level survey, when related to ordnance datum via the reference pin readings. These errors may reduce the accuracy by about $\pm 10\text{mm}$. The main physical differences between the readings on the reference pins and those within the access tube was elevation (1 to 1.5m difference) and environment, the latter being in the open air. The most likely cause of the inaccurate reference pin readings must therefore be temperature. This conclusion is further supported by calibrations carried out during Bank 1 construction, which showed no significant fall-off in the instrument's performance, despite the poor results obtained in the field.

The measured data for H.S.G.C., related to Ordnance Datum as described, and converted to vertical displacements without correction, are

DATE	AVGE PRECISION OF READINGS	LEVEL DIFFERENCE OF REFERENCE PINS, mm				DRIFT ON RETURN	COMMENTS		LEVEL DIFFERENCE ERROR
		S to N	N to S	AVGE	LEVEL SURVEY		mm	R.L.TAKEN AT PIN	
10/1/74	3	+48	+21	+35	+49	+27	N	Not Plotted	-1
15/1	2	+50	+35	+42	+45	+15	N		+5
22/1	10	+46	-2	+22	+45	+48	-	Readings Rejected	-
30/1	5	+28	+23	+26	+46	+5	N		-18
4/2	5	+16	+36	+27	+48	-13	S		-21
7/2	5	+21	+31	+26	+44	-10	S		-18
14/2	8	+36	+30	+33	+45	+6	S	Not Plotted	-12
22/2	2	+20	+25	+23	+45	-5	S	Not Plotted	-22
28/2	1	+34	+30	+32	+44	+4	S		-12
7/3	4	+40	+32	+36	+44	+8	S	Not Plotted	-8
22/3	-	+41	-	-	+39	0	S	Tape Broken	+2
4/4	2	+44	+44	+44	+41	0	S	Not Plotted	+3
16/5	8	+62	+41	+51	+41	0	S		+10
30/5	4	+36	+35	+35	+40	+1	S	Not Plotted	-5
14/6	6	+36	+41	+39	+44	+5	S	Not Plotted	-5
11/7	2	+34	+34	+34	+44	0	S		-10
23/8	6	+49	+14	+32	+49	+35	N		0
20/9	5	+59	+43	+51	+44	+16	S		+7
9/1/75	3	-272	-206	-239	+49	+66	-	Readings Rejected	-
12/6	2	+49	+61	+56	+50	-6	N		-1

TABLE 5.3.2.

Bank 2, H.S.G.C.: Accuracy and Precision of Vertical Displacement Measurements

presented in figure 5.3.5. together with the vertical displacements of the three settlement plates on Section C and the surface targets. Inspection of the results shows them to be far superior to those obtained for Bank 1, and compatible with the observed displacements of the surface targets and the settlement plates. The observed heave movements of the foundation to the south of Bank 2 were less than 30mm, and even smaller to the north. Visual inspection of the vertical displacement profiles in the heave regions suggests that, although 2 or 3 of the 12 profiles plotted* may have had accuracies as low as $\pm 20\text{mm}$, the majority were probably accurate to within $\pm 10\text{mm}$. This represents approximately 3.5% of the maximum observed settlements, and was particularly satisfactory in view of the poor results obtained previously.

(iv) Final Comments

The final observation procedure combined with the improved facilities at the observation stations produced H.S.G. readings compatible with the precision claimed by the manufacturers. However, the overall accuracy appears to be reduced by the lower accuracy associated with the readings on the reference pins; never-the-less the overall accuracy of the displacements for H.S.G.C. is probably better than $\pm 10\text{mm}$, compared to $\pm 25\text{mm}$ (after correction) for Bank 1.

*20 sets of observations were made, as shown in table 5.3.2. Of these 2 were rejected; 11 of the remainder are presented in figure 5.3.5. whilst the final 7 were only omitted for the sake of clarity. In addition the time of reading of some of the 6 was such that the displacement profiles were very similar to the previous measurements.

For any future use of this instrument it is suggested that metal collars be attached to the access tube at various locations outside of the embankment area; these collars would have reference pins welded to them such that the tops were above ground level and could be located in a level survey. Suitable locations might be at the embankment toe, the end of the initially horizontal portion of the access tube and mid-way between these positions. The access tube profile could then be related to Ordnance Datum without recourse to readings taken outside of the access tube. Such installations would also provide a useful additional check on the instruments overall behaviour.

Reference to table 5.3.2. reveals no trend towards more accurate readings being obtained at particular times of the year, and it would seem that the procedure adopted for Bank 2 minimised temperature effects, whereas that used for Bank 1 did not. That temperature, rather than air in the hydraulic system as a result of leakages etc., is the main factor in producing inconsistent results is indicated by the excellent data obtained over a long period, with no de-airing, for Bank 2, and the consistently good performance of the instrument when calibrated under constant temperature conditions.

Temperature effects could be minimised for the standard apparatus if a white cable were used instead of the normal black. Also a fluid exhibiting less marked variations in specific gravity with temperature could be used in the hydraulic system. Other possible improvements have been suggested by Green (1973(b)), with the

object of achieving a positively pressurised hydraulic system, as follows:-

1. Use compressed air to back pressurise the bladder.
2. Locate the transducer within the probe.
3. Use excavated datums.

5.3.5. Accuracy of Horizontal Displacements

(i) Precision of the Equipment

The manufacturers claim an accuracy of location of $\pm 1\text{mm}$ for the magnetic rings; as the sensitivity of the steel band is 1mm this would seem optimistic. Although the location of ring magnets by reed switch sensors can be very precise (section 5.11) under controlled conditions, the accuracy is largely dependent on the tape measurements and the repeatability of the line of passage of the probe through the magnet. The readings of magnet location suggested that the start and finish points of the signal could be defined to within $\pm 1\text{mm}$ on the tape. Examination of the initial readings for all the H.S.G. s (each magnet location being the average from four different readings) at Mucking revealed the standard error of location to be $\pm 1\text{mm}$ with a 99% confidence limit of $\pm 2.5\text{mm}$.

(ii) Accuracy of Measured Displacements

This, again, depends on the ability of the magnet plates to monitor the displacements of adjacent soil elements. Inaccuracies may also be introduced into the horizontal measurements due to settlement of the tube (as discussed in 5.3.4.) and movements of the plates relative

to it (i.e. if they do not remain perpendicular). The use of the H.S.G. to measure horizontal displacements has been fairly limited, and there do not appear to be sufficient data in the literature to enable this facet of its performance to be meaningfully assessed.

5.3.6. Observed Horizontal Displacements

(i) Bank 1, Stage 1

The location of the magnets did not present any real problems, although the following difficulties arose:-

- (1) Magnet 'H' on H.S.G.A. was not located after the 17.9.73.
- (2) On one occasion the lead to the buzzer came loose and some readings were lost.
- (3) Breakage of the steel band occurred on one occasion.

The measured horizontal displacements are presented in figures 5.3.2. and 5.3.3., wherein horizontal displacements interpolated from the inclinometer profiles, at the same initial elevations as the H.S.G. access tubes, are included for comparison. Such comparisons are largely indirect because of the interpolations required between reading locations, but where direct comparisons can be made (e.g. IA2 with magnet 'H' of H.S.G.A; IB2 with magnet 'D' of H.S.G.B.) the results can be seen to be in good agreement.

The overall precision of the inclinometer measurements is thought to be better than $\pm 2.5\text{mm}$ (section 5.4) and so differences of $\pm 5\text{mm}$ could be expected between the measurement sources. Comparison is made more difficult on the plots in question because only fill

height has been used to compare the displacements, which became increasingly time dependent with fill height. This is demonstrated by a comparison between the results of the final displacements before failure as measured by H.S.G.B. (8.10.73), the inclinometers (early afternoon, 9.10.73) and H.S.G.A. (late afternoon of 9.10.73), the latter relating to about 2.5 hours prior to failure. The three sets of data are, however, compatible on the basis of fill height and time.

Where the displacements can be compared directly differences vary from less than the combined precision of the observations (H.S.G.A.) to about 20mm (H.S.G.B.), in the latter case the magnets undergoing the larger displacements.

(ii) Bank 1, Stage 2

In this case both the elevation and distance measurements were made from the northern observation station and only H.S.G.B. was monitored. The tape measurements for Stage 2 were felt to be less accurate as a consequence of the modified observational approach.

The results are presented in figure 5.3.4., again with the inclinometer data for comparison. Again agreement appears reasonably good, although there is a maximum difference of about 25mm between the displacement of IB5 and magnet 'I', in this case the inclinometer movements being the greater. However, the incremental displacements are in very good agreement and it may be that there was a source of constant error between the two tape/probe configurations used. It is particularly interesting to note that the change in the direction of horizontal displacement at the location of IB4 (resulting from the change in

embankment geometry) has been picked up by both systems. This indicates that the H.S.G. was functioning properly as far as magnet 'F', despite the Stage 1 failure, and therefore that the access tube was able to undergo large local distortions without transmitting any influences to other sections.

(iii) Bank 2

As for Bank 1, tape breakage occurred during the observations, this time on two occasions, and also similarly a magnet was lost; magnet 'E' was located during the initial readings but not subsequently. The results, together with data from inclinometers IC1 and IC2, are presented in figure 5.3.5.

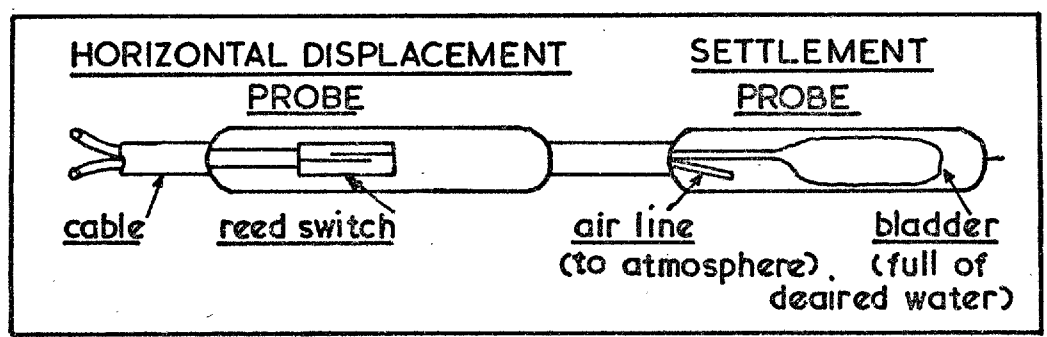
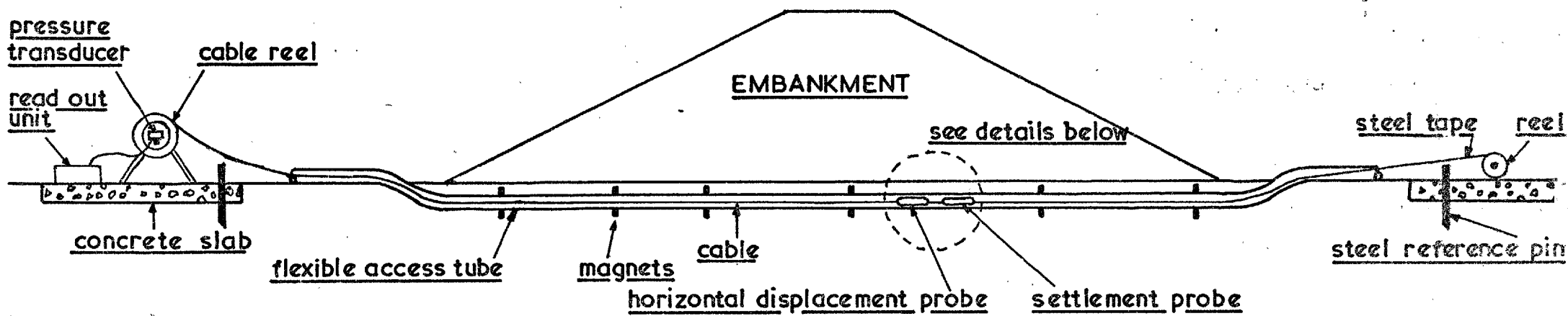
Unfortunately the differing locations of the inclinometers and the nearest magnets makes direct comparison impossible, but the linearly interpolated H.S.G. horizontal displacements during construction agree with those from the inclinometers to within the precision of the instruments. Thereafter, to the south of the embankment the H.S.G. displacements become progressively larger than those of the inclinometer whilst to the north the reverse is true, the respective differences being approximately 40 and 20mm. This may well be due to the linear interpolation of the H.S.G. displacements and it is suggested that the true agreement between the two measurement sources is of the order of ± 5 to ± 10 mm overall.

(iv) Final Comments

The comparisons between the measured horizontal displacements of the H.S.G. magnets and the inclinometer casings suggests to the writer that both instruments recorded horizontal displacements of the foundation

to an accuracy of between ± 5 and ± 10 mm, or between 5 and 10% of the observed values.

The monitoring of horizontal displacements using the H.S.G. s was thus simple and accurate using the observational procedure described. The equipment is robust, but even with careful use tapes can be easily twisted, kinked and snapped; if this happens good results will not be achieved (Wilkes, 1973). When tape breakage occurs it may be more convenient to relocate the reading positions for vertical displacements. This was done for Bank 2, as shown in figure 5.3.5.



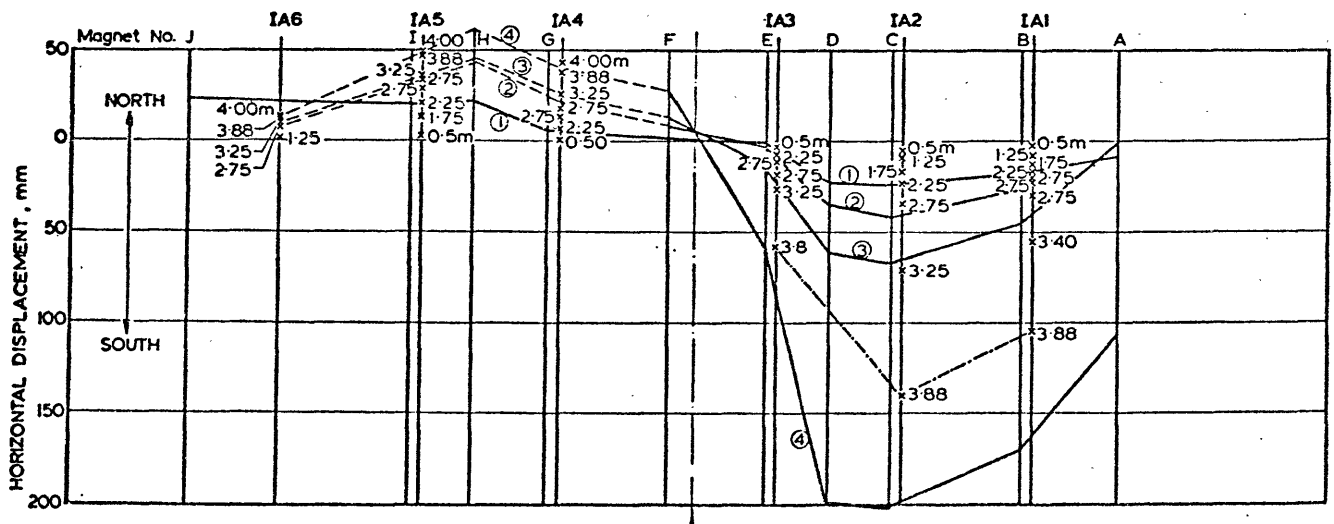
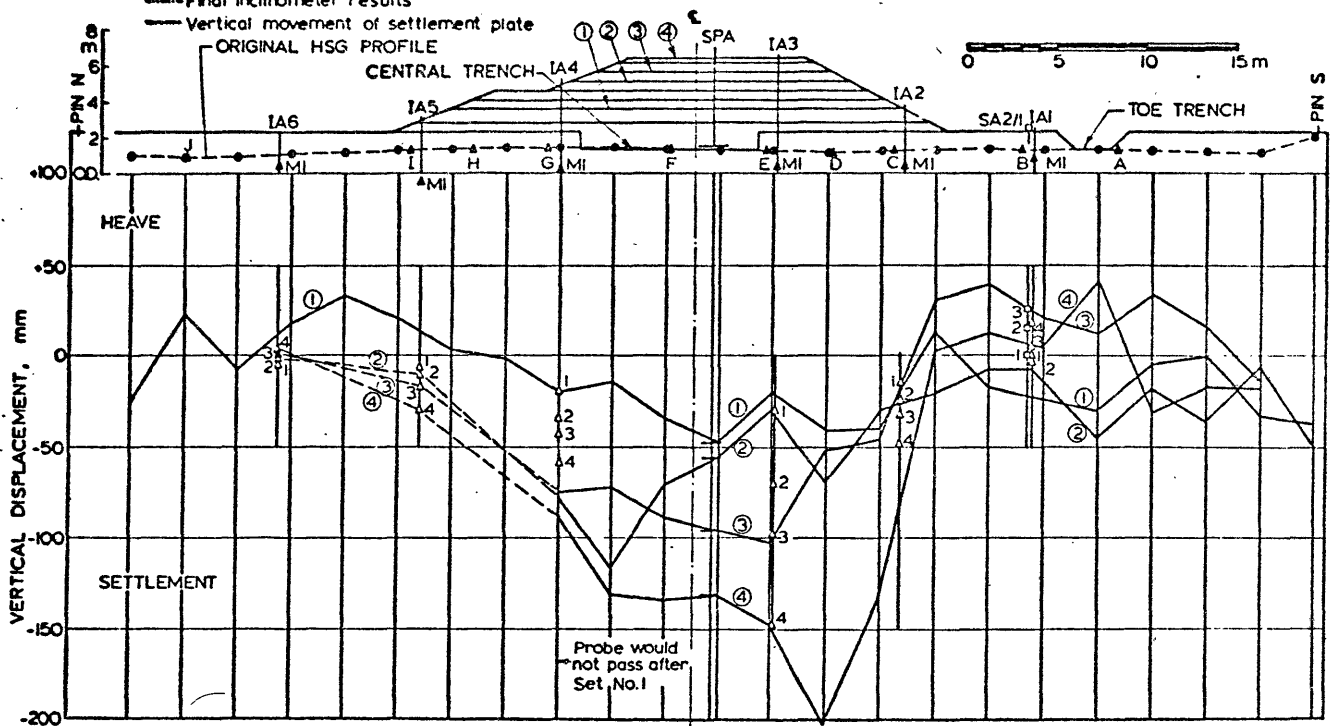
-338-

DIAGRAMMATIC REPRESENTATION OF HYDRAULIC SETTLEMENT GAUGE AS USED AT MUCKING (DRAWING ADAPTED FROM WERNECK, 1974)

- LEGEND:**
- Vertical movement reading position
 - ▲ Original magnet position
 - ▲ Vertical movement of inclinometer magnets (MI)
 - Vertical movement of surface target
 - Horizontal movement of inclinometers
 - Inclinometer results used
 - Final inclinometer results
 - Vertical movement of settlement plate

KEY TO READINGS:

Set No.	Fill Height	Date
1	2.25m	17/9/73
2	2.85	3/10
3	3.25	5/10
4	4.00	9/10



BANK I, STAGE I, HSGA.

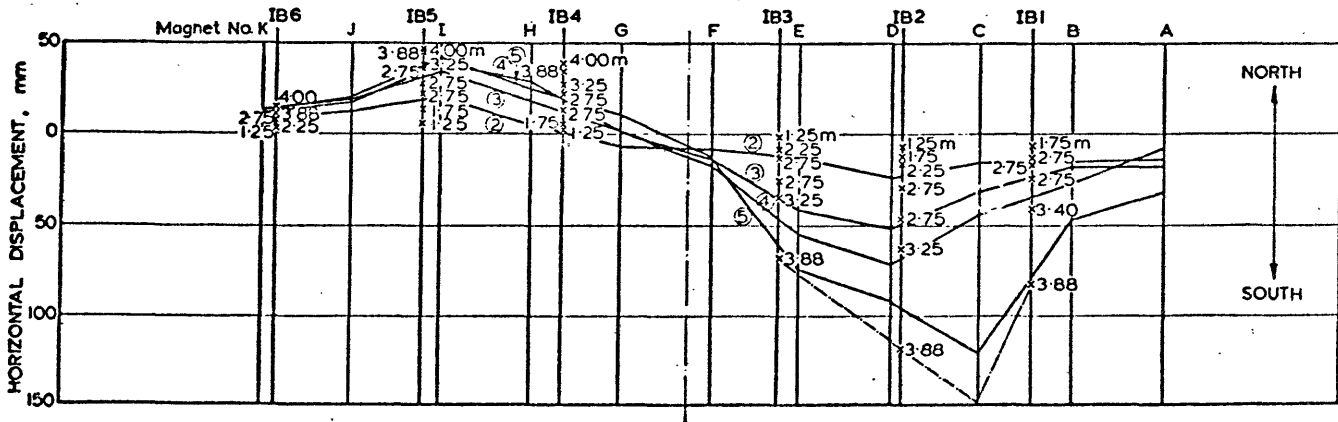
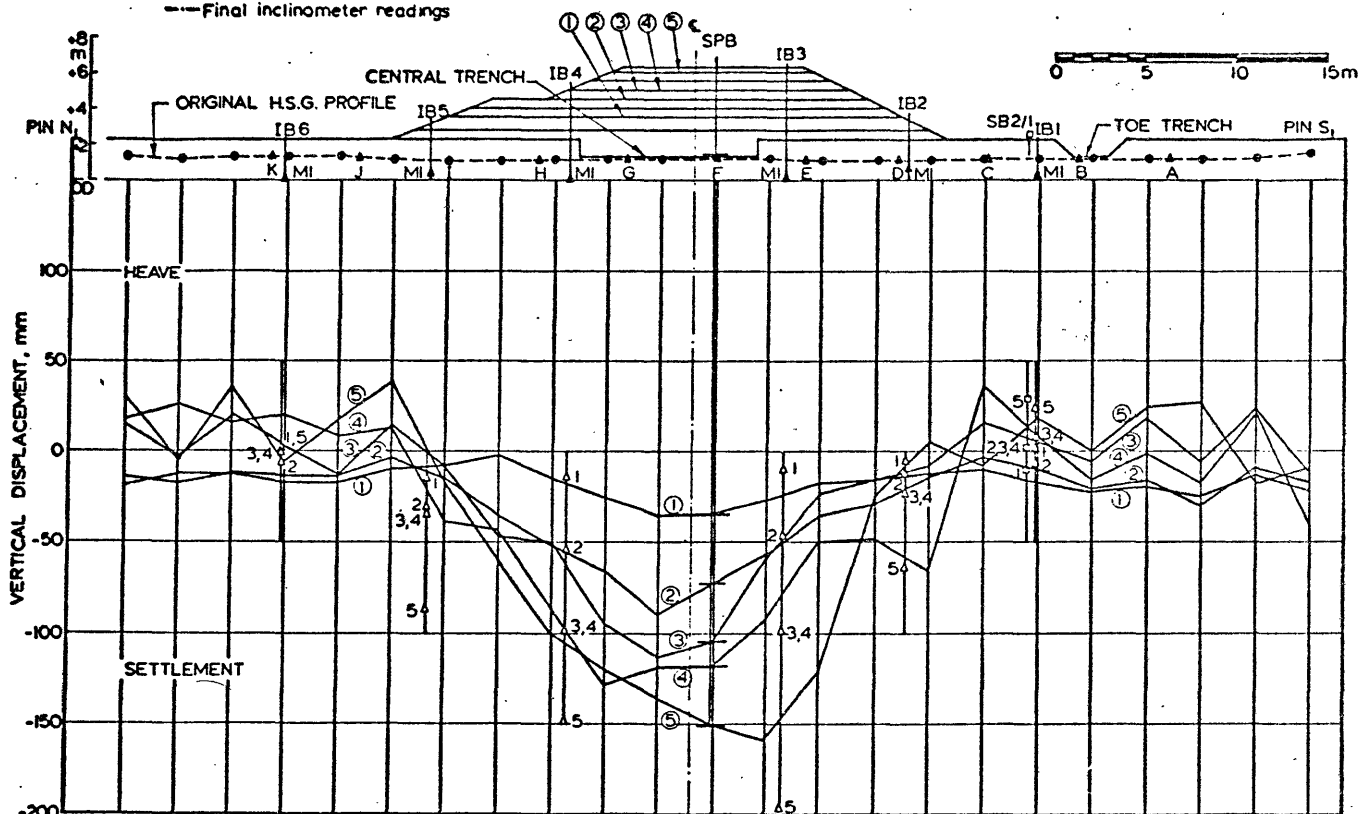
HORIZONTAL AND VERTICAL DISPLACEMENTS

Fig. 5.3.2

- LEGEND :**
- Vertical movement reading position
 - Vertical movement of settlement plate
 - ▲ Original magnet position
 - ▲ Vertical movement of inclinometer magnets (MI)
 - Vertical movement of surface targets
 - Horizontal movement of inclinometers
 - Final inclinometer readings

KEY TO READINGS:

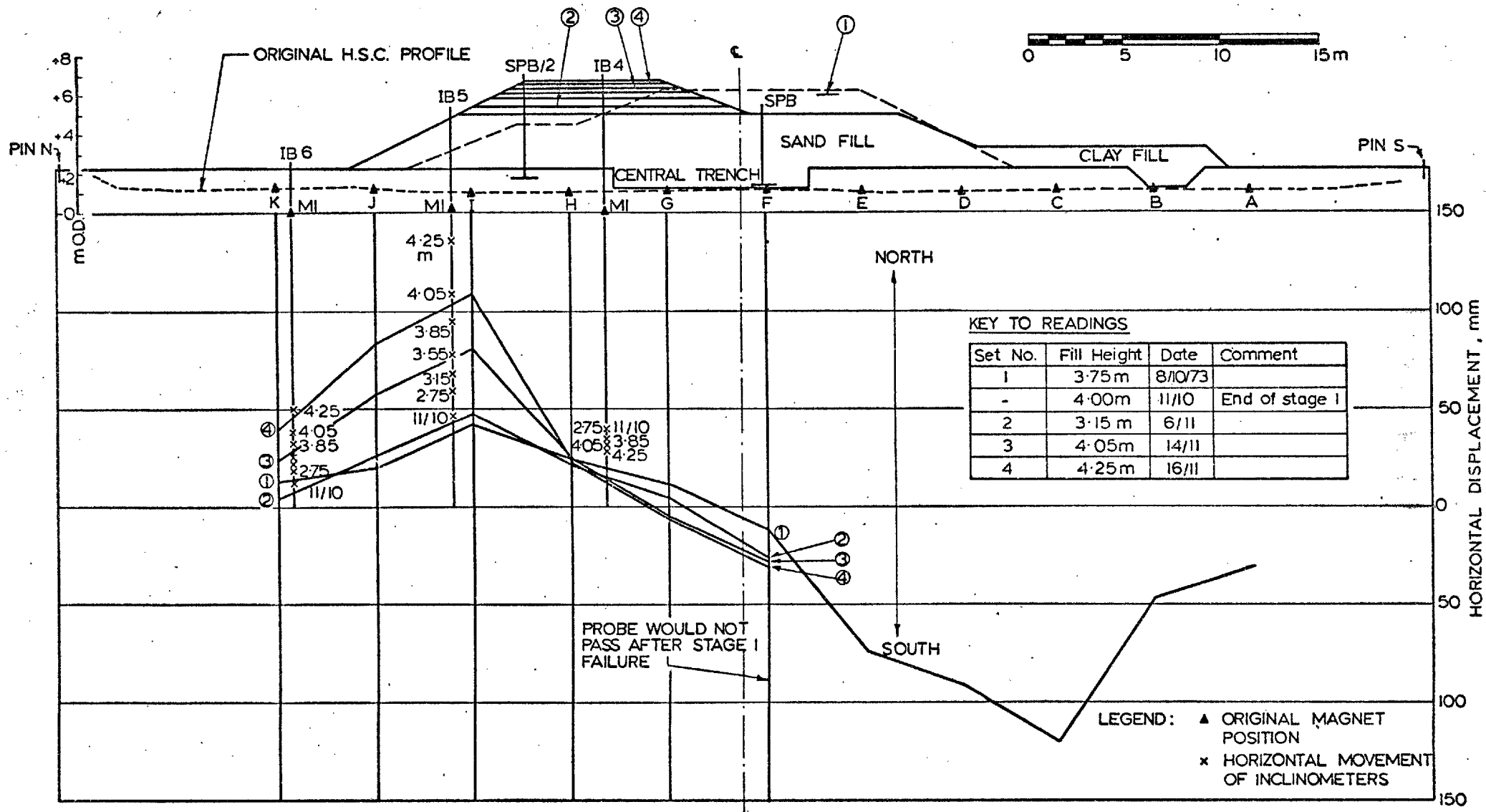
Set No.	Fill Height	Date
1	1.25m	5/9/73
2	2.25	17/9
3	2.75	24/9
4	2.75	2/10
5	3.75	8/10



BANK I, STAGE I, H.S.G.B.

HORIZONTAL AND VERTICAL DISPLACEMENTS

Fig. 5.3.3



BANK I, STAGE 2, H.S.G.B.

HORIZONTAL DISPLACEMENTS ONLY.

Fig. 5.3.4

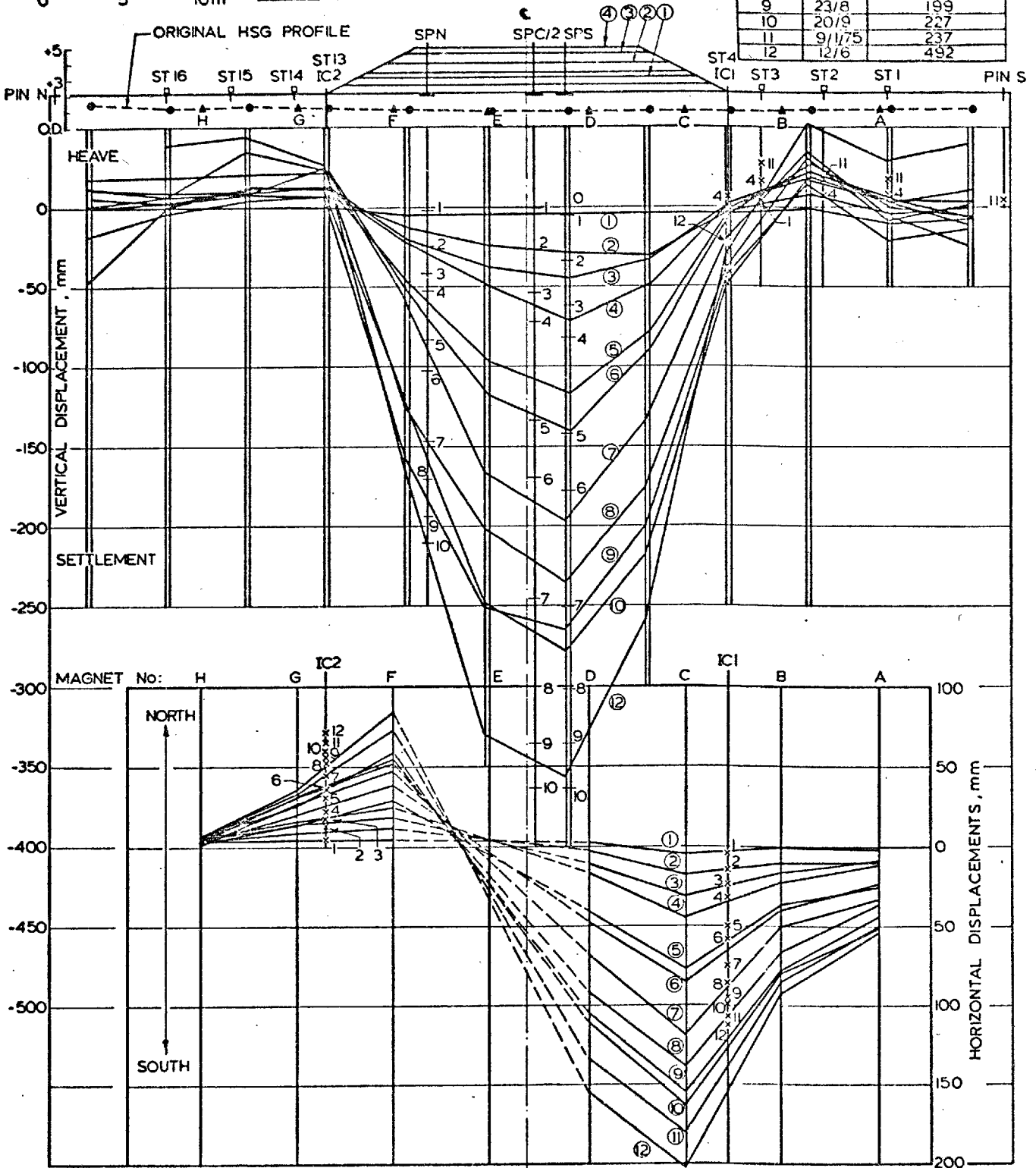
KEY TO READINGS:

DURING CONSTRUCTION

Set No.	Fill Height	Date
1	0.95m	15/1/74
2	1.85	30/1
3	2.45	4/2
4	2.80	7/2

POST CONSTRUCTION

Set No.	Date	Days from E.o.C
5	28/2/74	23
6	2/3	45
7	16/5	100
8	11/7	156
9	23/8	199
10	20/9	227
11	9/1/75	237
12	12/6	492



- LEGEND :
- Vertical movement reading position (NB. shifted 0.3m to N after set No.6)
 - ▲ Original magnet position
 - Vertical movement of surface targets

- × Horizontal movement of inclinometers
- Magnet E not located after initial readings
- Vertical movement of settlement plates

BANK 2, H.S.G.C. HORIZONTAL AND VERTICAL DISPLACEMENTS

Fig. 5.3.5

5.4. Inclinerometers

5.4.1. Installation

The inclinometer torpedo used was a Soil Instruments Ltd., Mk II, coupled to a 12 volt digital read-out unit complete with battery checking facilities. This torpedo operated inside an aluminium casing (50mm I.D.) with four keyways, ninety degrees apart, to orientate the instrument.

The casing was in 3m lengths, epoxy painted to resist corrosion after installation (Wilkes, 1973), although this is by no means an absolute form of protection (Fraser, 1972; Cole, 1973) and where ground/backfill conditions are particularly aggressive an additional coating of bitumastic material is recommended (Green, 1973(a)). The casings were assembled on site to the required lengths prior to installation and inspected for any signs of twist. Site conditions being essentially 7m of clay overlying gravel (into which the casing bases were installed) the assembly process comprised joining three lengths of casing. Penetration into the gravel stratum varied, but was on average between 1 and 1.5m. The individual lengths of casing were joined by 300mm long couplings which slid over them, these being a fairly tight fit. Each joint was formed so that there was a 100mm 'telescopic' gap to account for vertical movement. The couplings were secured to the main casings by four rivets mid-way between the keyways and 50mm from the end of the coupling. Finally the joint was wrapped with denso-tape to seal it against the ingress of soil, water or grout.

Ring magnets, mounted on couplings, were likewise fitted onto the main casing lengths above each of the two telescopic joints to be in the foundation. The casing bases were blocked by the insertion of an end cap and sealed with denso-tape. The complete casings, comprising three 3m lengths, two couplings, two coupling mounted ring magnets and the base cap, were installed into 150mm diameter flight augered boreholes. Each casing was filled with clean water prior to installation to counteract the buoyancy effects of the ground-water.

Having inserted a casing, it was orientated so that one pair of keyways lay along the bearing line of the instrumentation sections (320° ; figure 4.1). The space between the casing and the borehole sides was grouted up with a 3:1 bentonite:cement mix, pumped down via a tremie pipe.

Casings outside the proposed loaded areas were given a concrete surround at ground level to form a working surface. All the casings were cut off above ground level at convenient heights.

5.4.2. Horizontal Displacement Observations

(i) Reading System

A reading interval of 1m (twice the effective length of the torpedo) was selected as appropriate for the situation, mainly on the basis of reading and data reduction time. The first reading was taken with the torpedo's fixed wheels equidistant from a point 1m above the base of the casing. This entailed lifting the torpedo 640mm from, and implied zero horizontal displacements at a point 500mm above, the base. The use of a 1m reading

interval necessitates extrapolating the measured angle 250mm beyond the fixed wheels, in both directions. Full details of the installations and reading positions are provided with the measured horizontal displacements (figures 5.4.2. to 5.4.16).

The first reading in an inclinometer casing is generally taken at some distance above the base, to guard against this datum position being lost due to any backfilling of the casing. At Mucking the distance of 1m from the base was selected so that the torpedo wheels would never be in a coupling at a reading position in the foundation, no matter how much telescopic movement occurred. However, the combination of reading interval and starting position resulted in readings being taken across both couplings in the foundation, a practice which is usually avoided if at all possible. Thus at worst 2 readings out of the 8 per casing in the foundation might have to be discarded; the 2 reading positions across couplings were also those where the torpedo wheels could enter the joint if the vertical control was inadequate.

When angles are directly recorded using an inclinometer, the results are generally inspected for the different face error which occurs when a reading is taken with the wheels in a coupling and such readings are discarded. The read-out unit used enabled angles, as well as incremental or summed displacements to be recorded, the latter two being available for 0.5 and 1.0m reading intervals. The summed displacement facility used greatly reduces data reduction but does not permit such a ready appreciation of face error variations as angle or incremental displacement readings. This, plus the limited number

of readings in the foundation, made it desirable to avoid readings being taken with the torpedo wheels in a coupling, if this was going to lead to errors of such magnitude as to necessitate rejection of the readings. However, there is no *a priori* reason why the average angle recorded with a torpedo wheel in a coupling should not be the average angle of the casing, provided that:-

1. The 'depth' of the coupling is uniform.
2. Vertical control is good enough to enable correct location of the torpedo on both faces.
3. The casing has not dog-legged about the coupling.

At Mucking the basic displacement data were plotted and the face errors evaluated; inspection of both of these quantities was used as a basis for the acceptance or rejection of data, as will be discussed in due course.

Readings taken with the torpedo fixed wheels straddling a coupling are potentially a source of much greater error. When the casing deforms smoothly there are no problems, errors being introduced when the casing becomes dog-legged about the coupling. This form of deformation often occurs in aluminium casings (Green, 1969), although Werneck (1974) reported bending angles of $5^{\circ}/305\text{mm}$ (approximately $15^{\circ}/\text{metre}$), compared to maximum tilting angles of 6° , measured in aluminium casings. The error introduced, when a reading is taken across a bent coupling linking relatively straight casing lengths, is due to the recording of their average angle. This error is accentuated by the use of a reading interval greater than the torpedo wheel base, as at Mucking, and also because of

the rapid rate of angular change experienced by the torpedo. The latter means that vertical location errors may cause significant horizontal errors, although these may show up as face error variations.

All the coupling readings were carefully inspected to try and assess if a more accurate profile would be obtained by extrapolation of the angles either side of the coupling. It was hoped, in view of the relatively short installations, that the sacrifice of accuracy to enable rapid reading and data reduction would not be excessive

(ii) Reading Process

A pulley wheel attachment was fitted to the top of the casing, the cable drum and read-out unit being supported in a portable frame. The torpedo was then lowered to the base of the casing, which was maintained full of water, and left for at least ten minutes to cool to the ambient temperature (Green, 1973(a)). The read-out unit was connected to the cable drum, and hence to the torpedo, by a jack-plug socket; this connection was made and the unit switched on. This allowed the read-out unit to warm up and observation of the 'settling down' of the instrument if desired. Before commencing to take readings a steady angle was looked for at the base of the casing and the state of charge of the battery was checked. The torpedo was then pulled up 640mm from the casing base, to the first reading position. A marker post was placed adjacent to a convenient 1m or 0.5m mark on the torpedo cable at this first position; readings were then taken up the casing at 1m intervals from it. A few seconds were allowed at

each reading position for damping of the pendulum in the torpedo. This interval was based on observations of the settling time for angle measurements as no such observation is possible with displacement recording.

Having taken the uppermost reading the torpedo was speedily withdrawn, reinserted on the opposite face and lowered to the base again. The opposite face readings were taken in similar manner to that previously described. No delay was deemed necessary for temperature equalisation when changing face as the torpedo was only out of the water for a few seconds. When moving the equipment from one location to another the torpedo was always transferred first to minimise any raising of the temperature.

Only one pair of keyways was read per casing, this being along the instrumentation section lines, except for IA6 (Bank 1, Stages 1/2) where the misalignment during installation was excessive. As with all the instruments used, initial readings were taken in triplicate, angles and incremental displacements being recorded as well as summed displacements. Readings were also taken initially in the plane strain direction to allow for periodic checking of this design assumption.

During construction those inclinometers within the fill areas were extended by jointing in similar fashion to the foundation casings. In the fill, however, the couplings were only 150mm long and the telescopic gaps only 50mm; no magnets were used in the fill. The extension lengths were selected on the basis of fill height, convenience of operation of equipment and avoidance of the torpedo wheels entering the couplings at reading positions.

5.4.3. Accuracy of Horizontal Displacements

(i) Precision of the Instrument

The Soil Instruments Ltd. Mk II inclinometer torpedo operates by means of a steel leaf spring, to which are bonded 4 temperature compensated strain gauges, and from which hangs a tapered, oil damped, plumb bob. The fixed wheel base is 500mm and a pair of diametrically opposite sprung wheels locate the torpedo within the casing. The torpedo is completely sealed and has a transit locking device. The read-out unit functions on the normal wheatstone bridge arrangement, besides having the computational facilities previously described. Calibration of these instruments is carried out in a special frame, as described by Green (1969). The manufacturer's specification is briefly outlined in table 5.4.1.

QUANTITY	SPECIFICATION
Range	$\pm 19.99^\circ$ angle; $\pm 9.999\text{m}$ displacement
Sensitivity	$\pm 0.01^\circ$ angle; $\pm 3.6\text{seconds}$; $\pm 1.7545 \times 10^{-4}$ radians; $\pm 1\text{mm}$ displacement
Temperature	Better than $0.05\%/^\circ\text{F}$
Cross Sensitivity	Better than 0.3 minutes/degree for 20° cross deflection

Table 5.4.1.

Inclinometer Torpedo Specification (S.I.L. Mk.II)

(ii) Casing Characteristics

Tests carried out by Green (1969, 1973(a)) indicate twist in extruded aluminium casing to be random and generally less than $1^\circ/3\text{m}$ length.

Maintenance of a constant cross-section and formation of keyways with constant dimensions do not appear to present problems with this type of casing.

(iii) Accuracy of the Inclinometer System

In order to correctly approach the problem of assessing the accuracy of the inclinometer system, as used to measure horizontal displacements of soil masses, and the corrections that may need to be made to quantifiable errors, it is first necessary to consider the two fundamental sources of discrepancy:-

- (1) if the casing does not deform in exactly the same way as the soil the results are inaccurate. In this category is included the effect of the installation on the soil behaviour, and the tendency for aluminium casings to bend at the couplings.
- (2) if the casing is not exactly surveyed by the instrument the results are inaccurate.

Considering point (1) firstly, the effect of the perturbation caused by the installation is difficult to assess. Additionally, the aluminium casing is unlikely to exactly model the deformed soil profile with respect to horizontal or vertical movements. Plastic casing, being more flexible, is in theory more likely to follow the deformations of a soft clay but its practical application is limited by the large amounts of twist which may occur during extrusion.† Green (1969, 1973(a)) found 18° of twist in 25m of casing. Marsland (1973(a)) reports the use of cylindrical plastic casing, with no keyways, in soft clay. The torpedo

†This problem has now been overcome, according to Soil Instruments Ltd., (1975)

was kept correctly orientated by the use of rods instead of a cable, but this method appears too tedious for normal circumstances. The selection of a casing is thus a compromise between its having sufficient suppleness to deform with the soil, being sufficiently rigid to maintain a constant cross-section under stress and having the necessary material properties for precise extrusion.

Also under this heading consideration must be given to the effect of the grout column. This should ideally be of compatible stiffness to the ground. Various types of backfill have been used in preference to bentonite/cement grouts e.g. sand columns and plastic foams (Green, 1973(a)). Corrections for the relative stiffness of the grout column are not usually applied and its influence is a suitable topic for study, being uncertain at present.

Turning to point (2), if a continuous angular profile could be recorded within a constant cross-section casing, the correct relative displacements of the casing from its original position could be recorded. Typical inclinometer torpedos are restricted in their practical reading interval by the length between the fixed wheels, that is the effective torpedo length. The angle measured by the device is the average inclination to the vertical of the casing over the length of the wheel base. Probably the most realistic interval is the wheel base of the torpedo (Burland & Moore 1973; Gould and Dunnicliff, 1971; Bromwell et al, 1971). Intervals less than this enable more than one profile to be measured and should increase the accuracy, although not necessarily in proportion to the additional effort, whilst greater intervals will reduce accuracy. The first inaccuracy in the surveying procedure is thus introduced; the deformed

shape of the casing is represented by a series of constant angle lines which themselves represent the average inclination over the measured sections.

Such errors will obviously be greater, as the deformation of the casing increases and its shape departs from a series of smooth curves: one could be lucky or unlucky with the selection of reading position when using a larger reading interval. A good quantitative estimate of the likely errors in surveying the casing can be obtained by reference to the tests carried out at Imperial College by Green (1969). These indicated measurement errors within $\pm 5\%$ of the true displacements applied to casings over 25m lengths, using a 610mm reading interval (SINCO 200B SERIES and S.I.L. Mk I instruments used, both with 305mm wheel base). An interesting point to emerge from these tests was the difference in error patterns which resulted from the use of aluminium and plastic casings, as well as the twist problems discussed previously. Errors in calculated displacements for the aluminium casing were generally self cancelling with elevation whereas those for the plastic were cumulative. This was thought to be due to the different deformation modes of the two casing types. The relatively rigid aluminium casing with fairly flexible rivetted couplings tended to 'dog-leg' rather than bend, whilst the relatively supple plastic casing, with fairly rigid cemented couplings, deformed more smoothly.

(iv) Accuracy of the Reading System

Thus far the accuracy of the system as a whole has been considered, as well as the precision of the equipment. An appreciation of these quantities is necessary in order to decide upon the degree of accuracy required from the observational process itself, the specification of

this process being of major importance in inclinometer measurements.

The correct approach is to monitor the horizontal and vertical displacements of a particular soil element. This implies angle measurements at the same positions in the casing on each occasion that an inclinometer survey is carried out, and that the casing can follow both the horizontal and vertical displacements of the soil. In order to achieve measurements at the same point in the casing the vertical displacements of each casing length would need to be determined before each set of inclinometer readings; these are provided by the displacements of the settlement magnets and the base of the casing. Such an observational system will still produce inaccurate results if the magnet movements are not representative of the casing movements, or if one or both are not representative of the soil behaviour. In addition the reading process, when the overall casing length is changing due to telescopic movement at the couplings, is complicated: changes in reading interval will be necessary and therefore the reading of angles.

Such an approach is incompatible with rapid reading and data reduction, and in view of this was not used at Mucking. The adopted reading system, as described in section 5.4.2., implied that readings would be taken at constant elevations, provided that the casing bases did not move vertically, and therefore at different locations in the casing if telescopic movements occurred at the couplings. However, the likely errors resulting from such an approach can be quantified and the need for refinements in the observational system, or corrections to the measured data, assessed.

Major problems can arise, using this system, when coupling closures and the resultant reduction in the overall casing lengths are such that reading positions transfer from one casing length to another. Large errors will result from such occurrences if the casing develops a 'dog-leg' shape and the reading system, or method of data interpretation, then has to be modified (Werneck, 1974). The casing installations at Mucking were such that this problem could only arise for the readings across the couplings, which would in any case be closely scrutinised.

(v) Observational and Data Reduction Errors

Once a set of readings has been taken, the calculated horizontal displacements may be subject to errors deriving from the observational system as described previously, the calculation of the displacements and their plotting. Such errors should be avoided, or corrected, as they can in the main be quantitatively assessed (Gould and Dunnicliff, 1971; Green, 1973(a)). In general, problems arise when the measured displacements are either very small (Philips and James, 1973) or both vertical and horizontal displacements are large (Werneck, 1974). For the former category the precision of the equipment may be most important whilst for the latter correct observation and interpretation of the data may have highest priority. The major sources of error are considered briefly in the following sections, mainly with respect to the installations at Mucking.

(a) Displacement Calculation

The horizontal displacement (x_{hor}) is usually calculated as an arc length (x_{arc}) as follows:-

$$x_{hor} = x_{arc} = R.\theta^r$$

where 'R' is the reading interval along the casing and θ^r the inclination of the casing (in radians) to the vertical. At large inclinations the difference between x_{arc} and $x_{hor} = R \sin \theta = R_v \tan \theta$, where R_v is the vertical reading interval, becomes significant. For an inclinometer with a sensitivity of 2×10^{-4} radians a cumulative horizontal displacement error of less than 1.6mm might be expected for the foundation portions of the inclinometer casings at Mucking (section 5.4.4.). On this basis any observational or data reduction error may be considered significant when the integrated effect is greater than ± 1 mm (the sensitivity of the read-out unit).

The relationship between x_{arc} and x_{hor} is illustrated in figure 5.4.1.(a) and the difference $x_{arc} - x_{hor}$ presented, graphically, as a function of θ in figure 5.4.1. (c). The error is approximately 1mm at 10^0 , but thereafter increases rapidly. This source of error is therefore much more significant for casings initially installed non-vertically especially if the out of plumb exceeds 10^0 (Green, 1973(a)). Displacement calculation errors may be totally cumulative (figure 5.4.1.(d)), or self-cancelling to some extent (figure 5.4.1.(e)), depending on the profile of the casing. For a cumulative error, and constant casing angle of 5^0 , the error for a foundation inclinometer at Mucking would be less than 1mm.

(b) Misinterpretation of Depth

The basic displacement calculation described previously assumes each point in the inclinometer to rotate as shown in figure 5.4.1.(a), and this has been shown to be an acceptable approximation for small angles. If a non-telescopic casing was installed in a material which was displacing horizontally only, the use of a constant reading interval (R)

would imply a change in the elevation of the reading as shown in figure 5.4.1.(b). Thus the constant elevation approach is in error by a vertical amount ($V = R - R_V$), giving rise to a horizontal error (h) in the measured displacement at that elevation, and the same casing location approach is similarly in error as the casing cannot exactly follow the adjacent soil elements.

The vertical error is cumulative with distance from the base of the casing, but whether or not there is horizontal error and whether it is positive or negative depends on the casing inclination. This relationship is illustrated in figure 5.4.1.(c), the error being of opposite sign to $x_{arc} - x_{hor}$. For cumulative errors from this source and $\theta = 5^\circ$ an error of 2.4mm would result for a foundation inclinometer at Mucking. With the self-cancelling effect of the $x_{arc} - x_{hor}$ error this reduces to 1.6mm.

In order to assess the likely cumulative errors from these two sources, the two imaginary inclinometer profiles shown in figure 5.4.1.(d) and (e) were considered. The shapes are fairly representative of actual profiles at Mucking and both consist of 8 x 1m reading intervals. The total errors at the casing tops are 2.4mm (figure 5.4.1.(d)) and 0.4mm, with a maximum of 1.6mm (figure 5.4.1.(e)).

In practice, where the 'same casing location' approach is used, errors due to misinterpretation of depth are probably only significant for the case of zero vertical movement. Where telescopic casings are used to accommodate vertical displacements of the soil, these displacements will generally be much larger than induced by the rotation of the casing at

its base, and present a far greater threat to overall accuracy. If required the true vertical reading interval for a casing subjected to movement in two horizontal planes can be calculated as follows:-

$$R_V = \frac{R}{\sqrt{(1 + \tan^2 \theta_1 + \tan^2 \theta_2)}}$$

where θ_1 and θ_2 are the inclinations of the casing to two vertical orthogonal planes.

To term misinterpretation of depth an error is rather anomolous when considered in the context of the 'constant elevation' approach to readings in telescopic casings, when settlement is taking place. Any attempt to maintain a constant vertical reading interval, and hence constant elevation of reading locations, will move the reading locations further away from their original position in the casing. Only in the case of heave, and therefore extension of the casing length, would a correction improve the accuracy of the measurements.

It was therefore decided that in the case of settling casings that no corrections for misinterpretation of depth would be made, but that where heave occurred corrections would be made if the errors were significant. 'Constant elevation' was thus a slight misnomer on this basis. In the case of both horizontal displacement calculations and depth misinterpretation no significant errors were anticipated if tilting angles did not exceed 5° .

(c) Vertical Mislocation of the Torpedo

The tape markers on the inclinometer cable were within $\pm 10\text{mm}$ and generally better than $\pm 5\text{mm}$. The reading system enabled location of the markers to

within $\pm 5\text{mm}$ and their positions on the length of cable in use were periodically checked against a steel tape. For accurate location vertically, a steel tape is to be preferred to the cable markers (Burland & Moore, 1973; Vaughan, 1973(c)).

Mislocation of the torpedo within a casing length only affects the measured angle and hence the calculated horizontal displacement, if there is angular variation (i.e. bending) within the particular length. If it is assumed that the variation in angle between each pair of correct reading positions is linear, then it can readily be shown that the horizontal displacement error (Δx_{hor}) due to mislocation by a vertical interval of ΔR_V between two correct reading points whose angular difference is $\Delta\theta$, is as follows:-

$$\Delta x_{\text{hor}} = \Delta R_V \tan \Delta\theta \text{ or } \Delta x_{\text{arc}} = \Delta R_V \Delta\theta^r$$

The former expression has been used to calculate Δx_{hor} for a range of values of ΔR_V and $\Delta\theta$ as shown in table 5.4.2. Thus although the accuracy of the vertical location measurements was low, significant horizontal displacement errors would not be expected from this source using the 'same casing location' observational approach.

However the data in table 5.4.2. also represent the 'mislocation error' resulting from the 'constant elevation' reading procedure used, so that with a knowledge of the angular changes within the casings and their vertical displacements the magnitude of these errors can be evaluated and refinements made to the observational system if deemed necessary.

ANGLE DIFFERENCE	VERTICAL MISLOCATION mm						
DEGREES	5	10	20	30	50	75	100
0	0	0	0	0	0	0	0
1	0.1	0.2	0.3	0.5	0.9	1.3	1.8
2	0.2	0.3	0.7	1.0	1.7	2.6	3.5
3	0.3	0.5	1.0	1.6	2.6	3.9	5.2
4	0.3	0.7	1.4	2.1	3.5	5.2	7.0
5	0.4	0.9	1.8	2.6	4.4	6.6	8.8
6	0.5	1.0	2.1	3.1	5.2	7.8	10.9
7	0.6	1.2	2.5	3.7	6.1	9.2	12.3
8	0.7	1.4	2.8	4.2	7.0	10.5	14.0
9	0.8	1.6	3.2	4.8	7.9	11.9	15.8
10	0.9	1.8	3.5	5.3	8.8	13.2	17.6
11	1.0	1.9	3.9	5.8	9.7	14.6	19.4
12	1.1	2.1	4.3	6.4	10.6	15.9	21.3

Table 5.4.2.

Horizontal Displacement Errors Resulting From Vertical Mislocation of the Torpedo

(d) Settlement/Heave of the Base of the Casing

This introduces a further inconsistency into the 'constant elevation' approach. Vertical displacement of the casing base (ρ) results in a displacement calculation 'error' (e) of the form shown in figure 5.4.1.(f), due to the displacements being derived at different elevations to the

original measurements. However, as in the case of depth misinterpretation, to describe 'e' as an error is somewhat anomalous: as long as the vertical movements of the casing base are in the same direction as the other casing lengths these movements will tend to improve the accuracy of the results by shifting the reading positions closer to their original locations.

Therefore it was decided that no attempt would be made to maintain constant elevation of reading positions if vertical movements of casing bases occurred. Vertical mislocation errors could thus be assessed on the basis of the difference between the displacements of a particular casing length and the base.

(e) Horizontal Movement of the Base of the Casing

When this occurs the integrated displacements relative to the base will be less than the absolute values at any particular location. An independent measurement of the horizontal displacement of the top of the casing is always desirable in this respect.

(f) Misalignment and/or Twist of the Casing

Inclinometers are often installed to measure unidirectional displacements, as in the plane strain situation at Mucking. Hence if one keyway axis is aligned in the direction of movement the perpendicular axis need only be considered occasionally as a check. When misalignment of the casing occurs during installation, errors arise if only one vectorial component is recorded and then taken as being the resultant displacement. The nature of this error is illustrated in figure 5.4.1.(g) and quantified in table 5.4.3., wherein the resultant has been considered as a unit vector

acting at δ° to the recorded 'y' vector. Large angles of misalignment can be seen to be necessary to cause significant errors. The random twist of better than $1^{\circ}/m$ for extruded aluminium casings is obviously insignificant whereas the large cumulative twists in plastic casings could result in large errors.

δ°	% ERROR	δ°	% ERROR
1	0.02	11	1.84
2	0.06	12	2.19
3	0.14	13	2.56
4	0.24	14	2.97
5	0.38	15	3.41
6	0.55	16	3.87
7	0.75	17	4.37
8	0.97	18	4.89
9	1.23	19	5.45
10	1.52	20	6.03

Table 5.4.3.
Casing Twist and Misalignment Errors

(vi) Summary

The various problems associated with the use of inclinometers to measure horizontal displacements are not easy to categorise on a general basis, as they are largely inter-related and their significance dependent on the magnitude of the inclination and movements of the casing, as well as the accuracy required. The selection of an approach to reading

inclinometers also depends on these factors as well as the frequency of recording and available time. The foregoing attempt to rationalise these problems with respect to the Mucking site is a process which has to be carried through for any inclinometer installation. Hopefully some guidelines have been provided. Inclinometer measurements must always be related back to the basic behaviour of the casing: the integrated displacement read-out used enables displacement changes to be quickly calculated without recourse to casing angles, but could lead to serious errors in this respect.

5.4.4. Observed Horizontal Displacements

(i) General

The eight readings per inclinometer casing taken within the foundation material were assessed with a view to making corrections where necessary and to ascertain the overall performance and accuracy of the system. A brief review of the results of this assessment is given in the following sections and summarised in table 5.4.4., the measured data being presented in figures 5.4.2. to 5.4.16.

Displacements within the fill material were not of primary interest and considered to be somewhat unreliable due to the influence of the embankment construction. However, those inclinometers just in the fill, being in the embankment slopes (I.A/B.2/5), were little affected and the displacements of the fill surface recorded were used in comparisons with surface target observations.

NO.	QUANTITY	BANK 1		BANK 2	
		STAGE 1	STAGE 2	(1)	(2)
1	Total No. of sets of Readings	151	37	18	44
2	Total No. of readings in foundation	1208	296	144	352
3	<u>Face Errors</u>				
a.	Maximum variation of face error tolerated	±3mm	±3mm	±3mm	±3mm
b.	Total No. of times unacceptable face error variations encountered X	a=2+ b=4+3+	a=0 b=0	a=0 b=0	a=0 b=10
c.	Mean face error variation	±1mm	±1mm	±1mm	±1mm
d.	Standard deviation of face errors	±0.88mm	±0.74mm	±1.11mm	±0.63mm
e.	99.8% Confidence limit	±2.64mm	±2.22mm	±3.33mm	±1.89mm
f.	99% Confidence limit	±2.20mm	±1.85mm	±2.77mm	±1.57mm
4.	No. of Readings taken with wheels in coupling	7	0	0	8
5a.	Maximum casing angle	2°55'	5°34'	0°55'	2°04'
b.	Maximum angular variation (bending)	2°35'	4°34'	<0°55'	<2°04'
6.	Maximum bearing error with only one keyway read	9°	9°	3°	3°

(1) During construction (2) Post-construction

X Excluding wheels in joint a = explained b = unexplained

† Complete sets of readings

Sample sizes 96, 48, 48, 48 respectively

Table 5.4.4. Inclinator Results Summary

(ii) Face Errors

The statistical study of face errors, or reproducibility of readings, may be represented in various ways (Cornforth, 1973). The deviation from the mean, and the spread (twice the deviation from the mean), can be calculated directly in millimetres and thus related directly to horizontal displacements. This approach has been used to assess the accuracy of the Mucking results. Alternatively the deviation from the mean may be represented as a cumulative angular deviation with respect to the base of the casing. Detailed analyses of stationary casing (Green, 1969; Cornforth, 1973; Werneck, 1974) show the displacement deviation from the mean to increase with elevation, but at less than a linear rate such that the cumulative angular deviation is close to, but less than, the read-out resolution of the instrument.

With the equipment used the displacement deviation from the mean at original ground level, assuming a cumulative angular deviation of 2×10^{-4} radians, would be 1.6mm. On this basis deviations of face error from the mean greater than or equal to ± 3 mm were regarded unfavourably and the results rejected. In the event ± 3 mm emerged as being approximately 3.5 times the standard error of a single reading.

(a) Bank 1, Stage 1

Five complete sets of readings were discarded because of inconsistent face errors throughout. Two of these were due to temperature effects, the rest to causes unknown.

(b) Bank 1, Stage 2, Bank 2

Only individual readings with unacceptable face errors were rejected.

(c) Summary

The absolute value of the face error changed somewhat during the period of use of the inclinometer torpedo without seeming to affect the accuracy of the results. The average deviation of face error from the mean for all sets of readings, except the five rejected, was $\pm 1\text{mm}$. Samples of face errors were analysed statistically as indicated in table 5.4.4., these analyses showing that 1 in 100 results would have a variation greater than $\pm 2\text{mm}$ and 1 in 500 greater than $\pm 2.5\text{mm}$. This is essentially borne out by the results from Bank 1 where 4 results in 1464 considered were outside the $\pm 3\text{mm}$ criteria. Face errors caused by torpedo wheels in a joint do not reflect the system's accuracy and as such were not included in the analyses.

The results from Bank 2 indicate a similar level of accuracy, except that the number of unacceptable face errors in the post-construction period increased to a final total of 10. This may be a reflection on the infrequency of use of the instrument and variation in operators.

No study of the variation in face error or spread of results with elevation was made because of the relatively short lengths of casing and the limited number of results for stationary casings respectively. However it can be seen that the overall accuracy is very close to that predicted on such a basis.

The laboratory results of Green (1969), using the same instrument that Werneck (1974) used in the field, showed greater accuracy as might be expected. As deformation of the casing increases the accuracy may well fall off even more. That it did not at Mucking is largely a function of the relatively small horizontal displacements.

(iii) Torpedo Wheels in Coupling when Reading

(a) Bank 1, Stage 1

Despite all precautions examination of the face errors showed this to have occurred 7 times in 1208 readings. However the torpedo appeared to register the average angle of the relevant casing length even in these instances and the results were plotted. Face error variations caused by this occurrence were easily identified by their magnitude, this corresponding to the 2 to 2.5mm wall thickness of the casings.

(b) Bank 1, Stage 2

There were no errors from this source.

(c) Bank 2

No errors during construction but during the post-construction period the torpedo wheels entered the near surface joints on 8 occasions.

(iv) Casing Angles, Angular Changes, Coupling Readings and Reading Interval Errors

(a) Bank 1, Stage 1

The maximum recorded casing angle and angular variation (bending angle)

were $2^{\circ} 55'$ and $2^{\circ} 35'$ /metre respectively. On average pre-failure angles were closer to 1° . The readings across the couplings were inspected to see if they indicated angular changes intermediate between the adjacent casing lengths, and hence a 'dog-leg' shape, or similar to one or both of the casing lengths, thus indicating bending or rotation of the casing, respectively. A brief discussion of the results is presented in the following sections.

IA1, IB1 (figures 5.4.2., 5.4.3.)

The casings have rotated about their bases with only slight bending of the casing lengths above these locations.

IA2, IB2 (figures 5.4.4., 5.4.5.)

These casings were subjected to the largest displacements, tilting angles and bending angles. In both casings the upper coupling* appears to have bent whereas the lower one has not. If the upper coupling readings are ignored and the displacements predicted on the basis of the angles measured above and below the joints (i.e. extrapolated down to, and up to, the coupling respectively) the hatched profiles are obtained. These suggest that the casings have deformed relatively smoothly across the couplings and therefore that the coupling readings are perfectly valid measurements. Of particular interest is the final profile for IA2 which indicates the casing to have bent considerably below, but not at, the lower coupling as failure was approached.

*the upper and lower couplings herein refer to the lower two couplings in the foundation.

IA3, IB3 (figures 5.4.6., 5.4.7.)

The displacement profiles suggest that the upper coupling of casing IB3 has bent, but when the coupling reading is ignored the resulting profile (hatched lines, profile 7) indicates that, again, the angular change is reasonably smooth.

At larger displacements the profiles for IA3 indicate inconsistencies at both couplings, the upper one in particular appearing to develop a 'dog-leg' shape as shown by the hatched lines. The apparent discrepancy at the lower coupling is not compatible with such a mode of deformation, and it is suggested that the slight kinks in the displacement profiles at the lower coupling are within the accuracy of the measurements. The angular difference between the coupling and the casing length above is equivalent to a displacement variation of 2mm/metre.

Separate examination of the apparent 'dog-leg' developed at the upper coupling shows that it is more pronounced than the previous ones discussed, but still smooth enough to be adequately represented by the coupling reading.

IA4, IB4 (figures 5.4.8., 5.4.9.)

Displacement profile 8 for casing IB4 indicates bending at the upper coupling but as shown by the hatched line, the deformation is relatively smooth. The previous profiles show more bending to have occurred within the upper casing length than at the coupling.

The displacements of IA4, similarly to IA3, exhibit inconsistencies at the lower coupling; in this case the angular variation is equivalent to

3mm/metre. Again this is within the measurement accuracy, and the inconsistencies are incompatible with 'dog-legging' of the coupling.

The upper coupling of IA4 appears to develop a distinct 'dog-leg' shape with increasing fill height and it could be suggested that in the case of profiles 6 to 8 the hatched lines deriving from the omission of the coupling reading are the best estimates of displacement. However for profile 8 the coupling reading was taken with the upper wheels of the torpedo in the joint and, if this occurrence did not result in any angular error, there must have been bending in the length of casing below, as well as at, the coupling. The proximity of the torpedo wheels to the joint may mean that, although the casing bent at the coupling, the 'dog-leg' shape was adequately represented by the readings.

IA5, IB5, IA6, IB6 (figures 5.4.11. to 5.4.14)

There is no evidence of excessive bending at the couplings, or anomolous results, in any of the displacement profiles.

(b) Bank 1, Stage 2

The maximum recorded angle and angular variation were $5^{\circ} 34'$ and $4^{\circ} 34'/$ metre respectively, just prior to failure. Previously the maximum values were $3^{\circ} 30'$ and $2^{\circ} 00'/$ metre respectively, with average pre-failure tilting angles of about 2° .

The readings across the couplings were again individually assessed as follows:-

IA4, IB4 (figures 5.4.8., 5.4.10.)

Both casings showed signs of continuing bending at the upper couplings but, based on the observations for Stage 1 as discussed previously, it seems probable that the installations were adequately surveyed. The displacements of IA4 at the lower coupling still appear inconsistent with regard to the kink in the profile, but the 'error' remains less than the measurement accuracy.

IA5, IB5 (figures 5.4.11., 5.4.12)

Casing IB5 shows no signs of bending at the couplings although there is bending within the casing lengths.

Whereas the lower coupling of IA5 has not bent despite considerable bending of the casing length immediately above it, the upper coupling appears to have 'dog-legged' just prior to failure. However, the fact that there appears to be as much bending in the upper length of casing as at the coupling indicates that the measurements were within the accuracy of the system.

Similarly to the results for IA2 during Stage 1, the displacements of these casings show considerable bending to have occurred at locations within the casing which were close to, but not at, the couplings.

IA6, IB6 (figures 5.4.13., 5.4.14)

There is no evidence that bending has occurred at the couplings to a greater or lesser extent than within the individual casing lengths.

(c) Bank 2

IC1, IC2 (figures 5.4.15., 5.4.16)

The maximum tilting angle during construction was only $0^{\circ} 55'$ and post-construction was only $2^{\circ} 04'$. The data for IC2 indicate smooth bending to have occurred at the upper coupling despite the implied 'dog-leg' shape. Bending also appears to have taken place below the lower coupling rather than at the joint itself: this also seems to be the case for IC1.

The displacement observations for the upper coupling of IC1 are anomalous but do not indicate a 'dog-leg' type of deformation. A number, but by no means all, of the post-construction readings were taken with the torpedo wheels in the coupling, further suggesting that the inconsistent displacement patterns were not due to bending of the coupling. If the coupling reading is ignored for the final profile (19) the displacement at ground level increases by 10mm in 125mm or 8% (hatched line). However, there is no reason to suppose that this is a more correct profile, particularly as a comparison with the results of IC2 indicates that the first reading in the upper casing length may well be the anomalous result. With no direct evidence on which to base any corrections the results were accepted at face value.

(d) Summary

The maximum tilting and bending angles were not of sufficient magnitude to result in significant errors due to the method of horizontal displacement calculation or depth misinterpretation. The maximum recorded bending angle of $4^{\circ} 34'$ /metre is relatively small compared

to the manufacturer's claim for the geometrical imitation capacity of the torpedo, which is equivalent to about 20° /metre for a smoothly deformed casing. In practice the casings tend not to deform smoothly and Werneck (1974) found that, for a 305mm wheel base torpedo, access became difficult when bending angles exceeded $4^{\circ}/305\text{mm}$ (13° /metre).

The measured displacements indicate bending of the casing to have been as common as bending at the couplings. Where bending of a coupling did occur, it appears to have been relatively smooth and not resulted in any extreme 'dog-legging' of the casing. Readings across the couplings are thus thought to be no less accurate than those within the casing and no coupling readings were rejected.* Local bending of the couplings was mainly confined to the upper joints and to situations where the changes of inclination of the casing changed sign (i.e. from positive angular change to negative or vice versa). Any errors in the representations of the casing profiles could have been largely avoided by the use of a smaller reading interval.

The magnitude of possible errors due to extrapolating the measured angles 250mm from the torpedo wheels in either direction can be assessed from a consideration of the tilting and bending angles. The maximum bending angle of $4^{\circ} 34'$ /metre (tilting angles from $5^{\circ} 34'$ to $1^{\circ} 00'$) could produce an error of about 20mm if the incorrect angle was extrapolated over 250mm. Tilting and bending angles being generally less than 3° and 2° /metre respectively, overall errors were

*none of the unexplained face error variations discussed in sub-section ii, and summarised in table 5.4.4. were at the coupling locations.

less than $\pm 10\text{mm}$. In addition, the casings subjected to the severest tilting and bending angles often underwent both positive and negative changes of inclination so that the reading interval errors may have been largely self-cancelling. If this was the case the errors were probably closer to $\pm 5\text{mm}$ (i.e. $\pm 5\%$ approximately; Green, 1969).

Finally, reference has been made throughout this section to absolute casing angles whereas the displacement profiles relate to angle changes from the original inclinations. The latter, however, were only $1^{\circ} 30'$ maximum, and generally less than 1° . The displacement profiles thus give a reasonable approximation to the actual casing shapes, although at an exaggerated scale.

(v) Vertical Displacements of Casings

The results for Bank 1 are fully discussed in sections 5.4.5., to 5.4.7., illustrated in figures 5.4.18., to 5.4.22., and the maximum values summarised in table 5.4.5. The latter shows relative closures of up to the full 200mm to have occurred, but that the large closures, and hence torpedo mislocations, coincide with relatively low bending angles. Comparison of the total closures for the casings (representing the maximum vertical mislocation) with the calculated bending angles indicates maximum errors, due to vertical mislocation, to be of the order of $\pm 5\text{mm}$, and on average better than $\pm 2.5\text{mm}$.

The vertical displacements of inclinometer casings IC1 and IC2 were less than $\pm 10\text{mm}$ and no vertical mislocation errors were anticipated; no vertical displacement data are presented for these casings.

(vi) Errors in Keyway Bearings

As described previously only IA6 required the reading of both keyways. Elsewhere alignment errors were small as shown in table 5.4.4.

(vii) Horizontal Displacements of Casing Bases

(a) Bank 1, Stages 1 and 2

No independent measurements of the displacements of the tops of the casings were made and thus only indirect assessments of whether basal movement had occurred could be made. In some instances the inclinometer casings penetrated the gravel to a depth of about 1.5m and thus the first displacement reading was in, or very close to, that stratum. In these cases the evidence is (figures 5.4.7., to 5.4.12., and 5.4.14) that there was very little horizontal displacement (<5mm) in the gravel. Such an observation excludes the possibility of lateral translation of the whole of the length within the gravel.

Comparisons made between surface displacement recorded by inclinometer and surface target observations are discussed in section 5.7. The accurate surveying of the top of the casing enables an assessment of the accuracy of the casing survey by the inclinometer torpedo and any movements of the base of the casing to be made without bringing the ability of the instrument to monitor the actual soil deformations into question. Comparison with other instruments (see sections 5.3 and 5.7.) raises both questions, the evidence suggesting that significant movement of the casing bases did not occur.

(b) Bank 2

In this case the inclinometer casing tops were located within the triangulation survey, the results being presented in figures 5.2.1. and 5.2.2. Overall agreement between the ground survey and the inclinometer survey for inclinometer casing IC1 can be seen to be very good, with a difference of only 4mm in 78mm (5%) when the last triangulation survey was carried out. This agreement is certainly better than the combined accuracy of the two measurement systems. The ground survey displacements are nearly always greater than those from the inclinometer survey, indicating slight horizontal displacement of the casing base. However, casing IC1 only penetrated the gravel to a depth of 700mm and the results therefore suggest that in general there were no significant horizontal displacements of the casing bases.

(viii) Final Comments

(a) Performance of the Equipment

The figures in table 5.4.4. indicate this to have been very good and the manufacturer's claims regarding the precision of the torpedo were met. Over the main period (8 months) of site work the only maintenance required was the reconnection of the cables on two occasions, the breakages probably being caused by jarring the torpedo during raising or lowering.

The only unsatisfactory part of the recording equipment was the method of marking depth on the torpedo cable. The initial accuracy was not good and with use became worse. The transparent protective sleeves for the tape markers tended to be moved by the lowering pulley, leaving the

markers to deteriorate rapidly. Thus remarking of the cable was necessary at intervals: inadequate depth markings appears to be a common problem with inclinometer systems (Green, 1969).

Deterioration of the aluminium casings is often accompanied by froth forming on top of the water within it (Werneck, 1974; McKenna and Roy, 1973). No evidence of any deterioration of the casing used was visible, on this basis, after 24 months of use (IC1, IC2).

(b) Accuracy of the Measured Displacements

Table 5.4.4. shows the precision of the measurements to have been about $\pm 2.5\text{mm}$. However, the reading interval chosen probably reduced the accuracy by a further $\pm 5\text{mm}$ which, when added to the likely errors due to vertical mislocation ($\pm 2.5\text{mm}$), produces an overall accuracy of $\pm 10\text{mm}$. The accuracy with which the torpedo can survey the casing has been shown to decrease as the casing deforms and telescopes. Thus the accuracy of the early readings was probably closer to $\pm 5\text{mm}$, falling off to $\pm 10\text{mm}$ as deformation increased. Close to failure, for those casings subjected to large displacements, the accuracy could be expected to be even worse than $\pm 10\text{mm}$.

The accuracy of the displacements as horizontal movements of the foundation can only be ascertained by comparison with other observations. The inclinometer displacements have already been compared to those of the H.S.G. magnets (section 5.3) and shown to be compatible with an overall accuracy of $\pm 10\text{mm}$. In general this comparison was also compatible with a fall off in the accuracy of the inclinometer results with increasing deformation (figures 5.3.2. to 5.3.5.), and an overall figure of $\pm 10\%$

for the accuracy appears reasonable. On this basis the accuracy of the horizontal displacements of the H.S.G. may be nearer $\pm 5\%$. Good agreement was also found between the inclinometer displacements and those of adjacent surface targets, as exemplified by ICI and ST4 for Bank 2 (figures 5.2.1., and 5.2.2.).

The close correspondence of the various sources of data suggests that the combination of aluminium casings and bentonite: cement grout was supple enough to enable accurate monitoring of the horizontal displacements of the very soft Mucking clay.

(c) Overall Performance of the System

The inclinometer data could have been improved in two ways in particular. The termination of the casings just in the gravel layer did not significantly affect the results but was rather inappropriate. Allowing a reasonable length of casing in what is assumed to be the inactive zone has two main advantages, besides proving or disproving that assumption. Firstly it enables the exact depth at which measurable deformation commences to be determined, and secondly it provides a constant set of readings which can be used to assess the precision of the instrument for each set of readings. At Mucking an extra two lengths of casing (6m) could have provided considerable benefit without a great sacrifice to additional reading time (or much financial outlay).

In the event the reading system and process were adequate and the time saved was possibly worth the sacrifice in accuracy. That this was so can be largely attributed to the small tilting and bending angles, short overall casing lengths and modest amounts of telescopic movement. In

such cases, armed with a knowledge of the likely errors that will be incurred, this sort of reading system is justifiable.

However, for any future installations the writer would definitely use a reading interval equal to, or less than, the wheel base of the torpedo and an angular read-out. The advantages of the displacement read-out, in the writer's opinion, are outweighed by its inflexibility. Angle measurements necessitate more calculations but are fundamental to really accurate results. The time necessary to take inclinometer readings is relatively short compared to many instruments and it is therefore also recommended that a reading interval equal to half the effective torpedo length could be used and therefore duplicate profiles obtained.

For any installations where angles and telescopic movements may be large the best approach is probably to attach the magnets to each casing length, as at Mucking, and then use the sensing probe to enable accurate re-location of the torpedo at the same reading positions in the casing. Each casing length could then be surveyed independently and accurately, and the final profile obtained by assembling and integrating the results.

The combination of the magnet sensing probe, inclinometer torpedo and a steel tape in essentially one unit, as described by Vaughan (1973(c)) increases the practicability of such a system. Even when reading and data reduction time are at a premium, the additional effort required to accurately survey inclinometer casings is well spent in view of the time which may be wasted in attempting to 'back-analyse' results from integrated displacement measurements over large reading intervals.

5.4.5. Reading Process for Vertical Displacements

The ring magnets were located with the same probe used to locate the magnets on the vertical settlement unit (V.S.U.), but with a cylindrical plastic sleeve (45mm O.D.) fitted to keep the probe axis central within the larger diameter inclinometer casings. The reading process was identical to that described in section 5.11 for the V.S.U., the bases of the casings being plumbed and the tops picked up in the level survey for each set of readings.

5.4.6. Accuracy of Vertical Displacement Observations

This depends on the precision with which the probe is able to detect the magnets as well as the overall accuracy of the vertical location measurements (tape plus level survey). A full discussion of these aspects is presented in section 5.11: however, from the three sets of initial readings, the overall accuracy of location of an individual magnet was within $\pm 2\text{mm}$, this figure being in agreement with data presented by Gould and Dunnicliff (1971), Burland et al (1972) and Burland and Moore (1973).

5.4.7. Observed Vertical Displacements

(i) Displacements of Magnets in Relation to Soil

The magnets were attached to the casing lengths in the foundation, as described in section 5.4.1., in order to monitor vertical displacements of the casings; these were required in order to estimate vertical

mislocation errors. These vertical displacements of the casings are very unlikely to represent vertical displacements of the surrounding soil except, possibly, near the top of a casing length and then only when it has become independent due to telescoping of its joints. The magnet holders can alternatively be used as couplings, in which case they may reflect settlement of the adjacent foundation after the coupling has telescoped. However, there is no physical contact between the magnet and the soil and the accuracy of the settlement measurements will depend on the compatibility of the displacements of the grout and the foundation (see e.g. Werneck, 1974). There is also a distinct possibility that, although the coupling is telescopic, the magnet may be influenced by movements of the casing lengths.

Because of the low degree of accuracy of the vertical displacements from the H.S.G. measurements it was decided to study the inclinometer magnet movements to see if they would corroborate the H.S.G. profiles. It was necessary to first consider the physical behaviour of the magnets and casings in order to assess their relevance to foundation movements.

An inclinometer casing installation under the central portion of the embankment, where all vertical components of displacement may be assumed to be settlement, is now considered by way of an illustration of the possible mechanism of movement.

Initially, as the soil compresses under the loading, the casing moves down as a 'rigid' pile. During this period the only part of the casing to move similar vertical distances to the surrounding soil is the upper part. Hence, initially the upper magnet may give a reasonable account

of soil movements (although on the high side), whilst the lower magnet and casing base reflect exaggerated movements, the grout being assumed to deform in similar fashion to the foundation material.

At some stage the shear stresses induced in the couplings by the differential displacements of the soil/grout along the casing length, are sufficient to shear the rivets, and the couplings become telescopic. For the case in hand the upper coupling would be likely to become telescopic first. The upper magnet (M1) thus continues to reflect the movements of its length of casing, these being over estimates of the displacements of the foundation at the actual magnet position. However, this upper magnet is also still prone to influence from the lengths of casing which are being added above it as the fill height increases, until the joint above it becomes telescopic.

The lower magnet (M2) is now independent of casing movements above the telescopic coupling and may be expected to similarly reflect exaggerations of the movement at its location. Due to the continuing pile action of the lower two casing lengths the base of casing movements are still atypical for its elevation.

Finally the lower coupling becomes telescopic such that the movements of the two magnets and the casing base are all independent, each reflecting the total movement of the length of casing at whose base it is situated. Complete independence of the magnets could only be achieved by the shearing of the rivets attaching them to the casing: this would seem to be a remote possibility.

(ii) Observed Displacements for Bank 1 and Extrapolated Data for Stage 1

The observations of the magnet and casing base vertical displacements during the construction of Bank 1, Stages 1 and 2 are presented versus fill height in figures 5.4.18 to 5.4.22 and the maximum values summarised in table 5.4.5. The last reading taken during Stage 1 was with the fill height at 2.75m and the trench excavated, after which the breakdown of the probe prevented further observations. Thus in order to plot vertical displacement profiles from the magnet data, some extrapolation was necessary.

The upward vertical movements of the settlement plates (figure 5.10.2) upon the reduction in fill height at their locations from 4m to 2.75m were very small (2-4mm). Thus for those inclinometers which remained in service during Stages 1 and 2 the assumption was made that the initial readings for Stage 2 (fill height = 2.75m) were the same as the final readings for Stage 1 (fill height = 4m). The Stage 1 readings for inclinometers IA/B4-6 inclusive were thus completed by a straight line from the 2.75m plus trench observations to the 4m level, as shown in figure 5.4.17 and figures 5.4.18 to 5.4.22. In order to complete the data for inclinometers IA/B1-3 inclusive during Stage 1 the relative similarity of their locations to IA/B6-4 respectively, during Stage 2 was utilised. The relative similarity of location between these same inclinometers up to a fill height of 2.25m during Stage 1 was also considered. Thus the Stage 1 results for IA/B1-3 were completed by direct comparison with IA/B6-4 during Stage 2. This simple process is illustrated in figure 5.4.17 and led to the extrapolated results of figures 5.4.18 to 5.4.22.

I	M1	M2	BASE	-(M1 - M2)		-(M2-BASE)		-(M1-BASE)	STAGE*
	Δz	Δz	Δz	d Δz	ϵz	d Δz	ϵz	d Δz TOTAL	
	mm	mm	mm	mm	%	mm	%	mm	
A1	+18	+18	+18	-	-	-	-	-	1
B1	+30	+30	+30	-	-	-	-	-	1
A2	-47	-37	-19	+10	+0.3	+18	+0.5	+28	1
B2	-74	-74	-119	-	-	-45	-1.4	-45	1
A3	-148	-64	-46	+84	+2.7	+18	+0.5	+102	1
B3	-220	-112	-64	+108	+3.5	+48	+1.4	+156	1
A4	-59	-59	-35	-	-	+24	+0.7	+24	1
	-180	-115	-69	+65	+2.1	+46	+1.4	+111	2
B4	-163	-70	-58	+93	+3.0	+12	+0.4	+105	1
	-318	-222	-109	+96	+3.1	+113	+3.4	+209	2 ⁺
A5	-29	-29	-20	-	-	+9	+0.3	+9	1
	-64	-58	-13	+6	+0.2	+45	+1.3	+51	2
B5	-101	-101	-94	-	-	+7	+0.2	+7	1
	-149	-149	-140	-	-	+9	+0.3	+9	2 ^x
A6	+3	+3	+3	-	-	-	-	-	1
	+66	+66	+66	-	-	-	-	-	2
B6	+3	+3	+3	-	-	-	-	-	1
	+26	+26	+26	-	-	-	-	-	2

Table 5.4.5.

Maximum Vertical Displacements of Inclinator Magnets and Casings,
and Implied Average Vertical Linear Strains

*Data extrapolated to 4.00m fill height for Stage 1, and recorded at 4.25m fill height for Stage 2, except:-

+Fill height, 4.50m and x fill height = 4.05m

NB. Settlement - ve, compression +ve

Before turning to the vertical displacement profiles derived from these results, the actual observations are considered. The inclinometer casings are grouped together in the pairs on each section line used for the extrapolation of the Stage 1 results.

Inclinometer Casings 3 and 4 (figures 5.4.21 and 5.4.22)

The similarity of location of these inclinometers during Stage 1, up to 2.25m fill is reflected in the observations. The likeness of position of IA/B4 during Stage 2 to IA/B3 during Stage 1 enabled a fairly positive comparison to be made. A summary of the observations is provided below:-

SECTION A

<u>IA3 Stage 1</u>	M1 independent after 1.75m fill
	M2 and base together at 2.75m fill
<u>IA4 Stage 1</u>	Base independent after 2.25m fill
<u>IA4 Stage 2</u>	M1 and M2 independent after 3.55m fill

SECTION B

<u>IB3 Stage 1</u>	M1 independent after 1.75m fill
	M2 and base together at 2.75m fill
<u>IB4 Stage 1</u>	All independent after 2.25m fill
<u>IB4 Stage 2</u>	All independent.

These results generally corroborate the mechanism of magnet and casing behaviour postulated earlier in this section. Due to independence of movement being achieved by the three lengths of casing their vertical displacements may be considered as reasonably representative of average foundation movements.

Inclinometer Casings 2 and 5 (figures 5.4.19 and 5.4.20)

The similarity of location is not as great as for IA/B,3/4 but a reasonable comparison can be made. A summary of the observations is provided below:-

SECTION A

IA2 Stage 1 All independent after 2.25m fill
IA5 Stage 1 All together at 2.75m fill
IA5 Stage 2 Base independent at 2.75m fill
 M1 and M2 independent after 4.05m fill

SECTION B

IB2 Stage 1 Base independent after 1.75m fill
 M1 and M2 together at 2.75m fill
IB5 Stage 1 Base independent after 2.25m fill
IB5 Stage 2 M1 and M2 together at 4.05m fill (last reading)

The results show a lack of telescopic movement, despite quite large overall vertical displacements. The movements probably only approach the actual soil behaviour for the upper casing lengths, the displacements on Section A being much less than those on Section B.

Inclinometer Casings 1 and 6 (figure 5.4.18)

The comparison between these casings was fairly positive and the recorded displacements relatively small, these being heave in the latter parts of the construction stages. No independence of movement of either magnets or casings (tops as well as bases) was observed,

the installations acting as 'rigid' piles throughout.

(iii) Displacement Profiles

Using the vertical displacements of the magnets, vertical displacement profiles were plotted as shown in figures 5.4.23 to 5.4.26. Smooth curves were used to link the data, there being only 6 displacement values per profile for Stage 1, and 3 for Stage 2. The profiles are further approximated by the nature of the extrapolated data in the case of Stage 1 and the differing initial elevations of the magnets, as shown in the figures. The displacement profiles are probably best considered as representing the average displacements of the casing lengths. The average length of the upper piece of casing was 2.20m and the average mid-height corresponded to +1.10m O.D. for both sections. The displacement profiles for the upper (M1) magnets could thus be expected to approximate to the vertical displacements of the settlement plates, H.S.G. s and surface targets. The 'mid-foundation' casing lengths were all 3m long and average mid-height for these corresponded to -1.60m O.D. for both sections.

The results from Stage 2 (figures 5.4.25 and 5.4.26) are best considered first as the displacement profiles were constructed from measured data. A comparison between the displacements of the upper magnets on Section B and those of settlement plate SPB/2 shows the former to progressively over-estimate the settlement. This appears to be mainly due to the large settlements of IB5; the non-telescopic behaviour of this inclinometer also had an adverse effect on the already exaggerated displacements of

the lower (M2) magnets. Although there was no settlement plate to enable a direct comparison of displacements, similar comments probably apply to the results for Section A. In the case of both sections a comparison between the displacements of the central settlement plates and the upper magnets of IA/B4 indicates that the settlements of the latter may be reasonable approximations to the near surface movements. The settlements of the lower magnets give an approximate average settlement for the 'mid-foundation' casing length only in the case of IA/B4, the other casings being virtually non-telescopic. The vertical heave displacements of inclinometers IA/B6 are in reasonable agreement with those of the adjacent surface targets.

The displacement profiles for Stage 1 are based on extrapolation but the results for the upper magnets on Section A, when compared to those from the settlement plate and surface target, appear to be very good. The vertical displacements of the magnets are also in good general agreement with the settlement profiles for H.S.G.A. (figure 5.3.2.), particularly for the south side of the embankment. Due to non-telescopic casing displacements during Stage 2 the extrapolated displacements of the lower magnets are doubtless largely exaggerated, the results for IA3 being the best approximation to the average settlements of a particular location.

The displacement profiles for Section B again indicate reasonable early agreement with the settlement plate results, followed by progressive over-estimation of the settlements by the magnet displacements. This is related to the extrapolation from the Stage 2 results, but may also have occurred in reality. However, agreement

with the settlement profiles of H.S.G.B. (figure 5.3.3.) is generally good, again particularly for the southern side of the embankment, as it also is with the surface target data. The settlement data for the lower magnets only approximate to the true displacements over the central part of the embankment, as on Section A.

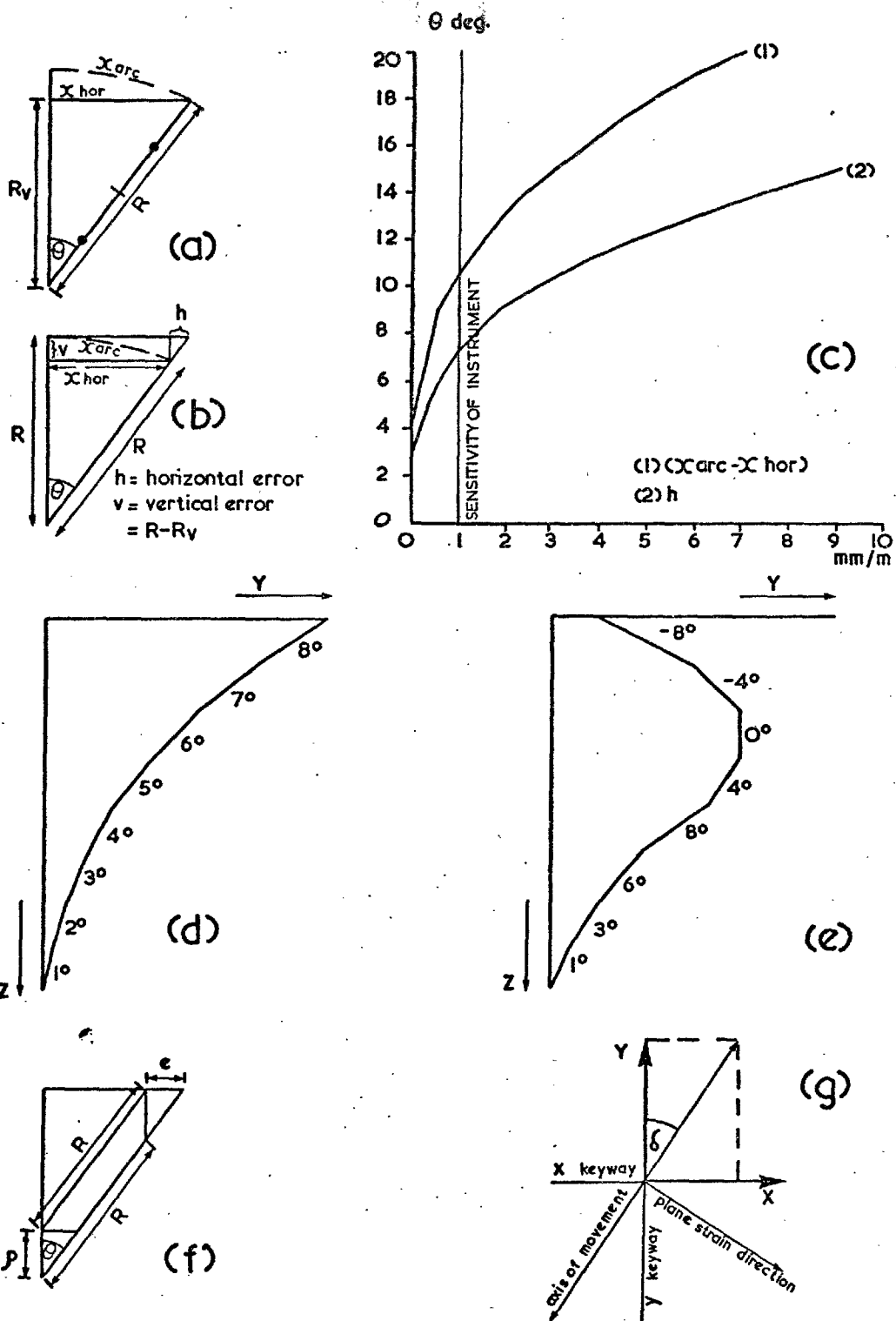
(iv) Final Comments

Comparisons with the settlement plates, H.S.G. s and surface targets indicate that the extrapolated vertical displacements of the upper (M1) magnets, during Stage 1 of Bank 1, approximate to the displacements of the foundation adjacent to the upper length of casing. The most accurate results appear to be those for Section A and particularly, in the case of both sections, for the southern side of the embankment. The profiles are obviously approximate, accuracy probably being of the order of ± 15 to ± 25 mm.

The displacements of the upper magnets during Stage 2 provide the only data from which vertical displacement profiles can be constructed. Although appearing to over-estimate the settlements beneath the northern slope of the embankment, these profiles may at least provide a reasonable estimate of settlements beneath the crest.

For both construction stages the displacements of the lower magnets only provide an approximation to average foundation movements over the 'mid-foundation' casing lengths for those installations beneath the central part of the embankment. Such average displacements are of little real value for analysis purposes, but the vertical strains calculated in table 5.4.5., based on the relative movements of the magnets and the casing base, provide an indication of the likely order of magnitude of such quantities.

The use of magnets, attached to inclinometer casings as at Mucking, has already been advocated as a system of vertical control to enable accurate angle measurements. In addition it would be very simple to install magnets at intermediate positions around the casing, but positively linked to the soil by shoot-out devices (see section 5.11). Such installations proved very successful at Mucking and would enable accurate vertical displacements and strains to be determined at the inclinometer locations. These measurements would also be useful in relating the vertical foundation movements to those of the casings, and thus in further assessing the accuracy of the horizontal displacements.



INCLINOMETERS : DATA REDUCTION ERRORS

Fig. 5.4. I.

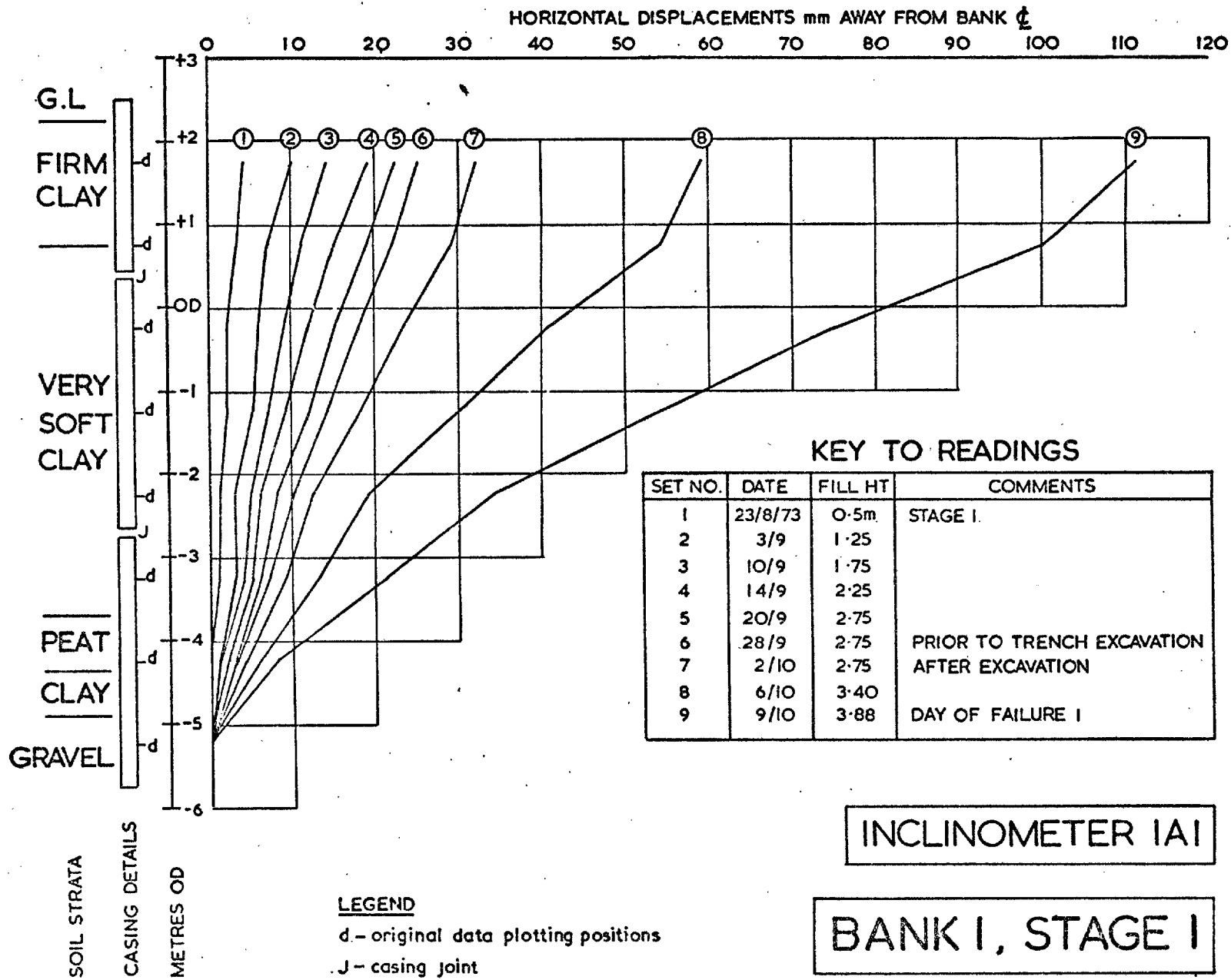


Fig. 5.4.2

HORIZONTAL DISPLACEMENTS mm AWAY FROM BANK ζ

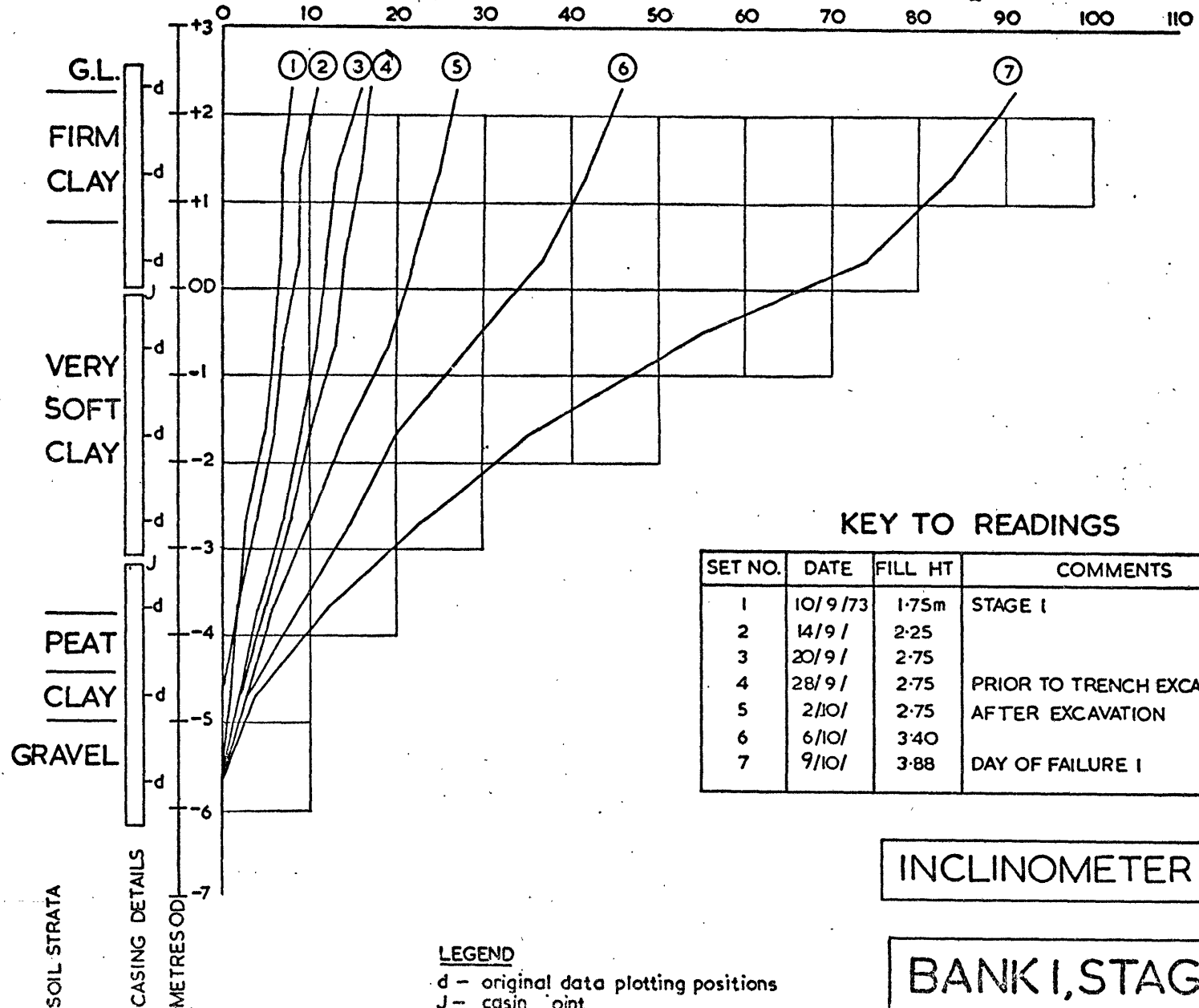


Fig. 5.4.3

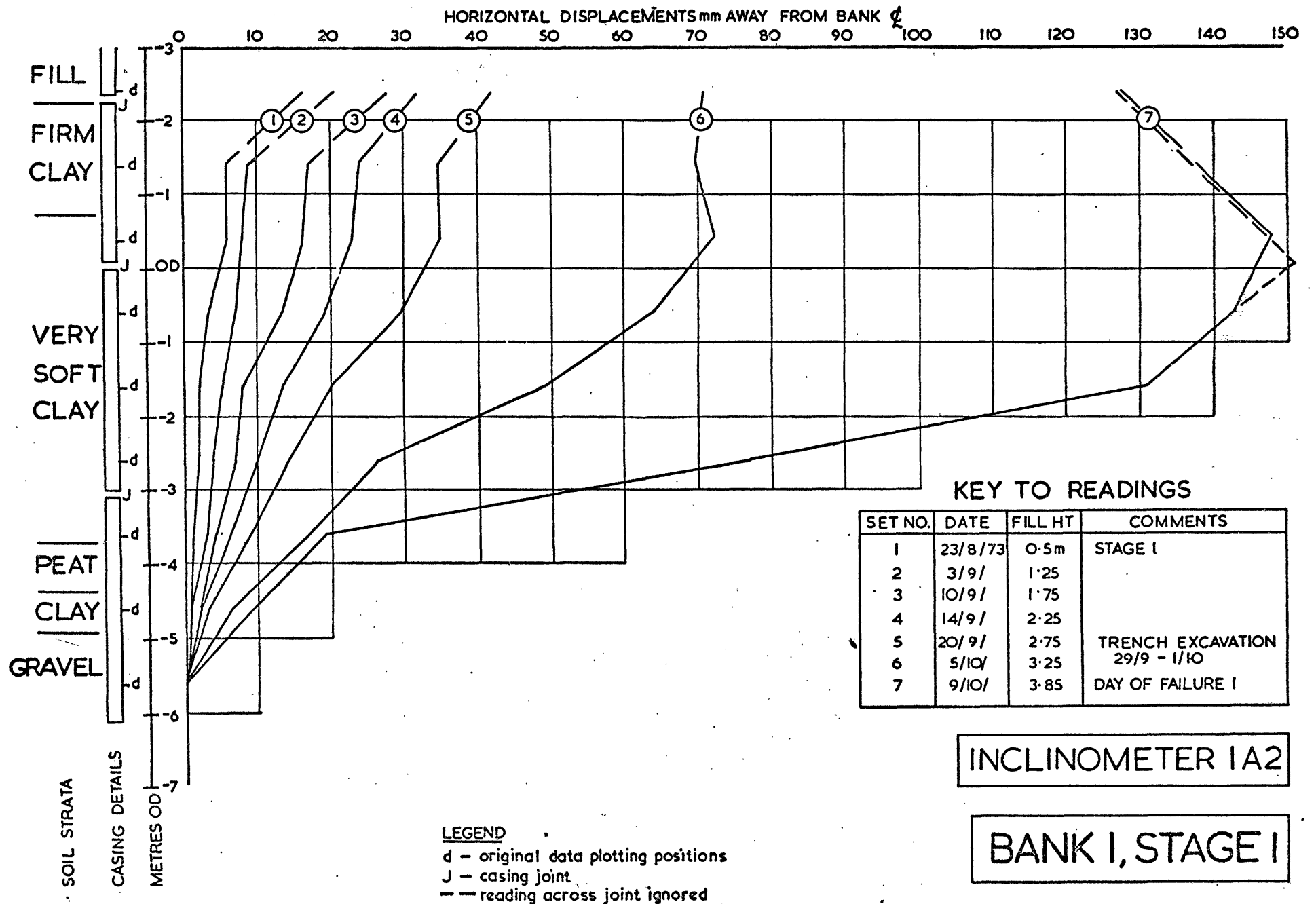


Fig. 5.4.4.

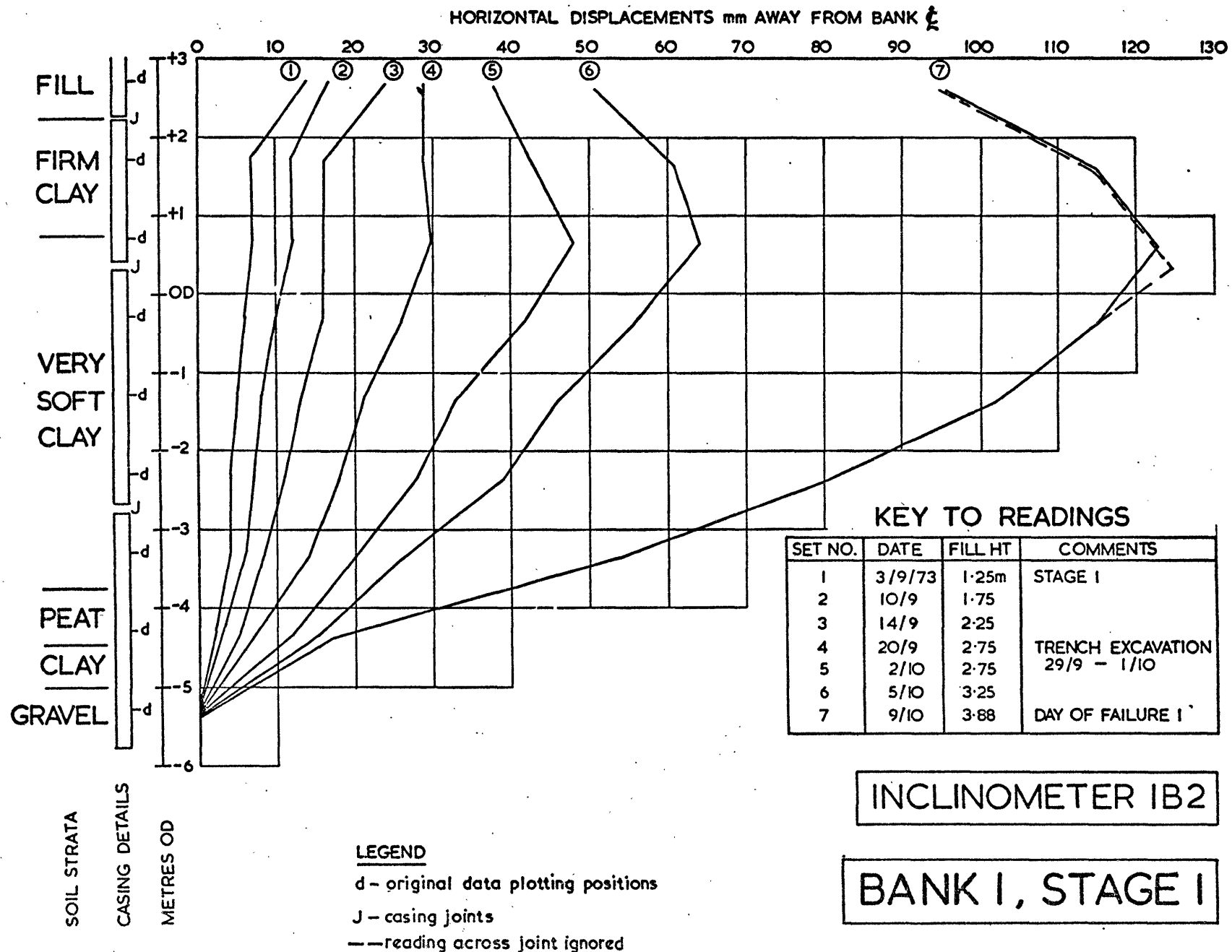


Fig. 5.4.5.

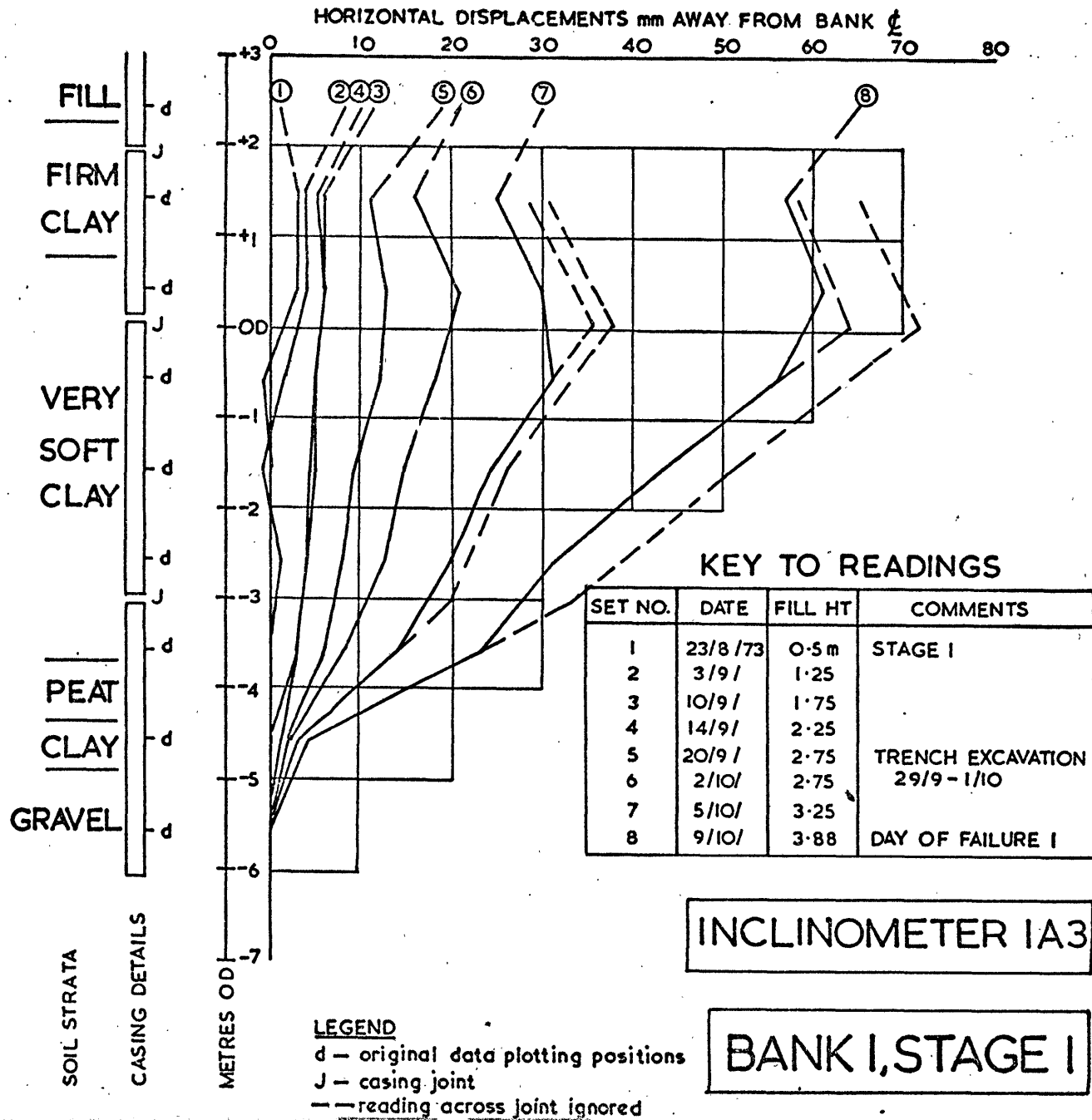


Fig. 5.4.6

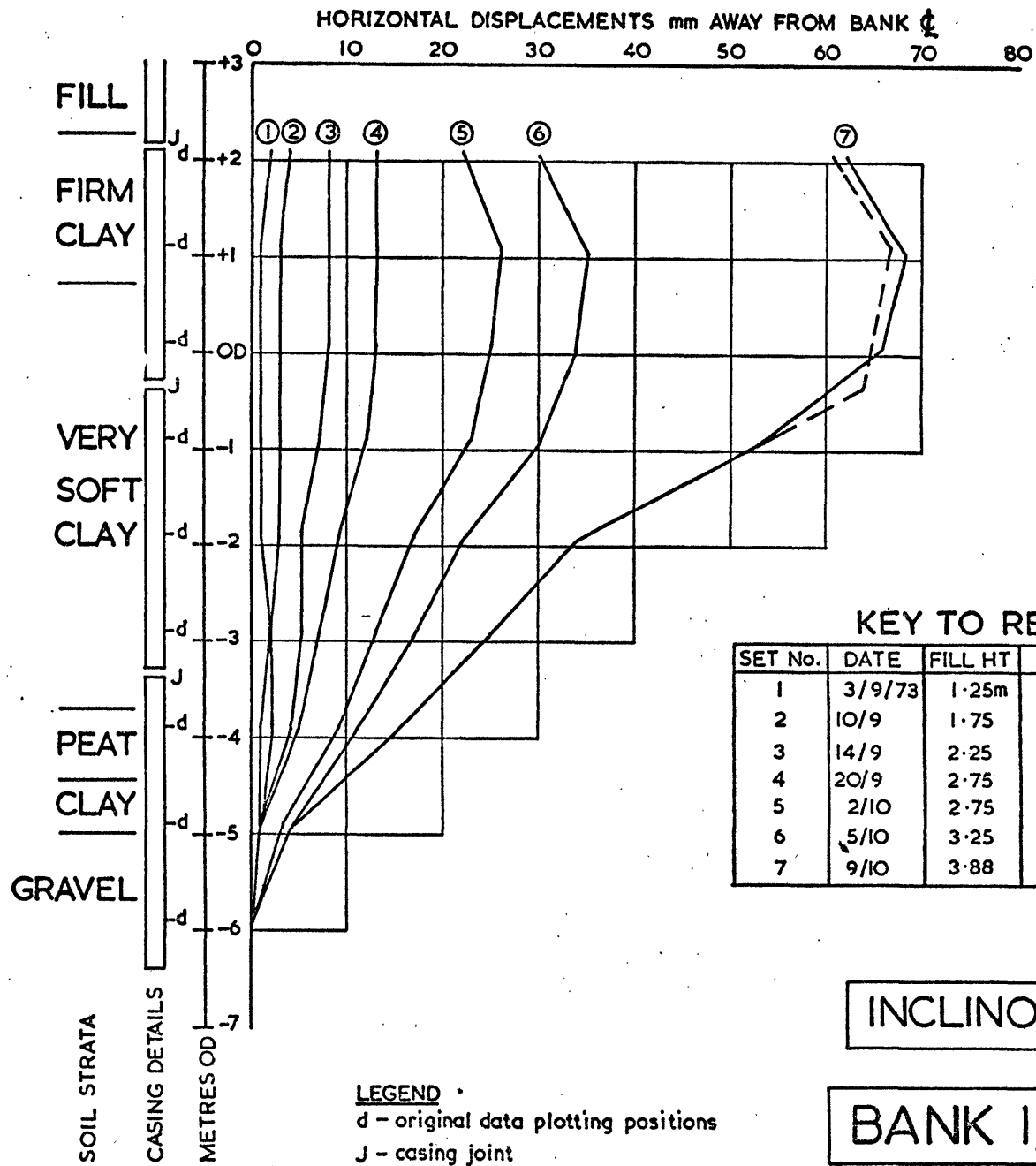


Fig. 5.4. 7.

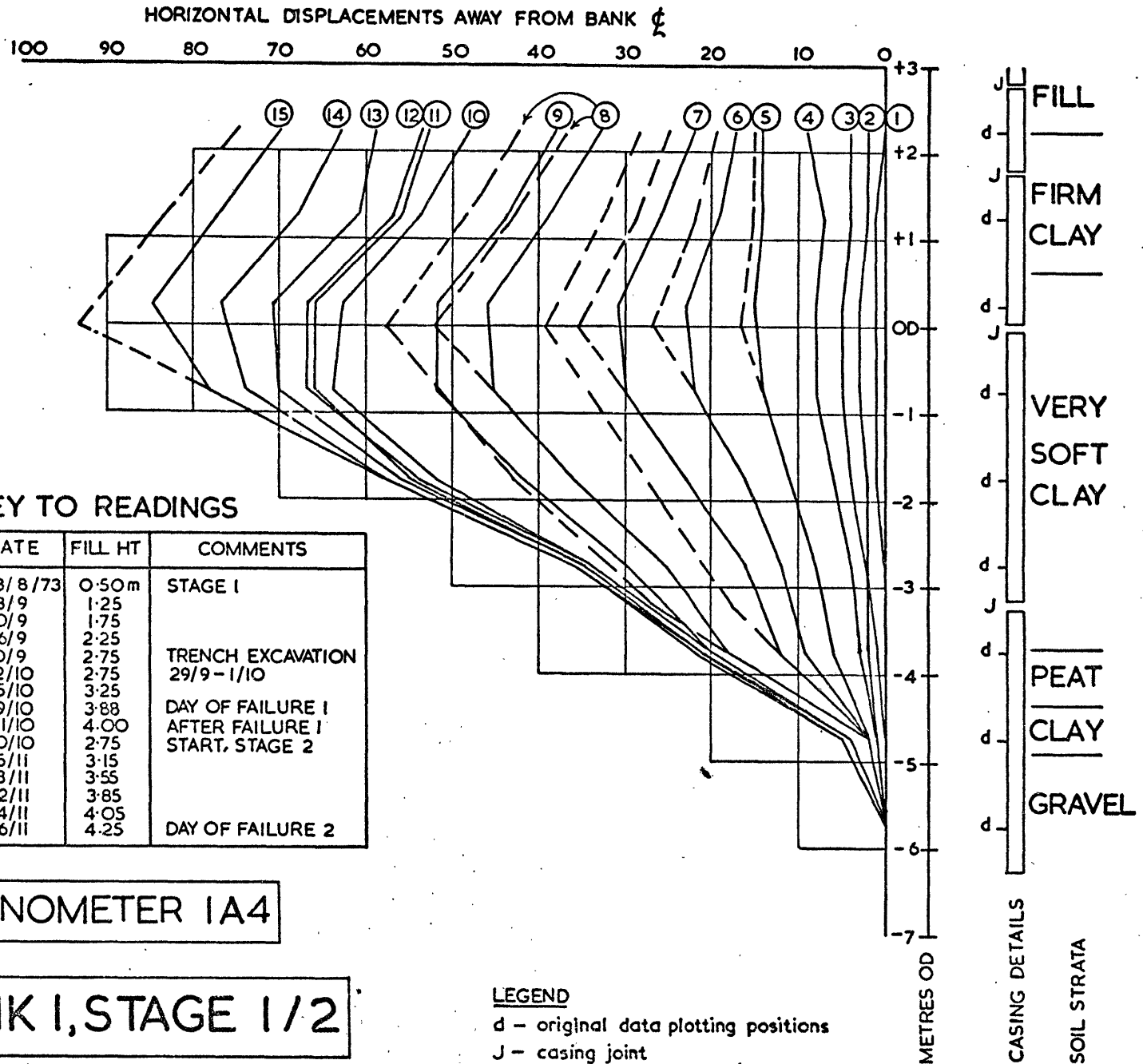
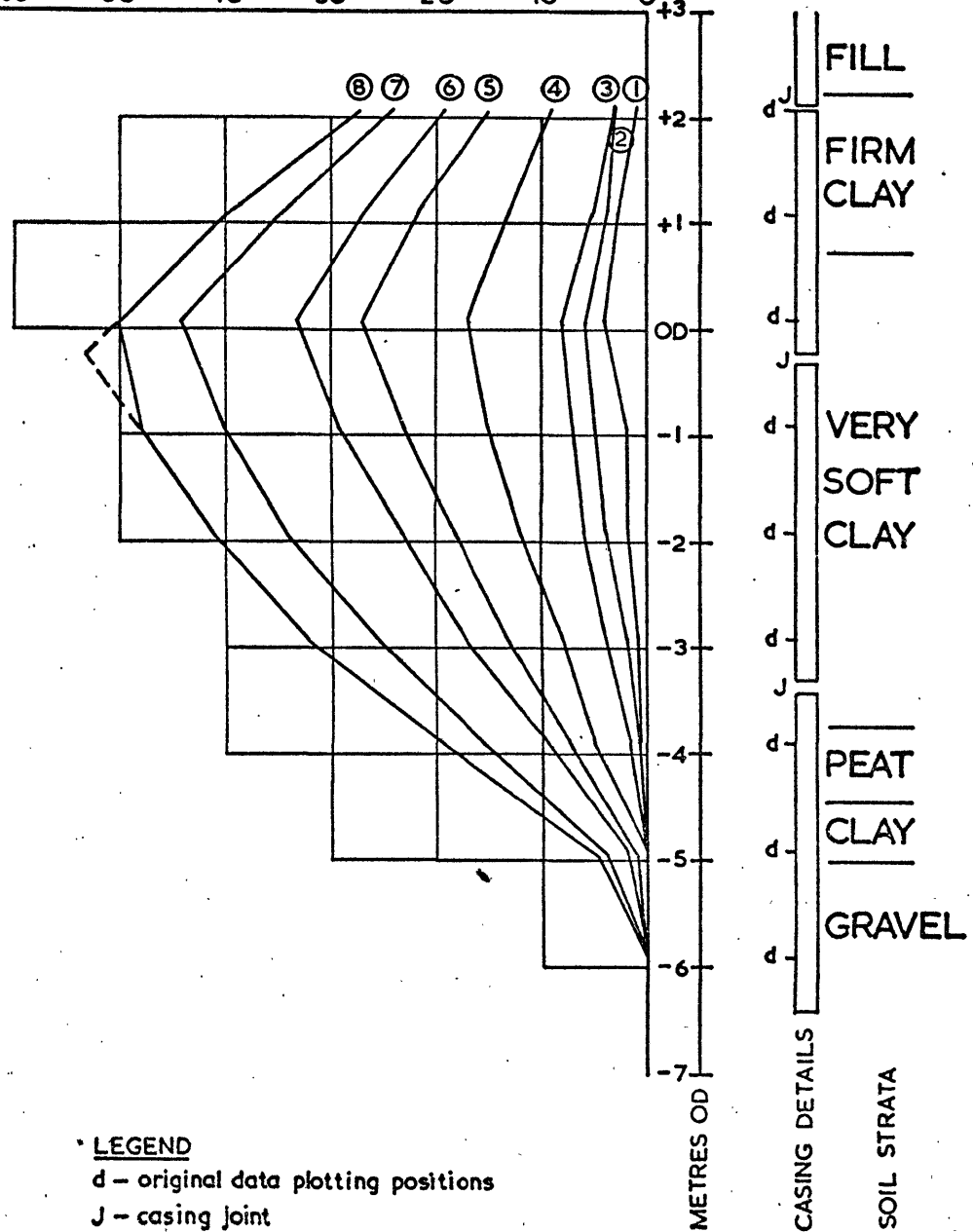


Fig. 5.4.8

HORIZONTAL DISPLACEMENTS mm AWAY FROM BANK $\frac{1}{2}$

70 60 50 40 30 20 10 0



KEY TO READINGS

SET No.	DATE	FILL HT	COMMENTS
1	3/9/73	1.25m	STAGE I
2	10/9	1.75	
3	14/9	2.25	
4	20/9	2.75	TRENCH EXCAVATION 29/9 - 1/10
5	2/10	2.75	
6	5/10	3.25	
7	9/10	3.88	DAY OF FAILURE!
8	11/10	4.00	AFTER FAILURE!

INCLINOMETER IB4

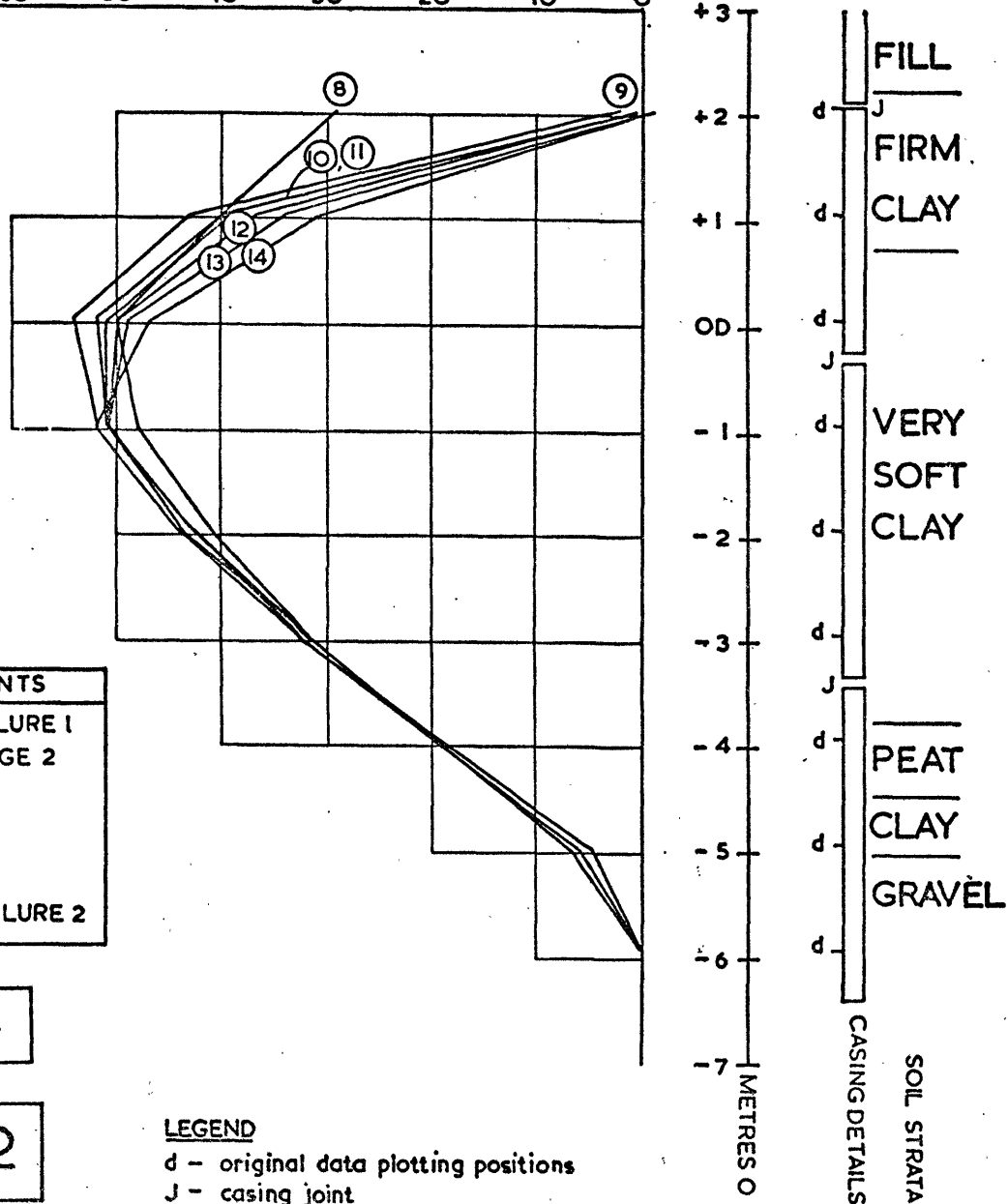
BANK I, STAGE I

LEGEND
 d - original data plotting positions
 J - casing joint
 --- reading across joint ignored

Fig. 5.4.9.

HORIZONTAL DISPLACEMENTS mm AWAY FROM BANK ζ

70 60 50 40 30 20 10 0



KEY TO READINGS

SET NO.	DATE	FILL HT	COMMENTS
8	11/10/73	4.00m	AFTER FAILURE 1
9	30/10/	2.75	START, STAGE 2
10	5/11/	3.15	
11	8/11/	3.55	
12	12/11/	3.85	
13	14/11/	4.05	
14	16/11/	4.25	DAY OF FAILURE 2

INCLINOMETER IB4

BANK I, STAGE 2

LEGEND

d - original data plotting positions
 J - casing joint

Fig. 5.4.10

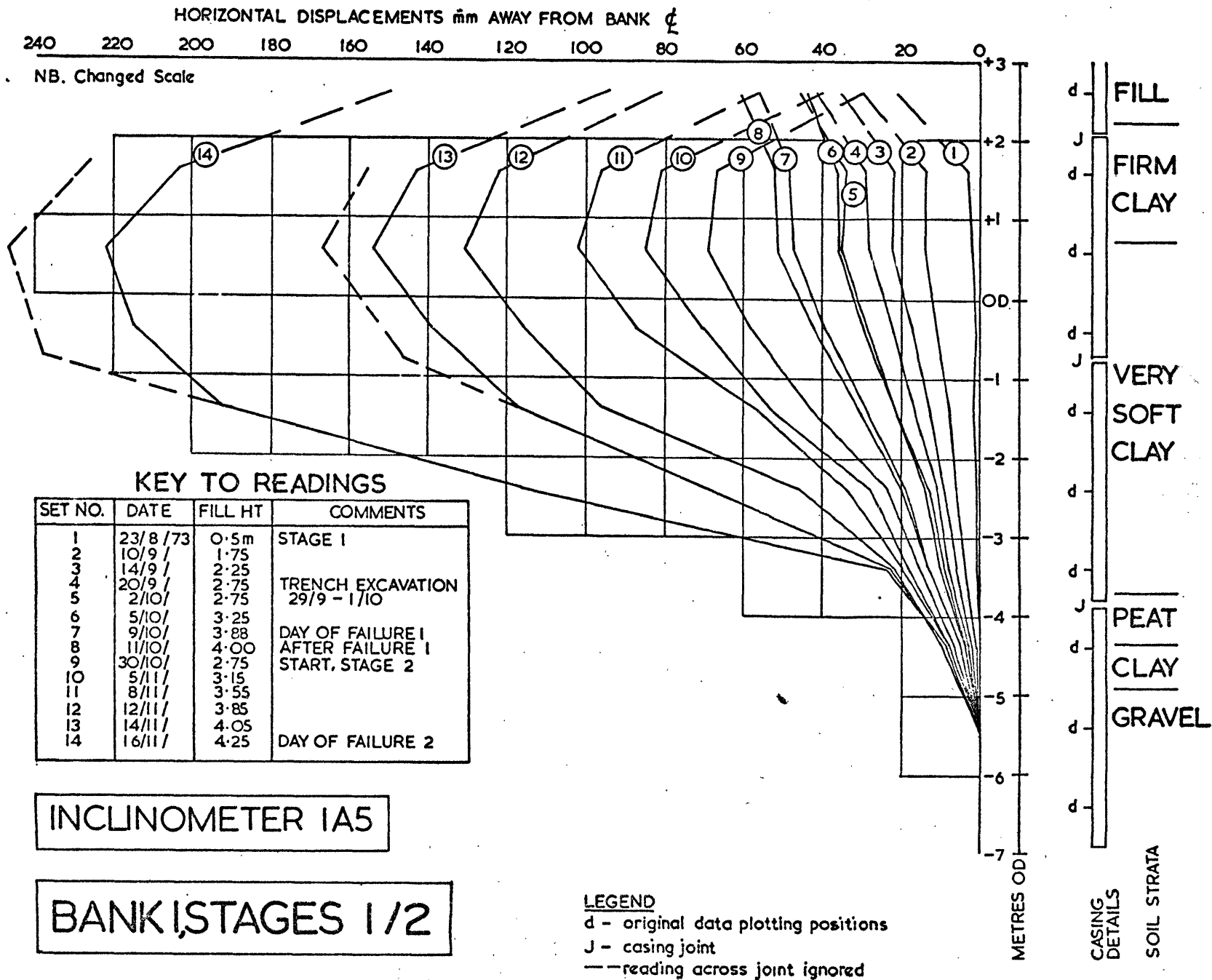


Fig. 5.4.11.

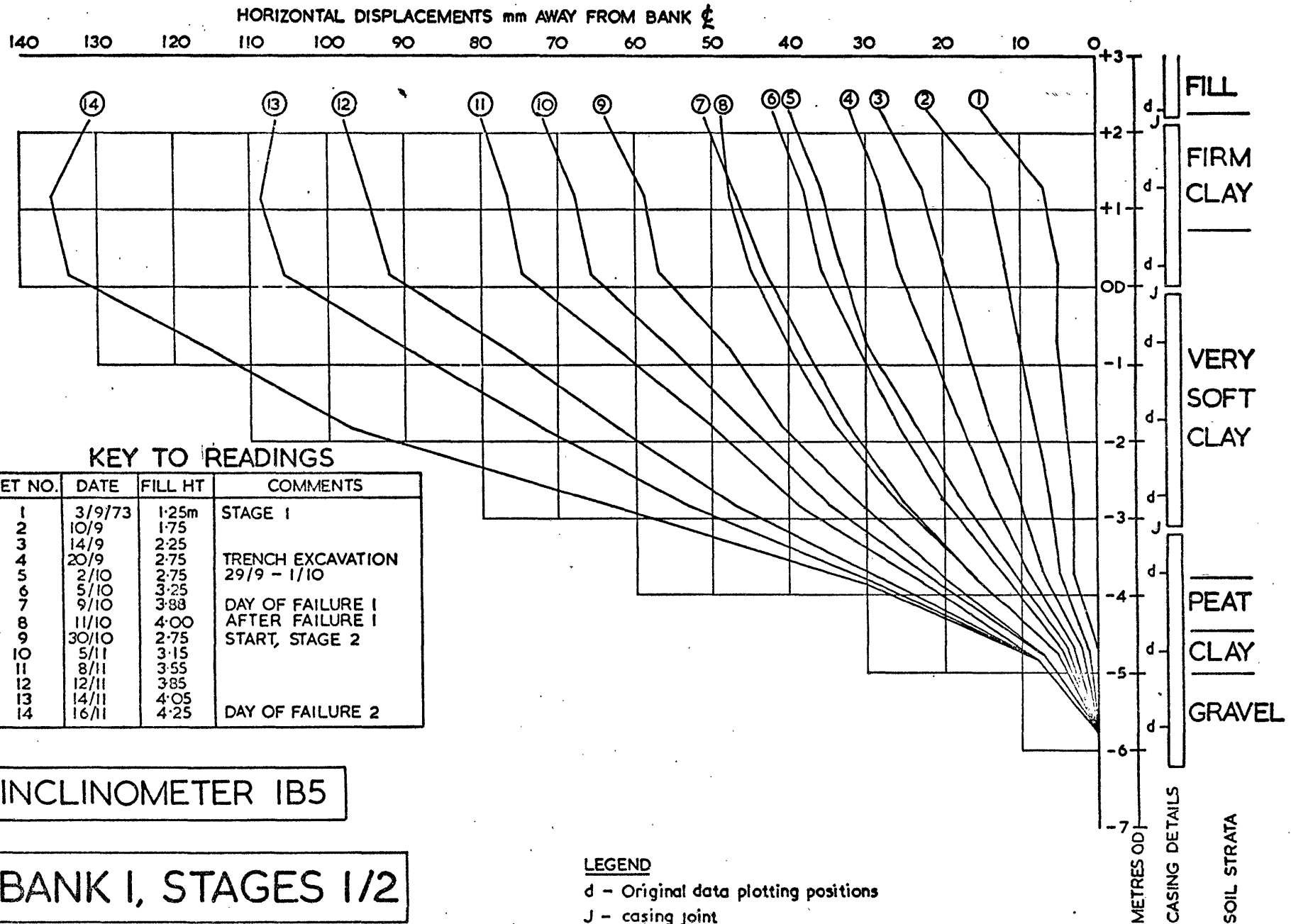


Fig 5.4.12

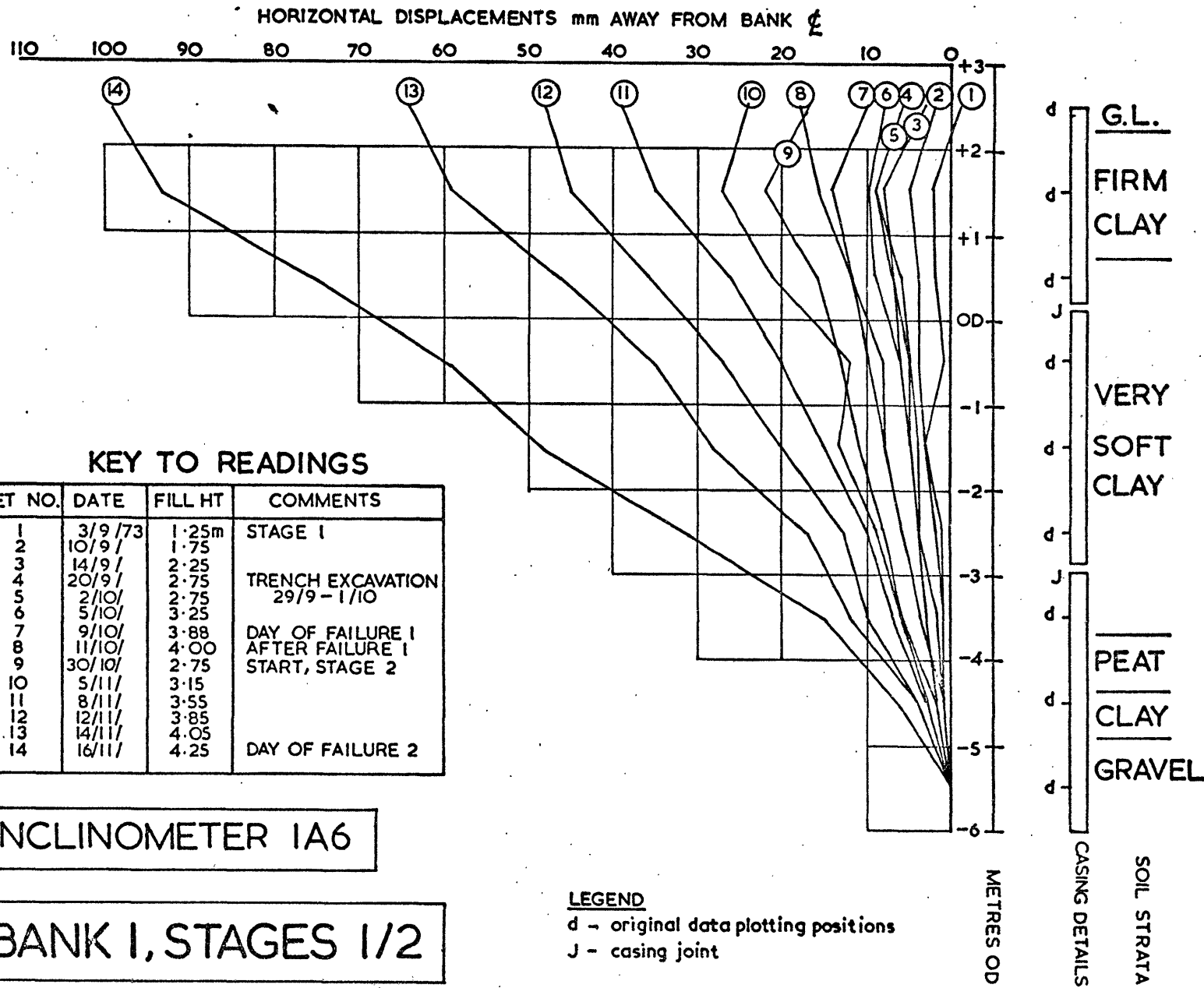
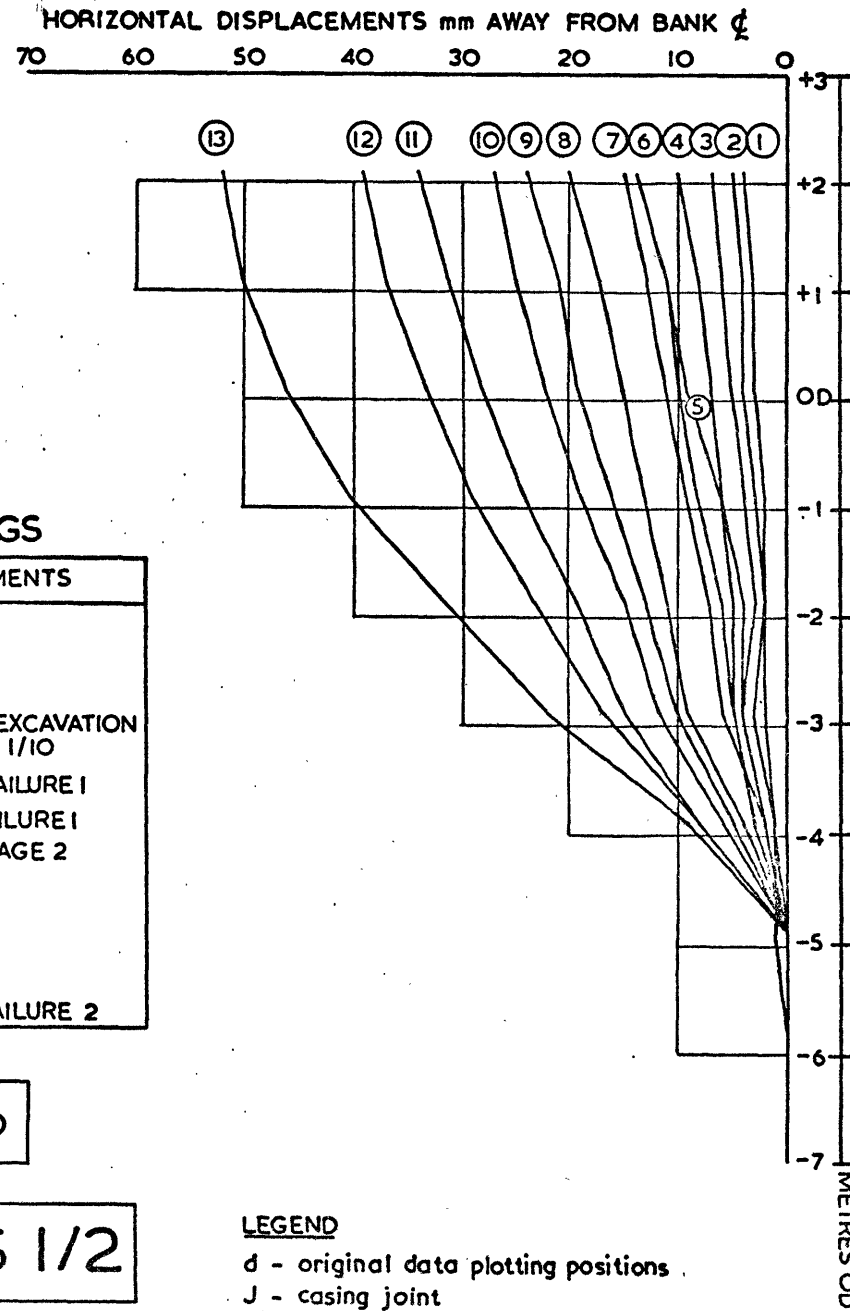


Fig. 5.4.13



KEY TO READINGS

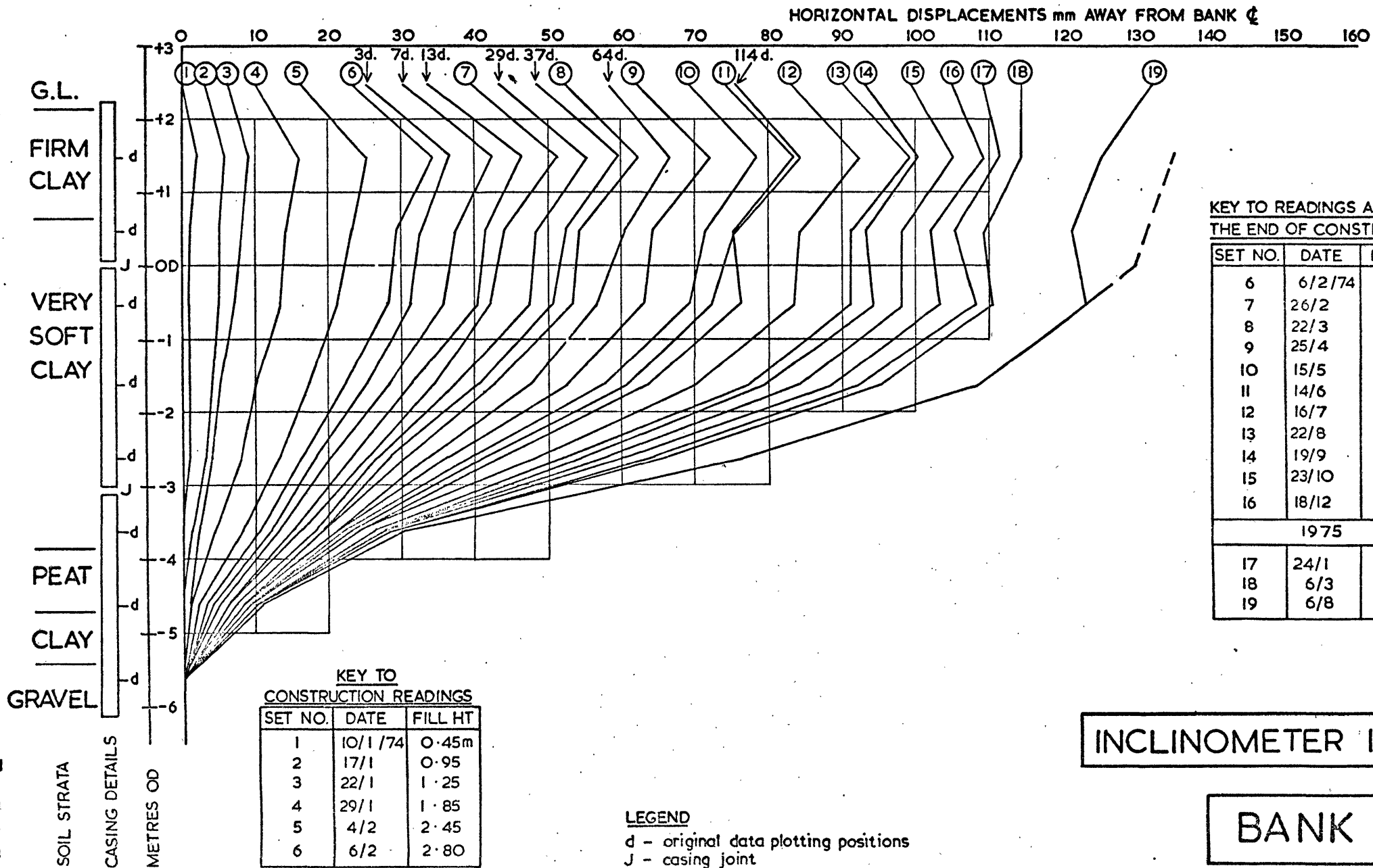
SET NO.	DATE	FILL HT	COMMENTS
1	3/9/73	1.25m	STAGE I
2	10/9/	1.75	
3	14/9/	2.25	
4	20/9/	2.75	TRENCH EXCAVATION
5	2/10/	2.75	29/9 - 1/10
6	9/10/	3.88	DAY OF FAILURE I
7	11/10/	4.00	AFTER FAILURE I
8	30/10/	2.75	START, STAGE 2
9	5/11/	3.15	
10	8/11/	3.55	
11	12/11/	3.85	
12	14/11/	4.05	
13	16/11/	4.25	DAY OF FAILURE 2

INCLINOMETER IB6

BANK I, STAGES 1/2

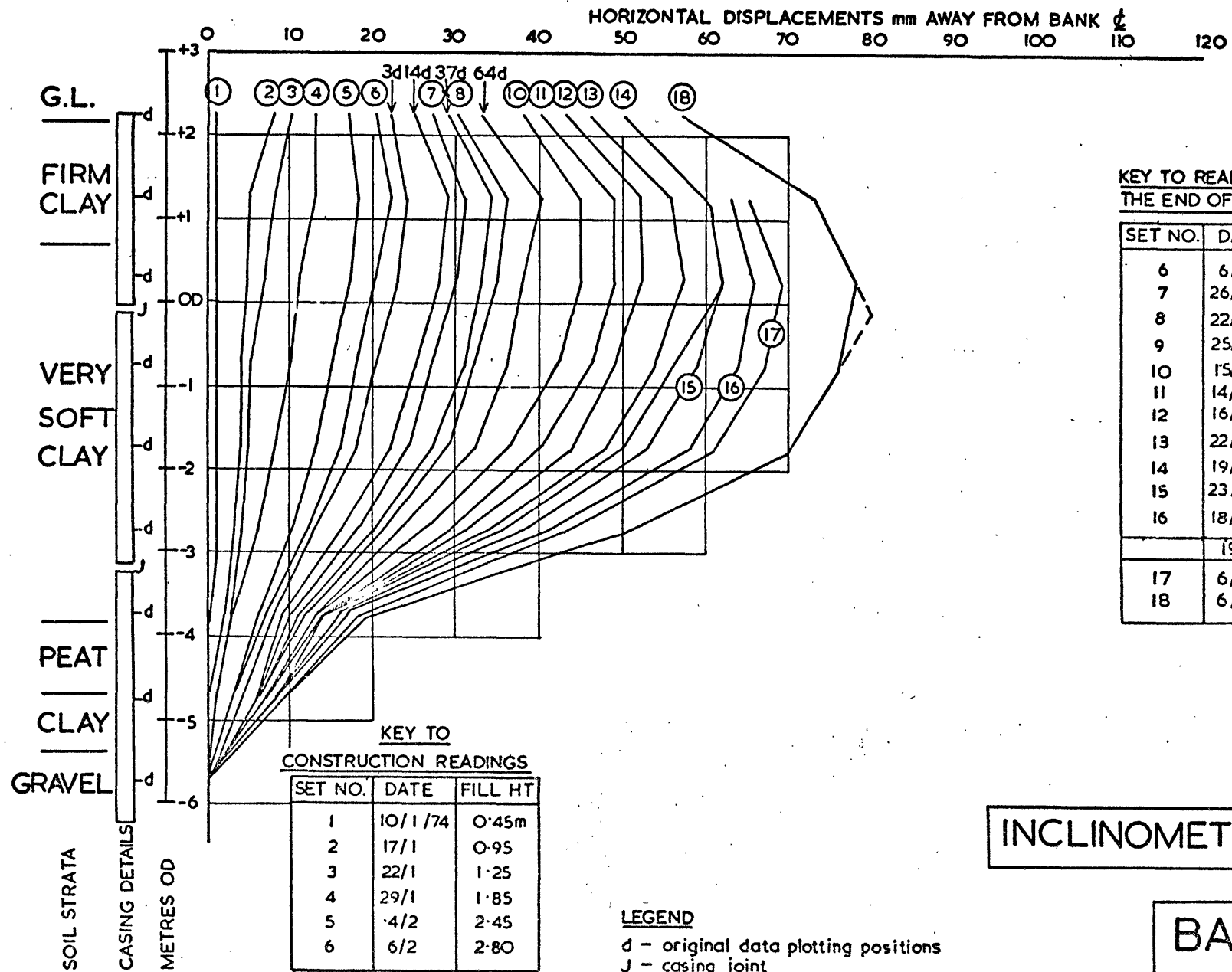
LEGEND
d - original data plotting positions
J - casing joint

Fig. 5.4. 14



-404-

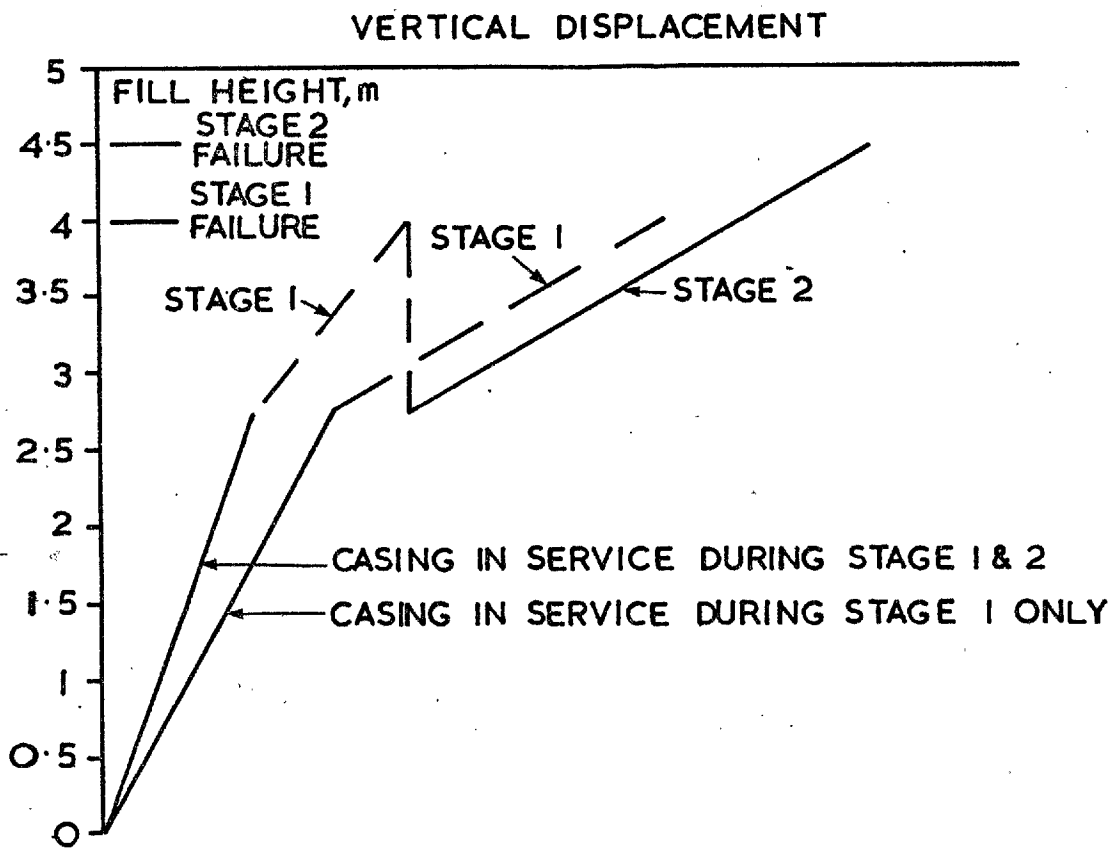
Fig 5.4.15



INCLINOMETER IC2

BANK 2

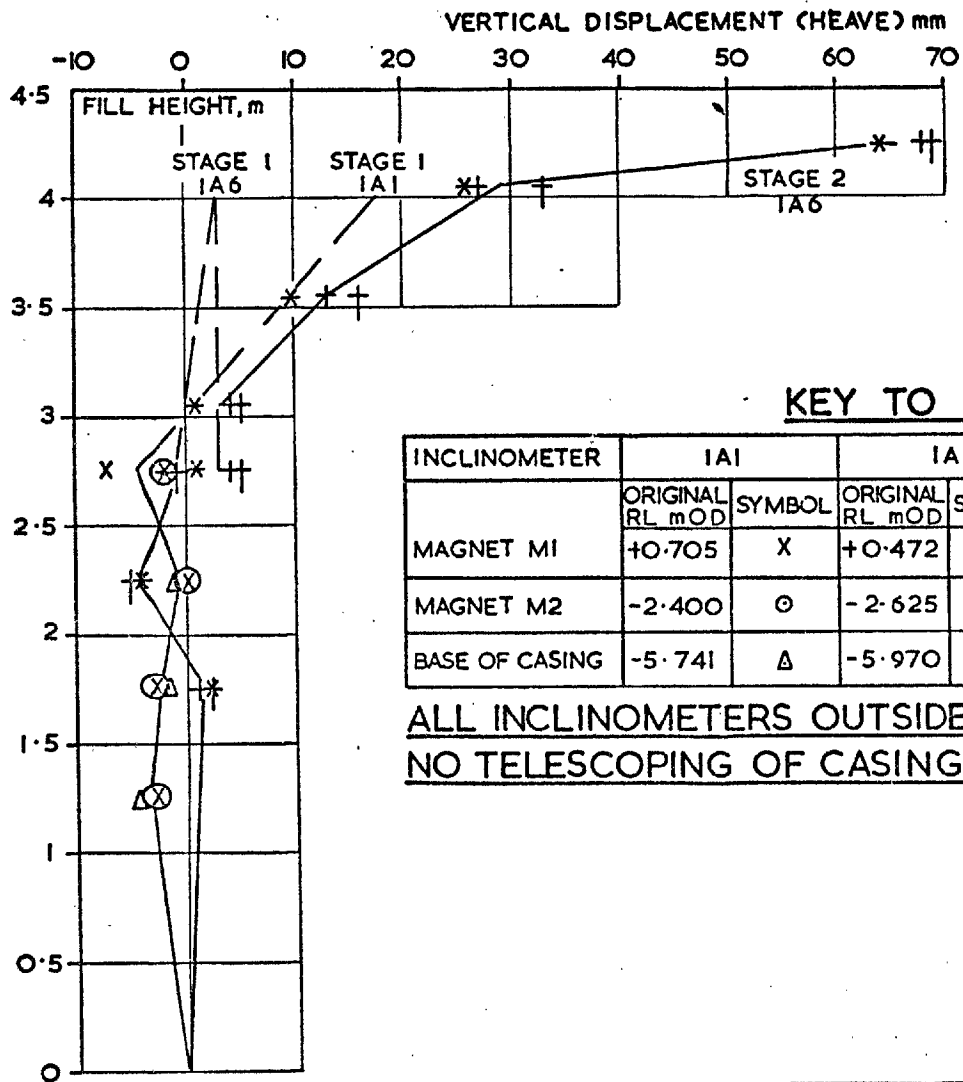
Fig. 5.4.16



LEGEND	
—	OBSERVED
- -	EXTRAPOLATED

BANK I, STAGE I:
EXTRAPOLATION OF INCLINOMETER MAGNET DISPLACEMENTS

Fig. 5.4.17

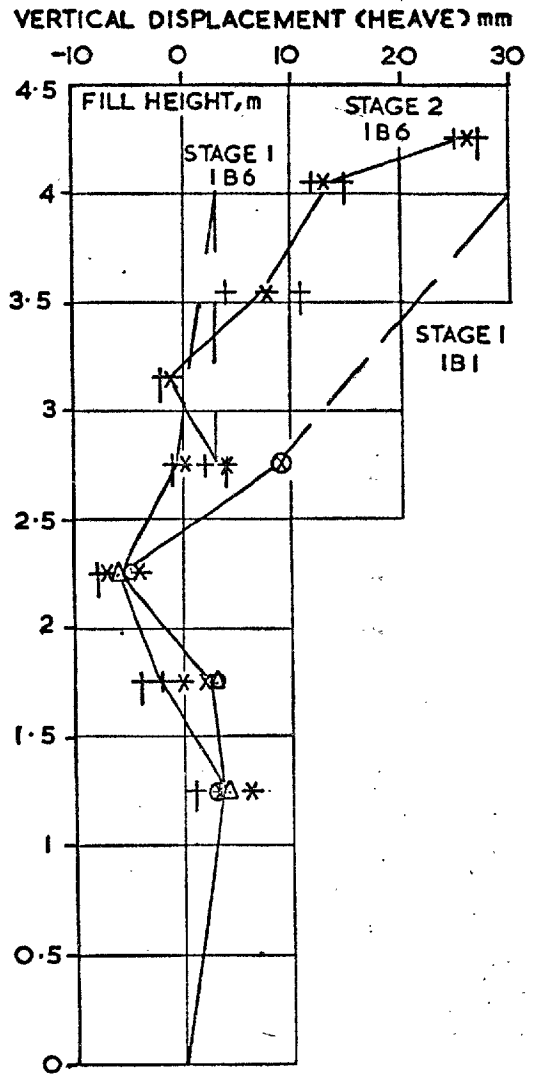


LEGEND
 — OBSERVED
 - - - EXTRAPOLATED

KEY TO READINGS

INCLINOMETER	IA1		IA6		IB1		IB6	
	ORIGINAL RL mOD	SYMBOL	ORIGINAL RL mOD	SYMBOL	ORIGINAL RL mOD	SYMBOL	ORIGINAL RL mOD	SYMBOL
MAGNET M1	+0.705	X	+0.472	+	+0.242	X	+0.051	+
MAGNET M2	-2.400	⊙	-2.625	*	-2.854	⊙	-3.064	*
BASE OF CASING	-5.741	Δ	-5.970	+	-6.196	Δ	-6.398	+

ALL INCLINOMETERS OUTSIDE FILL AREA:
NO TELESCOPING OF CASINGS



INCLINOMETERS IB1/6

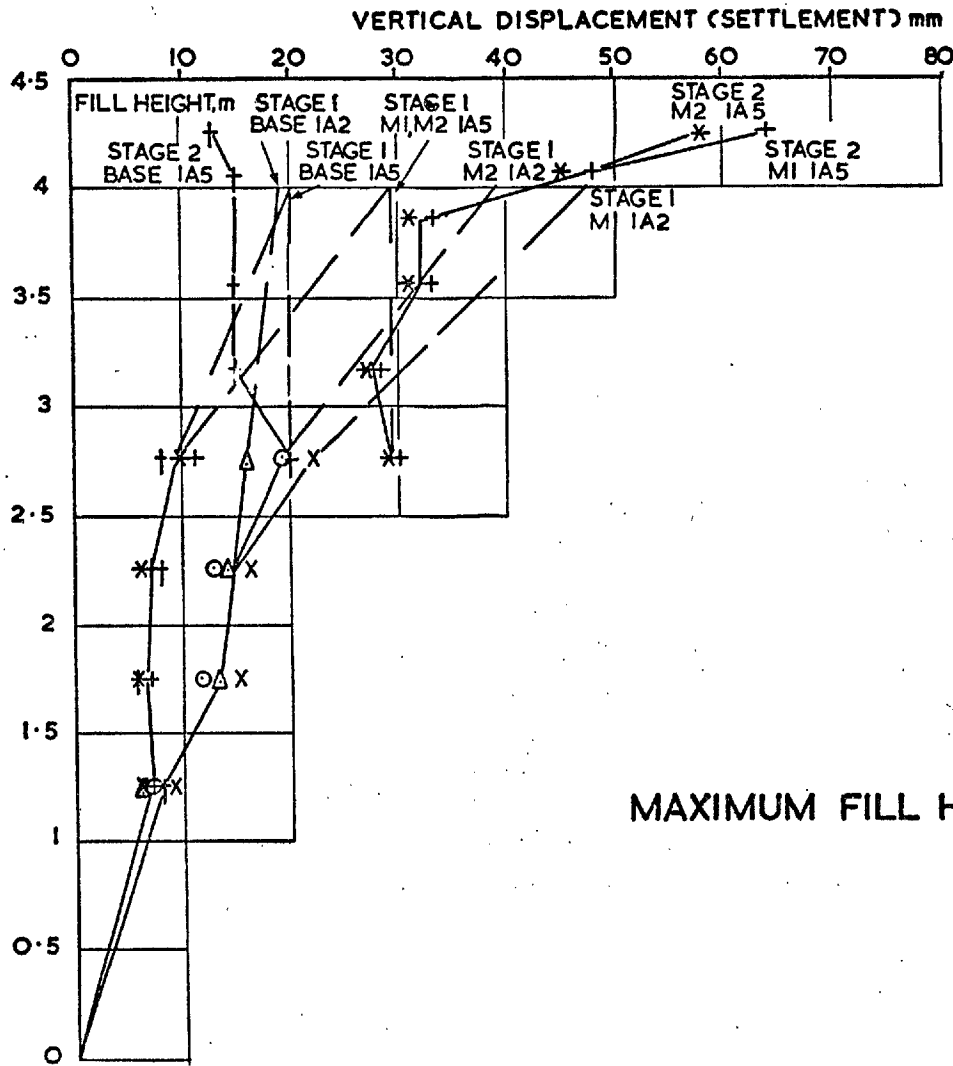
BANK I, STAGES 1/2

INCLINOMETERS IA1/6

VERTICAL DISPLACEMENTS OF MAGNETS AND CASING BASES VERSUS FILL HEIGHT

Fig. 5.4.18

-407-



LEGEND	
—	OBSERVED
- - -	EXTRAPOLATED

KEY TO READINGS

INCLINOMETER	IA2		IA5	
	ORIGINAL RL m OD	SYMBOL	ORIGINAL RL m OD	SYMBOL
MAGNET MI	+0.320	X	-0.455	+
MAGNET M2	-2.763	O	-3.553	*
BASE OF CASING	-6.108	Δ	-6.897	†

MAXIMUM FILL HEIGHT AT INCLINOMETER LOCATIONS

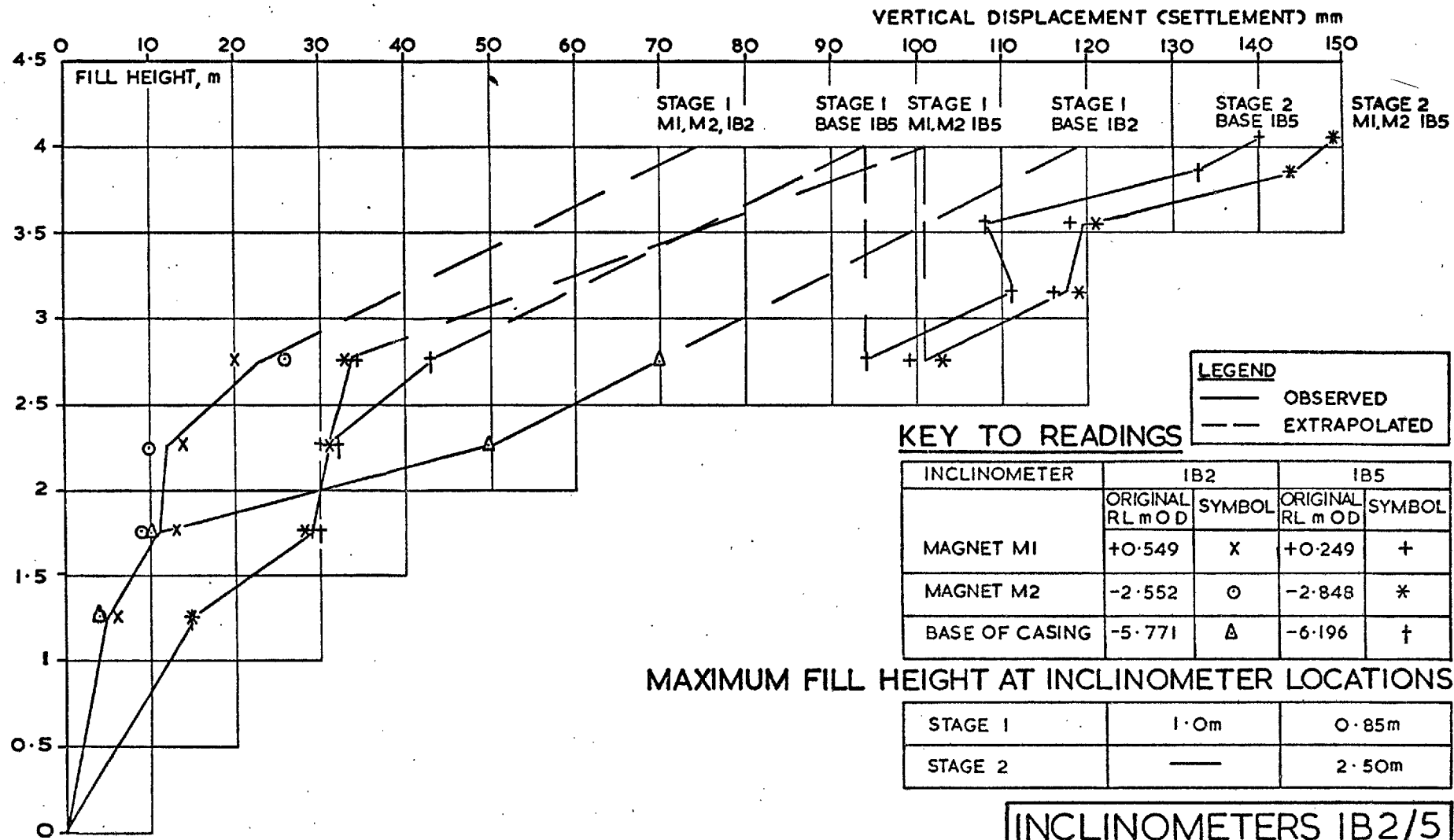
STAGE 1	1.0m	0.85m
STAGE 2	—	2.50m

INCLINOMETERS IA2/5

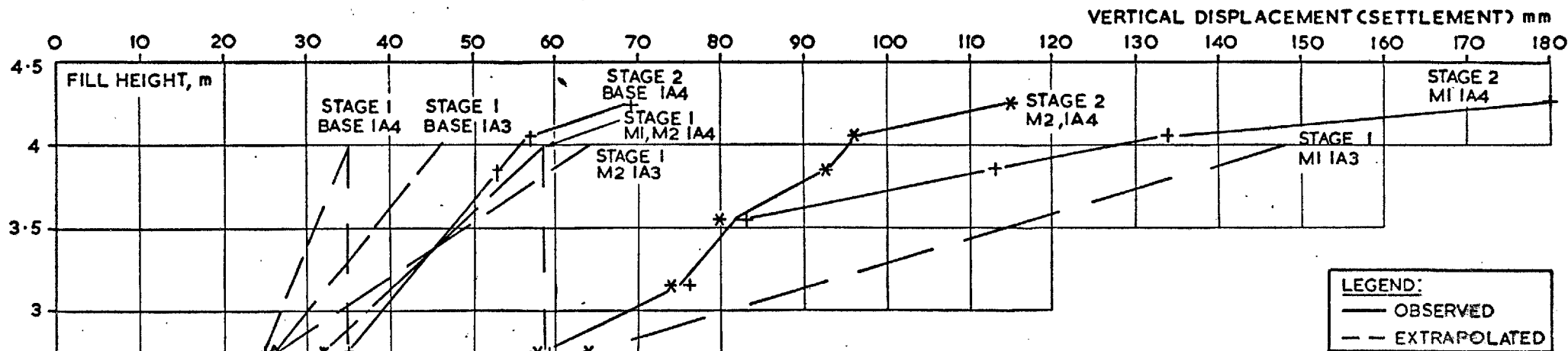
BANK 1, STAGES 1/2

VERTICAL DISPLACEMENTS OF MAGNETS AND CASING BASES VERSUS FILL HEIGHT

Fig. 5.4.19



VERTICAL DISPLACEMENTS OF MAGNETS AND CASING BASES VERSUS FILL HEIGHT



LEGEND:
 — OBSERVED
 - - - EXTRAPOLATED

KEY TO READINGS

INCLINOMETER	IA3		IA4	
	ORIGINAL RL mOD	SYMBOL	ORIGINAL RL mOD	SYMBOL
MAGNET M1	+0.379	X	+0.193	+
MAGNET M2	-2.738	o	-2.903	*
BASE OF CASING	-6.077	Δ	-6.244	†

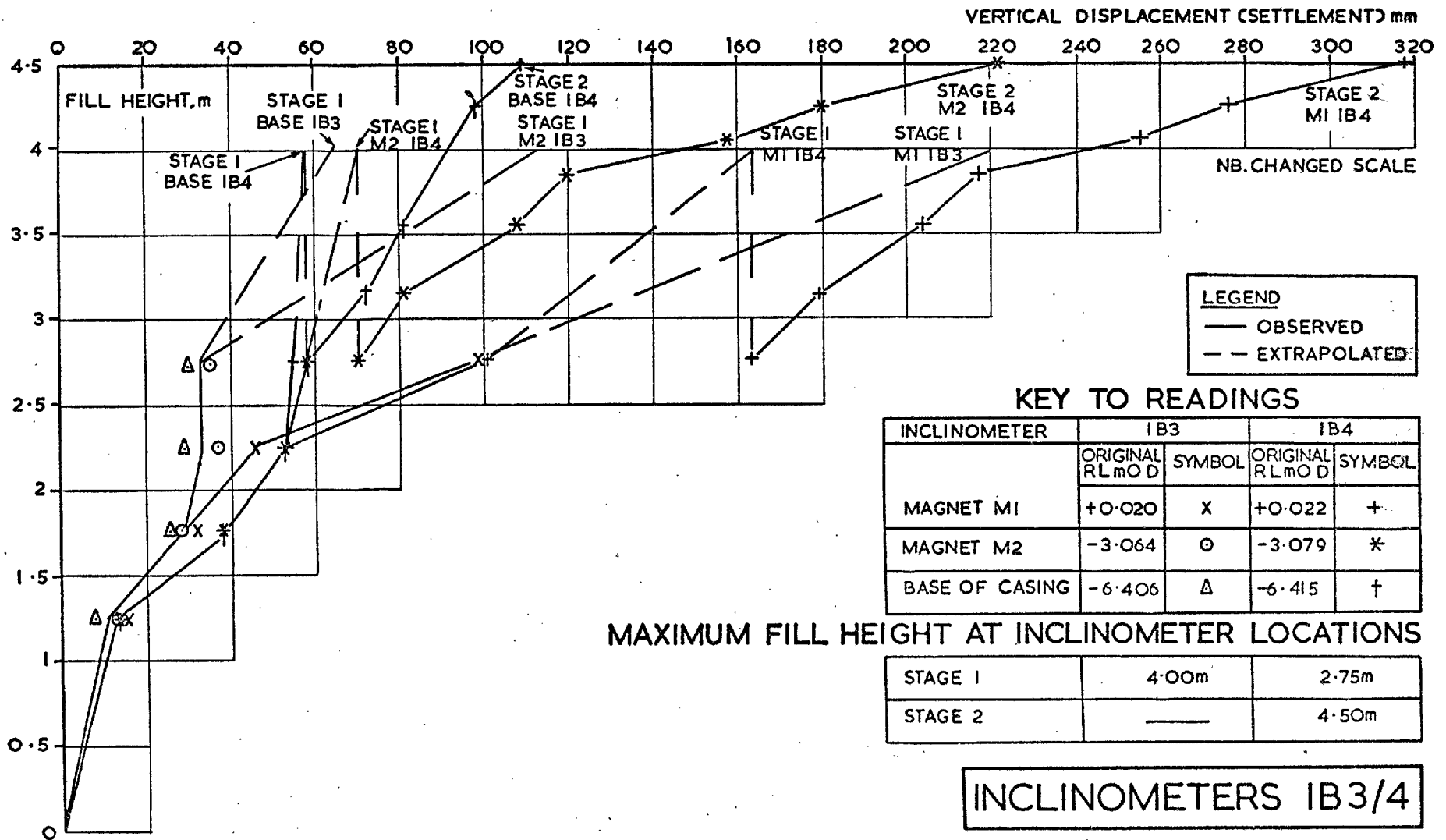
MAXIMUM FILL HEIGHT AT INCLINOMETER LOCATIONS

STAGE	IA3	IA4
STAGE 1	4.00m	2.75m
STAGE 2	—	4.50m

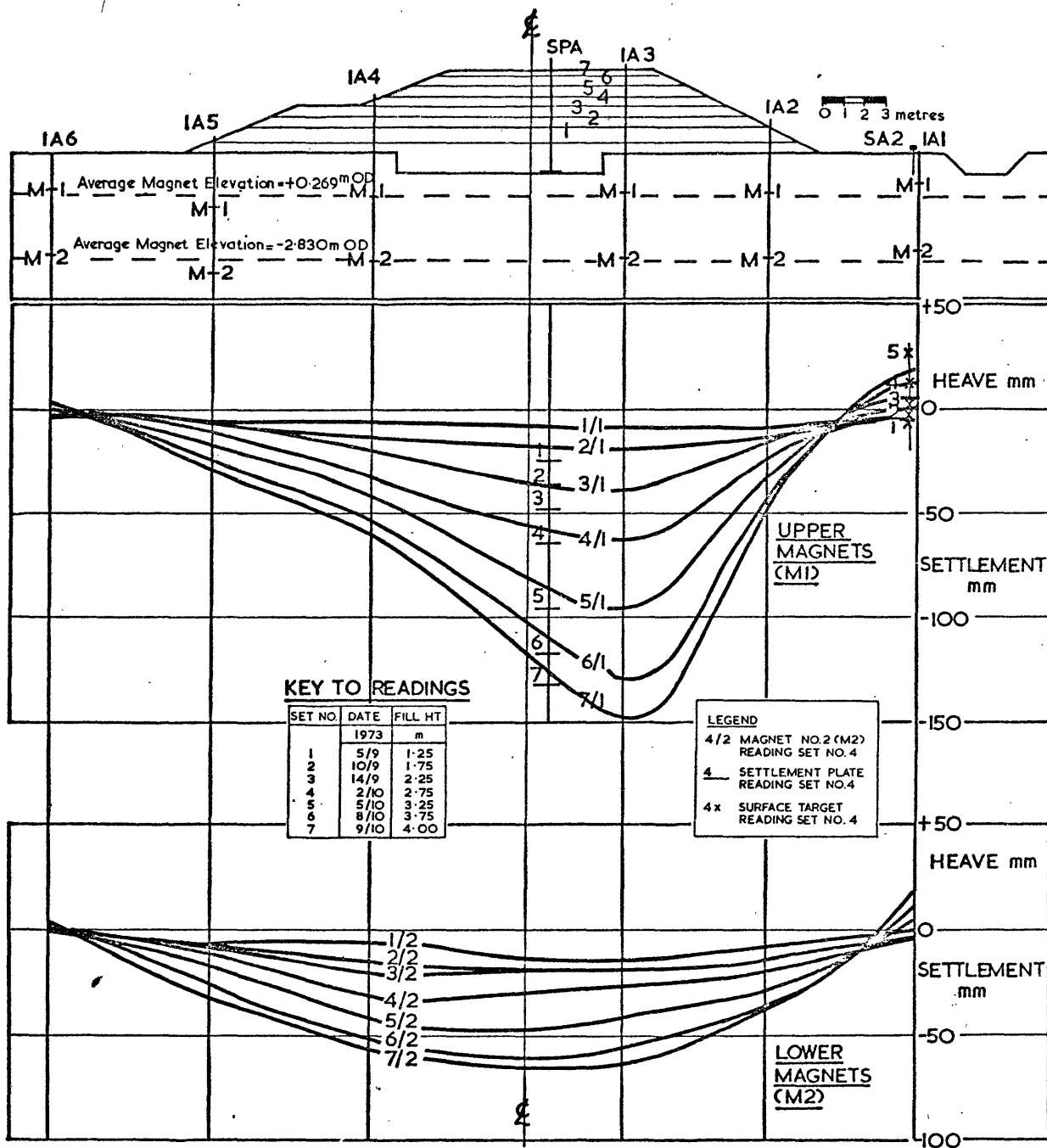
INCLINOMETERS IA3/4

BANK I, STAGES 1/2

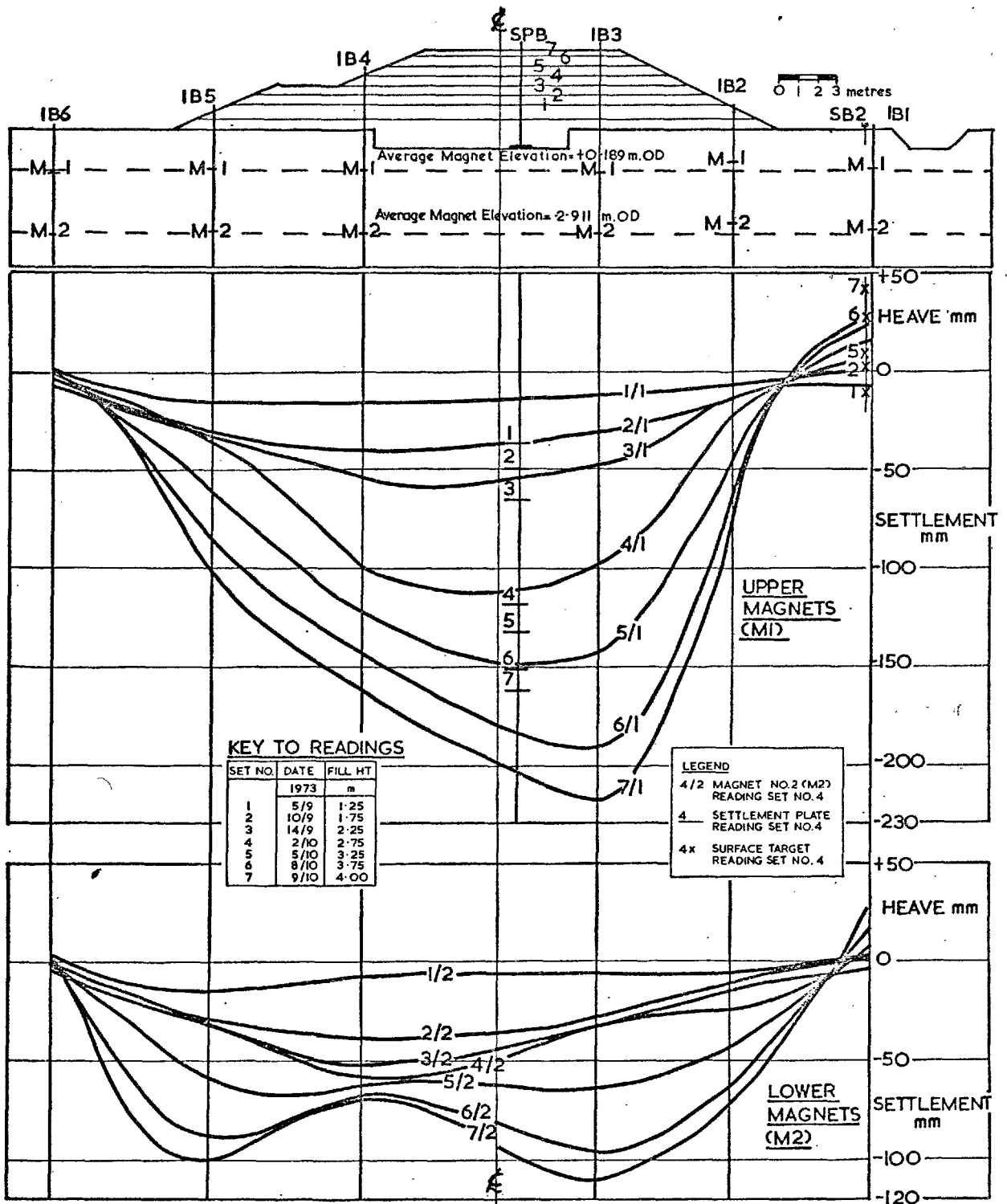
VERTICAL DISPLACEMENTS OF MAGNETS AND CASING BASES VERSUS FILL HEIGHT



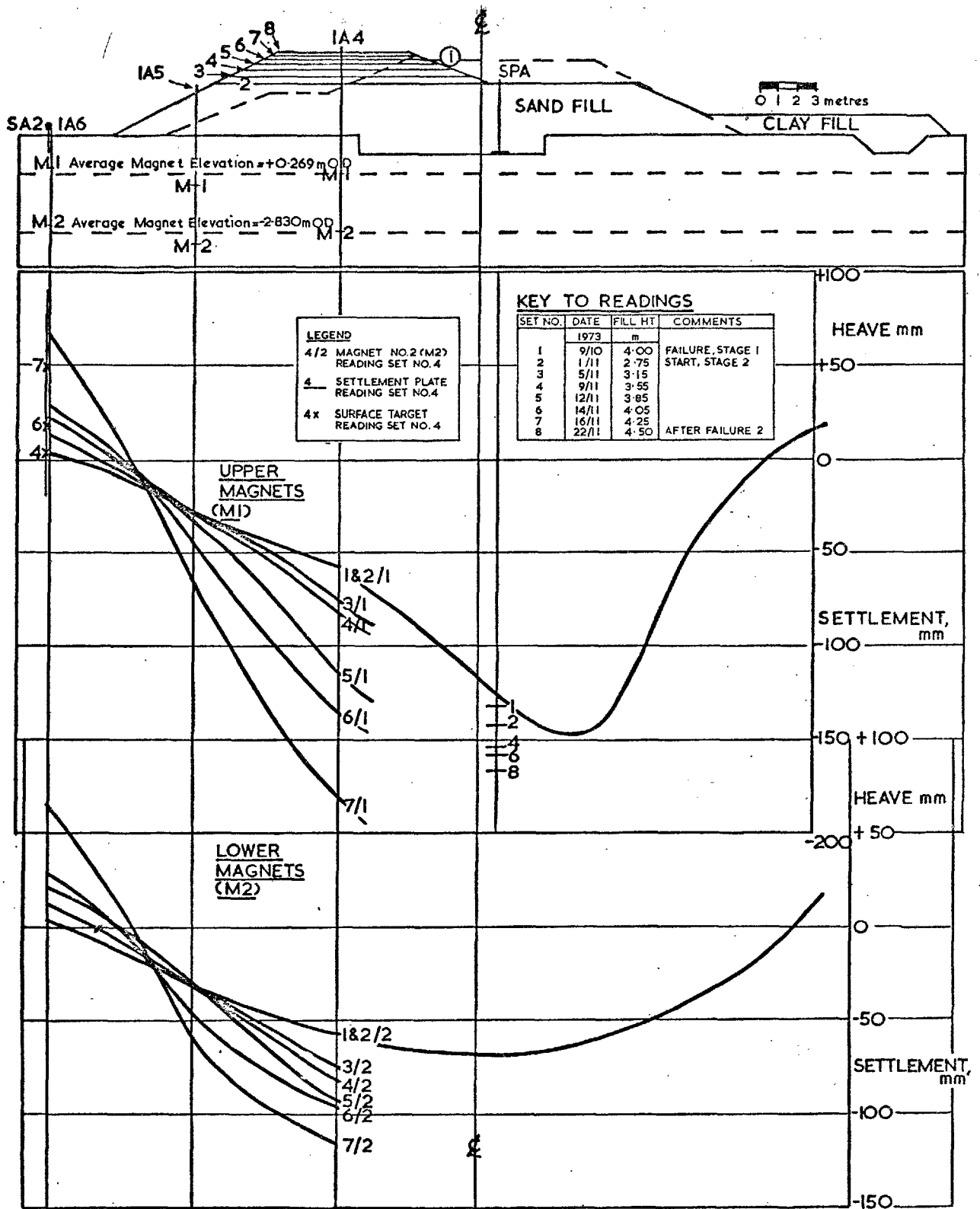
VERTICAL DISPLACEMENTS OF MAGNETS AND CASING BASES VERSUS FILL HEIGHT



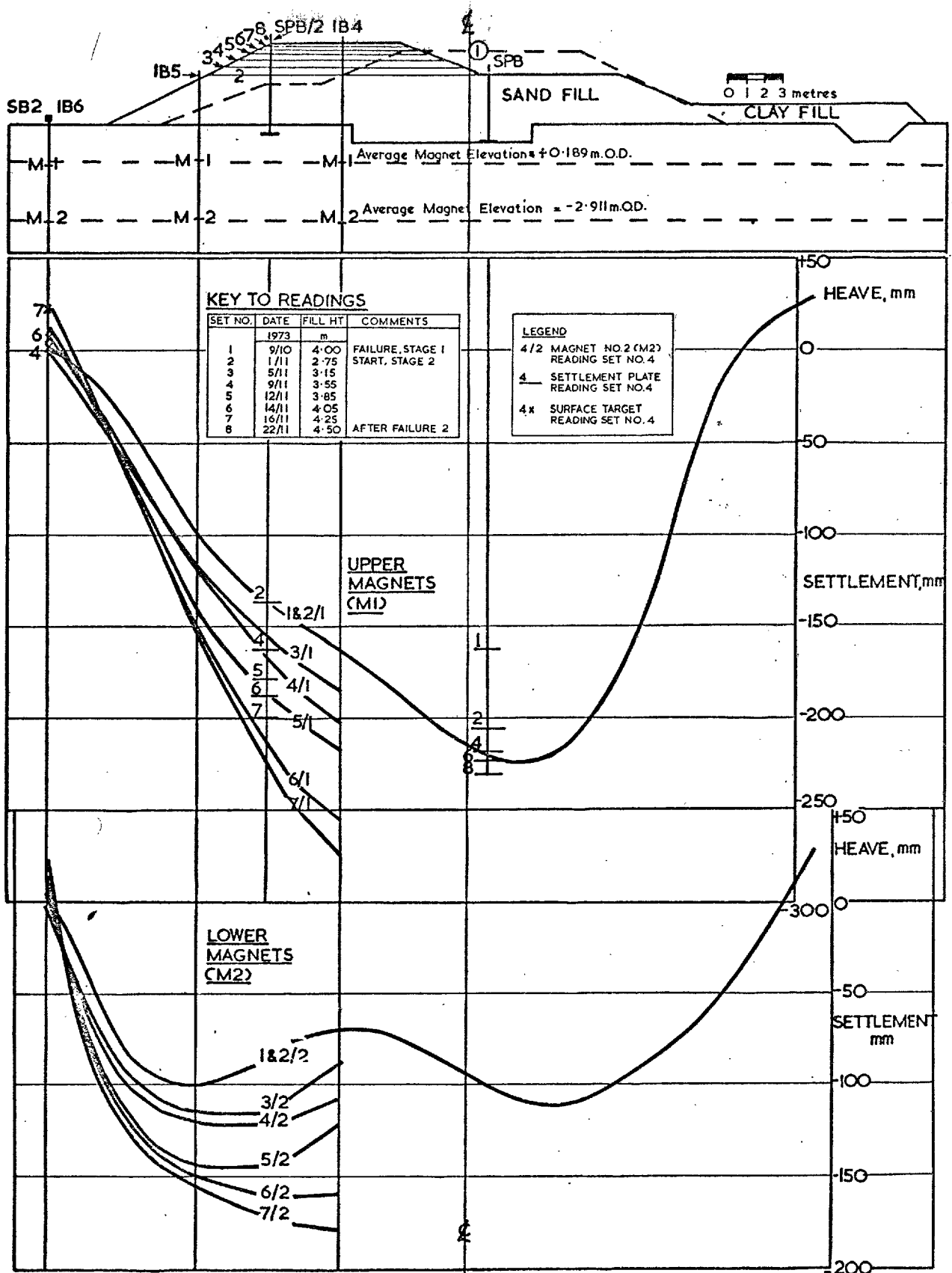
BANK I, STAGE I - SECTION A. VERTICAL DISPLACEMENT PROFILES FOR INCLINOMETER MAGNET



BANK I, STAGE I - SECTION B. VERTICAL DISPLACEMENT PROFILES FOR INCLINOMETER MAGNETS



BANK I, STAGE 2 : SECTION A. VERTICAL DISPLACEMENT PROFILES FOR INCLINOMETER MAGNETS



BANK I, STAGE 2 - SECTION B. VERTICAL DISPLACEMENT PROFILES FOR INCLINOMETER MAGNETS

5.5. Piezometers

5.5.1. Installation

Hydraulic twin tube 'push-in' piezometers, with high air-entry value ceramic filters (pore diameter 1 micron, permeability 2×10^{-8} m/s, air-entry value 1 atmosphere) were installed in the foundation material beneath, and adjacent to, all the test fills constructed at the site. The high air-entry ceramic filters were used because of the possibility of there being pockets of marsh gas within the essentially saturated clay. In fact the only reason for not using a low permeability ceramic in a clay is that interpretation of in-situ permeability tests may be difficult (Gibson, 1966; Marsland 1973(a)).

The 125mm long, by 38mm diameter, ceramic filters were located between neoprene washers and plastic end caps attached to a central threaded brass rod. The lower end caps were conical and the upper ones, complete with nut and olive fittings and through which the rod protruded a short distance, cylindrical. This particular type of 'push-in' piezometer was developed for use in conjunction with a trial embankment on a soft clay foundation at King's Lynn, as described by Wilkes (1970), who also describes the installation process summarised as follows.

The piezometers were installed from the bottom of 75mm diameter boreholes, drilled with a continuous flight auger. The boreholes were terminated 300mm from the intended piezometer location, and the piezometer lowered to the base by means of a special placing tool. This was a nominal 100mm long by 12mm I.D. aluminium casting, extended in 3m lengths, into which the central rod of the piezometer fitted; recesses at the nose enabled

the piezometer tubes to be taken along the outside of the tool without excessive bending at the couplings, and there were holes in the body through which grout could be pumped. Thus the piezometer, complete with cross-coupled tubing slightly longer than the depth of the borehole, was pushed 300mm into position. Installation was completed by grouting up the borehole with a 3:1 bentonite:cement mix, using the placing tool as a tremie pipe.

This procedure was adopted to keep smear effects to a minimum, this being particularly important for materials with a definite structure in which in-situ permeability measurements are to be made, and for response time generally (Wilkinson, 1968; Bishop and Al-Dhahir, 1969); to obtain intimate contact with the soil* and thus avoid air being trapped between the piezometer and the soil (Wilkinson, 1968); and to ensure a good seal (Hvorslev 1951; Bishop et al, 1960; Vaughan, 1965 and 1969). Wilkes (1970) also points out that this type of installation is quick, economical and less prone to damage than normal borehole installations (see also McKenna and Roy, 1973). The only problem encountered at Mucking was a tendency for material to fall back into the hole on withdrawal of the flight auger.

Wilkes (1970) also advised installation of dry (low air-entry value) piezometers to further lessen the risk of smear: this is the reverse of normal practice for high air-entry value tips. The piezometers at

*this can also be achieved by installing the piezometer in Plaster of Paris (Walbancke, 1976).

Mucking were left standing in buckets of de-aired water for at least one day before installation. Immediately prior to installation they were connected up to the appropriate lengths of tubing (2.8mm I.D., 4.8mm O.D. nylon 11, coated with 1mm polythene) and de-aired whilst in the buckets. Six piezometers on Section A of Bank 1 (PA25-30, figure 4.3) were installed dry and de-aired subsequently; no difference was noticed in the behaviour of these tips.

Vertical location of the piezometer tips was achieved by tape measurement from the top of the placing tool extension rods to mid-height of the ceramic filter before installation, followed by a level survey of the former before withdrawal. The installations on the trial bank section lines were in near vertical sets (the boreholes were 500mm apart) of three at approximately 1.50, 3.50 and 5.50m depth. Having installed the piezometer tip the short lengths of tubing were uncoupled and connected up to the main lengths which led, via a common trench to the gauge house. The positions of the trenches for the piezometer tubing (figure 4.1) were given careful consideration, especially for the multi-stage construction of Bank 1. Prior to installation a colour coding system was devised to individually label each pair of tubes at regular intervals. This is obviously necessary to avoid confusion during the installation of such a large number (75) of piezometers, and is also invaluable when damage necessitates excavation and repair of tubing (McKenna and Roy, 1973).

Having placed the tubes loosely in the trenches, leaving loops of tubing at sub-surface coupling positions, and made the connections at the gauge house the trenches were carefully backfilled and

compacted. This installation procedure appears to have been perfectly satisfactory, although one improvement could be advocated. That would be to de-air the tubing from the gauge house prior to connection to the piezometer tubing and, possibly, as suggested by Wilkes (1970), to de-air the tips at the same time as the connections were being made.

Five Casagrande standpipe piezometers, comprising low air-entry value ceramic filters (permeability 3×10^{-4} m/s) and 19mm I.D., 26mm O.D., rigid P.V.C. standpipe tubing were installed in 150mm diameter shell and auger boreholes. The 50mm diameter by 250mm long piezometer tips were installed in 1m long sand pockets, following standard practice, to monitor pore pressures in the gravel layer, as described in section 2.5.

Finally five Bishop piezometers (Bishop et al, 1960), comprising 100mm long, tapering from 50 to 38mm diameter, high air-entry value ceramic filters* located between brass end caps, were installed at varying depths in the soft clay layer to monitor seasonal fluctuations in ground-water conditions (also as discussed in section 2.5). Installation was in 102mm diameter hand-augered boreholes, using the same placing technique as for the 'push-in' piezometers.

All the piezometer tubes terminated in a wooden gauge house (figure 4.1); the tubing was brought into the gauge house via 350mm P.V.C. ducts which were finally backfilled with sand. The latter is particularly important in order to prevent animals from damaging the tubing or entering the

*properties as for the filters of the 'push-in' piezometers.

gauge house. In a similar installation at the site a ferret was found to have taken up residence after gaining entry via the piezometer ducts, and was observed listening intently to a discussion on constant head permeability tests!

The individual lines from the piezometers terminated in a standard busbar (1.6mm I.D. stainless steel tubing) layout incorporating Hoek zero volume change valves, a header tank, back-pressure unit, transducer and read-out unit. De-airing facilities were provided by a semi-automatic unit which could circulate a predetermined volume of de-aired water through a piezometer at selected constant values of pressure and vacuum.

5.5.2. De-Airing

(i) General Concepts

In theory the aim of de-airing is the circulation of de-aired water around the piezometer system at constant velocity and with no flow into the ground (Little and Vail, 1960), such that contact is established between the air-free water in the measuring system and the pore water in the soil. As pointed out by Vaughan (1973(c)) it is desirable to maintain a small excess head at the tip to avoid drawing in gas-saturated water from the soil, and to avoid excessive pressure reductions which could lead to cavitation in the leads. The difficulties associated with successful de-airing of a particular system are mainly a function of the relative elevations of the gauge house and the tip, and the existing total stresses and pore pressures at the tip. Vaughan (1973(c))

has illustrated the typical situation for an embankment dam where the gauge house is below tip level. For foundation piezometers, as at Mucking, the reverse was true and the relatively low in-situ total stresses meant that hydraulic fracture was a possibility at small excess pressures.*

Figure 5.5.1.(A) shows the relative positioning of a typical piezometer to gauge level at Mucking, and the pressures involved in de-airing. Considering the following notation:-

- Δh = head difference (gauge level - tip level)
- h_w = head of water at tip = u_o/γ_w
- P_H = pressure head on inflow side of de-airing unit
- v_H = vacuum head on return side of de-airing unit
- F_{OUT}, F_{IN} = outward/inward friction head losses in piezometer tubes
- v = velocity of flow through the system (= constant); the de-airing

process can be considered in terms of Bernouilli's equation. Thus for the inflow side:-

$$P_H + \Delta h + v^2/2g = h_w + F_{IN} + v^2/2g \dots\dots\dots(5.5.1.)$$

and for the outflow side:-

$$h_w + v^2/2g = F_{OUT} + \Delta h + v^2/2g - v_H \dots\dots\dots(5.5.2.)$$

where 'g' is gravitational acceleration. As the velocity is assumed constant and the inflow and outflow distances are equal F_{IN} can be equated to F_{OUT} and thus solving for equations 5.5.1. and 5.5.2. leads to:-

$$P_H = 2(h_w - \Delta h) + v_H \dots\dots\dots(5.5.3.)$$

Equation 5.5.3. thus represents the relationship between pressure head, vacuum head, pore pressure and elevation difference for de-airing of a

*this is further discussed in section 5.5.6.(iv).

piezometer below gauge level, with zero flow into the ground. It is necessarily approximate when applied to the flow of air/water mixtures through small bore tubing.

(ii) De-Airing Under Initial Hydrostatic Conditions

The ground-water conditions prevailing during initial de-airing of the piezometers were approximately as shown in figure 5.5.1. with $h_w - \Delta h = \text{constant} = -2.25\text{m}$. Thus from equation 5.5.3:-

$P_H = -4.50 + v_H$ i.e. the magnitude of the vacuum head needed to be 4.50m greater than the pressure head. This situation is represented by the solid lines in figure 5.5.1.(B) with de-airing being carried out by the application of a vacuum head of 4.50m to the return limb, whilst opening the inflow limb to atmospheric pressure at gauge level. However, as stated previously a small flow into the ground is desirable, but in a situation such as is illustrated in figure 5.5.1. care must be taken to avoid hydraulic fracture. For the minimum piezometer depth of 1.5m, figure 2.13 shows p_o to be 22.5 kN/m^2 and p_o' , with the G.W.L. at 1m depth, was therefore 17.6 kN/m^2 . Assuming K_o to be 0.55 leads to $\sigma_H' = 9.7 \text{ kN/m}^2$ and $\sigma_H = 14.6 \text{ kN/m}^2$. Thus an increase in pressure at the tip of 9.7 kN/m^2 (or approximately 1m of water) would produce a cavity pressure equal to the total lateral stress. An additional problem is that the vacuum head of 4.5m, applied as in figure 5.5.1.(B) could well result in air coming out of solution in the return limb.

In such circumstances de-airing is best carried out by opening the inflow limb to atmospheric and applying a smaller vacuum to the outflow limb, as depicted by the hatched lines in figure 5.5.1.(B) wherein a

vacuum head of 2.5 m has been applied resulting in an excess head (Δh_w) of 1m. De-airing using small pressure differences is time consuming and the semi-automatic unit used at Mucking was particularly valuable in this respect. Inflow could have been achieved by simply connecting to a bucket of water at gauge level; in fact a small pressure (about 1m head) was applied using the de-airing unit, and an outflow vacuum head of about 2.5m. There was thus a danger of hydraulic fracture occurring at the near surface tips, although the likelihood of K_0 values in excess of 0.55 (figure 2.13) reduced this possibility. In addition data presented by, among others, Al-Dhahir (1967), Bjerrum et al (1972), Penman (1975) and Walbancke (1976) indicate that such an occurrence should not influence subsequent pore-pressure readings at the tip once the excess pressures so generated have dissipated.

De-airing of all 75 piezometers initially installed was completed between 1 and 2 months prior to construction. Other than some problems associated with the de-airing unit* in the early stages the operation was successfully completed without undue difficulty. De-airing of the water was carried out by boiling, followed by cooling under a vacuum, a process which should lead to a dissolved oxygen content of between 2 and 5 p.p.m. (Gould and Dunicliff, 1971).

(iii) De-Airing During and After Construction

The pressures for zero flow into the ground were calculated using equation 5.5.3., incorporating the new pore pressures at the tips.

*in addition this unit was not well suited for use at low values of pressure and vacuum head.

As the pressure heads rose above gauge level, the pressure head required for de-airing becomes greater in magnitude than the vacuum. De-airing could then be carried out using a small pressure increase and zero vacuum, or a small back pressure, in the return limb.

5.5.3. Response Times

(i) General

The hydraulic response time of a piezometer system may be defined as the time required for the soil to furnish the necessary amount of water to change the initial pressure in the system to that of the soil's pore pressure. It has been considered analytically by Hvorslev (1951) and Gibson (1963), investigated experimentally by Penman (1960) and reviewed by Bishop et al (1969) and Vaughan (1973(a)).

Penman (1960) installed various piezometer tips in saturated remoulded London Clay, to which known increments of all round total stress were applied. The intake and volume factors of the various systems tested were determined and the theoretical response times calculated using Hvorslev's (1951) formulation for an incompressible soil. Comparison of these values with the observations showed that although good agreement was achieved at high degrees of equalisation (95%+), the predicted values were otherwise much slower. Gibson (1963) provided the theoretical explanation for these observations in his solution for the response times of piezometers installed in compressible media, using Terzaghi's (1943) one-dimensional consolidation theory.

The relationship between degree of equalisation and time elapsed, derived from either theory, is for the situation where the water pressure in the cavity is initially different from the correct pore pressure in the ground. However, initially the pore pressure in the ground will have been altered by the installation of the instrument, resulting in a stress-adjustment time lag (Hvorslev, 1951), and, as has been indicated previously, by subsequent de-airing. These factors influence the time required for the piezometer cavity to register the true pore-water pressure as not only has the cavity pressure to equalise but so has the perturbed pore pressure around the cavity. If equalisation of the perturbed pore pressure is slow initial erroneous pore pressures will be recorded.

Soderberg (1962) considered the equalisation of a perturbed pore-pressure zone around an expanded impermeable cylinder (this being analogous to the installation of a 'push-in' piezometer, although the latter is permeable) and found 95% equalisation at the cylinder radius to correspond to a time of $30r_p^2/C^*$ (where r_p is the radius of the cylinder). That initial equalisation of pore pressures can be dominated by reconsolidation (or swelling) of the perturbed zone around the piezometer was realised by Hvorslev (1951). This is particularly important for compressible soils and rapidly responding measuring systems (Walbancke, 1976).

During construction, pore pressures around the tip may be different from the correct pore pressure in the soil because of the different total stresses set up around the tip. Vaughan (1973(a)) considered that the changes in average total stress are probably small compared

*C = C_v or C_s

to the changes in the principal stresses, and that the effects on pore pressures around the piezometer tip are correspondingly small. Examination of the effect of a rigid impermeable spherical inclusion in an infinite elastic medium led Sandroni (1977) to suggest that equalisation of the perturbed pore pressures in this case may be approximately 15 times quicker than for that considered by Soderberg (1962).

The theories thus apply to idealised situations, but Penman's (1960) work enables evaluation of ultimate response times to proceed with some confidence.

For the rapid construction of trial (or prototype) embankments under undrained conditions, such as were anticipated at Mucking, rapid response* of the piezometer system is required so that pore pressure/total stress relationships can be established and stability analyses performed in terms of effective stresses. Response of the in-situ pore pressures to total stress changes is commonly assumed to be instantaneous; however, if the development of undrained shear strains is time dependent (as was suggested in section 3.4), then so will be the generated pore pressures. Thus another uncertainty is introduced into the measurement of pore pressures.

When large numbers of piezometers have to be frequently monitored it is also very important that the response of the measurement side of the system is very rapid when connected to an equalised piezometer. There were 54 piezometers installed for Bank 1 and thus the response of the measuring system needed to be of the order of 1 minute.

*better than 1 hour.

The piezometers in the foundation beneath and adjacent to Banks 2 and 4 were required to monitor not only the pore pressures during construction (undrained loading) but also those during the consolidation of the foundation. In this case, as opposed to that of undrained loading, the rate of change of pore pressure as well as the piezometer's response time is governed by the soil's compressibility and permeability. Thus any time lag during the drainage period is mainly a function of the piezometer's intake and volume factors. As long as it has not been installed close to a drainage boundary, where pore pressure changes may be quite rapid, an ordinary standpipe piezometer would be adequate for monitoring consolidation pore pressures (Vaughan, 1973(a)).

There were 9 piezometers beneath Bank 2 and 12 beneath Bank 4, as well as the 5 installed to monitor seasonal ground-water movements. Thus, although the requirements with regard to response of the piezometer cavity and tubing were not so demanding as for Bank 1, it was still desirable to have a rapidly responding measuring system.

(ii) Calculation From Theory

The basic theories presented herein relate to the response time resulting from hydraulic time lag only.

(a) Incompressible Soil (Hvorslev, 1951)

A piezometer element was considered, having an intake factor 'F' installed in a saturated incompressible soil, the initial cavity pressure being different to that of the adjacent ground-water. Darcy's Law was used to determine the rate of flow to or from the cavity, which was taken

to be sufficiently small to prevent drawdown of the phreatic surface.

Thus:-

$$Q = F.k. h_{wt} \dots\dots\dots(5.5.4.)$$

where 'Q' is the flow to, or from, the piezometer cavity; h_{wt} is the head difference between the piezometric level and G.W.L. after time 't' since the start of the equalisation process.

In a time interval 'dt' the flow into the piezometer standpipe (area 'a') is thus:-

$$Q.dt = a(-dh_w)^* \dots\dots\dots(5.5.5.)$$

which from equation 5.5.4. leads to the basic differential equation governing equalisation:-

$$\frac{-dh_w}{h_{wt}} = \frac{F.k dt}{a} \dots\dots\dots(5.5.6.)$$

At time 't' the total volume of flow required for equalisation of the head difference h_{wt} is $a.h_{wt}$, and Hvorslev defined the basic time lag T_L as the time required for equalisation of this head difference if the corresponding flow rate was maintained. Thus:-

$$T_L = \frac{a.h_{wt}}{F.k.h_{wt}} = \frac{a}{F.k} \dots\dots\dots(5.5.7.)$$

and from equation (5.5.6.)

$$\frac{-dh_w}{h_{wt}} = \frac{dt}{T_L} \dots\dots\dots(5.5.8.)$$

*considering flow into the piezometer, and taking the G.W.L. as datum for head measurement and +ve downwards.

which leads directly to:-

$$\frac{h_{wt}}{h_{wt=0}} = e^{-\frac{t}{T_L}} \dots\dots\dots(5.5.9.)$$

Hvorslev defined the equalisation ratio (E_H) as follows:-

$$E_H = \frac{h_{wt=0} - h_{wt}}{h_{wt=0}} = 1 - e^{-\frac{t}{T_L}} \dots\dots\dots(5.5.10)$$

and termed $\frac{h_{wt}}{h_{wt=0}}$ the head ratio.

(b) Compressible Soil (Gibson, 1963)

A spherical piezometer element of radius r_p was considered to be installed in a saturated homogeneous isotropic soil obeying Terzaghi's (1943) one-dimensional consolidation theory. The permeability of the tip was taken to be large compared to that of the soil, and the depth of installation to be similarly large in comparison to r_p (which includes the dimensions of any sand or Plaster of Paris around the tip, as does 'F'). In common with the Hvorslev formulation the initial cavity pressure is different to that of the adjacent ground-water, but in contrast the radial variation of pore pressure (u_{rt}) is now a function of the radial distance from the tip (r), and the time elapsed since the start of the equalisation process (t), and is governed by the spherically symmetrical form of the consolidation equation as follows:-

$$c \left(\frac{\delta^2 u}{\delta r^2} + \frac{2}{r} \frac{\delta u}{\delta r} \right) = \frac{\delta u}{\delta t}, \quad r > r_p^* \dots\dots\dots(5.5.11)$$

* $c = c_v$ or c_s

with the following boundary conditions:-

1. as $r \rightarrow \infty$, $u \rightarrow u_0$
2. $u = u_0$ at $t = 0$ for $r > r_p$
3. $u(r_p, t) = \gamma_w (h_{wt=0} - h_{wt})$ for $t > 0$

Flow at the tip can again be expressed in terms of Darcy's Law, assuming continuity between the tip and the soil, as follows:-

$$4\pi r_p^2 \frac{k}{\gamma_w} \left(\frac{\delta u}{\delta r} \right)_{r=r_p} = a \left(-\frac{dh_w}{dt} \right)^* \dots\dots\dots(5.5.12)$$

Gibson defined the equalisation ratio as follows:-

$$E_G = \frac{h_{wt}}{h_{wt=0}} \quad (\text{which is Hvorslev's head ratio}) = 1 - E_H \dots\dots\dots(5.5.13)$$

and solved for E_G such that $E_G = f(\mu, T)$, where μ characterises the stiffness of the soil/piezometer system as follows:-

$$\mu = \frac{4\pi r_p^3 M_V \gamma_w}{a} \dots\dots\dots(5.5.14)$$

and 'T' is the time factor. The relationship between E_G , μ and 'T' is expressed graphically in figure 4 of Gibson's paper, so that response times can be predicted. For an incompressible soil $M_V = \mu = 0$ and the formulation reverts to that of Hvorslev (1951).

When a closed piezometer system is used the volume change required for equalisation is represented by the volume factor 'V', defined as the volume change of the system per unit pressure increase. Thus $a = V \cdot \gamma_w$ and equations 5.5.7. and 5.5.14 respectively become:-

*same flow conditions and nomenclature as for Hvorslev.

$$T = \frac{V_{Y_W}}{F \cdot k} \dots\dots\dots(5.5.7.(a))$$

$$\text{and } \mu = \frac{4\pi r_p^3 \cdot M_V}{V} \dots\dots\dots(5.5.14(a))$$

and for rapid response of a closed system the requirements are:-

1. large intake factor (or equivalent spherical radius)
2. low volume factor
3. high consolidation/swelling coefficient, implying a high 'k' and low M_V (equation 2.1).

(iii) Intake Factors and System Flexibility

(a) Intake Factor

A knowledge of the piezometer's intake factor, as defined by equation 5.5.4., and reflected by the $4\pi r_p^3$ term in equation 5.5.14(a), is necessary for the determination of response time and/or permeability from in-situ tests. Equation 5.5.4. shows the intake factor to reflect the influence of the piezometer's physical dimensions on the flow into or out of the cavity. A number of flow situations may be envisaged at the intake (Al-Dhahir, 1967), broadly grouped as follows:-

1. Steady State
 - constant head, incompressible soil
 - constant head, compressible soil after long time interval.
2. Unsteady State
 - constant head, compressible soil
 - varying head, compressible soil
 - varying head, incompressible soil

The intake factor for a cylindrical cavity of finite dimensions, forming an extension to a lined borehole installed in a saturated incompressible medium, under steady state conditions was derived by Dachler (1936), and presented by Hvorslev (1951), together with the approximating assumptions, as follows:-

$$F = \frac{2\pi L}{\log_e \left[\frac{L}{D} + \sqrt{1 + \left(\frac{L}{D}\right)^2} \right]} \dots\dots\dots(5.5.15.)$$

where 'L' is the length, and 'D' the diameter, of the intake.

Al-Dhahir (1967) compared numerical, analogue and approximate analytical solutions for the intake factor of a finite length cylinder with one or both ends impermeable, and with or without an impermeable borehole above the cylinder. Little difference was found between these steady state solutions and that of Dachler (1936).

The intake factors for a spherical cavity and an infinitely long sand drain in an incompressible medium under steady state conditions can be derived directly by solution of the Laplace equations governing flow, together with the appropriate boundary conditions (Al-Dhahir, 1967).

The solution for the spherical tip is as follows:-

$$F = 4\pi r_p \dots\dots\dots(5.5.16.)$$

Al-Dhahir (1967) also numerically analysed unsteady flow into finite length cylindrical cavities and spherical cavities in a compressible medium. The results indicated that the flow into a cylindrical cavity was almost identical to that into a spherical cavity of the same surface area. This result was found to hold for constant head conditions

regardless of L/D, but for varying heads only if L/D < 4. As L/D increased above 8 the intake factor of the cylinder approached that of an infinite sand drain. Wilkinson (1968) also presented a numerical solution to this problem, which showed that $F = 4\pi r_p$ could be taken as $F(\text{cylinder})$ in Gibson's (1963) equation (5.5.14(a)) for isotropic conditions and L/D < 4.

The intake factors for the site piezometers (L/D < 4) could thus be calculated using equation 5.5.15, or 5.5.16 with r_p being the radius of an equivalent surface area sphere (Al-Dhahir, 1967) or radius of an equivalent spherical intake (Wilkinson, 1968), as shown in table 5.5.1.

Thus far conditions of isotropic permeability have been considered whereas the laboratory data (section 2.4.3.) indicated that $k_v/k_H = 2$. At the in-situ stress levels C_{v1} was $63\text{m}^2/\text{year}$ and M_{v1} was $4.6 \times 10^{-4} \text{m}^2/\text{kN}$ (section 2.6) for vertical samples. From equation 2.1. $k_v = 9 \times 10^{-9} \text{m/s}$ and therefore $k_H = 4.5 \times 10^{-9} \text{m/s}$. For steady state conditions and an incompressible soil, anisotropic permeability can be taken into account in the derivation of the intake factors by the use of transformation factors (Taylor, 1948; Hvorslev, 1951). The intake factor for the cylindrical tip becomes:-

$$F = \frac{2\pi L}{\log_e \left[\frac{m \cdot L}{D} + \sqrt{1 + \left(\frac{mL}{D} \right)^2} \right]} \dots\dots\dots (5.5.17.)$$

*i.e. $r_p \equiv F(\text{cylinder})/4\pi$

and for the spherical tip:-

$$F = \frac{4\pi r_p}{\log_e \left[m + \sqrt{1 + m^2} \right]} \dots\dots\dots(5.5.18.)$$

where $m = \sqrt{k_H/k_V}$ and in both equations equation 5.5.4. becomes

$Q = F \cdot k_H \cdot h_{wt}$. Intake factors and equivalent radii for $k_V/k_H = 2$ have been derived and are presented in table 5.5.1.

PIEZOMETER TYPE		'PUSH-IN'		BISHOP	
Length (L)	mm	125		100	
Diameter (D)	mm	38		44(mean)	
L/D		3.3		2.3	
k_V/k_H		1	2	1	2
F(Cylinder)	mm	412	497	403	502
r_p corresponding to F_{CYL}	mm	32.8	26.0	32.1	26.2
r_p of equiv. surface area sphere	mm	34.5	34.5	33.2	33.2
F (Sphere)	mm	433	658	417	634

Table 5.5.1

Intake Factors for Cylindrical and Spherical Intakes

The equivalent surface area sphere representation (Al-Dhahir, 1967) can be seen, as would be expected, to only apply for the isotropic case.

(b) System Flexibility

(1) Volume Factor for Polythene Coated Nylon 11 Piezometer Tubing

$V = 4.9 \times 10^{-11} \text{ m}^3/\text{kN/m}^2/\text{m.run}$ (Penman, 1960; Al-Dhahir, 1967)

(2) Volume Factor for Stainless Steel Busbar Tubing

$$V = 9.1 \times 10^{-13} \text{ m}^3/\text{kN/m}^2/\text{m.run. (Bishop and Henkel, 1962*)}$$

(3) Volume Factor for Transducer

$$V = 4.7 \times 10^{-17} \text{ m}^3/\text{kN/m}^2 \text{ (Bishop and Henkel, 1962)}$$

(iv) Calculation of Theoretical Response Times

(a) 'Push-In' Piezometers to Hoek Valves

(1) Incompressible Soil - Isotropic Permeability ($=k_v$)

'V' for 2 x 100m of piezometer tubing = $9.8 \times 10^{-9} \text{ m}^3/\text{kN/m}^2$. Using equation 5.5.7.(a), $T_L = 26$ seconds and thus:-

$$E_H = 95\%, \quad t = 3 T_L = 78 \text{ seconds}$$

$$E_H = 99\%, \quad t = 4.6 T_L = 120 \text{ seconds}$$

(2) Incompressible Soil-Anisotropic Permeability ($k_v/k_H = 2$)

Using equation 5.5.7(a), $T_L = 43$ seconds and thus:-

$$E_H = 95\%, \quad t = 129 \text{ seconds}$$

$$E_H = 99\%, \quad t = 198 \text{ seconds}$$

(3) Compressible Soil-Isotropic Permeability ($=k_v$)

Using equation 5.5.15(a) with $r_p = 32.8\text{mm}$ and $M_{v1} = 4.6 \times 10^{-4} \text{ m}^2/\text{kN}$

$\mu = 21$. From figure 4 of Gibson's (1963) paper:-

$$E_G = 5\%, \quad T = 1.3 \times 10^{-1}; \quad t = 70 \text{ seconds} \dagger$$

$$E_G = 1\%, \quad T = 7 \times 10^{-1}; \quad t = 377 \text{ seconds} \dagger$$

*the value is in fact for the same diameter copper tubing; the authors state that the volume change is largely due to the compressibility of water
†assuming $C_v = 63\text{m}^2/\text{year}$.

There is no evidence to suggest that the anisotropic spherical radii, corresponding to F_{CYL} , derived in table 5.5.1. are applicable in other than steady state conditions.

The calculated theoretical response times of the piezometers can be seen to be excellent; values for the Bishop tips are comparable to those for the 'push-in' variety. It is interesting to note that the anisotropic permeability analysis predicts a longer response time ($\times 1.65$) due to the influence of k_H on flow into a cylindrical cavity (Wilkinson, 1968). Agreement between the Hvorslev (1951) and Gibson (1963) formulations is very good at 95% (E_H) equalisation, but the latter predicts 3 x longer is required for 99% equalisation. This is consistent with the different assumptions made in the analysis (Gibson, 1963).

(b) Busbar System and Transducer

'V' for 2m of stainless steel tubing between the Hoek valve and the transducer is $1.82 \times 10^{-12} \text{ m}^3/\text{kN/m}^2$, compared to which the volume factor of the transducer is negligible. When the zero volume change Hoek valves are opened in order for the pressure response to travel from the valve to the transducer, water must enter the tip from the ground at a rate governed by the consolidation/swelling characteristics of the soil. However, only the section of the system between the valve and the transducer is not at the same pressure as the ground-water, so that only this part is subjected to further volume change.

(1) Incompressible Soil-Isotropic Permeability ($=k_v$)

Using equation 5.5.7(a), $T_L = 0.005$ seconds and thus:-

$$E_H = 95\%, \quad t = 0.015 \text{ seconds}$$

$$E_H = 99\%, \quad t = 0.023 \text{ seconds}$$

(2) Compressible Soil-Isotropic Permeability ($=k_v$)

Using equation 5.5.14(a), $\mu = 110,000$, and from figure 4 of Gibson's (1963) paper:-

$$E_G = 1\%, \quad T = 35 \times 10^{-5}; \quad t = 0.19 \text{ seconds.}$$

Thus the response time of the measuring system was theoretically compatible with the rapid monitoring of a large number of piezometers.

(v) Summary

The overall predicted performance of the system has been shown to be more than adequate for the situation. However, the inclusion of gas in a piezometer measuring system causes large increases in response time (Vaughan, 1973(a)). The volume factor of 1cc of air is about $2.65 \times 10^{-9} \text{ m}^3/\text{kN/m}^2$, which is of the same order as 50m of piezometer tube; thus only 4cc of air in the system would approximately double the basic response time.

5.5.4. Site Procedure For Reading

The portable read-out unit was linked via D.I.N. plug connectors to the transducer: in common with all the digital read-outs it required a few minutes to warm up. During this warm-up period the busbar system was flushed with de-aired water. The unit was then set to zero and subsequently switched to read over the appropriate scale. The transducer was then checked by venting it to atmosphere at gauge level and also applying a known head from the header tank and checking the readings. Zero and span adjustments could be made to the transducer if required.

The piezometers were then read one limb at a time in the normal fashion. When the pattern of pore pressures was established after the first few readings the piezometers were read in order of decreasing head so that the pressure change in the busbar system between readings was small. This way it was hoped that even if a piezometer was responding slowly due to gas in the system, and thus read at a low degree of equalisation, the error would not be great. The lowest heads were read last to avoid air coming out of solution when the pressure in the system was tensile.

5.5.5. Measured Pore-Water Pressures

(i) Equalisation After Installation

An attempt to monitor the equalisation of the zone of perturbed pore pressure created by pushing the piezometers into the foundation (and by advancing the borehole and grouting it up) was made using the 'I' piezometers. These were installed fully de-aired and very close to the gauge house (figure 4.1): overall response time of 2 to 3 minutes could thus be anticipated. Soderberg's (1962) work indicates approximately 1.5 hours would be needed for 95% equalisation and 0.5 hours ($10 r_p^2 / C_v$) for 80% equalisation of the perturbed pore pressures. Figure 5.5.2. shows the results obtained which are rather inconclusive due to the lack of results between 1 and 16 hours after installation. However, it can be said that at worst the values predicted by Soderberg (1962) may be about an order of magnitude low, and at best may be a very good approximation to reality. In addition, on the basis of Sandroni's (1977) work the results suggest that the dissipation of pore pressures due to stress perturbations around piezometers may be very rapid.

(ii) Equalisation After De-Airing

The equalisation time after de-airing or carrying out an in-situ test depends on the period for which the excess or reduced head has been applied. In the limit, steady state conditions will be reached. When the flow of water to or from the tip is stopped and readings attempted a falling or rising head situation will develop until equalisation occurs, as demonstrated analytically by Gibson (1963). If, however, the estimated pore pressure is then applied to the tip, flow can occur both into the piezometer and into the ground (assuming an excess head exists around the tip). This reduction in drainage path length should significantly improve the equalisation time. Walbancke (1976) reported response times reduced by 1.5 orders of magnitude when using this procedure.

At Mucking it was never necessary to monitor pore pressures immediately after de-airing and no special procedures were adopted; however, the basic reading process tended towards such an approach.

(iii) Performance of the System

No attempt was made to monitor the response time of the overall system; however, after initial de-airing, the response of the measuring system was of the order of 10 to 15 seconds. With air in the system response times slowed appreciably, and this was found to be the best guide as to when de-airing was required. The difference in the head recorded in the two limbs of a piezometer was often negligible even when response times had lengthened enormously. This indicates that the gas was either in the piezometer cavity or in the form of bubbles within, but not continuous across the section of, the tubing. Fortunately this was not a common occurrence.

Initially, with near steady state conditions in situ, all the measurements were suctions at gauge level of about 2m (see figure 5.5.1.(B)). Under these sort of conditions some de-airing was anticipated until the heads became positive with respect to gauge level. George and Parry (1973) reported such occurrences under similar conditions, although this may have been partly due to the use of low air-entry value ceramic filters in soils containing methane.

No de-airing was deemed necessary during the construction of Bank 1, Stage 1. Those few piezometers which did show a slowing of response time were allowed a longer period (up to 15 minutes) than the standard 2 minutes for reading. As this was only necessary for a few tips it was considered preferable to de-airing and consequent disturbance of the in-situ pore-pressure regime.

Similarly no de-airing was carried out during Bank 1, Stage 2 construction although all the piezometers remaining in service were de-aired between the construction stages. De-airing was carried out during the long-term observations for Banks 2 and 4 as deemed necessary by slow response times or inconsistent readings, and occasionally as a matter of course.

Finally it is interesting to note that although the response time of the measuring system was very rapid (10 to 15 seconds at best) it was still nearly 2 orders of magnitude greater than predicted by Gibson's (1963) theory. Similar discrepancies have been noted in laboratory measurements (Maguire, 1975). According to Sandroni (1977) the major part of this increase in laboratory response time may be

attributed to the time required for flow through the piezometer ceramic.

(iv) Construction Pore Pressures

(a) Bank 1 (figures 5.5.3. to 5.5.5.)

The results have been plotted as piezometric elevations versus time with the fill elevation above the middle piezometer in each vertical group of three superimposed on the plots. Where the fill elevation above each tip is different (i.e. beneath the embankment slopes) this involves a maximum inconsistency for the other two tips of $\pm 250\text{mm}$ of fill. Individual fill elevations were not plotted in order to avoid further complication of the figures. In general the results appear very consistent in relation to the construction sequence. Some slightly erratic behaviour can be observed in the response of PA/B 1 to 3 and 22 to 24; the piezometric level at these positions was generally such that there was tension in the measuring system. The only piezometer not to function throughout Stage 1 was PA1 which was damaged during the excavation of the toe trench, although PA18 (and PA21 to some extent) recorded values of pore pressure which appear low. Response times of the latter were also slow.

Only 6 piezometers (PA/B 10 to 12) were lost during the Stage 1 failure and a further 6 (PA/B 13 to 15)* during the Stage 2 failure, demonstrating the robustness of the installations. As failure was approached in both construction stages a few selected piezometers were monitored on a day to day basis to see if any indications of failure would be provided by the measured pore pressures. The

* plus the duplicate piezometers PA28 to 30

selected piezometers were as follows:-

Stage 1 - PA1, 5, 7, 8, 9, 10, 21

Stage 2 - PA16, 17, 18, 19, 20, 24

The results for the duplicate piezometers (installed dry) PA25 to 30 have not been presented as they were indistinguishable from their counterparts on the 'A' section line (figure 4.3).

(b) Bank 2, Bank 4 (figure 5.5.6.)

The measured pore pressures all appear consistent with the construction process except for the low values recorded by PE9.

(v) Long-Term Observations - Bank 2, Bank 4 (figures 5.5.7. to 5.5.13)

These had been in progress for over two years at the time of writing and the observations appear to be, on the whole, consistent with all the piezometers still functioning*. Some fluctuations can be observed in the dissipation curves; these may possibly be due in part to changes in boundary conditions caused by the seasonal fluctuations in ground-water conditions and/or the performance of in-situ tests. The limited de-airing carried out does not appear to have had any significant influence on the measured pore pressures. All the piezometers were de-aired in November 1975 after the repairs to the gauge house installations. The seasonal pore-pressure observations have been discussed in Chapter 2.

*the gauge house was vandalised in the summer of 1975 but all the installations were subsequently repaired only to be completely destroyed the following winter.

(vi) Summary

The measurement of pore pressures was achieved with the minimum of trouble and, the plots indicate, to a reasonable degree of accuracy (possibly $\pm 100\text{mm}$). Continuous pore-pressure records were obtained during the construction, post-construction and post-failure stages of the various embankments, thus fulfilling the objectives of the installations.

5.5.6. In-Situ Permeability Tests

(i) General

Hvorslev's (1951) hydraulic time lag theory also enables the permeability, of incompressible soils, to be determined from in-situ rising or falling head tests. Equation 5.5.10 enables the calculation of T_L and equation 5.5.7.(a) can then be used to determine the permeability.

Gibson (1963) produced plots of E_G versus $\mu.T$ ($\mu = 0$ to 10) and E_G versus $\mu^2 T$ ($\mu = 2$ to ∞) which can be used as the basis for the analysis of in-situ variable head tests in compressible soils. The test results are plotted as E_G versus T and an overlay of Gibson's curves is used to determine μ and T by obtaining the best fit. Thus M_V (expansion or compression) $C_{V/S}$ and k can all be determined, in theory, from the results of variable head tests.

However a consideration of the mechanics of flow involved shows that the soil consolidates initially and then swells (rising head test), or swells initially and then consolidates (falling head test). Thus the theory, by assuming a constant value of C_V is more appropriate for overconsolidated clays ($C_V \neq C_S$) and falling head tests (swelling followed by reconsolidation).

The analysis of variable head tests in compressible soils is thus indirect and it may be difficult to achieve a good fit to Gibson's (1963) curves due to in-situ changes in 'C'. The analysis additionally requires a knowledge of the volume factor; if $\mu < 2$ it is found that the curves coincide with $\mu = 0$ at $E_H = 90\%$ so that Hvorslev's (1951) equations can be used to determine 'k'; although a value for 'V' is still required. These particular difficulties do not manifest themselves in the constant head test (C.H.T.), wherein a constant pressure head is maintained above or below the ambient value* at the tip and the changes in flow rate are observed over a period of time.

(ii) Theory for the Constant Head Test

In a saturated incompressible soil a constant head test is associated with steady state seepage conditions, and can be directly analysed in terms of Hvorslev's (1951) equation 5.5.4., wherein h_{wt} applies at any time after the start of the test.

The analysis of a constant head test in a saturated compressible soil was performed by Gibson (1963) as follows:-

1. Equation 5.5.11. governs the variation of pore pressure in space and time, and boundary conditions 1. and 2. defined in sub-section 5.5.3.(ii)(b) still apply.
2. $u(r_p, t) = u_0 + \Delta u$ for $t > 0$ where $\Delta u/\gamma_w$ is the applied head change = h_w .

*generally above to avoid air coming out of solution during the test (Wilkinson, 1968; Raymond and Azzouz, 1969).

Equation 5.5.12 may be expressed as follows:-

$$Q_t = 4\pi r_p^2 \frac{k}{\gamma_w} \left(\frac{du}{dr} \right)_{r=r_p}$$

and Gibson showed that:-

$$u = u_0 + \Delta u \left(\frac{r_p}{r} \right) \operatorname{erfc} \left(\frac{r - r_p}{2\sqrt{Ct}} \right) \dots\dots\dots(5.5.19.)$$

where erfc is the complimentary error function (Carslaw and Jaeger, 1959)

$$= 1 - \frac{2}{\sqrt{\pi}} \int_0^r e^{-\left(\frac{r - r_p}{\sqrt{4 Ct}} \right)^2} \frac{1}{2\sqrt{Ct}} dr$$

Differentiation of 5.5.19 and substitution into 5.5.12 leads directly to:-

$$Q_t = 4\pi r_p \frac{k}{\gamma_w} \left(1 + \frac{1}{\sqrt{\pi T}} \right) \Delta u \dots\dots\dots(5.5.20.)$$

After a large time interval steady state conditions are achieved and:-

$$Q_{\infty} = 4\pi r_p \frac{k}{\gamma_w} \Delta u \dots\dots\dots(5.5.21.)$$

and equation 5.5.19 reverts to:-

$$u = u_0 + \Delta u \frac{r_p}{r} \dots\dots\dots(5.5.22.)$$

which describes the radial steady state pore-pressure distribution.

This solution suggested that, by plotting the results of a C.H.T. as Q_t versus $1/\sqrt{t}$, the coefficient of permeability could be found from the extrapolated intercept on the ordinate (Q_{∞}) and the coefficient of consolidation or swelling from the slope ($4\pi r_p^2 k/\gamma_w \Delta u/\sqrt{\pi C}$) of the linear relationship.

Gibson (1966) extended the analysis of the C.H.T. to include the influence of the permeability of the piezometer's ceramic filter and any surrounding filter material. This analysis showed that Q_t was also a function of λ where:-

$$\lambda = \frac{k}{k_c} \left(\frac{r_p}{r_c} - 1 \right) \dots\dots\dots(5.5.23.)$$

for the case of a piezometer cavity in direct contact with the soil, k_c being the ceramic permeability and r_c , the radius of the cavity.

A plot of Q_t/Q_∞ versus $1/\sqrt{t}$ for various values of λ (0 to 10) revealed that significant errors in permeability measurements would result if $\lambda > 0.2$ and that reliable estimates of 'C' are unlikely if $\lambda > 0.01$ to 0.02.

For a Bishop tip $\left(\frac{r_p}{r_c} - 1 \right) \approx 0.5$ and for the Mucking installations $k/k_c = 2.25 \times 10^{-1}$ (for $k = k_H$) and thus $\lambda = 0.1$. The piezometer tips were therefore considered permeable enough for permeability measurements* but not for estimating the value of 'C'. Gibson's (1966) data showed that as λ increases the time of running of the test needs to be increased to account for the curved nature of the Q_t vs $1/\sqrt{t}$ plot obtained, which would tend to result in over-estimation of the soil permeability. For a piezometer in a soil of comparable permeability Gibson (1966) extended his analysis to allow a corrected value of 'k' to be obtained. Such a formulation can also be used to indicate the influence of a smeared zone around a driven piezometer tip (Wilkinson, 1968).

*this was subsequently shown (section 6.3) to only be true for the permeability values post-construction and not for those relevant to the initial in-situ conditions or the early stages of construction.

However, actual test data (Wilkinson, 1968; Bishop and Al-Dhahir, 1969; Al-Dhahir et al, 1969; Wilkinson et al, 1969; Raymond and Azzouz, 1969) diverged from Gibson's (1963) theory in that curved Q_t vs $1/\sqrt{t}$ plots were obtained which could not be attributed to piezometer permeability effects. Gibson (1969, 1970) then extended the constant head theory by demonstrating that equation 5.5.20 was only applicable to elastic soils ($A = 0.33$), in which case the total-stress change in the soil caused by the application of the head change $\Delta u/\gamma_w$ at the piezometer tip did not generate any excess pore pressures.* Gibson (1970) also considered that the changes in σ_r and σ_θ (radial and hoop (circumferential) stresses) would be very small for a rigid tip in intimate contact with the soil, and Δu negative; and also for both $\pm \Delta u$ if a rigid piezometer tip was pushed into position (thus pre-stressing the soil) provided that the pore pressures so generated were allowed to dissipate and that $+\Delta u$ was not sufficient to cause hydraulic fracture. Thus in these cases the undrained pore pressures caused by the application of Δu would be small and equation 5.5.20 is valid.

Nevertheless for a borehole piezometer and $+\Delta u$ applied, positive pore pressures can be expected in a normally consolidated soil ($A \approx 1$) and negative pore pressures in an overconsolidated deposit ($A \approx 0$). For normally consolidated soils this means that a plot of Q_t vs $1/\sqrt{t}$ may predict reasonable values of 'k', even after a short time, but cannot be used to measure 'C'. In the case of overconsolidated soils although a reasonable estimate of the latter may be achieved after a short time,

*the original theory assumes there to be no total stress changes in the soil as a result of the induced pore-pressure change.

in order to get an accurate assessment of permeability C.H.T. s have to be run for a long time. In such soils variable head tests are less time consuming, being generally easier to perform than C.H.T. s, and should yield 'k' values of similar accuracy (Walbancke, 1976).

(iii) Test Procedure

A wooden staging was built on to the gauge house so that a large plastic tank (approximate capacity 100 litres) could be positioned to provide a constant head source at a number of elevations. The tank was connected to a triple burette system (total capacity 150ml) inside the gauge house by 6.35mm polythene piezometer tubing. This was connected to a junction block at the base of the burettes such that the constant head source could be applied upwards through the burettes or by-pass them and be linked directly into the return line of the busbar system. The constant head back-pressure unit was connected to the top of the burette system enabling pressure to be applied individually to each burette. The latter each had a paraffin/water interface to enable flow measurements to be made, and were connected to the inflow line of the busbar system.

In order to perform a C.H.T. the existing head at the piezometer was recorded in the usual way and the constant head tank adjusted to provide an excess head of about +1m. The excess heads were kept relatively small with the intention of avoiding hydraulic fracture (as outlined in section 5.5.2.) of the foundation (see also figure 5.5.1. and table 5.5.4.). The constant head tank was then connected into the return busbar system and the pressure head recorded by the

transducer. The back-pressure unit was adjusted to the same pressure and finally the constant head tank was switched to the return limb of the piezometer.

When a flow measurement was required the return limb of the piezometer was isolated from the constant head tank and the inflow limb switched so that flow to the tip was from the back-pressure unit, via one of the burettes. The flow through the burette was monitored for a period of between 5 and 60 minutes generally,* although flow periods of up to 1000 minutes were used after large time intervals. Tests were carried out over periods of 2 to 4 days, flow readings being commenced at the same time as the test. Flow of the interface was always downwards in the burettes, the total capacity of which was adequate for a single test. Having completed a measurement, flow was reverted to the constant head tank which could also be used to push the paraffin/water interfaces in the burettes back to the top against a reduced back pressure.

Measurements of volumetric flow could be interpolated to 0.05ml and flow rates were calculated to the nearest 0.001ml/minute. No allowance was made for any settling period after switching the flows although this was indirectly accounted for by the relatively long flow measuring intervals used with increasing time from the start of the test. The applied heads were regularly checked throughout the test period.

*increasing with time elapsed because of the decreasing flows.

(iv) Discussion of Results

C.H.T. s were carried out at 7 piezometer locations, 6 of these being beneath embankments 2 and 4 after the end of construction. The results are presented as plots of Q_t vs $1/\sqrt{t}$ (Gibson, 1963) and from these the extrapolated Q_∞ values have been used to calculate the permeability values summarised in table 5.5.4. The values range from 0.4 to 5.0×10^{-9} m/s with an average value of 1.6×10^{-9} m/s. This compares reasonably well with the laboratory value for k_H of 4.5×10^{-9} m/sec, but is nearly an order of magnitude lower than the laboratory value for k_V of 9×10^{-9} m/s, relevant to the initial in-situ effective stresses.

Use of equation 5.5.21 and an assumed k_V/k_H of 2 to predict the intake factor under steady state conditions produces a mean k_H of 1.3×10^{-9} m/s and hence a vertical permeability of 2.6×10^{-9} m/s. The in-situ permeability test using a cylindrical tip can be seen from these values of 'k'(mean) and k_H to yield permeability values in closer approximation to k_H in this instance. Wilkinson (1968) has shown that permeability anisotropy is only significant in the interpretation of results when the ratios k_H/k_V and L/D are both large (>4). The former is generally small unless the soil contains pronounced laminations (Raymond and Azzouz, 1969).

In many cases k_H may control consolidation (Wilkinson, 1968; Rowe 1972(a)), but at Mucking the higher vertical permeabilities, combined with essentially one-dimensional vertical consolidation (due to the thin clay layer) under the central areas of the embankments, meant that the laboratory permeability measurements on vertical samples could be considered more representative of prototype behaviour than typical in-situ permeability tests. The close

agreement between the laboratory and in-situ values of k_H reinforces the view that there is no horizontal fabric in the Mucking clay which could lead to more rapid pore-pressure dissipation than would be indicated on the basis of laboratory test results. The scatter in the permeability results of about an order of magnitude would not seem unreasonable for such an inhomogeneous deposit (Bjerrum et al, 1972). Smearing of the clay around the tips may have caused a slight reduction in permeability due to local destruction of the fabric (i.e. blocking drainage channels in the form of root holes).

Figure 5.5.17 shows the measured in-situ permeabilities plotted versus vertical effective overburden pressure at the tips, and as can be seen there is no apparent trend for 'k' to vary with effective stress over the fairly limited range of the latter.

The relationship between 'k', M_v , C_v and effective stress is of some importance with respect to the prediction of field behaviour. Whilst laboratory measurements of 'k' and C_v may often be inappropriate to the field situation (Rowe, 1968 and 1972(a)) field permeability tests in virgin ground relate only to relatively low values of effective stress. As 'k', M_v and C_v may all be significantly effective stress dependent (Wilkinson et al, 1969; Bishop and Al-Dhahir, 1969) such measurements may be of limited value (Wilkinson, 1968). As pointed out in Chapter 1 trial embankments form a valuable means of assessing laboratory and field permeability and compressibility data.

In Chapter 2 data were presented showing M_{V1} for the Mucking clay to increase from $4.6 \times 10^{-4} \text{ m}^2/\text{kN}$ to $1.2 \times 10^{-3} \text{ m}^2/\text{kN}$ when measured over effective stress increments of 15 - 30 kN/m^2 and 60 - 120 kN/m^2 respectively. The corresponding values of C_{V1} were 63 m^2/year and 4 m^2/year . Using equation 2.1., these values imply a reduction in k_v from 9 to $1.5 \times 10^{-9} \text{ m/s}$.* For relatively structureless soils M_v may decrease significantly with increasing effective stress whilst 'k' decreases rather less (in terms of order of magnitude) resulting in a slight increase in C_v (Bishop and Al-Dhahir, 1969). The behaviour of the Mucking clay is, in contrast, typical of a structured, lightly overconsolidated clay (Al-Dhahir et al, 1969) for which a significant decrease in permeability occurs with increasing effective stress as a consequence of a closing up of the structure. This is accompanied by an increase in M_v (when p_c' is exceeded) resulting in a significant decrease in C_v .

All of the permeability tests, except one, were carried out beneath embankments after the end of construction and the results indicate that sufficient pore-pressure dissipation had occurred for the effective stresses to exceed the preconsolidation pressure. It would thus appear that the measured permeabilities were not relevant to the initial in-situ effective stresses. Consideration of the total stress changes resulting from the construction of Banks 2 and 4, and thus a better assessment of the effective stresses at the piezometer locations, is given in Chapter 6. Wilkinson (1968) considered the influence of C_v , 'k' and M_v changing during a constant head test and concluded that Gibson's (1963) theory would produce average values for such a situation, and these would not be significantly in error.

*This latter value is thus very similar to the C.H.T. value of k_v of $2.6 \times 10^{-9} \text{ m/s}$ indicating that the vertical effective stresses in the field had exceeded p_c' at the time the C.H.T. s were performed, as is further discussed in section 6.3.

Returning to the Q_t vs $1/\sqrt{t}$ plots, these can be seen to take two distinct forms, as follows:-

1. For piezometers PI4, PE5, PE8, PC4 and PC5 the flows were very small and there was considerable scatter in the results. The latter was probably largely due to the flow measuring system being insufficiently sensitive for the measured quantities. The permeabilities recorded at these piezometers were between 0.4 and 1.1×10^{-9} m/s and, although the slopes of the 'best fit' straight lines were a matter of some conjecture the Q_∞ values were well defined because of the test duration, and the accuracy of the permeability values should not have suffered. No attempt was made to derive C_s values because of the scatter in the results, the low permeability of the piezometer ceramic (Gibson, 1966) and the general uncertainty regarding the slope of the Q_t vs $1/\sqrt{t}$ plot (Gibson, 1970).

2. For piezometers PE2 and PC6 the flows were much greater as were the slopes of the plots, and there was far less scatter in the results. Again, the latter may be attributed to the relationship between the flows and the sensitivity of the burette system. The permeabilities recorded at these tips were 2.8 and 5×10^{-9} m/s respectively.

The difference in the slopes of the plots for the two sets of data is consistent with a change in the pore-pressure response parameter, 'A' of the soil (i.e. steeper slope, lower 'A'; Gibson, 1970) but as the over-consolidation ratio of the clay appears to decrease with depth this explanation is not consistent with the elevation of the piezometers or the fact that they were pushed into place. The differences are also inconsistent with the effects of low ceramic permeability as predicted by Gibson (1966) and demonstrated by Walbancke (1976).

However, the increased slope of the Q_t vs $1/\sqrt{t}$ plots combined with higher measured permeabilities for the tests of PE2 and PC6 are similar to data presented by Wilkes (1974) for C.H.T. s in the soft alluvial clay at King's Lynn, where hydraulic fracture was thought to have occurred during the test.*

Bjerrum et al (1972) reported large increases in 'k' values (10^{-9} m/s to 10^{-6} m/s) determined from C.H.T. s when the ratio $\Delta u/p_{oi}$ ('i' denotes initial) exceeded values of 0.5 and 0.8 for the soft clay core of an embankment and a natural soft clay deposit respectively.

Furthermore the values of Δu appeared to be similar to the anticipated values of the minor principal effective stress (Bjerrum and Anderson, 1972). Laboratory tests showed that at a certain value of Δu a crack opened up along the minor principal plane, at which point there was a large increase in the flow from the tip.

Bjerrum et al (1972) analysed the hydraulic fracture situation by firstly considering the stresses set up by pushing the piezometer into position. They considered the effective stress changes to be as outlined in table 5.5.2. assuming no pore pressures to be generated during insertion† of the piezometer.

The values of α and β depend on E' , K_0 , ν and ϕ' , and for a highly compressible normally consolidated clay Bjerrum et al (1972) suggest $\alpha = 0.2$ to 0.4 and $\beta = 0.5$ to 1.1 . They then considered the application of an excess pressure ($+\Delta u$) at the tip as described in the following paragraph.

*although Wilkes considers this not to have affected the measured values of 'k'
†modelled as elastic, followed by plastic, expansion of a long cylindrical cavity.

	BEFORE INSTALLATION	AFTER INSTALLATION
σ_v'	p_o'	p_o'
σ_r'	$K_o p_o'$	$(1+\beta) K_o p_o'$
σ_θ'	$K_o p_o'$	$(1-\alpha) K_o p_o'$

Table 5.5.2.

Vertical (v), Radial (r) and Hoop (θ) Stresses in a Normally Consolidated Clay Before and After the Installation of a 'Push-in' Piezometer (after Bjerrum et al, 1972)

Gibson (1970) has previously indicated that, with the soil 'pre-stressed' in such a manner, the total stress changes prior to fracture would be small, and in addition that for a saturated isotropic elastic soil (as considered by Bjerrum et al (1972)) no undrained pore pressures would be set up by any total stress changes. Thus seepage occurs under the applied hydraulic gradient, with associated swelling of the clay and reduction in the effective radial and hoop stresses. If Δu is gradually increased until $\sigma_r' = 0$ (i.e. $\Delta u = \sigma_{rj}'$; $u = \sigma_{rj}$) the soil mass moves away from the tip and a cavity is formed. This is referred to as 'blow-off'. At this point a permeability test is still valid, providing that no preferential drainage paths are created and noting that the intake factor has increased to that of the cavity (Wilkes, 1974), and:-

$$\Delta u/p_o' = (1 + \beta) K_o \dots\dots\dots(5.5.24.)$$

Whether or not 'blow-off' occurs, at some value of $\Delta u / \sigma_{\theta}'$ becomes zero and a crack forms:-

$$\Delta u / p_0' = (1/\nu - 1) \left[(1 - \alpha) K_0 + \frac{p_t'}{p_0'} \right] \dots\dots\dots(5.5.25.)$$

where p_t' is defined as the maximum tensile effective stress the soil can sustain and:-

$\Delta u / p_0' \leq (1 + \beta) K_0$ which implies that fracture precedes 'blow-off.'

If the reverse is true then:-

$$\Delta u / p_0' = (1 - \nu) \left[(2 + \beta - \alpha) K_0 + \frac{p_t'}{p_0'} \right] \dots\dots\dots(5.5.26.)$$

The analysis assumed plane radial strain and indicated that the critical applied head at fracture was independent of E' . Equations 5.5.24 - 26 lead to the values of $\Delta u / p_0'$ presented in table 5.5.3. for a highly compressible soil and a driven piezometer, taking $\nu = 0.33$ (after Bjerrum et al (1972)) and $p_t' = 0$.

	EQN 5.5.24.	EQN 5.5.25.	EQN 5.5.26.
K_0	'Blow-off'	Fracture Before 'Blow-off'	Fracture After 'Blow-off'
0.5	0.8 - 1.0	0.6 - 0.8	0.7 - 1.0*
0.7	1.0	0.8 - 1.0*	1.0*

Table 5.5.3.

Values of $\Delta u / p_0'$ For 'Blow-off' and Fracture at a Driven Piezometer Location in a Highly Compressible Normally Consolidated Clay

*denotes horizontal crack.

A comparison of the values of $\Delta u/p_0'$ in table 5.5.4. with those in table 5.5.3. shows that on this basis the most likely test for fracture to have occurred in, was that on PC4, followed by PE2, PC5 and PI4 respectively. Of these only PI4 was not subjected to embankment loading conditions, and there is no evidence of fracture in the permeability test result (figure 5.5.14.). For the remainder of the piezometers K_0 conditions did not apply at the time of the permeability tests and values of $\Delta u/p_{oi}'$ and $\Delta u/p_0'$ cannot be related to the data in table 5.5.3.

The situation considered by Bjerrum et al (1972) was for a gradual increase in Δu , with a flow pattern into the soil being established at the time of 'blow-off' or fracture. If an excess pressure, greater than that required for fracture, was applied directly to a piezometer tip an undrained fracture would be expected upon opening the valve to the piezometer. This is the situation which is relevant for an excessively high head applied in a C.H.T.

Wilkes (1974) performed C.H.T. s with various applied heads and noted that above a certain value the relationship between Q_t and $1/\sqrt{t}$ changed from one very similar to that observed for PE5 (eg), to one very similar to that for PC6 (eg). However, there are important differences between Wilkes (1974) data and those for Mucking, these being as follows:-

1. When much higher initial flow rates, and steeper gradients of the Q vs $1/\sqrt{t}$ plots, were observed at King's Lynn, they were accompanied by an increase in the scatter of the results.

2. At a particular value of l/\sqrt{t} the plots changed gradient, becoming flatter*, and the results plotted much closer to a straight line.

Consistent values of 'k' were obtained from tests with both high and low applied heads. Wilkes (1974) postulated the formation of a crack at the high heads, and stabilisation of flow into the crack at the gradient change point. Such a stabilisation is only possible if the crack does not propagate to a free surface or more permeable zone.

By plotting excess head versus crack volume (obtained indirectly from the flow readings), or time to stable flow, Wilkes was able to determine the critical head at which a crack was just formed. He equated this to $K_0 p_0'$ (equations 5.5.24 - 25 with $\alpha = \beta = p_t' = 0$ and $\nu = 0.5$) and obtained K_0 values in good agreement with those obtained using the Camkometer (Wroth and Hughes, 1973). The results also agreed well with hydraulic fracture tests wherein the 'close-up' pressure was noted from falling head observations (Bjerrum and Andersen, 1972; Werneck, 1974; Penman, 1975).

(v) Summary

On the basis of the work carried out by Bjerrum et al (1972), Bjerrum and Andersen (1972), Wilkes (1974) and Penman (1975) there is no evidence to suggest that, where higher 'k' values were recorded, these were due to anything other than natural variations in the material. It is interesting to note the high values of $\Delta u/p_0'$ for PC4 which was 1.5m below O.G.L., beneath the centre of Bank 2. During construction

*the initial slope indicating a negative Q_t intercept.

K_0 would be expected to decrease towards K_a (coefficient of active earth pressure) for such a location and the fact that there is no evidence of hydraulic fracture at this tip suggests a high K_0 value as indicated in figure 2.13. For $\alpha = \beta = p_t' = 0$ and $\nu = 0.5$, the $\Delta u/p_0'$ value for PI4 shows that K_0 at a depth of 3m was greater than 0.5. Bjerrum and Andersen (1972) obtained in-situ K_0 values for a number of Norwegian 'normally consolidated' clays by equating the 'close-up' pressure to $\sigma_3 = \sigma_H$. Their results gave K_0 values of 0.6 to 0.8, whereas laboratory K_0 consolidation tests yielded values of 0.45 to 0.5. This agrees very well with the data for the Mucking clay presented in Chapter 2.

The accurate determination of permeability from C.H.T. s depends primarily on obtaining, or being able to extrapolate accurately to, steady flow conditions. Factors such as low ceramic permeability (Gibson, 1966), smear zones around the tip, head losses and/or gas within the system (Wilkinson, 1968) and excessive positive pressure increments (Wilkes, 1974) appear to be generally less influential on the result the longer the test is run. In this respect it is interesting to note that a large intake factor, whilst speeding up response time, increases the time necessary to achieve steady conditions in a constant head test (Bishop and Al-Dhahir, 1969). The test periods of up to 4 days used at Mucking were certainly beneficial in monitoring small flows and in the accurate determination of 'k'!

TIP NO.	INITIAL CONDITIONS AT TIP				CONDITIONS AT TIP AT TIME OF C.H.T.				TEST DATA			
	p_{oi}^{\dagger}	u_i	p_{oi}'	$K_o p_o'^*$	p_{ot}^{\dagger}	u_t	p_{ot}'	Δ_u^x	$\frac{\Delta_u}{p_{oi}'}$	$\frac{\Delta_u}{p_o' t}$	Q_{∞}	k
-	kN/m ²	kN/m ²	kN/m ²	kN/m ²	kN/m ²	kN/m ²	kN/m ²	kN/m ²	-	-	ml/min	m/s x 10 ⁹
PI4	45.75	24.62	21.13	11.62	45.75	24.62	21.13	+10.79	0.51	0.51	0.011	0.414
PE2	45.0	19.5	25.50	14.03	76.50	39.33	36.77	+17.95	0.70	0.49	0.125	2.76
PE5	45.0	19.52	25.45	14.01	88.75	50.03	38.72	+9.32	0.37	0.24	0.010	0.426
PE8	45.0	18.44	26.56	14.61	88.75	47.58	41.17	+11.28	0.42	0.27	0.030	1.06
PC4	22.50	8.34	14.16	7.79	71.5	44.05	27.45	+16.19	1.14	0.59	0.030	0.735
PC5	52.50	27.47	25.03	13.77	101.5	65.73	35.77	+13.93	0.56	0.39	0.021	0.598
PC6	82.50	46.89	35.61	19.59	131.5	85.94	45.56	+13.24	0.37	0.29	0.165	4.95

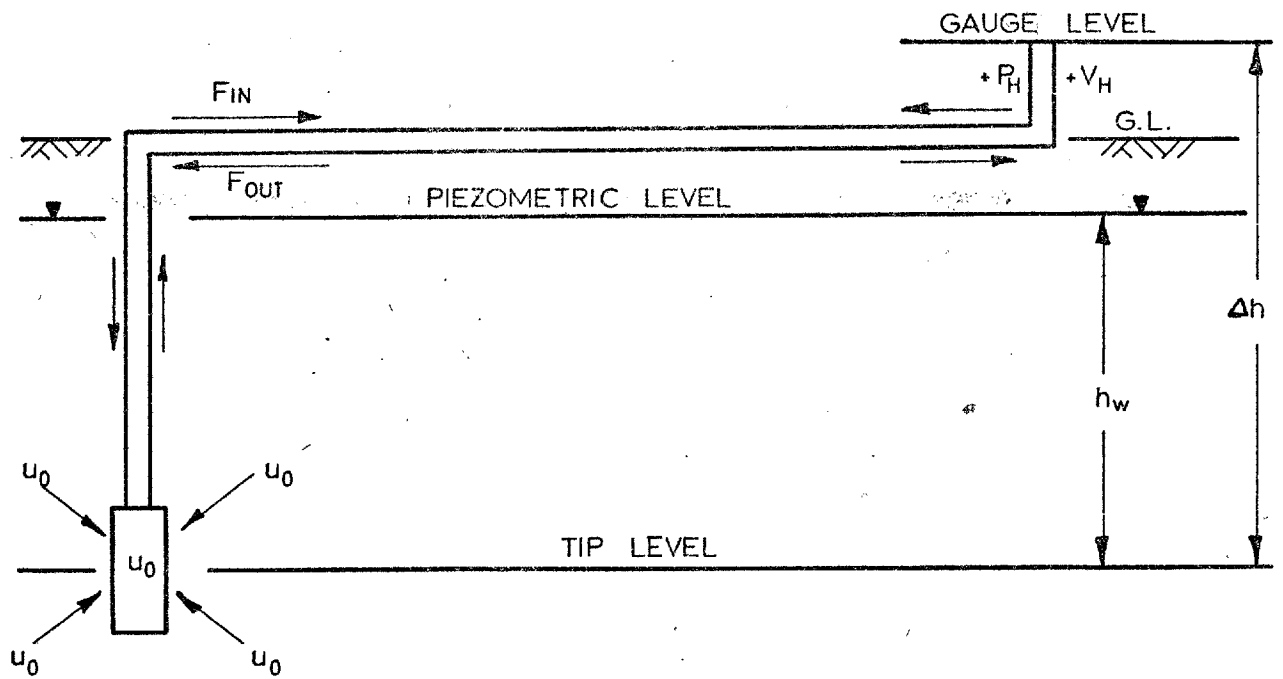
Table 5.5.4.

Results of Constant Head Permeability Tests

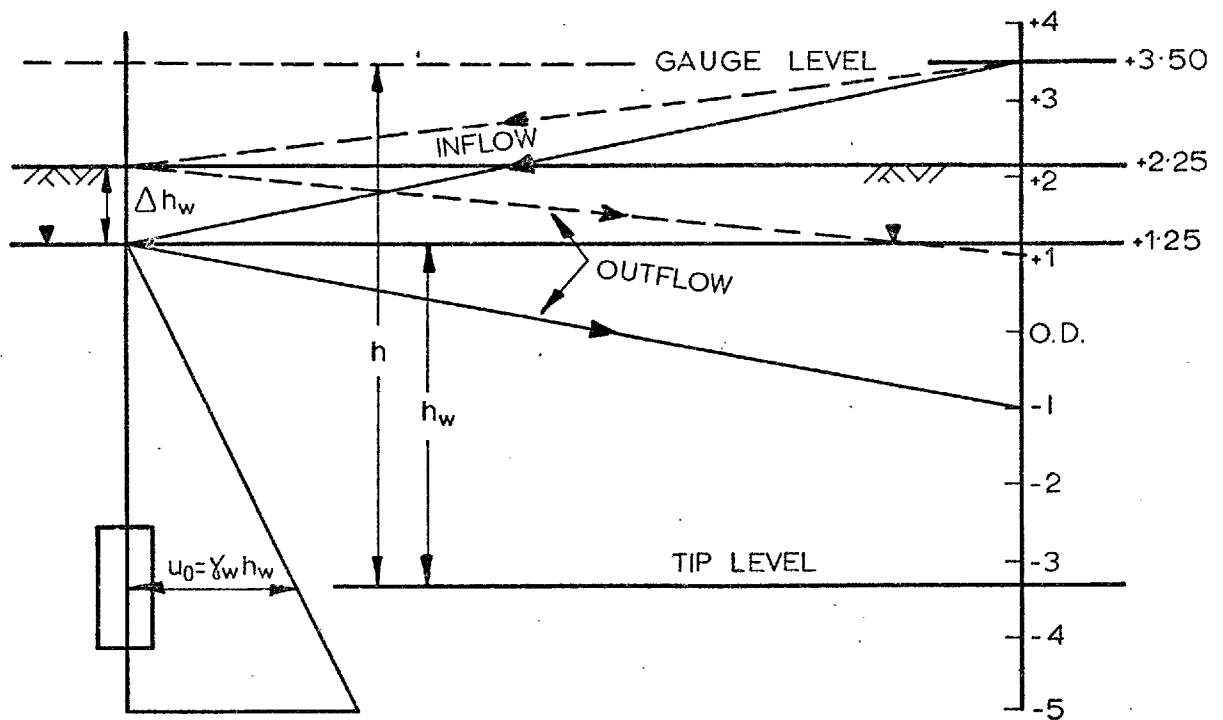
† p_o taken as $\Sigma \gamma h$ above tip

* K_o assumed = 0.55

x Δ_u = excess pressure applied at tip during C.H.T.



A) INITIAL DE-AIRING OF FOUNDATION PIEZOMETER



B) HEADS IN CIRCULATING TUBES DURING DE-AIRING

Fig.5.5.1

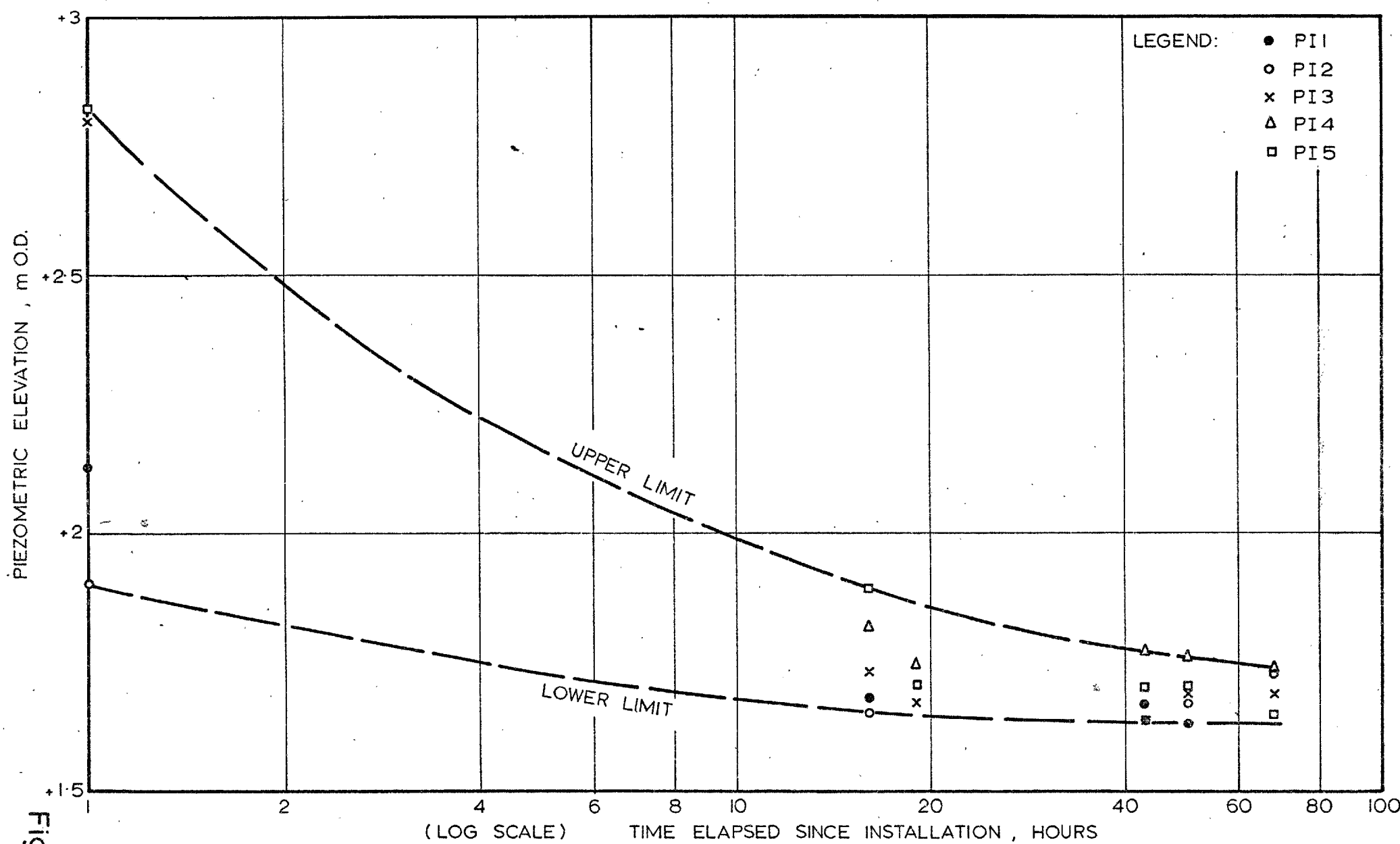
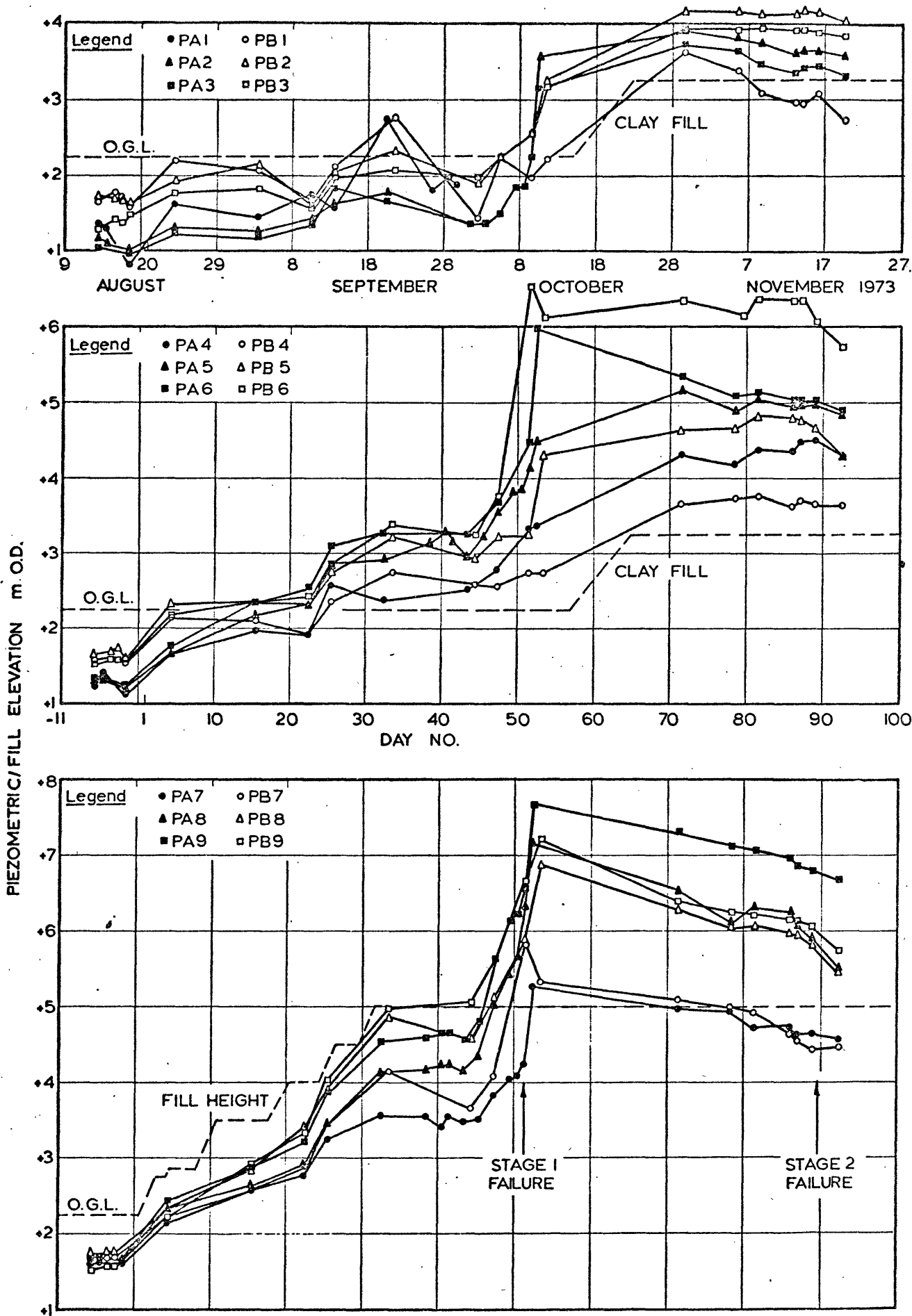


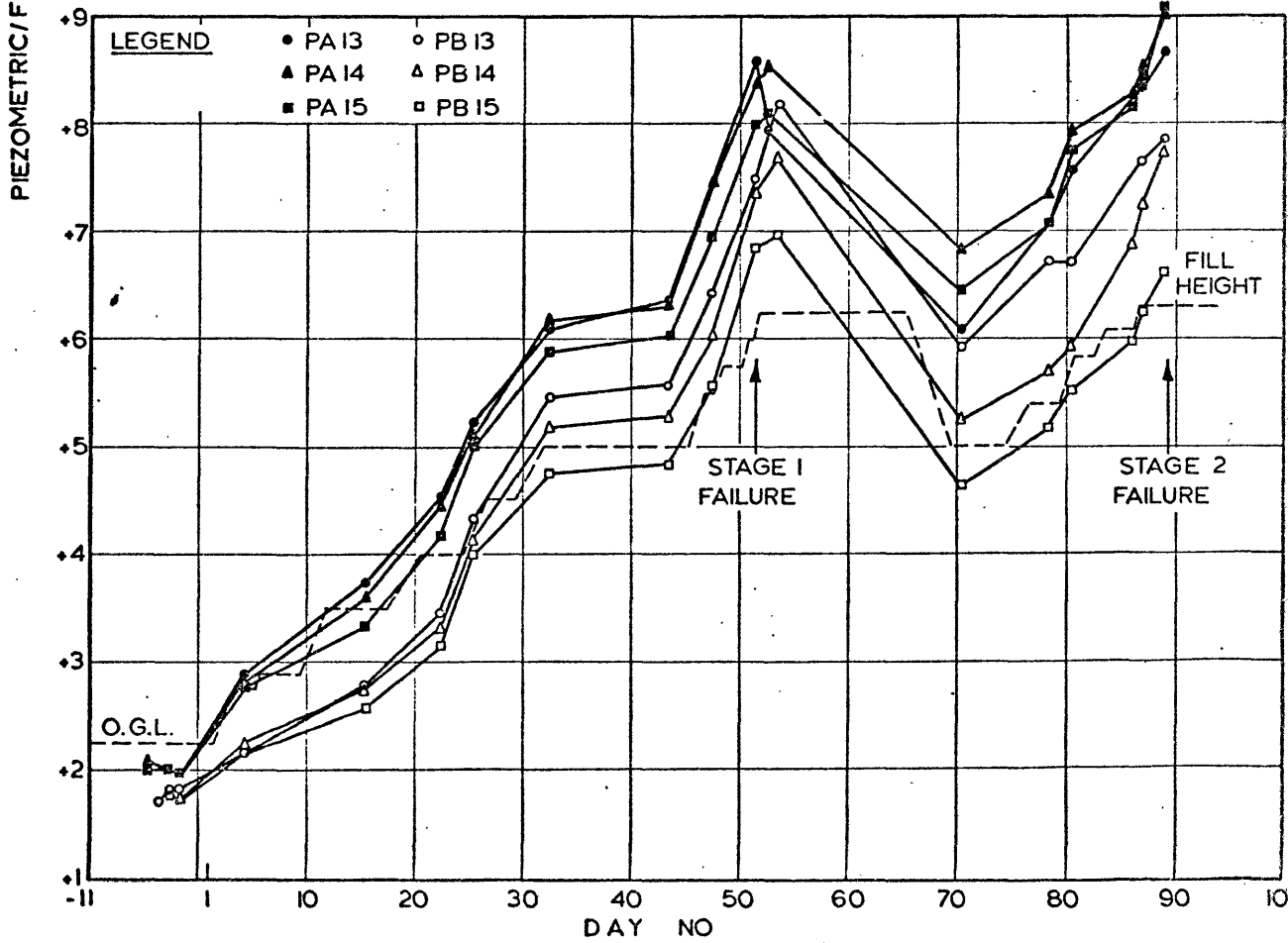
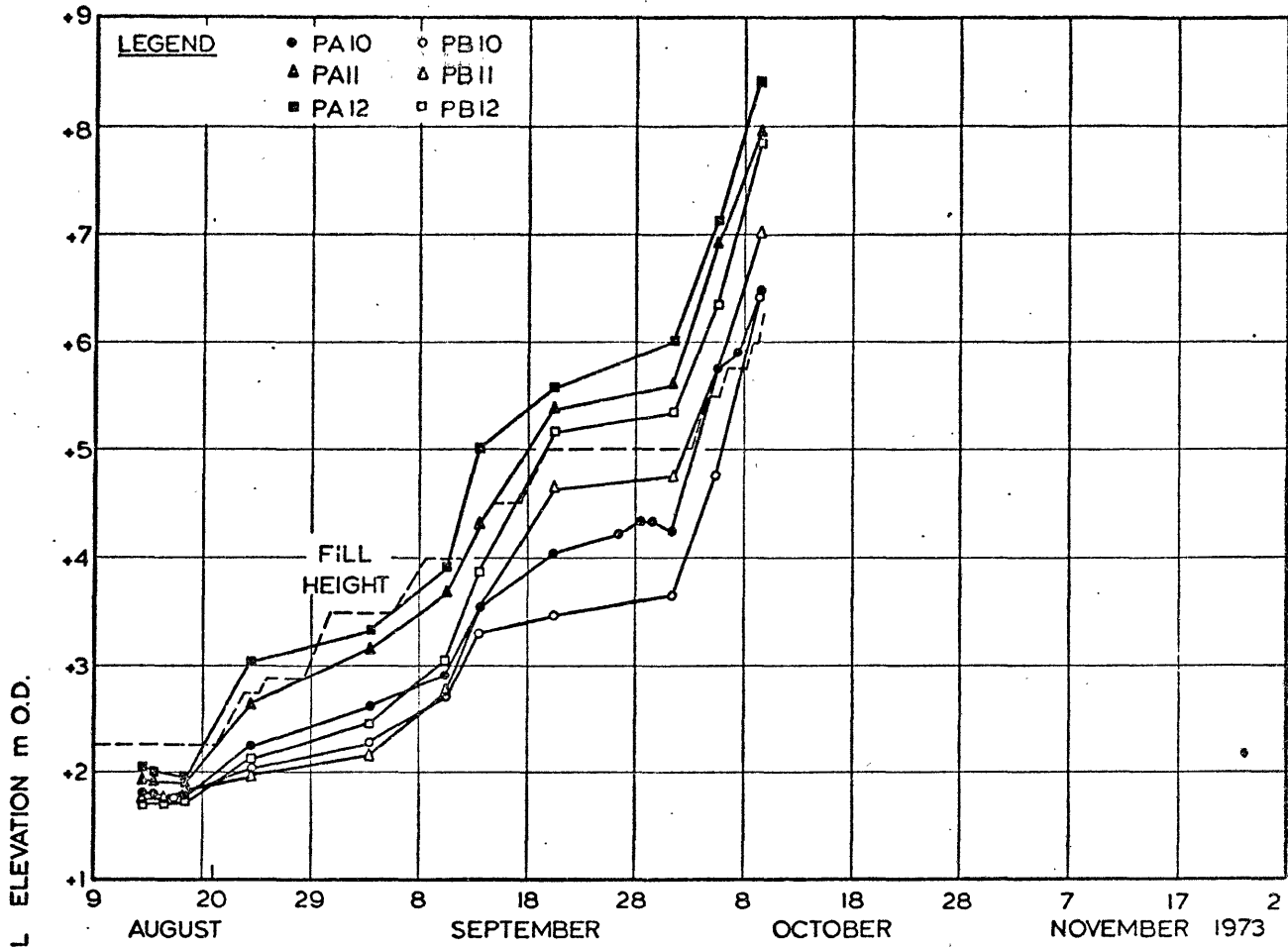
Fig. 55.2.

DISSIPATION OF PORE PRESSURES GENERATED DURING INSTALLATION



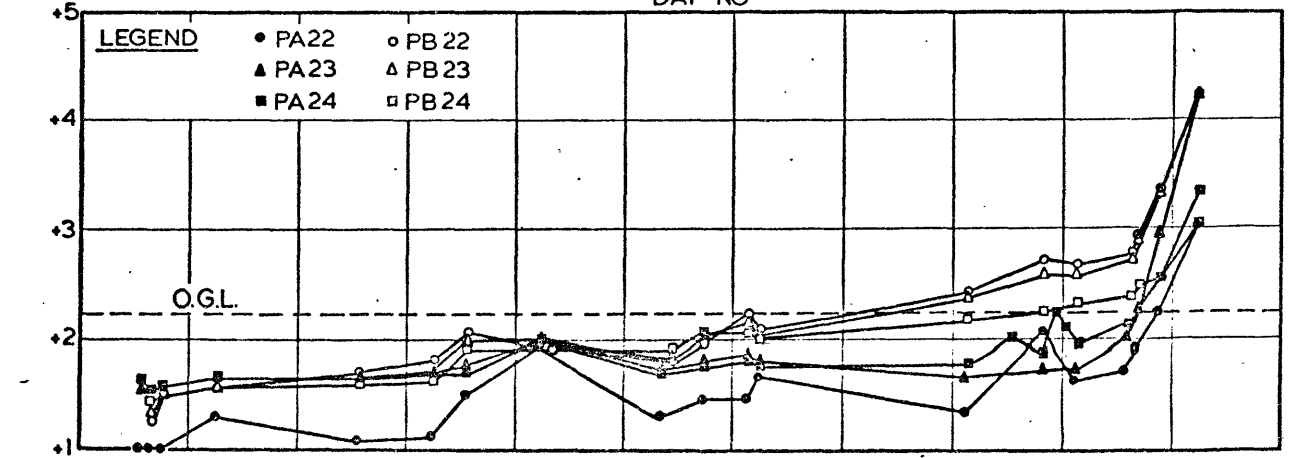
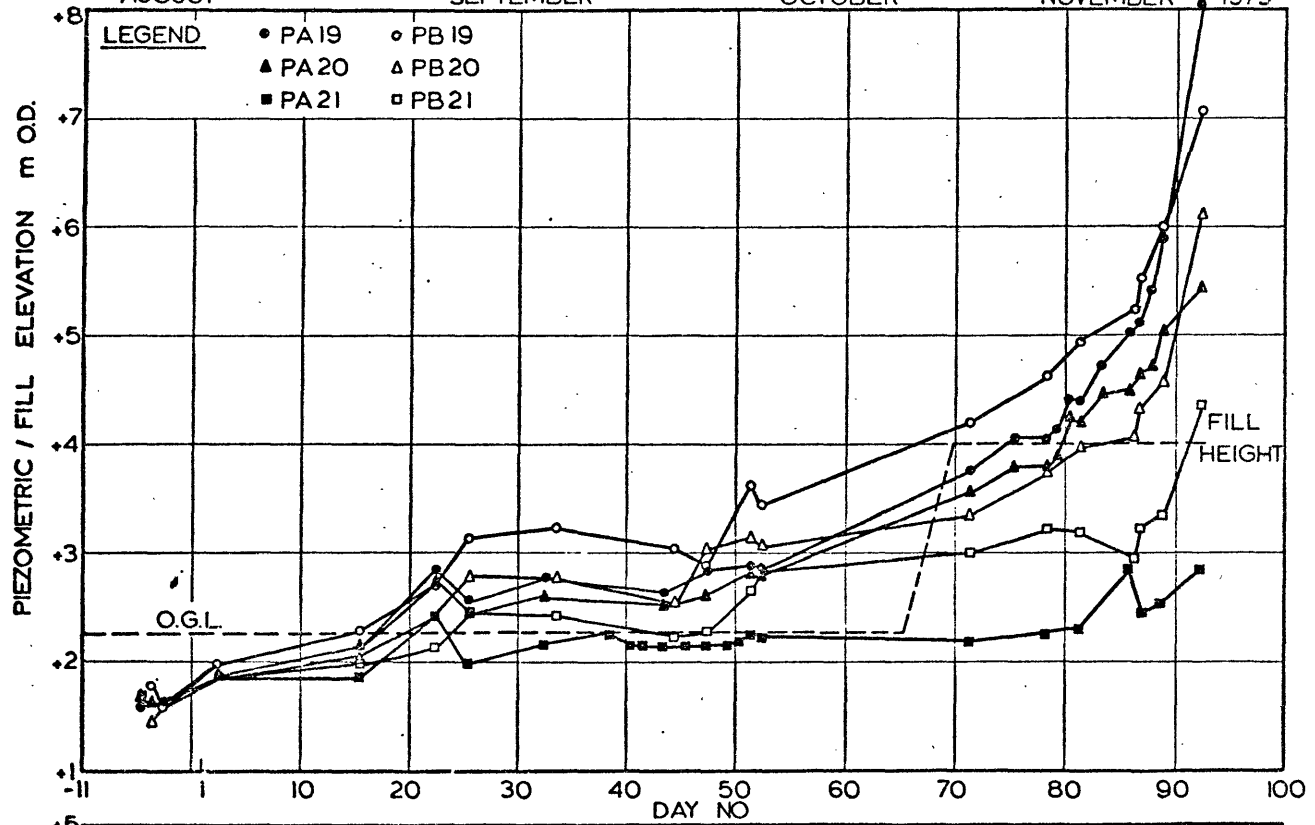
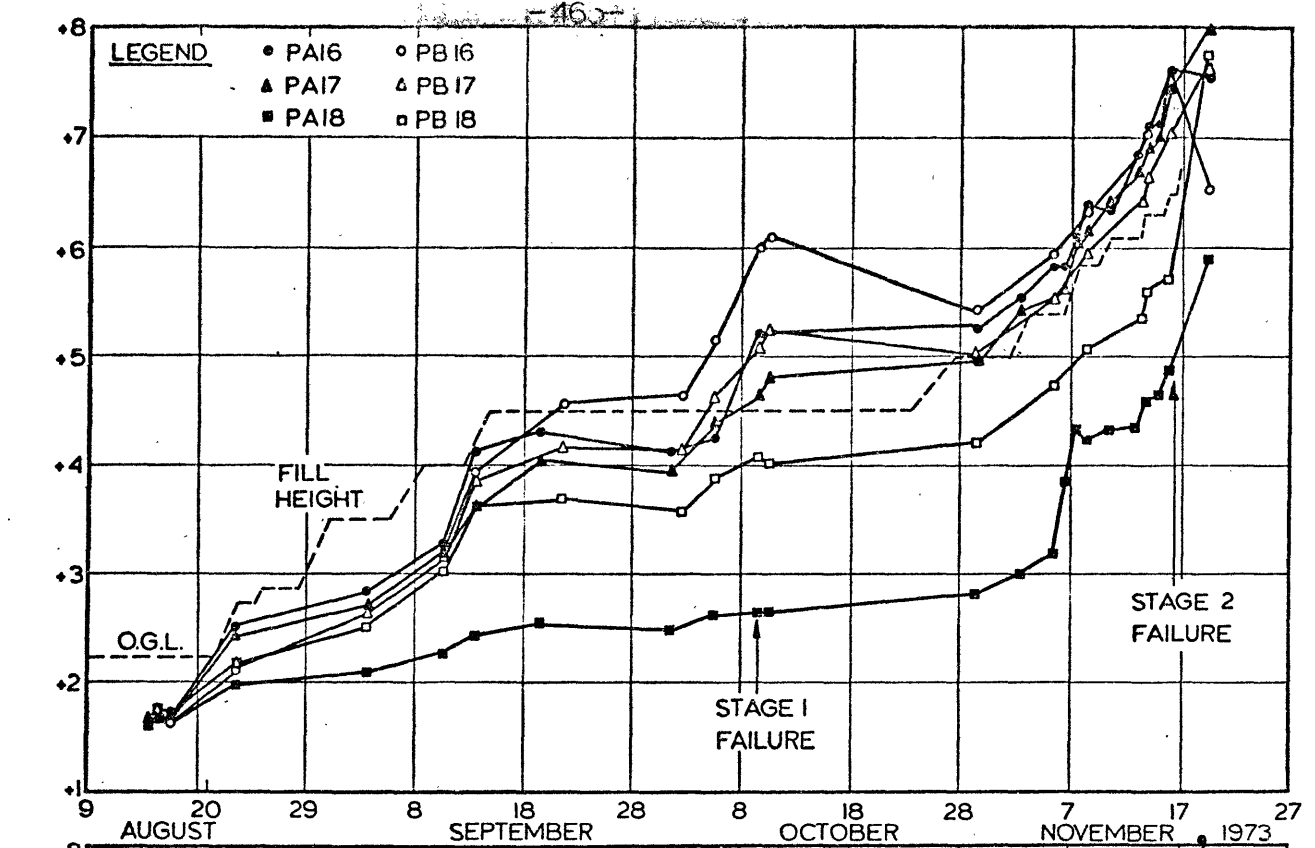
BANK I : PIEZOMETRIC RECORDS, PIEZOMETERS PA/B 1-9

Fig. 5.5.3



BANK I: PIEZOMETRIC RECORDS, PIEZOMETERS PA/B 10-15

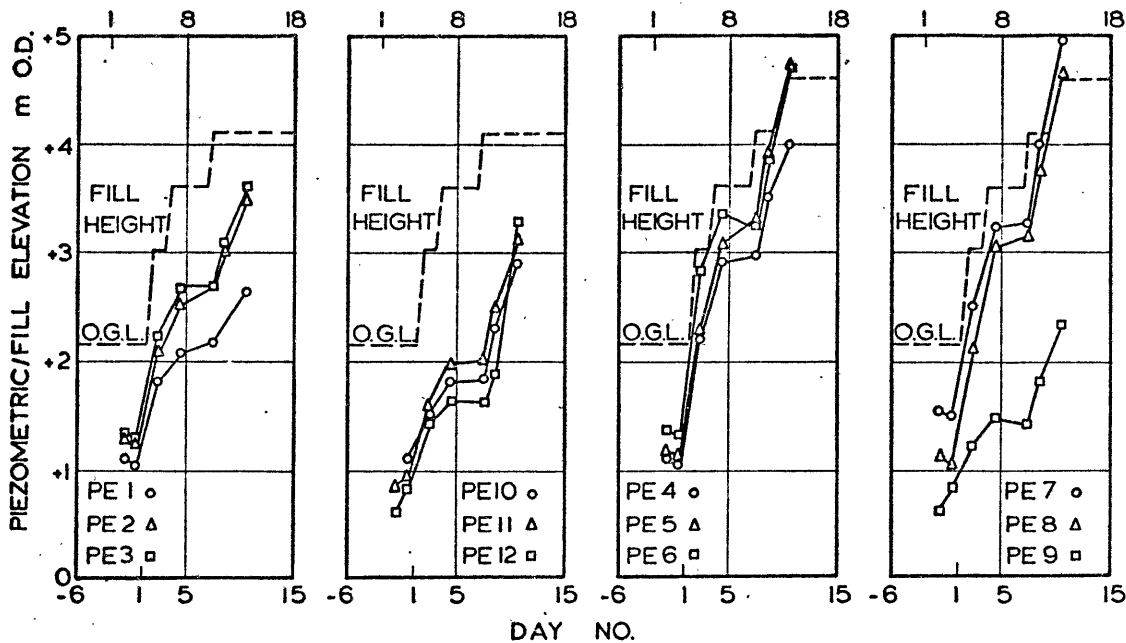
Fig. 5.5.4



BANK I : PIEZOMETRIC RECORDS , PIEZOMETERS PA/B 16 - 24

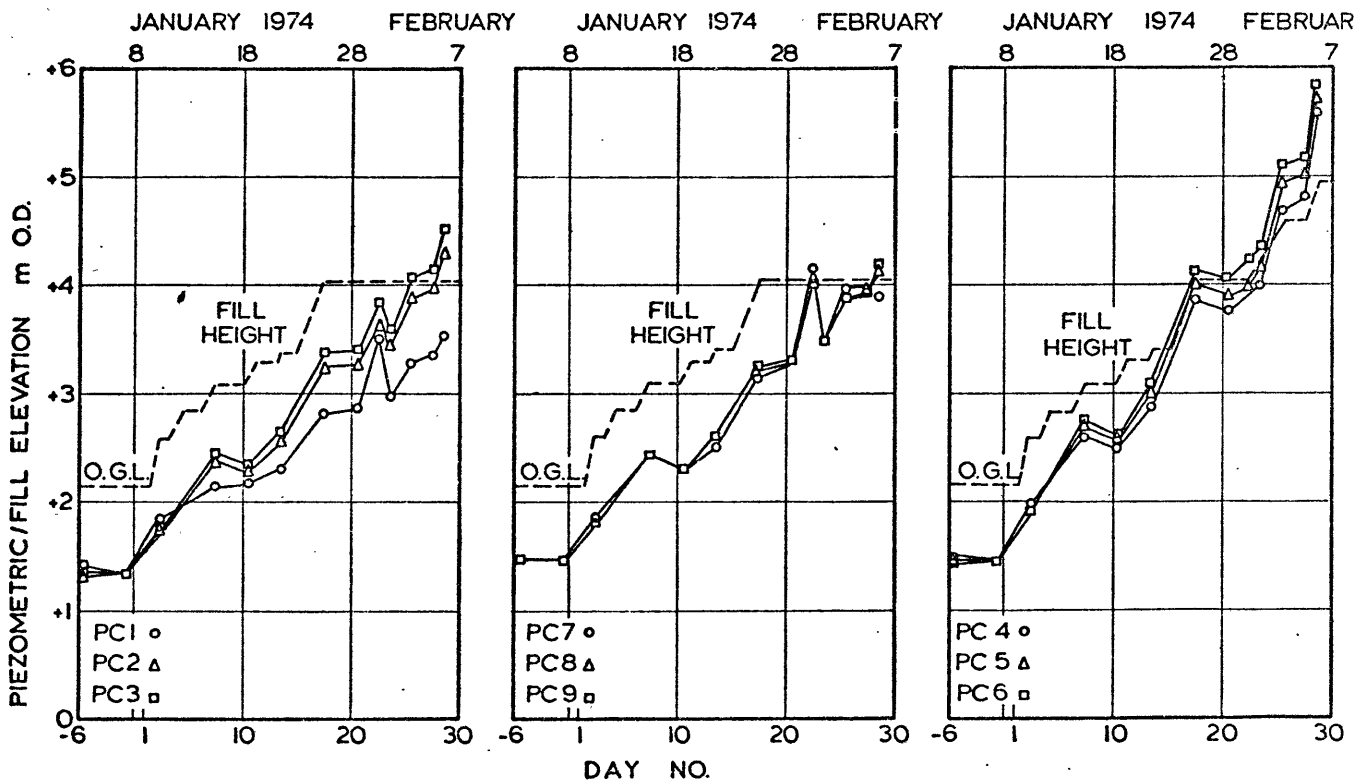
BANK 4

DATE, DECEMBER 1973



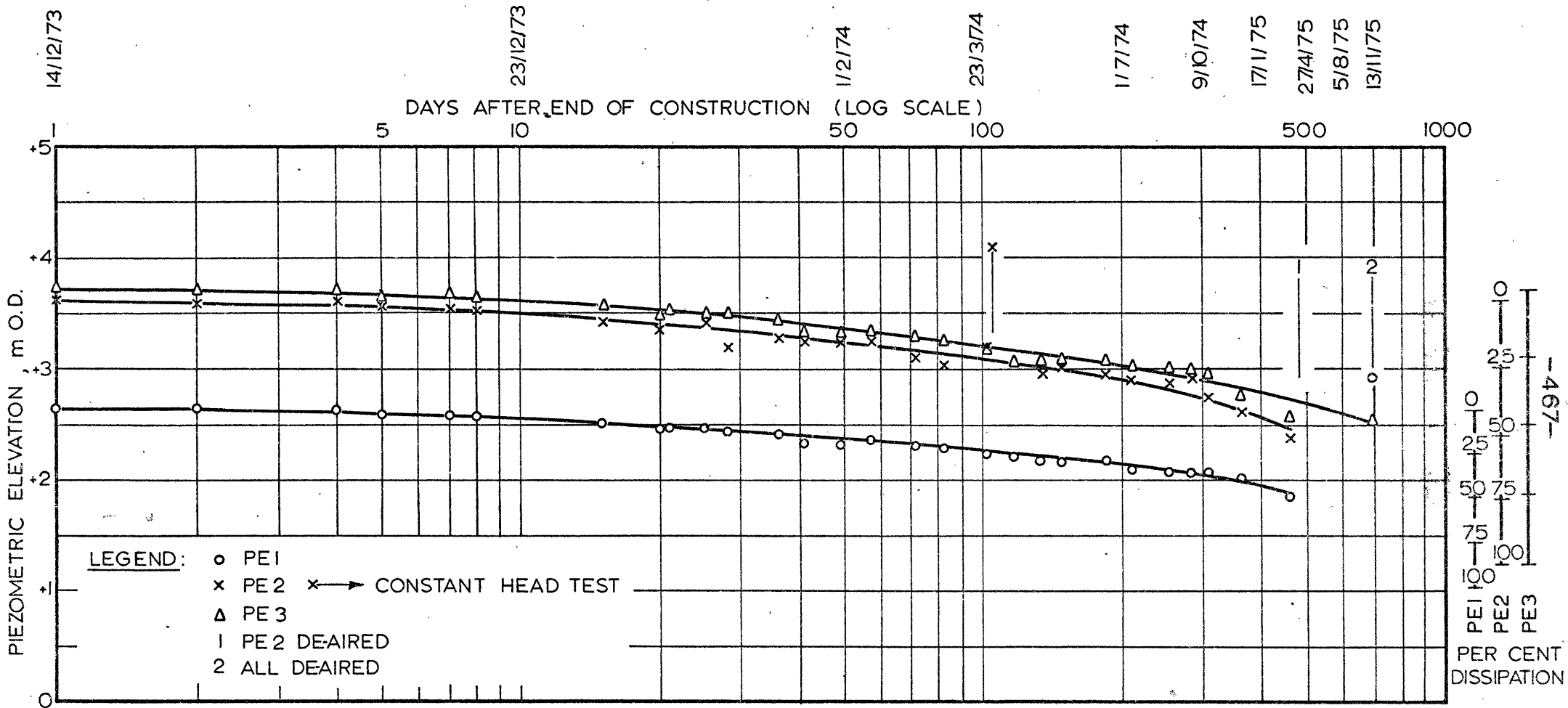
BANK 2

DATE



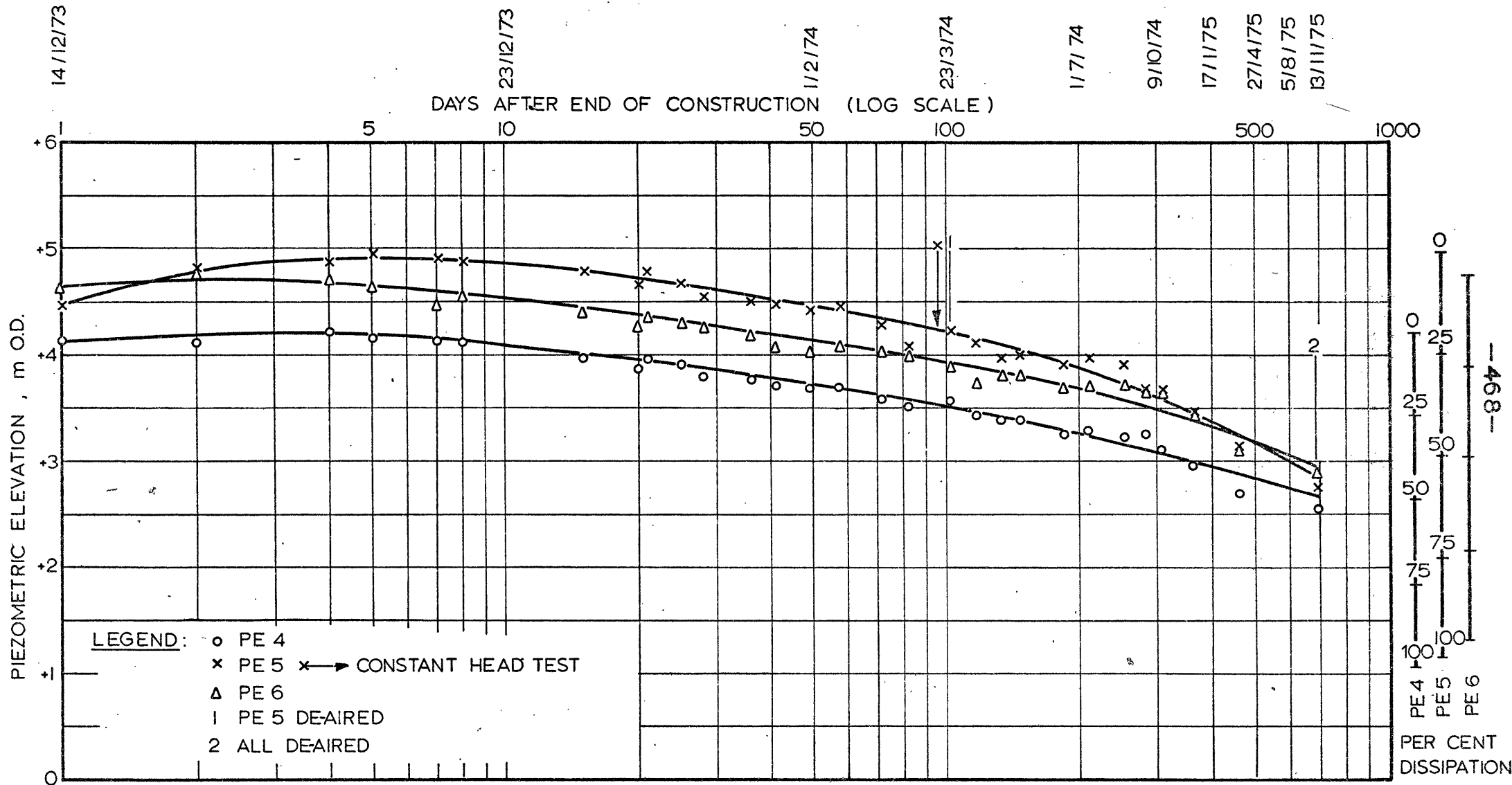
BANK 2, BANK 4: CONSTRUCTION PORE PRESSURES

Fig. 5.5.6



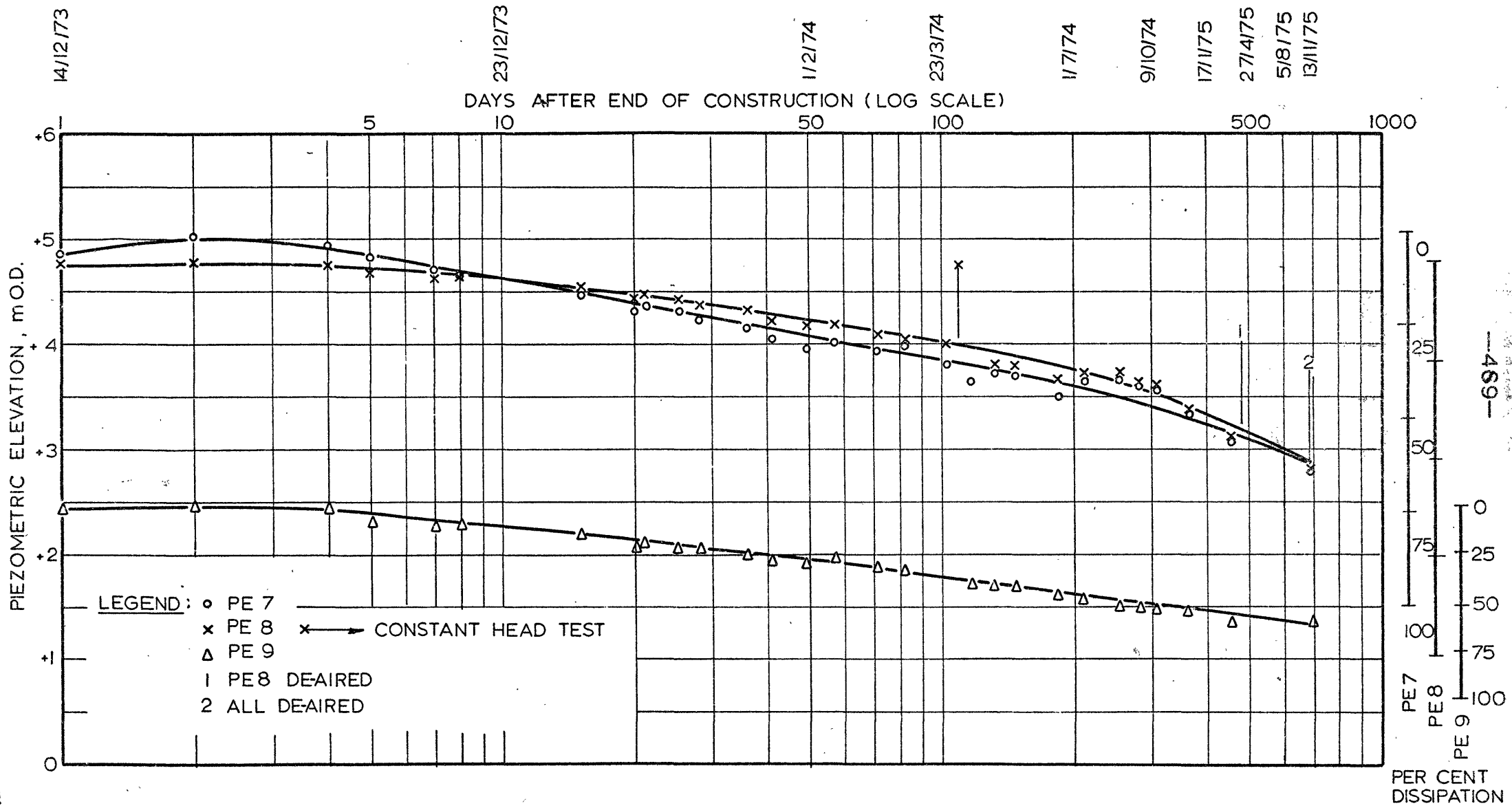
BANK 4, PIEZOMETERS PE 1-3

Piezometric elevation versus log time after the end of construction



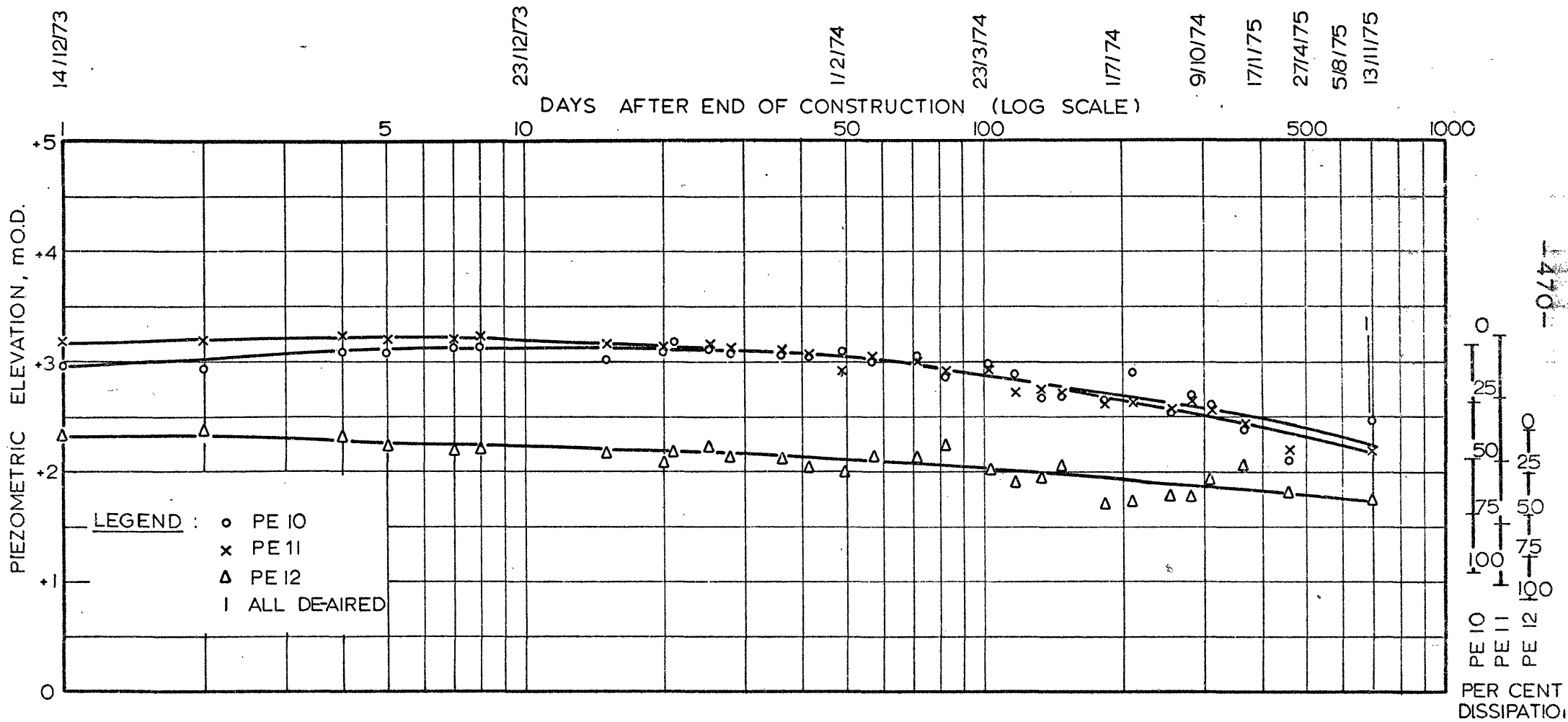
BANK 4, PIEZOMETERS PE 4-6

Piezometric elevation versus log time after the end of construction



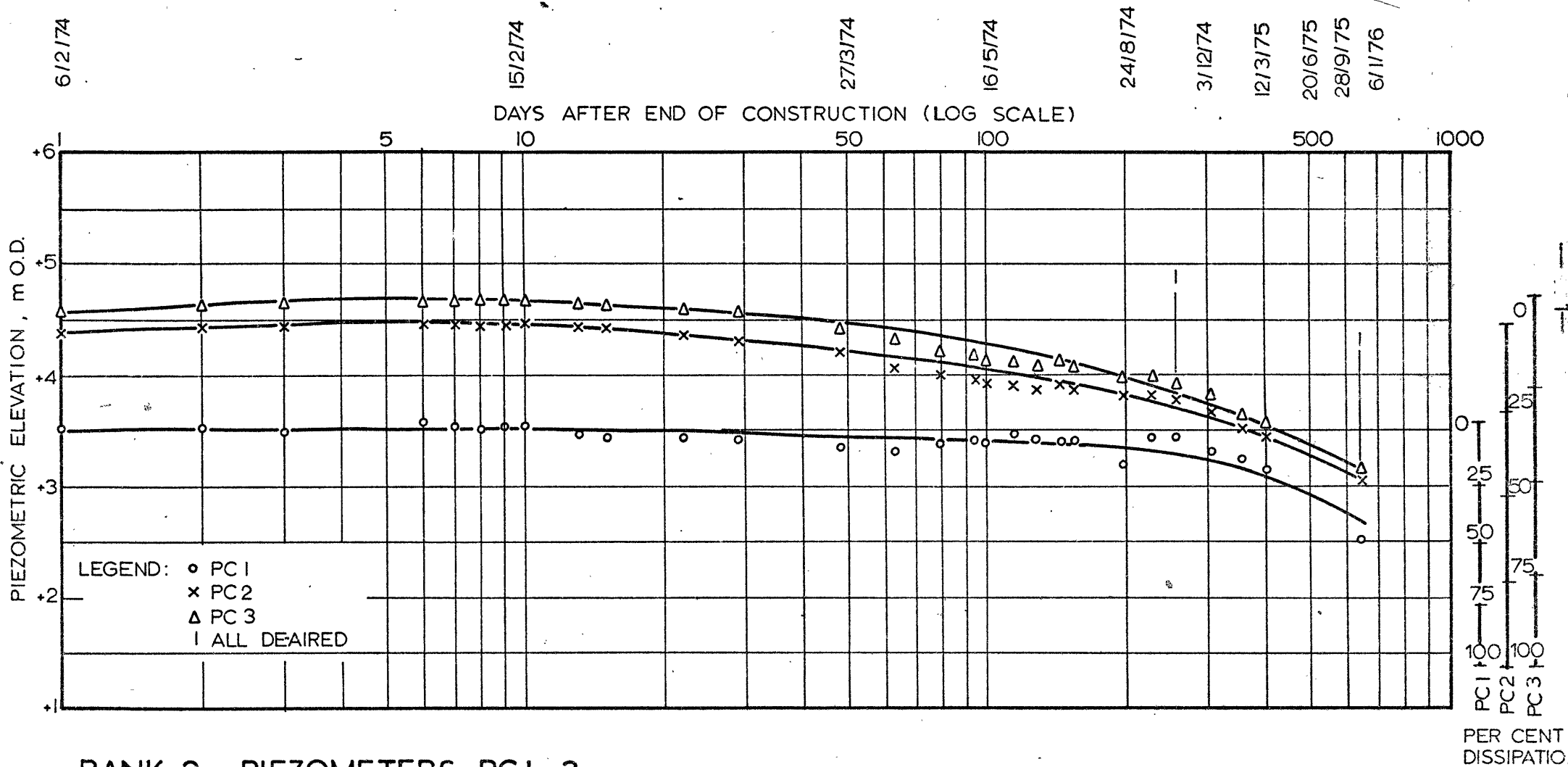
BANK 4, PIEZOMETERS PE 7-9

Piezometric elevation versus log time after the end of construction



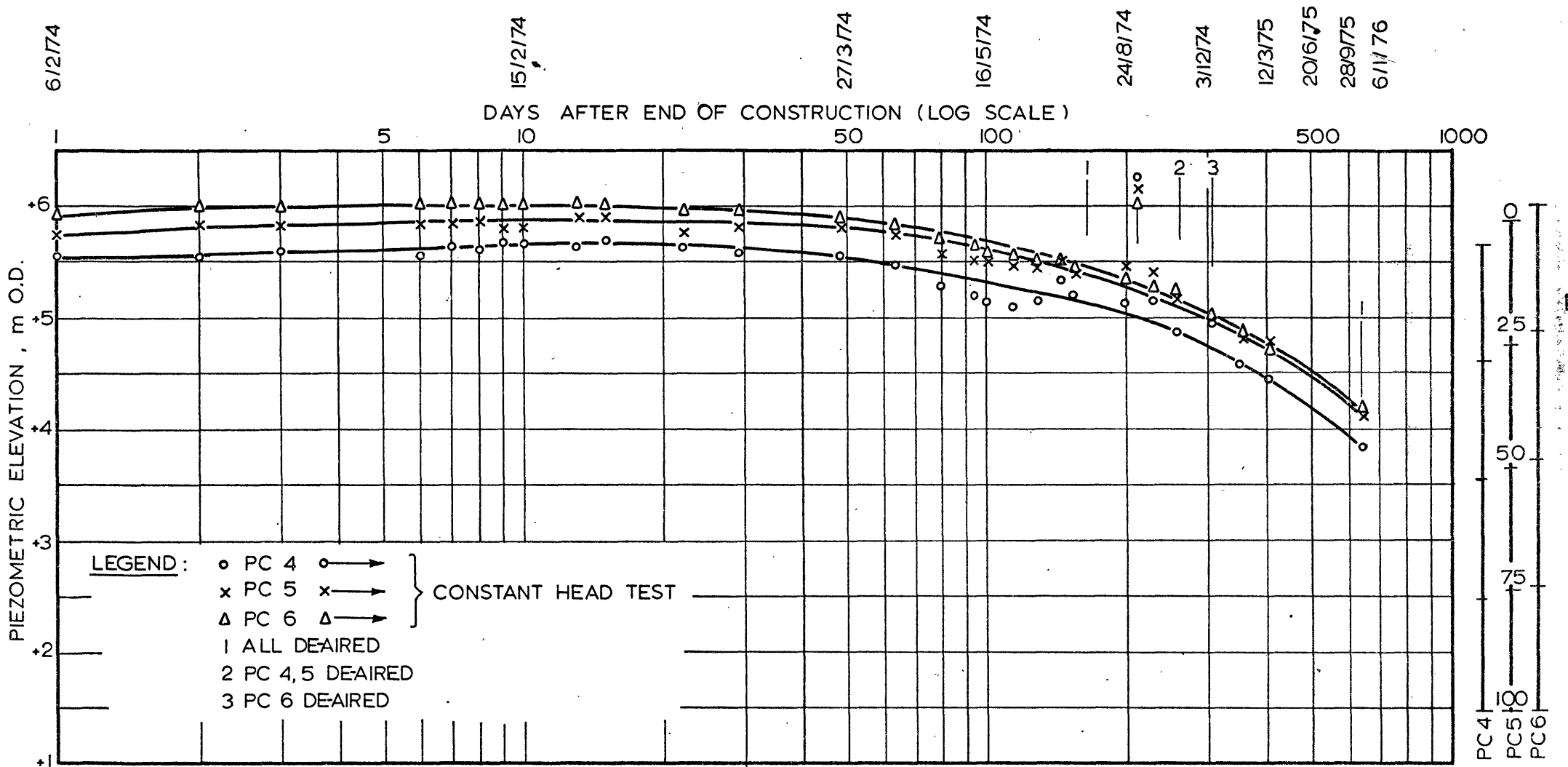
BANK 4 , PIEZOMETERS PE 10 - 12

Piezometric elevation versus log time after the end of construction



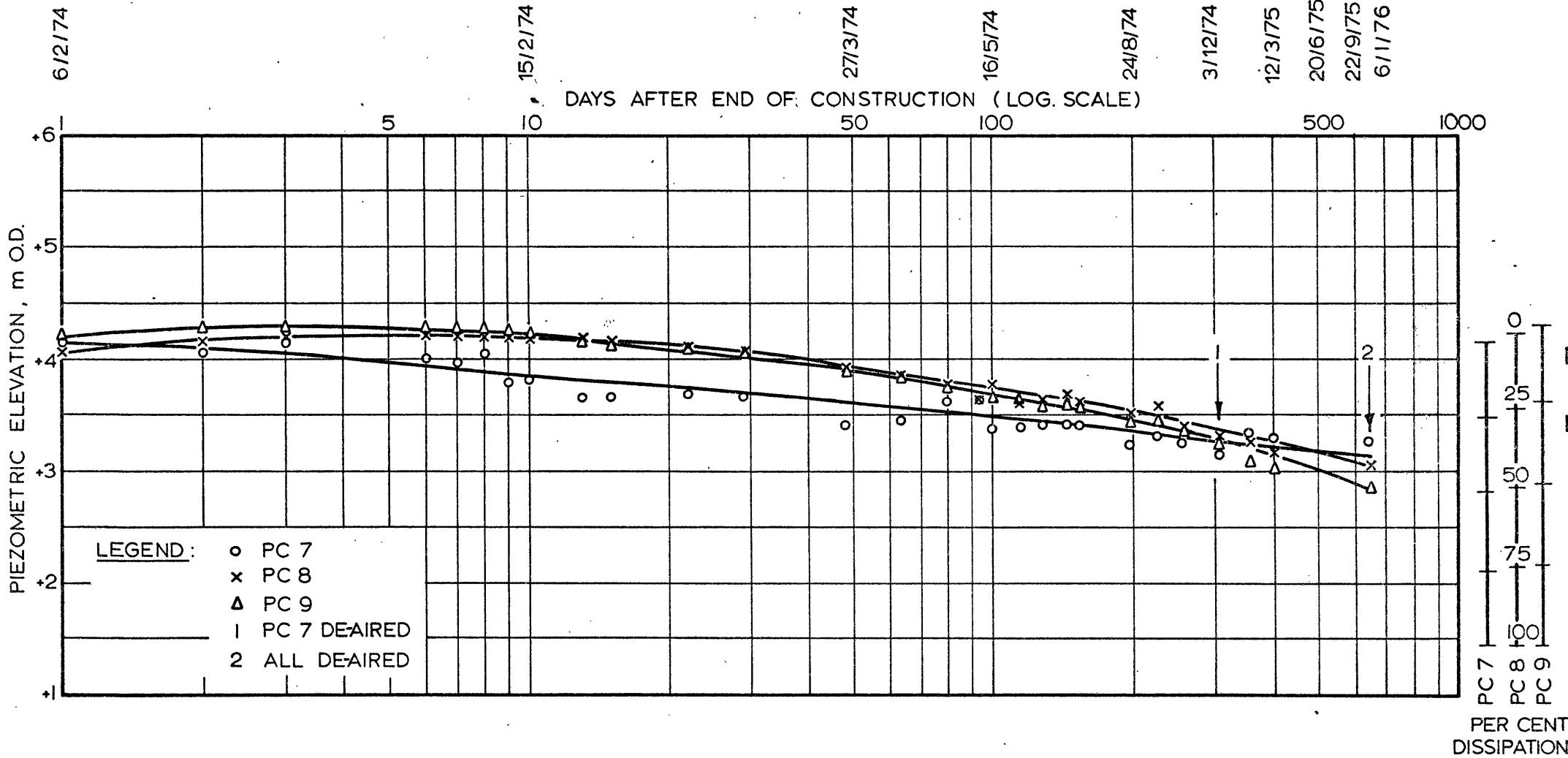
BANK 2 , PIEZOMETERS PC1-3

Piezometric elevation versus log time after the end of construction



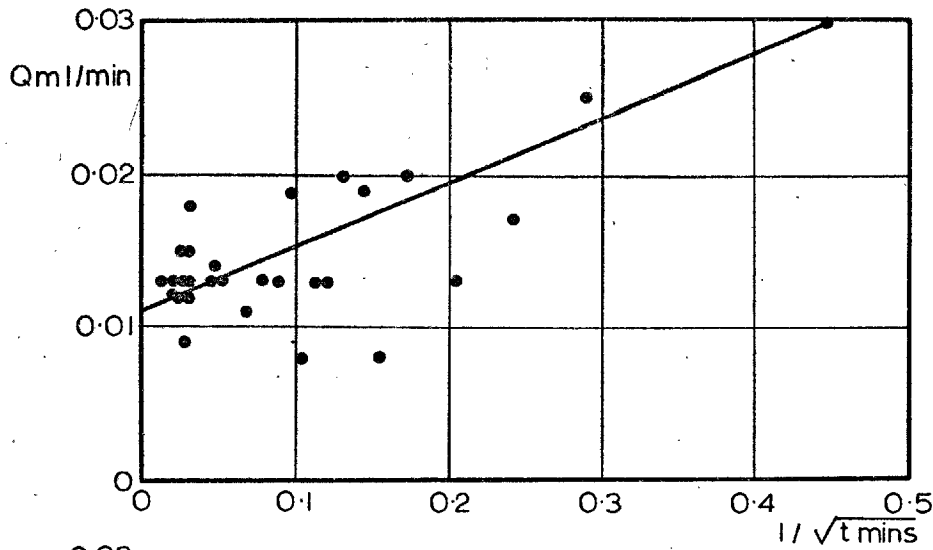
BANK 2, PIEZOMETERS PC 4-6

Piezometric elevation versus log time after the end of construction

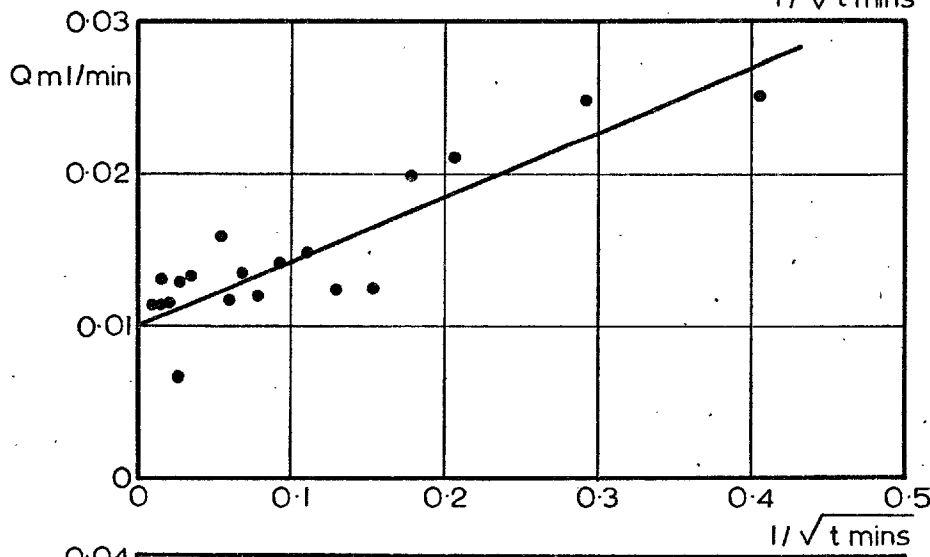


BANK 2, PIEZOMETERS PC 7-9

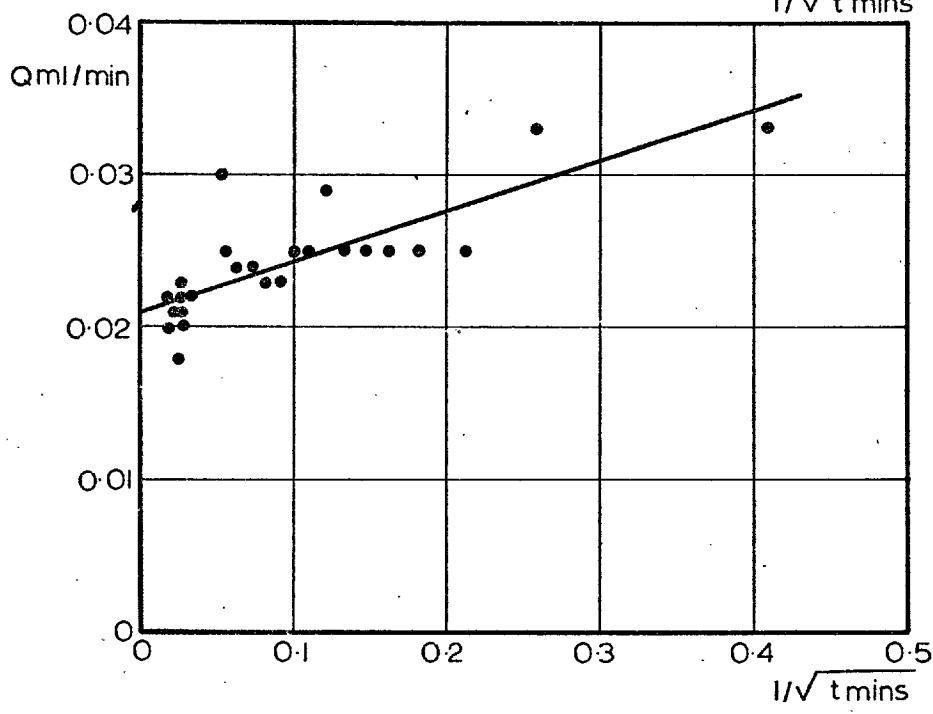
Piezometric elevation versus log time after the end of construction



PI4

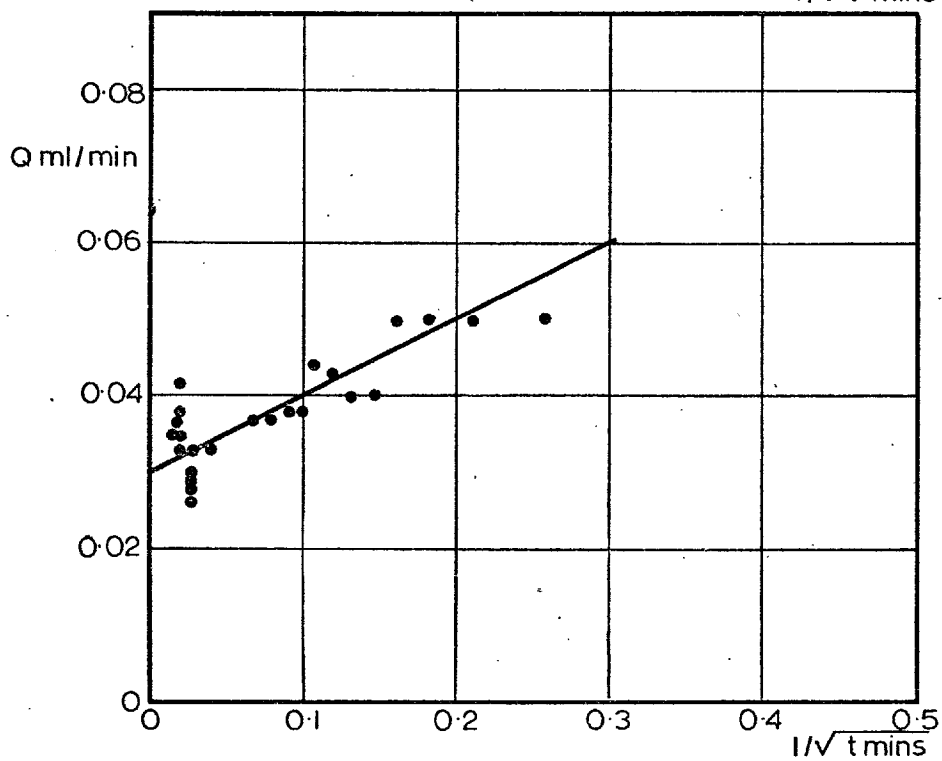
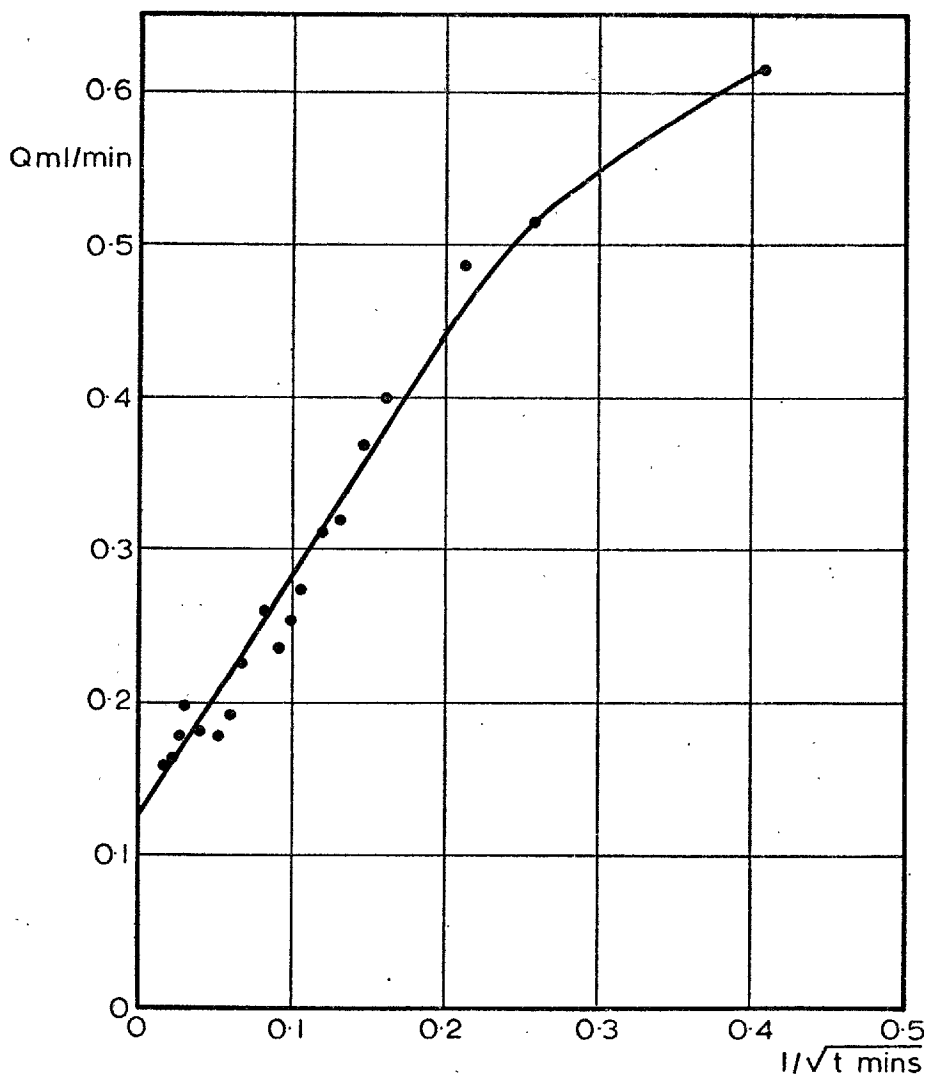


PE5

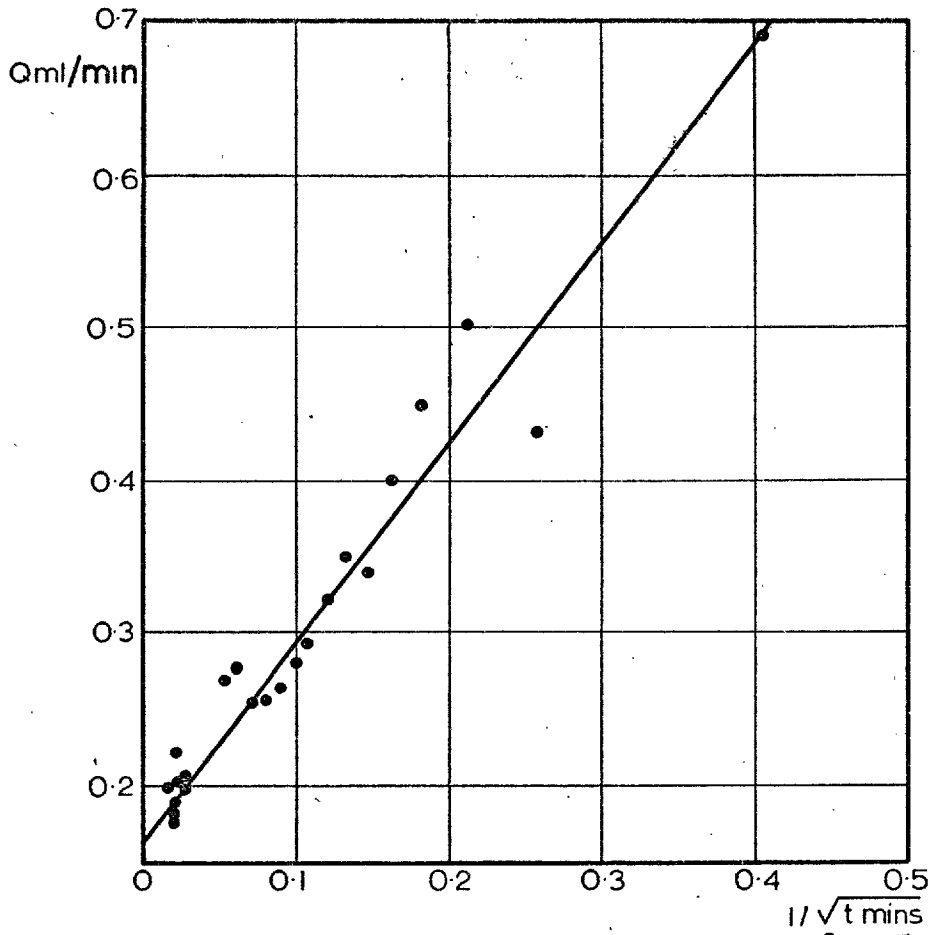


PC5

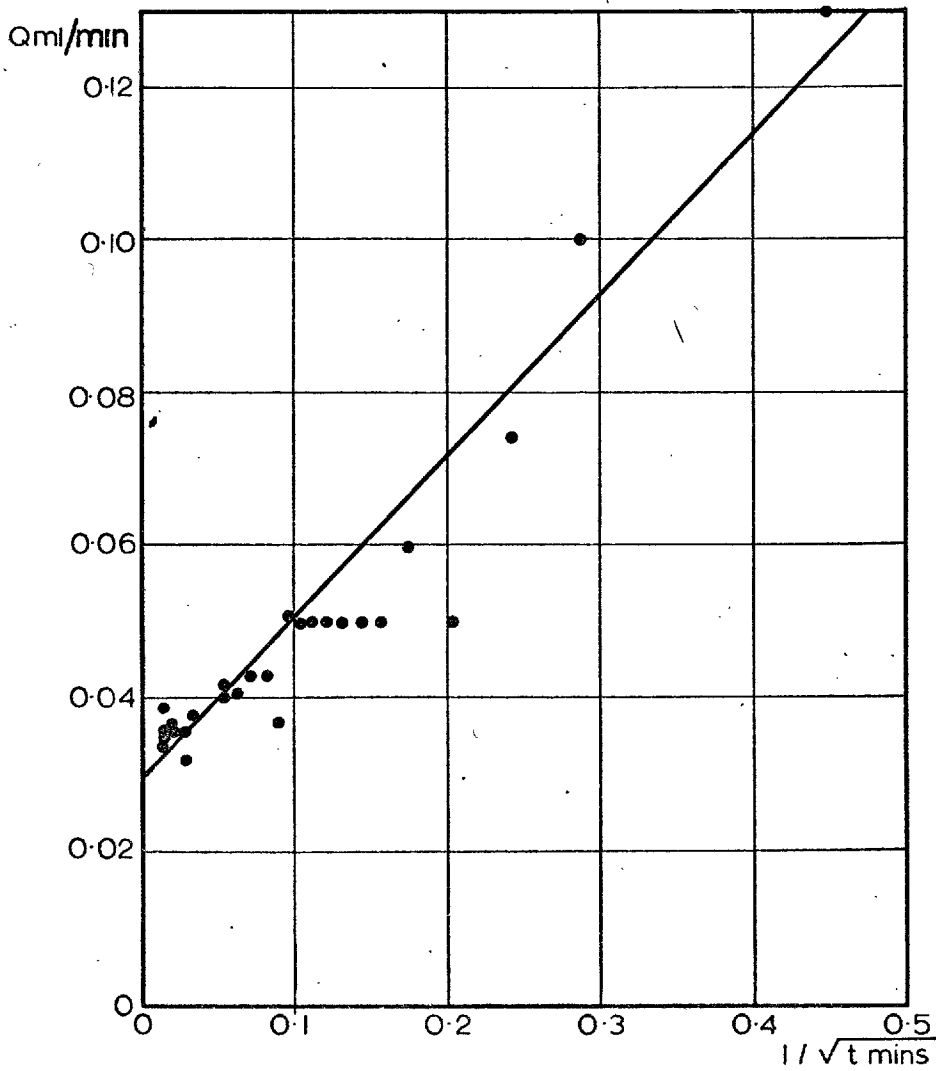
CONSTANT HEAD PERMEABILITY TESTS



CONSTANT HEAD PERMEABILITY TESTS

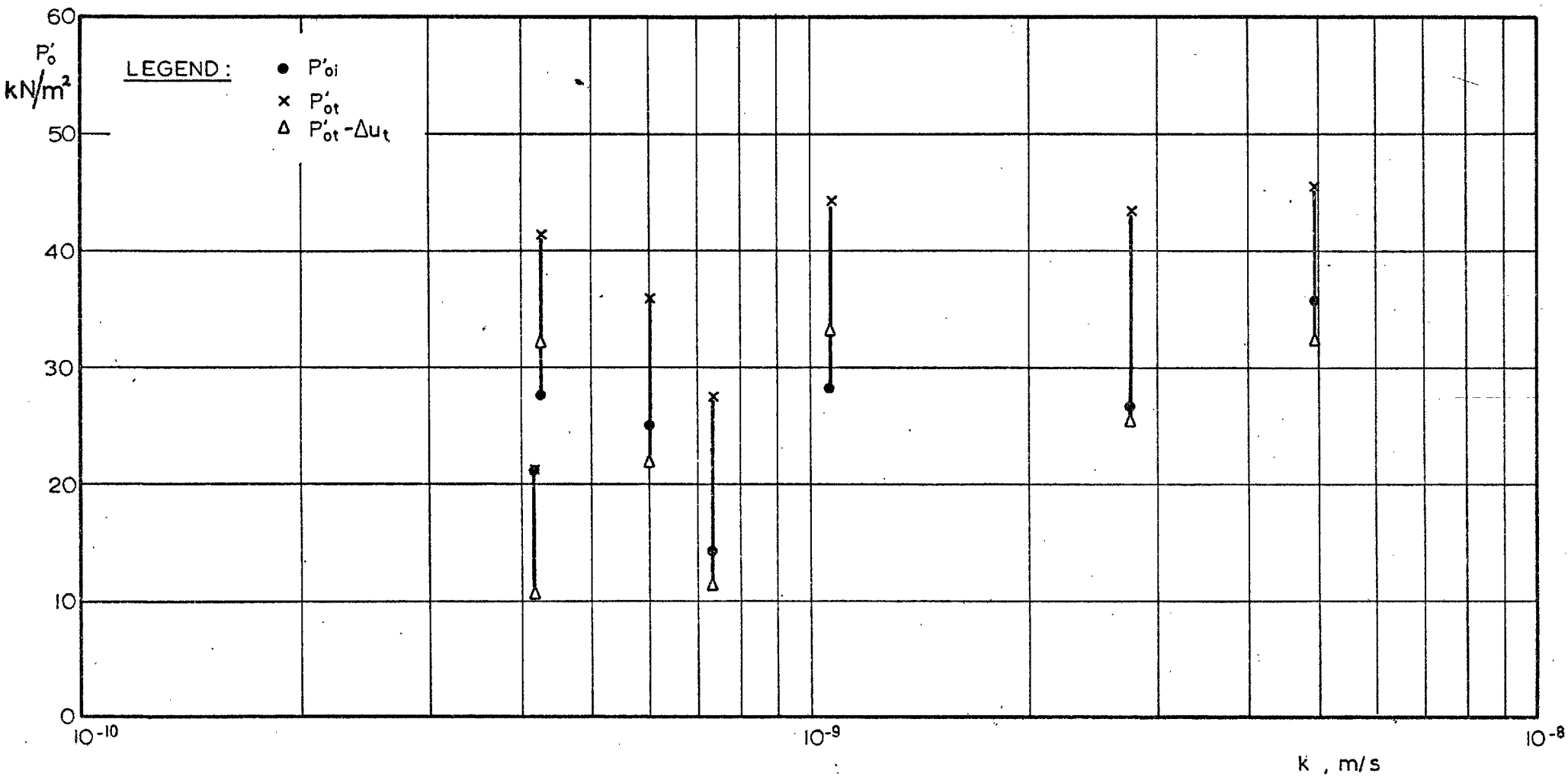


PC 6



PE 8

CONSTANT HEAD PERMEABILITY TESTS



IN-SITU PERMEABILITY VERSUS EFFECTIVE OVERBURDEN PRESSURE

5.6. Slip Surface Indicators

5.6.1. Installation

Slip surface indicators were installed at the site of Bank 1 only, being located on the 'A' and 'B' section lines as shown in figures 4.1 and 4.3. They comprised 12mm I.D. alkathene tubes supplied in 10m lengths and were installed in 75mm diameter flight augered boreholes, these being grouted up with a 3:1 bentonite:cement mix. Extension through the fill was by means of additional, shorter, lengths of tubing interconnected by cemented plastic couplings.

A 750mm long, 5mm diameter, steel rod was installed to the base of each access tube; the bases were capped and of known reduced level, being approximately 1m into the gravel as were the bases of the inclinometer access tubes. The steel rods were connected to the top caps via lengths of nylon line, sufficient extra line being allowed to accommodate instrument extension during construction.

5.6.2. Slip Surface Detection

After each of the Bank 1 failures the rods were pulled up as far as possible to locate the lower limit of the zone of maximum shear distortion: similarly another rod was lowered to locate the upper limit.

The lower rods were pulled during the actual failure of Stage 1, as it was feared that if the tubes sheared they would be inoperable. This was not the case, however, but it proved prudent to read during the failure as the indicator tubes in the heave zones gradually disappeared below ground level due to insufficient tube length having been left above ground level in the

foundation. Even so one upper reading was lost, as was also the case for Stage 2 when pressure of events resulted in the slip surface indicators being read some hours after the main period of movement. Some excavation was necessary to make those readings where the tubes were still reasonably accessible.

The results obtained are presented, discussed and compared to the data from other instruments in Chapter 6 where the location of the failure 'surfaces' is considered in detail.

Some doubt arises with regard to the lower readings. It appears that the access tubes deformed rather than sheared and as the shear zones passed relatively close to the fixed ends of the tubes they would be expected to be at fairly steep inclinations to the vertical in such locations. Thus pulled distances taken as vertical may over-estimate that dimension, and the lower limit of any zone of extreme deformation may be lower than indicated. However, in conclusion, it must be said that these instruments were simple to install and operate and reasonably effective.

5.7. Surface Movement Targets

5.7.1. General

The surface targets were used to record surface movements of the foundation and fill during construction and, during and after failure. They comprised 100mm square, by 20mm thick, pieces of marine plywood, the faces of which were marked with a cross made up of two white and two black triangles (plate 5.8.1.): the centre of the cross was taken as the target position. The targets were attached to 1m lengths of 20mm diameter steel rod by adjustable friction clamps. Installation was by simply pushing the rod into the soil such that the target was, in general, a few centimetres clear of the surface.*

The installations were obviously crude in comparison to the surface targets used to monitor the displacements of embankment dams (Penman and Charles, 1973) and other important structures (Penman and Charles, 1971; Burland and Moore, 1973). However, at Mucking, displacements of the fill were of secondary importance and the surface targets in the foundation were not the sole means of displacement measurement. It was hoped that these inexpensive and simple installations, coupled with a fairly accurate method of location would yield results of comparable accuracy to commonly used displacement measuring systems ($\pm 5 - 10\text{mm}$).

*Unfortunately quite a few of the targets installed on and adjacent to Bank 1 were rather higher with respect to adjacent ground/fill level. This makes interpretation of their displacements less certain, as is further discussed in section 5.8.

The targets for Bank 1 were installed on section lines 'A' and 'B', as well as the centre-line section (figures 4.2 and 4.4). Initial installations were in the foundation material, and later, as construction proceeded, in the fill. Similar installations were made along the entire centre-line section of Bank 2 (figures 4.1 and 4.5), the surface targets in the foundation being clamped to the heave pins in this case, as described in section 5.2.

Reference targets were installed remote from the embankments (but between them and the triangulation/photogrammetry base lines) on all of the Bank 1 section lines.

5.7.2. Location by Triangulation Survey

(i) Procedure

Base lines were established at suitable distances from the embankments, complete with triangulation stations at their extremities (figure 4.1). The triangulation stations for the Bank 1, Stage 1 base line consisted of concrete pads to provide bases for the theodolites, with steel pins (concreted in at depth) marking the ends of the base line. This arrangement proved inadequate, as weather conditions were often unsuited to accurate theodolite work. Unfortunately, when constructing trial embankments of this kind, if readings are not taken at the requisite time there is no second chance: thus the accuracy of the results and their frequency suffered in consequence.

The remainder of the triangulation stations were enclosed on all but one side by wooden framed shelters, covered with canvas and polythene.

These allowed rapid setting up of the instruments and greater speed and accuracy of triangulation, almost irrespective of weather conditions. A complete set of vertical and horizontal angles, with all targets in position, still took about 2 hours for Bank 1. Only horizontal angles were recorded for Bank 2, but due to there being two embankment faces to monitor, approximately double the reading time for Bank 1 was required. The repetition of readings in order to increase the precision was thus not a practical proposition during construction.

The base lines were each measured three times using a steel tape graduated in millimetres. The tape was subjected to a standard tension and supported in a series of short (5m) catenaries by wooden pegs. Measurements of, and corrections for, tension, temperature, catenary and slope were made. The variation in the three results for each base line in the field was within $\pm 1\text{mm}$ of the average and, after correction, less than the accuracy of the tape. The measured lengths of the base lines were thus considered to be within $\pm 1\text{mm}$ of the true distance.

(ii) Precision of Target Location

The Zeiss theodolite used had a sensitivity of 6 seconds of arc; it was not equipped with an optical plumb bob. From the recorded angles of each set of readings (average of face left and face right) the target coordinates were calculated using a simple triangulation computer program.

It can be shown that for the location of targets installed relative to a base line, as described, the measurement of angles only, from the known stations, is accurate and efficient (Ashkenazi, 1973; figure 5.7.1.). This has been verified in tests reported by Maughan (1972), wherein

6 sets of readings were taken on two targets at approximately 50m from the theodolite stations. The three dimensional location of the targets was by pure triangulation (vertical and horizontal angles measured, plus known station coordinates). The observed accuracy (standard error) was within ± 1 mm in all three directions (4 seconds of arc) using an instrument reading to 1 second of arc. These tests, performed under very stringent conditions, represent an upper bound to the precision that could have been achieved under site conditions at Mucking.

The precision of the triangulation was assessed from the repeatability of the reference target locations. These were the closest targets to the triangulation stations, and were installed in the foundation. They were thus susceptible to any movements due to moisture content changes but not in so great a danger of being disturbed by construction activities as those in the fill. When locating the targets by triangulation survey the accuracy of location should not have been significantly lower for the distant targets than for the reference targets (figure 5.7.1.).

Table 5.7.1. shows the standard deviation, 99% confidence level and the number of observations made for each coordinate direction during the construction of Bank 1. As discussed in section 5.2., the surface targets in the foundation adjacent to Bank 2 were combined with heave pins; there were no reference pins and vertical location of the targets was by level survey. However, a comparison of the Bank 2 results (figure 5.2.2.) with those for Bank 1, Stage 1 (figures 5.7.2. to 5.7.4.) and Bank 1, Stage 2 (figures 5.7.5. and 5.7.6.) suggests that the Bank 2 results represent the greatest accuracy achieved.

The data in table 5.7.1. reflect not only the precision of the triangulation procedure but also the susceptibility of the targets to influences unrelated to the construction process. The standard errors are very reasonable, the improvement from Bank 1, Stage 1 to Stage 2 (and to Bank 2) being mainly a function of the improved set-up used; this was also reflected in the lack of lost data due to inclement weather during Bank 1, Stage 2 and Bank 2.

It is interesting to note that the least accurate result by a long way is the vertical (Z) coordination for Stage 1. This almost certainly reflects the near surface volume changes which occurred during the period of observations, although the effects are nowhere near as drastic as those experienced by the heave pins (section 5.2). The accuracy of vertical location of the heave pins adjacent to Bank 2 by level survey (table 5.2.1) was only slightly less than that for the triangulation of the Bank 1, Stage 2 targets.

In conclusion, the average standard errors in the 'X', 'Y' and 'Z' directions, for the Bank 1 triangulation, of $\pm 3.9.$, $2.7.$, and 4.2mm are very acceptable for such a measurement system.

5.7.3. Location by Stereo Photogrammetry

(i) Introduction

Terrestrial photogrammetry is carried out using two phototheodolites such that pictures taken at the two camera stations cover a common area of interest. The coordinates of points within this common area may be determined from a knowledge of the three dimensional coordinates and

LOCATION AND TYPE OF MEASUREMENT	COORDINATE DIRECTION	NUMBER OF OBSERVATIONS	STANDARD DEVIATION ±mm	99% CONFIDENCE LEVEL ±mm
Bank 1, Stage 1; Triangulation	X	9	3.6	9
	Y	9	2.8	6.9
	Z	9	6.6	16.5
Bank 1, Stage 1; Photogrammetry	X	17	9	22
	Y	17	8	20
	Z	17	10	25
Bank 1, Stage 2; Triangulation	X	18	4.3	10.6
	Y	18	2.6	6.5
	Z	18	1.8	4.6
Bank 1, Stage 2; Photogrammetry	X	14	10	25
	Y	14	7	17
	Z	14	7	17

Table 5.7.1.

Accuracy of Surface Target Location Using Triangulation and Photogrammetric Surveys

inclination of the cameras, together with their optical characteristics. Whilst in theory the coordination of such points can be ascertained by the application of simple geometrical principles, accurate three-dimensional coordination is usually carried out in a stereo-comparator. This restitution of the stereoscopic plates in the comparator involves either direct measurement of coordinates from the photographs, followed by analytical computation of the field coordinates or, more commonly, direct measurement from a stereoscopic model.

The procedure used at Mucking, whereby the photogrammetric set up was specified, and restitution of the stereo pairs carried out, by a commercial organisation, whilst the actual photography and analysis of the recorded displacements were carried out by the Engineer's staff, has been successfully used elsewhere (Moore, 1973 and 1974). The photographic restitution is generally the most difficult part of the procedure, requiring specialist equipment and skills, although obviously good restitution cannot compensate for inaccurate photography. This aspect of the analysis is beyond the scope of this thesis; if further information is required reference should be made to standard texts on photogrammetry e.g. American Society of Photogrammetry (1968), or Air Surveys (Kilford, 1973). Less detailed discussions of photogrammetry may be found in standard texts on surveying e.g. Bannister and Raymond (1965).

However, certain terminology relevant to this section and section 5.8 will now be defined for ease of discussion. The line of collimation of a camera is a line normal to the photographic plane and passing through the optical centre of the lens. It is thus unique, intersecting the photographic plane at a point known as the principal point of the

photograph, and defines the orientation of the photograph with respect to the subject matter. The vertical axis of the theodolite in a phototheodolite, lies in the vertical plane of collimation of the camera enabling its precise location to be determined.

The principal or optical axis of a lens is the line passing through the optical centre and normal to both surfaces of the lens. The line of collimation and the principal axis thus only coincide when the lens and the photographic plane are in identical orientations. Coincidence of the principal point and the centre of the photograph is a further special case.

In order to coordinate points on the photographs the collimation must be known as must the focal length of the camera. The collimation is defined on the photographic plate by the principal point, which is, in turn, defined by the fiducial marks. These are internal camera markings which should appear on the photograph either as complete axes of intersection or marks at the extremities of the axes. Other data commonly shown on the plates are the photograph number and the camera's identification.

The principal distance is the length between the photographic plane and the optical centre of the lens measured along the line of collimation, and is thus a property of the camera (equals the image distance for an in focus image when the collimation and principal axes coincide). On the other hand the focal length is measured along the optical (or principal) axis of the lens, and is a property of the lens. However, the focal length and principal distance are commonly assumed to be identical in

survey photography, for which coincidence of collimation and principal axes is the norm; this aspect is further discussed in section 5.8.

Stereo photogrammetry is the name given to photogrammetric surveys wherein the collimation lines of the cameras are parallel, as at Mucking: the photographic plates are in the same vertical plane and also parallel to the base line. The cameras are also usually at similar elevations. Although in theory the coordinates of points in a stereo model can be determined from the basic positional and photographic data, the scale* of the photographs and the extrapolation to points of intersection renders the process relatively inaccurate (compared to conventional survey methods) over long distances. The accuracy is also closely related to the ratio between the base line length and the target distance (base: depth ratio). Thus most photogrammetry exercises involve the accurate coordination, by triangulation, of a series of control points which are so arranged as to define a three-dimensional spatial volume within the overlapping areas of the photographs, and within which the observation targets are positioned.

The stereo model is thus set up in a comparator to provide the best fit to the known control points and the observation targets are then located directly from the model. This process of inner orientation, or setting up of the photographs to represent the actual camera positions, is also of prime importance as far as accuracy is concerned.

*A long focal length camera increases the scale, and thus the accuracy, for a given distance.

(ii) Procedure

The Wild P32 phototheodolites were positioned as shown in figures 4.2 and 4.4 during Stages 1 and 2 of Bank 1, respectively; in both cases the base :depth ratio varied from 1:1.2 to 1:3.5 over the depth of field, and was, therefore, within acceptable limits. The surface targets installed for Bank 2 were not located by photogrammetry. The photogrammetry base lines can be seen to be parallel to the embankment toes; they were established by triangulation from the main survey base lines, as were the phototheodolite elevations. The phototheodolite stations were exactly the same as the triangulation stations described in section 5.7.2 for Bank 1, Stage 2 and Bank 2. Having established the base line and the stations the theodolites were set up and directed along horizontal lines perpendicular to, and towards the embankments. The cameras were then mounted on the theodolites and linked to a single shutter release control.

The phototheodolites were left thus set up, but covered to keep out the damp, and with a bag of silica gel in the covering as added protection. Photographs were generally taken daily, as the procedure was very simple. Having established the reflected light reading from the targets the camera shutter speed was set to correspond to an aperture of between f8 and f11 in order to maintain a reasonable depth of field. The focus was preset to include the desired depth of field at these apertures and did not often require adjustment. The angle and elevation of the lines of sight were always checked, as were the position and level of the theodolites.

With the cameras ready for operation the photographic plates were inserted and the covering shields removed (as were the lens caps, most of the time!). The coupled shutter release mechanism was then activated and the plates recovered, removed and labelled to complete the operation. The photographs were timed, whenever possible, to coincide with other measurements taken on the site, but light conditions, particularly the position of the sun, tended to be the main criteria.

R.20 plates, rated at 50 A.S.A. were used for daytime photography. In order to enable the use of photogrammetric, as well as time-lapse photographic, observations during a night time failure, two mobile floodlight towers were installed during Stage 1 construction. These had their own generators and produced a combined lighting power of 12 k.W. By marking the targets with reflective tape (as used on bicycles etc), using very fast plates (HP3, rated at 400 A.S.A.) and the maximum aperture size (f2), and careful positioning of the floodlights it was just possible to carry out night time photogrammetry.

During Stage 2 construction it was possible to obtain only one of the floodlight towers used for Stage 1, the additional tower used being of substantially less output. However, careful positioning of calor gas work lamps, and 'motorists torches' placed under each target, again made the operation just feasible.

Determination of the target coordinates from selected stereo photographic pairs was carried out by Meridian Air Maps Ltd (1974(a) and (b)) using a Wild A40 stereoplotter.

(iii) Precision of Target Location

Photogrammetric techniques should be capable of accuracies (in terms of standard error) of the order of $\pm 8\text{mm}$ over a distance of 40m (1 in 5000) with good control and the right equipment. Planicka and Nosek (1970), for example, reported accuracies of ± 5 to 10mm over 50m distance (1 in 10,000 to 1 in 5000) for observations of the displacements of a dam. The order of accuracy markedly increases with decreasing distance to the target location or base:depth ratio: with a constant base width and inner orientation the variation in accuracy with distance is approximately linear (Moore, 1973).

The Wild P32 phototheodolites used are capable of accuracies of the order of $\pm 15\text{mm}$ at 40m distance (1 in 2500), but in conjunction with the Wild A40 stereoplotter the accuracy drops to $\pm 80\text{mm}$ (1 in 500; Meridian Air Maps Ltd., 1974(a)). The latter is obviously inadequate for the order of magnitude of the pre-failure displacements recorded at Mucking.

Moore (1973) reported standard errors of ± 20 , 40 and 10mm for the 'X', 'Y' and 'Z' coordinates respectively, of targets located by photogrammetry (base:depth $\approx 1:5$) at Llyn Brianne Dam using Wild P30 phototheodolites and an A7 stereoscope. Overall accuracy decreased to $\pm 60\text{mm}$ at 400m, and $\pm 70\text{mm}$ at 450m, distance.

As for the triangulation, the accuracy of the results was assessed from the repeatability of the reference target coordinates, and the corresponding data are included in table 5.7.1. to enable a direct comparison between the two methods. Although the standard errors for the photogrammetric coordination compare reasonably well with the triangulation results,

unlike the latter they increase considerably with distance from the observation stations. Thus accuracy decreases to about $\pm 40\text{mm}$ (estimated) over the entire depth of field (Meridian Air Maps Ltd., 1974(a)).

The photogrammetry was thus considerably inferior to the triangulation in respect of the accuracy achieved. There were, however, extenuating circumstances, which may be summarised as follows:-

- (1) There is equipment available which is capable of yielding superior results to those obtained. This is particularly true of the plotter.
- (2) The equipment was not used to best advantage. Errors of alignment occurred between the cameras and the phototheodolites; these had to be deduced by orientating the photographic plates in the stereoplotter until the best fit with the control points was achieved.
- (3) The reference targets were not always positioned to best advantage; in particular SCR/1 was outside of the overlapping portion of the photographs and its position had to be constructed analytically.
- (4) The lack of any reference targets beyond the furthest target positions meant that the latter were located by extrapolation outside of the spatial volume defined by the reference targets.
- (5) Due to lack of internal illumination in the Wild P32 s both the plate labels and the fiducial marks were, at best, poorly defined and, at worst, non-existent for the night time photographs.
- (6) The targets were also much more difficult to locate on the night time photographs because of the combination of poor lighting and a very fast film. Any type of surveying is obviously very difficult under such conditions.

5.7.4. Discussion of the Results

(i) During Construction

As a consequence of weather conditions and working pressures, the triangulation results for Bank 1, Stage 1 only cover the construction period up to 2.75m fill height, with a final reading being taken after failure. The results are plotted in figures 5.7.2. to 5.7.4. together with the displacements of adjacent inclinometers, where applicable. The photogrammetry results were very erratic and indicated much larger displacements than the inclinometers. Upon inspection of the original plots it was noticed that the large variations in displacement predicted by the photogrammetry were systematic and confined to the early part of construction. Furthermore, from 2.75m fill height upwards the incremental displacements of the targets were, at worst, in the same direction as indicated by the inclinometers and, at best, (e.g. SB2/1, IB1; SB3/1, IB2) very similar to the inclinometer displacements. Thus it was decided to plot the vertical (ΔZ) and horizontal (ΔY) displacements of the targets from the triangulation data as far as they went, and to link the photogrammetry data to these at a fill height of 2.75m, as shown in figures 5.7.2. to 5.7.4.

The horizontal displacements at ground/fill level of the inclinometer casings and the vertical displacements of the tops of the inclinometer casings are in good agreement with the horizontal and vertical displacements of the targets from the triangulation results. The differences are certainly within the cumulative effects of the accuracy of the measurements ($\pm 15\text{mm}$ approximately) and the differences in location of the measurements.

No vertical movement readings were taken of the inclinometers after 2.75m fill height and the photogrammetry provides the only source of data from this point on. The results from Bank 1, Stage 2, as discussed subsequently, indicate that these are reliable. The horizontal displacements from those photogrammetry data used, show agreement with the inclinometer results which varies from very good (SB3/1, IB2; SB2/1, IB1) to poor (SA3/1, IA2), although the time dependence of movements near failure must be borne in mind when comparing displacements on a fill height basis.

During the construction of Bank 1, Stage 2 both photogrammetry and triangulation results were obtained throughout. Again vertical (ΔZ) and horizontal (ΔY) displacements have been plotted against fill height (figures 5.7.5., and 5.7.6). The agreement between the triangulated displacements and the inclinometer results is again very good for both the vertical and horizontal directions. The photogrammetry results are generally in reasonable agreement with the other two sets of data in the vertical direction. The horizontal displacements from the photogrammetry are not so good, although up to a fill height of 4.05m the differences are not great. Thereafter, however, the results exhibit consistent variations, for all the targets, of the type observed in the Stage 1 results, although of lesser magnitude. In neither set of data does there appear to be any great improvement in the agreement between the photogrammetry and triangulation results with decreasing distance to the base lines.

It is worth re-emphasising at this point that Bank 1, Stage 2 was essentially constructed in one lift up to 2.75m. The foundation movements represented by the targets are thus only a part of the total displacements at any particular point. Likewise, the inclinometer displacements plotted

for comparison purposes relate only to events after the first location of the surface targets. Targets SA/B/C1-4/2 were all installed with the fill height at 2.75m.

The surface targets installed for Bank 2 (figures 4.1 and 4.5) were located by triangulation survey throughout construction and then at intervals for a limited period post-construction as discussed in section 5.2. The displacements of the targets, as derived from triangulation survey and physical measurements, are plotted versus fill height in figure 5.2.1., and against time in figure 5.2.2.

These results appear to represent the greatest accuracy achieved using the triangulation survey, as can be seen from a comparison with the results for Bank 1.

(ii) During and After Failure

The movements of the surface targets during the failure of Bank 1, Stage 1 as determined by photogrammetry are shown in figure 5.7.7. Straight line approximations of the total construction and failure displacement vector for each target have also been drawn to scale on the post-failure profiles presented in section 6.2., to enable a comparison to be made between the photogrammetric measurements and those obtained from the ground survey. To further aid this comparison the ground surface movements at the target locations have been superimposed on the plots of figure 5.7.7., assuming the ground to have moved in the same overall direction as indicated by the target. These ground surface movements are to convey a better idea of the scale of the displacement vectors on the post-failure sections, and should not be interpreted as representing the accuracy or otherwise of either set of measurements. This is because the basis on which the ground surface vectors have been drawn is only representative for certain

locations. Also included in figure 5.7.7. are the final vectorial positions of the targets as located by triangulation survey.

The key to the times of the readings presented in figure 5.7.7. is given in table 5.7.2; the times of the final measurements made with the various location systems are compared in table 5.7.3.

DATA POINT	1	2	3	4	5	6	7	8	9	10
STEREO PAIR	30	31	33	34	35	37	38	40	41	42 .
TIME, DATE	1930/9	1945/9	2005/9	2012/9	2020/9	2030/9	2034/9	0100/10	0400/10	0700/10

Table 5.7.2.

Key to Photogrammetric Displacements During Failure of Bank 1, Stage 1

(figure 5.7.7; end of construction was at approximately 1730 hours and has been represented by stereo pair number 30, which was the first of the failure sequence for all targets except SA2/1, for which the last construction data are at a fill height of 3.50m and stereo pair number 34 represents the first data of the failure sequence).

It can be seen that the final triangulation survey was carried out on the second day following the failure and the ground survey three days after the failure. A comparison of the final photogrammetric locations with those from the triangulation survey indicates continuing movements of the soil mass during the 10 and 11/10/73. The results from the two sources appear fully compatible, the continuing movements indicated by the triangulation

being in the same directions as the photogrammetric displacements. Any comparisons with ground survey measurements should be made with due regard to the approximate nature of the latter.

MEASUREMENT	STAGE 1	STAGE 2
Last Stereo Pair	0700/10/10/73	0524/17/11/73
Last Time Lapse	2210/9/10/73	2327/16/11/73
Triangulation	A.M. 11/10/73	A.M. 19/11/73
Ground Survey	12/10/73	20-22/11/73

Table 5.7.3.

Comparison of Times of Final Measurements for Bank 1

The corresponding results for Bank 1, Stage 2 are presented in figures 5.7.8. to 5.7.10, and the key to the readings in table 5.7.4.

DATA POINT	1	2	3	4	5	6	7	8
STEREO PAIR	17	18	19	20	21	23	25	27
TIME, DATE	1550/16	2250/16	2307/16	2320/16	2334/16	0004/17	0104/17	0524/17

Table 5.7.4.

Key to Photogrammetric Displacements During Failure of Bank 1, Stage 2

(figures 5.7.8. to 5.7.10; end of construction was at approximately 1700 hours, the final data being from stereo pair number 17 taken when the fill height was 4.40m. The start of the failure was at 2240 hours. Targets SA/B/C5/2 were first observed on 14/11/73 when the fill height was 4.05m).

In the case of targets SA/B/C4/2 comparisons with the ground surface movements were inappropriate, as can be seen from the post-failure sections. The comments made for the Stage 1 data are also applicable for Stage 2 and the order of timing of the final measurements can be seen in table 5.7.3. to be the same. The final triangulation locations were again fully compatible with continuing movements of the slipped mass. However, in the case of targets SC5/2 and SB4/2 sensible final triangulation locations were not obtained; this is thought to be due to disturbance of the targets following the failure. This was a problem with all the post-failure observations as large numbers of people visited the site following the failures and some disturbance of the instruments doubtless occurred.

The photogrammetry results provide a unique set of data for the trial embankments in that displacements were monitored both during construction as well as during and after failure. The precision of the data was much more amenable to the magnitude of the displacements during failure than to those during construction. The displacements of the surface targets during failure are further discussed in section 5.8., which deals with the results of the time-lapse photography.

5.7.5. Final Comments

The use of conventional survey methods provides a very precise method of location of surface targets. The achieved accuracy of location of about ± 7 mm (99% confidence level) was of the order required for the observations at Mucking, and was compatible with the data from the other horizontal displacement observations. Comparisons with such data, particularly the

inclinometer results, suggest that this precision closely approached the accuracy of representation of the foundation and fill measurements.

Precise survey measurements are not difficult to make with the right equipment.* However, the importance of the observation stations (as has been amply demonstrated) and accurate base line measurement must not be overlooked. Finally, of course, the measurements are only as accurate as the target movements are representative of the ground/fill displacements; this point has been well demonstrated in section 5.2.

The main disadvantage of precise surveying is the time it takes, particularly when the number of stations and targets is large and/or if readings have to be repeated to achieve the required precision.

Photogrammetry, on the other hand, is a very powerful survey method when large numbers of points are to be located in a relatively short time, and it can be used, as at Mucking, to provide a near continuous record of displacements during construction and failure. A prerequisite for precise photogrammetric work is the accurate location, by conventional survey methods, of sufficient control points to define the spatial volume containing the targets. This is not always easy for close observations of long structures (Moore, 1974). The provision of an elevated target at the rear of the embankment, as was incorporated in the time-lapse photography for Bank 1, Stage 2 (figure 4.4), might have improved matters at Mucking, although this would not have been a stationary control point. The control points should ideally be surveyed before each photographic exercise.

*A more sensitive theodolite than that used is recommended for target location.

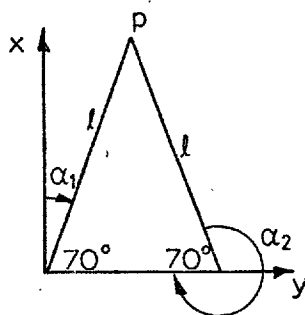
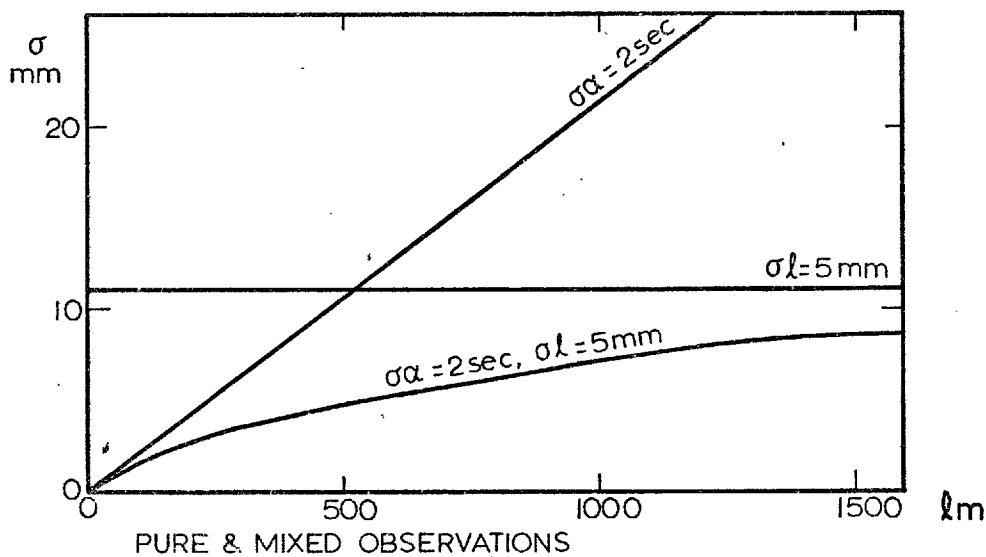
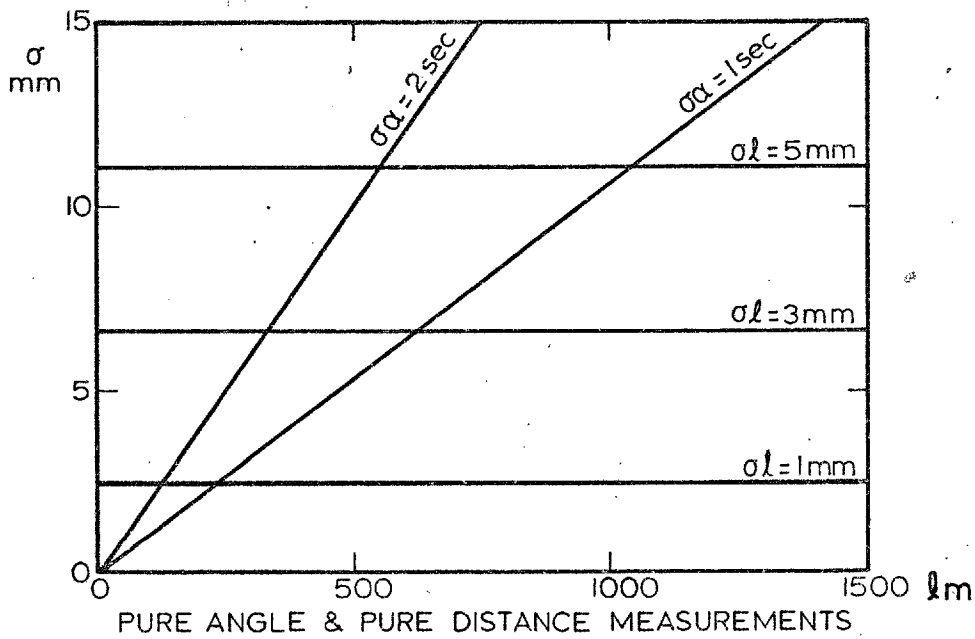
One of the main operational limitations on photogrammetry is its dependence on weather conditions (Moore, 1973) although this was not a great problem at Mucking. However, some photographs were incorrectly exposed and even a small amount of under- or over-exposure can make the restitution process very difficult. As the latter is the most expensive part of the operation the use of at least 3 shutter speeds with the chosen aperture makes good economic, as well as technical, sense.

Never-the-less the success of the night time photogrammetry shows the technique to be capable of good results even under the most arduous conditions. For target location at night and with rapid movements such as those associated with embankment failures, photographic survey methods are very well suited.

The use of photogrammetry to measure construction displacements has the disadvantage that the results cannot be immediately processed. Triangulation survey data can, on the other hand, be rapidly computed using a desk-top calculator. The overall accuracy of the photogrammetric surveys is hard to assess; the data plotted suggest it to be better than the $\pm 40\text{mm}$ overall quoted by Meridian Air Maps (1974 (a)), but significantly worse than the $\pm 7\text{mm}$ for the triangulation. A figure of between ± 10 to $\pm 25\text{mm}$ appears compatible with the plotted data, this representing the lower limit which would be acceptable for the order of magnitude of the pre-failure displacements. However, for the failure movements such an order of accuracy was more than adequate.

A large number of the targets were installed in the fill. Measurements of fill displacements always present problems because of the difficulty of obtaining datum readings i.e. locating the measuring point when the fill height is at the elevation of the target (Werneck, 1974; Moore, 1973). At Mucking this problem was overcome for the Stage 1 targets by installing them at the top of the embankment slopes after a layer of fill had been placed, and then surveying them. The Stage 2 targets, however, as stated previously, only recorded part of the total displacements at their locations. The inclinometers were extended prior to filling so that zero readings could be taken, although in this case a zero reading for the fill surface level at the instrument location was not possible. Thus the comparisons between the inclinometer and surface target displacements were made on an incremental basis following the fill lift corresponding to the target installations.

Finally, it will not be apparent on what basis the stereo pairs were selected for analysis. Initially, reasonable coverage of events using the best (photographically) pairs was attempted. However, due to the difficulties described, quite a number of pairs were unsuitable for analysis and the resulting coverage was the best that could be achieved. Whereas it was initially anticipated spending a couple of hours analysing each pair, inner orientation difficulties meant that up to a day was spent on some pairs. This also meant a rather drastic increase in the cost of the restitution process.

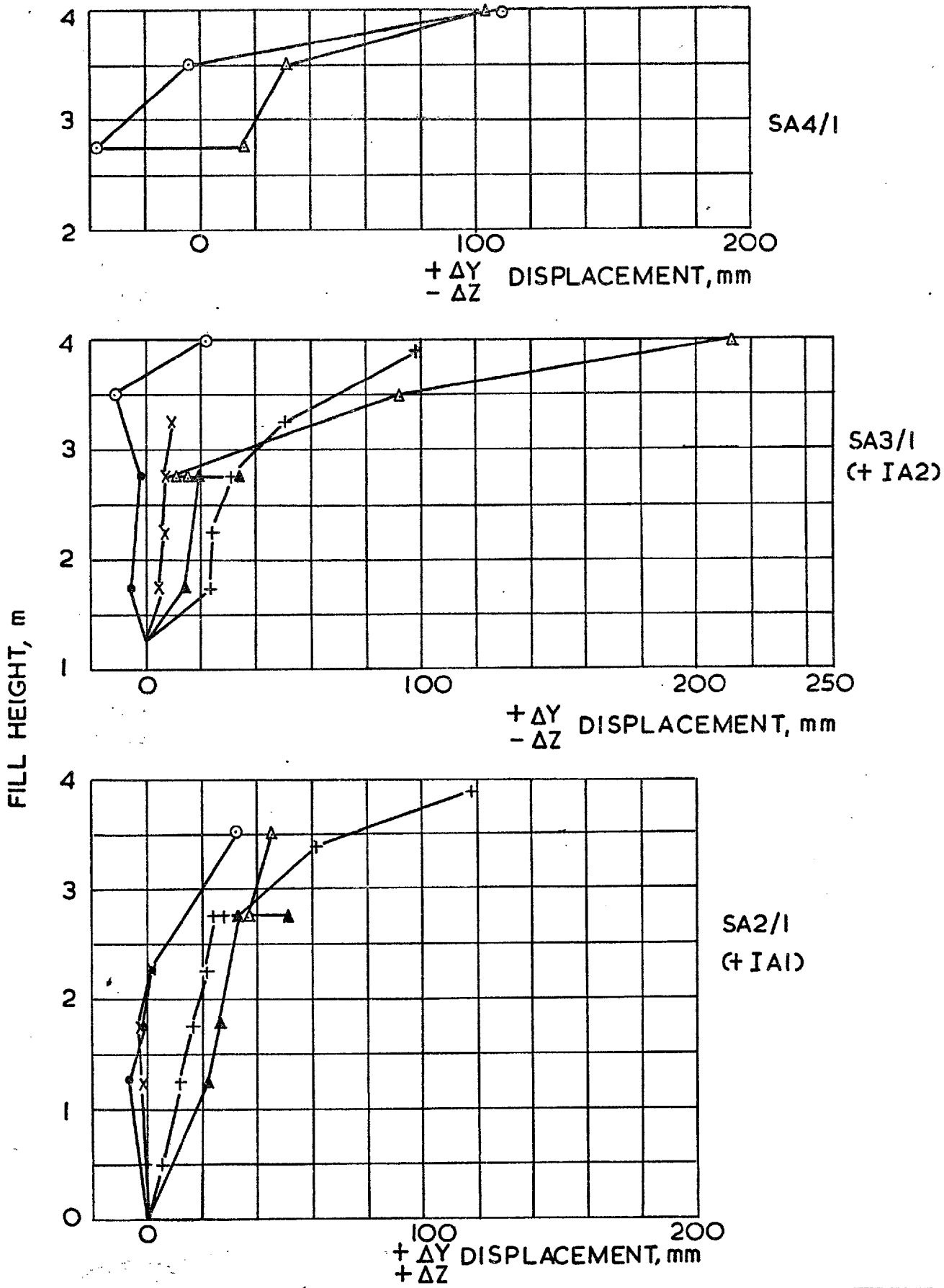


TARGET LOCATION

LEGEND : $\sigma(\alpha)$ = STANDARD ERROR OF ANGULAR (α)
 OR DISTANCE (l) MEASUREMENT

σ = OVERALL STANDARD ERROR
 FOR TARGET LOCATION

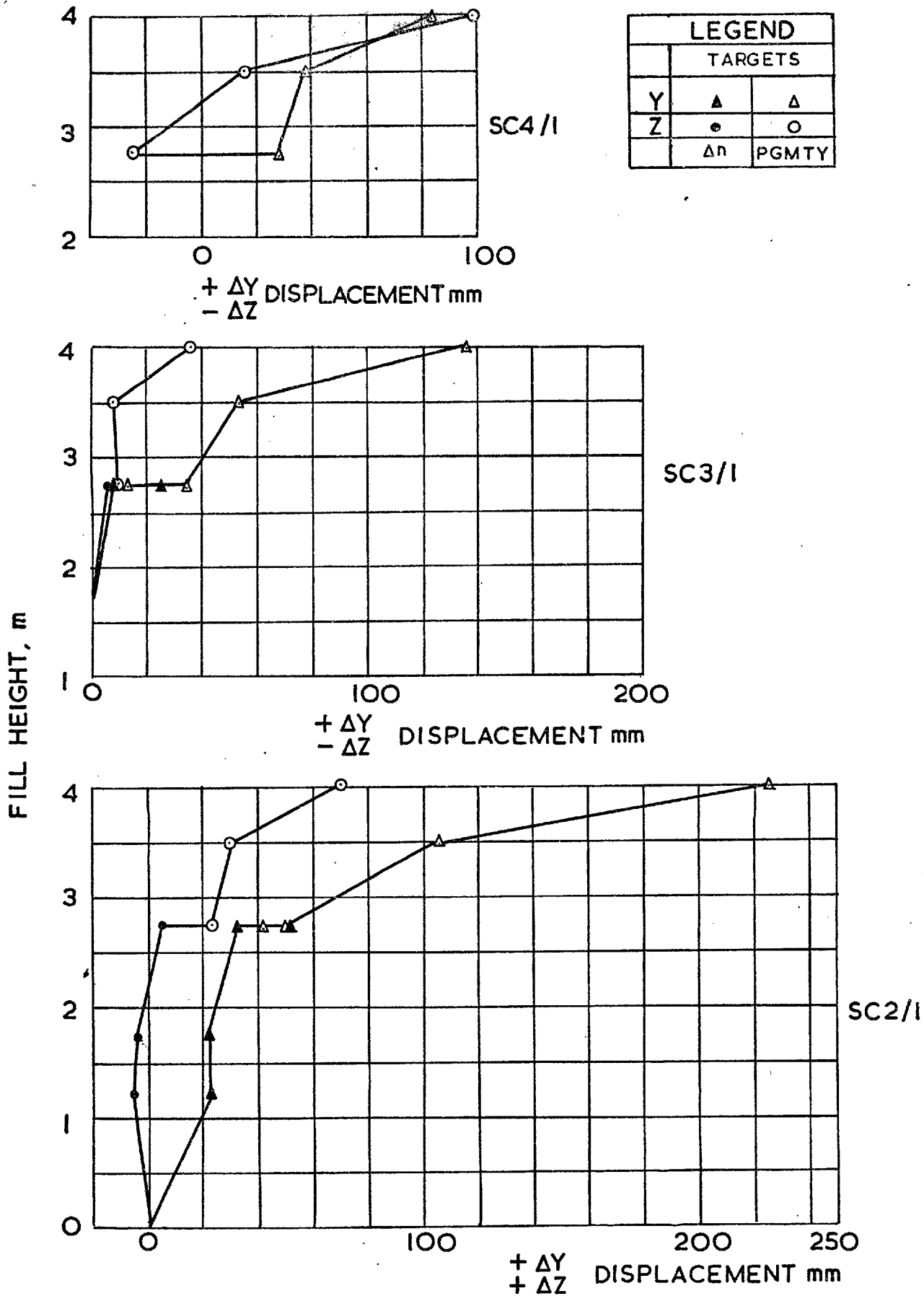
TYPICAL ACCURACIES FOR LOCATION OF SURFACE TARGETS (after Ashkenazi, 1973)



**BANK I, STAGE I
SECTION A
DISPLACEMENTS OF SURFACE TARGETS DURING
CONSTRUCTION**

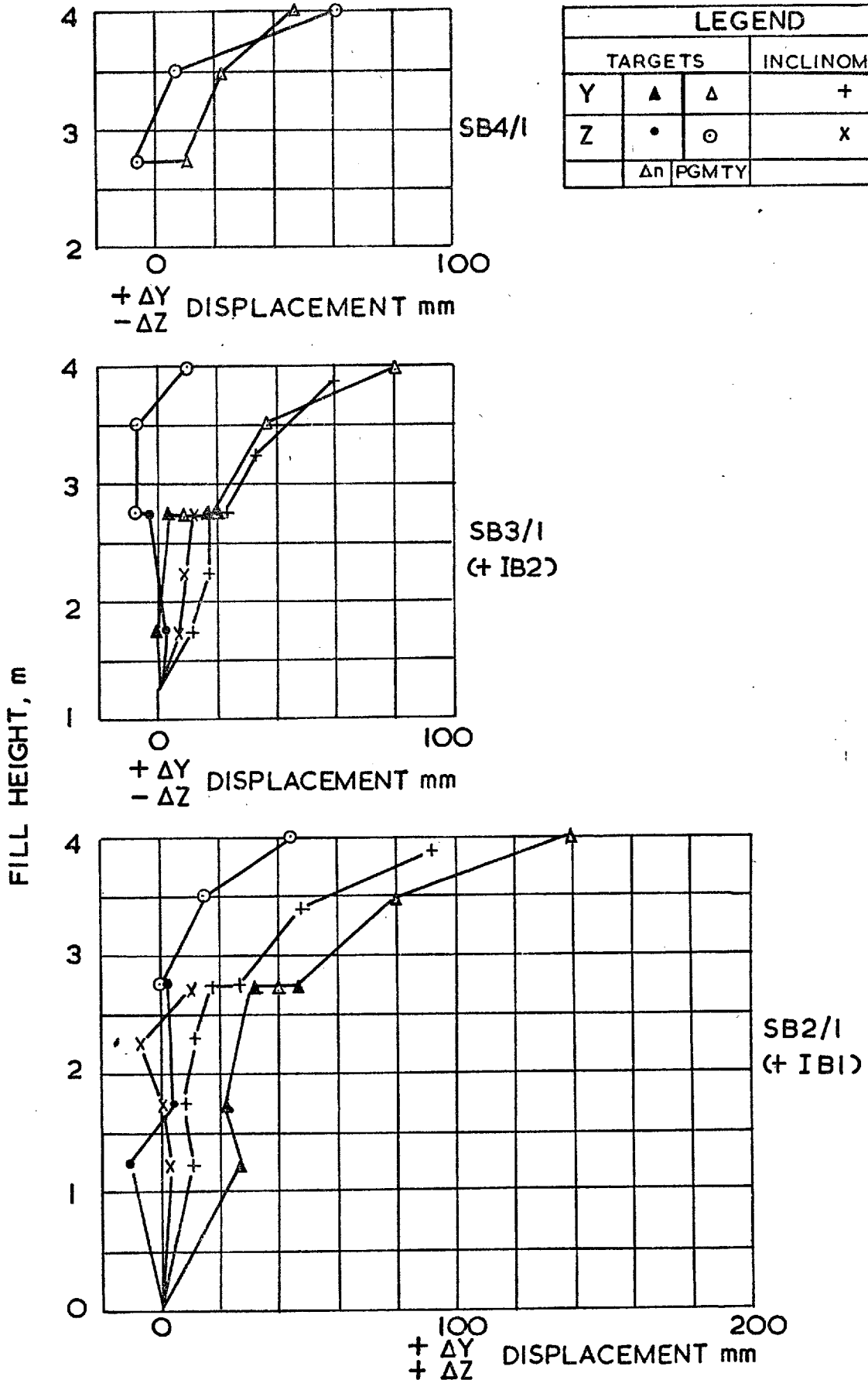
LEGEND	TARGETS	INCLINOMETERS
Y	▲ △	+
Z	• ○	X
	Δn PGMTY	

Fig. 5.7.2



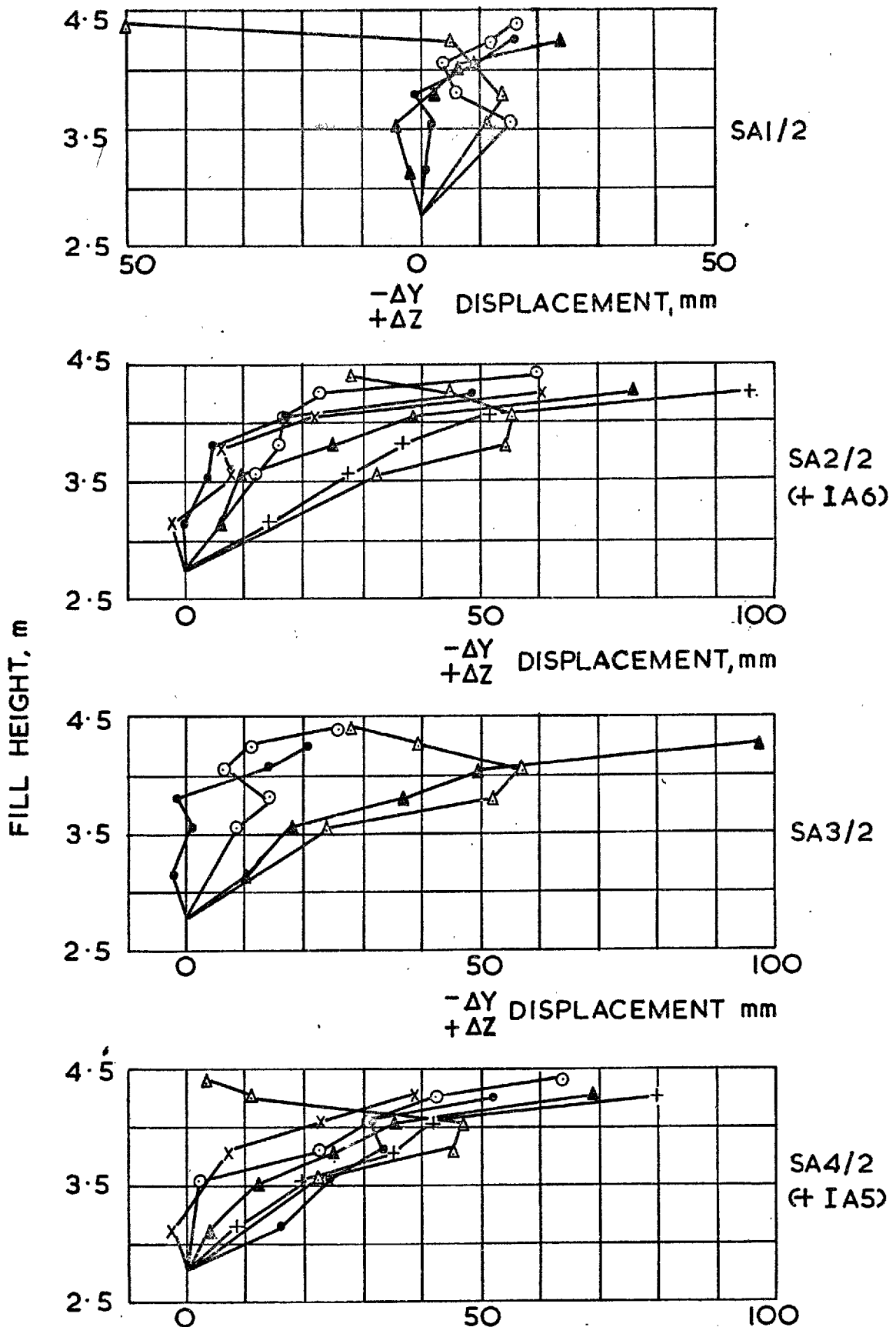
BANK I, STAGE I, SECTION ϕ
 DISPLACEMENTS OF SURFACE TARGETS DURING
 CONSTRUCTION

Fig. 5.7.3



BANK I, STAGE I, SECTION B
 DISPLACEMENTS OF SURFACE TARGETS DURING
 CONSTRUCTION

Fig. 5.7.4

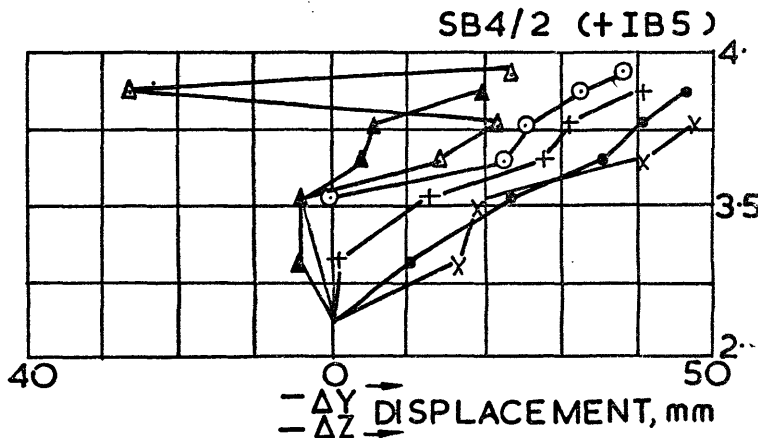
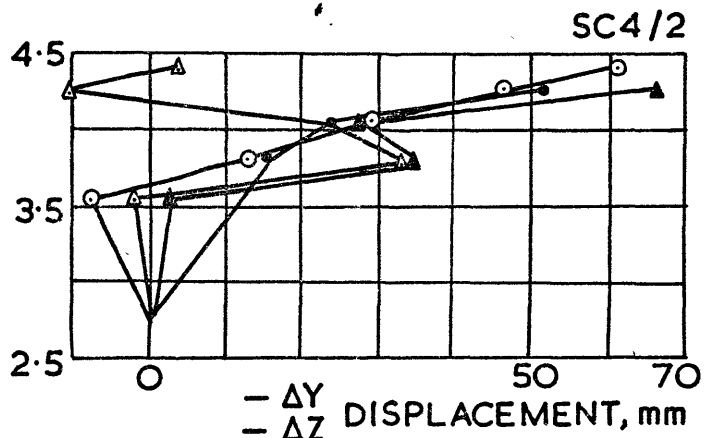
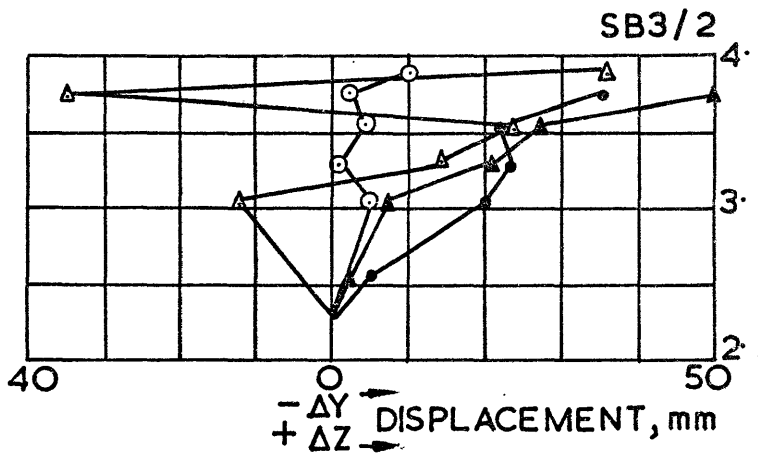
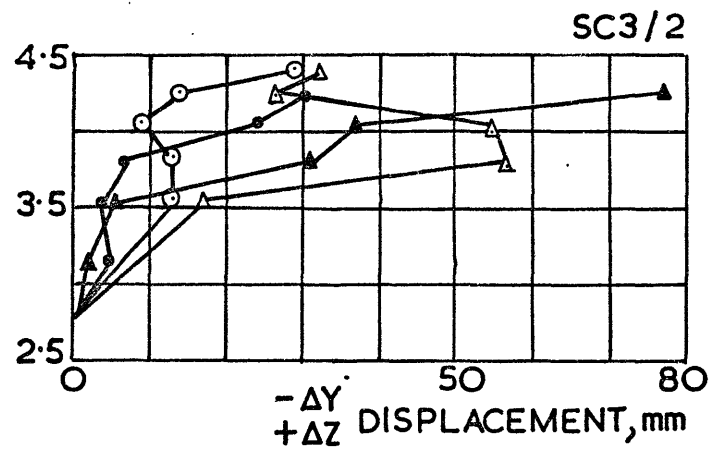
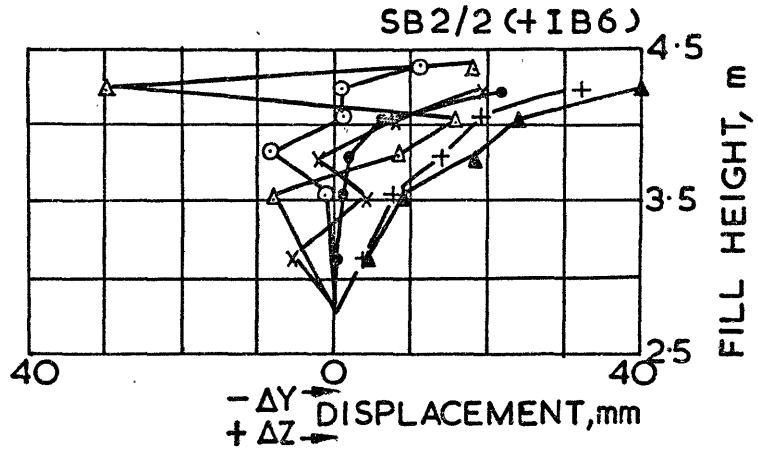
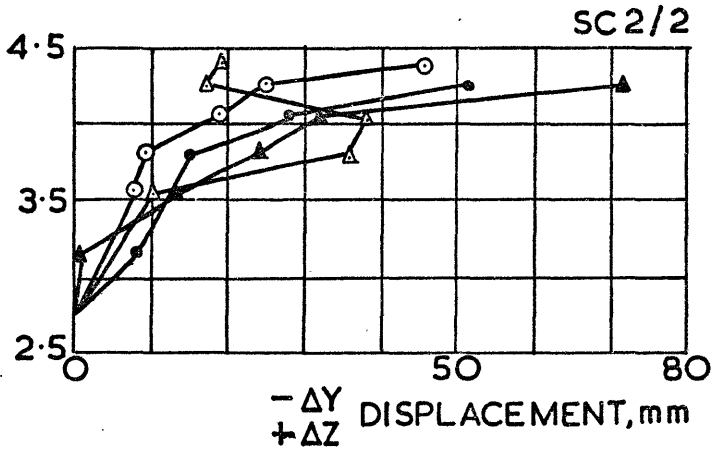
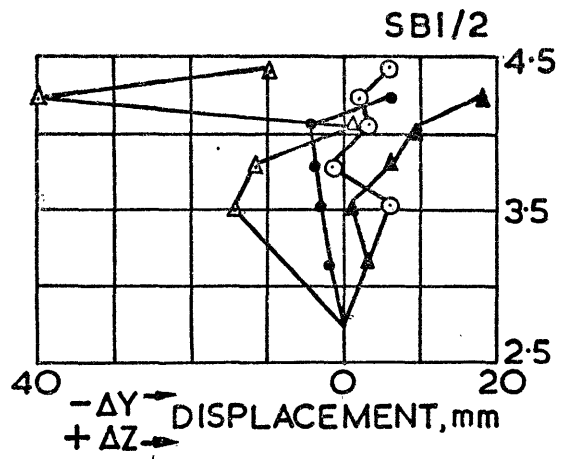
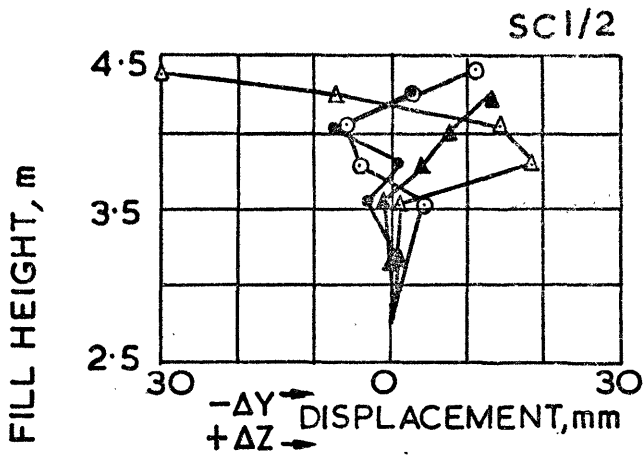


LEGEND			
	TARGETS		INCLINOMETERS
Y	▲	△	+
Z	●	○	×
	Δn	PGMTY	

-ΔY DISPLACEMENT mm
+ΔZ

BANK I, STAGE 2 SECTION A

DISPLACEMENTS OF SURFACE TARGETS DURING CONSTRUCTION

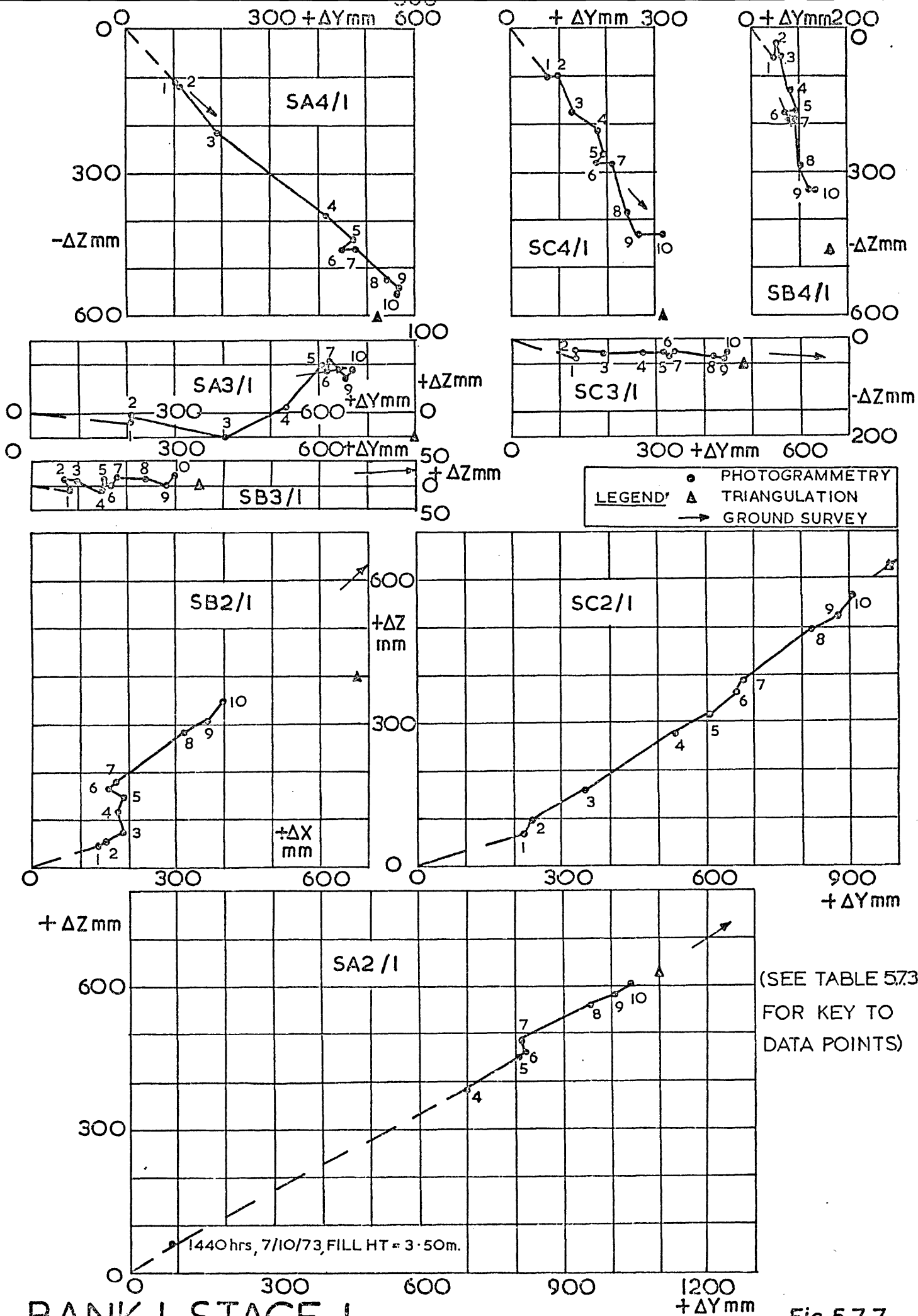


LEGEND			
	TARGETS		INCLINOMETERS
Y	▲	△	+
Z	●	○	x
	Δn	PGMTY	

BANK I, STAGE 2 SECTIONS C & B

DISPLACEMENTS OF SURFACE TARGETS DURING CONSTRUCTION

Fig. 5.7.6

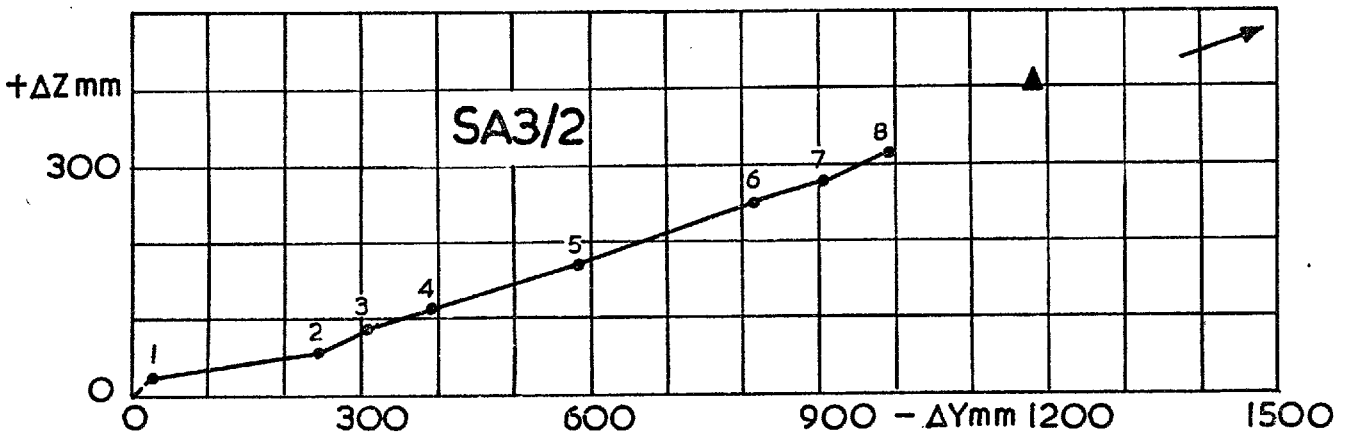
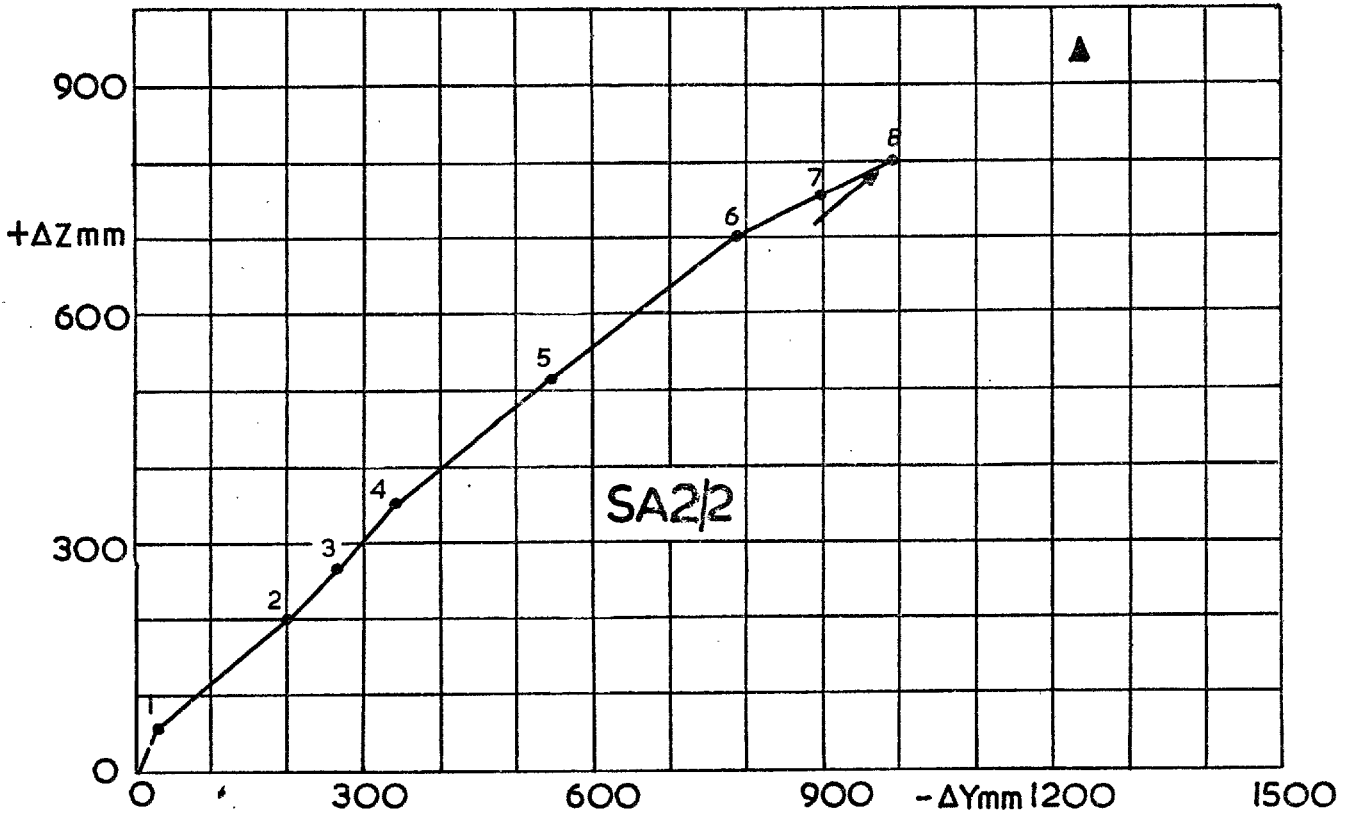
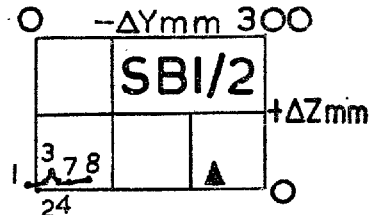
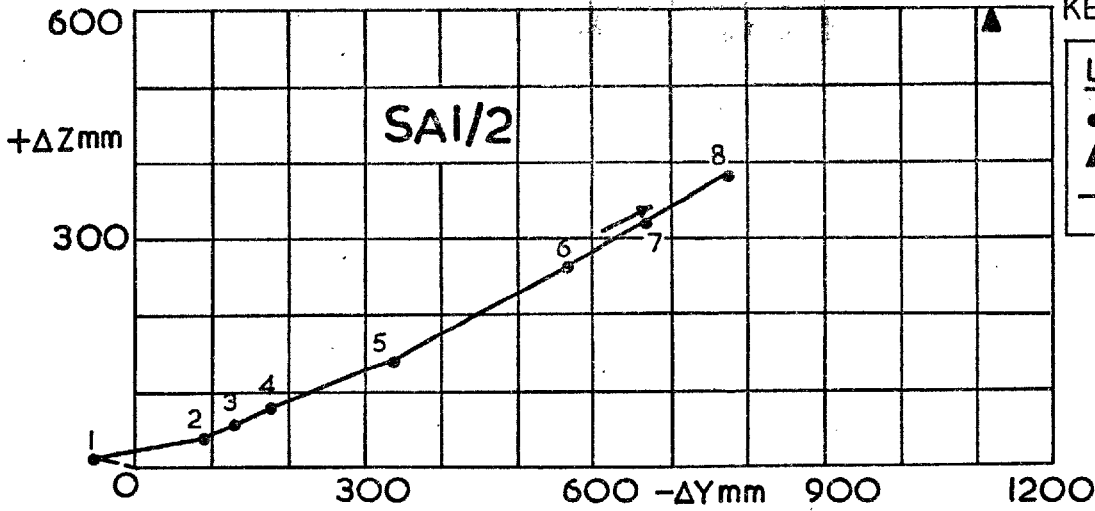


BANK I, STAGE I

DISPLACEMENT VECTORS FOR SURFACE TARGETS DURING FAILURE

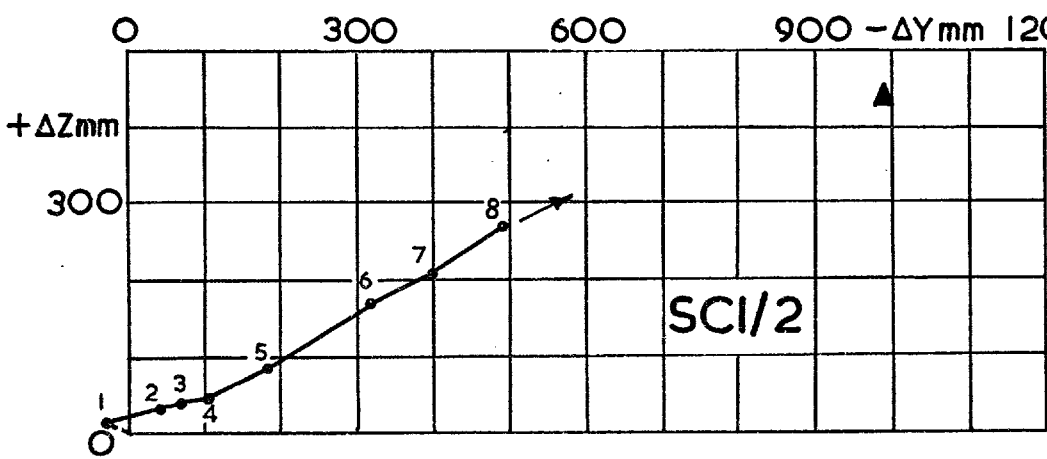
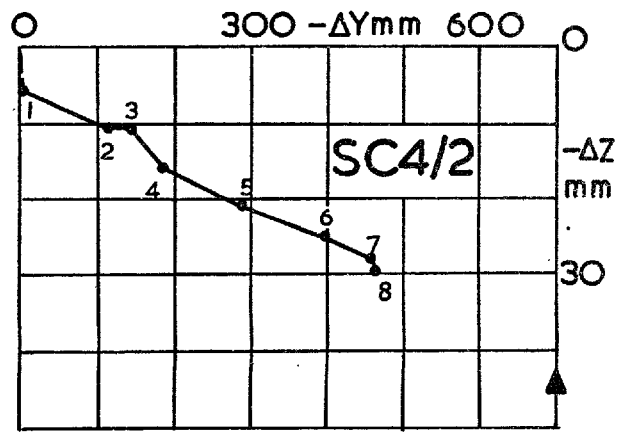
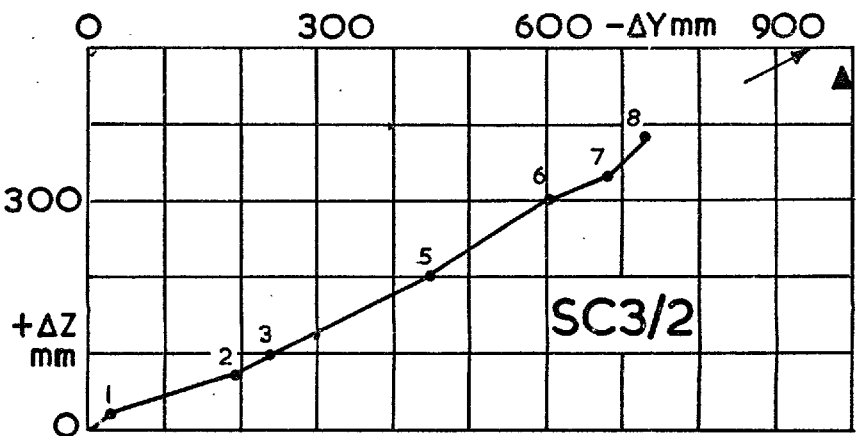
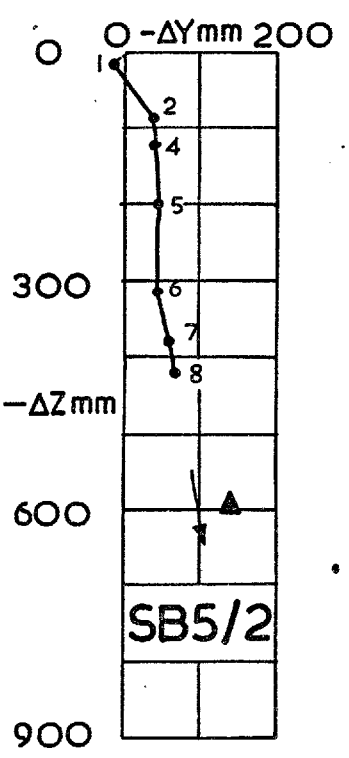
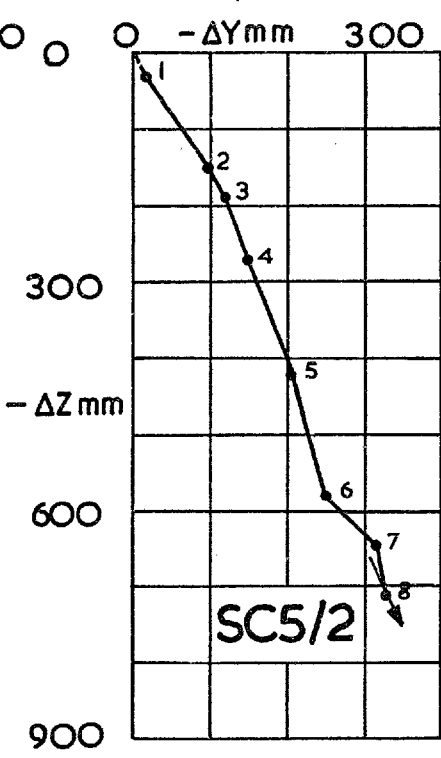
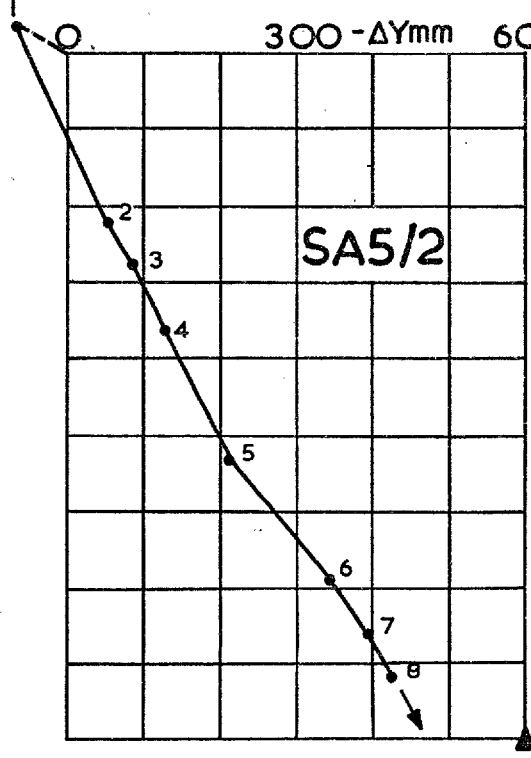
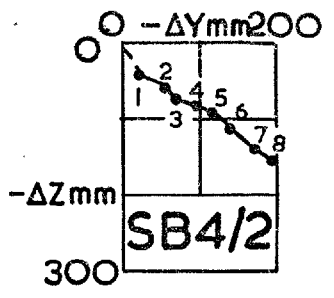
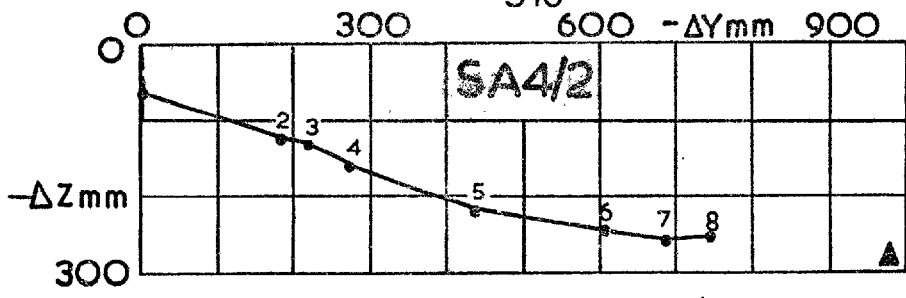
Fig. 5.7.7

(SEE TABLE 57.5 FOR KEY TO DATA POINTS)



**BANK I, STAGE 2 : SECTIONS A & B
DISPLACEMENT VECTORS FOR SURFACE TARGETS
DURING FAILURE**

Fig. 5.7.8

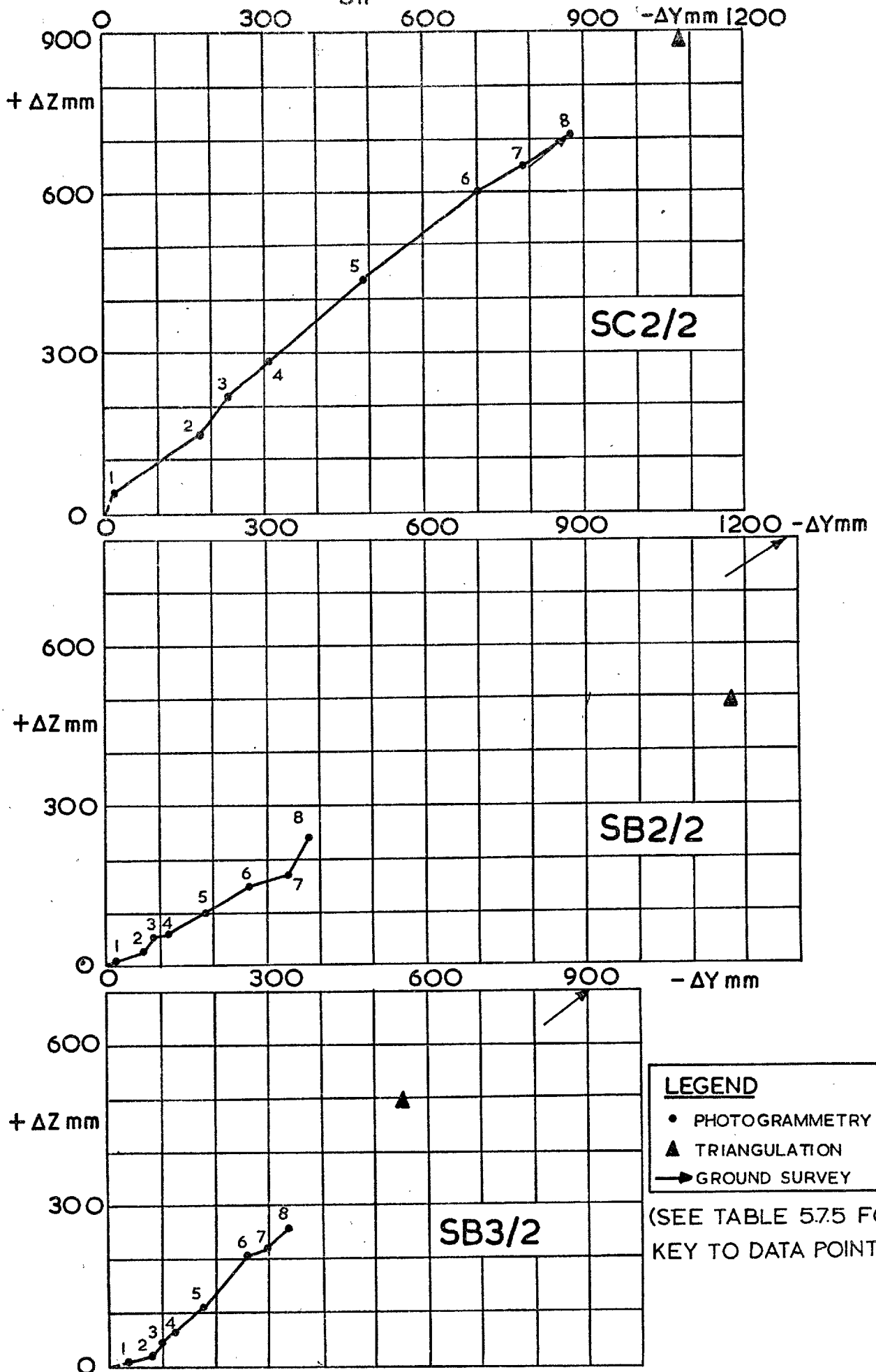


LEGEND

- PHOTOGAMMETRY
- ▲ TRIANGULATION
- GROUND SURVEY

(SEE TABLE 575 FOR KEY TO DATA POINTS)

BANK I, STAGE 2 : SECTIONS A, C & B
DISPLACEMENT VECTORS FOR SURFACE TARGETS
DURING FAILURE
 Fig. 5. 7. 9



BANK I STAGE 2: SECTIONS C & B
DISPLACEMENT VECTORS FOR SURFACE
TARGETS DURING FAILURE

5.8. Time-Lapse Photography

5.8.1. General

Inspection of the available literature concerning failures of trial embankments on soft clay foundations reveals that many failures have occurred outside of normal working hours (see e.g. Wilkes, 1972(a); Ladd 1972; Dasgal et al, 1972; Wroth, 1976). Whilst one might postulate that this was due to extra-terrestrial or climatic factors, the time dependence associated with the development of shear strains in many soft clays, as suggested by Bjerrum (1972 and 1973) and discussed in Chapter 3, is a likely reason for such occurrences.

In order to obtain the maximum benefit from the foundation trials it was decided that, in addition to 24 hour manning of the site during the latter parts of Stages 1 and 2 of the Bank 1 construction program, and photogrammetric monitoring of the failures of the latter, a near continuous photographic record of the anticipated failures should be aimed for. The photography was to be triggered automatically by movements of the embankment, and continued on a time-lapse basis throughout the periods of major movement. The exercise would thus be fully automatic, and not dependent for operation on the site staff other than in the initial setting up and in checking that the system was operational.

The photographic record of the failures would not pose any major problems if the latter occurred during daylight hours, but for the almost inevitable night time failure some form of luminous target was required. The mono photography obviously needed to record movements

of the embankment in (short) section, as closely as possible, for maximum analytical (qualitative or quantitative) benefit. At the distances involved the general illumination provided by the floodlights had no effect. It was, therefore, decided to use tunnel lights, attached to poles installed across the central section of the embankment, as targets for night time photography (figures 4.2 and 4.4; plates 5.8.1. and 5.8.2.).

Initially the time-lapse photography was intended to provide information on the timing of the failures, as well as to enable a qualitative interpretation of the failure mechanisms. In the event quantitative analyses were attempted, providing very encouraging results.

5.8.2. The Automatic Triggering System

This, when activated, set off an alarm bell and set the time-lapse camera in motion. The system comprised three mercury filled 48mm O.D. nylon tubes installed through the body of the embankment, at the base, approximately mid-height and close to the final crest level* (figure 5.8.1.(A)). The tubes were part of a composite cable containing electrical wires, and protected by a P.V.C. sleeve. Each tube was connected, at each end, to the base of a 6.4mm I.D. perspex cylinder, approximately 150mm long; the cylinders were clipped onto pieces of board so that they could be easily removed, or raised and lowered in situ, the boards being clamped to scaffold poles driven into the fill at approximately the same level as the mercury line (figure 5.8.1. and plate 5.8.1.).

*different levels were used for Stage 1 and Stage 2. (see tables 4.2. and 4.4.)

The connections at the bases of the cylinders were made with nuts and olives, to which were attached tags to enable the electrical wires to be connected. The tops of the cylinders were threaded to accommodate steel screws which could thus be raised or lowered so as to be just in contact with the mercury in the cylinders. A current was passed through the mercury in the cylinders via the tags and the screws: any differential movement of the two cylinders at the extremities of a mercury line would thus result in a break in the circuit at one end; this break activated the alarm bell and the camera.

The I.D., of the cylinders, required to provide a rapidly responding system, was determined by carrying out proving trials. The screws were set with a few millimetres of thread below the mercury meniscus; the response time was a matter of seconds. Thus a small differential movement across any of the three lines would break the circuit (figure 5.8.1.(A)), which was completed by a junction box wherein the break in the triggering circuit switched the power supply to the main circuit containing the alarm bell and the camera.

The junction box, alarm bell and camera were installed in a large weatherproof shelter (plate 5.8.1.), located as shown in figures 4.2 and 4.4 for Stages 1 and 2, respectively, of Bank 1, and to which a power line was run from the main generator.

It was found impractical to maintain a very sensitive setting on the triggering system during construction of the embankments as the shear strains induced in the foundation resulted in frequent alarm signals. Thus the screws were set about 10mm into the mercury, and

the positions of the screws and cylinders were observed, and adjusted as necessary to maintain the settings. However, after the end of each day's construction activity the settings were adjusted down to a few millimetres for the overnight period, during which they were again frequently checked, as was the overall functioning of the system.

5.8.3. Operation and Layout of the Photographic System

The camera used was a Hasselblad E.L. (plate 5.8.1.), this being clamped to a scaffold pole set in a mound of sand in order to achieve the required elevation. A working platform inside the camera shelter allowed easy access to the camera, alarm bell and the sensing/switching equipment. When activated, the camera could take photographs at one of several set time intervals completely automatically, each roll of film being approximately 70 exposures long; manual operation was also possible.

The tunnel lights were tied, using steel wire, to 3m long steel poles pushed approximately 1.5m into the foundation or fill (plate 5.8.1.). The lights were installed up the side of the embankment as construction proceeded and, as the critical height was approached, across the crest; they were also installed in the foundation to a distance well clear of any likely disturbance. Movements of construction plant necessitated those targets on the crest being taken down during working hours. The ground level at the pole bases, and the light bulb elevations, were determined by level survey, and the horizontal locations of the poles from the embankment centre line by tape measurements. Reference pictures were taken manually, as changes occurred in the numbers and positions, for the assessment of the displacements during failure.

Photographic trials were carried out under both daylight and night light conditions in order to ascertain a suitable exposure for each situation. This was desirable as the benefits of automation would have been somewhat reduced if the site staff had been required to re-set the camera as the light conditions changed. A film speed of 125 A.S.A. was used in conjunction with an aperture size of f.8. and a shutter speed of 1/30 second. This combination furnished excellent results, the targets being readily visible throughout the day and night, as illustrated in plate 5.8.2.

The camera locations were chosen so that the assumed line of collimation (based on assumed principal points, as discussed in section 5.8.4.) was as near to horizontal and parallel to the plane strain axis of Bank 1, as possible. The former condition was readily approximated to, as shown in figures 4.2. (Stage 1) and 4.4. (Stage 2), the collimation lines being 1.5° sub-horizontal and horizontal respectively. However, it did not prove possible to set up the collimation axes perpendicular to the 'Y' coordinate axis because of target visibility problems created by the embankment geometry. This fact is illustrated in more detail in figures 5.8.2. and 5.8.3., and its implications are discussed in section 5.8.4. The camera was, however, lined up so that the targets were near central in the frame, as shown in plate 5.8.2.

5.8.4. Analysis of the Results

(i) Determination of Target Image Coordinates

The developed negatives were firstly transferred to polyester based films, these being much more stable and thus better suited for measurement purposes. The coordinates of the target images on the negatives were determined using

a stereo comparator with only one viewing channel in operation. The machine used had output facilities in the form of punch tape as well as a digital display.

The photographic base line was established relative to which the targets were coordinated. This was done by orientating the film so that the horizontal axis of the comparator was parallel to a line passing through the extremities of the line of targets i.e. t22/1 to t1/1 for Stage 1 and tref/2 to t1/2 for Stage 2. For each frame analysed the primary reference target (t22/1 or tref/2) was assigned the same vertical and the same horizontal coordinates and the secondary reference target (t1/1 or t1/2) by necessity was assigned the same vertical coordinates as the primary. The coordinates of all the targets were thus determined, at various time intervals (i.e. for various frames), relative to the photographic axes.

(ii) Accuracy of Measured Coordinates

The measurement sensitivity of the stereo comparator was 1 micron; repeated location of a single light bulb image indicated an overall precision of ± 2 microns*. At the scale of the photography (see sub-section (iii)) this was equivalent to ± 2 mm of real target movement.

The other main errors which manifest themselves at this stage arise directly from the photographic process, due to misrepresentation of the target positions. Film stretch is probably the main source of error in this category, the image quality being very good due to the relatively

*the light bulb targets appeared on the negatives as circles of light with small 'tails'. Experimentation showed that the circle centres could be located most precisely.

slow film speed used. Any stretch could have been quantitatively assessed if the camera had been equipped with fiducial markings, but in their absence no estimate could be made of likely errors from such sources.

(iii) From Image Coordinates to Field Displacements

The basic data of target image coordinates, related to the photographic base line, were firstly converted to vertical and horizontal displacements in the plane of the film by transformation to the field axes and the application of a scale factor to the photographic displacements.

The relationship between object distance (u), image distance (v) and focal length (f) of a lens is usually expressed as follows:-

$$\frac{1}{u} + \frac{1}{v} = \frac{1}{f} \dots\dots\dots(5.8.1.)$$

and the scale is defined as v/u. For a camera with the lens focused at infinity the image can be seen to be in focus at the focal point (i.e. v = f) and the plane of the film is the focal plane of the lens and hence the scale is f/u. In fact the camera was focused just short of infinity, the average object distance being approximately 80m, for both construction stages.

However, recourse to equation 5.8.1. shows that when the object distance is less than infinity the scale is defined as:-

$$\text{scale} = \frac{v}{u} = \frac{f}{u - f} \dots\dots\dots(5.8.2.)$$

and therefore if u >> f, the scale is still approximately given by the ratio f/u.

Considering an average, in focus, object distance of 80m, the Hasselblad having an 80mm focal length, equation 5.8.2. leads to a scale factor of 1/999 as opposed to 1/1000 from the ratio f/u. The latter figure is thus

in error by 0.1% and was used for computation purposes.

As shown in figures 5.8.2. and 5.8.3. the object distances for Stage 1 varied between 75.4 and 84.3m, and for Stage 2 between 75.2 and 85.5m with distances along the assumed collimation lines of 77.2m and 78.9m respectively. The scales thus varied from 1/943 to 1/1054 for Stage 1, and from 1/940 to 1/069 for Stage 2. Assuming a mean scale of 1/1000 for both stages would thus involve errors of approximately $\pm 6\%$ in the determination of the field displacements in the plane of the film.

As discussed in section 5.7 the plane of the film is defined by the principal point which, together with the optical centre of the lens, in turn defines the line of collimation of the camera. With no fiducial marks to define the principal point, the collimation of the camera was unknown as was the plane of the film. With no other information to go on, it was assumed that the principal point was at the centre of the photographs, and thus the line of collimation was derived. For most terrestrial photogrammetry and air survey applications the optical or principal axis of the lens coincides with the collimation line of the camera (Kilford, 1973); the principal point is also more commonly within the central area of the photograph. The lens/camera axes shown in figures 4.2., 4.4., 5.8.2 and 5.8.3. are based on the assumption of a central principal point and coincident lens/camera axes.

Before proceeding further with the analyses it was decided to investigate the likely range of magnitude of error involved if the 'Y' and 'Z' field displacements were taken to be the horizontal and vertical displacements, respectively, in the plane of the film, as defined by the assumed collimation. As shown in figures 4.2. and 4.4., and discussed in section 5.8.3., the likely errors in the 'Z' direction were negligible. However, the situation

for the 'Y' direction, as depicted in figures 5.8.2., and 5.8.3., was rather different. The simple analyses graphically illustrated in these latter figures indicated errors of between -9% and +6% for Stage 1, and from -11% to +4% for Stage 2. It was considered that such errors were acceptable in view of the necessary assumptions made, and, additionally, that the average errors would be less than these extremes, particularly for those targets that actually moved.

A check on the validity of the various assumptions was made by comparing the length of the photographic base lines, as derived directly from the target image coordinates (assuming a scale of 1/1000), with the distances obtained from the ground surveys. The results, shown in table 5.8.1., indicate differences of 2.7% and 1% between the measurement sources for Stages 1 and 2 respectively. It was thus decided to adopt a constant scale of 1/1000 and to consider the displacements in the plane of the film as representative of the true displacements. This conveniently enabled the results to be plotted directly from the stereo comparator output coordinates, with rotation from the photographic to the field axes, one micron displacement on the negatives representing 1mm in the field. The results are presented in figures 5.8.4. to 5.8.8. for Stage 1, and figures 5.8.13 and 5.8.14 for Stage 2.

STAGE	PHOTOGRAPHIC BASE LINE LENGTH, m	
	PHOTOGRAPHS	GROUND SURVEY
1	45.63	44.46
2	38.18	37.80

Table 5.8.1.

Lengths of Photographic Base Lines Determined from Time-Lapse Photography and Ground Survey Measurements

(iv) Precision of the Observations

The method of restitution produced a measurement sensitivity of 1mm. The overall precision of target coordination was ascertained from the data for various targets outside the zone of influence of the embankment failures. The results are presented, in the form of standard errors and 99% confidence levels, in table 5.8.2., the average 'Y' and 'Z' standard errors being $\pm 9.8\text{mm}$ and $\pm 5.7\text{mm}$ respectively for Stage 1 and $\pm 6.9\text{mm}$ and $\pm 5.1\text{mm}$ respectively for Stage 2. The accuracy of location thus compared very favourably with the photogrammetry results, but it must be remembered that the time-lapse photography was a purely 2-dimensional exercise. The least accurate aspect of photogrammetry is, in general, coordination in the direction perpendicular to the base line.

Further examination of the measured coordinates of the light bulbs shows the scatter in the positions of the 'stationary' targets to be within $\pm 20\text{mm}$ and mostly better than $\pm 15\text{mm}$; figures which compare very favourably with the size of a light bulb! The positional changes were largely consistent and may therefore have been the result of slight movements of the camera caused by the automatic rewind and shutter release sequence. The calculated standard errors include the influence of any actual movements of the targets due to wind etc.

5.8.5. Discussion of the Results

(i) Bank 1, Stage 1

The construction and failure of Bank 1, Stage 1 have been discussed in section 4.3.3., and the sequence of events detailed in tables 4.2., and 4.3. In particular, the unqualified success of the automatic triggering

TARGET	COORDINATE DIRECTION	NUMBER OF OBSERVATIONS	STANDARD DEVIATION	99% CONFIDENCE LEVEL
			\pm mm	\pm mm
t1/1	Y	22	11.2	28.1
	Z	22	3.2	7.8
t5/1	Y	22	13.9	34.8
	Z	22	6.4	16.1
t8/1	Y	22	10.3	25.7
	Z	22	6.6	16.6
t21/1	Y	22	3.6	9.1
	Z	22	6.7	16.8
t18/2	Y	16	3.7	9.1
	Z	16	5.8	14.6
t17/2	Y	16	5.1	12.8
	Z	16	5.0	12.6
t3/2	Y	16	7.1	17.7
	Z	16	5.4	13.6
t1/2	Y	16	11.8	29.4
	Z	16	4.2	10.4

Table 5.8.2.

Accuracy of Target Location Using Time-Lapse Camera

system in detecting the incipient failure was most rewarding. It is very doubtful if the first signs of failure would have been observed without it, and even with staff on site full time an important part of the movements would almost certainly have gone unrecorded. Indeed, on reflection, even had the embankment been inspected every half an hour or so, most of the major movement could have been missed without the automatic system.

Following the triggering of the alarm bell and camera at 1930 hours on the 9/10/73, the first film in the camera was exposed automatically at the selected, nominal, 2 minute (1.87 minute actual) time-lapse sequence. This covered the period from 1930 hours (frame number 9) to 2124 hours (frame number 70). A second film was then loaded and exposed at the same sequence for 26 frames (2132 hours to 2224 hours; frame numbers 71 - 96 inclusive). At this point the automatic mechanism failed to operate (for unknown reasons) and this fault was not discovered until 2400 hours. The photographs were then taken manually at 10 minute intervals (0010 hours to 0100 hours, 10/10/73; frame numbers 97 - 102 inclusive) and thereafter at 15 minute intervals until 0900 (frame numbers 103 - 134). The automatic mechanism was repaired and the remainder of the film exposed at the 2 minute sequence (0920 to 0936 hours; frame numbers 135 - 148 inclusive). Finally a third film was exposed with a time-lapse interval of 5 minutes (1000 hours 10/10/73 to 0315 hours 11/10/73; frame numbers 149 to 218 inclusive).

The time-lapse negatives analysed were selected to give a reasonably detailed coverage of the failure; no problems were encountered regarding the quality of the photographs. The displacement vectors for all the

targets are presented in figures 5.8.4. to 5.8.8. The initial and final displacements of the moving targets and the total displacements of the 'stationary' targets have been plotted to a larger scale to enable a more detailed analysis of the development of the failure as well as the detection of any systematic errors. The initial coordinates of the moving targets also indicate how the starting points of the displacement vectors were arrived at.

Inspection of the coordinates for the 'stationary' targets, in addition to indicating the high degree of the accuracy of location, reveals that there were certain systematic trends running through the data. These are thought to be the result of camera movements, as outlined previously. There also appeared to be some discrepancy between the coordinates obtained from the first (up to frame 70) and second (frame 70 onwards) films. This was almost certainly due to movement of the camera when the films were changed. However, as can be seen from the figures, the results were very encouraging; the vectorial plots also indicated that sufficient data had been analysed to cover the movements detectable within the accuracy of the measurements. Therefore, frame 90, taken 160 minutes after the start of the failure, was the final time-lapse negative analysed.

Plots were then prepared of displacement versus time, as shown in figures 5.8.9. to 5.8.11. These revealed just how well the time-lapse photography had captured the development of the failure from the first small movements through the acceleration to a maximum velocity, and then the deceleration. However, the plots also showed that, within the time span considered, the latter process was not complete and that as indicated by the surface target observations, significant movements

continued to take place after the main period of the failure.

Figure 5.8.12 shows similar plots for the surface targets on the centre-line section, both over the time scale of the main movements and over the 12 hours following the failure. The photogrammetric data also recorded the development of the failure very well, although not in such detail as the time-lapse photographs. The displacements plotted over the 12 hour period show that the 160 minute period covered by the time-lapse photographs analysed did in fact represent the major part of the failure movement. As the photogrammetric and triangulation data appeared to adequately cover the continuing movements, and because of uncertainties regarding disturbances of the time-lapse camera during repairing and reloading, it was decided not to analyse any more photographs.

Table 5.8.3. indicates the scale of the continuing movements as well as the good general agreement between the displacements of the surface targets and the time-lapse camera targets.

The post-failure profiles presented in section 6.2. include straight line approximations to the displacement vectors of the time-lapse targets; figures 5.8.4. to 5.8.8. show this to be, in general, a reasonable approximation. As for the surface movement targets, the displacement vectors of the targets have also been drawn at the bases of the target poles to enable direct comparisons with the ground surface movements. The assumption implicit in such a representation is only valid if the target pole and the soil had undergone a translational motion. If the motion was essentially rotational the targets and the bases of the poles would move in concentric circular paths, and for this case the errors

may be estimated.

Considering the critical slip circle for the effective stress analyses (Chapter 7) plus targets SC3/1 and t15/1, indicates the surface target and time-lapse target to under estimate the movements by 5% and 15% respectively. Internal distortion of the slipped mass at the target locations would obviously introduce much more serious errors.

TIME ELAPSED	RESULTANT DISPLACEMENTS OF TARGETS, mm					
	SC4/1	t16/1	SC3/1	t15/1	SC2/1	t12/1
2 hrs 40 mins	270 ⁺	355	260 ⁺	135	695 ⁺	600
12 hours	405 ⁺	-	325 ⁺	-	850 ⁺	-
27 hours	555 ^x	-	350 ^x	-	945 ^x	-

+ Photogrammetry

x Triangulation

Table 5.8.3.

Long-Term Movements of Slipped Mass, After the Start of Failure -

Bank 1, Stage 1

Comparisons of the movements of the surface targets with the post-failure sections derived from the ground survey show good general agreement with respect to magnitude and direction. It should be borne in mind that the ground survey was approximate and the profiles thus involve a fair amount of interpolation, as well as remembering the time differences between the measurements.*

*the vectors represent the total displacements recorded by the photogrammetry, and not the triangulation.

The time-lapse camera targets only represent the movements during failure and the latter can only be compared in magnitude to the surface targets; table 5.8.3. indicates good general agreement. The vectorial directions show very good agreement with the movements of the foundation and reasonable agreement in the fill. In the latter case, however, it appears that the poles toppled to some extent, being influenced by internal distortion within the fill. The pole of target t10/1 almost certainly straddled the 'slip surface', resulting in the inconsistent displacements of the target.

It is difficult to assess the accuracy of the ground surface movements depicted by the displacements of the time-lapse camera targets because of the lengths of the poles. However, it would seem that in the foundation, if rotational errors were accounted for (assuming a circular slip), the accuracy was similar to that of the surface targets, whereas in the fill the latter were more accurate by virtue of their shorter pole lengths.

The overall¹ vectorial picture of the failure movements provided by the time-lapse photography was highly satisfactory; a more detailed discussion of the movements of individual targets, as well as the development and mechanism of the failure, follows in section 6.2.

(ii) Bank 1, Stage 2

The construction and failure of Bank 1, Stage 2 have similarly been discussed in section 4.3.3., the sequence of events being detailed in tables 4.4. and 4.5. Once again the automatic triggering system was

invaluable, the first alarm being signalled at 1705 hours on the 16/11/73, just 5 minutes after construction had finished for the day and a reference photograph (frame number 19) had been taken with the time-lapse camera. Only one frame (number 20) was taken before the system was reset; the next frame marked the start of the failure sequence which ran from 2240 to 2327 hours (frame numbers 21 to 46 inclusive) at the nominal 2 minute setting. At this point the camera ceased to function, possibly as a result of the sub-zero temperature. When this was discovered (at 2340 hours) manual operation was attempted but the winding mechanism was inoperative. Thus unfortunately only the first 47 minutes of the failure were recorded by the time-lapse photography.

The displacement vectors of the time-lapse camera targets have been plotted in figures 5.8.13 and 5.8.14, in similar fashion to the Stage 1 results. The comments made with respect to the latter, regarding accuracy of location, systematic errors and the overall highly satisfactory appearance of the results similarly apply to the Stage 2 results, as far as they go.

Presented in terms of displacement versus time (figures 5.8.15 and 5.8.16) the results again show how well the time-lapse photography recorded the development of the failure up to the point when the camera malfunctioned. Unfortunately this can be seen to be just at the time when the rate of movement was at a maximum.

Another interesting point to emerge from figures 5.8.13 to 5.8.16 concerns the magnitudes of the displacements which took place in the 340 minute interval between the end of construction and the onset of the main failure. This appears to be in contrast to Stage 1, for which the displacements of the surface targets recorded when the alarm was first sounded were plotted

as part of the construction displacements (figures 5.7.2. to 5.7.4.), and the failure developed much more abruptly. In other words, there was only a very short period (the 10 to 20 minutes following the sounding of the alarm bell) of transition, between the 'construction scale' displacements and the 'failure scale' displacements.

The longer period of build up to the Stage 2 failure is equally well shown by the displacements which occurred between the last photogrammetric survey of the construction sequence and the first of the failure sequence (figures 5.8.17. and 5.8.18). The photogrammetric data again provide an excellent picture of the before, during and after-failure displacements of the embankment. The limited time-lapse data were of great use in supplementing the latter, by providing a much more detailed account of the development of the major movement.

The different displacement/time build-up to the Stage 1 and Stage 2 failures is further illustrated in figure 5.8.19., wherein the resultant displacements of surface targets SC2/1 and SC2/2 are plotted over a 70 hour period up to and including the major movements of the failures. The Stage 2 results show a definite period of about 7 hours during which the movements were accelerating towards failure. Although the pre-failure curve is not as well defined in terms of photogrammetric data for Stage 1, its shape, as drawn, is supported by the general observations of the foundation instrumentation and the time-lapse photographic data. The Stage 1 results indicate a more rapid build up of construction displacements leading into a more abrupt failure. This apparent difference in the transition from the 'construction scale' displacements to the 'failure scale' displacements is further discussed in section 6.2., with particular reference to the

presence of the desiccated layer during Stage 2, as is the development and mechanism of the Stage 2 failure.

The length of the deceleration period is again evident from the figures in table 5.8.4., as is the excellent agreement between the surface target displacements and those of adjacent time-lapse camera targets.

Reference to the post-failure profiles for Stage 2 presented in section 6.2. indicates the good overall agreement between the vectorial displacements of the targets and the embankment, bearing in mind the various uncertainties, discussed in relation to the Stage 1 results, and the partial nature of the surface target vectors in this case. The limited time-lapse data again look good, although the target poles in the foundation nearest to the toe of the slip appear to have been disturbed in similar fashion to t10/1, whereas the surface targets have functioned perfectly. The rotational errors for Stage 2 are approximately the same as those calculated for Stage 1, for similarly placed targets.

TIME ELAPSED	RESULTANT DISPLACEMENTS OF TARGETS, mm							
	SC5/2	t13/2	SC3/2	t10/2	SC2/2	t8/2	SC1/2	t6/2
40 mins	135 ^{+*}	140	140 ^{+*}	135	215 ⁺ *	250	70 ⁺ *	165
6.7 hours	610 ⁺ *	-	635 ⁺ *	-	920 ⁺ *	-	510 ⁺ *	-
60 hours	-	-	900 ^{x*}	-	1195 ^{x*}	-	1035 ^{x*}	-

*start of failure extrapolated back on figure 5.8.17.

⁺photogrammetry

^xtriangulation

Table 5.8.4.

Long-Term Movements of Slipped Mass, After the Start of Failure -

Bank 1, Stage 2

5.8.6. Final Comments

The monitoring of surface targets during failure was very successful, particularly when the difficulties involved are considered. The photogrammetric data were almost certainly more accurate than the time-lapse data by virtue of the targets being better able to follow the ground movements. The precision of both methods was acceptable for the magnitude of the measured displacements.

The time-lapse photography, by providing detailed information on the development of both failures was invaluable as was the automatic triggering system which enabled both the time-lapse and photogrammetric work to be carried out successfully.

The use of triangulation/photogrammetry to monitor construction displacements with photogrammetry being used to monitor the failure and triangulation to finally locate the targets was very successful. Time-lapse photography supplemented these measurements by providing much more detailed coverage of the more rapid displacements, and the use of both methods was fully justified. The time-lapse photography, whilst inherently less sophisticated, was very simple to operate and to process; it has been shown to be capable of comparable accuracy to photogrammetry.

For future work certain suggestions can be made to improve a time-lapse photographic installation, as follows:-

1. the use of poles of similar length to the surface target poles, with the light bulbs tied firmly in position.

2. the use of a camera with fiducial markings in conjunction with polyester based films
3. any surface targets should be as close to the ground surface as is practicable
4. when analysing the Stage 1 results it was at first feared that target t22/1 might not have been far enough from the slipped mass to provide a reference datum. However, detailed examination of the movements of targets t22/1 and t/1 showed that no relative displacement between the targets was detectable within the accuracy of the data. However, for Stage 2 it was decided to install a more positive reference target in the form of tref/2; this was mounted on a long length of scaffold pole set into the rear berm. The use of such a target enabled the photographic base line to be established at the start of the photography, and this base line was not disrupted by the construction process. The establishment of such a base line is recommended for any future work.

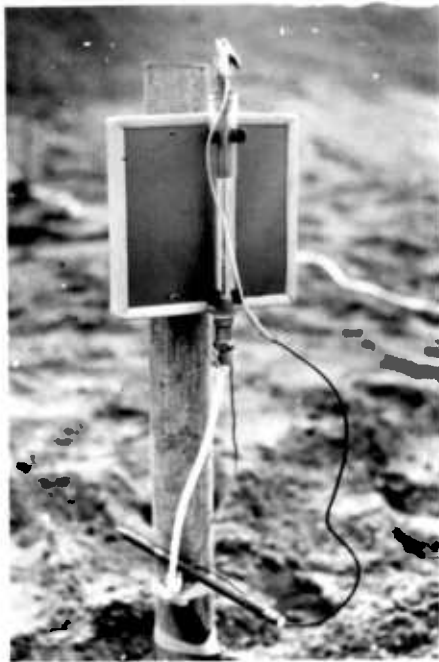


PLATE 5.8.1 INSTALLATIONS FOR TIME LAPSE PHOTOGRAPHY

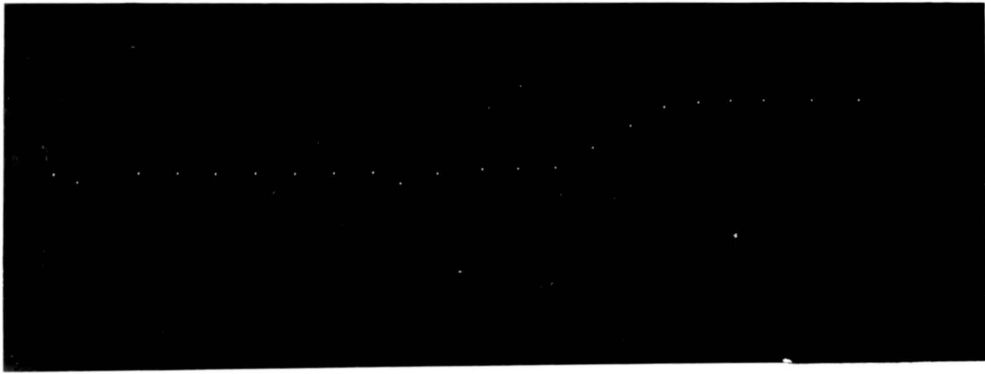
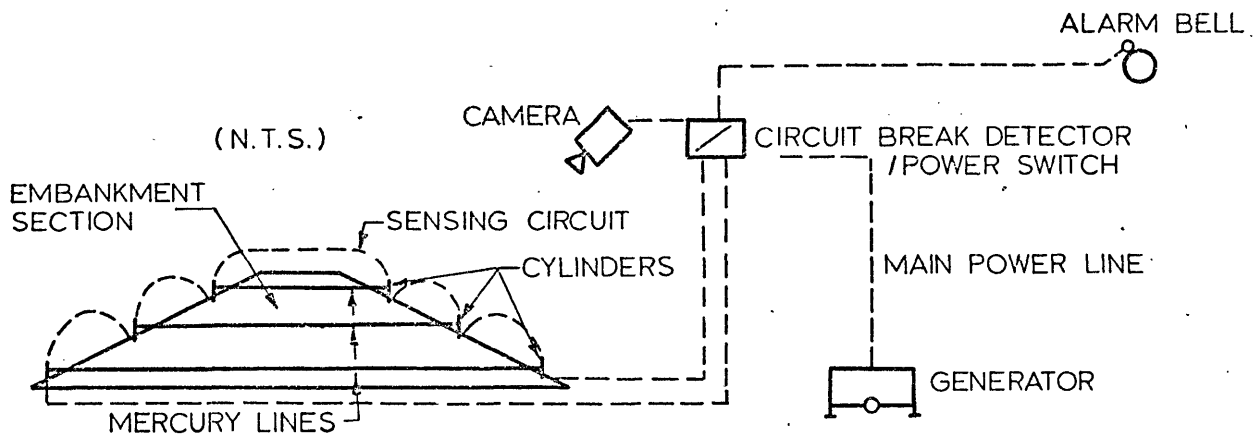
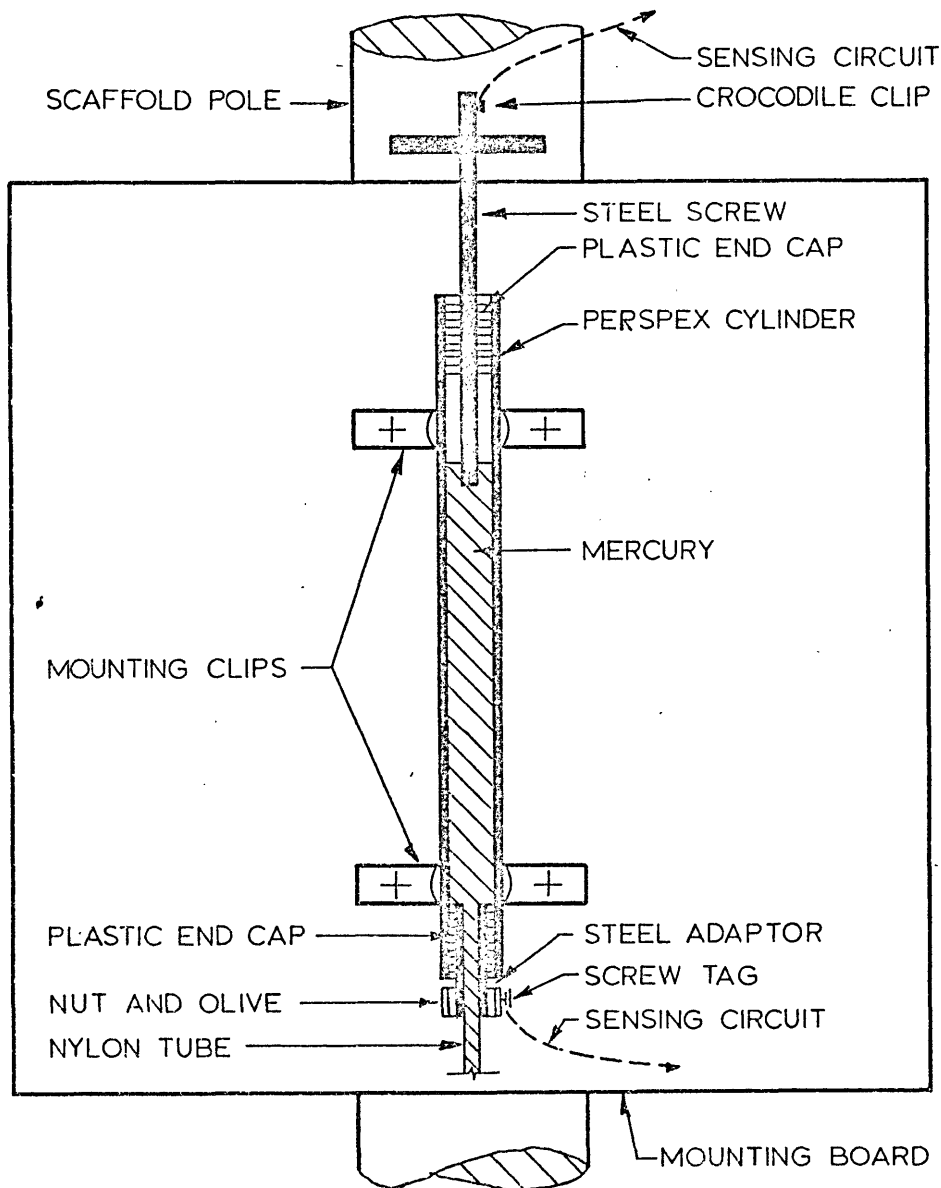


PLATE 5.8.2 INSTALLATIONS FOR TIME LAPSE PHOTOGRAPHY

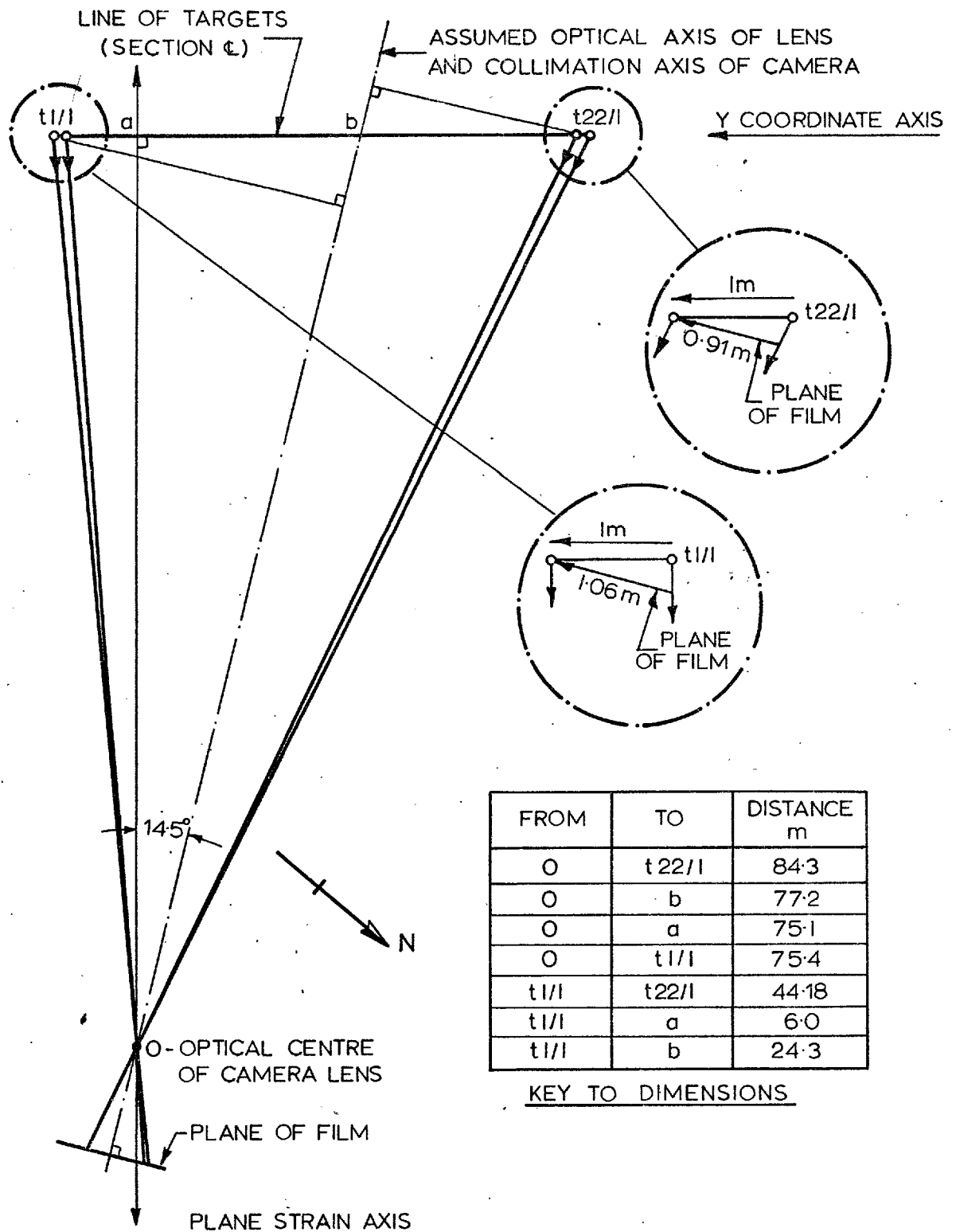


A) SCHEMATIC LAYOUT OF AUTOMATIC TRIGGERING DEVICE FOR ALARM BELL AND TIME-LAPSE CAMERA

B) DETAIL OF CYLINDERS (APPROXIMATELY TO SCALE)



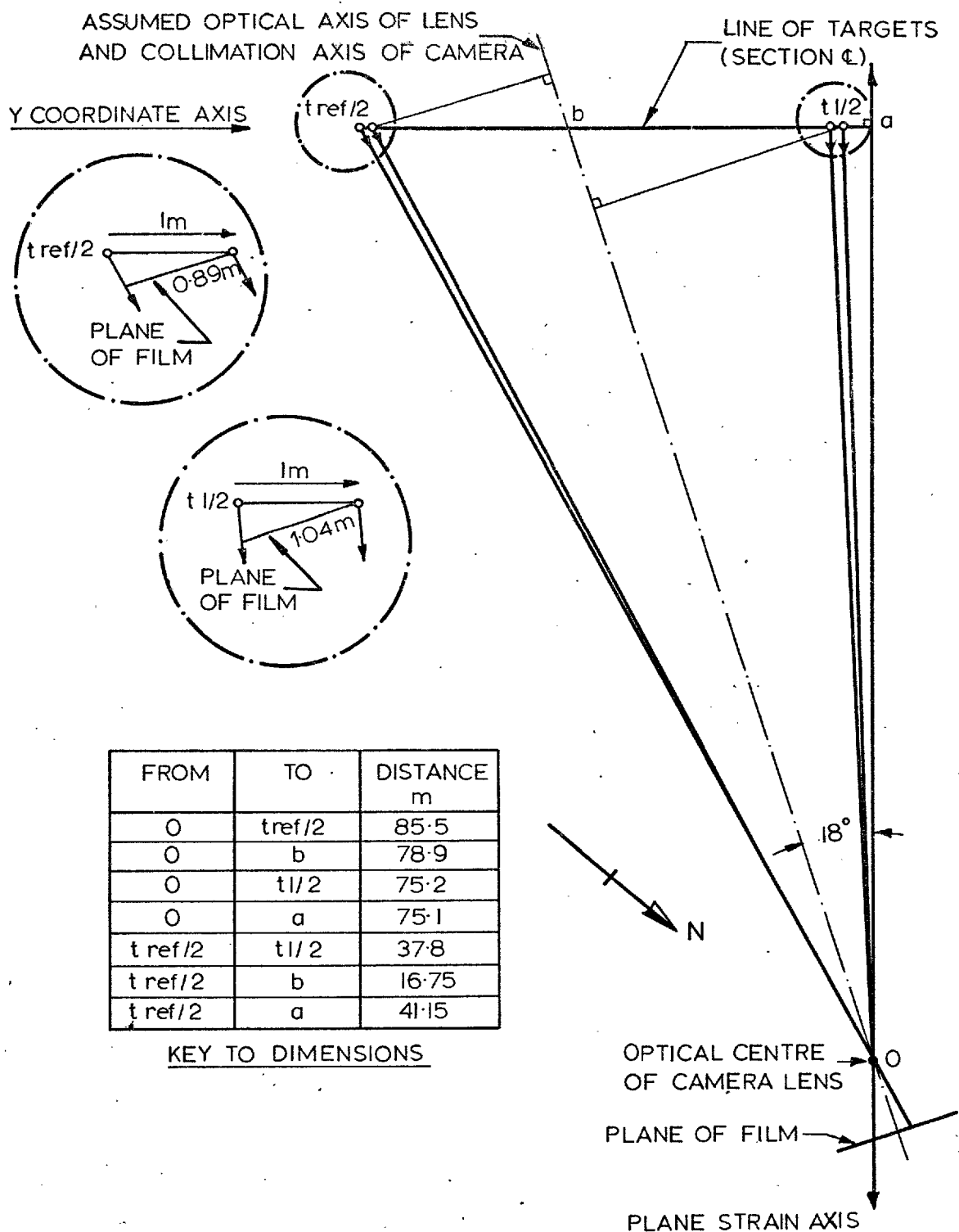
AUTOMATIC TRIGGERING SYSTEM



BANK I, STAGE I

Schematic relationship between horizontal displacements in the film plane and the site 'y' axis

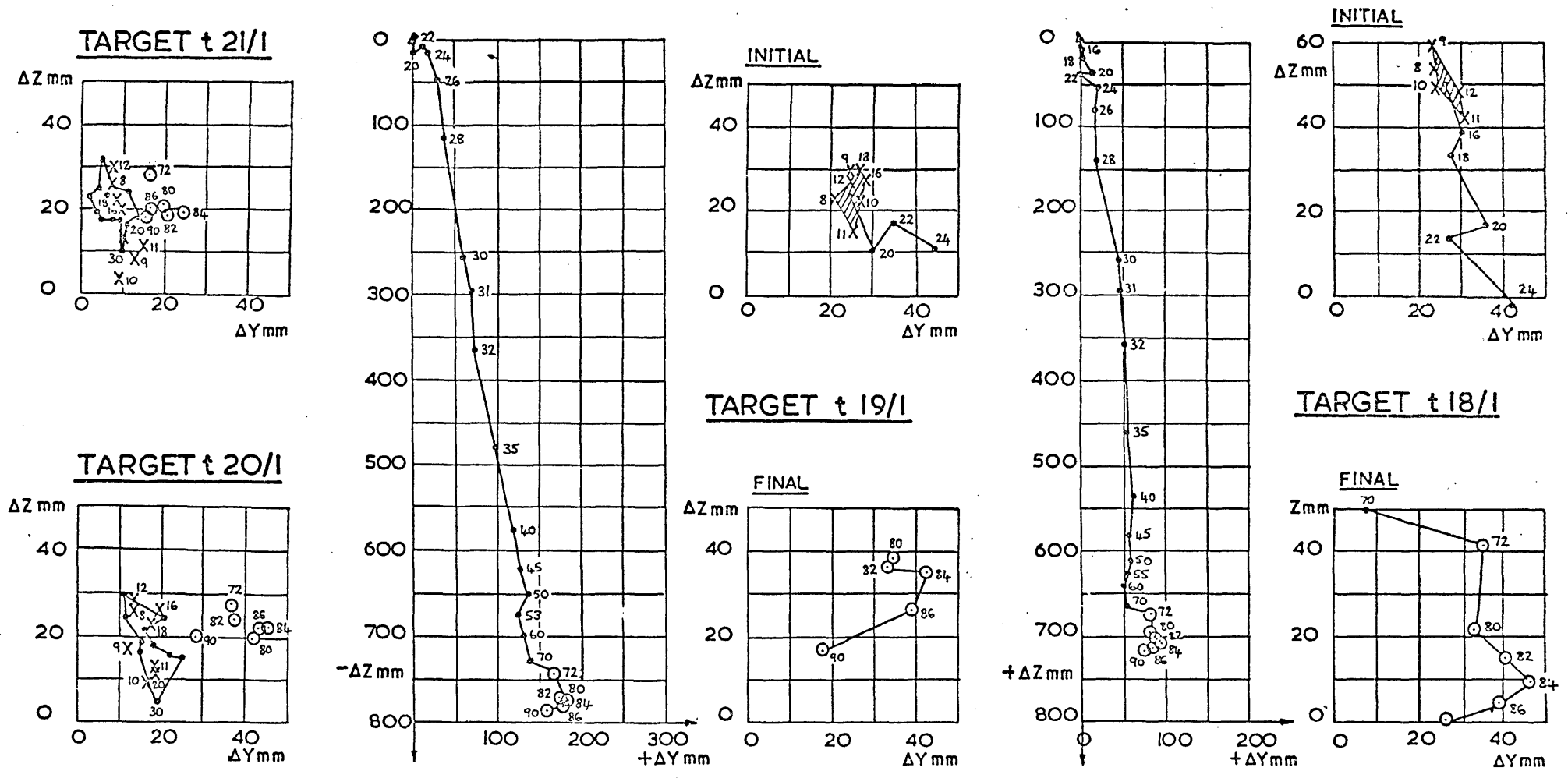
FIG. 5.8.2.



BANK I, STAGE 2

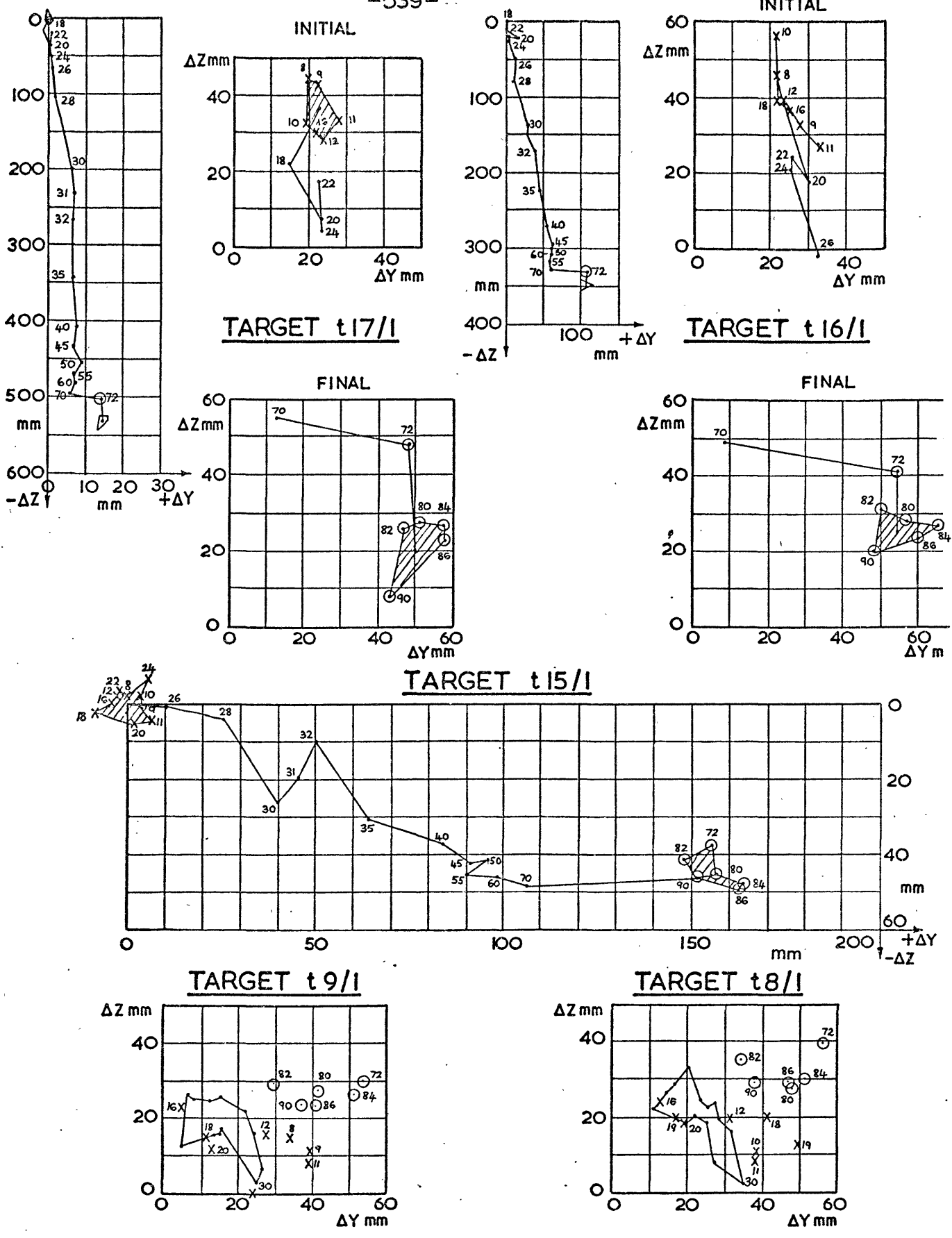
Schematic relationship between horizontal displacements in the film plane and the site 'y' axis

FIG. 5.8.3.



BANK I, STAGE I
TIME-LAPSE CAMERA TARGETS- DISPLACEMENT VECTORS DURING FAILURE

Fig 5.8.4



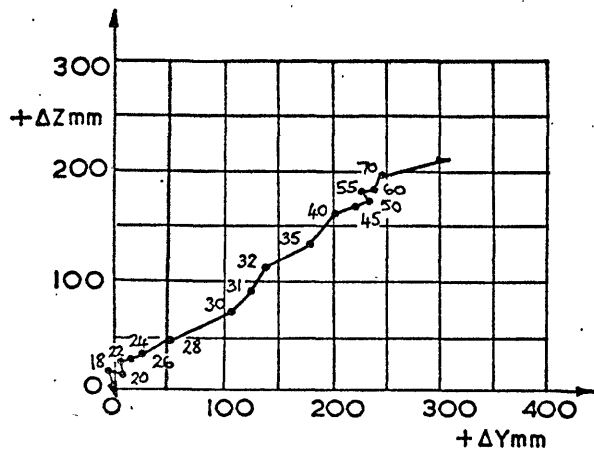
BANK I, STAGE I

LEGEND

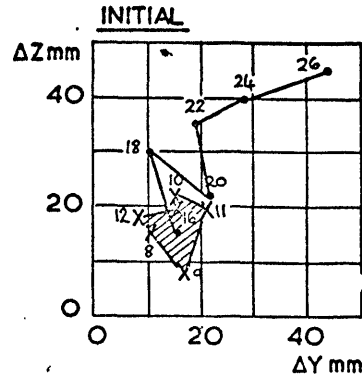
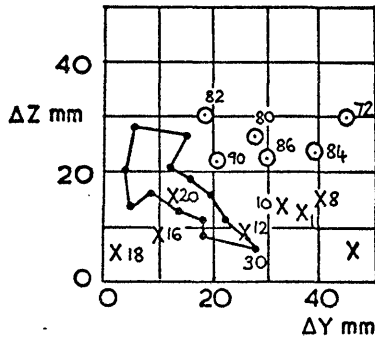
- X PRIOR TO MAIN MOVEMENT
- MAIN PERIOD OF MOVEMENT
- AFTER MAIN MOVEMENT; FILM No.2
- 9 FRAME No. 9 etc

TIME-LAPSE CAMERA TARGETS - DISPLACEMENT VECTORS DURING FAILURE

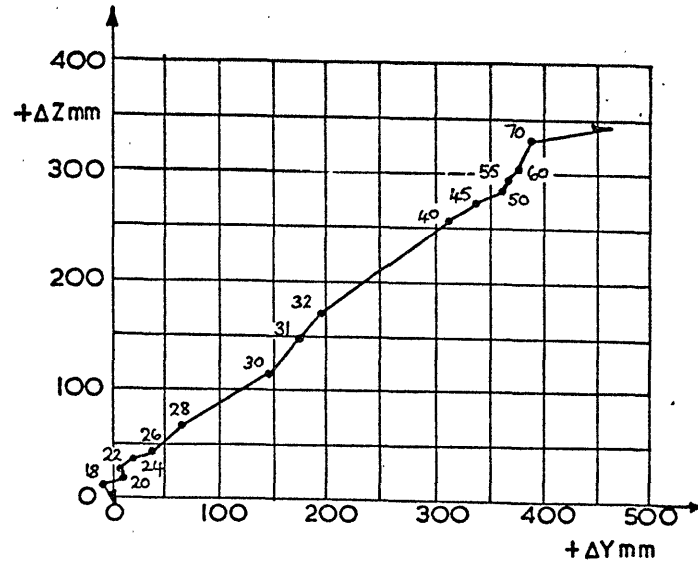
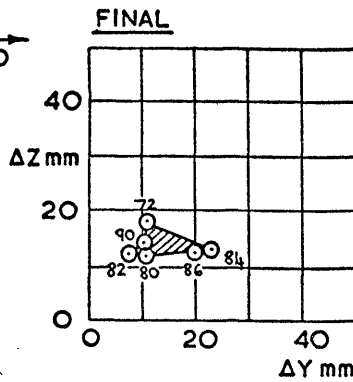
Fig. 5. 8. 5



TARGET t7/1

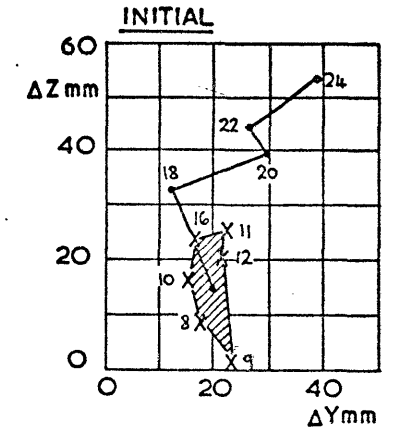
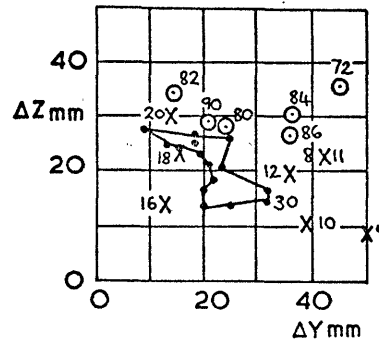


TARGET t14/1

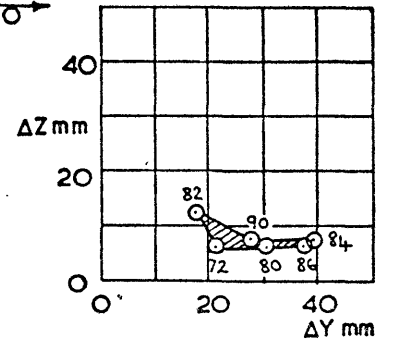


TARGET t13/1

TARGET t6/1



FINAL

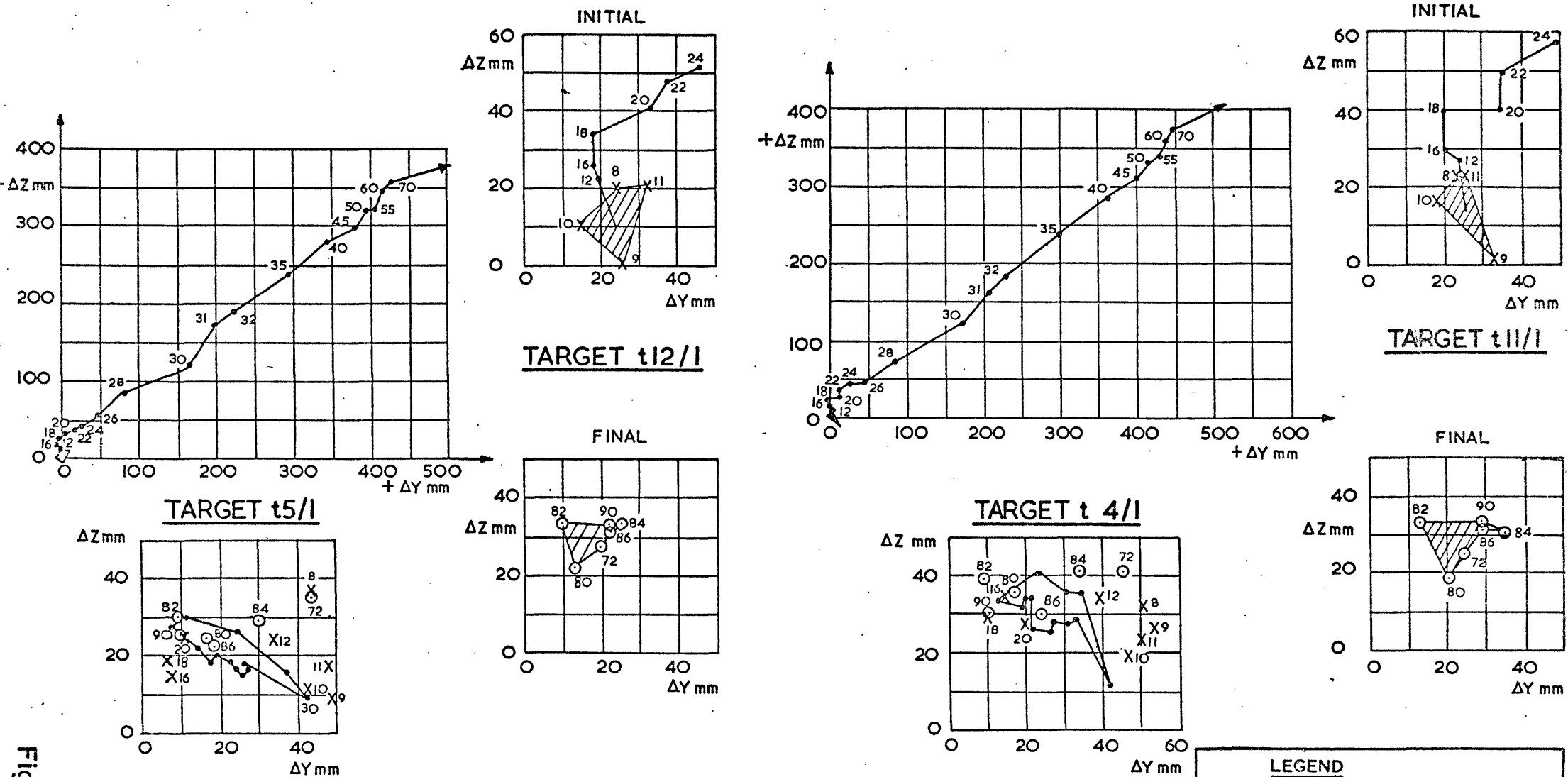


LEGEND	
X	PRIOR TO MAIN MOVEMENT } FILM No. 1
•	MAIN PERIOD OF MOVEMENT
○	AFTER MAIN MOVEMENT } FILM No. 2
9	FRAME No. 9 etc.

BANK I, STAGE I

TIME-LAPSE CAMERA TARGETS-DISPLACEMENT VECTORS DURING FAILURE

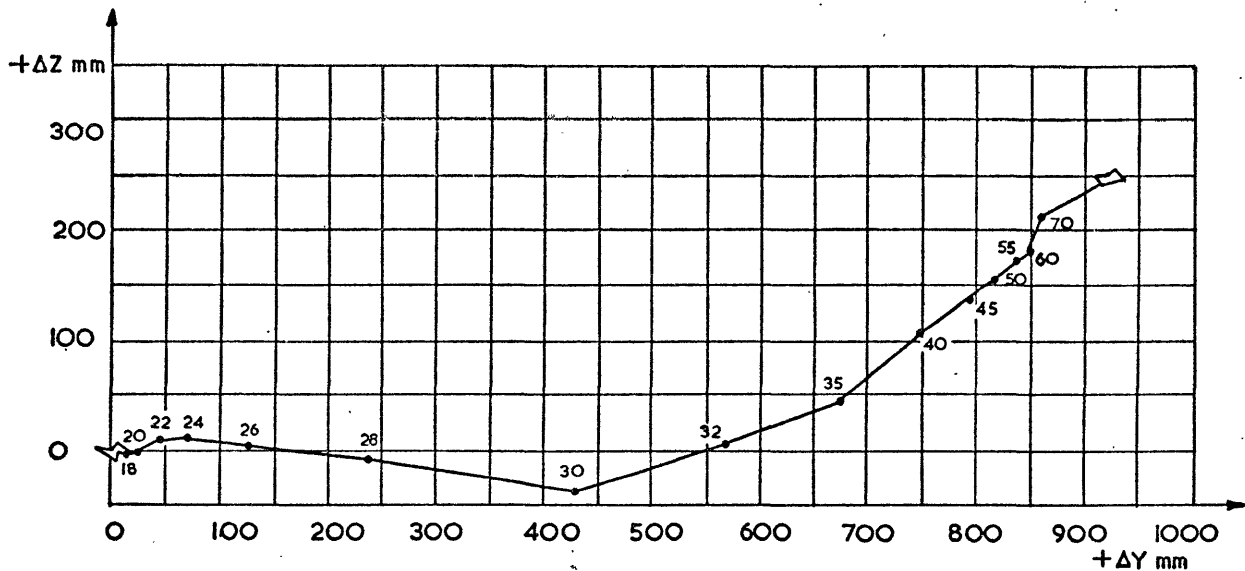
Fig. 5.8.6



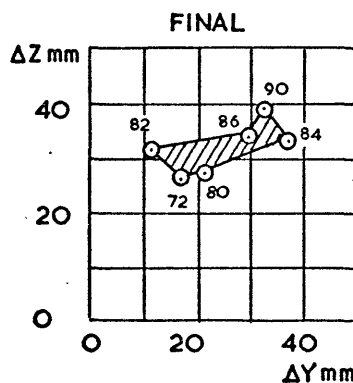
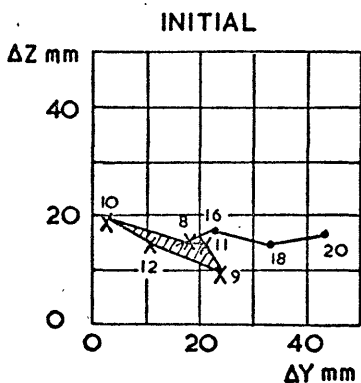
BANK I, STAGE I

TIME-LAPSE CAMERA TARGETS—DISPLACEMENT VECTORS DURING FAILURE

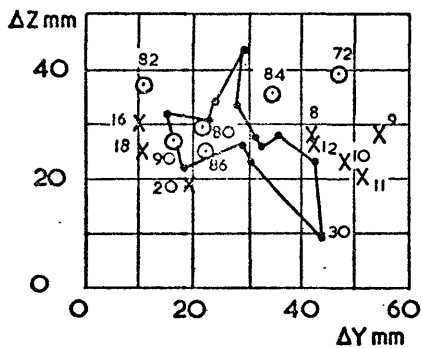
Fig. 5.8.7



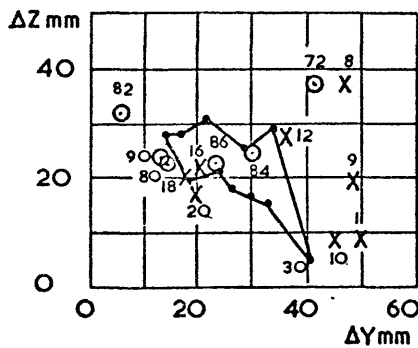
TARGET t10/I



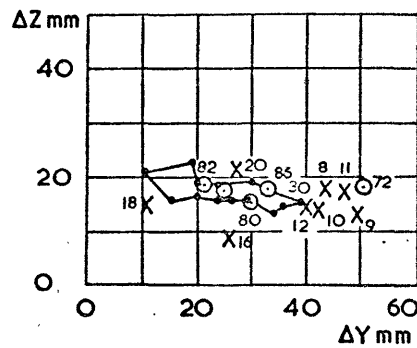
TARGET t3/I



TARGET t2/I



TARGET t1/I

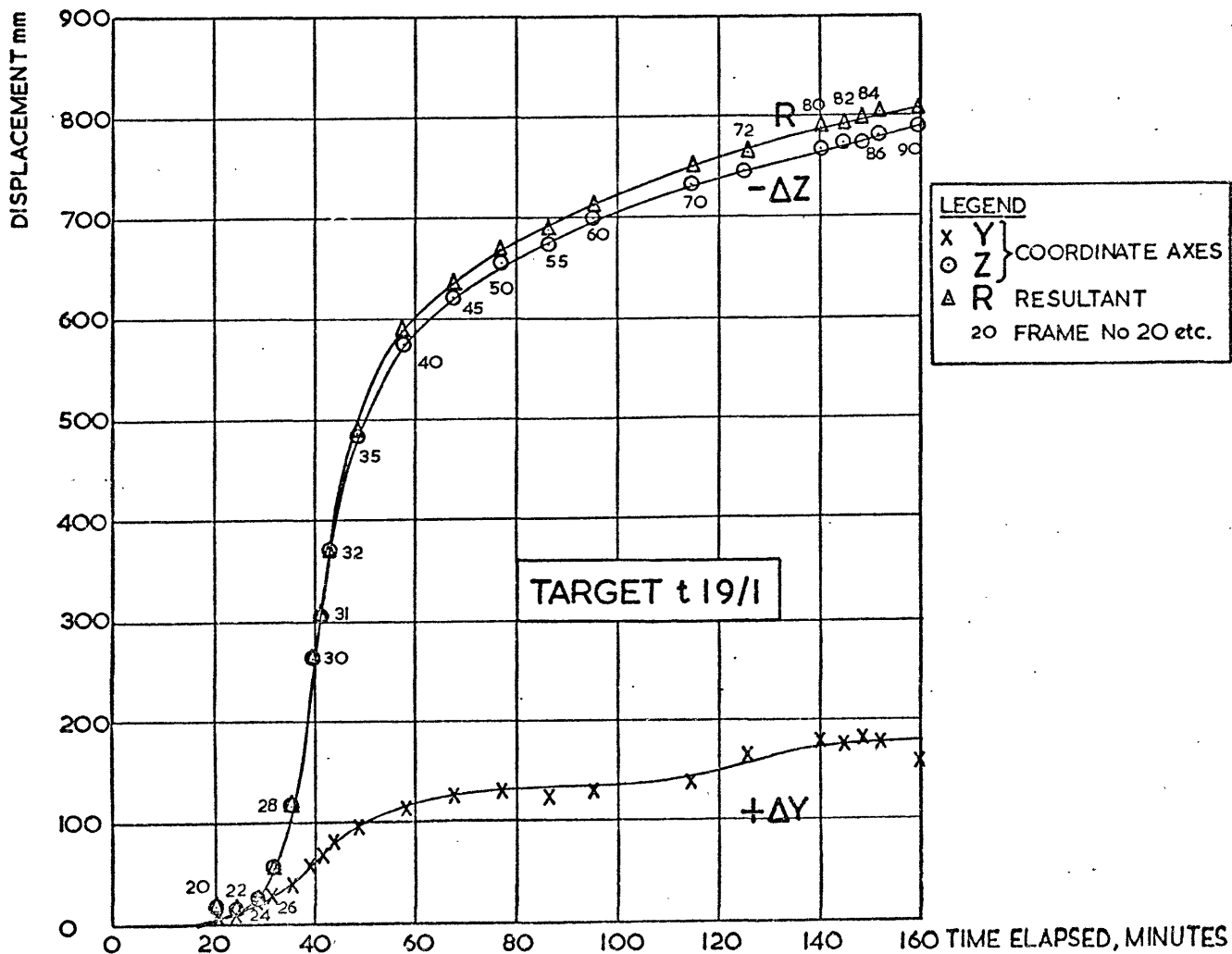
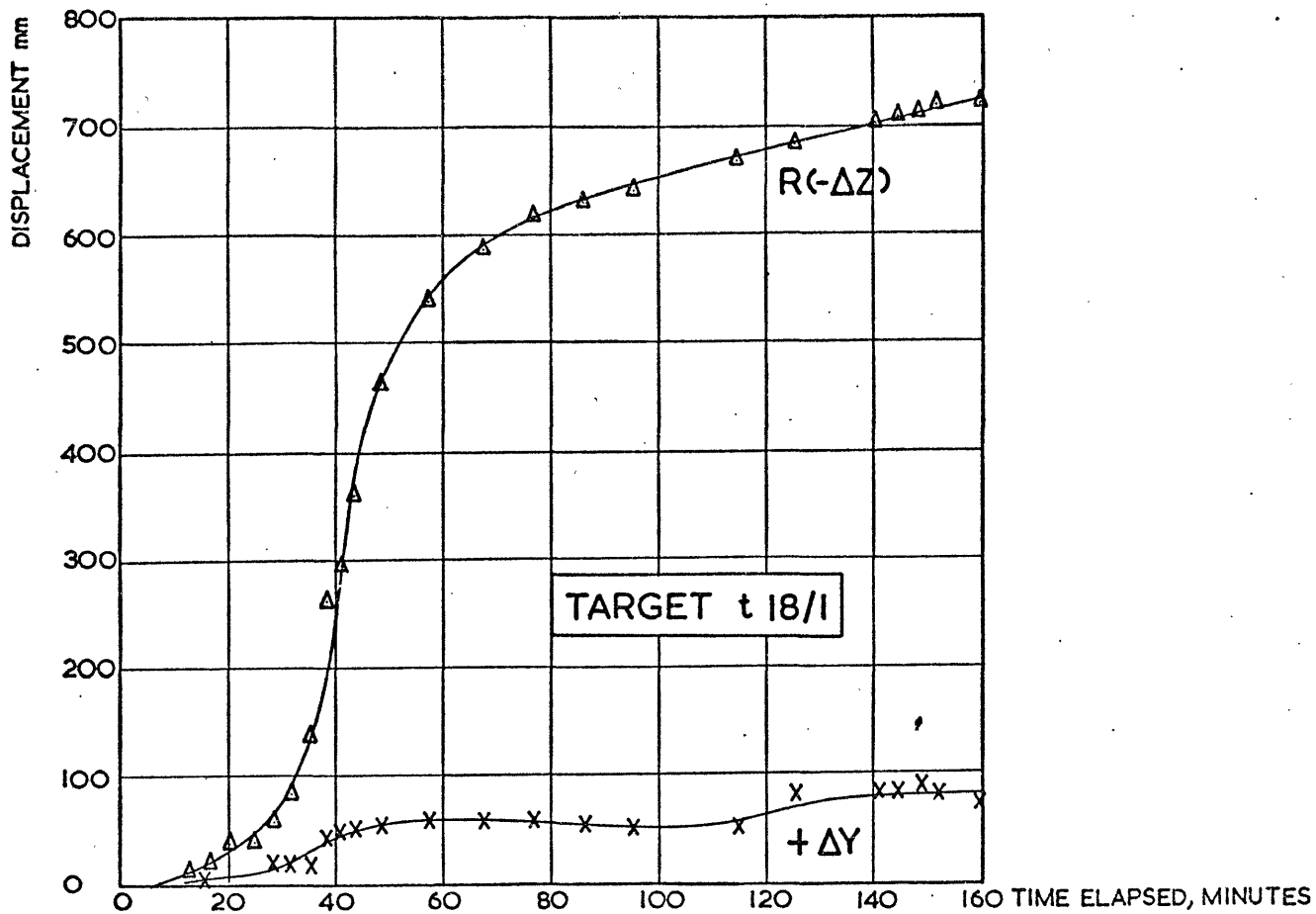


LEGEND	
X	PRIOR TO MAIN MOVEMENT } FILM No1
•	MAIN PERIOD OF MOVEMENT } FILM No2
○	AFTER MAIN MOVEMENT ; FILM No2
9	FRAME No 9 etc

BANK I, STAGE I

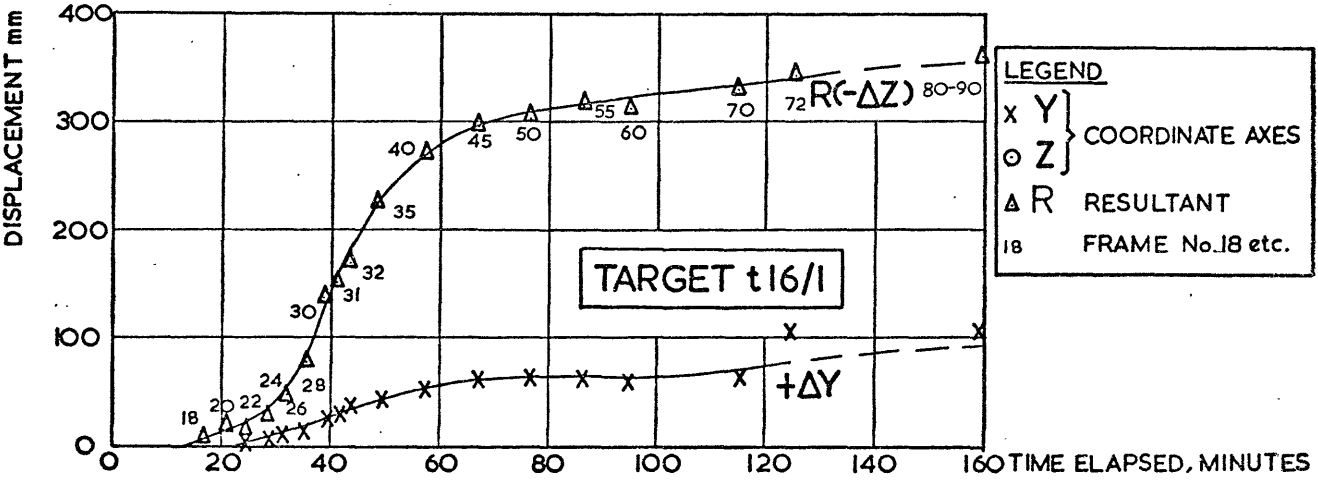
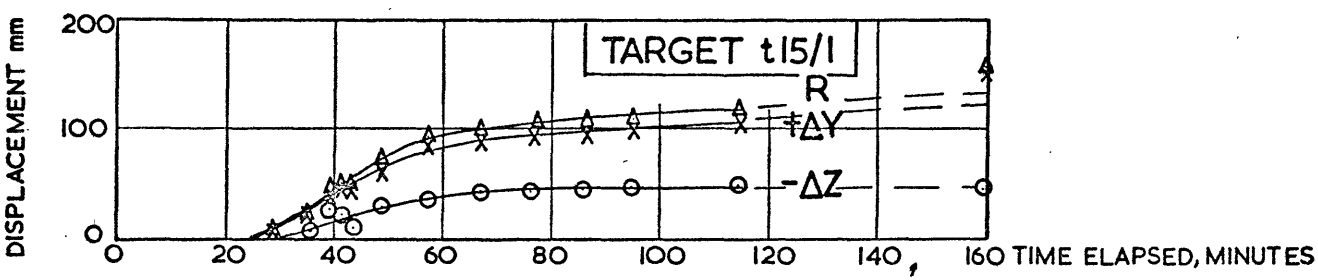
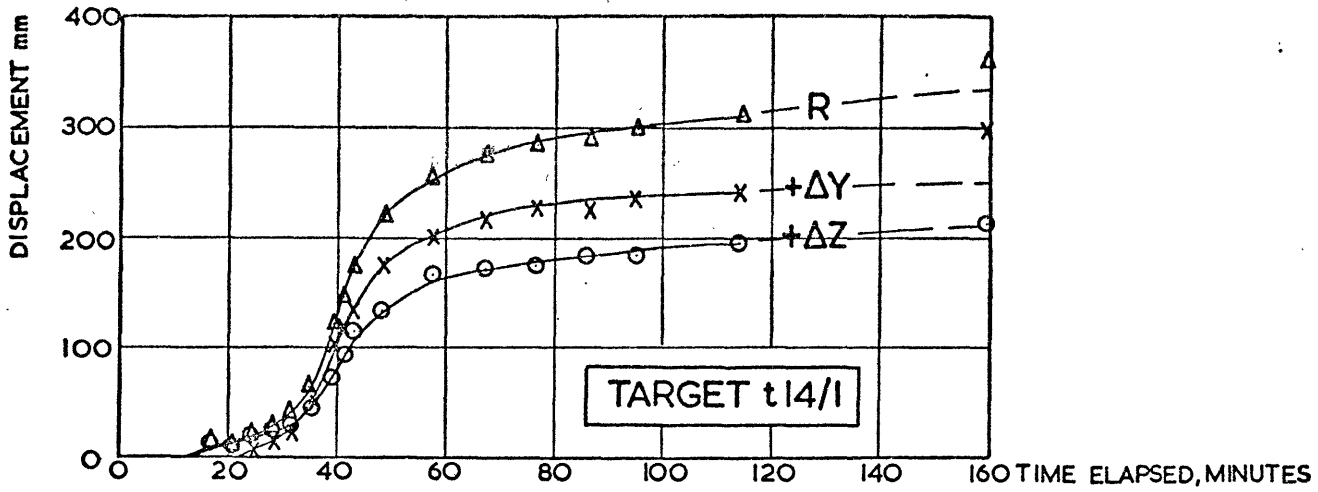
TIME-LAPSE CAMERA TARGETS-DISPLACEMENT VECTORS DURING FAILURE

Fig. 5.8.8



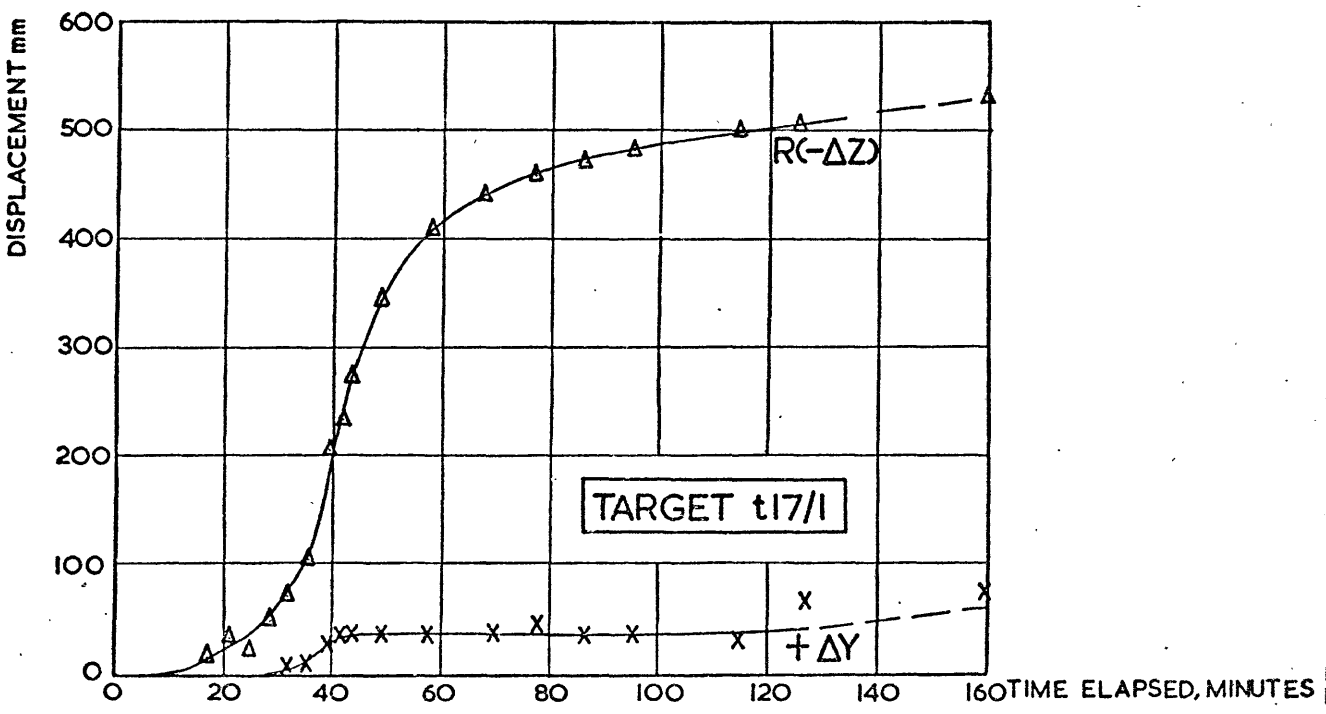
LEGEND
 X Y } COORDINATE AXES
 O Z }
 Δ R RESULTANT
 20 FRAME No 20 etc.

BANK I, STAGE I: TIME-LAPSE CAMERA TARGETS - DISPLACEMENT VERSUS TIME ELAPSED FROM START OF FAILURE

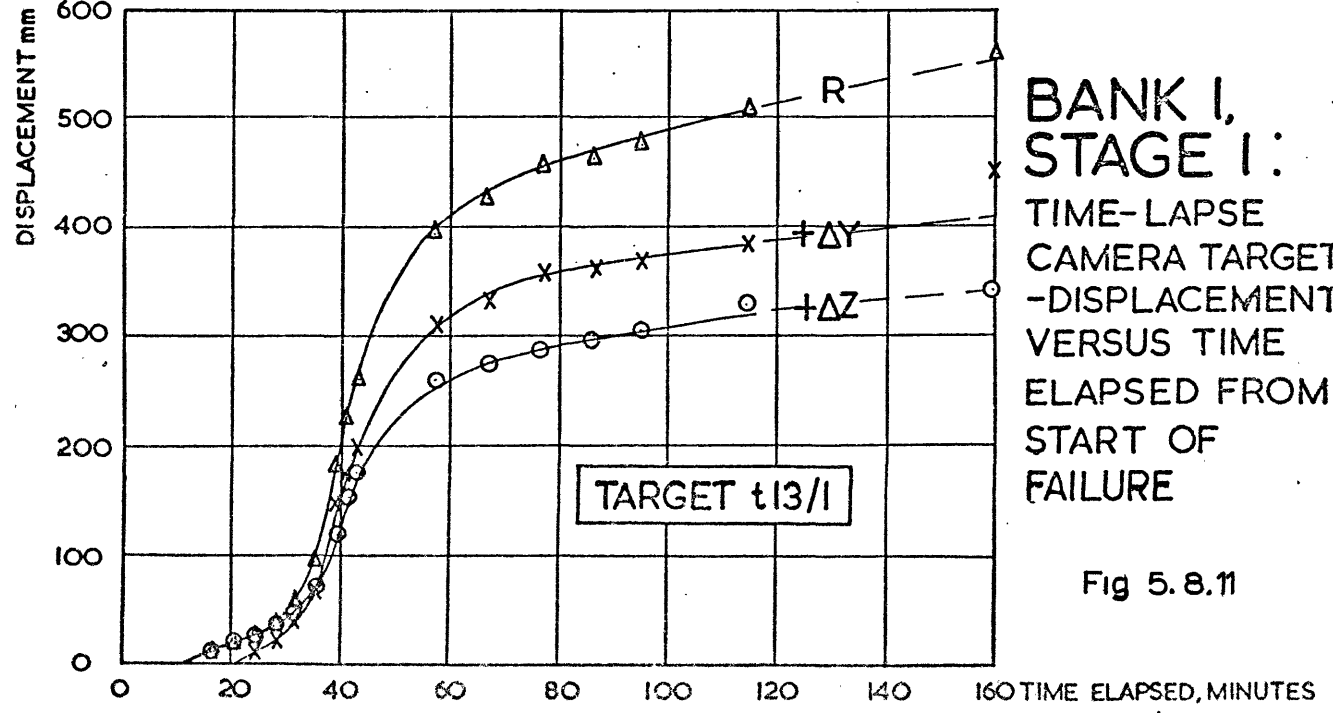
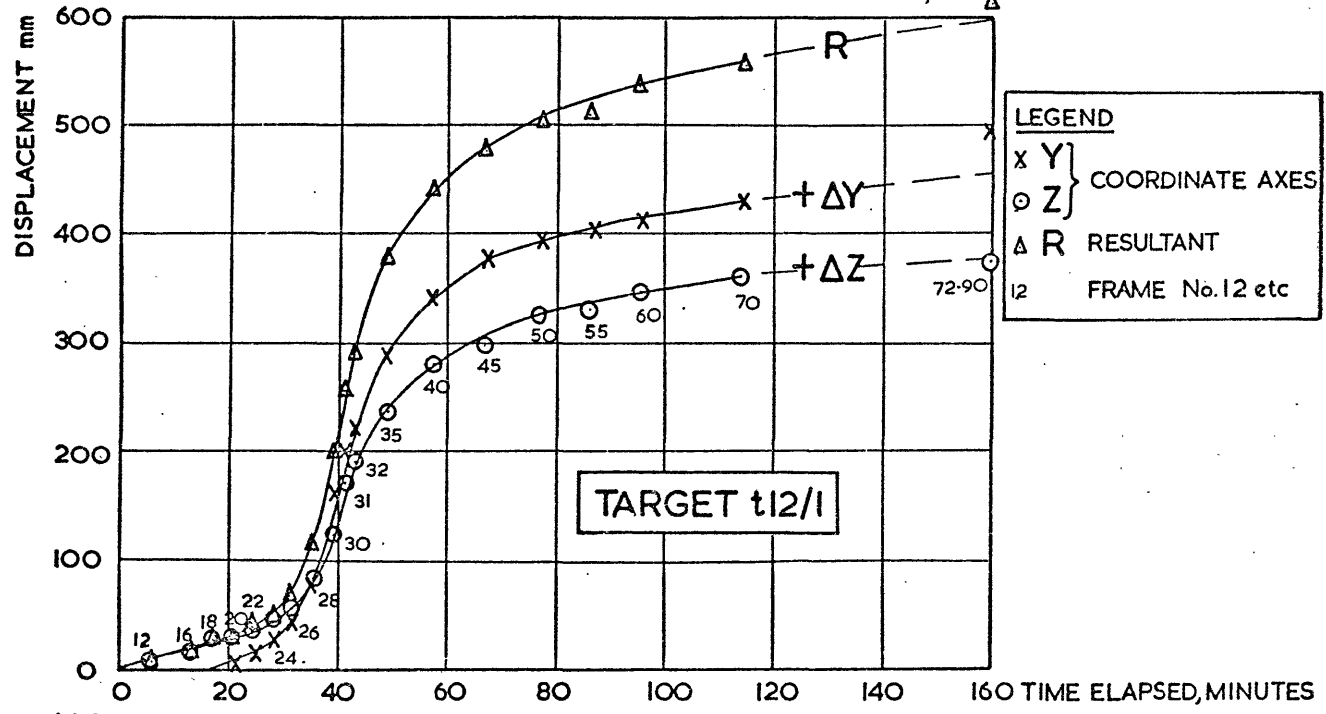
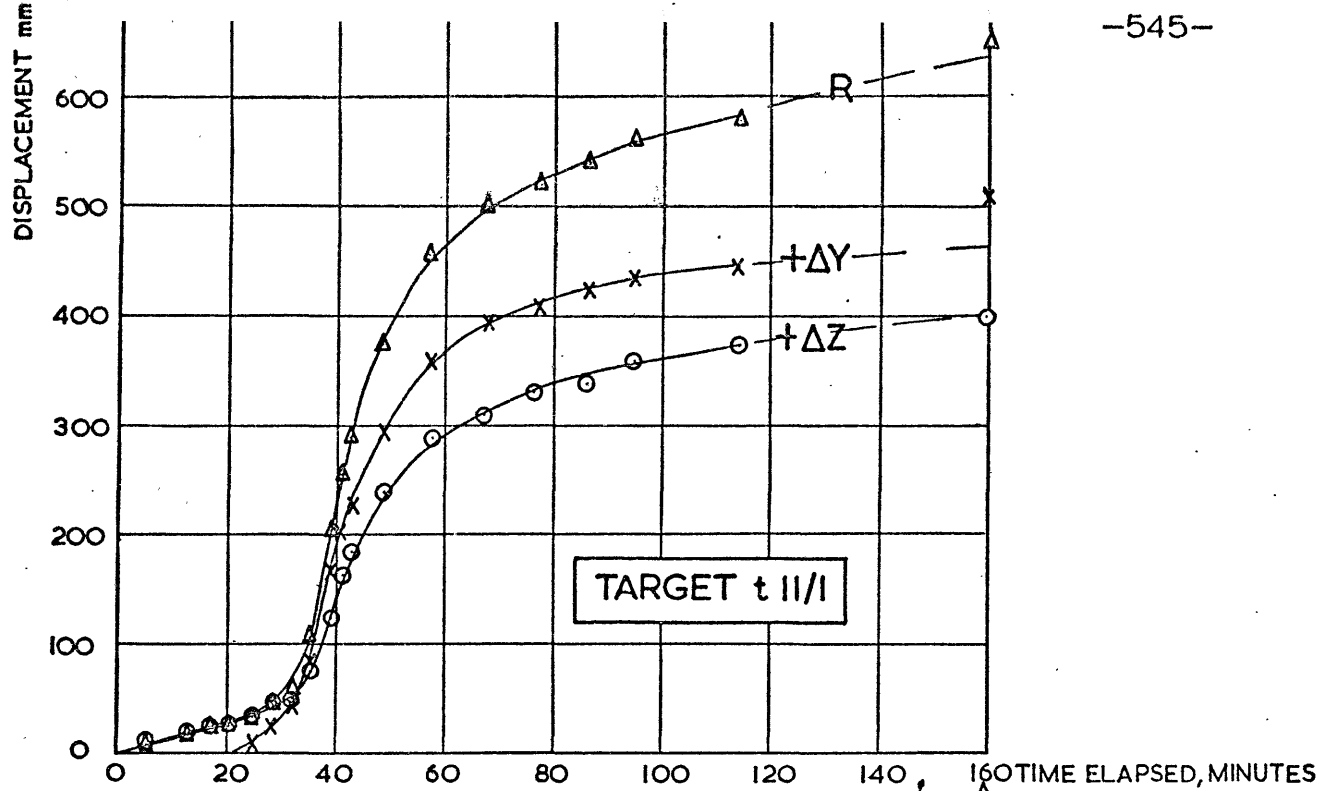


LEGEND

- X Y } COORDINATE AXES
- Z }
- △ R RESULTANT
- 18 FRAME No.18 etc.

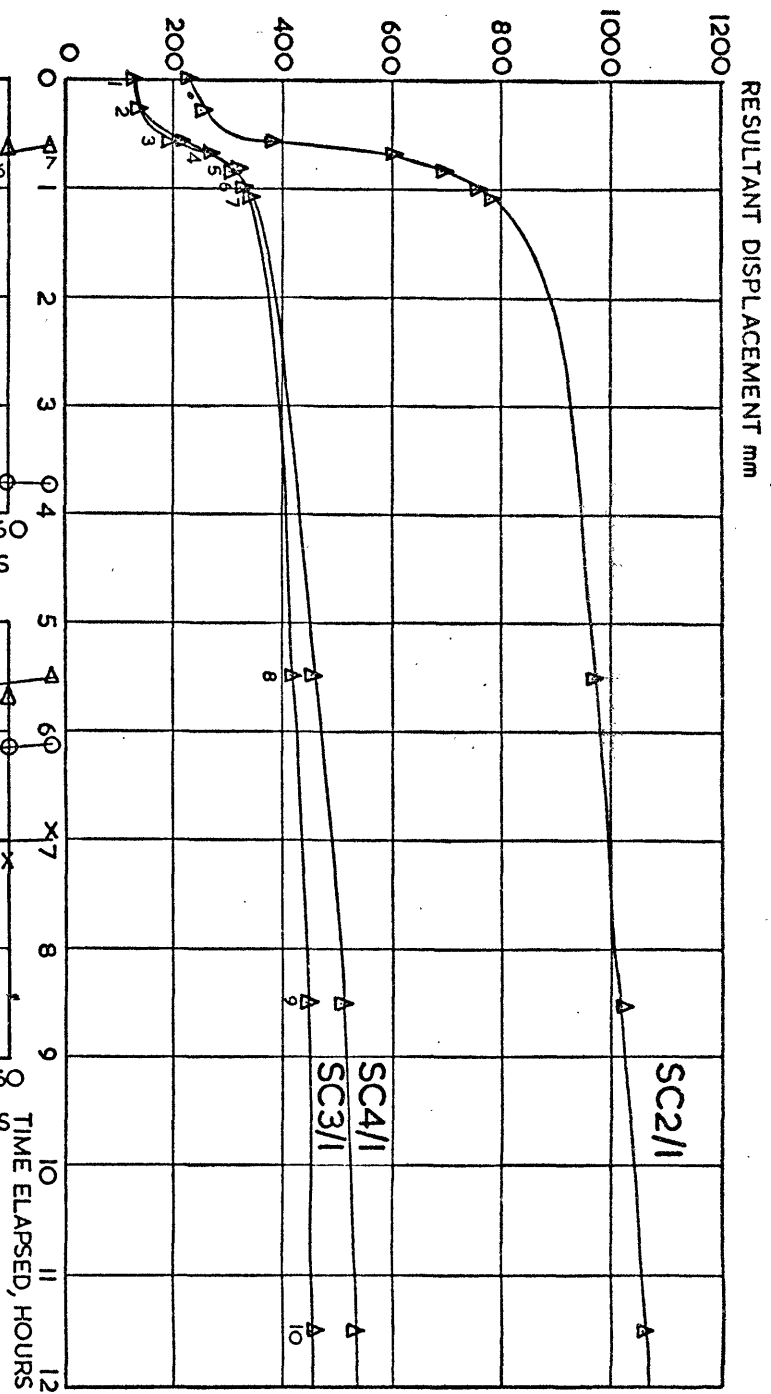
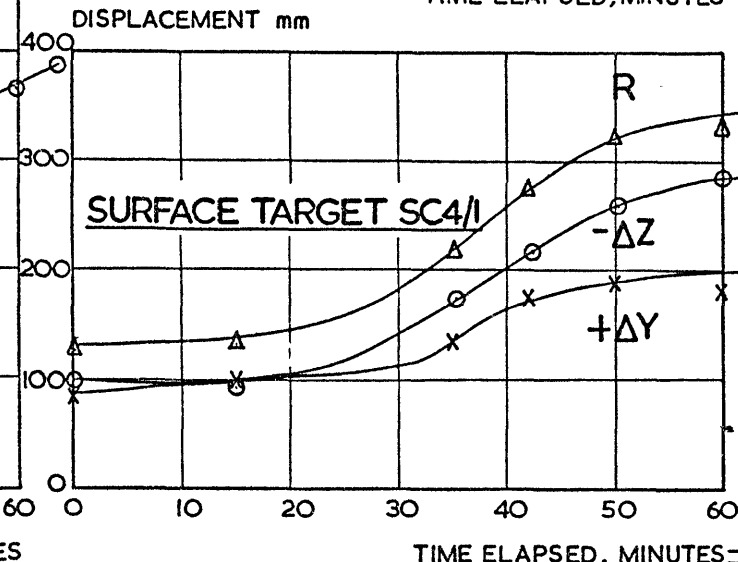
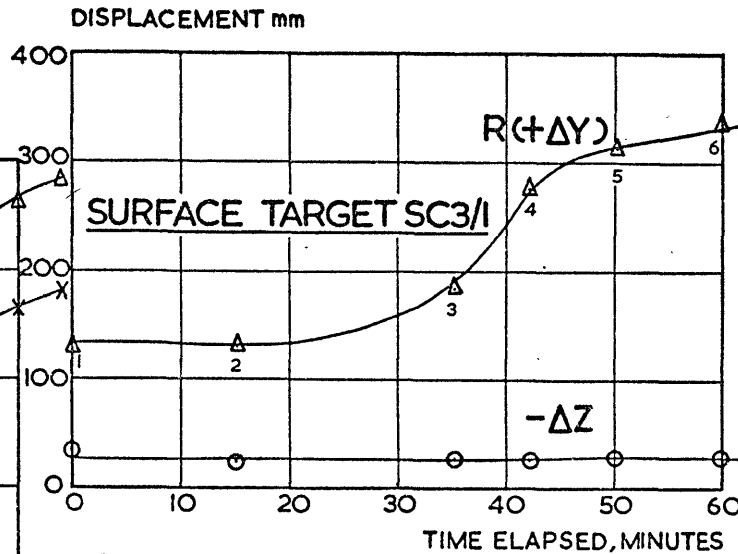
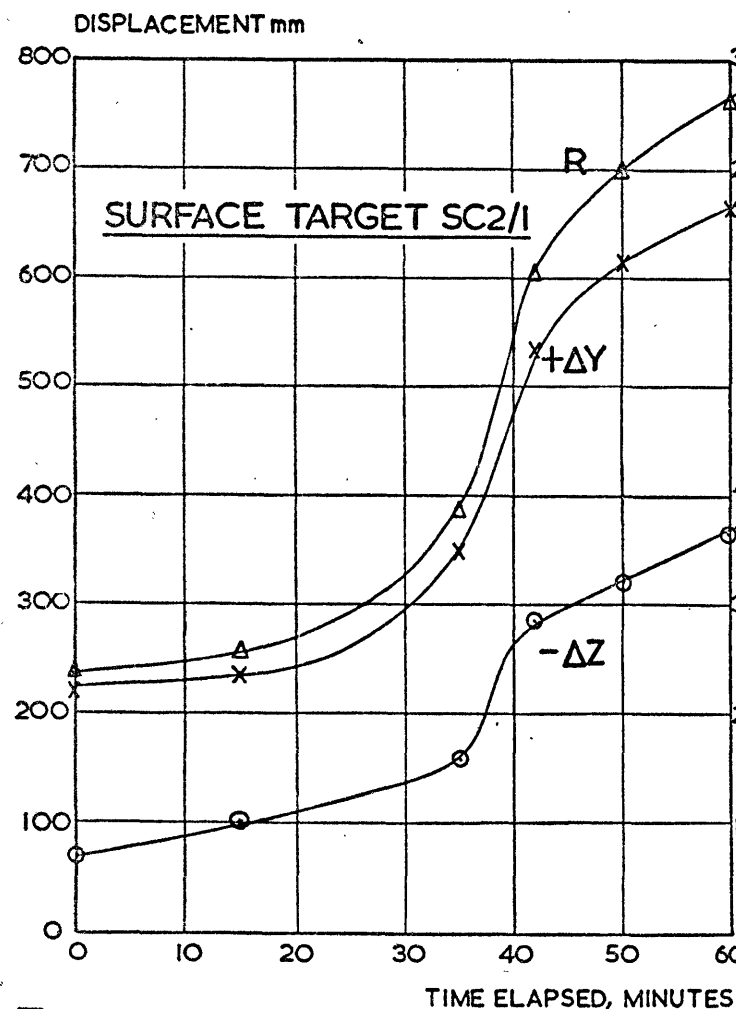


BANK I, STAGE I TIME-LAPSE CAMERA TARGETS -
DISPLACEMENT VERSUS TIME ELAPSED
FROM START OF FAILURE



**BANK I,
STAGE I:**
TIME-LAPSE
CAMERA TARGET
-DISPLACEMENT
VERSUS TIME
ELAPSED FROM
START OF
FAILURE

Fig 5.8.11



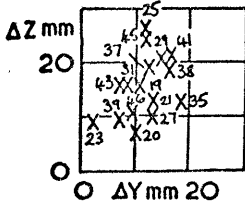
LEGEND
 X Y } COORDINATE AXES
 O Z }
 Δ R RESULTANT

(SEE TABLE 573 FOR KEY TO DATA POINTS)

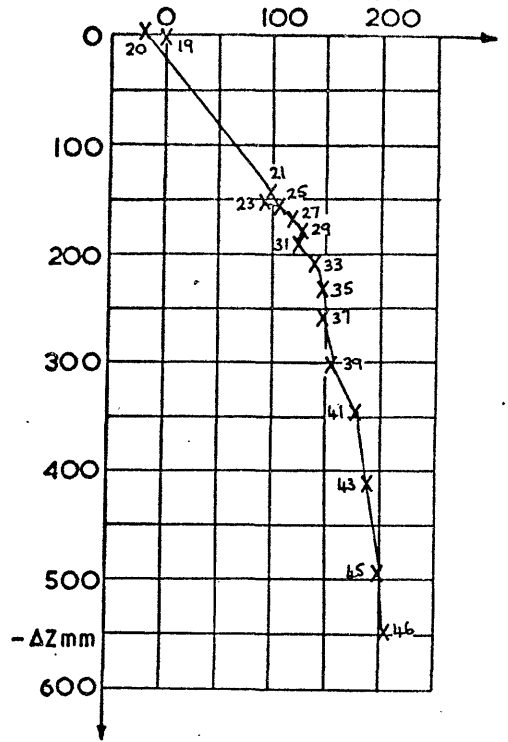
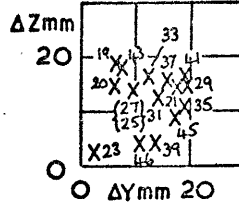
Fig. 5.8.12

BANK I, STAGE I: SURFACE TARGETS - DISPLACEMENT VERSUS TIME ELAPSED FROM START OF FAILURE

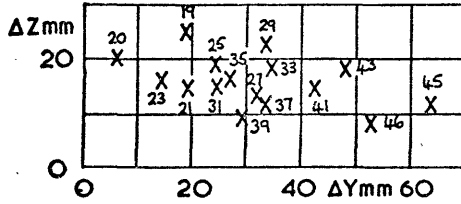
TARGET t18/2



TARGET t17/2



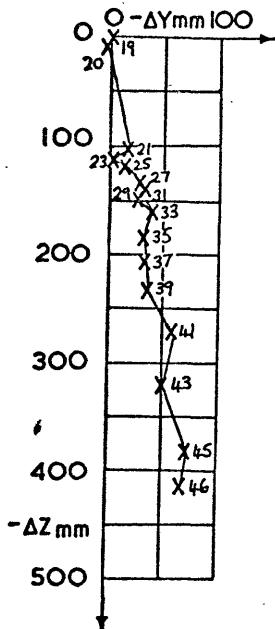
TARGET t16/2



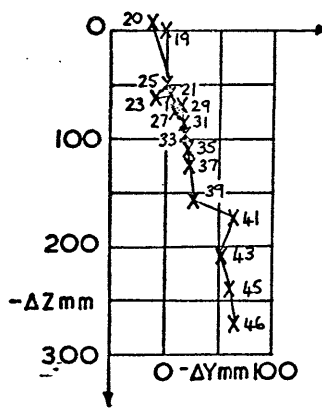
LEGEND

19 FRAME No.19 etc.

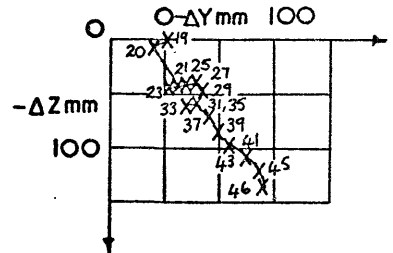
TARGET t14/2



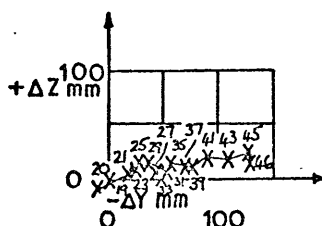
TARGET t13/2



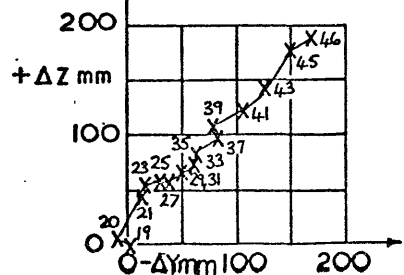
TARGET t12/2



TARGET t11/2



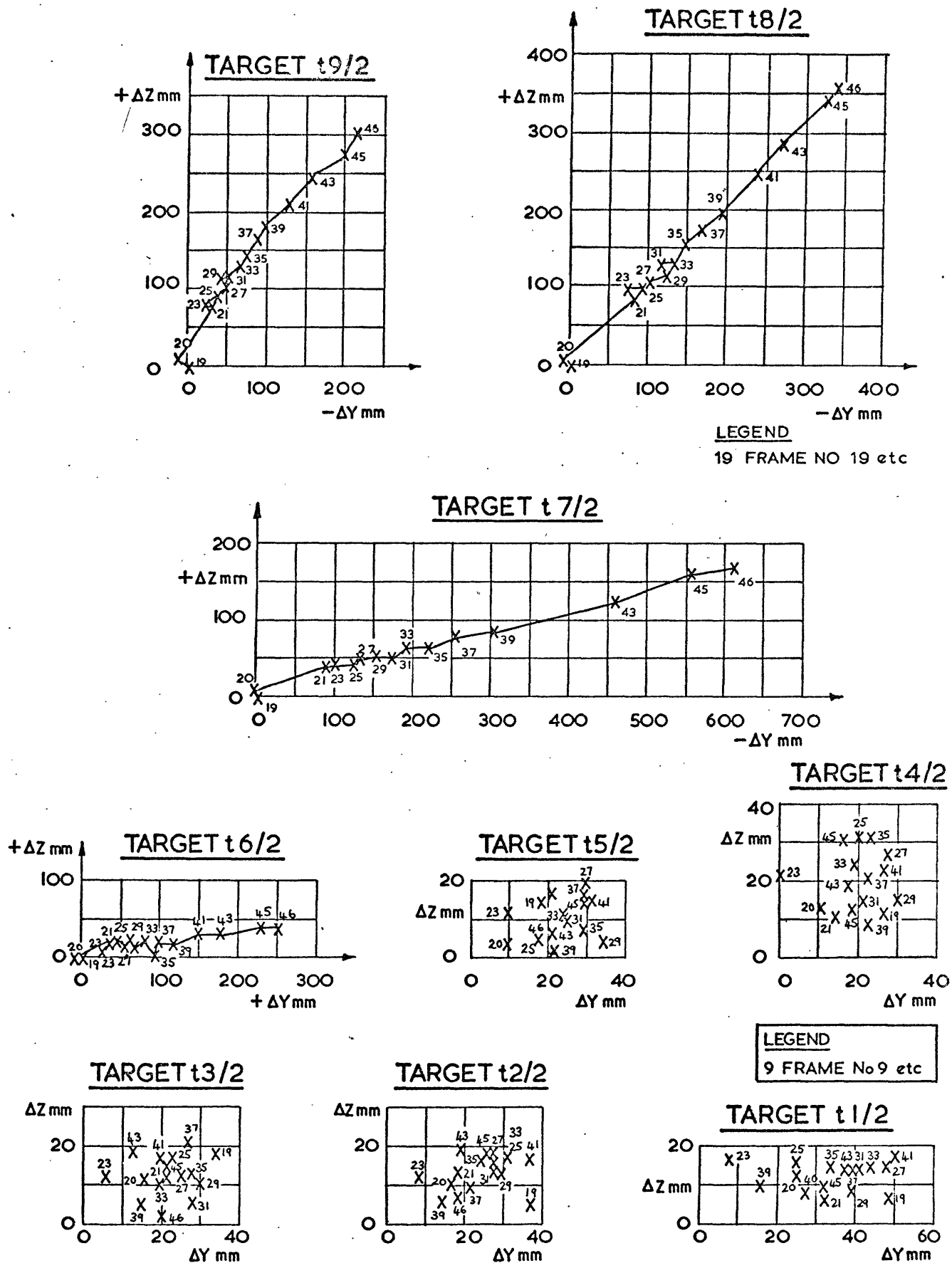
TARGET t10/2



BANK 1, STAGE 2

TIME-LAPSE CAMERA TARGETS - DISPLACEMENT VECTORS DURING FAILURE

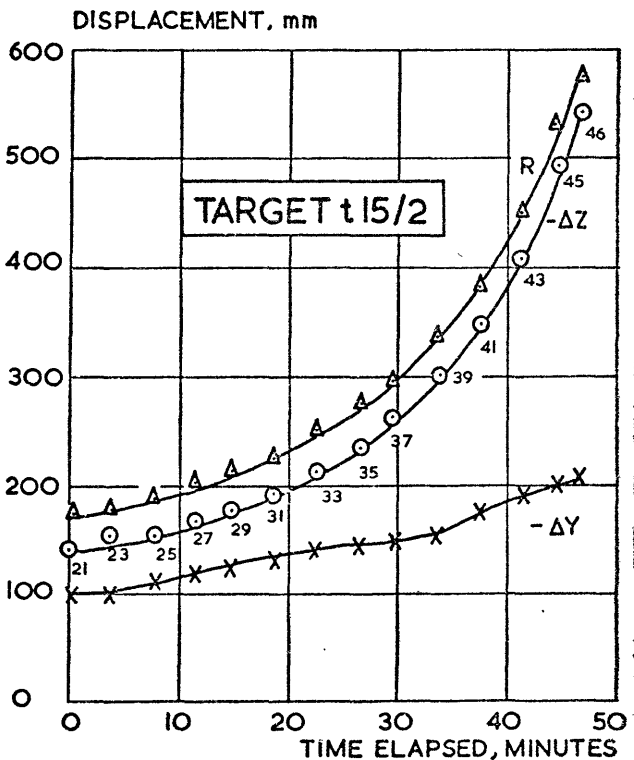
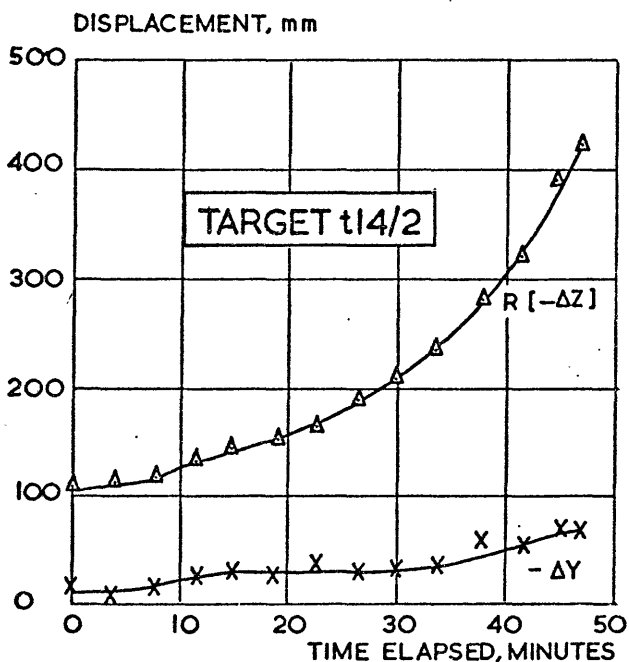
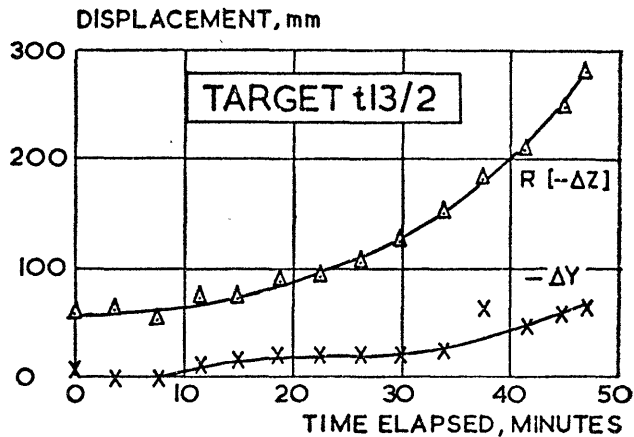
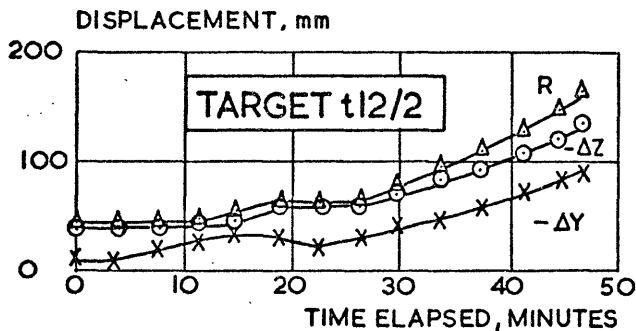
Fig 5.8.13



BANK I, STAGE 2

TIME-LAPSE CAMERA TARGETS-DISPLACEMENT VECTORS DURING FAILURE

Fig. 5. 8.14



LEGEND

X Y } COORDINATE AXES
 O Z }
 Δ R RESULTANT
 21 FRAME No. 21 etc.

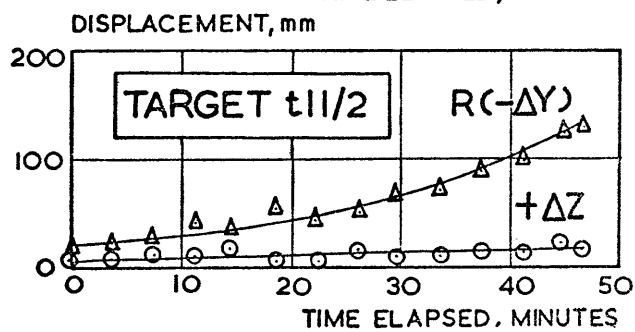
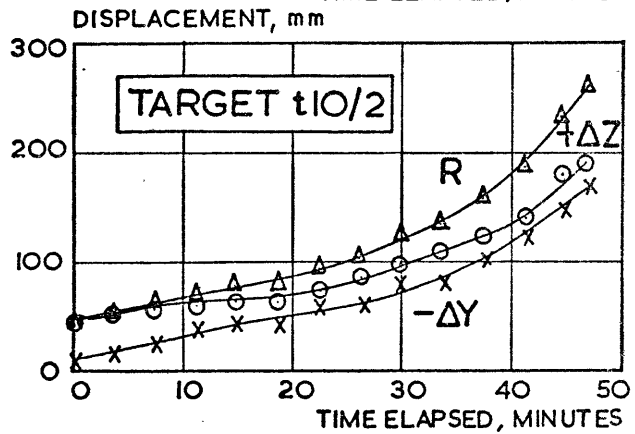
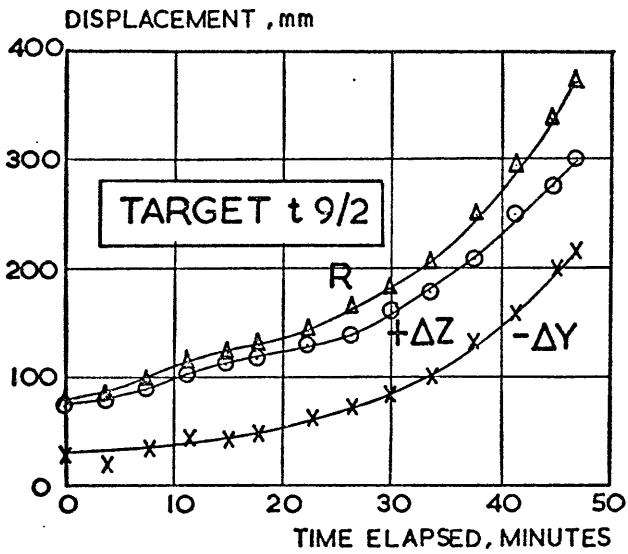
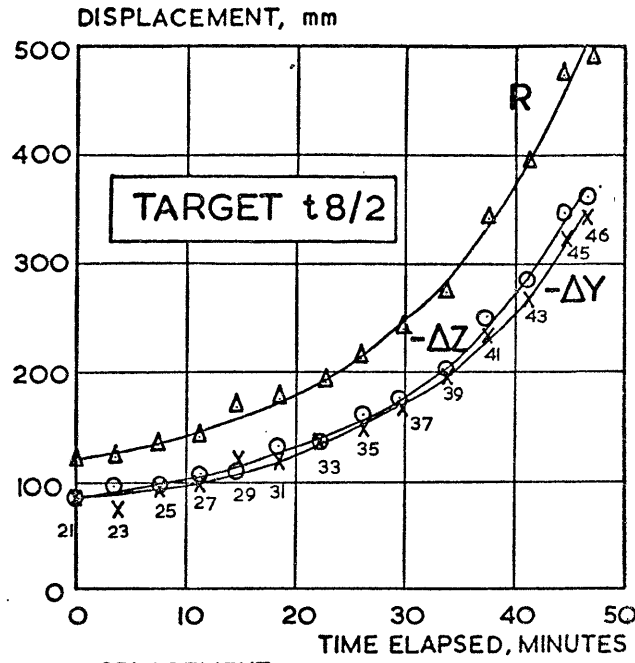
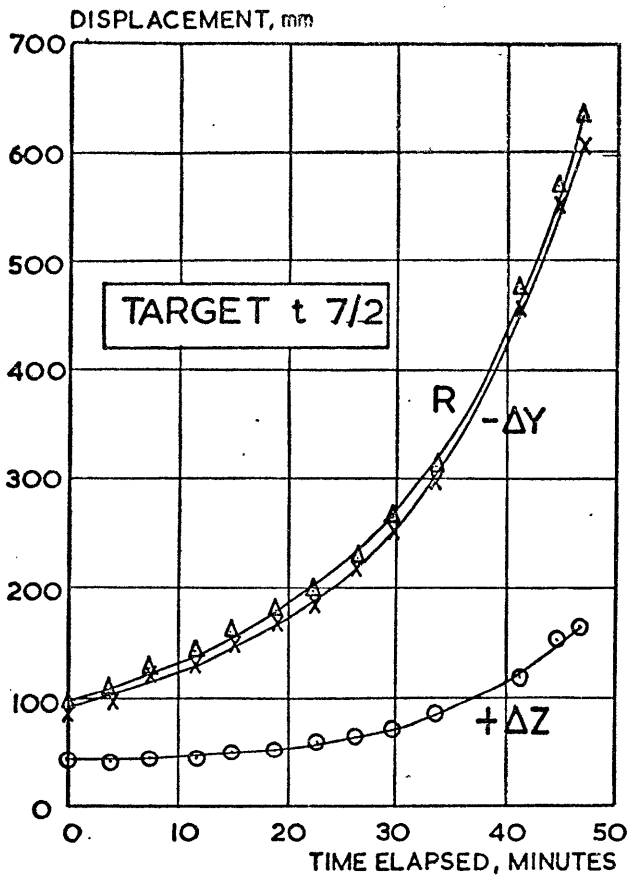
NB

INTERCEPTS ON DISPLACEMENT AXES ARE MOVEMENTS WHICH OCCURRED BETWEEN FIRST AND SECOND ALARM SIGNALS [A PERIOD OF 340 MINUTES]

BANK I, STAGE 2

TIME-LAPSE CAMERA TARGETS - DISPLACEMENTS VERSUS TIME ELAPSED FROM START OF FAILURE

Fig. 5.8.15



LEGEND

X Y } COORDINATE AXES

o Z }

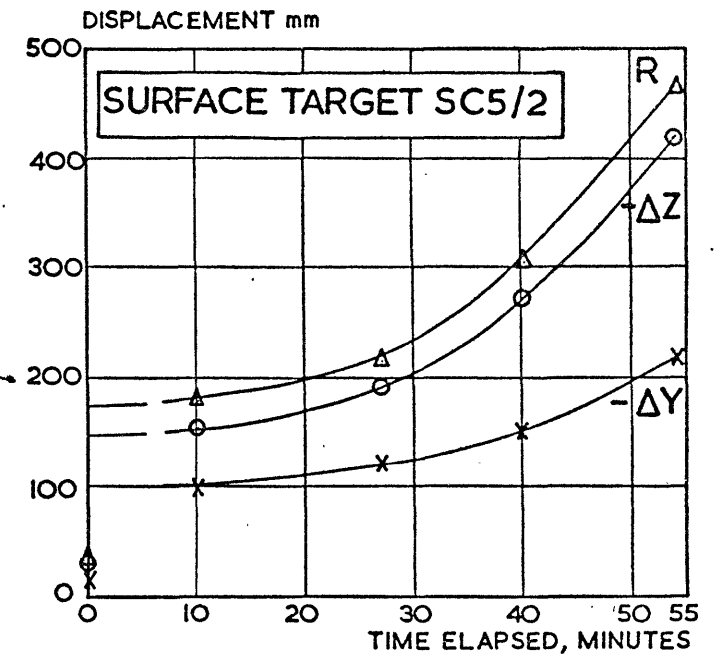
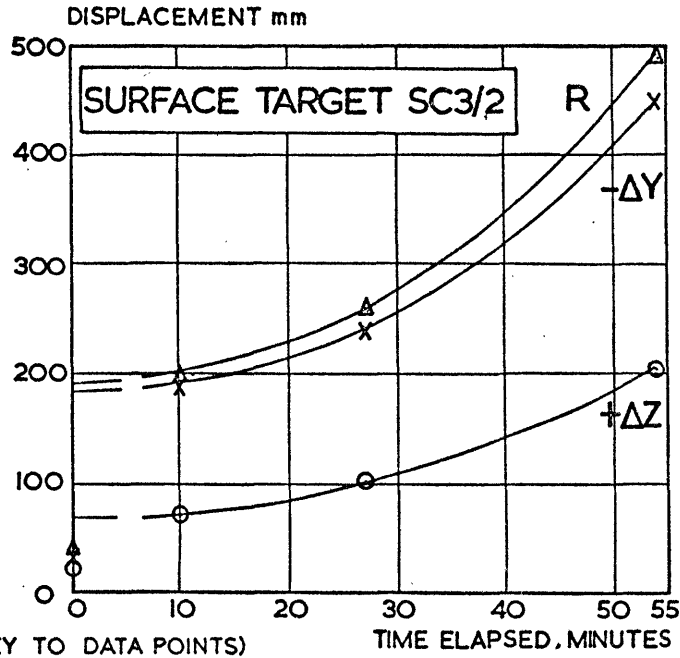
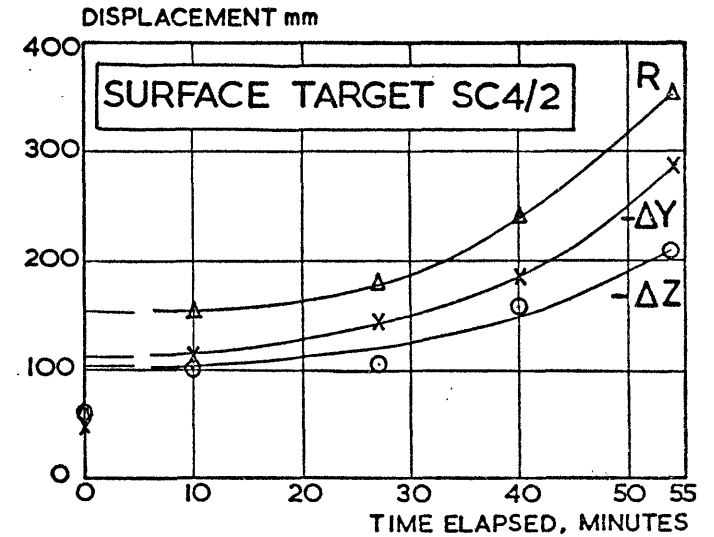
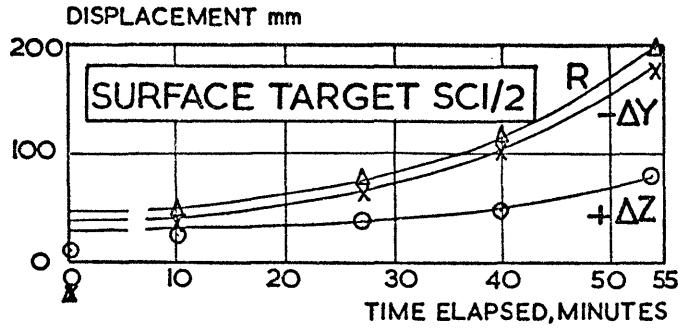
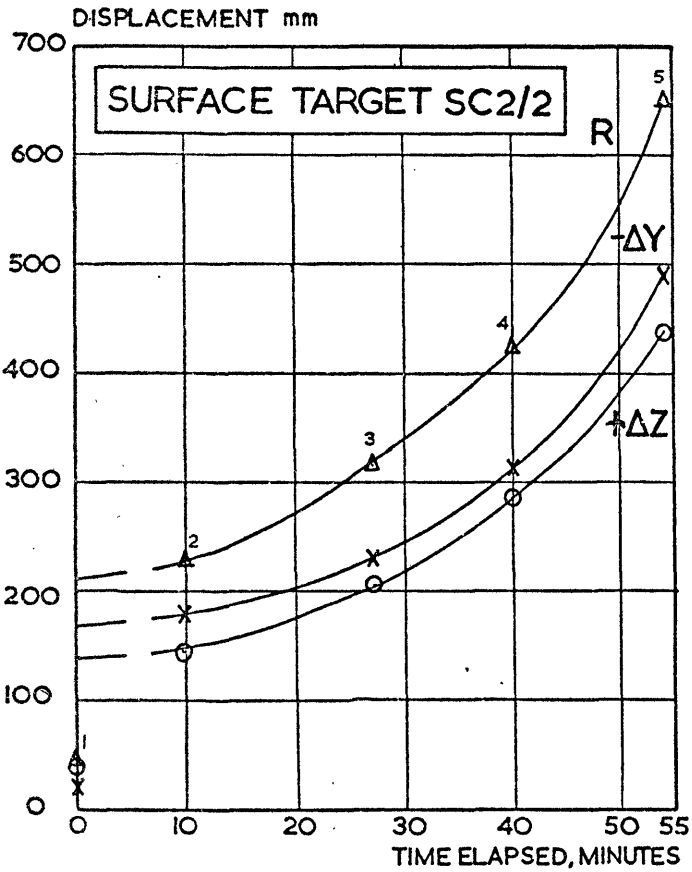
Δ R RESULTANT

21 FRAME No.21 etc

NB INTERCEPTS ON DISPLACEMENT AXES ARE MOVEMENTS WHICH OCCURRED BETWEEN FIRST & SECOND ALARM SIGNALS. (A PERIOD OF 340 MINUTES)

BANK I, STAGE 2

TIME-LAPSE CAMERA TARGETS - DISPLACEMENTS VERSUS TIME ELAPSED FROM START OF FAILURE

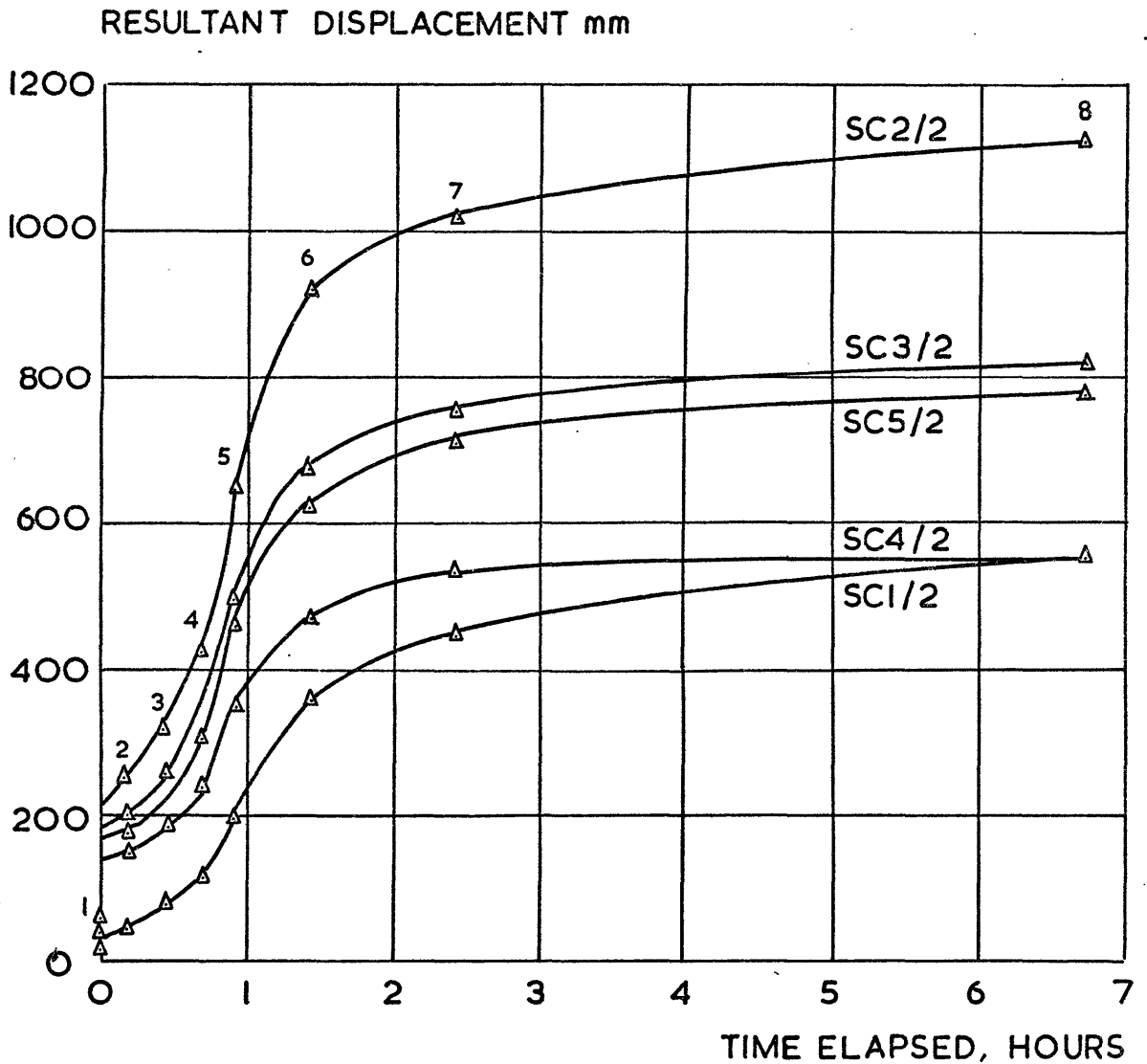


LEGEND
 X Y } COORDINATE AXES
 O X }
 Δ R RESULTANT

(SEE TABLE 57.5 FOR KEY TO DATA POINTS)

FIG. 5.8.17

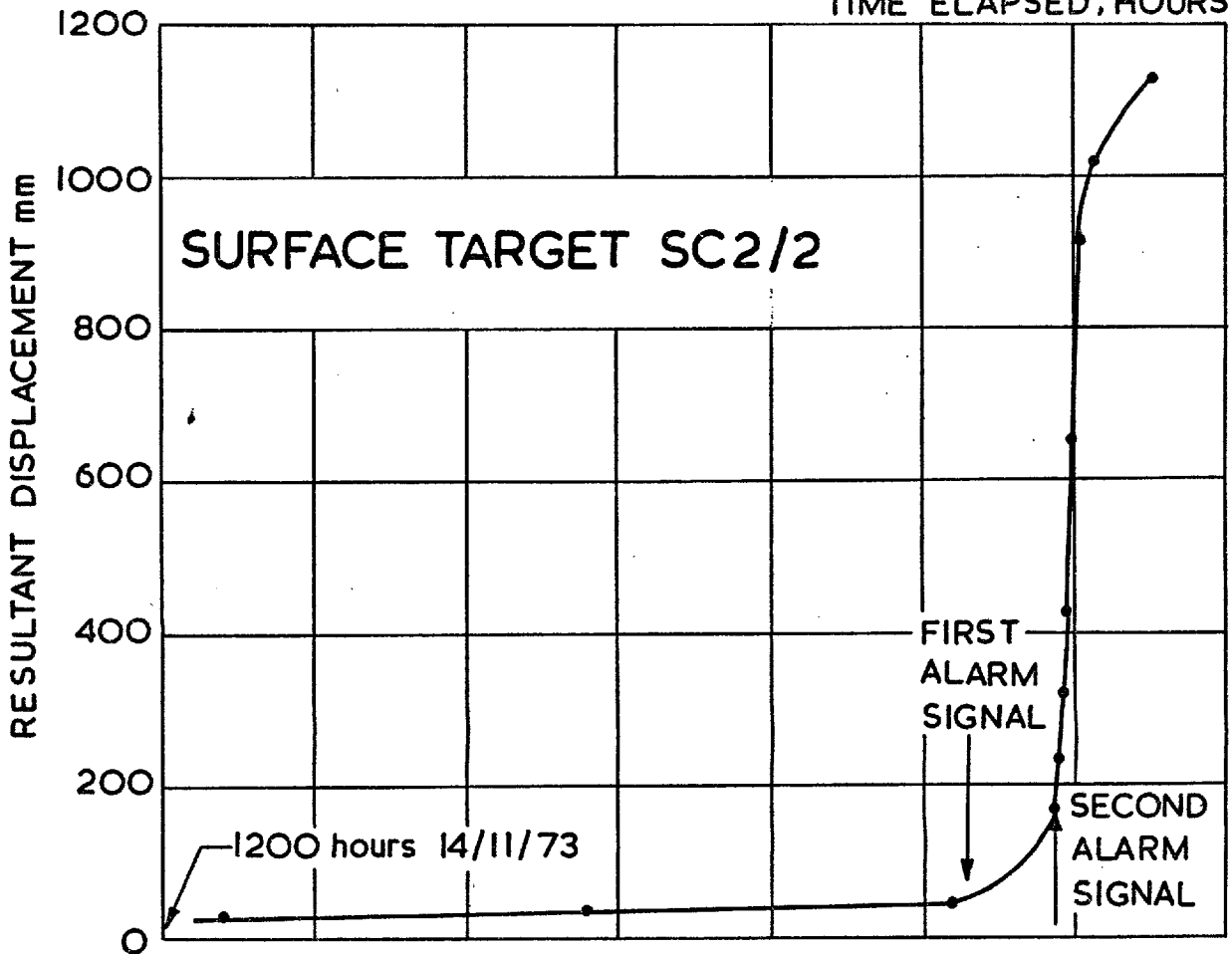
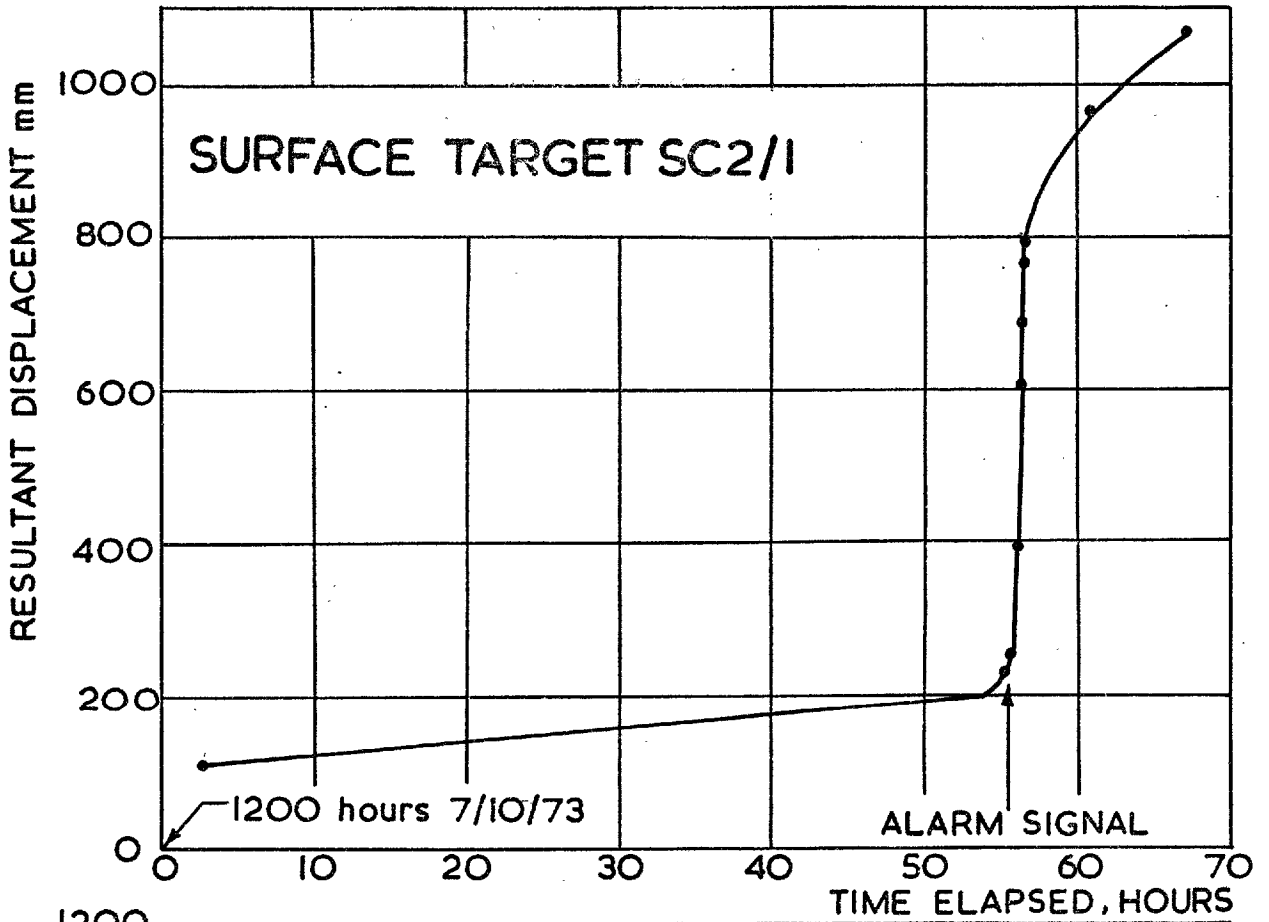
BANK 1, STAGE 2: SURFACE TARGETS-DISPLACEMENTS VERSUS TIME ELAPSED FROM START OF FAILURE



(SEE TABLE 57.5 FOR KEY TO DATA POINTS)

BANK I, STAGE 2
SURFACE TARGETS - RESULTANT DISPLACEMENTS VERSUS TIME ELAPSED FROM START OF FAILURE

Fig.5.8.18



**BANK I STAGES 1 & 2
DEVELOPMENT OF FAILURE**

Fig. 5.8.19

5.9. Temporary Bench Marks (T.B.M. s) and Level Surveys

5.9.1. Description and Installation

Two temporary bench marks were installed at the site as a basis for construction and instrumentation levels. The installation process, including a description of the bench mark components, is summarised below and illustrated in figure 5.9.1.

A 203mm diameter shell and auger boring was sunk through the soft clay and terminated in sand and gravel at approximately 12.25m depth. A 60mm O.D. steel tube, in 3m lengths joined with screw threaded collars, was then lowered into position in the centre of the borehole and sand/cement grout pumped, via a tremie pipe, to the base of the borehole. Sufficient grout was injected to form a reasonable size 'concrete' plug, the borehole being grouted up to about 2m from the base upon completion of this operation. Highly compressible polystyrene backfill was added next, filling the annulus between the steel tube and the borehole wall for a further 1m or so. This was followed by a 150mm O.D. P.V.C. tube, in 3m lengths joined with force fit couplings, which was lowered into place over the steel tube so that it rested on the polystyrene. Similarly to the vertical settlement gauge sleeves (section 5.10) this P.V.C. sleeve was designed to prevent downdrag of the steel tube, and the polystyrene to minimise any tendency for the P.V.C. tube to transmit downdrag forces to the 'concrete' base plug.

An annular rubber packing ring was placed between the inner and outer tubes at the top of the installation, this being in a small circular excavation about 150mm deep by 750mm diameter. The annulus between the P.V.C. tube and the borehole walls was then grouted up with a 3:1 bentonite : cement

grout placed via a tremie pipe, the P.V.C. tube being held in place to prevent ingress of grout between it and the steel tube at the junction with the polystyrene. To complete the installation the steel tube was capped with a level-staff location point and the bottom of the pit covered with an annular wooden plate.

5.9.2. Level Surveying and Stability of Bench Marks

The same Zeiss automatic level was used for all the level surveys carried out. The locations of the two temporary bench marks meant that only short distances needed to be traversed when setting out construction levels, or taking instrument levels, on any of the embankments. Even with the loss of T.B.M.N. under Bank 4 (figure 4.1.) this was still essentially the case. However, due to the nature of the construction, a round of instrument levels generally involved between four and eight change points. Each level survey, whether for instrument or construction levels, was closed back onto a T.B.M. The precision of closure back onto the T.B.M., as well as the repeatability of levels for fixed positions (e.g. initial instrument readings) was used to assess the overall accuracy of the level surveys. On this basis closures of worse than $\pm 3\text{mm}$ led to rejection of the particular round of levels, the results accepted being generally better than $\pm 2\text{mm}$. Levelling was found to be very quick and problems only arose under adverse weather conditions, particularly high winds.

The reduced levels of the T.B.M. s were initially established by carrying a level survey from an Ordnance Survey bench mark on a nearby (750m distant) railway bridge to the site and back again. A second Ordnance Survey bench mark on a sluice gate, only about 200m from the site, was picked up in the same survey and was subsequently used for much of the early site work. This bench mark and the T.B.M. s were independently checked in relation to the

railway bridge bench mark about one year later, and appeared to have remained stable within the accuracy of the survey (i.e. $\pm 3\text{mm}$).

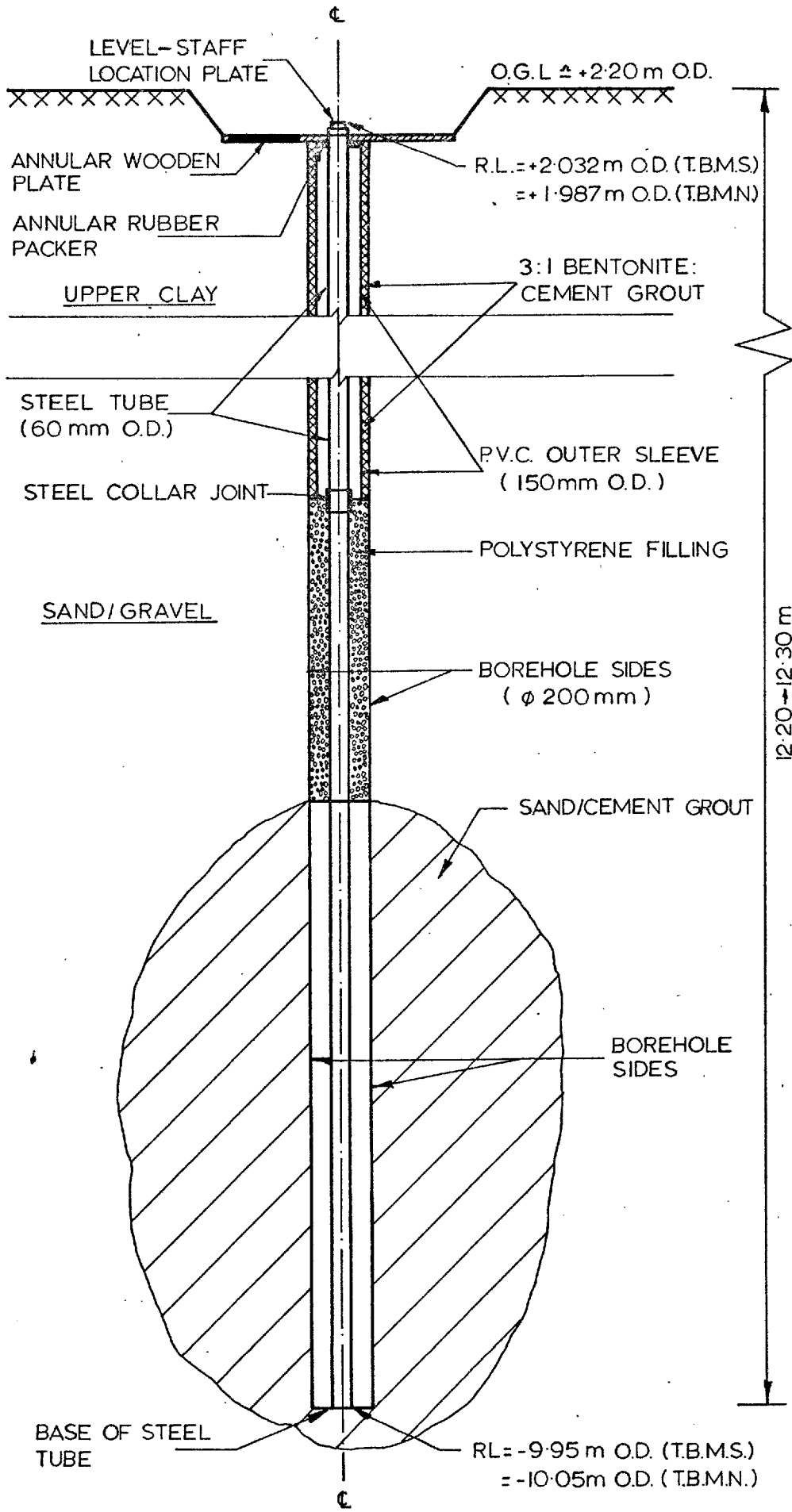
Finally, T.B.M.N. was turned into a deep settlement measuring point for the purposes of Bank 4, near the centre of which it happened to be located. This was achieved by welding a vertical settlement gauge collar to the top of the steel tube and then extending it through the fill as per the plate gauges (section 5.10). The results of this adaptation are presented, together with those for the V.S.U., in section 5.11 (figures 5.11.2. to 5.11.5.).

5.9.3. Accuracy of Level Survey

The level staff used was only calibrated in 5mm intervals, although readings were always interpolated to 1mm and it was not difficult to read to $\pm 1\text{mm}$. A good indication of the overall accuracy of the level survey is provided by the data in figure 5.9.2. These show the differences in observed settlement of the vertical settlement gauges in the foundation and the adjacent settlement plates on the surface of the sand fill. The results yield standard errors of between ± 2 and $\pm 3\text{mm}$ (± 5 to $\pm 7.5\text{mm}$ 99% confidence level) for single observations with the level.

The accuracy of location of the reference heave pins, adjacent to Bank 2 and Bank 4, has been discussed, and the data presented, in section 5.2. Standard errors of ± 2.5 to $\pm 3\text{mm}$ and ± 4.5 to $\pm 5.5\text{mm}$ were recorded for Bank 2 and Bank 4 respectively, the drop in accuracy between the two embankments probably being a function of the increased number of change points. These data obviously include effects unrelated to the level survey; the average 99% confidence level was $\pm 9.5\text{mm}$.

The results as a whole would thus suggest an overall accuracy of about $\pm 7\text{mm}$, which, as stated in section 5.2., is less than was required. The required accuracy (better than $\pm 5\text{mm}$) could easily have been achieved with a staff reading to 1mm , this being rather overlooked in the preoccupation with the sub-surface measurements.



(APPROX. SCALE 1:20)

TEMPORARY BENCH MARK INSTALLATION

FIG. 5.9.1.

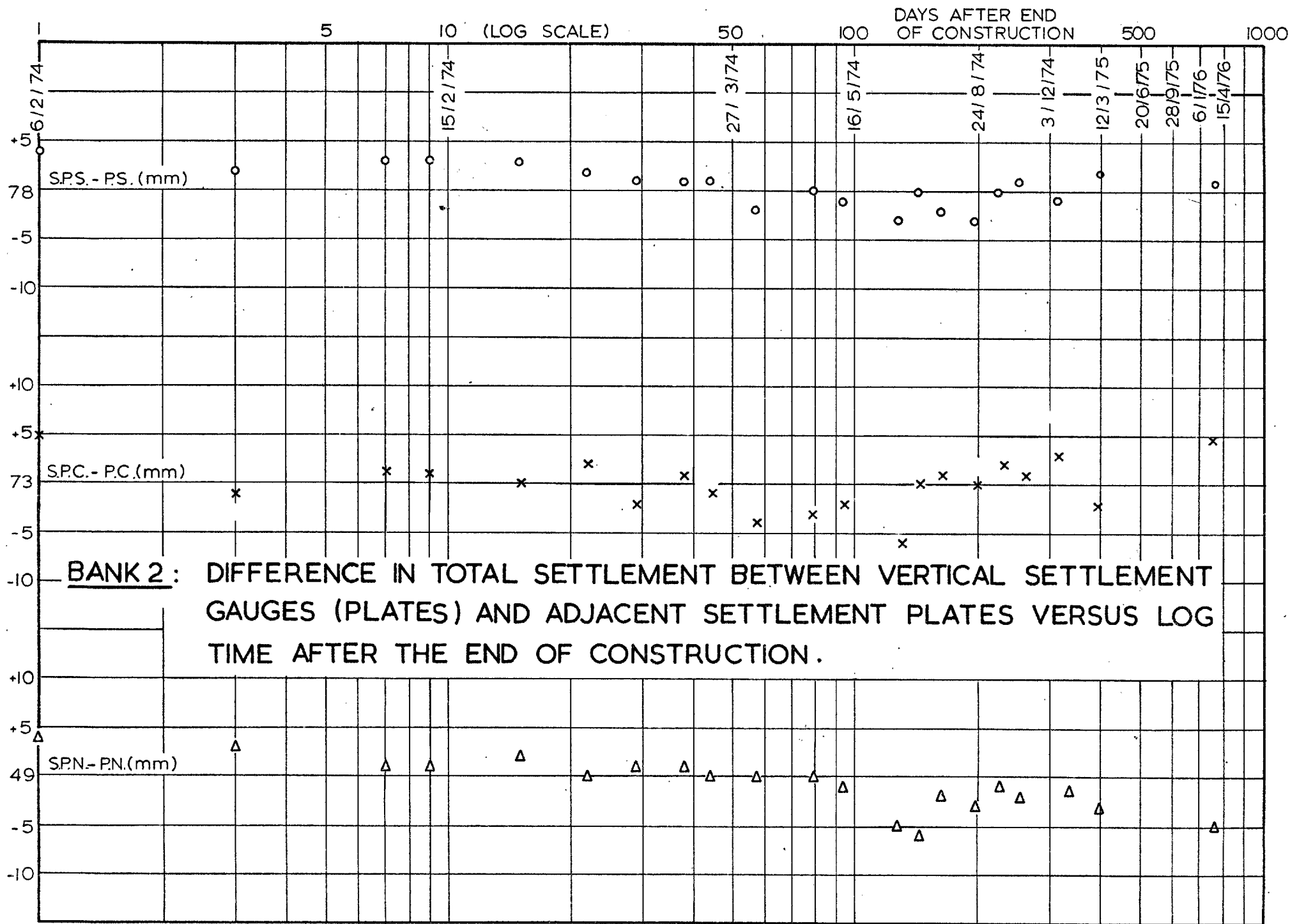


FIG. 5.9.2.

5.10 Vertical Settlement Gauges (Plates)

5.10.1. Description, Installation and Reading

The 1m square by 5mm thick steel plates each had a threaded collar welded centrally on its upper surface to accommodate instrument extension as construction proceeded. The extensions were 1m lengths of steel tubing, approximately 100mm O.D., with screw threaded collar joints. The plates were installed, with the first 1m length of tube attached, up to 1m below existing ground level. Having excavated to the required depth, a flat level surface, slightly greater in area than the plate, was prepared by hand and the plate positioned and checked for level and stability. An outer sleeve of 150mm O.D. P.V.C. downpipe, with force-fit couplings, was used to prevent downdrag of the steel tubing by the sand fill. In order to minimise any tendency for this outer sleeve to bear on the plate, and hence itself transmit downdrag forces, it was stopped about 200mm short of the plate and the gap packed with highly compressible polystyrene. Prior to the installation of the packing, the annulus between the lower end of the outer sleeve and the inner tube was filled with greasy rags to prevent ingress of sand fill. In addition this annular filling served to centralise the sleeve around the tube at its lower end and to locate it vertically (figure 5.10.1.).

At each stage of the extension, including the initial installation, the outer sleeve was stopped just short of the inner tube to enable easy levelling of the latter. Polystyrene packers were placed in the annular gaps of each joint to maintain their symmetry. The plates were initially located by level survey on three separate occasions, as was the top of the

first length of extension tube. The plate was then backfilled with sand and its subsequent elevations obtained by relating to the top of the extension tubes. Reduced levels were always taken immediately before and after extension in order to accurately determine the new total length of tubes and collars above the plate. As readings consisted of taking levels they were very quick to do and posed no problems. For the long-term installations under Banks 2 and 4 the tops of the extension tubes were fitted with top plates and level-staff location points. The outer sleeves were fitted with top caps which were locked in position in an attempt to protect the installations from vandalism.

5.10.2. Accuracy, and Assessment, of Results

The accuracy of the measurements was quite simply the accuracy of the level survey, which was assessed to be of the order ± 7 mm (section 5.9). The only likely source of discrepancy between the movements of the plate and the actual foundation settlements would be if compression within the fill resulted in downdrag on the extension tubes and punching of the plate into the foundation i.e. a bearing capacity failure of the plate. The only instruments to provide direct comparison with the plate gauges were the H.S.G. s, these being installed at approximately similar elevations. The only good results from the H.S.G. s were still thought to be inherently less accurate than the plates (section 5.3.) and thus the plates were used to assess the H.S.G. results rather than vice versa. However, there appears to be no reason to doubt the validity of the settlements recorded by the plate observations. The movements of SPC/4 were wholly compatible with those of the upper magnet (M1) of the V.S.U. (see figures 5.11.2 to 5.11.5), suggesting that the installation technique had been successful in

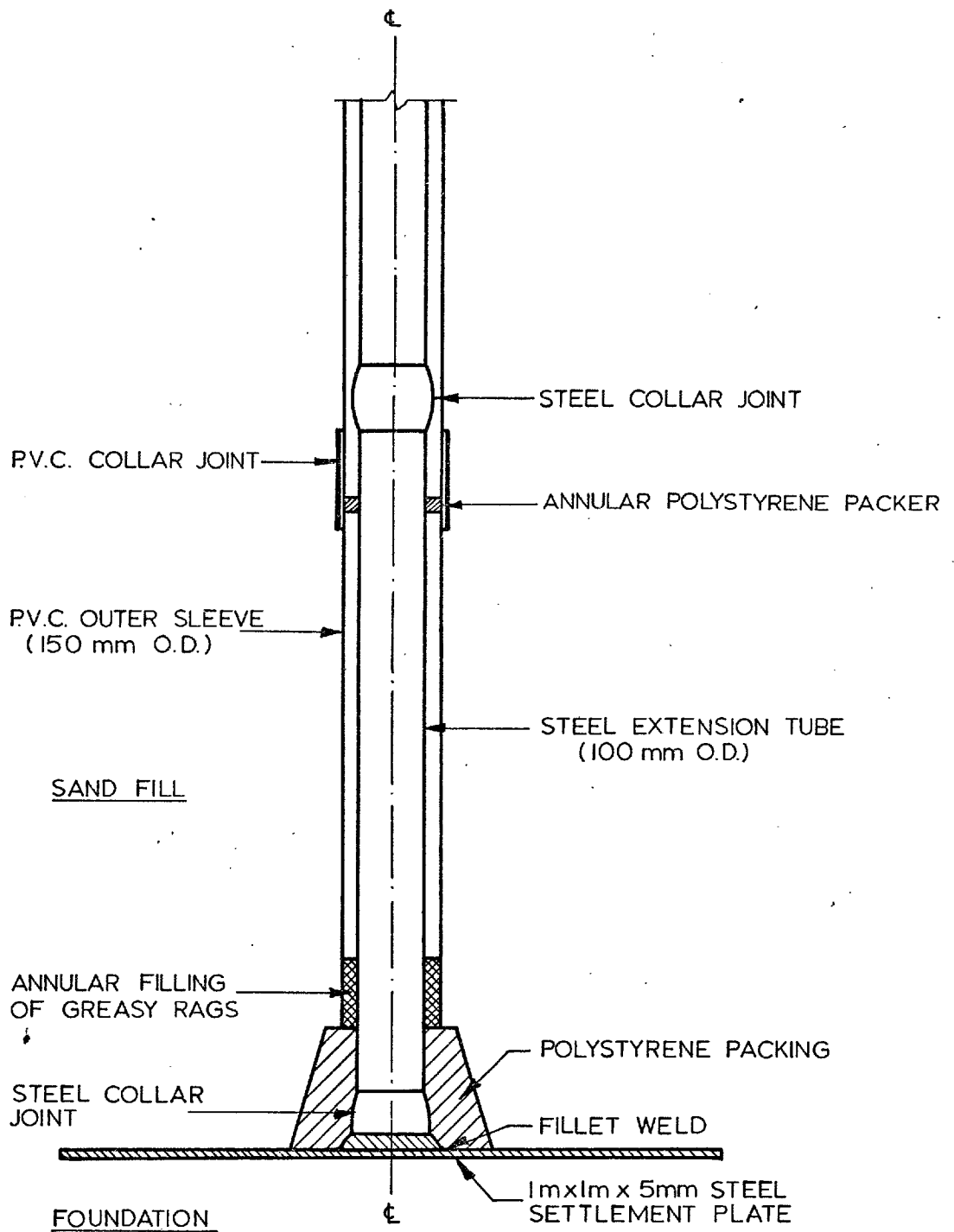
its aims. The results from the vertical settlement gauge observations during the construction of Bank 1 (Stages 1 and 2), Bank 2 and Bank 4 are presented in figure 5.10.2. whilst the long-term observations for Banks 2 and 4 are shown in figures 5.10.3 and 5.11.4/5 respectively.

Surface settlement plates, consisting of approximately 150mm square by 2.5mm thick pieces of steel plate with small welded level-staff location points at their upper face centres, were placed on top of Bank 2 at the end of construction. These were positioned adjacent to the tops of the extension tubes from the three vertical settlement gauges to provide a check on the movement of the latter as well as of the actual readings. The results are presented in figures 5.9.3. and 5.10.3, the former providing a direct comparison between the movements of the two types of plate. The differences would seem to largely represent level survey errors, as discussed in section 5.9., possibly combined with small differentials in the movements of the plates. However, it is noticeable that these differences become greater with time after the end of construction, although there is no common trend for the three pairs of plates. The larger variations occur after the end of permanent site work and it is possible that with different personnel taking the readings discrepancies have occurred. It should also be noted that the surface settlement plates rested on the embankment surface and were thus very exposed to any possible disturbances.

5.10.3. Final Comments

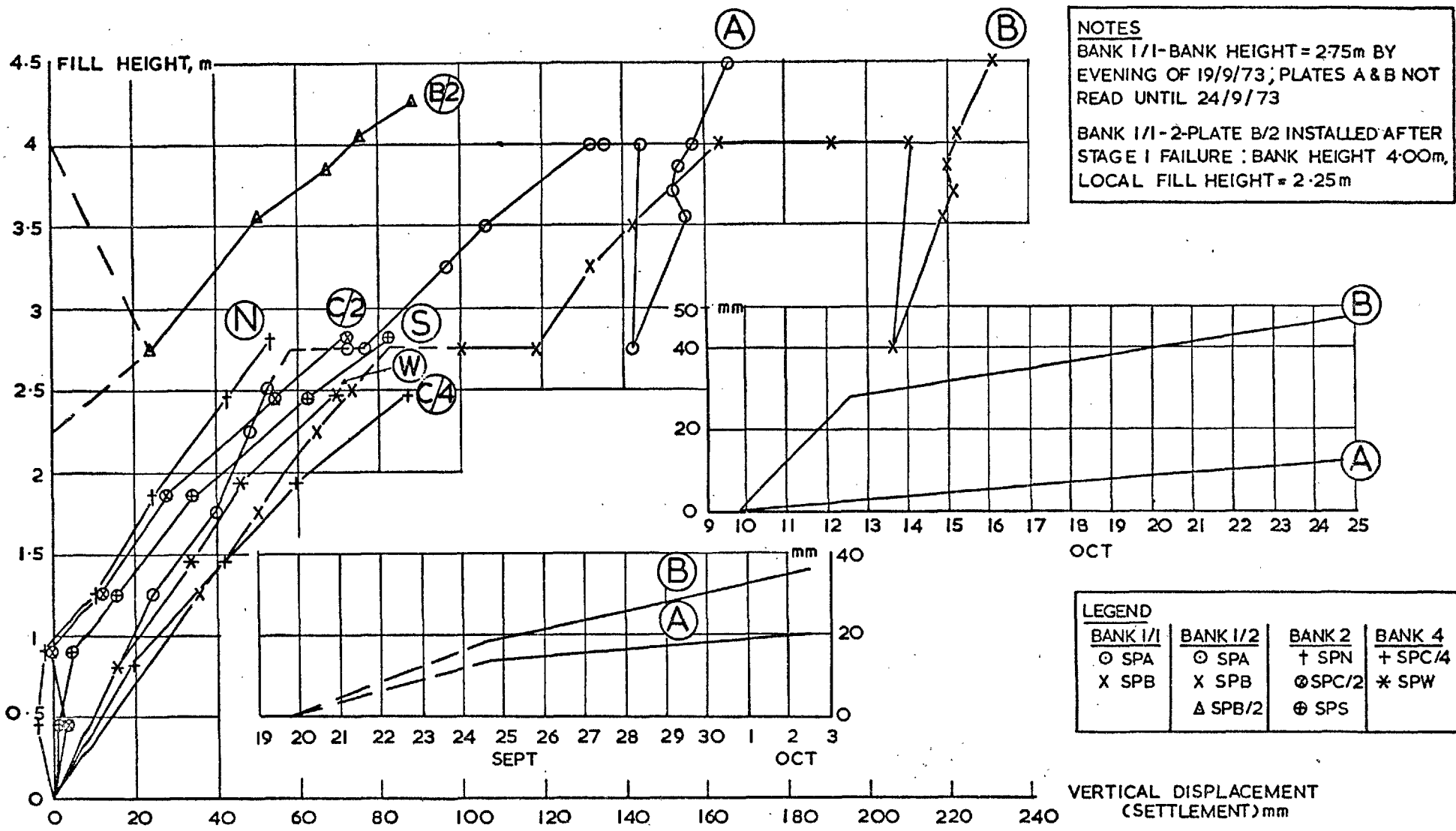
These instruments were found to be quick and easy to install, extend and read and to provide reliable foundation surface settlement data. In comparison the H.S.G. cannot match these points but it does provide a

continuous settlement profile as well as horizontal displacement data. Instruments which have to be extended through fill are always at risk from construction plant as well as making the construction operation more difficult. Despite the care taken the extension tubes from the two vertical settlement gauges in position during Bank 1, Stage 1 were knocked by construction plant and the welded joint on top of the plate was broken; this could occur with only a slight knock because of the long lever-arm provided by the extension tubes as fill height increased. In both these cases construction was at an early stage (the fill height was 1.25m) and the plates were excavated and repaired. Unfortunately due to levelling errors the absolute vertical location of the plates was lost and readings were recommenced at 1.25m fill height. Settlements during the placing of the initial 1.25m of fill were estimated by linear extrapolation of the fill height/settlement relationships obtained (figure 5.10.2.). As discussed in Chapter 6 this has almost certainly resulted in an over-estimate of the absolute settlements, the true behaviour during the initial stages of filling being represented by the data for Bank 2 (figure 5.10.2.).



(APPROX. SCALE 1:10)

VERTICAL SETTLEMENT GAUGE (PLATE)
INSTALLATION



BANK I STAGES 1/2, BANK 2, BANK 4; VERTICAL SETTLEMENT GAUGES (PLATES): VERTICAL DISPLACEMENTS VERSUS FILL HEIGHT & AT CONSTANT FILL HEIGHT DURING CONSTRUCTION

FIG. 5.10.2.

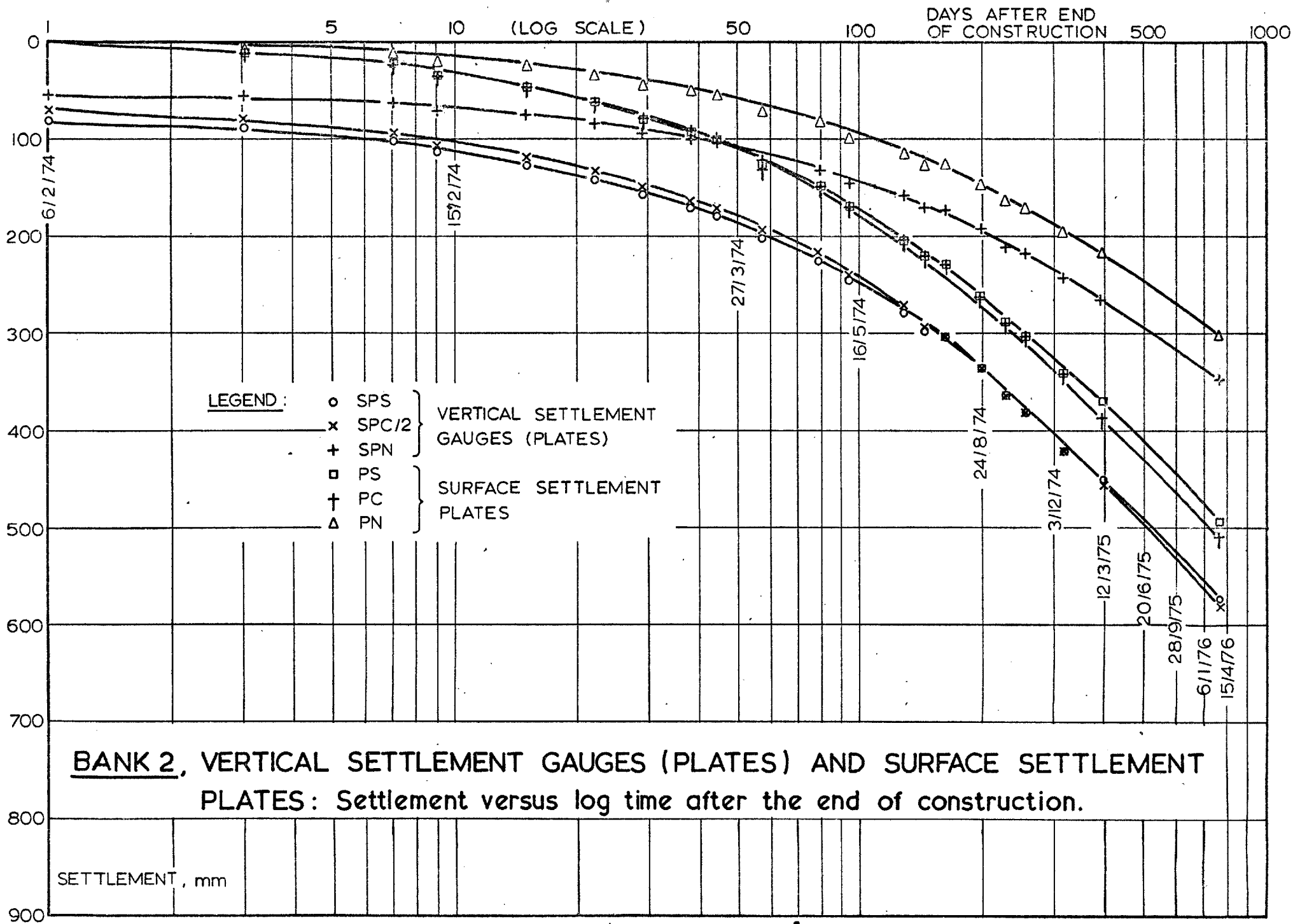


FIG.5.103

5.11. Vertical Settlement Unit

5.11.1. Description, Installation and Reading

This type of instrument is alternatively referred to as a borehole extensometer (Burland et al, 1972) or a multipoint magnetic extensometer (Marsland and Quarterman, 1974). The version described by Burland et al (1972) consisted of axially magnetised permanent ring magnets set at various levels in a borehole and located by a probe containing a reed switch. The magnets were mounted on short lengths of tubular (76mm O.D.) P.V.C., to which were attached three strong springs for the purpose of permanently locating them to the borehole walls. A rigid P.V.C. access tube, passed centrally through all the holders, enabled the probe to sense the magnet locations. This type of installation was used in conjunction with 100mm to 250mm diameter boreholes, which were grouted up after completion of the installation process. Various magnet holders have been designed for this system (Burland and Moore, 1973), which was originally intended for use in stiff clays and soft rocks.

Problems have been encountered with the use of this type of instrument in soft clay foundations, for three main reasons, as listed below:-

(i) The springs were not entirely satisfactory for positive location of the magnets to the borehole walls and incidences of magnet holders sliding down the access tube have been reported (Marsland, 1973(a); George and Parry, 1973). Such occurrences are not necessarily confined to soft soils (see e.g. Hallows, 1973).

(ii) The rigid P.V.C. access tube was subject to downdrag forces from the grout and deformed to such an extent that passage of the sensing probe was impossible (George and Parry, 1973).

(iii) This is to some extent a combination of the two previously described occurrences. The magnet holders may become locked onto the access tube, by the grout (Marsland, 1973(b)) or deformation of the access tube (George and Parry, 1973), and hence independent of the foundation material at their location.

In order to overcome these problems a modified multi-point settlement device has been suggested (Marsland 1973(c)). This incorporates a very flexible, wire reinforced, plastic tube to which the magnet holders are attached, and through which the rigid P.V.C. access tube passes. The latter is thus isolated from the soil and grout. The spring fixity has been improved such that the same springs can be used in a variety of borehole sizes and the installation method made more sophisticated. Initial results appear encouraging (Marsland and Quarterman, 1974).

A second system for use in soft clays consists of locating the ring magnets to the borehole walls with shoot-out devices; this was adopted at Mucking. The epoxy coated magnets were attached to rectangular plates, with cylinders running along two opposite sides. These cylinders were linked, via standard piezometer tubing, to a compressed air source, and contained steel pistons fitted with arrow heads which could be shot out, in opposite directions, into the borehole wall. When a piston had travelled the requisite distance for full penetration of the arrow head, a pressure-relief hole was exposed in the cylinder and the drop in

pressure indicated this occurrence to the installers. A central P.V.C. access tube (24mm I.D.) was made telescopic by the use of 36mm, I.D. couplings, the joints being made with double O-ring seals.

The actual design of the assembly, with regard to position of magnets and position and length of telescopic joints, is of some importance. It was decided to position four magnets at approximately 1m intervals within the soft clay, and one magnet in the gravel (as an experiment to see if any fixity could be achieved). The total length of telescopic joints was such that 600mm (4 x 150mm) of settlement could be accommodated within the foundation. The actual length of the telescopic joints is of some importance, as previous experience with this instrument (Bank 3) had shown that where this length exceeded that of the probe, some difficulty may be experienced when the probe has to pass from the larger diameter coupling tube back into the smaller diameter main access tube. The telescopic couplings were thus made 150mm long compared to the probe length of nearly 250mm. Finally the position of the magnets needs to be such that they are a greater distance below the telescopic joint above them than the length of the telescopic joint itself; if not, the telescopic coupling can bear down on the magnet and influence its movements (Wilkes, 1973).

The V.S.U. was assembled on site and installed in a 203mm diameter shell and auger borehole, with its base penetrating about 1m into the gravel stratum. The magnet holders were loosely taped in position on the access tube and the air lines attached to the cylinders. The telescopic joints were made up as required and the base of the access tube capped off. The assembled V.S.U. was then lowered into position. This operation involved careful handling in order

to keep the air lines manageable and to avoid telescoping any of the joints. The latter consideration precluded any pushing or pulling of the instrument during installation. Having successfully vertically located the unit in the borehole, the air lines were attached in turn to the compressed air source and the arrow heads shot into the borehole walls. Finally a tremie pipe was very carefully lowered to the base of the borehole and grouting carried out using 3:1 bentonite : cement mix (figure 5.11.1.).

The sensing probe containing the reed switch, which closed on passing into a magnetic field, was linked, via the circuit wire, to a buzzer and battery located in the cable drum holding the wire. The weight of the probe was taken, and its depth from the top of the access tube determined, by a steel tape attached to its upper end. The top of the access tube, which was extended through the fill using telescopic joints was picked up in the level survey at the time of each set of readings. Readings were taken of beginning and end of the buzzer signal, for each magnet, with the probe passing down the access tube and again on the way up the access tube, the actual position being taken as the average of these four readings. The base of the tube was also plumbed during each set of readings.

5.11.2. Accuracy, and Assessment, of Results

The basic system, whereby a reed switch moves axially into the magnetic field of a ring magnet and snaps closed, hence activating a circuit, is capable of sensitivities of the order of 0.02mm (Burland et al, 1972).

However, very strict control is needed to attain such high orders of accuracy, the following points being of particular importance (Burland, 1973(b)):-

- (i) The ring magnets may not always be symmetrically magnetised and thus centring of the probe is important.
- (ii) The position of the reed switch, with respect to its inclination to the vertical axis of the magnet and its orientation about this vertical axis, also affects the closure position.
- (iii) The reed switch will not close at the same position as it opens, when entering and leaving respectively, the same point in a magnetic field.

Providing the reed switch is confined to the middle third of the magnetic field an accuracy of location of $\pm 0.2\text{mm}$ is suggested by Burland et al (1972). Thus in a typical field situation the accuracy is largely controlled by the accuracy with which the position of the probe can be related to a datum i.e. the accuracy of the steel-tape measurements and the level survey. From the three sets of initial readings taken for each magnet this was found to be always better than $\pm 2\text{mm}$.

The readings taken during the construction of Bank 4 are shown in figures 5.11.2. and 5.11.3. whilst the post-construction readings are presented in figures 5.11.4. and 5.11.5. The latter also shows the relative displacements of the various settlement measuring points beneath the centre of Bank 4; the magnets can be seen to have moved independently. Marsland (1973(b)) suggested that even telescopic tubing may be ineffective when in direct contact with grout, due to locking of the magnets onto the access tube or of the joints themselves. The data indicated that the telescopic joints

had functioned as intended. If the magnets had become locked onto the access tube the results would only be seriously affected when the settlement of a particular magnet was sufficient to close the telescopic coupling below it, and hence start to move the next section of access tube and if, in addition, the magnet on this latter section was also unable to move independently. The relative settlements observed were not great enough to close the telescopic joints.

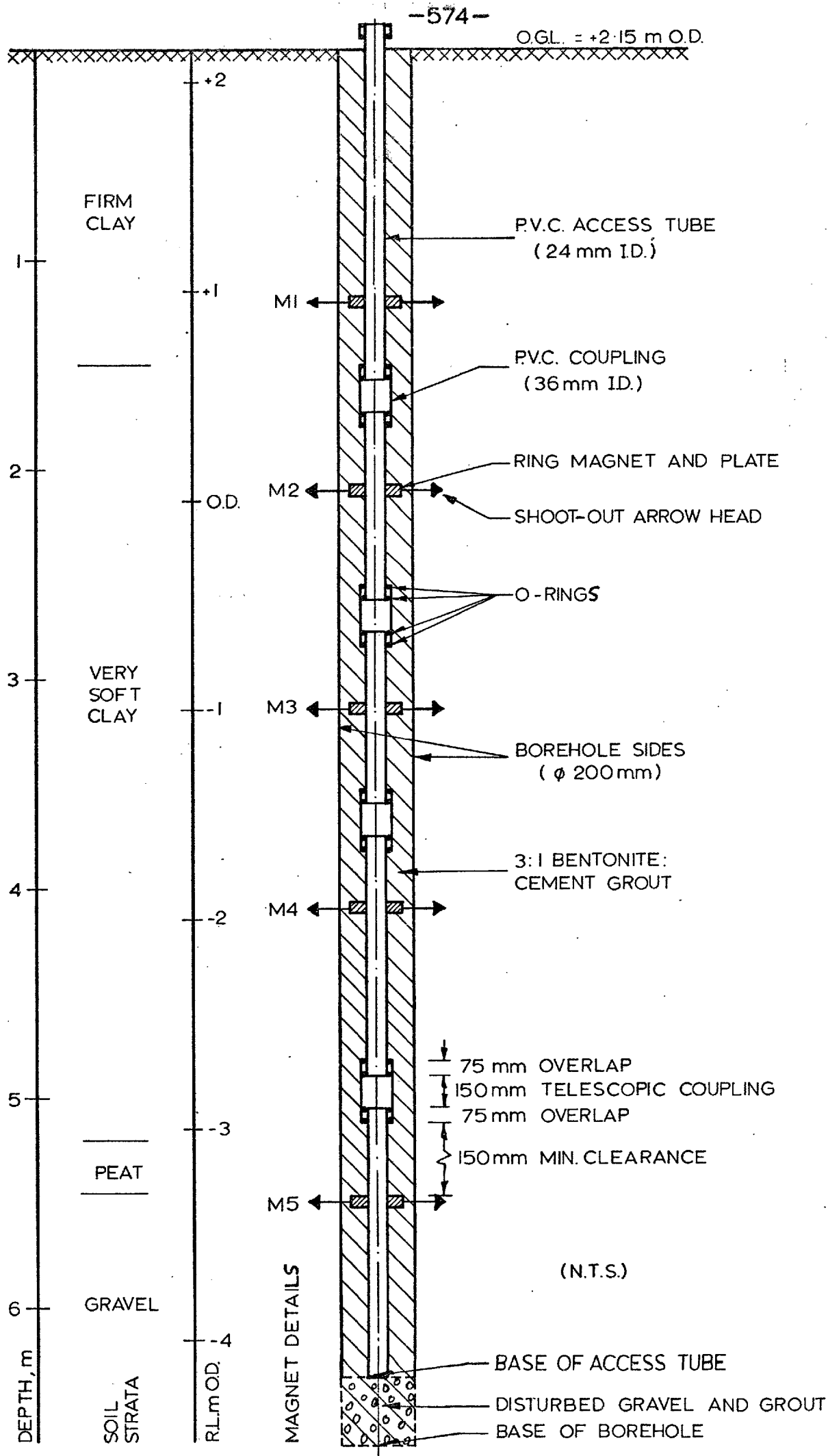
The overall pattern of vertical displacements recorded appears very acceptable when plotted against fill height during construction or versus logarithm of time for the long-term results. The consolidation curves resulting from the latter are particularly satisfactory (figures 5.11.4. and 5.11.5.). The data are also consistent with the vertical displacements of the settlement plates and T.B.M.N. Errors in the level survey can be seen to manifest themselves occasionally on all the plots, being particularly noticeable for those points where relatively small displacements have occurred e.g. T.B.M.N. base of V.S.U. and magnet M5.

The base of the V.S.U. and magnet M5 appear to have moved approximately together, the latter probably floating in the grout rather than being attached to the gravel in any way. As indicated in the inclinometer section (5.4.) it is hard to assess these movements because of the uncertainty regarding conditions at the base of a shell and auger borehole terminating in gravel. They may be compression of the grout and disturbed gravel at the base of the borehole (see figure 5.11.1.) or real movements of the gravel as underlying materials compress. The T.B.M. has certainly settled to some extent, but whether this is due to consolidation at depth or failure of the outer sleeve to prevent downdrag of the base, or a combination of both, is uncertain.

5.11.3. Final Comments

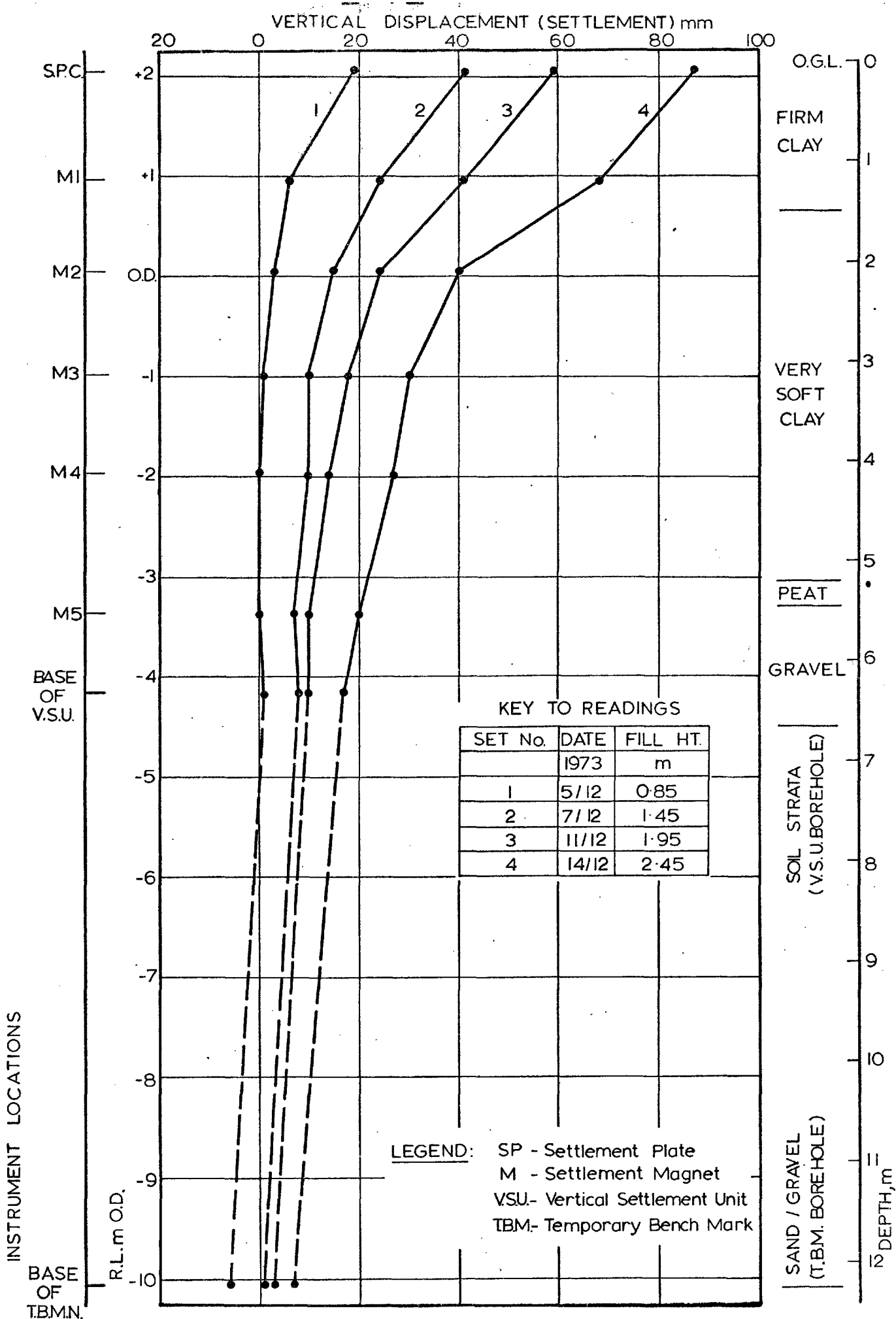
The V.S.U. appears to have functioned well over a period of some two years and there is no evidence to suggest that the magnets did not follow the adjacent foundation movements. The instrument facilitated quick and easy reading and results are readily processed. Provided adequate forethought is given to the design of the installation, and suitable care taken when installing it, this type of extensometer would seem well suited to the monitoring of vertical displacements within a soft clay foundation. It should be borne in mind that the experiences related herein are for a limited depth of compressible material. With greater thicknesses and longer installations some of the problems described may be accentuated.

Finally, the probe itself has to be treated with some care as the reed switch is installed in a very delicate glass capsule. Breakage of this only occurred once during about two and a half years use, but resulted in the absence of inclinometer magnet settlement data for the latter part of construction of Bank 1, Stage 1, as reported in section 5.4.

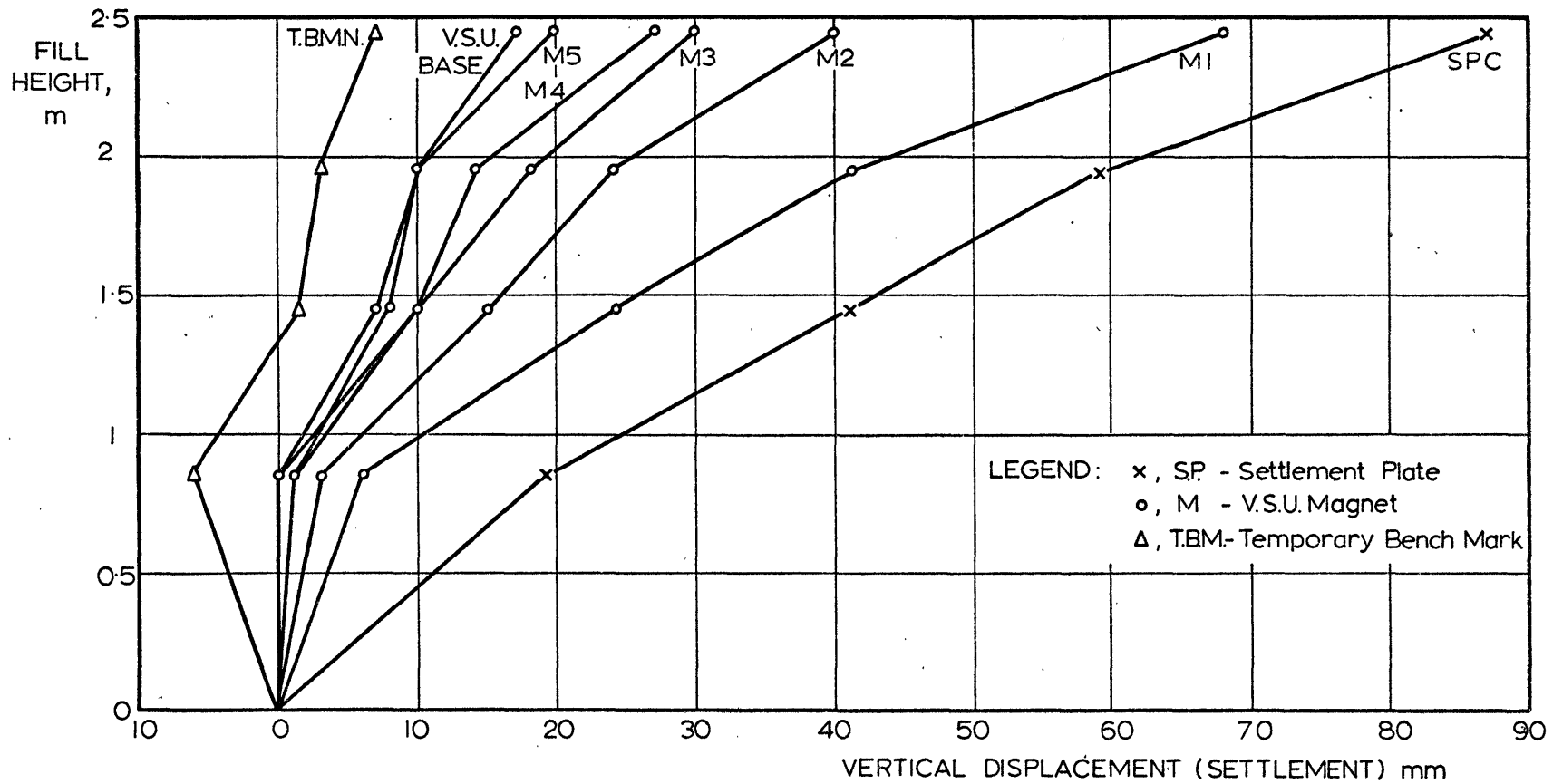


VERTICAL SETTLEMENT UNIT INSTALLATION

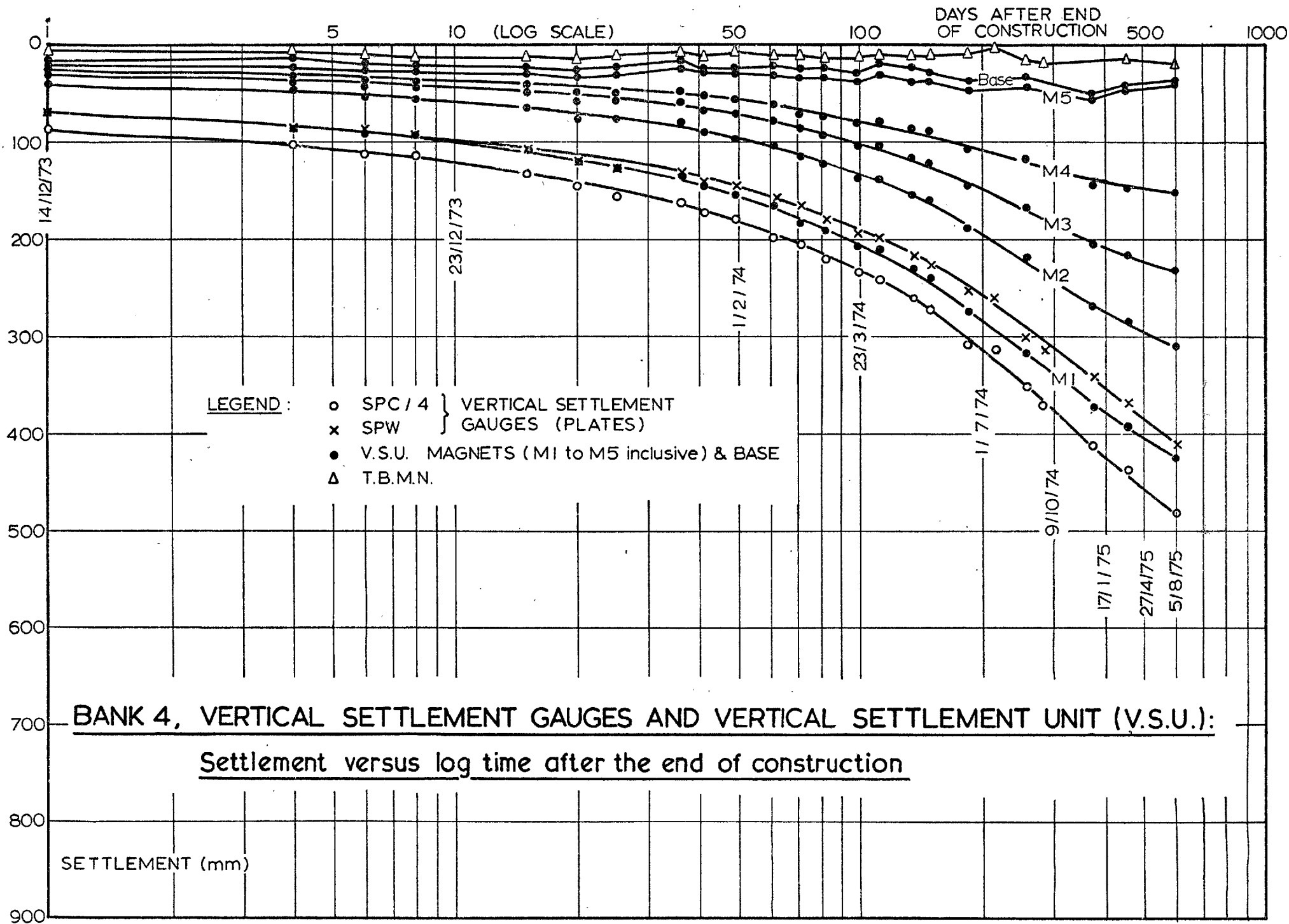
FIG. 5.II.I.

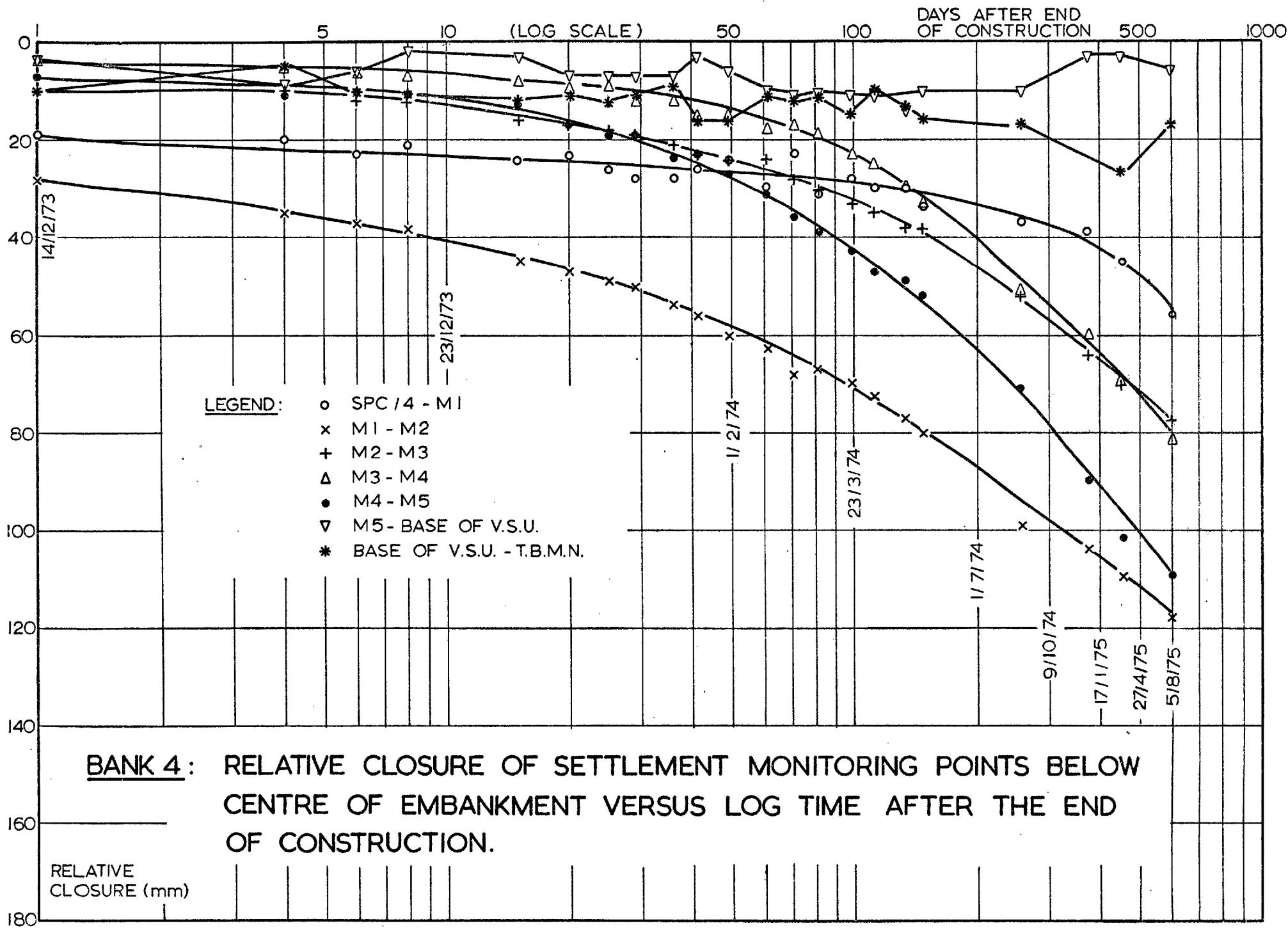


BANK 4: SETTLEMENT / DEPTH PROFILE DURING CONSTRUCTION



BANK 4 : SETTLEMENTS DURING CONSTRUCTION





5.12. Conclusions

Detailed conclusions dealing with each item of instrumentation have already been drawn, and it only remains to summarise the data obtained and assess the overall order of confidence. This has been done for the displacement measurements in table 5.12.1. The measured pore pressures were, with a few exceptions, considered to be reliable.

This opportunity can be used to list some of the main lessons learnt from the instrumentation program, as follows:-

- (1) The benefits yielded by duplication of instrumentation at a number of locations, and in some cases (e.g. the surface targets) the advantages of two separate methods of measurement.
- (2) The experience gained by trials of this nature in assessing the various forms of instrumentation, leading to possible improvements in equipment and/or the associated installation, reading and data reduction processes.
- (3) The importance of establishing, absolutely, zero readings on all instruments, and also of accurately surveying all details of the installations.
- (4) The need to adopt carefully thought-out reading procedures and data-reduction processes and additionally to record any changes in the instrumentation or the procedures followed. Optimisation of construction and instrument readings along critical path lines, as outlined in Chapter 4, is of considerable advantage.

(5) The data reduction process should always relate to the fundamental behaviour of the instrument and include an assessment of its likely accuracy. Ideally analysis of the results is best carried out by the person taking the readings; in the writer's opinion such continuity enormously enhances the value of the data (see also Green, 1973(b); Burland, 1975).

Items 1 to 5 have all enormously enhanced the instrumentation of the prototype structures now under construction.

Finally the problem of using a grout of compatible stiffness characteristics to the soil deserves some attention. This aspect of field instrumentation has received recent attention from Werneck (1974), Marsland (1973(b)) and Vaughan (1973(b)), and is particularly pertinent in soft clay foundations (McKenna and Roy, 1973).

Marsland (1973(b)) showed that high water : cement ratios were needed to achieve strengths compatible with even the stiffer soils, and also pointed out that typical cement-based grouts exhibit significant strength gains with time. Vaughan (1973(b)) similarly showed the high water contents required in a 1:1 bentonite : cement grout in order to achieve compatible compressibilities with soft clays (approximately 450% water content to give an M_v of $2 \times 10^{-3} \text{ m}^2/\text{kN}$ over an effective stress range from 0 to 200 kN/m^2).

Unfortunately the water content of the 3:1 bentonite : cement grout used at Mucking was not specified, but rather gauged to give a mix which could be readily placed by tremie pipe; however it was of the order of 200 to 400%.

EMBANKMENT	HORIZONTAL DISPLACEMENTS	VERTICAL DISPLACEMENTS
Bank 1, Stages 1/2	<ol style="list-style-type: none"> 1. Inclinometers H.S.G. s 2. Surface Targets Time-Lapse Targets 	<ol style="list-style-type: none"> 1. Vertical Settlement Gauges 2. Surface Targets Time-Lapse Targets 3. Inclinometers H.S.G. s
Bank 2	<ol style="list-style-type: none"> 1. Inclinometers H.S.G. Surface Targets Heave Pins 	<ol style="list-style-type: none"> 1. Vertical Settlement Gauges Vertical Settlement Plates H.S.G. Surface Targets Heave Pins
Bank 4	<ol style="list-style-type: none"> 1. Heave Pins 	<ol style="list-style-type: none"> 1. Vertical Settlement Gauges V.S.U. T.B.M.

Table 5.12.1.

Data Obtained from Instrumentation and Indications of Order of Reliability

Key Numbers 1, 2, 3 indicate decreasing order of accuracy. Where several instruments are listed under one number, this indicates all are of approximately same accuracy, the order implying the writer's preference.

Inspection of the grout in situ, some months after placing, revealed it to have a consistency very similar to that of the soil; the results obtained also indicated that there was no grout stiffness problem.

Vaughan (1969) showed that the grout backfill to a piezometer installation could be up to two orders of magnitude more permeable than the surrounding soil before serious errors in measured pressures would arise. The same author (Vaughan (1973(b))) also quoted a permeability of 5×10^{-10} m/s, for a 1:1 bentonite : cement grout with a water content of about 200%, which would suffice for clay soils. Viggiani (1973) reported tests wherein the seals of piezometers installed in soft clay were checked, these tests showing a 3:1 bentonite : cement mix to be satisfactory in all cases. Thus the grout used at Mucking would appear appropriate to soft clay foundations from both the stiffness and permeability points of view, although this is an area clearly ripe for further research.

THE STRENGTH AND DEFORMATION CHARACTERISTICS OF A SOFT ALLUVIAL CLAY
UNDER FULL SCALE LOADING CONDITIONS

A Thesis Submitted to the
University of London
for the Degree of
Doctor of Philosophy in the Faculty of Engineering

by

Richard Stewart Pugh

Volume III



June 1978

CHAPTER 6

BEHAVIOUR OF THE FOUNDATION MATERIAL UNDER THE APPLIED LOADING CONDITIONS

6.1. Undrained Loading

6.1.1. Displacements

(i) Bank 1

The vectorial pattern of displacements of the foundation and fill during construction Stages 1 and 2 is presented in figure 6.1.1., for Sections A and B. The data were derived from the inclinometers, surface targets and horizontal settlement gauges. Similar behaviour of the foundation at the two cross-sections is evident, although overall, the horizontal displacements tended to be greater at 'A' and the vertical displacements greater at 'B'. The inclinometer and surface target data confirmed that plane strain conditions existed at these two cross-sections during both construction stages; displacements in the 'X' coordinate direction were generally less than $\pm 10\%$ of those in the 'Y' and 'Z' coordinate directions.

The displacement vectors presented in figure 6.1.1. illustrate the build-up to the failure of the southern side of Bank 1 during construction Stage 1. The mechanism of movement suggested, commenced within the vicinity of the corner of the central trench, extended well down into the foundation and emerged within the toe trench. Also depicted is the build-up to the Stage 2 failure of the northern side of the embankment. In this case the major movement appears to initiate well clear of the central trench. Both failures are discussed in more detail in section 6.2.

*as were the pore pressures.

Displacements recorded by the individual instruments were discussed in detail in Chapter 5, and reference is now made to these data (H.S.G. s - figures 5.3.2. to 5.3.4; inclinometers - figures 5.4.2. to 5.4.14., and 5.4.17 to 5.4.26; surface targets - figures 5.7.2. to 5.7.6. vertical settlement gauges - figure 5.10.2).

Figures 5.3.2., 5.3.3. and 5.7.2. to 5.7.6. illustrate that pre-failure heave of the foundation beyond the toe of the embankment was very small. Figures 5.3.2., 5.3.3., 5.4.23 and 5.4.24 show the maximum construction settlements of the Stage 1 embankment to coincide with maximum horizontal displacements of the foundation, both occurring beneath the southern slope of the embankment. During undrained loading both horizontal and vertical displacements are directly caused by the applied shear loadings; thus maximum shear strains and therefore displacements are induced at the localities subjected to the maximum shear stresses. Furthermore under undrained plane strain conditions, vertical and horizontal linear strains will be equal and opposite and equal to half the shear strain (see section 6.1.2.), leading to the similar magnitudes of the observed horizontal and vertical foundation displacements.

The combination of small pre-failure heave (and thus, by implication, lateral compression) beyond the embankment toe, and large displacements beneath the embankment fill is in agreement with the loading conditions; progressive failure (Bishop, 1967) of a brittle foundation material would thus be anticipated.

Figures 5.7.2. to 5.7.6., wherein displacements of the surface targets have been plotted versus fill height clearly illustrate the acceleration of movement as failure was approached in both construction stages. This

aspect is further emphasised in figures 6.1.3. to 6.1.7; horizontal displacements interpolated from the inclinometer profiles at .1m intervals of depth have been plotted versus fill height. Excavation of the toe trench at a Stage 1 fill height of 2.75m appears to have exerted considerable influence upon the pattern of behaviour.

Although the relationship between fill height and horizontal displacement is generally non-linear from the early stages of construction, in many cases the divergence from linear is not great for fill heights below 2.75m. However, the relationship becomes distinctly non-linear for the foundation to the south of the embankment centre line, following excavation of the toe trench. Also shown in the figures are the horizontal displacements at constant fill height; these indicate that creep is a function of stress level, as might be expected (Bishop and Lovenbury, 1969; Bjerrum, 1973). The toe trench excavation can be seen to have dramatically increased creep rates to the south of the embankment centre line, whilst having no significant effect to the north.

It is of interest to consider the displacement/fill height relationships in the light of the critical shear stress concept discussed in Chapter 2 (Bjerrum 1973) and the concept of a current yield locus as incorporated, for example, in the Cam Clay Model (Wroth, 1976). These concepts advocate yielding of the foundation when the maximum previous shear stress in the former case, and a combination of the maximum previous shear and normal effective stress in the latter case, are exceeded. These aspects are discussed in relation to the values of $p_c' - p_o'$ for the foundation (see section 2.6.), and the observed pore pressures during the initial loading stages, in sections 6.1.3. and 6.3.

On the basis of the fill height/horizontal displacement relationships yielding occurred beneath the embankment centre almost from the outset of construction; initial behaviour closest to linear was exhibited by the foundation beyond the fill area.

Another point of interest is that following the excavation of the toe trench the fill height/horizontal displacement relationships for the foundation beneath the northern part of the embankment exhibited an increase in stiffness, suggesting that shear unloading or consolidation, or both had taken place. This is confirmed by the 'field' effective stress paths (figures 6.1.40 and 6.1.42).

Figures 6.1.1. and 6.1.3. to 6.1.6. show that despite the 1:2.5 northern slope of the Stage 1 embankment and construction of the berm at 2.25m fill height, the pattern of displacements was near symmetrical: only the excavation of the toe trench led to major asymmetry of the displacement pattern and thus, ultimately, to failure of the southern side of the embankment. However, figures 6.1.5. and 6.1.6. indicate that considerable yielding of the foundation beneath the northern side of the embankment had occurred by the time Stage 1 failure was reached; figure 6.1.7. shows the fill height/horizontal displacement relationships to have been highly non-linear from the outset of Stage 2 construction.

The vertical settlement gauges all indicated near linear fill height/vertical displacement relationships (figure 5.10.2: although as noted in section 5.10 the results for Stage 1 are suspect) throughout both construction stages, with virtually no elastic recovery between the end of Stage 1 and the start of Stage 2.

(ii) Bank 2

Figure 6.1.2. depicts the vectorial displacement pattern for the Bank 2 foundation, being similar, during the construction stage, to that for Bank 1 at the same fill height. Despite the embankment's symmetrical geometry, both the vertical and horizontal displacements were greater to the south of the embankment centre line.

Again, reference is made to the data presented in Chapter 5 (heave pins/surface targets - figure 5.2.1; H.S.G. - figure 5.3.5; inclinometers - figures 5.4.15 and 5.4.16; vertical settlement gauges - figure 5.10.2).

As in the case of Bank 1, heave of the foundation beyond the embankment toes was very small during the construction period.

Horizontal displacements of the inclinometers, when plotted versus fill height (figure 6.1.8.) also reflect the behaviour observed for Bank 1, Stage 1, by exhibiting non-linear characteristics from the start of construction.

The fill height/vertical displacement relationships derived from the settlement gauge data (figure 5.10.2) indicated distinct 'yield points' for all three gauges at 0.85m fill height, below which very little settlement occurred and above which the fill height/settlement relationship was approximately linear. The initial readings for the Bank 1 settlement gauges (see section 5.10.) were regarded as somewhat suspect and it seems likely that similar behaviour was exhibited by the Bank 1 foundation.

(iii) Bank 4

Heave adjacent to Bank 4 (figure 5.2.3.) was again very small during construction. The relationship between fill height and settlements recorded by the settlement gauges (figure 5.10.2) was similar to that for the Bank 1 gauges, being essentially linear, and showing no signs of the apparent yield point observed for the Bank 2 foundation. At this point it is worth noting the close correspondence between the fill height/settlement relationships at the sites of the different test fills (figure 5.10.2).

Vertical displacements within the foundation beneath Bank 4 are shown in figure 5.11.2. for the construction period. Although the vertical settlement gauge data showed no signs of a yield point in the fill height/settlement relationship, the V.S.U. magnet data indicated a definite yielding at 0.85m fill height, followed by near linear behaviour.

6.1.2. Strains

(i) Horizontal Strains

Average horizontal linear strains* were derived for the foundation material from the relative displacements of the H.S.G. magnets. These measurements were considered as accurate as any others with respect to near surface horizontal displacements (see table 5.12.1), and were the obvious ones from which to derive horizontal strains. It was not considered worthwhile deriving average horizontal linear strains for the foundation at depth,

*in the 'Y' coordinate direction i.e. $\epsilon_y; \epsilon_x$ being zero for plane strain conditions which were seen to apply in section 6.1.1.

from the relative horizontal displacements of the inclinometers because of the large base lengths this would involve.

The results for both stages of Bank 1 are presented in figures 6.1.9. and 6.1.10 for H.S.G.A. (Stage 1 only) and H.S.G.B. respectively. Figure 6.1.9. shows compressive strains (considered +_{ve} herein) to have developed from magnet 'C'southwards, and tensile strains (considered -ve herein) from magnet 'C'northwards, from the outset of Stage 1 construction. At a fill height of 2.85m (and the toe trench excavated) the maximum tensile strain was less than 1% (between magnets 'E' and 'D') and the maximum compressive strains less than 0.5% (between magnets 'A' and 'B').

Maximum tensile and compressive strains continued to develop at these same locations, until, at a fill height of 4m, just prior to failure, the values were -3.9% and +1.2% respectively. Incremental strains at a particular location were either wholly tensile or wholly compressive throughout construction with one exception; this being the area between magnets 'C' and 'D' which exhibited small compressive strain increments, after initial tensile ones up to 2.85m fill height. During this part of the construction sequence the embankment crest moved from south of 'C' to north of 'D'. At failure, however, the average linear strain of gauge length 'CD' was small and tensile.

The horizontal strains indicate that failure developed beneath the embankment centre with maximum horizontal tensile strains occurring close to the southern extremity of the central trench, above which point the initial tension crack was observed to open at the start of failure (see section 6.2).

The final set of data for H.S.G.A. were, very fortunately, obtained only 2.5 hours prior to failure of the Stage 1 embankment and thus provide an excellent indication as to the amount of tensile strain required to form a crack in the fill, this being at least 4%. As stated by Bjerrum (1972) the formation of cracks in fills is an important consideration in the back-analysis of failures using limit equilibrium methods.

The effect of the toe trench on the compressive strains beyond the embankment toe, and thus on the failure in general, is self evident.

Strains derived from the observations of H.S.G.B. permit a more complete picture to be constructed, readings being available over the entire length of the instrument; an extra magnet was also located close to the southern toe of the embankment. Maximum tensile strains again developed in the vicinity of the southern corner of the central trench (magnets 'E' and 'F'), whilst the maximum compressive strains are more precisely located, being in the area immediately adjacent to the embankment side of the toe trench. Strains beneath the embankment batter were again, small (magnets 'E' and 'D') and strain increments unidirectional except for the embankment toe (magnets 'D' and 'C') where overall compression was reversed by a large tensile strain increment just prior to failure.

Excavation of the toe trench exerted an approximately symmetrical influence on the near surface pattern of horizontal strains, except in its immediate vicinity. Indeed, at this stage of the embankment construction the overall strain pattern was likewise near symmetrical, but with the trend towards failure of the southern side of the embankment just commencing. This trend became increasingly evident with increasing fill height and was clearly

defined by the 3.75m fill height stage. At this point both the maximum compressive and tensile horizontal strains to the north of the embankment centre line were still less than 0.5%.

The build up to the Stage 2 failure of Bank 1, as depicted in figure 6.1.10., was similar in pattern to that for Stage 1. Maximum tensile strains developed between magnets 'I' and 'H', well to the north of the central trench and supporting other evidence (see section 6.2) that the Stage 2 failure resulted in shearing of the desiccated layer. A maximum compressive strain of 0.9% was recorded between magnets 'J' and 'K'; larger values may have existed beyond the embankment toe, in which area no measurements were made.

Once again average horizontal linear strains beneath the embankment slopes were small, and the incremental strains unidirectional except for the very small increments between magnets 'I' and 'J', which went from tension to compression as the embankment crest moved from north to south.

The patterns of deformation leading to the two failures could thus be considered as comprising three modes of strain, viz:-

- (a) an active (tensile horizontal strain) zone.
- (b) an intermediate (very small tensile/compressive horizontal strain) zone.
- (c) a passive (compressive horizontal strain) zone.

This theme is further expanded in sub-section (iv), wherein the complete state of strain, of selected points, within each of these zones is considered.

Horizontal strains developed at Section B were smaller than at Section A, which was more centrally located within both failures (section 6.2).

A comparison of the strains developed during the two construction stages at Section B indicates that the tensile strains developed within the foundation at Section A prior to the Stage 2 failure may have been significantly greater than those developed prior to the Stage 1 failure. This hypothesis is supported by the correspondingly larger settlements.

Average horizontal linear strains have been plotted versus fill height and time for selected pairs of H.S.G. magnets in figure 6.1.12. During Stage 1 construction, significant strain development commenced at a fill height of 2.25m, with a second increase in strain development subsequent to the excavation of the toe trench. A similar pattern developed during Stage 2 construction, with the corresponding fill heights being 3.15m and 4.05m respectively.

Figure 6.1.11. depicts the development of near-surface average horizontal linear strains for the Bank 2 foundation, based on data from H.S.G.C. The horizontal strain pattern at the end of construction was almost identical, in both magnitude and distribution, to that for Bank 1, Stage 1 at the same fill height. In the case of each embankment, the maximum horizontal, and therefore vertical, strain was recorded in the embankment crest/shoulder region (see also figures 5.3.2., 5.3.3., 5.3.5., 5.4.23 and 5.4.24 and section 6.1.1.) where the shear stresses induced in the foundation would be greatest, rather than beneath the embankment centre

where the vertical stress would attain its maximum value. However, as consolidation of the Bank 2 foundation proceeded, the zone of maximum settlement and maximum horizontal tensile strain migrated to the central area of the embankment, as depicted in figures 5.3.5. and 6.1.11.

Consolidation is, of course, largely the result of vertical strains and allied to vertical stress. Figure 6.1.11. indicates, however, that significant horizontal strains also developed during the post-construction period, as is discussed further in section 6.3. However, it is worth noting at this juncture that, 492 days after the end of construction, the tensile strain beneath the embankment centre had increased from 0.35% to 2% (a factor of 5.7 times) and the maximum compressive strain beneath the embankment toe from 0.35% to 1.85% (a factor of 5.3 times).

Similarly to Bank 1, Bank 2 also induced larger foundation strains to the south of the embankment, this trend continuing throughout the post-construction period. Yet again, horizontal strain increments were unidirectional.

Figure 6.1.13. depicts the horizontal strains for selected pairs of H.S.G. magnets in the Bank 2 foundation plotted versus fill height and time. As in the case of Bank 1 there is a fill height above which significant strains develop, in this case being 1.85m. The strain rate steadily decreased following the end of construction.

Finally, it is of interest to relate the previous discussions to the data presented by Werneck (1974), relating to horizontal strains in the over-

consolidated Lias Clay during the construction of a trial embankment at the site of Empingham Dam. Werneck observed that:-

- (a) initial strains were small
- (b) significant strain developed at a particular location during the construction of the embankment slope above that location
- (c) the strains 'in (b)' were proportional to the fill height at the particular location
- (d) post-construction strains were greatest at those locations where the strain rate at the end of construction had been greatest i.e. close to the embankment crest.

Observation (a) has also been made for the Mucking results. The geometries of the Mucking trial embankments were such that condition (b) was not discernable, although the largest strains were generally within the vicinity of the embankment crest (observation (c)).

Observation (d) is of particular interest with respect to the arguments relating to strain rate effects on shear strength, as discussed in section 3.4. and depicted in figure 3.24; and is in agreement with the data presented in figure 6.1.11., although the influence of any consolidation strains is superimposed therein.

(ii) Vertical Strains

Average vertical linear strains could only be computed for the foundation material beneath Bank 1 by using the displacement observations for the inclinometer magnets. These data, as discussed in section 5.4., are not considered reliable; however, average vertical linear strains were computed, and presented in table 5.4.5. Maximum vertical compressive

strains beneath the centre of Bank 1, just prior to the Stage 1 failure, were about 3.5%, and just prior to the Stage 2 failure, about 3.1%. These figures, as would be expected*, are of similar magnitude to the maximum horizontal tensile strains beneath the embankment centre (figures 6.1.9 and 6.1.10). The data in these figures can be used to assess the variation in average vertical linear strain across the embankment section, during construction. They indicate compressive strains beneath the Stage 1 embankment to be greatest in the area between the crest and the central trench, reducing to zero in the vicinity of the embankment toe. Tensile strains are implied beyond the toe, reaching maximum values in the vicinity of the toe trench. The magnitude of these strains should obviously be equal, but of opposite sign*, to the horizontal strains.

During Stage 2 construction, maximum compressive vertical strains appear to have been induced just behind the embankment crest, with tensile vertical strains apparently developing beneath the embankment toe.

Average vertical linear strains within the Bank 2 foundation, prior to the end of construction, may be assessed from the average linear horizontal strains depicted in figure 6.1.11. Maximum compressive vertical strains again occur within the vicinity of the embankment crest, and, as in the case of Bank 1, Stage 2 maximum tensile vertical strains appear to occur close to the embankment toe.

The data from the V.S.U. and T.B.M. enabled average vertical linear strains to be derived for the full depth of the foundation beneath Bank 4; the results for the clay foundation being presented in figure 6.1.14. together

*Under undrained ($\Delta V = 0$) plane strain ($\epsilon_2 = \epsilon_x = 0$) conditions $\epsilon_1 = -\epsilon_3$ and $\epsilon_z = -\epsilon_y$, $\epsilon_x + \epsilon_y + \epsilon_z$ being invariant

with those for the underlying sands and gravels. As discussed in section 5.11 the validity of the strains in these latter materials is somewhat suspect. However, it is reasonable to conclude that significant vertical strains were confined to the clay and peat strata.

At the end of construction (fill height 2.45m), the maximum vertical strain within the Bank 4 foundation was +2.8% immediately below the desiccated layer, whilst being +1.8% within the crust itself. The former figure had increased to +12.2%, 602 days from the end of construction.

The overall pattern of vertical strains during construction indicates a relatively stiff crust underlain by less stiff material. It should, however, be noted that initially the reverse was true, this point being further discussed in section 6.3. Below approximately 3m depth, construction strains were small (<0.5%).

Figure 6.1.15 shows the vertical strains within the Bank 4 foundation plotted versus fill height and time. In both cases the behaviour of the desiccated crust is markedly different to that of the underlying materials. The large strains during construction suggest the possibility of rapid consolidation within the crust; its post-construction behaviour was relatively stiff, although after day 300 there was an apparent increase in the strain rate experienced by the desiccated layer. The underlying materials exhibited small construction strains; only the layer immediately beneath the crust undergoing a two stage behaviour with significant strains developing once the fill height exceeded 0.85m.

Overall, the pattern of post-construction vertical strains (figures 6.1.14 and 6.1.15) indicated the compressibility of the clay foundation to increase with depth; both the post-construction behaviour and that during construction are further discussed in section 6.3.

(iii) Shear Strains

As discussed by Burland and Roscoe (1969) the derivation of strain at 'a point' within a plane strain system requires a knowledge of the displacement vectors of three points. Assuming uniform strain across the triangle (or 'point') defined by the three measurement locations (i.e. $\Delta Y = f(Y)$, $\Delta Z = f(Z)$ and $\Delta X = 0$) the horizontal strain (ϵ_Y), the vertical strain (ϵ_Z) and the shear strain (γ_{YZ}) can be determined for the 'point'. These three strain components completely define the state of strain at the point and thus the principal strain vectors can be derived (Timoshenko and Goodier, 1951; Jaeger, 1956).

The only locations within the Bank 1 foundation, at which such an analysis was possible were the intersections between the inclinometer casings and the H.S.G. access tubes, i.e. the constant strain triangle would be defined by two H.S.G. magnets and one inclinometer magnet; for each of which the displacement vector was known. However, as discussed in Chapter 5, some of the displacement components, notably the vertical ones, were not considered sufficiently accurate to warrant strain determinations.

Alternatively, the state of strain at a 'point' may be defined by direct determinations of ϵ_Y , ϵ_Z and γ_{YZ} i.e the average linear strains

of, and angular change between, any two originally orthogonal axes. The 'Z' axis was thus represented by the inclinometers and the 'Y' axis by the H.S.G. s. As outlined in the preceding sections, the H.S.G. s enabled reliable values of average horizontal linear strains to be computed. In the case of undrained plane strain $\epsilon_Z = -\epsilon_Y$ and the vertical strains were thus also derived from the H.S.G. data.

The angular change comprises two components, viz $\frac{d\Delta Z}{dY}$ (the gradient of the H.S.G. access tube) and $\frac{d\Delta Y}{dZ}$ (the inclination of the inclinometer casing). The former is referred to herein as vertical shear strain, γ_Z , and the latter as horizontal shear strain, γ_Y .

Reference to section 5.3. (and figures 5.3.2. and 5.3.3.) indicates that there was no location at which γ_Z could be reliably evaluated at various stages throughout construction. However, Werneck (1974) had previously observed that for the Empingham trial bank foundation γ_Z was everywhere very small when compared to γ_Y , and therefore that in this case γ_Y could be taken to represent γ_{YZ} . As γ_Y could be readily derived from the inclinometer profiles $\gamma_Y(\max)$ was compared to $\gamma_Z(\max)$ for Bank 1, Stage 1 and the values found to be 5.6% and 4.5% respectively. Thus γ_Y could not be taken as reasonably representing γ_{YZ} for the Mucking clay foundation.

It was thus decided to evaluate γ_{YZ} for selected points on Section A (Bank 1, Stage 1), and for one point on Section C (Bank 2), at maximum fill heights, as is illustrated in figures 6.1.16 and 6.1.17.

Figure 6.1.16 depicts the state of strain of three points, designated 01, 02 and 03, within the Bank 1, Stage 1 foundation at Section A, just prior to failure. Figure 6.1.17 depicts the state of strain within the Bank 2 foundation at the junction of inclinometer IC1 and HSGC at the end of construction and at intervals thereafter. In all cases the principal strain vectors have been derived from the average linear strains and the shear strains; the latter are further discussed in the following section.

(iv) Principal Strains

As only three points within the Bank 1, Stage 1 foundation were selected for interpretation, and then only at maximum fill height, the state of strain at each point is dealt with separately in the following discussion of figure 6.1.16. The principal strains were derived by construction of Mohr's circle of strain; compression was considered positive and positive shear strains to be associated with positive shear stresses. The latter are linked to clockwise couples for the tension positive case (Timoshenko and Goodier, 1957) and thus in figures 6.1.16 and 6.1.17 positive shear stresses are linked to counter clockwise couples about the soil element, as per the notation of Poulos and Davis (1974). The associated sign convention for the shear stress on any soil element is that a shear stress is positive if acting in a positive cartesian coordinate direction on a plane whose inward normal is also in a positive cartesian coordinate direction, or in a negative direction on a plane whose inward normal is also in a negative direction.

a. Point 01

As would be expected the maximum principal strain (ϵ_1) is near vertical and therefore of similar magnitude to ϵ_z (about 4%), with $\gamma_{\max} = 8.2\%$.

The slight inclination to the vertical is, however, in the opposite sense to that which might be anticipated. γ_Z is small, but in the expected direction, whereas γ_Y , whilst also small, is in the reverse direction to that anticipated; a cumulative γ_{YZ} ($= \gamma_Z + \gamma_Y$) of 2.25% results. For ϵ_Y and ϵ_Z to be principal strains γ_Y would have to be equal and opposite to γ_Z (i.e. in the reverse direction to that observed). Had γ_Y been in the anticipated direction and exceeded γ_Z in magnitude ϵ_1 would have rotated to the embankment side of vertical. All four points for which the state of strain was evaluated, were located at the base of the desiccated layer and the presence of this layer appears to have been responsible for the observed γ_Y direction; similar behaviour was confirmed by finite element analyses (figures 6.1.41 and 6.1.43.).

b. Point 02

γ_Y is again in the reverse direction to that which might have been expected in the absence of the desiccated zone. In this case γ_Y is in the same direction as γ_Z , reducing γ_{YZ} ($= \gamma_Z - \gamma_Y$) to 1.3%. The values of ϵ_Z and ϵ_Y are close to zero, leading to significant rotation of the principal strains; ϵ_1 is +0.65% at 41° to the embankment side of vertical and $\gamma_{YZ} \approx \gamma_{\max} = 1.3\%$. The principal strain rotation is thus in the opposite direction to that observed for point 01, but approximately as anticipated.

c. Point 03

The shear strain components are as might be expected, producing a cumulative γ_{YZ} of 3.4%. The major principal strain has rotated even further, being 63° to the vertical, and having a magnitude of 2.1%, corresponding to $\gamma_{\max} = 4.2\%$.

The analyses presented in figure 6.1.16 and discussed in the preceding paragraphs are mainly based on horizontal displacements and are therefore considered reasonably accurate ($\pm 10\%$). However, the three locations considered do not necessarily represent the locations of maximum shear strain within the foundation, with the exception of point 01 which is very close to the point of initiation of the failure surface (see section 6.2.) and may thus be taken to represent failure conditions. The major principal strain is in fact in good agreement with the laboratory values reported in section 2.8. Point 03 was probably also close to an area of maximum shear strain, whilst point 02 was fairly remote.

If the axes of principal stress and strain coincide* then figure 6.1.16 reveals that the conditions of points 01, 02 and 03 approach respectively those of active shear, simple shear and passive shear, thus confirming the observations made in Chapter 2 with respect to test methods for shear strength determinations (section 2.7 and figure 2.14).

d. Bank 2

The state of strain at the junction of H.S.G.C. and I.C.1, as depicted in figure 6.1.17, for the end of construction situation is compatible with that observed for Bank 1, although the strains were very small.

*The assumption that the axes of principal stress coincide with those of principal strain is only correct for a homogeneous isotropic elastic material. As briefly outlined in section 2.8 the laboratory behaviour of the Mucking clay could not be modelled by either isotropic or anisotropic elastic behaviour.

The state of strain was also evaluated from the displacements 156 and 492 days after the end of construction, as shown in figure 6.1.17. In these cases undrained conditions no longer applied and ϵ_z was thus unknown. However, reference to the vertical movements at the inclinometer location (figure 5.2.2.) indicates that, in the long term, ΔZ (post-construction) was negligible and it was therefore assumed that $\Delta\epsilon_z$ was also zero. On this basis, the increasing horizontal and shear strains post-construction resulted in an increase in ϵ_1 from 0.55% to 2.3% (a factor of 4.2 times) and γ_{\max} from 1.1% to 3% (a factor of 2.7 times); these increases were accompanied by little rotation of the principal axes. It should also be noted that, as analysed, the increase in γ_{\max} from 156 to 492 days after the end of construction was only 0.3%, being entirely the result of $\Delta\epsilon_y$; $\Delta\gamma_{yz} = 0$.

6.1.3. Pore Pressures

(i) General

(a) Bank 1, Stage 1

Ground-water conditions at the site were discussed in section 2.5, particular attention being focused on the seasonal pore-pressure variations (figure 2.12). Both the lateral and vertical variations of pore pressure within the alluvial clay at the location of Bank 1, prior to construction, are depicted in figure 6.1.18. Site work prior to construction of the embankment (section 4.2), in the form of excavation, and backfilling, of the central trench resulted in the observed pattern. Pore pressures recorded by piezometers PA1-3 were typical of the seasonal norm (figure 2.12), whereas those closer to the trench were higher; the maximum increase of 7.35 kN/m^2 (or 750mm of water) occurring directly beneath the trench. A maximum increase in total stress of about 4.5 kN/m^2 resulted from the trenching operations and thus a

significant part of the pore-pressure rise was probably as a result of rainfall being more readily able to infiltrate the sand surface; much of that falling on the clay surface would have evaporated during the summer months. Any rises in pore pressure would have been the more rapid because of the equivalent reduction in drainage path length brought about by the presence of sand within the trench.

Construction pore pressures within the Bank 1 foundation were discussed in section 5.5.5. and illustrated in figures 5.5.3. to 5.5.5. An alternative presentation, as excess pore pressure* ($\Sigma\Delta u$, being the excess related to the initial situation as illustrated in figure 6.1.18) versus fill height (h' , being the maximum height of the fill above O.G.L.) is given in figures 6.1.19 and 6.1.20. The following points are of importance:-

- (1) the pore pressures corresponding to the maximum fill height for each stage ($h = 4\text{m}$ - Stage 1; $h = 4.5\text{m}$ - Stage 2) were recorded post-failure
- (2) $\Sigma\Delta u$ has everywhere been expressed as metres of water. However, the ratios $\Sigma\Delta u/\gamma_B \cdot h$ and $\Delta u/\gamma_B \Delta h$ are dimensionless, as is normal and correct, when discussed in the text.

The ratios $\Delta u/\Delta h$ and $\Sigma\Delta u/h$ varied both vertically and laterally, total variations during construction being summarised in figure 6.1.21. and discussed in the following using the same categorisation as in the figure:-

*When more than one measurement of pore pressure was made at a particular fill height the maximum value of $\Sigma\Delta u$ was plotted. The $\Sigma\Delta u$ values are generally for Section A where maximum values were recorded, except when doubts existed regarding the validity of the readings e.g. PA7, PA18 (Stages 1/2) and PA21 (Stage 2) - see section 5.5.5.

(1) Beneath the major part of the embankment fill (piezometer locations 7 - 15) $\Delta u/\gamma_B \Delta h$ was initially close to unity; this suggests conditions of undrained zero lateral yield as would be expected (see also figure 6.1.9) at shallow depth beneath the centre of a wide uniform load, particularly in view of the relatively thin compressible layer (Giroud and Watissee, 1972). A saturated foundation having a pore-pressure parameter 'B' (Skempton, 1954) = 1 is also suggested.

However, close to O.G.L. Δu was generally less than $\gamma_B \Delta h$, possibly as a result of a combination of the highly permeable desiccated layer (section 2.5; Marsland, 1957(a)) and the proximity of the near surface piezometers to the drainage boundary formed by the central trench. Symons (1976(b)) observed that near surface piezometers rarely record Δu values approximating to $\gamma_B \Delta h$ when alluvial clays with desiccated surface layers are subjected to the initial stages of embankment loading (see also Lewis et al 1975; Symons 1974). However the finite element analyses also predicted a reduction in the total stresses in this area (see figures 6.1.35 and 6.1.36).

The ratio $\Delta u/\gamma_B \Delta h$ then decreased to a new, near constant, value, before increasing to values close to, and sometimes in excess of unity. This second change in the $\Delta u/\Delta h$ slope occurred predominantly at fill heights of between 1.25 and 2.25m, being more pronounced in some locations than in others (figures 6.1.19 and 6.1.20). Beneath the embankment centre (locations 10 - 15) $\Sigma \Delta u/\gamma_B h$ was in many cases close to unity as failure approached.

(2) In the berm area (piezometer locations 16 - 18) the excess pore-pressure pattern was initially similar to that described in (1); subsequently, however, $\Delta u/\Delta h$ remained near constant at the lower value, with no indication of an increased pore-pressure response with increasing fill height.

(3) In the toe areas (piezometer locations 4 - 6, 19 - 21) $\Delta u/\gamma_B \Delta h$ was less than unity from the outset; $\Delta u/\Delta h$ remained essentially constant beneath both toes, although to the south, where the ratio was similar in value to the berm area, there were indications of an increased pore-pressure response when the fill height exceeded 3.25m. Beneath the northern toe $\Delta u/\Delta h$ was much lower.

(4) Beyond the embankment toes (piezometer locations 1 - 3, 22 - 24) $\Delta u/\gamma_B \Delta h$ was also less than unity from the outset, remaining near constant to the north, but showing a definite increase, at 3.5m fill height, to the south. Initial values of $\Delta u/\gamma_B \Delta h$ were very small in both cases, as were the overall values to the north.

In summary, the observations suggest that (ignoring the initial response) $\Delta u/\Delta h$ increases from one near constant value to another, the change point occurring at increasing fill heights the further the observation point from the embankment centre. A 'progressive' type of failure (or yielding) with overstress (or yielding) commencing beneath the embankment centre and spreading outwards towards the toe trench, is thus indicated. Similar behaviour has been observed by, among others, Hoeg et al (1969), D'Appolonia et al (1971), and Leroueil et al (1978(a)). Piezometers located beyond the toe of the embankment may thus provide the best guide to approaching failure as discussed in section 6.4; unfortunately such

piezometers tend to be the least reliable because of their low piezometric elevations relative to gauge level (section 5.5.5).

Figure 6.1.22 depicts the lateral and vertical variations in excess pore pressure with increasing fill height; clearly visible is the consistent overall trend of increasing $\Delta u/\gamma_B \Delta h$ with depth.

Finally, r_u^* values have been calculated from the recorded pore pressures at 3.75m fill height, and pore pressures linearly extrapolated, using the $\Sigma \Delta u/h$ relationships, to 4m fill height: the r_u values are presented in figure 6.1.22. Beneath the main fill area r_u values reached 0.6 to 0.8, prior to failure, over a large part of the foundation; maximum values slightly in excess of unity were recorded beneath the southern toe.

(b) Bank 1, Stage 2

The construction pore pressures have been discussed in section 5.5.5. and were presented in figures 5.5.3. to 5.5.5. Reference is now made to figures 6.1.19, 6.1.20 and 6.1.21, and using the categorisation of the latter:-

(1) Pore pressures recorded at locations which were beneath the embankment centre during both construction stages (piezometer locations 13-15) showed $\Delta u/\gamma_B \Delta h$ to be close to unity during both the Stage 1 - Stage 2 unloading and the Stage 2 filling.

* r_u being as defined by equation 5.1.1., and therefore noting that $r_u > 1$ does not imply a negative effective stress state.

(2) At those locations beneath the embankment centre during Stage 2 only (piezometers 16 - 18) $\Delta u/\gamma_B \Delta h$ was slightly negative during the Stage 1 - Stage 2 unloading*. During Stage 2 construction $\Delta u/\gamma_B \Delta h$ approximated to unity.

(3) Beneath the embankment's northern slope (piezometer locations 19-21) unloading was such that $\Delta u/\gamma_B \Delta h$ was again negative.* During Stage 2 construction $\Delta u/\gamma_B \Delta h$ was initially less than unity, but increased to approximately unity at about 4m fill height.

(4) Beyond the northern toe of the embankment (piezometer locations 22-24) $\Delta u/\gamma_B \Delta h$ was very small (both positive and negative) during the Stage 1 - Stage 2 unloading. During Stage 2 construction $\Delta u/\gamma_B \Delta h$ increased from a low value to near unity, also at about 4m fill height.

In summary, the observed response of the pore pressures to the applied changes in total stress was very similar to that for Stage 1, as discussed in sub-section (a) previously. The pore-pressure changes during the interval between the end of Stage 1 construction and the start of Stage 2 construction resulted from a combination of total stress changes and consolidation. As for Stage 1 a consistent overall trend of increasing $\Delta u/\gamma_B \Delta h$ with depth is depicted for Stage 2 in figure 6.1.22.

*In both these cases the reduction in shear stress due to embankment unloading was accompanied by an increase in fill height at the piezometer locations. The pore-pressure changes are therefore not surprising; in both cases Δu was less than Δh at the piezometer location, particularly for piezometers 16 - 18.

Finally, values of r_u (equation 5.1.1.) were calculated from the recorded pore pressures at 4.25m fill height, and pore pressures linearly extrapolated, using the $\Sigma\Delta u/h$ relationship, to 4.5m fill height; the results are presented in figure 6.1.22. Beneath the main fill area r_u values prior to failure were in the range 0.7 to 0.9 over a large part of the foundation. However, considering the foundation as a whole the r_u values appear to be slightly lower than those for the Stage 1 construction (see also Chapter 7).

(c) Bank 2 and Bank 4

The construction pore pressures, which were briefly mentioned in section 5.5.5. and presented in figure 5.5.6., have been plotted as excess pore pressure versus fill height in figure 6.1.23. Similar behaviour to that observed for Bank 1 is in evidence, except that Δu beneath the centres of these smaller loaded areas was less than $\gamma_B \Delta h$ at the start of construction. It will subsequently be postulated that significant dissipation of the excess pore pressures occurred during the early stages of construction, prior to yielding of the foundation. Reference to figure 2.12. indicates that the average ground-water level was significantly lower prior to construction of Bank 1 when compared to Banks 2 and 4; it is thus a possibility that dissipation beneath Bank 1 was delayed somewhat by the necessity of developing positive pressures within the desiccated zone and the sand filled central trench, thus leading to the initial apparently undrained pore pressure response observed for Bank 1 (see figure 6.1.21) but not for Banks 2 and 4.

An increase in the ratio $\Delta u/\gamma_B \Delta h$ with increasing fill height was observed for nearly all of the piezometers; the change in the slope of the $\Sigma\Delta u/h$ relationships for both embankments occurred at fill heights of about 1m.

The data for Bank 4 were less conclusive in this respect than those for Bank 2.

Figure 6.1.24 depicts the lateral and vertical variations in excess pore pressure with increasing fill height; once again the trend of increasing $\Delta u/\gamma_B \Delta h$ with depth is clearly defined for Bank 2 and the upper part of the foundation beneath Bank 4. The smaller excess pore pressures of the deepest piezometers beneath Bank 4 are considered to be the result of rapid dissipation, these piezometers being very close (less than 500mm) to the lower drainage boundary (i.e. the gravel).

Values of r_u (equation 5.1.1.), corresponding to the end of construction, are shown in figure 6.1.24, being generally between 0.6 and 0.7 for Bank 2 and between 0.5 and 0.6 for Bank 4.

As in the case of Bank 1, the excess pore pressures depicted in figures 6.1.23. and 6.1.24. were the maximum recorded values at each fill height with the exception of the end of construction values, which were just that. Reference to figures 5.5.7. to 5.5.13., wherein the post-construction pore pressures within the foundation materials beneath Banks 2 and 4 are depicted, shows that the maximum pore pressures were recorded between 1 and 15 days after the end of construction. It is postulated that during this period the pore pressures generated by the continuing development of shear strains (see section 3.4.2. and figure 6.1.17) were greater than the reductions in pore pressure resulting from consolidation. Similar rises in excess pore pressure were observed beneath the toe of the New Liskeard embankment (Lo and Stermac, 1965) following the end of construction,

although in this case the rises were both greater in magnitude and over an extended time scale. The foundation clay at New Liskeard was varved and Raymond (1972) has suggested lateral drainage and/or undrained creep (Walker, 1969) as possible causes for the observed pore-pressure increases. Similar post-construction rises in pore pressure have also been reported for other embankments on soft clay foundations (e.g. Leroueil et al 1978(a); Jamiolkowski, 1975).

(ii) Pore-Pressure Predictions

(a) General Theories

Probably the best known relationship between pore-pressure change and change in the applied total stresses is equation 2.5., proposed by Skempton (1948(e) and 1954) who derived it via the elastic pore-pressure changes predicted by equation 2.9; the pore-pressure parameter 'B' is usually assumed to be unity, this assumption being implicit in the following formulations.

The Skempton equation for predicting pore-pressure changes in the triaxial compression test is thus:-

$$\Delta u = \Delta \sigma_3 + A (\Delta \sigma_1 - \Delta \sigma_3) \dots\dots\dots(6.1)$$

As pointed out by Skempton (1954 and 1960) the parameter 'A' is stress path and stress system dependent even for isotropic elastic soils as was demonstrated in table 2.4; equation 6.1. may thus be better rearranged as follows:-

$$\Delta u = \frac{\Delta \sigma_1 + 2\Delta \sigma_3}{3} + (A - \frac{1}{3})(\Delta \sigma_1 - \Delta \sigma_3) \dots\dots\dots(6.2)$$

for triaxial compression,

$$\Delta u = \frac{\Delta\sigma_3 + 2\Delta\sigma_1}{3} + (A - \frac{2}{3})(\Delta\sigma_1 - \Delta\sigma_3) \dots\dots\dots(6.3)$$

for triaxial extension and,

$$\Delta u = \frac{\Delta\sigma_1 + \Delta\sigma_2 + \Delta\sigma_3}{3} + (A - \frac{1}{2})(\Delta\sigma_1 - \Delta\sigma_3) \dots\dots\dots(6.4)$$

for plane strain, assuming equation 2.10 to be valid.

Thus in each case the pore-pressure change is composed of a component due to the change in octahedral normal stress (equation 2.9., noting that this reduces to equation 2.11., for conditions of elastic plane strain) and a change in deviator stress*. In the case of an elastic isotropic soil, noting the 'A' values in table 2.4., it can be seen that equations 6.2. to 6.4., reduce to equation 2.9., there being no component of pore pressure as a result of changes in shear stress.

Skempton (1960) proposed that a relationship of the form:-

$$\frac{\Delta v}{v} = -C \frac{(\Delta\sigma_1' + \Delta\sigma_2' + \Delta\sigma_3')}{3} + 3.D\Delta\tau_{OCT} \dots\dots\dots(6.5)$$

was required to predict volumetric strain ($\epsilon_v = \frac{\Delta v}{v}$), where 'C' is a coefficient of compressibility and 'D' is a coefficient of dilation and τ_{OCT} is the octahedral shear stress:-

$$\Delta\tau_{OCT} = \frac{[(\Delta\sigma_1 - \Delta\sigma_2)^2 + (\Delta\sigma_2 - \Delta\sigma_3)^2 + (\Delta\sigma_3 - \Delta\sigma_1)^2]^{\frac{1}{2}}}{3} \dots\dots(6.6)$$

*The deviator stress component is always positive, the pore pressures generated being independent of the sign of the shear stress (Skempton, 1960)

Thus $\Delta u = \Delta\sigma_{OCT} + 3.a.\Delta\tau_{OCT} \dots\dots\dots(6.7)$

and $a = -\frac{D}{C} \dots\dots\dots(6.8)$

Equation 6.7. is that presented by Henkel (1960(b)), and which reduces to:-

$\Delta u = \frac{\Delta\sigma_1 + 2\Delta\sigma_3}{3} + a\sqrt{2} (\Delta\sigma_1 - \Delta\sigma_3) \dots\dots\dots(6.9)$

for triaxial compression,

$\Delta u = \frac{2\Delta\sigma_1 + \Delta\sigma_3}{3} + a\sqrt{2} (\Delta\sigma_1 - \Delta\sigma_3) \dots\dots\dots(6.10)$

for triaxial extension, and

$\Delta u = \frac{\Delta\sigma_1 + \Delta\sigma_2 + \Delta\sigma_3}{3} + \frac{a\sqrt{3}}{\sqrt{2}} (\Delta\sigma_1 - \Delta\sigma_3) \dots\dots\dots(6.11)$

for plane strain, assuming equation 2.10 to be valid.

Henkel's 'a' parameter may thus be related to Skempton's 'A' parameter as follows:-

$a\sqrt{2} = A - \frac{1}{3} \dots\dots\dots(6.12)$

for triaxial compression,

$a\sqrt{2} = A - \frac{2}{3} \dots\dots\dots(6.13)$

for triaxial extension, and

$\frac{a\sqrt{3}}{\sqrt{2}} = A - \frac{1}{2} \dots\dots\dots(6.14)$

for plane strain, assuming equation 2.10., to be valid.

Equation 6.7., is sometimes written in the alternative form:-

$$\Delta u = \Delta \sigma_{OCT} + \alpha \Delta \tau_{OCT} \dots \dots \dots (6.15)$$

wherein $\alpha = 3a$ $\dots \dots \dots (6.16)$

The use of the pore-pressure parameter 'A' to predict pore-pressure changes in the field is restricted, in particular, by the following factors:-

(i) it is stress path and stress system dependent (Bishop, 1954) and thus, like C_u , not a true soil parameter. Ideally it should be used in conjunction with a stress path type method of design (Lambe, 1967); however, as pointed out by Burland (1971) the stress paths which can be followed in laboratory apparatus currently available are of limited practical application.

(ii) it is strain level dependent (see e.g. Lambe 1962; Raymond, 1972; Wesley, 1975) and is commonly evaluated only for the failure condition i.e.

$$A = A_f.$$

(iii) whilst for settlement studies (Skempton and Bjerrum, 1957) of building foundations, which are commonly associated with factors of safety of the order of three against total collapse, elastic solutions are reasonable (Terzaghi, 1943) the problem of embankments on soft clay dictates that some account of yield and or local failure be taken (Parry, 1971(a)). In addition, the total stresses are seldom independent of the material properties (Burland, 1971; Gibson, 1974).

The aforementioned factors place similar restrictions on the use of 'a' (or α), although Henkel (1960(b)) found similar values of $a/\sqrt{2}$ for triaxial compression and extension tests carried out on normally consolidated remoulded specimens of Weald Clay. Tests on overconsolidated specimens, however, produced higher values of $a/\sqrt{2}$ in triaxial compression than in

triaxial extension, although the differences were less than that between the respective 'A' values. It may thus be that for normally and lightly overconsolidated unstructured clays equations 6.7., or 6.15., can be used to predict pore-pressure changes irrespective of stress path or stress system, but never-the-less subject to the limitations of points (ii) and (iii) discussed previously.

Henkel (1959, 1960(a) and (b)) extended the early work of Rendulic (1937) on saturated remoulded clays by demonstrating the existence of unique water content/effective stress relationships for these materials; the exact form of the relationship being a function of the O.C.R. Thus the volume changes under drained conditions and the pore-pressure changes under undrained conditions could be predicted for any total stress path. A new approach to the prediction of pore pressures was thus possible which eliminated the strain dependency and, for isotropic materials, the stress path dependency problems associated with the use of pore-pressure parameters.

Unfortunately, undisturbed clays in nature seldom exhibit similar behaviour when remoulded (Bishop, 1971(a)). Henkel (1971) and Atkinson (1973(a) and (b)) demonstrated that cross-anisotropic elasticity could be used to predict the deformations of undisturbed London Clay at small strains, such a model involving stress path dependency on the direction of the principal stresses. As was shown in section 2.7., lightly overconsolidated soft clays such as the Mucking clay (Wesley, 1975) may exhibit marked effective stress path variations with rotation of the principal stresses. Raymond (1972) formulated Skempton's 'A' parameter within the framework of cross-anisotropic elastic theory, but as discussed by Raymond (1970), Atkinson 1973(b) and Wesley (1975) this is unlikely to be a realistic soil

model for soft clays. Variation in pore-pressure response with the direction of the principal stresses thus poses a problem to all of the methods of pore-pressure prediction.

The concept of a line of critical states, representing, for a particular material, a unique relationship between void ratio and effective stress (figures 6.1.25., and 6.1.26) which is independent of the initial consolidation history of the material and the stress path followed to reach the critical state, has been advocated by Roscoe et al (1958), Roscoe and Schofield (1963) and Schofield and Wroth (1968). Critical state soil mechanics led to the formulation of a generalised model for the prediction of the stress-strain behaviour of 'wet' (i.e. normally consolidated and lightly overconsolidated - again see figures 6.1.25 and 6.1.26) clays known as Cam Clay (Roscoe et al, 1958). This model was subsequently modified; hence Modified Cam Clay (Roscoe and Burland, 1968; Burland 1969 and 1971). The essential features of the elasto-plastic Cam Clay* soil model are depicted in figures 6.1.25., and 6.1.26; a brief outline of the model is now given.

The parameters p' and q' are defined as:-

$$p' = \frac{\sigma_1' + \sigma_2' + \sigma_3'}{3} \dots \dots \dots (6.17)$$

$$q' = \sigma_1' - \sigma_3' \dots \dots \dots (6.18)$$

* The modifications concern the formulation of the model in terms of plasticity theory and do not affect the simple physical picture presented in the figures.

The critical state concept predicts that a soil subjected to continuous shear will eventually reach a state at which continuous deformation accompanies a constant applied shear stress, and also at which the soil undergoes no further changes in volume or effective stress. It is thus akin to the concept of critical void ratio as discussed by e.g. Taylor, (1948).

If the critical state is assumed to be coincident with Mohr-Coulomb failure the slope of the critical state line, q'/p' , may be defined as:-

$$\frac{q'}{p'} = \frac{6 \sin \phi'}{3 - \sin \phi'} = M \dots\dots\dots(6.19)$$

in triaxial compression,

$$\frac{q'}{p'} = \frac{6 \sin \phi'}{3 + \sin \phi'} \dots\dots\dots(6.20)$$

in triaxial extension and

$$\frac{q'}{p'} = \frac{6 \sin \phi'}{2(1 + m)} \dots\dots\dots(6.21)$$

in plane strain where:-

$$m = \frac{\sigma_2'}{\sigma_1' + \sigma_3'} \dots\dots\dots(6.22)$$

and in p'/e space by:-

$$e = \Gamma - C_c \log_{10} p' \dots\dots\dots(6.23)$$

where Γ is the critical void ratio for the material, corresponding to a p' of unity and being analogous to the liquid limit (Schofield and Wroth, 1968), and C_c is the slope of the normally consolidated $e/\log_{10} p'$ relationship.

It is of interest to note that in q'/p' stress space elastic behaviour (equation 2.9) is characterised by a unique vertical (i.e. $\Delta u = \Delta p = \Delta \sigma_{OCT}$; $\Delta p' = 0$) undrained effective stress path. Thus elastic samples having the same initial value of p' reach the critical state line at the same value of p' , whereas inelastic materials having the same initial value of p' (or e) reach the critical state line at a different, but common, value of p' . This is why the ratios C_{UTE}/C_{UTC} and $C_{UPSA/P}/C_{UTC}$ predicted by elastic theory combined with Mohr-Coulomb failure in section 2.7 were the same (given the same value of 'm' - equation 6.22) as those predicted by Parry (1971(b)) using critical state theory.

Coincidence of Mohr-Coulomb failure and the critical state is of course restricted to non-brittle materials (as defined by Bishop (1971(b)) having particular stress-strain characteristics (Parry, 1971(b)): the relevance of the critical state to the study of deformation and failure of real soil masses has also been critically discussed by Bishop (1971(c)), Green (1971) and Wroth (1971). However, in the prediction of pore pressures using Modified Cam Clay the Mohr-Coulomb failure criterion may be used in place of the critical state line (Burland, 1971).

A yield point is considered as a stress (or limit) state beyond which irrecoverable plastic strains (γ_p), together with recoverable elastic strains (γ_e), occur, and below which only recoverable elastic strains occur. Thus after unloading from point 'A' in figures 6.1.25 and 6.1.26 'A' becomes a current yield point; upon reloading to 'G', and subsequent unloading, 'G' becomes the new current yield point. Yield points can therefore be defined in q'/γ relationships and in e/p' relationships for which the preconsolidation pressure p_c' is synonymous with the current yield point.

In $q'/p'/e$ space (figure 6.1.26) a yield locus can be defined within which the soil behaves elastically and outside of which yield occurs, being associated with plastic volumetric and shear strains. The yield surface incorporated in the Cam Clay model is elliptical, and cuts the critical state line on its minor axis, the major axis being defined by p'_c (point 'A' or 'G').

Thus, under drained conditions stress changes beneath the state boundary surface result in elastic strains (predicted using C_r - the slope of the unload-reload part of the $e/\log_{10} p'$ relationship - to derive the bulk modulus, 'K', together with ν). Stress increments which cross the state boundary surface result in expansion of the yield surface, being accompanied by both elastic and plastic strains. The latter are predicted using an associated flow rule (normality condition) to predict the plastic strain increment vector and a hardening law, derived from the slope of the normal consolidation line, to predict the plastic volumetric strains. For drained analyses it is necessary, therefore, to define ϕ' , C_c , C_r , Γ and ν .

Under undrained conditions the pore pressures generated are predicted using elastic theory (equation 2.9) until the effective stress path reaches the state boundary surface; it is then forced to follow the current yield locus (to cross it implying plastic volumetric strains) round towards the critical state, thus defining the pore pressures generated. A current yield locus is thus an effective stress path in p'/q' stress space and equivalent to the constant void ratio path described by Henkel, (1959; 1960(a) and (b)). Depending on the degree of overconsolidation undrained effective stress paths thus comprise an initial linear elastic path followed by an elliptical plastic path.

In order to use the Cam Clay model as described it is thus necessary to solve the particular boundary value problem in terms of the elasto-plastic constitutive laws; finite element formulations have been described by Zienkiewicz and Naylor (1971), Smith (1971), Wroth and Simpson (1972) and Wroth (1976). The formulation described in the latter reference is in terms of effective stress, regardless of the drainage conditions, pore pressures being evaluated by means of a consideration of the relative stiffnesses of the soil skeleton and the pore fluid. A similar formulation was also presented by Naylor and Hooper (1974) based on the work of Bishop (1966(b)).

Burland (1971) suggested a simplified method of pore-pressure prediction, combining elastic and critical state theories in such a manner as to enable hand calculations. The analysis is for plane strain conditions, following Roscoe and Burland (1968), and the following definitions are used herein:-

$$q'_p = \frac{\sigma_1' - \sigma_3'}{2} \dots\dots\dots(6.24)$$

$$p'_p = \frac{\sigma_1' + \sigma_3'}{2} \dots\dots\dots(6.25)$$

and in q'_p/p'_p stress space the critical state line is given by:-

$$\frac{q'_p}{p'_p} = \frac{M}{\sqrt{3}} \dots\dots\dots(6.26)$$

'M' having been previously defined by equation 6.19. Equation 6.26 predicts considerably higher stress ratios at failure (i.e. critical state) than Mohr-Coulomb (equation 2.14) as indicated in figure 6.1.32. The general

validity of equation 2.14. for undisturbed soils has been demonstrated by Bishop (1966(a)) and in Burland's (loc cit) analysis equation 2.14. replaces equation 6.26. for the purpose of defining failure.

The yield locus is defined by the equation:-

$$p_{op}' = p_p' \left[1 + \frac{3 \left[\frac{q_p'}{p_p'} \right]}{M^2} \right] \dots\dots\dots(6.27)$$

where p_{op}' is the intersection of the yield locus with the p_p' axis, a series of such loci being shown in figure 6.1.32. For points whose initial stresses plot beneath the appropriate yield locus (i.e. to the right of points such as 'X' in figure 6.1.25) the effective stress path is vertical within the elastic region (the pore-pressure changes being given by equation 2.11), subsequently following the yield locus to its intersection with the Mohr-Coulomb envelope. At this point the analysis assumes no further change in q_p' or p_p' , and thus no strain softening, to occur.

As the initial stresses move towards the origin of the stress path plot the soil (assuming a constant yield surface location) becomes increasingly overconsolidated; at points to the left of point 'X' in figure 6.1.25. (i.e. on the dry side of the critical state) the effective stress path encounters the failure line (be it Mohr-Coulomb or critical state) prior to reaching the yield surface. In this region Burland (loc cit) also assumed that, upon reaching the failure line, there was no further change in q_p' or p_p' . Thus, as pointed out by Wroth (1976), the model is restricted to normally consolidated and lightly overconsolidated soils;

it contributes nothing to the prediction of pore pressures under completely undrained conditions for soils on the dry side of the critical state save in the prediction of the total stresses during contained plastic flow.

Burland (1971) recommends that the Mohr-Coulomb failure envelope be defined in terms of C_u/p'_{pi} i.e. assume vertical effective stress paths in the overconsolidated stress space. As Burland (loc cit) points out, laboratory triaxial tests on a number of lightly overconsolidated clays have demonstrated that such materials exhibit only small changes in C_u with O.C.R. (in the range 1 to 2.5; see e.g. Parry (1968), Mitchell (1970) and Wesley (1975)). However, as depicted in figure 2.17 this is precisely because of the considerable variation in the inclinations of the undrained effective stress paths with O.C.R. and thus assuming that $\sin \phi' = C_u/p'_{pi}$ is likely to lead to considerable error in determining ϕ' ; but will correctly predict local failure as required by the analysis.

Finally, based on the work of Hoeg et al (1968) and Hoeg et al (1969) which suggested that vertical stresses calculated using elastic theory may be valid under conditions of local failure, Burland (1971) suggested the following method of calculating the horizontal and shear stresses during failure, as depicted in figure 6.1.27:-

$$\tau_{\max.e} = \left[\left(\frac{\sigma_{ve} - \sigma_{he}}{2} \right)^2 + (\tau_{vhe})^2 \right]^{\frac{1}{2}} \dots\dots\dots(6.28)$$

$$\tau_{\max.p} = C_u = \left[\left(\frac{\sigma_{ve} - \sigma_{hp}}{2} \right)^2 + (\tau_{vhp})^2 \right]^{\frac{1}{2}} \dots\dots\dots(6.29)$$

noting that subscripts 'e' and 'p' denote elastic and plastic respectively.

Assuming that there is no further rotation of the principal stress axes because of local failure, implies:-

$$\frac{\tau_{vhe}}{\sigma_{ve} - \sigma_{he}} = \frac{\tau_{vhp}}{\sigma_{ve} - \sigma_{hp}} \dots\dots\dots(6.30)$$

and thus:-

$$\sigma_{hp} = \sigma_{ve} - \frac{c_u}{\tau_{max.e}} (\sigma_{ve} - \sigma_{he}) \dots\dots\dots(6.31)$$

and:-

$$\tau_{vhp} = \tau_{vhe} \left(\frac{\sigma_{ve} - \sigma_{hp}}{\sigma_{ve} - \sigma_{he}} \right) \dots\dots\dots(6.32)$$

For points beneath the centre line of an embankment:-

$$\tau_{vhe} = 0, \tau_{max.e} = \frac{\sigma_{ve} - \sigma_{he}}{2}$$

$$\text{and } \sigma_{hp} = \sigma_{ve} - 2c_u \dots\dots\dots(6.33)$$

$$\text{i.e. } \Delta\sigma_{hp} = \Delta\sigma_{ve} \dots\dots\dots(6.34)$$

$$\text{or } \Delta\sigma_3 = \Delta\sigma_1 \dots\dots\dots(6.35)$$

which is also true for all locations post-plastic failure. Elastic theory thus predicts:-

$$\Delta u = \frac{\Delta\sigma_1 + \Delta\sigma_3}{2} \dots\dots\dots(2.11)$$

pre-failure and

$$\Delta u = \Delta\sigma_1 \dots\dots\dots(6.36)$$

post-failure, which is equivalent to putting Skempton's 'A' parameter equal to unity in equations 6.2. to 6.4. Equations 2.11. and 6.36. represent the approach to pore-pressure prediction advocated by Hoeg et

al (1969), $\Delta\sigma_1$ being calculated from elastic theory directly. Lambe (1962) predicted the pore-pressure changes beneath the Lagunillas test fill by a number of methods, including the use of equation 6.35. ($\Delta\sigma_1$ again being calculated directly from elastic theory) combined with equation 6.1. It should be noted, however that the use of equations 2.11. and 6.36. as proposed by Hoeg et al (1969) produces identical results to Burland's (1971) method only for points both dry of the critical state and beneath the centre line of an embankment.

Finally, Leroueil et al (1978(a)) proposed a method of pore-pressure prediction based on the YLIGHT (Yield Locus Influenced by Geological History and Time) model of soil behaviour (Tavenas and Leroueil, 1977). However, they limit themselves to the prediction of pore pressures beneath the centre line of embankments, whereas in practice the pore-pressure distribution within the entire region of the foundation likely to be affected by a failure is required in order to carry out effective stress stability analyses. The main areas of difficulty in the prediction of pore pressures that are reasonably representative are usually beneath the shoulders and beyond the toes of embankments. If stability control is being based on pore-pressure predictions (Symons, 1976(a)) these areas will be particularly pertinent (Raymond, 1972) and, as indicated herein, may also provide the best guide to impending failure.

As used in the prediction of pore pressures the YLIGHT model is essentially similar to Modified Cam Clay as presented by Burland (1971), in that it is a 'cap' model, but with a different yield locus. The shape of the yield locus, which is variable, is typically symmetrical about the K_0 consolidation line in q'_p/p'_p stress space; this means that effective stress paths which

join the yield locus between the K_0 line and the failure line are subsequently defined by $\sigma_v' = \sigma_1' = p_c' = \text{constant}$. In other words, the issue of principal stress rotation having been sidestepped, initial pore pressures are given by elastic theory until at some point (depending on the initial stresses and drainage conditions during loading) σ_v' becomes equal to p_c' . At this point the behaviour of the material is assumed to revert to that of a normally consolidated soil and the pore pressures are given by equation 6.36 as the effective stress path becomes the yield locus. Similarly to Cam Clay, failure is reached on the normally consolidated effective stress envelope.

When a particular stress path reaches failure the pore pressures are controlled by p'_p and q'_p being constant for an elastic-plastic material, or by the strain softening of the yield locus towards the critical state. Linear elastic theory is used to predict the total vertical stresses following Hoeg et al (1968)

Leroueil et al (1978(a) and (b)) noted that the foundation pore pressures for the Saint-Albans test fill, together with those from numerous case records reported in the literature, were initially less than predicted by elastic theory. They postulated this was because of rapid pore-pressure dissipation associated with the high C_v values exhibited by the clays in their overconsolidated state. Using the work of Schiffman (1958 and 1960) to enable the initial C_v values to be back-calculated led to values of the order of $500 \text{ m}^2/\text{year}$ for the Saint-Albans foundation. Thus vertical effective stresses may initially rise rapidly until equal to p_c' ; analysis of a number of case records showed good agreement between σ_v' corresponding to the 'yield point' in the excess pore pressure/fill height relationships and p_c' .

The main difference between the method of Leroueil et al (1978(a)), accepting that the models incorporate different yield loci, and Cam Clay is therefore in the consideration of drainage during the early stages of construction. This has the interesting result that materials on the dry side of critical state may experience yielding prior to failure whilst materials on the wet side of critical state may experience yielding at significantly lower shear stresses than would be predicted on the basis of an entirely undrained elastic stress path. An allowance for drainage could of course be incorporated in any of the methods of pore-pressure prediction but this involves a knowledge of C_v and its variation with effective stress and the construction time-scale for the embankment. As was seen in section 2.4, C_v is likely to vary considerably within the relevant effective stress range and additionally the shear component of the pore-pressure response will increase with decrease in the O.C.R.

In conclusion, apart from the consolidation aspects which are not an integral part of the soil model (an empirical allowance is suggested by Leroueil et al (1978(b))), the YLIGHT model seems little different in concept from Cam Clay except that the latter does at least offer a complete solution to a particular boundary value problem and in a satisfyingly elegant form.

A number of fundamentally different pore pressure/fill height (or total stress) relationships are thus predicted by the different theories. The limit state models (Cam Clay and YLIGHT) may predict elastic (with or without consolidation), yielding and plastic phases or simply

elastic-plastic behaviour similar to that predicted by Hoeg et al (1969), whilst in their simplest form the pore-pressure parameter formulations predict single phase behaviour. The interpretation of the observations presented in figure 6.1.21 indicates in general a two-phase system although closer inspection of figures 6.1.19 and 6.1.20 reveals that a further phase close to overall failure is also in evidence.

(b) Bank 2

In examining the observed pore pressures at Mucking in the light of the various theories outlined in the preceding section, due account has been taken of the fact that a class 'C1' prediction (Lambe, 1973) was being made. Thus, rather than attempt to present yet another method of pore-pressure prediction which fitted the observations perfectly, it has been attempted to assess the sensitivity of the major variables in such an analysis.

Even the Cam Clay model (Wroth, 1976), which works in terms of effective stresses, relies upon the correct interpretation of the total stress field resulting from the applied loading, and thus total stress-change predictions are at the heart of the various pore-pressure prediction methods. Elastic solutions (Poulos and Davis, 1974) have been much used in the past, particularly, for embankments, that derived by Jurgenson (1940). As the total stresses induced in the Bank 1/1 foundation, which was the object of the major pore-pressure assessment exercise, were obtained from a non-linear finite element solution, those induced by the simple geometry of Bank 2 were calculated using a homogeneous linear elastic solution (Giroud and Watissee, 1972). This solution applies to an embankment

founded on a compressible stratum underlain by a rigid base; solutions were available with a maximum ν value of 0.3. Thus the first two variables considered were the type of stress-strain law and the value of ν incorporated in the solution.

The construction of Bank 2 was considered in three stages as shown in figures 6.1.28 and 6.1.31. The former depicts the calculated maximum shear stresses at the piezometer locations assuming K_0 to be 0.55; this is lower than is anticipated to occur at the site at the present time (figure 2.13) based on the work of Brooker and Ireland (1965). Figure 6.1.31 illustrates the changed situation having assumed K_0 to vary with depth; the actual distribution used is presented in Chapter 8, being an extreme variation based on the vane test results shown in figure 2.13. Thus two extremes of K_0 value were considered; ground-water level prior to construction of Bank 2 was about 650mm B.G.L. (figure 2.12) and thus the best estimate of the K_0 distribution would lie between these extremes.

Adopting $\nu = 0.3$ for a limited foundation having $\nu = 0.5$ leads to an under-estimate of the octahedral normal stresses and an over-estimate of the maximum shear stress. These 'errors' are further amplified if, for example, a K_0 of 0.55 is assumed, when in fact a value of unity exists (Leroueil et al 1978(a)).

Superimposed on figures 6.1.28 and 6.1.31 is the profile of undrained strength derived from a very thorough back-analysis of the trial embankment failures using limit equilibrium techniques (see Chapter 7).

Figure 6.1.29 presents values of Skempton's (1954) 'A' parameter and Henkel's (1960(b)) 'a' parameter corresponding to the seasonal extremes

of O.C.R. at the site; as can be seen the differences are significant. It should be noted that these are failure values from triaxial tests on isotropically consolidated vertical samples; no account of stress level or anisotropy has therefore been included. Wesley's (1975) data indicate that the value of ' A_f ', with the major principal stress in the horizontal direction, may be up to 60% greater than when the major principal stress is vertical. In both cases the pore-pressure response to shear is stress level dependent (see figure 6.1.39), being more so in the former case.

Figure 6.1.30 presents the pore pressures predicted by equations 6.1 and 6.11., together with the observed values. Both equations predict reasonable values beneath the embankment centre, but agreement is not so good beneath the shoulder; overall, equation 6.11 yields the most satisfactory predictions in this case. Variations in K_0 did not affect the use of equations 6.1 and 6.11 except in the case of piezometers 1 and 4, the principal stresses rotating through 90° at these locations when the variable K_0 distribution was used (i.e. $K_0 > 1$). The 'variable K_0 ' predictions for piezometers 1 and 4 are presented in figure 6.1.33.

Predictions based on equations 2.11 and 6.36., following the method of Hoeg et al (1969) are given in figure 6.1.33. As can be seen the predicted and observed pore pressures are generally in good agreement especially when it is remembered that the actual in-situ conditions approximate to a position between the cases considered. However, the agreement must be considered highly fortuitous as the use of $\nu = 0.3$ will have resulted in the premature prediction of local failure (see e.g. figure 6.1.28) and an under-estimate of the elastic pore-pressure response. K_0 can be seen to have a significant influence on the predicted pore pressures using this method.

A comparison of the pore pressures predicted using Henkel's equation (6.11) and elastic theory (equation 2.11) indicates that the major contribution to the predicted pore pressure is provided by the change in octahedral normal stress; the contribution from changes in deviator stress being relatively small. Thus the influence of the pore-pressure parameter is not great. This leads to the important conclusion that pore-pressure variation with principal stress rotation will be relatively less marked in the field than in a conventional laboratory triaxial or plane strain test.

Finally, figure 6.1.32 shows the predicted effective stress paths based on the Cam Clay model (Burland, 1971). The yield loci were constructed using equation 6.27, together with a knowledge of p_c' (figure 2.13. - K_0 being taken as 0.55 in the normally consolidated state); the normally consolidated part of the effective stress failure envelope (figure 2.25) was approximated to $\phi' = 35^\circ$ on the basis of the data presented by Wesley (1975). The slope of the critical state line could then be established from equations 6.19 and 6.26. The overconsolidated failure envelope was constructed by assuming $\phi' = 25^\circ$ (as obtained in the laboratory (figure 2.17) and by limit equilibrium back-analysis of the embankment failures) and that the 'change' from normally consolidated to overconsolidated behaviour coincided with the intersection of the yield locus and the normally consolidated failure envelope. This construction led to c' values increasing with depth (and hence with p_c') from 3.5 kN/m^2 at 1.5m depth to 5 kN/m^2 at 5.5m depth, thus being in good general agreement with values obtained by back-analysis of the embankments using the limit equilibrium method.

In this case the in-situ stresses were derived from figure 2.13 using the actual values of σ_v' and the appropriate O.C.R: as shown in figure 6.1.32., the points fall both wet and dry of the critical state; however the imposition of the Mohr-Coulomb failure envelope (Burland, 1971) results in the prediction of only a two phase elastic-plastic pore-pressure response as illustrated in figure 6.1.33. The reason for the difference between the Cam Clay predictions and the simple elastic-plastic predictions is that in the latter case the back-analysed values of C_u were used to define local failure directly whereas the effective stress envelope used in the Cam Clay model, coupled with the assumed vertical effective stress paths, predicts slightly higher undrained strengths (i.e. the field stress paths exhibit an overall decrease in p_p') and hence local failure at higher values of the maximum shear stress.

Finally, the effective stress paths predicted by the Cam Clay model are compared to the 'field' paths, based on linear elastic total stress changes and observed pore pressures, in figure 6.1.34. Under-estimation of $\Delta\sigma_{OCT}$ combined with an over-estimate of the maximum shear stress has resulted in the 'field' paths crossing the Mohr-Coulomb failure envelope even though the embankment had a factor of safety, in terms of effective stress, of about 1.5 at the end of construction.

If the 'field' paths which are in error are envisaged being brought back to the right of the failure envelope the inference is that they move initially to the right and then yield to the left. Partial dissipation of the excess pore pressures during construction is thus a possibility which is also suggested by the good agreement between the pore pressures predicted using

$\nu = 0.3$ and the observed values, and the field records themselves (figure 5.5.6). The importance of use of the correct value of ν in undrained elastic analyses is thus self-evident.

(c) Bank 1, Stage 1

Total stress changes were obtained using a non-linear finite element solution (Hamza, 1976) as is further discussed in Chapter 8. The two solutions considered at this stage both incorporated stress-strain data from ~~unconsolidated undrained~~ laboratory triaxial tests on specimens cut at varying inclinations, but with peak deviator stress defined via the C_u values obtained from the limit equilibrium back-analysis of the embankment failures. An initial undrained Young's Modulus, $E_{ui} = 2700 \text{ kN/m}^2$ was common to all of the stress-strain relationships, but the relationships themselves varied with depth. Two extreme variations of K_0 were considered, as discussed previously (and in Chapter 8), and ν was taken to be 0.4999.

Pore-pressure predictions using equations 6.1., 6.11 and 2.11 are compared to the observed values in figures 6.1.35 and 6.1.36. Values of the pore-pressure parameters 'A' and 'a' were selected on the basis of the O.C.R. s existing prior to construction (figures 2.13 and 6.1.29). In all of the methods used the total stress changes were influenced by the 'yielding' of the stress-strain function and by local plastic failure; strain softening was not possible in the model used.

It is perhaps worth pointing out that the pore pressures have been predicted for all 24 piezometers beneath and beyond the embankment on one cross-section; the piezometer locations thus encompassing a wide range of principal stress rotations (figures 6.1.41 and 6.1.43). In addition the predictions cover the

entire construction period during which elastic, yielding plastic, perfectly plastic and strain softening behaviour have probably all contributed to the observed pore pressures; as indeed has partial dissipation.

In terms of an overall pore-pressure field for use in effective stress stability analyses the results are certainly very reasonable. Once again, on an overall basis the predictions based on Henkel's equation (6.11) and elastic theory (equation 2.11) are the most satisfactory and also very similar confirming the lack of influence of shear stress change on the pore-pressure predictions.

Figures 6.1.37 and 6.1.38 illustrate the effect of K_0 on the elastic predictions and more clearly depict the successes and shortcomings of the predictions. Considering particular locations, separately, and using the categorisation of figure 6.1.21:-*

1. Beneath Embankment Fill; piezometers 7 - 15

Little principal stress rotation and, overall, good predictions, especially close to failure. However the initial pore-pressure changes are over-predicted and those during the later stages are under-predicted; the tendency for the octahedral normal stress to drop as an element approached failure is a function of the finite element formulation. Thus the initial drop in the rate of pore-pressure response, the apparent 'yield' in the pore pressure/fill

*reference to principal stress rotation and E.S.P. s herein relates to the finite element analysis with $K_0 = 0.55$; although varying K_0 influences both rotation and E.S.P. the $K_0 = 0.55$ case provides a reasonable basis for discussion.

height relationship and the subsequent increases in the rate of pore-pressure response were not predicted by non-linear elastic theory.

2. Beneath Embankment Berm; piezometers 16 - 18

Little principal stress rotation, but the over-prediction during the early construction stages is particularly bad. Piezometers 16 and 18 exhibited a decrease in pore-pressure response during the latter stages of construction which was correctly predicted. Piezometer 16, on the other hand exhibited a 'yield', followed by an increased rate of response which was not predicted.

3. Beneath Embankment Toes; piezometers 4 - 6, 19 - 21

Large principal stress rotations but reasonably good predictions. Beneath the southern toe the pore pressures are well predicted during the early part of construction but subsequently under-predicted as failure is approached, although the increased pore-pressure response is correctly predicted. It is interesting to note that the increase in $\Delta\sigma_{OCT}$ at this location corresponds to a decrease following local failure beneath the main part of the embankment. The predictions beneath the northern toe were excellent.

4. Beyond Embankment Toes; piezometers 1 - 3; 22 - 24

Again large rotations of the principal stresses coupled with excellent agreement particularly to the north of the embankment. The increases in pore pressure beneath the toe trench just prior to failure were under-predicted.

At first glance it thus appeared that a major improvement in the non-linear elastic prediction technique was required during the early part of construction for those piezometers beneath the embankment fill (piezometers 7 - 18). However, before proceeding further the 'field' effective stress paths were plotted from the finite element total stress paths and the observed pore pressures (figures 6.1.40 and 6.1.42). The associated principal stress rotations for these cases ($K_0 = 0.55$ and $K_0 = f(\text{depth})$) are presented in figures 6.1.41 and 6.1.43. Also shown in figure 6.1.40 are the appropriate Cam Clay yield loci, constructed as described previously, together with the normally consolidated and overconsolidated Mohr-Coulomb failure envelopes.

An interesting aspect of the effective stress paths is the coincidence of a number of points, corresponding to 4m fill height, with the overconsolidated Mohr-Coulomb failure envelope obtained from the limit equilibrium back-analysis of the embankment failures. Figure 6.1.44 depicts the latter failure envelope, together with the final points of the 'field' effective stress paths for those piezometer locations at which the maximum shear stress had reached the undrained strength. It should be noted that the pore pressures at 4m fill height, as presented in figures 6.1.35 to 6.1.38, were extrapolated from 3.75m fill height. The measured values at 4m fill height (figures 6.1.19 and 6.1.20) relate to the failure condition and are thus not appropriate to the analysis in question.

The effective stress shear strength parameters 'back-analysed' using the finite element method are thus in good overall agreement with those from the limit equilibrium analyses. These results thus tend to support the validity of the predicted total stresses and therefore the elastic pore-pressure predictions. This point is of some importance as data presented by

D'Appolonia et al (1971) suggest significant increases in $\Delta\sigma_{OCT}$ can result when a bi-linear soil model ($E_u = f(\text{depth})$, $\tau_{max} = C_u$) is used in place of a homogeneous elastic solution.

In Chapter 8 it will be proposed that the stress-strain model used, based on *unconsolidated undrained* triaxial test specimens, was inappropriate to some areas of the foundation (beneath the embankment centre in particular); it being considered that the actual soil when loaded, beneath the embankments, from K_0 conditions in situ was initially stiffer than predicted by the model and also, initially, essentially, homogeneous and linearly elastic. Thus in situ the initial stress changes may have been similar to those predicted using a homogeneous elastic solution whereas those presented herein are for a non-homogeneous elastic medium and may, therefore, over-estimate $\Delta\sigma_{OCT}$. Unfortunately this aspect has not been investigated further; never-the-less it remains as a possible source for the type of errors observed.

Also considered was the possibility that the use of equation 2.10 to predict the intermediate principal stress may have resulted in an over-estimate of $\Delta\sigma_{OCT}$. However, even putting $\Delta\sigma_2 = \Delta\sigma_3$ resulted in only a slight reduction in $\Delta\sigma_{OCT}$.

The error in pore-pressure prediction can be seen to decrease with increasing fill height, and in figure 6.1.39 the errors have been plotted versus major principal strain, clearly illustrating this trend. Also shown in the figure is the average variation, from triaxial tests on horizontal and vertical specimens, of Henkel's 'a' parameter with major principal strain, indicating a similar trend. However, reference to figures 6.1.35 and 6.1.36 reveals once more that

the contribution to the pore-pressure prediction of the shear stresses is minimal, as therefore, is the influence of 'a'.

Returning to the effective stress paths in figures 6.1.40. and 6.1.42., the piezometer locations at which the measured and predicted pore pressures differ most during the early stages of construction (i.e. 7 - 18) can be seen to exhibit broadly similar effective stress paths, moving initially to the right in the proximity of the K_0 line and then yielding sharply to the left in the cases of piezometers 7 to 16. Thus initial drained shear, approximating to K_0 conditions in some cases, is suggested, in accordance with the hypothesis of Leroueil et al (1978(a) and (b)); and indeed the stress paths are remarkably similar to a typical YLIGHT yield surface (Tavenas and Leroueil, 1977; see also section 6.3 and figure 6.3.4).

It is thus of interest to examine the changes in effective stress which occurred during construction prior to the 'yield' point in the pore pressure/fill height relationships and in the effective stress paths. Table 6.1.1. presents such an examination for piezometers 7 - 16; the principal stress rotations at these locations were small (figure 6.1.41, $K_0 = 0.55$ analysis) and the change in σ_v' evaluated thus corresponds closely to $\Delta\sigma_1'$. The vertical effective stresses at yield can be seen to approach, in some cases, the laboratory preconsolidation pressure, p_c' (see figure 6.1.45), whilst, except in the case of piezometer 7, the maximum shear stresses were less than C_u . The fill heights at which the maximum shear stress reached the undrained strength for those piezometers within areas of local failure are indicated in figures 6.1.35. and 6.1.36*. As stated previously, in some cases this

*The fill heights indicated correspond to first failure within the element 'containing' the piezometer. As there were not insignificant stress variations between the Gauss Points these values should be regarded with some caution.

height corresponds to a further increase in the pore-pressure response. Figures 6.1.35 and 6.1.36 also show the large over-estimate of change in maximum shear stress resulting from the use of $\nu = 0.3$ in the Bank 2 analysis.

Thus although initially consolidated to a state in the vicinity of the 'wet/dry' boundary, it is postulated that the Mucking clay was able to consolidate sufficiently* to reach a limit state at which point C_v was sufficiently reduced to result in a continuation of undrained behaviour, the effective stress path subsequently following a current yield surface to failure. The fact that failure occurred on the overconsolidated Mohr-Coulomb envelope is not inconsistent with normally consolidated yield as the yield surface should define the meeting of the normally consolidated and overconsolidated failure envelopes as illustrated in figure 6.1.32. It is unlikely that such well defined changes of state occur in practice.

As predicted by the various 'cap' models and observed for real soils (Ladd and Lambe, 1963; Parry, 1968; Mitchell, 1970; Wesley, 1975) relatively little change in C_u results from increasing consolidation within the lightly overconsolidated 'wet' stress space due to convergence of the effective stress paths at failure. Thus for soils initially close to the wet/dry boundary, as was the Mucking clay, elastic theory would be expected to predict the correct pore pressures at failure even if drainage and subsequent yield, as postulated, were to occur. This is confirmed by the excellent predictions for piezometers 7 - 15 at fill heights of between 3.5m and 3.75m. The tendency to under-predict at 4m fill height may be the result of an increased pore-pressure response, following local failure.

*Rapid dissipation of excess pore pressures at low effective stresses has already been predicted by the laboratory consolidation tests, observations of seasonal pore-pressure fluctuations in the field and the results of the large vane tests.

Furthermore, at the locations of piezometers 17 and 18 dissipation occurred, but was not sufficient to result in yield, and thus elastic theory over-predicted the pore pressures. The behaviour at these locations suggests that the reduction in C_v with increasing effective stress may have been sufficient to prevent yield and result in the continued generation of elastic pore pressures.

The effective stress paths for piezometers 4-6 signify yielding from the start of construction and thus, as would be expected, the elastic pore pressures are under-estimates. It will be remembered that the yield point in the oedometer test on the horizontal sample (section 2.6) was considerably lower than p_c' , and also that larger pore pressures are associated with the major principal stress inclined more towards the horizontal. Figure 6.1.37 also suggests that local failure occurred in the locality of piezometers 4 - 6 at about 3.25m fill height, although not predicted by the finite element solution.

As depicted in figures 6.1.19 to 6.1.21 the observed pore pressures for Bank 1, Stage 2 corroborate the behaviour pattern postulated for Stage 1. Data for piezometers 16 - 18 during Stage 2, added to figure 6.1.45 confirm this as do those for Banks 2 and 4 (also shown in figure 6.1.45 and summarised in table 6.1.2).

(d) Conclusions

The literature contains numerous case histories for which the pore pressures have been back-analysed, and occasionally forward-analysed (Wroth, 1976) to make a Class 'A' prediction (Lambe, 1973); most of the methods considered herein have found favour at some time or another. Skempton's (1954)

equation (6.1) and Henkel's (1960(b)) equation (6.11) have been combined with both linear elastic and non-linear elastic total stresses, to give reasonable predictions (Lambe, 1962; Raymond, 1972; D'Appolonia et al, 1971; Croce et al, 1973; Wu et al, 1975). The elastic-plastic formulation of Hoeg et al (1968) has been used by Hoeg et al (1969) and D'Appolonia et al (1971). Most soft clays are lightly overconsolidated as a result of the processes outlined by Parry (1970) and Bjerrum (1973), and it has been shown that predictions based on elastic theory will be good for undrained behaviour without yield and also reasonable at failure when drainage is sufficient to cause yield. More serious departures from elastic theory will be encountered if drainage is insufficient to cause yield and as the initial stress state becomes 'wetter'. Burland (1971) used a simplified form of Cam Clay to predict the behaviour of normally consolidated and lightly overconsolidated clays with some success* and this technique was further explored by Symons (1974). Wroth and Simpson (1972) acknowledged that the pore pressures predicted for the Kings Lynn trial embankment (Wilkes, 1972(a)) using a finite element version of Cam Clay, were poor; in fairness the ground conditions at the site were variable and only conventional site investigation data were available. However, the same formulation produced better results for the M.I.T. prediction symposium with respect to the pore pressures beneath the Interstate I-95 'road' embankment (Wroth, 1976) although data for only three piezometers, two of which were beneath the centre line, were published.

Based on observations at a large number of sites (Lewis et al, 1975; Symons and Murray, 1975; Murray and Symons, 1974) Symons (1974 and 1976(a)) proposed the use of $\Delta u = \Delta \sigma_1$ for pore-pressure predictions at all stages

*Although this has been questioned with respect to Burland's (loc cit) input data by Raymond (1973) and Lacasse and Ladd (1973).

of embankment construction, for use in effective stress stability control charts. The attractions of such a simple method are obvious and a similar approach was used by Parry (1968). However, the limitations of elastic theory still apply.

Leroueil et al (1978(b)) found that for a large number of embankments on soft clays, as at Mucking, initial consolidation was followed by normally consolidated yield. They only consider pore pressures beneath the centres of embankments, for which their model (YLIGHT) predicts $\Delta u = \Delta \sigma_v = \Delta \sigma_1$ i.e. ($A = 1$) post-yield. In terms of practical application the model is thus much less self-contained than Cam Clay.

The assessment of the observed pore pressures at Mucking leads to the conclusion that the Mucking clay behaviour may be predicted by a limit state model. Pore-pressure prediction thus requires:-

- (i) A method of predicting the elastic-plastic-failure stresses.
- (ii) Definition of the limit state surface. Although this surface will not be unique, but depend on principal stress rotation, the overall effect on pore pressures will probably be such that an average (as used to obtain the mean field value of C_u) would be sufficiently realistic for design purposes.
- (iii) Prediction of the in-situ stresses. Despite the misgivings of Tavenas et al (1975) it seems that, using the work of Brooker and Ireland (1965), hydraulic fracture tests (see section 5.5) or the Camkometer (Wroth, 1975(b)) reasonable estimates of K_0 for lightly overconsolidated clays may be obtained.

- (iv) The prediction of the amount of dissipation during construction and thus a knowledge of C_v and its variation with effective stress.
- (v) Working in terms of effective stress.
- (vi) Definition of the failure envelope for the soil.
- (vii) An allowance for the pore pressures generated by undrained creep.

These requirements are considered likely to be valid for most soft clay deposits. Thus although the difficulties in predicting correct pore pressures at all stages of construction are self evident the foregoing analysis, by revealing the fundamental behaviour of the clay, enables the use of approximate methods with some certainty as to their actual limitations. In this respect a knowledge of the in-situ stresses and the consolidation history of a lightly overconsolidated clay are of prime importance in enabling reasonable pore-pressure predictions to be made using approximate methods.

6.1.4. Summary

The 'undrained' behaviour of the Mucking clay was characterised by small displacements and strains, coupled with elastic pore pressures, under initial loading conditions. Pore-pressure dissipation, leading to increases in the mean effective stresses, resulted in plastic yielding, associated with increased displacements, strains and pore pressures per unit of fill height. Prior to yielding, conditions beneath the centre of Bank 1, Stage 1 resembled drained K_0 loading. When consolidation and shear unloading were observed, reduced displacements and elastic pore pressures resulted. Local failure was indicated by further increases in

the rates of displacement, strain and pore-pressure generation. Local failure appeared to progress outwards from the crest of Bank 1, Stage 1 towards the toe trench.

The unloading following Bank 1, Stage 1 failure and preceding Stage 2 construction produced elastic pore-pressure responses and virtually no recoverable displacements. Bank 1, Stage 2 produced a similar behaviour pattern to Stage 1 except that the tensile strains developed beneath the embankment prior to failure appear to have been larger.

Banks 2 and 4 also behaved similarly but local failure was not in evidence. Undrained creep was observed at higher stress levels, post-yield, and increased with the onset of local failure. The undrained creep was associated with pore-pressure generation.

PIEZOMETER	C_u^+ kN/m ²	p_c^+ kN/m ²	σ_{vi}^+ kN/m ²	h m	σ_v^* kN/m ²	τ_{max}^* kN/m ²	$\Delta\sigma_v^+$ kN/m ²	σ_v^+ max kN/m ²
7	9.7	35	14.1	3.25	27.6	9.7	13.5	31.5
8	10.9	45	24.1	1.75	37.6	9.7	13.5	43.5
9	13.9	55	34.4	2.05	45.0	11.7	10.6	45.0
10.	9.7	35	12.3	1.75	25.5	7.6	13.2	31.0
11	10.9	45	21.5	1.75	34.1	8.7	12.5	41.5
12	13.9	55	31.5	1.75	44.5	10.0	13.0	44.5
13	13.9	55	31.2	1.25	38.0	9.4	6.8	47.5
14	10.9	45	20.8	1.25	28.0	7.9	7.2	39.5
15	9.7	35	10.7	1.25	19.6	4.8	8.9	31.5
16	13.9	55	34.2	2.05	51.7	11.0	17.5	53.0

Table 6.1.1.

Bank 1, Stage 1. Vertical Effective Stresses and Maximum Shear Stresses at Yield Plus Maximum Vertical Effective Stresses

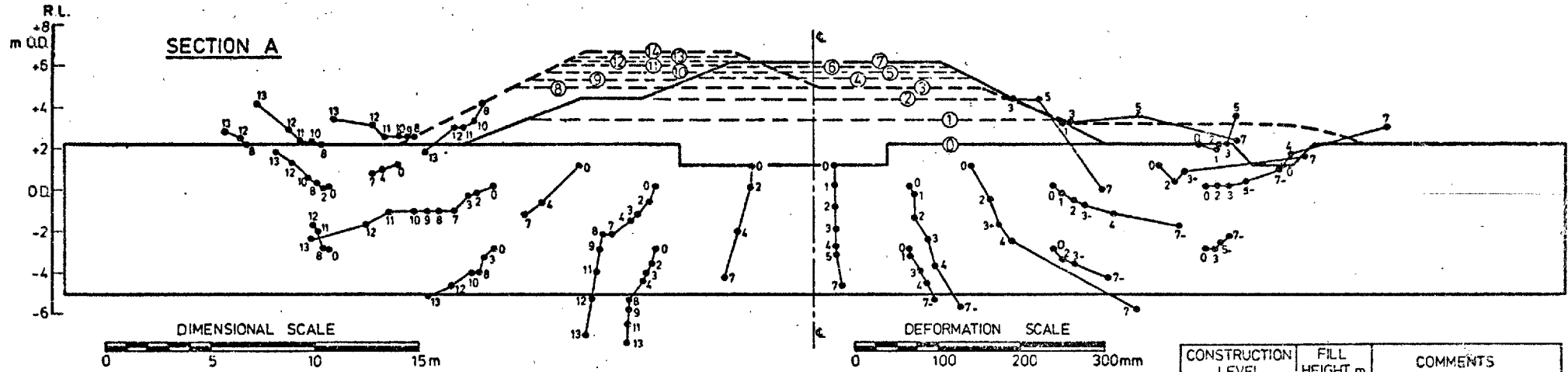
⁺ C_u values correspond to Gauss Points closest to piezometers under consideration and not to piezometer locations.

*based on finite element analysis F.E.2. ($K_0 = 0.55$), noting that F.E.3. ($K_0 = f(\text{depth})$) results in lower values of τ_{max} in general

PIEZOMETER	p_c^+ kN/m ²	σ_{vi}^+ kN/m ²	h m	σ_v^+ kN/m ²	$\Delta\sigma_v^+$ kN/m ²
PA16	55	34.2	2.75	47.1	12.9
PA17	45	24.1	2.75	39.2	15.1
PB18	35	14.1	2.75	27.2	13.1
PC4	35	14.2	0.95	17.2	3.0
PC5	45	25.0	0.95	30.3	5.3
PC6	55	35.6	0.95	41.0	5.4
PE4	31	15.0	0.85	15.0	0
PE5	41	25.5	0.85	28.5	3.0
PE6	51	34.2	0.85	37.9	3.7

Table 6.1.2

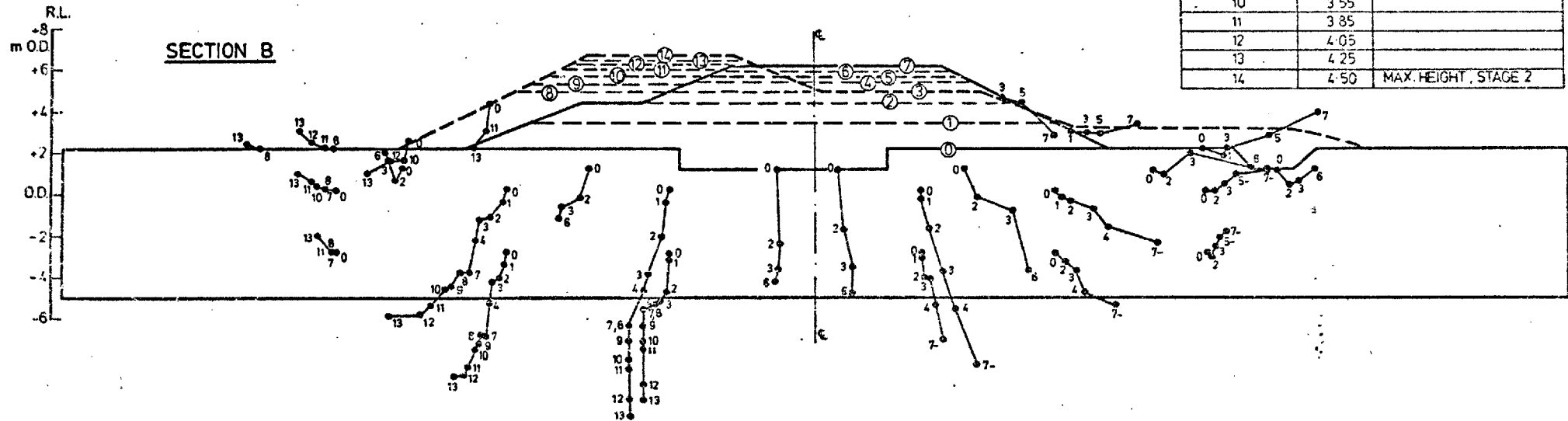
Bank 1, Stage 2, Bank 2 and Bank 4. Vertical Effective Stresses at Yield

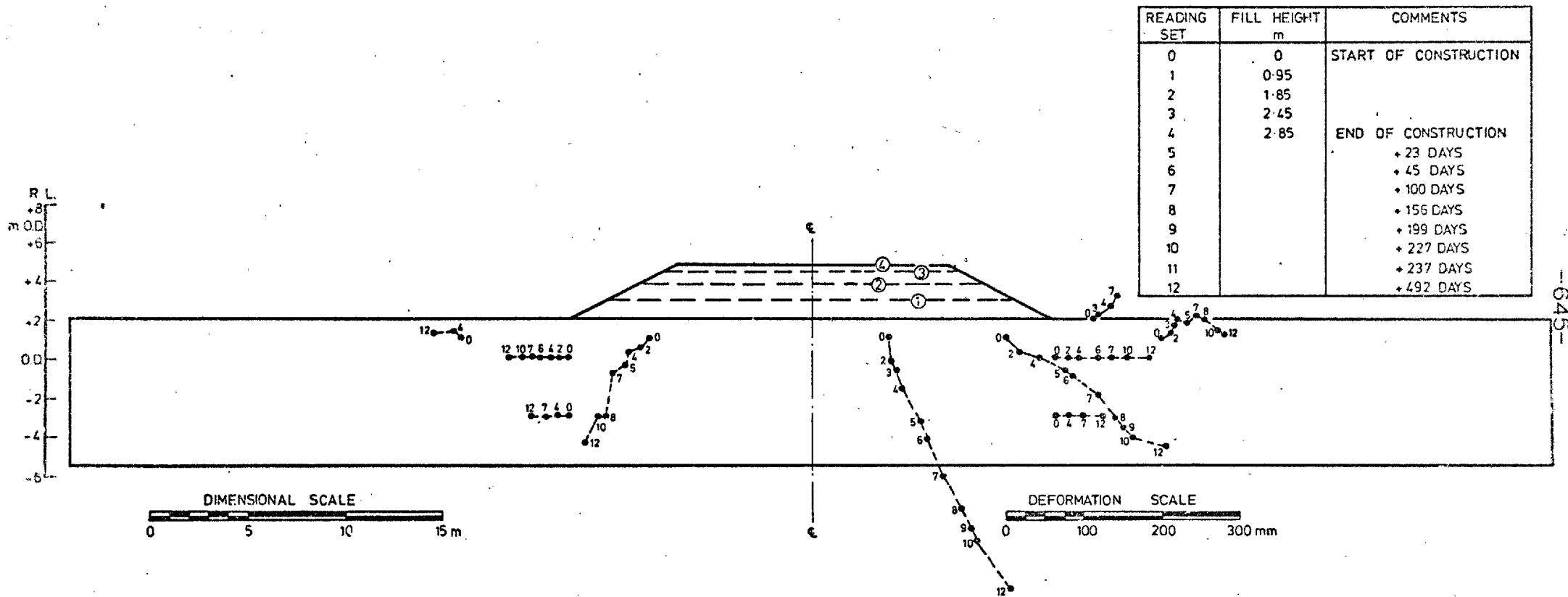


BANK 1, STAGES 1 & 2

DISPLACEMENT VECTORS, DURING CONSTRUCTION, WITHIN FOUNDATION AND FILL.

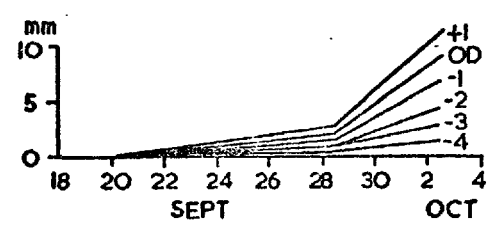
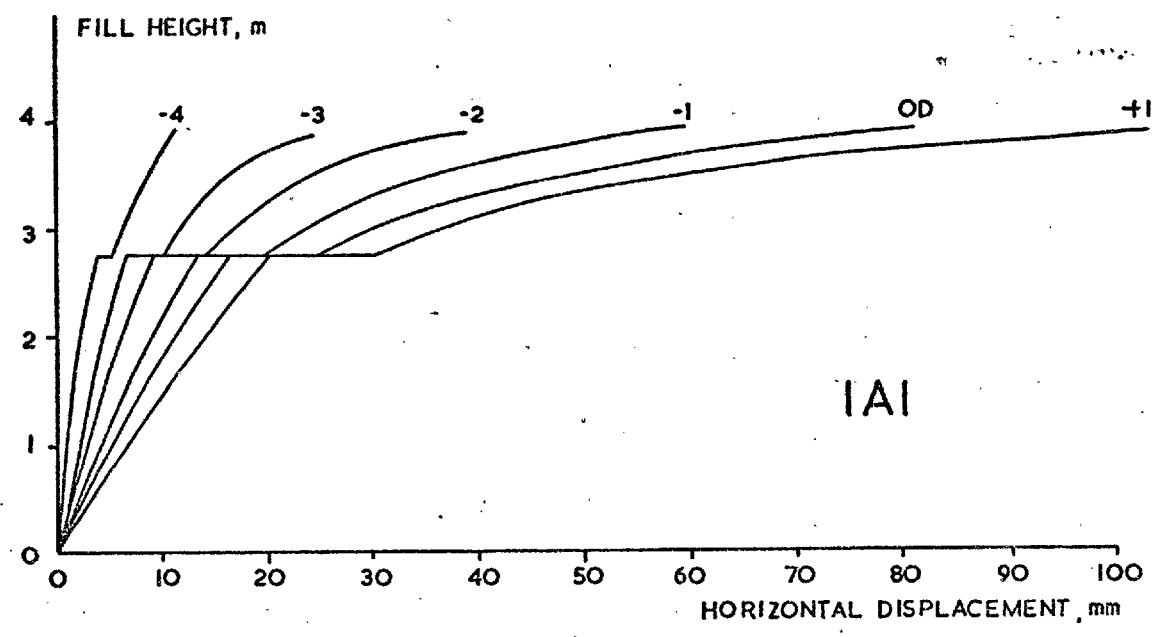
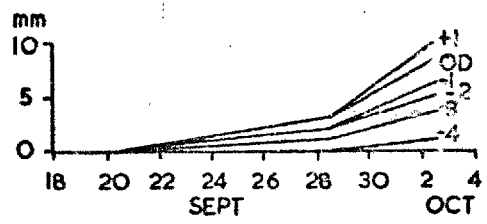
CONSTRUCTION LEVEL	FILL HEIGHT, m	COMMENTS
0	0	START OF STAGE 1
1	1.25	
2	2.25	
3	2.75	TOE TRENCH EXCAVATED
4	3.25	
5	3.50	
6	3.75	
7	4.00	MAX. HEIGHT, STAGE 1
8	2.75	START OF STAGE 2
9	3.15	
10	3.55	
11	3.85	
12	4.05	
13	4.25	
14	4.50	MAX. HEIGHT, STAGE 2



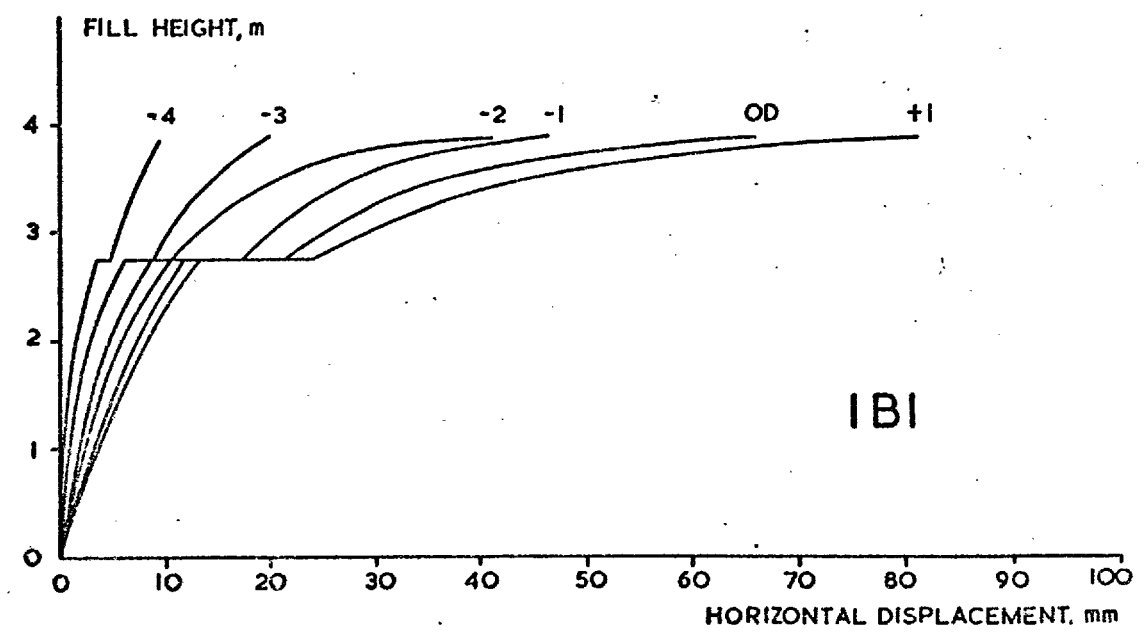


BANK 2

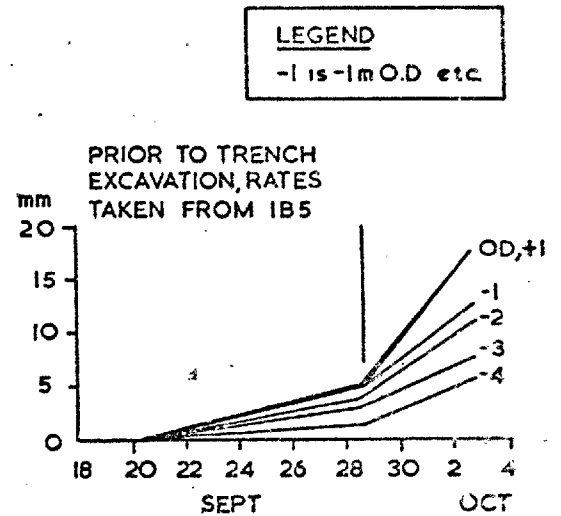
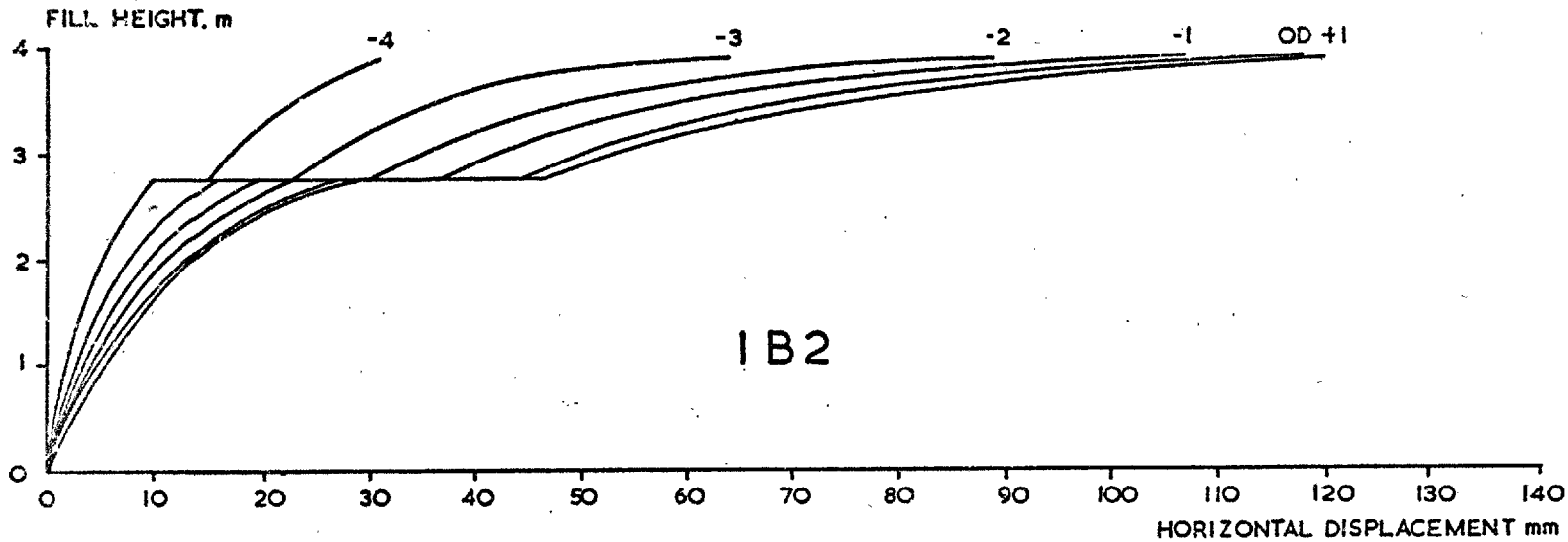
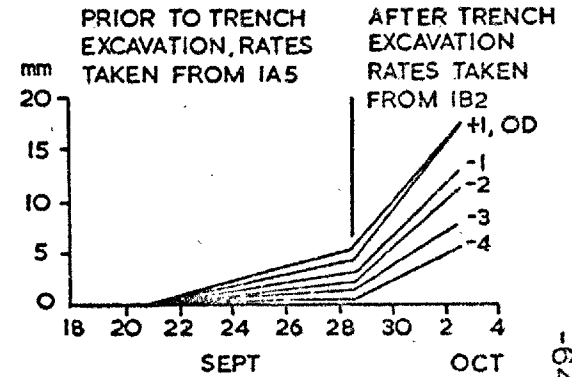
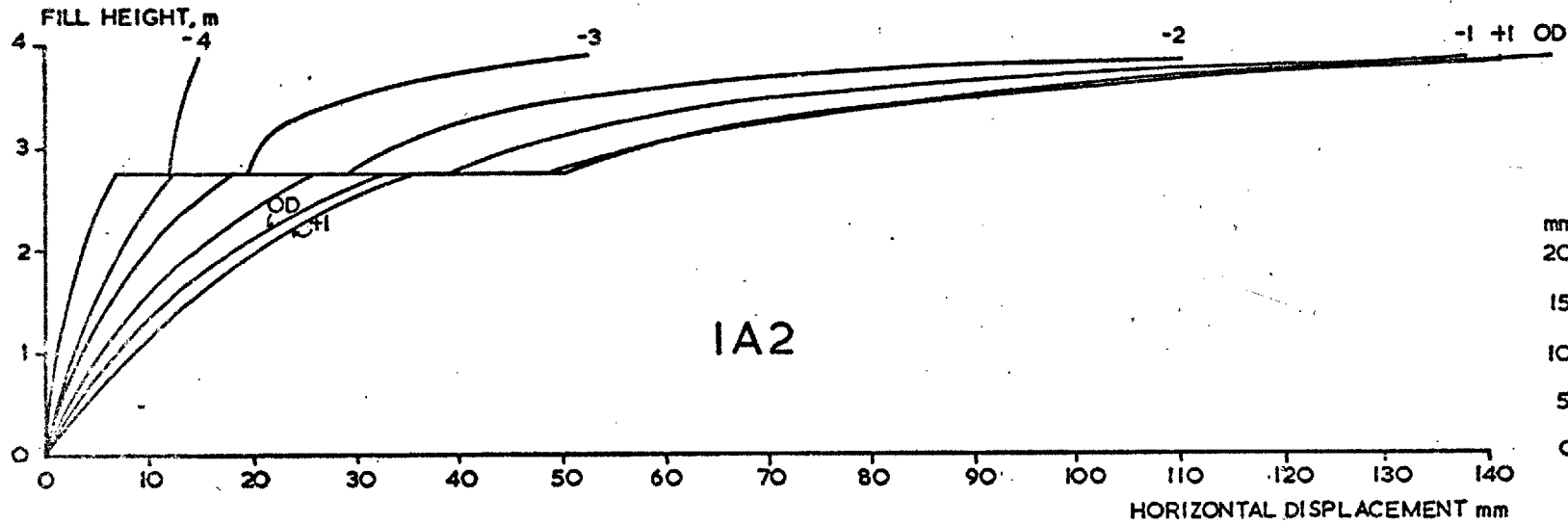
DISPLACEMENT VECTORS WITHIN THE FOUNDATION, DURING AND POST-CONSTRUCTION



LEGEND
-1 is -1m O.D. etc.



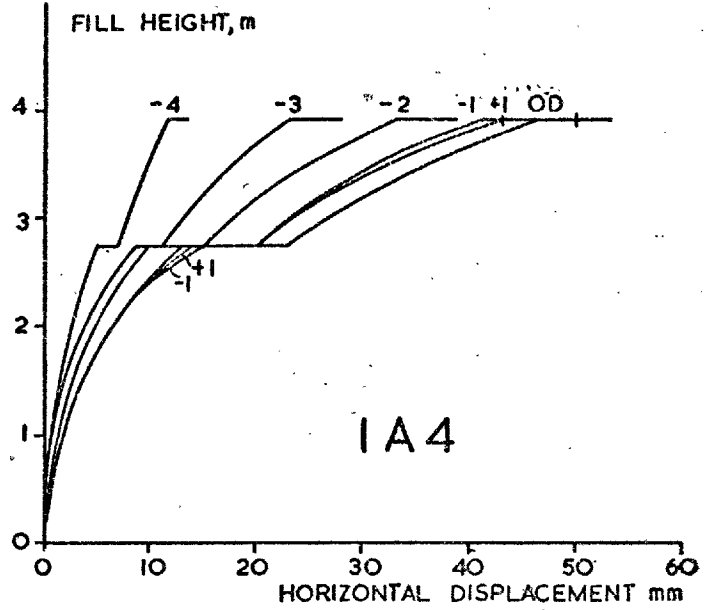
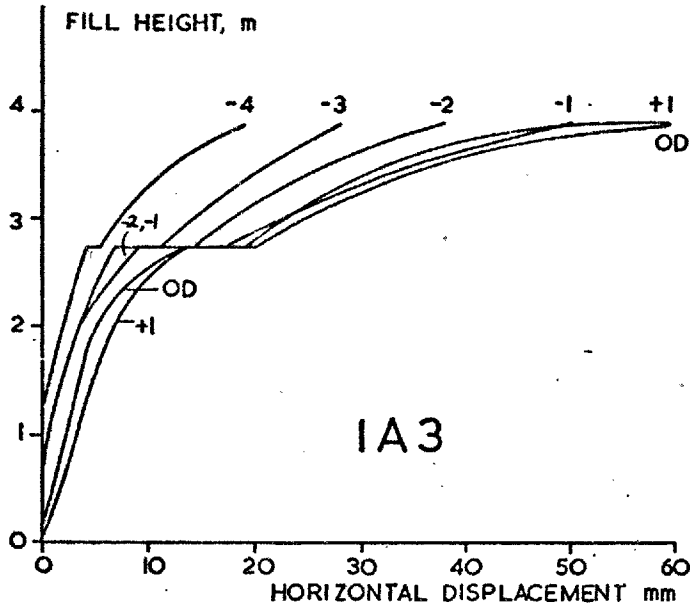
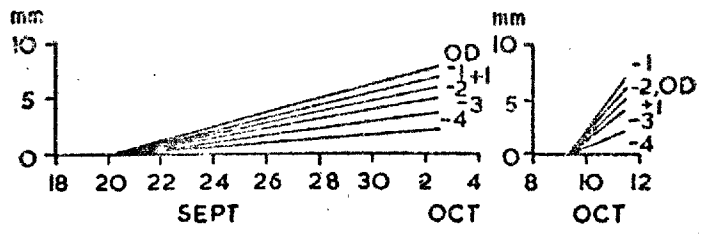
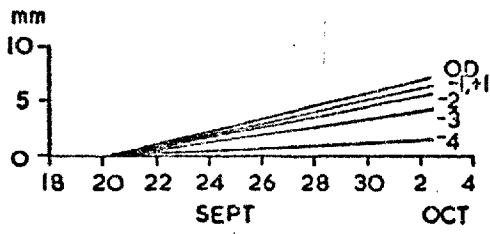
BANK I, STAGE I, INCLINOMETERS:
HORIZONTAL DISPLACEMENTS VERSUS FILL HEIGHT AND AT
CONSTANT FILL HEIGHT



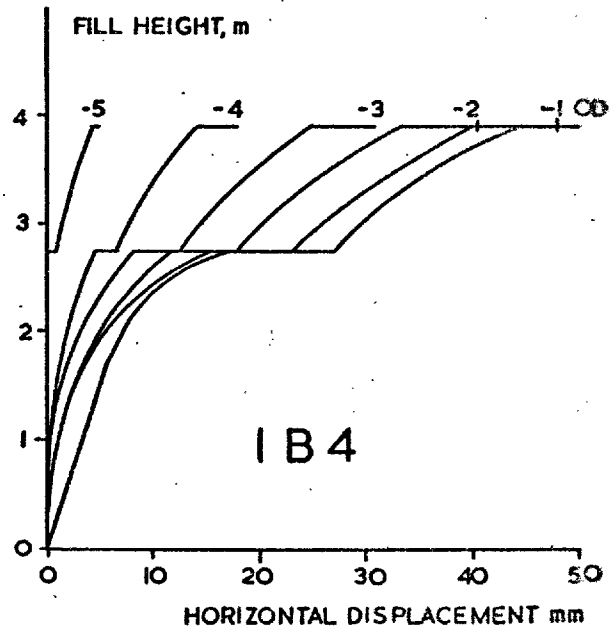
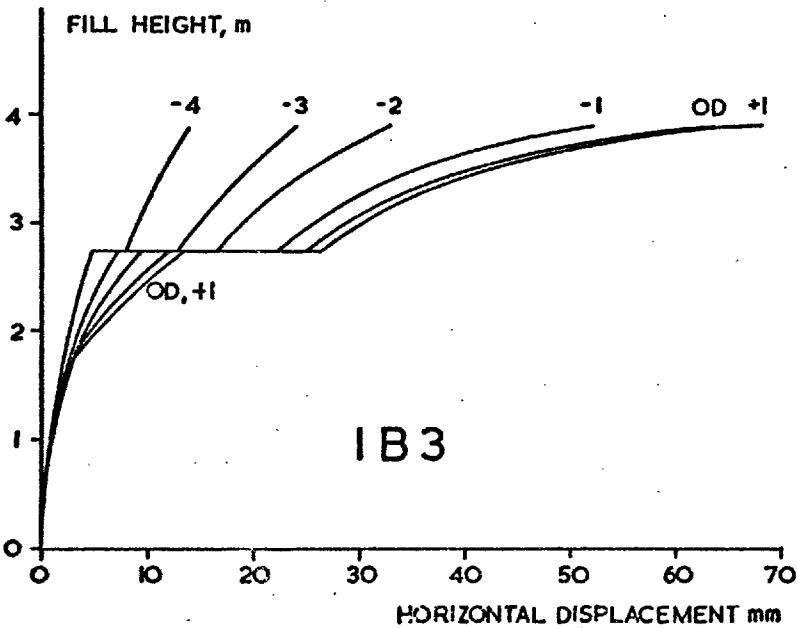
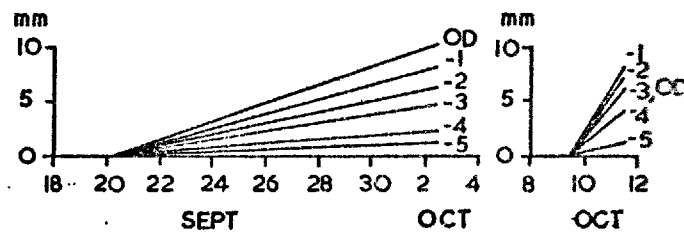
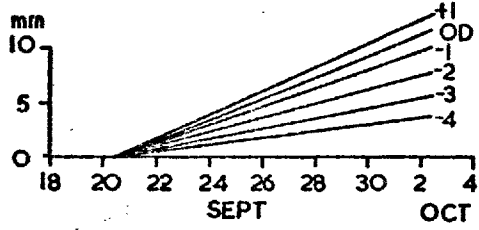
BANK I, STAGE I, INCLINOMETERS: HORIZONTAL DISPLACEMENTS VERSUS FILL HEIGHT AND AT CONSTANT FILL HEIGHT

Fig 6.14

-647-

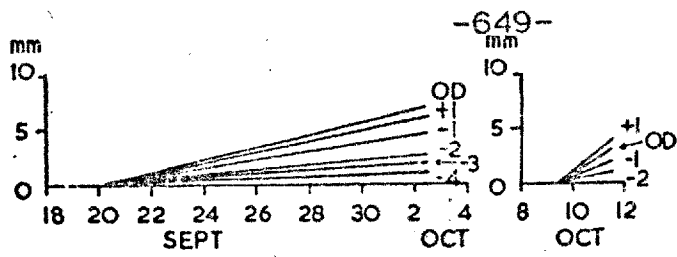


LEGEND: -1 is -1m O.D. etc

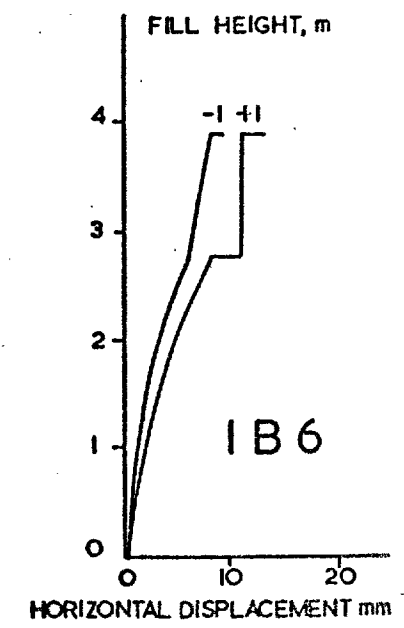
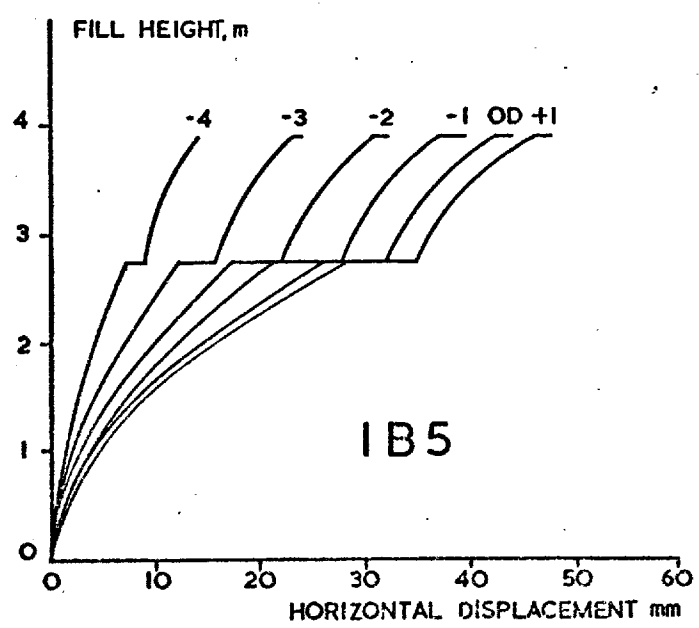
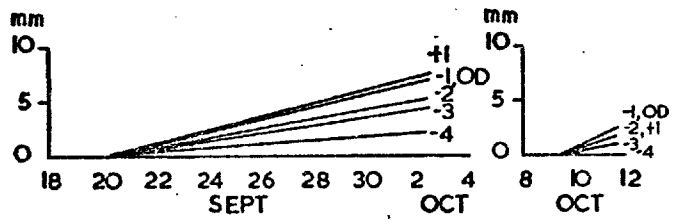
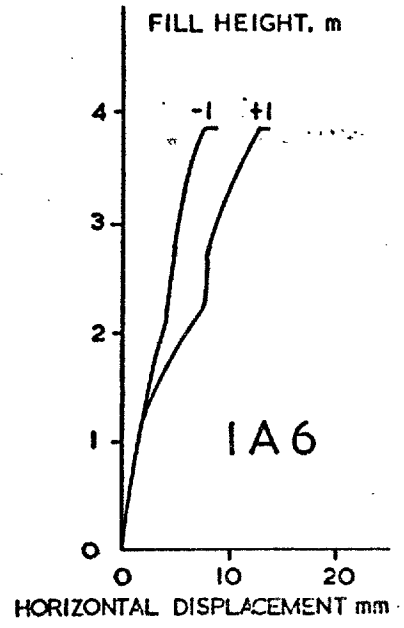
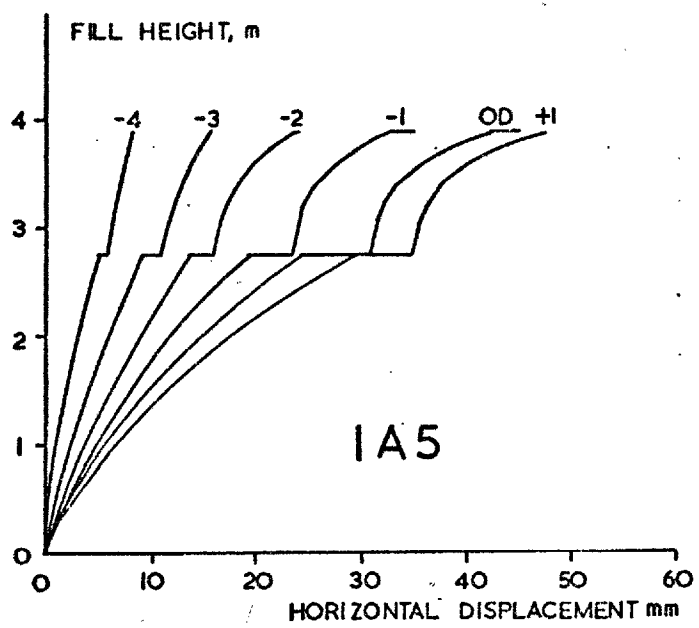


BANK I STAGE I, INCLINOMETERS: HORIZONTAL DISPLACEMENTS VERSUS FILL HEIGHT AND AT CONSTANT FILL HEIGHT

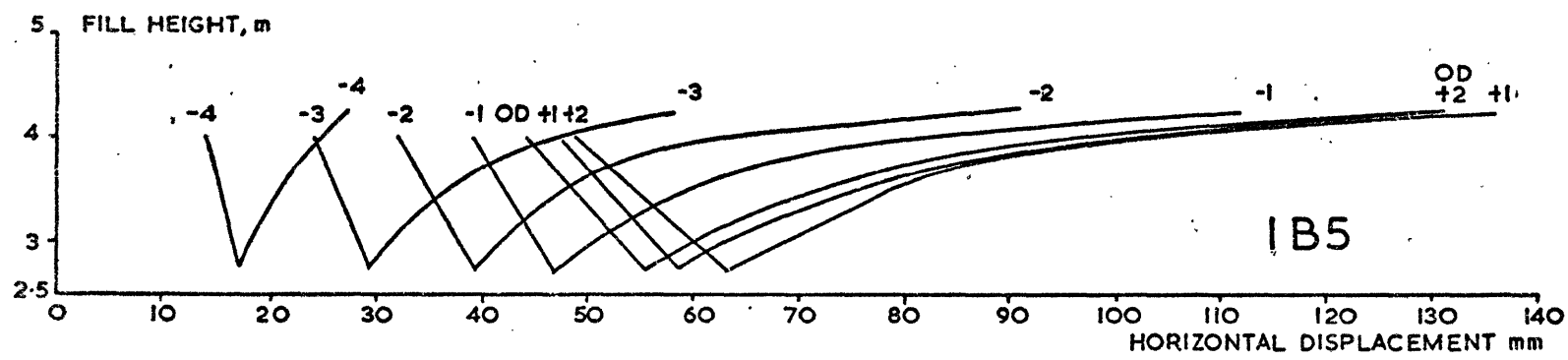
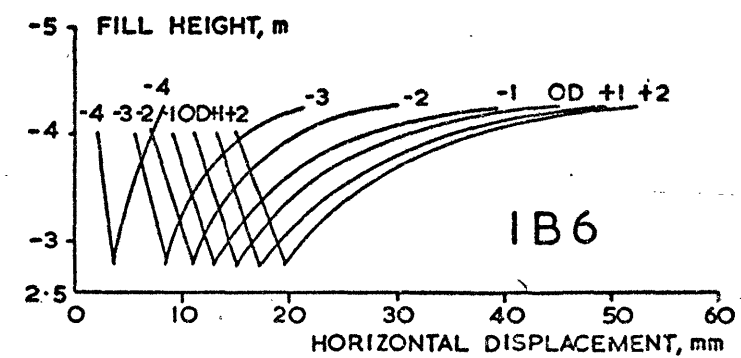
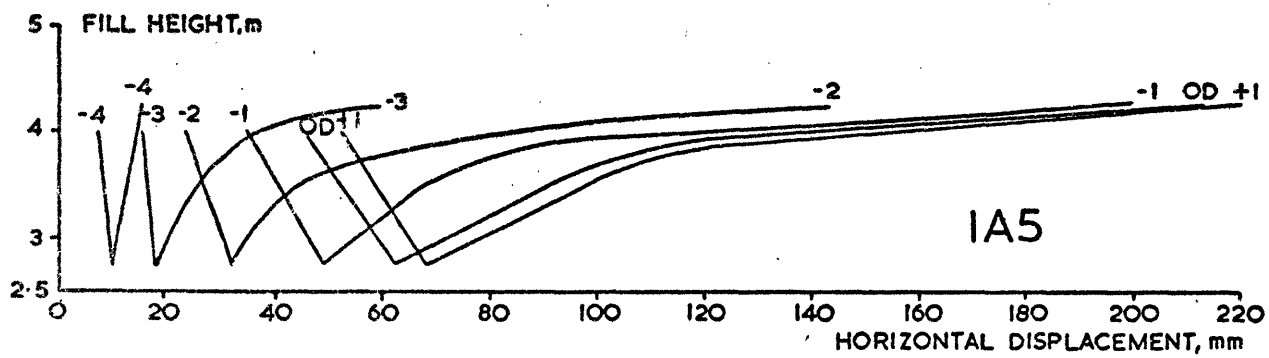
Fig 6.1.5



LEGEND
-1 is -1 m.O.D. etc.



BANK I, STAGE I, INCLINOMETERS:
HORIZONTAL DISPLACEMENTS VERSUS FILL HEIGHT AND AT
CONSTANT FILL HEIGHT



NO SIGNIFICANT DISPLACEMENTS
RECORDED ON IB4

LEGEND
-1 is -1m O.D. etc.

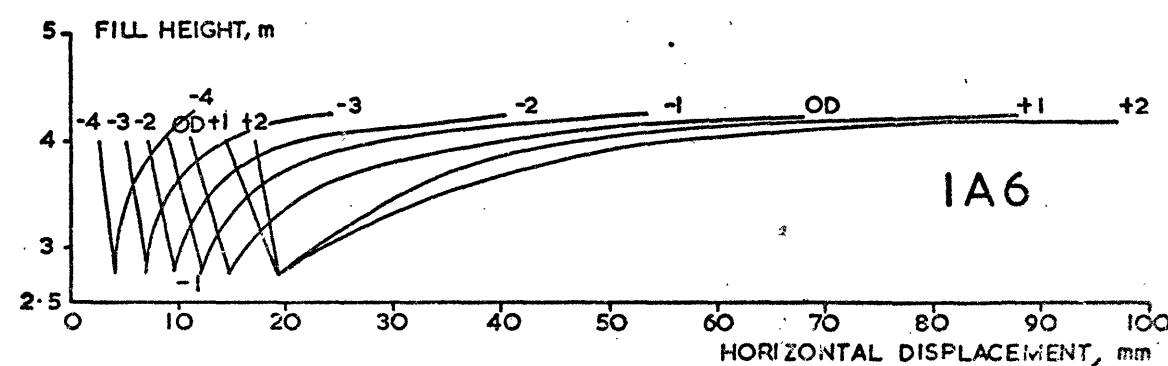
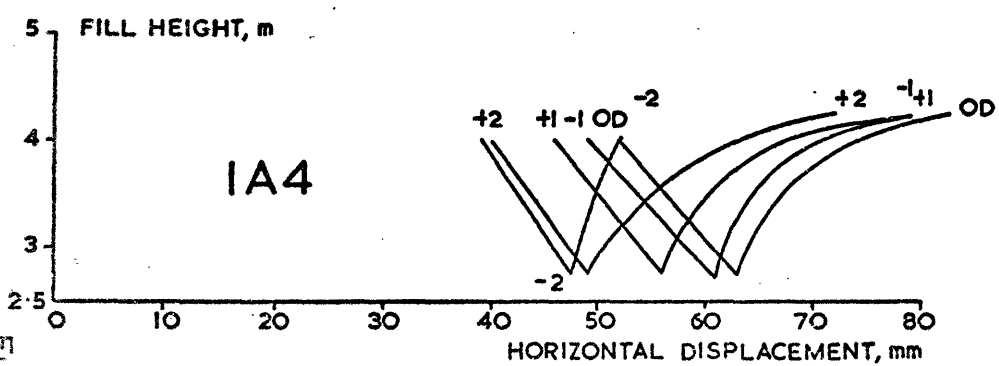
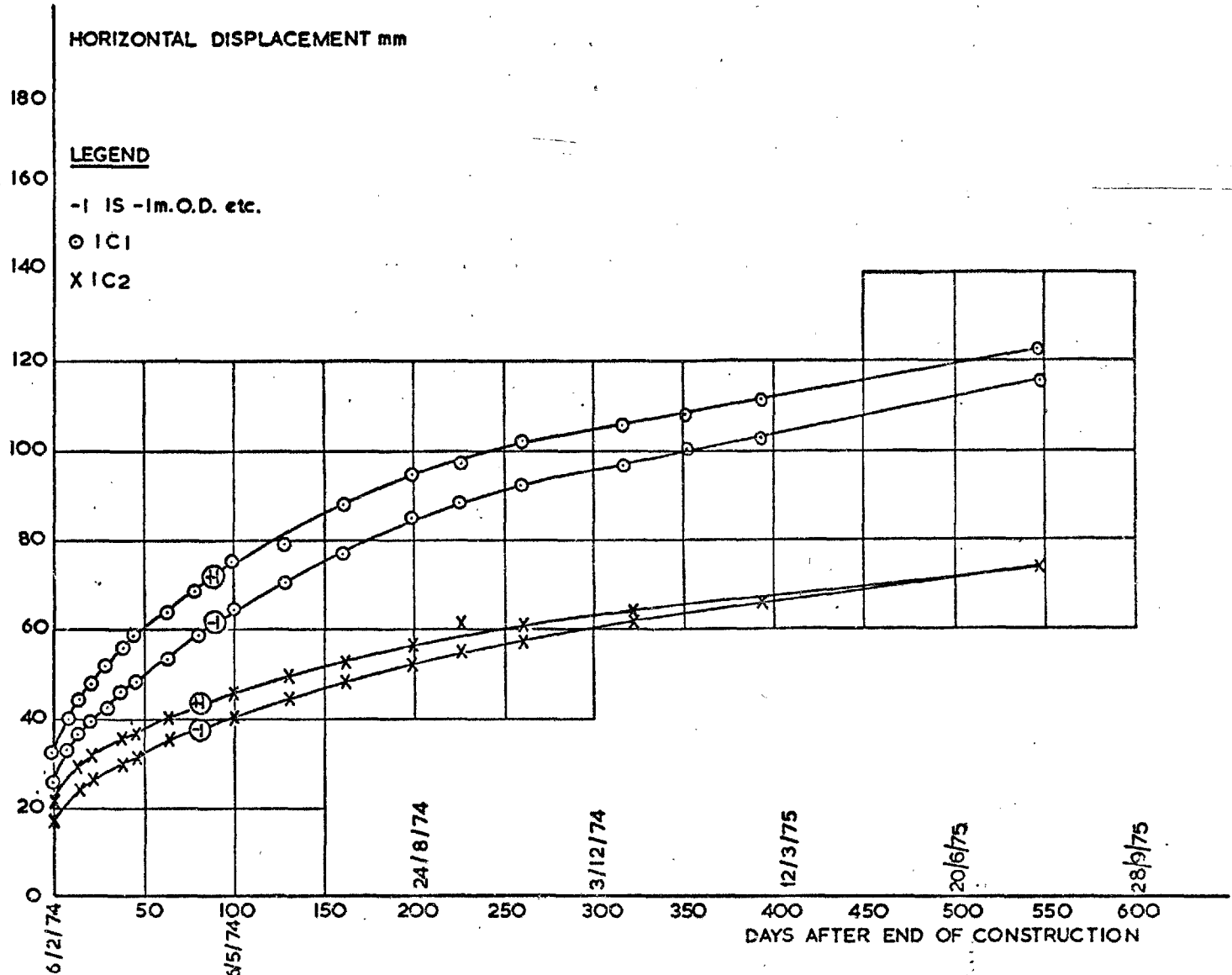
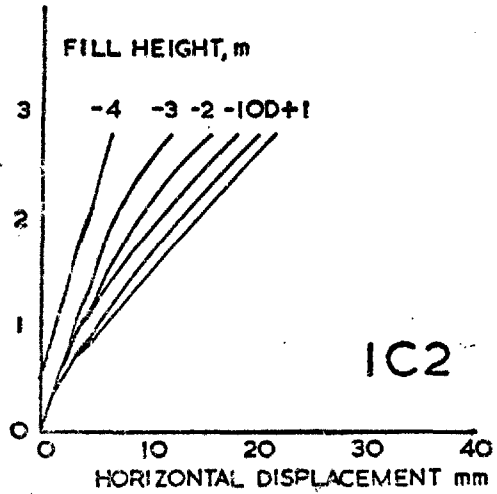
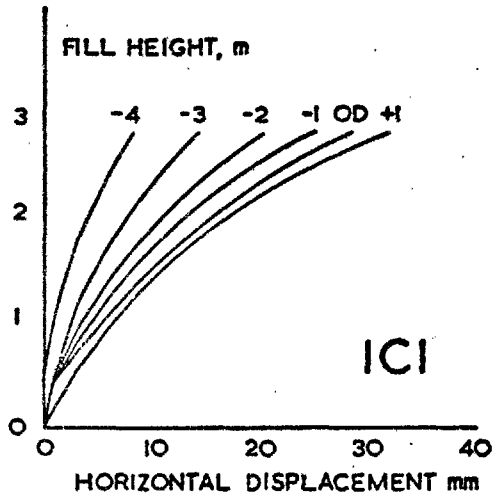


FIG 6.17

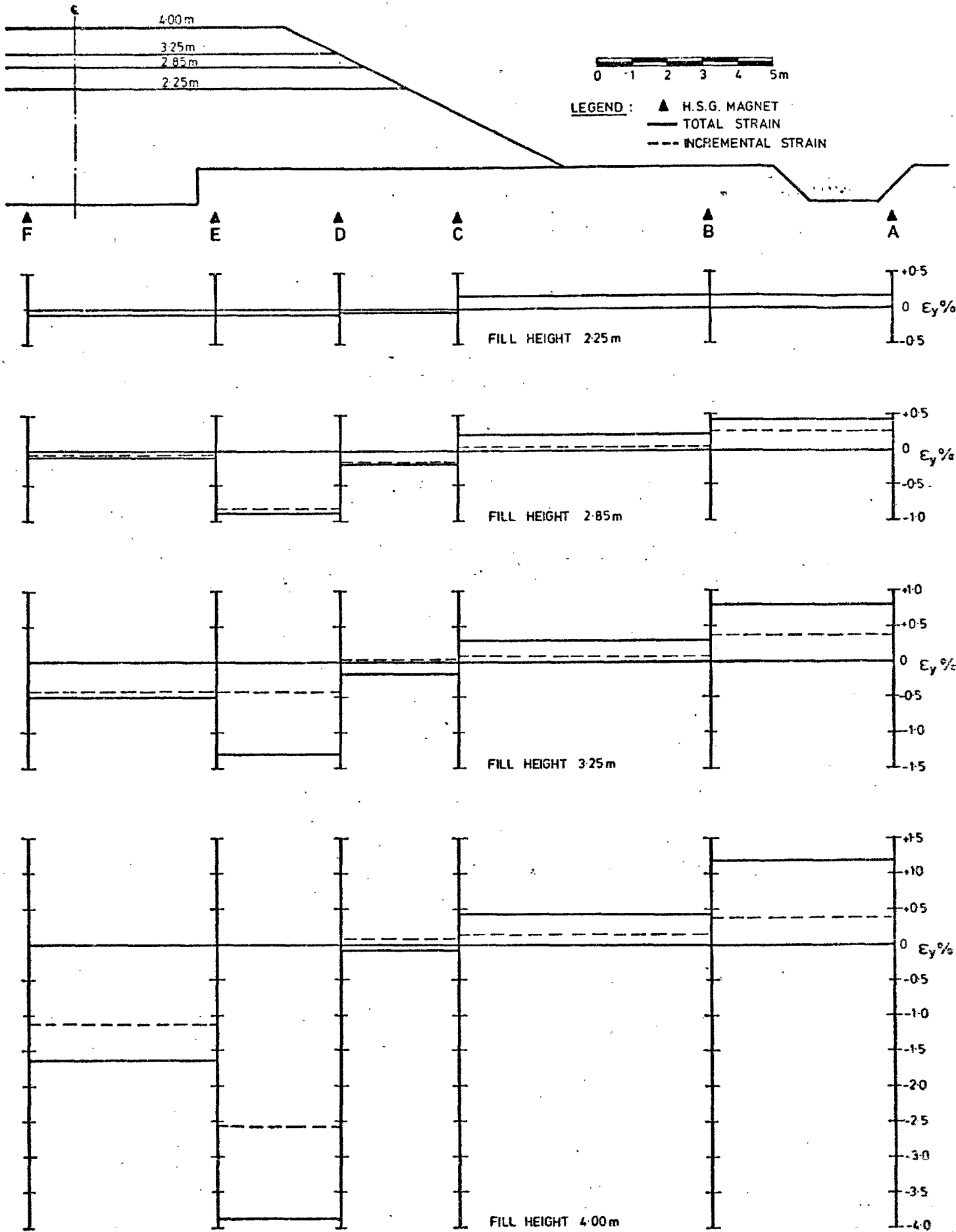
BANK I, STAGE 2, INCLINOMETERS : HORIZONTAL DISPLACEMENTS VERSUS FILL HEIGHT



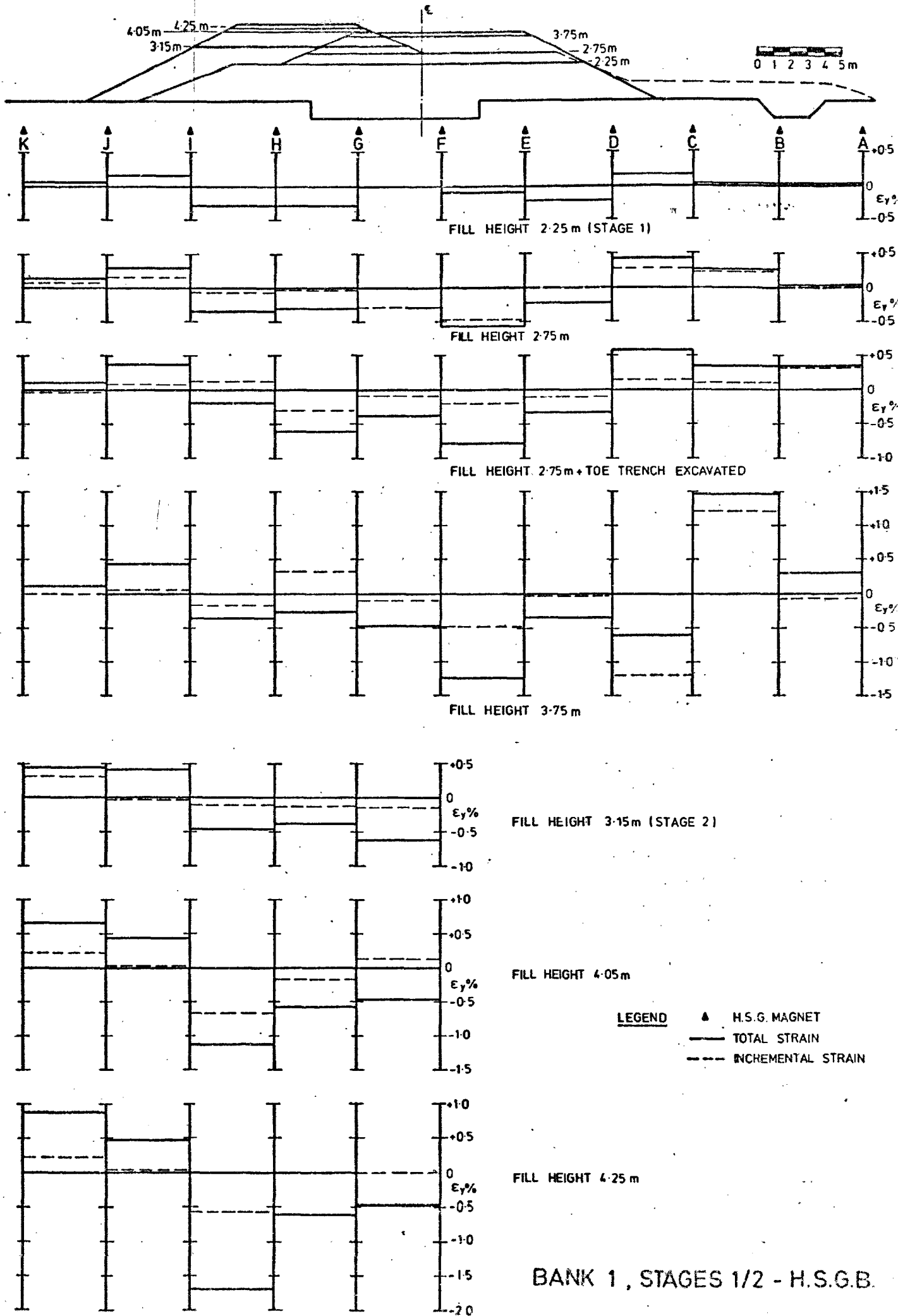
BANK 2, INCLINOMETERS : HORIZONTAL DISPLACEMENTS DURING CONSTRUCTION VERSUS FILL HEIGHT & HORIZONTAL DISPLACEMENTS VERSUS TIME AFTER THE END OF CONSTRUCTION

Fig 6.1.8

-651-

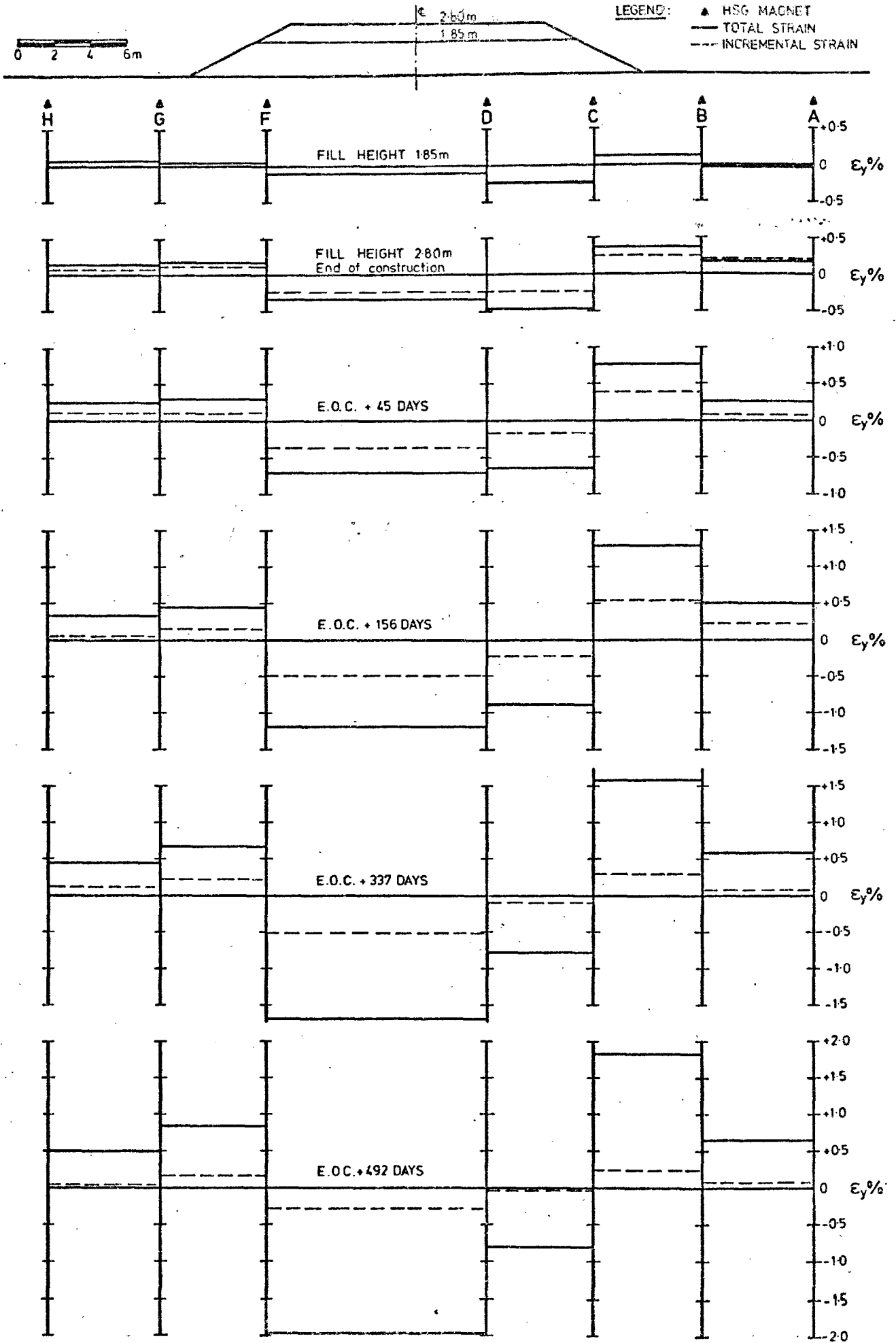


BANK 1, STAGE 1 - H.S.G.A.
AVERAGE HORIZONTAL LINEAR STRAINS



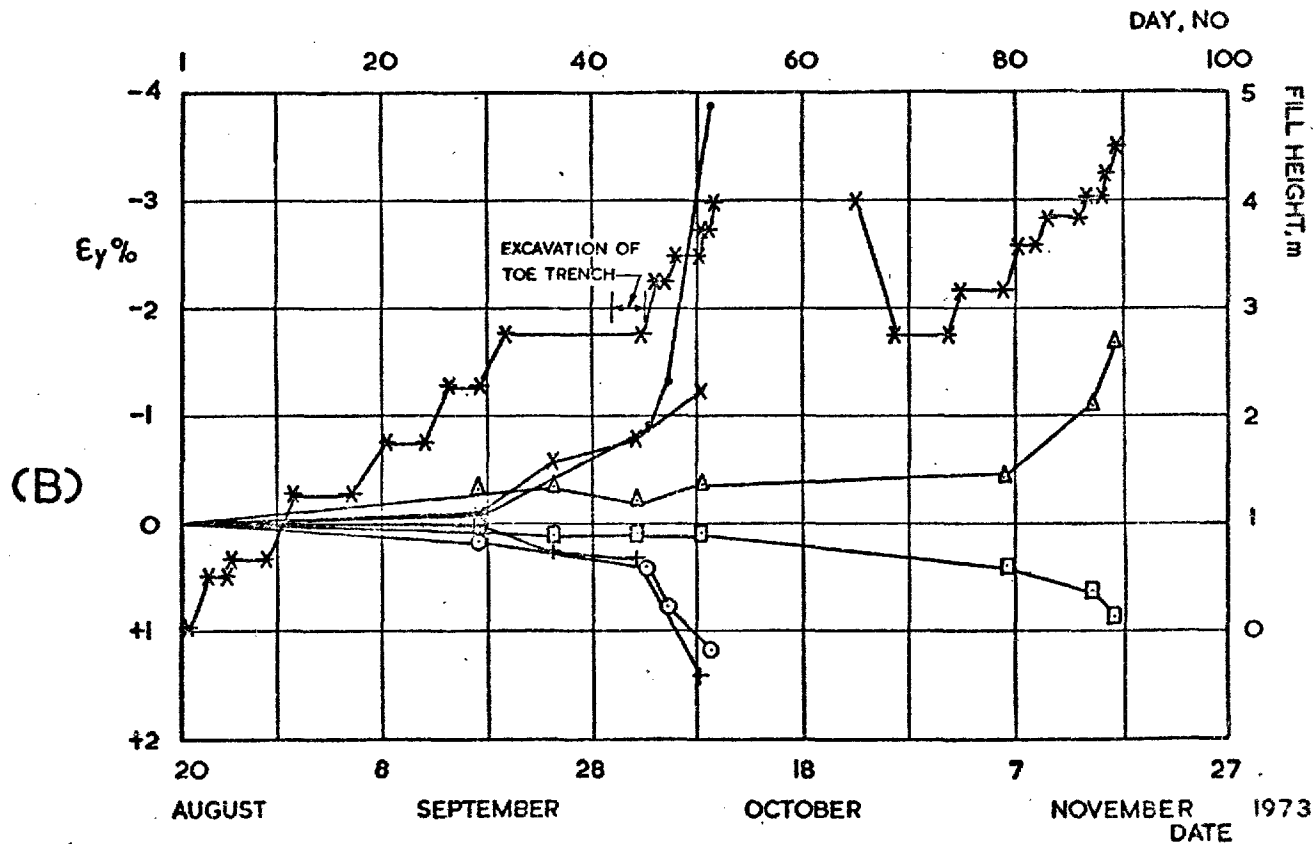
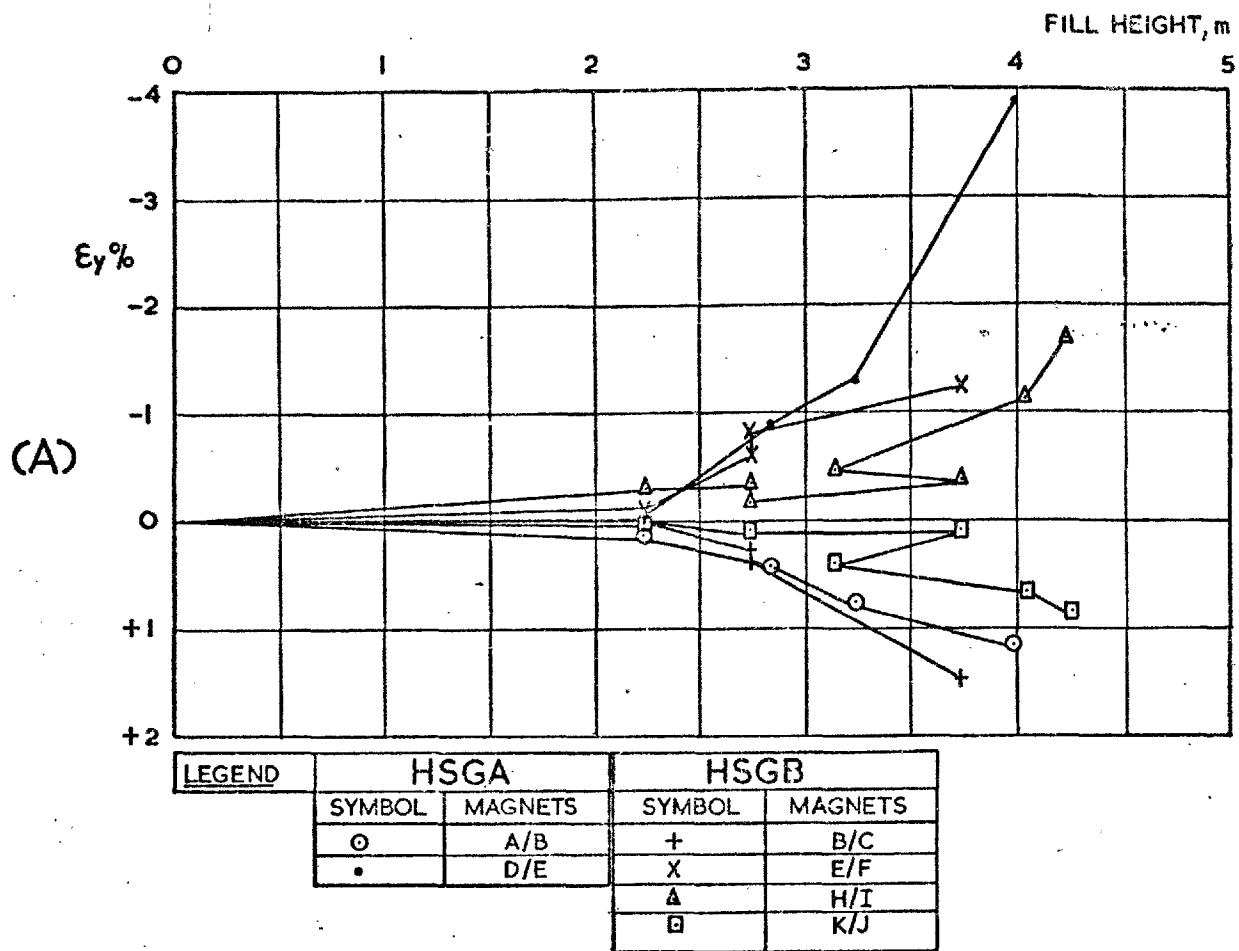
AVERAGE HORIZONTAL LINEAR STRAINS

Fig. 6.1.10



BANK 2 - HSGC
AVERAGE HORIZONTAL LINEAR STRAINS

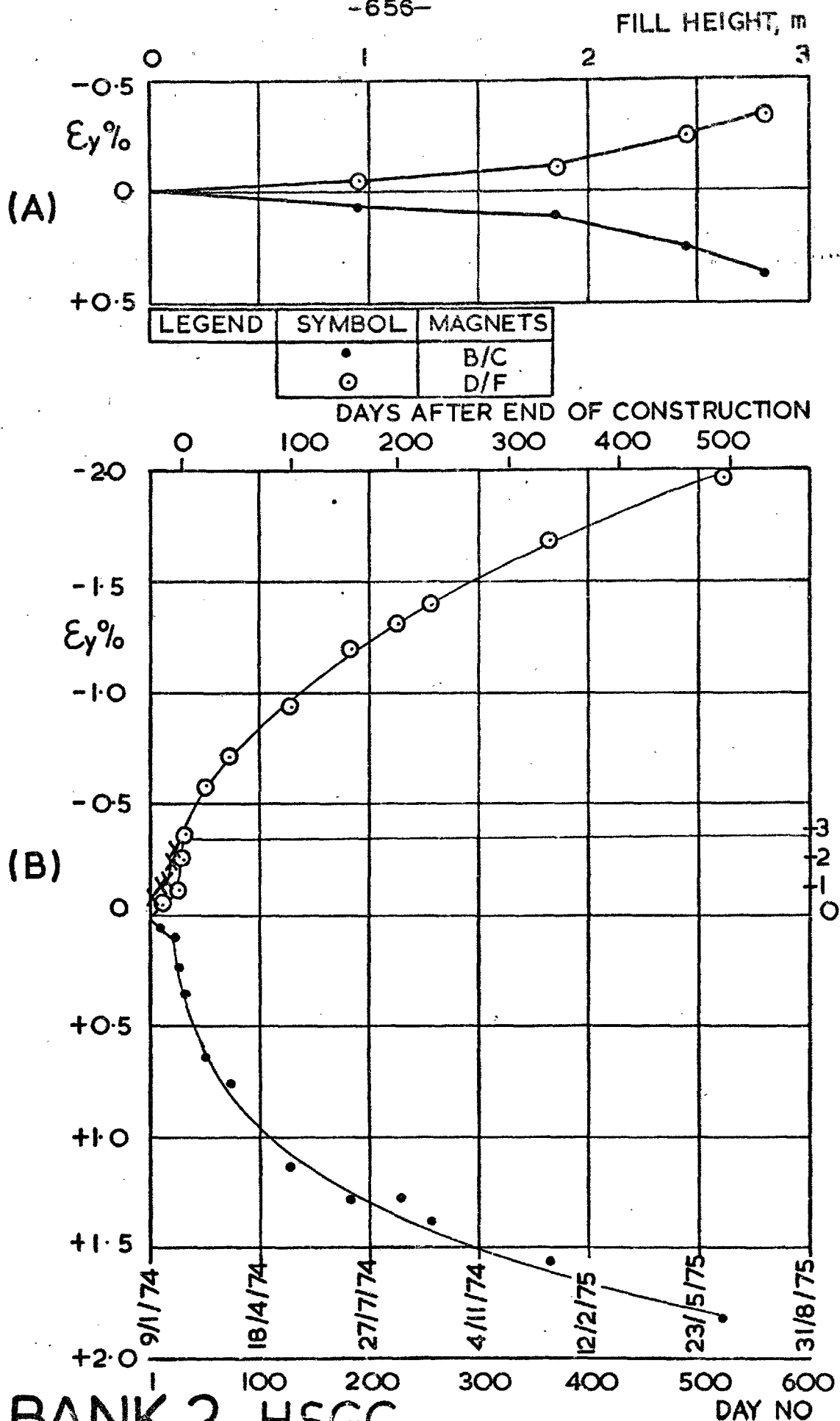
Fig. 6.1.11



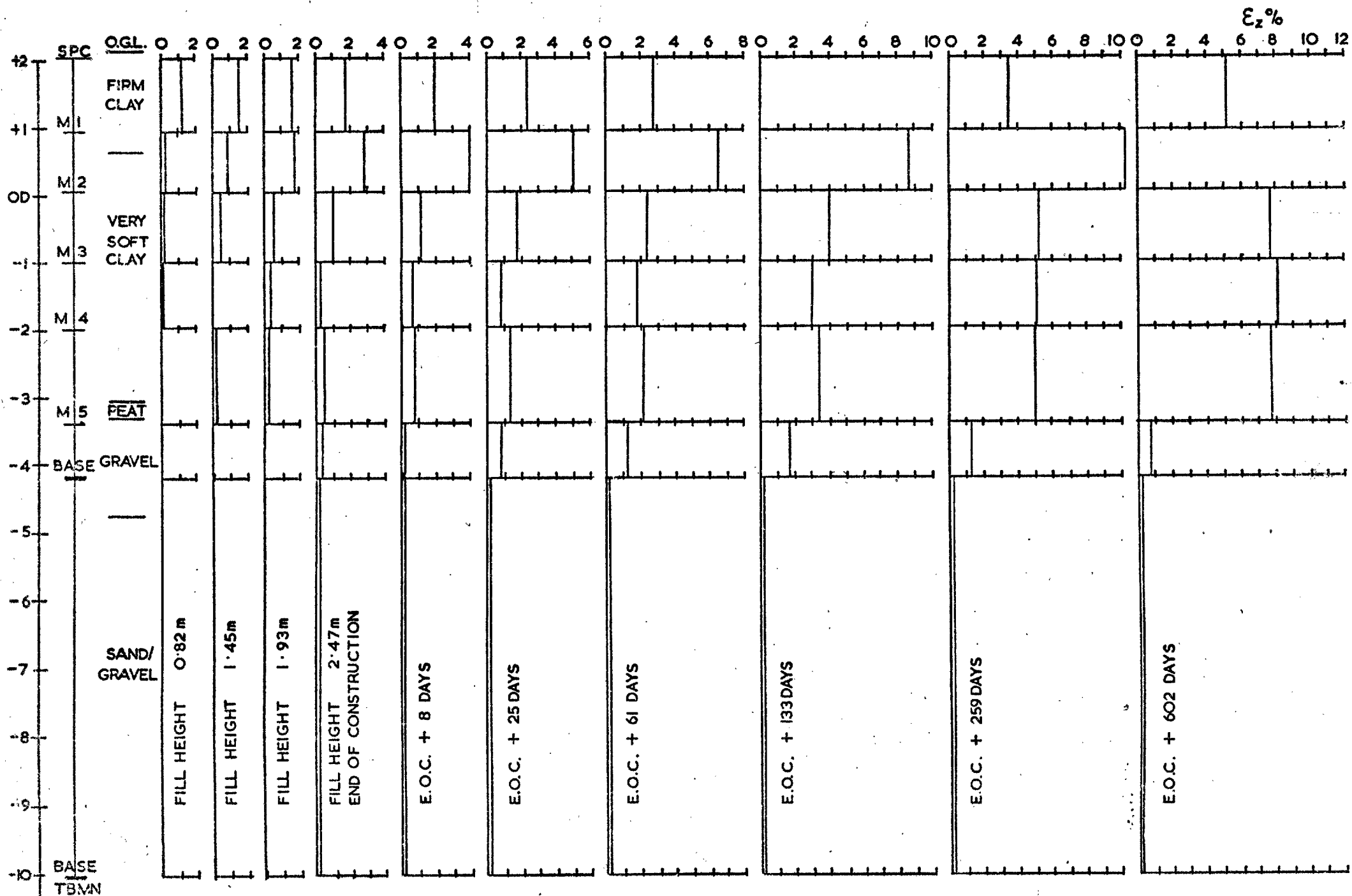
BANK I, STAGES 1/2-HSGs A & B

AVERAGE HORIZONTAL LINEAR STRAINS VERSUS FILL HEIGHT (A)
AND TIME FROM THE START OF CONSTRUCTION (B)

Fig. 6.1.12



BANK 2-HSGC
AVERAGE HORIZONTAL LINEAR STRAINS VERSUS
FILL HEIGHT (A)
AND TIME FROM START OF CONSTRUCTION (B)

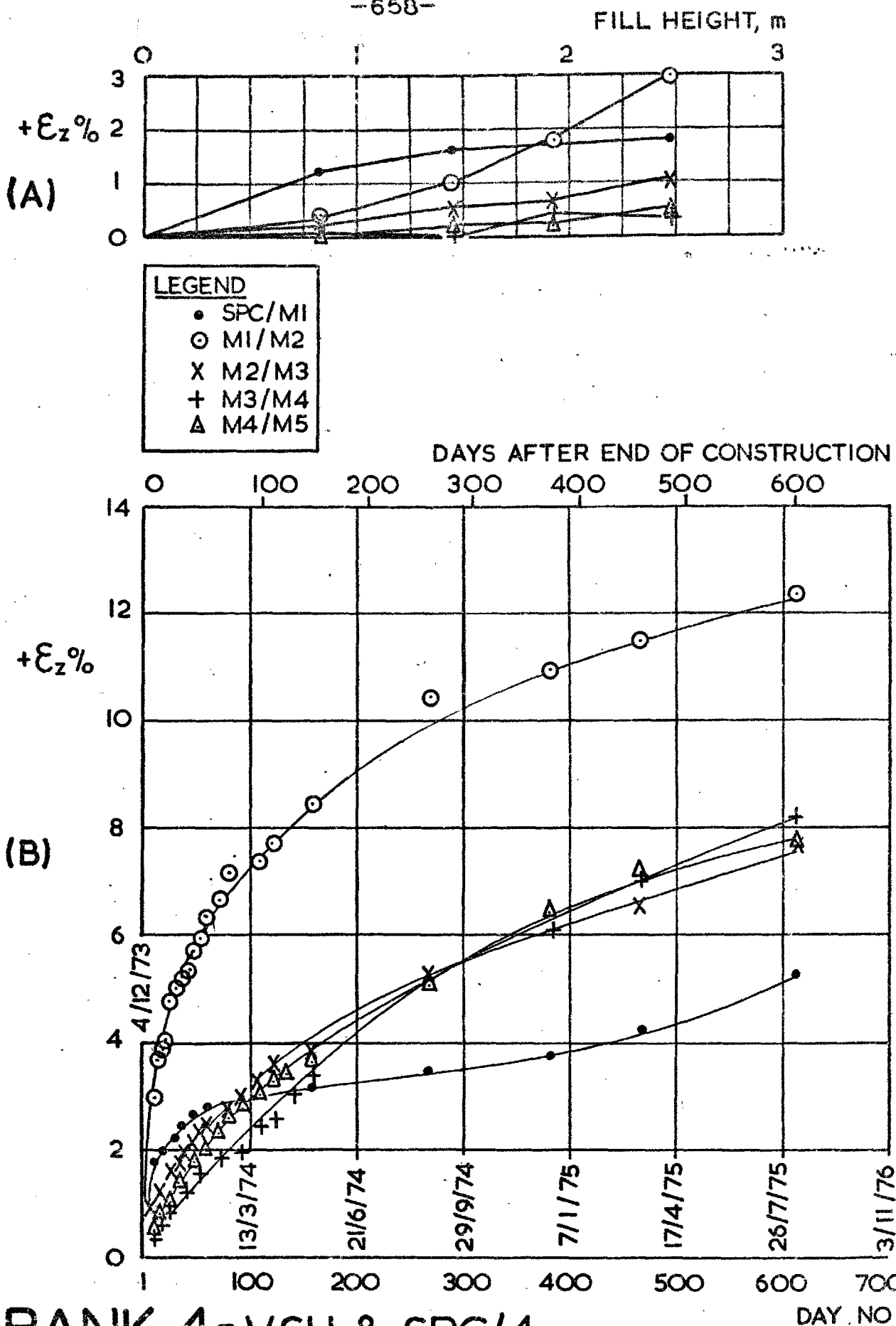


-657-

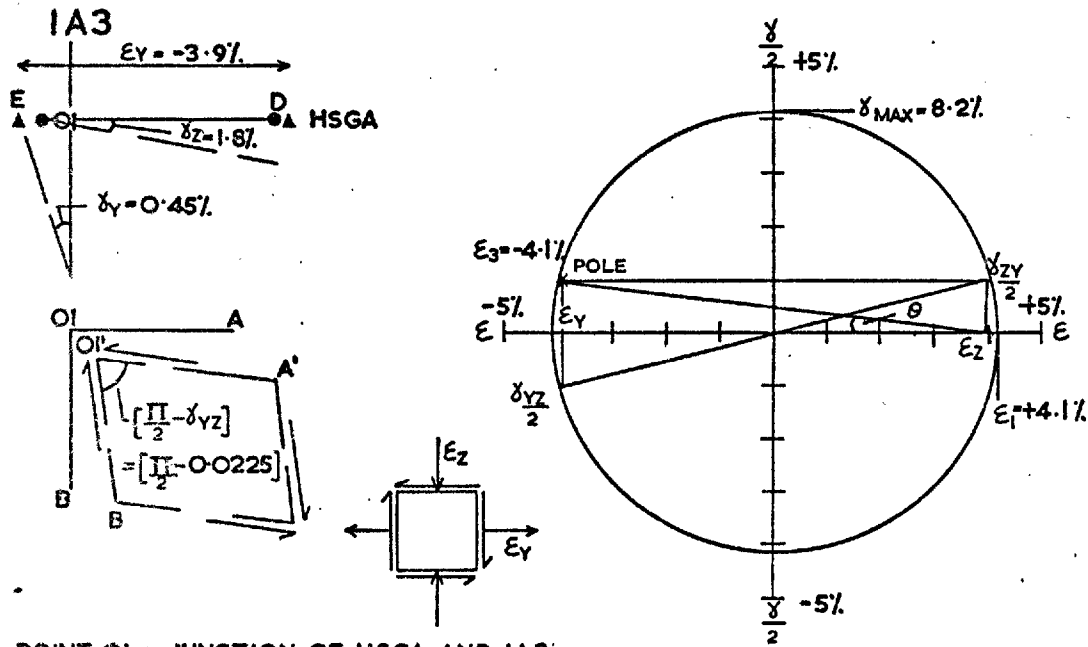
Fig. 6.1.1A

BANK 4 - V.S.U. SPC/4 & TBMN

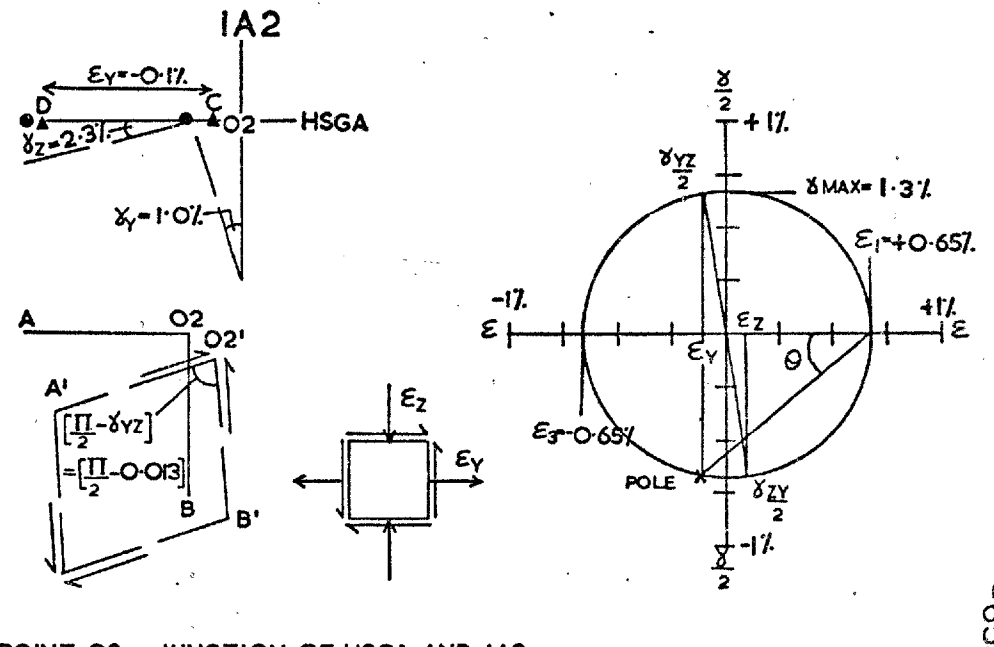
AVERAGE VERTICAL LINEAR STRAINS



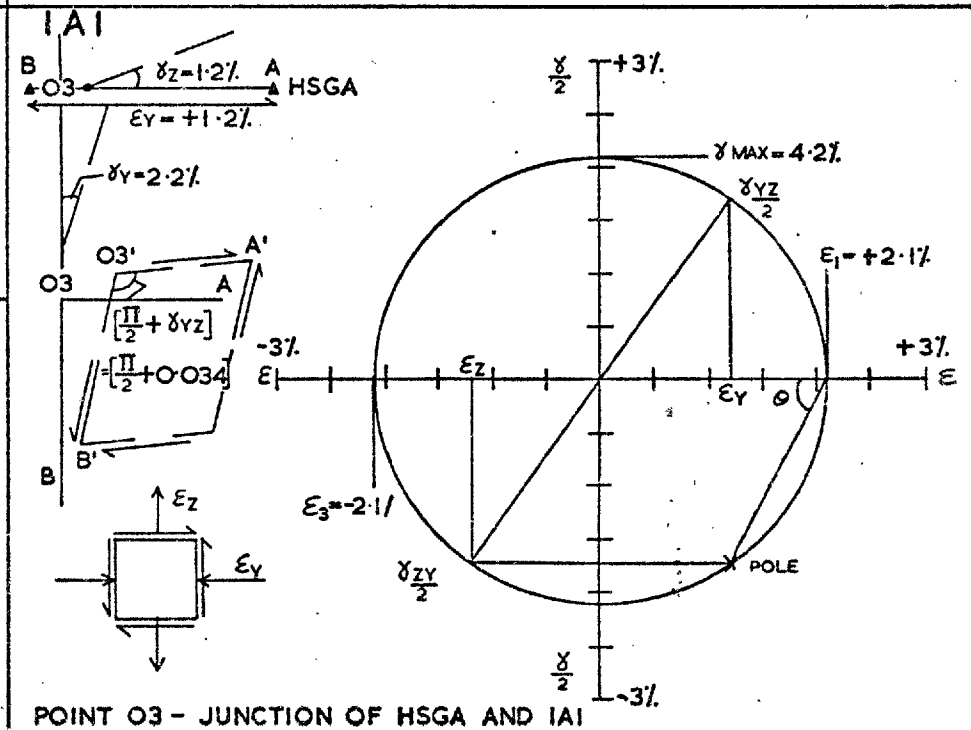
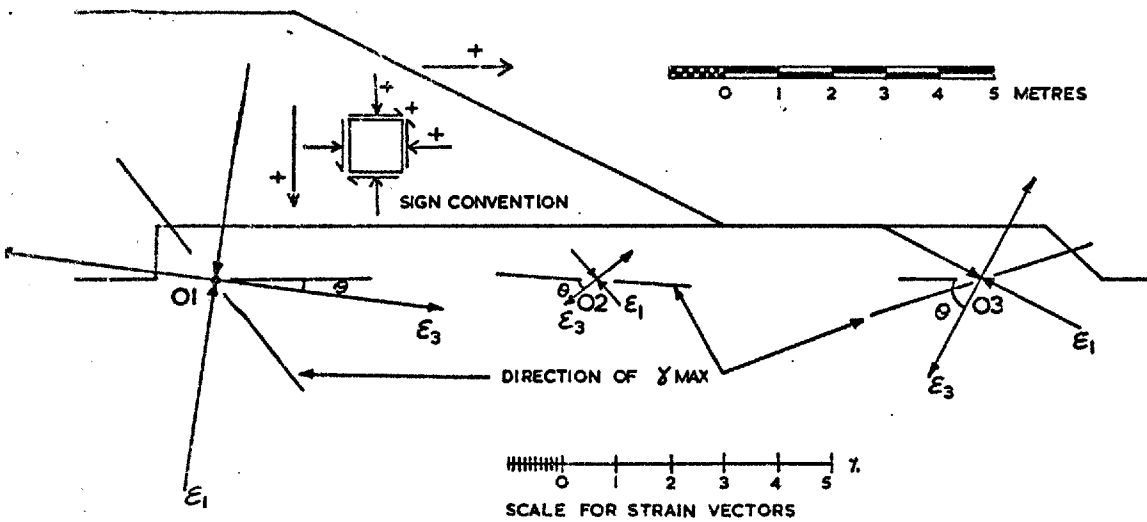
BANK 4-VSU & SPC/4
AVERAGE VERTICAL LINEAR STRAINS VERSUS
FILL HEIGHT (A)
AND TIME FROM START OF CONSTRUCTION (B)



POINT O1 - JUNCTION OF HSGA AND IA3



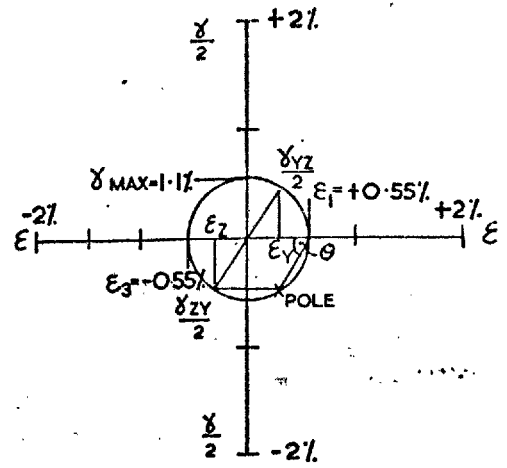
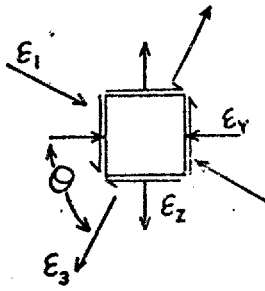
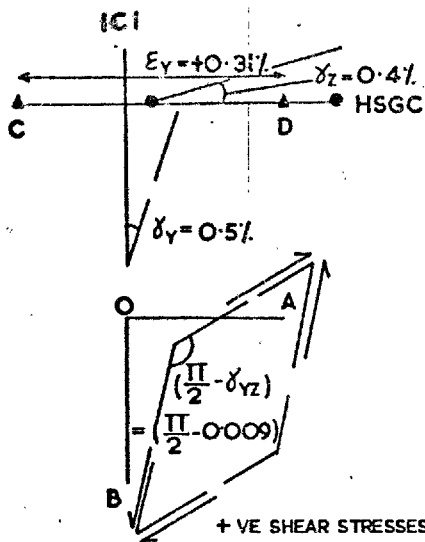
POINT O2 - JUNCTION OF HSGA AND IA2



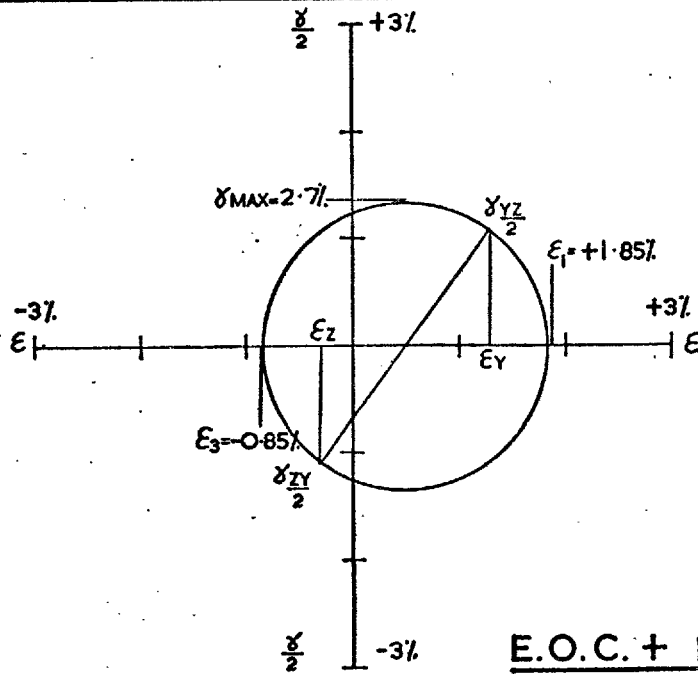
POINT O3 - JUNCTION OF HSGA AND IA1

BANK I, STAGE I - SECTION A
STATE OF STRAIN JUST PRIOR TO FAILURE

[NB. ONLY EMBANKMENT SECTION AND MOHR DIAGRAMS ARE TO SCALE]

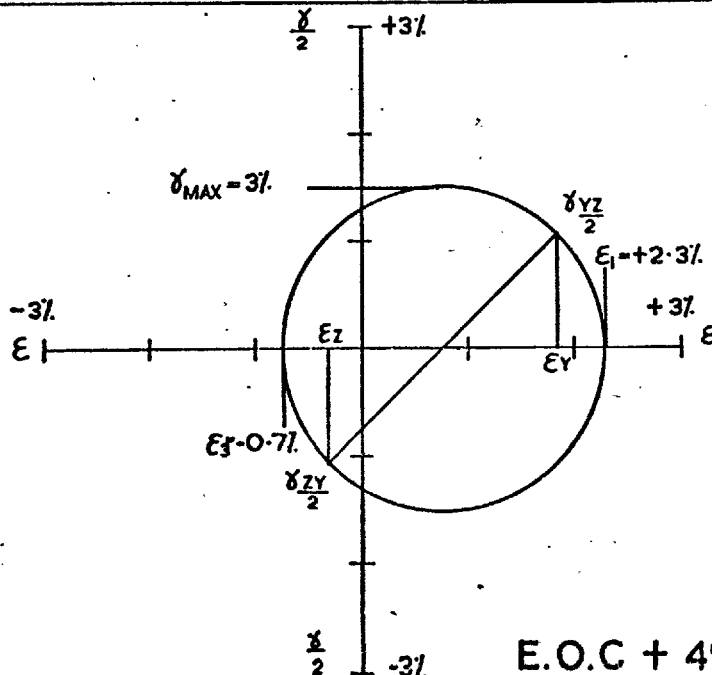


END OF CONSTRUCTION



- $\epsilon_y = +1.3\%$
- $\epsilon_z = -0.3\% (\Delta\epsilon_z = 0)$
- $\delta_z = 1.35\%$
- $\delta_y = 0.8\%$
- $\delta_{yz} = 2.15\%$

E.O.C. + 156 DAYS



- $\epsilon_y = +1.85\%$
- $\epsilon_z = -0.3\% (\Delta\epsilon_z = 0)$
- $\delta_z = 1.64\%$
- $\delta_y = 0.5\%$
- $\delta_{yz} = 2.15\%$

E.O.C. + 492 DAYS

BANK 2

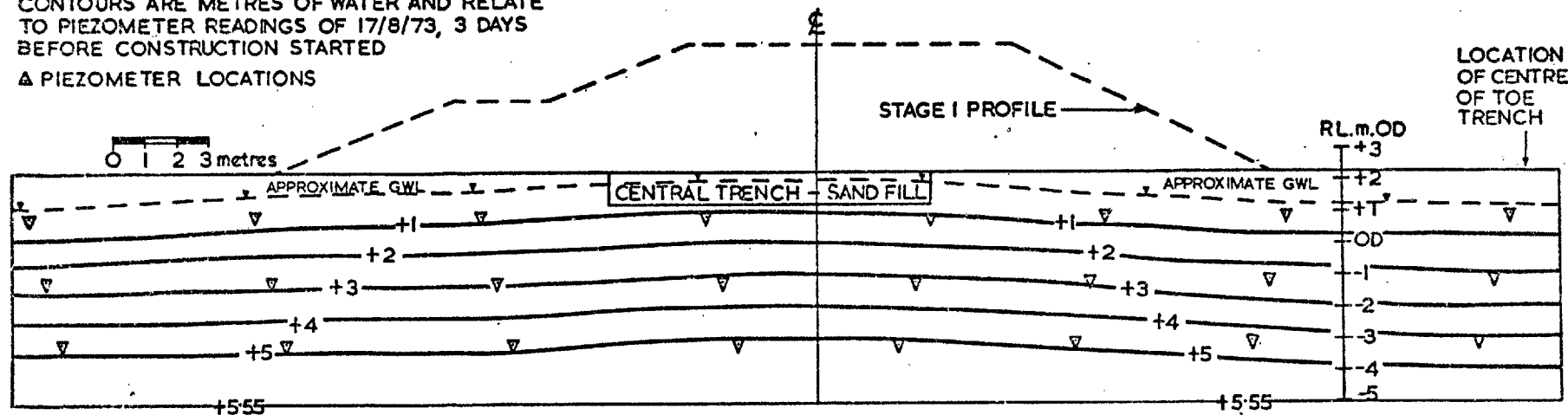
STATE OF STRAIN AT JUNCTION OF ICI AND HSGC
 (NB. ONLY MOHR DIAGRAMS ARE TO SCALE)

Fig. 6.1.17

KEY

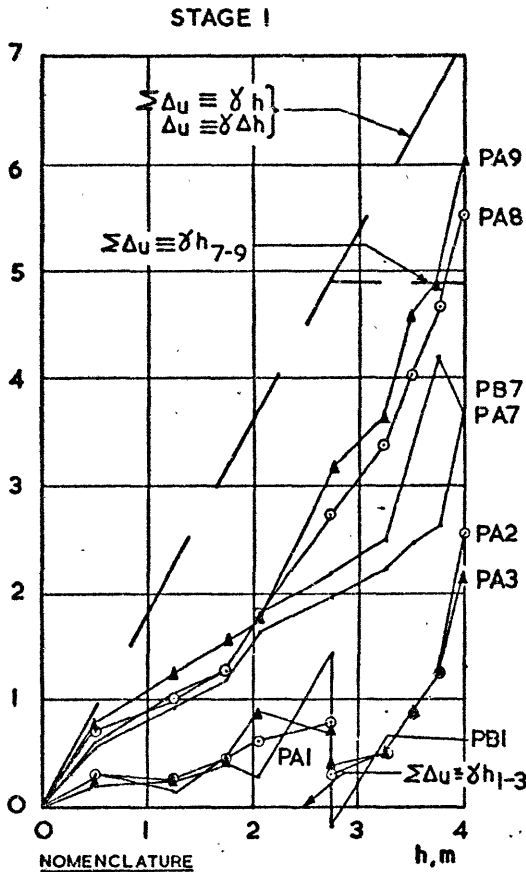
CONTOURS ARE METRES OF WATER AND RELATE TO PIEZOMETER READINGS OF 17/8/73, 3 DAYS BEFORE CONSTRUCTION STARTED

▲ PIEZOMETER LOCATIONS



BANK I LOCATION. PORE-PRESSURE CONTOURS PRIOR TO CONTRUCTION

EXCESS PORE-WATER PRESSURE, $\Sigma \Delta u$ m OF WATER



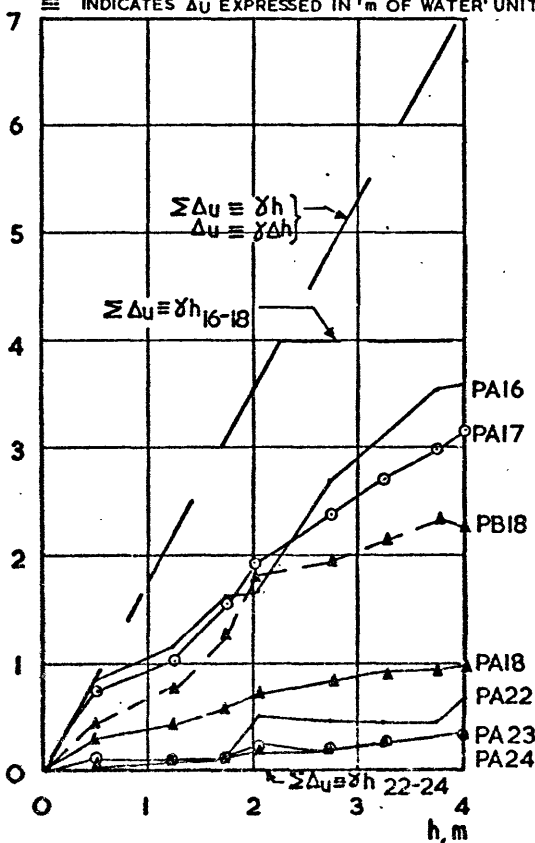
NOMENCLATURE

$\gamma = \gamma_B$ BULK UNIT WT OF FILL = 17.5 kN/m³

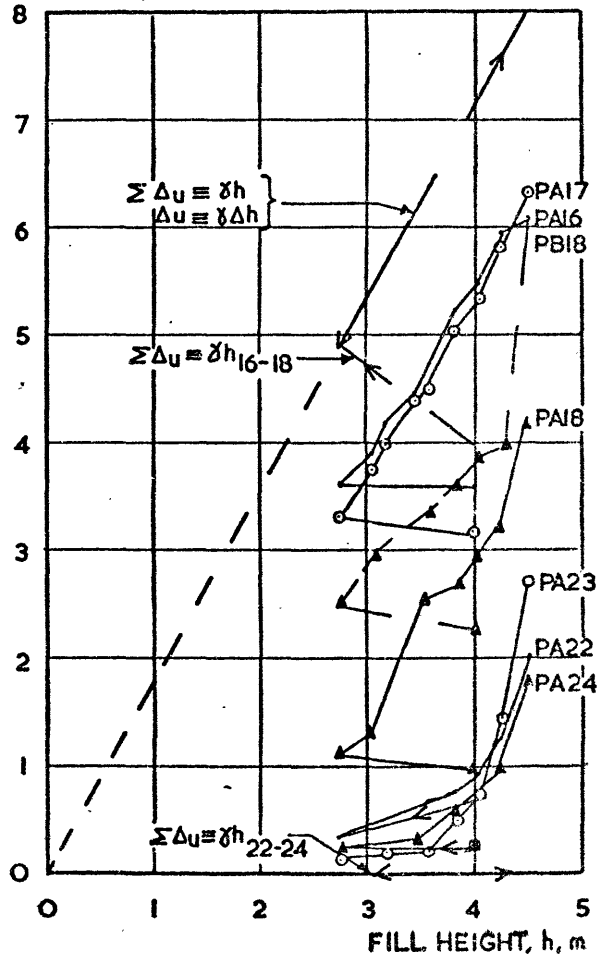
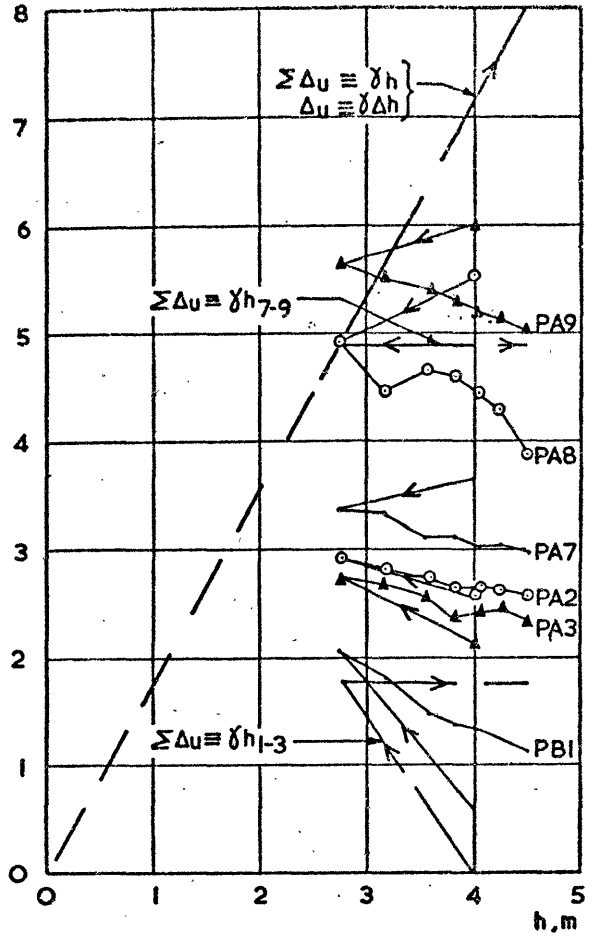
h_{x-z} = FILL HEIGHT ABOVE PIEZOMETERS X, Y, Z

FINAL READINGS FOR EACH STAGE ARE POST-FAILURE

\equiv INDICATES Δu EXPRESSED IN 'm OF WATER' UNITS



STAGE 1 → STAGE 2 AND STAGE 2

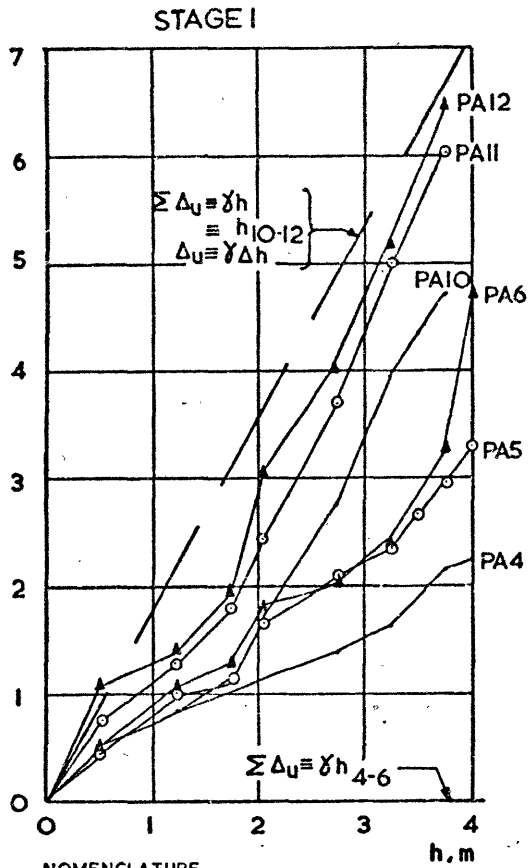


BANK I SECTION A

EXCESS PORE-WATER PRESSURE VERSUS FILL HEIGHT

Fig. 6.1.19

EXCESS PORE-WATER PRESSURE $\Sigma \Delta u$, m OF WATER



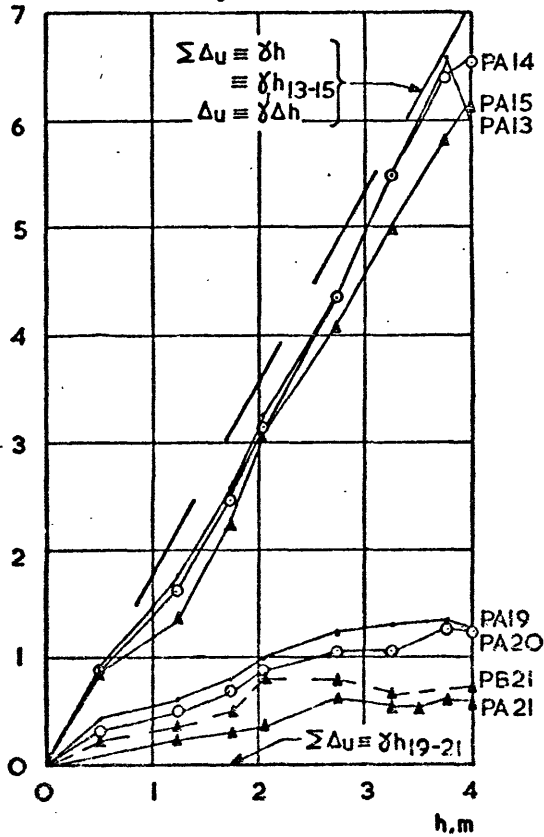
NOMENCLATURE

$\gamma = \gamma_B$ BULK UNIT WT OF FILL = 17.5 kN/m³

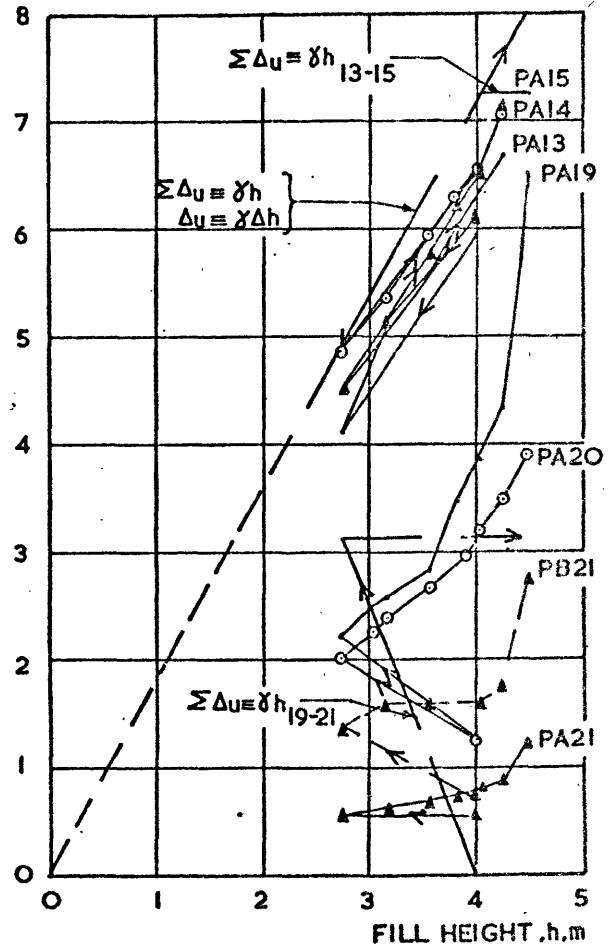
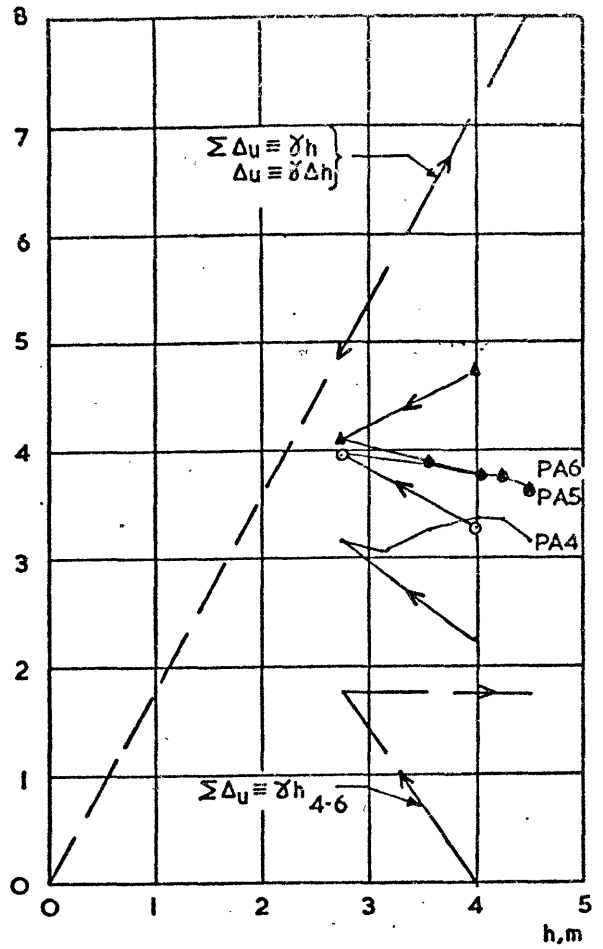
h x-z FILL HEIGHT ABOVE PIEZOMETERS X, Y, Z

FINAL READINGS FOR EACH STAGE ARE POST-FAILURE

\equiv INDICATES Δu EXPRESSED IN 'm OF WATER' UNITS



STAGE 1 → STAGE 2 AND STAGE 2

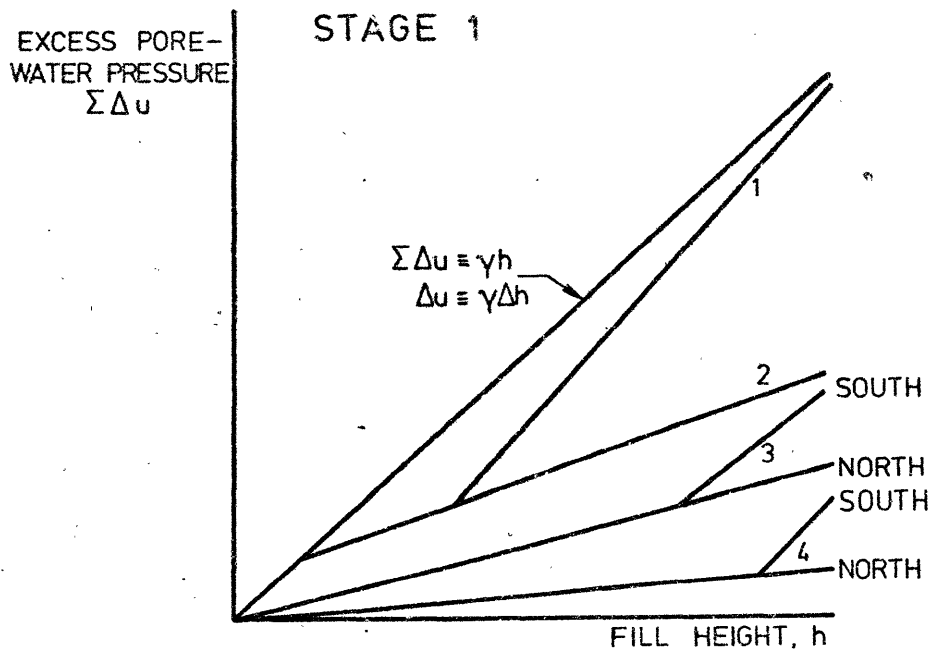


BANK I SECTION A

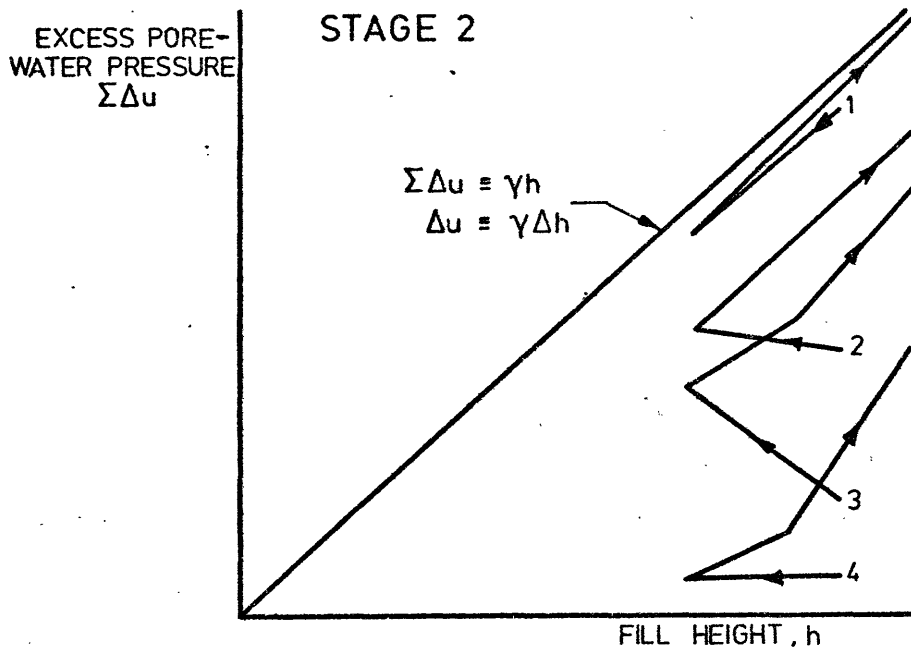
EXCESS PORE-WATER PRESSURE VERSUS FILL HEIGHT

Fig.6.1.20

NB. $\gamma = \gamma_b =$ BULK UNIT WEIGHT OF FILL = 17.5 kN/m^3
 Δu EXPRESSED IN 'm. OF WATER' UNITS



- LEGEND**
- 1 Beneath embankment fill ; piezometers 7-15
 - 2 Beneath embankment berm ; piezometers 16-18
 - 3 Beneath embankment toe ; piezometers 4-6, 19-21
 - 4 Beyond embankment toe ; piezometers 1-3, 22-24



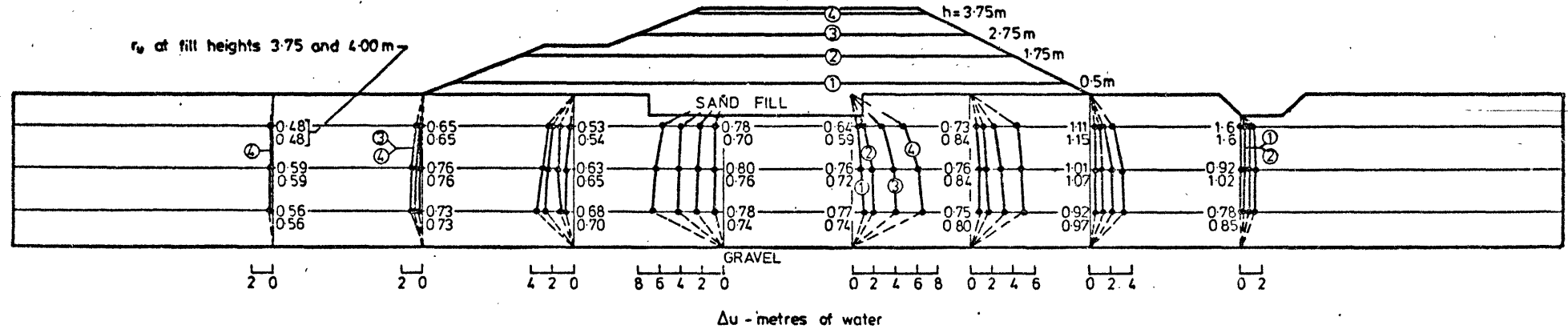
- LEGEND**
- 1 Beneath embankment centre during both stages ; piezometers 13-15
 - 2 Beneath embankment centre during Stage 2 ; piezometers 16-18
 - 3 Beneath embankment side slope ; piezometers 19-21
 - 4 Beyond embankment toe ; piezometers 22-24

BANK 1

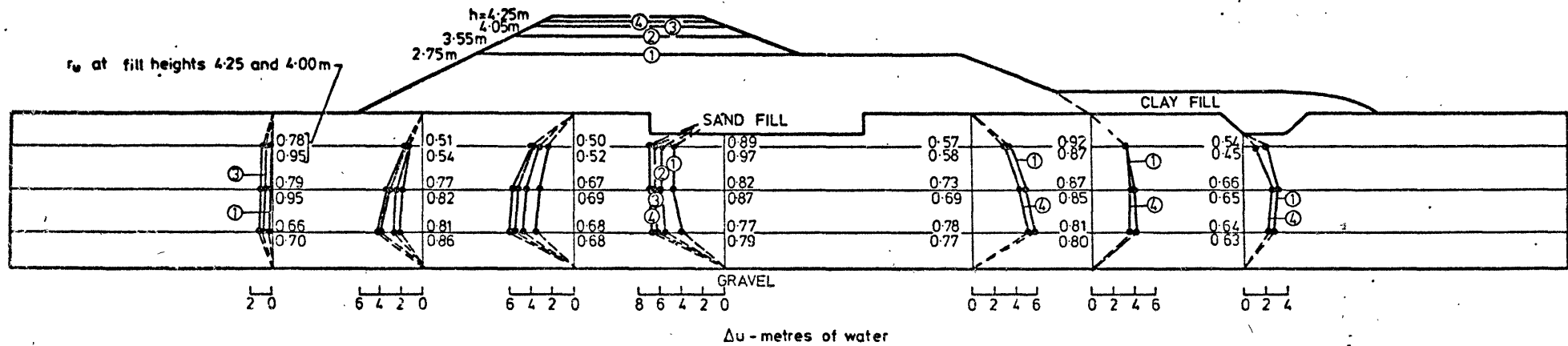
TYPICAL EXCESS PORE-WATER PRESSURE / FILL HEIGHT RELATIONSHIPS DURING CONSTRUCTION

Fig. 6.1.21

STAGE 1 (SECTION A, EXCEPT PIEZOMETERS PB 1,7,18 and 21)



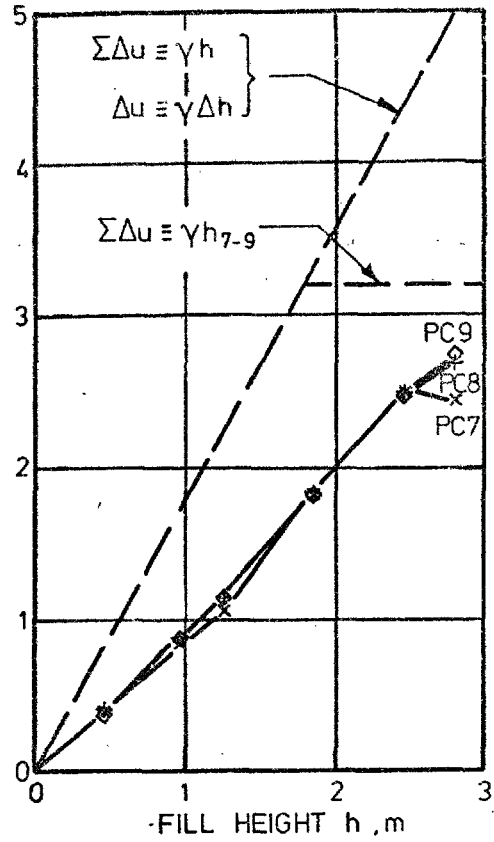
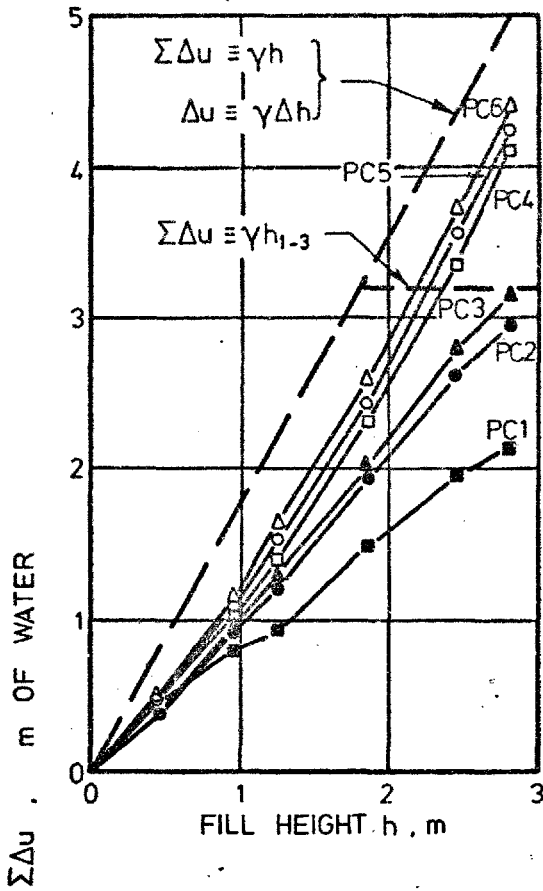
STAGE 2 (SECTION A, EXCEPT PIEZOMETERS PB 1,18 and 21)



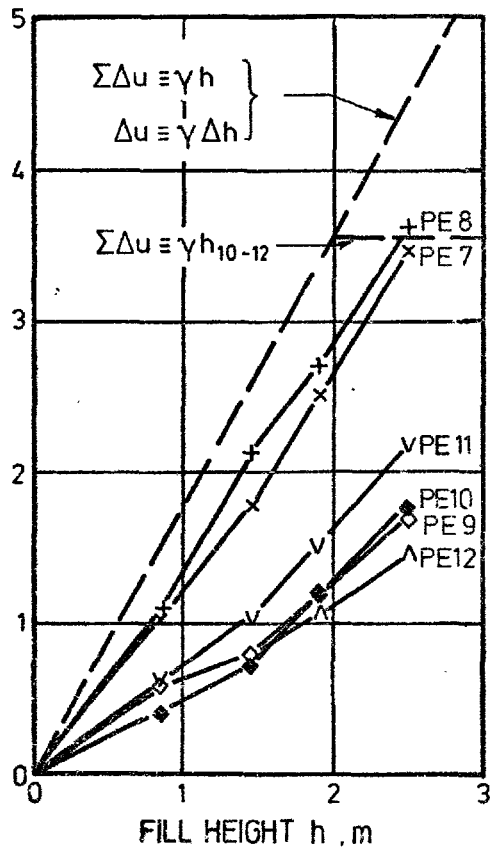
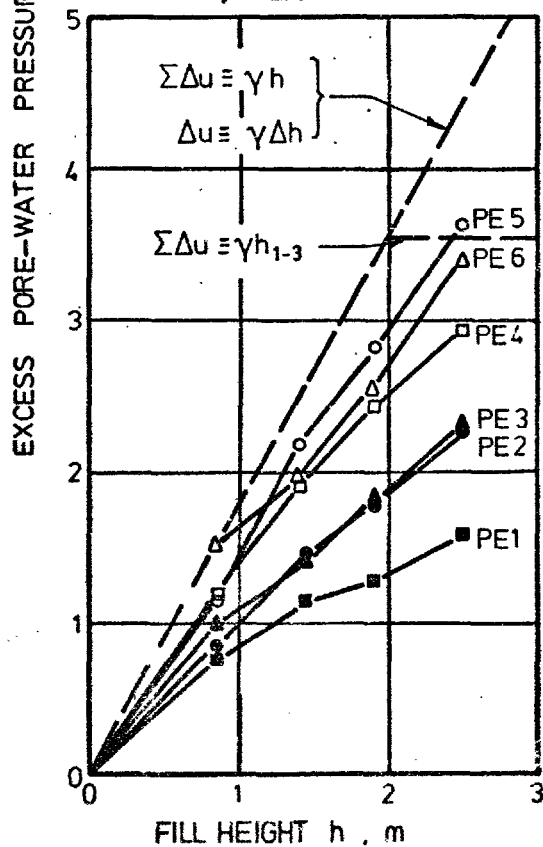
BANK 1
EXCESS PORE-WATER PRESSURES

NOMENCLATURE $\gamma = \gamma_B =$ BULK UNIT WT OF FILL = 17.5 kN/m³
 h_{x-z} = FILL HEIGHT ABOVE PIEZOMETERS X, Y, Z

BANK 2, SECTION C

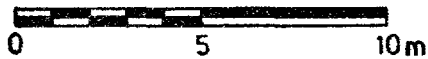
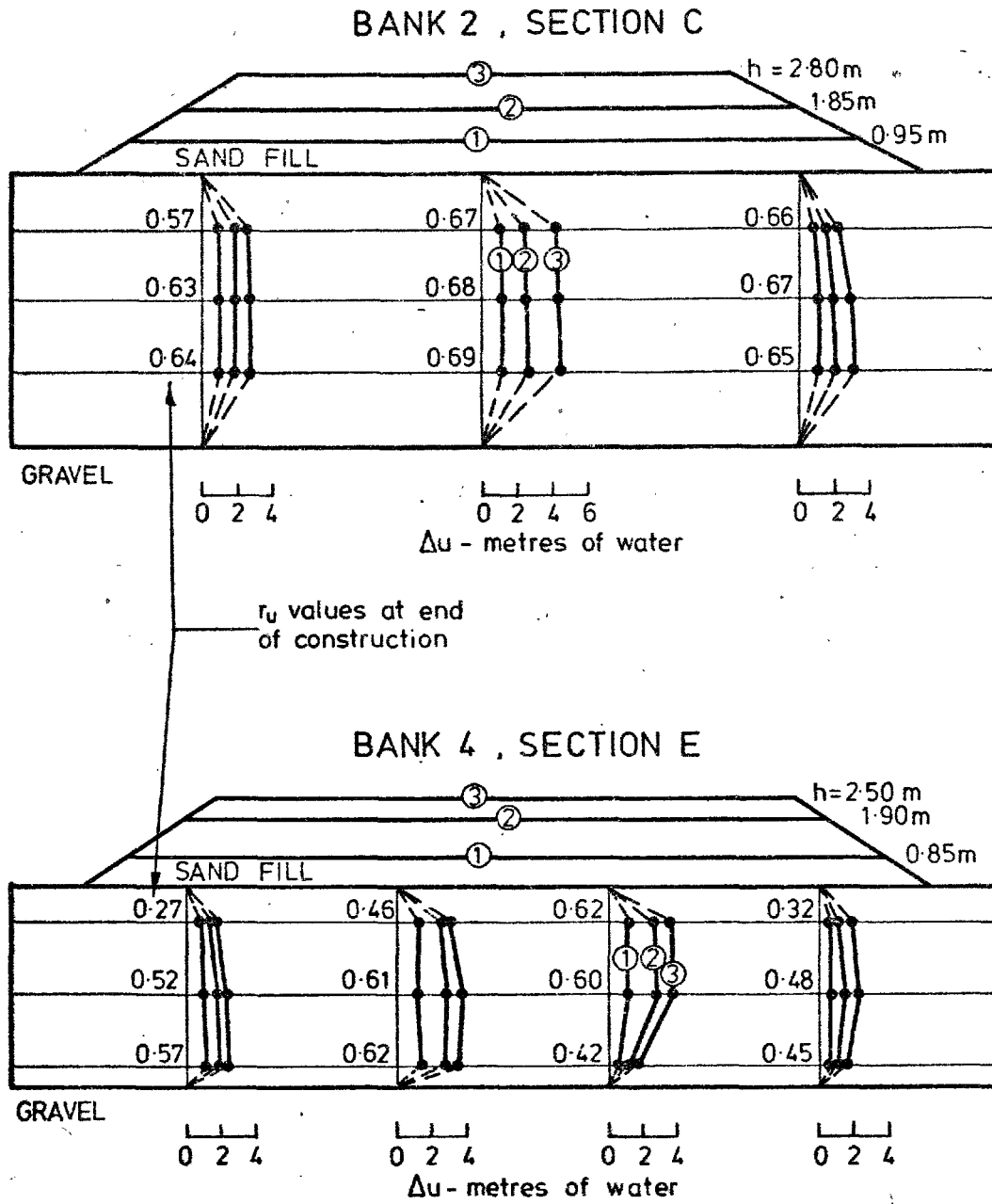


BANK 4, SECTION E

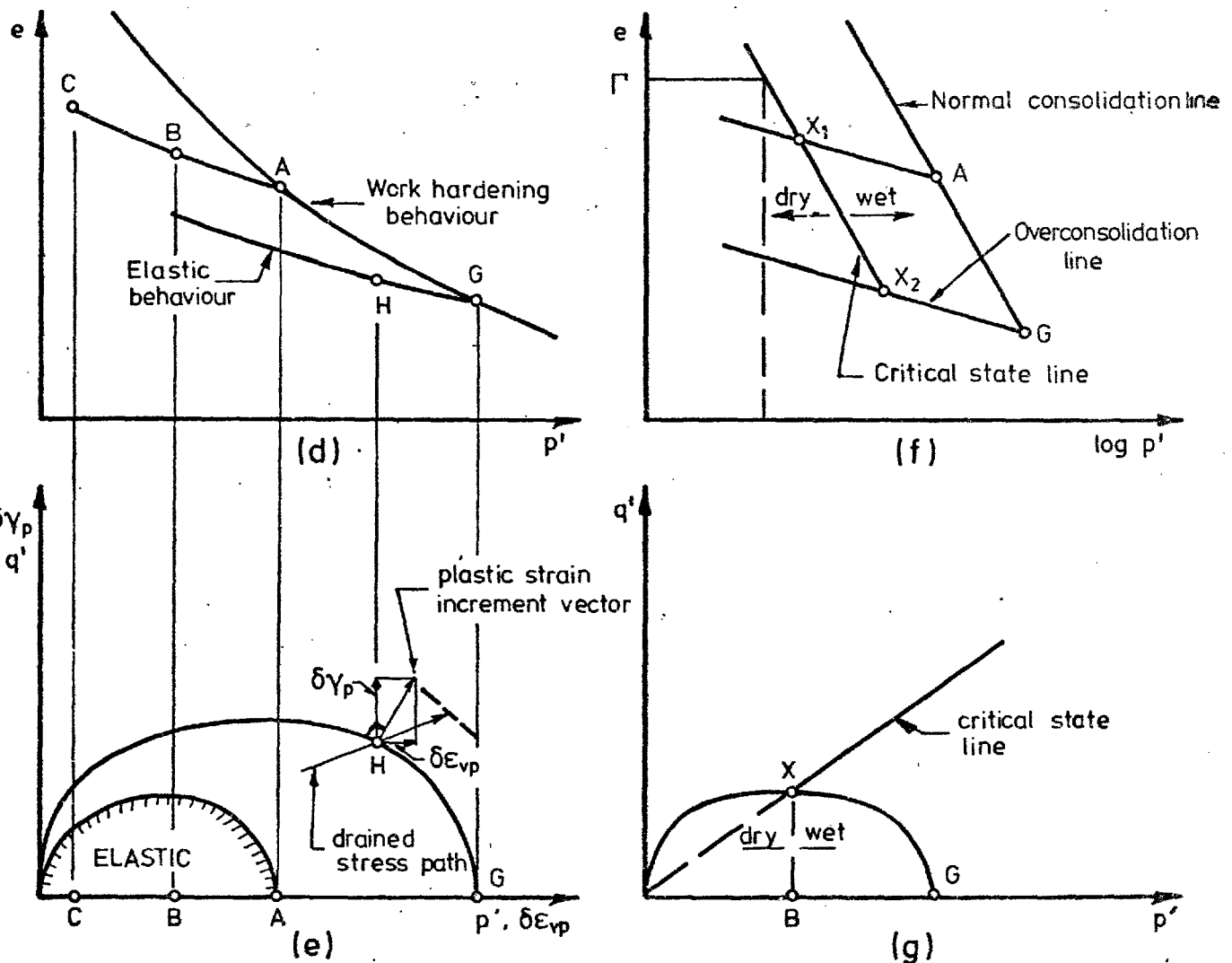
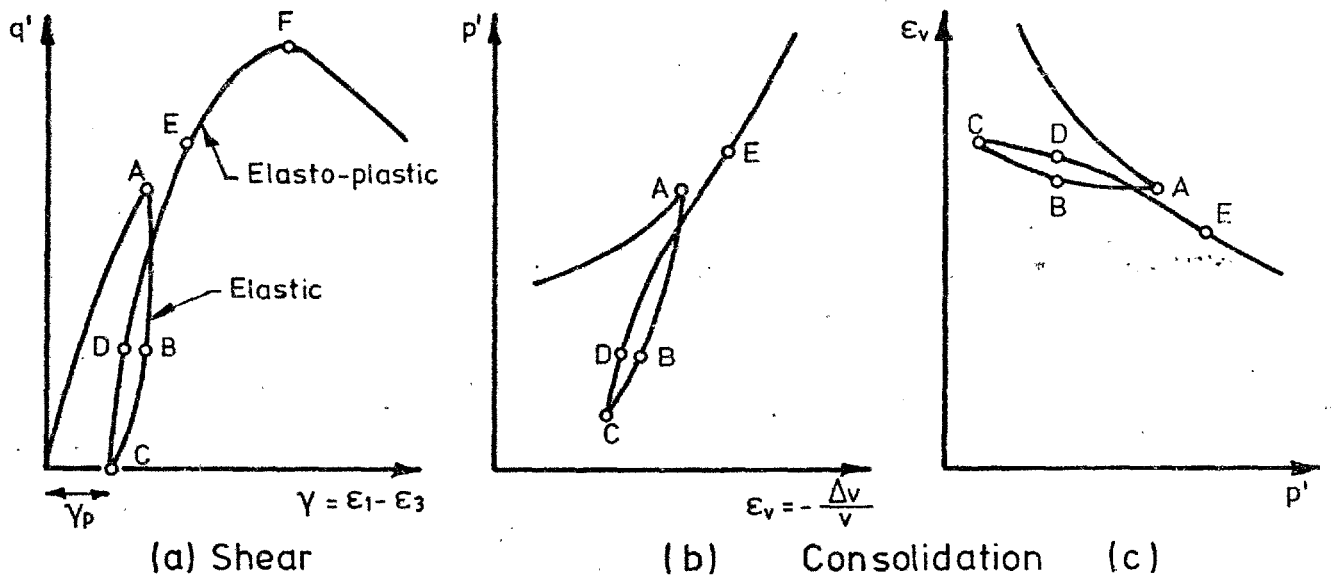


BANK 2 AND BANK 4

EXCESS PORE-WATER PRESSURE VERSUS FILL HEIGHT

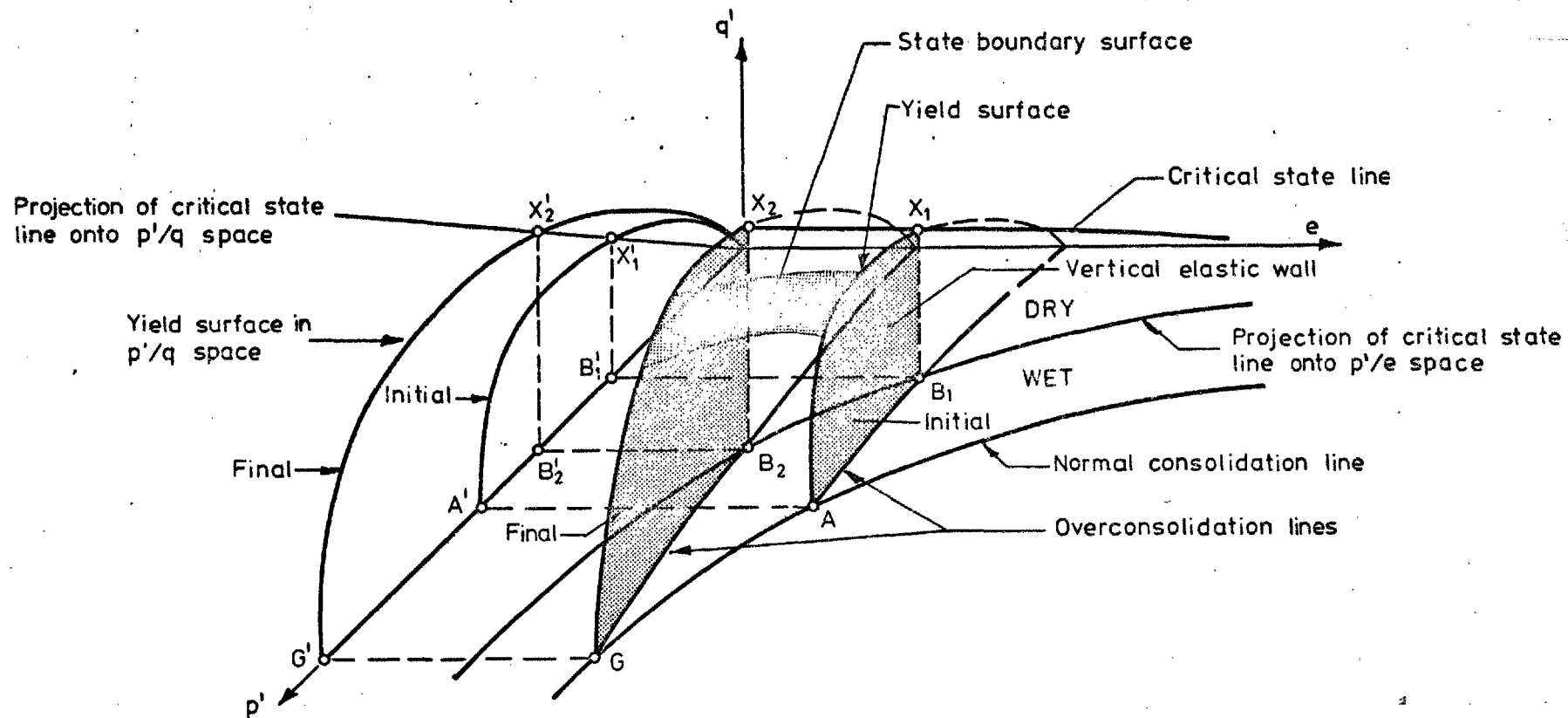


BANK 2 AND BANK 4
EXCESS PORE-WATER PRESSURES

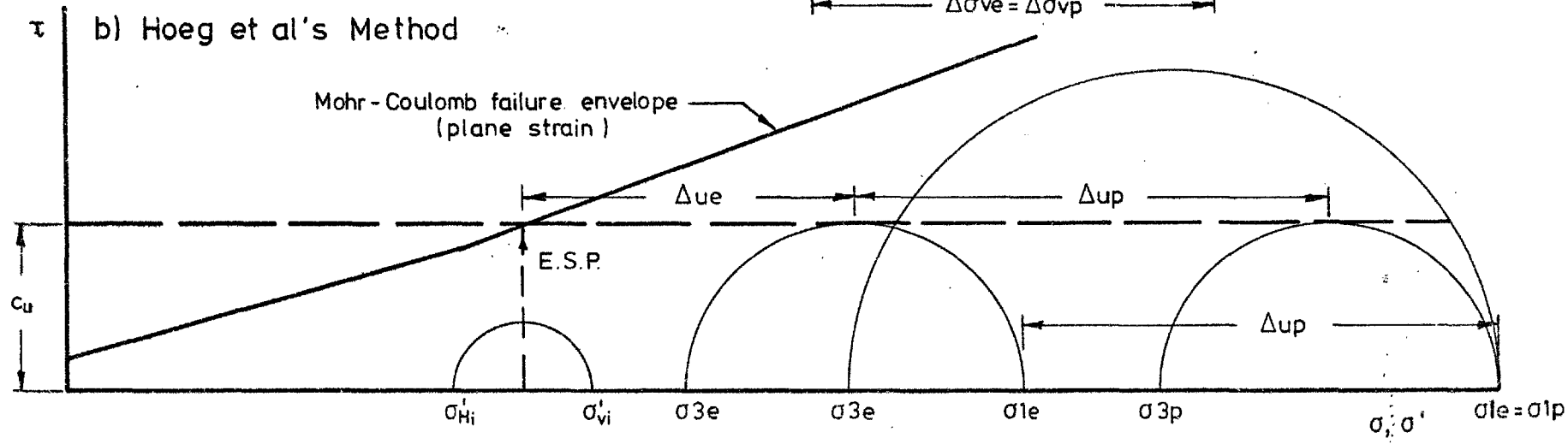
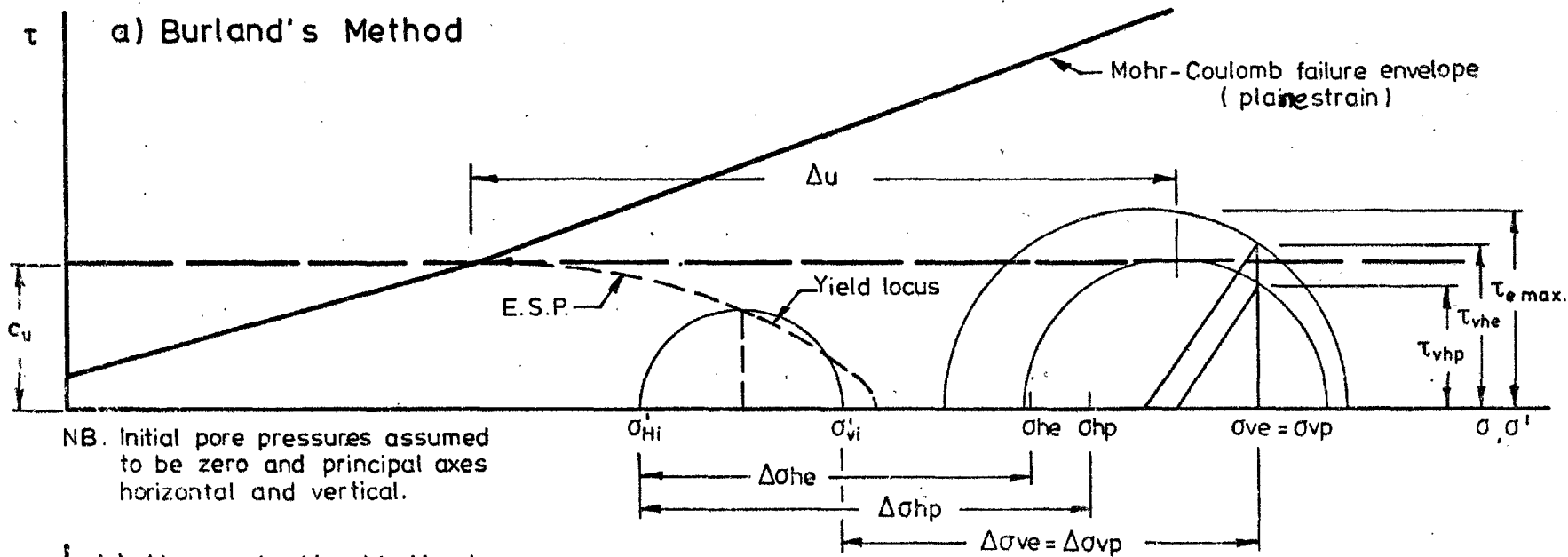


Variation of yield surface with consolidation history

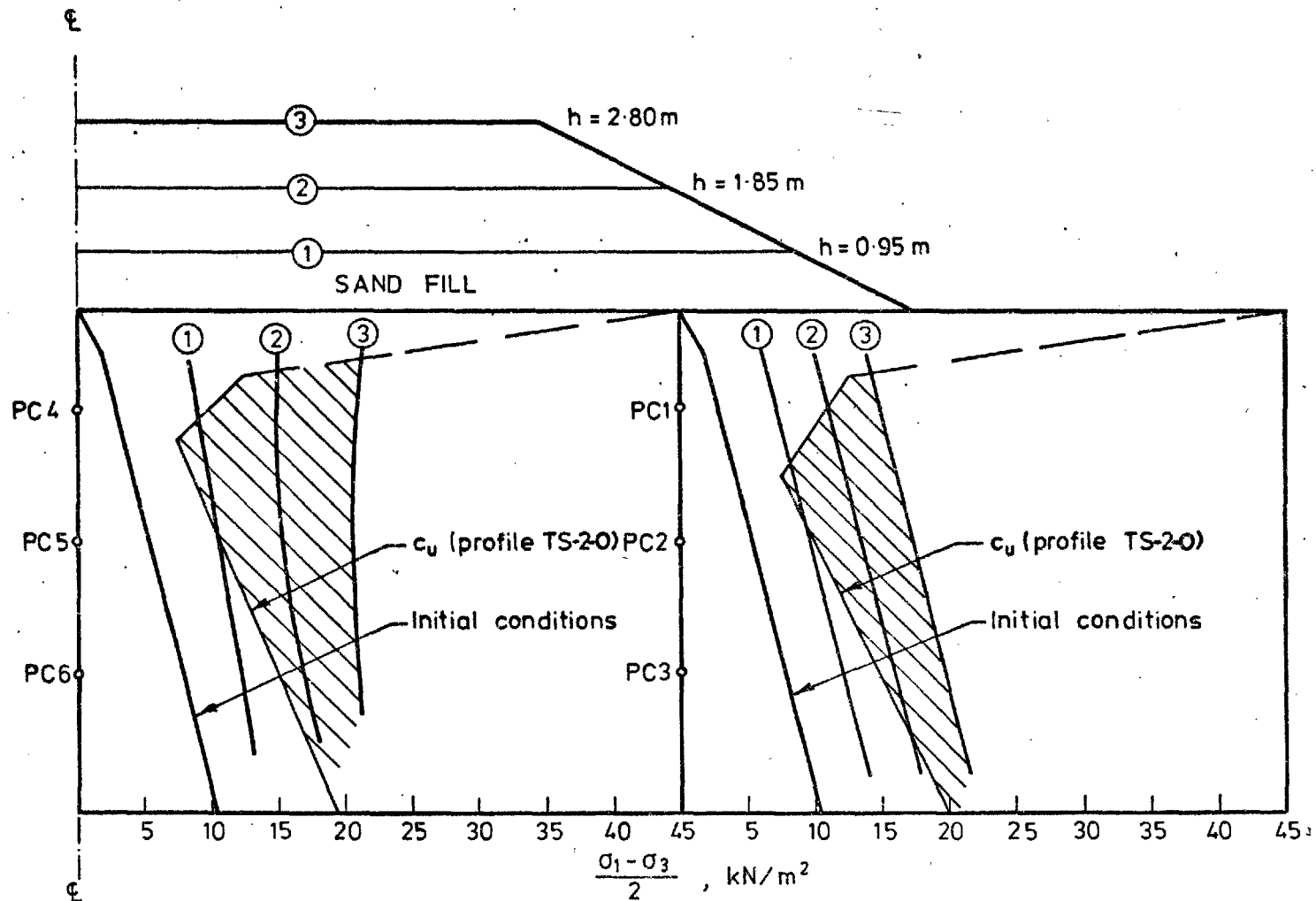
FUNDAMENTALS OF CRITICAL STATE SOIL MECHANICS AS INCORPORATED IN THE ELASTO-PLASTIC CAM CLAY SOIL MODEL (based on Wroth, 1976)



ELASTO-PLASTIC CAM CLAY SOIL MODEL
 SCHEMATIC REPRESENTATION OF STATE BOUNDARY SURFACE
 (based on Roscoe and Burland, 1968)

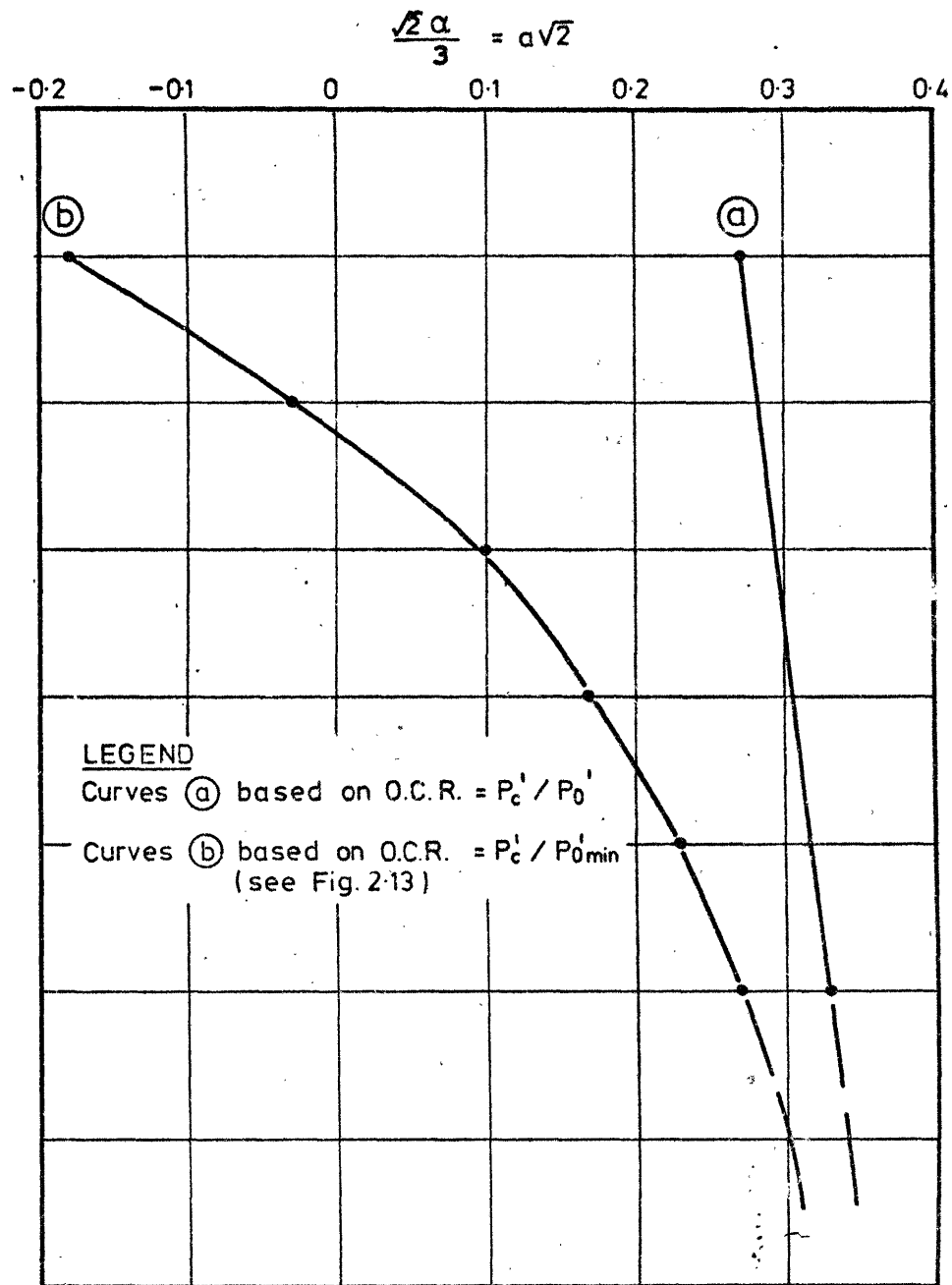
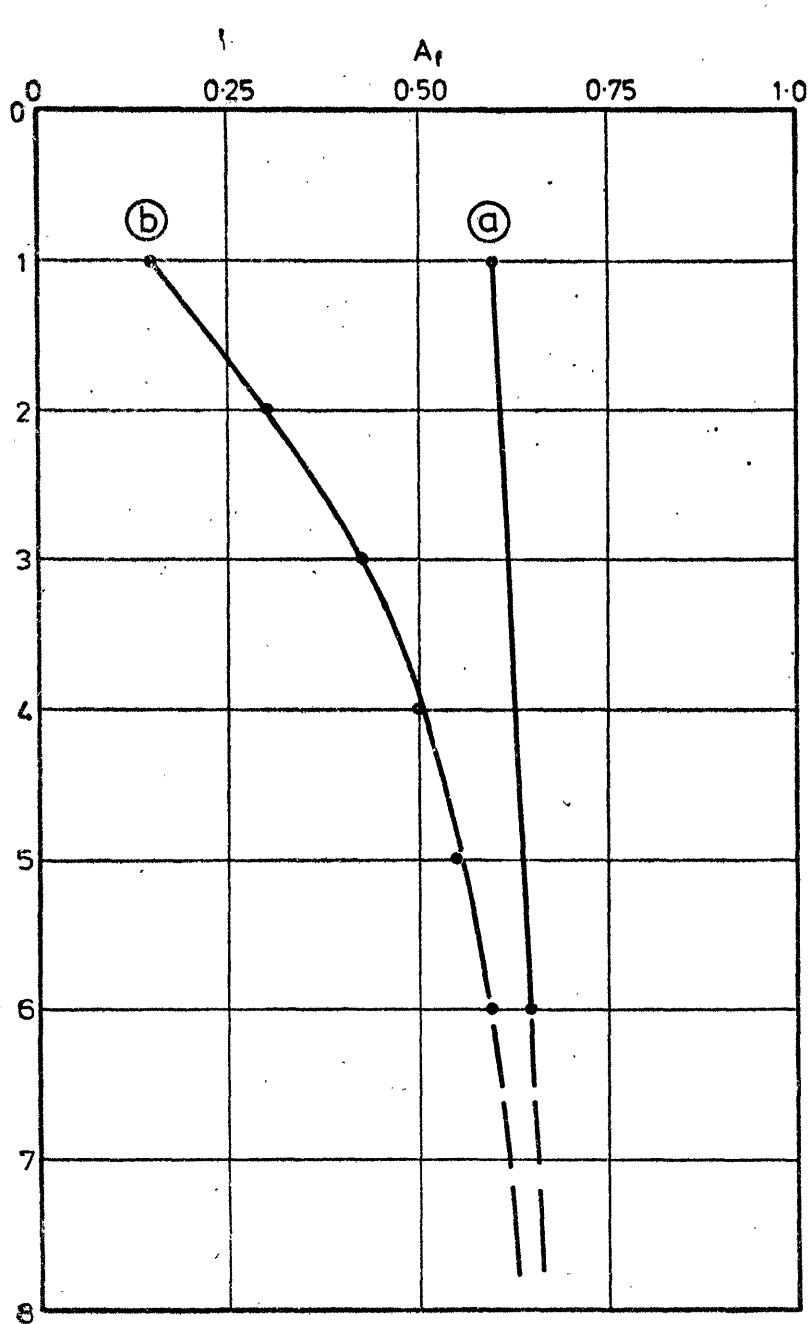


METHODS USED TO ESTIMATE PLASTIC STRESS CHANGES AND THE ASSOCIATED PORE-PRESSURE CHANGES

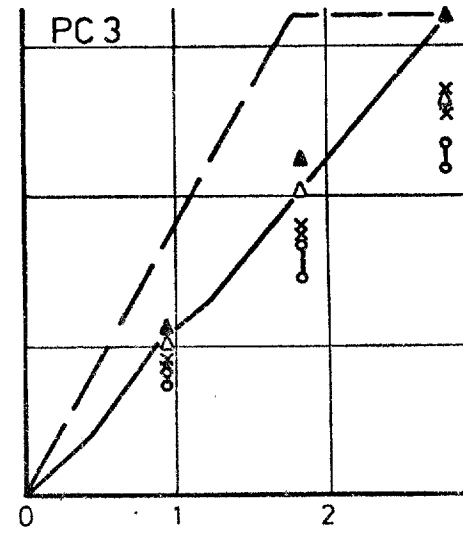
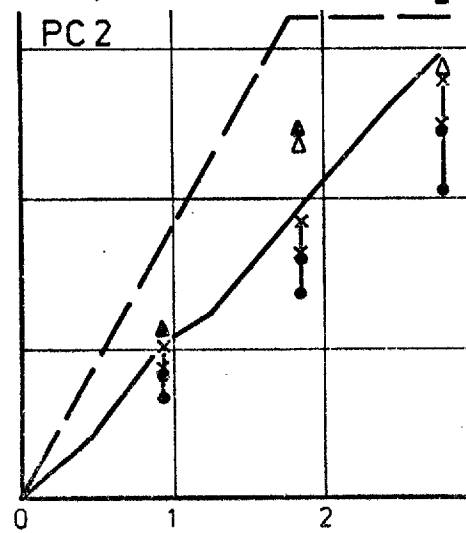
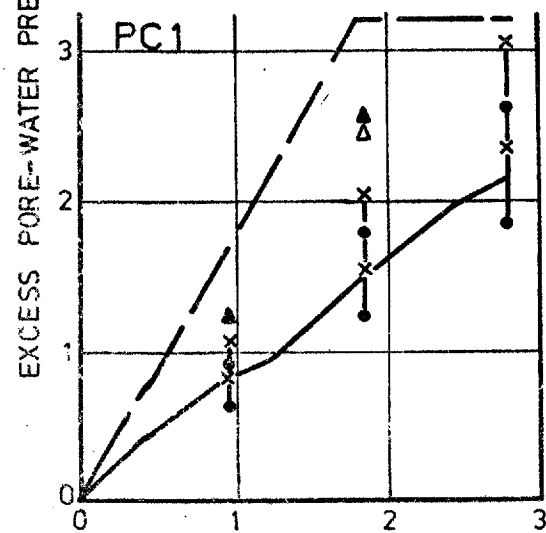
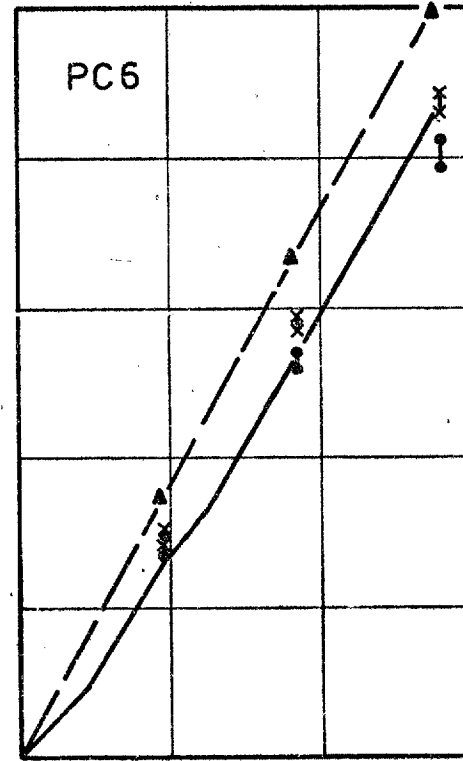
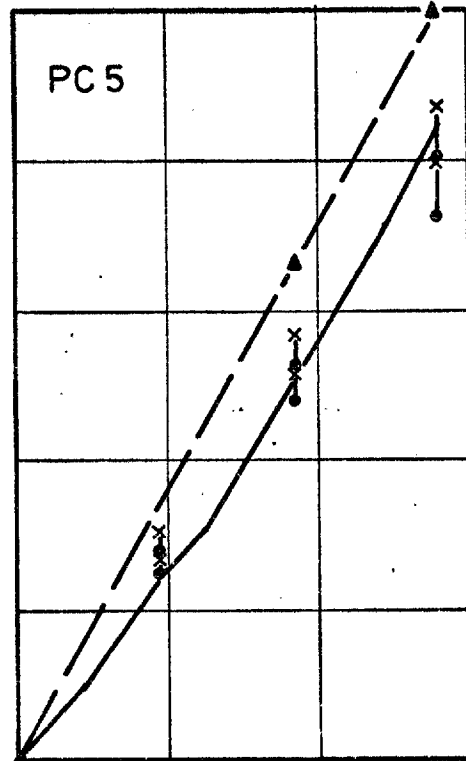
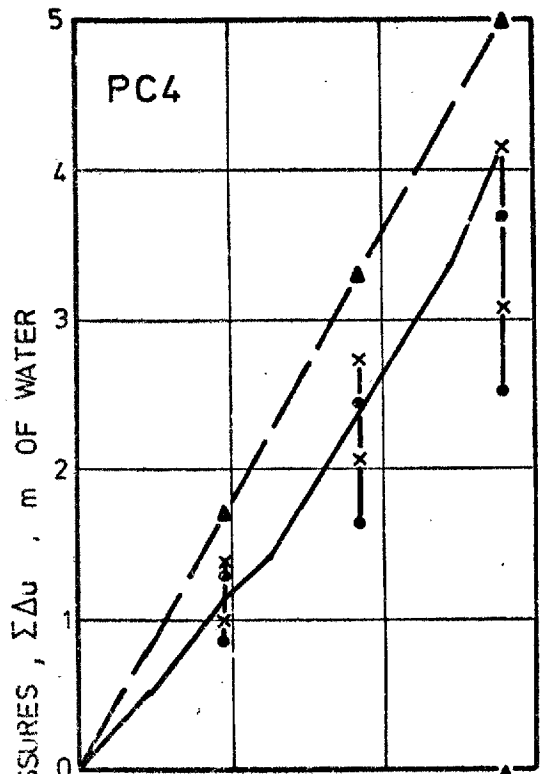


BANK 2

MAXIMUM SHEAR STRESSES AT PIEZOMETER LOCATIONS AS PREDICTED USING ELASTIC THEORY - $K_0 = 0.55$, $\nu = 0.3$.



THE PORE-PRESSURE PARAMETERS A_f , α and a .



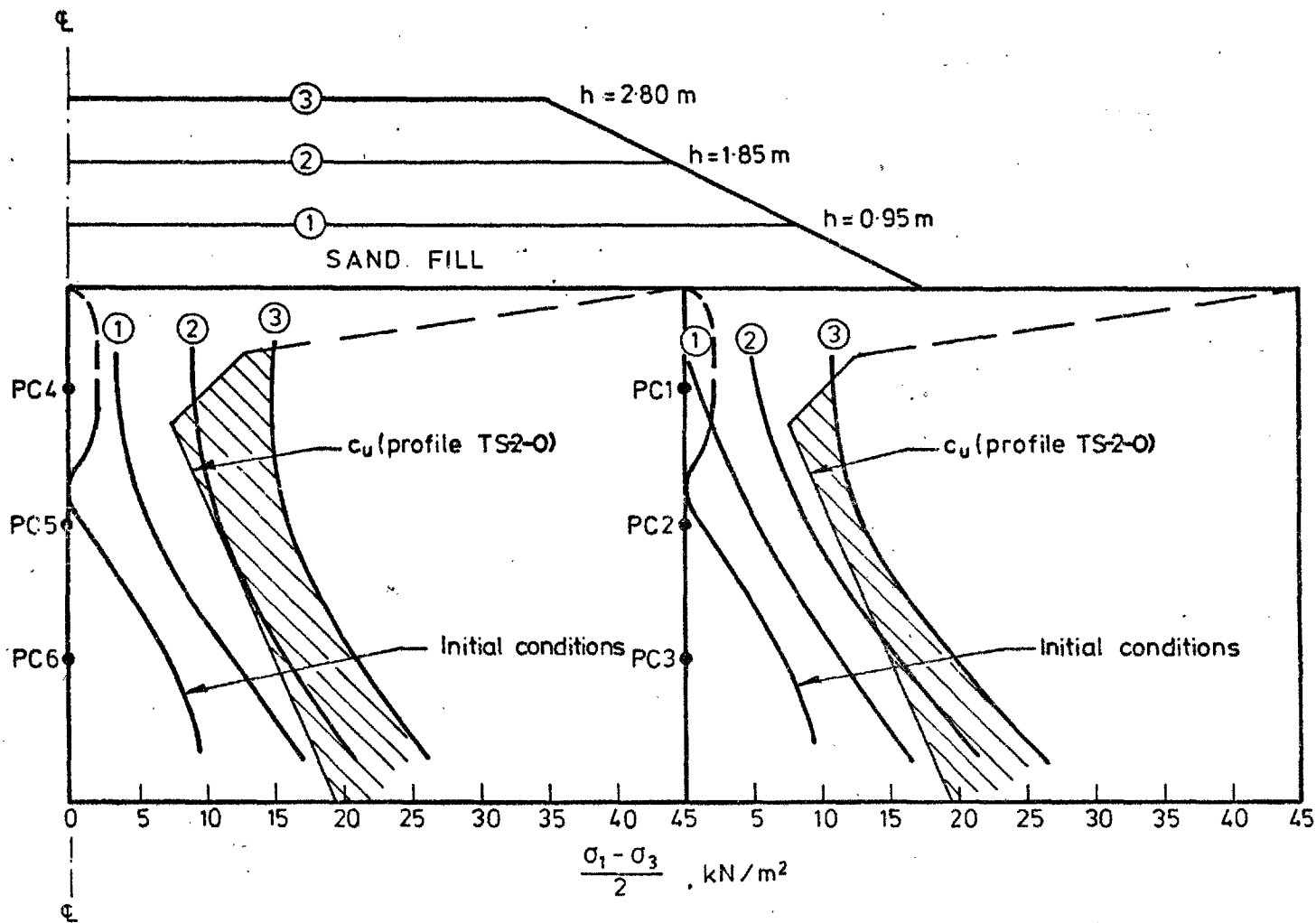
LEGEND

- Observed pore pressures
- - - $\Sigma \Delta u \equiv \gamma h$
- △ $\Delta u = \Delta \sigma_v$
- ▲ $\Delta u = \Delta \sigma_1$
- a ○ $\Delta u = \Delta \sigma_3 A_f (\Delta \sigma_1 - \Delta \sigma_3)$
- b ○ $\Delta u = \frac{\Delta \sigma_1 + \Delta \sigma_3}{2} + \frac{\alpha}{\sqrt{2} \sqrt{3}} (\Delta \sigma_1 - \Delta \sigma_3)$
- a x
- b x

'a' and 'b' refer to values of A_f and α used, as per Fig. 6.1.29

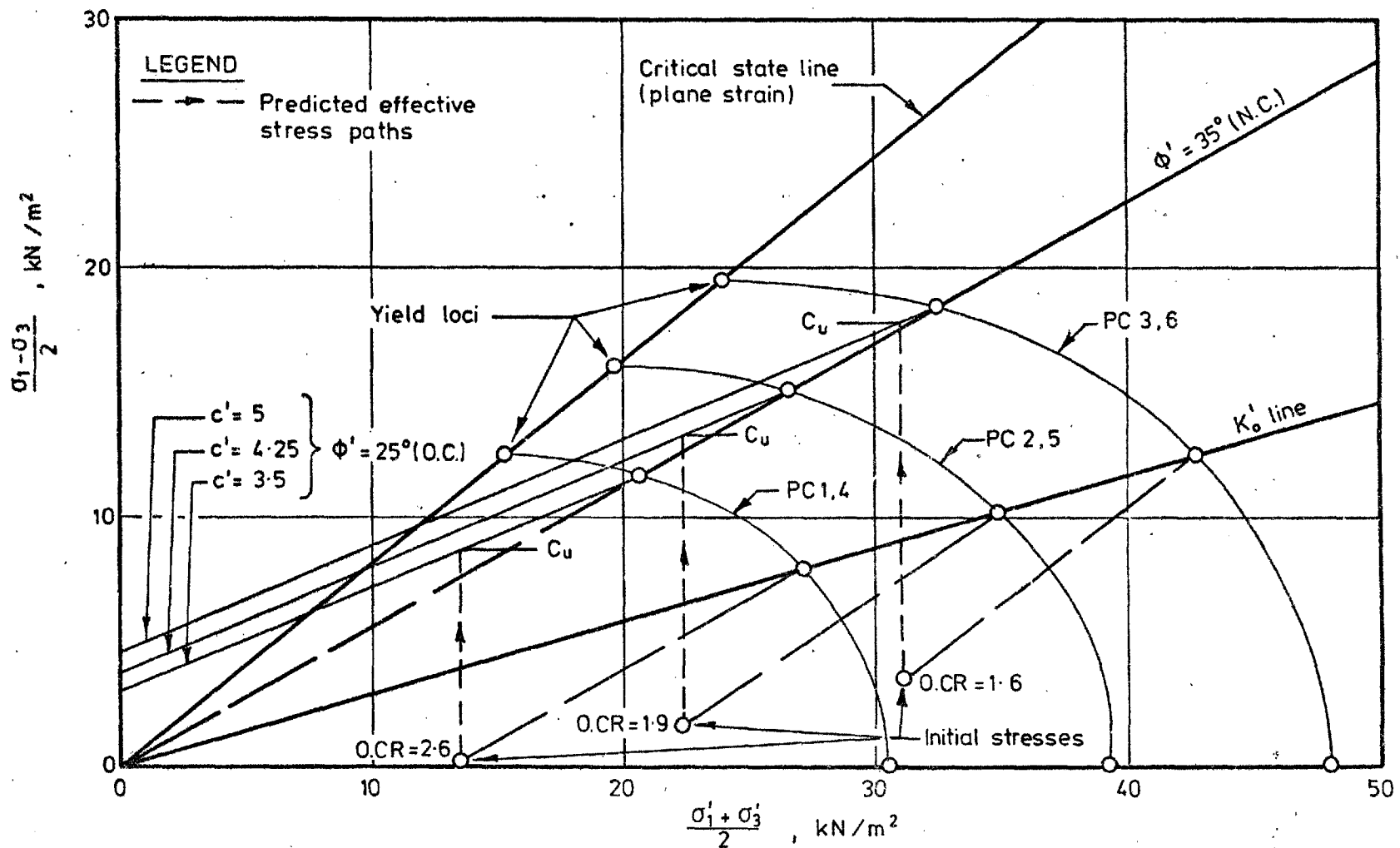
BANK 2 - COMPARISON

OF OBSERVED AND PREDICTED PORE PRESSURES



BANK 2

MAXIMUM SHEAR STRESSES AT PIEZOMETER LOCATIONS AS PREDICTED USING ELASTIC THEORY - K_0 DECREASING WITH DEPTH, $\nu = 0.3$.

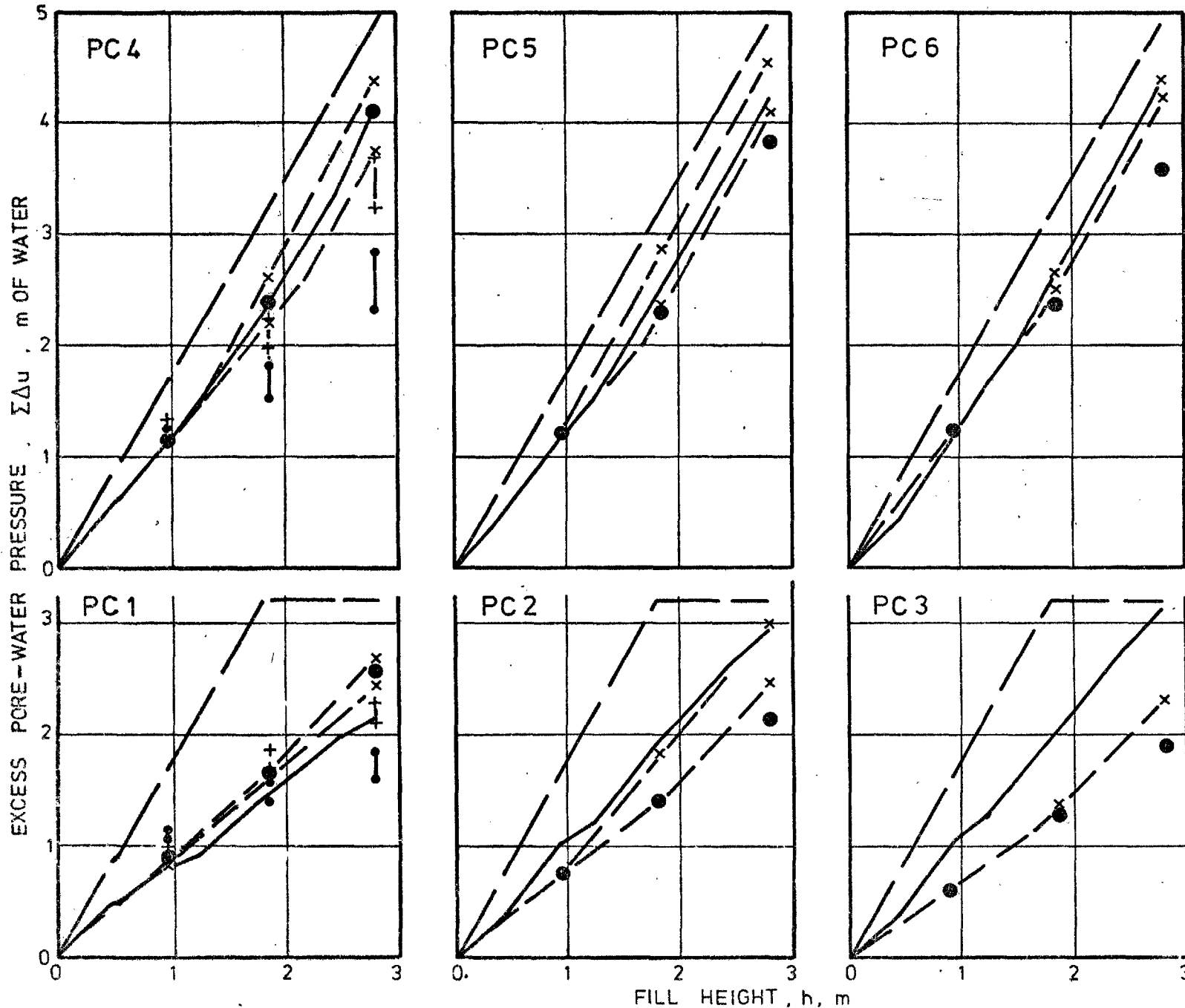


BANK 2

PREDICTION OF PORE-WATER PRESSURES USING MODIFIED CAM CLAY MODEL

Fig. 6.132

-675-



LEGEND

- Observed pore pressures
- $\Sigma\Delta u = \gamma h$
- $\Delta u = \frac{\Delta\sigma_1 + \Delta\sigma_3}{2}$ (elastic)
- $\Delta u = \frac{\Delta\sigma_1 + \Delta\sigma_3}{2} + \Delta\sigma_1$ (plastic)

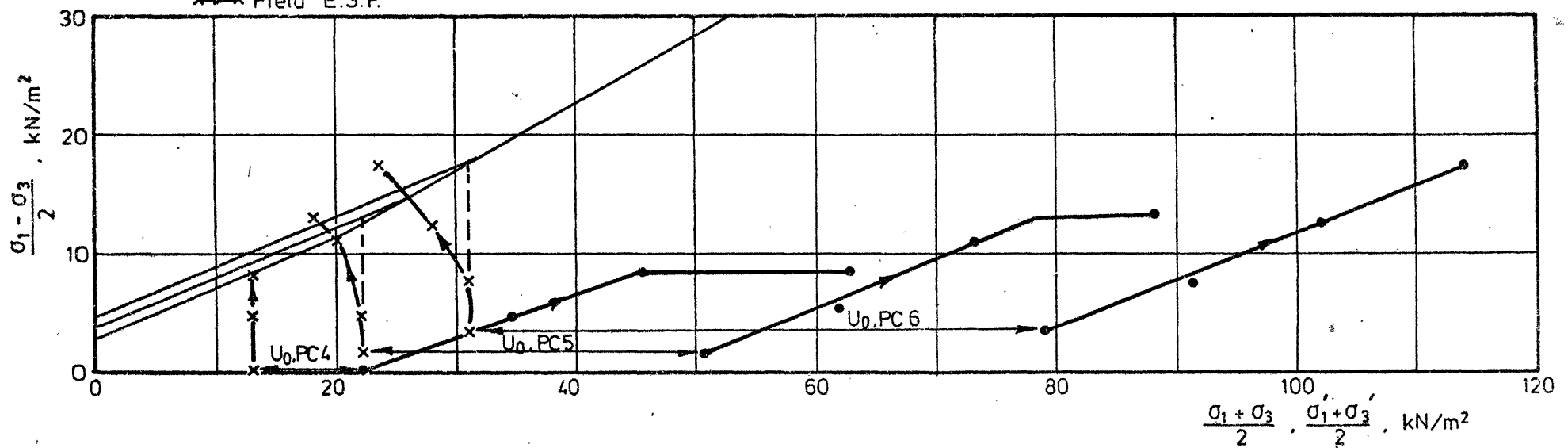
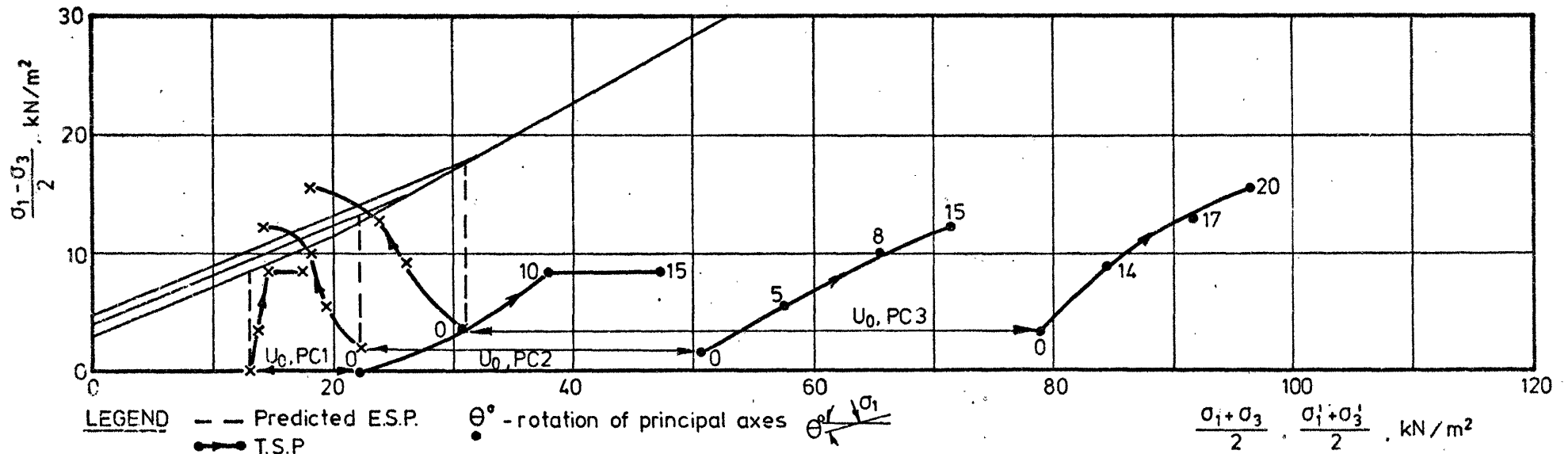
(max. values correspond to $K_0 = 0.55$, min. values to K_0 decreasing with depth)

- Modified cam clay model
- a | b | $\Delta u = \Delta\sigma_3 + A_f (\Delta\sigma_1 - \Delta\sigma_3)$
- a | b | $\Delta u = \frac{\Delta\sigma_1 + \Delta\sigma_3}{2} + \frac{\alpha}{\sqrt{2}\sqrt{3}} (\Delta\sigma_1 - \Delta\sigma_3)$

'a' and 'b' refer to values of A_f and α used, as per Fig. 6.1. 29.

BANK 2 - COMPARISON OF OBSERVED AND PREDICTED PORE PRESSURES

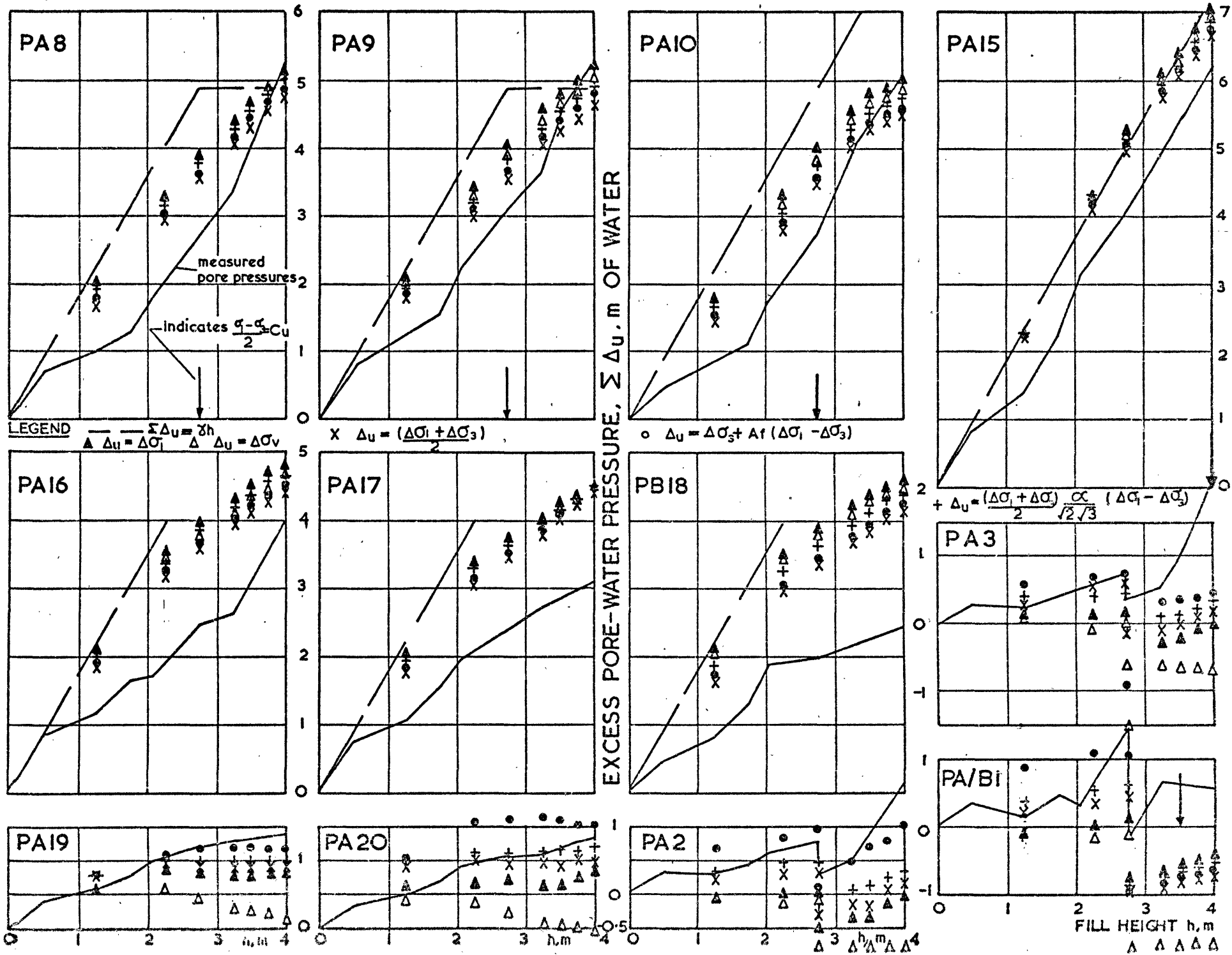
Fig. 6.1.33



BANK 2

COMPARISON OF EFFECTIVE STRESS PATHS PREDICTED BY MODIFIED CAM CLAY MODEL AND BASED ON MEASURED PORE-WATER PRESSURES

BANK 1, STAGE 1
COMPARISON OF OBSERVED AND PREDICTED PORE PRESSURES (K₀ = 0.55)



BANK I, STAGE 1
 COMPARISON OF OBSERVED AND PREDICTED PORE PRESSURES ($K_0=0.55$)

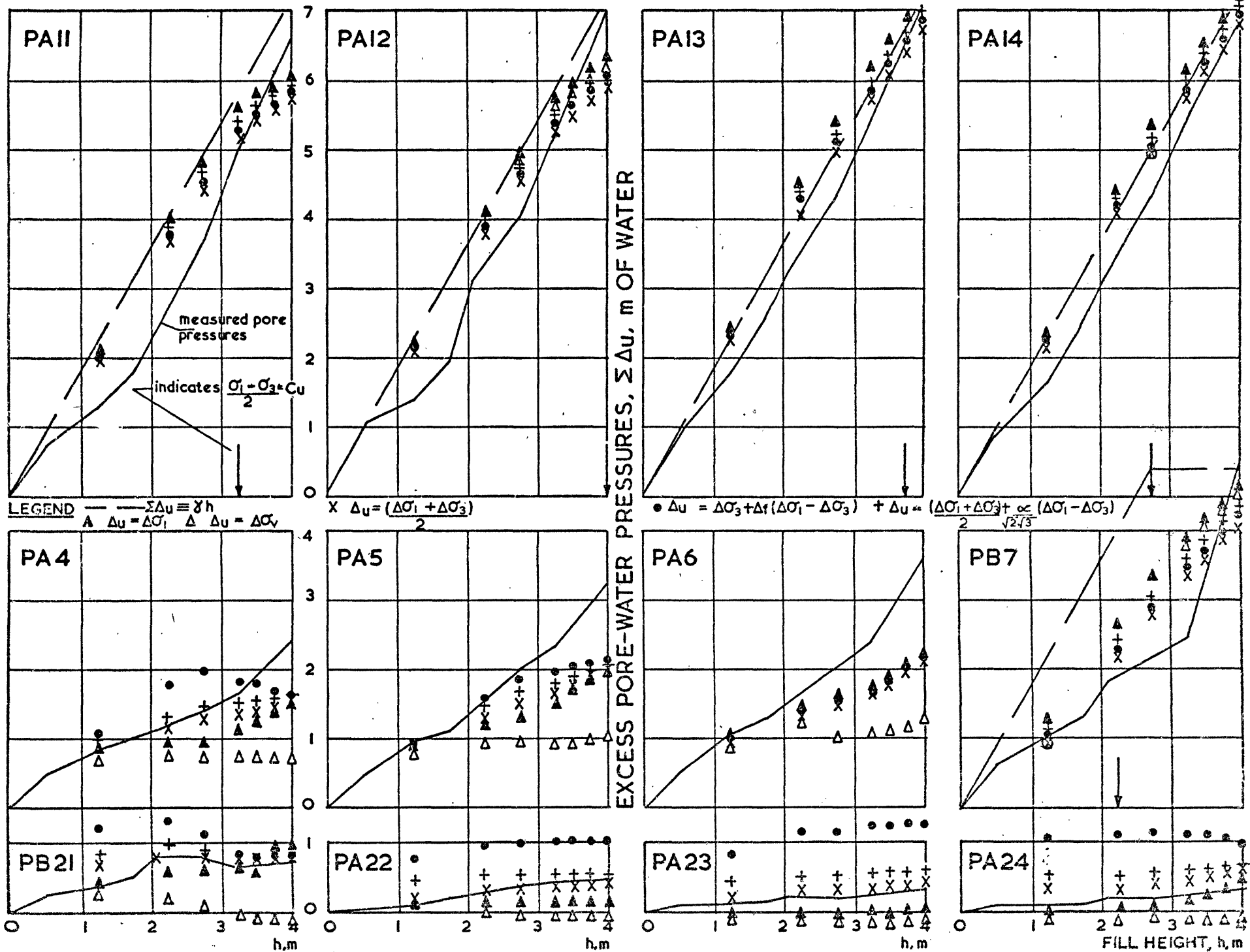


Fig. 6.1.36

BANK I, STAGE 1
INFLUENCE OF K_0 ON PREDICTED PORE PRESSURES

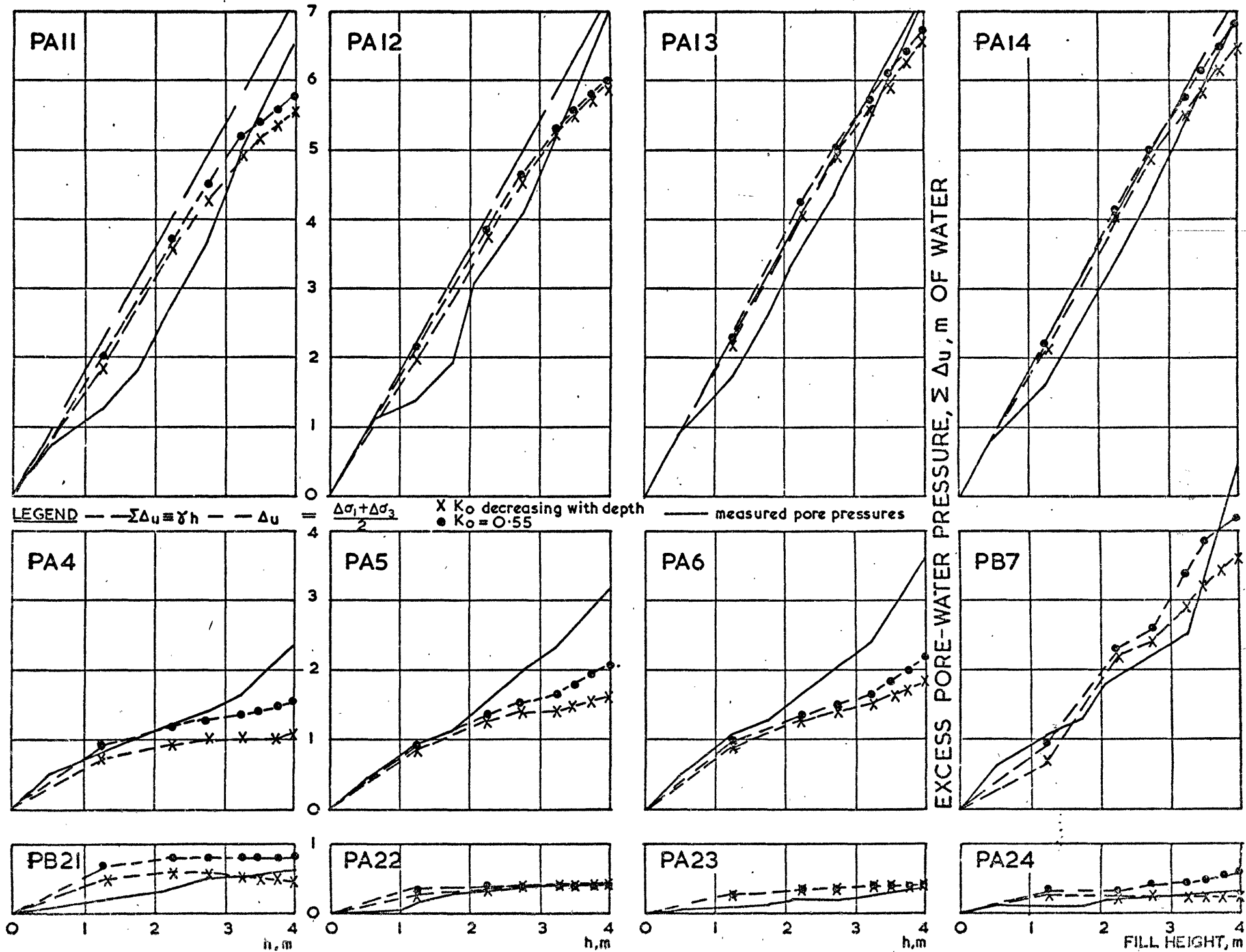


Fig 6.1.37

BANK I, STAGE I
 INFLUENCE OF K_0 ON PREDICTED PORE PRESSURES

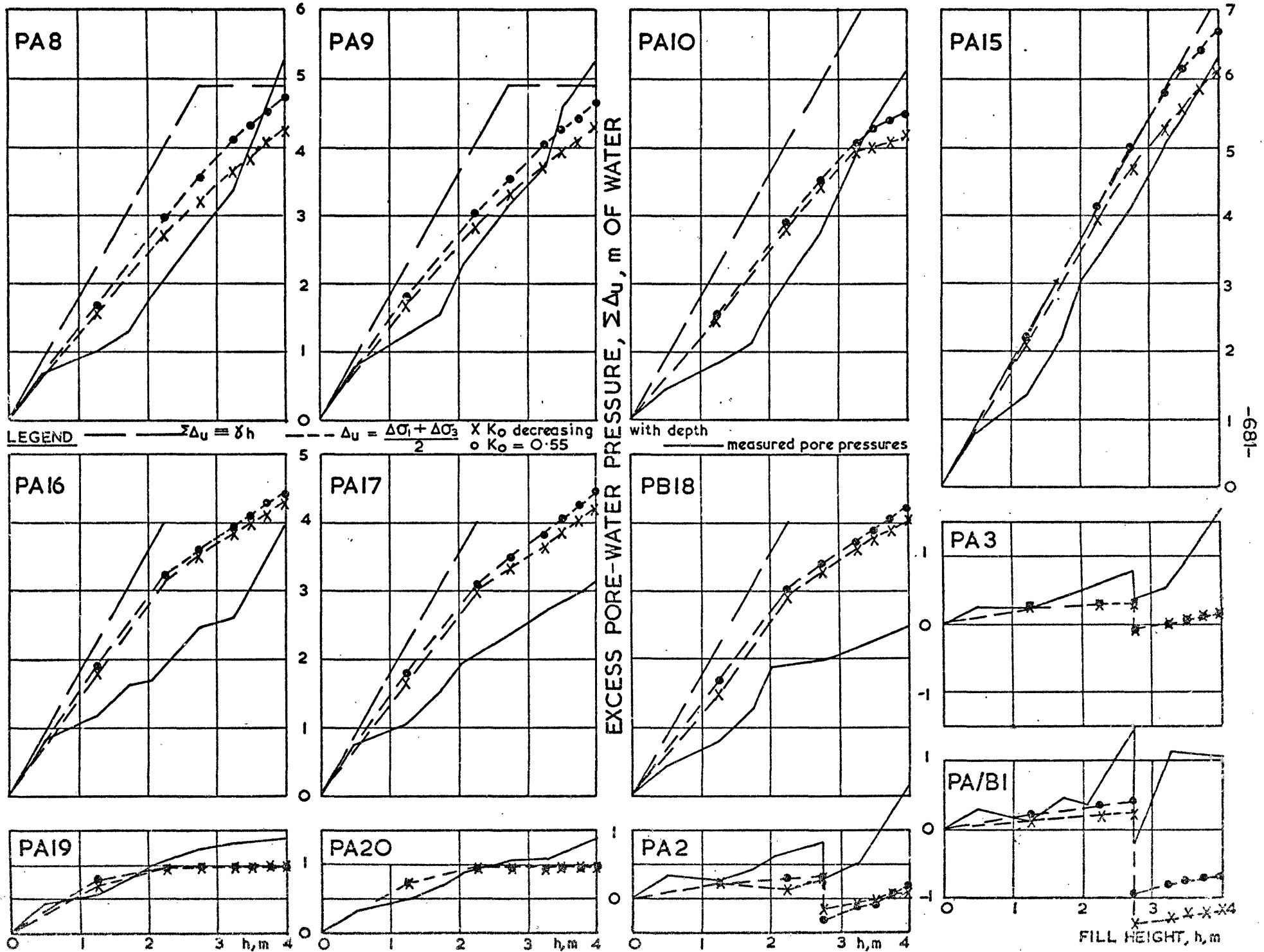
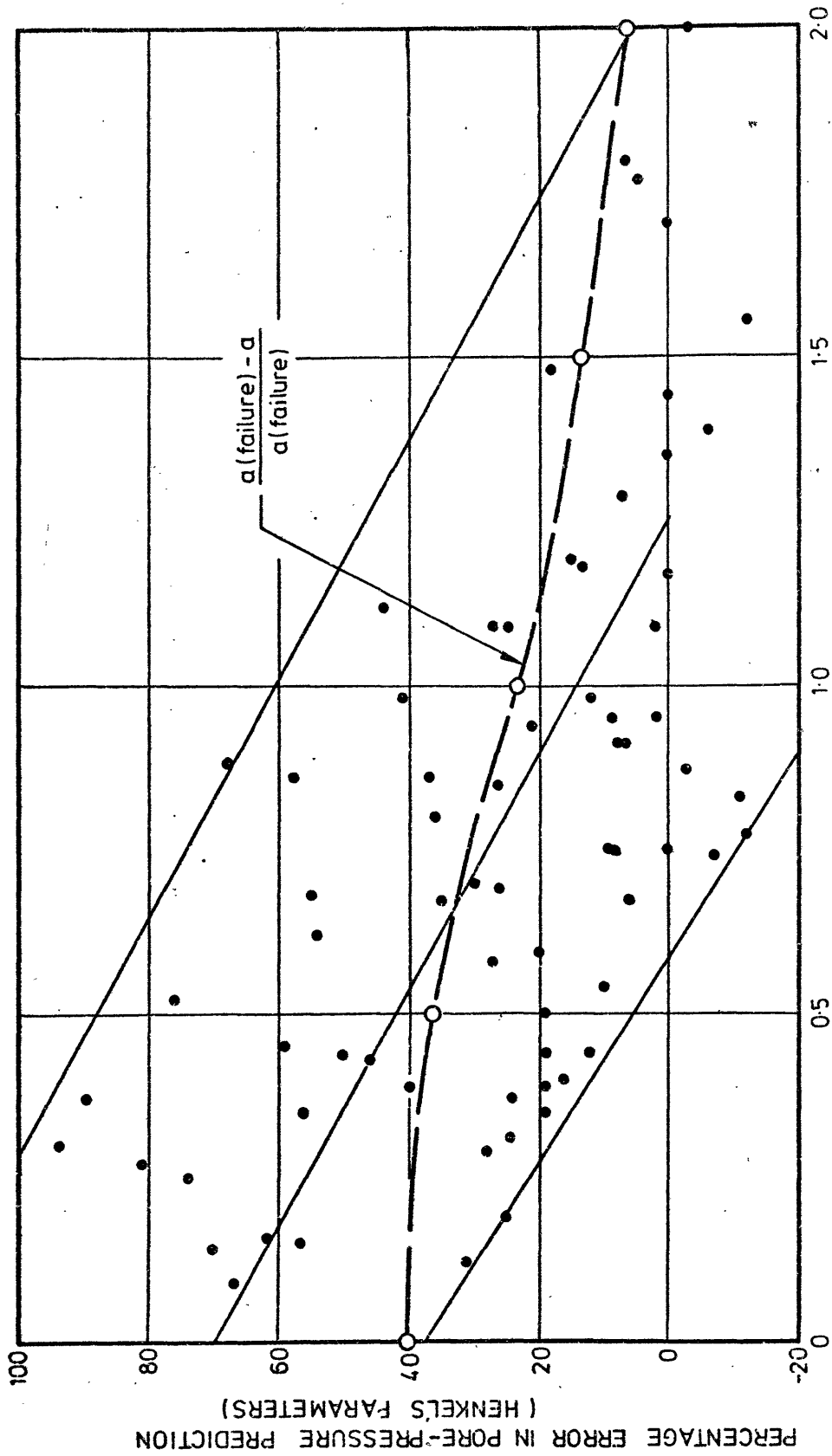
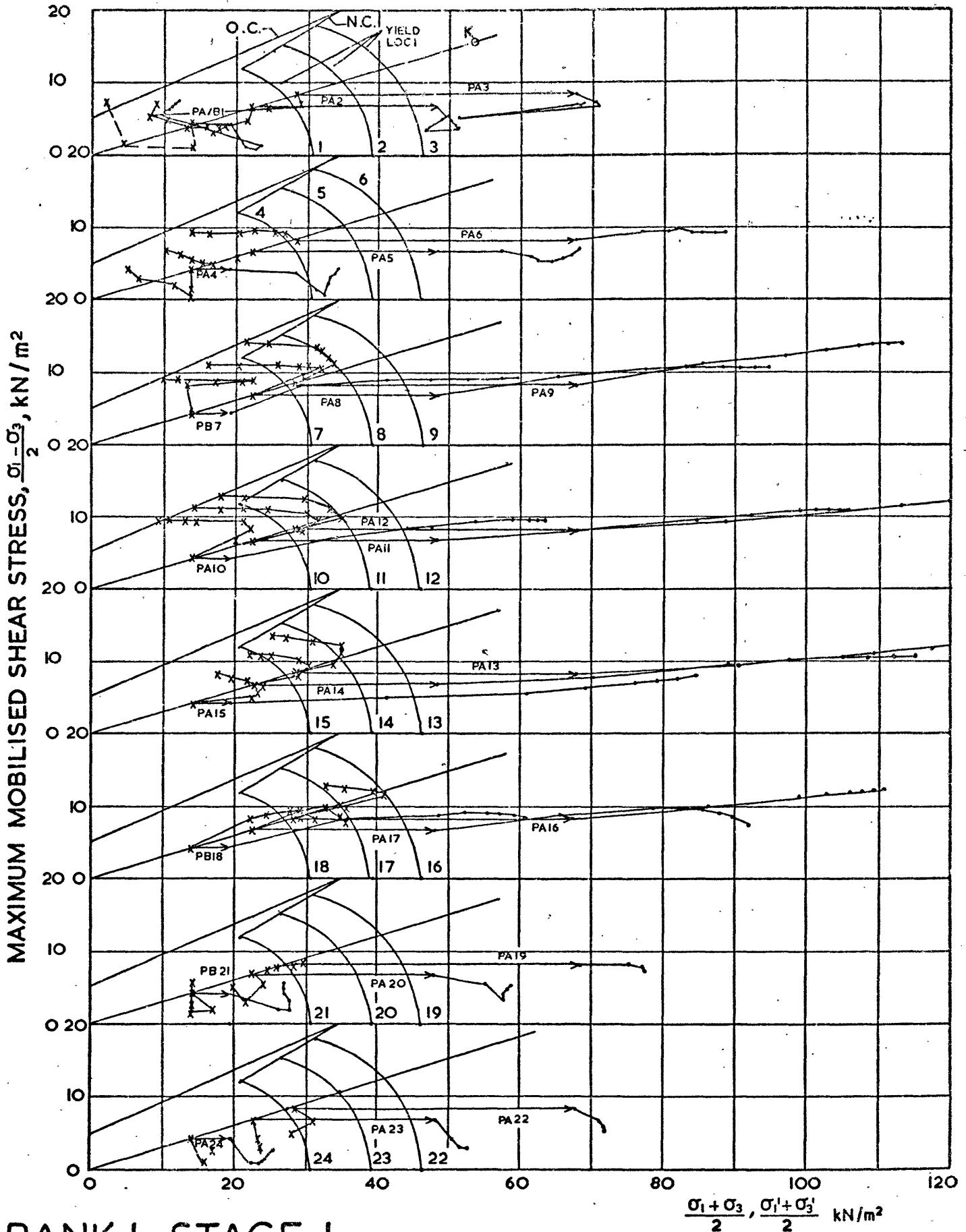


Fig. 6.1.38



INFLUENCE OF MAJOR PRINCIPAL STRAIN ON PORE-PRESSURE PREDICTION

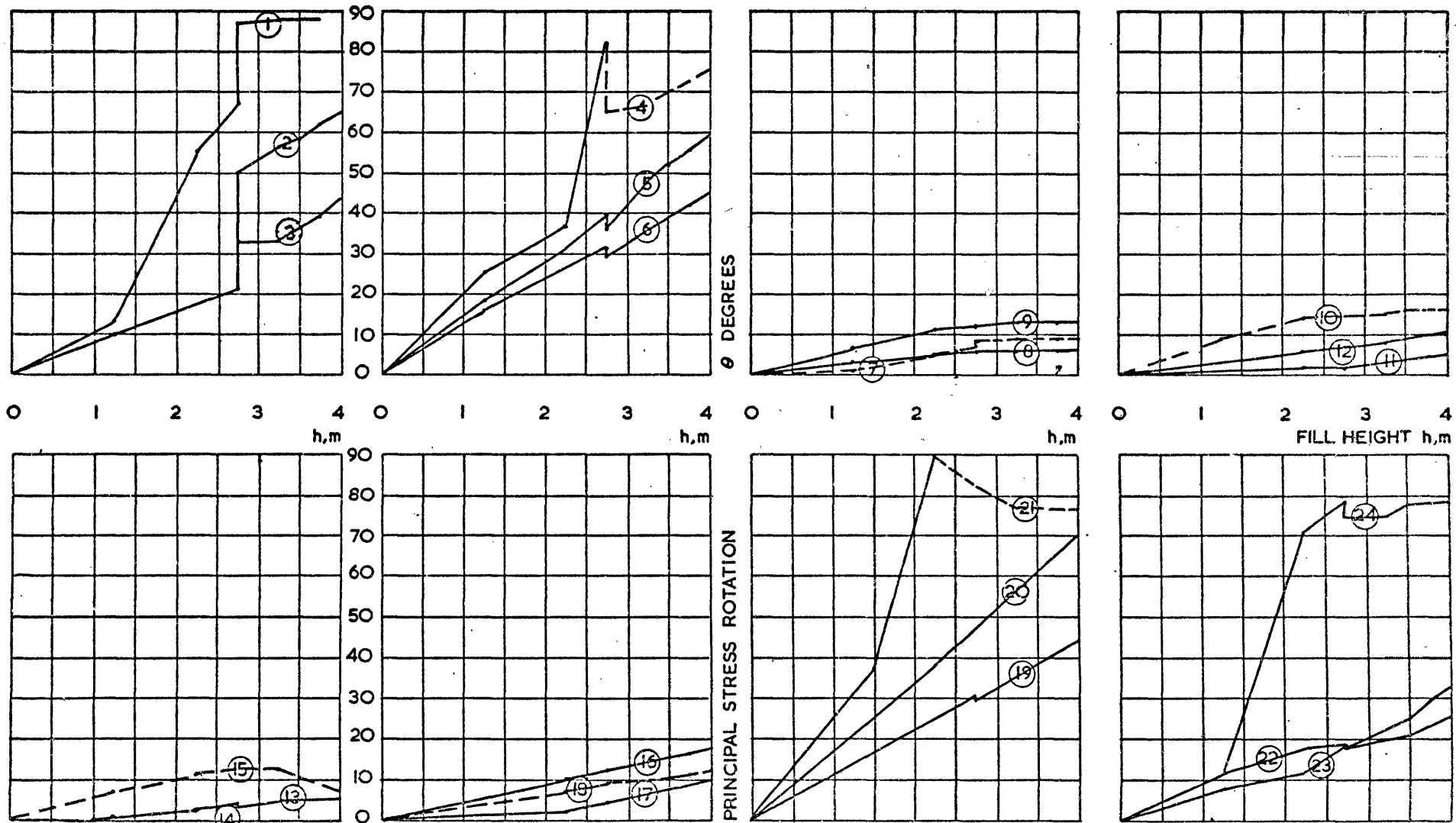
Fig. 5.1.39



BANK I, STAGE I
 FIELD STRESS PATHS ($k_0 = 0.55$)

LEGEND \times Initial Stresses \rightarrow ESP \rightarrow TSP

Fig. 6.1.40



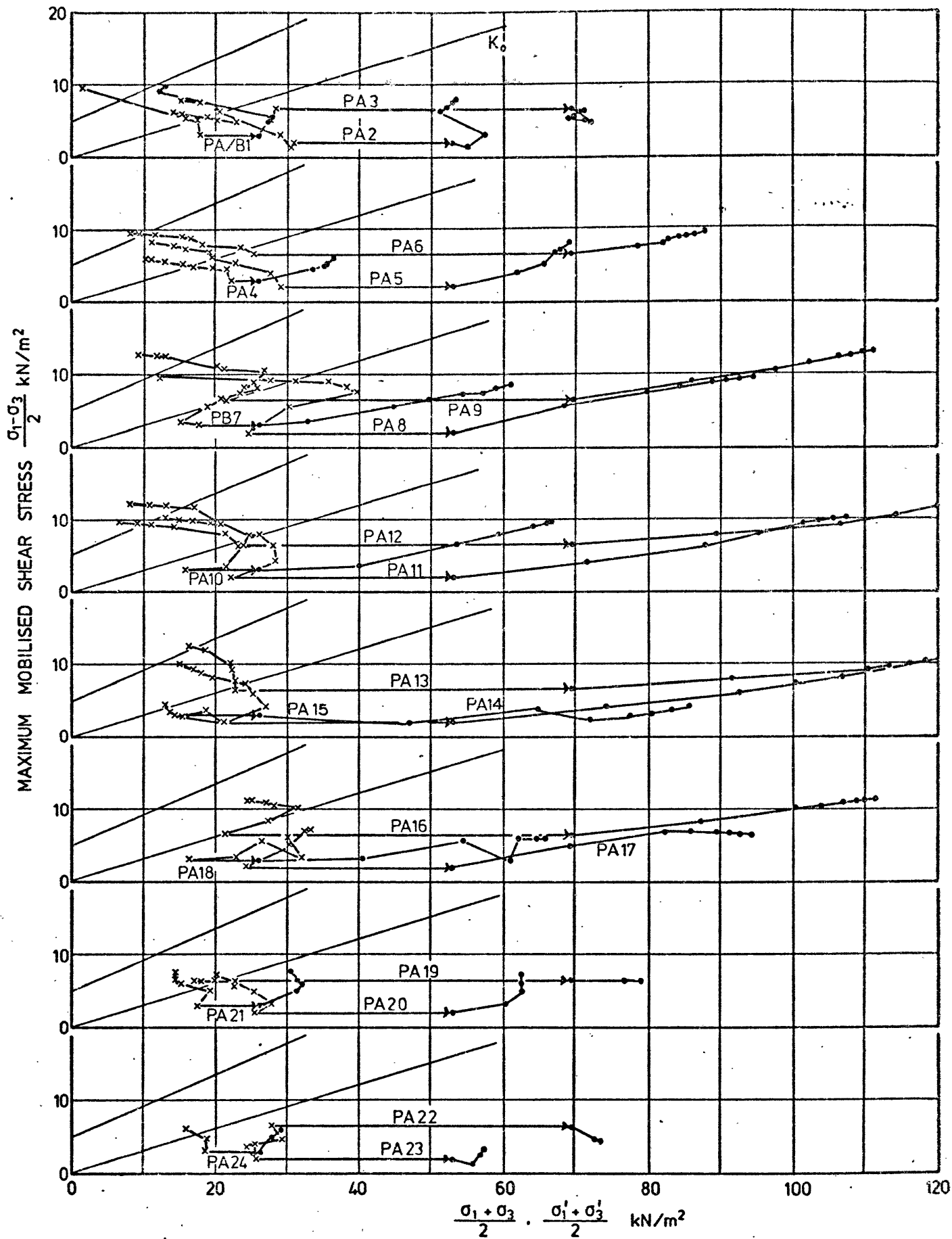
BANK I, STAGE I

ROTATION OF PRINCIPAL STRESS AXES AT PIEZOMETER LOCATIONS ($K_0=0.55$)



- | | | |
|-------|-------------------------|-------|
| — | θ anti-clockwise | 1-12 |
| — | clockwise | 13-24 |
| - - - | θ clockwise | 1-12 |
| - - - | anti-clockwise | 13-24 |

Fig. 6.1.41



LEGEND:
 x — Initial stresses — ESP
 ● — TSP

BANK 1, STAGE 1
FIELD STRESS PATHS ($K_0 = f(\text{depth})$)

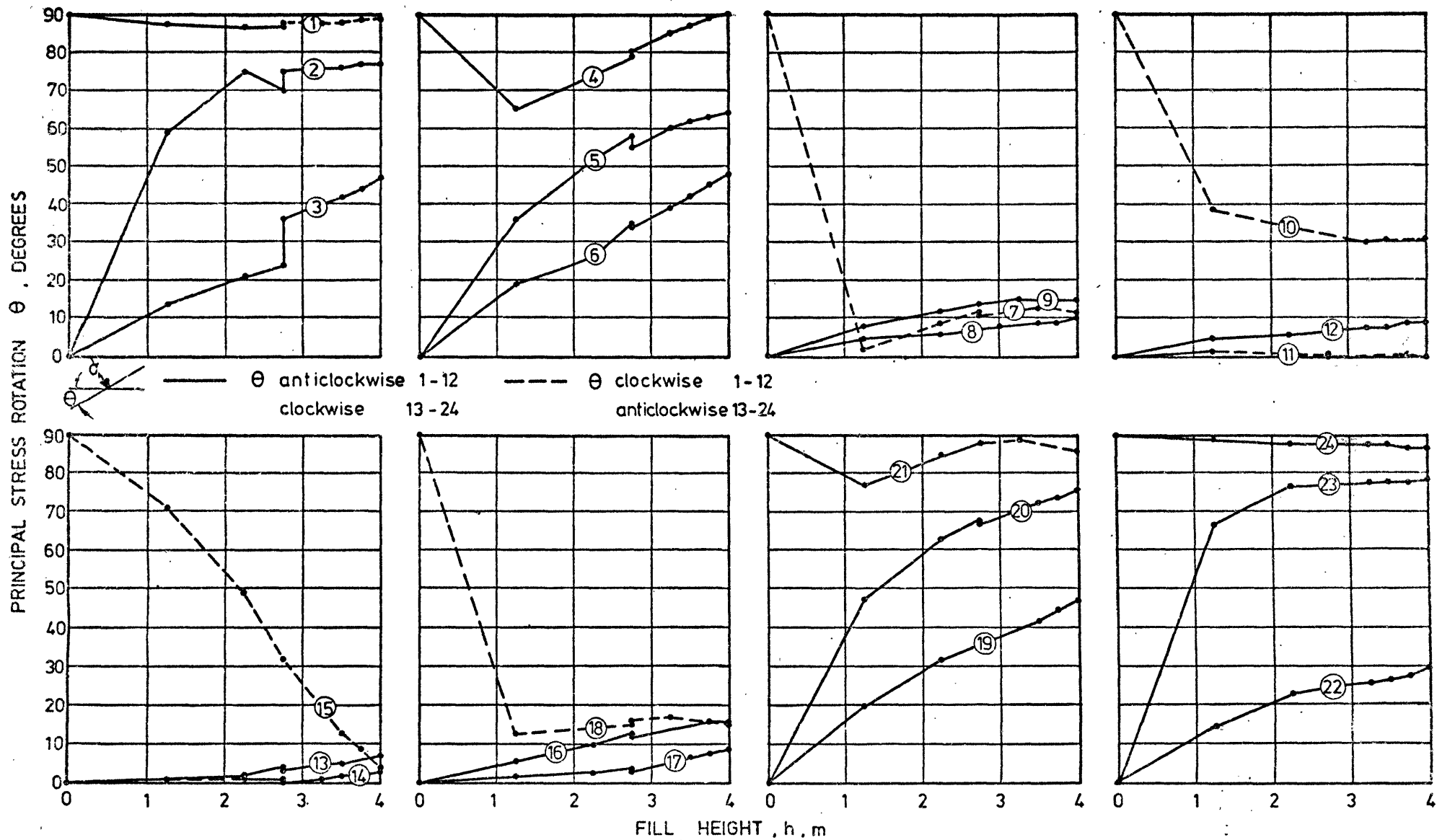
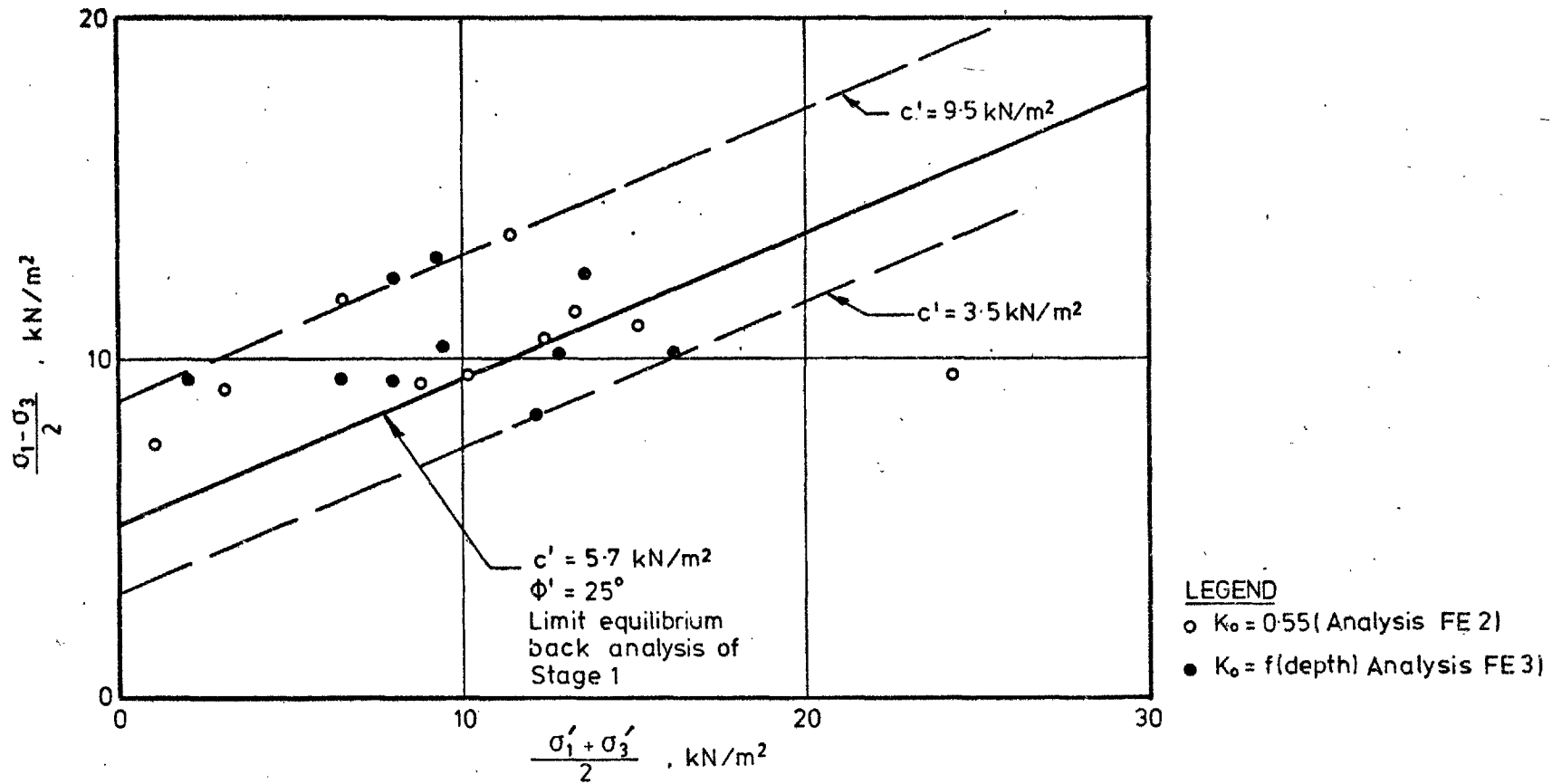


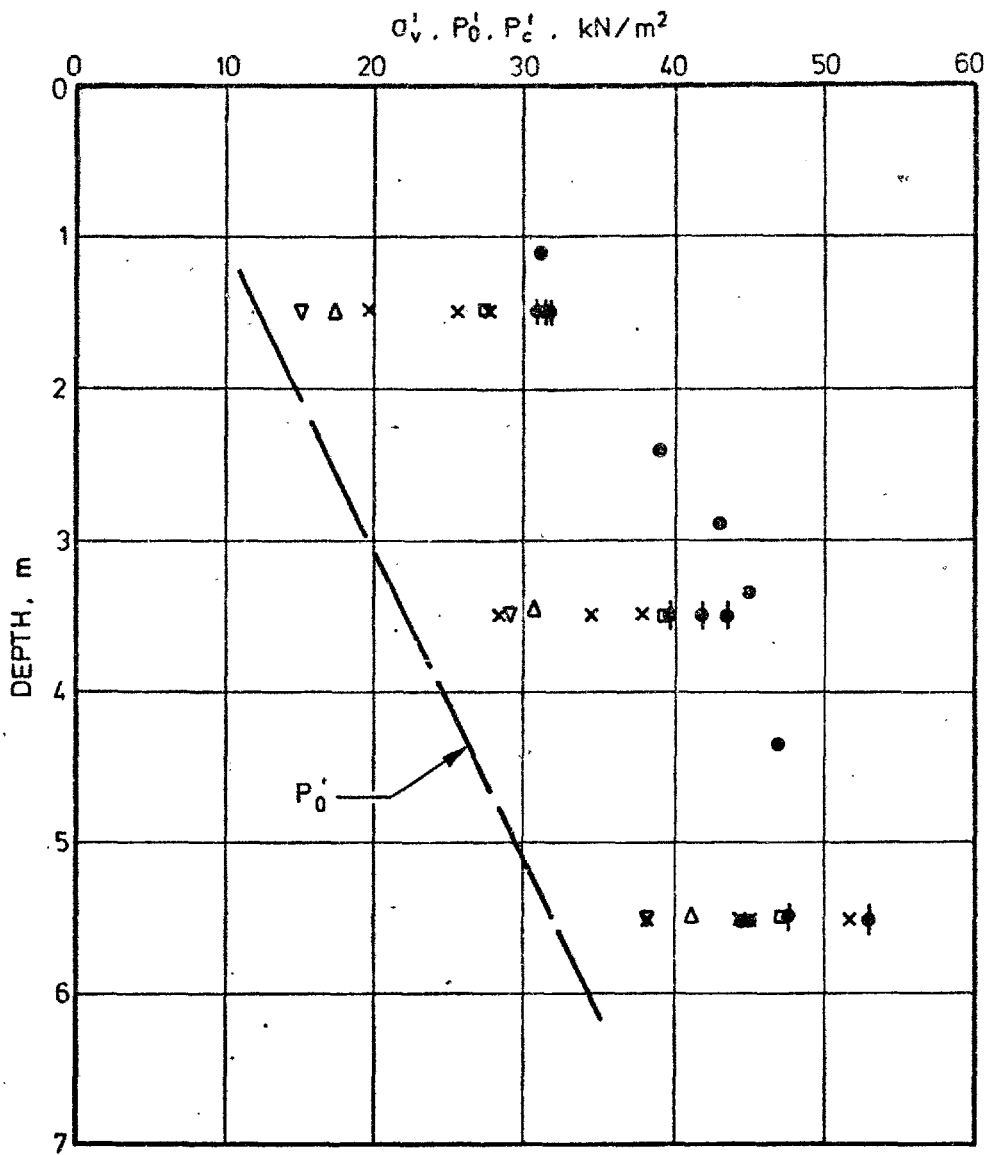
Fig. 6.1.43.

BANK 1, STAGE 1
ROTATION OF PRINCIPAL STRESS AXES AT PIEZOMETER LOCATIONS ($K_0 = f(\text{depth})$)



BANK 1 , STAGE 1

END POINTS OF 'FIELD' EFFECTIVE STRESS PATHS FOR PIEZOMETER LOCATIONS, AT WHICH FAILURE WAS PREDICTED BY THE FINITE ELEMENT ANALYSES



- LEGEND :**
- P'_c FROM LABORATORY TESTS
 - ◆ σ'_v MAXIMUM VALUE ON YIELD LOCUS (PIEZOS.7-16, BANK 1/1)
 - × σ'_v CORRESPONDING TO YIELD POINT ON 'FIELD' EFFECTIVE STRESS PATHS (PIEZOS. 7-16, BANK 1/1)
 - DITTO (PIEZOS. 16-18, STAGE 2)
 - △ DITTO (PIEZOS. 4-6, BANK 2)
 - ▽ DITTO (PIEZOS. 4-6, BANK 4)

YIELD POINTS ON FIELD EFFECTIVE STRESS PATHS IN TERMS OF σ'_v AND MAXIMUM VALUES OF σ'_v ON YIELD LOCUS

6.2. Undrained Failure

6.2.1. Introduction

In the previous section the development of displacements, strains and pore pressures during construction were considered. During the two failures of Bank 1 (see section 4.3.3. and tables 4.3 and 4.5) most of the instruments installed to record 'construction scale' displacements within those areas actively involved in the failures were lost (see section 4.3.4.); however, these instruments, together with the slip surface indicators (section 5.6), pore pressures recorded after the failures and the changes in sectional geometry of the embankment were used to deduce the 'boundaries' of the main rupture zones within the foundation and fill. Additional data in this respect were provided by the surface target (section 5.7) and time-lapse photography target (section 5.8) observations; these two data sources also provided the only continuous links between the displacements during construction and those during failure.

6.2.2. Bank 1, Stage 1

(i) General Observations

The post-failure survey plan for Bank 1, Stage 1 is presented in figure 6.2.1. and post-failure Sections A, C and B in figures 6.2.2. to 6.2.4. respectively. The following general observations are considered pertinent to an appreciation of the failure mechanism:-

a. a crack in the fill, up to 5mm wide, opened up 15 minutes prior to any discernable relative vertical displacements occurring across it. This crack had widened to a maximum of 100mm before relative vertical movements were observed. In a study of numerous case histories Bjerrum (1972) concluded

that, where there was little or no desiccation of the near surface material, failures of embankments on soft clay were generally preceded by the opening of a crack within the fill. It will be recalled that some 2.5 hours prior to failure, tensile horizontal strains (section 6.1.2) of about 4% had developed within the near surface foundation adjacent to the central trench; indications are, thus, that this figure was nearer 10% when relative vertical displacements commenced. The evidence (tables 4.2 and 4.3) suggests that during this period of horizontal movements of the embankment the foundation beyond the toe was experiencing heave movements of a similar magnitude.

b. the initial failure was followed by the development of secondary failure surfaces on the top of the embankment (figure 6.2.1), behind the main surface. These secondary surfaces developed subsequent to the period of maximum velocity and when the maximum vertical displacement was about 750mm.

c. although the failure of the embankment was more pronounced towards the western end (figure 6.2.1), it extended along virtually the entire crest length of the embankment (74m). The visual evidence suggested that the failure, similarly to the construction (section 6.1.1), was under essentially plane strain conditions. Maximum displacements in the 'X' coordinate direction (ΔX) were some 15% of those in the 'Y' direction (ΔY), although generally much less.

d. the geometry of the slip, particularly in the area of the embankment toe, where the slipped mass was disrupted by tension cracks (indicating some internal distortion), and the rear scarp of the slip surface suggested a non-circular failure surface. The tension cracks in the fill and the foundation were restricted to a plan area extending about 4m to the 'north' and 'south' of the toe; they were well developed and clearly visible.

- e. the main rear scarp of the slip was a vertical face, about 1m high, located above the central trench.
- f. the shear surface within the foundation was clearly defined (and planar) where it entered the toe trench.

(ii) Foundation Instrumentation

Figures 6.2.2. and 6.2.4. show the upper and lower limits of the rupture zone as defined by the slip surface indicators; also shown are the upper limits defined by the access limits to the inclinometers and observation wells.

Ignoring SSB5, which was to the rear of the main body of the movement, the foundation instrumentation at Section B presents a very consistent picture; being of a 'narrow' rupture zone (about 500mm wide) composed of two inclined zones meeting beneath the embankment toe and having their opposite extremities within the toe, and central, trenches respectively.

A similar picture is presented by the data for Section A, although in this case both the movement within, and the width of, the implied rupture zone are greater.

In figure 6.2.3. the data from figures 6.2.2. and 6.2.4. have been combined to define the limits of a zone of extreme deformation; this rupture zone can be seen to be generally compatible with the observed changes in geometry and the movements of the various surface targets. Additionally, the maximum horizontal shear strains (γ) at the inclinometer locations (figures 5.4.2. to 5.4.13) coincided with this zone. Of the piezometers which exhibited marked increases in pore pressure post-failure, three (nos 2, 6 and 7) were within, or close to, the rupture zone whilst one (no 3) was remote. Also

of relevance is the fact that only piezometers 10 - 12 were lost during the failure indicating the major movement to have been south of the vertical line in which they were installed, this being compatible with the postulated location of the rupture zone.

The major movement was thus confined to the very soft clay, as was intended for Stage 1 of Bank 1.

(iii) Surface Movements

As depicted in figures 6.2.2. to 6.2.4., these derive from three sources, viz the surface targets, the time-lapse photography targets and the ground survey. Any comparison must take note of the fact that the ground survey displacements simply relate the geometry of the embankment post-failure, to the design profile.

The displacement vectors of the surface targets (figure 5.7.7), the time-lapse photography targets (figures 5.8.4 to 5.8.8) and the ground surface, support the orientation and location of the postulated rupture zone. It is of interest to note that the time-lapse photography targets beyond the embankment toe all moved, initially, approximately vertically upwards by some 30 to 40mm.

(iv) Mechanism of Failure

The evidence presented indicates that the failure was preceded by the formation of a vertical tension crack through the fill, the horizontal linear strains within the foundation beneath the centre of the embankment being in excess of 4% at this stage. A large part of the foundation beneath the embankment is anticipated to have been in a state of active

local failure prior to the formation of the crack, which possibly precipitated passive local failure occurring beyond the toe. It would appear probable that during the period of horizontal spreading of the embankment, coupled with heave of the foundation beyond the toe, the areas of local failure were coalescing into a continuous rupture zone, the bounds of which are delineated in figure 6.2.3.

Attempts to define a centre of rotation from a computer analysis of the time-lapse target movements did not prove fruitful.

(v) Rates of Movement

These have already been discussed in some detail in section 5.8., displacement/time plots for the surface targets (figures 5.8.12) and for the time-lapse photography targets (figures 5.8.9. to 5.8.11) being presented therein, especially with respect to the rapid acceleration up to a peak velocity, followed by a prolonged period of deceleration. The variation in velocity with time of the slipped mass is indicated in figure 6.2.5., the data indicating, for the particular location, resultant surface velocities of between 25 and 45mm/minute some 40 minutes after the formation of the initial tension crack in the fill, and therefore some 25 minutes after the commencement of the major movement. Maximum resultant velocities at the time-lapse photography target locations varied between 10 and 45mm/minute.

6.2.3. Bank 1, Stage 2.

(i) General Observations

The post-failure survey plan for Bank 1, Stage 2 is presented in figure 6.2.6 and post-failure Sections A, C and B in figures 6.2.7 to 6.2.9 respectively. The following general observations are considered pertinent to an appreciation of the failure mechanism:-

- a. the failure was preceded by a period of some 6 hours during which the displacements increased from 'construction scale' to 'failure scale'; the top of the embankment noticeably settled during this period. The formation of a crack in the fill was simultaneous with the development of major horizontal and vertical displacements of the embankment.
- b. the initial failure was followed by the development of secondary failure surfaces on top of the embankment, behind the main surface. The pattern of secondary scarps was even more complex than for Stage 1: formation of these secondary features, as in the case of Stage 1, was subsequent to the period of maximum velocity; the coincidental maximum vertical displacement was about 550mm.
- c. failure of the embankment was definitely more pronounced towards the western end (figure 6.2.6.), extending from the western toe to approximately mid-way between Section B and the eastern crest. The visual evidence that the failure was under essentially plane strain conditions was supported by the surface target data, which showed the maximum 'X' direction movements (ΔX) to be about 20% of ΔY , although, as for Stage 1, generally much less.
- d. the geometry of the slip, together with the extensive signs of internal distortion, suggested a non-circular failure surface.
- e. the major rear scarp was again a vertical face about 1m high; on Section A this was located above the central trench whereas on Sections C and B the major movements were clear of the trench.

(ii) Foundation Instrumentation

Figures 6.2.7. and 6.2.9. show the upper and lower limits of the rupture zone, as defined by the slip surface indicators; also shown are the upper limits defined by the inclinometers and observation wells.

In this case a much wider rupture zone is suggested, as is a 'more circular' failure mode. At Section A the zone appears to commence within the confines of the central trench and pass down to the clay/gravel interface before rising up towards the toe of the slipped mass.

At Section B the picture is similar, except that the shear zone appears to have initiated in front of the central trench.

In figure 6.2.8. the data from figures 6.2.7. and 6.2.9. have been combined to define the limits of a zone of extreme deformation. As for Stage 1, this zone is generally compatible with the observed changes in geometry and movements of the various surface targets. The inclinometers suggest that large horizontal shear strains developed within a considerable part of the foundation, particularly the upper part of the postulated rupture zone. Of the piezometers which exhibited marked increases in pore pressure post-failure six (nos 14, 15, 19 and 22 - 24) were within the postulated rupture zone, whilst two (nos 18 and 21) were above it. These data thus support the existence of a wide zone of extreme deformation during failure. The loss of piezometers 13 - 15 (and 28 - 30) means that the rupture zone must have passed to the north of their location.

Although the shear zone encompasses part of the peat and lower clay layers, the evidence, particularly the inclinometer data (see e.g. figures 5.4.11 and 5.4.12), suggest that the major shearing occurred within the very soft clay. The rupture zone certainly passed through the desiccated crust beyond the embankment toe but beneath the embankment it appears to have encompassed both the desiccated crust and the central trench.

(iii) Surface Movements

The displacement vectors of the surface targets (figures 5.7.8. to 5.7.10), the time-lapse photography targets (figures 5.8.13 to 5.8.14) and the ground surface support the orientation and location of the postulated rupture zone.

(iv) Mechanism of Failure

The evidence presented suggests that failure was preceded by a transitional period during which large shear strains developed over a wide area of the foundation, which consequently moved to failure; it is almost as if the desiccated layer was increasingly having to maintain the embankments integrity, and when it also reached the limit of its shearing resistance a crack formed in the fill as overall failure occurred. Thus, unlike Stage 1, at the point of limiting equilibrium there does not appear to have been a fully developed tension crack through the fill.

(v) Rates of Movement

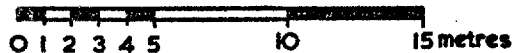
These have already been discussed in some detail in section 5.8., displacement versus time plots for the surface targets (figures 5.8.17 and 5.8.18) and for the time-lapse photography targets (figures 5.8.15 and 5.8.16) being presented therein. As for Stage 1, once the main failure had commenced there was rapid acceleration to a peak velocity, followed by a prolonged period of deceleration. However, as depicted in figure 6.2.10 the acceleration of the Stage 2 failure was not quite so rapid as for Stage 1. Velocities are of similar order, being possibly slightly less overall, varying between 20 and 30mm/minute at the location illustrated some 50 minutes after the formation of the initial tension crack in the fill (which also coincided with the commencement of major movement).

6.2.4. Summary

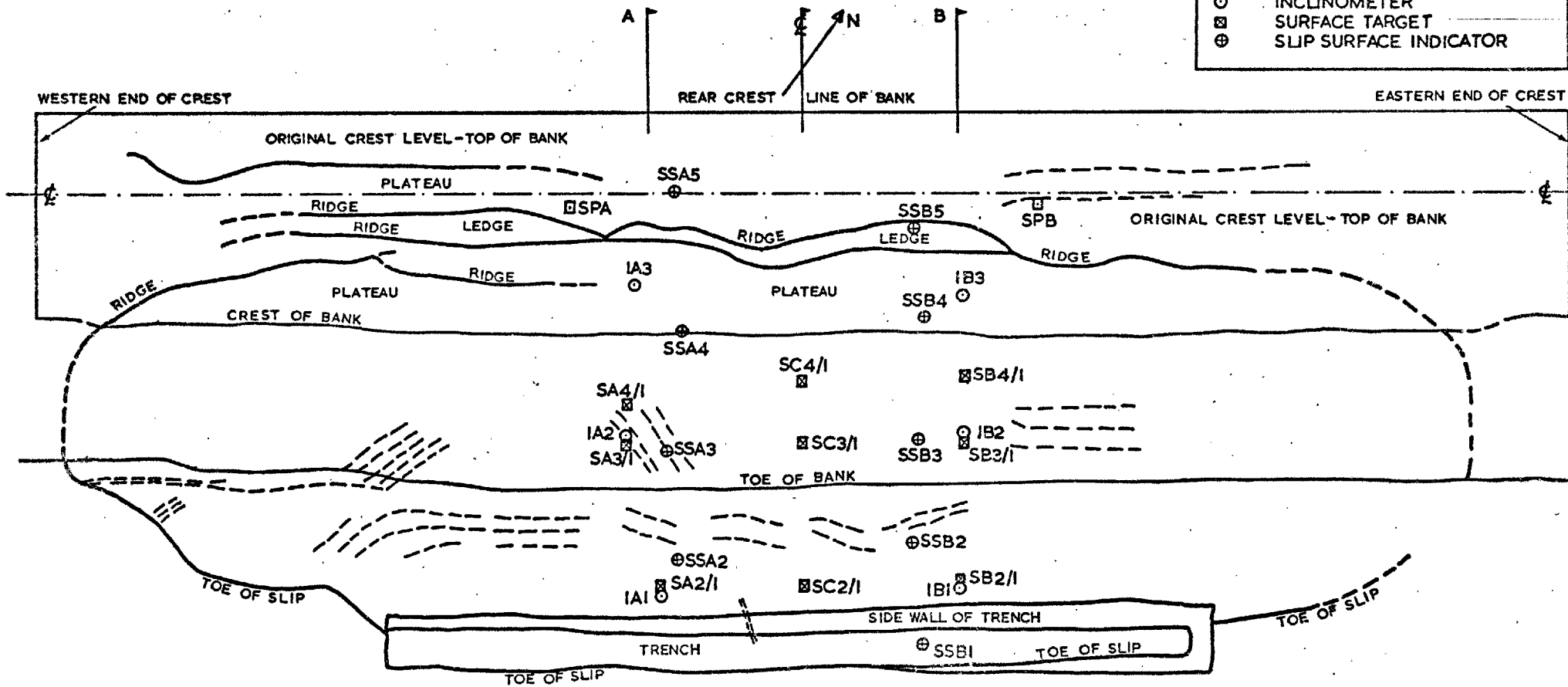
By the time that overall failure was imminent, the Stage 1 embankment appears to have induced a local active failure zone beneath the main area of fill. Shear strain rates within the passive zone beyond the toe increased, and at some point the horizontal tensile strains beneath the fill were sufficient to induce a near vertical crack through the fill. The embankment initially moved outwards, widening the crack, whilst the foundation beyond the toe heaved; this period is thought to coincide with the merging of the areas of local failure into a continuous rupture zone. Movements then rapidly built to a maximum and slowly subsided over a number of days. The rupture zone was 'relatively' narrow (500 to 1500mm).

The presence of the continuous desiccated layer beneath the Stage 2 embankment appears to have maintained stability even though a large part of the foundation was in a state of failure, and possibly, a continuous rupture zone within the soft clay already existed. Failure of the desiccated layer then took place; this marked the start of overall failure (at which point a tension crack developed), movements building rapidly to a maximum and subsiding over a number of days. The rupture zone was 'relatively' wide (3.5m average) and following a vertical crack through the fill could be sub-divided into active, simple and passive shear areas, unlike Stage 1 where the rupture zone location was largely dictated by the two trenches. The lack of cracking prior to failure together with wide shear zones when a desiccated surface layer is present has also been noted by Kaufman and Weaver (1967), Dasca1 et al (1972), Ladd (1972), Lacasse and Ladd (1973) and Dasca1 and Tournier (1975).

The difference in the build-ups to the two failures is clearly depicted in figure 5.8.19.



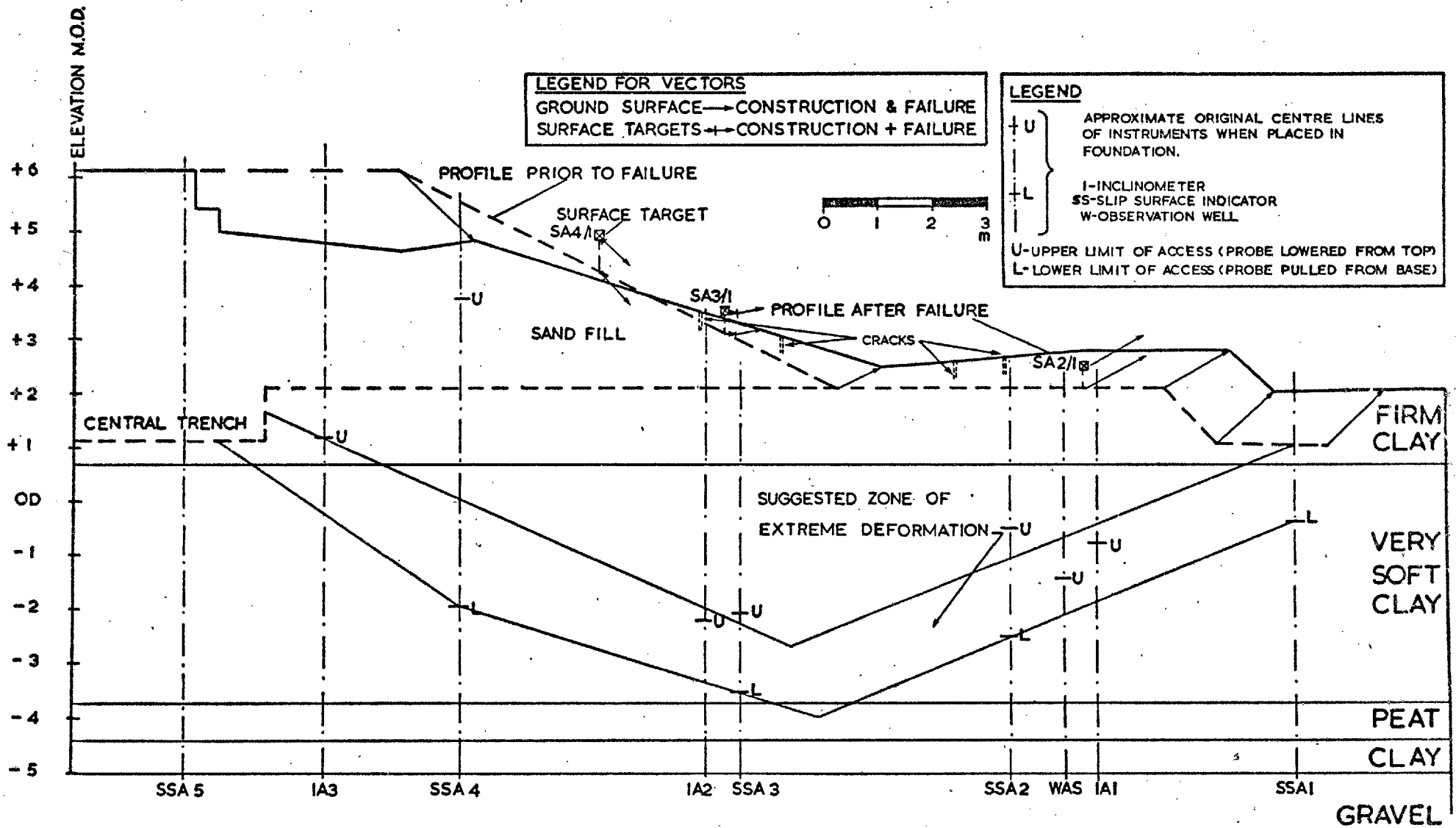
LEGEND	
—	MAIN FEATURES
- - -	CRACKS
□	SETTLEMENT GAUGE (PLATE)
○	INCLINOMETER
⊠	SURFACE TARGET
⊕	SLIP SURFACE INDICATOR



BANK I, STAGE I: POST-FAILURE SURVEY PLAN

Fig. 6.2.1

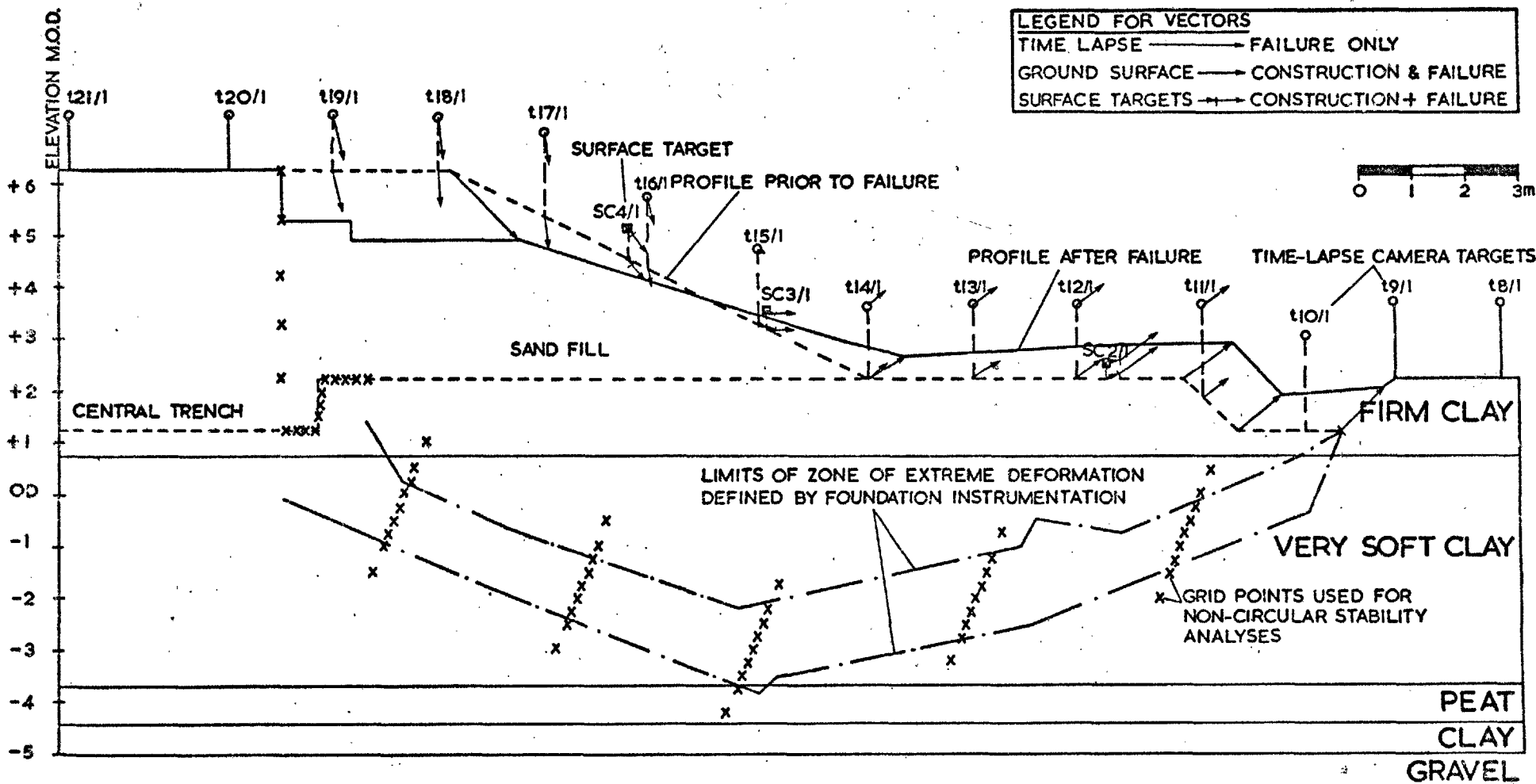
-669-



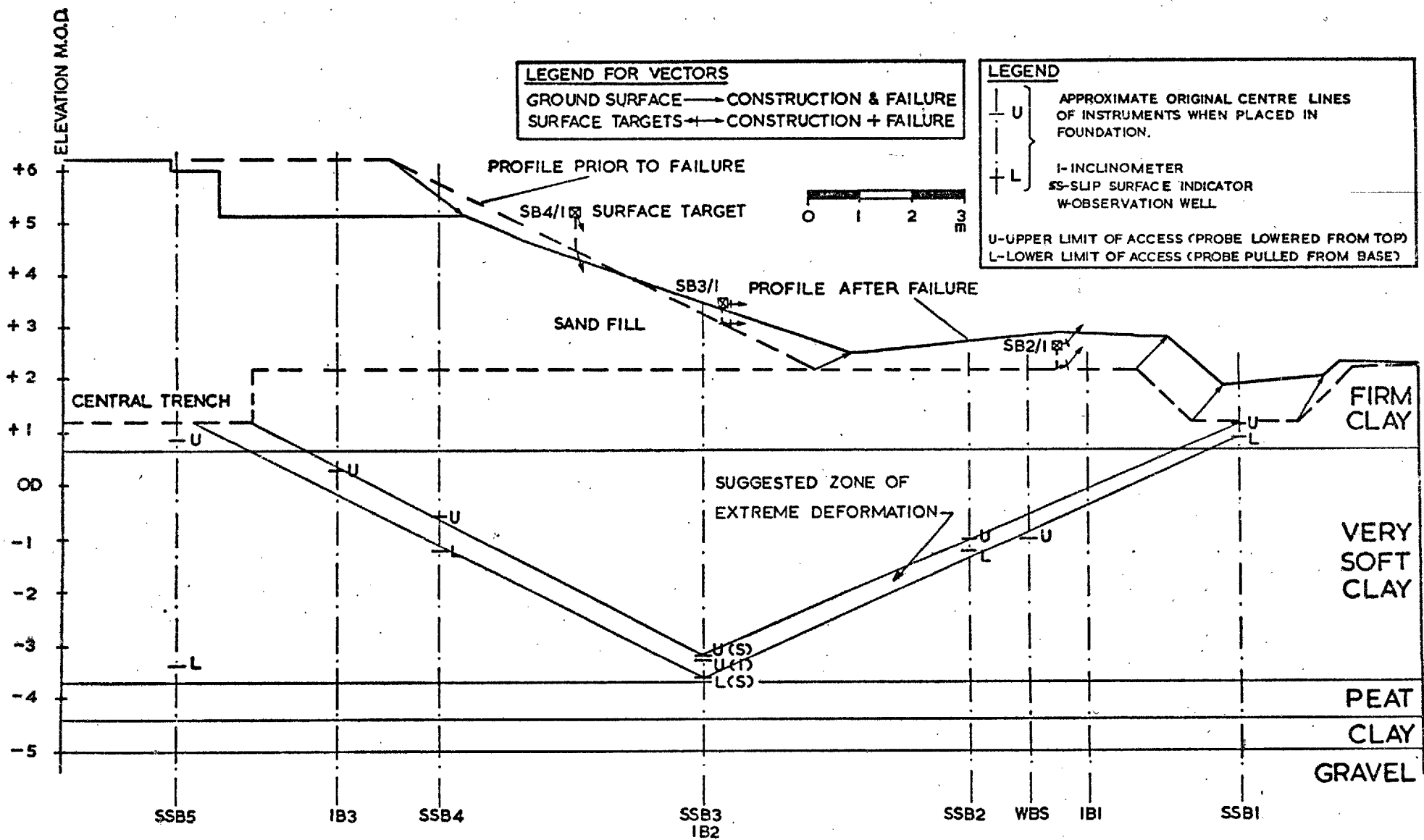
-700-

BANK I/I, SECTION A: PRE- & POST-FAILURE PROFILES, AND SURFACE MOVEMENT VECTORS

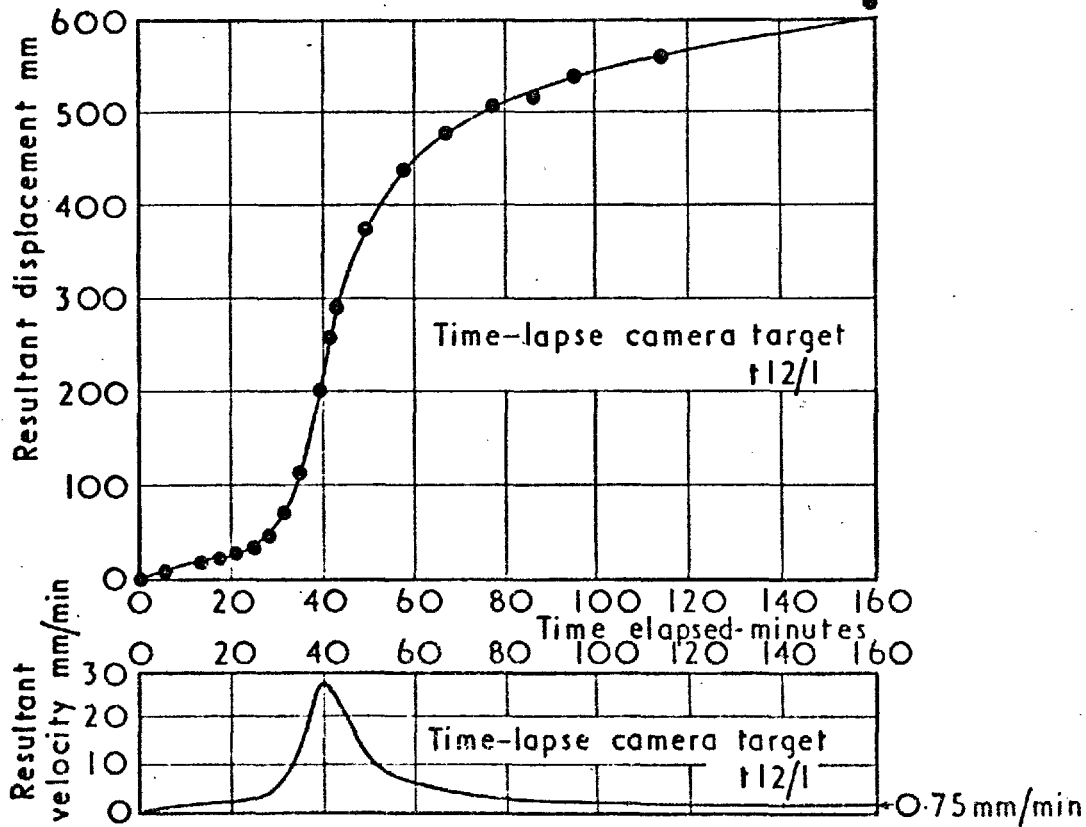
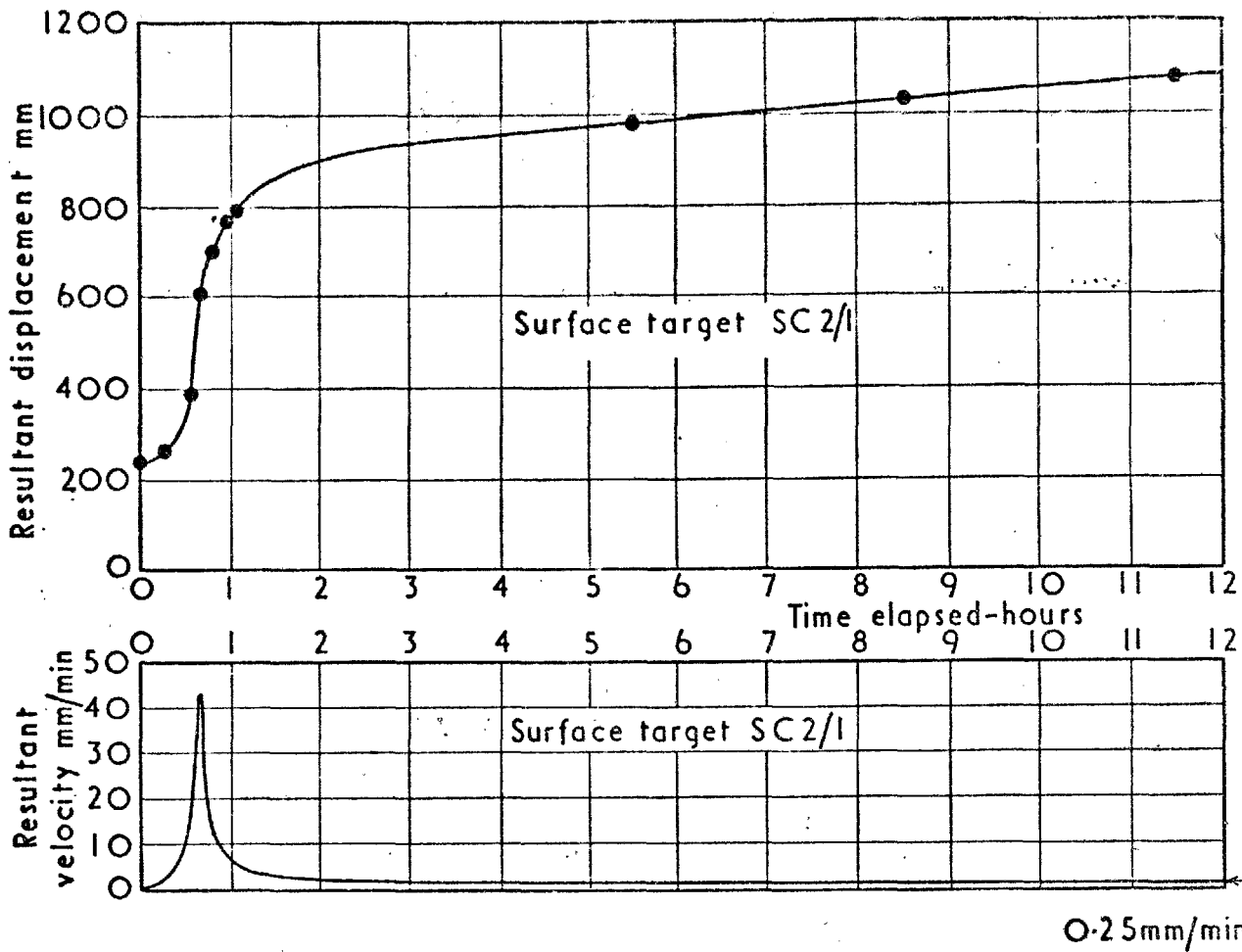
FIG. 5.2.2



BANK I/I, SECTION C: PRE-& POST-FAILURE PROFILES, AND SURFACE MOVEMENT VECTORS

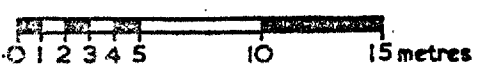


BANK I/I, SECTION B : PRE-& POST-FAILURE PROFILES AND SURFACE MOVEMENT VECTORS

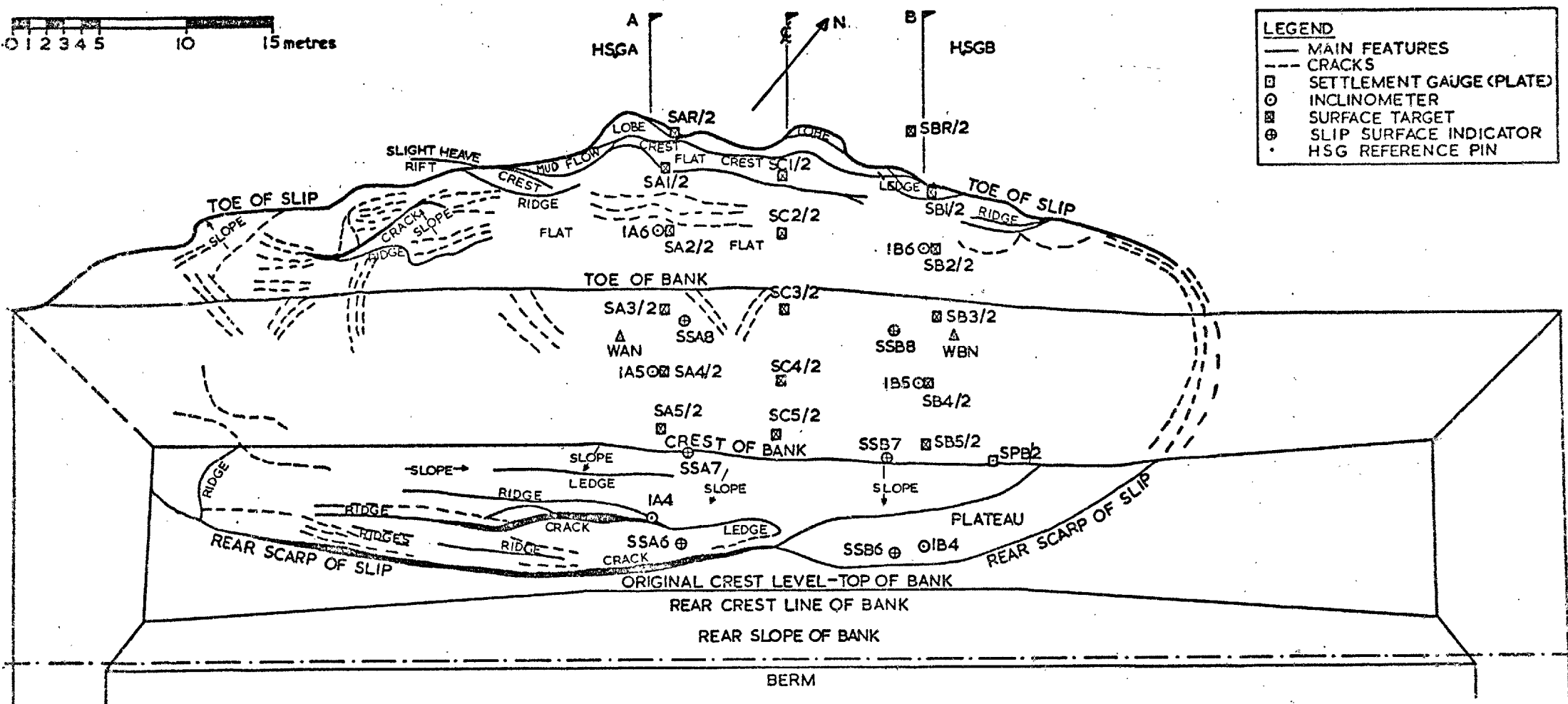


BANK I, STAGE I.- RESULTANT DISPLACEMENTS AND VELOCITIES OF PHOTOGRAMMETRY AND TIME-LAPSE CAMERA TARGETS VERSUS TIME FROM START OF FAILURE

Fig. 6.2.5



LEGEND	
—	MAIN FEATURES
- - -	CRACKS
□	SETTLEMENT GAUGE (PLATE)
○	INCLINOMETER
⊗	SURFACE TARGET
⊕	SLIP SURFACE INDICATOR
•	HSG REFERENCE PIN



BANK I, STAGE 2 : POST-FAILURE SURVEY PLAN

Fig. 6.2.6

704-

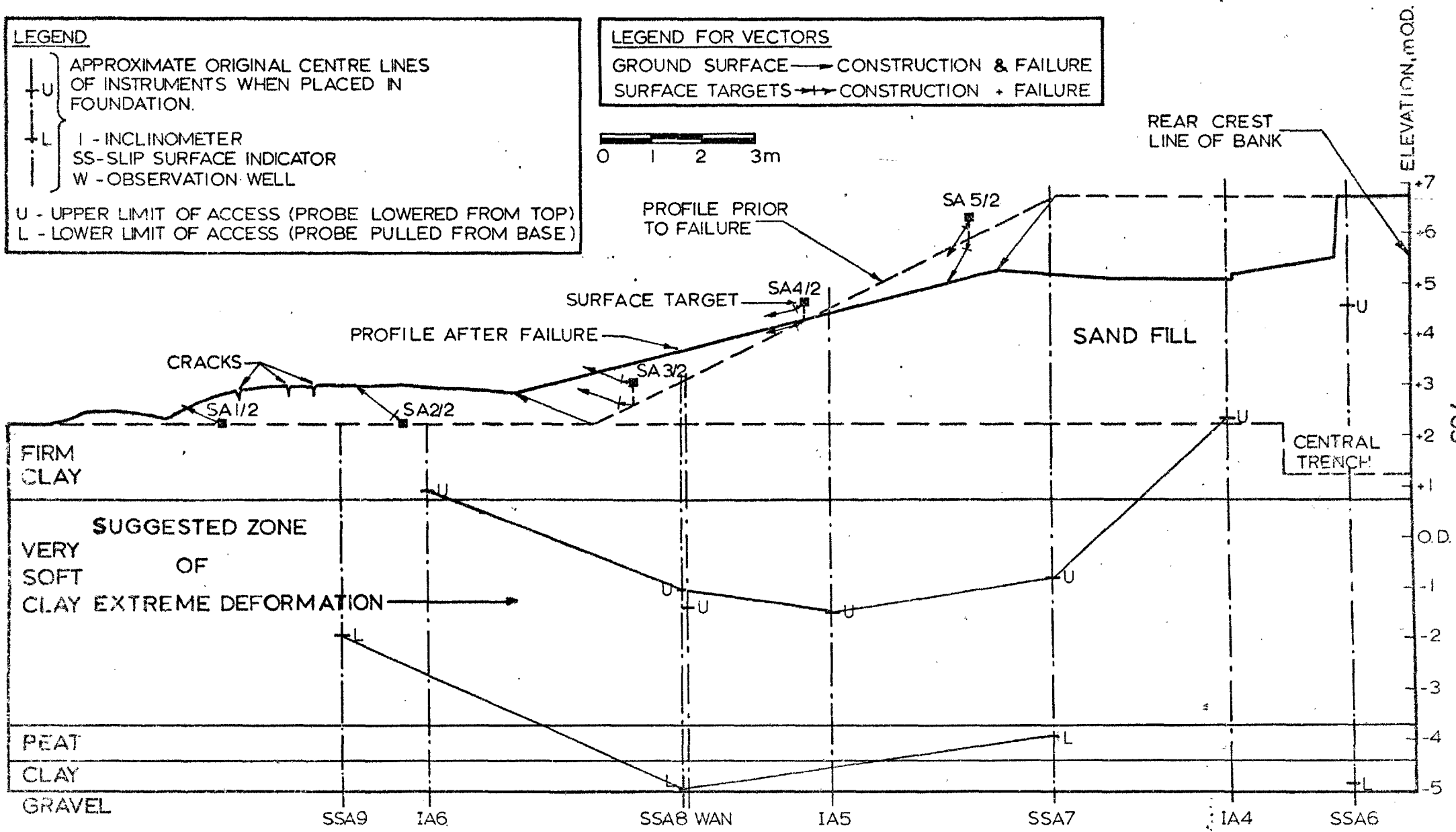
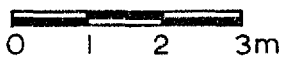
LEGEND

+U } APPROXIMATE ORIGINAL CENTRE LINES
 OF INSTRUMENTS WHEN PLACED IN
 FOUNDATION.
 +L } I - INCLINOMETER
 SS - SLIP SURFACE INDICATOR
 W - OBSERVATION WELL

U - UPPER LIMIT OF ACCESS (PROBE LOWERED FROM TOP)
 L - LOWER LIMIT OF ACCESS (PROBE PULLED FROM BASE)

LEGEND FOR VECTORS

GROUND SURFACE → CONSTRUCTION & FAILURE
 SURFACE TARGETS ↔ CONSTRUCTION + FAILURE



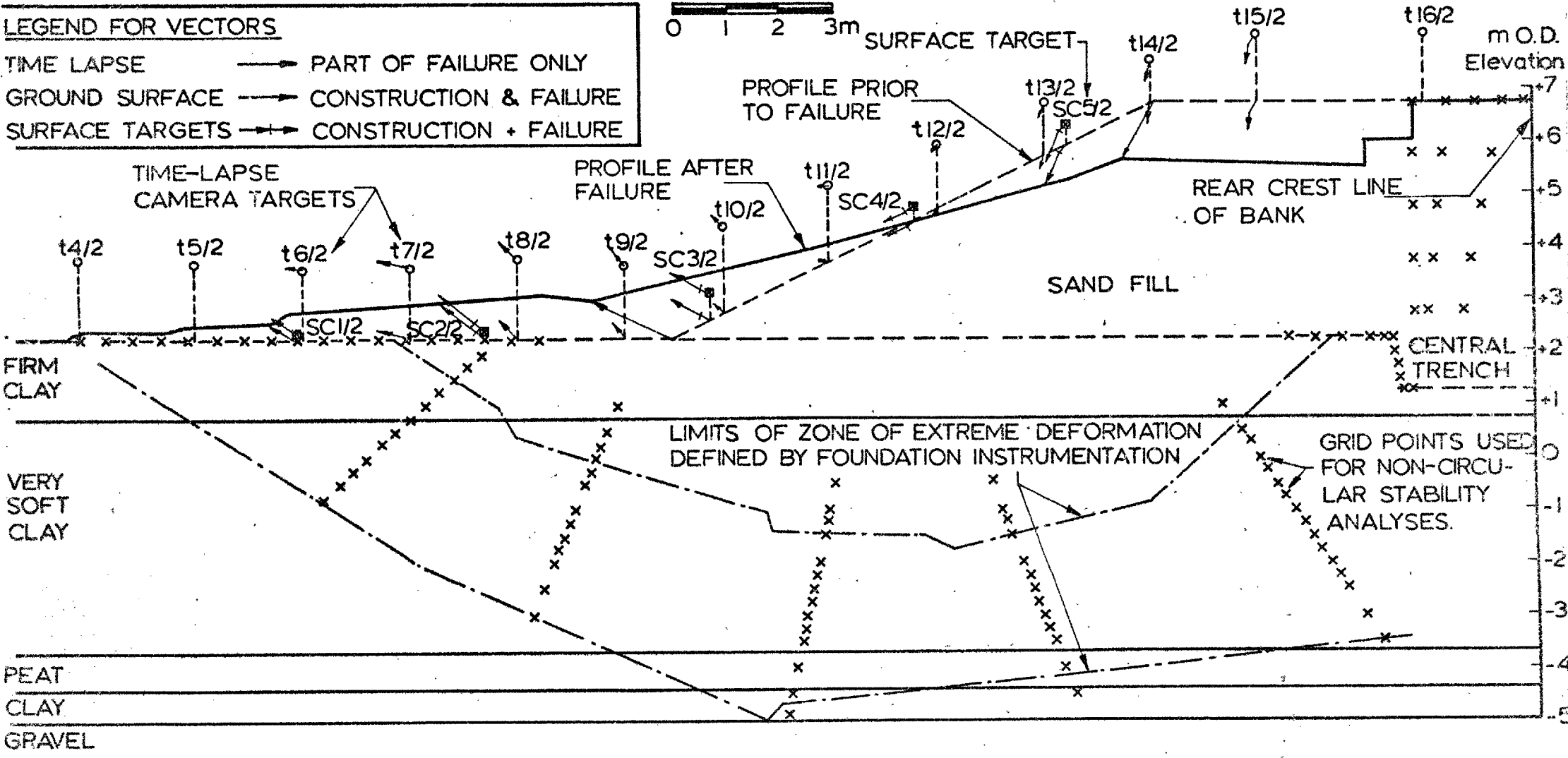
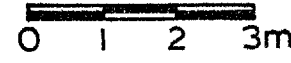
BANK 1/2, SECTION A: PRE- & POST-FAILURE PROFILES, AND SURFACE MOVEMENT VECTORS

LEGEND FOR VECTORS

TIME LAPSE \rightarrow PART OF FAILURE ONLY

GROUND SURFACE \rightarrow CONSTRUCTION & FAILURE

SURFACE TARGETS \rightarrow CONSTRUCTION + FAILURE



BANK 1/2, SECTION C: PRE-& POST-FAILURE PROFILES, AND SURFACE MOVEMENT VECTORS

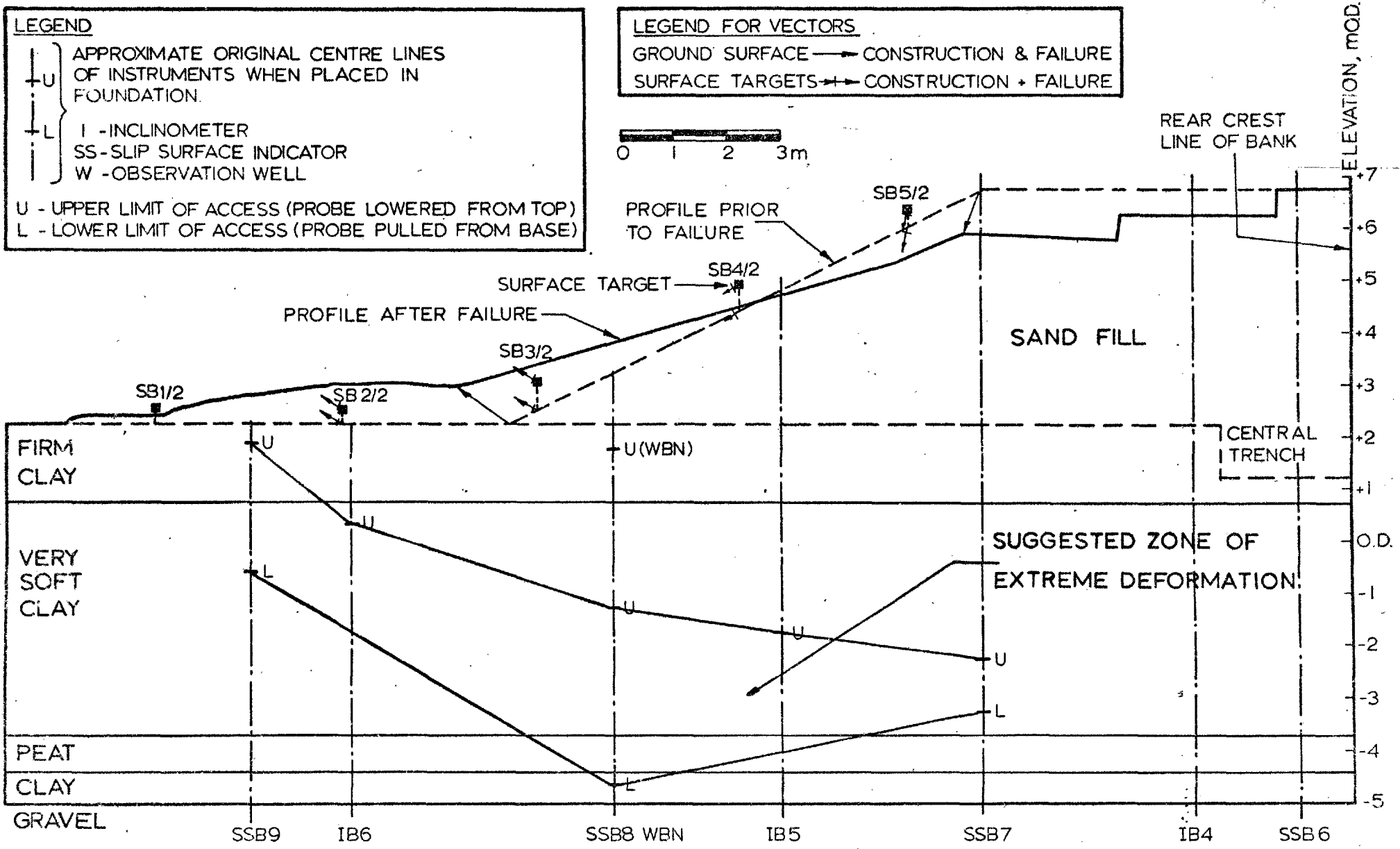
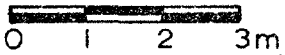
FIG. 3.50

LEGEND

+U } APPROXIMATE ORIGINAL CENTRE LINES
 OF INSTRUMENTS WHEN PLACED IN
 FOUNDATION.
 +L } I - INCLINOMETER
 SS - SLIP SURFACE INDICATOR
 W - OBSERVATION WELL
 U - UPPER LIMIT OF ACCESS (PROBE LOWERED FROM TOP)
 L - LOWER LIMIT OF ACCESS (PROBE PULLED FROM BASE)

LEGEND FOR VECTORS

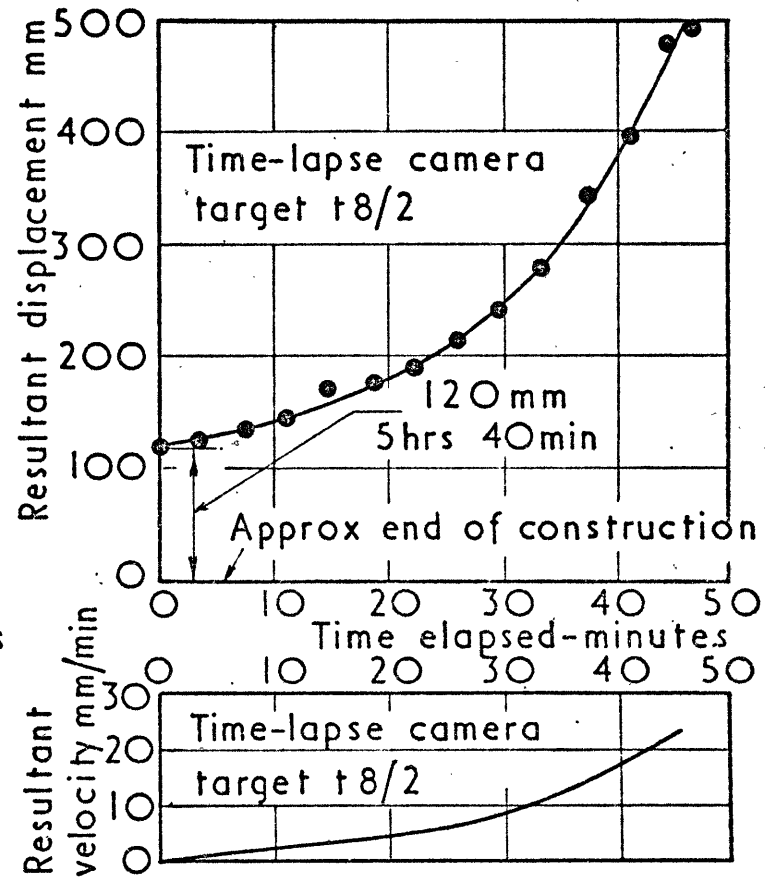
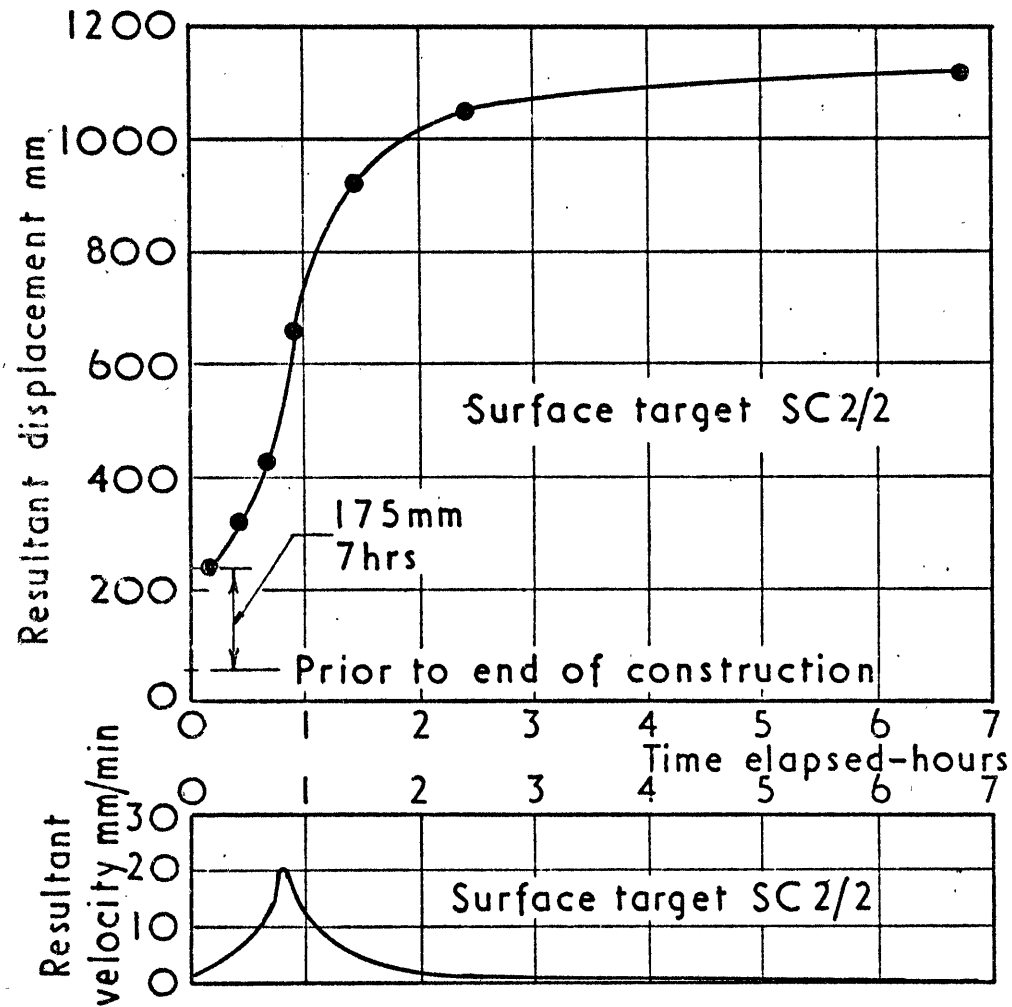
GROUND SURFACE → CONSTRUCTION & FAILURE
 SURFACE TARGETS → CONSTRUCTION + FAILURE



-707-

Fig. 6.23

BANK 1/2, SECTION B: PRE-& POST-FAILURE PROFILES, AND SURFACE MOVEMENT VECTORS



BANK 1, STAGE 2 RESULTANT DISPLACEMENTS AND VELOCITIES OF PHOTOGRAMMETRY AND TIME-LAPSE CAMERA TARGETS VERSUS TIME ELAPSED FROM START OF FAILURE

6.3. Consolidation, Settlement and Creep

6.3.1. Consolidation

(i) During Construction

In section 6.1.3. it was suggested that significant consolidation of the clay foundation had occurred during construction of the embankments, this consolidation primarily taking place prior to yielding of the foundation. Assuming a constant rate of embankment construction, coupled to a constant rate of generation of elastic pore pressures, C_v values (assumed to be constant) relevant to the pre-yield consolidation were evaluated using the analysis presented in table 6.3.1., indicating C_v values in the range 93 - 369 $m^2/year$. Yield of the foundation beneath Bank 1/1 (piezometers 10 - 12) and Bank 2 (piezometers 4 - 6) occurred at fill heights of 1.75m (table 6.1.1) and 0.95m (table 6.1.2) respectively, based on the pore-pressure observations: for Bank 4 these data did not indicate a definite yield point; however, yield was assumed to occur at 0.85m fill height, as indicated by the settlement records (figure 5.11.3).

Schiffman's (1958) method was also used to analyse the end of construction situation for Bank 2 and 4 (figure 6.1.24), C_v values of 26 $m^2/year$ and 33 $m^2/year$ being obtained as shown in table 6.3.1. These values are obviously only averages, the analyses assuming a constant C_v during construction, whereas the data indicate a significant reduction in C_v at yield, as illustrated in table 6.3.1.

The laboratory data, as discussed in section 2.4.3., are summarised in table 6.3.2. The field values of C_v were of the same order as those from the block sample specimens but some two orders of magnitude higher than those from the piston sample specimens; this is not unusual behaviour for

soft clays (Davis and Poulos, 1967; Symons and Murray, 1975).

The result of the single in-situ constant head permeability test (section 5.5.6; table 5.5.4) carried out at pre-yield effective stresses indicated no difference in permeability, within the scatter of the results, from those tests performed after the end of construction. No significance can be attached to this and, in hindsight, it was remiss of the writer not to have carried out a program of C.H.T. s at the in-situ effective stresses. At the time the significance of yield on the permeability was not appreciated, the C.H.T. s being geared to an assessment of 'k' relevant to post-construction consolidation.

As discussed in section 5.5.6. the laboratory data indicate a reduction in k_v of about sixfold to be associated with yielding; thus the in-situ value of k_v can be estimated to be $1.6 \times 10^{-8} \text{ m/s} * (2.6 \times 10^{-9} \times 6)$. When linked to the pre-yield laboratory value of M_{v1} ($4.6 \times 10^{-4} \text{ m}^2/\text{kN}$), this suggests a pre-yield field value of C_v of $109 \text{ m}^2/\text{year}$, being in good agreement with the back-analysed field values in table 6.3.1., especially the value of $93 \text{ m}^2/\text{year}$ for Bank 1/1, this being based on the most reliable estimate of the elastic pore pressures. The vertical total stress changes for Bank 2 were based on the solution of Giroud and Wattissee (1972) and for Bank 4 on that of Milović (1974).

*this k_v corresponds to a k_H of $8 \times 10^{-9} \text{ m/s}$ and thus a ratio $k/k_c = 0.4$. Based on equation 5.5.23 (Gibson, 1966) λ would thus be 0.2, which is close to the limit for accurate permeability measurements and some doubt must therefore exist as to whether reliable values of 'k' at in-situ stress levels could have been obtained from C.H.T. s using the grade of piezometer ceramic installed.

(ii) Post-Construction

The post-construction pore pressures for Banks 2 and 4 (figures 5.5.7 to 5.5.13) were analysed on two separate bases; firstly by continuing the analysis on the basis of Schiffman's (1958) method produced average C_v values of $3.1 \text{ m}^2/\text{year}$ for the two years or so from the start of construction, as indicated in table 6.3.3. Secondly, individual piezometers beneath the centre lines of the embankments were considered in relation to the pore-pressure isochrones presented by Taylor (1948); the back-calculated C_v values are shown in table 6.3.3., mean values of $1.8 \text{ m}^2/\text{year}$ and $0.87 \text{ m}^2/\text{year}$ being obtained for Banks 2 and 4 respectively. These values are based on the assumption that all of the dissipation took place post-construction and would therefore be expected to be lower than those obtained by the Schiffman method.

The consolidation analyses presented herein are obviously simplified; the continued generation of pore pressures as a result of undrained creep together with the seasonal changes in the boundary drainage conditions are complicating factors which have not been considered. Divergence of the observed isochrones from those predicted by Terzaghi's (1943) one-dimensional consolidation theory are apparent from table 6.3.3.

The use of the post-yield field k_v ($2.6 \times 10^{-9} \text{ m/s}$, from the C.H.T. s) together with the post-yield laboratory value of M_{v1} ($1.2 \times 10^{-3} \text{ m}^2/\text{kN}$) to predict the post-yield field C_v leads to a value of $5 \text{ m}^2/\text{year}$. The field value of k_v (full scale) was thus within the scatter of the results obtained from the C.H.T. s.

Back-calculated C_v values are compared to the laboratory data (table 6.3.2.) in figure 6.3.1.

6.3.2. Settlement

The normal practice of assuming entirely undrained settlements to occur during construction, followed by consolidation settlements post-construction is clearly inappropriate to the trial embankments at Mucking. The data from the V.S.U. beneath Bank 4 permitted a simple analysis of the settlements within the foundation both during (figures 5.11.2. and 5.11.3) and post-construction (figures 5.11.4. and 5.11.5).

Pre-yield settlements were considered to be entirely consolidation; as the 'field' effective stress paths beneath the centre of Bank 1/1 have been seen (figure 6.1.40) to approximate to K_0 conditions pre-yield, this may not be an unreasonable assumption.

The average pre-yield increase in vertical effective stress of about 3.5 kN/m^2 , together with the observed settlements, suggested M_v values as presented in table 6.3.4. With the exception of the desiccated layer the pre-yield field values of M_v are similar to those measured in the laboratory. The desiccated layer appears to have yielded from the start of construction, as was suggested in section 6.1.3., the pre-yield value of M_v being similar to the post-construction value. For the remainder of the foundation the post-construction values were approximately an order of magnitude greater than the pre-yield values, and also slightly greater than the laboratory values ($4.25 \times 10^{-3} \text{ m}^2/\text{kN}$ cf $1.2 \times 10^{-3} \text{ m}^2/\text{kN}$) of Wesley (1975). However, laboratory M_v values closely approximating to the field values were obtained by Buri (1978) from tests lasting much longer, indicating the importance of secondary consolidation. It is of particular interest to note that no difference in compressibility or permeability characteristics is in evidence for the peat layer.

The use of the post-yield field k_v (C.H.T.) plus the mean post-yield field M_v leads to a corresponding C_v of $2.0 \text{ m}^2/\text{year}$, compared to $2.1 \text{ m}^2/\text{year}$ from the pore-pressure dissipation data using Schiffman's (1958) method.

Finally, the settlements of Bank 4 between the fill heights of 0.85m and 2.50m were considered as undrained and used to back-calculate an undrained Young's Modulus, E^T . The vertical settlement beneath a rigid circular load on a finite elastic layer can be estimated using the formulation of Milovic (1970):-

$$\Delta Z = \frac{2\Delta\sigma_v R.I}{E^T} \dots\dots\dots(6.37)$$

where 'R' is the radius of the loaded area and 'I' is an influence factor. For $\nu = 0.45$, E^T was found to be 2378 kN/m^2 ; this value is compatible with the laboratory initial secant modulus (E_{u50}) of 2700 kN/m^2 (section 2.8), it being anticipated that, post-yield, the Bank 4 foundation would be on the non-linear portion of the field stress-strain relationship.

6.3.3. Secondary Consolidation/Creep

The relatively high plasticity (figure 3.3) of the Mucking clay would suggest significant secondary consolidation (or drained creep) at in-situ stress levels (Bjerrum, 1967), and, indeed, such behaviour has been observed in the laboratory (Wesley, 1975; Buri, 1978). However, it will be recalled from section 2.6 that the apparent overconsolidation of the Mucking clay appears more likely to have been caused by previous lowering of the ground-water level (Parry, 1970).

Undrained creep has been suggested by the strain rate effects observed in the laboratory (section 2.7) and in the large field vane tests (section 3.3) as well as by the continuing build-up of pore pressures and horizontal displacements at constant fill height during the construction of Bank 1 (figures 5.5.3 to 5.5.5 and 6.1.3 to 6.1.6).

It would thus seem likely that following the end of construction the foundation was undergoing consolidation combined with both drained and undrained creep. The post-construction settlement records for Bank 2 (figure 5.10.3) show no signs of an end to the settlement some 760 days after the end of the construction, pore-pressure dissipation being about 60% complete after some 650 days. On the other hand the settlement records for Bank 4 (figure 5.11.4) show signs of nearing completion by 600 days after the end of construction when the average pore-pressure dissipation was about 70% complete.

Horizontal displacements of inclinometers IC1 and IC2 (Bank 2) were presented versus a natural time scale in figure 6.1.8 and are replotted versus log time in figure 6.3.2., wherein the ultimate relationships are approximately linear (maximum of 70mm per log cycle of time in days). Similarly horizontal strains for Bank 2 were presented versus natural time in figure 6.1.13., being replotted versus a log time scale in figure 6.3.3; again the ultimate relationships are linear (maximum of -1.75% per log cycle of time in days). On this basis, 50 years after the end of construction one might anticipate some 4.7% tensile strain beneath the embankment, about 175mm of horizontal movement at the toe and, extrapolating the settlement records in figure 5.10.3., some 1.45m of settlement beneath the centre of the embankment i.e. reducing the crest height from 2.8m to 1.35m!

Comparing the pore-pressure dissipation records for Bank 2 (figures 5.5.11 to 5.5.13) with the data in figures 5.11.5, 6.3.2 and 6.3.3., shows that during the 50 days or so before the pore pressures reduced to the end of construction values, 100mm of surface settlement, 27mm of horizontal movement at the toe and 0.48% horizontal strain beneath the embankment had occurred; these figures compare to end of construction values of 85mm, 32mm and 0.24% respectively i.e. the settlement and horizontal movements approximately doubled whilst the strain trebled. Thus undrained creep and secondary consolidation are highly significant to the prediction of both short-term and long-term deformations of the Mucking clay.

6.3.4. Summary

The laboratory investigations (Wesley, 1975) were mainly confined to shear strength studies and only limited consolidation and creep data were available. Likewise, only a superficial study of the field consolidation, settlement and creep data has been attempted herein. However, the analyses performed suggest some significant conclusions, as summarised in the following:-

(1) the early stages of construction, prior to first yield of the foundation, were characterised by high C_v values (of the order of $100\text{m}^2/\text{year}$) and significant pore-pressure dissipation. These high C_v values were predicted by the laboratory data from large diameter block samples (see figure 6.3.1) but not by the data from the piston sample specimens (see table 6.3.2). Sample disturbance is the most likely cause of this discrepancy (Davis and Poulos, 1967). Based on the available evidence it would also seem likely that these high C_v values would also be predicted using equation 2.1,

together with the field value of k_v from C.H.T. s (using piezometers having a ceramic permeability, $k_c > 2 \times 10^{-7}$ m/s) at the in-situ effective stresses and the pre-yield laboratory value of M_{v1} (Murray, 1971 and 1973; Lewis et al, 1975). Assessment of the former requires a knowledge of the permeability anisotropy which, in this case, appears to have been reliably assessed by laboratory tests on the large diameter samples. Obviously, in other materials k_H may be more relevant (see e.g. Rowe 1968 and 1972(a) and (b)).

(ii) pre-yield settlements of the foundation may be adequately predicted on the basis of consolidation settlements incorporating pre-yield laboratory values of M_{v1} from either large diameter block samples or piston samples (tables 6.3.2 and 6.3.4).

(iii) little pore-pressure dissipation would be anticipated during the post-yield stages of construction.

(iv) post-construction consolidation was characterised by low C_v values (of the order of $1 \text{ m}^2/\text{year}$). The associated field permeability, k_v , could be adequately determined using C.H.T. s at the correct post-yield effective stresses. The laboratory data from the block samples tended to over-estimate C_v (figure 6.3.1) and under-estimate M_v (table 6.3.4); thus a combination of k_v from C.H.T. s and the post-yield laboratory M_v over-estimated the field C_v . Excellent agreement was found, however, between the field values of k_v , M_v and C_v obtained respectively from C.H.T. s, settlements and pore-pressure dissipation.

(v) post-construction settlements were under-estimated by the laboratory values of M_v ; the influence of secondary consolidation and undrained creep are significant factors in this respect (Buri, 1978).

At this point it should also be noted that the vertical effective stresses at yield, beneath the centres of the embankments, varied considerably at any one depth, and, as mentioned in section 6.1.3., and illustrated in tables 6.1.1. and 6.1.2. and figure 6.1.45., were in many cases considerably lower than p_c' . However, as shown in table 6.1.1. and figure 6.1.45. the maximum values of σ_v' on the 'field' effective stress paths for Bank 1/1 (figures 6.1.40 and 6.1.42) were very similar to p_c' * despite varying values of σ_v' at yield. It is thus necessary to consider the consolidation histories which have led to the observed behaviour.

Beneath Bank 2 the O.C.R. at the start of construction varied from 2.6 at 1.5m depth to 1.6 at 5.5m depth; corresponding values for Bank 4 were 2.1 to 1.5 and for Bank 1/1 0.8 to 0.95 beyond the toe and, significantly, 3.3 to 1.8 beneath the central trench. This latter variation was a result of the varying initial ground-water levels, being partly a function of the central trench excavation as illustrated in figure 6.1.18 and discussed in section 2.5. Thus based on the tests of Brooker and Ireland (1965), as illustrated in figure 2.13, calculated K_0 values varied between 1 and 0.8 for Bank 2, 0.9 and 0.8 for Bank 4 and 0.95 and 0.8, and 1.1 and 0.85 respectively for Bank 1/1.

Using the data from the finite element analysis of Bank 1/1 combined with the preceding best estimates of K_0 , the positions of the yield points in p_p'/q_p' stress space have been plotted in figure 6.3.4. The yield points for Banks 2 and 4 were similarly evaluated, assuming that the total stress changes beneath their centres corresponding to the fill height at yield

*the laboratory values of p_c' from oedometer tests on the piston sample specimens, similarly to the M_v values, thus appear reliable, unlike the C_v values.

(0.95m and 0.85m respectively) were the same as for Bank 1; considering the low height/width ratios of the embankments at yield this is not considered an unreasonable approximation. The further approximation that the Bank 1/1 total stress changes, relating to $K_0 = 0.55$, also apply to other values of K_0 is also indicated to be reasonable for locations beneath the embankments at low fill heights by figures 6.1.37 and 6.1.38.*

The data presented in figures 6.1.40., 6.1.42 and 6.1.45., and table 6.1.1 suggest that following yield the effective stress paths subsequently reach a point at which the vertical effective stress approximates to p_c' ; normal consolidation is then assumed and a further point on the yield surface may be defined. The suggested form of a possible yield locus for the Mucking clay has been drawn for the three main piezometer depths in figure 6.3.4., the picture being completed by the normally consolidated effective stress failure envelope, the overconsolidated effective stress failure envelope (c' being a function of p_c') and the 'critical state' line. The intersection of the normally consolidated and the overconsolidated effective stress envelopes marks another point on the yield surface as does the undrained strength which is shown on the overconsolidated envelope[†]; as shown a small amount of progressive failure is indicated.

*the influence of the assumed K_0 on the effective stress paths is further investigated in Chapter 8.

[†]indicating that the writer considers the soil to have a 'memory' despite having been reconsolidated back onto the 'normally consolidated yield locus'.

The postulated yield locus, which is similar to YLIGHT (Leroueil et al, 1978(b)), thus suggests that with increasing O.C.R. smaller effective stress changes are required for yield; hence the early yield beneath the central trench of Bank 1/1 when compared to other locations beneath the embankment, but more remote from the trench. The shape of the proposed yield surface below the normally consolidated K_0 line can be seen to be typical of a decreasing effective stress level path under conditions of zero lateral yield (see e.g. Lambe, 1967; Brooker and Ireland, 1965).

As in the case of the pore pressures (section 6.1.3) the consolidation/settlement behaviour of the Mucking clay has been seen to be rather different to that which would be predicted by conventional methods. In order to correctly predict construction settlements it would be necessary to define the yield surface and, hence, from a knowledge of the consolidation history, in-situ effective stresses, C_v and the rate of construction to calculate the increase in vertical effective stress prior to yield. Thus using the pre-yield value of M_v the consolidation settlements during construction may be calculated. The remaining construction settlements would probably approximate to undrained deformation, but as yielding had already taken place these are unlikely to be predicted using linear elastic theory. An exact solution to the consolidation/settlement problem thus requires the use of sophisticated numerical techniques (Murray, 1974).

BANK NO.	YIELD			END OF CONSTRUCTION*			FINAL READINGS		
	t	U	C _v	t	U	C _v	t	U	C _v
	days	%	m ² /year	days	%	m ² /year	days	%	m ² /year
1/1	23	50	93	-	-	-	-	-	-
2	10	60	369	40	33	26	670	61	3.1
4	2	34	286	15	33	38	700	69	2.1

*Values relate to maximum excess pore pressures

t is time elapsed from start of construction

Table 6.3.1.

Field Values of the Coefficient of Consolidation

(Based on data presented by Schiffman, 1958)

BLOCK SAMPLE - OEDOMETER TEST			
VERTICAL EFFECTIVE STRESS			
0 - 15 kN/m ²	15 - 30 kN/m ²	30 - 60 kN/m ²	60 - 120 kN/m ²
287	63	19	4.1
BLOCK SAMPLE - TRIAXIAL DISSIPATION TEST			
MEAN EFFECTIVE STRESSES			
0 - 25 kN/m ²		50 - 100 kN/m ²	
110		13	
PISTON SAMPLES - OEDOMETER TESTS			
VERTICAL EFFECTIVE STRESS			
20 kN/m ²	50 kN/m ²	100 kN/m ²	
0.47 - 4.7	0.32 - 1.1	0.32 - 0.69	

A) C_v m²/year

BLOCK SAMPLE - OEDOMETER TEST		
VERTICAL EFFECTIVE STRESS		
15 - 30 kN/m ²	60 - 120 kN/m ²	
4.6×10^{-4}	1.2×10^{-3}	
BLOCK SAMPLE - TRIAXIAL DISSIPATION TEST		
MEAN EFFECTIVE STRESS		
0 - 25 kN/m ²	50 - 100 kN/m ²	
7.0×10^{-4}	1.1×10^{-3}	

B) M_v m²/kN

Table 6.3.2.

Laboratory Consolidation Test Data

PIEZOMETER	σ_{vi}^1	σ_v^*	$\sigma_v - u_i$	$\sigma_v^1 (\text{min})^+$	$\Delta\sigma_v^1$	t	u_t	U_z	C_v	$\sigma_v - u_t$
	kN/m ² (2)	kN/m ²	kN/m ²	kN/m ² (1)	kN/m ² (1)-(2)	days	kN/m ²	%	m ² /year	kN/m ²
PC4	14.2	71.5	63.2	22.2	8.0	625	31.4	44	1.1	40.1
PC5	25.0	101.5	74.0	30.6	5.6	630	53.5	40	2.5	48.0
PC6	35.6	131.5	84.8	39.8	4.2	630	73.8	40	1.7	57.7
PE4	15.0	58.8	58.8	28.9	13.9	687	14.7	50	0.60	44.1
PE5	25.5	88.8	69.3	32.4	6.9	685	36.3	55	1.8	52.5
PE6	34.2	118.8	78.0	44.7	10.5	688	56.9	52	0.21	61.9

* End of construction value

+ Value relating to maximum excess pore pressure

't' is time elapsed between recording of maximum excess pore pressure and final readings

Table 6.3.3.

Field Values of the Coefficient of Consolidation

(Based on data presented by Taylor, 1948)

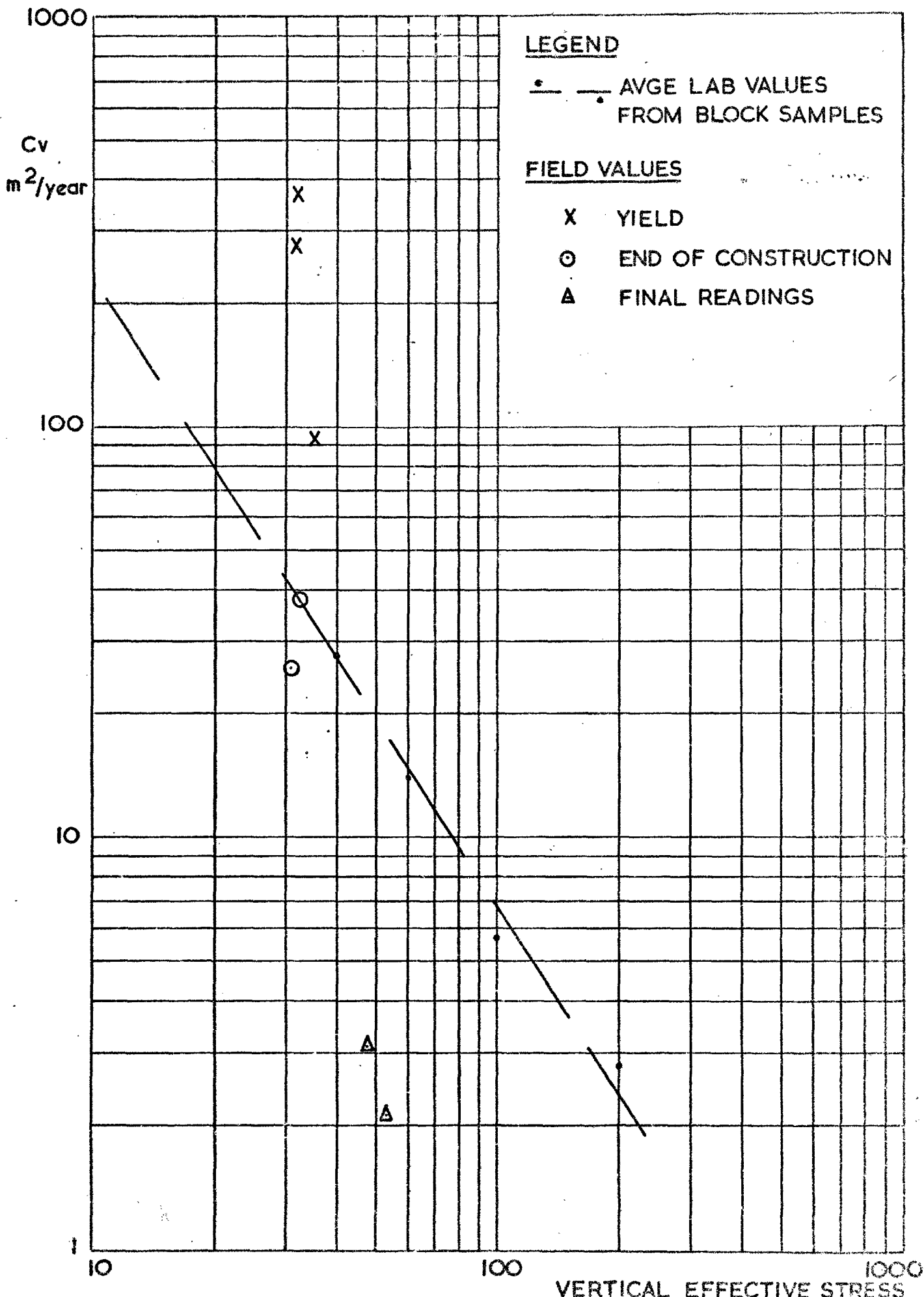
LOCATION*	PRE-YIELD	POST-CONSTRUCTION
SPC - M1	3.0×10^{-3}	2.0×10^{-3}
M1 - M2	7.8×10^{-4}	4.4×10^{-3}
M2 - M3	5.0×10^{-4}	4.0×10^{-3}
M3 - M4	2.5×10^{-4}	4.5×10^{-3}
M4 - M5	-	4.1×10^{-3}

*see figure 5.11.1. for key to locations

Table 6.3.4.

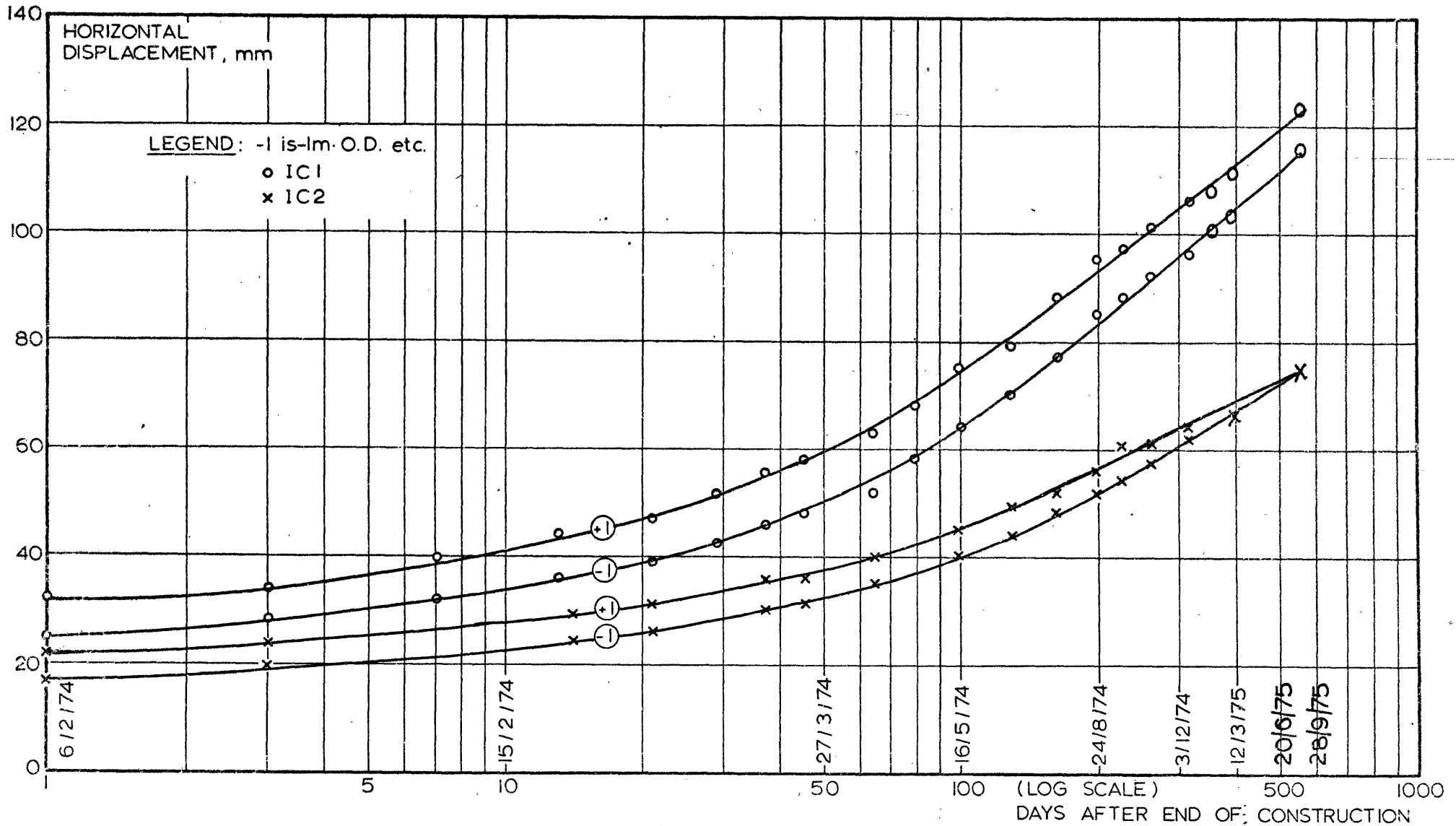
Field Values of the Coefficient of Compressibility,

$M_v, m^2/kN$ - Bank 4

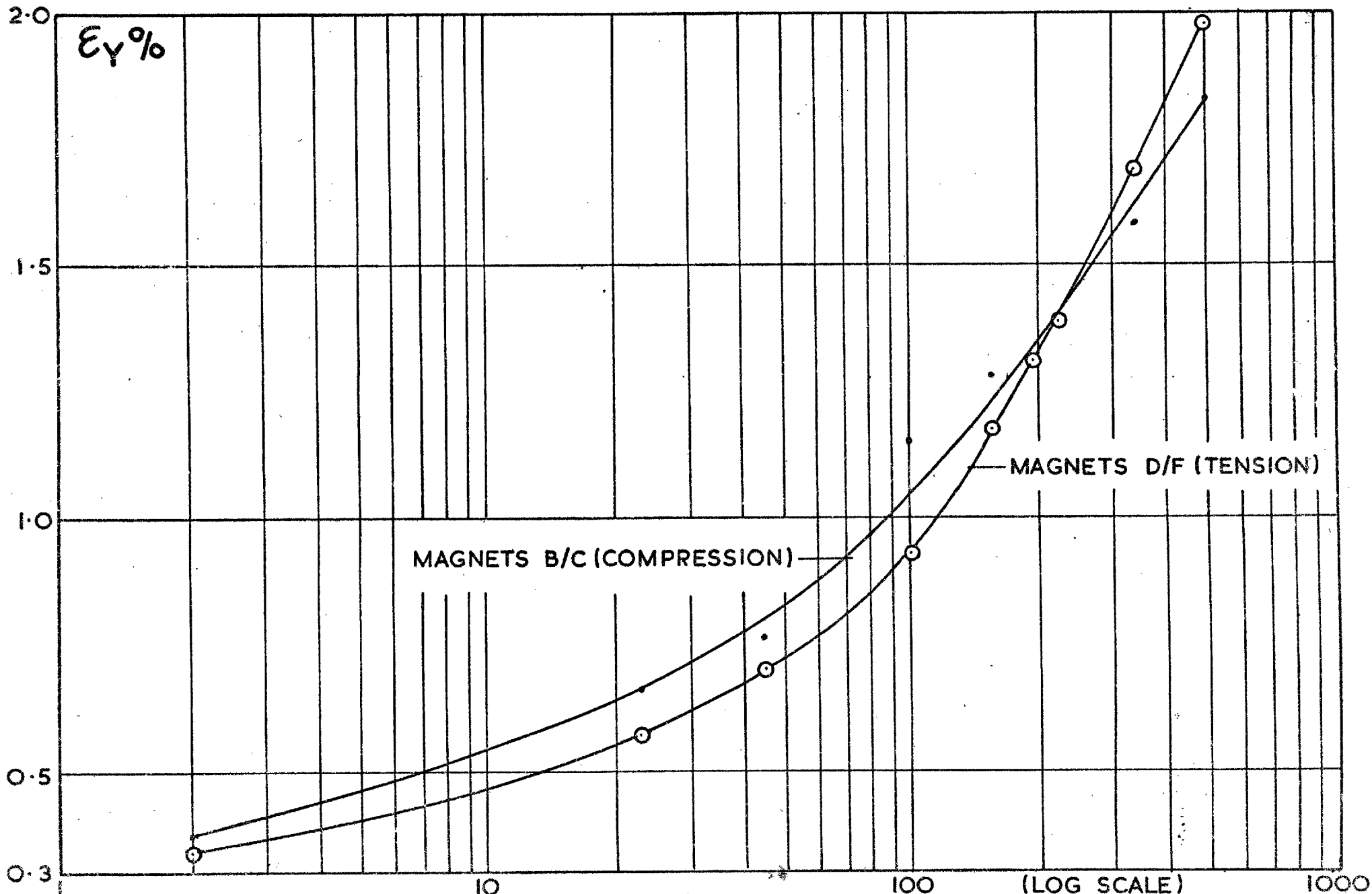


FIELD AND LABORATORY VALUES OF THE COEFFICIENT OF CONSOLIDATION

Fig. 6.3. 6



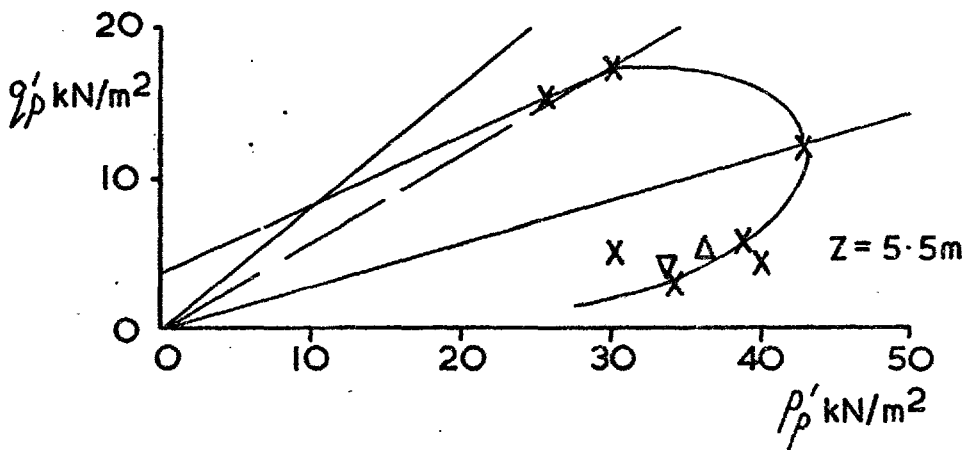
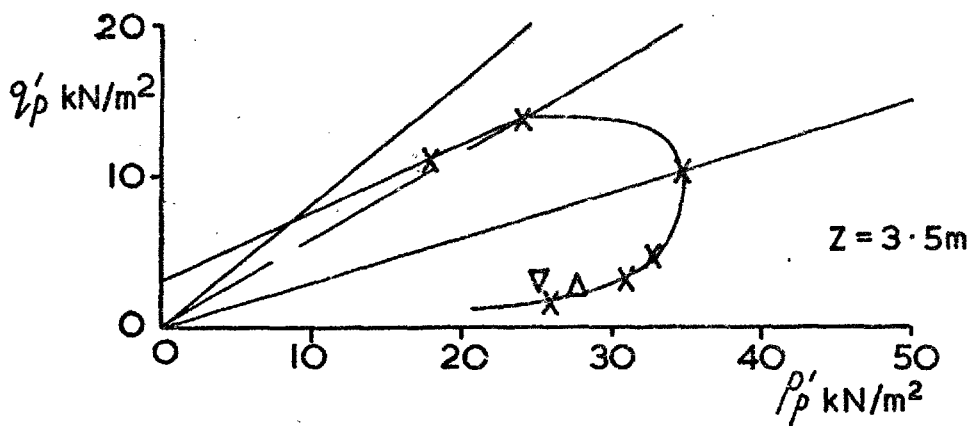
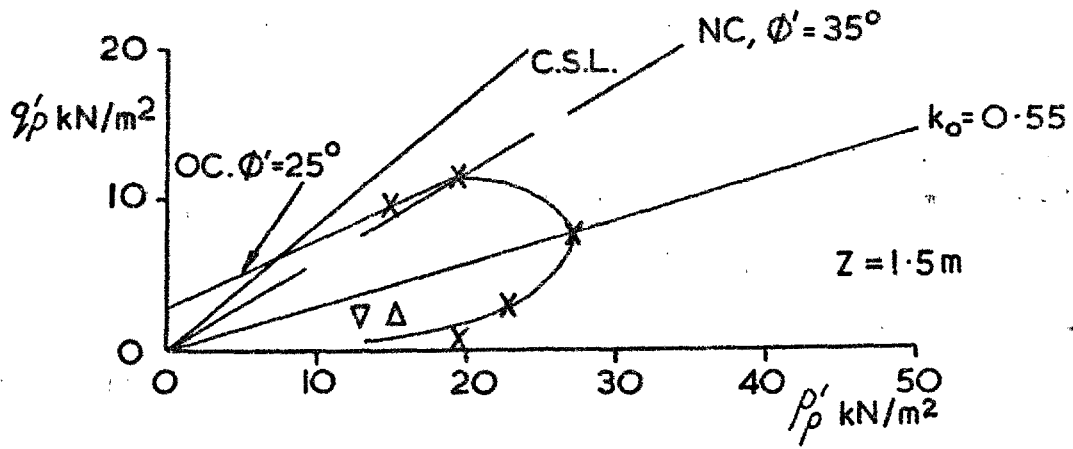
BANK 2, INCLINOMETERS: Horizontal displacements versus log time after the end of construction.



BANK 2-HSGC: AVERAGE HORIZONTAL LINEAR STRAINS VERSUS LOG TIME AFTER THE END OF CONSTRUCTION

(LOG SCALE) DAYS AFTER END OF CONSTRUCTION

Fig. 6.3.3



LEGEND	
X	BANK 1/1
Δ	BANK 2
∇	BANK 4

SUGGESTED FORM OF POSSIBLE YIELD LOCUS FOR MUCKING CLAY BASED ON OBSERVED YIELD UNDER FULL SCALE LOADING CONDITIONS

Fig. 6.3.4.

6.4. The Direct Use of Field Measurements To Control Construction

6.4.1. Introduction

As discussed in Chapters 1 and 4, it was hoped that the full scale foundation trials at Mucking would enable the direct use of field instrumentation to provide advance warning of instability during construction of the main works. In the following a brief assessment of the success of the various measurement systems in enabling the detection of incipient instability is given.

6.4.2. Displacements

Only horizontal displacements are considered for construction control purposes, in order to avoid the consolidation problem associated with the interpretation of vertical movements. Horizontal displacements of the Mucking foundation have been plotted, indirectly, versus time in the form of displacement profiles (figures 5.3.2. to 5.3.4. and 5.4.2. to 5.4.14) and, directly, versus fill height (figures 5.2.1. to 5.2.3., 5.7.2. to 5.7.6. and 6.1.3. to 6.1.7). As discussed in section 6.1.1. the latter indicate early yield of the foundation and subsequent non-linear behaviour. However, major non-linearity of the relationships developed at fill heights of 3.25m and 3.85m for Stages 1 and 2, respectively, of Bank 1 and possibly at close to maximum fill height for Bank 2. Thus, construction may have been stopped, of a main works embankment, at these fill heights, on the basis of the relationships between horizontal displacement and fill height.

The early yield of the foundation suggests that the best hope of predicting overall failure is to detect local failure. It has been postulated (section 6.1.4) that local failure progressed outwards from beneath the

embankment crest, and its detection at such a locality would be advisable to prevent local failure spreading into overall failure.

The foundation has also been seen to undergo significant undrained creep at higher stress levels and thus a plot of $\Delta Y/h$ versus time (see e.g. Wilkes, 1973) suggests itself as being more amenable to the detection of local failure. Figure 6.4.1. shows such a plot; the radical changes in the relationships at 2.75 - 3.25m fill height for Bank 1/1, at 3.8m for Bank 1/2 and, possibly, at 2.45m for Bank 2 are clearly visible. Based on these plots construction would have been stopped at 3.5m, 4.25m and 2.8m for the respective embankments. Continuing observations would then have been required in the case of both stages of Bank 1 to see if, as appears likely, the displacements were continuing to accelerate towards failure or, as in the case of Bank 2, gradually diminishing.

This type of plot thus appears suitable for the detection of local failure from horizontal displacement observations. However, it is obviously important to detect local failure beneath the embankment crest/shoulder to provide sufficient time for observations to be made at constant fill height. By the time local failure has spread beyond the embankment toe overall failure may well be unavoidable unless remedial measures are taken.

Finally, it has been noted that the development of significant heave beyond the embankment toe closely precedes failure.

6.4.3. Strains

Average horizontal linear strains for Banks 1/1, 1/2 and 2 were presented as profiles in figures 6.1.9 to 6.1.11 and plotted versus fill height and time in figures 6.1.12 and 6.1.13. As discussed in section 6.1.2., the latter indicated definite changes in the development of strains from negligible, to significant, to relatively large. Large strains developed beneath Bank 1/1 at between 2.75m and 3.25m fill height and beneath Bank 1/2 at 4.05m fill height; large strains were not developed beneath Bank 2 during construction. These data thus tell a similar story to the horizontal displacements, local failure beneath Bank 1/1 probably developing between 2.75m and 3.25m fill height, spreading out beyond the toe as the fill height reached 3.5m and finally reaching the toe trench at 4m. Corresponding values for the Bank 1/2 construction are 3.85m, 4.25m and 4.50m; local failure beneath Bank 2 had probably also commenced at the maximum fill height of 2.80m.

When plotted as ϵ_y/h versus time (figure 6.4.2) the average linear horizontal strains clearly depict the probability of local failure beneath Banks 1/1 and Banks 1/2 at the fill heights mentioned above. Thus average horizontal linear strains derived from H.S.G. data provide a further means to control construction.

6.4.4. Excess Pore Pressures

Excess pore pressures have been plotted versus time in figures 5.5.3. to 5.5.6. and versus fill height in figures 6.1.19., 6.1.20 and 6.1.23. As discussed in some detail in section 6.1.3. the latter plots indicate early yielding of the foundation, with signs of an increase in pore-pressure

response as local failure commenced. However, the interpretation is not easy, the only definite indication of failure being provided by those piezometers beyond the embankment toes; even in these instances the separation of yield from local failure would not always be easy in practice. Thus, piezometers 1 - 3 indicated local failure during the construction of Bank 1/1 at 3.75m fill height and piezometers 22 - 24 indicated local failure of Bank 1/2 at 4.25m fill height. However, similarly to heave measurements (section 5.2), pore pressures at these locations tend to be unreliable as a result of the low absolute values (section 5.5).

Plotting $\Delta u/h$ versus time, as in figure 6.4.3., can be seen to provide no assistance in the task of predicting the onset of instability.

6.4.5. Summary

The data presented in this section illustrate the trends, during construction of the embankments, summarised previously in section 6.1.4. i.e. of early yield followed by 'progressive' local failure. It has been possible to identify the fill height at which local failure commenced and to monitor its progress towards overall failure.

The writer's suggestions for construction control using 'direct' measurements are as follows:-

(i) Plotting of average horizontal (near surface) linear strains divided by fill height, versus time, for locations across the entire width of the embankment.

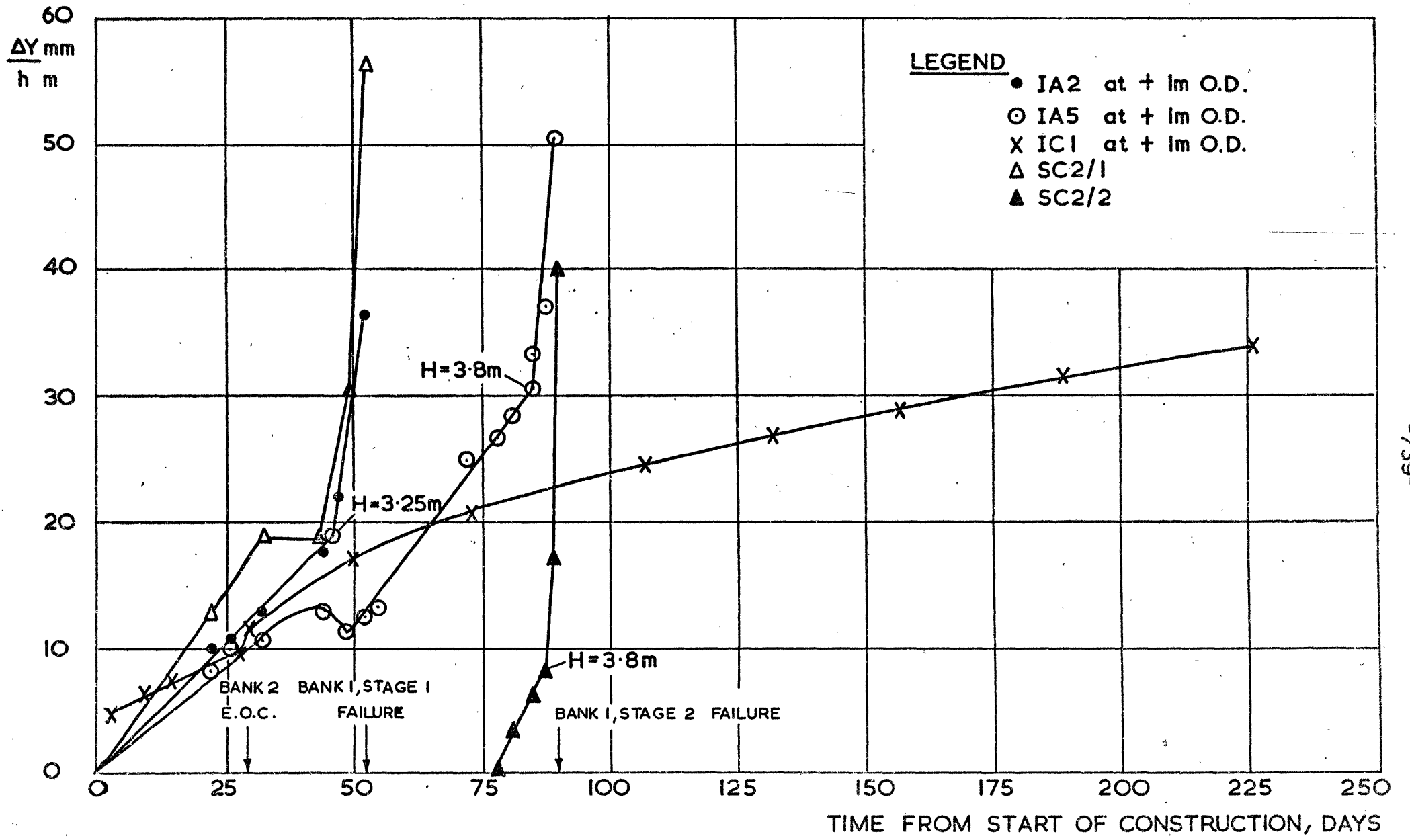
(ii) Plotting of maximum horizontal displacements divided by fill height, versus time, from inclinometer observations across the entire width of the embankment.

(iii) Plotting of excess pore pressure versus fill height for piezometers across the entire width of the embankment.

(iv) Plotting of heave beyond the toe, divided by fill height, versus time.

Plots (i) and (ii) would hopefully detect the initial local failure beneath the embankment, possibly supported by the data plotted in (iii). If local failure then continued to spread its progress would be monitored by plots (i) and (ii), corroborated by (iii) and (iv); by which time rapid preventative action would be required to prevent a total collapse.

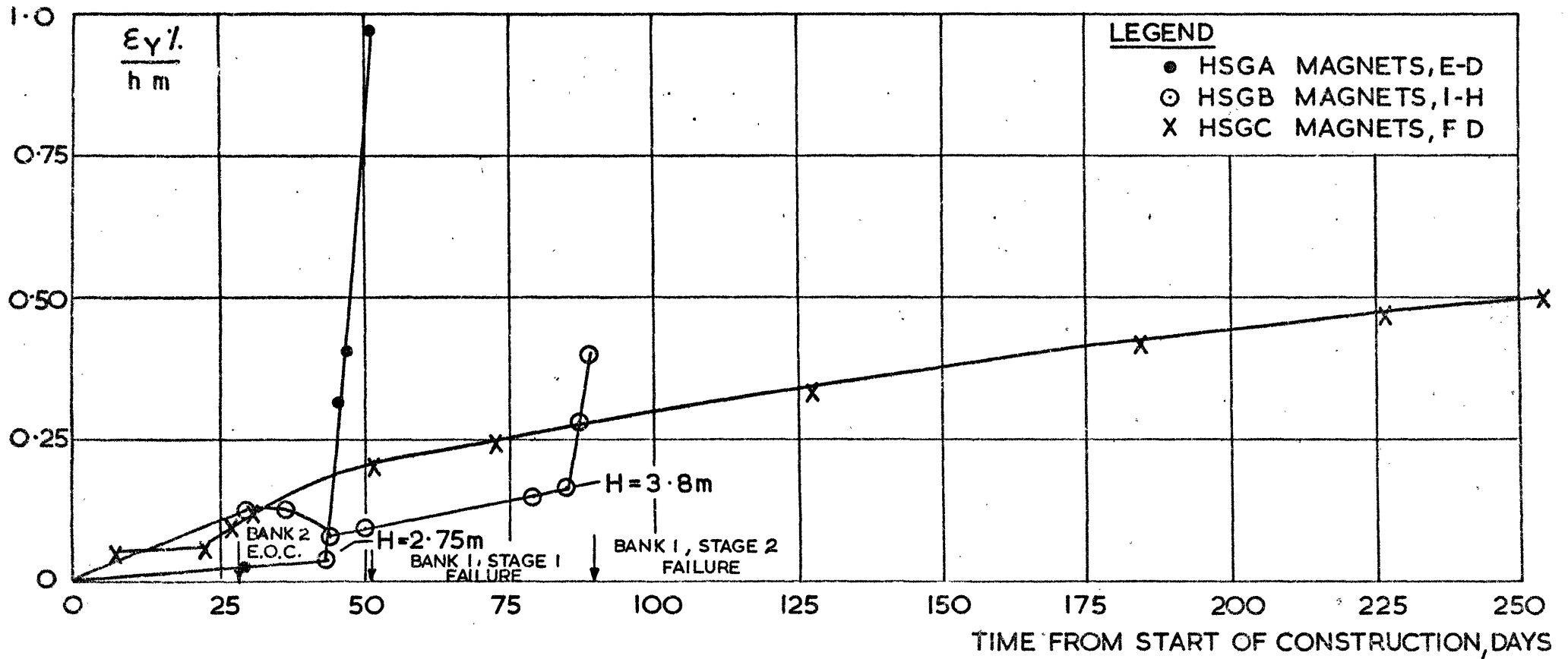
The use of pore-pressure measurements together with effective stress stability charts (Cook and Ingold, 1973; Symons, 1974 and 1976(a)) is an 'indirect' use of field data to control construction and as such has not been considered herein; comment on this technique is, however, made in section 7.7.



-739-

USE OF HORIZONTAL DISPLACEMENT MEASUREMENTS TO PREDICT FAILURE

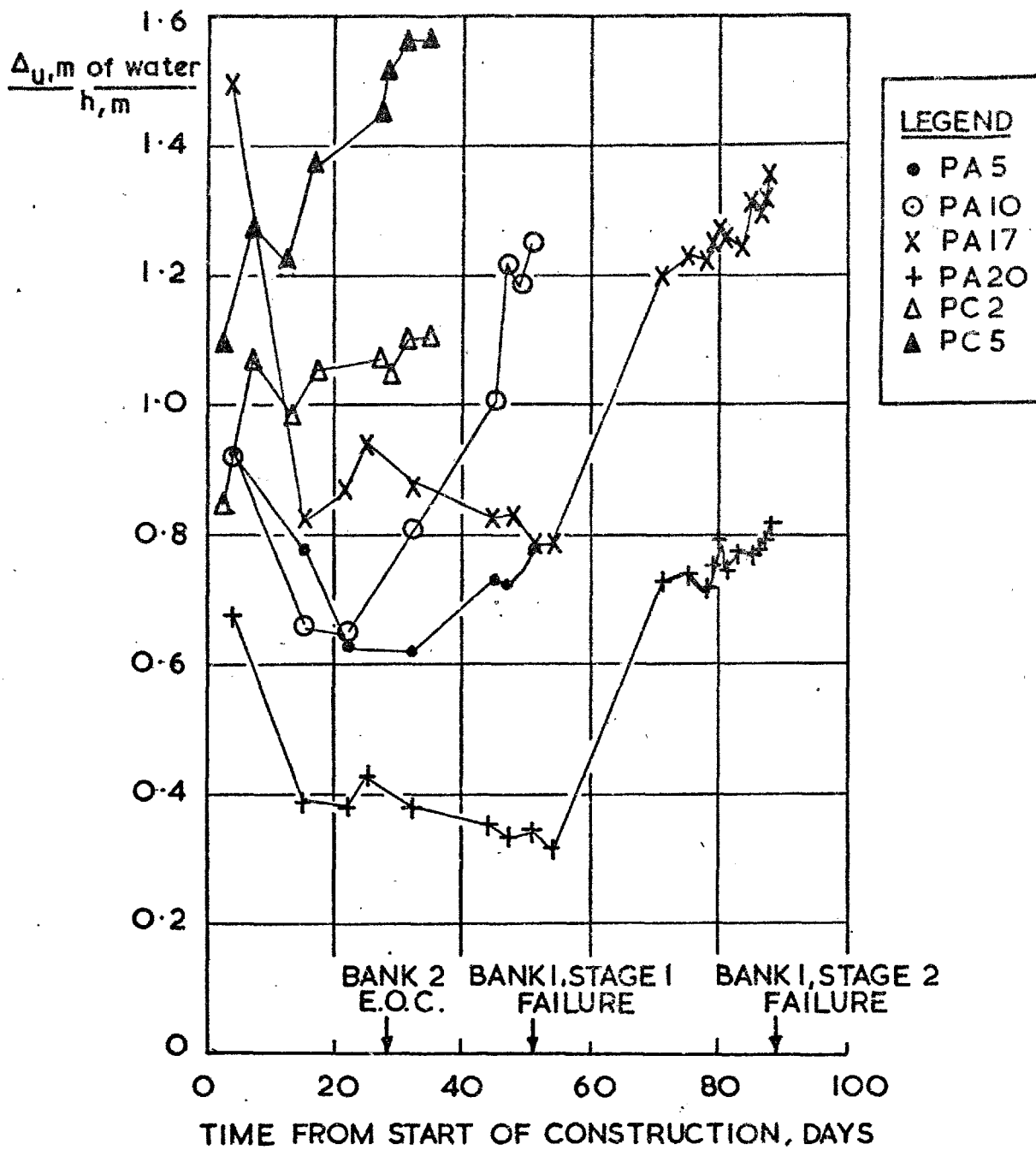
Fig. 6.4.1.



-740-

Fig. 6.4.2.

USE OF AVERAGE HORIZONTAL LINEAR STRAINS TO PREDICT FAILURE



USE OF EXCESS PORE-WATER PRESSURES TO 'PREDICT' FAILURE

Fig.6.4.3

CHAPTER 7

ANALYSIS OF EMBANKMENT STABILITY USING LIMIT EQUILIBRIUM METHODS

7.1. Methods, and Extent, of Analyses

7.1.1. Methods Used

Two methods of limit equilibrium analysis were used, both based on the method of slices (Fellenius, 1936); Bishop's Routine Method (1955) was used to analyse circular arc failure surfaces and Sarma's Method (1973) to analyse general slip surfaces.

In its 'Rigorous' form the method proposed by Bishop (1955) satisfies all the equations of force and moment equilibrium. The simpler 'Routine' method incorporates the assumption that:-

$$\sum \left[(X_n - X_{n+1}) \frac{\sec \theta \tan \phi'}{1 + \frac{\tan \phi' \tan \theta}{F}} \right] = 0 \dots\dots\dots(7.1)$$

where X_n is the shear force on slice boundary 'n', θ is the angle of the slip surface to the horizontal and 'F' is the F.o.S.

and does not consider the interslice forces further, save that the horizontal (E) interslice forces are implicit in the formulation of the normal effective stress on the slip surface which is obtained by resolving vertically. Whitman and Bailey (1967) interpret the 'Routine' method as assuming horizontal resultant interslice forces, although Bishop (1955) does not actually assume (equation 7.1) that $\Delta X (= X_n - X_{n+1}) = 0$, or that $X_n = X_{n+1} = 0$; of course, in general, $\sum \Delta X = 0$.

In practice (Bishop, 1955; Johnson, 1975) the assumption of equation 7.1 has little influence on the calculated F.o.S. As 'F' appears on both sides of Bishop's equation an iterative solution is required.

The analyses performed using Bishop's Routine Method made use of a computer program written by Mr. E. N. Bromhead of Kingston Polytechnic. The section to be considered was divided into zones, thus separating the various soil types, each zone being assigned shear strength parameters, a bulk unit weight and a value of r_u . Slip surfaces were specified by centres of rotation plus an initial radius and radius increment.

The initial F.o.S. for input into the Bishop Routine calculation was determined using the Conventional (or U.S.B.R.) method (Daehn and Hilf, 1951). For a circular arc failure surface the Conventional Method is derived from the equations of force and moment equilibrium, together with the assumption that:-

$$\sum \tan \phi' \left[(X_n - X_{n+1}) \cos \theta - (E_n - E_{n+1}) \sin \theta \right] = 0 \dots\dots\dots(7.2)$$

This assumption, which Whitman and Bailey (1967) interpret as being equivalent to the assumption of interslice forces parallel to the base of the slice (the normal effective stress being obtained by resolving perpendicular to the base of the slice), is in fact valid for planar slip surfaces (i.e. θ constant) and constant ϕ' . In the latter case the formulation can be derived from a consideration of the equations of force equilibrium only. For circular arc slip surfaces with wide central angles of arc, particularly when the pore pressures are high, the Conventional Method may lead to highly conservative safety factors (Bishop, 1955; Whitman and Bailey, 1967; Johnson, 1975).

In the computer program used, convergence of the iterative process was deemed to have occurred when the F.o.S. at the start and finish of an iteration differed by less than 0.001.

Whitman and Bailey (1967) have suggested that the inherent assumption in the Bishop Routine Method occasionally results in the calculation of erroneous normal effective stresses. They suggested that in any analysis it should be checked that both the numerator and denominator of this term were positive, i.e.:-

$$W - u.b. - \frac{c'b \tan \theta}{F} > 0 \dots\dots\dots(7.3)$$

and,

$$1 + \frac{\tan \theta \tan \phi'}{F} > 0 \dots\dots\dots(7.4)$$

where 'W' is the weight of a slice whose width is 'b'

These checks were provided in the computer program, although contrary to Whitman and Bailey (1967), Bromhead (1976), considered that, on the rare occasion such errors are found, the erroneous effective stresses generally result in only small errors in the calculated F.o.S.

Satisfaction of all of the physical requirements on an arbitrary slip surface, together with non-failure at the interslice boundaries, has been attempted by, among others, Kenney (1956), Janbu (1957), Nonveiller (1965) and Morgenstern and Price (1965). The equations derived by the latter satisfied all conditions of equilibrium but were obviously statically

indeterminant: however, static determinancy can be achieved by many means, including the assumption that the relationship between 'E' and 'X' is known; this being the basis of the Morgenstern - Price Method (1965), wherein:-

$$X_n = \lambda f(x) E_n \dots\dots\dots(7.5)$$

f(x) determining the variation in the angle (α) of the resultant interslice force from slice to slice, thus:-

$$\tan \alpha_{(n)} = \frac{X_n}{E_n} = \lambda(f(x)) \dots\dots\dots(7.6)$$

λ being a constant (additional unknown) scale factor which determines the absolute value of α .

In the Morgenstern - Price Method f(x) is assumed and λ calculated; a constant f(x) = 1 is commonly assumed, thus leading to parallel interslice forces. An iterative solution is required to arrive at 'E' and 'X' forces satisfying overall equilibrium and the final solution must be checked to ensure that the derived line of thrust is reasonable and that the F.o.S. against vertical shear between the slices (F_L) is adequate. However, the derived F.o.S. is not unique and a lot of iterations are usually required for solution; in addition convergence problems are not uncommon (Bromhead, 1976) and satisfaction of all the physical requirements may be difficult (Whitman and Bailey, 1967).

Sarma (1973) also formulated a rigorous solution to the general slip surface problem, but in terms of the critical earthquake acceleration (K_c), corresponding to a static F.o.S. of unity; no iterations are necessary to determine K_c . The static F.o.S. is determined by reducing

the shear strength parameters around the slip surface by a certain factor until $K_c = 0$, at which point the factor is the static F.o.S.; only a few iterations are required to determine the latter by interpolation and convergence is not a problem. Alternatively, when searching for a critical surface in terms of static F.o.S. initial analyses can be run to determine the surface having the lowest value of K_c thus making a substantial saving in computational effort. Sarma and Bhawe (1974) have demonstrated that, for a particular problem, a simple relationship between K_c and static F.o.S. exists, and that the surface for which K_c is a minimum is very close to that for which the static F.o.S. is a minimum. Similarly to the Bishop Routine Method (but unlike the Morgenstern - Price Method) hand calculations can be used to perform Sarma's Method.

Similarly to Morgenstern and Price (1965), Sarma (1973) considered force and moment equilibrium for each slice; however, Sarma (loc cit) simplified the moment equation by taking moments about the centre of gravity of *the mass*. Similarly to Bishop (1955), Sarma (loc cit) used the force equilibrium equations to eliminate $DE (= E_n - E_{n+1})$; a solution for DX and K_c was then possible. However, the distribution of 'X' forces also has to satisfy $\sum DX = 0$ and thus Sarma (loc cit) assumed:-

$$DX_x = \lambda F_x \dots\dots\dots(7.7)$$

$$\text{with } \sum F_x = 0 \dots\dots\dots(7.8)$$

i.e. an assumed distribution of DX is used which satisfies $\sum DX = 0$ and the constant scale factor (noting this to be different to the Morgenstern - Price λ) calculated, leading to the value of K_c without iteration. The

actual values of 'X' and 'E' for each slice boundary can then be calculated, again without iteration, and F_L determined; the position of the line of thrust is also evaluated at this stage.

Thus, whereas the Morgenstern - Price Method necessitates the assumption of a distribution of the inclination of the thrust line, Sarma's Method depends on a knowledge of F_x . Sarma (loc cit) simply derived 'E' from a consideration of the Mohr circle of stress for the failure plane relevant to each slice (i.e. by deriving σ_y and σ_x) and was thus able to define 'X' as:-

$$X_n = C_n \frac{1}{F_L} = C_n \lambda f(x) \dots\dots\dots(7.9)$$

where C_n represents the Mohr-Coulomb failure criterion. From equation (7.7) and (7.9) it follows that:-

$$F_x = C_n f(x) - C_{n+1} f(x) \dots\dots\dots(7.10)$$

In order to analyse a problem an assumed variation of the local F.o.S. ($=F_L$), as represented by $f(x)$ (again noting that this is not the same as the Morgenstern - Price $f(x)$), must be input; a value of 1 is usually chosen for initial purposes.

Sarma's Method was used in the form of a computer program written by Dr. S. K. Sarma of Imperial College, University of London. The section to be considered was divided into zones comprising the various soil types, each being assigned shear strength parameters and a bulk unit weight. Pore pressures were input on a grid basis, as were the points used to define the slip surfaces; pore pressures relevant to the base and sides of a slice were determined by linear interpolation as part of the computer

solution. An $f(x)$ value of unity was used throughout; all critical solutions were checked for physical acceptability.

Although a brief outline of the rather esoteric applied mechanics of the limit equilibrium methods used has been attempted it should be borne in mind that the variations in 'accuracy' resulting from the use of the different accepted methods is likely to be small when compared to the differences in F.O.S. which may result from variations in shear strength data (Bishop, 1955; Johnson, 1975) and different interpretations thereof. A striking example of the latter is presented by Lacasse and Ladd (1973) in their reappraisal of the New Liskeard case history (Lo and Stermac, 1965).

Comprehensive reviews of the available methods of limit equilibrium analyses have been presented by Whitman and Bailey (1967), Lowe (1967), Skempton and Hutchinson (1969), Wright et al (1973) and Johnson (1975).

7.1.2. Extent of Analyses

(i) Circular Arc Failure Surfaces

Back-analyses of the Bank 1 failures were carried out employing both total and effective stress parameters; slip surfaces restricted to fit, as closely as possible, the field observations, and unrestricted (within the limit that they emerged within the top part of the embankment) surfaces were both considered. The end-of-construction stability of Bank 2 was analysed in terms of both total and effective stresses, no restrictions being placed on the slip surface locations; post-construction stability was assessed in terms of effective stress only.

With $\phi' = 0$ and $c' = C_u$ the formulations of both the Conventional and Bishop Routine Methods revert to that of the $\phi_u = 0$ Analysis (Skempton, 1948(c); Skempton and Golder, 1948).

The nomenclature used to describe the critical surfaces is presented in table 7.1.1.

(ii) Non-Circular Failure Surfaces

Back-analyses of the Bank 1 failures were again made employing both total and effective stress parameters, but in this case only surfaces approximating to the field observations were considered for Stage 1, although unrestricted surfaces were investigated for Stage 2.

The stability of the critical surfaces (as designated in table 7.1.1) was also investigated in conjunction with the post-failure profiles, assuming a state of limiting equilibrium to have been re-established, in order to assess the field residual shear strength parameters and hence the brittleness index, I_B , in terms of both total and effective stresses. I_B is defined (as by Bishop, 1967 and 1971(b)) in figure 7.1.1.

V W X / Y Z

- V - S = Sarma's Method; Non-Circular Surface
- B = Bishop's Routine Method; Circular Surface

- W - T = Total Stress Analysis of Foundation
- E = Effective Stress Analysis of Foundation

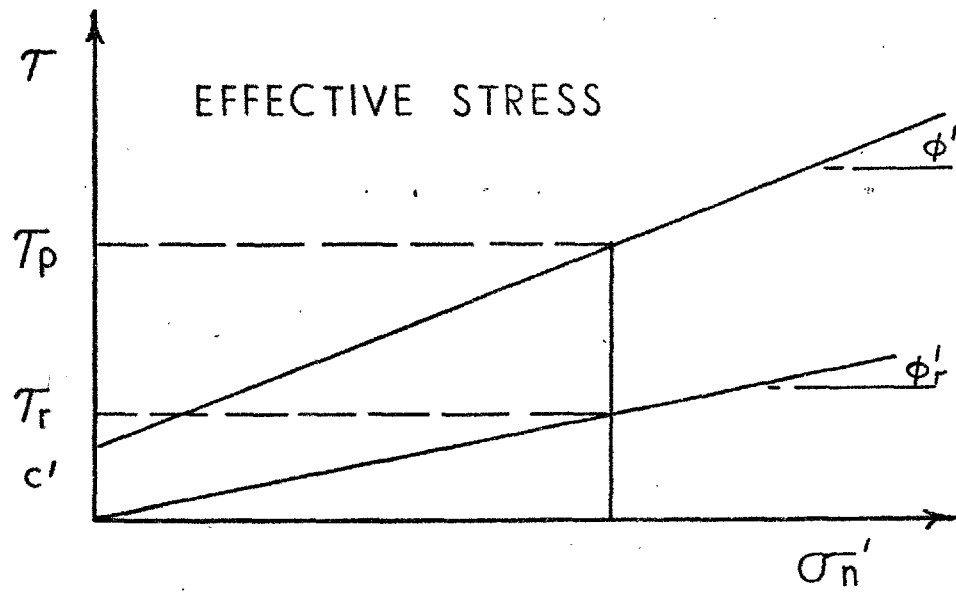
- X - 1 = Weak Crust Assumption
- 2 = Strong Crust Assumption

- Y - 1 = Critical Surface for Stage 1
- 2 = Critical Surface for Stage 2

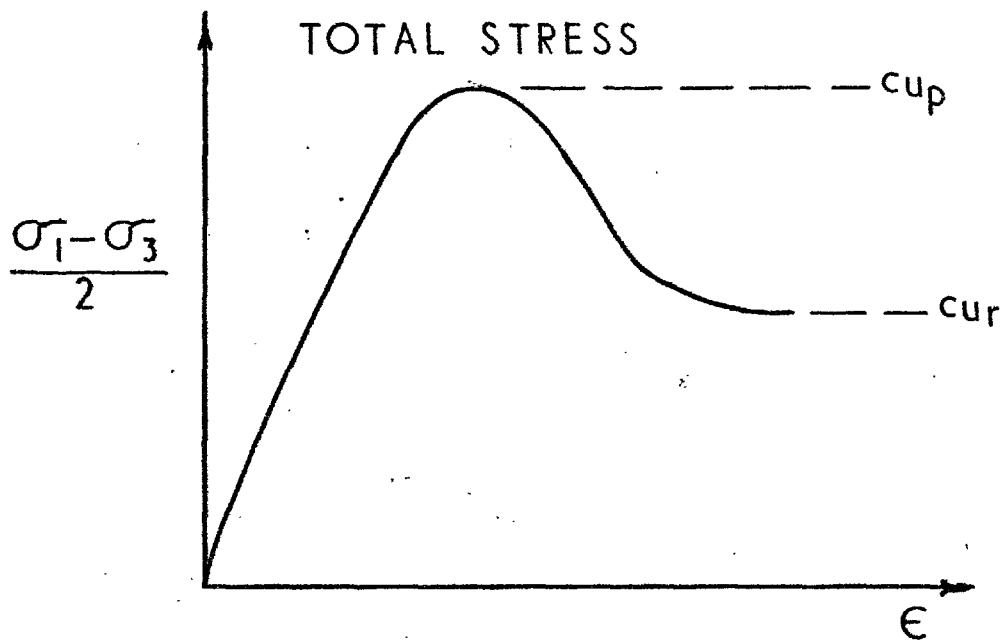
- Z - = Surface Restricted to Fit Field Observations
- A = Unrestricted Surface
- (A) = Unrestricted Surface Fits Field Observations

Table 7.1.1.

Key to Critical Slip Surfaces



$$I_B = \frac{\tau_p - \tau_r}{\tau_p}$$



$$I_B = \frac{c_{up} - c_{ur}}{c_{up}}$$

BRITTLENESS INDEX (I_B) IN TERMS OF EFFECTIVE & TOTAL STRESS

Fig. 7.1.1

7.2. Shear Strength Data for Limit Equilibrium Analyses

7.2.1. General

A detailed account of the factors influencing the relevance of the laboratory measured undrained shear strength to the analysis of full scale structures was provided in section 2.7. In conclusion, a design profile of C_u versus depth was presented in figure 2.23 (see also figures 3.18 and 3.23), derived via a consideration of the influence of stress path (including initial stresses and undrained strength anisotropy), stress system, sample size and sample disturbance. As illustrated in figure 2.21 and summarised in table 3.11, a major reduction in the undrained strength measured in a 10-15 minute laboratory test would be anticipated in a field trial lasting some 50 - 90 days. Although, as outlined in section 3.4., the writer was uncertain as to the validity of a direct extrapolation of the laboratory data to the field case it was decided to apply such a reduction factor (=0.65) to the laboratory data in order to obtain a best estimate of the relevant field undrained strength (Skempton and Bishop (1950) suggested 0.70 to 0.85 in general). Finally, the data in figure 2.27 suggested that progressive failure might cause a considerable reduction in the field mobilised undrained strength although, as illustrated in table 3.11., no allowance could be derived from the existing data.

A detailed account of the factors influencing the relevance of the undrained shear strength measured with the field vane has been given in Chapter 3. In conclusion, it was considered that only tests carried out with the new large vane apparatus, and conducted fairly rapidly, actually measured an undrained strength. The undrained strength measured with the field vane was, in this case, concluded to at least partially account for the undrained

strength anisotropy anticipated to be relevant to the full scale field situation. However, as in the case of the laboratory undrained strengths a considerable undrained strain rate effect was anticipated (figure 3.3); the estimated full scale field value of the undrained strength being some 61% to 70% of that measured with the field vane. Once again the effects of progressive failure could not be quantitatively assessed. In this context it is relevant to note that the majority of the case histories considered by Bjerrum (1972) related to foundation materials with a liquidity index equal to or in excess of unity. Dascal and Tournier (1975) considered that Bjerrum's (loc cit) correction factor needed modification to account for progressive failure in sensitive soils having liquidity indices in excess of unity. The values of the liquidity index for the Mucking clay (figure 2.7) are more in keeping with the values suggested by Skempton (1970) for clays normally consolidated by gravitational compaction in the range of vertical effective stresses representative of typical failure surfaces.

The laboratory effective stress shear strength parameters of $c' = 8 \text{ kN/m}^2$ and $\phi' = 25^\circ$ (figures 2.17 and 2.25) were also discussed in detail in section 2.7 and arrived at after an assessment of the same factors considered to influence the undrained strength. As illustrated in figure 2.22 the effective stress shear strength parameters were also strain rate dependent and although this dependency was partially a function of pore pressure (figure 2.22) it also involved a significant drop in c' (assuming ϕ' constant) as shown in figure 7.2.1.,* which can be directly compared to figure 2.21.

*some doubt may be cast on the validity of the effective stress path for the 3.8 minute duration test, but as the average laboratory t_f was 9 hours this does not affect the portion of the curve relevant to extrapolation from laboratory to field conditions.

The shear strength, in terms of effective stress, mobilised under full scale loading conditions may also be reduced as a result of progressive failure, although there were no laboratory data to substantiate this. Certainly, the data presented by Skempton (1964) and Vaughan and Walbancke (1975) suggest that, on the basis of percentage clay fraction and plasticity index respectively, ϕ'_r for the Mucking clay could be substantially less than ϕ'_p .

Finally, the results of the large vane tests at test levels 1 and 2 (figure 3.20) indicated that a significant drained strain rate effect may also be anticipated in the field.

The influence of strain rate effects, as observed in the laboratory and in the field, on the full scale field behaviour was discussed in section 3.4 and considered to be a function of the field stress-strain-time path (Bjerrum, 1973). Rapid consolidation during the initial stages of embankment construction was predicted by both small scale laboratory (section 2.4.3) and field (section 3.3) tests and by field observations of seasonal ground-water movements (section 2.5) and confirmed by analysis of the full scale behaviour (sections 6.1.3. and 6.3). Thus at this stage a re-assessment of the anticipated strain rate effect is appropriate.

Although the existence of strain rate effects has long been appreciated (Taylor, 1948; Skempton and Bishop, 1950; Casagrande and Wilson, 1951; Skempton and Bishop, 1954; Casagrande, 1960) the successful use of the $\phi_u = 0$ Analysis using both laboratory (Skempton and Golder, 1948; Bishop and Bjerrum, 1960) and, in some cases (as discussed in section 3.1.1.), field vane shear strengths suggested that such effects were not of major importance. However, compensating factors such as sample disturbance,

sample size, consolidation in the field and the possibility of higher field strengths as a result of stress path effects (Hansen and Gibson, 1949) may have been influential in this success (Bishop and Henkel, 1962).

Test embankments are normally constructed as rapidly as possible, to minimise dissipation and /or redistribution of pore pressures, until failure occurs and the back-calculated shear strength taken as the best approximation to the field value of C_u . While this may be true in clays of low plasticity it is based on the assumption that the minimum F.o.S. pertains to the end-of-construction situation (Bishop and Bjerrum, 1960; Bjerrum 1972): an assumption which may not be justified for clays of higher plasticity; this fact, as discussed in section 3.4.3., is obscured by the normal practice of continuous construction until failure occurs but demonstrated by delayed failures of the type reported by Golder and Palmer (1955) and Kaufman and Weaver (1967)*. It is interesting that in both of these cases the failures were attributed to progressive failure, which is time independent (Bishop, 1967).

Figure 7.2.2.(A) diagrammatically represents (after Taylor, 1948) the relationship between shear strength and test duration for a specimen of clay, drainage from which is controlled by both C_v and the drainage path length, assuming that:-

(i) dissipation of excess pore pressure, which is always, on average, positive with respect to the base value, increases C_u and the drained strength corresponding to a particular effective stress is greater than the consolidated undrained strength for the same test duration.

*Stability of the Atchafalaya Levees is reconsidered by Foott and Ladd (1977), who discount progressive failure and make no mention of strain rate effects. Their use of the SHANSEP design method may provide another example of compensatory errors.

(ii) both C_u and the drained strength are time dependent.

(iii) the major increase in strength as a result of pore pressure dissipation occurs within two log cycles of time.

Taking figure 7.2.2.(A) to be relevant to the construction of a trial embankment* on a plastic clay three representative cases (labelled 1 to 3) may be considered.

(1) the shear strength/time relationship for a foundation subject to rapid consolidation throughout construction; this implies that no dramatic decrease in C_v occurs as a result of the increase in effective stress and/or that drainage path lengths remain very short i.e. that the soil fabric is not altered by the shear and consolidation strains which develop. Such a soil would contain sand/silt lenses of relatively high permeability (see e.g. Rowe, 1968 and 1972(a) and (b)). In this case even a rapidly constructed test embankment would not provide a true measure of the field undrained strength, point 'C' being relevant to the field failure rather than point 'D' which might have been measured in the laboratory. However, significantly, the back-calculated field value of the shear strength may be similar to that measured in a quick undrained laboratory test.

(2) the opposite extreme is represented by a foundation of considerable depth having a low in-situ C_v value, being typical of entirely normally consolidated deposits, and which therefore experiences little, if any, gain in shear strength during construction (see e.g. Kaufman and Weaver, 1967; Foott and Ladd, 1977). The shear strength back-calculated from a typical trial embankment failure is therefore the relevant undrained strength for the particular stress-strain-time path. However, main works embankments having a significant F.O.S. against short-term failure may undergo a delayed failure, as outlined in Chapter 1.

*as qualified in section 3.4.3.

(3) most typically, significant dissipation takes place during construction but may result in only a slight over-estimate of the undrained strength (point 'E' being relevant to the field situation, point 'F' being a truly undrained strength). This would be typical behaviour for the lightly overconsolidated clays considered by Leroueil et al (1978(b)) in their study of some 30 case histories and, as shown in sections 6.1.3. and 6.3., of the Mucking clay. However, the net strength change is still a loss and the minimum field shear strength may not be reached until some considerable time after the end of construction, as is illustrated in section 7.6.

A typical curve 'AA' was established from the laboratory data, as illustrated in figure 2.21; although a similar curve for fully drained behaviour was not established, figures 2.22 and 7.2.1. suggest its likely existence. The time dependency of C_u and c' are compared in figure 7.5.2.

Time dependent field behaviour was clearly demonstrated by the large vane tests (section 3.3) and it is instructive to compare figure 3.20(B) with figure 7.2.2.(A). The large vane test data at levels 1 and 2 indicate behaviour typical of curve 1 (i.e. a shear strength/time relationship such as 'ACB' whilst at levels 3 and 4 the behaviour is more typical of curve 3 (i.e. a shear strength/time relationship such as 'ADEB').

The influence of a yield stress on the partially drained tests is unknown, but these tests together with the observed pore-pressure/consolidation behaviour during construction suggest that the full scale behaviour may well be characterised by a curve such as 3 (figure 7.2.2.(A)).

Figure 7.2.2.(B) depicts the variations in F.o.S. which would accompany the variations in the field shear strength discussed previously; only in the case of curve 1, representing rapid pore-pressure dissipation throughout construction, does the end-of-construction situation coincide with the minimum F.o.S. as predicted by Bishop and Bjerrum (1960).

The selection of shear strength data for stability analyses has also been considered in some detail by Bishop and Bjerrum (1960), Lowe (1967), Skempton and Hutchinson (1969), Parry (1971(a)), Bjerrum (1972 and 1973) and Johnson (1975).

7.2.2. Summary of Data Used

(i) Total Stress Analyses

The property sets used in the analyses are listed in Appendix 6 (table A.6.2.), a key to the nomenclature used being provided in the Appendix (table A.6.1.); table A.6.2. provides a key to the figures illustrating the various undrained strength/depth profiles.

The weak crust assumption was based on an extrapolation of the laboratory data (figure 2.23) whilst the strong crust assumption was based on a combination of the data presented in section 2.7.5.(ii) and the back-analysis of the Bank 1, Stage 1 failure using non-circular failure surfaces, as discussed in section 7.3.1.

By necessity (being a function of the computer programs used) the undrained strength/depth profiles had to be approximated to zones having average properties. Bulk unit weights for the zones were derived directly from figure 2.23.

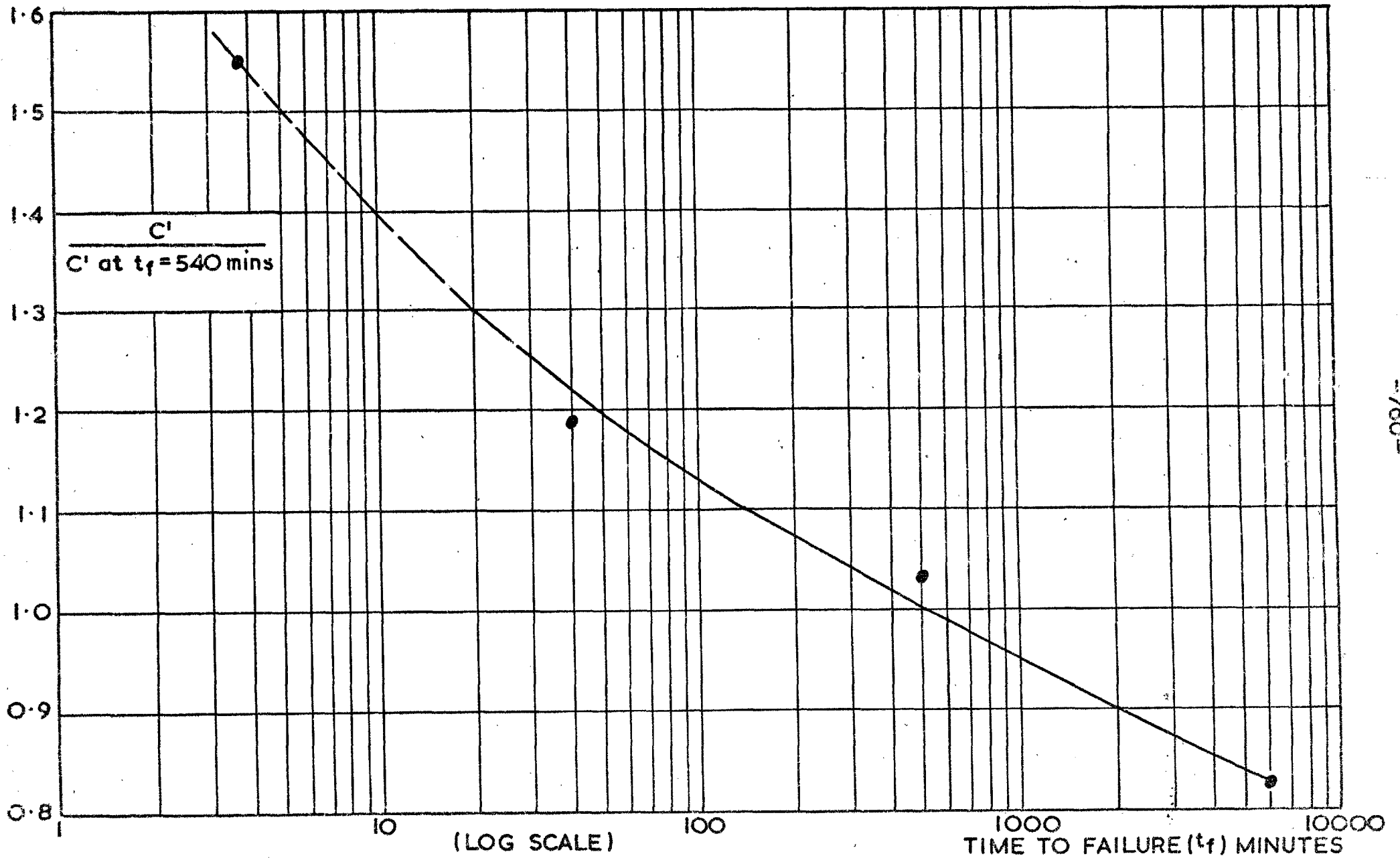
(ii) Effective Stress Analyses

The initial laboratory design values of c' and ϕ' , as presented in Appendix 6 (table A.6.3.) were different from the final design values (figures 2.17 and 2.25) selected upon completion of the laboratory testing program. However, parametric studies in terms of c' and ϕ' were made enabling the F.o.S. for the critical surfaces to be assessed in terms of the final design values. In this case the effects of strain rate were considered subsequently.

The weak crust assumption was based on constant effective stress parameters throughout the foundation, whilst for the strong crust an undrained strength was assigned to the uppermost zone of the foundation. An identical approach to this problem was adopted by Ladd (1972) and Lacasse and Ladd (1973).

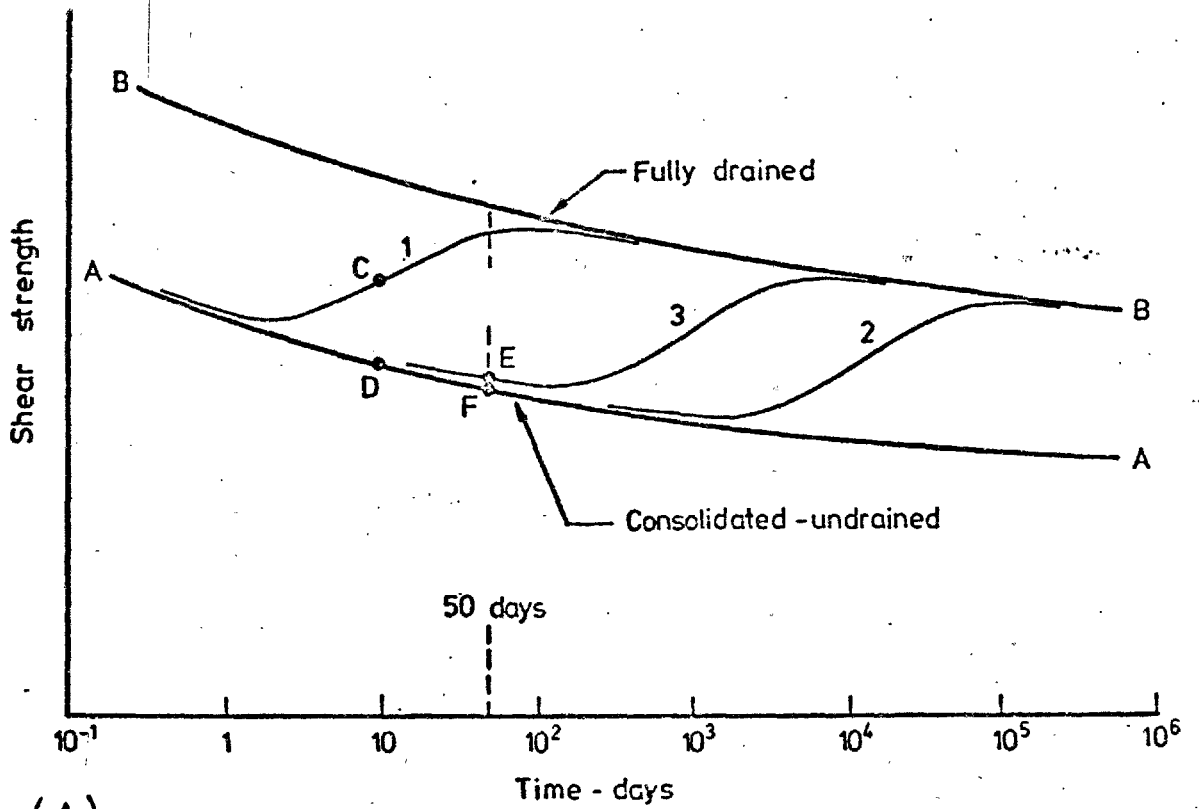
In both the total and effective stress analyses of the foundation the fill was considered in terms of drained shear strength parameters (Appendix 6; table A.6.3); the influence of various depths of tension crack was investigated for the Stage 1 analysis.

Based on the in-situ density measurements a γ_B of 17.5 kN/m^3 was adopted for the fill, except within the saturated central trench for which a γ_B of 19.2 kN/m^3 was assigned to the sand.

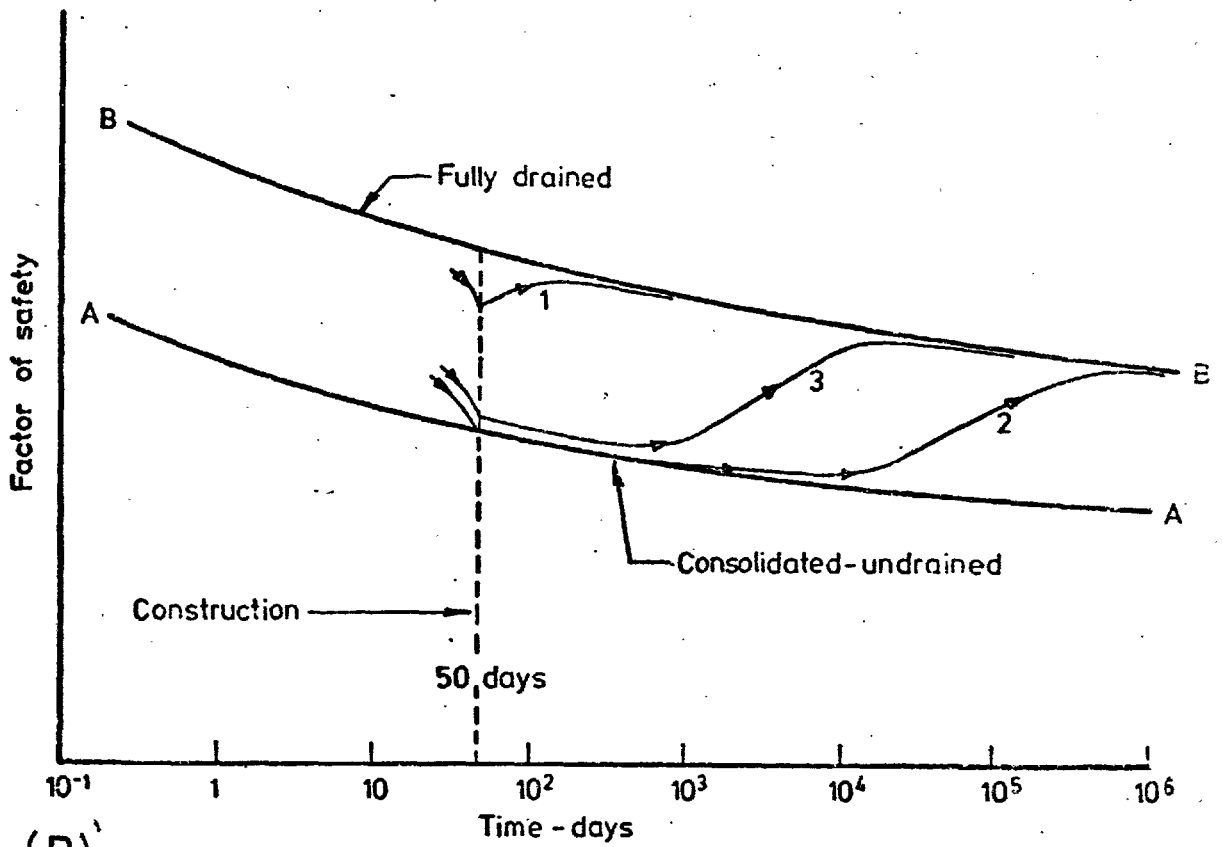


STRAIN RATE INFLUENCE ON APPARENT COHESION (DERIVED FROM FIGURE 2.21; $\phi' = 25^\circ$)

Fig. 7.21



(A)



(B)

RELATIONSHIPS BETWEEN SHEAR STRENGTH/FACTOR OF SAFETY AND TIME (LOG SCALE)

7.3. Analysis of Bank 1, Stage 1 Failure

7.3.1. Maximum Fill Height - Total Stress Analyses

(i) General

Figure 6.2.3. shows both the limits of the zone of extreme deformation defined by the foundation instrumentation and the grid points used to define the non-circular slip surfaces. Using the laboratory design undrained strengths (figure 2.23; properly set TS-LD-1, table A.6.2.) a critical restricted slip surface (ST1/1) was located (figure 7.3.1; also depicted are the zones into which the foundation and fill were divided and the centres of rotation for the circular arc failure surfaces). This surface passed through the crust (zone 3) whereas the actual slip surface is considered (section 6.2.2.) to have passed through the central trench. Although the $\phi_u = 0$ Analysis would not be expected to predict the true slip surface (Skempton, 1948(c)) the critical total stress surface must be influenced by the presence of stronger and weaker layers within a foundation.

Thus, in order to assess the undrained strength of the crust, C_u for zone 3 was increased until the critical surface was forced into the central trench, this being surface ST2/1. The 'critical strength' of the desiccated crust was found to be 45 kN/m^2 , being in excellent agreement with the data presented in section 2.7.5., and with that published by Cox (1970), Ladd (1972), Lacasse and Ladd (1973), DascaI and Tournier (1975) and Hughes et al (1975) for similar desiccated near-surface materials. In the various case histories referred to, the assignment of an undrained strength to the crust has always been a stumbling block, values usually being taken from vane tests, whereas at Mucking a direct full scale field assessment was possible.

Surface ST1/1 (figure 7.3.1) was associated with a 1m deep tension crack and ST2/1 with a 3m deep crack; introduction of the tension cracks reduced the respective safety factors by 0.03 and 0.06, and was in agreement with the field observations that the formation of a tension crack preceded the limiting equilibrium condition.

The undrained shear strength of the foundation was then reduced until a F.o.S. of unity was achieved on each of the critical restricted surfaces, resulting in property sets TS-1-1 and TS-2-1 for surfaces ST1/1 and ST2/1 respectively.

Stability was reconsidered using circular arc failure surfaces, initially restricted to pass through the observed toe of the failure. These critical surfaces (BT1/1 - property set TS-LD-1; BT2/1 - property set TS-LD-2) were in good agreement with the limits defined by the foundation instrumentation (figure 7.3.1), although forced to outcrop to the rear of the observed tension crack.

Finally an analysis was performed with no restrictions on the circular arc locations, using the laboratory design data, with and without a strong desiccated layer; this being a genuine $\phi_u = 0$ analysis. Critical surfaces BT1/1A (property set TS-LD-1) and BT2/1A (property set TS-LD-2) resulted, as depicted in figure 7.3.2; perhaps surprisingly these surfaces were also in good agreement with the locations predicted by the field instrumentation. Both surfaces outcropped within the toe trench and to the rear of the observed tension crack. The undrained shear strength of the foundation was then reduced (except for the derived $C_u = 45 \text{ kN/m}^2$ for the strong crust analysis) until a F.o.S. of unity was achieved on each of the unrestricted critical

surfaces, resulting in property sets TS-1-0 and TS-2-0 for surfaces BT1/1A and BT2/1A respectively, being the true back-calculated shear strengths in terms of total stress.

(ii) Discussion of Results

The various undrained strength/depth profiles obtained from the laboratory and field vane test data were subsequently used to assess 'stability' on, among others, all of the critical surfaces.

Calculated safety factors for all of the property sets considered, as applied to all of the critical surfaces located, are presented in Appendix 6 (table A.6.4) and summarised in tables 7.3.1 and 7.3.2. Considering the assumption of a weak crust first (table 7.3.1) the $\phi_u = 0$ Analysis (unrestricted surfaces) revealed that:-

(a) the quick undrained laboratory triaxial test data, relating to the block samples, led to a minimum F.o.S. of 1.33 for vertical specimens, reducing to 1.21 having made allowance for undrained strength anisotropy, and further reducing to 0.79 when corrected for strain rate effects. The piston sample (vertical) specimens indicated a F.o.S. of 1.25; thus the increased sample disturbance associated with these specimens approximately compensated for the estimated effects of undrained strength anisotropy. Such compensatory factors have been previously discussed in section 7.2 and are further investigated in section 7.5.

(b) the critical surface for the vane test data was not the same as for the laboratory data, and in fact passed through the central trench (surface BT2/1A; Appendix 6, table A.6.4).

(c) the vertical Geonor vane test data suggested a F.o.S. of 1.39, reducing to 1.10 after correction for plasticity (i.e. $\times \mu$, after Bjerrum, 1972; figure 3.3).

(d) the large vane test data at a time to failure corresponding to that of the Geonor vane tests led to a F.o.S. of 1.12, reducing to 0.91 after correction for plasticity.

(e) the minimum strengths from the large vane tests produced a F.o.S. of 1.06, reducing to 0.84 when corrected for plasticity.

The restricted circular arc and non-circular failure surfaces produced higher safety factors. A maximum difference in F.o.S. between the unrestricted circular arcs and the restricted non-circular surfaces of 0.11 was found, compared to 0.05 between the two classes of circular arcs.

Turning to the strong crust assumption (table 7.3.2), the $\phi_u = 0$ Analysis (unrestricted surfaces) revealed that:-

(a) there was little difference in the minimum F.o.S. for the various sets of laboratory data from that predicted by the analyses incorporating a weak crust, because the strong crust assumption merely changed the critical surface from BT1/1A to BT2/1A; the latter of course at no point passed through the crust.

(b) the critical surface for the vane test data, and hence the minimum values of F.o.S., remained unchanged.

The restricted failure surfaces again resulted in increasing safety factors with increasing restriction, the maximum difference in F.o.S. being 0.16, whilst being only 0.03 between the two classes of circular arc.

Finally, parametric studies to determine the influence of ϕ' for the fill showed that a $\pm 1^\circ$ change in ϕ' produced a ± 0.005 change in the F.o.S. Thus the analyses were reasonably insensitive to the value of ϕ' for the fill, although the introduction of a tension crack made a significant difference to the calculated F.o.S.

7.3.2. Maximum Fill Height - Effective Stress Analyses

(1) General

The division of the strata into zones, the grid points for the non-circular surfaces and the centres for the circular arc surfaces were all as described in the previous section.

Figure 7.3.3. depicts pore-pressure contours based on the last set of observations prior to the Stage 1 failure; these were used for the initial analyses, being input on a grid basis along the zone lines. Using the initial laboratory design effective stress parameters (property set ES-LD-1; Appendix 6 - table A.6.3) a critical restricted non-circular surface SE1/1 was located (figure 7.3.4: this passed through the desiccated layer; in this case it would be expected to locate the observed surface from the analysis, being considered to have passed through the central trench).

In terms of effective stress the shear strength of the crust could be derived directly from the existence of desiccation stresses (Parry, 1970) or bonding (produced by weathering (Bjerrum, 1967)), or indirectly by dissipation of large pore suctions leading to a high O.C.R. and a substantial c' . As the suctions which existed in the upper layer prior to construction must have dissipated to atmospheric pressure at the ground surface in order that the observed consolidation could take place (as pointed out in section 6.1.3) it was decided to investigate the effect of increasing c' within zone

3 (zero pore pressures having been input at O.G.L. throughout the section).

In order to force the critical surface through the central trench a c' approximating to the back-calculated C_u was necessary for zone 3. It was decided to put $\phi_u = 0$ and $C_u = 45 \text{ kN/m}^2$ for zone 3 in the effective stress analyses, resulting in critical surface SE2/1.*

As in the total stress analyses, the critical restricted non-circular surfaces were associated with tension cracks, the influence on the F.o.S. being similar in both cases.

The laboratory design value of c' was reduced until a F.o.S. of unity was achieved for each of the critical restricted surfaces, resulting in property sets ES-1-1 and ES-2-1 for surfaces SE1/1 and SE2/1 respectively.

Circular arc surfaces restricted to pass through the observed toe of the failure were then considered. In these analyses the pore pressures were converted to r_u values (section 6.1.3 and figure 6.1.22) and the average r_u found for each zone; this was a fairly gross approximation, as can be seen by comparing the average r_u values with the range for each zone (Appendix 6 - table A.6.8; see also figure 6.1.22). The resulting critical surfaces BE1/1(A) and BE2/1(A) were in good agreement with the limits defined by the foundation instrumentation, although forced to outcrop to

*noting that the use of $C_u = 45 \text{ kN/m}^2$ for zone 3 was to force the critical surface through the central trench and thus that the mobilised shear strength on the critical surface was entirely dependent on effective stress parameters.

the rear of the observed tension crack; furthermore, these surfaces were also critical when the analyses were extended to include unrestricted surfaces and were close to limiting equilibrium (i.e. F.o.S. ≈ 1) when considered in conjunction with the appropriate c' for the foundation i.e. the value back-calculated using the critical non-circular surfaces.

Analysis of the non-circular surfaces was then repeated incorporating pore pressures extrapolated to a fill height of 4m, using the data in figures 6.1.19 and 6.1.20. No change in the critical surfaces was found, but a significantly smaller reduction of the laboratory c' was required to produce a F.o.S. of unity in each case.

Parametric studies in terms of c' and ϕ' for the foundation, together with the two pore-pressure distributions, were carried out for the critical surfaces.

(ii) Discussion of Results

The calculated safety factors for all of the property sets considered, as applied to the various critical surfaces, are presented in Appendix 6 (table A.6.5) and summarised in tables 7.3.3 to 7.3.6. Considering, firstly, the weak crust assumption it was found that:-

(a) in conjunction with the measured pre-failure pore pressures (table 7.3.3) the initial laboratory design data produced a F.o.S. of 1.23, reducing to 1.09 if the pore pressures extrapolated to maximum fill height were used (table 7.3.4). Only a small reduction in c' (1 kN/m^2) was required to achieve a F.o.S. of unity, in the latter case, for the critical surface.

(b) there was excellent agreement between the safety factors on the critical circular and non-circular surfaces, and also excellent agreement between their locations and the field observations, the critical circular surfaces actually passing through the observed toe of the failure (figure 7.3.4).

The assumption of a strong crust produced the following findings:-

(a) a F.o.S. of 1.39 resulted from the use of the observed pre-failure pore pressures and the initial laboratory design data (table 7.3.5), reducing to 1.25 if the extrapolated pore pressures were incorporated (table 7.3.6). A 2.75 kN/m^2 reduction in c' was required, in the latter case, to achieve a F.o.S. of unity for the critical surface.

(b) agreement between the safety factors on the critical circular and non-circular surfaces was not as good as that associated with the weak crust assumption, although the critical circular arcs still passed through the observed toe of the failure.

Parametric studies showed the influence of the fill's strength to be as described for the total stress analyses.

7.3.3. Post-Failure Embankment Profile

Analysis of this case was restricted to the four critical restricted non-circular surfaces, as depicted in figure 7.3.5; also shown is the simplified zoning of the foundation assumed for analysis purposes.

Tension cracks were assumed to have remained open to the critical depths established in the previous studies. Pore pressures for the post-failure effective stress analyses were based on figure 7.3.3., representing the observations made immediately after the failure.

The shear strength parameters were reduced for each of the property sets relevant to a particular critical surface until limiting equilibrium was re-established. Property sets TS-1(R)-1, TS-2(R)-1, ES-1(R)-1 and ES-2(R)-1 were thus obtained for critical surfaces ST1/1, ST2/1, SE1/1 and SE2/1 respectively. In these analyses it was considered justified to carry out a total stress analysis of an 'actual' slip surface.

Using the back-calculated peak shear strength parameters in conjunction with post-failure conditions led to safety factors of 1.85, 1.63, 1.36 and 1.32 for the respective surfaces, the peak effective stress parameters being based on the extrapolated pore pressures.

SOIL PROPERTIES	FACTOR OF SAFETY		
	CIRCULAR ARC SURFACES		NON-CIRCULAR SURFACES
	Passing into toe trench (1)	Passing into actual toe	Passing through actual toe and crest
<u>LABORATORY DATA</u>			
1. Block samples; with allowance for anisotropy (2)	1.21	1.26	1.27
2. Block samples; as 1, but corrected for strain rate effect (2)	0.79	0.82	0.83
3. Block samples; vertical specimens only (2)	1.33	1.38	1.42
4. Piston samples; vertical specimens (2)	1.25	1.31	1.34
<u>FIELD VANE DATA</u>			
1. Vertical Geonor Vane (2)	1.39	1.41	1.50
2. Vertical Geonor Vane; corrected for plasticity (3)	1.10	1.12	1.20
3. Large Vane; at same (2) time to failure as Geonor	1.12	1.15	1.21
4. Large Vane; as 3, but corrected for plasticity (3)	0.91	0.93	0.99
5. Large Vane; min.values (2)	1.06	1.07	1.14
6. Large Vane; as 5, but corrected for plasticity (3)	0.84	0.85	0.90
<u>DERIVED DATA</u>			
1. Based on lab. data 1.	1.02	1.08	1.09

(1) No restrictions imposed on surface location

(2) Extrapolated lab. data used for crust.

(3) Derived data used for crust.

Table 7.3.1.

Bank 1, Stage 1

Results of Total Stress Stability Analyses for Critical Surfaces, Assuming A Weak Desiccated Crust

SOIL PROPERTIES	FACTOR OF SAFETY		
	CIRCULAR ARC SURFACES		NON-CIRCULAR SURFACES
	Passing into toe trench (1)	Passing into actual toe	Passing through actual toe and crest
<u>LABORATORY DATA</u>			
1. Block samples; with allowance for anisotropy	1.25	1.27	1.36
2. Block samples; as 1, but corrected for strain rate effect	0.81	0.83	0.89
3. Block samples; vertical specimens only	1.37	1.38	1.50
4. Piston samples; vertical specimens	1.30	1.31	1.42
<u>FIELD VANE DATA</u>			
1. Vertical Geonor Vane	1.39	1.41	1.55
2. Vertical Geonor Vane; corrected for plasticity	1.10	1.12	1.22
3. Large Vane; at same time to failure as Geonor	1.12	1.15	1.23
4. Large Vane; as 3, but corrected for plasticity	0.91	0.93	0.99
5. Large Vane; min. values	1.06	1.07	1.15
6. Large Vane; as 5, but corrected for plasticity	0.84	0.85	0.90
<u>DERIVED DATA</u>			
1. Based on lab. profile 1.	0.99	1.01	1.06

(1) No restrictions imposed on surface location.

Derived data used for crust.

Table 7.3.2.

Bank 1, Stage 1

Results of Total Stress Stability Analyses for Critical Surfaces, Assuming A Strong Desiccated Crust

SOIL PROPERTIES	FACTOR OF SAFETY	
	CIRCULAR ARC SURFACES	NON-CIRCULAR SURFACES
	Passing into actual toe (1)	Passing through actual toe and crest
Initial laboratory design data from test pit samples $c' = 6.5 \text{ kN/m}^2 \quad \phi' = 26.5^\circ$	1.25	1.23
Data derived from stability analysis for Bank 1/1 $c' = 3.75 \text{ kN/m}^2 \quad \phi' = 26.5^\circ$	1.04	1.01
Data derived from stability analysis for Bank 1/2 $c' = 2.75 \text{ kN/m}^2 \quad \phi' = 26.5^\circ$	0.96	0.93

(1) No restrictions imposed on surface location

Table 7.3.3.

Bank 1, Stage 1

Results of Effective Stress Stability Analyses For Critical Surfaces, Assuming

A Weak Desiccated Crust, and Measured Pore Pressures At 3.75m Fill Height

SOIL PROPERTIES	FACTOR OF SAFETY
	NON-CIRCULAR SURFACES
	Passing through actual toe and crest
Initial laboratory design data from test pit samples $c' = 6.5 \text{ kN/m}^2$, $\phi' = 26.5^\circ$	1.09
Data derived from stability analysis for Bank 1/1 $c' = 5.5 \text{ kN/m}^2$, $\phi' = 26.5^\circ$	1.01
Data derived from stability analysis for Bank 1/2 $c' = 5.25 \text{ kN/m}^2$, $\phi' = 26.5^\circ$	0.98

Table 7.3.4.

Bank 1, Stage 1

Results of Effective Stress Stability Analyses for Critical Surfaces, Assuming A Weak Desiccated Crust, and Pore Pressures Extrapolated to 4.00m Fill Height

SOIL PROPERTIES	FACTOR OF SAFETY	
	CIRCULAR ARC SURFACES	NON-CIRCULAR SURFACES
	Passing into actual toe (1)	Passing through actual toe and crest
Initial laboratory design data from test pit samples $c' = 6.5 \text{ kN/m}^2$ $\phi' = 26.5^\circ$	1.29	1.39
Data derived from stability analysis for Bank 1/1 $c' = 1.85 \text{ kN/m}^2$ $\phi' = 26.5^\circ$	0.95	1.01
Data derived from stability analysis for Bank 1/2 $c' = 0$ $\phi' = 21^\circ$	0.64	Solution did not Converge

(1) No restrictions imposed on surface location.
Strong crust as in total stress analysis.

Table 7.3.5.

Bank 1, Stage 1

Results of Effective Stress Stability Analyses for Critical Surfaces, Assuming A Strong Desiccated Crust, and Measured Pore Pressures at 3.75m Fill Height

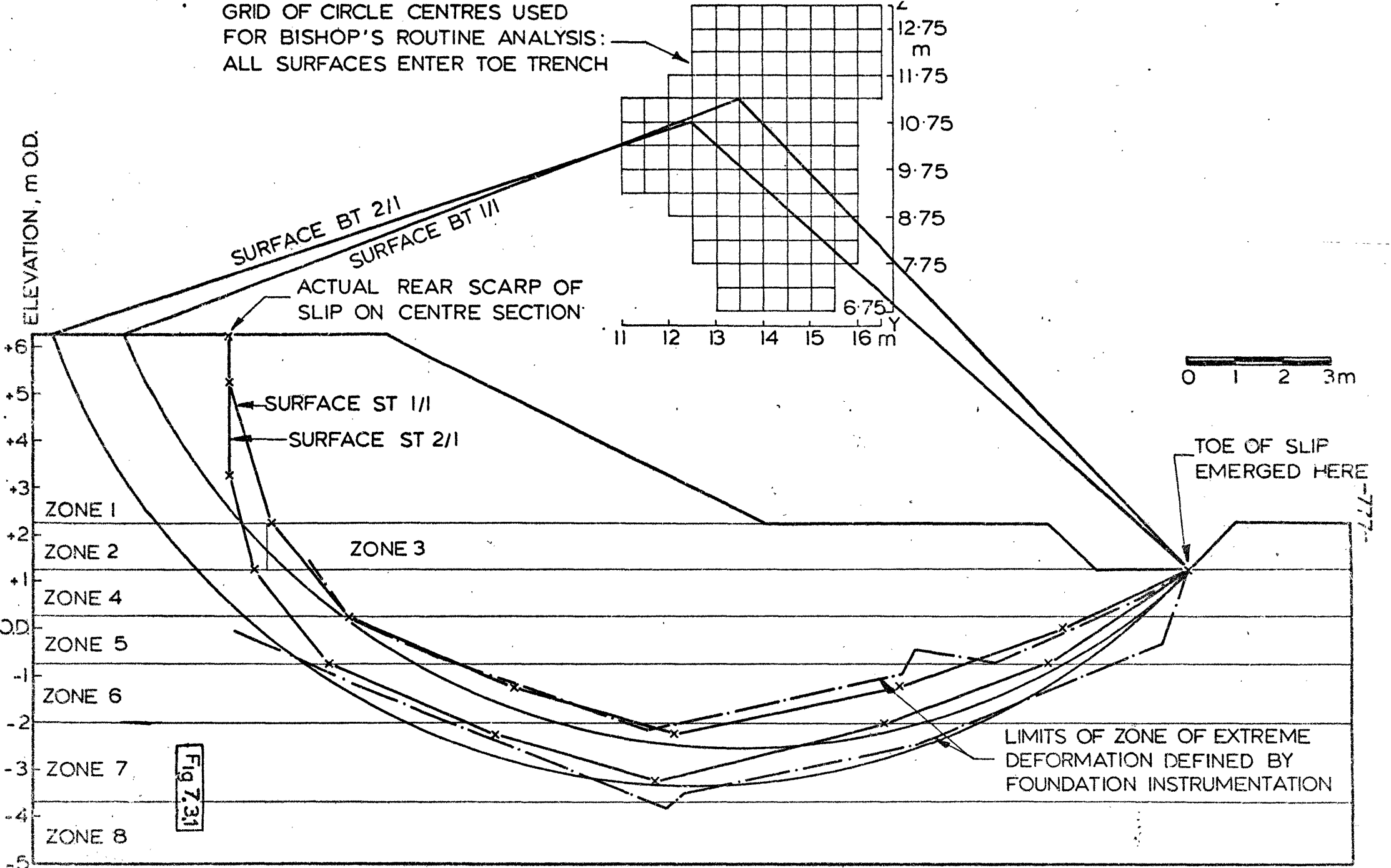
SOIL PROPERTIES	FACTOR OF SAFETY
	NON-CIRCULAR SURFACES
	Passing through actual toe and crest
Initial laboratory design data from test pit samples $c' = 6.5 \text{ kN/m}^2, \phi' = 26.5^\circ$	1.25
Data derived from stability analysis for Bank 1/1 $c' = 3.75 \text{ kN/m}^2, \phi' = 26.5^\circ$	1.01
Data derived from stability analysis for Bank 1/2 $c' = 0.7 \text{ kN/m}^2, \phi' = 26.5^\circ$	0.73

Strong crust as in total stress analysis.

Table 7.3.6.

Bank 1, Stage 1

Results of Effective Stress Stability Analyses for Critical Surfaces,
Assuming a Strong Desiccated Crust and Pore Pressures Extrapolated
to 4.00m Fill Height



BANK I/I: STABILITY ANALYSES IN TERMS OF TOTAL STRESSES - Critical 'restricted' surfaces predicted by Sarma's, and Bishop's routine, method.

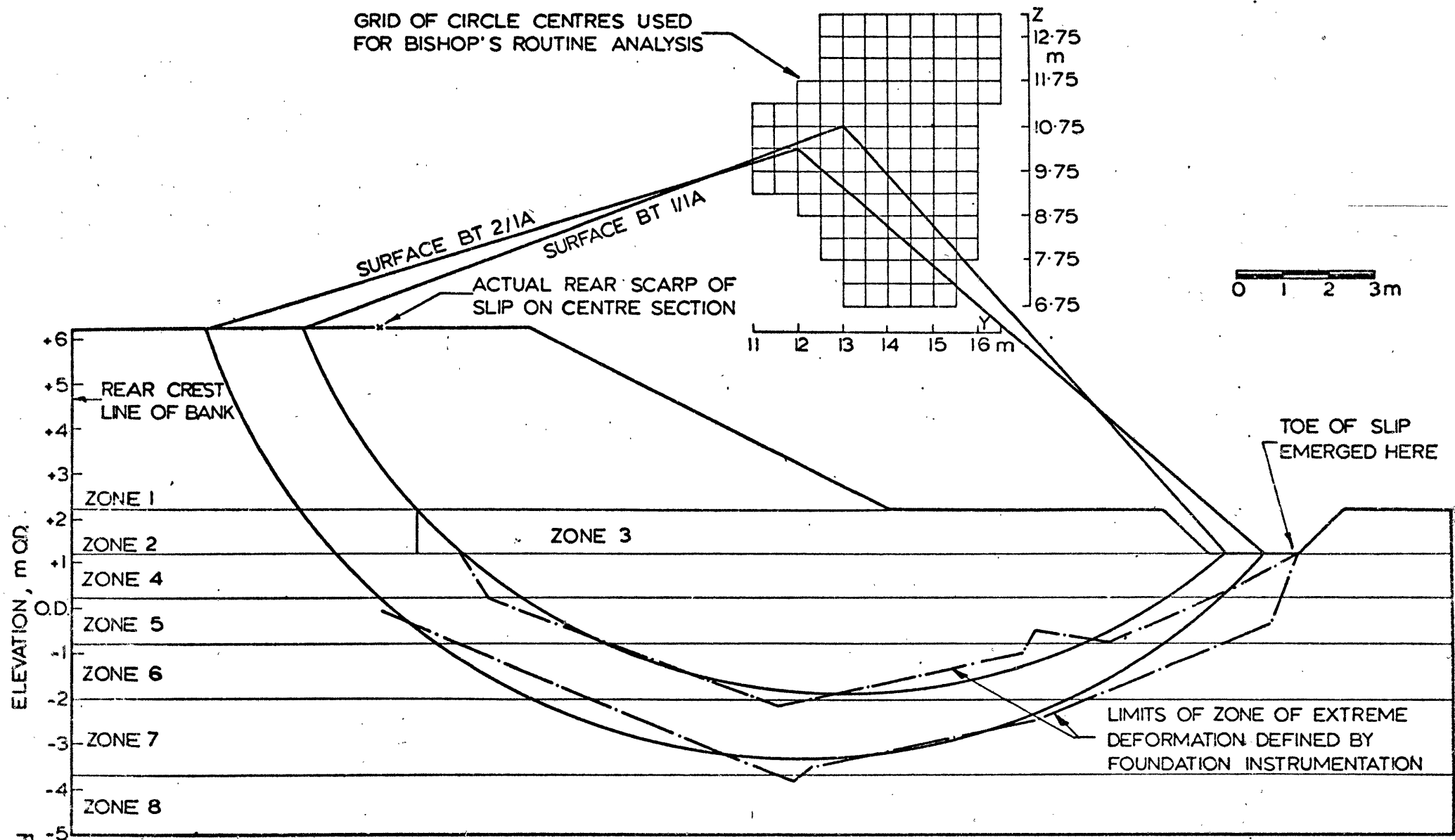


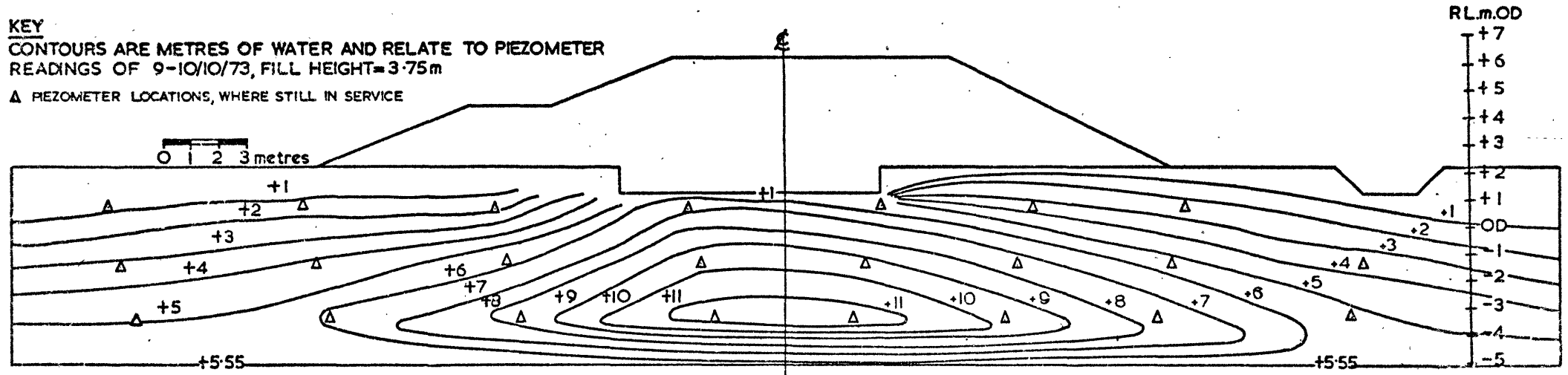
Fig 7.3.2

BANK 1/1: STABILITY ANALYSES IN TERMS OF TOTAL STRESSES – Critical 'unrestricted' surfaces predicted by Bishop's routine method.

KEY

CONTOURS ARE METRES OF WATER AND RELATE TO PIEZOMETER READINGS OF 9-10/10/73, FILL HEIGHT=3.75m

Δ PIEZOMETER LOCATIONS, WHERE STILL IN SERVICE

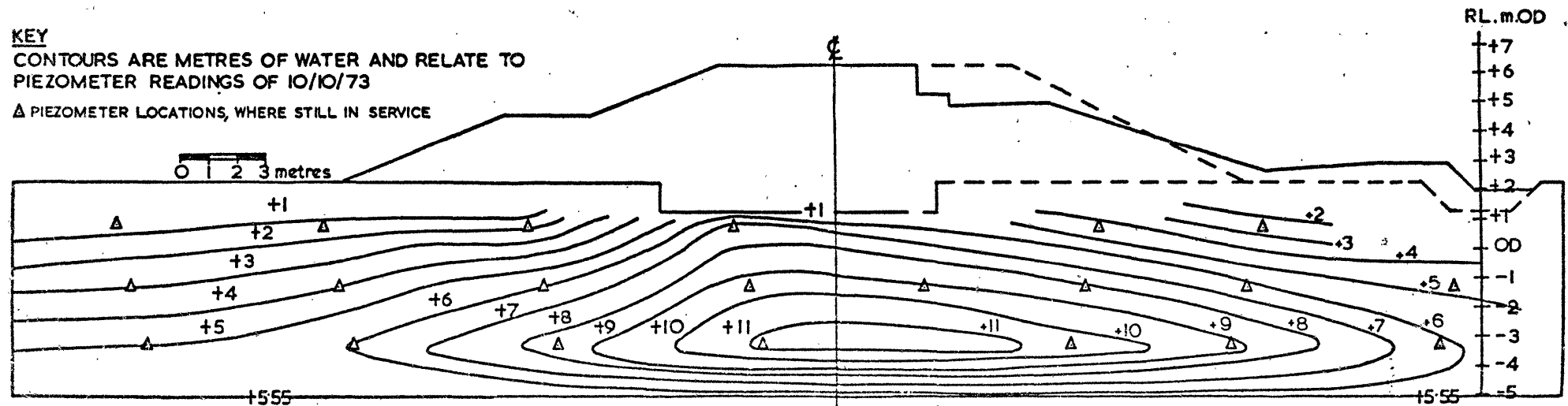


BANK I, STAGE I PORE-PRESSURE CONTOURS PRIOR TO FAILURE

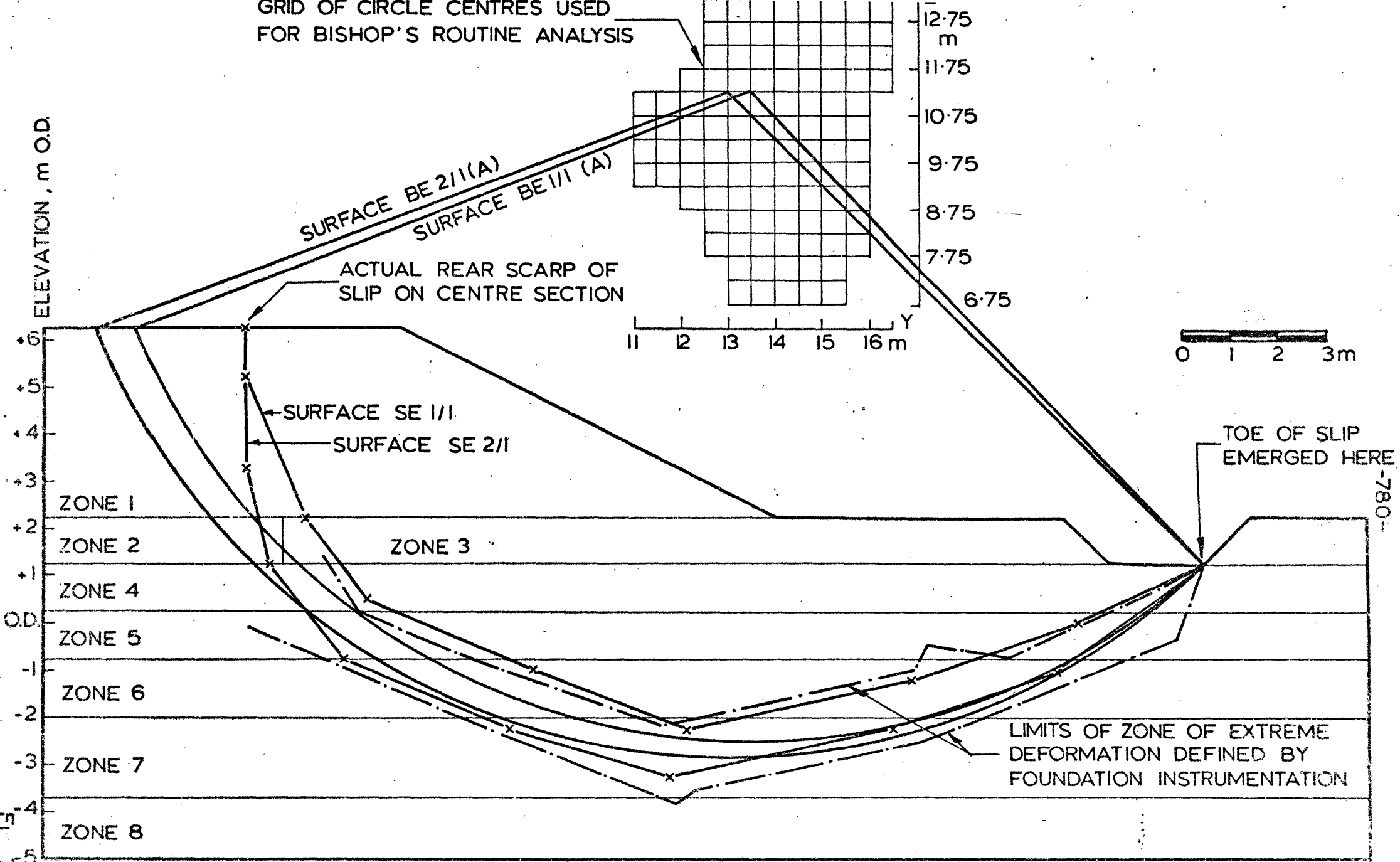
KEY

CONTOURS ARE METRES OF WATER AND RELATE TO PIEZOMETER READINGS OF 10/10/73

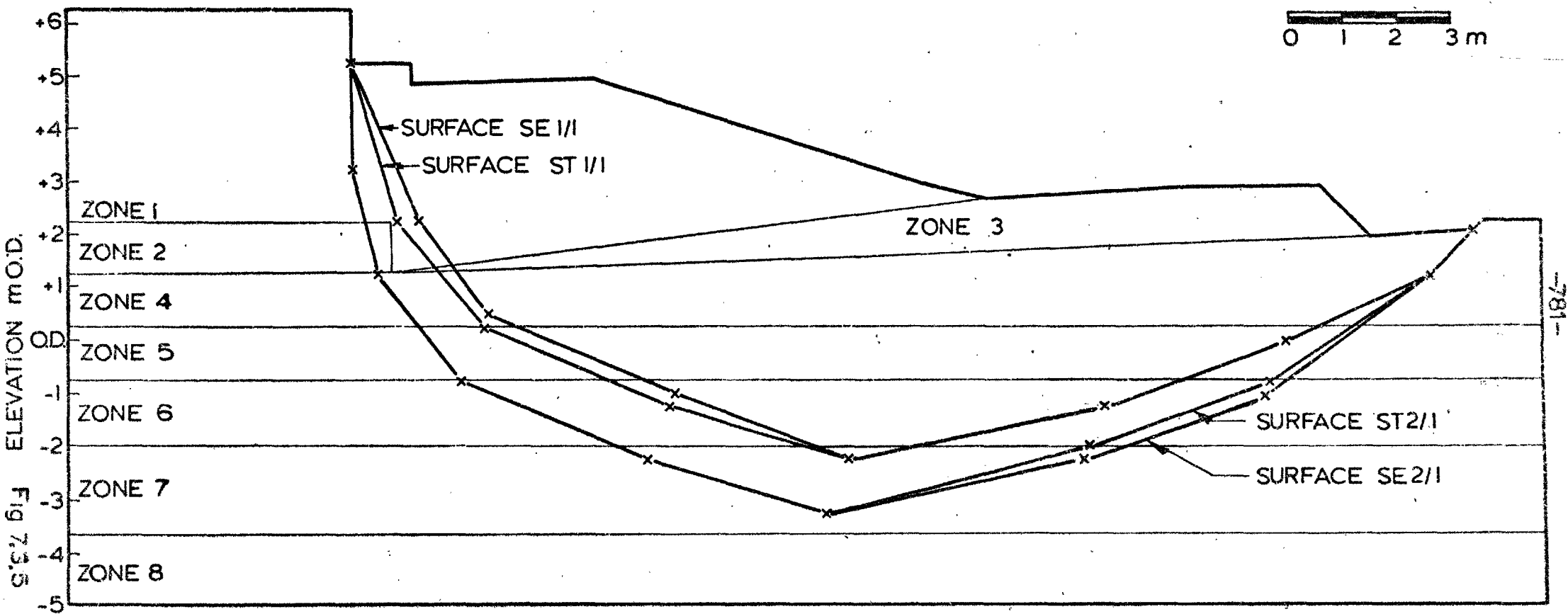
Δ PIEZOMETER LOCATIONS, WHERE STILL IN SERVICE



BANK I, STAGE I PORE-PRESSURE CONTOURS AFTER FAILURE



BANK 1/1: STABILITY ANALYSES IN TERMS OF EFFECTIVE STRESSES – Critical 'restricted' surfaces predicted by Sarma's method and critical 'unrestricted' surfaces predicted by Bishop's routine method



BANK I/I: STABILITY ANALYSES, INCORPORATING POST-FAILURE PROFILE (SECTION E) AND CRITICAL 'RESTRICTED' SURFACES PREDICTED BY SARMA'S METHOD.

7.4. Analysis of Bank 1, Stage 2 Failure

7.4.1. Maximum Fill Height - Total Stress Analyses

(i) General

Figure 6.2.8. shows both the limits of extreme deformation defined by the foundation instrumentation and the grid points used to define the non-circular slip surfaces. The rupture zone for Stage 2 was less well defined than that for Stage 1 both with respect to location and the points of emergence (section 6.2.3.).

Using the data derived from the back-analysis of Stage 1 (TS-1-1 and TS-2-1) a single critical restricted (at the observed crest point only) non-circular surface ST1/2 (= ST2/2) was located. This surface (figure 7.4.1.) was very close to the upper limit of extreme deformation and did not pass through the central trench. It will be recalled from section 6.2.3. that, unlike Stage 1, the Stage 2 fill is not considered to have cracked completely until a state of limiting equilibrium was reached; thus only a small tension crack was introduced into the analysis over the initial portion of the slip surface within the fill. The shear strength data derived from the Stage 1 restricted surfaces resulted in safety factors both greater and less than unity for Stage 2 and two additional sets of parameters (TS-1-2 and TS-2-2) were derived to achieve a F.o.S. of unity on critical surface ST1/2.

Unrestricted circular and non-circular surfaces were then considered; property set TS-1-0 led to a critical circular arc BT1/2A and a non-circular surface ST1/2A (figure 7.4.2). The safety factors on these surfaces were close to unity. Similarly property set TS-2-0 led to critical surfaces BT2/2A and ST2/2A, both having safety factors close to unity.

In common with the restricted total stress surfaces the unrestricted ones were also close to the upper limit of extreme foundation deformation.

(ii) Discussion of Results

The various undrained strength/depth profiles obtained from the laboratory, and field vane, test data were subsequently used to assess the 'stability' of, among others, all of the critical surfaces.

Calculated safety factors for all of the property sets considered, as applied to all of the critical surfaces, are presented in Appendix 6 (table A.6.6) and summarised in tables 7.4.1 and 7.4.2.

Considering, firstly, the weak crust assumption (table 7.4.1) the following points are evident from the $\phi_u = 0$ Analyses (unrestricted surfaces):-

(a) the quick undrained laboratory triaxial test data, relating to the block samples, led to a minimum F.o.S. of 1.23 for vertical specimens reducing to 1.14 having made an allowance for undrained strength anisotropy and further reducing to 0.75 having corrected for strain rate effect. Data from the piston sample (vertical) specimens indicate a F.o.S. of 1.16; thus, as for Stage 1, the increased sample disturbance associated with the piston samples compensated for the estimated effects of undrained strength anisotropy.

(b) the safety factors predicted by the laboratory data are some 0.07 to 0.10 lower for the Stage 2 failure.

(c) as for Stage 1 the critical surface for the vane test data was not the same as for the laboratory test data, being, as shown in Appendix 6 (table A.6.6.), surface BT2/2A.

- (d) the vertical Geonor vane test data suggested a F.o.S. of 1.32; correction of the data for plasticity reduced the F.o.S. to 1.08 compared to values of 1.39 and 1.10 respectively for Stage 1.
- (e) the large vane test data, at a time to failure corresponding to that of the Geonor tests, led to a F.o.S. of 1.06, reducing to 0.89 after correction for plasticity; the respective Stage 1 values were 1.12 and 0.91.
- (f) the minimum strengths from the large vane tests produced a F.o.S. of 1.01, reducing to 0.83 when corrected for plasticity; the respective Stage 1 values were 1.06 and 0.84.
- (g) the vane test data thus produced similar safety factors for both stages, but consistently lower for Stage 2, as was also the case for the laboratory data.

Table 7.4.1. shows that agreement between Bishop's Routine Method and Sarma's Method for the unrestricted surfaces was better than ± 0.01 in terms of F.o.S., thus providing a useful check on the computer programs used. A maximum increase in F.o.S. of only 0.04 resulted if the slip surfaces were restricted to the observed rear scarp of the failure.

Unlike the case of Stage 1, for which the assumption of a strong desiccated layer merely served to deter the critical slip surface from passing through the crust, all of the critical surfaces for the Stage 2 analyses passed through the crust beneath the embankment centre, as well as remote from its toe. Therefore, the strong crust assumption had a much more marked effect on the calculated F.o.S. for Stage 2 (table 7.4.2), the following points being evident from the $\phi_u = 0$ Analyses (unrestricted surfaces):-

(a) using the laboratory data the safety factors obtained are up to 0.14 higher than those for the corresponding weak crust analyses, but are very similar to the corresponding analyses for Stage 1. Although the embankments (i.e. Stage 1 and Stage 2) were of differing geometries, a fact which may result in different 'safety factors at failure' using the same undrained strength data (Eide and Holmberg, 1972), it is considered that the undrained shear strength of the crust was considerably higher than that of the remainder of the clay foundation, and approximated to 45 kN/m^2 .

(b) Likewise, the safety factors obtained using the vane test data are about 0.12 to 0.15 higher than those for the corresponding weak crust analyses.

(c) safety factors obtained from the uncorrected vane test data are in reasonable agreement with the corresponding values for Stage 1, but about 0.06 higher. The corrected data for Stage 2 produce safety factors which are higher by some 0.11 to 0.13.

(d) the critical surface for the vane tests (BT2/2A) was unchanged from the weak crust analysis.

Table 7.4.2. indicates reasonable agreement between Bishop's Routine Method and Sarma's Method for the unrestricted surfaces but, at ± 0.05 in terms of F.o.S., not as good as for the weak crust assumption. Restriction of the slip surfaces increased the F.o.S. by a maximum of 0.15.

Finally, parametric studies to determine the influence of ϕ' for the fill led to findings similar to those previously discussed for Stage 1.

7.4.2. Maximum Fill Height - Effective Stress Analyses

(i) General

The division of the strata into zones, the grid points for the non-circular surfaces, the centres for the circular arc surfaces and the limits of extreme foundation deformation, being as for the total stress analyses, are shown in figures 7.4.1. and 7.4.4.

Figure 7.4.3. illustrates the pore-pressure contours based on the last set of observations prior to the Stage 2 failure; these were used for initial analysis purposes, being input on a grid basis along the zone lines as for the Stage 1 analysis.

A critical restricted non-circular surface (SE1/2(A)) was determined for the initial laboratory design effective stress parameters, and a similar surface (SE2/2) using these same parameters in conjunction with a strong crust assumption (property set ES-LD-2). In common with the corresponding total stress surfaces, the critical effective stress surfaces were close to the upper limit defined by the foundation instrumentation; only nominal tension cracks were introduced into the analysis (see figure 7.4.1.).

The relevant parameters derived from the Stage 1 restricted non-circular surfaces (i.e. property sets ES-1-1 and ES-2-1) produced safety factors in excess of unity for Stage 2 and two additional sets of parameters (property sets ES-1-2 and ES-2-2) were derived to achieve limiting equilibrium on surfaces SE1/2(A) and SE2/2 respectively, by reducing c' and, in the latter case, ϕ' .

Non-circular analyses were then extended to unrestricted surfaces; using the weak crust assumption SE1/2(A) remained the critical surface whereas for the strong crust a new critical surface (SE2/2A; figure 7.4.4) was found.

Unrestricted circular arc failure surfaces were finally investigated, the pore pressures, as for Stage 1, being converted to r_u values (see section 6.1.3. and figure 6.1.22) and averaged for each zone (Appendix 6; table A.6.8). The resulting critical surfaces, BE1/2(A) and BE2/2(A), derived using the laboratory data with and without, respectively, a strong crust, were similarly located (figure 7.4.4) to the previously derived critical surfaces.

Finally, the non-circular analyses were repeated using pore pressures extrapolated to a fill height of 4.5m, using the data in figures 6.1.19 and 6.1.20. This resulted in the same critical surfaces (SE1/2(A) and SE2/2; figure 7.4.1) but far greater consistency in the results, as discussed in the following sub-section.

(ii) Discussion of Results

Calculated safety factors for all of the property sets considered, as applied to all of the critical surfaces, are presented in Appendix 6 (table A.6.7) and summarised in tables 7.4.3 to 7.4.6. Considering the weak crust assumption first, the main conclusions are that:-

- (a) in conjunction with the observed pre-failure pore pressures (table 7.4.3) the initial laboratory design data yielded a F.o.S. of 1.31, being somewhat higher than the corresponding value for Stage 1 of

1.25. However, if the extrapolated pore pressures are used (table 7.4.4), excellent agreement between the F.o.S. for Stage 1 (1.09) and that for Stage 2 (1.11) resulted. Thus using the extrapolated pore pressures there was also excellent agreement between the back-calculated effective stress shear strength parameters for each Stage.

(b) the safety factors on the critical circular and non-circular surfaces differed by about ± 0.05 .

(c) there was good agreement between the locations of the critical restricted and unrestricted non-circular surfaces, and the unrestricted circular arc surfaces, all corresponding to the upper limit of extreme deformation defined by the foundation instrumentation. This finding corroborates the views advanced in section 6.2.3.

The strong crust analyses revealed that:-

(a) in conjunction with the observed pre-failure pore pressures (table 7.4.5) the initial laboratory design data produced a F.o.S. of 1.65, being significantly higher than the corresponding value of 1.39 for Stage 1. Even when the extrapolated pore pressures were incorporated in the analysis the Stage 2 F.o.S. was 1.45 compared to 1.25 for Stage 1. A significant difference in the back-calculated values of c' , being 3 kN/m^2 , thus resulted for the two stages, even in the latter case, whereas in the former case widely different parameters were back-calculated.

(b) agreement between the safety factors for the unrestricted circular arc and non-circular surfaces was excellent, the critical circular arc passing through the observed crest.

The influence of ϕ' for the fill on the analyses was as described previously.

7.4.3. Post-Failure Embankment Profile

Analysis of this case was again restricted to the four critical restricted non-circular surfaces, as depicted in figure 7.4.5; also shown is the simplified zoning of the foundation assumed for analysis purposes. The tension cracks can be seen to have disappeared as a result of the downward movement of the embankment crest; pore pressures relevant to the post-failure effective stress analyses were as shown in figure 7.4.3.

The shear strength parameters were reduced for each of the property sets relevant to the particular critical surface until limiting equilibrium was re-established for the post-failure profile. Property sets TS-1(R)-2 (= TS-1(R)-1), TS-2(R)-2, ES-1(R)-2 and ES-2(R)-2 were thus obtained for critical surfaces ST1/2, ST2/2, SE1/2(A) and SE2/2 respectively.

Only in the case of the total stress analyses were the property sets derived from the post-failure conditions of the two stages in close agreement. Inconsistencies associated with the effective stress analyses almost certainly relate to the difficulty in determining the pore pressures relevant to the post-failure limiting equilibrium condition. Whereas pore-pressure observations were made immediately following the Stage 1 failure (i.e. the next day) the corresponding observations for Stage 2 were made three days after the failure. In addition, no allowance was made for the effects of the displacements undergone by the piezometers during failure.

Using the back-calculated peak shear strength parameters in conjunction with post-failure conditions resulted in safety factors of 1.83, 1.69, 1.65 and 1.85 for the respective surfaces, the peak effective stress parameters being based on the extrapolated pore pressures. Agreement between the total stress analyses for the two stages is seen to be excellent; the indications

are that the observed post-failure pore pressures for Stage 2 were lower than those relevant to the limiting equilibrium condition.

SOIL PROPERTIES	FACTOR OF SAFETY		
	CIRCULAR ARC SURFACES	NON-CIRCULAR SURFACES	
	Unrestricted	Unrestricted	Passing through actual crest
<u>LABORATORY DATA</u>			
1. Block samples; with allowance for anisotropy (1)	1.14	1.14	1.15
2. Block samples; as 1 but corrected for strain rate effect (1)	0.75	0.75	0.77
3. Block samples; vertical specimens only (1)	1.23	1.23	1.26
4. Piston samples; vertical specimens (1)	1.16	1.15	1.19
<u>FIELD VANE DATA</u>			
1. Vertical Geonor Vane (1)	1.32	1.33	1.36
2. Vertical Geonor Vane; corrected for plasticity (2)	1.08	1.07	1.09
3. Large Vane; at same time to failure as Geonor (1)	1.06	1.09	1.13
4. Large Vane; as 3, but corrected for plasticity (2)	0.89	0.89	0.93
5. Large Vane; min. values (1)	1.01	1.02	1.04
6. Large Vane; as 5, but corrected for plasticity (2)	0.83	0.83	0.84
<u>DERIVED DATA</u>			
1. Based on lab. data 1.	0.98	0.96	0.97

(1) Extrapolated lab. data used for crust.

(2) Derived data used for crust.

Table 7.4.1.

Bank 1, Stage 2

Results of Total Stress Stability Analyses for Critical Surfaces, Assuming A Weak Desiccated Crust

SOIL PROPERTIES	FACTOR OF SAFETY		
	CIRCULAR ARC SURFACES	NON-CIRCULAR SURFACES	
	Unrestricted	Unrestricted	Passing through actual crest
<u>LABORATORY DATA</u>			
1. Block samples; with allowance for anisotropy	1.28	1.32	1.40
2. Block samples; as 1, but corrected for strain rate effect	0.83	0.86	0.91
3. Block samples; vertical specimens only	1.37	1.41	1.51
4. Piston samples; vertical specimens	1.30	1.33	1.44
<u>FIELD VANE DATA</u>			
1. Vertical Geonor Vane	1.44	1.53	1.58
2. Vertical Geonor Vane; corrected for plasticity	1.21	1.30	1.36
3. Large Vane; at same time to failure as Geonor	1.20	1.27	1.38
4. Large Vane; as 3, but corrected for plasticity	1.04	1.14	1.20
5. Large Vane; min. values	1.13	1.20	1.29
6. Large Vane; as 5, but corrected for plasticity	0.97	1.04	1.11
<u>DERIVED DATA</u>			
1. Based on lab. data 1.	1.01	1.08	1.15

Derived data used for crust.

Table 7.4.2.

Bank 1, Stage 2

Results of Total Stress Stability Analyses for Critical Surfaces, Assuming

A Strong Desiccated Crust

SOIL PROPERTIES	FACTOR OF SAFETY	
	CIRCULAR ARC SURFACES	NON-CIRCULAR SURFACES
	Passing through actual crest (1)	Passing through actual crest (1)
Initial laboratory design data from test pit samples $c' = 6.5 \text{ kN/m}^2$ $\phi' = 26.5^\circ$	1.39	1.31
Data derived from stability analysis for Bank 1/1 $c' = 3.75 \text{ kN/m}^2$ $\phi' = 26.5^\circ$	1.19	1.09
Data derived from stability analysis for Bank 1/2 $c' = 2.75 \text{ kN/m}^2$ $\phi' = 26.5^\circ$	1.12	1.00

(1) No restrictions imposed on surface location

Table 7.4.3.

Bank 1, Stage 2

Results of Effective Stress Stability Analyses for Critical Surfaces, Assuming

A Weak Desiccated Crust and Measured Pore Pressures At 4.25m Fill Height

SOIL PROPERTIES	FACTOR OF SAFETY
	NON-CIRCULAR SURFACES
	Passing through actual crest
Initial laboratory design data from test pit samples $c' = 6.5 \text{ kN/m}^2$, $\phi' = 26.5^\circ$	1.11
Data derived from stability analysis for Bank 1/1 $c' = 5.5 \text{ kN/m}^2$, $\phi' = 26.5^\circ$	1.03
Data derived from stability analysis for Bank 1/2 $c' = 5.25 \text{ kN/m}^2$, $\phi' = 26.5^\circ$	1.01

No restrictions imposed on surface location.

Table 7.4.4.

Bank 1, Stage 2

Results of Effective Stress Stability Analyses for Critical Surfaces, Assuming A Weak Desiccated Crust and Pore Pressures Extrapolated to 4.5m Fill Height

SOIL PROPERTIES	FACTOR OF SAFETY		
	CIRCULAR ARC SURFACES	NON-CIRCULAR SURFACES	
	Passing through actual crest (Unrestricted)	Unrestricted	Passing through actual crest
Initial laboratory design data from test pit samples $c' = 6.5 \text{ kN/m}^2 \phi' = 26.5^\circ$	1.61	1.62	1.65
Data derived from stability analysis for Bank 1/1 $c' = 1.85 \text{ kN/m}^2 \phi' = 26.5^\circ$	1.23	1.24	1.27
Data derived from stability analysis for Bank 1/2 $c' = 0 \phi' = 21^\circ$	0.94	0.98	1.01

Strong crust as in total stress analysis

Table 7.4.5.

Bank 1, Stage 2

Results of Effective Stress Stability Analyses, for Critical Surfaces, Assuming

A Strong Desiccated Crust and Measured Pore Pressures at 4.25m Fill Height

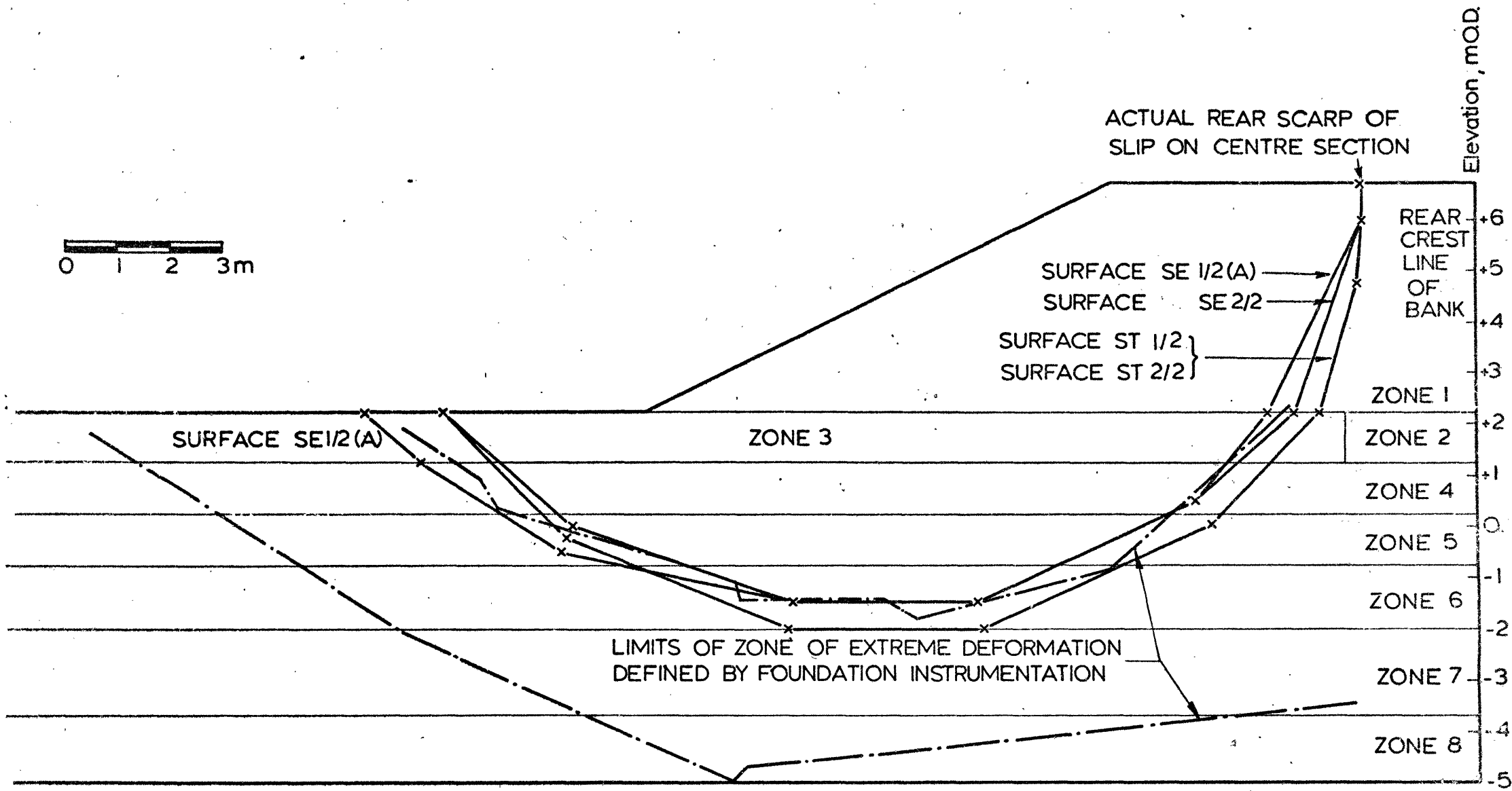
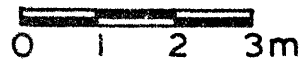
SOIL PROPERTIES	FACTOR OF SAFETY
	NON-CIRCULAR SURFACES
	Passing through actual crest
Initial laboratory design data from test pit samples $c' = 6.5 \text{ kN/m}^2 \quad \phi' = 26.5^\circ$	1.45
Data derived from stability analysis for Bank 1/1 $c' = 3.75 \text{ kN/m}^2 \quad \phi' = 26.5^\circ$	1.22
Data derived from stability analysis for Bank 1/2 $c' = 0.7 \text{ kN/m}^2 \quad \phi' = 26.5^\circ$	0.99

Strong crust as in total stress analysis

Table 7.4.6.

Bank 1, Stage 2

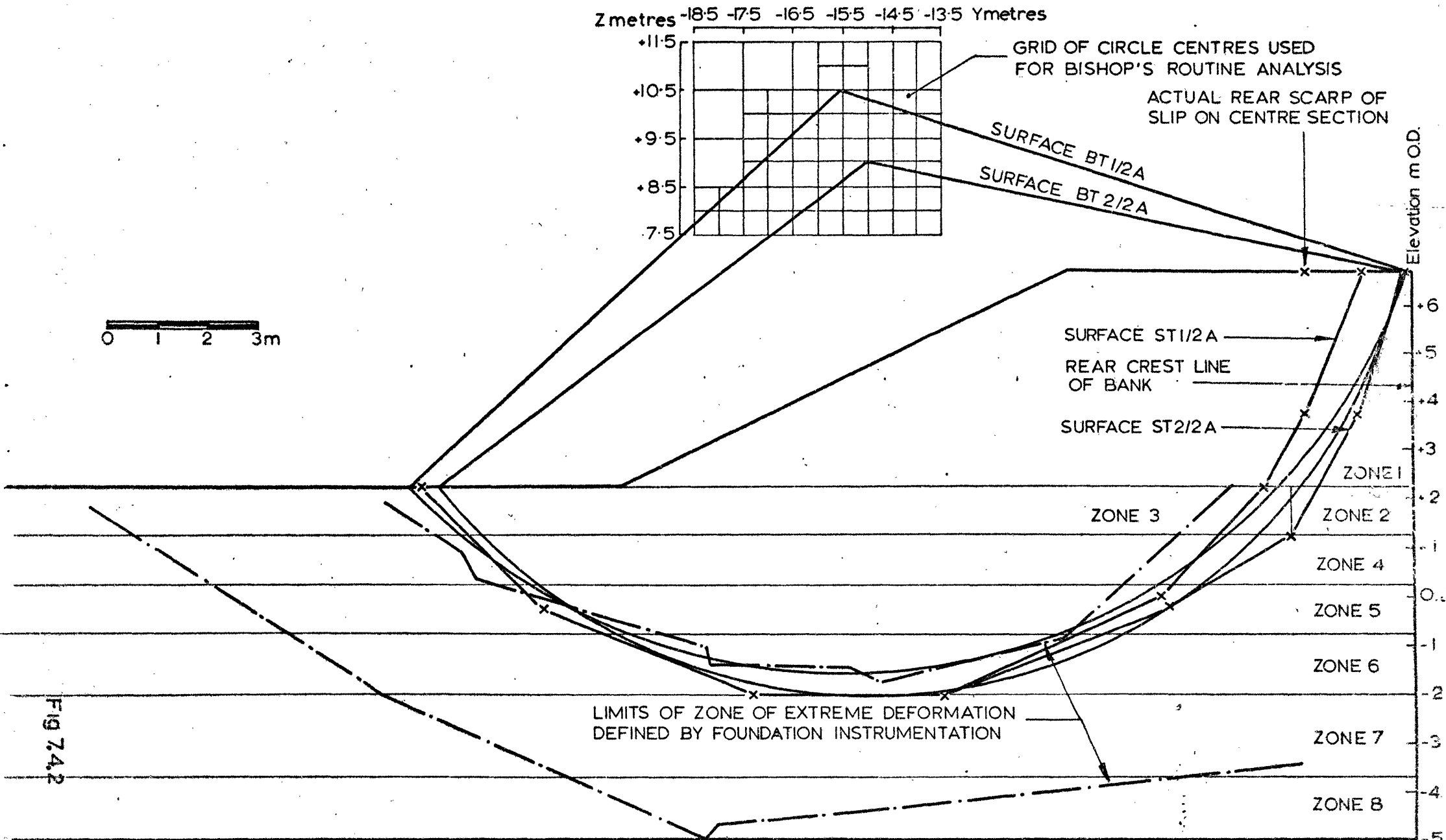
Results of Effective Stress Stability Analyses for Critical Surfaces, Assuming A Strong Desiccated Crust and Pore Pressures Extrapolated to 4.5m Fill Height



BANK 1/2: STABILITY ANALYSES IN TERMS OF TOTAL AND EFFECTIVE STRESSES - CRITICAL 'RESTRICTED' SURFACES PREDICTED BY SARMA'S METHOD.

Fig 7.41

-797-

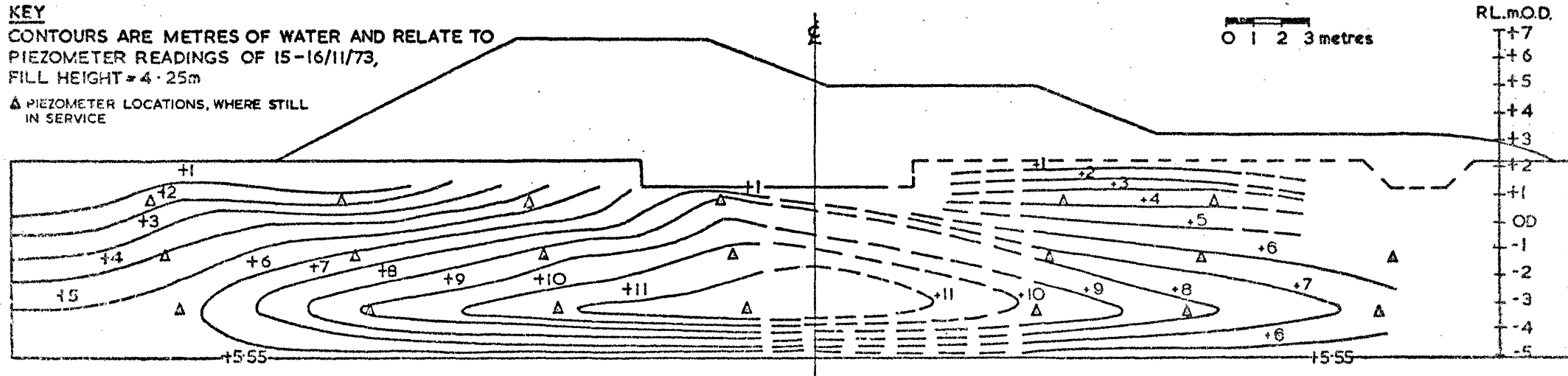


BANK 1/2: STABILITY ANALYSES IN TERMS OF TOTAL STRESSES - CRITICAL 'UNRESTRICTED' SURFACES PREDICTED BY SARMA'S, AND BISHOP'S ROUTINE, METHOD.

KEY

CONTOURS ARE METRES OF WATER AND RELATE TO
PIEZOMETER READINGS OF 15-16/11/73,
FILL HEIGHT = 4.25m

△ PIEZOMETER LOCATIONS, WHERE STILL
IN SERVICE

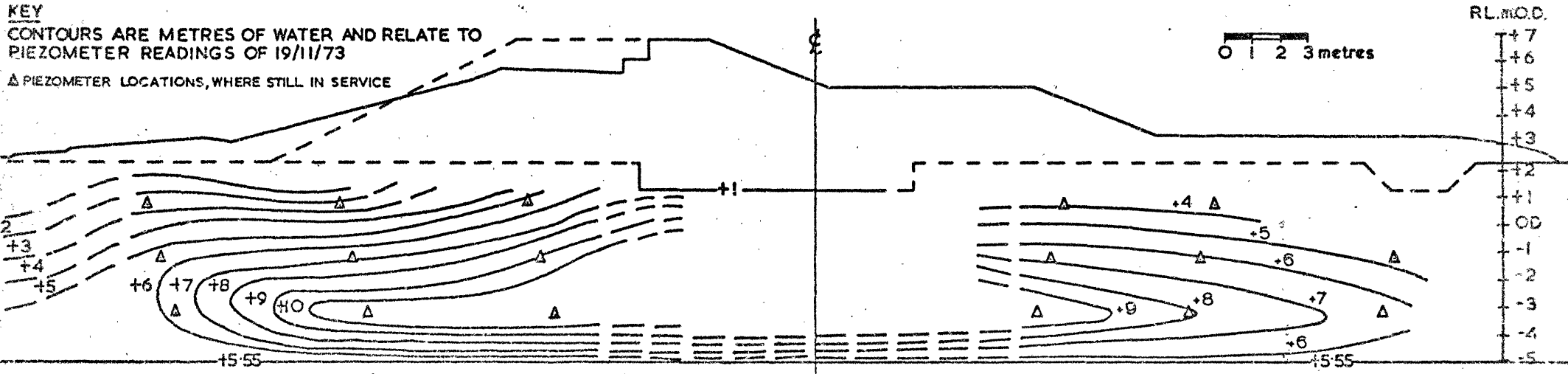


BANK I, STAGE 2 PORE-PRESSURE CONTOURS PRIOR TO FAILURE

KEY

CONTOURS ARE METRES OF WATER AND RELATE TO
PIEZOMETER READINGS OF 19/11/73

△ PIEZOMETER LOCATIONS, WHERE STILL
IN SERVICE



BANK I, STAGE 2 PORE-PRESSURE CONTOURS AFTER FAILURE

799

FIG 7.4.3

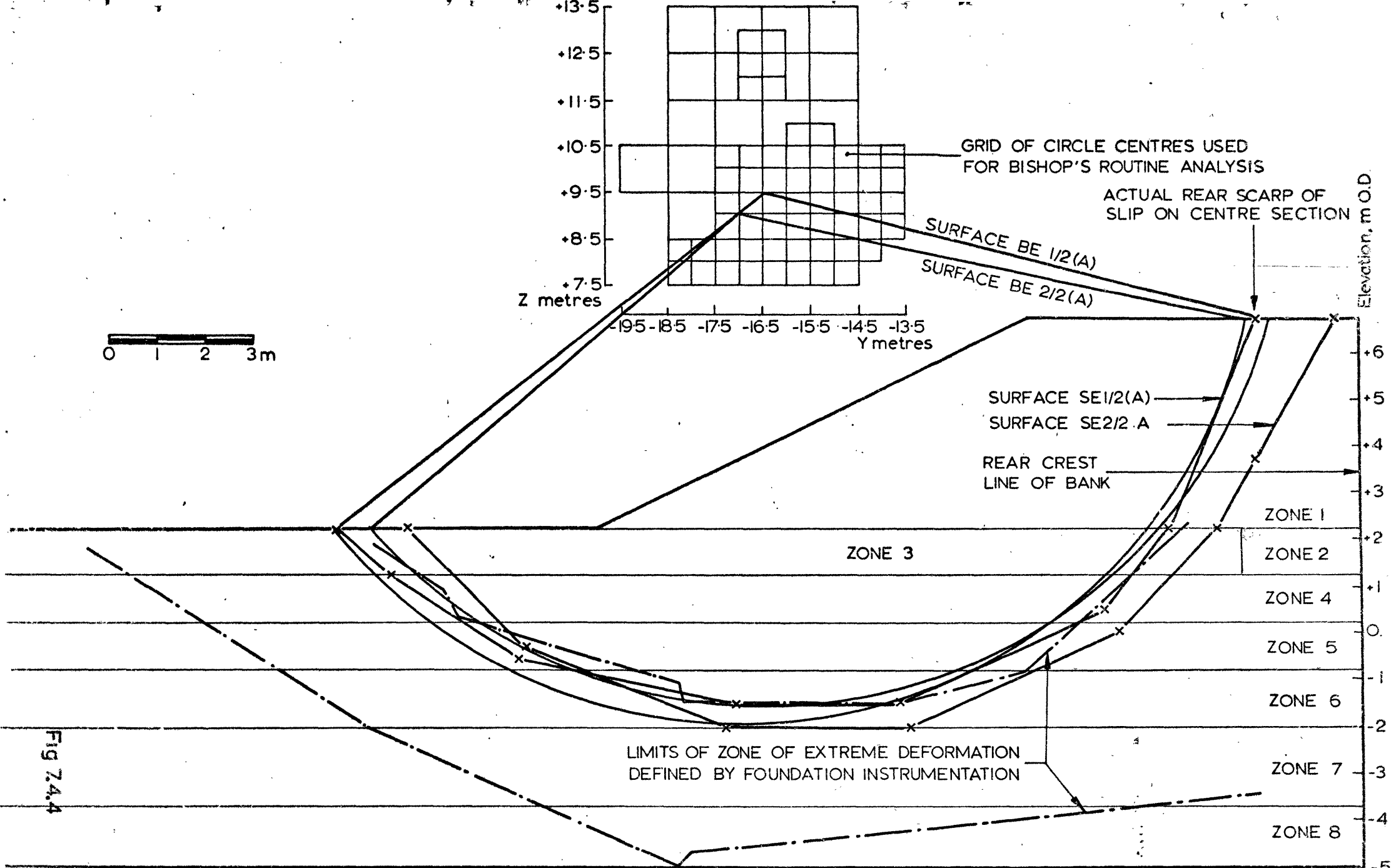
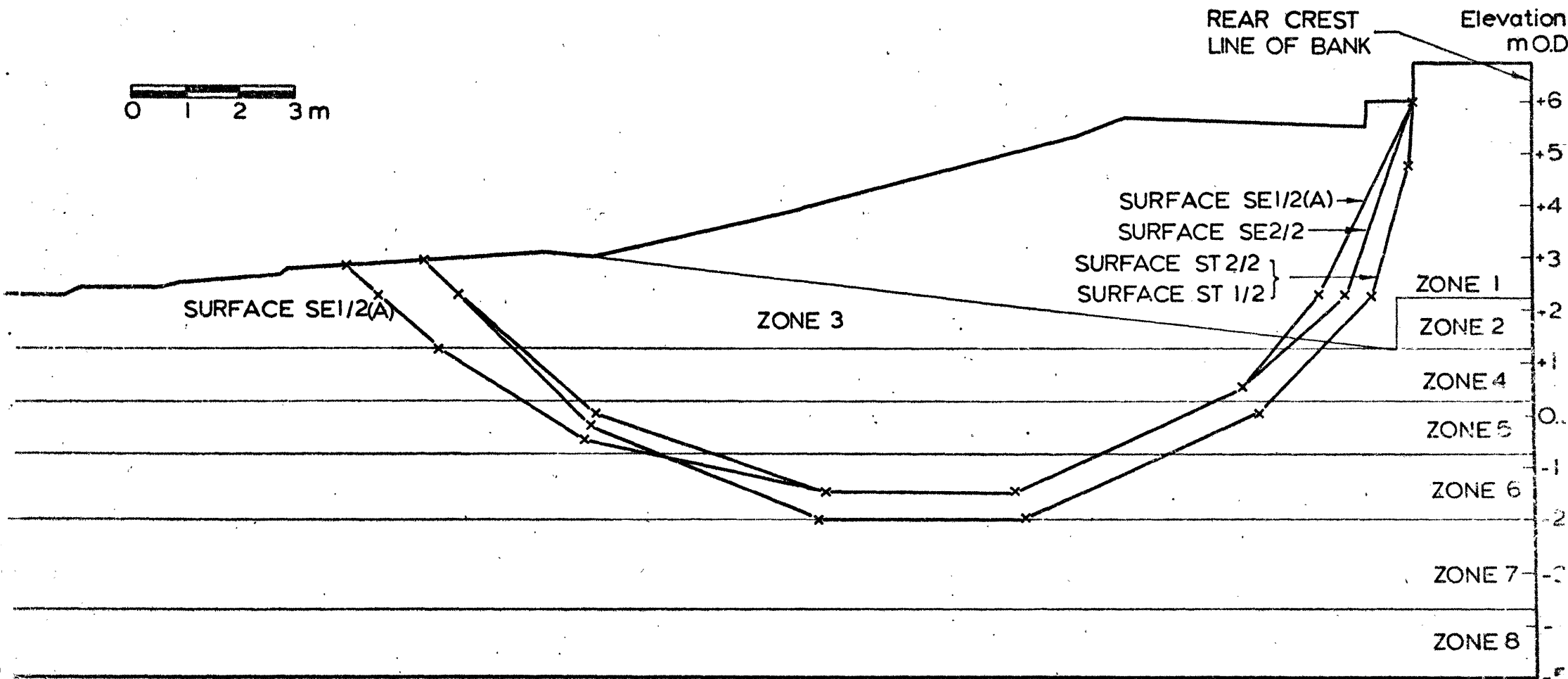


FIG 7.4.4

BANK 1/2: STABILITY ANALYSES IN TERMS OF EFFECTIVE STRESSES - CRITICAL 'UNRESTRICTED' SURFACES PREDICTED BY SARMA'S, AND BISHOP'S ROUTINE, METHOD.

1000



BANK 1/2 : STABILITY ANALYSES ,INCORPORATING POST-FAILURE PROFILE (SECTION C) AND CRITICAL 'RESTRICTED' SURFACES PREDICTED BY SARMA'S METHOD.

FIG 7.4.5

1-801-1

7.5. Summary of Results of Stability Analyses for Bank 1

7.5.1. Introduction

Before considering the back-calculated shear strengths (in terms of both total and effective stress) in relation to those determined from laboratory and small scale field tests, certain general observations regarding the limit equilibrium analyses will be made:-

- (i) the critical unrestricted slip surfaces (both circular and non-circular) for the effective stress analyses were in excellent agreement with the field observations (described in section 6.2).
- (ii) although, as would be expected, the critical unrestricted slip surfaces for the total stress analyses were not in such good agreement with the field observations, they were not dramatically different to those for the effective stress analyses.
- (iii) the critical unrestricted slip surfaces (effective stress analyses) for Stage 2 confirmed the view that the major movement took place within the upper part of the detected 'zone of extreme deformation', being clear of the peat layer.
- (iv) the results of analyses performed using Bishop's Routine Method and Sarma's Method, for the same degree of restriction applied to the critical slip surface, were in excellent agreement (maximum absolute difference in F.o.S. = 0.10; mean difference in F.o.S. = 0.01) despite the cruder assumptions forming the basis of the pore-pressure input data for the former method. The high degree of accuracy associated with Bishop's Routine Method has been observed elsewhere (Whitman and Bailey, 1967; Johnson, 1975; Foott and Ladd, 1977).

- (v) the safety factors derived using the Conventional Method, being the starting point for the iterative process of Bishop's Routine Method, were a maximum of 0.44 lower than the final F.o.S. Even in the case of the $\phi_u = 0$ Analysis, the Conventional Method produced lower safety factors by up to 0.09, noting that in all cases the fill was considered in terms of effective stress.
- (vi) for the critical surfaces, Bishop's Routine Method converged after some 3 to 4 iterations and Sarma's Method after only 2 iterations.
- (vii) between 30 and 50 slices were used to analyse each section, the larger number being associated with the Bishop analyses.
- (viii) the physical acceptability of the solutions using Sarma's Method was always checked. It was found that 'the closer to critical the better the solution' for a particular surface. For all of the critical surfaces $F_L > 1$ on all slice boundaries and the 'E' and 'X' forces were physically acceptable as was the average position of the line of thrust, being always between 0.3 and 0.4 times the height of the section above the slip surface. The thrust line always remained within the section, except for the final 500mm of the section within the fill.
- (ix) the effect of a tension crack on the analysis of Stage 1 was not particularly dramatic, but more significant than the likely errors in assignment of shear strength parameters to the fill. A knowledge of the actual mechanism of tension crack formation/failure formed an integral part of the stability analysis. The value of many case histories is reduced by a lack of such knowledge (Bjerrum, 1972).
- (x) restriction of the critical surface in a $\phi_u = 0$ analysis results in a significant over-estimate of the F.o.S. Back-calculated 'undrained strengths' on such surfaces are lower than the true undrained strength, and do not appear to be consistent for different geometries of trial

embankment. As pointed out by Cox (1975) there is an increasing incidence in the literature of case histories for which the field C_u has been associated with the observed failure surface (see e.g. Wilkes, 1972(a); Ladd 1972; Dascal et al, 1972; Lacasse and Ladd, 1973; Wu et al, 1975). This is particularly dangerous when the back-calculated C_u is used to derive empirical reduction factors (see e.g. Dascal and Tournier, 1975) of the type proposed by Bjerrum (1972). The previously mentioned case histories all relate to embankments on soft clays.

However, there may be cases where the straightforward approach of the $\phi_u = 0$ Analysis is not possible (Leonards, 1976).

(xi) the undrained strength/depth profiles, both with and without a stronger desiccated upper layer, derived using the $\phi_u = 0$ Analysis were equally satisfactory when applied to the differing geometries of the two stages of construction.

(xii) different critical surfaces may result from a change in the undrained strength/depth profile.

(xiii) in terms of total stresses the analyses incorporating a strong desiccated layer were considered to be the most satisfactory. The undrained strength of the desiccated crust is thus considered to be, on average, 45 kN/m^2 .

(xiv) comparisons between back-calculated undrained strengths and those predicted by laboratory and small scale field tests can be reliably made using the Stage 1 data, the complicating effects of the crust having been eliminated.

(xv) the most consistent effective stress analyses were those based on pore pressures extrapolated to correspond to the fill height at failure.

The difference between the latter analyses and those based on the observed pre-failure pore pressures goes a long way to explaining the lack of convincing effective stress analyses, for embankments on soft clay, in the literature. Difficulties have been experienced by, among others, Lo and Stermac (1965), Parry (1968), Ladd (1972), Lacasse and Ladd (1973), Wu et al (1975) and Foott and Ladd (1977); the case histories referred to include both main works structures, for which the pore-pressure data would not be expected to be complete, and trial embankments for which comprehensive pore-pressure data were available. As pointed out by Brooker (1965), and evident from the data of Ladd (1972), it is the pore pressures at failure which are relevant to an effective stress analysis; the success of the analyses reported herein largely hinges on the accurate determination of those pore pressures using a carefully executed instrumentation scheme.

(xvi) the least satisfactory aspect of the effective stress analyses was the incorporation of an undrained strength for the desiccated layer; these analyses also proved to be the least consistent. However, as in the total stress case, the Stage 1 analyses eliminated the uncertainties associated with the crust which have plagued many of the reported case histories in the literature (Seymour-Jones, 1975).

(xvii) consistent results were achieved from the total, but not the effective, stress analyses of restricted non-circular surfaces in conjunction with the post-failure profiles. This is considered to be a result of the delay in making the post-failure pore-pressure observations for Stage 2 and thus the analyses of Stage 1 are considered to be the most reliable.

7.5.2. Peak Shear Strength Parameters

(i) Total Stress Analyses

The derived undrained strength/depth profile, assuming a strong desiccated crust, is compared to the main laboratory and field vane test data in figure 7.5.1. These data are also summarised in table 7.5.1., wherein the average undrained strengths, around the critical unrestricted circular arc failure surface (BT2/1A), relating to the various profiles are given; surface BT2/1A did not pass through the desiccated crust.

Table 7.5.1. also gives the average correction factors which would be required to reduce the various measured undrained strengths to the field value, together with Bjerrum's (1972) correction factor (μ) as applied to the vane test data. These factors should be compared to those presented in table 3.11 as a summary of the possible correction factors to be applied to the field vane and laboratory test data.

Considering the laboratory data, figure 7.5.2.(A) depicts the back-calculated undrained strength for Bank 1 (being an average for both stages i.e. property set TS-2-0) plotted at a mean construction time of 70 days, in comparison to the laboratory undrained strain rate effect curve; the laboratory C_u value is based on the design profile and thus includes an allowance for anisotropy. The required average reduction factor of 0.79 is significantly larger than the value of 0.65 based on direct extrapolation of the laboratory data (table 3.11 and table 7.5.1.). This discrepancy could be the result of the different stress-strain-time path followed in the field and/or an increase in

undrained strength as a result of consolidation. It is interesting to note that the factor of 0.75, postulated in table 3.11 on the basis of the rate effect component of Bjerrum's μ factor, is closer to the correct value: this again suggests that the stress-strain-time path is important and/or that the embankment foundations considered by Bjerrum (1972) were also partially drained; the latter hypothesis is supported by the data of Leroueil et al (1978(b)).

Tables 7.5.1. and 3.11 both illustrate the difference obtained by the use of the averaging technique to account for undrained strength anisotropy, as compared to a slip circle analysis with the undrained strength assigned to each segment of the slip surface according to the principal stress directions implied by the slip surface orientation (see figure 2.14(A)). It is important to note that in the analysis the critical $\phi_u = 0$ surface was assumed to be at 45° to the major principal plane (i.e. $\beta = 45^\circ$), in accordance with the theoretical justification of the ϕ_u Analysis (Skempton, 1948(c)). The undrained strength associated with the relevant direction of major principal stress was obtained using Bishop's equation (2.15), the parameters 'a' and 'b' being as defined and evaluated in figure 2.20. In the analysis presented by Lo (1965) the surface considered is always equated to an actual failure surface (i.e. $\beta = 45 + \phi'/2$) to which the undrained strength is, inconsistently, applied. Using Lo's (loc cit) method an average C_u of 14.25 kN/m^2 was found, compared to 14.85 kN/m^2 for the true $\phi_u = 0$ Analysis. On the actual failure surface the mobilised shear strength would be expected to be $C_u \cdot \cos\phi'$, and not C_u as proposed by Lo (1965) and used in the case histories discussed previously; in fact the mobilised shear stress on the critical effective stress surface

(see table 7.5.2) was almost exactly equal to $C_u \cos \phi'$.

The averaging technique, as used herein to account for undrained strength anisotropy, was equivalent to a reduction factor (applied to C_{uv1}) of 0.87; a straight average of the results of triaxial tests on vertical and horizontal specimens would have yielded a factor of 0.85, the inclusion of 45° specimens lowering this to 0.83. The difference between the design profile and the latter was because of the upper part of the profile being based solely on vertical specimens as discussed in section 2.7.5. An average undrained strength based on vertical, 45° and horizontal specimens would thus make a realistic approximation to the effects of undrained strength anisotropy. The straight average proposed by Ladd and Foott (1974) is slightly unconservative and the average of the results of C_{UTC} and C_{UTE} tests, also as proposed by Ladd and Foott (1974), overconservative. Comparison of the data in tables 3.11., 7.5.1., and figure 7.5.2(A) suggests that the reduction factors proposed by Parry (1971(a)) for both undrained strength anisotropy and undrained strain rate effect err on the unsafe side.

The single point plotted for the Bank 1 failures, in figure 7.5.2.(A), is obviously an approximation. Reference to tables 7.3.1. and 7.4.1. shows that there was a very small increase in the available undrained strength between the failure of Stage 1 (on day 51) and the failure of Stage 2 (on day 89). Thus the Bank 1 failures probably occurred on a curve such as '3' in figure 7.2.1., as discussed in section 7.2.

The results of the Geonor vane tests have been seen to represent partially drained conditions and it is thus not surprising that the correction factor μ is insufficient to reduce the vane shear strength to the field value.

However, a combination of the appropriate rate effect reduction factor based on the laboratory data (0.61; table 3.11) and the anisotropy component of μ (1.08; table 3.11) yields, doubtless fortuitously, a factor of 0.66 compared to that required of 0.68. Thus the consolidation in the field appears to have been compensated for by the consolidation in the Geonor vane tests; another example of compensating errors. In this context it is interesting to note that in their re-appraisal of the New Liskeard Embankment, Lacasse and Ladd (1973) achieved a F.o.S. close to unity using the corrected vane strengths; now the New Liskeard Clay is varved (Lo and Stermac, 1965) and the vane test results in this case were, also, almost certainly influenced by consolidation (Townsend, 1965).

The results from the large vane tests, at the same time to failure as the Geonor tests, require less correction (reduction factor = 0.84) than suggested by μ (= 0.76) or the combined factor of 0.66 derived in the preceding paragraph. This further suggests, as do the New Liskeard data, that some of the vane test data analysed by Bjerrum (1972) were also influenced by consolidation during the test.

(ii) Effective Stress Analyses

The analyses relating to entirely effective stress conditions are summarised in figure 7.5.3., which enables the final laboratory design values of $c' = 8 \text{ kN/m}^2$ and $\phi' = 25^\circ$ to be related to the two failures. Using the extrapolated pore pressures the F.o.S. for Stage 1 is 1.21 and for Stage 2, 1.22; these values are thus in excellent agreement with each other and with the safety factors based on the laboratory total stress design data in conjunction with the strong crust assumption (i.e. 1.21 for Stage 1 and 1.28 for Stage 2).

The back-calculated values of c' , for a F.o.S. of unity in each case, were 5.7 kN/m^2 (Stage 1) and 5.4 kN/m^2 (Stage 2). These data are compared to the laboratory values extrapolated on a strain rate basis in figure 7.5.2.(B), wherein it may be seen that the field values of c' are entirely consistent with the values which would be predicted from the laboratory data.

Now both the values of C_u and c' presented in figure 7.5.2. represent 'best' estimates based on the laboratory data, the only major uncertainty (other than the relevance of the laboratory strain rate curve to the field situation) not considered being progressive failure. The data in figure 7.5.2. suggest that the differences in stress-strain-time path experienced by the laboratory sample and the foundation material under full scale loading conditions do not significantly influence the mobilised shear strength. Two conclusions follow:-

- (a) the increase in C_u obtained in the field, relative to the laboratory strain rate curve, was the result of consolidation.
- (b) the values of c' and ϕ' mobilised at failure were not reduced by progressive failure and therefore any undrained brittleness could only be as a consequence of pore-pressure generation. No evidence of significant strain softening as a result of pore-pressure generation was in evidence from the pore-pressure data (section 6.1.3), and thus the data overall support the progressive failure 'reduction' factor of unity proposed by Dasgal and Tournier (1975) for materials with a liquidity index less than unity (table 3.11).

7.5.3. Residual Shear Strength Parameters

The average shear stresses on the critical total stress restricted non-circular surfaces (figures 7.3.5. and 7.4.5.), both pre-failure and post-failure are presented in table 7.5.2; also shown are the corresponding shear and normal effective stresses for the corresponding effective stress analyses. These data, which are summarised in figure 7.5.4*, have been used to calculate the field values of I_B in terms of total and effective stresses.

In terms of total stress I_B was between 40% and 50%, and thus much lower than the figures of 80% to 90% obtained in the laboratory (section 2.7.6) and using the field vane (section 3.2.4); this discrepancy could well be the result of pore-pressure dissipation during the field failures.

The back-calculated values of the field I_B , in terms of total stress, for the two failures can be seen to be very consistent. As would be expected the average shear stress on the total stress surfaces is slightly greater than on the effective stress surfaces, but lower than on the critical unrestricted surface (table 7.5.1). In this context it should be noted that the points in figure 7.5.4. representing the total stress analyses are for restricted surfaces and thus do not represent a true $\phi_u = 0$ analysis. The residual undrained strength profile associated with a strong crust is compared to the peak strength data in figure 7.5.1.

*it is worth noting on the figure that the derived effective stress parameters at peak are equally valid for the strong crust assumption.

In terms of effective stress, I_B for Stage 1 was between 25% and 32% suggesting a considerable pore-pressure component to be associated with the undrained brittleness. The corresponding ϕ'_r was 35° with $c' = 0$; the large strains associated with the failure would thus appear to have resulted in a remoulding of the clay back to its normally consolidated state. The higher values of I_B in terms of effective stress resulting from the Stage 2 data are compatible with an under-estimate of the post-failure pore pressures as discussed in section 7.5.1.

In conclusion although progressive failure appears to have had little influence on the shear strengths mobilised at 'first' failure, a significant reduction in shear strength, in terms of both total and effective stresses, occurred during failure. This reduction appears to have comprised a complete loss of c' , accompanied by an increase in ϕ' . The implications for main works construction are that, should a failure occur, embankment construction to full height would still be possible given sufficient pore-pressure dissipation; however, a lengthy stage reconstruction would be necessary unless measures were taken to speed up the drainage process.

7.5.4. Conclusions

The results of the stability analyses confirm the previous findings (Chapter 6) that significant pore-pressure dissipation took place during construction, resulting in an increase of about 2.8 kN/m^2 in the average C_u of the foundation. Such an increase would result in an increase in the F.o.S. for a $\phi_u = 0$ analysis of about 0.23.

In Chapter 6 (see e.g. table 6.1.1) it was shown that the vertical effective stresses beneath the centre of Bank 1 increased to a maximum value, during the early stages of construction, closely corresponding to the preconsolidation pressure; being an average increase of some 20 kN/m^2 . Reference to figure 2.16 indicates that such an increase, followed by undrained shear, would be expected to produce an increase in C_u of about 5 kN/m^2 , C_u/p_c' being near constant in the sub- p_c' range (figure 2.24). However, the back-calculated increase of only 2.8 kN/m^2 suggests that the undrained strain rate effect partly cancelled (and diminished) the increase in strength resulting from consolidation. In this context it is of interest to speculate that, based on the large vane test data (figure 3.20), the separation of the drained and undrained rate effect curves (e.g. figure 7.2.2) was about 10 kN/m^2 .

The factors by which the undrained strength of vertical specimens, from high quality large diameter samples tested (unconsolidated) in triaxial compression, needs to be reduced have been seen (table 3.11) to be 0.82 for anisotropy and 0.65 for undrained strain rate effect (i.e. a combined reduction of 0.52) in order to achieve the field undrained strength corresponding to a 50 - 100 day construction period. However, to this considerably reduced undrained strength must be added the increase resulting from consolidation.

Now the average $C_{UV\eta}$ was 18.2 kN/m^2 (table 7.5.1); if, based on figure 2.16 and table 6.1.1., 5 kN/m^2 is added to allow for the effects of consolidation $C_{UV\eta}$ becomes 23.2 kN/m^2 . Correction for strain rate (0.65) and for anisotropy (0.82) leads to a design field shear strength

of 12.4 kN/m^2 compared to the back-calculated value of 12.5 kN/m^2 . The accurate prediction of the field undrained strength in cases where rapid consolidation occurs during the early part of construction, until p_c' is reached, would thus seem possible; according to Leroueil et al (1978(b)) such cases are the rule rather than the exception.

The only vane test data considered to represent undrained shear strengths were those from the large vane tests. Considering the results at a time to failure corresponding to that of the Geonor tests, the average C_u was 14.85 kN/m^2 . According to Bjerrum (1972) this value requires correction by a factor of 1.08 to account for undrained strength anisotropy, yielding a C_u of 16 kN/m^2 ; applying a rate effect correction of 0.93 to normalise this value to the laboratory data results in a C_u of 14.85 kN/m^2 which is exactly that obtained from the laboratory data when used with the inclination of specimen appropriate to the slip surface. Thus the same rate effect and consolidation allowances are appropriate to the laboratory and the field vane data.

Bjerrum's correction factor has been seen to be of far from universal application; this is thought to be because of the influence of varying amounts of consolidation on the vane test, and full scale field, data used in its derivation; in addition the rate effect factor must depend on the actual construction time or time to failure. Ladd and Foott (1977) recently re-appraised the stability of the Atchafalaya Levees (Kaufman and Weaver, 1967) for which the foundation behaviour would appear to correspond to curve 2 of figure 7.2.2.; strong time dependency of the undrained strength was evident (Kaufman and Weaver, 1967). In this case the vane tests, even when corrected for plasticity, produced a F.o.S.

well in excess of unity; however, the failure did not occur until some five months after the end of construction.

Perhaps somewhat surprisingly, therefore, the laboratory undrained strengths, based on the SHANSEP method of design (Ladd and Foott, 1974), with no apparent account being taken of strain rate effect, yielded safety factors close to unity. This method of design was outlined in section 2.7.2. and criticism made of the principle of testing at elevated stress levels. In addition Wesley (1975) has shown that consolidating the Mucking clay to a pressure in excess of p_c' , as defined by the change in gradient of the C_u/p_o' relationship, does not entirely remove the effects of previous stress history although this tends to increasingly occur at higher values of p_o' (section 2.6). More recently Buri (1978) demonstrated that different undrained strengths were measured at a particular void ratio, having arrived at that void ratio via secondary consolidation on the one hand and release of stress on the other hand. The success of Ladd and Foott's (1974) method may, thus, also be partly the result of compensating errors.

By way of a final comment on compensating influences in relation to undrained shear strength, it will be remembered that in Chapter 1 (table 1.3) C_u for the Essex marsh clay was estimated to be some 10 - 15 kN/m^2 *, a figure based on specimens which were doubtless disturbed to a lesser or, more probably, greater extent, tested in unconfined compression. Exercising engineering judgement one might select a mean value of 12.5 kN/m^2 (reference to table 7.5.1. indicating the extent of the judgement!). If the desiccated layer was ignored, and a clay embankment of similar strength to the foundation

*in fact not only C_u but also ϕ' and the post-yield value of C_v are accurately predicted by the data in table 1.3.

assumed, Taylor's (1948) stability numbers (figure 1.3) can be used to predict the critical height of an embankment (Bank 1, Stage 2) at Mucking; the critical height is 4.5m. In similar vein table 7.4.1. shows that using the data from the vertical piston samples and ignoring the true strength of the crust produces a F.o.S. for Bank 1, Stage 2 of 1.16, compared to 1.37 representing the 'best' estimate.

The effective stress analyses have shown that reliable values of c' and ϕ' can be determined from standard laboratory tests and likewise the time dependent drop in c' . Combined with the relevant pore pressures excellent predictions of stability were possible; in view of the almost complete lack of successful effective stress analyses of embankments on soft clay reported in the literature the analyses presented herein were particularly rewarding and justified the painstaking approach adopted with respect to the field observations. However, it has been seen that the effective stress analyses were very sensitive to the pore pressures and thus the success achieved using Bishop's Routine Method may have been to some extent fortuitous*.

Although it has been shown that dissipation of pore pressure can be accounted for in the prediction of undrained strength for construction failures, effective stress analyses are obviously attractive for partially drained cases. In addition failure of foundations whose shear strength is markedly time dependent may occur well after the end of construction, again pointing to an effective stress method of analysis. However, as shown in section 6.1.3., it is doubtful if available pore-pressure

*this comment reflecting on the method of pore-pressure input incorporated in the computer program and not on the applied mechanics of the method of stability analysis.

prediction methods are sufficiently refined to enable the effective stress end-of-construction analysis to better the total stress approach. Even after the end of construction, predictions based on effective stress analyses will be complicated by uncertainties regarding creep induced pore pressures, and a consolidated undrained method of analysis may be deemed appropriate.

DATA SOURCE	DATA LABEL	F.o.S.	C_u kN/m ²	REQUIRED CORRECTION FACTOR	APPLIED CORRECTION FACTOR
1. Laboratory; block samples, vertical specimens	TS-VB-2	1.37	18.20	0.69	1.00
2. Laboratory; block samples with allowance for anisotropy	TS-LD-2	1.25	15.85	0.79	0.87
3. Laboratory; block samples with correct inclination	-	1.17	14.85	0.84	0.82
4. Laboratory; as 2 but corrected for strain rate	TS-LD(r)-2	0.81	10.20	1.22	0.57
5. Laboratory; as 3 but corrected for strain rate	-	0.76	9.65	1.30	0.52
6. Vertical Geonor Vane	TS-GV-2	1.39	18.30	0.68	
7. As 6; but corrected for plasticity	TS-GV-2(μ)	1.10	13.95	0.90	0.76(μ)
8. Large Vane; at same time to failure as Geonor	TS-LV-2	1.12	14.85	0.84	-
9. As 8; but corrected for plasticity	TS-LV-2(μ)	0.91	11.65	1.07	0.76(μ)
10. Large Vane; min. values	TS-LM-2	1.06	13.15	0.95	-
11. As 10; but corrected for plasticity	TS-LM-2(μ)	0.84	10.30	1.21	0.76(μ)
<u>DERIVED DATA</u>					
1. Based on lab. profile 1.	TS-2-0	0.99	12.5	-	-

Table 7.5.1.

Bank 1, Stage 1

Comparison of Average Undrained Strengths on Critical Surface BT2/1A

SOIL PROPERTIES	PRE-FAILURE*			POST-FAILURE			I _B %
	τ_{av} kN/m ²	$\sigma'_{n\ av}$ kN/m ²	$\frac{\tau_{av}}{\sigma'_{n\ av}}$	τ_{av} kN/m ²	$\sigma'_{n\ av}$ kN/m ²	$\frac{\tau_{av}}{\sigma'_{n\ av}}$	
Weak crust	11.32	11.89	0.95	6.77	9.48	0.71	25
Strong crust	11.44	15.52	0.74	6.72	11.94	0.56	32
BANK 1, STAGE 1 EFFECTIVE STRESS RESULTS							

SOIL PROPERTIES	PRE-FAILURE*	POST-FAILURE	I _B %
	τ_{av} kN/m ²	τ_{av} kN/m ²	
Weak crust	11.45	6.00	48
Strong crust	11.62	6.89	41
BANK 1, STAGE 1 TOTAL STRESS RESULTS			

SOIL PROPERTIES	PRE-FAILURE*			POST-FAILURE			I _B %
	τ_{av} kN/m ²	$\sigma'_{n\ av}$ kN/m ²	$\frac{\tau_{av}}{\sigma'_{n\ av}}$	τ_{av} kN/m ²	$\sigma'_{n\ av}$ kN/m ²	$\frac{\tau_{av}}{\sigma'_{n\ av}}$	
Weak crust	12.53	14.86	0.84	6.46	13.95	0.46	45
Strong crust	13.48	15.82	0.85	6.25	16.50	0.38	55
BANK 1, STAGE 2 EFFECTIVE STRESS RESULTS							

SOIL PROPERTIES	PRE-FAILURE*	POST-FAILURE	I _B %
	τ_{av} kN/m ²	τ_{av} kN/m ²	
Weak crust	13.04	6.63	49
Strong crust	13.34	6.93	48
BANK 1, STAGE 2 TOTAL STRESS RESULTS			

* Pre-failure pore pressures extrapolated to:-

4.00m fill height for Stage 1

4.50m fill height for Stage 2

Table 7.5.2.

Brittleness Index In Terms of Total & Effective Stress

BANK 1 - STABILITY ANALYSES

SUMMARY OF UNDRAINED STRENGTH PROFILES

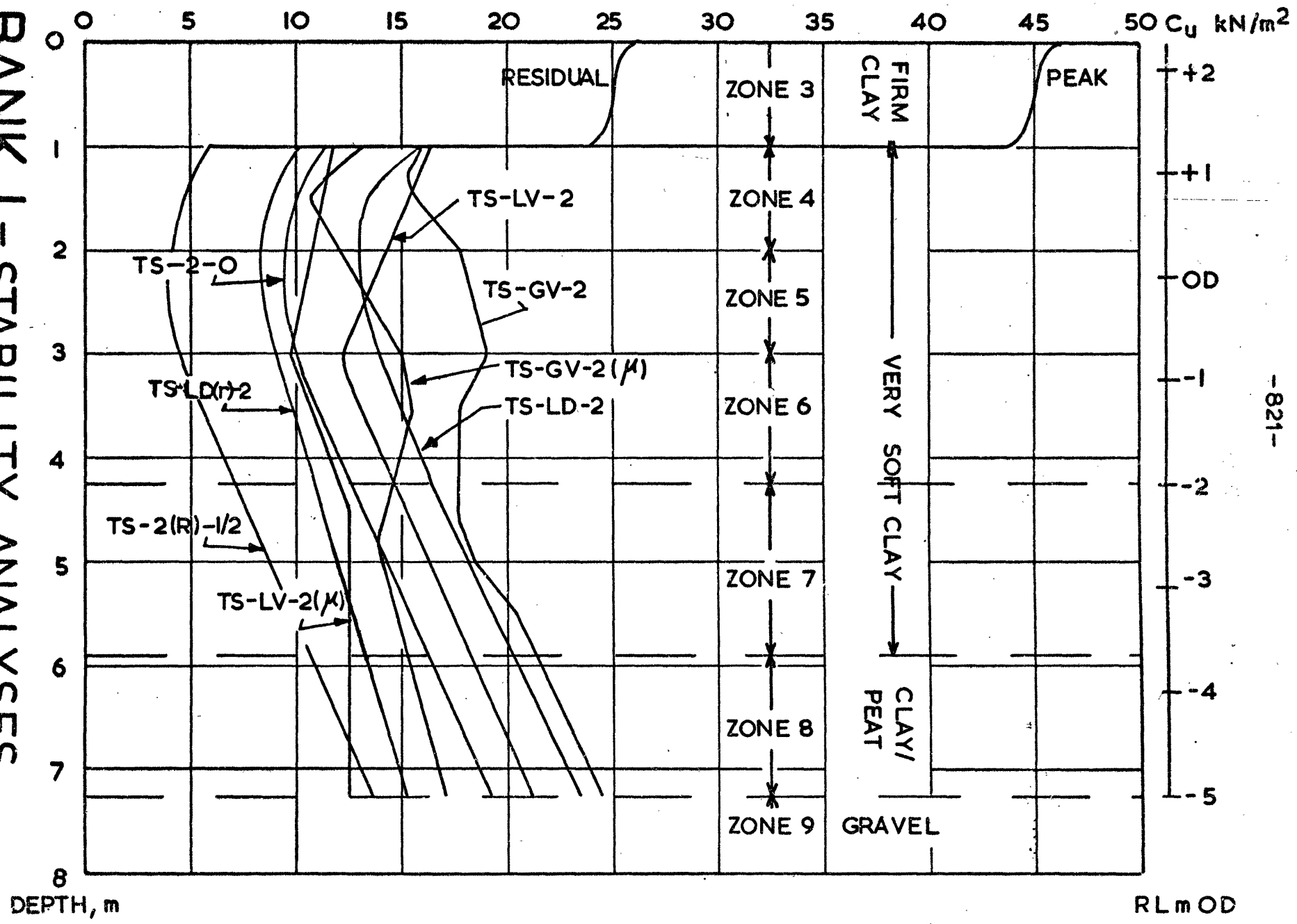
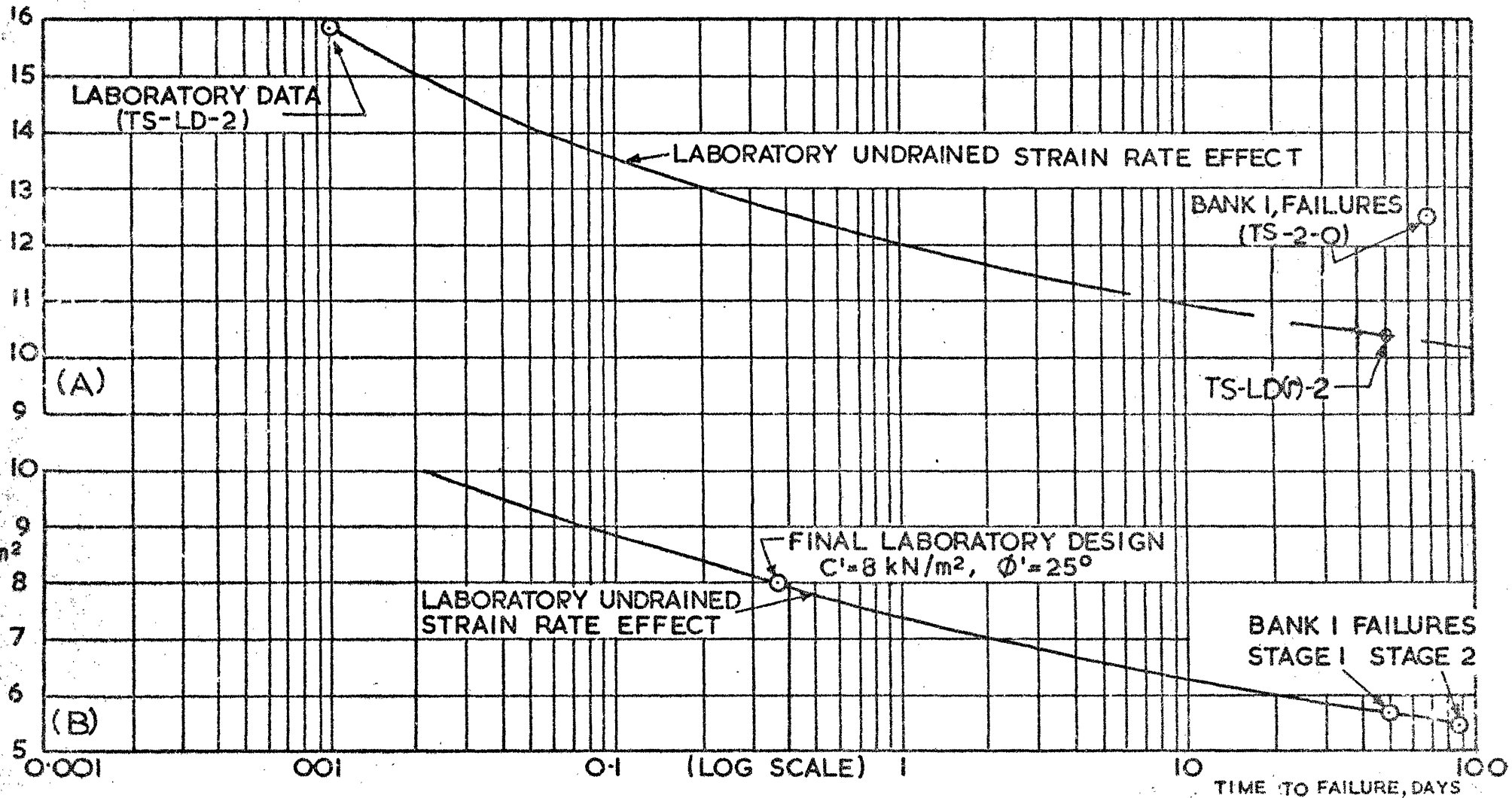


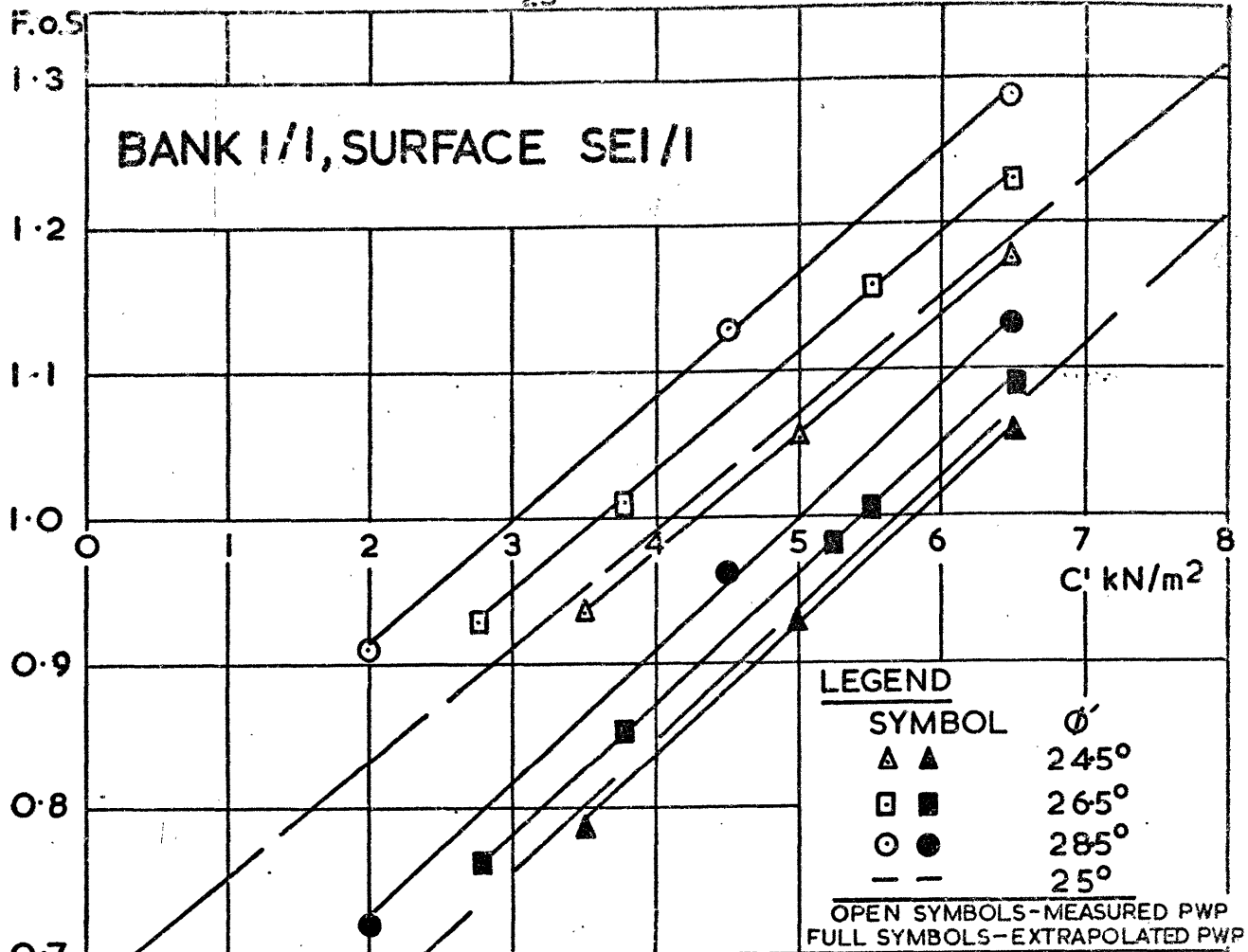
Fig. 7.5.1

Cu KN/m²



INFLUENCE OF TIME TO FAILURE ON LABORATORY AND FULL SCALE FIELD MEASUREMENTS OF A) UNDRAINED STRENGTH AND B) EFFECTIVE APPARENT COHESION

FIG. 7.5.2



F.o.S INFLUENCE OF C' ϕ' AND PORE PRESSURE ON THE FACTOR OF SAFETY FOR BANK 1, STAGES 1 & 2

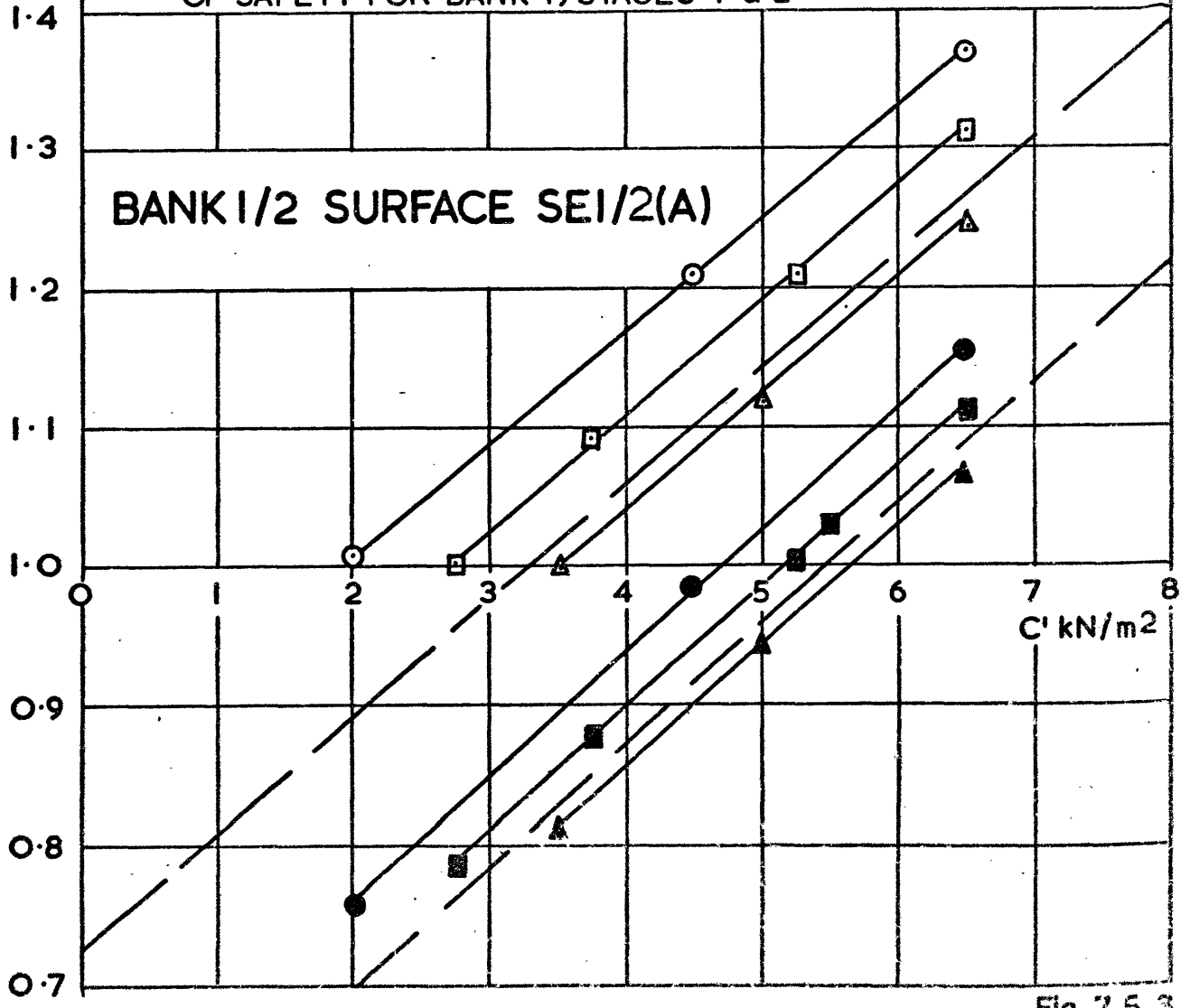


Fig. 7.5.3

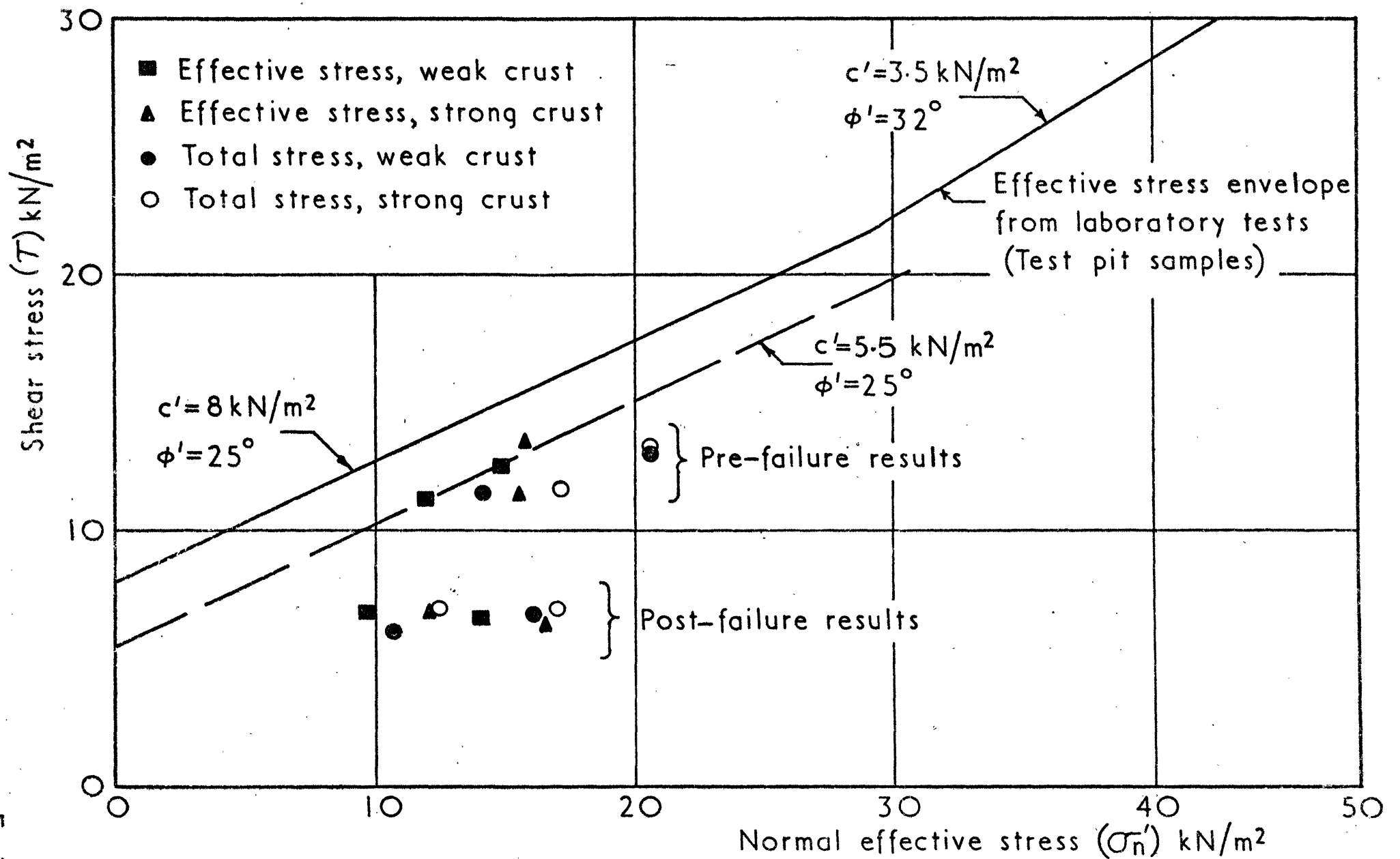


Fig 7.54

RESULTS OF STABILITY ANALYSES FOR NON-CIRCULAR SURFACES PASSING THROUGH ACTUAL SLIP LOCATIONS WITH PRE-FAILURE PORE PRESSURES EXTRAPOLATED TO MAXIMUM FILL HEIGHT

7.6. Analysis of Bank 2

7.6.1. Introduction

The back-analyses of Bank 1 enabled the stability of Bank 2 to be examined incorporating a time dependent loss of c' together with pore pressures which continued to rise post-construction. Using Bishop's Routine Method the stability was assessed for the end-of-construction situation and 5, 50, 200 and 600 days thereafter. The corresponding pore pressures, presented as contours of equal r_u , are depicted in figure 7.6.1. (see also figure 6.1.24). A constant ϕ' of 25° was adopted for the foundation, c' varying with time as shown in figures 7.5.2. and 7.6.3. A second analysis, assuming c' to be constant at the mean value of 5.5 kN/m^2 (figure 7.5.4.) back-analysed from the Bank 1 failure, was performed.

7.6.2. Results of Analyses

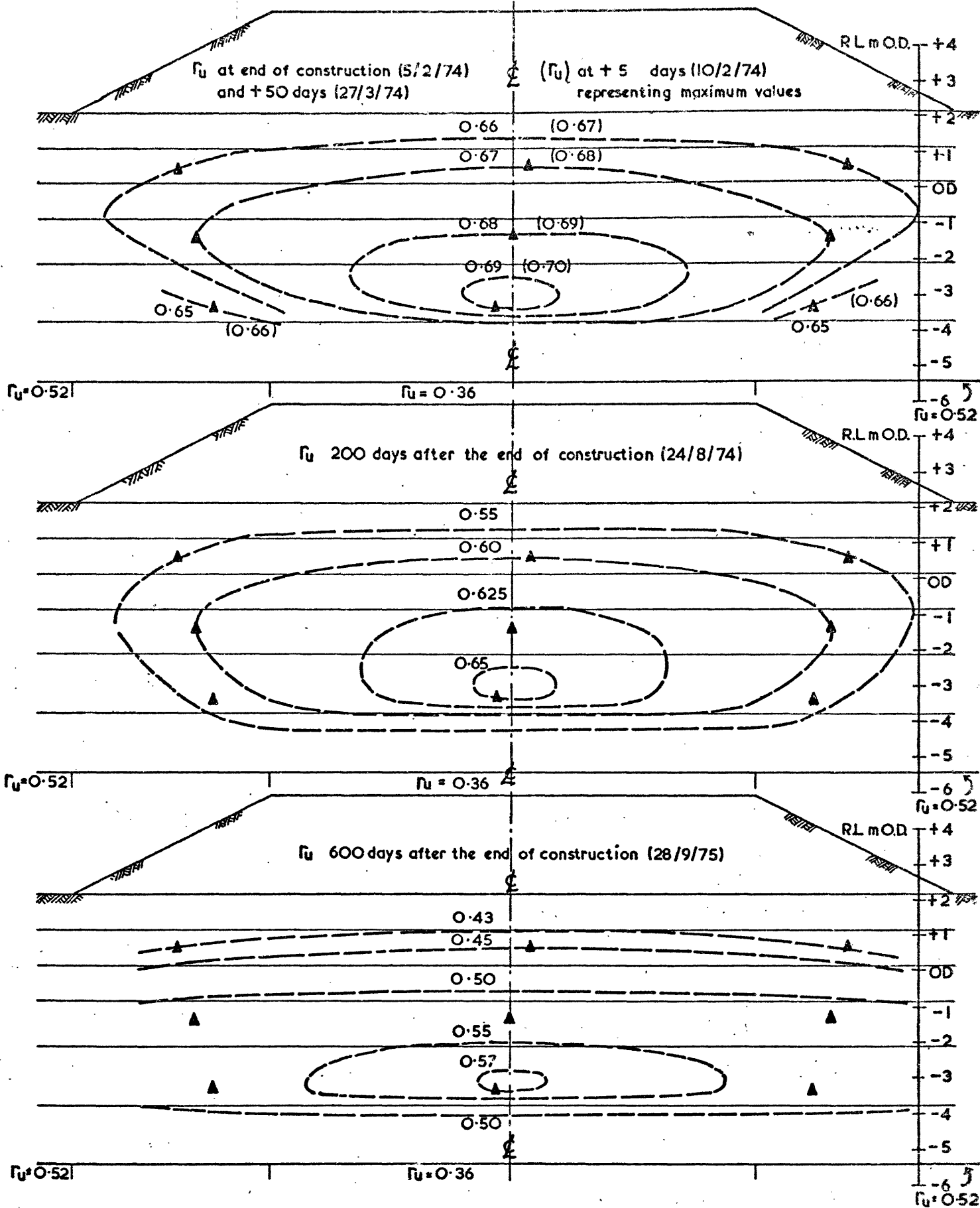
The results are presented as F.o.S. versus c' , corresponding to the changing pore-pressure regime, in figure 7.6.2.(A), and as F.o.S. versus time after the end of construction in figure 7.6.2.(B). The latter relationship is alternatively presented as F.o.S. versus log time from the start of construction in figure 7.6.3. (c.f. figure 7.2.2.).

Assuming c' to be constant, corresponding to the construction time for Bank 1, can be seen to be conservative initially, for the more rapidly constructed Bank 2 but unconservative in the long term (60+ days after the end of construction).

With c' reducing as a function of increasing time the F.o.S. of 1.56 at the end of construction reduced to a minimum of about 1.50 some 30 days afterwards. These data clearly show that for embankments constructed on

soft clay the end-of-construction case need not be the most critical.

Finally, it is important to note that, given the type of field E.S.P. derived in Chapter 6 the F.o.S. calculated using a total stress analysis will be different to that using an effective stress analysis, except at failure. In fact, with the E.S.P. s typically moving to the left in a stress path plot the effective stress analysis may suggest an unwarranted degree of confidence in the stability of an embankment. Thus, as suggested in section 7.5., the use of a consolidated undrained analysis has certain advantages.

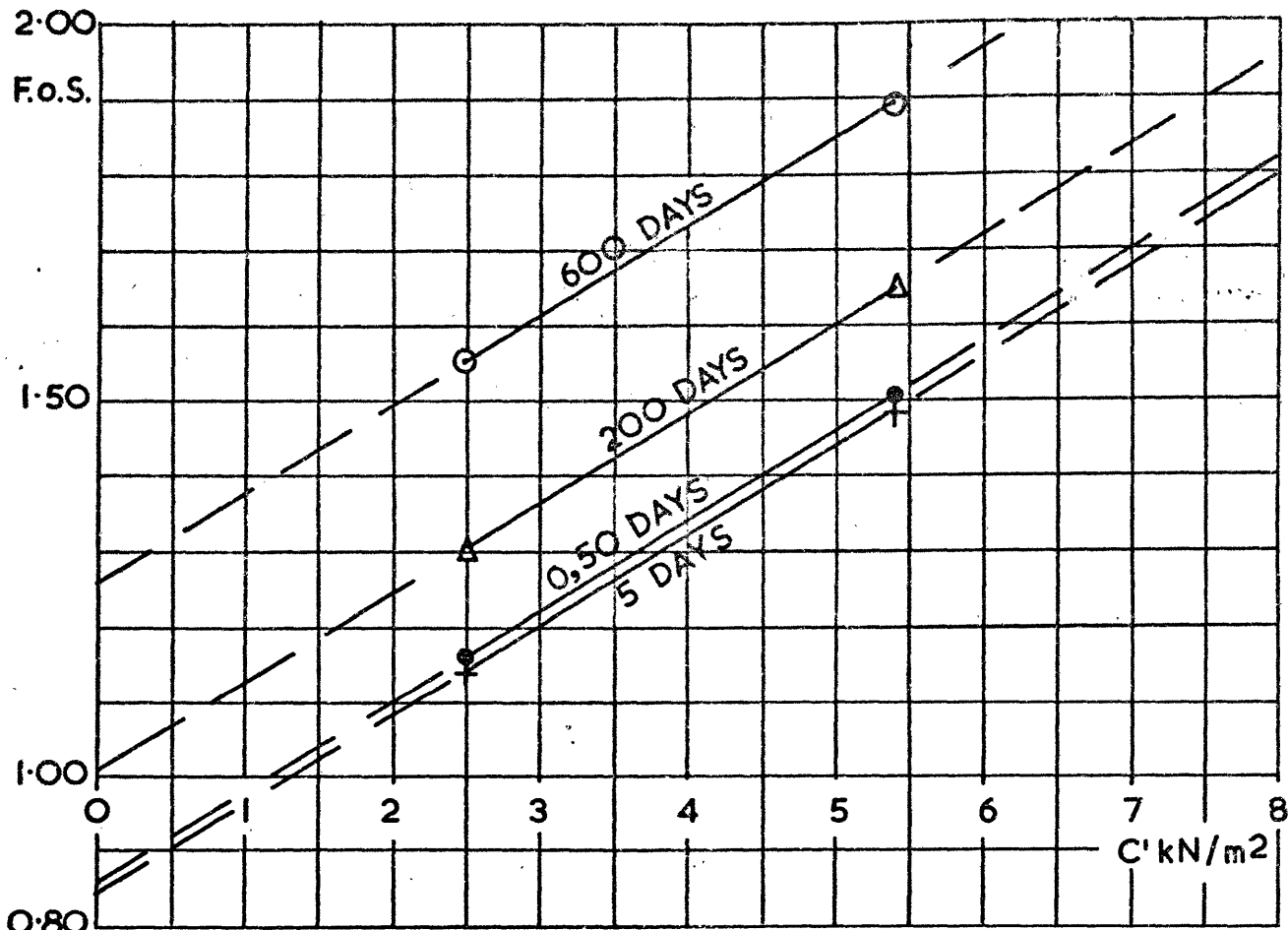


LEGEND ▲ PIEZOMETER LOCATION

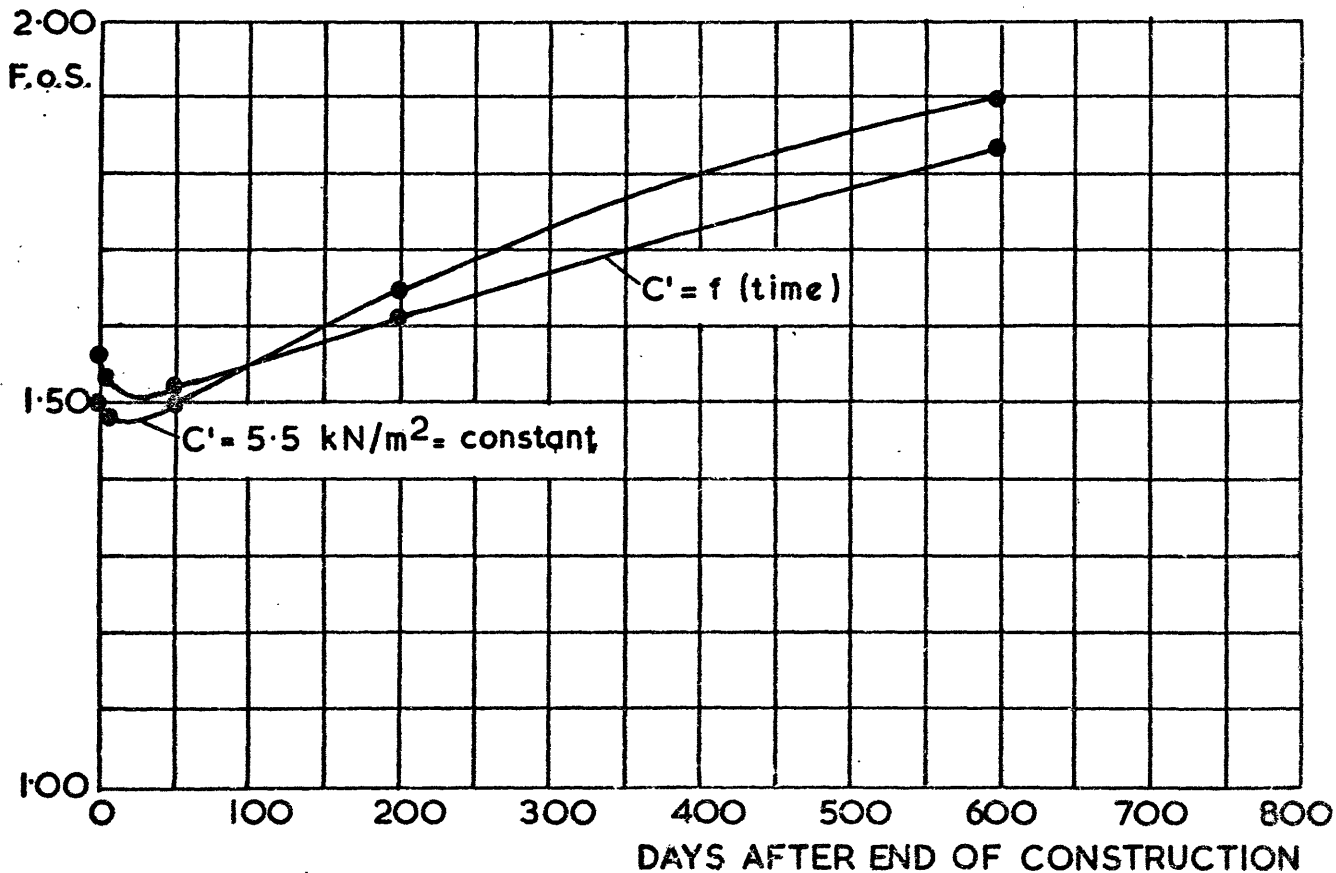
BANK 2

CONTOURS OF PORE-PRESSURE RATIO (r_u) AT VARIOUS TIMES AFTER THE END OF CONSTRUCTION

Fig. 7.6. 1

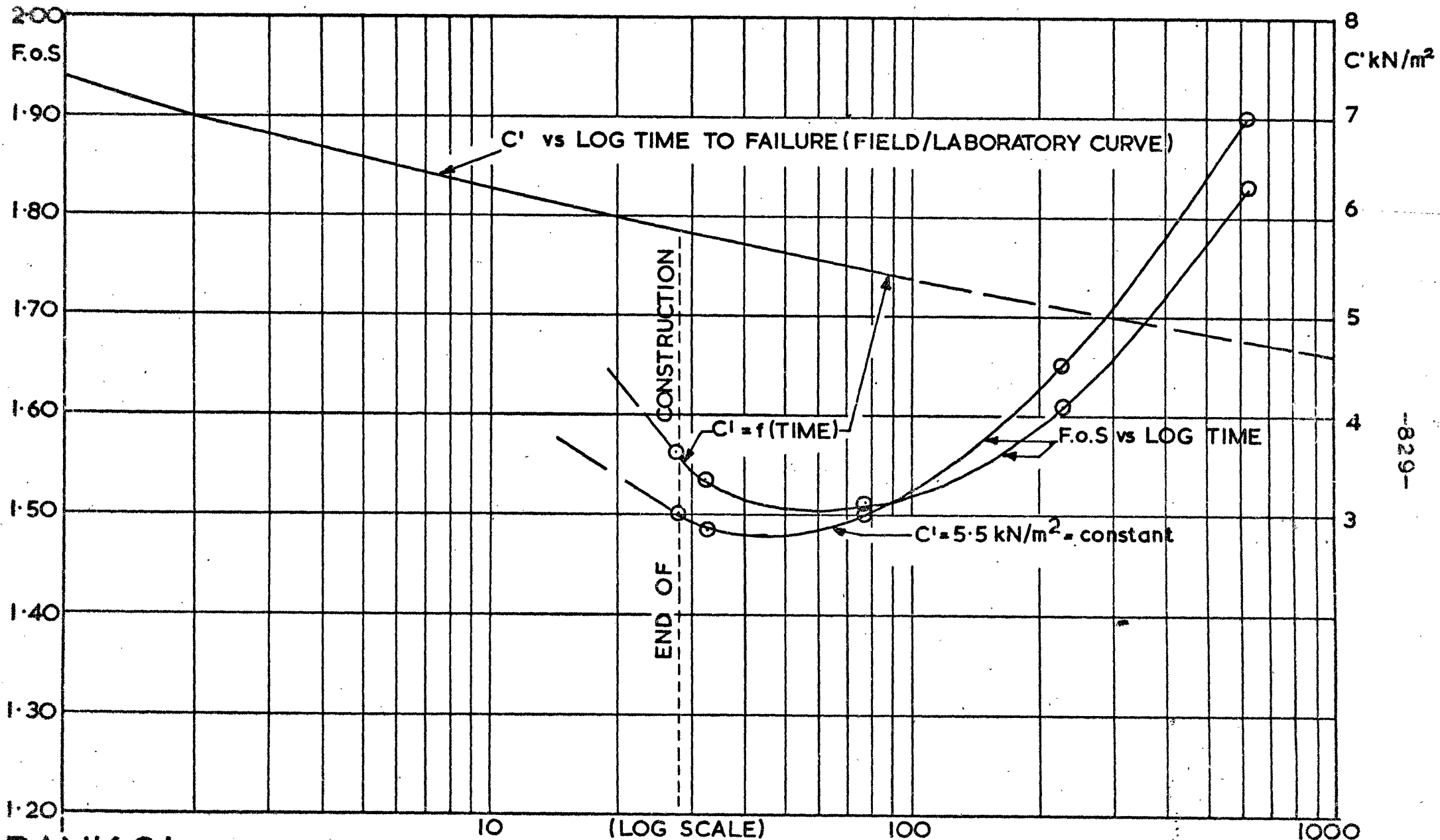


A) F.o.S vs C' AT VARIOUS TIMES AFTER THE END OF CONSTRUCTION



B) F.o.S vs TIME AFTER THE END OF CONSTRUCTION

BANK 2 EFFECTIVE STRESS STABILITY ANALYSES



-829-

BANK 2: VARIATION OF APPARENT COHESION AND FACTOR OF SAFETY WITH TIME

DAYS AFTER START OF CONSTRUCTION
TIME TO FAILURE, DAYS

Fig. 7.6.3

7.7. Assessment of the Stability of Embankments on Very Soft Lightly Overconsolidated Clays

7.7.1. Introduction

In this section an attempt is made to provide guidelines for the design of embankments on soft clay. Similar exercises have been presented by Bjerrum (1972 and 1973), with particular reference to the vane shear strength, and by Ladd and Foott (1974) in support of the SHANSEP approach to design; a more general, and therefore less specific, appraisal of the problem was also presented by Parry (1971(a)).

The guidelines set down herein relate specifically to the Mucking clay, although a survey of the available literature suggests that they may be of fairly wide application. However, the behaviour of soft clays under full scale loading conditions is strongly influenced by, among other things, the soil's fabric (Rowe, 1972), its sensitivity (Dascal and Tournier, 1975) and its O.C.R; obviously any design exercise must include a thorough investigation of these, and associated aspects.

The data presented have clearly illustrated the need for at least one profile of large diameter high quality samples, if at all possible, in order to assess the confidence which can be placed in the strength test results obtained from conventional piston sample specimens. Sample disturbance may result in considerable reductions in the laboratory measured undrained strengths of soft clays; whilst the SHANSEP approach may have some merit when applied to highly disturbed specimens it is no substitute for the testing of high quality samples at the correct effective stress levels. Sample disturbance may also influence the laboratory effective stress parameters.

Truly undrained field vane shear strengths are only likely to be obtained using the large vane equipment or similar; certainly an investigation of the effect of shear strain rate should become a routine part of both laboratory and field vane tests on soft clays (Parry 1971(a)). It has clearly been shown that Bjerrum's (1972) μ factor is of far from universal application; corrections for strain rate and anisotropy should, ideally, be determined directly in relation to the actual construction situation.

7.7.2. Total Stress Analyses

It has been shown that reliable field undrained strengths may be obtained from triaxial tests on high quality specimens taking into account the effects of undrained strength anisotropy and undrained strain rate, both of which may be directly assessed in the laboratory.

In many instances (Leroueil et al, 1978(b)) an increase in the field undrained strength may result from rapid dissipation of construction pore pressures during the early part of construction. The maximum vertical effective stress appears to closely correspond to p_c' so that the change in effective stress, $\Delta p_o'$, can be estimated; and thus ΔC_u determined from the C_u/p_o' relationship, noting that ΔC_u relates to quick laboratory tests on vertical samples.

Most soft clay deposits exhibit a strength increase close to the ground surface as a result of desiccation; this has been seen to be of some importance in an assessment of stability (see also Cox, 1970; Lacasse and Ladd, 1973; Seymour-Jones, 1975). The two-stage embankment construction used at Mucking enabled the strength of the desiccated layer to be directly

back-calculated, C_u being 45 kN/m^2 . This value agreed with the results of small laboratory vane tests.

Although theory (Hansen and Gibson, 1949; see also section 3.2.4) predicts that $C_{UFV} < C_{UTC}$ most case histories (except for clays of very low plasticity (Ladd, 1972)) reveal the reverse (Bjerrum, 1972), particularly close to the ground surface (Lo and Stermac, 1965). This has been shown to be partly because of the different times to failure associated with the two types of test, but mainly because of consolidation during the field vane test. $C_{UFV} < C_{UTC}$ was found when the results of large vane tests were used (the rate of strain in these tests being the same as for the standard (Geonor) vane tests and correction for strain rate being made to enable comparison with the laboratory data).

The results from the large vane tests, when corrected for anisotropy (after Bjerrum, 1973) and rate effect, as determined in the laboratory, produced a field undrained strength exactly corresponding to the value similarly derived from the laboratory. Reliable field undrained strengths based on large vane test results are thus as readily obtained as those from laboratory tests.

Finally $\phi_u = 0$ analyses should be carried out on unrestricted surfaces as originally intended by Skempton (1948(c)) if forward-analyses are not to be unsafe and back-analyses overconservative.

7.7.3. Effective Stress Analyses

The total stress method of analysis is often decried as unreliable (see e.g. Schmertmann, 1975) although this has been shown to be, at least partly, the

result of insufficient consideration of all the variables; C_u is, of course, not a soil parameter. However, although undrained analysis can adequately predict construction failure, the continuing stability of embankments post-construction is strictly speaking an effective stress problem, although a consolidated undrained approach has also been suggested. Whilst not significantly anisotropic, the effective stress shear strength parameters are strain rate dependent; however, reliable values for field use can be evaluated on the basis of laboratory tests.

The use of $c' = 0$ is often advocated (Parry 1971(a)) and adopted (Murray and Symons, 1974); this is considered to be an unrealistically conservative approach and should be superseded by the time dependent c' approach advocated herein. In the past $c' = 0$ has probably proved acceptable because combined with the higher ϕ' associated with the normally consolidated condition as a result of sample disturbance or testing at elevated effective stress levels.

The main problem with effective stress analyses is the difficulty of pore-pressure prediction; it is suggested that pore-pressure predictions be made and the stability monitored both during and after construction on the basis of observed pore pressures as suggested by Symons (1976(a)).

One only has to peruse the literature relevant to embankments on soft clay to realise the difficulty of predicting failure using effective stress methods even when observed pore pressures are available. The successful use of the effective stress method in conjunction with stability charts (Cook and Ingold, 1973; Lewis et al 1975; Symons 1976(a)) is of course related to the non-failure condition for which 'actual' accuracies and safety factors are not generally known with any certainty.

CHAPTER 8

ANALYSIS OF BANK 1, STAGE 1 USING THE FINITE ELEMENT METHOD

8.1. Introduction

As outlined in section 6.1.3., wherein the total stress predictions from the finite element analyses were utilised for pore-pressure prediction purposes, the analyses performed were intended to assess the influence of the major variables, rather than obtain a perfect fit to the observations. Only three complete solutions were obtained, each solution comprising construction of the embankment in eight stages, one stage being the excavation of the toe trench. The data presented and discussed herein thus only represent a preliminary back-analysis of the embankment's performance using the finite element method; however, sufficient work has been done to permit significant conclusions to be drawn and to detail the changes necessary in the analysis to achieve good overall agreement with the field observations.

8.2. Method of Analysis

8.2.1. The Finite Element Method

The finite element method is well documented in the literature (Desai and Abell, 1972; Zienkiewicz, 1977) and details of the method will not be discussed herein. The computer program used was a version of Finite Element System Swansea, modified by Dr. M.M.A.F. Hamza of Imperial College, University of London.

8.2.2. Type of Elements

The elements into which the continuum was divided were quadrilateral in shape: distortion of the elements was defined by a quadratic shape function and numerical integration of element volume was achieved with 2 x 2 Gauss integration points; such a combination has been shown (Pugh, 1973) to be both accurate and economical.

8.2.3. Constitutive Law

The relationship between stress and strain was defined by a non-linear isotropic elastic formulation, developed by Hamza (1976). Such formulations employ either a Young's Modulus (E) and Poisson's Ratio (ν) or a bulk modulus (K) and shear modulus (G). In the former case the Young's Modulus and, in the latter case, the shear modulus vary with stress or strain level; the remaining two parameters (ν and K) may also be stress or strain level dependent.

Hamza's (loc cit) technique is of the approximate step type employing a curve fitting technique, known as the 'Quasi Runge-Kutta One-Step Technique'; the non-linearity is expressed in terms of 'E' and a simple relationship allows the variation in 'E' to be defined as a function of stress level:-

$$E = E_i \frac{(1 - a.b.\sigma_r)}{(1 + a\sigma_r)} \dots\dots\dots(8.1)$$

$$\text{where } \sigma_r = \frac{(\sigma_1 - \sigma_3)}{(\sigma_1 - \sigma_3)_f} \dots\dots\dots(8.2)$$

and E_i is the initial value of 'E'.

The curve fitting technique is similar in principle to the tangent stiffness, or incremental, approach but generally gives a better* fit to the nominated stress-strain law (Hamza, 1976). In brief, from a particular starting stress the appropriate 'E' is used as the basis for a complete solution of the load increment; this is the pilot solution, being equivalent to the tangent stiffness solution. A new value of 'E' is then evaluated for the stress level mid-way between the starting stress level and the final stress level indicated by the pilot solution, to give the final solution for the load increment.

If at the starting stress, $\sigma_r > 0.95$ a nominal (very small) 'E' is assigned; and, if the pilot stress is such that $\sigma_r > 1$ the stress increment is successively sub-divided until $\sigma_r < 1$ and 'E' is then assigned accordingly.

8.3. Analysis of Bank 1, Stage 1

8.3.1. Discretisation of the Continuum

The finite element mesh is depicted in figure 8.3; reference to figure 4.6 indicates that the construction sequence was exactly simulated above a fill height of 2.25m, being approximated by two lifts up to that level. The vertical boundaries to the foundation were placed at distances from the embankment at which the field observations indicated there were no significant displacements during construction. The lower boundary to the foundation was located such that one row of well formed elements could be included to model the gravel stratum underlying the clay.

*increasing divergence from the stress-strain law is unavoidable with approximate step techniques; in general 'the smaller the step, the better the fit'.

It was decided, in view of the consolidation observed to have taken place during the early part of construction, to compare horizontal displacements in order to assess the adequacy of the finite element solutions. Thus both the inclinometer and H.S.G. locations were made coincident with element boundaries. As discussed in section 6.1.3. it was not considered worthwhile arranging the elements to achieve coincidence of the Gauss points (at which the stresses are considered to be most reliable) and the piezometers. In view of the fluctuations in total stress observed between Gauss point positions within individual elements, this decision appears to have been justified.

Finally, the mesh was designed to divide the clay foundation into the same zones as those used for the stability analysis, thus including a separate zone for the peat/lower clay layer. A total of 176, 8-noded, elements were used, being generally well formed although the aspect ratio (longest side/shortest side) increased to approximately 6 towards the lateral boundaries. The latter were fully restrained horizontally but free to move vertically whilst the lower boundary of the mesh was assumed completely fixed. A separate computer program was used to check the element/nodal data by plotting out the mesh; this program was also written by Dr. Hamza (see Hamza, 1976).

8.3.2. Soil Properties

(i) The Mucking Clay

The finite element solution for the displacements and stresses within the clay foundation was carried out entirely in terms of total stress; undrained shear strength and deformation characteristics were thus appropriate and a $\nu = 0.4999$ assigned. The laboratory undrained shear strength parameters

were discussed in section 2.7.5. (and further elaborated upon in section 7.2) and the corresponding deformation parameters in section 2.8.

Based on the observations discussed in section 2.8. average (normalised) stress-strain curves were prepared for each test level from the unconsolidated undrained triaxial compression test data. Separate curves were prepared for the vertical, 45° inclined and horizontal specimens, although each set of three curves had more or less common values of E_{u50} . From the three averaged curves for each depth a single normalised curve was prepared; this enabled a plot of E_{u50} versus elevation to be prepared. The latter exhibited no significant trend and a mean E_{u50} of 2700 kN/m^2 was selected for design purposes. In addition values of ϵ_A and σ_D (deviator stress) were plotted versus elevation, the values corresponding to σ_r values of 50, 70, 90, 95 and 100%. These relationships were consistent, being similarly shaped to the undrained strength/depth profile, in that for any particular stress level the values of deviator stress and axial strain increased above and below minimum values corresponding approximately to O.D. level.

It was thus possible to 'construct' a normalised stress-strain curve, and thus E/σ_r relationship, for each zone of the foundation and to derive the curve fitting constants 'a' and 'b' (equation 8.1). These were found not to vary significantly and were thus averaged for the whole of the clay foundation. In addition two constants were derived to define the linear increase in C_u above and below the minimum value at O.D. level. The value of 'E' at any elevation within the clay foundation was thus defined by one value of E_{u50} , one value of C_u (minimum), two curve fitting constants and two

constants defining the C_u /depth relationship. Using these data the average stress-strain curve for each zone was generated and compared to the 'constructed' normalised curve:

Now the constants 'a' and 'b' were derived by defining $E_i = E_{u50}$ and fitting the design stress-strain curve at $\sigma_r = 70\%$ and 100% . When the generated curves were compared to the design curves an exact fit was found up to $\sigma_r = 70\%$ and at $\sigma_r = 100\%$ in all cases, but also in all cases in the range $\sigma_r = 70 - 100\%$ the generated curves consistently underpredicted the strains, maximum errors occurring in the range $\sigma_r = 85 - 95\%$. However these errors were not considered significant and the derived data were used for initial analysis purposes.

As will be discussed further in subsequent sections the use of the previously described data in conjunction with a finite element analysis (denoted F.E.1) indicated that the embankment was stable at a fill height of 4m; the calculated maximum shear stresses in the foundation only occasionally equaling the undrained shear strength. This analysis (F.E.1) therefore confirmed the results of the limit equilibrium analyses that the laboratory design undrained strength profile without a rate effect correction (TS-LD-1) was an over-estimate of the field undrained strength, even though there had been significant consolidation of the foundation.

At the time this analysis was being performed the limit equilibrium analyses had already been completed and it was thus decided to incorporate the back-calculated undrained strength/depth profile (TS-2-0; figure 7.5.1) in the remaining finite element analyses (F.E.2 and F.E.3); unlike the initial analysis (F.E.1) these latter analyses thus included a stronger desiccated

layer. The new design stress-strain curves were simply obtained by scaling down the stresses assuming the relationship between σ_r and ϵ_A , derived initially, to still apply; E_{u50} was not changed. New values of the other five constants were derived and the generated stress-strain curves compared to the design curves; similar comments applied in this case to those made in respect of the data for F.E.1.

In view of the findings reported in Chapters 6 and 7 no attempt was made to separately model the parameters of the peat/lower clay layer.

(ii) The Gravel

The gravel was modelled as a linear elastic material having an $E' = 150,000 \text{ kN/m}^2$ (an arbitrary 50 times that of the clay) and a $\nu' = 0.25$.

(iii) The Sand Fill

The only laboratory data available on which to base a model for the fill were from one multi-stage consolidated drained triaxial test on a sand specimen compacted (at the placement water content) to the in-situ density; the consolidation pressures covered the effective stress range implied by the embankment loading.

On the basis of these data the fill was modelled as a linear elastic material with $E' = 85,000 \text{ kN/m}^2$ and $\nu' = 0.33$. Using the empirical relationship proposed by Parry (1971(d)) this figure suggests a medium dense sand, which is consistent with the observed placement bulk unit weight of 17.5 kN/m^3 .

During the finite element simulation of the embankment construction the layer being placed was treated as a dense liquid i.e. assigned a $\nu = 0.4999$,

a nominal $E = 5 \text{ kN/m}^2$ and the full bulk unit weight whilst the 'air' elements representing fill layers not yet placed were assigned $\nu' = 0.25$, $E' = 5 \text{ kN/m}^2$ and zero unit weight. Once placed each layer of fill was automatically assigned the design deformation parameters.

8.3.3. In-Situ Stresses

As discussed in section 6.1.3. σ_v was calculated directly from the bulk unit weights (figure 2.23) and σ_v' from the pore pressures recorded prior to construction (figures 2.12 and 6.1.18). The variation in σ_v' with depth was based on assumed, average, hydrostatic conditions relating to G.W.L. at 1m depth; no lateral variation in σ_v' at a particular depth was assumed.

As illustrated in figure 8.1., two extreme variations of K_0 were considered ($K_0 = 0.55$, F.E.1 and F.E.2; $K_0 = f(\text{depth})$, F.E.3), whereas, as discussed in section 6.1.3., the true distribution of K_0 with depth probably lay between the limits 'a' and 'b' defined in figure 2.13, and varied from one vertical section to another across the embankment site.

8.4. Results of Analyses

8.4.1. Comparison of Predicted and Observed Displacements

Figure 8.2. illustrates predicted and observed displacements at various locations within the foundation; these locations are on the inclinometer casing profiles and encompass the complete range of principal stress rotations encountered to the south of the embankment centre line (see figures 6.1.41 and 6.1.43) as well as the variations in the assumed K_0 distributions (figures 2.13 and 8.1).

As noted in Chapter 5 (table 5.12.1) the horizontal displacement observations recorded with the inclinometers were considered accurate to within $\pm 10\%$ of the actual displacements (see section 5.4). However, the differences in the horizontal displacements recorded at Sections A and B (see figures 5.3.2. and 5.3.3; and 5.4.2. to 5.4.7) should also be borne in mind when assessing the results of the F.E. analyses.

The influence of K_0 on the shear strength reserve of the foundation was briefly discussed in section 2.5. The two distributions of K_0 with depth incorporated in the analyses result in markedly different stress paths for the upper part of the foundation (see figures 6.1.40 and 6.1.42). In the constant K_0 ($= 0.55$) case, active loading beneath the embankment results in shear loading throughout construction, with little rotation of the principal stress axes, whereas beyond the toe the passive loading results in stress paths which are, initially, shear unloading paths, accompanied by large rotations of the principal stress axes (see figures 6.1.40 and 6.1.41).

In contrast the variable K_0 distribution (figure 8.1) results in initial shear unloading beneath the embankment, accompanied by large rotations of the principal stress axes; beyond the toe the reverse is true (see figures 6.1.42 and 6.1.43). The influence of these different initial stress states upon the predicted horizontal displacements is depicted in figure 8.2., but before discussing these data further some additional background information on the F.E. analyses is required.

All three F.E. analyses over-predicted the horizontal displacements at 1.25m fill height, by between 4mm (minimum - IA3 at +0.75m OD) and 26mm

(maximum - IA2 at +0.75m OD). Thereafter, in all three analyses performed the predicted fill height/horizontal displacement relationship then 'stiffened' and continued near parallel to the observed relationship. Now an increase in foundation stiffness could only occur, using the model adopted, if shear unloading were to occur from a value of σ_r in excess of 50%. In all of the analyses performed the major part of the foundation was initially operating on the linear part of the stress-strain curve and thus a constant, or decreasing 'E', applied during the early stages of construction.

Although no parametric studies were performed, it is considered that the initial over-prediction was the result of the 'dense liquid' analogy incorporated in the computer program to simulate the placement of the first construction lift, comprising 1.25m of fill. In the field it took some 11 days, and several lifts, to reach this stage of construction and the fill's presence doubtless restricted the horizontal displacements of the foundation from the start of construction. Thus although the computer simulation of the construction process appeared adequate for the remainder of the lifts it would seem entirely inappropriate for the first layer, particularly as the initial stages of construction were approximated by one fairly thick layer of fill.

It was thus decided to link the observed displacements to those predicted at 1.25m fill height, as shown in figure 8.2; this enabled a more realistic appraisal of the F.E. predictions. The initial analysis (FE1) predicted linear fill height/horizontal displacement relationships at all fill heights and locations and these results have been omitted from figure 8.2. for the sake of clarity. However, they may be readily envisaged as straight line extrapolations of the data for analysis FE2 from 1.25 to 2.75m fill height.

Overall impressions of the data from analyses FE2 and FE3, as presented in figure 8.2., may be summarised as follows:-

(i) the horizontal displacements are not overly sensitive to K_0 ; the higher values of K_0 within the upper part of the foundation (analysis FE3) generally resulting in less non-linearity, as a result of lower stress levels, and therefore smaller predicted horizontal displacements. As in the case of the pore-pressure predictions (section 6.1.3) the use of K_0 values derived (using the data of Brooker and Ireland, 1965) from the O.C.R.s pertaining to the start of construction (see figure 2.13) would have resulted in predictions somewhere between the two extremes considered. However, when considering the influence of K_0 on the predicted displacements, it should be remembered that only a single stress-strain curve was used to derive the relevant value of 'E'; there being no distinction made between shear loading and shear unloading or between compression and extension loading.

(ii) for fill heights up to 3.25m (at which point a F.o.S. of about 1.25 would apply) the observed and predicted displacements are in good agreement.

(iii) where significant non-linearity of the observed fill height/horizontal displacement relationships occurred, probably as a result of local failure (section 6.4), the F.E. model increasingly under-predicts the displacements.

Looking at the data in more detail, the following points are also evident:-

(i) at locations where there was little rotation of the principal stress axes (see figures 6.1.41 and 6.1.43) and the increase in maximum shear stress was dominated by increasing vertical stress (i.e. $+\Delta\sigma_v$; e.g. at IA2 and IA3; - 1m O.D. and - 3m O.D.) the model consistently *over*-predicted the displacements during the early part of construction when E_i largely controlled the soil's stiffness. It will be remembered (section 2.8) that the initial undrained

modulus measured in undrained triaxial compression tests on specimens consolidated (anisotropically) to the estimated in-situ stresses was about twice that for specimens which were isotropically consolidated. The F.E. model was of course based on unconsolidated undrained test data.

(ii) at locations where the increase in maximum shear stress was principally the result of increasing horizontal stress (i.e. $+\Delta\sigma_H$; e.g. at inclinometer IA1; + 0.75m HD and -1m HD), being accompanied by generally large rotations of the principal stress axes (see figures 6.1.41 and 6.1.43) excellent agreement between the model and the full scale behaviour was in evidence during the early stages of construction, again with E_i dominant in the determination of stiffness. In the case of extension tests the laboratory moduli (section 2.8) were not significantly influenced by the form of consolidation.

(iii) the model correctly predicted the onset of non-linearity during the early stages of construction and the development of major non-linearity at fill heights in excess of 2.75m (see figures 6.1.3. to 6.1.6; also section 6.1.1.).

(iv) in the majority of cases the model predictions of the horizontal displacements caused by the excavation of the central trench were excellent. Where under-predictions are in evidence, as e.g. IA2 at + 0.75m HD and - 1m HD the full scale displacements were strongly influenced by creep movements, as indeed were all of the displacements at higher stress levels (again see figures 6.1.3 to 6.1.6).

(v) under-prediction of non-linearity as failure was approached; now the F.E. stress-strain curves at stress levels in excess of 70% ($=\sigma_r$) have been seen (section 8.3.2.) to have been too steep, and this would therefore appear to be of some importance. Over-estimation of modulus

values at high stress levels is a problem associated with the particular algorithm used (equation 8.1) and has been observed elsewhere (Hamza, 1976). In order to overcome this problem it may be necessary to obtain a good fit to the stress-strain curve in the region $\sigma_r = 75\%$ to 95% at the expense of over-estimating the failure strain.

8.4.2. Predicted States of Stress Within the Foundation

As discussed in the preceding section, K_0 exerts a major influence on the value of σ_r at a particular location and stage of construction. The pattern of elements which had failed (being defined as $\sigma_r > 95\%$) in the F.E. analysis at 4m fill height is compared in figure 8.3. for the two K_0 profiles adopted. As anticipated, the adoption of higher K_0 values within the upper part of the foundation reduced the total number of failed elements and also gave the failure zone the more asymmetrical appearance associated with failure of the southern side of the embankment. Also superimposed onto the cross-sections is the critical failure surface and the average direction of the major principal stress for those elements through which the surface passes. In both cases the elements along the surface which had not reached failure in the analyses had values of σ_r in excess of 85% .

The development of local failure in the finite element model is depicted in figures 6.1.35 and 6.1.36; failure commenced in the area beneath the embankment shoulder and spread outwards in much the same way as was observed in the field (see sections 6.1., 6.2 and 6.4). As mentioned above, the variable K_0 profile delayed the onset of local failure, but spread it further outwards beyond the toe. The F.E. analyses thus clearly indicate that any change in behaviour associated with local failure could only have been observed towards the end of construction; and that yielding of the foundation is an entirely separate phenomenon.

In section 6.1.3. it was seen that the predicted total stresses agreed well with the observed pore pressures until local failure occurred. The model used results in a situation of contained plastic flow and it was evident that as failure occurred beneath the embankment, shear load was shed onto areas beyond the toe. This shedding of shear load was also accompanied by a proportionate lessening of the total stress carried by the failed elements and an increase in that carried by the unfailed elements; at the same time the field pore pressures exhibited an increased rate of generation. That the F.E. model behaviour is reasonably realistic is indicated by the good general agreement between the end points of the 'field' effective stress paths constructed (figures 6.1.40 and 6.1.42) and the failure envelope back-analysed using limit equilibrium methods (see figure 6.1.44).

The 'field' stress paths have already been discussed in sections 6.1.3 and 6.3; the different K_0 assumptions were seen to radically alter both the total and effective paths followed by the foundation, in particular the upper part, during construction.

Thus with $K_0 > 1$ near to O.G.L. the E.S.P. s for piezometers 1, 2, 4 and 5 became shear loading paths as opposed to shear unloading when K_0 was put equal to 0.55 throughout. In general the variable K_0 profile appears to provide a more consistent pattern of E.S.P. s; however, reference to figures 6.1.40 and 6.1.42 reveals just how sensitive the E.S.P. s are to the pore-pressure observations particularly where the absolute values of pore pressure are small, and therefore (see section 5.5) least reliable.

It is also of interest to note that the T.S.P. s clearly depict shear unloading to have taken place beneath the vicinity of the rear berm in the interval following its formation. This, it will be remembered, was predicted in section 6.1.1., on the basis of the observed increase in stiffness in the fill height/horizontal displacement relationships. However, this increase in stiffness would not be predicted by the F.E. model used because of the absence of an unload/reload modulus.

The rotations of the axes of principal stress associated with the various stress paths, were presented in figures 6.1.41 and 6.1.43. In general there is little difference in the results of the two analyses with the obvious exceptions of those locations at which the initial stresses were rotated through ninety degrees. Both K_0 assumptions confirm the field observations (figure 6.1.16; section 6.1.2) that, near surface beneath the embankment, the principal axes rotated in the opposite direction to that anticipated, as a result of the stiffness of the crust.

8.5. Summary

It has been shown that the laboratory data from conventional triaxial tests on high quality samples provide reliable estimates of the full scale undrained deformation characteristics of the lightly overconsolidated Mucking clay. In order to make successful predictions of the behaviour of the main works embankments the following are recommended:-

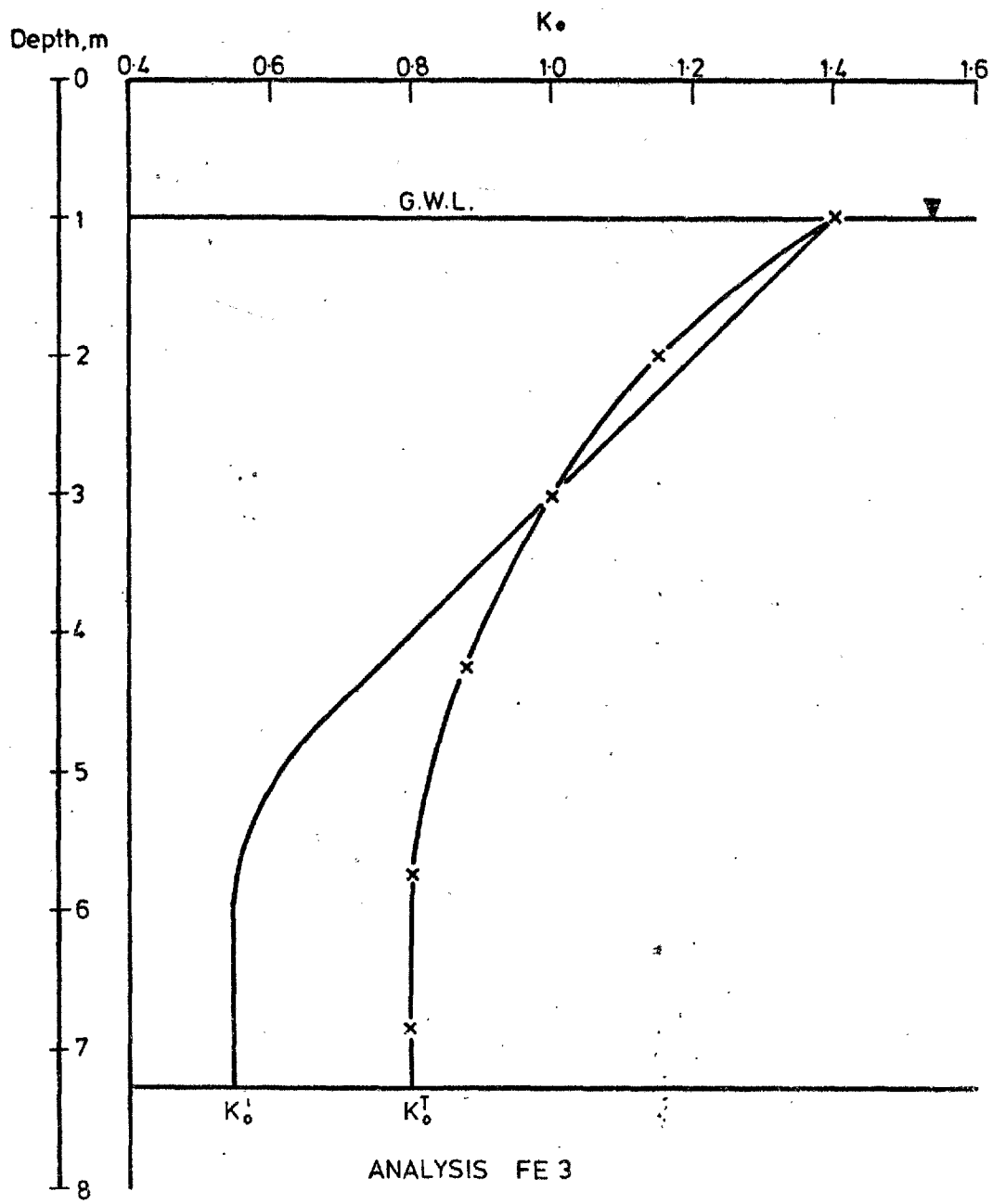
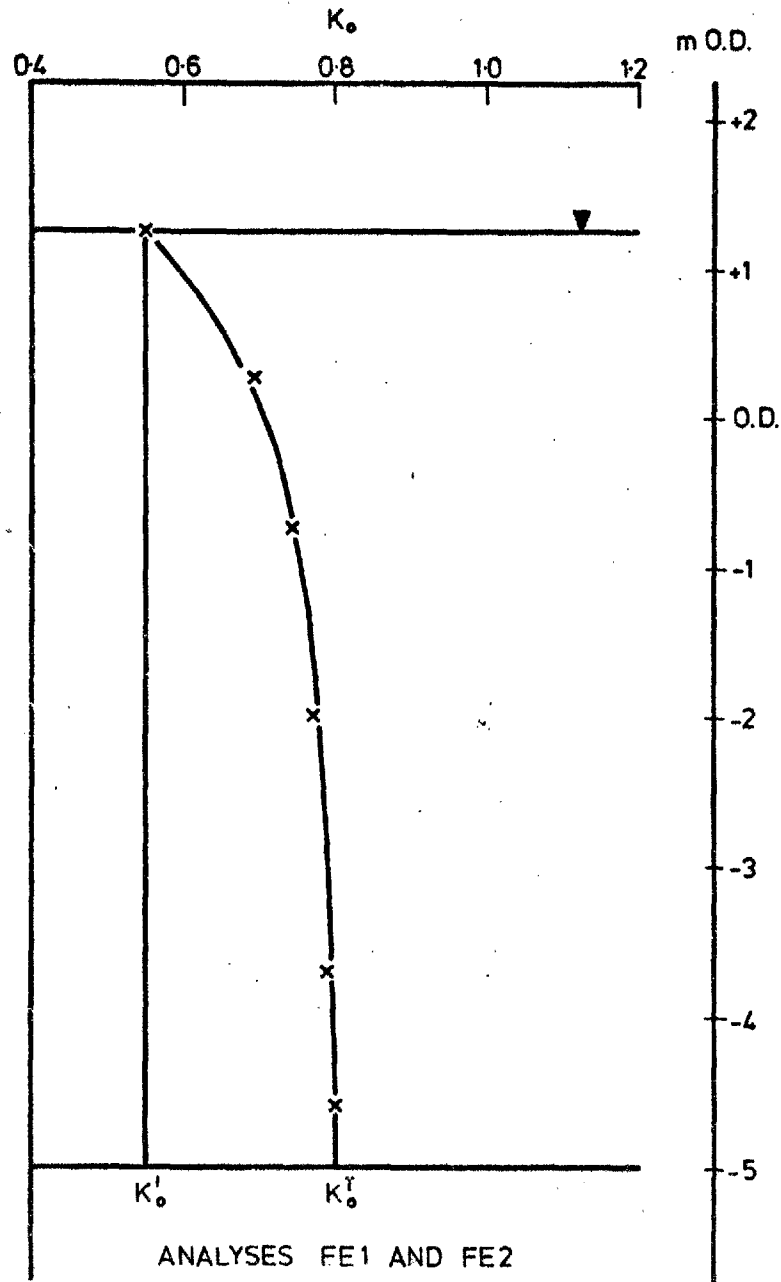
(i) K_0 values selected on the basis of O.C.R. at each location within the foundation, using the data of Brooker and Ireland (1965) - see also Ladd and Foott (1977).

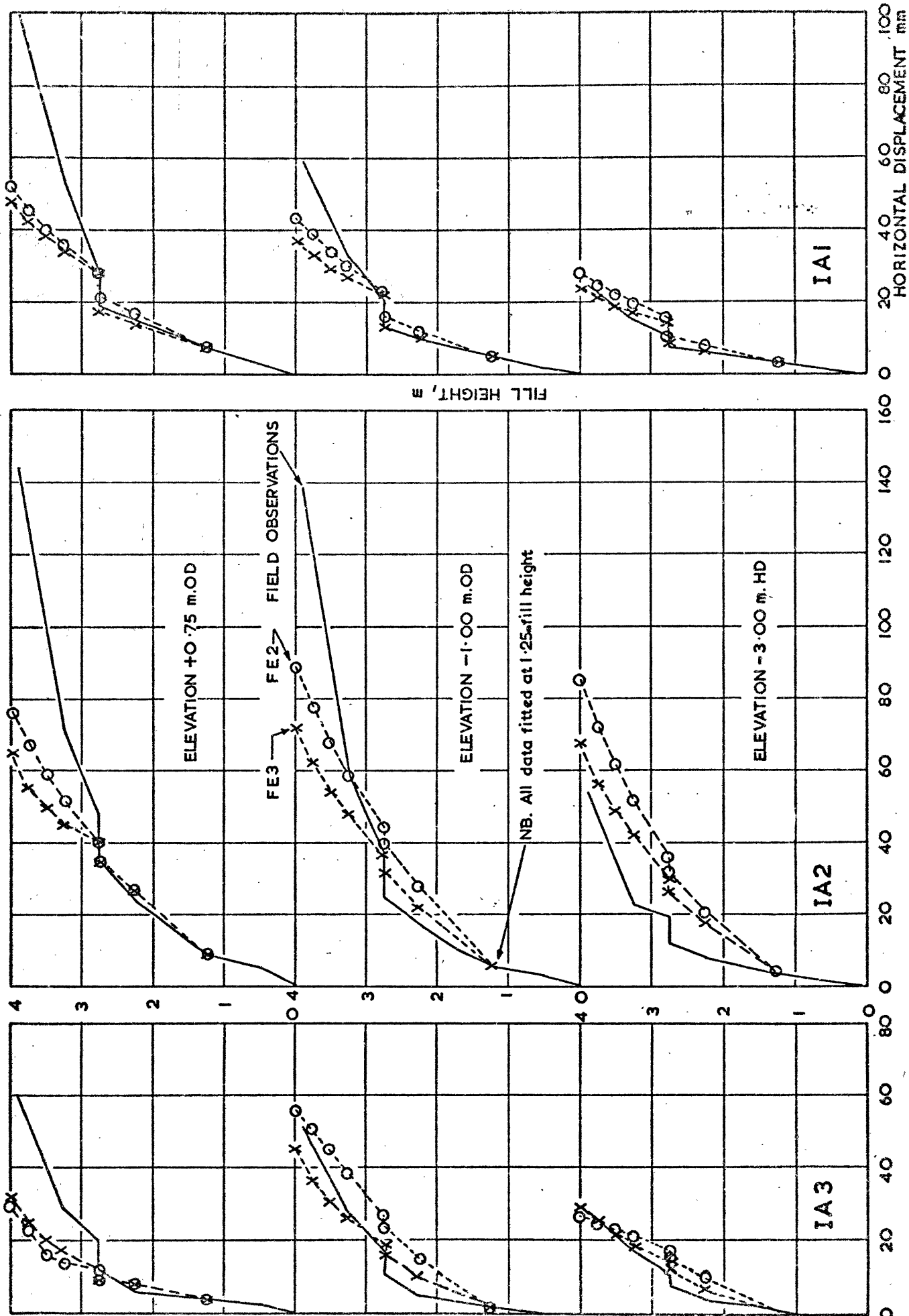
- (ii) undrained strengths evaluated from the laboratory data as outlined in Chapter 7.
- (iii) normalised stress-strain curves derived as outlined previously, but with different values of E_i for shear loading and shear unloading from the initial stress state.
- (iv) particular attention to be paid to the correct simulation, by the computer model, of the stress-strain curves in the range $\sigma_r = 75\%$ to 95% .
- (v) use of a separate unload/reload modulus for shear unloading following initial shear loading.
- (vi) placement of an initial, very thin, layer of fill as a 'dense liquid' or assignment of full stiffness to the initial layer of fill during placement.
- (vii) assignment of correct stress-strain properties to the fill materials.

Finally, the relatively good agreement between the results of the limit equilibrium and F.E. analyses is very encouraging. For main works construction both F.E. and limit equilibrium analyses should be considered for design purposes. Predicted effective stress paths and stability in terms of effective stress could be amended at instrumented cross-sections on the basis of observed pore pressures and used to control construction. Likewise predicted horizontal displacements and strains, plotted as recommended in section 6.4, could be used as a basis for a complementary approach to construction control; these predictions would be very useful in the prediction of local failure and thus concentrating field observations onto the particularly critical stage of construction.

K₀ DISTRIBUTIONS USED IN FINITE ELEMENT ANALYSES

BANK 1, STAGE 1

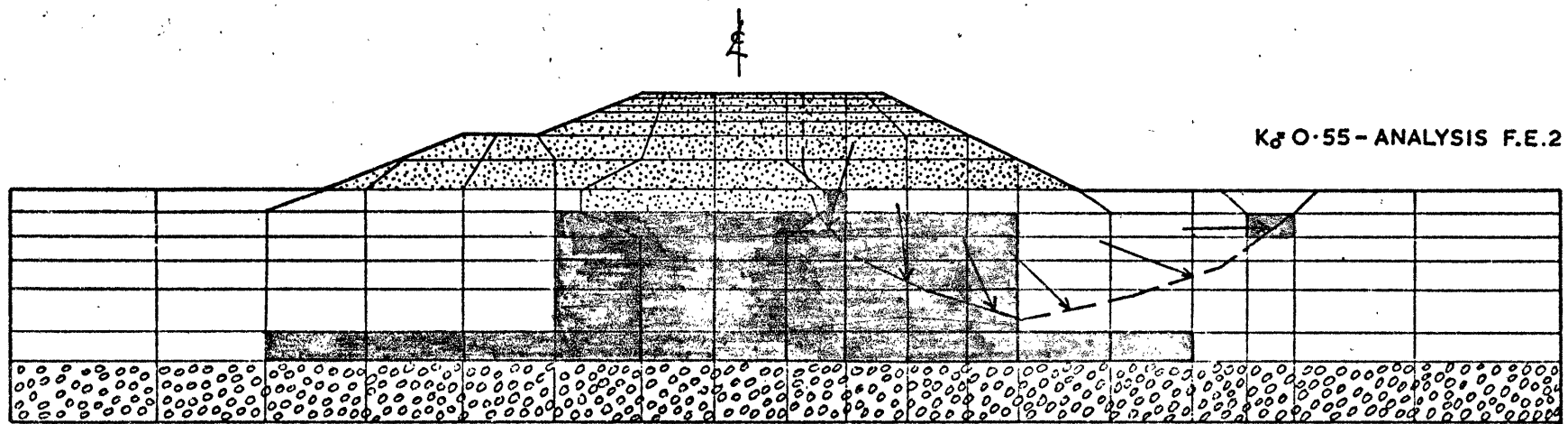




BANK I, STAGE I


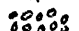
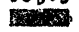
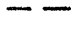
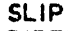
COMPARISON OF OBSERVED AND PREDICTED HORIZONTAL DISPLACEMENTS

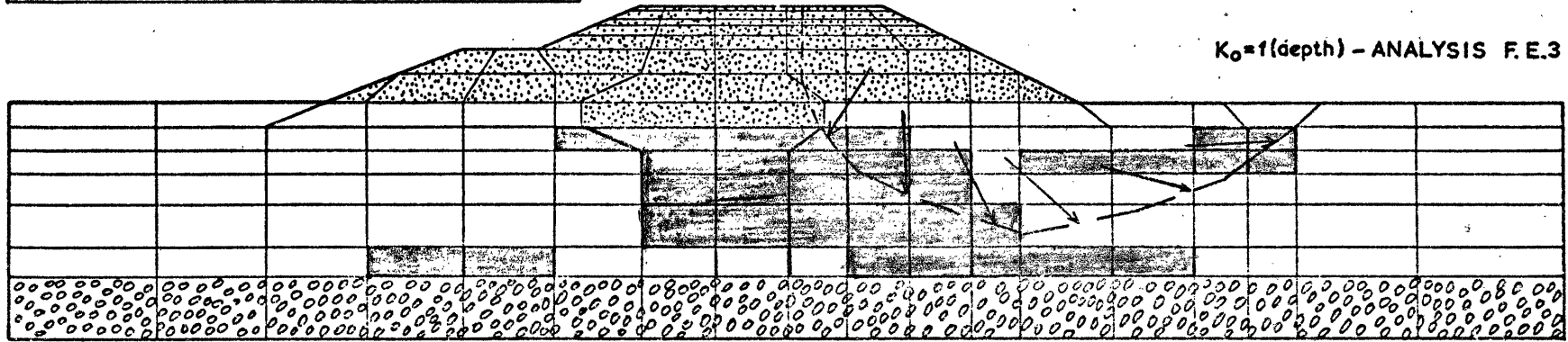
Fig. 8.2



$K_0 = 0.55$ - ANALYSIS F.E.2

LEGEND

-  SAND
-  GRAVEL
-  FAILED ELEMENTS
-  SLIP SURFACE SE2/I
-  DIRECTION OF MAJOR PRINCIPAL STRESS



$K_0 = 1(\text{depth})$ - ANALYSIS F.E.3

BANK I, STAGE I
FINITE ELEMENT MESH AND DISTRIBUTION OF FAILED ELEMENTS

Fig. 8.3

CHAPTER 9

CONCLUSIONS

The problems associated with the construction of the Thames Tidal Defences have been reviewed and seen to be largely a function of the marsh clay foundation, this being a very soft lightly overconsolidated organic silty clay of high plasticity, sensitivity and compressibility and of low permeability. The role of full scale field trials in the design process has been outlined and a detailed account of the construction and monitoring of the trial embankments at Mucking has been given. In this chapter only the main conclusions relating to the behaviour of the foundation material are reiterated. Detailed conclusions have been drawn in the body of the text whilst for comments on the performance of the instrumentation and the quality of the data obtained reference should be made to Volume 2 (Chapters 3 and 4). The data presented therein obviously comprise the major part of this work and form the basis for all of the major conclusions reached.

The Mucking clay was found to be typical in many ways of the marsh clay as a whole, being a very soft lightly overconsolidated silty clay; the organic content, however, was generally low and confined to a system of vertical root holes which constituted the major feature of the soil's fabric. Plasticity index (40 - 70), clay fraction (30% - 60%), liquidity index (0.1 - 1.0) and sensitivity (1 - 9) all varied with depth. The top one metre or so of the clay was firm and desiccated and also contained the highest proportion of organic matter. Pre-existing shear surfaces were also found within the upper 2m or so of the clay layer.

The light overconsolidation of the deposit appears to be the result of a combination of a previously lower G.W.L. and secondary consolidation. This overconsolidation, coupled with the soil's fabric, has resulted in high C_v values (circa $100 \text{ m}^2/\text{year}$) at in-situ (pre-yield) effective stresses; these high C_v values in turn result in the significant changes in pore pressure observed in the field over a complete seasonal cycle, with consequent changes in O.C.R. and K_0 , and the rapid dissipation of the pre-yield excess pore pressures observed during the initial stages of embankment construction.

Laboratory tests on good quality samples correctly predicted the order of the in-situ C_v values but much lower values were obtained from laboratory tests on conventional piston samples. However, both types of sample yielded essentially similar M_v and p_c' values; these laboratory M_v values together with field 'k' values from C.H.T.s (at pre-yield effective stresses) were also used to calculate C_v values in good agreement with those back-calculated from observations of the full scale trials.

The laboratory tests also revealed k_v to be approximately twice k_H , the field data from C.H.T.s and the full scale foundation trials being compatible with this observation. At in-situ (sub- p_c') stress levels the soil stiffness (measured in oedometer tests) in the vertical direction was found to be twice that in the horizontal direction, as was the drained value of 'E' (measured in T.C. tests). This anisotropic stiffness of the soil skeleton gradually disappeared when laboratory specimens were consolidated isotropically to stresses in excess of p_c' .

Considerable reduction in C_v with increasing effective stress was evident from the laboratory test data, as was a considerable increase in M_v at effective stresses in excess of p_c' . Similar behaviour was observed in the field although the yield point, defining a marked change in the permeability/compressibility characteristics, was observed to correspond to a vertical effective stress (beneath the embankment centre) significantly less than p_c' , the actual value depending upon the O.C.R. at the start of construction. However, the maximum vertical effective stresses reached on the 'field' effective stress paths for elements beneath the embankment centre were observed to be similar to the laboratory values of p_c' .

Post-yield, the laboratory M_v values appear to underestimate the field values (although pre-yield values appear reliable) unless the laboratory tests were of sufficient duration to allow secondary consolidation to take place; M_v values from such tests, combined with field 'k' values from C.H.T.s (at post-yield effective stresses) produced good estimates of the post-yield field C_v values under full scale loading conditions.

Yielding of the foundation in the full scale trials was indicated by an increased excess pore-pressure response (the more dramatic because of the associated reduction in the rate of dissipation) and an increase in the vertical displacements per unit of fill height. No marked change in the horizontal displacement response pattern was discernible. In general, pre-yield displacements and strains were small and the pore pressures probably similar to those predicted by elastic theory. The combination of a high value of ν and a thin compressible layer resulted in relatively large changes in octahedral normal stress and relatively small changes in octahedral shear stress; thus conventionally predicted pore pressures were largely dependent on the former. Further increases in the rate of response of excess pore pressure, displacement and strain to the applied

loading were observed to accompany local failure and methods of controlling construction on the basis of these increases were proposed.

Laboratory measurements of the undrained deformation characteristics resulted in considerable scatter and thus some difficulty in interpretation. In general, E^T appeared to be dependent on p_c' , there being relatively little increase in E_{U50} with increasing consolidation pressure over the greater part of the sub- p_c' range, and similar values were obtained under triaxial and plane strain testing conditions. However, the initial E^T of anisotropically consolidated specimens in T.C. tests was significantly greater than values obtained from T.E. tests and from tests on isotropically consolidated specimens. In addition at small strains E^T was less for horizontal than for vertical specimens.

However, E_{U50} values were essentially similar for all conditions of consolidation and specimen orientation and were used as a basis for non-linear finite element analyses. These showed that the field E^T was indeed greater when the soil was subjected to shear loading from K_0 conditions although, overall, the F.E.M. predictions at low stress levels were satisfactory. The importance of using the correct K_0 to predict the initial stresses and of correctly modelling the stress-strain function at high stress levels was evident from the results of the analyses.

The laboratory study of undrained shear strength clearly indicated that, given good quality samples, the most important factors to be considered in the use of T.C. test data to predict field C_u values under plane strain loading conditions were anisotropy, strain rate (i.e. time to failure) and progressive failure. Little difference was observed between undrained strengths measured in T.C. and P.S.A. tests on specimens cut at the same

inclination, or between those for specimens tested unconsolidated, isotropically consolidated or anisotropically consolidated. The latter observation was seen to be the result of the strong dependency of C_u upon p_c' for effective stresses in the overconsolidated range. Thus the undrained strength was much less affected by the effective stresses prior to testing than the undrained modulus; however, significantly lower undrained strengths were measured in T.C. tests on specimens from conventional piston samples. No sample size effects were observed.

Back-analysis of the full scale failures using limit equilibrium methods in terms of total stress showed that the field shear strength could be predicted using the laboratory T.C. test data on a consolidated undrained basis i.e. making allowance for the increase in undrained strength achieved as a result of the increase in effective stress during the early (pre-yield) part of construction. The increase in vertical effective stress approximated to $p_c' - p_o'$. Thus values of C_{UV} from quick T.C. tests factored according to the inclination of the critical rupture surface, and reduced to allow for the increase in t_f in the field, yielded a F.o.S. close to one in the analyses. The effect of undrained strength anisotropy on the critical $\phi_u = 0$ rupture surface could also be approximated by the use of an average C_u from the results of T.C. tests on vertical, 45 degree inclined and horizontal specimens. An average C_u from T.C. and T.E. tests did not approximate to the observed effects of anisotropy; in addition these tests were shown to yield different C_u values even for an isotropic elastic soil. Progressive failure appeared to have little influence on the peak undrained shear strength mobilised during first-time field failures.

A review of the vane test and the uncertainties associated with the interpretation of the data therefrom, have been presented; in particular the importance of careful calibration of the apparatus was demonstrated. The field vane apparatus was seen to be generally unsuitable for the measurement of remoulded shear strengths.

Consolidation has been shown to have significantly influenced the results of the Geonor (small) vane tests, all of the vane test data being subject to the effects of anisotropy (including the direction of shear) and strain rate. A detailed study of undrained strength anisotropy in relation to the field vane test showed that, although the direction of shear is inappropriate to the full scale field situation, the undrained strength measured in a vertical vane test only required a small correction for anisotropy when applied to the critical $\phi_u = 0$ rupture surface. The C_u values from horizontal vane tests were seen to be directly relevant to such a surface.

The form of undrained strength anisotropy observed in the laboratory T.C. and P.S.A. tests has been seen to be compatible with the field vane test data, although the more commonly (and less logically) adopted approach of associating maximum and minimum undrained strengths with vertical and horizontal planes was also seen to be tenable.

The only truly undrained strengths measured in field vane tests were those obtained in quick tests ($t_f \approx 5$ minutes) using the large vane apparatus. The latter was designed specifically to investigate the influence of t_f in field vane tests. This influence was seen to encompass the effects of consolidation and strain rate.

The values of C_{uFV} from the large vane tests (at $t_f = 5$ minutes) were used to successfully predict the field undrained strength, allowances for the increase in C_u as a result of consolidation during the field trials, anisotropy and strain rate being made. The influence of strain rate (i.e. time to failure) on C_u as determined in the laboratory T.C. test, the FV test and by back-analysis of the full scale failures appears to be identical in each case.

The data obtained clearly showed that it is unreasonable to expect a single vane test correction factor (albeit a function of plasticity) to be applicable in all situations; strain rate investigations should form part of any study of undrained strength, be it in the field or the laboratory.

The critical surfaces predicted by the $\phi_u = 0$ analysis differed in location, although not greatly, from the observed failure surfaces as would be expected. Significantly higher (total stress) safety factors were associated with the observed failure surfaces, which are not relevant to the $\phi_u = 0$ Analysis; although an increasing number of case studies involving back-analysis of actual failure surfaces using the $\phi_u = 0$ Analysis was noted in the literature. Likewise undrained strength anisotropy should be linked to $\phi_u = 0$ planes (i.e. $\beta = 45^\circ$) and not failure planes (i.e. $\beta = 45^\circ + \phi'/2$).

The effective stress shear strength parameters were not significantly dependent on specimen inclination or stress system. The observed undrained strength anisotropy was thus largely a pore-pressure phenomenon resulting from the anisotropic stiffness of the soil skeleton. Anisotropic excess pore-pressure generation was seen to be relatively less significant in the field than in the laboratory because of the larger changes in octahedral normal stress associated with the former.

However, the laboratory effective stress parameters were strain rate dependent, this dependency being modelled, for analytical purposes, as a drop in c' with increasing t_f . Back-analysis of the full scale failures using limit equilibrium methods in terms of effective stress revealed that, if the laboratory c' was extrapolated, on the basis of t_f , to the field situation, the laboratory and field effective stress parameters were identical. These results confirmed that progressive failure had little influence on the peak shear strength mobilised by first-time field failures. Excellent agreement between the observed failure surfaces and the critical back-analysed surfaces was obtained.

The end points (i.e. at failure) of 'field' effective stress paths, constructed from total stresses obtained by finite element analyses and observed pore pressures, exhibited good general agreement with the effective stress failure envelope and with the predicted undrained strengths. The sensitivity of any form of effective stress analysis to the pore-pressure data was noted, the successful analyses reported herein being largely dependent on the high quality of the field observations.

A very different mode of embankment failure was observed when the desiccated surface layer was removed. With the crust excavated a tension crack developed over the full height of the embankment prior to limiting equilibrium being reached, failure commencing abruptly within a relatively narrow rupture zone. On the other hand, with the crust left in place tension cracks did not develop until limiting equilibrium had been reached, the failure building up slowly within a wide rupture zone. Rates of displacement were monitored during failure, revealing relatively rapid acceleration to peak velocities of about 40mm/minute followed by a deceleration period spanning several days.

Limit equilibrium analyses in terms of both total and effective stress were performed for the post-failure embankment profiles. In this case progressive failure was a possibility, the observed I_p being about 50% in terms of total stress and about 30% in terms of effective stress. A complete loss of c' accompanied by increased excess pore-pressure generation was suggested by the data; in addition the effect of continuing shear appears to have been an increase in ϕ' from the peak value of 25° in the overconsolidated state to the normally consolidated value of 35° .

Progressive failure may well be a significant factor in the assessment of the stability of reconstructed sections of embankments which fail during, or after, construction.

REFERENCES

The following abbreviations have been used throughout:-

A.C.S.M.F.E. Proceedings of the Asian Conference on Soil Mechanics and Foundation Engineering

A.N.C.S.M.F.E. Proceedings of the Australia-New Zealand Conference on Soil Mechanics and Foundation Engineering

A.N.C.G. Proceedings of the Australia-New Zealand Conference on Geomechanics

A.S.C.E. Proceedings/Transactions of the American Society of Civil Engineers

A.S.T.M. American Society for Testing and Materials

A.S.T.M.(1957) Symposium on Vane Shear Testing of Soils. Special Technical Publication No. 193

A.S.T.M.(1964) Procedures for Testing Soils. Committee D-18 on Soils and Rocks for Engineering Purposes

A.S.T.M.(1966) Vane Shear and Cone Penetration Resistance Testing of In-situ Soils. Special Technical Publication No. 399

Austin Conf.(1974) Proceedings of the A.S.C.E. Conference on Analysis and Design in Geotechnical Engineering. 2 Volumes. University of Texas, Austin, Texas (published, 1974)

Berkeley Conf.(1967) Proceedings of the A.S.C.E. Conference on Stability and Performance of Slopes and Embankments. University of California, Berkeley, California (published 1967)

B.G.S. Conf.(1969) Proceedings of the British Geotechnical Society Conference on In-situ Investigations in Soil and Rock (published 1970)

B.G.S. Symp.(1973) Proceedings of the British Geotechnical Society
Symposium on Field Instrumentation in Geotechnical Engineering
(published 1974)

B.G.S. Conf.(1975) Proceedings of the British Geotechnical Society
Conference on Settlement of Structures (published 1975)

Boulder Conf.(1960) Proceedings of the A.S.C.E. Research Conference
on Shear Strength of Cohesive Soils. University of Colorado, Boulder,
Colorado (published 1961)

B.R.E. C.P. Building Research Establishment. Current Paper

Brussels Conf.(1958) Proceedings of the Brussels Conference on Earth
Pressure Problems. 2 Volumes. (published 1958)

C.G.J. Canadian Geotechnical Journal

Cornell Conf.(1970) Proceedings of the A.S.C.E. Speciality Conference
on Lateral Stresses in the Ground and Design of Earth-Retaining
Structures. State-of-the-Art Volume. Cornell University, Ithaca, New York
(published 1970)

E.C.S.M.F.E. Proceedings of the European Conference on Soil Mechanics
and Foundation Engineering

Geot Geotechnique

I.C.E. Proceedings/Transactions of the Institution of Civil Engineers,
London

I.C.E. Conf.(1960) Proceedings of the I.C.E. Conference on Pore Pressure
and Suction in Soils (published 1961)

I.C.S.M.F.E. Proceedings of the International Conference on Soil
Mechanics and Foundation Engineering

J.S.M.F.E.D. Journal of the Soil Mechanics and Foundation Engineering Division (of A.S.C.E.)

J.G.E.D. Journal of the Geotechnical Engineering Division (of A.S.C.E.)

Oslo Conf.(1967) Proceedings of the Geotechnical Conference on the Shear Strength Properties of Natural Soils and Rocks. 2 Volumes. Oslo (published 1967)

N.S.F.Conf.(1953) Proceedings of the I.C.E. Conference on the North Sea Floods of 31 January/1 February 1953 (published 1954)

P.C.S.M.F.E. Proceedings of the Pan-American Conference on Soil Mechanics and Foundation Engineering

Purdue Conf. (1972) Proceedings of the A.S.C.E. Speciality Conference on Performance of Earth and Earth-Supported Structures. 3 Volumes. Purdue University, Lafayette, Indiana (published 1972)

Q.J.E.G. Quarterly Journal of Engineering Geology

Q.J.G.S. Quarterly Journal of the Geological Society of London

Raleigh Conf.(1975) Proceedings of the A.S.C.E. Conference on In-situ Measurement of Soil Properties. 2 Volumes. North Carolina State University, Raleigh, North Carolina (published 1975)

Roscoe Symp.(1971) Stress-Strain Behaviour of Soils. Proceedings of the Roscoe Memorial Symposium, Cambridge University. (published 1972)

T.R.R.L. L.R. Transport and Road Research Laboratory. Laboratory Report

Aas, G. (1965) A Study of the Effect of Vane Shape and Rate of Strain on the Measured Values of In-situ Shear Strength of Clays.

6th I.C.S.M.F.E., 1, 141-145

Aas, G. (1967) Vane Tests for Investigation of Anisotropy of Undrained Shear Strength of Clays.

Oslo Conf., 1, 3-8

Agarwal, K.B. (1967) The Influence of Size and Orientation of Sample on the Undrained Strength of London Clay

Ph.D. Thesis, Imperial College, University of London

Al-Dhahir, Z.A.R. (1967) Correlation Between Field and Laboratory Measurements on Earth Dams

Ph.D. Thesis, Imperial College, University of London

Al-Dhahir, Z.A.R., Kennard, M.F. and Morgenstern, N.R. (1969)

Observations of Pore Pressures Beneath the Ash Lagoon at Fiddler's Ferry Power Station

B.G.S. Conf., 265-276

American Society of Photogrammetry (1966) Manual of Photogrammetry

Andresen, A. and Bjerrum, L. (1957) Vane Testing in Norway

A.S.T.M.

Andresen, A. and Sollie, S. (1966) An Inspection Vane

A.S.T.M.

Apted, J.P. (1977) Some Effects of Weathering on Some Geotechnical Properties of London Clay

Ph.D. Thesis, Imperial College, University of London

Arthur, J.R.F. (1973) Principles of Measurement

B.G.S. Symp., 510-516

Ashkenazi, V. (1973) The Measurement of Spatial Deformations by
Geodetic Methods

B.G.S. Symp., 1-12

A.S.T.M. (1964) The In-Place Vane Shear Test

A.S.T.M.

Atkinson, J.H. (1973(a)) The Deformation of Undisturbed London Clay

Ph.D. Thesis, Imperial College, University of London

Atkinson, J.H. (1973(b)) Elasticity and Plasticity in Soils

Geot., 23, 4, 565-571

Bannister, A and Raymond, S. (1965) Surveying

Pitman

Bergdahl, U. and Broms, B.B. (1967) New Methods of Measuring In-situ

Settlements

A.S.C.E., J.S.M.F.E.D., 93, SM5, 51-57

Berre, T. and Bjerrum, L. (1973) Shear Strength of Normally Consolidated

Clays

8th I.C.S.M.F.E., 1.1, 39-49

Bishop, A.W. (1948) A New Sampling Tool for Use In Cohesionless Sands

Below Ground-Water Level

Geot., 1, 2, 125-131

Bishop, A.W. (1952) The Stability of Earth Dams

Ph.D. Thesis, Imperial College, University of London

Bishop, A. W. (1954) The Use of Pore-Pressure Coefficients in Practice

Geot., 4, 4, 148-152

Bishop, A.W. (1955) The Use of The Slip Circle in the Stability
Analysis of Slopes
Geot.,5, 1, 7-17

Bishop, A.W. (1958) Test Requirements for Measuring the Coefficient
of Earth Pressure at Rest
Brussels Conf., 1, 2-14

Bishop, A.W. (1966(a)) The Strength of Soils as Engineering Materials
Geot.,16, 2, 89-130

Bishop, A.W. (1966(b)) Soils and Soft Rocks as Engineering Materials
Inaugural Lecture, Imperial College, University of London

Bishop, A.W. (1967) Progressive Failure - With Special Reference
to the Mechanism Causing It.
Oslo Conf., 2, 142-150

Bishop, A.W. (1971(a)) Shear Strength Parameters for Undisturbed and
Remoulded Soil Specimens
Roscoe Symp., 3-58

Bishop, A.W. (1971(b)) The Influence of Progressive Failure on the
Choice of the Method of Stability Analysis
Geot., 21, 2, 168-172

Bishop, A.W. (1971(c)) Discussion
Roscoe Symp., 125-133

Bishop, A.W. and Al-Dhahir, Z.A.R. (1969) Some Comparisons Between
Laboratory Tests, In-situ Tests and Full Scale Performance, With
Special Reference to Permeability and Coefficient of Consolidation
B.G.S. Conf., 251-264

Bishop, A.W. and Bjerrum, L. (1960) The Relevance of the Triaxial Test to the Solution of Stability Problems
Boulder Conf., 437-501

Bishop, A.W., and Green, P.A. (1973) The Development and Uses of Trial Embankments
B.G.S. Symp., 13-37

Bishop, A.W. and Henkel, D. J. (1962) The Measurement of Soil Properties in the Triaxial Test
Arnold

Bishop, A.W. and Hight, D. W. (1977) The Value of Poisson's Ratio in Saturated Soils and Rocks Stressed Under Undrained Conditions
Geot., 27, 3, 369-384

Bishop, A.W., Kennard, M.F. and Penman, A.D.M. (1960) Pore-Pressure Observations at Selset Dam
I.C.E. Conf., 91-102

Bishop, A.W., Kennard, M.F. and Vaughan, P.R. (1964) Developments in the Measurement and Interpretation of Pore Pressure in Earth Dams
Trans. 8th Cong. Large Dams, 1, 47-69

Bishop, A.W. and Lovenbury, H.T. (1969) Creep Characteristics of Two Undisturbed Clays
7th I.C.S.M.F.E., 1, 29-39

Bishop, A.W., Vaughan, P.R. and Green, G.E. (1969) Pore-Pressure Measurements in the Field and in the Laboratory
7th I.C.S.M.F.E., 3, 427-444

Bishop, A.W., Webb, D.L. and Lewin, P.I. (1965) Undisturbed Samples of London Clay from the Ashford Common Shaft: Strength-Effective Stress Relationships.

Geot., 15, 1, 1-31

Bjerrum, L. (1954) Geotechnical Properties of Norwegian Marine Clays

Geot., 4, 2, 49-69

Bjerrum, L. (1961) The Effective Shear Strength Parameters of Sensitive Clays

5th I.C.S.M.F.E., 1, 23-28

Bjerrum, L. (1967) Engineering Geology of Norwegian Normally Consolidated Marine Clays as Related to Settlements of Buildings

Geot., 17, 2, 81-118

Bjerrum, L. (1971) Private Communication to Bishop 1971(a)

Bjerrum, L. (1972) Embankments on Soft Ground

Purdue Conf., 2, 1-54

Bjerrum, L. (1973) Problems of Soil Mechanics and Construction on Soft Clays and Structurally Unstable Soils (Collapsible, Expansive and Others)

8th I.C.S.M.F.E., 3, 111-159

Bjerrum, L. and Anderson, K.H., (1972) In-situ Measurements of Lateral Pressures in Clay

5th E.C.S.M.F.E., 1, 11-20

Bjerrum, L. and Kenney, T.C. (1967) Effect of Structure on the Shear Behaviour of Normally Consolidated Quick Clays

Oslo Conf., 2, 19-27

Bjerrum, L. and Kjaernsli, B. (1957) Analysis of the Stability of
Some Norwegian Natural Clay Slopes

Geot., 7, 1, 1-16

Bjerrum, L. and Landva, A. (1966) Direct Simple Shear Tests on a
Norwegian Quick Clay

Geot., 16, 1, 1-20

Bjerrum, L., Nash, J.K.T.L., Kennard, R.M. and Gibson, R.E. (1972)
Hydraulic Fracturing in Field Permeability Testing

Geot., 22, 2, 319-332

Bjerrum, L., Simons, N. and Torblaa, I. (1958) The Effect of Time
on the Shear Strength of A Soft Marine Clay

Brussels Conf., 1, 148-158

Bourges, F., Chiappa, J., Legrand, J. and Paute, J.L. (1969)

Etude de Tassement des Vases Supportant des Remblair

7th I.C.S.M.F.E., 2, 35-43

Bozuzuk, M. and Leonards, G.A. (1972) The Gloucester Test Fill

Purdue Conf., 1, 299-317

Bromham, S.B. (1971) The Measurement of Disturbance in Samples of
Soft Clay

4th A.C.S.M.F.E., 68-72

Bromhead, E.N. (1976) Private Communication

Bromwell, L.G., Ryan, C.R. and Toth W.E. (1971) Recording Inclinator
for Measuring Soil Movements

4th P.C.S.M.F.E., 2, 333-343

Brooker, E.W. (1965) Discussion of Lo and Stermac (1965)

C.G.J., 2, 3, 254-258

Brooker, E.W. and Ireland, H.O. (1965) Earth Pressures at Rest Related
to Stress History

C.G.J., 2, 1, 1-15

B.S.970 (1947) Wrought Steels, En Series

British Standards Institution

B.S.971 (1950) Commentary on British Standard Wrought Steels, En Series

British Standards Institution

B.S.4019 (1966) Specification for Rotary Core Drilling Equipment

Part 1 : Basic Equipment

British Standards Institution

Buri, P.B. (1978) Influence of Secondary Consolidation and Overconsolidation
on the Behaviour of a Soft Alluvial Clay

Ph.D. Thesis, Imperial College, University of London

Burland, J.B. (1969) Deformation of Soft Clay Beneath Loaded Areas

7th I.C.S.M.F.E., 1, 55-63

Burland, J.B. (1971) A Method of Estimating the Pore Pressures and
Displacements Beneath Embankments on Soft Natural Clay Deposits

Roscoe Symp., 505-536

Burland, J.B. (1973(a)) The Interpretation of Field Observations

B.G.S. Symp., 607-613

Burland, J.B. (1973(b)) Discussion

B.G.S. Symp., 569-570

Burland, J.B. (1975) Some Examples of the Influence of Field Measurements on Foundation Design and Construction

B.R.E. C.P. 11/77 (also Proceedings of the 6th Regional Conference for Africa on Soil Mechanics and Foundation Engineering, 2, 267-284)

Burland, J.B. and Moore, J.F.A. (1973) The Measurement of Ground Displacement Around Deep Excavations

B.G.S. Symp., 70-84

Burland, J.B., Moore, J.F.A. and Smith, P.D.K. (1972) A Simple and Precise Borehole Extensometer

Geot., 22, 1, 174-177

Burland, J.B. and Roscoe, K.H. (1969) Local Strains and Pore Pressures in a Normally Consolidated Clay Layer During One-Dimensional Consolidation
Geot., 19, 3, 335-356

Cadling, L. and Lindskog, G. (1957) Some Notes on Five Years Experience from Field Vane Tests in Sweden

A.S.T.M.

Cadling, L. and Odenstad, S. (1950) The Vane Borer
Proceedings Royal Swedish Geotechnical Institute, Publication No.2.

Carlson, L. (1948) Determination In-situ of the Shear Strength of Undisturbed Clay by Means of a Rotating Auger

2nd I.C.S.M.F.E., 1, 265-270

Carslaw, H.S. and Jaeger, J.C. (1959) Conduction of Heat in Solids

Clarendon Press

Casagrande, A. (1960) An Unsolved Problem of Embankment Stability on

Soft Ground

1st P.C.S.M.F.E., 2, 721-746

Casagrande, A. and Carrillo, N. (1944) Shear Failure of Anisotropic

Materials

Journal. Boston Society of Civil Engineers, 31, 74-87

Casagrande, A. and Wilson, S.D. (1951) Effect of Rate of Loading on

the Strength of Clays and Shales at Constant Water Content

Geot., 2, 3, 251-263

Cole, K.W. (1973) Discussion

B.G.S. Symp., 589-594

Cook, D.A. and Ingold, T.S. (1973) A Practical Method for Field Control

of Loading

B.G.S. Symp., 100-111

Cooling, L.F. and Marsland, A. (1953) Soil Mechanics Studies of the Sea

Defence Banks of Essex and Kent

N.S.F. Conf., 58-73

Cornforth, D.H. (1973) Performance Characteristics of the Slope

Indicator Series 200-B Inclinator

B.G.S. Symp., 126-135

Cox, J.B. (1967) A Review of the Vane Test

The Institution of Engineers, Australia. Civil Engineering Transactions,

CE9, 19-30

Cox, J.B. (1970) Shear Strength Characteristics of the Recent Marine Clays in South East Asia

Journal. South East Asia Society of Soil Engineering, 1, 1, 1-28

Cox, J.B. (1971) Engineering Characteristics of the Soils Along the Thon Buri-Pak Tho Highway, Thailand

4th A.C.S.M.F.E., 1, 249-255

Cox, J.B. (1975) Discussion of Dascal and Tournier (1975)

A.S.C.E., J.G.E.D., 101, GT11, 1173-1174

C.P.2001 (1957) British Standard Code of Practice- Site Investigations
British Standards Institution

Croce, A., Viggiani, C. and Calabresi, G. (1973) In-situ Investigation of Pore Pressures in Soft Clays

8th I.C.S.M.F.E., 2.2., 53-60

Dachler, R. (1936) Flow of Ground-Water

Springer

Daen, W.W. and Hilf, J.W. (1951) Implications of Pore Pressure in Design and Construction of Rolled Earth Dams

Trans. 4th Cong. Large Dams, 1, 259-270

Dallard, N.J. (1971) Design and Construction of Embankments on an Alluvial Plain

I.C.E., 49, 157-170

D'Appolonia, D.J., Lambe, T.W. and Poulos, H.G. (1971) Evaluation of Pore Pressures Beneath an Embankment

A.S.C.E., J.S.M.F.E.D., 97, SM6, 881-897

Dascal, O. and Tournier, J.P. (1975) Embankments on Soft and Sensitive Clay Foundation

A.S.C.E., J.G.E.D., 101, GT3, 297-314

Dascal, O., Tournier, J.P., Tavenas, F. and La Rochelle, P. (1972)

Failure of a Test Embankment on Soft Sensitive Clay

Purdue Conf., 1, 129-158

Davis, E.H. and Christian, J.T. (1971) Bearing Capacity of Anisotropic Cohesive Soil

A.S.C.E., J.S.M.F.E.D., 97, SM5, 753-769

Davis, E.H. and Poulos, H.G. (1967) Laboratory Investigations of the Effects of Sampling

The Institution of Engineers, Australia. Civil Engineering Transactions, CE9, 86-94

De Lory, F.A. and Lai, H. N. (1971) Variation in Undrained Shearing Strength by Semi-Confined Tests

C.G.J., 8, 4, 538-545

Denness, B. and Green, M.W. (1971) A New Technique of Vane Testing

Q.J.E.G., 4, 1, 75-85

Desai, C.S. and Abel, J.F. (1972) Introduction to the Finite Element Method Van Nostrand Reinhold

Duncan, J.M. (1967) Undrained Strength and Pore-Water Pressures in Anisotropic Clays

5th A.N.C.S.M.F.E., 68-71

Duncan, J.M. and Seed, H.B. (1966(a)) Strength Variation Along Failure Surfaces in Clay

A.S.C.E., J.S.M.F.E.D., 92, SM6, 81-104

Duncan, J.M. and Seed, H.B. (1966(b)) Anisotropy and Stress Reorientation
in Clay

A.S.C.E., J.S.M.F.E.D., 92, SM5, 21-50

Dunnicliff, C.J. (1971) Equipment for Field Deformation Measurements

4th P.C.S.M.F.E., 2, 319-332

Eden, D.J. and Hamilton, J.J. (1957) The Use of A Field Vane Apparatus
in Sensitive Clay

A.S.T.M.

Eide, O. (1968) Discussion

Oslo Conf., 2, 133-135

Eide, O. and Holmberg, S. (1972) Test Fills to Failure on the Soft
Bangkok Clay

Purdue Conf., 1, 159-180

Evans, G. (1965) Intertidal Flat Sediments and Their Environments of
Deposition in the Wash

Q.J.G.S., 121, 209-245

Evans, I., Sherratt, G.G. and Calderwood, W. (1948) A Simple and
Convenient Instrument for Measuring the Shearing Resistance of Clay
Soils

Army Operational Research Report No.74

Farquharson, W.I. (1953) Storm Surges on the East Coast of England

N.S.F. Conf., 14-27

Fellenius, W. (1936) Calculation of the Stability of Earth Dams

Trans. 2nd Cong. Large Dams , 4, 445-462

Fenske, C.W. (1957) Deep Vane Tests in Gulf of Mexico

A.S.T.M.

Flaate, K. (1966) Factors Influencing the Results of Vane Tests

C.G.J., 3, 1, 18-31

Foott, R. and Ladd, C.C. (1977) Behaviour of Atchafalaya Levees

During Construction

Geot., 27, 2, 137-160

Foundation Engineering Ltd. (1973) Thames Tidal Defences - Sector I

Report on Site Investigation

Foundation Engineering Ltd. (1974(a)) Thames Tidal Defences - Sector II

Report on Site Investigation

Foundation Engineering Ltd. (1974(b)) Thames Tidal Defences - Contract

No. III

Report on Site Investigation for Foundation Tests

Fraser, W. S. (1972) Certificate of Analysis No. 114

Ove Arup and Partners (Unpublished)

George, P.J. and Parry, R.H.G. (1973) Field Loading Tests at Canvey

Island

B.G.S. Symp., 152-165

Gibbs, H.J. (1957) An Apparatus and Method of Vane Shear Testing of Soils

A.S.T.M.

Gibbs, H.J. (1960) Discussion

Boulder Conf., 1067-1069

Gibson, R. E. (1953) Experimental Determination of the True Cohesion and True Angle of Internal Friction in Clays

3rd I.C.S.M.F.E., 1, 126-130

Gibson, R.E. (1963) An Analysis of System Flexibility and Its
Effect on Time Lag in Pore-Water Pressure Measurements
Geot., 13, 1, 1-11

Gibson, R.E. (1966) A Note on the Constant Head Test to Measure
Soil Permeability In Situ
Geot., 16, 3, 256-259

Gibson, R.E. (1969) Discussion
B.G.S. Conf., 297-298

Gibson, R.E. (1970) An Extension to the Theory of the Constant Head
In-situ Permeability Test
Geot., 20, 2, 193-197

Gibson, R.E. (1974) The Analytical Method in Soil Mechanics
Geot., 24, 2, 115-140

Gibson, R.E. and Morgenstern, N.R. (1962) A Note on the Stability of
Cuttings in Normally Consolidated Clays
Geot., 12, 3, 212-216

Giroud, J.P. and Watisee, H. (1972) Stresses Due to an Embankment
Resting on a Finite Layer of Soil
Proc. 6th Conf. Australian Road Research Board, 6, 4, 109-121

Godwin, H., Willis, E.H. and Switsur, V.R. (1965) Cambridge University
Natural Radiocarbon Measurements, vii
Radiocarbon 7

Golder, H.Q. (1953) Discussion
N.S.F. Conf., 96-98

Golder, H.Q. and Palmer, D.J. (1955) Investigation of a Bank Failure at
Scrapsgate, Isle of Sheppey, Kent.
Geot., 5, 1, 55-73

Gould, J.P. and Dunicliff, C.J. (1971) Accuracy of Field Deformation Measurements

4th P.C.S.M.F.E., 1, 313-366

Green, G.E. (1969) Report on Tests on the Performance of the Wilson Slope Indicator and the Soil Instruments Inclinator
Imperial College, University of London (Unpublished)

Green, G.E. (1971) Discussion

Roscoe Symp., 401-409

Green, G.E. (1973(a)) Principles and Performance of Two Inclinator for Measuring Horizontal Ground Movements

B.G.S. Symp., 166-179

Green, G. E. (1973(b)) Equipment

B.G.S. Symp., 517-526

Greensmith, J.T. and Tucker, E.V. (1973) Holocene Transgressions and Regressions on the Essex Coast, Outer Thames Estuary

Geologie En Mijnbouw, 52, 4, 193-202

Grieve, H. (1959) The Great Tide

County Council of Essex

Hallowes, G.R. (1973) Discussion

B.G.S. Symp., 568

Hamza, M.M.A.F. (1976) Analysis of Embankment Dams Using Non-Linear Finite Element Method

Ph.D. Thesis, Imperial College, University of London

Hansen, J. Brinch and Gibson, R.E. (1949) Undrained Shear Strengths of Anisotropically Consolidated Clays

Geot., 1, 3, 189-204

Henkel, D.J. (1959) The Relationship Between the Strength, Pore-Water Pressure and Volume Change Characteristics of Saturated Clays
Geot., 9, 3, 119-135

Henkel, D.J. (1960(a)) The Relationships Between the Effective Stress and Water Content in Saturated Clays
Geot., 10, 2, 41-54

Henkel, D.J. (1960(b)) The Shear Strength of Saturated Remoulded Clays
Boulder Conf., 533-554

Henkel, D.J. (1970) Geotechnical Considerations of Lateral Stresses
Cornell Conf., 1-49

Henkel, D.J. (1971) The Relevance of Laboratory Measured Parameters in Field Studies
Roscoe Symp., 669-675

Hill, R. (1950) The Mathematical Theory of Plasticity
Clarendon Press

Hill, W.C. (1957) Vane In-Place Soil Shear Device Developed and Applied by Oregon State Highway Department
A.S.T.M.

Hoeg, K.H., Andersland, O.B. and Rolfsen, E.N. (1969) Undrained Behaviour of Quick Clay Under Load Tests at Asrum
Geot., 19, 1, 101-115

Hoeg, K.H., Christian, J.T. and Whitman, R.V. (1968) Settlement of Strip Load on Elastic-Plastic Soil
A.S.C.E., J.S.M.F.E.D., 14, SM2, 431-445

Holtz, R.D. and Broms, B. (1972) Long-Term Loading Tests at Ska Edeby,
Sweden

Purdue Conf., 1, 435-464

Holtz, R.D. and Lindskog, G. (1972) Soil Movements Below a Test
Embankment

Purdue Conf., 1, 273-284

Hughes, J.M.O. (1969) Culvert Elongations in Fills Founded on Soft
Clays

C.G.J., 6, 2, 111-117

Hughes, J.M.O., Wroth, C.P. and Pender, M.J. (1975) A Comparison of
the Results of Special Pressuremeter Tests with Conventional Tests on a
Deposit of Soft Clay at Canvey Island

2nd A.N.C.G., 292-296

Hutchinson, J.N. (1973) Discussion

B.G.S. Symp., 557

Hutchinson, J.N. (1975) Private Communication

Hutchinson, J.N. and Gostelow, T.P. (1975) The Development of an Abandoned
Cliff in London Clay at Hadleigh, Essex.

Phil. Trans. Royal Soc., A.283, 557-604

Hvorslev, M.J. (1951) Time Lag and Soil Permeability in Ground-Water
Observations

Bulletin No. 36., U.S. Waterways Experimental Station

Hvorslev, M.J. (1960) Physical Components of the Shear Strength of
Saturated Clays

Boulder Conf., 437-501

Institute of Geological Sciences (1960) British Regional Geology.
London and Thames Valley

Irwin, M.J. (1973) Instruments Developed by the T.R.R.L. for Studying
the Behaviour of Earthworks
B.G.S. Symp., 194-206

Jaeger, J.C. (1956) Elasticity, Fracture and Flow
Methuen

Jain, G.S. and Mohan, D. (1957) Field Vane Shear Tests
Civil Engineering & Public Works Review, 52, 618, 1387-1388

Jaky, J. (1944) The Coefficient of Earth Pressure at Rest
Journal of the Society of Hungarian Architects & Engineers, Budapest,
355-258

Jaky, J. (1948) Pressure in Silos
2nd I.C.S.M.F.E., 1, 103-107

Jamiolkowski, M. (1975) Discussion
B.G.S. Conf., 690-694

Janbu, N. (1957) Earth Pressures and Bearing Capacity Calculations by
Generalised Procedure of Slices
4th I.C.S.M.F.E., 2, 207-212

Johnson, S.J. (1975) Analysis and Design Relating to Embankments
Austin Conf., 2, 1-48

Jurgenson, L. (1940) The Application of Theories of Elasticity and
Plasticity to Foundation Problems
Contributions to Soil Mechanics 1925-40, Boston Society of Civil Engineers

Justo, J.L. (1969) Instrumentation of a New Channel in Soft Ground
7th I.C.S.M.F.E., 2, 599-607

Kallstenius, T. (1957) Swedish Vane Borer Design
A.S.T.M.

Karlsson, R. and Pusch, R. (1967) Shear Strength Parameters and
Microstructure Characteristics of a Quick Clay of Extremely High
Water Content
Oslo Conf., 1, 35-42

Kaufman, R.I. and Weaver, F.J. (1967) Stability of Atchafalaya Levees
A.S.C.E., J.S.M.F.E.D., 93, SM4, 157-176

Kenney, T.C. (1956) An Examination of the Methods of Calculating the
Stability of Slopes
M.Sc. Thesis, Imperial College, University of London

Kenney, T.C. (1968(a)) Shear Strength of Soft Clay
Oslo Conf., 2, 49-58

Kenney, T.C. (1968(b)) A Review of Recent Research on Strength and
Consolidation of Soft Sensitive Clays
C.G.J., 5, 2, 97-119

Kenney, T.C. and Landva, A. (1965) The Vane Triaxial Apparatus
6th I.C.S.M.F.E., 1, 269-272

Kidson, C. and Heyworth, A. (1975) The Quaternary Deposits of the
Somerset Levels
Q.J.E.G., 9, 3, 217-236

Kilford, W.K. (1973) Elementary Air Survey
Pitman

La Rochelle, P., Trak, B., Tavenas, F. and Roy, M. (1974) Failure of a
Test Embankment on a Sensitive Champlain Clay Deposit

C.G.J., 11, 1, 142-164

Lacasse, S.M. and Ladd, C.C. (1973) Behaviour of Embankments on New
Liskeard Varved Clay

Dept. of Civ. Eng., M.I.T. Research Report R73-44 (Soils Publication
No. 327)

Ladd, C.C. (1969) The Prediction of In-situ Stress-Strain Behaviour of
Soft Saturated Clays During Undrained Shear

Bolkesjo Symp. on Shear Strength and Consolidation of Normally Consolidated
Clays, Norwegian Geotechnical Institute, 14-19

Ladd, C.C. (1972) Test Embankment on Sensitive Clay

Purdue Conf., 1, 101-128

Ladd, C.C., Aldrich, H.P. and Johnson, E.G. (1969) Embankment Failure on
Organic Clay

7th I.C.S.M.F.E., 2, 627-634

Ladd, C.C. and Foott, R. (1974) New Design Procedure for Soft Clays

A.S.C.E., J.G.E.D., 100, GT7, 763-786

Ladd, C.C. and Lambe, T. W. (1963) The Strength of 'Undisturbed' Clay
Determined from Undrained Tests

A.S.T.M. - N.R.C. Symp. Lab. Shear Testing of Soils, S.T.P. No. 361,
342-371

Lambe, T.W. (1962) Pore Pressures in a Foundation Clay

A.S.C.E., J.S.M.F.E.D., 88, SM2, 19-47

Lambe, T. W. (1967) Stress Path Method

A.S.C.E., J.S.M.F.E.D., 93, SM6, 117-141

Lambe, T.W. (1973) Predictions in Soil Engineering

Geot., 23, 2, 149-202

Lambe, T. W., D'Appolonia, D.J., Karlsrud, K. and Kirby, R.C. (1971)

The Performance of the Foundation Under a High Embankment

Dept. of Civ. Eng., M.I.T. Research Report R71-22 (Soils publication No.277)

Leonards, G.A. (1976) Some Fundamental Misconceptions in Soil Mechanics

Lecture at Imperial College

Leroueil, S., Tavenas, F., Trak, B., La Rochelle, P. and Roy, M. (1978(a))

Construction Pore Pressures in Clay Foundations Under Embankments

Part I: The Saint Alban Test Fills

C.G.J., 15, 2, 54-65

Leroueil, S., Tavenas, F., Mieussens, C. and Piegnaud, M. (1978(b))

Construction Pore Pressures in Clay Foundations Under Embankments

Part II: Generalised Behaviour

C.G.J., 15, 1, 66-82

Lewis, A.W., Murray, R.T. and Symons I.F. (1975) Settlement and Stability

of Embankments Constructed on Soft Clay

I.C.E., 2, 59, 571-593

Little, A.L. and Vail, A.J. (1960) Some Developments in the Measurement

of Pore Pressure

I.C.E., Conf., 75-80

Lo, K.Y. (1965) Stability of Slopes in Anisotropic Soils

A.S.C.E., J.S.M.F.E.D., 91, SM4, 85-106

Lo, K.Y. and Stermac, A. G. (1965) Failure of an Embankment Founded
on Varved Clay

C.G.J., 2, 3, 234-253

Lo, K.Y. and Stermac, A. G. (1966) Discussion of Lo and Stermac (1965)

C.G.J., 3, 1, 42-45

Lowe III, J. (1967) Stability Analysis of Embankments

Berkeley Conf., 1-33

Maguire, W.M. (1975) The Strength and Stress-Strain Characteristics of
Brecciated Upper Lias Clay

Ph.D. Thesis, Imperial College, University of London

Marsland, A. (1957(a)) The Design and Construction of Earth Flood Banks

Journal of the Institution of Water Engineers, 11, 3, 236-258

Marsland, A. (1957(b)) Discussion

4th I.C.S.M.F.E., 3, 257

Marsland, A. (1961) A Study of A Breach in an Earth Embankment Caused
by Uplift Pressure

5th I.C.S.M.F.E., 2, 663-668

Marsland, A. (1966) The Design and Construction of Earth Flood Banks

Chapter 24, River Engineering and Water Conservation Work,

Ed. R.B. Thorn, Butterworths

Marsland, A. (1973(a)) Instrumentation of Flood Defence Banks Along the
River Thames

B.G.S. Symp., 287-303

Marsland, A. (1973(b)) Discussion

B.G.S. Symp., 530

Marsland, A. (1973(c)) Discussion

B.G.S. Symp., 587

Marsland, A. and Quarterman, R. (1974) Further Development of Multipoint
Magnetic Extensometers for Use in Highly Compressible Ground

Geot., 24, 3, 429-433

Massarsch, K.R., Holtz, R.D., Holm, B.G. and Frederikson, A. (1975)

Measurement of Horizontal In-situ Stress

Raleigh Conf., 1, 266-286

Maughan, J.D. (1972) Measurement of Structural Deformations

B.Sc. Thesis, University of Nottingham

Menzies, B.K. and Mailey, L.K. (1976) Some Measurements of Strength

Anisotropy Using Diamond Shaped Shear Vanes

Geot., 26, 3, 535-538

Meridian Air Maps Ltd. (1974(a)) Thames Tidal Defences - Mucking Bank 1,

Stage 1

Report to Binnie & Partners

Meridian Air Maps Ltd. (1974(b)) Thames Tidal Defences - Mucking Bank 1,

Stage 2

Report to Binnie & Partners

Mesri, G. (1975) Discussion of Ladd and Foott (1975)

A.S.C.E., J.G.E.D., 101, GT4, 409-412

Milović, D.M. (1970) Constraints et Deplacements dans Une Couche Elastique
D'epaisseur Limitee, Produits Par Une Foundation Circulaire

Le Genie Civil, T.147, 5, 281-285

Mitchell, R.J. (1970) On the Yielding and Mechanical Strength of Leda Clays

C.G.J., 7, 3, 297-312

Moh, Z.C., Brand, E.W. and Nelson, J.D. (1972) Pore Pressures Under a
Bund on Soft Fissured Clay

Purdue Conf., 1, 243-272

Moore, J.F.A. (1973) The Photogrammetric Measurement of Constructional
Displacements of a Rockfill Dam

B.R.E. CP 34/74 (also Photogrammetric Record, 7, 42, 628-648)

Moore, J.F.A. (1974) Mapping Major Joints in the Lower Oxford Clay Using
Terrestrial Photogrammetry

B.R.E. CP 82/74 (also Q.J.E.G., 7, 1, 57-67)

Morgenstern, N.R. and Price, V. E. (1965) The Analysis of the Stability
of General Slip Surfaces

Geot., 15, 1, 79-93

Morgenstern, N.R. and Tchalenko, J.S. (1967) Microscopic Structures in
Kaolin Subject to Direct Shear

Geot., 17, 4, 309-328

Murray, R. T. (1971) Embankments Constructed on Soft Foundations:
Settlement at Avonmouth

T.R.R.L. LR 443

Murray, R. T. (1973) Embankments Constructed on Soft Foundations:
Settlement Studies Near Oxford

T.R.R.L. LR 538

Murray, R.T. (1974) Two-Dimensional Analysis of Settlement by Computer
Program

T.R.R.L. LR 617

Murray, R.T. and Symons, I.F. (1974) Embankments on Soft Foundations:
Settlement and Stability Study at Tickton, Yorkshire.

T.R.R.L. LR 643

McKenna, J.M. and Roy, M. (1973) Performance of the Instrumentation Used
to Monitor the M5 Motorway Embankments Built on Soft Ground Between
Edithmead and Huntworth

B.G.S. Symp., 275-286

Naylor, D.J. and Hooper, J.A. (1975) An Effective Stress Finite Element
Analysis to Predict the Short- and Long-Term Behaviour of a Piled Raft
Foundation on London Clay

B.G.S. Symp., 394-402

Nonveiller, E. (1965) The Stability Analysis of Slopes with A Slip Surface
of General Shape

6th I.C.S.M.F.E., 2, 522-525

Noorany, I. and Seed, H.B. (1965) In-situ Strength Characteristics of
Soft Clays

A.S.C.E., J.S.M.F.E.D., 91, SM2, 49-80

Odenstad, S. (1948) Loading Tests on Clay

2nd I.C.S.M.F.E., 1, 299-303

O'Riordan, N. (1978) The Consolidation and Settlement Characteristics
of Inter-Bedded Alluvial Deposits

Ph.D. Thesis, King's College, University of London

Osterberg, J.O. (1957) Introductory Remarks

A.S.T.M.

Parry, R.H.G. (1968) Field and Laboratory Behaviour of a Lightly
Overconsolidated Clay

Geot., 18, 2, 151-171

Parry, R.H.G. (1969) Discussion

B.G.S. Conf., 245-246

Parry, R.H.G. (1970) Overconsolidation of Soft Clay Deposits

Geot., 20, 4, 442-446

Parry, R.H.G. (1971(a)) Stability Analysis for Low Embankments on Soft
Clays

Roscoe Symp., 643-668

Parry, R.H.G. (1971(b)) Undrained Shear Strength in Clays

1st A.N.C.G., 11-15

Parry, R.H.G. (1971(c)) A Simple Driven Piezometer

Geot., 21, 2, 163-167

Parry, R.H.G. (1971(d)) A Direct Method of Estimating Settlement in
Sands from S.P.T. Values

Proc. Symp. Interaction of Structure and Foundation, Midlands Soil
Mechanics and Foundation Engng Soc., 29-37

Parry, R.H.G. (1973) Discussion

B.G.S. Symp., 614

Parry, R.H.G. and McLeod, J.H. (1967) Investigation of Slip Failure
in Flood Levee at Launceston, Tasmania

5th A.N.C.S.M.F.E., 294-300

Peters, S.P. (1953) Some Meteorological Aspects of North Sea Floods
with Special Reference to February 1953

N.S.F. Conf., 28-35

Picknett, J.K., Gudgeon, D.L. and Evans, E.P. (1974) Ground-Anchored
Sea Walls for Thames Tidal Defences

Conference on Diaphragm Walls and Anchorages, I.C.E., London, 195-202

Penman, A.D.M. (1960) A Study of the Response Times of Various
Piezometers

I.C.E. Conf., 53-58

Penman, A.D.M. (1975) Earth Pressures Measured with Hydraulic Piezometers

B.R.E. CP 39/75 (also Raleigh Conf., 2, 361-381)

Penman, A.D.M., Burland, J.B. and Charles, J.A. (1971) Observed and
Predicted Deformations in a Large Embankment Dam During Construction

I.C.E., 49, 1-21

Penman, A.D.M. and Charles, J.A. (1971) Measuring Movements of Engineering
Structures

B.R.E. CP 32/71 (also Proc. 13th Int. Congress of Surveyors, Wiesbaden,
Commission 6, Paper 605.4)

Penman, A.D.M. and Charles, J.A. (1973) Measuring Movements of Embankment
Dams

B.G.S. Symp., 341-358

Philips, S.H.E. and James, E.L. (1973) An Inclinator for Measuring the
Deformation of Buried Structures with Reference to Multi-Tied Diaphragm
Walls

B.G.S. Symp., 359-369

Pilot, G. (1972) Study of Five Embankment Failures on Soft Soils

Purdue Conf., 1, 81-100

Planicka, A. and Nosek, L. (1970) Terrestrial Photogrammetry in Measurement
of Deformations of Rockfill Dams

Trans. 10th Cong. Large Dams, 1, 207-215

Poulos, H.G. and Davis, E.H. (1974) Elastic Solutions for Soil and
Rock Mechanics

Wiley

Pugh, R.S. (1973) Appraisal of the Finite Element Method for the
Solution of Displacements and Stresses Within an Isotropic Elastic
Medium Loaded by a Smooth Flexible Strip

Imperial College, University of London (Unpublished)

Raymond, G.P. (1970) Discussion on Stresses and Displacements in a Cross-
Anisotropic Soil

Geot., 20, 4, 456-458

Raymond, G.P. (1972) Prediction of Undrained Deformations and Pore Pressures
in Weak Clay Under Two Embankments

Geot., 22, 3, 381-401

Raymond, G.P. (1973) Foundation Failure of New Liskeard Embankment

Highway Research Record No. 453, 1-17

Raymond, G.P. and Azzouz, M.M. (1969) Permeability Determination for Predicting
Rates of Consolidation

B.G.S. Conf., 285-293

Rendulić, L. (1937) Ein Grundgesetz der Tonmechanik und Sein Experimentaler
Beweis

Bauingenieur, 18, 459-467

Robertson, N.F. (1974) The Design of Instrumentation Installations for
Soft Foundations

M.Sc. Thesis, Imperial College, University of London

Roscoe, K.H. and Burland, J.B. (1968) On the Generalized Stress-Strain Behaviour of Wet Clay
Engineering Plasticity, Ed. Heyman and Leckie, Cambridge University Press, 535-609

Roscoe, K.H. and Schofield, A.N. (1963) Mechanical Behaviour of An Idealised 'Wet' Clay
2nd E.C.S.M. F.E., 1, 47-54

Roscoe, K.H., Schofield, A.N. and Wroth, C.P. (1958) On the Yielding of Soils
Geot., 8, 1, 22-53

Rowe, P.W. (1968) The Influence of Geological Features of Clay Deposits on the Design and Performance of Sand Drains
I.C.E., 1, 1-72

Rowe, P.W. (1972(a)) The Relevance of Soil Fabric to Site Investigation Practice
Geot., 22, 2, 195-300

Rowe, P.W. (1972(b)) Embankments on Soft Alluvial Ground
Q.J.E.G., 5, 2, 127-141

Sandroni, S.S. (1977) The Strength of London Clay in Total and Effective Stress Terms
Ph.D. Thesis, Imperial College, University of London

Sarma, S.K. (1973) Stability Analysis of Embankments and Slopes
Geot., 23, 3, 423-433

Sarma, S.K. and Bhawe, M.V. (1974) Critical Acceleration Versus Static Factor of Safety in Stability of Earth Dams and Embankments
Geot., 24, 4, 661-665

Schiffman, R.L. (1958) Consolidation of Soil Under Time Dependent Loading and Varying Permeability
Highway Research Board, 37, 584-617

Schiffman, R.L. (1960) Field Applications of Soil Consolidation Under Time Dependent Loading and Varying Permeability
Highway Research Board, Bulletin 248

Schmertmann, J.H. (1955) The Undisturbed Consolidation Behaviour of Clay
A.S.C.E., 120, 1201-1233

Schmertmann, J.H. and Osterberg, J.O. (1960) An Experimental Study of the Development of Cohesion and Friction with Axial Strain in Saturated Cohesive Soils
Boulder Conf., 643-694

Schofield, A.N. and Wroth, C.P. (1968) Critical State Soil Mechanics
McGraw-Hill

Scott, R.F. (1963) Principles of Soil Mechanics
Addison-Wesley

Seymour-Jones, A.A. (1975) Discussion of Ladd and Foott (1975)
A.S.C.E., J.G.E.D., 101, GT7, 81-83

Shanley, F.R. (1957) Strength of Materials
McGraw-Hill

Sherwood, D.E. and Currey, B. (1973) Experience in Using Electrical Tiltmeters
B.G.S. Symp., 382-395

Simons, N.E. (1960) The Effect of Overconsolidation on the Shear Strength Characteristics of an Undisturbed Oslo Clay
Boulder Conf., 747-763

Schmertmann, J. H. (1975) Measurement of In-situ Shear Strength
Raleigh Conf., 2, 57-138

Simons, N.E. (1975) Normally Consolidated and Lightly Overconsolidated
Cohesive Materials

B.G.S. Conf., 500-530

Skempton, A.W. (1945) A Slip in the West Bank of the Eau Brink Cut

I.C.E., 24, 7, 267-287

Skempton, A.W. (1948(a)) Geotechnical Properties of Post-Glacial Clays

Geot., 1, 1, 7-22

Skempton, A.W. (1948(b)) Vane Tests in the Alluvial Plain of the River

Forth Near Grangemouth

Geot., 1, 2, 1-16

Skempton, A.W. (1948(c)) The $\phi_u = 0$ Analysis for Stability and Its

Theoretical Basis

2nd I.C.S.M.F.E., 1, 72-78

Skempton, A.W. (1948(d)) A Study of the Immediate Triaxial Test on

Cohesive Soils

2nd I.C.S.M.F.E., 1, 192-196

Skempton, A.W. (1948(e)) The Effective Stresses in Saturated Clays

Strained at Constant Volume

7th Int. Cong. Applied Mechanics, 1, 378-392

Skempton, A.W. (1953) The Colloidal Activity of Clays

3rd I.C.S.M.F.E., 1, 57-61

Skempton, A.W. (1954) The Pore-Pressure Coefficients A and B

Geot., 4, 4, 143-147

Skempton, A.W. (1957) Discussion

I.C.E., 7, 305-307

Skempton, A.W. (1960) The Pore-Pressure Coefficients in Saturated Soils
Geot., 10, 4, 186-187

Skempton, A.W. (1961) Horizontal Stresses in An Overconsolidated Eocene
Clay
5th I.C.S.M.F.E., 1, 351-357

Skempton, A.W. (1964) Long-Term Stability of Clay Slopes
Geot., 14, 2, 77-101

Skempton, A.W. (1970) The Consolidation of Clays by Gravitational Compaction
Q.J.G.S., 125, 373-412

Skempton, A.W. and Bishop, A. W. (1950) The Measurement of the Shear
Strength of Soils
Geot., 2, 2, 90-108

Skempton, A. W. and Bishop, A.W. (1954) Soils. Chapter X of 'Building
Materials, Their Elasticity and Inelasticity', Ed. M. Reiner
North-Holland Publishing Co.

Skempton, A. W. and Bjerrum, L. (1957) A Contribution to the Settlement
Analysis of Foundations on Clay
Geot., 7, 2, 168-178

Skempton, A. W. and Golder, H.Q. (1948) Practical Examples of the
 $\phi_u = 0$ Analysis of Stability of Clays
2nd I.C.S.M.F.E., 2, 63-70

Skempton, A. W. and Henkel, D.J. (1953) The Post-Glacial Clays of the
Thames Estuary at Tilbury and Shellhaven
3rd I.C.S.M.F.E., 1, 302-308

Skempton, A. W. and Hutchinson, J.N. (1969) Stability of Natural Slopes and
Embankment Foundations
7th I.C.S.M.F.E., State-of-the-Art Volume, 291-340

Skempton, A. W. and Northey, R. D. (1952) The Sensitivity of Clays
Geot., 3, 1, 30-53

Skempton, A. W. and Ward, W.H. (1952) Investigations Concerning a Deep
Cofferdam in the Thames Estuary at Shellhaven
Geot., 3, 3, 119-139

Smith, A.H.V. (1945) Some Preliminary Trials with the Army Operational
Research Group Vane Apparatus
Army Operational Research Group, Memorandum No. 540

Smith, A.H.V. (1947) The Measurement of Shear Strength of Soils in the Field
Army Operational Research Group, Report No. 352

Smith, I.M. (1971) Plane Plastic Deformation of Soil
Roscoe Symp., 537-547

Snell, E.L. (1953) Damage to the Essex Coastline, and Restoration Works
N.S.F. Conf., 155-164

Soderberg, L.O. (1962) Consolidation Theory Applied to Foundation Pile-
Time Effects
Geot., 12, 3, 217-225

Soil Instruments Ltd., (1975) Private Communication

Soil Mechanics Ltd., (1972) Thames Tidal Defences-Site Investigation for
Sector III

Symons, I.F. (1974) Stability of Embankments on Soft Foundations
M.Sc. Thesis, University of Birmingham

Symons, I.F. (1976(a)) Assessment and Control of Stability for Road
Embankments Constructed on Soft Subsoils

T.R.R.L. LR 711

Symons, I.F. (1976(b)) Private Communication

Symons, I.F. and Murray, R.T. (1975) Embankments on Soft Foundations:
Settlement and Stability Study at Over Causeway By-Pass
T.R.R.L. LR 675

Tavenas, F., Blanchette, G., Leroueil, S., Roy, M. and La Rochelle, P. (1975)
Difficulties in the In-situ Determination of K_0 in Soft Sensitive Clays
Raleigh Conf., 1, 450-476

Tavenas, F., Chapeau, C., La Rochelle, P. and Roy, M. (1974)
Immediate Settlements of Three Test Embankments on Champlain Clay
C.G.J., 11, 1, 109-141

Tavenas, F. and Leroueil, S. (1977) Effects of Stresses and Time on
Yielding of Clays
9th I.C.S.M.F.E., 1, 319-326

Taylor, D.W. (1948) Fundamentals of Soil Mechanics
Wiley

Taylor, H.T. and Buchignani, A.L. (1972) Field Test of Debris Fill Over
Soft Soil
Purdue Conf., 1, 395-414

Terzaghi, K. (1943) Theoretical Soil Mechanics
Wiley

Timoshenko, S. and Goodier, J.N. (1951) Theory of Elasticity
McGraw-Hill

Townsend, D.L. (1965) Discussion of Lo and Stermac (1965)
C.G.J., 2, 3, 254-258

Vaid, Y.P. and Campanella, R.G. (1974) Triaxial and Plane Strain Behaviour
of Natural Clay

A.S.C.E., J.G.E.D., 100, GT3, 207-224

Vaughan, P.R. (1965) Field Measurements in Earth Dams

Ph.D. Thesis, Imperial College, University of London

Vaughan, P.R. (1969) A Note on Sealing Piezometers in Boreholes

Geot., 19, 3, 405-413

Vaughan, P.R. (1973(a)) The Measurement of Pore Pressures with Piezometers

B.G.S. Symp., 411-422

Vaughan, P.R. (1973(b)) Discussion

B.G.S. Symp., 539-543

Vaughan, P.R. (1973(c)) Discussion

B.G.S. Symp., 558-563

Vaughan, P.R. (1973(d)) The Applications of Instrumentation

B.G.S. Symp., 599-606

Vaughan, P.R. and Walbancke, H.J. (1975) The Stability of Cut and Fill
Slopes in Boulder Clay

Proc.Symposium on the Behaviour of Glacial Materials, Midlands Geotechnical
Society, 209-219

Vaughan, P.R., Werneck, M.L.G. and Hamza, M.M.A.F. (1973) Discussion

B.G.S. Symp., 617-623

Viggiani, C. (1973) Discussion

B.G.S. Symp., 563-565

Walbancke, H.J. (1968) Holocene Sea Levels in Southern Britain

M.Sc. Thesis, Imperial College, University of London

Walbancke, H.J. (1976) Pore Pressures in Clay Embankments and Cuttings

Ph.D. Thesis. Imperial College, University of London

Walker, F.C. (1967) Willard Dam-Behaviour of a Compressible Foundation

A.S.C.E., J.S.M.F.E.D., 92, SM4, 177-198

Walker, L.K. (1969) Undrained Creep in a Sensitive Clay

Geot., 19, 4, 575-529

Weisel, C.E. (1968) Discussion

Oslo Conf., 1, 130

Weisel, C.E. (1971) Discussion

A.S.C.E., J.S.M.F.E.D., 97, SM2, 483-489

Weisel, C.E. (1973) Some Factors Influencing In-situ Vane Test Results

8th I.C.S.M.F.E., 1, 473-479

Werneck, M.L.G. (1974) Field Observations of the Behaviour of the Upper

Lias Clay at the Empingham Dam Site

Ph.D. Thesis, Imperial College, University of London

Wesley, L.D. (1975) The Influence of Stress Path and Anisotropy on the

Behaviour of a Soft Alluvial Clay

Ph.D. Thesis, Imperial College, University of London

Whitman, R.V. and Bailey, W.A. (1967) Use of Computers for Slope Stability

Analysis

Berkeley Conf., 519-542

Wilkes, P.F. (1970) A Note on the Installation of Piezometers in Small

Diameter Boreholes

Geot., 20, 3, 330-333

Wilkes, P.F. (1972(a)) An Induced Failure at a Trial Embankment at
Kings Lynn, Norfolk, England

Purdue Conf., 1, 29-64

Wilkes, P.F. (1972(b)) Kings Lynn Trial Embankment

Journal of the Institution of Highway Engineers, 14, 8, 9-16

Wilkes, P.F. (1973) Instrumentation for the Kings Lynn Southern By-Pass

B.G.S. Symp., 448-461

Wilkes, P.F. (1974) Permeability Tests in Alluvial Deposits and the
Determination of K_0

Geot., 24, 1, 1-11

Wilkinson, W.B. (1968) Constant Head In-situ Permeability Tests in Clay
Strata

Geot., 18, 2, 172-194

Wilkinson, W.B., Barden, L. and Rocke, G. (1969) An Assessment of In-situ and
Laboratory Tests in Predicting the Pore Pressure in an Earth Dam

B.G.S. Conf., 277-284

Wilson, S.D. (1973) Discussion

B.G.S. Symp., 556-557

Wright, S.G., Kulhawy, F.H. and Duncan, J.M. (1973) Accuracy of Equilibrium
Slope Stability Analyses

A.S.C.E., J.S.M.F.E.D., 99, SM10, 783-792

Wroth, C.P. (1971) Discussion

Roscoe Symp., 122-124

Wroth, C.P. (1975(a)) Private Communication

Wroth, C.P. (1975(b)) In-situ Measurement of Initial Stresses and Deformation Characteristics

Raleigh Conf., 2, 181-230

Wroth, C.P. (1976) The Predicted Performance of Soft Clay Under a Trial Embankment Loading Based on the Cam Clay Model

Finite Elements in Geomechanics, Ed. G. Gudehus, Wiley

Wroth, C.P. and Hughes, J.M.O. (1973) An Instrument for the In-situ Measurement of the Properties of Soft Clays

8th I.C.S.M.F.E., 1, 487-494

Wroth, C.P. and Simpson, B. (1972) An Induced Failure at a Trial Embankment: Part II - Finite Element Computations

Purdue Conf., 1, 65-80

Wu, T.H., Thayer, W. B. and Sheng, S.L. (1975) Stability of Embankment on Clay

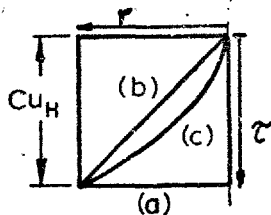
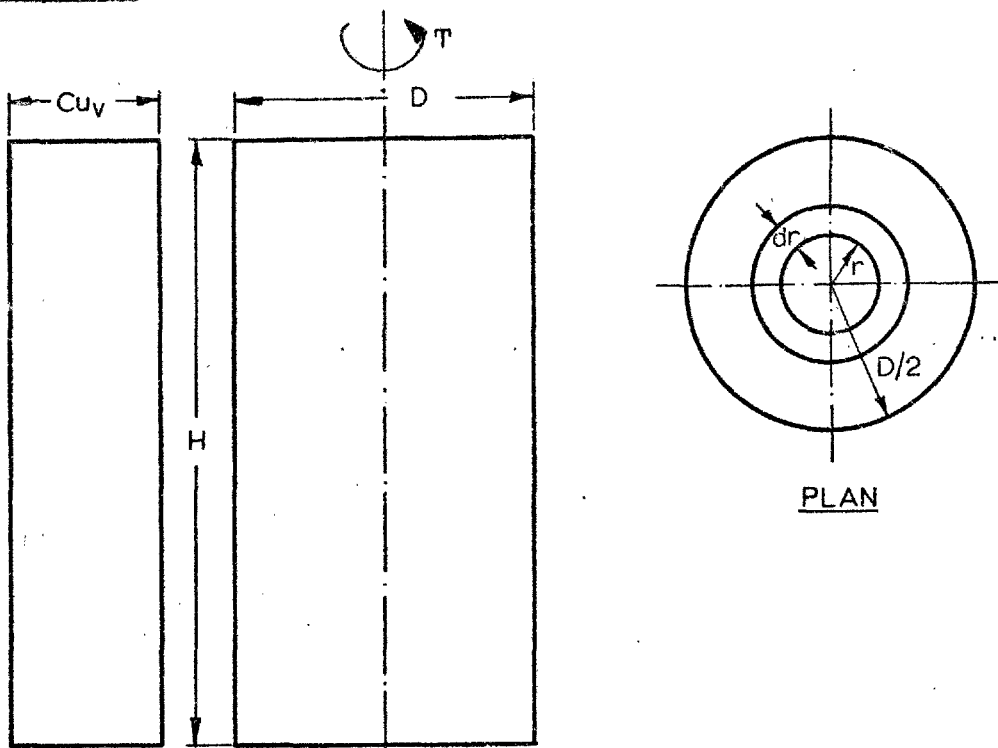
A.S.C.E., J.G.E.D., 101, GT9, 913-932

Zienkiewicz, O.C. (1977) The Finite Element Method

McGraw-Hill

Zienkiewicz, O.C. and Naylor, D.J. (1971) Discussion on the Adaptation of Critical State Soil Mechanics Theory for Use in Finite Elements

Roscoe Symp., 537-547



ELEVATION

- a) uniform distribution, $f(r) = 1$
- b) linear variation, $f(r) = 2r/D$
- c) parabolic variation, $f(r) = (2r/D)^{1/2}$

Component of torque from horizontal surfaces: (end)

$$T_e = \int_0^{D/2} 2 \cdot 2\pi r \cdot C_{uH} \cdot f(r) \cdot r \cdot dr$$

Component of torque from vertical surface: (cylindrical)

$$T_c = C_{uV} \pi D H \cdot D/2$$

Thus

$$T_{VER} = T_e + T_c = \frac{\pi D^2 H}{2} \cdot C_{uV} + 4\pi C_{uH} \int_0^{D/2} f(r) \cdot r^2 \cdot dr$$

which leads to:

$$T_{VER} = \frac{\pi D^2 H}{2} \left(C_{uV} + \frac{\alpha_V D}{H} C_{uH} \right) \dots (A.1.1)$$

- where a) $\alpha_V = 0.33$
- b) $\alpha_V = 0.25$
- c) $\alpha_V = 0.29$

For an isotropic soil and full mobilisation of shear stress over the entire surface area of the cylinder we have the basic formulation:

$$T = \frac{\pi D^2 H C_u}{2} \left(1 + \frac{D}{3H} \right) \dots (A.1.2)$$

VANE TORQUE / SOIL SHEAR STRENGTH RELATIONSHIP:
VERTICAL VANE TESTS.

APPENDIX 2

CALIBRATION OF GEONOR VANE

A.2.1. VERTICAL CALIBRATION

The set up used in the vertical calibration is represented diagrammatically in figure A.2.1.(A), the operation being carried out from a wooden platform about 2.5m above floor level. The vane casing passed through a hole in the platform and was held vertically by a lathe chuck, resistance to rotation being provided by stilsons reacting against the platform supports. The vane was advanced beyond the protection shoe in the normal way and an aluminium cross-arm fitted. This was a force fit on the taper of the vane shaft, such that its position was mid-height on the vane. Equal horizontal forces, and hence a pure moment, were applied to the arm by means of the weight pans and system of wires illustrated in figure A.2.1.(A). Having added the required weights equally to the pans the vane was rotated by the torsion head until the forces T_T were perpendicular to the cross arm. These forces were maintained horizontal by adjusting the length of the inclined wires, using the screw pegs. These were located in uprights attached to a solid wooden base, the uprights having had slots cut in them to allow the weight pans to hang vertically without interference. Several large weights were placed on the base of the frame to prevent its rotation as the torque was applied. The angle of inclination of the non-horizontal wires (θ_c) was measured with a protractor and hence by consideration of the triangle of forces involved the applied torque was related to the torsion head dial divisions (figure A.2.1.(A)).

The vertical calibration was carried out with one and two lengths of casing (and rods) additional to the vane head. Both these calibrations were carried out twice and each individual calibration carried out by applying weights in 1.kg.f. intervals up to a maximum value using whole kg.f. units (i.e. 1, 2, 3, 4, 5) and then dismantling, resetting up and repeating in 0.5 kg.f. units (i.e. 1.5, 2.5, 3.5, 4.5, 5.5). The weight pans were initially weighed and balanced using lead shot to facilitate the use of the same standard weights with each pan.

A.2.2. HORIZONTAL CALIBRATION

This was carried out with the vane lying on a bench, rotation again being resisted by stilsons. The torque was applied to the vane using the same cross-arm as previously, but with the weight pans acting directly on it in a vertical direction, one pan acting upwards by incorporating a pulley as shown in figure A.2.1.(B). The required weights were applied equally to the pans and the vane then rotated until the torque arm was horizontal. In this position only one calibration (although again in two increments) was carried out, using the vane plus one length of casing.

A.2.3. DISCUSSION OF RESULTS

Figure A.2.2. shows the relationship obtained between applied torque and torsion head dial divisions. As can be seen the relationship is unaffected, within the scatter of the results, by the position of the vane or the number of sections used. The friction in the apparatus at zero load is indicated by the intercept with the abscissa.

Figure A.2.3. shows the calibration curve derived for the Geonor vane. Again, there appears to be no definable difference between the various calibrations within the scatter, which is generally better than $\pm 3\%$. Also indicated are the average calibration factors deriving from the best fit straight line of figure A.2.2. and Geonor's calibration chart for the torsion head.

From equation A.1.1. the torsion head dial reading can be related to the undrained strength of an isotropic soil, as below:-

$$\begin{array}{l} C_u = 16.081 \times CF \times \text{dial divisions} \\ C_u = 16.680 \times CF \times \text{dial divisions} \end{array} \left. \begin{array}{l} \alpha_v = 0.33 \\ \alpha_v = 0.25 \end{array} \right\} \begin{array}{l} 55 \times 110\text{mm vane} \end{array}$$

$$\begin{array}{l} C_u = 9.742 \times CF \times \text{dial divisions} \\ C_u = 10.106 \times CF \times \text{dial divisions} \end{array} \left. \begin{array}{l} \alpha_v = 0.33 \\ \alpha_v = 0.25 \end{array} \right\} \begin{array}{l} 65 \times 130\text{mm vane} \end{array}$$

where CF is the relevant calibration factor from figure A.2.3. in units of kg.f.m./dial division and C_u is in kN/m^2 . A calibration chart, relating undrained strength to dial divisions, for field use is shown in figure A.2.4. based on the average calibration factors described previously.

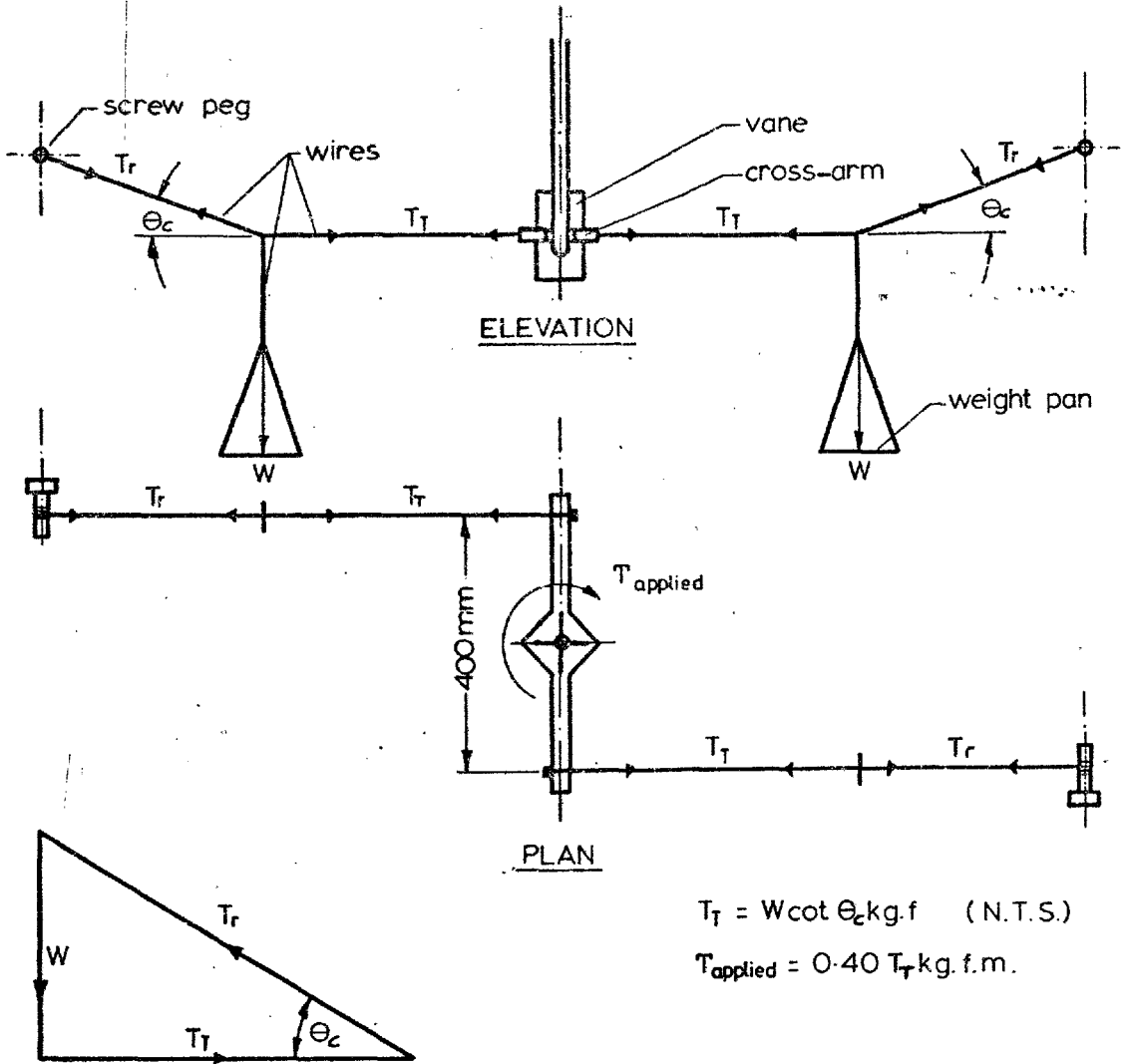
Inspection of the Mucking results shows peak undisturbed vane strengths to have been mobilised at torsion head readings of between 20 and 60 divisions, the average being about 30. A reading of 20 divisions represents the maximum error in this range, the calibration factor being 0.0551 kg.f.m./division compared to the average value of 0.0570 and Geonor's value of 0.0610. These latter values are overestimates by 3.5% and 11% respectively.

At the average value of 30 divisions the calibration factor is 0.0560, giving in this case respective errors of 2% and 9%. It was thus considered acceptable to use the average calibration factor, and hence the field calibration chart, in deriving the undisturbed undrained strength values from the Geonor vane test results.

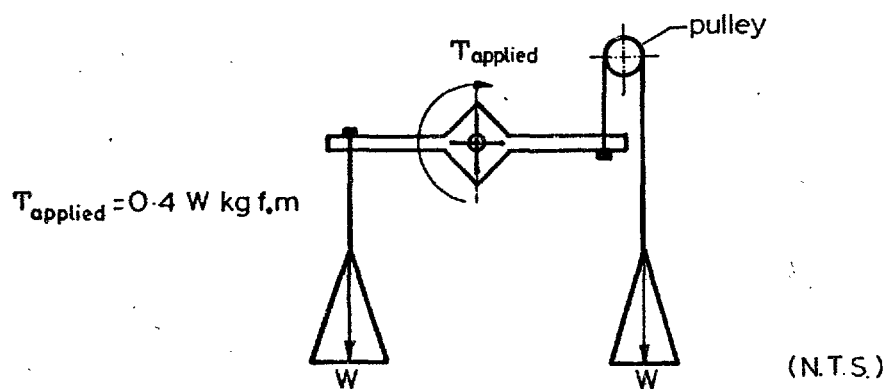
The remoulded strength tests produced torsion head readings between 5 and 15 divisions with an average of about 7.5. The average calibration factor overestimates by between 7% and 58% in this region, the average error being about 30%. In addition the values of the calibration factor are obviously less reliable in this area. Because of the very low values of the remoulded undrained strength these relatively large errors are in fact comparable to the precision of the equipment and the field calibration chart was used for these results as well.

Use of the calibration chart for the torsion head alone would thus result in an overestimate of the undisturbed undrained strength by about 10% i.e. 1.75 kN/m^2 at the average vane undrained strength value of about 17.5 kN/m^2 . At the time of receiving the equipment for calibration the torsion head had been recalibrated since manufacture, in this country. This calibration, which was in use at the time, was 15 - 20% on the low side. Subsequent recalibration of the torsion head on the same calibration frame resulted in values very nearly identical to the original Geonor ones. The Geonor calibration was assumed to be based on $\alpha_v = 0.33$ and these results substantiated this supposition.

The calibration exercise was thus seen to be fully justified and it may be asked how many vane test results have been misinterpreted because of poor calibration. Internal friction in the apparatus and the adoption of the correct calibration factor are thus important points to account for if further uncertainty is not to enter the interpretation of field vane results. A 10% increase in the average undrained shear strength of the Mucking clay will be seen, in Chapter 7, to correspond to an increase of around 10% in the safety factor for a critical total stress slip surface. Thus whereas the $\pm 3\%$ accuracy of the calibration may be acceptable the 10% error on the unsafe side, resulting from calibration of the torsion head alone, is not.



(A) Vertical Calibration



(B) Horizontal Calibration

CALIBRATION OF GEONOR VANE

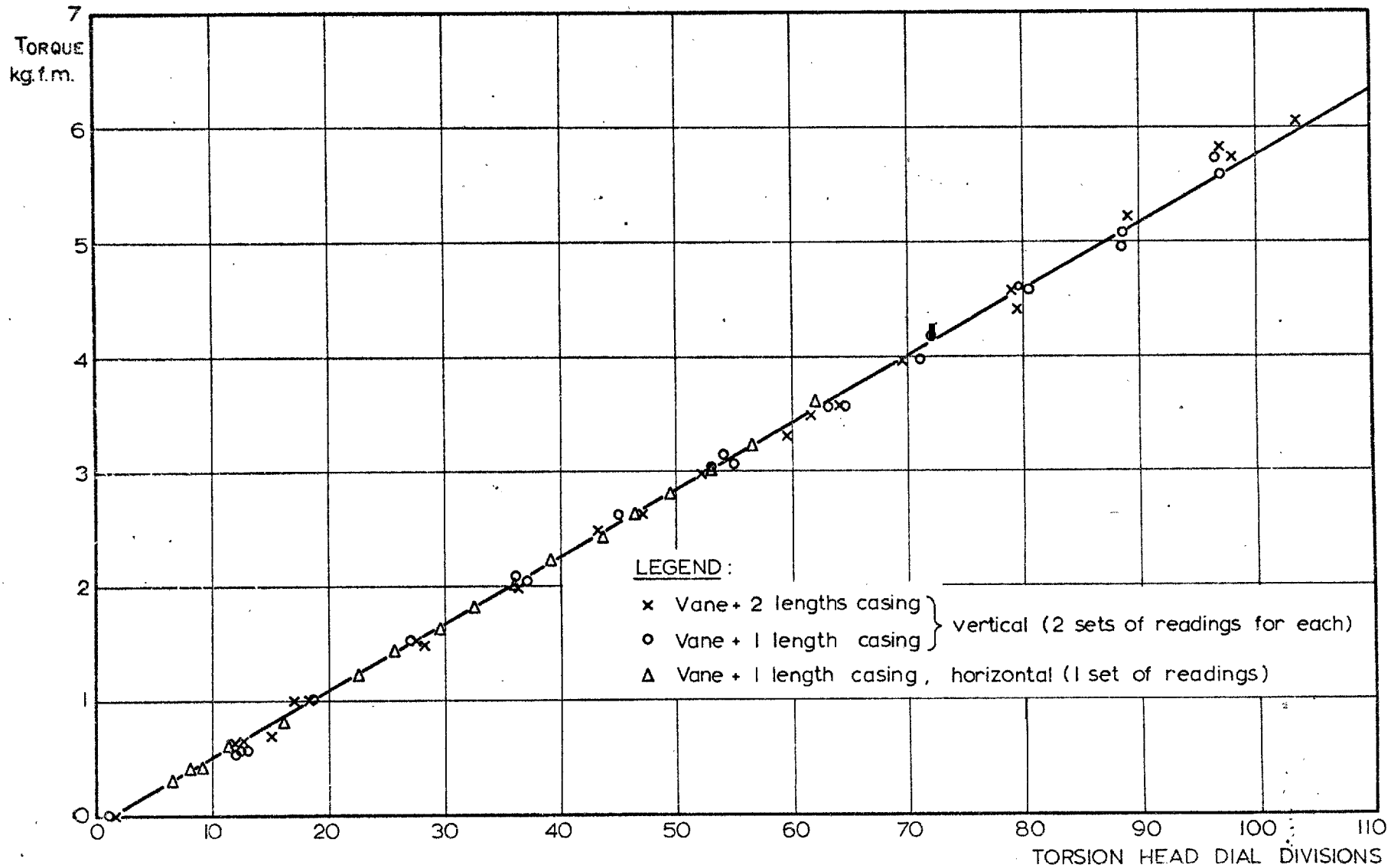
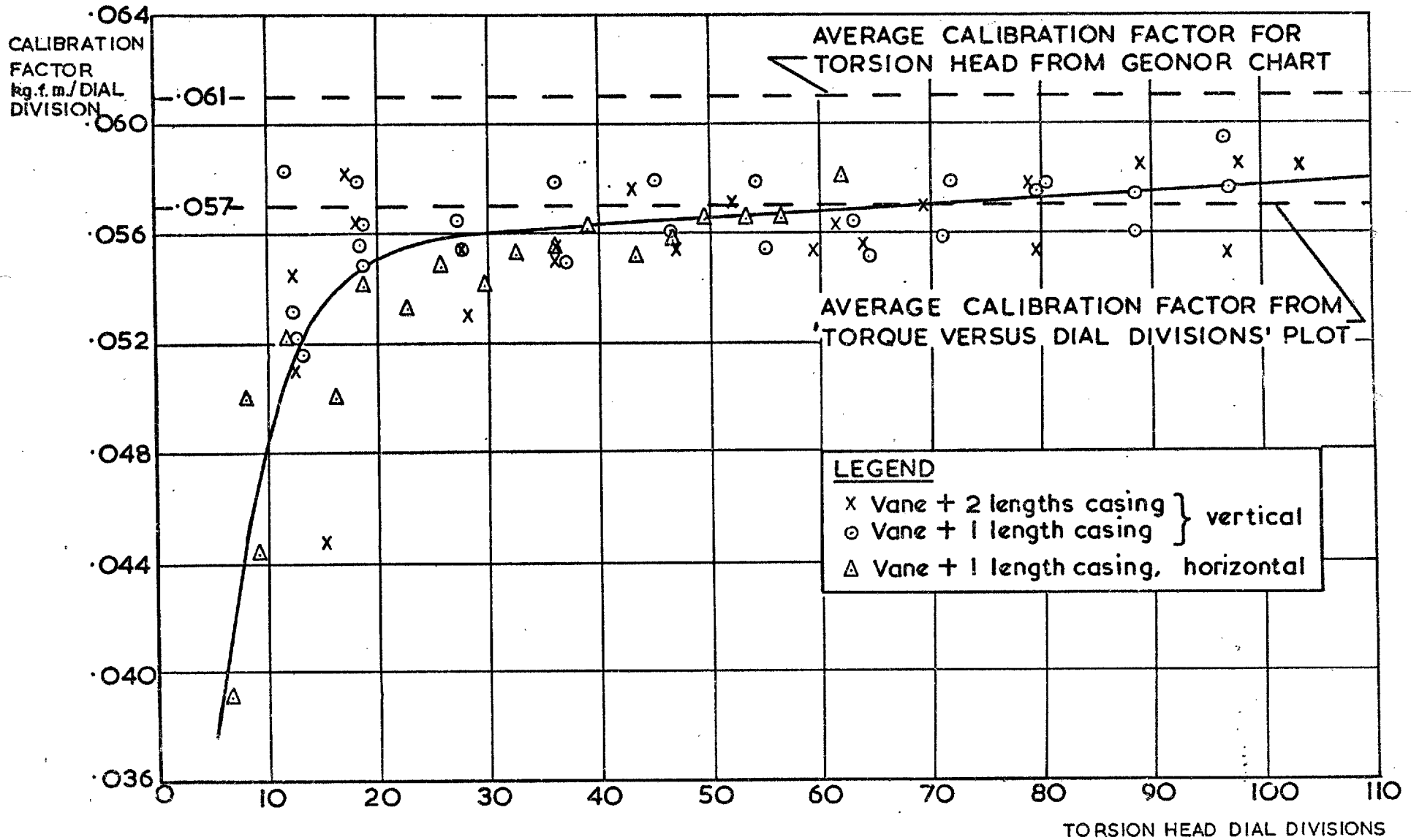
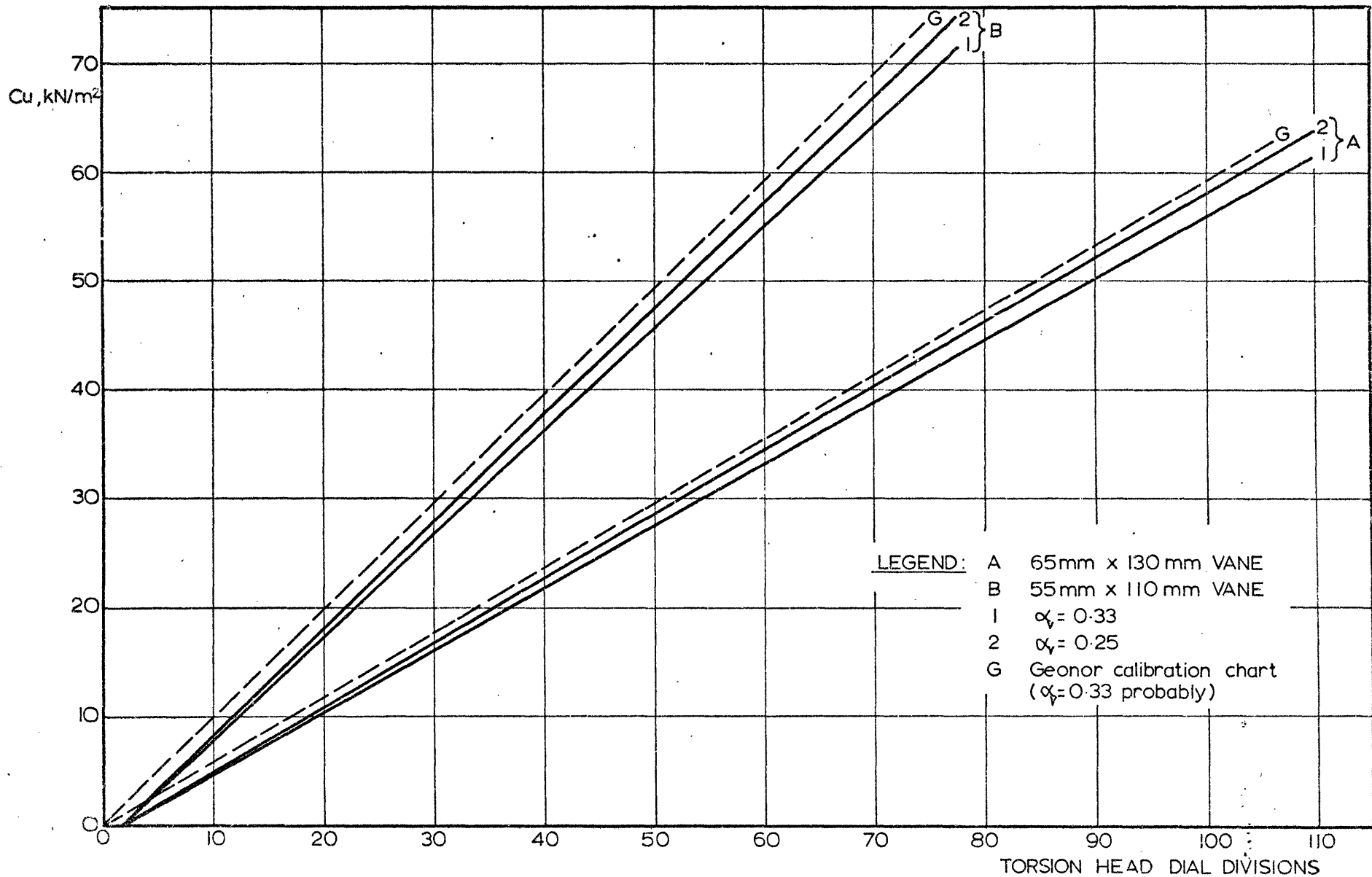


Fig. A. 2.2

CALIBRATION OF GEONOR VANE: TORQUE VERSUS DIAL DIVISIONS



CALIBRATION CURVE FOR GEONOR VANE



CALIBRATION OF GEONOR VANE: UNDRAINED STRENGTH VERSUS DIAL DIVISIONS

APPENDIX 3

ANISOTROPIC ANALYSES FOR FIELD VANE TESTS

A.3.1. ANALYSIS OF HORIZONTAL VANE TEST USING EQUATION 2.15 (See figure A.3.1.)

(i) The Cylindrical Surface

Although equation 2.15 has a wavelength of π , the half wavelengths ($\theta = 90^\circ$ to 0° and $\theta = 90^\circ$ to 180°) are identical and of the same sign, and it is thus only necessary to integrate over one quadrant and then summate for four quadrants. The axes in figure A.3.1., for this analysis represent principal stress directions and are rotated clockwise 30° ($90 - \beta = \alpha$) from those depicted in figure 3.8(C).*

Denoting the applied torque necessary to cause shear failure on the cylindrical surface by T_c , the analysis proceeds as follows:-

$$\begin{aligned}
 T_c &= 4 \cdot \frac{D}{2} \cdot \frac{H}{2} \cdot \frac{D}{2} C_{uv1} \int_0^{\frac{\pi}{2}} (1 - a \sin^2 \theta) (1 - b \sin^2 2\theta) d\theta \\
 &= D^2 H C_{uv1} \left[\int_0^{\frac{\pi}{2}} 1 \cdot d\theta - \int_0^{\frac{\pi}{2}} a \sin^2 \theta d\theta - \int_0^{\frac{\pi}{2}} b \sin^2 2\theta d\theta + \int_0^{\frac{\pi}{2}} ab \sin^2 \theta \sin^2 2\theta d\theta \right] \\
 &= D^2 H C_{uv1} \left[\theta - a \left[\frac{\theta}{2} - \frac{1}{4} \sin 2\theta \right] - b \left[\frac{\theta}{2} - \frac{1}{8} \sin 4\theta \right] + \frac{ab}{4} \left[\theta - \frac{\sin 2\theta}{2} - \frac{\sin 4\theta}{4} + \left(-\frac{1}{2} \sin 2\theta + \frac{1}{6} \sin 6\theta \right) \right] \right]_0^{\frac{\pi}{2}} \\
 &= D^2 H C_{uv1} \left[\frac{\pi}{2} - \frac{\pi a}{4} - \frac{\pi b}{4} + \frac{ab\pi}{8} \right] \\
 T_c &= \frac{\pi D^2 H C_{uv1}}{2} \left[\left(1 - \frac{a}{2}\right) \left(1 - \frac{b}{2}\right) \right]
 \end{aligned}$$

*as long as the complete half wavelength is integrated the solution is independent of the assumed axes and therefore of the assumption as to whether the cylindrical surface is a failure surface or a $\phi_u = 0$ surface.

(ii) The End Surfaces

For these $C_u = C_{uV}$ and thus $\alpha = 0^\circ$ (or 180°) and $\theta = 150^\circ$. Thus from equation 2.15:-

$$C_{uV} = C_{uV1} \left[\left(1 - \frac{a}{4}\right) \left(1 - \frac{3b}{4}\right) \right]$$

From Appendix 1 and equation A.1.1. the component of torque from the end surfaces, T_e , can be defined as follows:-

$$T_e = \frac{\pi D^3 \alpha_v \cdot C_{uV1}}{2} \left[\left(1 - \frac{a}{4}\right) \left(1 - \frac{3b}{4}\right) \right]^*$$

and therefore the torque developed in a horizontal vane test may be expressed as:-

$$T_{HOR} = T_c + T_e = \frac{\pi D^2 H C_{uV1}}{2} \left[\left(1 - \frac{a}{2}\right) \left(1 - \frac{b}{2}\right) + \left(1 - \frac{a}{4}\right) \left(1 - \frac{3b}{4}\right) \frac{\alpha_v D}{H} \right] \dots (A.3.1.)$$

which, for the case when $a = b = 0$ reduces to equation A.1.1 with $C_{uV} = C_{uH}$.

*Consideration of the vertical $\phi_u = 0$ plane (see figure 3.8(C)) leads to $\theta = 135^\circ$ and thus from equation 2.15:-

$$C_{uV} = C_{uV1} \left(1 - \frac{a}{2}\right) (1 - b)$$

If incorporated in equation A.3.1. this expression leads to a decrease in T_{HOR} of approximately 1%.

A.3.2. ANALYSIS OF HORIZONTAL VANE TEST USING EQUATION 2.15(A)(See figure A.3.1.)

(i) The Cylindrical Surface

In this case the axes in figure A.3 1. are as indicated, but with $\theta = \alpha$.
 Integration can again be carried out over one quadrant and summated.
 The substitution of α for θ can be seen from Appendix A.3.1. to lead directly to:-

$$T_c = \frac{\pi D^2 H \cdot C_{uV}}{2} \left[\left(1 - \frac{a_\alpha}{2}\right) \left(1 - \frac{b_\alpha}{2}\right) \right]$$

(ii) The End Surfaces

For the end surfaces $C_u = C_{uV}$ and thus:-

$$T_e = \frac{\pi D^3 \alpha_v C_{uV}}{2} \quad \text{which leads directly to:-}$$

$$T_{HOR} = \frac{\pi D^2 H \cdot C_{uV}}{2} \left[\left(1 - \frac{a_\alpha}{2}\right) \left(1 - \frac{b_\alpha}{2}\right) + \frac{\alpha_v D}{H} \right] \dots\dots\dots (A.3.1.(A))$$

which, for the case when $a_\alpha = b_\alpha = 0$ reduces to equation
 A.1.1. with $C_{uV} = C_{uH}$.

A.3.3. ANALYSIS OF HORIZONTAL VANE TEST USING EQUATION 3.3. (see figure A.3.1.)

(i) The Cylindrical Surface

The axes in figure A.3.1. represent principal stress directions, and integration over one quadrant, followed by summation to four quadrants is expressed as follows:-

$$T_c = 4 \cdot \frac{D}{2} \cdot \frac{H}{2} \cdot C_{uV1} \int_0^{\frac{\pi}{2}} \left[1 - \frac{2}{\pi} \theta r (1 - x) \right] d\theta$$

$$= D^2 H C_{uV1} \left[\theta - \frac{2}{\pi} \frac{\theta^2}{2} (1 - x) \right]_0^{\frac{\pi}{2}}$$

$$T_c = \frac{\pi D^2 H C_{uV1}}{2} \left[1 - \frac{1}{2} (1 - x) \right]$$

(ii) The End Surfaces

For the end surfaces $C_u = C_{uV}$ and $\alpha = 0^\circ$ (or 180°) and $\theta = 150^\circ$. As equation 3.3 only applies to one quadrant ($\theta = 0$ to 90°) $\theta \equiv 30 = \frac{\pi}{6}$ and thus:-

$$C_{uV} = C_{uV1} \left[1 - \frac{1}{3}(1 - x) \right]$$

and $T_e = \frac{\pi D^3 \alpha_V C_{uV1}}{2} \left[1 - \frac{1}{3}(1 - x) \right]$ which leads directly to:-

$$T_{HOR} = \pi D^2 H C_{uV1} \left[1 - \frac{1}{2} (1 - x) + (1 - \frac{1}{3}(1 - x)) \frac{\alpha_V D}{H} \right] \dots \dots \dots (A.3.2.)$$

which, for the case when $x = 1$, reduces to equation A.1.1. with $C_{uH} = C_{uV}$.

A.3.4. ANALYSIS OF HORIZONTAL VANE TEST USING EQUATION 3.3.(A)(See figure A.3.1.)

(i) The Cylindrical Surface

The axes in figure A.3.1. are as indicated, but with $\theta = \alpha$. From Appendix A.3.3. the substitution of α for θ can be seen to lead directly to:-

$$T_c = \frac{\pi D^2 H \cdot C_{uV}}{2} \left[1 - \frac{1}{2} (1 - x_\alpha) \right]$$

(ii) The End Surfaces

$C_u = C_{uV}$ and thus:-

$$T_e = \frac{\pi D^3 \alpha_v C_{uV}}{2} \text{ and therefore:-}$$

$$T_{HOR} = \frac{\pi D^2 H \cdot C_{uV}}{2} \left[1 - \frac{1}{2} (1 - x_\alpha) + \frac{\alpha_v D}{H} \right] \dots\dots\dots (A.3.2.(A))$$

which, for the case when $x_\alpha = 1$, reduces to equation A.1.1. with

$$C_{uH} = C_{uV}$$

A.3.5. ANALYSIS OF VERTICAL VANE TEST USING EQUATION 2.15

For the vertical surface:-

$\alpha = 0^\circ$ (or 180°) and $\theta = 150^\circ$. Thus from equation 2.15:-

$$C_{uV} = C_{uV1} \left[\left(1 - \frac{a}{4}\right) \left(1 - \frac{3b}{4}\right) \right]$$

For the horizontal surfaces:-

$\alpha = 90^\circ$ and $\theta = 60^\circ$. Thus from equation 2.15:-

$$C_{uH} = C_{uV1} \left[\left(1 - \frac{3a}{4}\right) \left(1 - \frac{3b}{4}\right) \right]$$

and therefore by direct substitution into equation A.1.1. (Appendix 1.)

$$T_{VER} = \frac{\pi D^2 H}{2} C_{uV1} \left[\left(1 - \frac{a}{4}\right) \left(1 - \frac{3b}{4}\right) + \frac{\alpha_V D}{H} \left(1 - \frac{3a}{4}\right) \left(1 - \frac{3b}{4}\right) \right] \dots\dots\dots (A.3.3.)$$

which for the case when $a = b = 0$ reduces to equation A.1.1 with $C_{uV} = C_{uH}$.

A.3.6. ANALYSIS OF COMBINED RESULTS OF HORIZONTAL AND VERTICAL VANE TESTS

From equation A.1.1., the torque developed in a vertical vane test, T_{VER} , can be expressed as:-

$$T_{VER} = \frac{\pi D^2 H C_{uV}}{2} \left[1 + \frac{\alpha_V D}{H} (1 - a_\alpha) \right] \dots\dots\dots (A.3.4.)$$

using equation 2.15(A), or using equation 3.3(A) as:-

$$T_{VER} = \frac{\pi D^2 H C_{uV}}{2} \left[1 + \frac{x \alpha_V D}{H} \right] \dots\dots\dots (A.3.5.)$$

As $x_\alpha = 1 - a_\alpha = C_{uH}/C_{uV}$ equations A.3.4., A.3.5. and A.1.1. are identical. If α_V , x_α and b_α are fixed then, for a particular vane size, it can be seen from equations A.3.1.(A), A.3.2.(A) and A.1.1. that:-

$$T_{HOR} = (\text{CONSTANT A}) C_{uV} \cdot \frac{\pi D^2 H}{2} \quad \text{and}$$

$$T_{VER} = (\text{CONSTANT B}) C_{uV} \cdot \frac{\pi D^2 H}{2}$$

where from a combination of equations A.3.1.(A) and A.3.4.

$$A = \left(1 - \frac{a_\alpha}{2}\right) \left(1 - \frac{b_\alpha}{2}\right) + \frac{\alpha_V D}{H} \quad \text{and}$$

$$B = 1 + \frac{\alpha_V D}{H} (1 - a_\alpha)$$

and using equations A.3.2.(A) and A.3.5.

$$A = 1 - \frac{1}{2} (1 - x_\alpha) + \frac{\alpha_V D}{H}$$

$$B = 1 + \frac{x_\alpha \alpha_V D}{H}$$

For both sets of equations the torque ratio from adjacent horizontal and vertical tests may be expressed as:-

$$\frac{T_{MAX} - T_{MIN}}{T_{MAX}} = \frac{A - B}{A} \quad (\text{when } T_{HOR} = T_{MAX}) \quad \text{or}$$

$$\frac{T_{MAX} - T_{MIN}}{T_{MAX}} = \frac{B - A}{B} \quad (\text{when } T_{VER} = T_{MAX})$$

It should also be noted that if horizontal and vertical tests are conventionally analysed (i.e. on the basis of isotropic undrained strength) then:-

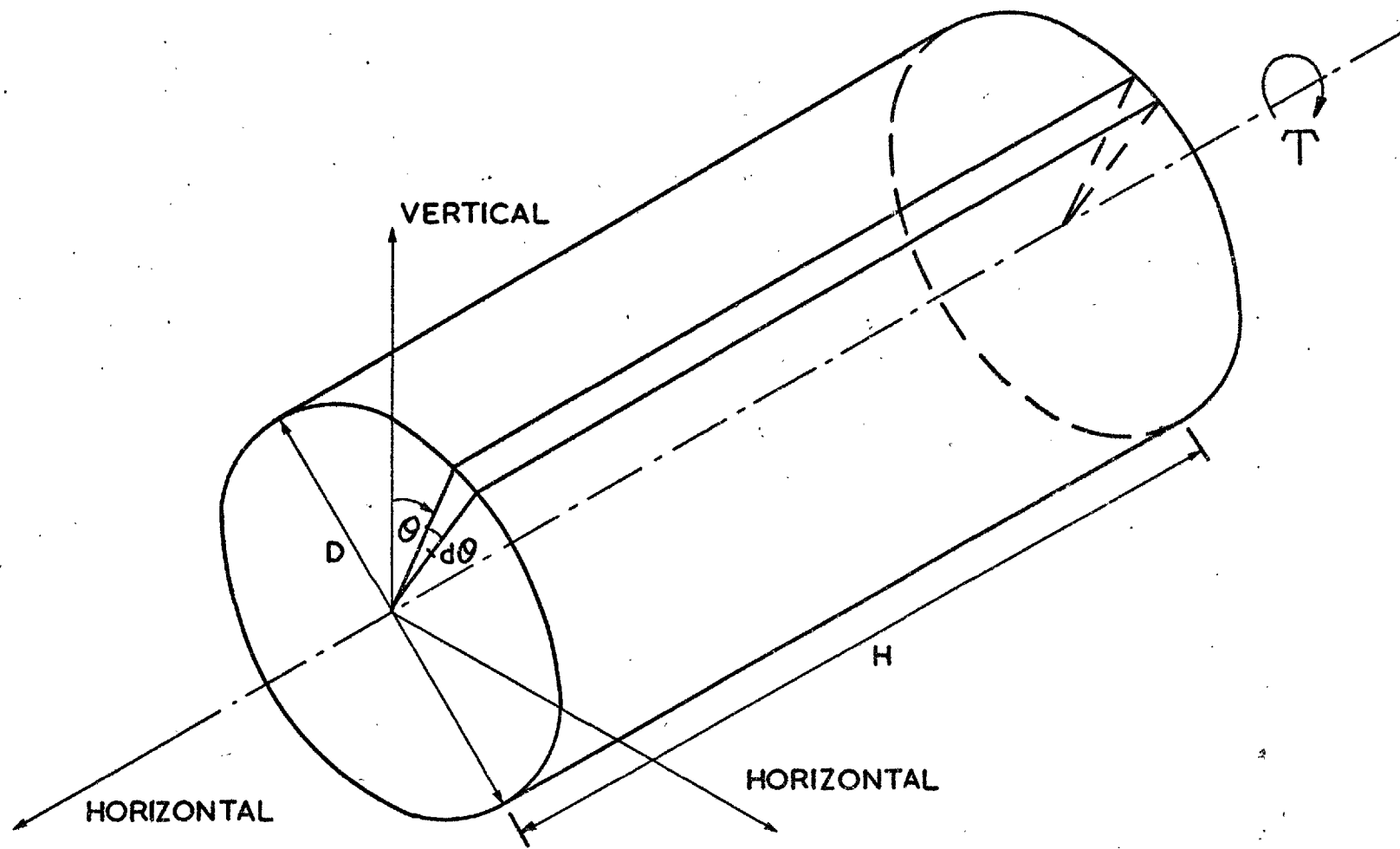
$$T_{HOR} = (\text{CONSTANT C}). C_{u.FV.(H)}$$

$$T_{VER} = (\text{CONSTANT C}). C_{u.FV.(V)}$$

where $C = \frac{\pi D^2 H}{2} \left(1 + \frac{\alpha_v D}{H} \right)$ and thus:-

$$\frac{T_{MAX} - T_{MIN}}{T_{MAX}} = \frac{C_{u.FV.(V)} - C_{u.FV.(H)}}{C_{u.FV.(V)}} \quad \text{or} \quad \frac{C_{u.FV.(H)} - C_{u.FV.(V)}}{C_{u.FV.(H)}}$$

Thus if α_v and b_α are assigned values the torque ratio can be directly related to C_{uH}/C_{uV} as presented graphically in figure 3.10. The value of b_α was taken as 0.065, which was the value of 'b' determined from the laboratory tests (section 2.7.3.). It should be noted that equations 2.15 and 2.15(A) do not revert to isotropic strength predictions unless b , and b_α , respectively are equal to zero. Thus when $b \neq a = 0$ equation 2.15 does not reduce to a circular arc on a polar diagram (figure 3.9). This has the effect that the torque ratio is zero (i.e. $T_{HOR} = T_{VER}$) when $C_{uH}/C_{uV} = 1.10$ (see figure 3.10), if the undrained strength anisotropy is represented by equation 2.15(A).



ANALYSIS OF HORIZONTAL VANE TESTS

Fig. A.3.1

APPENDIX 4

DESIGN, CONSTRUCTION, TESTING AND CALIBRATION OF THE LARGE VANE

APPARATUS

A.4.1. GENERAL

The apparatus was designed for use in soft clays only and as such a design soil shear strength of 36 kN/m^2 (750 p.s.f.) was adopted (C.P.2001, 1957). From equation A.1.2. this infers a design torque of 2.17 kN.m. (1600 lb. ft.).

A.4.2. DESIGN OF THE VANE

The design torque was assumed to be the summation of four equal components, and thus simply related to a total load on each vane blade. The assumption of a simple load distribution function enabled shear forces and bending moments to be calculated. Elastic bending theory showed that a maximum fibre stress of $158,000 \text{ kN/m}^2$ (23,000 p.s.i.) could be expected in vane blades constructed of 6.35mm (0.25 ins) thick mild steel plate. The properties of mild steel assumed for the overall design are presented in table A.4.1.

PROPERTY	VALUES	
	kN/m ²	P.S.I.
Youngs Modulus (E)	193×10^6	28×10^6
Shear Modulus (G)	69×10^6	10×10^6
Ultimate Tensile Strength	379,000	55,000
Yield Stress	248,000	36,000
Ultimate Shear Strength	241,000	35,000

Table A.4.1.

Properties of Mild Steel (after Shanley, 1957)

The 6.35mm mild steel plate was thus acceptable on the basis of ultimate strength and yield stress criteria. The rigidity of the blades under load was investigated by assuming each blade to be a cantilever, to which an equivalent point load was applied through the centroid of the loading diagram. A deflection of 1.02mm (0.04 ins) was predicted under a load corresponding to the design torque.

In order to test the design calculations with respect to both the strength and rigidity of the blades, a test piece of the 6.35mm steel plate was set up in cantilever and a line load appropriately applied to produce bending moments up to 2.5 x the design values. The plate behaved elastically throughout both the loading and unloading sequences, but the measured deflections were up to 30% higher than calculated. This discrepancy was thought to be mainly attributable to the inadequacy of the clamping arrangement at the cantilever support. However, if the whole of the difference was genuine deflection it would still only mean a maximum deflection for any vane blade of 1.33mm under the design loading.

A.4.3. CONSTRUCTION OF THE VANE

The vane was thus constructed from two pieces of 508(H) x 254(D) x 6.35mm mild steel plate, these being free from any twisting or warping. Each plate had a 6.35mm wide slot cut centrally over half its height, so that the pair could be slotted together to form a cruciform vane, the bottom of each plate being fashioned to form a knife edge. In addition a 66.675mm (2.625 ins) wide x 50.8mm (2 ins) deep slot was cut centrally in the top of each blade to accommodate the vane-rod adaptor. This was

a cylindrical (66.675mm diameter) piece of mild steel, with two perpendicular diametric 12.7mm (0.5 ins) deep slots cut into its base to locate it over the vane blades. A tapered central shaft (444.5mm (17.5 ins) long, tapering from 66.675mm to 6.35mm diameter) was made in sections from four pieces of square section mild steel. These were turned as one piece by clamping them to a pair of dummy 6.35mm thick plates.

The vane was constructed by welding the central tapered shaft to the blades and finally welding the vane-rod adaptor to the top of the assembly. To complete the vane a 0.4mm (0.015 ins) thick steel edging strip was bonded (with araldite) to the base of each vane blade face. This was to remould the clay passing over it and onto the blade faces during insertion, and hence facilitate the jacking of the vane into position. Having completed the manufacture of the vane it was rotated and checked to see if the blades were still true, which they were. The final vane configuration had an area ratio (measured at mid-height of the vane) of 7.4%.

A.4.4. DESIGN OF THE VANE RODS

Data on the specification of rotary core drilling rods were obtained from B.S.4019 (1966). These rods are made from EN.8.40 carbon, normalised steel (B.S.970, 1947; B.S.971, 1950) which has a yield stress of 276,000 kN/m^2 (40,000 p.s.i.) and an ultimate tensile strength of 538,000 kN/m^2 (78,000 p.s.i.). The strength properties used in the design (table A.4.1.) were thus slightly conservative for the drilling rods. An analysis of the suitability of 'W' series drilling rods

showed that under the design torque NW (66.675mm (2.625 ins) diameter) rods would be subjected to a maximum shear stress of $83,000 \text{ kN/m}^2$ (12,000 p.s.i.) which was judged to be acceptable. The twist, under this loading, however, was approximately $2^\circ/\text{metre}$ ($0.6^\circ/\text{ft}$) which is greater than recommended by the commonly adopted design rule that twist shall not exceed 1° in a length equal to 20 rod diameters. For any steel rod, assuming $G = 69 \times 10^6 \text{ kN/m}^2$ ($10 \times 10^6 \text{ p.s.i.}$) (table A.4.1.), this limits the shear stress to a maximum of $31,000 \text{ kN/m}^2$ (4,500 p.s.i.) which is possibly slightly conservative on a stress level basis. The torque in an N W drilling rod would be limited to 0.8 kN.m (600 lb. ft.) which is equivalent to a soil shear strength of 14 kN/m^2 (2.p.s.i.).

The next larger size of 'W' series rod is H W , which, at 88.9mm (3.5 ins) diameter was thought to be excessively heavy for the loads involved, although even this rod size would be subjected to a maximum shear stress of $34,000 \text{ kN/m}^2$ (4,900 p.s.i.) under the design torque and thus falls outside the limits imposed by the twist rule. As rotary drilling rigs used in this country commonly develop torques in excess of twice the vane design value, and are used in conjunction with all 'W' series drilling rods, NW rods were selected although the twists might be large at high torques. This decision was also influenced by three main factors, other than their size being compatible with that of the vane, namely:-

- (1) the low strength of the Mucking clay meant that the maximum shear stress developed in N W rods would not be greatly in excess of $31,000 \text{ kN/m}^2$.
- (2) it was anticipated using standard piston sample jacking equipment to advance the vane into position and this incorporates N W threads

- (3) rod twist only presented a problem regarding the travel of the loading system and hence the actual time to failure
- (4) if at any stage in the future the vane were to be used in firmer materials, and it was decided that the twist in N W rods would be excessive, H W rods could be used with the aid of two simple adaptors.

The vane-rod adaptor terminated in a male N W thread; the drilling rods having female threads at both ends are used in conjunction with 'double male' adaptors.

A.4.5. DESIGN OF THE LOADING FRAME AND TORQUE MEASURING SYSTEM

(i) General

The main aspects of field vane design were discussed in section 3.1.2., and in particular, the application and measurement of torque was covered in some detail in sub-section (iv). In common with previous borehole vane designs (Skempton, 1948(b); Gibbs, 1957; A.S.T.M., 1964) it was decided to derive the main reaction for the loading frame from the borehole casing. The standard American borehole vane design (A.S.T.M., 1964) has been shown in section 3.1.2 to have much to commend it, and a scaled-up version of the loading frame and torque measuring system used therein would have been very satisfactory for the new large vane. However, two main factors influenced the final design to a considerable extent, these being as follows:-

- (1) The calibration of the Geonor vane had shown the importance of correct calibration in vane testing, and the large vane would

thus need to be likewise calibrated. The use of a torsional load cell would enable the applied torque at the vane to be related to that applied by the loading frame. There was, therefore, no need to eliminate mechanical friction from the main torque measuring system, or to use sophisticated measuring systems in the field (as described by Weisel, 1973) in order to obtain good results. The adoption of standard drilling rods with well defined sectional and torsional properties also meant that the actual rotation of the vane could be calculated with reasonable accuracy, again without recourse to sophisticated on-site systems.

- (2) The design and construction of any new piece of equipment involves considerable financial outlay. It had to be borne in mind that the large vane test, because of the associated drilling costs, would be relatively expensive, compared to the Geonor vane test and, as such, would probably only be used on a limited number of occasions. The use of existing components enabled not only a cost saving but the construction of a very simple loading frame as shown in figure 3.11.

The loading system is best described by working around the system, starting at the uppermost N W drilling rod as follows. Reference should also be made to plates A.4.1. and 3.1. For any particular field test the top of the uppermost N W rod was at some distance between 1.436m (4.71 ft) and 38.1mm (1.5 ins) below the top of the borehole. The latter was in fact a 228.6mm (9 ins) long hanger head, this being a standard item of cable tool boring equipment. The rod sequence was completed, and brought above the top of the hanger head, by a 1.524m (5ft.) long, 63.5mm (2.5 ins) diameter, solid mild steel drive rod with a 1.486m

(4.875 ft) long, 8.73mm (11/32 ins) wide by 8.73mm deep vertical keyway, and male threads at either end. This passed through a circular borehole top plate, having an upper lip with an outer diameter equal to the O.D. of the hanger head (323.85mm (12.75 ins)) and the main body of which had an O.D. equal to the I.D. of the hanger head (304.8mm (12 ins)) into which it fitted. The drive rod was located at the centre of the borehole top plate within a self aligning ball race, which enabled the vane to operate (if so desired) even when the rod and plate were not at right angles. This part of the apparatus was completed by a 304mm (12 ins) pitch circle diameter (P.C.D.) plate wheel bolted to an annular, cylindrical (152.4mm (6 ins) O.D., 63.5mm I.D.) boss having a vertical British Standard Key (B.S.K. - 17.46mm x 17.46mm (11/16 ins x 11/16 ins)) running down its inner cylindrical surface. The boss and plate wheel fitted over the drive rod, with the key located in the keyway of the drive rod and the under-reamed base of the boss sitting on the housing of the borehole top plate central bearing. The bearing was fitted with removable rubber covers and packed with grease to prevent ingress of soil and water.

The loading frame was constructed from 76.2mm x 76.2mm (3 ins square) mild steel box section attached to a 304.8mm nominal diameter clamping ring, all joints being fillet welded. The frame was clamped to the top of the hanger head using this ring, as shown in figure 3.11 and plate A.4.1. The torque was applied to the drive rod, via the drive plate wheel, by the open ended main chain drive, the load in the chain being monitored by means of a proving ring and applied by a screw jack.

The proving ring can be seen to be loaded in tension and the ring mountings were modified to facilitate this, the original design being for compression. It was mounted within a yoke comprising a universal joint through which it was located to the loading frame by a horizontal (11.11m (7/16 ins) diameter) pin, held in place by circlips and therefore easily removed. The other end of the yoke was a rigid mounting for a 114.3mm (4.5 ins) P.C.D. plate wheel running on a needle bearing.

Having passed around the proving ring plate wheel, the drive chain can be seen to pass around a 114.3mm P.C.D. bearingless jockey wheel, attached directly to the loading frame by means of a vertical welded spindle. This jockey wheel aligned the drive chain with the axis of travel of the jack. The screw jack was of the conventional worm and wheel type and was mounted in a horizontal position on a vertical 19.05mm (0.75 ins) thick mild steel plate which was attached to the loading frame as shown in figure 3.11. Both the jack and proving ring were standard items of laboratory equipment.

(ii) Applied Forces and Component Specification

Figure A.4.1. shows a diagrammatic representation of the configuration used for the torque application. A list of all the components incorporated in the large vane design, together with their specifications is given in table A.4.2., while the individual items of the apparatus are also shown in plate A.4.1.

The design torque ($T = 2.17 \text{ kN.m}$) corresponds to a chain tension ' T ', where:-

$$T = \frac{T \times 2}{D_{DW}} = 14.24 \text{ kN compared to the chain's load capacity of } 26.69 \text{ kN}$$

(6000 lb f.), where D_{DW} is the drive wheel diameter. ' T ' is also the maximum load on the borehole top plate bearing, which likewise has a load capacity of 26.69 kN.

The load on the proving ring at anytime is ' P ', where:-

$P = 2.T.\cos 3^{\circ} 48' = 28.42 \text{ kN}$ maximum, compared to its nominal capacity of 26.69 kN. However, the proving ring assembly was successfully tested and calibrated to 29.89 kN (3 tons f.) as described in section A.4.7. (ii). The capacity of the needle bearing assembly for the plate wheel was 30.90 kN (7000 lb. f.) for static, and 31.88 kN (7,150 lb.f.) for dynamic, loading.

The load on the jackey wheel pivot is ' C ', where:-

$C = 2.T.\cos 46^{\circ} 54' = 19.46 \text{ kN}$ maximum, the capacity of this component being unknown, although an approximate analysis using elastic bending theory indicated it to be well below yield stress at this load.

The load on the jack was obviously equal to ' T ', and thus a maximum of 14.24 kN compared to its capacity of 29.89 kN. On the basis of the design calculations the individual components considered are suitable for loads developed when the vane is used in soils with shear strengths up to 36 kN/m^2 . For soil strengths greater than this it would appear inadvisable to use either the proving ring assembly or N W drilling rods.

A.4.6. DESIGN OF THE MECHANICAL DRIVE SYSTEM

The apparatus was intended to enable tests to be carried out both faster and slower than in the Geonor vane test, but predominantly interest was to be focused on the slower tests. Due to the inevitability of different rod twists etc., occurring in tests with the two types of vane, the rate of rotation of the large vane which could be readily applied manually was only approximately related to the 6° per minute of the Geonor vane test. In addition any manually controlled rate of rotation is by definition only approximate. Rotation of the large vane at a rate of 6° per minute corresponds to a travel rate of 15.96mm per minute for the jack. The gearing of the jack was such that one revolution of the handle (i.e. of the worm) produced 0.127mm (0.005 ins) travel of the shaft. Thus to produce a vane rotation of 6° per minute† required the worm to be rotated at 126 revolutions per minute (r.p.m.), this being approximately twice the 60 r.p.m. used for the Geonor apparatus.

The gear reduction between the main drive wheel and the crank handle is thus approximately 1:7500 (c.f. 1:3600 for the Geonor vane), this likewise being the reduction in torque between the two locations, only in the opposite sense. The torque at the jack handle corresponding to the design torque at the vane was therefore only 0.289 N.m. (0.2 lb.ft). The large vane apparatus is thus easily operated manually over the design range of soil shear strengths. The horse power (H.P.) required for its operation at this rate (which is close to the maximum required) under

† rod twist effects etc., being ignored.

design loading can be evaluated from the torque at the main drive wheel:-

$$\text{H.P.} = \frac{2.\pi.n.T}{33,000} = \frac{2.\pi.0.017.1600}{33,000} = 0.005$$

where 'n' is the r.p.m. at the drive wheel, or from the work done at the jack:-

$$\text{H.P.} = T \times \text{displacement rate of jack}$$

$$= \frac{3200 \text{ lb.} \times 0.0524 \text{ ft./min.}}{33,000} = 0.005,$$

these calculations being purposely performed in Imperial units for more ready comprehension.

A standard laboratory gearbox, driven by a 0.25 H.P. electric motor, was mounted with the main axis vertical (as opposed to horizontal in the laboratory) on a frame constructed from the same box section as the loading frame (see plate A.4.1.). The drive frame had two lugs on the base section which enabled it to be located correctly relative to the rear 'T piece' of the loading frame. The two frames were held together by a pair of G-clamps. Drive from the gearbox was by a closed secondary chain (17.79 kN (4000 lb.f.) capacity), there being a 2:1 reduction from the gearbox output plate wheel (127mm (5 ins) P.C.D.) to that mounted on the worm shaft of the jack. A readily removable chain guard, linking the jack to the gearbox, completed the assembly.

The mechanical drive system had 6 gears (numbered 1 to 6) each one being a reduction of 1/5 on the previous. This enabled the large vane to be motor driven over a range of angular rotations from approximately

1.5 x faster to 0.0048 x slower than the Geonor vane. Full details of the gearing and corresponding testing rates are given in table A.4.3.

A.4.7. TESTING AND CALIBRATION OF THE LARGE VANE APPARATUS

(i) Testing

Before using the equipment on site it was obviously desirable not only to test the components up to the design loads, but also to gain some experience handling, assembling and operating the equipment. The test set up is shown in plate A.4.1. A short (864mm (2ft. 10 ins)) length of casing was installed in a tank which was subsequently filled with dry sand, this then being vibro-compacted. The vane was connected directly to the drive rod by a double female adaptor (part of the vane equipment) and the assembly positioned vertically, and centrally, within the casing, the bottom 100mm or so of which had also been filled with sand. For the purpose of testing the design specification of the apparatus components the casing was filled with sand, whilst to simulate field tests a remoulded clay was used.

The use of the casing to resist the applied torsion means that the load frame tends to unscrew the hanger head from the uppermost piece of casing. To prevent this a pair of borehole casing clamps were tightened around the joint. The loading frame was lowered over the hanger head, but was not clamped onto it until the borehole top plate was in position. This is very important as the hanger head is easily distorted and even slight burrs prevented the top plate from fitting. The hanger head used for all the vane tests described in this thesis was specially machined to take the top plate and used only in

conjunction with the vane tests. The normal use of a hanger head in cable tool boring means that the loading frame as well as the top plate may not fit because of distortion and burring. This was only discovered during the testing operation and obviously saved subsequent trouble on site. The loading frame and drive frame were mounted on a tank as shown in plate A.4.1., for the purposes of testing and calibration.

The main drive wheel was fitted over the drive rod and lowered into position. Again the tolerances were such that the drive rod, the boss and the keyway system had to be kept clean and free from damage. The proving ring assembly was positioned on the frame using the locating pin and initially maintained slightly sub-horizontal by placing a support under the plate wheel yoke. This support was removed as soon as the proving ring rose clear of it during the test. The jack was set in the fully extended position, either manually or, preferably, using the mechanical drive. In order to connect the chain from the output plate wheel on the gearbox to that on the worm, it was necessary to tilt the drive frame forward. Having connected the chain, the drive frame was gently lowered back until the correct chain tension was achieved, and then held in position by means of wooden wedges. The assembly was completed by fitting the main drive chain from the jack around the jockey, proving ring plate and main drive, wheels. Final connection to the latter was made by means of a link which could be bolted to the plate wheel.

Before commencing a test the proving ring dial gauge was set to zero and the jack set in motion at the fastest rate (which was always used for

jack adjustment) until the dial gauge indicated that loading had commenced. At this point the jack was stopped, the appropriate gear selected and the test proper commenced. Laboratory tests were carried out, both manually and mechanically, with perfectly satisfactory results, but the strength of the soils used limited the tests to an applied torque of 1.6 kN.m.

One of the problems anticipated in the field operation of the vane was the 'breaking' of the drilling rods after tests involving high torques. In normal drilling practice this is achieved by the drilling machine operating in reverse, but for the field vane would have to be done manually, using chain wrenches. This was perfectly satisfactory for the drilling rods but not for the drive rod which would have been damaged by wrenches. Experimentation with the laboratory set up showed that, as with conventional drilling practice, the main drive wheel operated in reverse could be used to unscrew the drive rod. Rather than use the jack to pull directly on the wheel (in which case the applied forces would not be known) a long piece of steel angle section was bolted onto the top of the drive wheel. This enabled two people to readily 'break' the joint when the next rod down was securely clamped.

The apparatus was found to be easily set up and handled. Two people could lift the loading frame and manhandle the drive frame, although three to four people are necessary to lift and transport the latter any distance.

(ii) Calibration

(a) The Proving Ring Assembly.

This was tested in its entirety (i.e. the ring, its mountings, the yoke, the plate wheel and its needle bearing, and the locating pin) in an Amsler (35 ton) testing machine. The assembly was located to the testing rig by means of the actual frame locating pin at one end, the plate wheel load being applied through a length of the main drive chain looped around another pin at the other end. The proving ring assembly was thus loaded in tension up to 29.89 kN and the chain, therefore, to 14.945 kN. The calibration was carried out, in 2.5 kN (0.25 tons. f.) intervals of loading and unloading, three times and the average loading and unloading results are shown in figure A.4.2., where load is plotted against the proving ring deflection (the dial gauge on the ring was calibrated in 0.0001 ins divisions). The related calibration curves for the proving ring are presented in figure A.4.3., wherein the calibration factors can be seen to vary over the whole loading range. The proving ring is best suited for loads in excess of 4 kN, which corresponds to an apparatus torque of 0.3 kN.m and a soil shear strength of 5 kN/m². Below these figures the results cannot be expected to be very accurate. The results show the proving ring to be suitable for accurate measurement of loads from 4 kN up to design loads.

The torque applied to the drive wheel can be calculated from the results presented in figure A.4.3. using the expression:-

$$T = \frac{\text{Proving Ring Dial Divisions} \times \text{C.F.}}{2 \times \cos 3^{\circ} 48'} \times \frac{D_{DW}}{2} \dots\dots\dots(\text{A.4.1.})$$

where C.F. is the proving ring calibration factor (see also figure A.4.1.). The use of this expression to predict the torque at the vane itself is in error by an amount equal to the torsional component of the friction force in the top plate bearing and any other frictional forces (e.g. rod skin friction).

(b) The Torsional Load Cell

In order to calibrate the apparatus as a whole a simple torsional load cell was developed (figure A.4.4.). This consisted of a 228.6mm (9 ins) long tubular mild steel N.W. section, with female threads at either end and the central, 76.2mm (3 ins) long, section turned down to an O.D. of 61.976mm (2.440 ins) and an I.D. of 51.562mm (2.030 ins). On the circumferential centre line of the central section two micro-measurement foil gauges were bonded diametrically opposite each other, using 'M-bond 610' adhesive. These strain gauges were designed particularly for the measurement of strains resulting from pure torsion, each 'gauge' consisting of two orthogonal gauge wires such that each was at 45° to the axis of the load cell. Thus each gauge comprised one tension and one compression element, the total configuration being wired into a full bridge circuit. The gauges were type EA-06-125TH-120 (manufactured by Welwyn Electrics Ltd), these being mild steel temperature compensated, with a gauge factor of 2,065. The load cell output was monitored directly in microstrain ($\mu\epsilon$) on a standard readout unit.

When the load cell is subjected to a pure torsion the tension and compression gauge elements are respectively subjected to the major and minor principal strains (tension +ve), these being of equal magnitude

and opposite sign, and thus half the maximum shear strain. From a consideration of the test piece geometry and elastic theory it can be shown that the design torque corresponds to a maximum shear stress of $88,600 \text{ kN/m}^2$ (12,850 psi), and thus a maximum shear strain of $1285\mu\epsilon$ (G' as in table A.4.1.) and a maximum principal strain of $642.5\mu\epsilon$. Conforming to the limit on twist of 1° per 20 diameters has been shown to limit the maximum shear stress to $31,000 \text{ kN/m}^2$, and hence the maximum shear and principal strains in the load cell to 450 and $225\mu\epsilon$ respectively. The strain gauge configuration was such that the potential drop across the bridge circuit was proportional to the strain in any one gauge, although this was magnified by a factor of 4 on the readout.

The load cell was calibrated in an Avery (30,000 lb. in.) torsion machine to a torque of approximately 1.4 kN.m producing a shear strain of about $700\mu\epsilon$ and therefore a gauge strain of $350\mu\epsilon$ and a readout of $1400\mu\epsilon$. This corresponded to a maximum shear stress of $48,300 \text{ kN/m}^2$ (7000 psi) in the load cell and a soil shear strength of 22.5 kN/m^2 . The load cell behaved perfectly elastically during the calibration, which was carried out, in 0.113 kN.m (1000 lb. in.) intervals of loading and unloading, twice. Before calibration, the load cell was cyclically loaded a number of times to check for any hysteresis effects, but none were observed. From a consideration of the shear strain - torque relationship obtained it is possible to calculate a value of ' G' ', this being $82 \times 10^6 \text{ kN/m}^2$ ($12 \times 10^6 \text{ psi}$), again indicating that the design parameters were slightly conservative.

The loading and unloading results of torque versus output are presented in figure A.4.5. whilst the calibration curves are plotted in figure A.4.6. The calibration factors are constant above 550 $\mu\epsilon$ output and well defined down to 200 $\mu\epsilon$ output, the latter corresponding to a torque of 0.2 kN.m and a soil shear strength of 3 kN/m². Again below these values accurate results cannot be expected. The overall results from the torsional load cell calibration are very good and its performance, which was also compatible with that of the proving ring, more than justified the decision to use this means of measuring the torque applied to the field vane.

The calibration of the load cell was to sufficiently high torques for the use of the vane in the Mucking clay, whereas for future use in firmer materials further calibration would be required. The design calculations suggest that the load cell capacity is compatible with the design torque although quite large twists would result.

(c) The Vane Apparatus

The vane was set up in the laboratory in exactly the same way as described in the section on testing, except that the mechanical drive was not used. The double female adaptor, between the vane and drive rod, previously used was replaced by the torsional load cell. This was fitted with a thin steel cover to protect the strain gauges, there being a small slot through which the gauge wires passed. These were taken out of the casing, by way of the hole in the hanger head, and connected to the readout unit (plate A.4.1.). The calibration was carried out, in 0.0050 inch loading and unloading increments of the proving ring dial gauge, twice and the average loading and

unloading values of torque are plotted versus proving ring dial divisions in figure A.4.7. Also shown in this figure is the average applied torque derived from equation A.4.1., the difference between the torques being the frictional component of the top plate bearing. This increases with load to a maximum of about 10% at the maximum calibration torque of nearly 1.4 kN.m, the apparatus as a whole being calibrated over the same torsion range as the load cell.

The loading and unloading calibration factors for the apparatus are shown in figure A.4.8., best fit lines having been drawn through the results. The wavy nature of the variation between calibration factor and torque level is due to the calibration factor for the whole apparatus reflecting the calibration curves for the proving ring (figure A.4.3.) and the torsional load cell (figure A.4.6.). The average calibration factor for the vane apparatus derived from figure A.4.7. (using the torsional load cell results) is 1.885 N.m. per dial division compared to 2.04 N.m. per dial division if the average factor is derived from equation A.4.1. (as represented in figure A.4.7.). The bearing friction thus makes a significant contribution to the applied torque and must be taken into account in any calculations to derive soil shear strength values.

The calibration factors for the vane apparatus are well defined down to 100 proving ring dial divisions (figure A.4.8.), thus corresponding to approximately the same limits of accuracy as the torsional load cell and the proving ring, as might be expected. The range of soil strengths measured with the large vane at Mucking corresponded to proving ring

readings of between 200 and 600 divisions; the apparatus was therefore entirely functioning on the well defined part of the 'torsional' calibration characteristics. In addition, typical remoulded strengths, measured in the laboratory and with the Geonor vane, would produce readings of between 75 and 125 divisions, these corresponding to reasonably well defined calibration factors. The apparatus is thus superior in this respect to the Geonor vane (see figure A.2.3.) and should enable accurate determinations of remoulded strength values as low as 2.5 kN/m^2 .

(iii) Calculations

(a) Mobilised Shear Stress in Soil

From equation A.1.1. for an isotropic soil, the mobilised shear stress at any stage of a large vane test can be evaluated as follows:-

$$\tau_{\text{MOB}} = 16.650 \times 10^{-3} \times \text{C.F.} \times \text{proving ring dial divisions, where}$$

$$\alpha_v = 0.33$$

or

$$\tau_{\text{MOB}} = 17.265 \times 10^{-3} \times \text{C.F.} \times \text{proving ring dial divisions, where}$$

$$\alpha_v = 0.25$$

and C.F. is the appropriate calibration factor (figure A.4.8.) in N.m. per dial division, τ_{MOB} being in kN/m^2 .

For field use a calibration chart relating C_u to proving ring dial divisions has been prepared (figure A.4.9.). The values of C_u obtained therefrom relate to the average calibration factor of 1.885 N.m per dial

division and therefore closely approximate to the rigorously obtained values over most of the testing range. Typically for a proving ring reading of 350 divisions (either loading or unloading) the error incurred by using figure A.4.9. as opposed to figure A.4.8. would be 1%.

(b) Angular and Circumferential Displacement of Vane

The circumferential displacement of the vane (d_c) is given as follows:-

$d_c = \frac{D}{D_{DW}} \times d_{DW}$ where d_{DW} is the circumferential displacement of the drive wheel and may be expressed as follows:-

$d_{DW} =$ Travel of jack-rod twist component of travel -

$\frac{2 \times (\text{proving ring dial divisions})}{\cos 3^\circ 38'}$ - displacement due to other causes

The displacements due to other causes comprise such things as bending of the vane blades (which has been shown to result in a maximum displacement of the order of 1mm, and for the Mucking clay even less) and the various pivots plus chain stretch etc. These might be expected to be insignificant compared to the first three components influencing d_{DW} , which may thus be expressed as above but ignoring the last term, to a good approximation. The circumferential displacement and hence the true angular rotation of the vane can thus be calculated as follows:-

$$\omega_o = \frac{2 \cdot d_c}{D} \text{ radians}$$

The travel of the jack is simply calculated from table A.4.3. and the rod twist may be evaluated for any torque directly from figure A.4.10.,

wherein the cumulative rod twist for various standard combinations of N W drilling rods is presented as a function of torque. The rod twist (G assumed as in table A.4.1.) has also been expressed for convenience as an equivalent component of d_{DW} (i.e. as an equivalent jack travel or chain displacement).

ITEM NO.	DESCRIPTION/SPECIFICATION
1	254mm(D) x 508mm(H) vane with male NW vane-rod adaptor.
2	double female NW adaptor.
3	torsional load cell and adaptors for torsional calibration machine.
4	1.524m long x 63.5mm dia. drive rod.
5	borehole top plate with self aligning ball race (S.K.F., No. RM20, capacity 26.69 kN).
6	305mm P.C.D. drive plate wheel (Renold, No.219620, 19.05mm pitch) attached to boss (152.4mm OD., 63.5mm ID) with fitted B.S.K.
7	main drive chain (Renold, No.110066, 19.05mm pitch, capacity 26.69 kN) plus connecting links, connecting plate and nut/bolt for latter.
8	Loading frame complete with screw jack (capacity 26.89 kN), handle and 63.5mm P.C.D. plate wheel (Renold, No.213461, 12.7mm pitch) and nuts/bolts/washers (2 sets) for the clamping ring.
9	29.89 kN capacity proving ring assembly, comprising the ring with tension mountings, universal joint assembly, yoke and the 114.3mm P.C.D. plate wheel (Renold, No.213461, 19.05mm pitch) mounted on a needle bearing (INA No. NA6905, static capacity 30.90 kN), plus locating pin and circlips.
10	0.25 H.P. electric motor (Hoover, No.22519HA) plus integral gearbox (S.E. Opperman Ltd. No.61F1042) and 6 speed gearbox complete with output wheels and 127mm P.C.D. drive plate wheel (Renold, No.219058, 12.7mm pitch) mounted on drive frame.
11	2 G-clamps for locating item 10 to item 8.
12	secondary drive chain (Renold, No.110046, 12.7mm pitch, capacity 17.79 kN) plus connecting links.
13	chain guard for item 12.
14	dynamic drive head with male N W thread
15	wooden borehole top plate.

Table A.4.2.

Inventory of Large Vane, and Ancilliary, Equipment

POSITION (COG NO) Δ	R.P.M. OF JACK PLATE WHEEL	DISPLACEMENT RATE OF CHAIN		DISPLACEMENT RATE OF VANE [†] CIRCUMFERENCE*		ω_{LV}	$\frac{\omega_{LV}}{\omega_{GV}}$
		ins/min	mm/min	ins/min	mm/min	°/min	
1	190	0.9500	24.13	0.7917	20.108	9.05	1.5
2	38	0.1900	4.826	0.1583	4.022	1.81	0.3
3	7.6	0.0380	0.965	0.0317	0.804	0.363	0.06
4	1.5	0.0076	0.193	0.0063	0.161	0.0726	0.012
5	0.3	0.0015	0.039	0.0012	0.032	0.0145	0.0024
6	0.06	0.0003	0.0078	0.0002	0.006	0.0029	0.00048

Nomenclature

- Δ Position 2 corresponds to standard rate for large vane
- [†] No account taken of rod twist in these calculations
- * Rate of circumferential displacement of Geonor vane (65(D) x 130(H)mm) rotated at 6°/min is 3.4 mm/min.

LV Large Vane
GV Geonor Vane

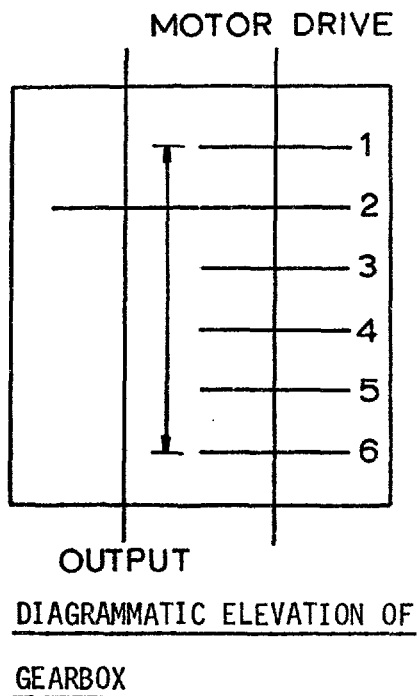


Table A.4.3.

Gearbox Calibration For Large Vane Apparatus

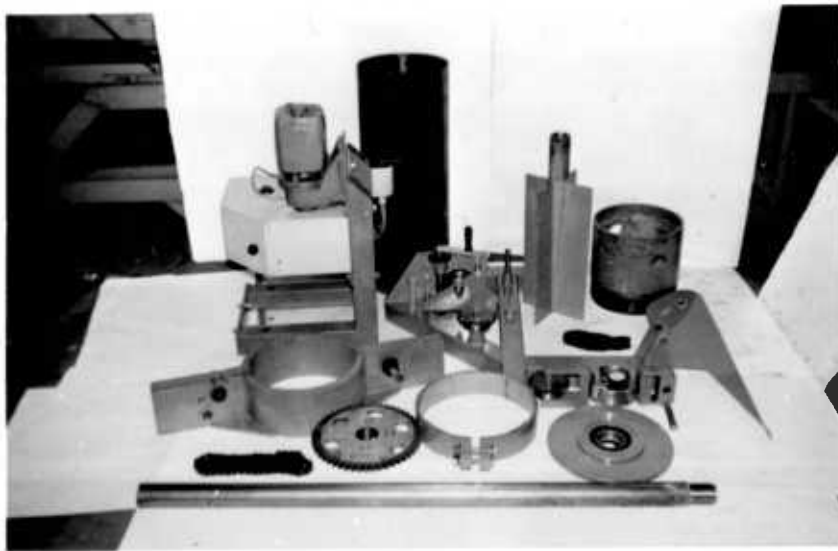
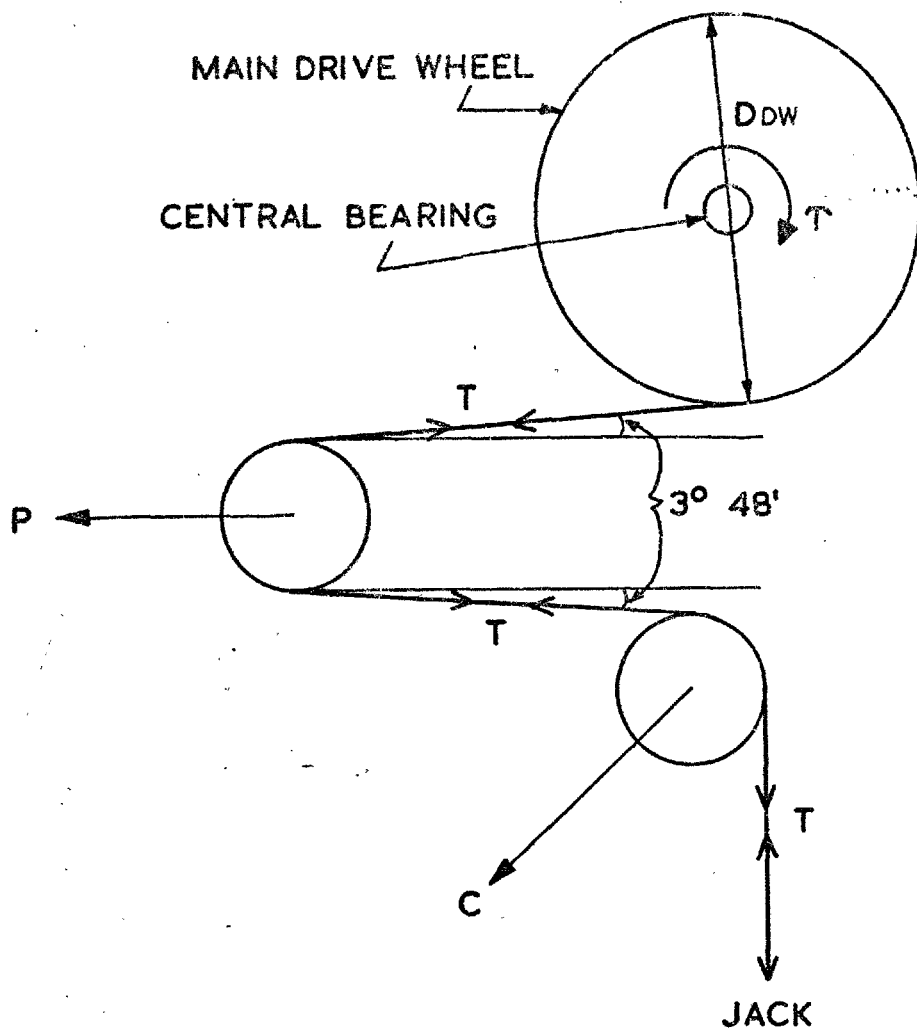


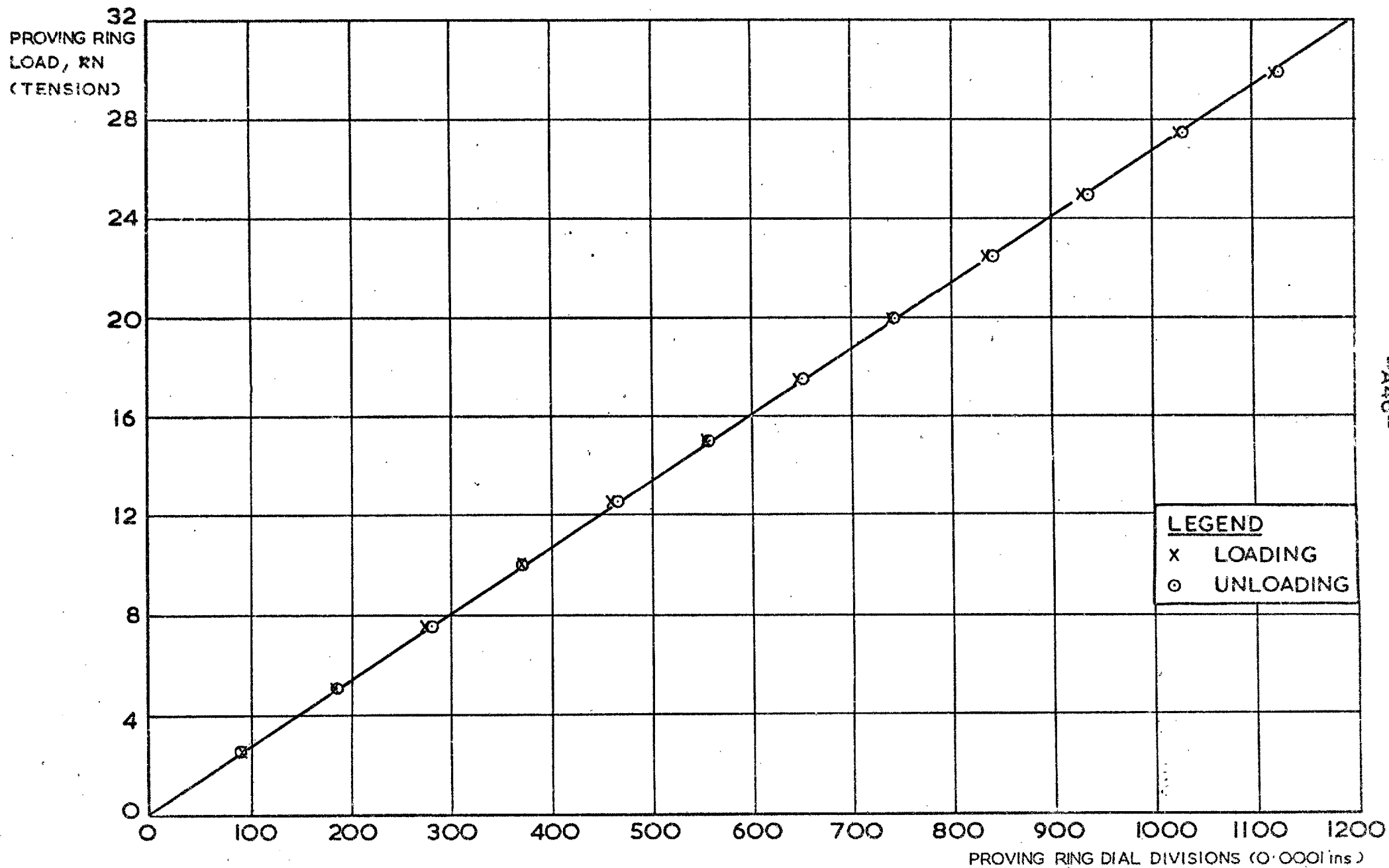
PLATE A.4.1 TESTING AND CALIBRATION OF LARGE VANE



<u>LEGEND</u>	
T	APPLIED TORQUE
P	PROVING RING LOAD
T	CHAIN TENSION
C	JOCKEY WHEEL PIVOT LOAD

LARGE VANE APPARATUS FORCES DEVELOPED DURING TORQUE APPLICATION

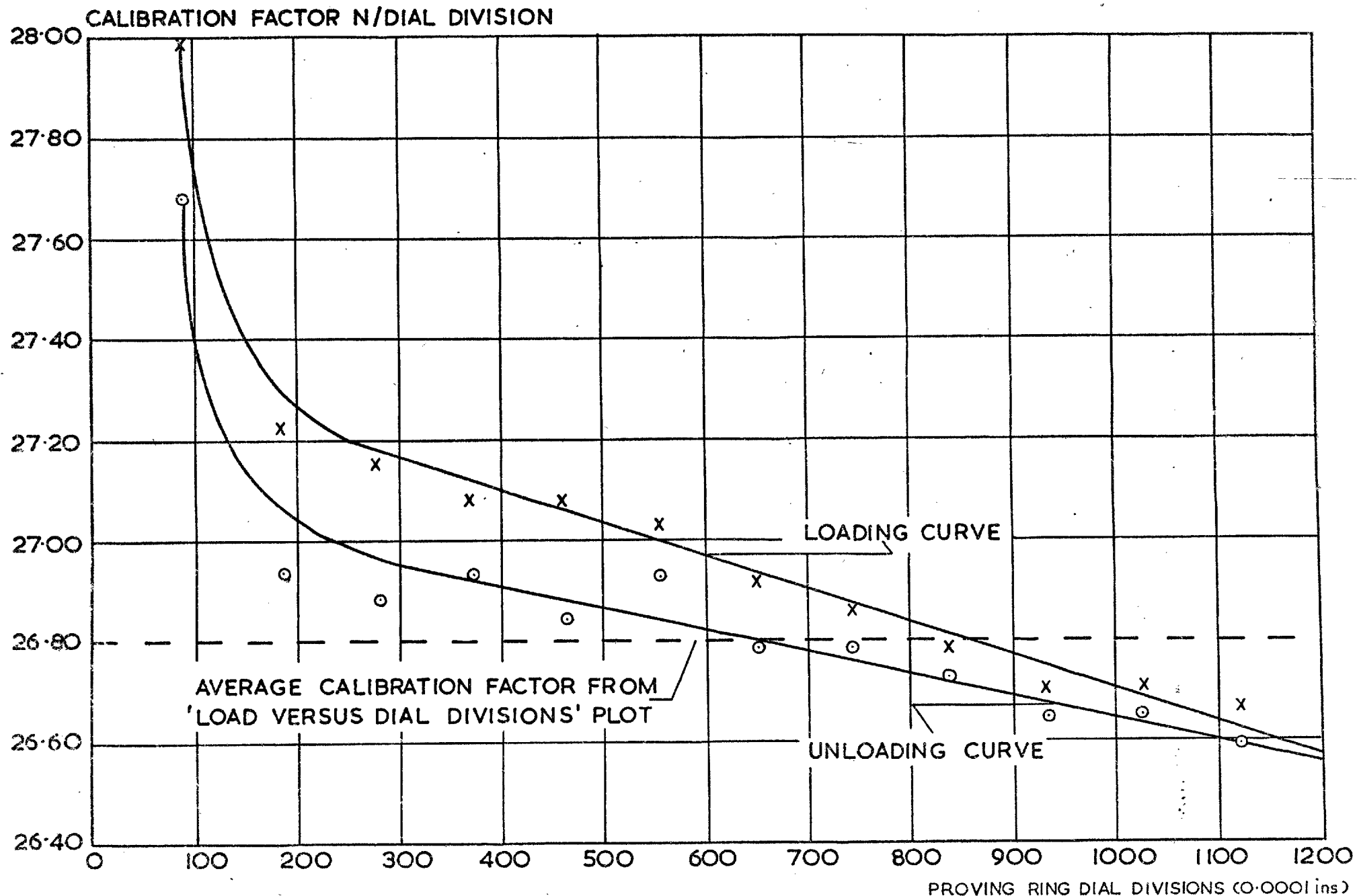
Fig.A.4.1



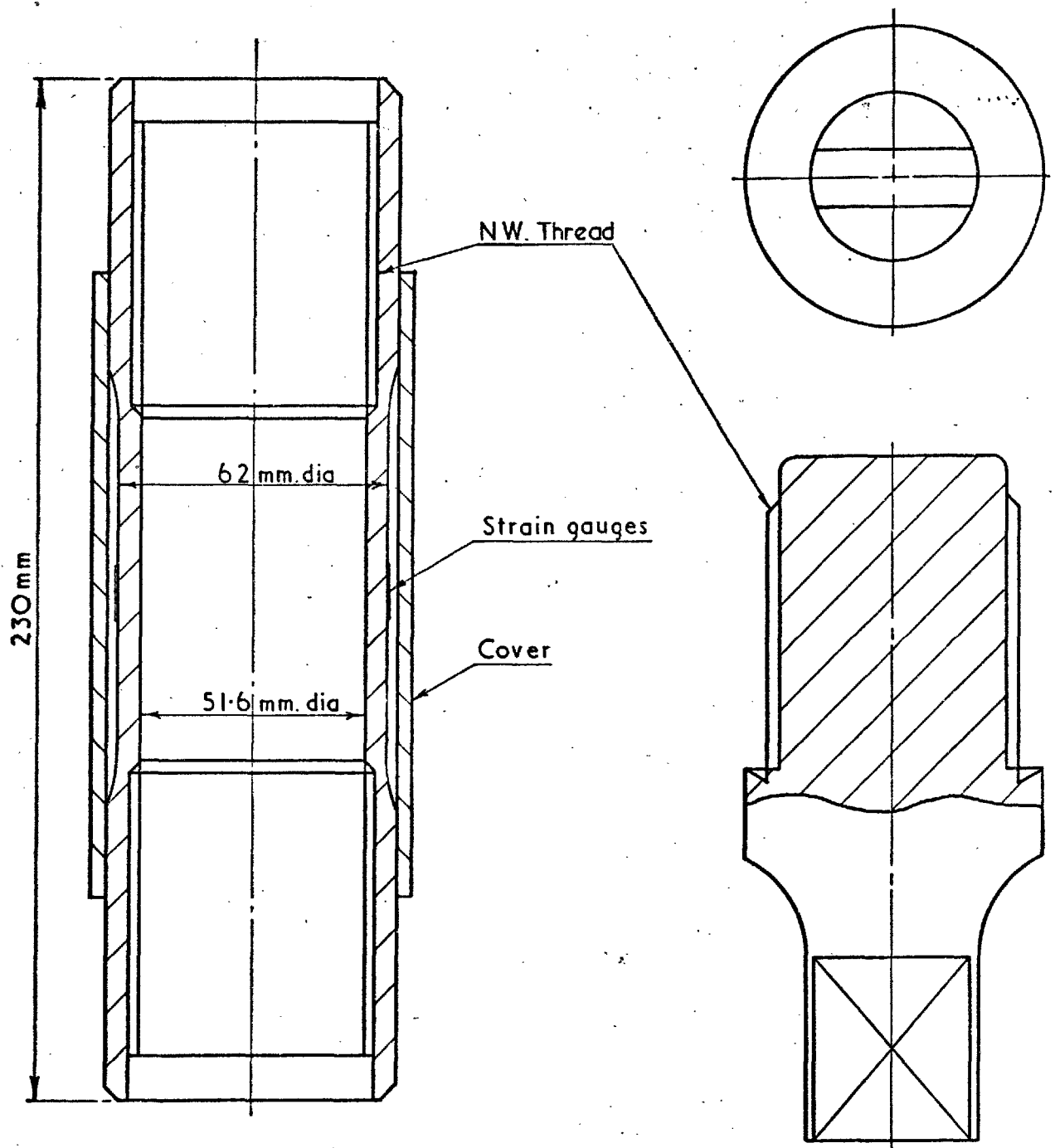
--A46--

Fig. A.4.2

CALIBRATION OF PROVING RING : LOAD VERSUS DIAL DIVISIONS

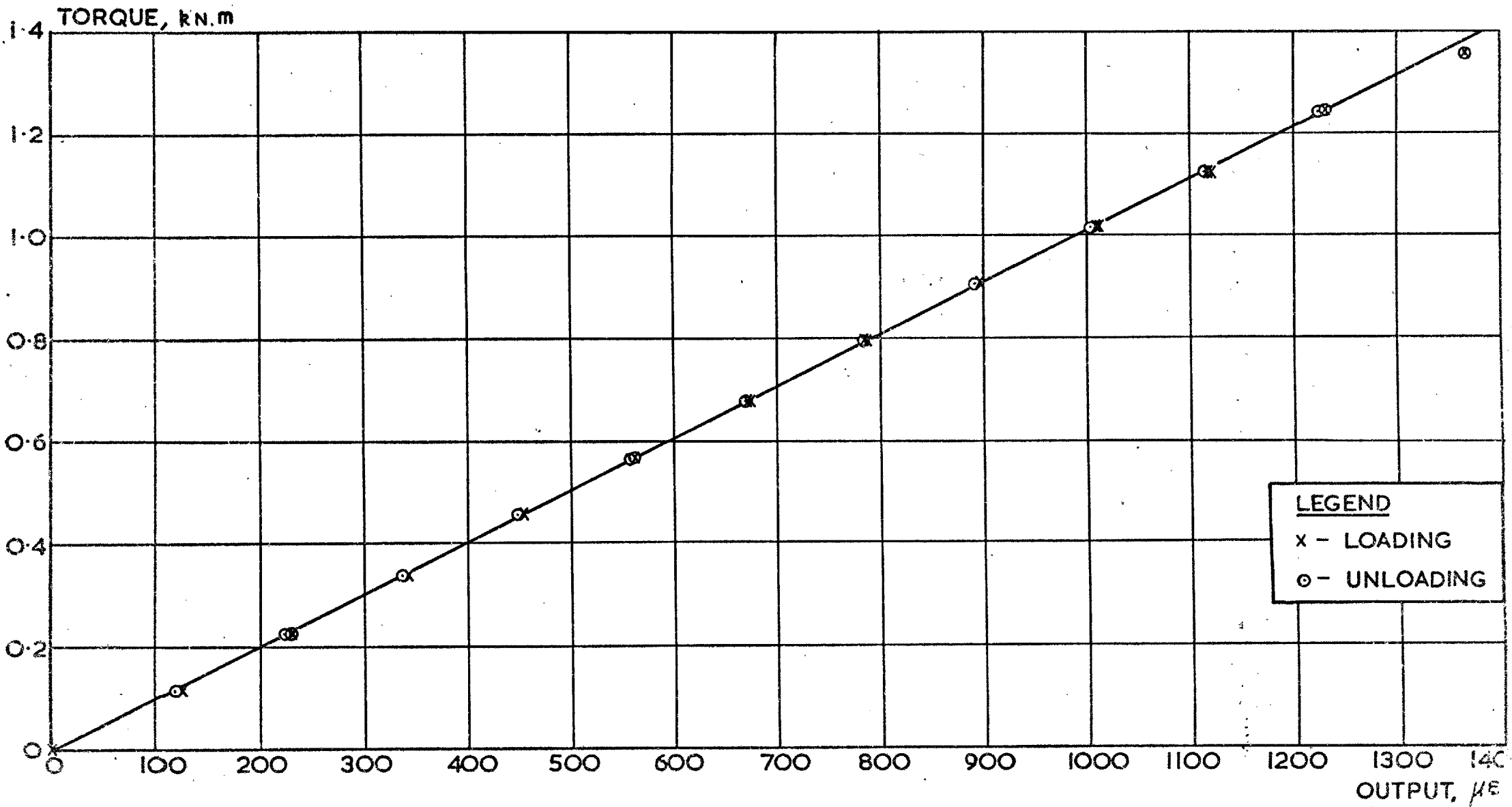


CALIBRATION CURVES FOR PROVING RING



TORSIONAL LOAD CELL

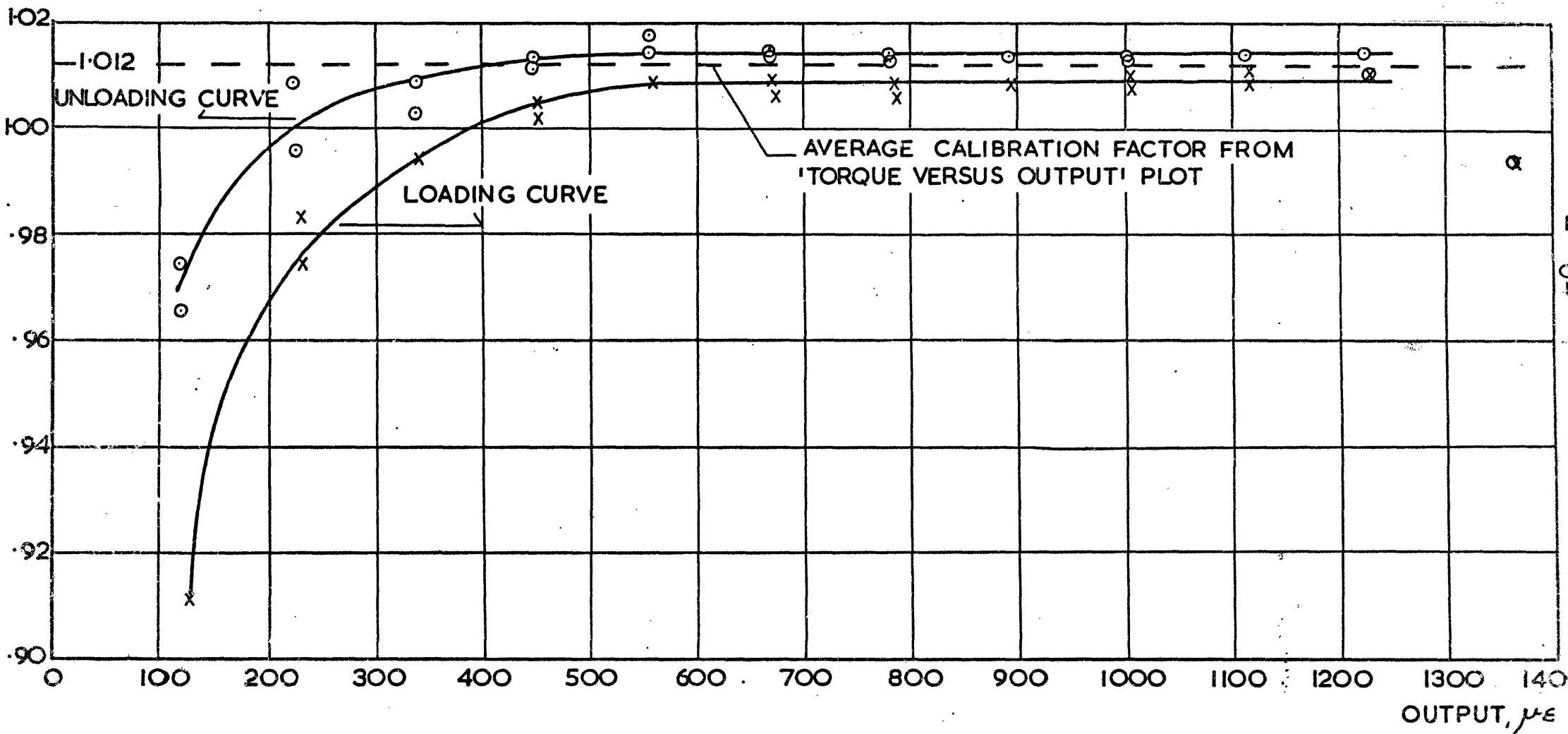
ADAPTORS FOR CALIBRATOR



CALIBRATION OF TORSIONAL LOAD CELL: TORQUE VERSUS OUTPUT (μE)

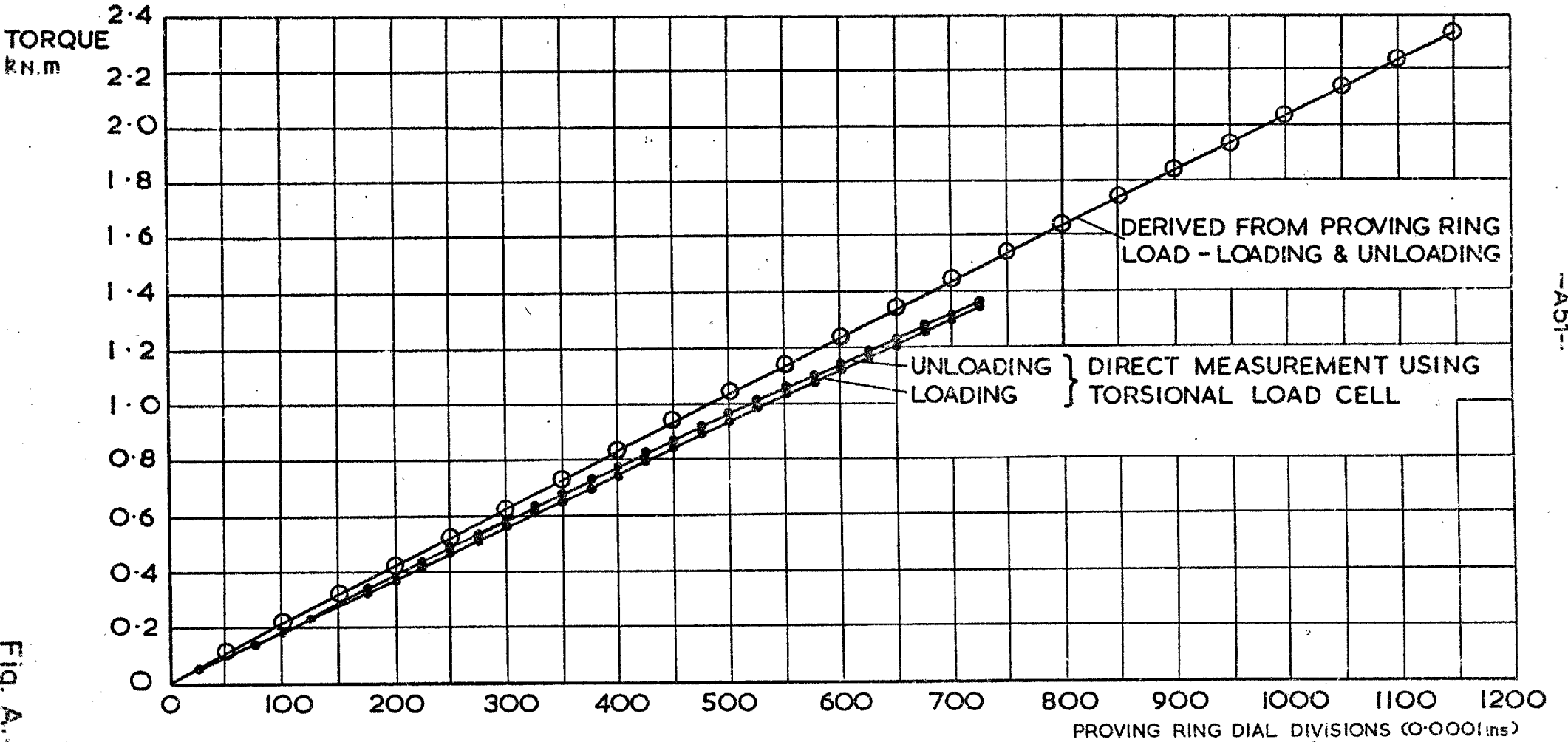
Fig. A.4.5

CALIBRATION FACTOR Nm/ $\mu\epsilon$



CALIBRATION CURVES FOR TORSIONAL LOAD CELL

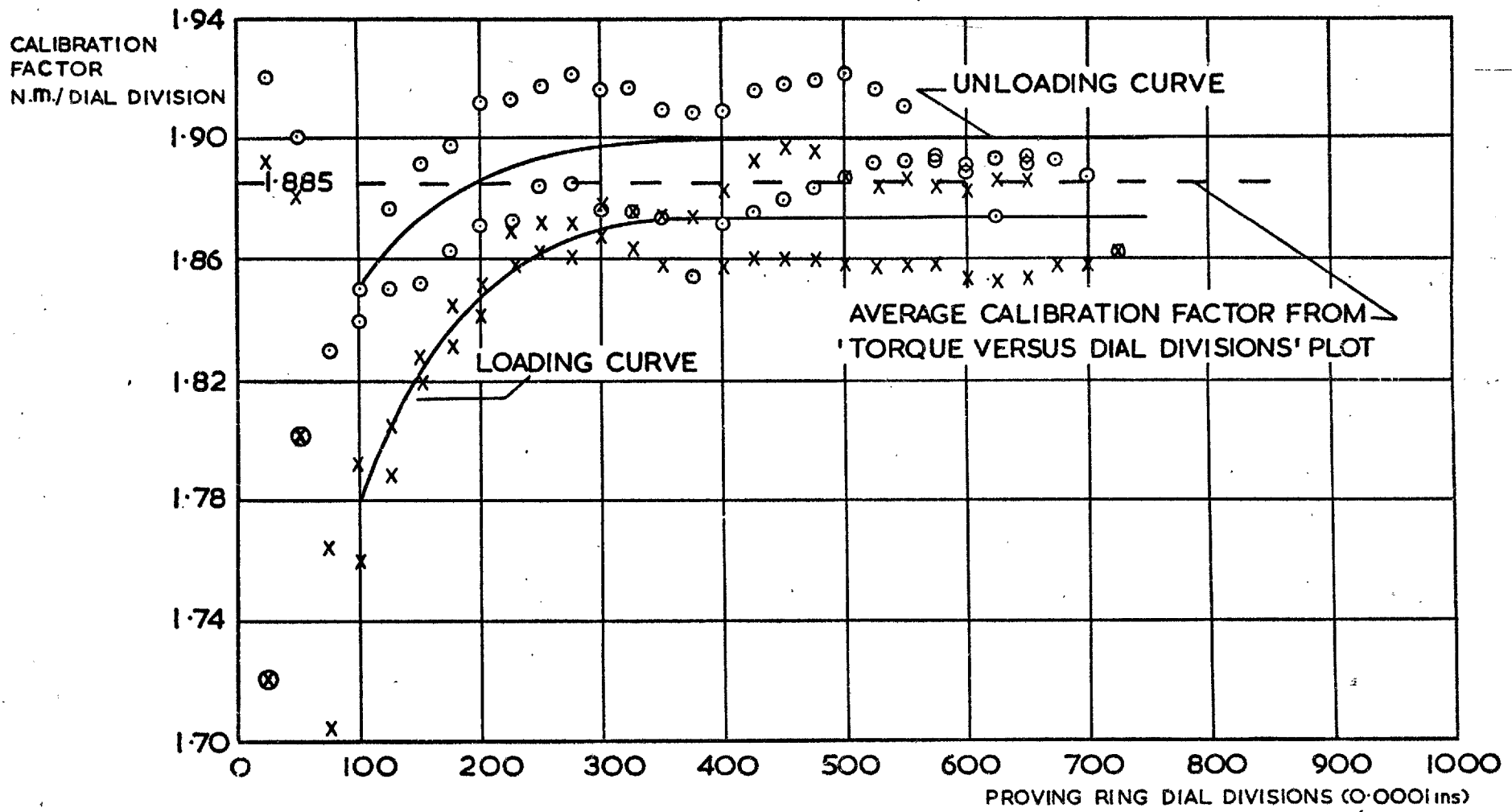
Fig. A. 4.6



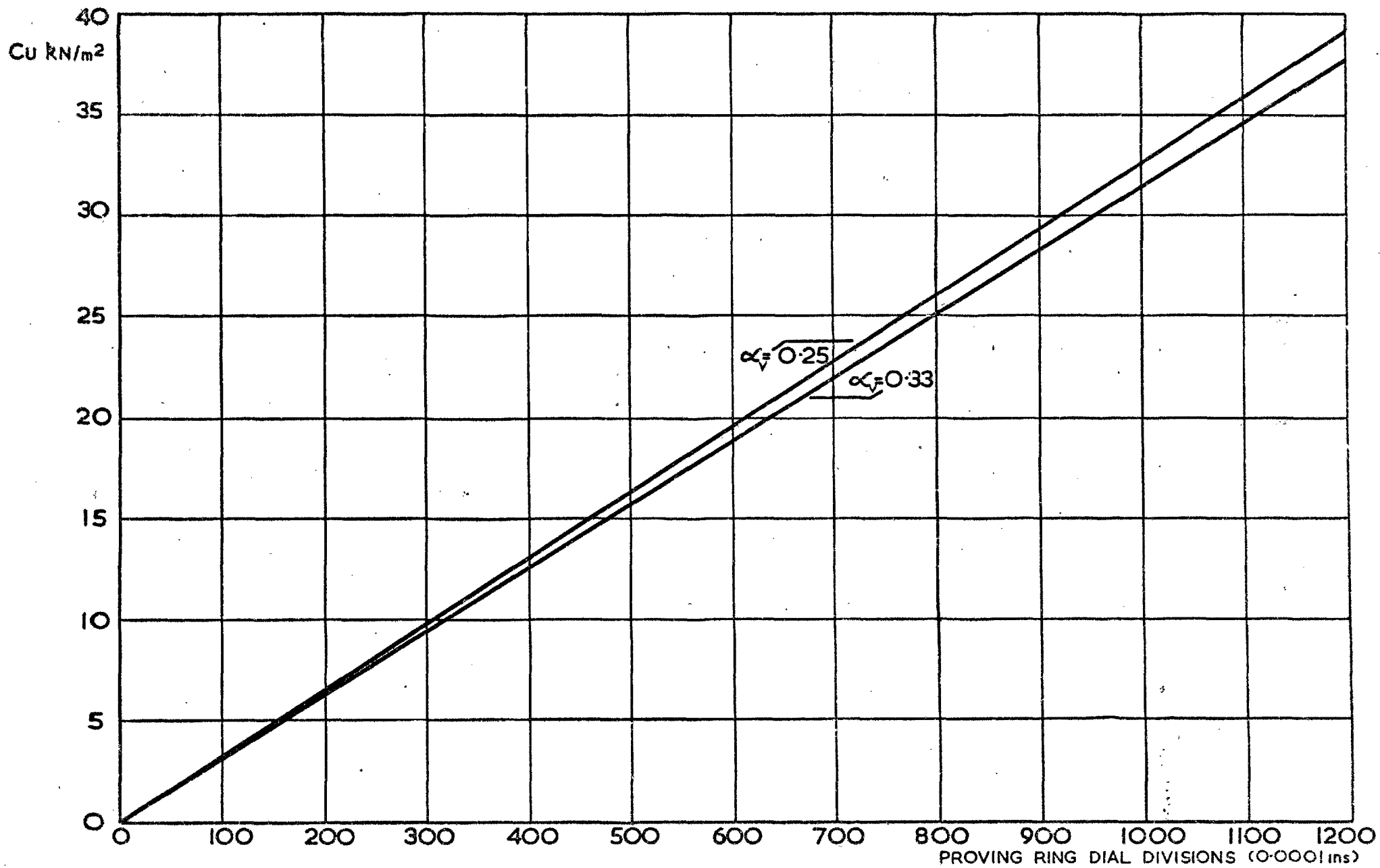
-A51-

Fig. A.4.7

CALIBRATION OF 254 x 508mm VANE EQUIPMENT : TORQUE VERSUS DIAL DIVISIONS



CALIBRATION CURVES FOR 254x508mm VANE EQUIPMENT



-A53-

Fig. A.4.9.

CALIBRATION OF 254 x 508mm VANE EQUIPMENT: UNDRAINED STRENGTH VERSUS DIAL DIVISIONS

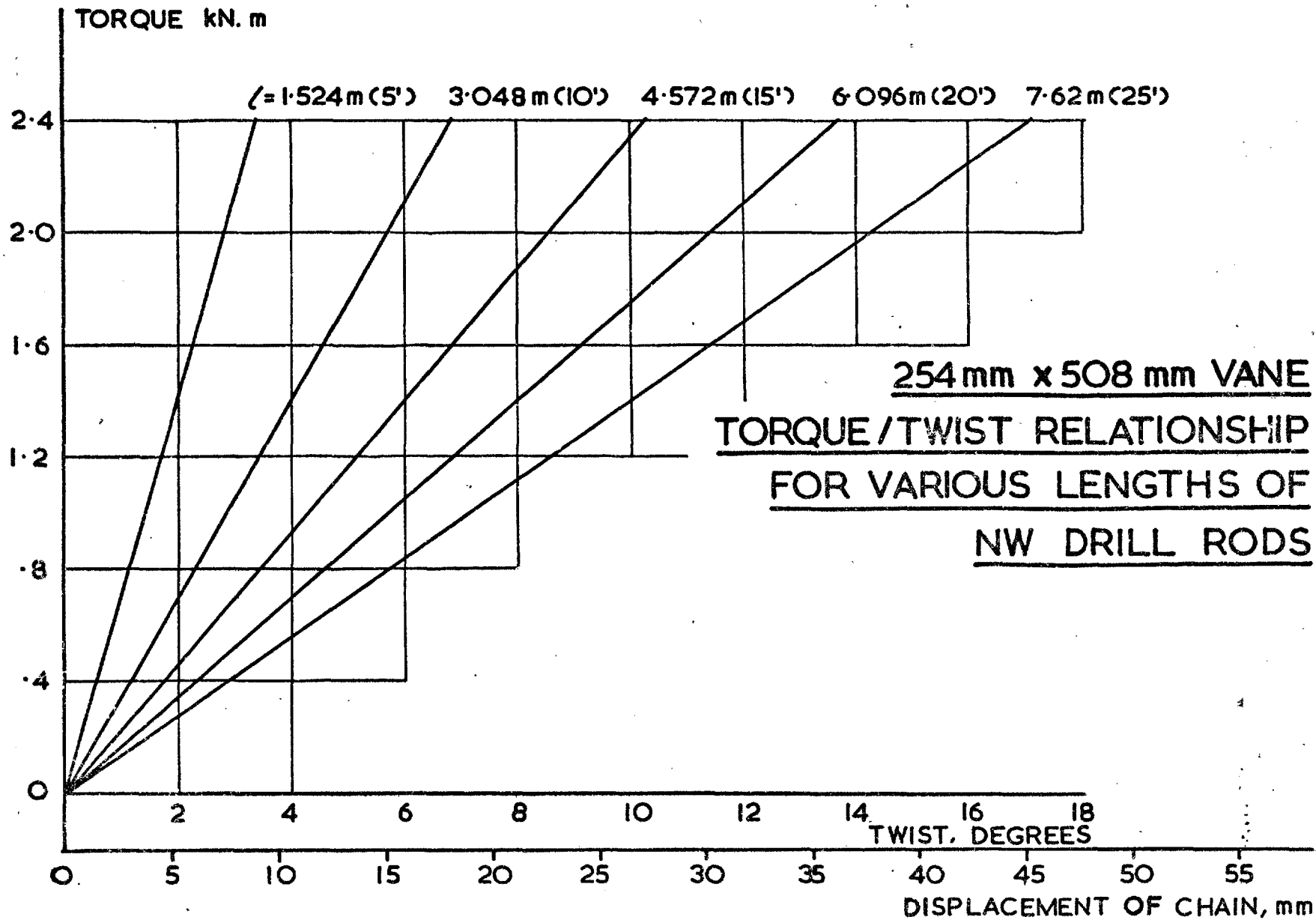
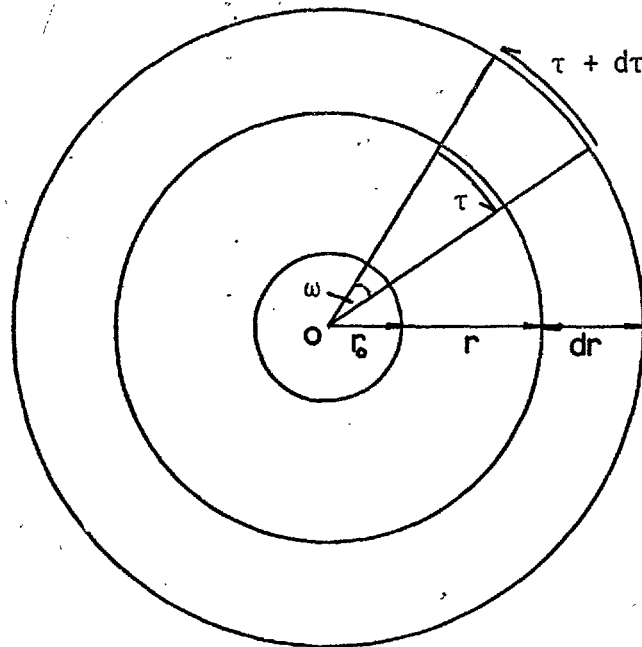


Fig. A.410

APPENDIX 5

STRESSES AND STRAINS ASSOCIATED WITH A VANE TEST IN AN ELASTIC SOIL

This calculation follows the analysis of Cadling and Odenstad (1950); the vane is represented by a rigid cylinder having the same radius (r_0) as the vane and extending axially to infinity, with the clay assumed to adhere to the surface of this cylinder (as below):-



Considering the equilibrium of a small element at a radial distance r (as above): by taking moments about O:-

$$(\tau + d\tau)(r + dr) \omega (r + dr) - \tau r \omega r = 0$$

which leads to $d\tau = -2\tau dr$ if differential products are ignored

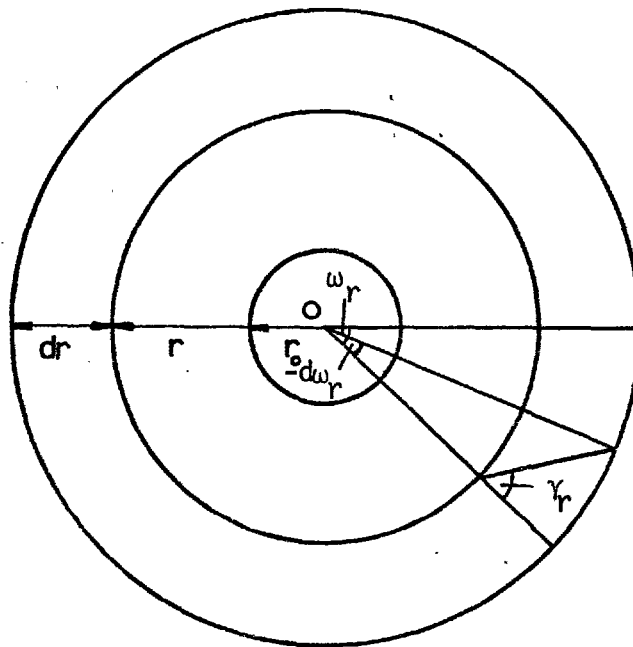
$$\therefore \frac{d\tau}{\tau} = -\frac{2dr}{r} \text{ and } \tau_0 \left(\frac{d\tau}{\tau} \right) = -2 \left(\frac{r_0}{r} \right) dr$$

$$\therefore \log \tau_0 - \log \tau_r = -2(\log r_0 - \log r)$$

$$\therefore \frac{\tau_0}{\tau_r} = \left(\frac{r}{r_0} \right)^2 \text{ and } \tau_r = \frac{r_0^2}{r^2} \tau_0 \dots\dots\dots(\text{A.5.1.})$$

and as $\tau = G \cdot \gamma$ $\gamma_r = \frac{r_0^2}{r^2} \gamma_0$

During deformation each point in the clay is assumed to move in a circular arc, the centre of which is the vane's centre (O). If the movement of the soil at radius r subtends an angle ω_r at the centre, the movement of the soil at radius (r + dr) subtends an angle $\omega_r - (-d\omega_r)$ thus inducing a shear strain γ_r in the soil, as follows:-



$$\therefore \gamma_r = \frac{(r + dr)\omega_r - (r + dr)(\omega_r + d\omega_r)}{dr} = -r \frac{d\omega_r}{dr} = \frac{r_0^2}{r^2} \gamma_0$$

$$\therefore \frac{d\omega_r}{dr} = -\frac{r_0^2}{r^3} \gamma_0 \quad \text{and} \quad \omega_r = \gamma_0 \int -\frac{r_0^2}{r^3}$$

$$\therefore \omega_r = \frac{\gamma_0}{2} \frac{r_0^2}{r^2} + C; \quad \text{when } r = \infty, \omega_r = 0 \text{ and } \therefore C = 0$$

$$\therefore \omega_r = \frac{1}{2} \frac{r_0^2}{r^2} \gamma_0 \quad \dots\dots\dots (A.5.2.)$$

which leads directly to $\omega_0 = \frac{1}{2} \gamma_0 \quad \dots\dots\dots (A.5.3.)$

and therefore to $G = \frac{\tau_0}{2\omega_0} \quad \dots\dots\dots (A.5.4.)$

APPENDIX 6

DETAILED DATA RELATING TO LIMIT EQUILIBRIUM ANALYSES

1. Table A.6.1. - Key to property sets used in stability analyses.
2. Table A.6.2. - Material property sets used in total stress stability analyses.
3. Table A.6.3. - Material property sets used in effective stress stability analyses.
4. Table A.6.4. - Bank 1, Stage 1. Summary of results of total stress stability analyses.
5. Table A.6.5. - Bank 1, Stage 1. Summary of results of effective stress stability analyses.
6. Table A.6.6. - Bank 1, Stage 2. Summary of results of total stress stability analyses.
7. Table A.6.7. - Bank 1, Stage 2. Summary of results of effective stress stability analyses.
8. Table A.6.8. - r_u values for Bishop's Routine Method.

1. LABORATORY AND FIELD TEST DATA XX-YY-Z(Z)

- XX - TS = Total Stress, ES = Effective Stress
- YY - LD = Laboratory Design Values With (r), and Without, A Strain Rate Correction
- VB = Vertical Specimens from Block Samples
- VP = Vertical Specimens from Piston Samples
- GV = Geonor Vane
- LV = Large Vane (Corresponding to t_f of Geonor Vane)
- LM = Large Vane, Minimum Values
- Z - 1 = Weak Crust Assumption
- 2 = Strong Crust Assumption
- (Z) - (μ) = Bjerrum's (1972) Correction Factor Applied (Vane Tests Only)

2. DERIVED PEAK STRENGTH DATA XX-YY-Z(Z)

(i.e. F.O.S. = 1.0 on critical surface for section at max. fill height)

- XX - TS = Total Stress, ES = Effective Stress
- YY - 1 = Weak Crust Assumption
- 2 = Strong Crust Assumption
- Z - 0 = Applies to Both Failures; No Restrictions on Slip Surface Location
- 1 = Applies to Stage 1 Only; Slip Surface Restricted to Fit Field Observations
- 2 = Applies to Stage 2 Only; Slip Surface Restricted to Fit Field Observations
- (Z) - (a) = Pore Pressures in Effective Stress Analyses Extrapolated to Correspond to Fill Height at Failure

3. DERIVED RESIDUAL STRENGTH DATA XX-YY-Z

(i.e. F.O.S. = 1.0 on critical restricted surface for post-failure section)

- XX - TS = Total Stress, ES = Effective Stress
- Y - 1 = Weak Crust Assumption
- 2 = Strong Crust Assumption
- (Y) - (R) = Residual Strength Analysis
- Z - 1 = Applies to Stage 1 only
- 2 = Applies to Stage 2 only

Table A.6.1.

Key to Property Sets Used in Stability Analyses

ZONE	3	4	5	6	7	8	
PROPERTY SET							SEE FIG.
TS-LD-1	20	14.0	13.25	15.0	18.5	21.5	2.23
TS-LD-2	45	14.0	13.25	15.0	18.5	21.5	7.5.1.
TS-LD(r)-1	13	9.1	8.6	9.75	12.0	14	2.23
TS-LD(r)-2	45	9.1	8.6	9.75	12.0	14	7.5.1.
TS-VB-1	20	13.5	15.25	17.5	20.5	23.5	3.7
TS-VB-2	45	13.5	15.25	17.5	20.5	23.5	
TS-VP-1	20	13.0	13.75	16.25	19.5	22.75	2.23
TS-VP-2	45	13.0	13.75	16.25	19.5	22.75	
TS-GV-1	20	16.25	18.25	18.0	19.25	22.75	3.7
TS-GV-1(μ)	17.5	11.5	13.5	15.0	14.75	16.25	3.7
TS-GV-2	45	16.25	18.25	18.0	19.25	22.75	7.5.1.
TS-GV-2(μ)	45	11.5	13.5	15.0	14.75	16.25	7.5.1.
TS-LV-1	20	15.0	13.25	13.25	16.25	19.25	3.18
TS-LV-1(μ)	17.5	11.25	10.25	10.75	12.5	12.5	3.23
TS-LV-2	45	15.0	13.25	13.25	16.25	19.25	7.5.1.
TS-LV-2(μ)	45	11.25	10.25	10.75	12.5	12.5	7.5.1.
TS-LM-1	20	13.1	11.9	12.65	14.5	16.5	3.18
TS-LM-1(μ)	17.5	10.1	9.0	10.25	11.0	11.0	3.23
TS-LM-2	45	13.1	11.9	12.65	14.5	16.5	
TS-LM-2(μ)	45	10.1	9.0	10.25	11.0	11.0	
1. LABORATORY AND FIELD VANE TEST DATA							
TS-1-0	17.5	11.5	10.8	12.5	16.0	19.0	
TS-2-0	45	10.2	9.5	11.2	14.7	17.7	7.5.1.
TS-1-1	16.4	10.4	9.65	11.4	14.9	17.9	
TS-2-1	45	9.7	8.95	10.7	14.2	17.2	
TS-1-2	17.8	11.8	11.05	12.8	16.3	19.3	
TS-2-2	45	7.95	7.2	8.95	12.45	15.45	
2. DERIVED PEAK STRENGTH DATA							
TS-1(R)-1	11.25	5.25	4.5	6.25	9.75	12.75	
TS-2(R)-1	30	5.0	4.25	6.0	9.5	12.5	7.5.1.
TS-1(R)-2	11.25	5.25	4.5	6.25	9.75	12.75	
TS-2(R)-2	20	4.5	3.75	5.5	9.0	12.0	
3. DERIVED RESIDUAL STRENGTH DATA							

Note: For key to property sets see table A.6.1.

Table A.6.2.

Material Property Sets Used in Total Stress Stability Analyses

PROPERTY SET	ES-LD-1/2	'FINAL' DESIGN*		
c' kN/m ²	6.5	8		
φ' DEG	26.5	25		
1. LABORATORY DATA				
PROPERTY SET	ES-1-1	ES-1-1(a)	ES-2-1	ES-2-1(a)
c' kN/m ²	3.75	5.5	1.85	3.75
φ' DEG	26.5	26.5	26.5	26.5
PROPERTY SET	ES-1-2	ES-1-2(a)	ES-2-2	ES-2-2(a)
c' kN/m ²	2.75	5.25	0	0.7
φ' DEG	26.5	26.5	21	26.5
2. DERIVED PEAK STRENGTH DATA				
PROPERTY SET	ES-1(R)-1	ES-2(R)-1	ES-1(R)-2	ES-2(R)-2
c' kN/m ²	2.25	0.65	0	0
φ' DEG	26.5	26.5	24	20
3. DERIVED RESIDUAL STRENGTH DATA				

- Notes:**
1. Effective stress parameters for fill (ZONES 1 and 2) were $c = 0$, $\phi' = 38^\circ$.
 2. Property sets tabulated refer to ZONES 3 to 8 except for strong crust analyses (table A.6.1.) in which properties for ZONE 3 are as per table A.6.2.
 3. For key to property sets see table A.6.1.
- * No strain rate effect correction of c' was made at the input stage.

Table A.6.3.

Material Property Sets Used in Effective Stress Stability Analyses

SURFACE	BT1/1A	BT2/1A	BE1/1(A) BT1/1	BE2/1(A)	BT2/1	ST1/1	ST2/1	SE1/1	SE2/1
PROPERTY SET									
TS-LD-1	1.21	1.25	1.26	1.21	1.27	1.27	1.36	1.30	1.37
TS-LD-2	1.30	1.25	1.34	1.31	1.27	1.37	1.36	1.39	1.37
TS-LD(r)-1	0.79	0.81	0.82	0.84	0.83	0.83	0.89	0.85	0.90
TS-LD(r)-2	0.86	0.81	0.88	0.84	0.83	0.90	0.89	0.91	0.90
TS-VB-1	1.33	1.37	1.38	1.42	1.38	1.42	1.50	1.43	1.51
TS-VB-2	1.46	1.37	1.45	1.42	1.38	1.51	1.50	1.52	1.51
TS-VP-1	1.25	1.30	1.31	1.35	1.31	1.34	1.42	1.35	1.43
TS-VP-2	1.36	1.30	1.38	1.35	1.31	1.43	1.42	1.45	1.43
TS-GV-1	1.42	1.39	1.44	1.46	1.41	1.50	1.55	1.52	1.56
TS-GV-1(μ)	1.16	1.10	1.14	1.17	1.12	1.20	1.22	1.22	1.22
TS-GV-2	1.56	1.39	1.56	1.46	1.41	1.64	1.55	1.65	1.56
TS-GV-2(μ)	1.32	1.10	1.28	1.17	1.12	1.39	1.22	1.43	1.22
TS-LV-1	1.13	1.12	1.15	1.20	1.15	1.21	1.23	1.21	1.24
TS-LV-1(μ)	0.96	0.91	0.96	0.97	0.93	1.01	0.99	1.02	0.99
TS-LV-2	1.26	1.12	1.28	1.20	1.15	1.35	1.23	1.33	1.24
TS-LV-2(μ)	1.13	0.91	1.07	0.97	0.93	1.14	0.99	1.13	0.99
TS-LM-1	1.08	1.06	1.08	1.13	1.07	1.14	1.15	1.16	1.15
TS-LM-1(μ)	0.89	0.84	0.87	0.91	0.85	0.92	0.90	0.93	0.90
TS-LM-2	1.22	1.06	1.21	1.13	1.07	1.27	1.15	1.29	1.15
TS-LM-2(μ)	1.05	0.84	1.01	0.91	0.85	1.07	0.90	1.09	0.90
TS-1-0	1.02	1.08	1.08	1.14	1.10	1.09	1.16	1.11	1.17
TS-2-0	1.09	0.99	1.12	1.05	1.01	1.14	1.06	1.16	1.07
TS-1-1	0.94	1.00	1.00	1.05	1.02	1.00	1.07	1.01	1.07
TS-2-1	1.06	0.95	1.09	1.00	0.97	1.10	1.01	1.12	1.02
TS-1-2	1.05	1.10	1.10	1.16	1.12	1.11	1.18	1.13	1.19
TS-2-2	0.94	0.83	0.97	0.88	0.85	0.97	0.87	0.99	0.87

Table A.6.4.

Bank 1, Stage 1

Summary of Results of Total Stress Stability Analyses

SURFACE	BT1/1A	BT2/1A	BE1/1(A) BT1/1	BE2/1(A)	BT2/1	ST1/1	ST2/1	SE1/1	SE2/1
PROPERTY SET									
ES-LD-1	1.26	1.30	1.25	1.29	1.30	1.25	1.42	1.23	1.39
ES-LD-2	1.42	1.30	1.38	1.29	1.30	1.40	1.42	1.40	1.39
ES-1-1	1.05	1.10	1.04	1.09	1.10	1.03	1.19	1.01	1.17
ES-1-1(a)	-	-	-	-	-	1.18	1.34	1.16	1.33
ES-2-1	1.04	0.96	1.00	0.95	0.97	1.01	1.01	1.01	1.01
ES-2-1(a)	-	-	-	-	-	1.17	1.17	1.16	1.17
ES-1-2	0.98	1.03	0.96	1.02	1.03	0.94	1.10	0.93	1.09
ES-1-2(a)	-	-	-	-	-	-	-	-	-
ES-2-2	0.77	0.65	0.73	0.64	0.66	0.73	*	0.73	*
ES-2-2(a)	-	-	-	-	-	-	-	-	-
A) PORE PRESSURES MEASURED AT 3.75m FILL HEIGHT									
ES-LD-1	-	-	-	-	-	1.11	1.27	1.09	1.25
ES-LD-2	-	-	-	-	-	1.26	1.27	1.26	1.25
ES-1-1	-	-	-	-	-	0.87	1.03	0.85	1.01
ES-1-1(a)	-	-	-	-	-	1.03	1.18	1.01	1.17
ES-2-1	-	-	-	-	-	0.86	0.84	0.85	0.84
ES-2-1(a)	-	-	-	-	-	1.02	1.01	1.02	1.01
B) PORE PRESSURES EXTRAPOLATED TO 4.0m FILL HEIGHT									

Table A.6.5.

Bank 1, Stage 1

Summary of Results of Effective Stress Stability Analyses

SURFACE	BT1/2A	BT2/2A	BE1/2(A)	BE2/2(A)	ST1/2A	ST2/2A	SE1/2(A)	SE2/2A	ST1/2 ST2/2	SE2/2
PROPERTY SET										
TS-LD-1	1.14	1.15	1.17	1.15	1.14	1.20	1.20	1.14	1.15	1.17
TS-LD-2	1.39	1.28	1.41	1.30	1.45	1.32	1.46	1.36	1.40	1.43
TS-LD(r)-1	0.75	0.76	0.77	0.76	0.75	0.78	0.78	0.75	0.77	0.78
TS-LD(r)-2	0.91	0.83	0.92	0.85	0.95	0.86	0.96	0.88	0.91	0.93
TS-VB-1	1.23	1.24	1.26	1.26	1.23	1.31	1.26	1.23	1.26	1.26
TS-VB-2	1.47	1.37	1.50	1.40	1.55	1.41	1.51	1.45	1.57	1.52
TS-VP-1	1.16	1.17	1.20	1.18	1.15	1.24	1.16	1.15	1.19	1.19
TS-VP-2	1.40	1.30	1.45	1.32	1.44	1.33	1.43	1.36	1.44	1.45
TS-GV-1	1.33	1.32	1.36	1.35	1.33	1.41	1.41	1.33	1.36	1.38
TS-GV-1(μ)	1.08	1.08	1.10	1.10	1.07	1.15	1.14	1.07	1.09	1.10
TS-GV-2	1.60	1.44	1.62	1.48	1.54	1.53	1.65	1.53	1.58	1.62
TS-GV-2(μ)	1.39	1.21	1.40	1.25	1.33	1.30	1.43	1.32	1.36	1.40
TS-LV-1	1.13	1.06	1.13	1.20	1.10	1.13	1.10	1.09	1.13	1.12
TS-LV-1(μ)	0.94	0.89	0.95	0.91	0.91	0.95	0.89	0.90	0.93	0.93
TS-LV-2	1.40	1.20	1.37	1.33	1.41	1.27	1.35	1.31	1.38	1.38
TS-LV-2(μ)	1.26	1.04	1.22	1.16	1.35	1.20	1.30	1.14	1.20	1.23
TS-LM-1	1.05	1.01	1.06	1.03	1.02	1.08	1.09	1.02	1.04	1.05
TS-LM-1(μ)	0.87	0.83	0.88	0.85	0.83	0.89	0.89	0.84	0.84	0.86
TS-LM-2	1.32	1.13	1.32	1.16	1.24	1.20	1.34	1.24	1.29	1.31
TS-LM-2(μ)	1.18	0.97	1.17	1.00	1.09	1.04	1.18	1.09	1.11	1.16
TS-1-0	0.98	0.98	0.99	0.98	0.96	1.02	1.02	0.96	0.97	0.99
TS-2-0	1.21	1.01	1.20	1.04	1.13	1.08	1.22	1.13	1.15	1.20
TS-1-1	0.90	0.90	0.91	0.90	0.88	1.10	0.93	0.88	0.89	0.90
TS-2-1	1.18	0.98	1.17	1.08	1.10	1.04	1.20	1.10	1.12	1.16
TS-1-2	1.00	1.00	1.01	1.00	0.97	1.04	1.04	0.98	0.99	1.01
TS-2-2	1.09	0.86	1.07	0.90	1.00	0.93	1.08	1.00	1.01	1.06

Table A.6.6.

Bank 1, Stage 2

Summary of Results of Total Stress Stability Analyses

SURFACE	BT1/2A	BT2/2A	BE1/2(A)	BE2/2(A)	ST1/2A	ST2/2A	SE1/2(A)	SE2/2A	ST1/2 ST2/2	SE2/2
PROPERTY SET										
ES-LD-1	1.45	1.47	1.39	1.42	1.35	1.47	1.31	1.34	1.37	1.32
ES-LD-2	1.80	1.66	1.74	1.61	1.63	1.67	1.66	1.62	1.65	1.65
ES-1-1	1.26	1.28	1.19	1.22	1.13	1.26	1.09	1.13	1.15	1.10
ES-1-1(a)	-	-	-	-	-	-	-	-	-	-
ES-2-1	1.42	1.28	1.36	1.23	1.25	1.29	1.28	1.24	1.27	1.27
ES-2-1(a)	-	-	-	-	-	-	-	-	-	-
ES-1-2	1.19	1.21	1.12	1.15	1.05	1.17	1.00	1.05	1.06	1.01
ES-1-2(a)	-	-	-	-	1.24	1.38	1.21	1.25	1.27	1.22
ES-2-2	1.16	0.97	1.10	0.94	0.98	0.98	1.02	0.98	1.02	1.01
ES-2-2(a)	-	-	-	-	1.18	1.20	1.20	1.17	1.19	1.19
A) PORE PRESSURES MEASURED AT 4.25m FILL HEIGHT										
ES-LD-1	-	-	-	-	1.15	1.28	1.11	1.15	1.17	1.12
ES-LD-2	-	-	-	-	1.44	1.45	1.47	1.43	1.44	1.45
ES-1-2	-	-	-	-	0.82	0.95	0.79	0.82	0.82	0.76
ES-1-2(a)	-	-	-	-	1.05	1.18	1.01	1.05	1.06	1.02
ES-2-2	-	-	-	-	0.83	0.83	0.88	0.82	0.84	0.87
ES-2-2(a)	-	-	-	-	0.98	0.99	1.01	0.97	0.98	0.99
B) PORE PRESSURES EXTRAPOLATED TO 4.5m FILL HEIGHT										

Table A.6.7.

Bank 1, Stage 2

Summary of Results of Effective Stress Stability Analyses

ZONE	1	2	3	4	5	6	7	8
RANGE	-	0-0.11	0-0.47	0.11-1.36	0.58-1.36	0.58-0.97	0.61-0.91	0.31-0.82
AVERAGE	0	0.05	0.16	0.61	0.81	0.78	0.75	0.58

Bank 1/1 - Fill Height 3.75m

ZONE	1	2	3	4	5	6	7	8
RANGE	-	0-0.11	0-0.97	0.1-1.1	0.39-1.1	0.52-1.03	0.55-0.94	0.29-0.74
AVERAGE	0	0.05	0.20	0.56	0.71	0.71	0.67	0.57

Bank 1/2 - Fill Height 4.25m

Table A.6.8.

r_u Values for Bishop's Routine Method